frontiers | Research Topics

Cellular CNS repair strategies, technologies and therapeutic developments

Edited by
Jorg Dietrich, Tim-Henrik Bruun, Ulrich - Bogdahn and Anna Klingseisen

Published in
Frontiers in Cellular Neuroscience

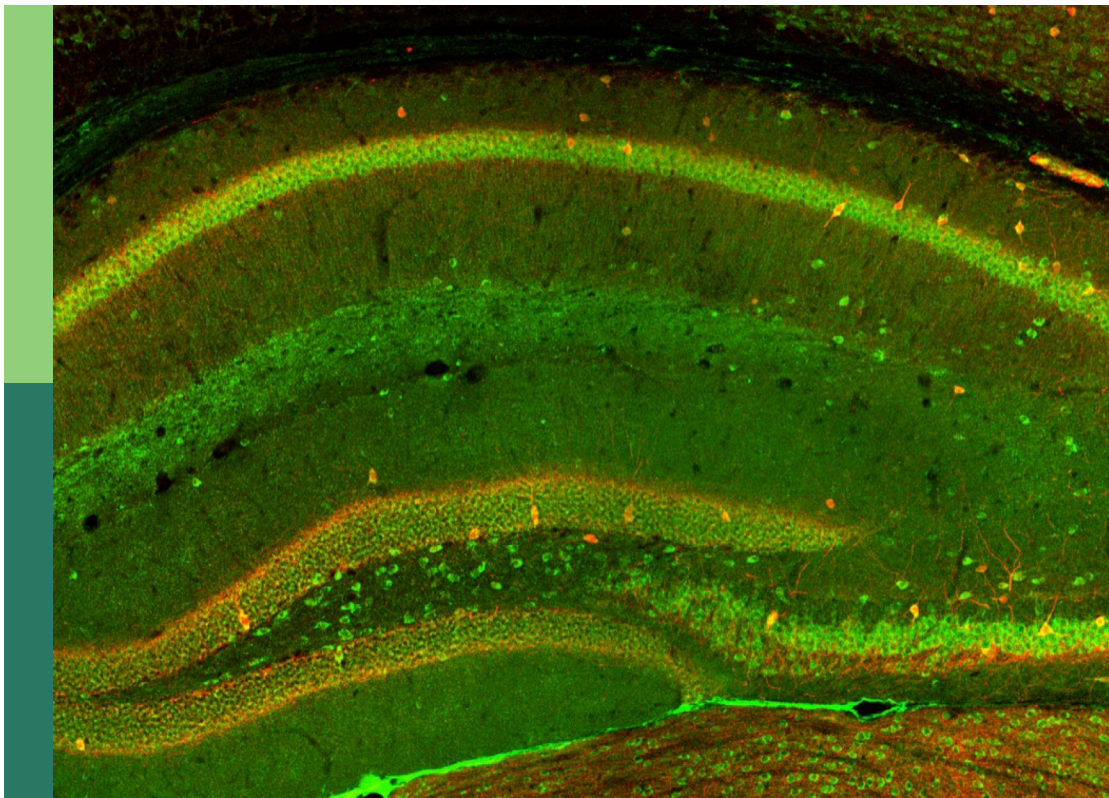

FRONTIERS EBOOK COPYRIGHT STATEMENT

The copyright in the text of individual articles in this ebook is the property of their respective authors or their respective institutions or funders. The copyright in graphics and images within each article may be subject to copyright of other parties. In both cases this is subject to a license granted to Frontiers.

The compilation of articles constituting this ebook is the property of Frontiers.

Each article within this ebook, and the ebook itself, are published under the most recent version of the Creative Commons CC-BY licence. The version current at the date of publication of this ebook is CC-BY 4.0. If the CC-BY licence is updated, the licence granted by Frontiers is automatically updated to the new version.

When exercising any right under the CC-BY licence, Frontiers must be attributed as the original publisher of the article or ebook, as applicable.

Authors have the responsibility of ensuring that any graphics or other materials which are the property of others may be included in the CC-BY licence, but this should be checked before relying on the CC-BY licence to reproduce those materials. Any copyright notices relating to those materials must be complied with.

Copyright and source acknowledgement notices may not be removed and must be displayed in any copy, derivative work or partial copy which includes the elements in question.

All copyright, and all rights therein, are protected by national and international copyright laws. The above represents a summary only. For further information please read Frontiers' Conditions for Website Use and Copyright Statement, and the applicable CC-BY licence.

ISSN 1664-8714
ISBN 978-2-8325-2404-6
DOI 10.3389/978-2-8325-2404-6

About Frontiers

Frontiers is more than just an open access publisher of scholarly articles: it is a pioneering approach to the world of academia, radically improving the way scholarly research is managed. The grand vision of Frontiers is a world where all people have an equal opportunity to seek, share and generate knowledge. Frontiers provides immediate and permanent online open access to all its publications, but this alone is not enough to realize our grand goals.

Frontiers journal series

The Frontiers journal series is a multi-tier and interdisciplinary set of open-access, online journals, promising a paradigm shift from the current review, selection and dissemination processes in academic publishing. All Frontiers journals are driven by researchers for researchers; therefore, they constitute a service to the scholarly community. At the same time, the *Frontiers journal series* operates on a revolutionary invention, the tiered publishing system, initially addressing specific communities of scholars, and gradually climbing up to broader public understanding, thus serving the interests of the lay society, too.

Dedication to quality

Each Frontiers article is a landmark of the highest quality, thanks to genuinely collaborative interactions between authors and review editors, who include some of the world's best academicians. Research must be certified by peers before entering a stream of knowledge that may eventually reach the public - and shape society; therefore, Frontiers only applies the most rigorous and unbiased reviews. Frontiers revolutionizes research publishing by freely delivering the most outstanding research, evaluated with no bias from both the academic and social point of view. By applying the most advanced information technologies, Frontiers is catapulting scholarly publishing into a new generation.

What are Frontiers Research Topics?

Frontiers Research Topics are very popular trademarks of the *Frontiers journals series*: they are collections of at least ten articles, all centered on a particular subject. With their unique mix of varied contributions from Original Research to Review Articles, Frontiers Research Topics unify the most influential researchers, the latest key findings and historical advances in a hot research area.

Find out more on how to host your own Frontiers Research Topic or contribute to one as an author by contacting the Frontiers editorial office: frontiersin.org/about/contact

Cellular CNS repair strategies, technologies and therapeutic developments

Topic editors
Jorg Dietrich — Harvard Medical School, United States
Tim-Henrik Bruun — Velvio GmbH, Germany
Ulrich - Bogdahn — University of Regensburg, Germany
Anna Klingseisen — University of Edinburgh, United Kingdom

Citation
Dietrich, J., Bruun, T.-H., Bogdahn, U., Klingseisen, A., eds. (2023). *Cellular CNS repair strategies, technologies and therapeutic developments*. Lausanne: Frontiers Media SA. doi: 10.3389/978-2-8325-2404-6

UB is member of Neurovision Pharma GmbH. T-HB and UB are members of Velvio GmbH.

The remaining authors declare that the research was conducted in the absence of any commercial or financial relationships that could be construed as a potential conflict of interest

Table of contents

06 Editorial: Cellular CNS repair strategies, technologies and therapeutic developments
Tim-Henrik Bruun, Jorg Dietrich, Anna Klingseisen and Ulrich Bogdahn

07 Fully Characterized Mature Human iPS- and NMP-Derived Motor Neurons Thrive Without Neuroprotection in the Spinal Contusion Cavity
Zachary T. Olmsted, Cinzia Stigliano, Brandon Marzullo, Jose Cibelli, Philip J. Horner and Janet L. Paluh

24 Vav3-Deficient Astrocytes Enhance the Dendritic Development of Hippocampal Neurons in an Indirect Co-culture System
David Wegrzyn, Josephine Zokol and Andreas Faissner

44 Hearing Recovery Induced by DNA Demethylation in a Chemically Deafened Adult Mouse Model
Xin Deng and Zhengqing Hu

54 Metabolic Reprogramming in HIV-Associated Neurocognitive Disorders
Charles N. S. Allen, Sterling P. Arjona, Maryline Santerre, Claudio De Lucia, Walter J. Koch and Bassel E. Sawaya

75 Plasticity-Related Gene 5 Is Expressed in a Late Phase of Neurodifferentiation After Neuronal Cell-Fate Determination
Isabel Gross, Nicola Brandt, Danara Vonk, Franziska Köper, Lars Wöhlbrand, Ralf Rabus, Martin Witt, Axel Heep, Torsten Plösch, Mark S. Hipp and Anja U. Bräuer

92 Astroglia in the Vulnerability to and Maintenance of Stress-Mediated Neuropathology and Depression
José Javier Miguel-Hidalgo

102 Neuronal Redevelopment and the Regeneration of Neuromodulatory Axons in the Adult Mammalian Central Nervous System
Patrick Cooke, Haley Janowitz and Sarah E. Dougherty

120 Targeting C–C Chemokine Receptor 5: Key to Opening the Neurorehabilitation Window After Ischemic Stroke
Yi-Qi Feng, Zhen-Zhen Xu, Yan-Ting Wang, Yue Xiong, Wanli Xie, Yu-Yao He, Lu Chen, Guo-Yang Liu, Xia Li, Jie Liu and Qingping Wu

135 Ablation of GSDMD Attenuates Neurological Deficits and Neuropathological Alterations After Traumatic Brain Injury
Hao Du, Chang-Hong Li, Ruo-Bing Gao, Xiao-Qing Cen and Ping Li

151 Immune Cells in Subretinal Wound Healing and Fibrosis
Manon Szczepan, María Llorián-Salvador, Mei Chen and Heping Xu

164 MicroRNA-124/Death-Associated Protein Kinase 1 Signaling Regulates Neuronal Apoptosis in Traumatic Brain Injury *via* Phosphorylating NR2B
Yingwu Shi, Wenxing Cui, Qiang Wang, Jinpeng Zhou, Xun Wu, Jin Wang, Shenghao Zhang, Qing Hu, Liying Han, Yong Du, Shunnan Ge, Haixiao Liu and Yan Qu

177 Nicotine Facilitates Facial Stimulation-Evoked Mossy Fiber-Granule Cell Long-Term Potentiation *in vivo* in Mice
Li-Xin Cao, Yan-Hua Bing, Yin-Hua Xu, Guang-Jian Zhang, Chun-Ping Chu, Lan Hong and De-Lai Qiu

187 The role of enriched environment in neural development and repair
Yu Han, Mei Yuan, Yi-Sha Guo, Xin-Ya Shen, Zhen-Kun Gao and Xia Bi

205 Peripheral nervous system: A promising source of neuronal progenitors for central nervous system repair
Jessica L. Mueller, Rhian Stavely, Ryo Hotta and Allan M. Goldstein

212 The immune microenvironment and tissue engineering strategies for spinal cord regeneration
Yuan Feng, Yong Peng, Jing Jie, Yumin Yang and Pengxiang Yang

229 Mitochondrial behavior when things go wrong in the axon
Victorio M. Pozo Devoto, Isaac G. Onyango and Gorazd B. Stokin

245 LZK-dependent stimulation of astrocyte reactivity promotes corticospinal axon sprouting
Meifan Chen, Laura Ingle, Erik J. Plautz, Xiangmei Kong, Rui Tang, Neil Ghosh, Megan K. Romprey, William K. Fenske and Mark P. Goldberg

259 Oxytocin accelerates tight junction formation and impairs cellular migration in 3D spheroids: evidence from Gapmer-induced exon skipping
Benjamin Jurek, Lucia Denk, Nicole Schäfer, Mohammad Saied Salehi, Sareh Pandamooz and Silke Haerteis

276 Lithium promotes long-term neurological recovery after spinal cord injury in mice by enhancing neuronal survival, gray and white matter remodeling, and long-distance axonal regeneration
Zeynep Balçıkanlı, Irem Culha, Pelin Dilsiz, Mehmet Serif Aydin, Nilay Ates, Mustafa Caglar Beker, Saltuk Bugra Baltaci, Halil I. Koc, Ahmet Yigitbasi, Mustafa Gündogar, Thorsten R. Doeppner, Dirk M. Hermann and Ertugrul Kilic

290 Restoration of spinal cord injury: From endogenous repairing process to cellular therapy
Yaqi Wu, Zhijian Tang, Jun Zhang, Yu Wang and Shengwen Liu

frontiers | Frontiers in Cellular Neuroscience

TYPE Editorial
PUBLISHED 28 April 2023
DOI 10.3389/fncel.2023.1200639

Check for updates

OPEN ACCESS

EDITED AND REVIEWED BY
Enrico Cherubini,
European Brain Research Institute, Italy

*CORRESPONDENCE
Ulrich Bogdahn
✉ uli.bogdahn@ukr.de

RECEIVED 05 April 2023
ACCEPTED 06 April 2023
PUBLISHED 28 April 2023

CITATION
Bruun T-H, Dietrich J, Klingseisen A and Bogdahn U (2023) Editorial: Cellular CNS repair strategies, technologies and therapeutic developments.
Front. Cell. Neurosci. 17:1200639.
doi: 10.3389/fncel.2023.1200639

COPYRIGHT
© 2023 Bruun, Dietrich, Klingseisen and Bogdahn. This is an open-access article distributed under the terms of the Creative Commons Attribution License (CC BY). The use, distribution or reproduction in other forums is permitted, provided the original author(s) and the copyright owner(s) are credited and that the original publication in this journal is cited, in accordance with accepted academic practice. No use, distribution or reproduction is permitted which does not comply with these terms.

Editorial: Cellular CNS repair strategies, technologies and therapeutic developments

Tim-Henrik Bruun[1], Jorg Dietrich[2], Anna Klingseisen[3] and Ulrich Bogdahn[1,4]*

[1]Velvio GmbH Regensburg, Regensburg, Germany, [2]Harvard Medical School Boston, Boston, MA, United States, [3]UK Dementia Research Institute, University of Edinburgh, Edinburgh, United Kingdom, [4]Department of Neurology, University Hospital Regensburg, Regensburg, Germany

KEYWORDS

neurodegeneration, drug-development, CNS-repair, biomarker, study-design in CNS

Editorial on the Research Topic
Cellular CNS repair strategies, technologies, and therapeutic developments

The central nervous system (CNS) plays a key role in controlling and coordinating the body's functions and movements. Damage to the CNS may have devastating effects, including paralysis, sensory loss, and cognitive impairment. However, recent advances in cellular CNS repair strategies have brought new hope for patients suffering from CNS injuries or neurodegenerative disorders. The Research Topic "*Cellular CNS repair strategies, technologies and therapeutic developments*" featured in Frontiers in Neuroscience, highlights several novel aspects and advances in this exciting field.

The special Research Topic includes contributions from 20 committed scientists and researchers from around the world, providing valuable insights into some of the latest technologies and therapeutic developments in cellular CNS repair. The articles range from basic science to clinical applications, covering a broad spectrum of topics that are crucial for advancing our understanding of CNS repair.

One of the main themes that emerge from the Research Topic is the use of stem cells for CNS repair. Stem cells have the potential to differentiate into various cell types, making them ideal for repairing damaged or diseased tissue. In their article, Feng et al. discuss the use of neural stem cells in the treatment of spinal cord injury (SCI), demonstrating the promising results of preclinical studies.

Another major theme in the Research Topic is the role of neurotrophic factors for CNS repair. Neurotrophic factors are proteins that promote the growth and survival of neurons and some non-neuronal cells, and they have been shown to play a crucial role in the regeneration of damaged CNS tissue (Chen et al.). In their article, Olmstedt et al. describe how the outcome of neural cell-based therapies in SCI might be improved.

Several articles in this Research Topic also explore the use of novel technologies for CNS repair. For example, Feng et al. discuss the use of immune microenvironment and tissue engineering strategies for CNS repair, highlighting the potential of this approach for improving the efficacy and specificity of SCI therapies. Jurek et al. used a 3D culture model and found that Oxytocin (OXT) decreases cellular migration but increases cell-cell contacts and therefore improves nutrient supply, which might have implications for degenerating CNS disorders and tumor formation in various tissues.

The Research Topic also includes articles that focus on clinical applications of cellular CNS repair strategies. For example, Wu et al. summarizes cell types involved in the repair process and the common repair mechanisms of spinal cord injury, emphasizing the importance of clinical trial design and patient selection for the success of SCI therapies. Shi et al. also describe the use of miRNA targets for traumatic brain injury (TBI), demonstrating a potential target for the treatment of TBI related dysfunction.

Overall, the Research Topic "*Cellular CNS repair strategies, technologies and therapeutic developments*" provides valuable examples of the current state of research in this exciting field. The featured contributions highlight several examples of the significant progress that has been made in recent years, as well as the challenges that lie ahead. By bringing together researchers from diverse disciplines and perspectives, the Research Topic provides a potential roadmap for future research in this critical area.

It is worth noting that the Research Topic also sheds light on some of the ethical considerations surrounding the use of cellular CNS repair strategies. As the field continues to advance, it is important to ensure that these therapies are developed and deployed in an ethical and responsible manner. Mueller et al. discusses the importance of considering the potential risks and benefits of stem cell therapies, as well as the need for standardized protocols in the manufacturing and testing of stem cell products.

Conclusion

In conclusion, the Research Topic "Cellular CNS repair strategies, technologies and therapeutic developments" is a valuable resource for researchers, clinicians, and policymakers interested in the field of CNS repair. This special edition and collection of articles provides a comprehensive overview of the latest technologies and therapeutic developments, as well as highlighting existing challenges and future perspectives. As the field continues to advance, there is increasing evidence that cellular CNS repair strategies will play an increasingly important role in the treatment of CNS injuries and degenerative disorders, bringing new hope to patients around the world, and bringing to our attention that we never had been dreaming of repairing the brain and spinal cord.

Author contributions

T-HB wrote the first draft of the manuscript. All authors contributed to manuscript revision, read, and approved the submitted version.

Conflict of interest

UB is member of Neurovision Pharma GmbH. T-HB and UB are members of Velvio GmbH.

The remaining authors declare that the research was conducted in the absence of any commercial or financial relationships that could be construed as a potential conflict of interest.

Publisher's note

All claims expressed in this article are solely those of the authors and do not necessarily represent those of their affiliated organizations, or those of the publisher, the editors and the reviewers. Any product that may be evaluated in this article, or claim that may be made by its manufacturer, is not guaranteed or endorsed by the publisher.

frontiers in Cellular Neuroscience

ORIGINAL RESEARCH
published: 03 January 2022
doi: 10.3389/fncel.2021.725195

Fully Characterized Mature Human iPS- and NMP-Derived Motor Neurons Thrive Without Neuroprotection in the Spinal Contusion Cavity

Zachary T. Olmsted[1], *Cinzia Stigliano*[2], *Brandon Marzullo*[3], *Jose Cibelli*[4,5], *Philip J. Horner*[2] *and Janet L. Paluh*[1]*

[1]Nanobioscience Constellation, Colleges of Nanoscale Science and Engineering, State University of New York Polytechnic Institute, Albany, NY, United States, [2]Center for Neuroregeneration, Department of Neurosurgery, Houston Methodist Research Institute, Houston, TX, United States, [3]SUNY Buffalo Genomics and Bioinformatics Core, New York State Center of Excellence in Bioinformatics and Life Sciences, Buffalo, NY, United States, [4]Department of Animal Science, College of Agriculture and Natural Resources, Michigan State University, East Lansing, MI, United States, [5]Department of Large Animal Clinical Sciences, College of Veterinary Medicine, Michigan State University, East Lansing, MI, United States

OPEN ACCESS

Edited by:
Haruyuki Kamiya, Hokkaido University, Japan

Reviewed by:
Arne Battefeld, Université de Bordeaux, France
Xifan Mei, First Affiliated Hospital of Jinzhou Medical University, China

***Correspondence:**
Janet L. Paluh
paluhj@sunypoly.edu

Specialty section:
This article was submitted to Cellular Neurophysiology, a section of the journal Frontiers in Cellular Neuroscience

Received: *15 June 2021*
Accepted: *04 November 2021*
Published: *03 January 2022*

Citation:
Olmsted ZT, Stigliano C, Marzullo B, Cibelli J, Horner PJ and Paluh JL (2022) Fully Characterized Mature Human iPS- and NMP-Derived Motor Neurons Thrive Without Neuroprotection in the Spinal Contusion Cavity. Front. Cell. Neurosci. 15:725195. doi: 10.3389/fncel.2021.725195

Neural cell interventions in spinal cord injury (SCI) have focused predominantly on transplanted multipotent neural stem/progenitor cells (NSPCs) for animal research and clinical use due to limited information on survival of spinal neurons. However, transplanted NSPC fate is unpredictable and largely governed by injury-derived matrix and cytokine factors that are often gliogenic and inflammatory. Here, using a rat cervical hemicontusion model, we evaluate the survival and integration of hiPSC-derived spinal motor neurons (SMNs) and oligodendrocyte progenitor cells (OPCs). SMNs and OPCs were differentiated *in vitro* through a neuromesodermal progenitor stage to mimic the natural origin of the spinal cord. We demonstrate robust survival and engraftment without additional injury site modifiers or neuroprotective biomaterials. *Ex vivo* differentiated neurons achieve cervical spinal cord matched transcriptomic and proteomic profiles, meeting functional electrophysiology parameters prior to transplantation. These data establish an approach for *ex vivo* developmentally accurate neuronal fate specification and subsequent transplantation for a more streamlined and predictable outcome in neural cell-based therapies of SCI.

Keywords: spinal cord injury, spinal motor neuron, neuromesodermal progenitor, oligodendrocyte progenitor cell, neuron transplantation, neuron survival, neuron maturation, contusion

INTRODUCTION

The feasibility to replace tissues damaged in spinal cord injury (SCI) *via* transplantation and to drive host-graft restored connectivity depends on optimizing therapeutic cell strategies. Central nervous system (CNS) cell replacement and regeneration initially used fetal tissue containing differently staged neural stem and progenitor cells (NSPCs), neurons and glia, and non-neuronal cell types (Reier et al., 1986; Bregman et al., 1993).

Multipotent NSPCs generated *via* mouse and human stem cell neurotechnologies have now replaced this source in order to address the complexity of damage and loss of diverse CNS cell types in spinal networks after traumatic injuries (Silva et al., 2014; Assinck et al., 2017). Historically, there is no evidence that a mature neuron survives or thrives after transplantation. However, as stem cell neurotechnologies advance, breakthroughs in early human brain and trunk CNS development as well as RNA-Seq analysis are now enabling advanced neuronal differentiation strategies for generation of regionally-matched spinal neuron types and subtypes (Dulin et al., 2018; Olmsted and Paluh, 2021). Here we demonstrate that spinal motor neurons (SMNs) differentiated and matured *in vitro* from pluripotent stem cells can survive when transplanted into the SCI microenvironment in a 10 day and 6 week study.

A renewed interest to more directly address brain and trunk CNS pathologies with neurons is occurring in parallel with continuing NSPC efforts. Parkinson's disease has seen great advancements by applying new stem cell neural differentiation technologies that provide anatomic regional matching and cell-type specific replacement (A9 dopaminergic neurons and their precursors; Kikuchi et al., 2017; Xiong et al., 2021). Pre-differentiated GABAergic spinal interneurons were recently tested for use in neuropathic pain models (Manion et al., 2020), although this study did not use an injury model and cells were injected into the intact dorsal horn. Due to a newly advanced understanding of human trunk and spine development (Henrique et al., 2015; Olmsted and Paluh, 2021; Wind et al., 2021), the spinal cord field is now poised to generate spinal neural cell types along the entire rostral-caudal neuraxis (Peljto et al., 2010; Kumamaru et al., 2018) and test these in a variety of animal SCI models. Developmentally directed neural cell types are expected to represent the gold standard for cell transplantation. The discovery of neuromesodermal progenitors (NMPs) as the multipotent building blocks of the human trunk and spine (Tzouanacou et al., 2009) revealed a novel pool of axial stem cells that give rise to the spinal cord neuroectoderm, mesodermal somites, and trunk neural crest cells (NCCs). The strategy of NMP-derived neural cells is gaining momentum as a possible optimized cell source for SCI therapeutics that is based in normal human progenitor development (Gouti et al., 2014) and could allow long-term survival in order to realize efficient host-graft interactions.

Stem cell pre-differentiated neurons for transplantation into traumatic models of SCI remain understudied but are emerging as a novel strategy in SCI cell therapeutics. Recently, a direct reprogramming approach bypassing the typical human developmental timeline was applied by Lee et al. (2020). In their acute transplantation study, de-differentiated autologous fibroblasts that were induced into motor neurons (iMNs) promoted functional recovery in a thoracic rodent spinal cord T9 compression model. Direct reprogramming of fibroblasts to iMNs vs. directed differentiation from pluripotent stem cells through developmental cascades results in inherent transcriptional differences with unknown long-term therapeutic impact (Burke et al., 2020; Carter et al., 2020) as well as cell variability that can impact reproducibility of SCI therapeutic outcomes. In this study, we differentiate spinal neurons from hiPSC-derived NMPs, which are yet to be evaluated in any postnatal mammalian SCI model, along with relevant spinal interneurons and oligodendrocyte progenitor cells (OPCs) in rat cervical hemicontusion SCI (C4-C5). By histological analysis at 10 days and 6 weeks, we show that NMP-derived homotypic neural cells delivered as suspensions survive in the harsh contusion injury microenvironment. Importantly, the SMNs survive without additional neuroprotective encapsulation or added facilitators, consistent with evidence that homotypic matching is a dominant factor in graft survival, integration and organization (Dulin et al., 2018). The ability to streamline cell therapeutics and achieve survival within the refractory lesion epicenter (Sontag et al., 2014), while bypassing the use of microenvironment regulators and/or encapsulation, is an important milestone for grafted neurons in SCI.

Ex vivo differentiation avoids the fate influence of the SCI microenvironment and gliogenic cues that are encountered *in vivo* by NSPCs, and instead employs more uniform differentiation to avoid variability in outcomes. We applied comprehensive analysis of SMNs by immunofluorescence imaging of biomarkers, RNA-Seq of temporally differentiating SMNs, and functional validation by co-culture assays with myotubes, phenotypic analyses of synaptic and ion channel repertoires, and functional microelectrode array (MEA) electrophysiology. Although the focus of this study is not oligodendroglia, we included hiPSC-derived OPCs that have been deemed necessary in other studies (Almad et al., 2011; Fan et al., 2017; Duncan et al., 2018). We assessed the microenvironment stability of homotypic SMNs and OPCs *in vivo* for SCI by transplanting co-cultures directly into the contusion cavity at the C4-C5 injury site, followed by immunohistochemistry of spinal cord sections 10 days and 6 weeks post-transplantation. Biomarker analysis revealed robust survival of the homotypic spinal neurons and OPCs, and rapid engraftment within the host tissue at both time points. We demonstrate emergent features of graft cell maturation over time such as OPC ramification and caudal axon navigation with anisotropic alignment in the host spinal cord. Transplanted OPCs lost progenitor biomarkers but did not yet obtain myelinating activity at 6 weeks, which classically occurs over a protracted time frame. This work is the first to assess unprotected NMP-derived homotypic SMNs and OPCs in a rodent model of SCI and demonstrates that these maturing cell types survive and consistently engraft within the subacute injury cavity. We propose that regional neural cell matching to the spinal cord will enable streamlining of SCI cell therapeutics to focus on neuronal connectivity and avoid variability introduced through *in vivo* NSPC reprogramming strategies.

MATERIALS AND METHODS

Human iPSC Maintenance

The self-designated African American hiPSC line F3.5.2 was previously derived by reprogramming with Yamanaka factors in the Paluh and Cibelli labs and comprehensively characterized

(Chang et al., 2015; Tomov et al., 2016). F3.5.2 hiPSC colonies were maintained in the pluripotency medium mTeSR Plus supplemented with 1× penicillin-streptomycin (P-S) on hESC-qualified Matrigel (1:100 dilution; Corning) at 37°C, 5% CO_2. Cultures were passaged 1:6 in 6-well plates every 4–7 days depending on confluency using Gentle Cell Dissociation Reagent (GCDR, STEMCELL Technologies). Cells were stored at low passage number in mFreSR cryopreservation medium (STEMCELL Technologies). G-band karyotype was performed (Cell Line Genetics, Madison, WI) and cells were certified free of pathogens and mycoplasma.

Lentivirus Transduction

GFP labeling of cells using lentivirus transduction was performed similarly to as described by Taylor et al. (2006) at the hiPSC pluripotent stage. Briefly, hiPSCs were seeded onto freshly coated 6-well plates 3 days prior to transduction with premade LV-CAG-eGFP lentivirus (Kerafast FCT149, 1×10^8 CFU/ml). Polybrene (2 μg/ml; Millipore Sigma) was added to 2 ml mTeSR Plus. hiPSCs were transduced at 5 × multiplicity of infection (MOI) by centrifugation with the mTeSR-PB-LV medium for 1 h at 32°C, 1,200× *g* and subsequent incubation at 37°C, 5% CO_2 for 18 h. Cultures were rinsed 2× with DMEM/F-12 and cultured in mTeSR Plus for 48 h prior to visual inspection by fluorescence microscopy. Transduced hiPSCs were selected and expanded in media with 2 μM puromycin. Cells were cryopreserved in mFreSR (STEMCELL Technologies) or further differentiated to OPCs described.

Neural Differentiation and Specification to SMNs and OPCs

SMNs with caudal spinal cord identity were differentiated as previously described (Olmsted et al., 2020). Briefly, colonies at ∼60–70% confluency were exposed to Neuromesodermal Progenitor Medium (NMPM). N2B27 basal medium: 1:1 DMEM/F-12:Neurobasal Plus medium, 2% (v/v) B-27 Plus supplement, 1% (v/v) N-2 supplement, 1× GlutaMAX, 1× MEM Non-Essential Amino Acids, 1× P-S (Gibco); NMPM: N2B27 supplemented with 40 ng/ml recombinant human (rh) FGF2 (R&D Systems), 40 ng/ml rhFGF8 (R&D Systems), 2 μM CHIR 99021 (Tocris Bioscience), 10 μM DAPT (Millipore Sigma), 10 μM SB431542 (Tocris Bioscience), 100 nM LDN193189 (Tocris Bioscience), and 0.36 U/ml heparin (Millipore Sigma). NMPM was changed daily. On day 5, NMPs were passaged using Gentle Cell Dissociation Reagent in Caudo-Ventral Patterning Medium (CVPM). CVPM: N2B27 supplemented with 100 nM Retinoic Acid (RA; Millipore Sigma), 200 nM Hh-Ag1.5. Y-27632 (Tocris Bioscience) was added at 10 μM during passages. Spinal cord NSC cultures were passaged 1:3 in 12-well plates and maintained at 90–100% confluency for 2–3 days before subsequent high-density passages (1:2). Neural cells were cultured on Matrigel for the entirety of differentiation. The NSCs were patterned in CVPM to day 25 and then transitioned to Terminal Differentiation Medium (TDM). TDM: N2B27 supplemented with 10 ng/ml rhBDNF, 10 ng/ml rhGDNF, 1 μM dibutyryl cyclic-AMP (dbcAMP; Millipore Sigma). Short-term 24–48 h neurosphere (NS) cultures were formed in 6-well plates (CELLTREAT) using a Scilogex MX-M microplate mixer at ∼120 rpm and freshly seeded onto Matrigel substrate.

OPCs were differentiated through NMP and scNSC stages with the omission of DAPT during the first 5 days (**Supplementary Figure 4A**). On day 19 short-term 24 h NS suspension culture was used as a purification strategy. NS were seeded at day 20 in OPC medium (OPCM; Khazaei et al., 2017). This strategy specifies OPCs by biasing with growth factors IGF1, FGF2, and PDGF-AA in addition to the thyroid hormone triiodothyronine (T3) at day 20. OPCM: N2B27 (no Vitamin A) supplemented with 10 ng/ml rhIGF-1 (R&D Systems), 20 ng/ml rhFGF2 (R&D Systems), 20 ng/ml rhPDGF-AA (R&D Systems), 60 ng/ml tri-iodothyronine (T3; Millipore Sigma), and 0.36 U/ml heparin (Millipore Sigma). We validated OPCs by immunofluorescence (IF) of OLIG2/PAX6, Nkx-2.2, A2B5 and the OPC-specific antigen O4 (**Supplementary Figure 4B**).

OPC Sorting and SMN-OPC Co-culture

We generated purified co-cultures of SMNs and OPCs prior to transplantation. The purification steps used were MACS separation of OPCs by the O4 antigen (**Supplementary Figures 4C,D**), and SMN-NS suspension culture and re-plating. Separated GFP-OPCs were mixed 1:2 with SMNs and co-cultured for in modified N2B27 medium for downstream SCI transplantation studies. GFP-OPCs were sorted manually using the MidiMACS kit (Miltenyi Biotec 130-090-312) with LS columns and Anti-PE MicroBeads (Miltenyi Biotec 130-048-801) according to manufacturer's instructions. Cells were labeled with IgM PE-O4 antibody (R&D Systems FAB1326P) at 10 μl/10^6 cells. GFP-OPCs were retained and mixed 1:2 with SMNs. Co-cultures were seeded and maintained for 1 week in modified N2B27 SMN-OPC medium prior to neural ribbon co-encapsulation. SMN-OPC Medium: N2B27 supplemented with 10 ng/ml rhBDNF, 10 ng/ml rhGDNF, 10 ng/ml rhNGF, 20 ng/ml rhPDGF-AA, 10 ng/ml rhIGF-1, 60 ng/ml T3, 100 μM dbcAMP, 25 μg/ml insulin, and 20 μg/ml ascorbic acid.

Neuromuscular Junctions

Neuromuscular junction (NMJ) assays were performed similarly to as described in previous studies (Harper et al., 2004; Miles et al., 2004). Briefly, rat L6 myoblasts (ATCC CRL-1458) were seeded into Matrigel-coated Lab-Tek II 4-chambered cover glass and grown to confluency in DMEM/F-12, 10% FBS, 1× P-S medium. At 100% confluency, myoblasts were cultured in N2B27 medium supplemented with 100 nM RA, 200 nM Hh-Ag1.5 to drive multinucleated skeletal myotube formation. Twenty-four hours NS (day 38) were seeded onto myotubes at 5–8 NS per well in TDM and cultured for four days prior to fixation and fluorescence microscopy (day 42 SMNs).

Phase Contrast Imaging and Immunofluorescence *In vitro*

Phase contrast images were acquired using a Zeiss Invertoskop 40C (5×/0.12 NA CP-Apochromat, 10×/0.25 NA Ph1 A-Plan and 20×/0.30 NA Ph1 LD A-Plan objectives; Olympus DP22 color camera). For immunofluorescence (IF), cells were

seeded into Matrigel-coated glass-bottom chambers (Lab-Tek II 4-chambered cover glass; Nunc, #155382) and fixed with 10% buffered formalin for 30 min at appropriate stages in differentiation. Samples were permeabilized for 5 min in 0.1% Triton-X-100 and blocked for 30 min in 1% BSA fraction V (1× PBS). Primary antibodies were applied in 1 ml fresh blocking buffer and incubated at 4°C overnight (**Supplementary Table 1**, list of primary antibodies). Samples were rinsed thoroughly in 1× PBS before applying AlexaFluor secondary antibodies (Invitrogen) for 1 h in the dark with DAPI (4°C). Cells were imaged directly in chambered cover glass wells (Invitrogen). Fluorescence microscopy was performed using a Zeiss Axio Observer.Z1 inverted fluorescence microscope (20× /0.8 NA air and 63×/1.4 NA oil Plan-Apochromat DIC objectives). Images were acquired using an Hamamatsu ORCA ER CCD camera and Zeiss AxiovisionRel software (ver. 4.8.2). *Z*-stacks were gathered at 1 μm separation distance and compressed using the Extended Focus feature. Uniform exposure times were maintained across samples for identical antibodies. If necessary, images were adjusted linearly for brightness in Keynote or ImageJ.

Calcium Imaging

SMN cultures were incubated at 37°C with 5 μM Fluo-4 AM (Invitrogen) for 30 min in DMEM/F12 (no supplements). Cultures were recovered in fresh medium for 30 min and imaged in HBSS using the Zeiss Axio Observer. Z1 system with the 20x air objective. Time lapse series were captured at an exposure time of 50 ms obtained in 200 ms intervals for a total duration of 1.5 min using the 488 nm LED. Frequency of transients and F/F_0 over time was determined using ImageJ.

Microelectrode Array Electrophysiology and Analyses

To monitor spontaneous neuronal activity in adherent SMN cultures, we seeded MNP-NS directly onto 60MEA200/30iR-Ti microelectrode arrays (MEA; Multi Channel Systems). MEA chips contained single wells with 60 electrodes per well, each of 30 μm diameter with 200 μm inter-electrode spacing (input impedance 30–50 kΩ). One electrode per MEA chip served as a reference electrode. To obtain recordings, we used an MEA2100 head stage system connected to an MCS-IFB-*in-vitro* interface board. Temperature was maintained at 37°C during recordings using a temperature controller. Arrays were coated with Poly-D-Lysine and 20 μg/ml Laminin. On day 28 of differentiation, 12–15 NS were seeded in TDM and allowed to adhere for 2 days, at which point one-half medium changes were made (1 ml total volume). One-half medium changes were subsequently made twice per week. Recordings were acquired after NS culturing for 6 days with Multi Channel Experimenter software (v2.14.0) sampled at 25 kHz for at least 5 min. Spike threshold for detection was automatically set to 5× above standard deviation over background noise (1 ms pre trigger, 2 ms post trigger). Burst detection parameters were set as follows: 50 ms interval to start and end burst, 100 ms minimum inter-burst interval, 50 ms minimum burst duration, four minimum spikes per burst. Spike and burst analyses were performed using Multi Channel Analyzer (v2.14.0) in conjunction with NeuroExplorer (v5.022), and are shown for days 35 and days 52 in differentiation in accordance with patch clamp experimental time points. For glutamate stimulation, we prepared a 10 mM solution in N2B27 medium and added glutamate to a final concentration of 50 μM. Recordings were taken for a minimum of 5 min and up to 14 min. N = 4–5 separate MEA chips were used for quantification per time point. Generation of raw data traces and statistical analyses were performed using GraphPad Prism 8 in conjunction with Microsoft Excel.

Bulk RNA-Seq

Detailed information of RNA-Seq biological samples is provided in **Supplementary Table 2**. The datasets for SMN differentiated cell time points are also posted on NCBI GEO (GSE178600). SMNs were differentiated as described. RNA was extracted using the PureLink RNA Mini Kit (Invitrogen) according to manufacturer's instructions. Neural cells from three wells of a 12-well plate were pooled for each sample for library preparation and RNA-Seq was performed at the SUNY Buffalo Genomics and Bioinformatics Core. Per-cycle basecall (BCL) files generated by the Illumina NextSeq were converted to per-read FASTQ files using bcl2fastq version 2.20.0.422 using default parameters and no lane splitting. The quality of the sequencing was reviewed using FastQC version 0.11.5 and FastqScreen version 0.11.1. Quality reports were summarized using MultiQC version 1.7 (Ewels et al., 2016). No adapter sequences were detected so no trimming was performed. Genomic alignments were performed using hisat2 version 2.1.0 using default parameters (Kim et al., 2015). The Illumina provided UCSC hg38 from their igenomes database was used for the reference genome and gene annotation set. Sequence alignments were compressed and sorted into binary alignment map (BAM) files using samtools version 1.7. Counting of mapped reads for genomic features was performed using Subread featureCounts version 1.6.2 using the parameters -p -s 2 –g gene_name -t exon -B -C -Q 60 the annotation file specified with –a was from UCSC hg38 (Liao et al., 2014). Alignment statistics and feature assignment statistics were again summarized using MultiQC. The unique alignment rate of the paired-end reads for all samples was around 85%. The number of mapped reads assigned to features ranged from about 8 million to 16 million. Differentially expressed genes were detected using the Bioconductor package DESeq2 version 1.24.0. DESeq2 tests for differential expression using a negative binomial generalized linear models, dispersion estimates, and logarithmic fold changes (Love et al., 2014). DESeq2 calculates log2 fold changes and Wald test *p*-values as well as preforming independent filtering and adjusts for multiple testing using the Benjamini-Hochberg procedure to control the false discovery rate (FDR). Histograms were generated using Microsoft Excel and GraphPad Prism.

Cell Encapsulation, Overnight Shipping, and Cell Collection

Cells were encapsulated in neural ribbons for overnight shipping from Albany, NY to Houston, TX as previously

described (Olmsted et al., 2020). Immediately after formation, neural ribbon quality was monitored by visual inspection. Shippable neural ribbons in 12-well plates were resuspended in N2B27 supplemented with 10 μM ROCK inhibitor, transferred to 1.8 ml cryovials using 1,000-μl pipette tips and immediately shipped on ice (4°C) *via* FedEx (20–22 h total in transit). At the destination laboratory, neural ribbons were recovered in a 37°C humidified cell culture incubator 1 day prior to transplantation. To collect cells for transplantation, alginate was rapidly dissolved in 1.6% sodium citrate solution and cells were pelleted by centrifugation and resuspended in HBSS supplemented with 20 ng/ml FGF2 and EGF and 5 mM glucose.

Rat Cervical Spinal Cord Hemi-Contusion Injury and Transplants

A total of $N = 6$ rats were used in SCI grafting experiments. We performed cervical C4-C5 hemi-contusion injuries as previously described (Mondello et al., 2015). Briefly, injuries were made using the electromagnetic spinal cord injury device (ESCID). Right-sided hemi-laminectomy was performed at C4 level in anesthetized animals that were then placed in a spinal frame to clamp the lateral processes of C3, C5. The ESCID electromagnetic probe was positioned at the surface of the dura with an initial sensing force followed by rapid displacement (0.8 mm with 14 ms dwell). Afterwards, muscles were sutured in layers and the skin was clipped. The immunosuppressant tacrolimus was administrated 1 week prior transplantation of human cells at the dosage of 3.4 mg/kg/day through using a slow-release subcutaneous pellet implant (Innovative Research of America). Human SMNs and OPCs were shipped overnight as encapsulated neural ribbon constructs on ice (Olmsted et al., 2020), and received in Houston one day prior to injections. Constructs were suspended in fresh N2B27 and maintained in a humidified tissue culture incubator overnight. Cell number and retained viability was validated with an automatic counter (Invitrogen) before transplantation. For transplants, the spinal cord was re-exposed at injury level 15 days post-injury in anesthetized animals. To stabilize the animal, the lateral process of C3 was secured in a custom spinal frame. For delivery of high dose cell suspensions ($N = 6$ animals), alginate was dissolved using 1.6% sodium citrate and cells collected by centrifugation. Cells were delivered at ∼200,000 cells per animal directly into the injury cavity by pulled glass pipette connected to Kopf micromanipulator in 2 μl of 5 mM glucose in HBSS vehicle with additional 20 ng/ml FGF and EGF for neurotrophic support. The glass pipette was retracted after delivery. The dura was sealed using a fibrin sealant made by mixing a 1:1 ratio of fibrinogen solution (20 mg/ml) with a bovine thrombin solution (10 U/ml; Millipore Sigma). Muscle and skin layers were closed, and animals received appropriate post-operative care. All rat experimental protocols were approved by Houston Methodist Research Institute IACUC and carried out in accordance with relevant ethical guidelines and regulations. This includes animal comfort, veterinary care, methods and reasons for euthanasia, and materials and hiPSC-derived neural injections.

Tissue Processing and Immunohistochemistry

Spinal cords were harvested at two time points for short term (10 days post-transplantation, $N = 3$) and long term (6 weeks post-transplantation, $N = 3$) analyses. Animals were sedated with isoflurane and transcardially perfused first with ice cold 0.1 M PBS with 10,000 U of heparin. Tissues were then fixed by perfusion of 4% paraformaldehyde in 0.1 M PBS (pH 7.4). Spinal cords were harvested for further fixation in 4% paraformaldehyde at 4°C overnight. They were passed through a sucrose buffer gradient (10%, 20%, 30%; 24 h per solution) at 4°C for cryoprotection and aligned longitudinally in a Tissue Tek OCT block (Sakura, Nederland) using dry ice, and stored at −80°C. Forty micrometer thick spinal cord sagittal sections were prepared using a Cryostar NX50 cryomicrotome (ThermoFisher Scientific). Serial sections of the entire spinal cord were then mounted onto positively charged slides (ThermoFisher Scientific). For immunohistochemistry, slides were blocked with 10% goat serum in 0.2% Triton-PBS (T-PBS) for 1 h at room temperature followed by primary antibody incubation in 1% serum, 0.2% T-PBS overnight at 4°C. Primary antibodies used for *in vivo* studies were mouse anti-STEM121 (1:500; Takara, #Y40410, RRID: AB_2801314), chicken anti-GFAP (1:2,000; Abcam, #ab4674, RRID: AB_304558), rabbit anti-Synapsin 1 (1:200; Abcam, #ab64581, RRID: AB_1281135), rabbit anti-TUJ1 (1:1,000; BioLegend, #802001, RRID: AB_2564645), rabbit anti-OLIG2 (1:500; EMD-Millipore, #AB910, RRID: AB_2149918), mouse anti-O4 (1:500; R&D Systems, #MAB1326, RRID: AB_357617), mouse anti-APC (1:50; EMD-Millipore, #OP80, RRID: AB_205371). GFP-OPCs retained GFP signal after fixation. After three additional wash steps with 1% serum T-PBS, slides were incubated with secondary antibodies in PBS for 1 h. Secondary antibodies used were goat anti-rabbit IgG Alexa Fluor (AF) 568 (ThermoFisher Scientific, #A-11011, RRID: AB_143157), goat anti-mouse IgM AF 647 (ThermoFisher Scientific, #A-21238, RRID: AB_2535807), goat anti-mouse IgG2b AF 647 (ThermoFisher Scientific, #A-21242, RRID: AB_2535811), goat anti-mouse IgG1 AF 568 (ThermoFisher Scientific, #A-21124, RRID: AB_2535766), goat anti-chicken IgY Cy5 (ThermoFisher Scientific, #A-21449). Secondaries were added at a dilution of 1:1,000. Slides were mounted with DAPI-Permount (ThermoFisher Scientific) and imaged with a Leica DMi8 confocal microscope.

Graft volume and area at the lesion site were calculated with the stereological probe Cavalieri using the software StereoInvestigator (MBF Bioscience). Specifically, the lesion area of the cord (4 mm), cavity, and graft size were determined on every five sections by tracing the different areas in the cords transplanted with cell suspensions and sacrificed at 6 weeks ($N = 3$). Transplant area was defined in STEM121/DAPI longitudinal sections 40 μm thick using a Zeiss Axioskop 2 microscope. For the Cavalieri method, the following parameters were chosen: grid size (μm): 100; Associated Area (μm^2): 10,000; Section Cut Thickness (μm): 40; Section

Evaluation Interval: five; Associated Volume (μm^3): 2,000,000; Number of Sections: four. The number of GFP-OPCs and GFP-OPCs/GFAP+ were estimated with stereology analysis using the Optical Fractionator probe in StereoInvestigator software and an Axioskop2plus Zeiss microscope. For further analysis, the percentage of GFP-OPCs/GFAP+ cells was calculated by dividing estimated population number of GFP-OPCs/GFAP+ by the estimated population total number of GFP-OPCs. Data are provided as averages of estimated population of cells using defined section thickness of three rats (6 weeks time point), five sections per rat with 40 μm section cut thickness.

Experimental Design and Statistical Analyses

Raw data were compiled in Microsoft Excel (v16.16.16) and exported to GraphPad Prism (v8.3.0) for plotting and statistical analyses. Data are reported as mean ± s.e.m.) and analyzed using unpaired two-tailed t-test unless otherwise specified. Cells were manually counted in ImageJ to quantify immunofluorescence data. $^{****}p < 0.0001$ $^{***}p < 0.001$ $^{**}p < 0.01$ $^{*}p < 0.05$ n.s. not significant ($\alpha = 0.05$). Power analysis was not performed. Detailed information for each experiment is provided in figure legends.

Figures

Figures for this manuscript were made in Keynote (v9.2.1), Canvas Draw (v4.0.1), Adobe Illustrator CC (v25.0.1), and BioRender.com. Data plots were generated using GraphPad Prism (v9) or Microsoft Excel (v16.16.19).

RESULTS

Generation of SMNs From hiPSCs Using Trunk-Biased Neuromesodermal Progenitors

To generate neurons appropriate for cervical SCI, spinal motor neurons (SMNs) were derived in three stages (**Figure 1**; **Supplementary Figure 1**), referred to here as: (1) neural induction; (2) caudo-ventral patterning; and (3) neuronal maturation (**Figure 1A**). Before neural induction, we first differentiated the hiPSC line F3.5.2 to neuromesodermal progenitors (NMPs) that are bipotent intermediates preceding spinal cord neuroectodermal development (Chang et al., 2015; Lippmann et al., 2015; Tomov et al., 2016). We previously showed that this protocol generates SOX2/Bra NMPs at high efficiency (Olmsted et al., 2020, 2021). Synergistic Wnt/β-catenin and FGF-mediated signaling pathways were stimulated using the small molecule CHIR 99021 and recombinant human FGF2/FGF8 proteins, respectively, in the context of dual SMAD inhibition with LDN 193189 and SB 431542 (Chambers et al., 2009, 2012) during the first 5 days of differentiation. The GSK-3β inhibitor DAPT was also included in the growth medium during this time. NMP transition to spinal cord NSC rosettes (scNSCs) was triggered by switching to caudo-ventral patterning medium containing 100 nM of the caudalizing morphogen, retinoic acid (RA), that promotes neuralization and 200 nM of the ventralizing morphogen, Hh-Ag1.5, a potent agonist of Sonic hedgehog (**Supplementary Figure 1A**). Continued exposure yields robust motor neuron progenitor (MNP) cultures by day 12 that were immunopositive for Nestin, OLIG2, TUJ1, and NeuN (**Supplementary Figures 1B–D**). Differentiating SMNs were validated using bulk RNA-Seq at seven time points including days 10, 19, 25, 28, 32, 37, and 42 (**Supplementary Figures 1E,F**). Day 32 cultures had an expression profile that was most indicative of desired SMNs (e.g., HB9/FOXP1/ISL1/PRPH/STMN2/VGF/CHAT/MAP2/TUBB3) and so we compared all other datasets to this stage individually, shown with volcano plots (**Supplementary Figure 1G**). Day 32 SMNs have perinuclear and polarized expression of STMN2 in GAP-43 positive neurites, also typical of developing SMNs (**Supplementary Figure 1H**, Klim et al., 2019).

We used short-term (24–48 h) neurosphere (NS) suspension cultures as a purification step prior to neuronal maturation. Plated NS cultures projected aligned axons radially outward along which neurons migrated to form distal 2D adherent regions, visualized by the pan-axonal marker SMI312 (**Figure 1B**). At day 25, cultures were transitioned to and subsequently maintained in terminal differentiation medium containing 10 ng/ml BDNF, GDNF, and 1 μM dbcAMP. Adherent neurons exhibited typical SMN morphology as assessed by trapezoidal soma shape, a prominent single nucleolus, and dendritic arborization (**Figure 1C**). The SMNs expressed a panel of characteristic biomarkers by immunofluorescence (IF) time course (**Figures 1D,E**). That is, the ventral motor neuron progenitor domain transcription factor NK6 homeobox 1 (Nkx-6.1), SMN-related ISL LIM homeobox 1 and 2 (ISL-1&2), SMN-specific homeobox 9 (HB9/*MNX1*), and choline acetyltransferase (ChAT). Growth associated protein 43 (GAP-43) localized to neuronal growth cone and branching structures (**Figure 1D**). By developmentally relevant differentiation cues, we generated the appropriate cervical SMNs through neuromesodermal progenitors reflecting characteristic morphological and biomarker expression.

Developmental Hallmarks of NMP-Derived Spinal Motor Neurons Validated By RNA-Seq, Biomarkers, and Functional Assays

SMNs derived through NMP intermediates were further validated by whole-transcriptome bulk RNA-Seq and IF on a differentiation time course (**Figure 1**; **Supplementary Figure 1**). SMNs primarily expressed lateral motor column (LMC) transcription factor FOXP1 (53 ± 12%, $n = 349$ cells) vs. the medial motor column (MMC) transcription factor LHX3 (5 ± 2%, $n = 304$ cells) that was downregulated over time (**Figures 1F,G**; Amoroso et al., 2013). We verified general biomarker expression for neuronal compartments that are somatic (NeuN), dendritic (SMI311R/MAP2), axonal (SMI312) and membrane (Pan-Cadherin/NCAM-1), and phenotypic regional specificity to the LMC (Hox-C6, RALDH2, Peripherin) by IF (**Figure 1H**). Caudal cervical

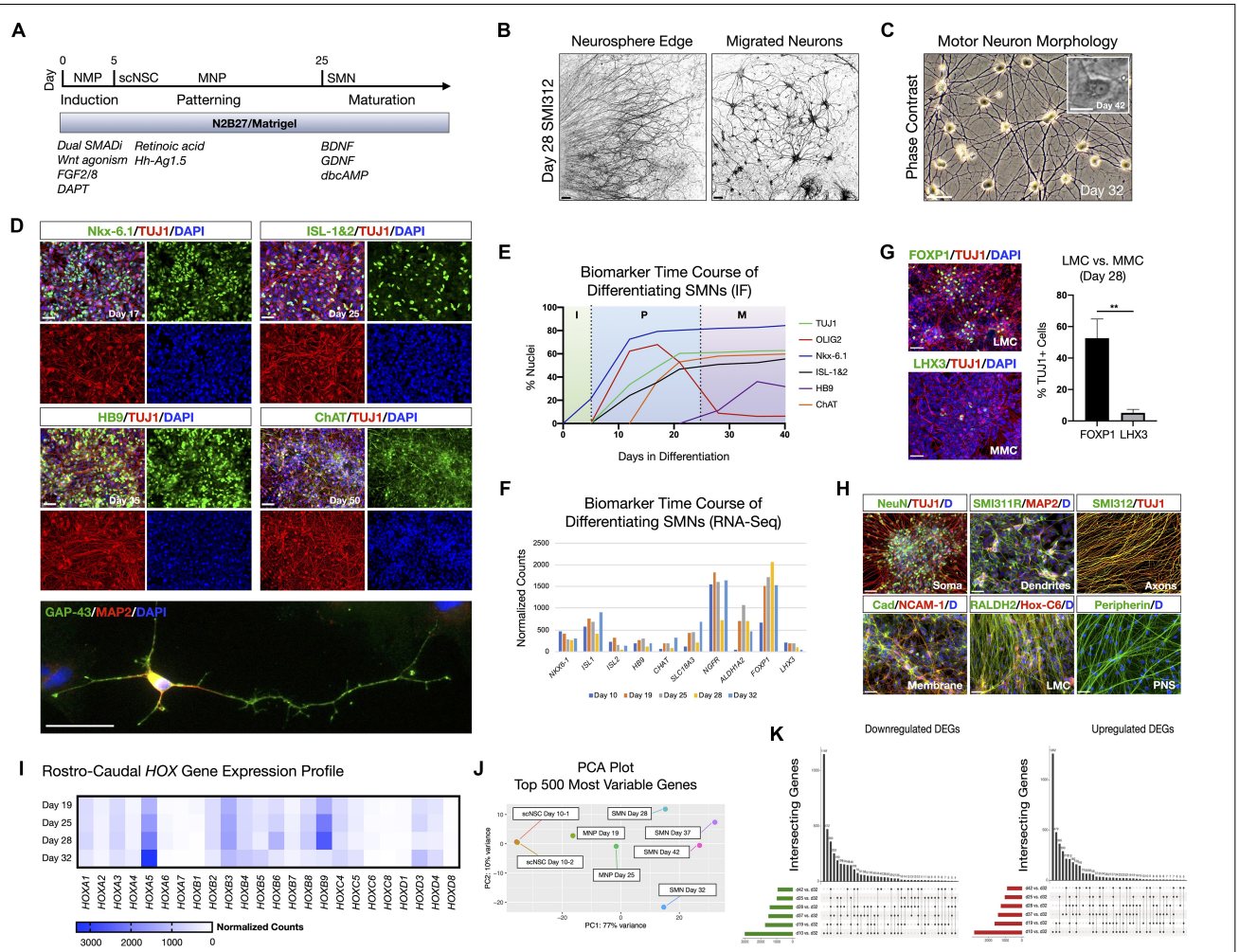

FIGURE 1 | hiPSC-derived scNSCs generate SMNs regionally-matched for the spinal cord. **(A)** Overview of differentiation protocol used to generate cervically-patterned SMNs through NMP, scNSC, and MNP stages. Small molecules and growth factors used in caudo-ventral patterning and maturation are listed. **(B)** Pan-axonal antibody SMI312 labeling of day 28 adherent neurosphere (NS) culture at NS edge (left) and more distal field of migrated neurons (right). SMI312 signal shown with inverted LUT. **(C)** Phase contrast images of day 32 SMN cultures. Inset is day 42 single SMN with characteristic trapezoidal shape and prominent nucleolus. **(D)** SMN hallmark biomarkers. Top: Motor progenitor spinal domain transcription factor Nkx-6.1 (day 17); SMN-related factors ISL-1&2 (day 25); Middle: SMN-specific HB9 (day 35); choline acetyltransferase enzyme ChAT (day 50); Cells are counterstained with TUJ1 and DAPI. Bottom: IF of single neuron. GAP-43/MAP2/DAPI (day 32). **(E)** Time course of biomarker expression in differentiating SMN cultures (I, induction; P, patterning; M, maturation). Percent of nuclei were counted from IF images. $N = 3$ fields were averaged per biomarker per time point (>100 cells per field). **(F)** Time course biomarker expression of differentiating SMN cultures by bulk RNA-Seq. **(G)** IF images and histogram of later motor column (LMC) SMN transcription factor FOXP1 (53 ± 12%; $n = 349$ cells) vs. medial motor column (MMC) SMN transcription factor LHX3 (5 ± 2%; $n = 304$ cells; two-tailed t test, $t = 6.629$, df = 4, $^{**}P = 0.0027$). **(H)** Visualizing neuronal compartments and SMN regional specificity by biomarker. **(I)**, RNA-Seq validation of cervical spinal cord identity by normalized Hox gene expression profile in differentiating SMN cultures. **(J)** PCA plot of 500 most variable genes during scNSC neuronal differentiation. **(K)** UpSet plots of intersecting downregulated (left) and upregulated (right) differentially expressed genes (DEGs) using individual time point comparisons in differentiation. Plot height represents the number of overlapping DEGs between the sets below marked with filled circles. Vertical lines connecting two or more dots denote the set of genes overlaps the connected sets. Data are reported as mean ± s.e.m. Scale bars are 50 μm, and 10 μm in **(C)** inset.

spinal cord identity is consistent with collinear *Hox* gene expression profiles using bulk RNA-Seq (**Figure 1I**). Principle component analysis (PCA) plots of the top 500 most variable genes revealed the similarities between scNSC biological replicates, but a progressive dissimilarity between time points in longer differentiated cultures (**Figure 1J**). UpSet plots for downregulated [$\log_2$(fold change) <0] and upregulated [$\log_2$(fold change) >0] differentially expressed genes (DEGs; $P_{adj} < 0.05$) enable visualization of multiple set intersections similarly to Venn or Euler diagrams (**Figure 1K**). However, unlike Venn or Euler diagrams, UpSet scales appropriately when comparing three or more groups and also maintains correct intersectional area proportions. Differentiating samples were compared to day 32 SMNs and the trend was the same for both downregulated and upregulated DEGs.

We further interrogated phenotypic maturation and functional hallmarks of the SMNs using numerous assays (**Figure 2**). At day 35 in differentiation, SMNs were

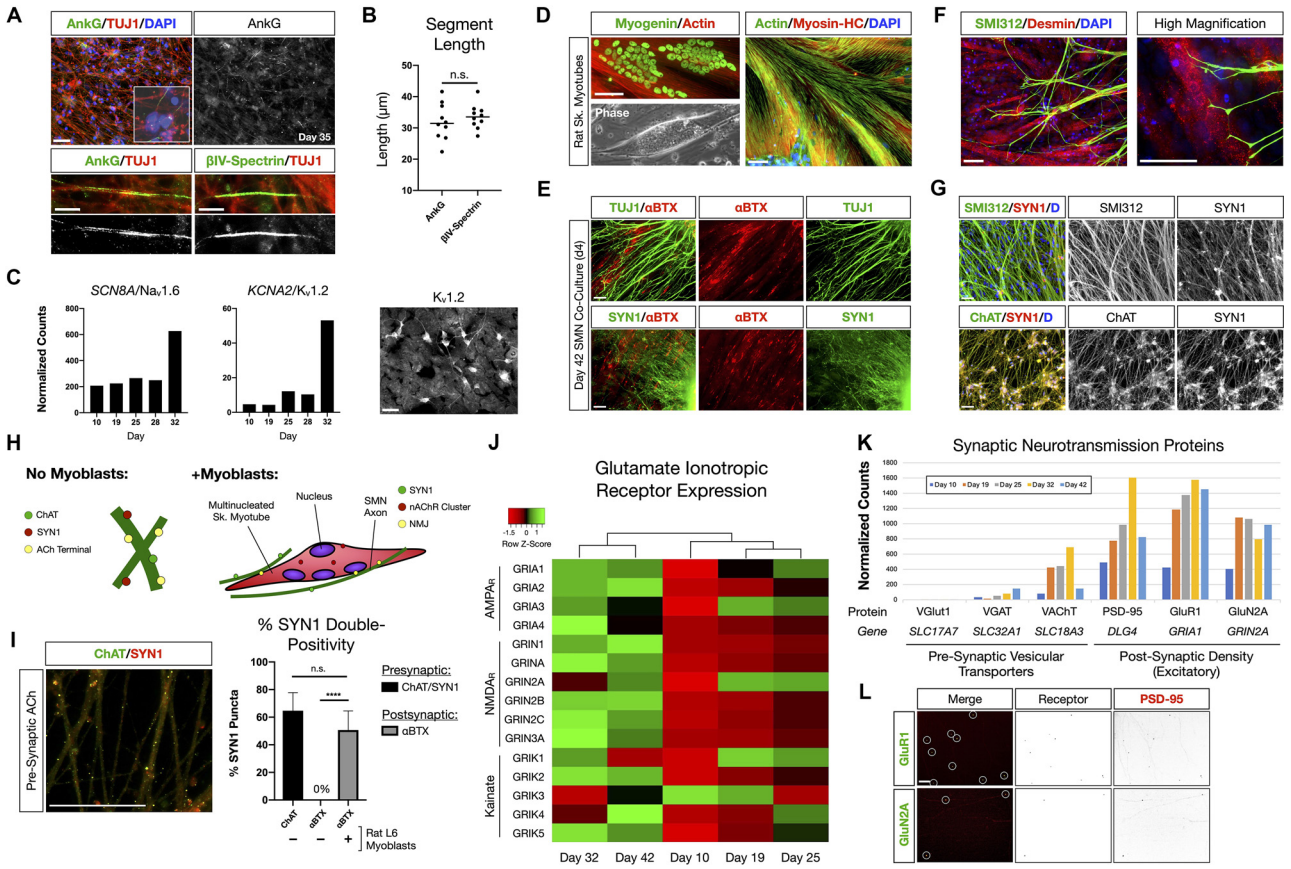

FIGURE 2 | NMP-derived SMNs are positive for axon initial segment proteins, assemble neuromuscular junctions, and develop characteristic synaptic profiles. **(A)** Maturing SMN-NS cultures exhibit short segments immunopositive for AIS proteins Ankyrin-G (AnkG) and βIV-Spectrin at day 35. Top: AnkG/TUJ1 counterstained with DAPI (nuclei). High-magnification image depicts AnkG+ staining distal to the soma. Bottom-left: AnkG immunopositive region along TUJ1+ filaments. Bottom-right: βIV-Spectrin immunopositive region along TUJ1+ filaments. **(B)** Length of AnkG (32 ± 2 μm) and βIV-Spectrin (34 ± 1 μm) segments by day 35 (two-tailed t test, $t = 0.7082$, df = 18, $P = 0.4879$, $n = 10$ segments measured per antibody). **(C)** Time course normalized expression of AIS-related voltage gated ion channels $Na_V1.6$ and $K_V1.2$ by RNA-Seq. IF showing cells positive for $K_V1.2$ on right. **(D)** Rat L6 multinucleated skeletal myotubes for NMJ formation assays. **(E)** Day 4 co-culture of SMN-NS (day 42) seeded onto rat myotubes. Top: TUJ1+ filament termination onto αBTX+ junctions (nAChR). Bottom: SYN1/αBTX. **(F)** SMI312 axon termination in Desmin+ myotubes resembling early motor end plates. **(G)** Co-localization of cholinergic terminals (ChAT, bottom) with SYN1 puncta along axons (SMI312, top). **(H)** Cartoon diagram of ChAT/SYN1 pre-synaptic ACh terminals and nAChR post-synaptic machinery. **(I)** IF image and histogram of ChAT/SYN1 (64.7 ± 13.1%, $n = 118$ puncta) and SYN1/αBTX co-localization in the absence (0%, $n = 48$ puncta) or presence (50.7 ± 13.8%, $n = 69$ puncta) of L6 myotubes (two-tailed t test, $t = 10.36$, df = 14, $^{****}P < 0.0001$). $N = 8$ fields were averaged for each condition. **(J)** Heatmap of glutamate ionotropic receptor expression ($AMPA_R$, $NMDA_R$, Kainate) during SMN differentiation. **(K)** Histogram of normalized gene expression for pre-synaptic vesicular transporters (VGlut1 excitatory, VGAT inhibitory, VAChT cholinergic) and post-synaptic density proteins/excitatory receptors. **(L)** Co-localization of $AMPA_R$ GluR1 (top) and $NMDA_R$ GluN2A (bottom) with scaffolding protein PSD-95. Individual channels provided as inverted LUT. Data are reported as mean ± s.e.m. Scale bars are 50 μm, and 10 μm in **(A)** high magnification images (bottom). n.s., not significant.

immunopositive for neuronal markers of the axon for axon initial segment (AIS) proteins Ankyrin-G (AnkG) and βIV-Spectrin (**Figure 2A**). As expected, immunostaining occurred as short segments along TUJ1 labeled microtubule neuronal filaments distal to the soma for both AnkG (32 ± 2 μm) and βIV-Spectrin (34 ± 1 μm; mean ± s.e.m.; **Figure 2B**). Maturation of signaling potential was reflected in time course RNA-Seq analysis of genes encoding the voltage-gated ion channels $Na_V1.6$ (*SCN8A*) and $K_V1.2$ (*KCNA2*) that additionally supports ongoing neuronal maturation in these cultures (**Figure 2C**).

The ability to assemble neuromuscular junction (NMJ) machinery was investigated between species by co-culturing hiPSC-derived SMNs with multinucleated skeletal myotubes formed from rat L6 myoblasts (**Figure 2D**). Co-culture of SMN-derived NS (day 38) with rat myotubes for 4 days resulted in marked co-localization of TUJ1 and Synapsin 1 (SYN1) neuronal filaments with α-bungarotoxin (αBTX), a high-affinity binding antagonist of nicotinic acetylcholine receptors (nAChR) that form the post-synaptic junction of NMJs (**Figure 2E**). SMN axons identified with SMI312 labeling terminated abruptly onto myotubes and formed structures resembling early motor end plates (**Figure 2F**). The NMJ presynaptic terminal contains a network of ion channels including those for release of acetylcholine (ACh). We further observed co-localization of the choline acetyltransferase enzyme,

ChAT, with SYN1 puncta along SMN axons, identifying the cholinergic pre-synaptic terminals (64.7 ± 13.1%, n = 118 SYN1 puncta; **Figures 2G–I**). Post-synaptic αBTX did not co-localize with SYN1 puncta in control SMN mono-cultures. Thus our SMNs reflect multiple functional hallmarks of NMJs.

SMN activity in the spinal cord is influenced by descending cranial motoneuron (MN) fibers *via* glutamatergic neurotransmission. We therefore also investigated the expression of glutamate ionotropic receptors by the SMNs (**Figures 2J–L**). Clustering analysis of RNA-Seq data revealed that SMNs cluster separately from scNSCs and MN progenitors with progressive activation of mRNA expression for genes encoding AMPA, NMDA and Kainate receptors from stages of scNSCs through to SMNs as a general trend (**Figure 2J**). In accordance with observed immunostaining and pre-synaptic co-localization of ChAT and SYN1 in SMN NMJs, RNA-Seq data reveals that the SMNs primarily expressed the acetylcholine vesicular transporter VAChT vs. inhibitory (VGAT) or excitatory (VGlut1) vesicular transporters. The post-synaptic density scaffolding protein PSD-95 (*DLG4*) was highly expressed along with excitatory receptors, AMPA receptor subunit GluR1 (*GRIA1*) and the NMDA receptor subunit GluN2A (*GRIN2A*; **Figure 2K**) and these are co-localized by immunostaining (**Figure 2L**). In summary, the RNA-Seq data along with biomarker immunostaining reflect the maturation of SMNs *in vitro* through analysis of pan-neuronal and SMN specific biomarkers, and formation of functionally specific NMJ structures.

Characterization of SMN Ventral Patterning Efficiency and Gliogenesis in scNSC-Differentiated SMNs

Ventral and dorsal spinal interneurons (INs) along with astrocytes that promote synaptogenesis are indispensable to normal neuronal circuit function *in vivo*. We previously investigated the identities and proportions of spinal interneurons generated using the NMP-derived, SMN-directed differentiation protocol by immunofluorescence (Olmsted et al., 2021). Here we investigated ventral vs. dorsal identity and the presence of glia in our differentiating neuronal cultures by RNA-Seq. As expected from our differentiation protocol, the cultures primarily exhibited ventral rather than dorsal spinal cord identity by RNA-Seq normalized counts of characteristic progenitor domain and neuronal subtype transcription factors (**Supplementary Figure 2A**, Sagner and Briscoe, 2019). Genes for oligodendroglial and astroglial lineages were also identified in differentiating SMN-directed cultures (**Supplementary Figures 2B,C**), although we refer to the SMN cultures as simply "SMNs" throughout the text. GFAP+ astrocytes were not observed until day 40 in differentiation, consistent with late waves of gliogenesis subsequent to an initial neurogenesis phase in human gestation. The day 32 neurons that we transplant prior to this differentiation time point did not contain GFAP+ astrocytes and therefore are expected to rely on host astrocytes for metabolism and sustained viability.

SMNs Develop Regular Spiking Patterns and Glutamate-Responsive Bursting

Neuronal firing was examined by calcium imaging as a proxy in addition to MEA extracellular recordings (**Figure 3**). We measured calcium transients in the soma and neurites of day 19 and 32 adherent SMNs using the cell-permeant calcium sensitive dye, Fluo-4 AM (**Figures 3A,B**). Cultures were imaged in HBSS medium without additional chemical stimulation (e.g., glutamate) and calcium transients quantified. At day 19, 6.6 ± 2.3% of SMNs imaged exhibited multiple calcium transients above threshold during the 1.5 min recording window as measured in the soma (n = 83 neurons, N = 5 repeat experiments). This increased to 37.6 ± 7.5% of SMNs at day 32 (n = 101 neurons, N = 5 repeat experiments, $^{**}P$ = 0.0043; **Figure 3B**, left). Representative examples of single and multiple transients in soma and neurite are provided (F/Fo; **Figure 3B**, right). Mean rate of calcium transients as measured in the soma was 6.6 ± 1.2 transients/min at day 32.

For MEA analysis, we seeded day 28 neurospheres (NS) onto single 60-electrode arrays (12–15 NS/array) in terminal differentiation medium (**Figure 3C**, day 34) and maintained adherent cultures to day 52. The firing activity recorded using MEAs is described for day 35 and day 52 time points (**Figures 3D–K**). Day 35 cultures exhibited high and irregular spontaneous firing (**Figures 3D–H**). By contrast, day 52 cultures displayed lower and more regular spontaneous firing rates (**Figures 3E–H**; mean firing rate, MFR; **Figures 3I–K**). The RNA-Seq data analysis of the SMNs reveals they have the receptor machinery to respond to glutamate. Notably, in both day 35 and in day 52 cultures, addition of 50 μM glutamate to the extracellular medium increased neuronal firing and produced robust bursting activity (day 35 $^{***}P$ = 0.0007, day 52 $^{**}P$ = 0.0048). Glutamate-stimulated bursting was more pronounced and became qualitatively rhythmic in day 52 SMNs, and this effect persisted for the entire duration of the experiment (**Figure 3K**). Network bursts were not detected during the time of recordings using 2D cultures. To supplement electrophysiological characterization, we also examined a differentiation time series of potassium and sodium ion channel gene expression known to be critical for neuronal function and maturation (**Supplementary Figures 3A,B**). Our findings reflect functional maturation of spiking activity over time advanced, but was not enhanced by substantially longer culturing times (day 52) beyond day 32 SMNs. This is consistent with our previous studies in which the three-dimensional context of cells seems to play a greater role (Olmsted et al., 2021).

Transplanted Homotypic SMN-OPCs Survive Within the Contused Injury Cavity and Demonstrate Long-Term Histological Evidence of Integration

We transplanted neurons without microenvironment modifying enzymes or encapsulation, but we included OPCs that are known to be susceptible to death in the injury microenvironment (Almad et al., 2011) and in addition have been shown to

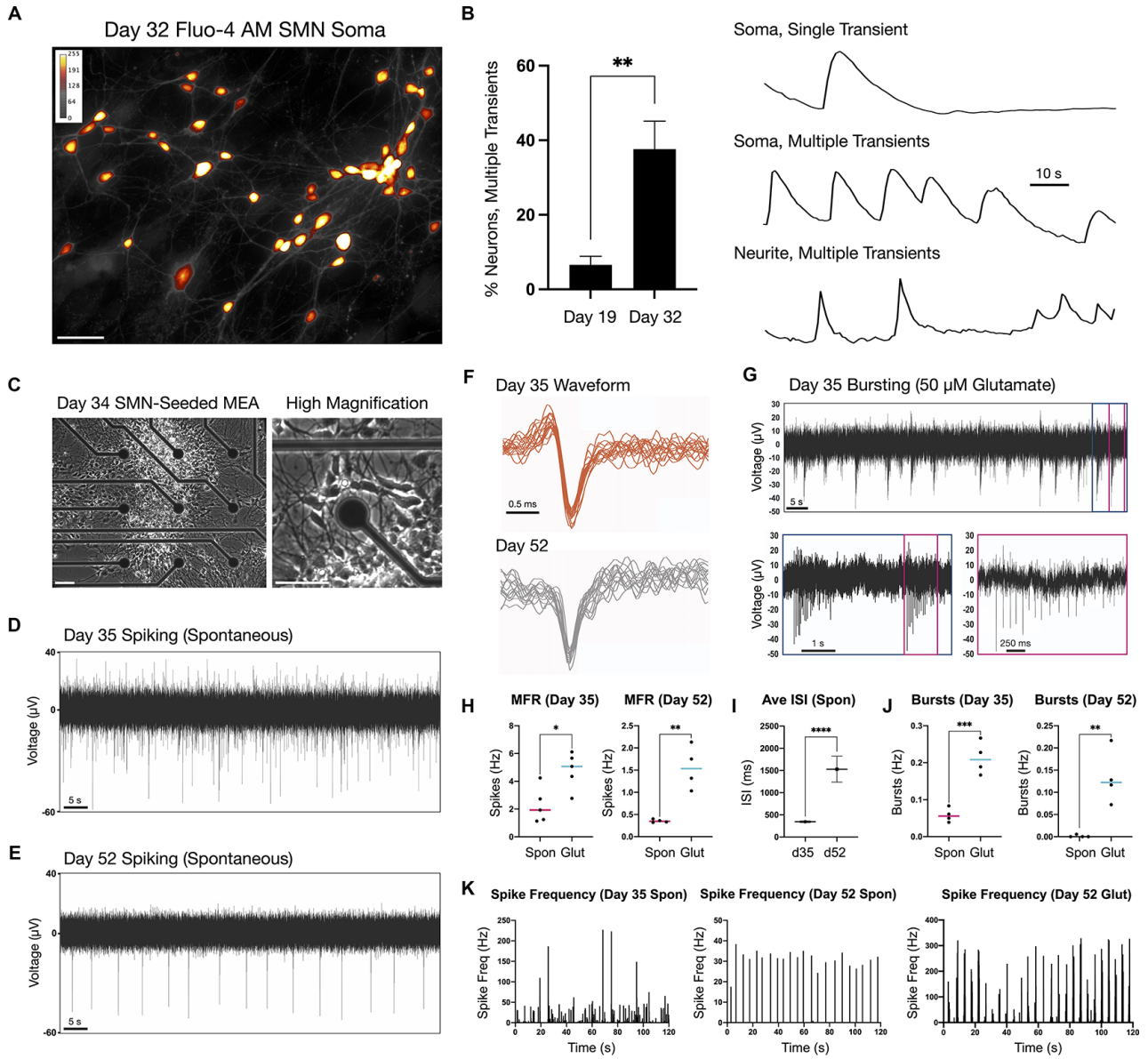

FIGURE 3 | Firing properties of adherent spinal neurons by calcium imaging and microelectrode arrays (MEA) at two time points. **(A)** Calcium dye Fluo-4 AM somatic signal in adherent SMNs (day 32). ImageJ Smart LUT fluorescence intensity (yellow high, gray low). **(B)** Left: Proportion of SMNs exhibiting multiple calcium transients above threshold in the 1.5 min recording window at day 19 (6.6 ± 2.3%, n = 83 neurons, N = 5 repeat experiments) and day 32 (37.6 ± 7.5%; n = 101 neurons, N = 5 repeat experiments). $^{**}P$ = 0.0043. Right: Representative examples of single and multiple transients in soma and neurite of day 32 SMNs over the 1.5 min recording window (F/Fo). Scale bar is 10 s. **(C)** Phase contrast images of SMN-seeded MEAs at day 34 in differentiation (seeded day 28). **(D,E)** Representative traces from single MEA channel depicting spontaneous SMN voltage spikes recorded at day 35 **(D)** and day 52 **(E)** in differentiation. **(F)** Representative overlay of spontaneous spike waveforms at day 35 and day 52 from traces in **(D,E)**. **(G)** Representative single electrode bursting in day 35 cultures stimulated with 50 μM glutamate. Three time scales are shown. Pink box depicts spikes within a single burst. **(H)** Quantification of mean firing rate (MFR, Hz) in day 35 and day 52 cultures. Spontaneous firing is compared to 50 μM glutamate stimulation (two-tailed t test; day 32 t = 3.096, df = 8, $^{*}P$ = 0.0148; day 52 t = 4.968, df = 6, $^{**}P$ = 0.0025). **(I)** Average inter-spike interval (ISI) in day 35 vs. day 52 SMNs under spontaneous conditions (t = 10.52, df = 499, $^{****}P < 0.0001$). **(J)** Single electrode burst rate (Hz) in day 35 vs. day 52 SMNs (day 32 t = 6.426, df = 6, $^{***}P$ = 0.0007; day 52 t = 4.356, df = 6, $^{**}P$ = 0.0048). **(K)** Spike frequency (Hz) vs. time (s) in day 35 vs. day 52 SMNs. Also shown is spike frequency for day 52 SMNs stimulated with 50 μM glutamate is shown (rightmost plot). Spontaneous (spon), glutamate (glut). Scale bars are 50 μm.

play a supportive role in recovery and myelination (Fan et al., 2017). OPCs were generated from hiPSCs expressing CAG-GFP by lentivirus transduction (Taylor et al., 2006) and were differentiated using a similar NMP protocol as for SMNs, except that DAPT was excluded during the first 5 days since this is used to favor generation of neurons. Validation and purification of OPCs derived through NMPs by this protocol (Olmsted et al., 2021) are described (**Supplementary Figure 4**)

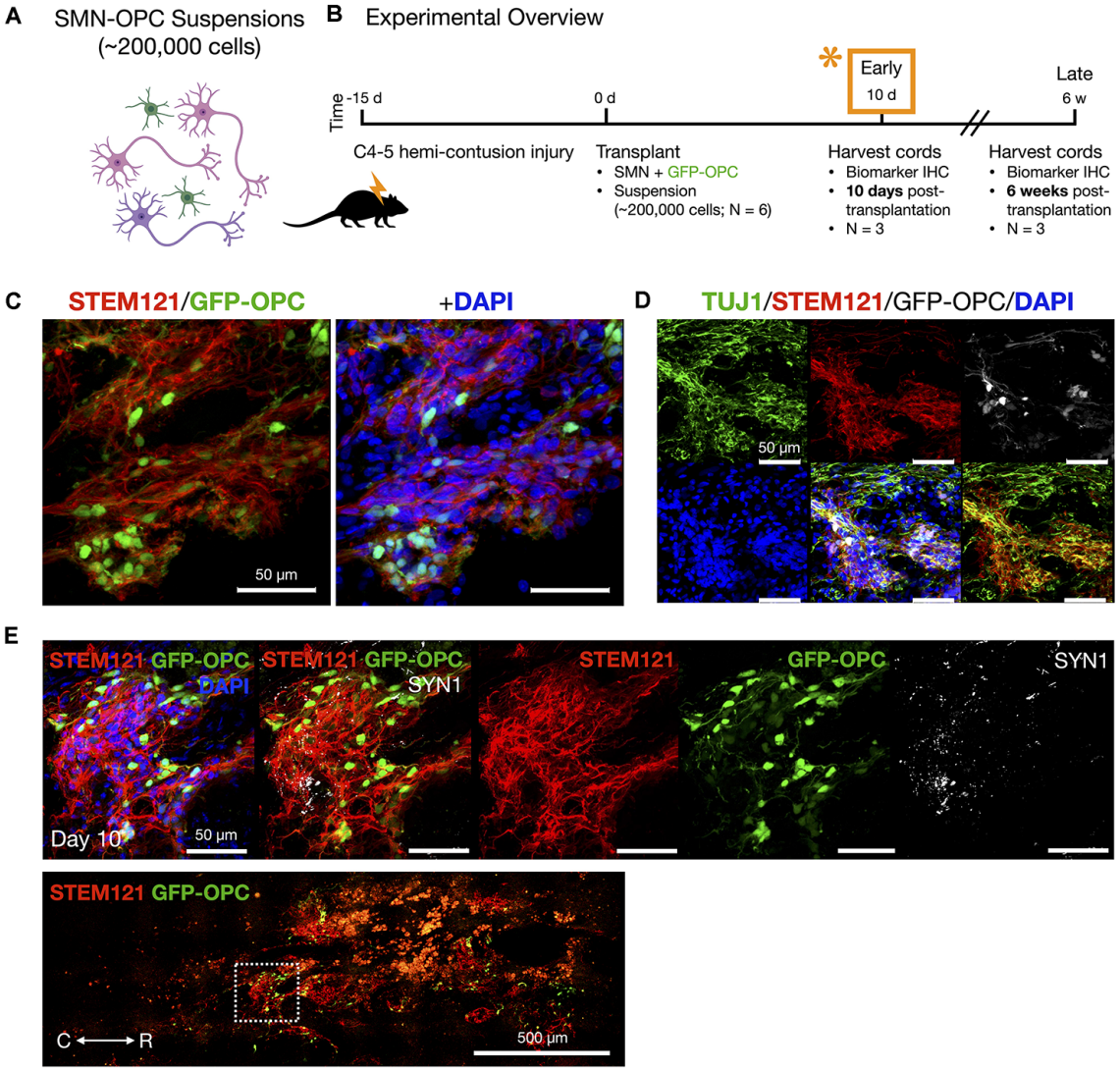

FIGURE 4 | *In vivo* delivery of SMN-OPC cell suspensions into the contusion cavity and survival at 10 days post-transplantation. **(A)** Schematic overview of the SMN-OPC cell suspension grafts. Pink depicts spinal motor neurons, purple depicts spinal interneurons that co-differentiate, and green is GFP-OPCs. **(B)** Schematic overview of SMN-OPC cervical hemicontusion grafting experiment (*N* = 6 animals). *Data provided in this figure are from the 10 days time point. **(C)** STEM121/GFP-OPC/DAPI merged image at the 10 days time point. **(D)** TUJ1 immunostain validates retention of the neuronal phenotype since this antibody detects the neuron-specific β-tubulin isotype, β-III-tubulin. **(E)** High magnification image of suspension SMN and GFP-OPC survival 10 days post-transplantation. SYN1 co-localization with STEM121 is shown. Low magnification STEM121/GFP-OPC image denotes position of field acquired caudal to the lesion epicenter (white box). R (rostral), C (caudal). Individual scale bars are provided.

and include biomarkers OLIG2/PAX6, NKX2–2, A2B5, and O4, along with MACS separation *via* the O4 antigen. We combined OPCs with SMNs in a 1:2 ratio for transplantation into the contused C4-C5 SCI cavity as a mixed-cell suspension (~200,000 cell dose per animal; **Figures 4**–7). The 1:2 ratio was chosen as opposed to a 1:1 ratio of OPCs to SMNs since single oligodendrocytes can myelinate multiple neuronal axons (Goldman and Kuypers, 2015). Neural co-cultures were encapsulated in 150 µm neural ribbons for overnight shipping on ice from Albany, NY to Houston, TX (Olmsted et al., 2020, 2021) for recovery and transplantation studies. Post-shipping release of the SMN-OPCs for transplantation was accomplished by dissolving the alginate in sodium citrate. The cells were injected in rats in HBSS supplemented with 5 mM glucose and 20 ng/ml FGF/EGF.

We used a well-characterized, reproducible rat model of cervical SCI (Mondello et al., 2015) wherein right-sided C4-C5 hemi-contusion injuries were made using the electromagnetic spinal cord injury device (ESCID). Fifteen days post-injury, female Long-Evans rats (*N* = 6) received cervical intraspinal injections of cell suspensions (~200,000 cells delivered). Grafts were successfully placed in all six animals. Half of the animals

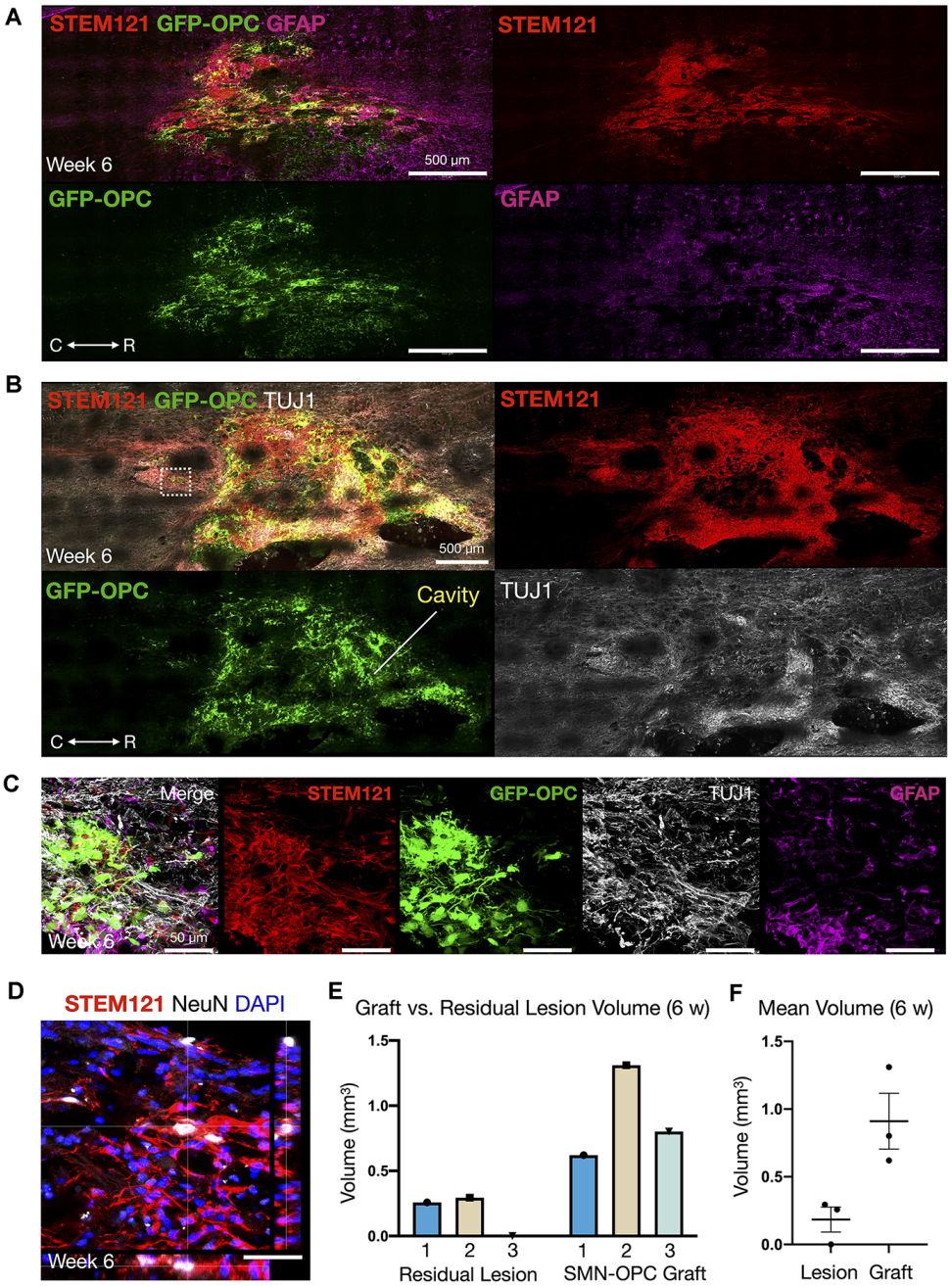

FIGURE 5 | Continued survival of SMN-OPC cell suspensions at 6 weeks post-transplantation. **(A)** Low power image of the graft at 6 weeks shown with STEM121/GFP-OPC/GFAP to depict host glial cells. **(B)** Low power image of the graft at 6 weeks shown with STEM121/GFP-OPC and TUJ1 to validate retention of the neuronal phenotype. White box denotes high magnification field shown in **(C)**, imaged caudal to the lesion epicenter. **(C)** High magnification merged image and individual channels (STEM121/GFP-OPC/TUJ1/GFAP) at 6 weeks post-transplantation. **(D)** STEM121 immunostain with mature neuronal marker NeuN co-localization. **(E,F)** Cavalieri volumetric analysis of the residual lesion and grafts. Color matching corresponds to the same animal. Shown are residual lesion vs. graft volume for individual spinal cords at 6 weeks (mm^3) **(E)** and mean ± s.e.m **(F)**. *N* = 3 animals were sacrificed at 6 weeks post-transplantation. R (rostral), C (caudal). Individual scale bars are provided.

were sacrificed 10 days post-transplantation (**Figure 4**), and the other half were sacrificed 6 weeks post-transplantation (**Figures 5**, **6**). Features of the SMNs such as TUJ1 positivity and synaptic connections were clearly visible at 10 days (**Figures 4D,E**). SMNs and OPCs survived in all animals at 10 days and 6 weeks time points. At the extended 6 weeks time point, grafted cells were again identified by immunohistochemistry that allowed discernment of host vs. transplanted human cells within the contusion cavity (GFAP, TUJ1, STEM121 comparisons in **Figure 5**) and neuronal

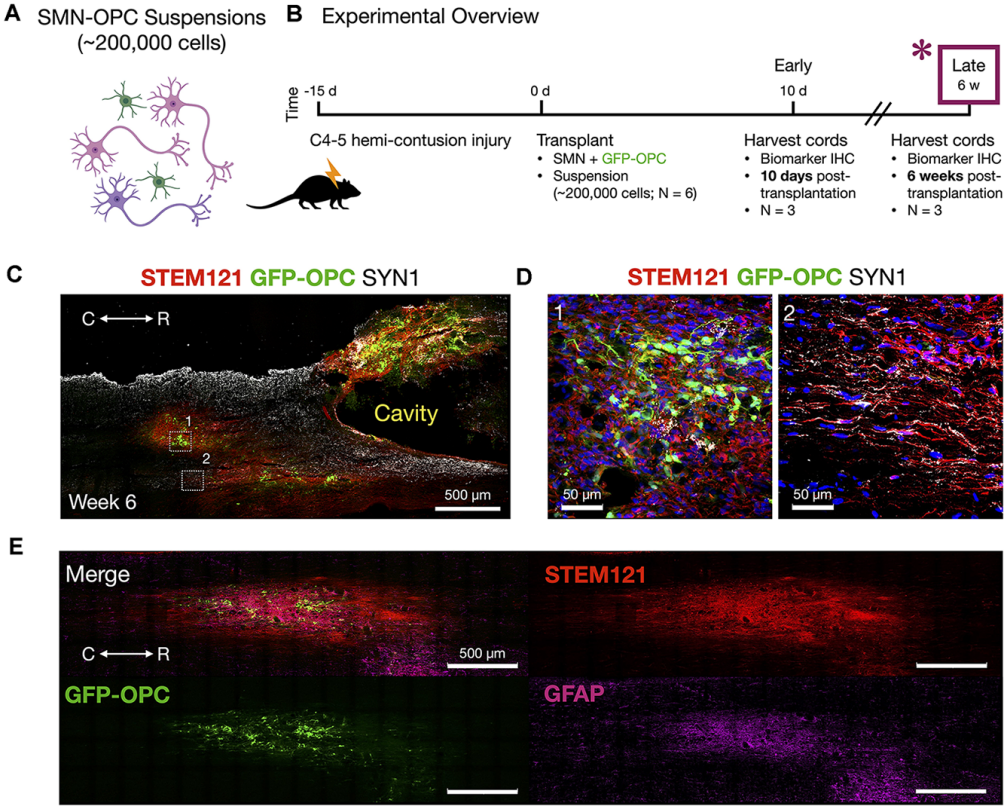

FIGURE 6 | Host tissue contusion site integration of SMN-OPC *in vivo* grafts. **(A)** Schematic overview of the SMN-OPC cell suspension grafts. Pink depicts spinal motor neurons, purple depicts spinal interneurons that co-differentiate, and green is GFP-OPCs. **(B)** Schematic overview of SMN-OPC cervical hemicontusion grafting experiment (N = 6 animals). *Data provided in this figure are from the 6 weeks time point. **(C)** Low magnification view of SMN-OPC suspension graft using STEM121 and SYN1 antibodies, and GFP to identify OPCs. White boxes (1, 2) denote high magnification fields shown in **(D)**. **(D)** Top: high magnification images of 6 weeks suspension grafts in the host spared spinal cord (1, 2) visualized with STEM121/GFP-OPC/SYN1/DAPI. Neuronal projections into spared host tissue have robust co-localization with SYN1. **(E)** Merged image and individual channels (STEM121/GFP-OPC/GFAP) demonstrates filling of the injury cavity and aligned fiber outgrowth in the host spared tissue. R (rostral), C (caudal). Individual scale bars are provided.

projections with aligned fiber outgrowth into spared host tissue (GFAP, SYN1, STEM121 comparisons in **Figure 6**). Grafted STEM121+ SMNs co-localized with Synapsin 1 and expressed NeuN at the extended 6 weeks time point. Transplanted neurons were measured to project a maximum of 2.12 mm caudal and 1.52 mm rostral to the lesion epicenter. We performed Cavalieri analysis of the spinal cord, lesion, and grafts to determine graft volumetrics at 6 weeks post-transplantation (**Figures 5E,F**). Every five sections (40 µm thick), the area of the cord, lesion cavity, and graft (STEM121) were determined and volumes were calculated (N = 3 spinal cords analyzed). The volumes (mm^3) for individual (N = 3) grafts and the corresponding residual lesions are provided in addition to the means. The volume of cell suspension injected was 2 µl (2 mm^3). The graft volume remained substantial at 6 weeks, consistent with our immunohistochemistry staining that indicates good viability of neurons and OPCs without neuroprotection or additional supportive measures within the contused SCI microenvironment (**Figures 5**, **6**).

Histological signs of OPC maturation over time are also evident comparing analyses at 10 days with 6 weeks (**Figure 7**) such as OPC ramification (**Figures 7A–D**). We also observed that in some frames the GFP-OPC signal appeared to be closely co-localized with that of GFAP (**Figures 7E,F**). Although the ability to count cells precisely is challenging in grafts, we quantified the total number of GFAP+ cells and determined the overlapping GFP-OPC/GFAP+ signals in 40 µm sections vs. GFP alone. The average estimated GFP-OPC population in three rats over five sections per animal is 50,570 ± 7,756 for GFP-OPCs where 6,717 ± 1,887 had GFP-OPC/GFAP+ co-localized signal (13.28%). GFP-OPC and GFAP signal overlap was only observed in subcellular compartments (neural processes) and not throughout entire cells. In most cases, distinct signals were identified in addition to regions of overlap (**Figures 7E,F**). Whether this result represents true transdifferentiation of OPCs to astrocytes, as has been reported in injury microenvironments (Valny et al., 2017), or instead the very close juxtaposition of these cells, cannot be easily discerned due to complex cell shape, disorganized tissue architecture at the injury site, and optical resolution restrictions for fine processes. Therefore, we cannot describe this as transdifferentiation based on the current data.

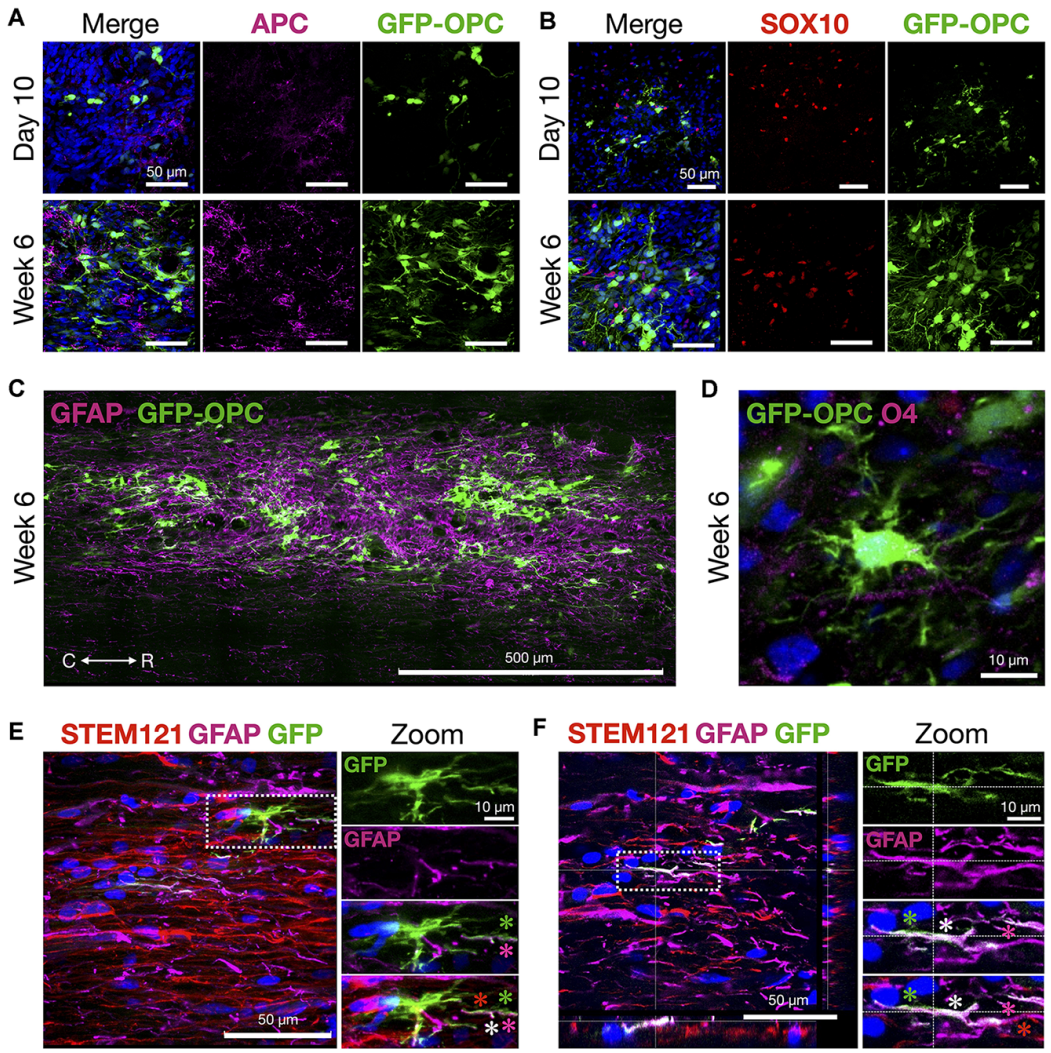

FIGURE 7 | OPCs thrive and morphologically develop in the contusion injury site. **(A)** Mature oligodendrocyte marker APC and transplanted GFP-OPCs at 10 days and 6 weeks time points, counterstained with DAPI. **(B)** GFP-OPCs increase in morphological complexity over 6 weeks in association with SOX10+ cells in the contusion injury microenvironment. Ten days and 6 weeks time points shown with DAPI. **(C)** GFP-OPCs survive and integrate within the GFAP+ injury milieu by 6 weeks. **(D)** GFP-OPCs arborize in the contusion injury microenvironment. O4 staining shown with DAPI. **(E,F)** Analysis of GFP-OPC and GFAP signal overlap at 6 weeks. GFAP and GFP signal is distinct with regions of overlap along STEM121 neural processes. Two examples are provided with zoom images. Asterisks depict GFP-OPC (green), GFAP (magenta), STEM121 (red), and signal overlap (white). R (rostral), C (caudal). Individual scale bars are provided.

DISCUSSION

The recent advanced ability to generate regionally matched spinal cord neurons for SCI *via* NMP lineage and developmental cues emboldens a re-evaluation of these cells *in vitro* to model neural circuit formation (Nedelec and Martinez-Arias, 2021; Olmsted et al., 2021) and their *in vivo* evaluation in animal models. The ability to graft spinal cord matched neuronal-glial cell types by applying these principles *ex vivo* through hiPSC and NMP technology and has not been tested in postnatal mammals outside of the current work. We demonstrate survival *in vivo* in a rat hemicontusion model of SCI and provide analysis to benefit their use in future SCI grafts for long-term behavioral analyses. Transplanted SMNs were comprehensively characterized *in vitro*, functionally and by RNAseq, and demonstrated to exhibit inherent hallmarks of neuronal maturity including expression of $Na_v1.6$ and $K_v1.2$, axon initial segment formation, cholinergic and glutamatergic synaptogenesis with NMJ formation, and spontaneous as well as glutamate-responsive spiking activity. Our findings are consistent with and underscore the importance of homotypic patterning in cell therapeutics for the spinal cord (Dulin et al., 2018; Olmsted et al., 2020), as has emerged in foundational CNS studies for brain pathologies (Lund and Hauschka, 1976; Lindvall, 1989; Das, 1990; Lindvall et al., 1990; Dunnett, 1991). *In vivo*, we observed robust survival, rapid engraftment, neuronal fiber anisotropic projections, and histological evidence for synaptogenesis of unprotected SMNs and OPCs delivered

in suspension into the challenging microenvironment of the hemicontusion injury cavity.

Neuronal grafting in the mammalian CNS has seen tremendous evolution, building from pre-stem cell studies with embryonic tissues across organisms (Bjorklund and Stenevi, 1984) to rapid innovation and discovery with stem cell technologies incorporating NSPCs (Thomson et al., 1998; Takahashi and Yamanaka, 2006). Trunk and spinal cord neural treatments with NSPCs could also adapt new NMP protocols used here vs. current methods that by default generate cells with obligate anterior telencephalic (Pankratz et al., 2007) rather than caudal trunk identity (Dulin et al., 2018; Kumamaru et al., 2018). The use of mature SMNs vs. trunk-directed NSPCs as a source for cell transplantation bypasses barriers inherent to multipotency and the potential for tumorigenicity.

Studies reveal that the refractory, immunoreactive SCI microenvironment generates inherent cell fate bias to differentiate along the astroglial lineage (Liu et al., 2019). Injury site modifiers applied with NSPCs, such as removal of inhibitory chondroitin sulfate proteoglycans (CSPGs) by use of the extracellular matrix glycosaminoglycan enzyme chondroitinase ABC (Bradbury and Burnside, 2019), may benefit grafts allowing NSPCs to differentiate towards neuronal outcomes and favor synaptogenesis and plasticity (Bradbury et al., 2002). We did not apply chondroitinase ABC in the current study. SMNs were co-transplanted with supporting NMP-derived OPCs purified by the OPC-specific biomarker O4. By immunohistochemistry we observed host GFAP+ astrocytes within the injury site, including a subset closely associated with the grafted GFP-OPCs. We evaluated merged fluorescent images to determine if transdifferentiation was occurring, as has been described previously in several studies (reviewed in Valny et al., 2017) in which OPCs can transdifferentiate to astrocytes in harsh CNS injury microenvironments. We determined that a significant fraction of co-signal overlap was due to merged signals from different planes as well as some very closely associated OPCs and GFAP+ staining cells along neuronal processes. It may still be possible that some transdifferentiation occurred at a very low frequency but will require future studies to validate such a transition in our graft-host contusion model.

An important step towards studying and fully achieving grafted complex circuit replacement in SCI is the development of greater reproducibility through improved methodologies. The use of homotypic, pre-defined neuronal and glial populations represents a new and exciting approach that allows immediate focus on circuitry regeneration. In the present study, we demonstrate that regionally appropriate stem cell-derived SMNs with maturing phenotype survive *in vivo* despite delivery into the challenging lesion cavity environment. The feasibility and reproducible methodologies for the delivery of pre-differentiated, functional cell types reported here constitute a critical step towards focused, targeted circuitry replacement in subacute lesions.

The findings of mature SMN engraftment as suspension-delivered cells are surprising and promising. Modern stem cell differentiation protocols are increasingly aided by newly revealed *in vivo* embryological principles for patterning spinal cord neural cells (Olmsted and Paluh, 2021) and are enabling alternative experimental strategies that combine encapsulation as a tool for pre-formation of transplantable neuronal networks (Olmsted et al., 2021). The *ex vivo* pre-differentiation of the cells allows comprehensive analysis by RNA-Seq, imaging of biomarkers, co-culture assays, and electrophysiology in order to ensure future reproducibility and to bypass NSPC-specific *in vivo* challenges of stochastic differentiation. Biomarker analysis of spinal cord sections in this study revealed robust survival of the homotypic neurons and OPCs, rapid engraftment within the host tissue at 10 days post-transplantation, and outgrowth at 6 weeks post-transplantation. Signs of graft cell maturation over time included OPC ramification, caudal axon anisotropic navigation, and increased co-localization with Synapsin within the spinal cord. The degree to which the electrophysiological profile of SMNs *in vitro* matches those *in vivo* is unknown. However, RNA-Seq revealed appropriate receptor profiles in the SMNs and functional *in vitro* assays confirmed neurotransmitter responsiveness. The robust survival and synaptic integration of the transplanted neurons *in vivo* is consistent with sufficient spinal cord matching.

The ability to fully interrogate SMNs and OPCs *in vivo* to restore circuitry and lost functional modalities will require larger cohorts and long-term circuitry evaluation with behavioral analyses. Our findings are expected to drive the field to develop advanced tools to address graft-host interconnectivity in circuitry reformation in real time, in addition to current methods of trans-synaptic labeling and transmission electron microscopy. As well, new strategies to boost OPC maturation and myelinating activity have been described through regulation of microRNAs (Fan et al., 2017). In our short-term study, the transplanted OPCs lost biomarkers for early progenitors but did not yet achieve myelinating activity at 6 weeks. Nevertheless, the cells remained in close contact with axons and became ramified. The precise role that grafted OPCs play in remyelination or support in regard to restored circuitry and functional behavior outcomes is unclear and not addressed this work. In a recent study, it was determined that myelinating activity of OPCs is not required for functional recovery (Duncan et al., 2018). We did not observe wrapping structures around axons in our GFP-OPCs, as were observed in Fan et al. (2017). Our approach may further benefit by incorporating additional defined cells such as ventral and/or dorsal spinal interneuron subtypes differentiated *in vitro* (Sagner and Briscoe, 2019; Zavvarian et al., 2020). Although we do not interrogate or quantify circuitry reformation, the functional pre-requisites of neuronal survival, synapse formation, and projection into the host are achieved. This work therefore demonstrates the exciting potential of transplanting pre-differentiated neurons within a lesion cavity to advance regionally specified circuit reconstruction and repair studies, as well as injury customization towards improved *in vivo* SCI therapeutic outcomes.

DATA AVAILABILITY STATEMENT

The datasets presented in this study can be found in online repositories. The names of the repository/repositories and

accession number(s) can be found below: https://www.ncbi.nlm.nih.gov/geo/query/acc.scgi?acc=GSE178600.

ETHICS STATEMENT

The animal study was reviewed and approved by the Houston Methodist Research Institute IACUC.

AUTHOR CONTRIBUTIONS

JP and ZO designed human stem cell experiments and wrote the manuscript with input from all co-authors. ZO compiled figures and performed hiPSC neural differentiation and analysis, *in vitro* imaging, mRNA sample preparation, and MEA experiments. BM assisted with RNA-Seq samples, analysis, and bioinformatics. PH and CS designed and conducted rat experiments for *in vivo* grafting. CS performed histology, data acquisition and analysis. The F3.5.2 hiPSC line was derived previously in collaboration with JC, who also provided key input for experiments and analysis. All authors contributed to the article and approved the submitted version.

FUNDING

This work was funded by the New York State Department of Health (NYS DOH) Spinal Cord Injury Research Board (NYSCIRB), Projects to Accelerate Research Translation (PART) award C33278GG, SUNY Polytechnic SEED award 917035-21, and used a published line developed through previous New York State stem cell research (NYSTEM) funding.

ACKNOWLEDGMENTS

RNA-Seq was performed at the SUNY Buffalo Genomics and Bioinformatics Core.

SUPPLEMENTARY MATERIALS

The Supplementary Material for this article can be found online at: https://www.frontiersin.org/articles/10.3389/fncel.2021.725195/full#supplementary-material.

REFERENCES

Almad, A., Sahinkaya, F. R., and McTigue, D. M. (2011). Oligodendrocyte fate after spinal cord injury. *Neurotherapeutics* 8, 262–273. doi: 10.1007/s13311-011-0033-5

Amoroso, M. W., Croft, G. F., Williams, D. J., O'Keeffe, S., Carrasco, M. A., Davis, A. R., et al. (2013). Accelerated high-yield generation of limb-innervating motor neurons from human stem cells. *J. Neurosci.* 33, 574–586. doi: 10.1523/JNEUROSCI.0906-12.2013

Assinck, P., Duncan, G. J., Hilton, B. J., Plemel, J. R., and Tetzlaff, W. (2017). Cell transplantation therapy for spinal cord injury. *Nat. Neurosci.* 20, 637–647. doi: 10.1038/nn.4541

Bjorklund, A., and Stenevi, U. (1984). Intracerebral neural implants: neuronal replacement and reconstruction of damaged circuitries. *Ann. Rev. Neurosci.* 7, 279–308. doi: 10.1146/annurev.ne.07.030184.001431

Bradbury, E. J., and Burnside, E. R. (2019). Moving beyond the glial scar for spinal cord repair. *Nat. Commun.* 10:3879. doi: 10.1038/s41467-019-11707-7

Bradbury, E. J., Moon, L. D. F., Popat, R. J., King, V. R., Bennett, G. S., Patel, P. N., et al. (2002). Chondroitinase ABC promotes functional recovery after spinal cord injury. *Nature* 416, 636–640. doi: 10.1038/416636a

Bregman, B. S., Kunkel-Bagden, E., Reier, P. J., Dai, H. N., McAtee, M., and Gao, D. (1993). Recovery of function after spinal cord injury: mechanisms underlying transplant-mediated recovery of function differ after spinal cord injury in newborn and adult rats. *Exp. Neurol.* 123, 3–16. doi: 10.1006/exnr.1993.1136

Burke, E. E., Chenowerth, J. G., Shin, J. H., Collado-Torres, L., Kim, S.-K., Micali, N., et al. (2020). Dissecting transcriptomic signatures of neuronal differentiation and maturation using iPSCs. *Nat. Commun.* 11:462. doi: 10.1038/s41467-019-14266-z

Carter, J. L., Halmai, J. A. N. M., and Fink, K. D. (2020). The iNs and outs of direct reprogramming to induced neurons. *Front. Genome Ed.* 2:7. doi: 10.3389/fgeed.2020.00007

Chambers, S. M., Fasano, C. A., Papapetrou, E. P., Tomishima, M., Sadelain, M., and Studer, L. (2009). Highly efficient neural conversion of human ES and iPS cells by dual inhibition of SMAD signaling. *Nat. Biotechnol.* 27, 275–280. doi: 10.1038/nbt.1529

Chambers, S. M., Qi, Y., Mica, Y., Lee, G., Zhang, X.-J., Niu, L., et al. (2012). Combined small-molecule inhibition accelerates developmental timing and converts human pluripotent stem cells into nocioceptors. *Nat. Biotechnol.* 30, 715–720. doi: 10.1038/nbt.2249

Chang, E. A., Tomov, M. L., Suhr, S. T., Luo, J., Olmsted, Z. T., Paluh, J. L., et al. (2015). Derivation of ethnically diverse human induced pluripotent stem cell lines. *Sci. Rep.* 5:15234. doi: 10.1038/srep15234

Das, G. D. (1990). Neural transplantation: an historical perspective. *Neurosci. Biobehav. Rev.* 14, 389–401. doi: 10.1016/s0149-7634(05)80061-2

Dulin, J. N., Adler, A. F., Kumamaru, H., Poplawski, G. H. D., Lee-Kubli, C., Strobl, H., et al. (2018). Injured adult motor and sensory axons regenerate into appropriate organotypic domains of neural progenitor grafts. *Nat. Commun.* 9:84. doi: 10.1038/s41467-017-02613-x

Duncan, G. J., Manesh, S. B., Hilton, B. J., Assinck, P., Liu, J., Moulson, A., et al. (2018). Locomotor recovery following contusive spinal cord injury does not require oligodendrocyte remyelination. *Nat. Commun.* 9:3066. doi: 10.1038/s41467-018-05473-1

Dunnett, S. B. (1991). Transplantation of embryonic dopamine neurons: what we know from rats. *J. Neurol.* 238, 65–74. doi: 10.1007/BF00315683

Ewels, P., Magnusson, M., Lundin, S., and Kaller, M. (2016). MultiQC: summarize analysis results for multiple tools and samples in a single report. *Bioinformatics* 32, 3047–3048. doi: 10.1093/bioinformatics/btw354

Fan, H.-B., Chen, L.-X., Qu, X.-B., Ren, C.-L., Wu, X.-X., Dong, F.-X., et al. (2017). Transplanted miR-219-overexpressing oligodendrocyte precursor cells promoted remyelination and improved functional recovery in a chronic demyelinated model. *Sci. Rep.* 7:41407. doi: 10.1038/srep41407

Goldman, S. A., and Kuypers, N. J. (2015). How to make an oligodendrocyte. *Development* 142, 3983–3995. doi: 10.1242/dev.126409

Gouti, M., Tsakiridis, A., Wymeersch, F. J., Huang, Y., Kleinjung, J., Wilson, V., et al. (2014). *in vitro* generation of neuromesodermal progenitors reveals distinct roles for Wnt signaling in the specification of spinal cord and paraxial mesoderm identity. *PLoS Biol.* 12:e1001937. doi: 10.1371/journal.pbio.1001937

Harper, J. M., Krishnan, C., Darman, J. S., Deshpande, D. M., Peck, S., Shats, I., et al. (2004). Axonal growth of embryonic stem cell-derived motor neurons *in vitro* and in motorneuron-injured adult rats. *Proc. Natl. Acad. Sci. U S A* 101, 7123–7128. doi: 10.1073/pnas.0401103101

Henrique, D., Abranches, E., Verrier, L., and Storey, K. G. (2015). Neuromesodermal progenitors and the making of the spinal cord. *Development* 142, 2864–2875. doi: 10.1242/dev.119768

Khazaei, M., Ahuja, C. S., and Fehlings, M. G. (2017). Generation of oligodendrogenic spinal neural progenitor cells from human induced pluripotent stem cells. *Curr. Protoc. Stem Cell Biol.* 42:2D.20.1–2D.20.14. doi: 10.1002/cpsc.31

Kikuchi, T., Morizane, A., Doi, D., Magotani, H., Onoe, H., Hayashi, T., et al. (2017). Human iPS cell-derived dopaminergic neurons function in a primate Parkinson's disease model. *Nature* 548, 592–596. doi: 10.1038/nature23664

Kim, D., Langmead, B., and Salzberg, S. L. (2015). HISAT: a fast spliced aligner with low memory requirements. *Nat. Methods* 12, 357–360. doi: 10.1038/nmeth.3317

Klim, J. R., Williams, L. A., Limone, F., San Juan, I. G., Davis-Dusenbery, B. N., Mordes, D. A., et al. (2019). ALS-implicated protein TDP-43 sustains levels of STMN2, a mediator of motor neuron growth and repair. *Nat. Neurosci.* 22, 167–179. doi: 10.1038/s41593-018-0300-4

Kumamaru, H., Kadoya, K., Adler, A. F., Takashima, Y., Graham, L., Coppola, G., et al. (2018). Generation and post-injury integration of human spinal cord neural stem cells. *Nat. Methods* 15, 723–731. doi: 10.1038/s41592-018-0074-3

Lee, H., Lee, H. Y., Lee, B. E., Gerovska, D., Park, S. Y., Zaehres, H., et al. (2020). Sequentially induced MNs from human fibroblasts facilitate locomotor recovery in a rodent SCI model. *eLife* 9:e52069. doi: 10.7554/eLife.52069

Liao, Y., Smyth, G. K., and Shi, W. (2014). featureCounts: an efficient general purpose program for assigning sequence reads to genomic features. *Bioinformatics* 30, 923–930. doi: 10.1093/bioinformatics/btt656

Lindvall, O. (1989). Transplantation into the human brain: present status and future possibilities. *J. Neurol. Neurosurg. Psychiatry* 52, 39–54. doi: 10.1136/jnnp.52.suppl.39

Lindvall, O., Brundin, P., Widner, H., Rehncrona, S., Gustavii, B., Frackowiak, R., et al. (1990). Grafts of fetal dopamine neurons survive and improve motor function in Parkinson's disease. *Science* 247, 574–577. doi: 10.1126/science.2105529

Lippmann, E. S., Williams, C. E., Ruhl, D. A., Esteves-Silva, M. C., Chapman, E. R., Coon, J. J., et al. (2015). Deterministic HOX patterning in human pluripotent stem cell-derived neuroectoderm. *Stem Cell Rep.* 4, 632–644. doi: 10.1016/j.stemcr.2015.02.018

Liu, C., Fan, L., Xing, J., Wang, Q., Lin, C., Liu, C., et al. (2019). Inhibition of astrocytic differentiation of transplanted neural stem cells by chondroitin sulfate methacrylate hydrogels for the repair of injured spinal cord. *Biomater. Sci.* 7, 1995–2008. doi: 10.1039/c8bm01363b

Love, M. I., Huber, W., and Anders, S. (2014). Moderated estimation of fold change and dispersion for RNA-Seq data with DESeq2. *Genome Biol.* 15:550. doi: 10.1186/s13059-014-0550-8

Lund, R. D., and Hauschka, S. D. (1976). Transplanted neural tissue develops connections with host rat brain. *Science* 193, 582–584. doi: 10.1126/science.959815

Manion, J., Khuong, T., Harney, D., Littleboy, J. B., Ruan, T., Loo, L., et al. (2020). Human induced pluripotent stem cell-derived GABAergic interneuron transplants attenuate neuropathic pain. *Pain* 161, 379–387. doi: 10.1097/j.pain.0000000000001733

Miles, G. B., Yohn, D. C., Wichterle, H., Jessell, T. M., Rafuse, V. F., and Brownstone, R. M. (2004). Functional properties of motorneurons derived from mouse embryonic stem cells. *J. Neurosci.* 24, 7848–7858. doi: 10.1523/JNEUROSCI.1972-04.2004

Mondello, S. E., Sunshine, M. D., Fischedick, A. E., Mortiz, C. T., and Horner, P. J. (2015). A cervical hemi-contusion spinal cord injury model for the investigation of novel therapeutics targeting proximal and distal forelimb functional recovery. *J. Neurotrauma* 32, 1994–2007. doi: 10.1089/neu.2014.3792

Nedelec, S., and Martinez-Arias, A. (2021). *in vitro* models of spinal motor circuit's development in mammals: achievements and challenges. *Curr. Opin. Neurobiol.* 66, 240–249. doi: 10.1016/j.conb.2020.12.002

Olmsted, Z. T., and Paluh, J. P. (2021). Stem cell neurodevelopmental solutions for restorative treatments of the human trunk and spine. *Front. Cell. Neurosci.* 15:667590. doi: 10.3389/fncel.2021.667590

Olmsted, Z. T., Stigliano, C. S., Badri, A., Zhang, F., Williams, A., Koffas, M. A. G., et al. (2020). Fabrication of homotypic neural ribbons as a multiplex platform optimized for spinal cord delivery. *Sci. Rep.* 10:12939. doi: 10.1038/s41598-020-69274-7

Olmsted, Z. T., Stigliano, C. S., Scimemi, A. S., Wolfe, T., Cibelli, J., Horner, P. J., et al. (2021). Transplantable human motor networks as a neuron-directed strategy for spinal cord injury. *iScience* 24:102827. doi: 10.1016/j.isci.2021.102827

Pankratz, M. T., Li, X.-J., Lavaute, T. M., Lyons, E. A., Chen, X., and Zhang, S.-C. (2007). Directed neural differentiation of human embryonic stem cells *via* an obligated primitive anterior stage. *Stem Cells* 25, 1511–1520. doi: 10.1634/stemcells.2006-0707

Peljto, M., Dasen, J. S., Mazzoni, E. O., Jessell, T. M., and Wichterle, H. (2010). Functional diversity of ESC-derived motor neuron subtypes revealed through intraspinal transplantation. *Cell Stem Cell* 7, 355–366. doi: 10.1016/j.stem.2010.07.013

Reier, P. J., Bregman, B. S., and Wujek, J. R. (1986). Intraspinal transplantation of embryonic spinal cord tissue in neonatal and adult rats. *J. Comp. Neurol.* 247, 275–296. doi: 10.1002/cne.902470302

Sagner, A., and Briscoe, J. (2019). Establishing neuronal diversity in the spinal cord: a time and a place. *Development* 146:dev182154. doi: 10.1242/dev.182154

Silva, N. A., Sousa, N., Reis, R. L., and Salgado, A. J. (2014). From basics to clinical: a comprehensive review on spinal cord injury. *Prog. Neurobiol.* 114, 25–57. doi: 10.1016/j.pneurobio.2013.11.002

Sontag, C. J., Uchida, N., Cummings, B. J., and Anderson, A. J. (2014). Injury to the spinal cord niche alters the engraftment dynamics of human neural stem cells. *Stem Cell Rep.* 2, 620–632. doi: 10.1016/j.stemcr.2014.03.005

Takahashi, K., and Yamanaka, S. (2006). Induction of pluripotent stem cells from mouse embryonic and adult fibroblast cultures by defined factors. *Cell* 126, 663–676. doi: 10.1016/j.cell.2006.07.024

Taylor, L., Jones, L., Tuszynski, M. H., and Blesch, A. (2006). Neurotrophin-3 gradients established by lentiviral gene delivery promote short-distance axonal bridging beyond cellular grafts in the injured spinal cord. *J. Neurosci.* 26, 9713–9721. doi: 10.1523/JNEUROSCI.0734-06.2006

Thomson, J. A., Itskovitz-Eldor, J., Shapiro, S. S., Waknitz, M. A., Swiergiel, J. J., Marshall, V. S., et al. (1998). Embryonic stem cell lines derived from human blastocysts. *Science* 282, 1145–1147. doi: 10.1126/science.282.5391.1145

Tomov, M. L., Olmsted, Z. T., Dogan, H., Gongorurler, E., Tsompana, M., Otu, H. H., et al. (2016). Distinct and shared determinants of cardiomyocyte contractility in multi-lineage competent ethnically diverse iPSCs. *Sci. Rep.* 6:37637. doi: 10.1038/srep37637

Tzouanacou, E., Wegener, A., Wymeersch, F. J., Wilson, V., and Nicolas, J.-F. (2009). Redefining the progression of lineage segregations during mammalian embryogenesis by clonal analysis. *Dev. Cell* 17, 365–376. doi: 10.1016/j.devcel.2009.08.002

Valny, M., Honsa, P., Kriska, J., and Anderova, M. (2017). Multipotency and therapeutic potential of NG2 cells. *Biochem. Pharmacol.* 141, 42–55. doi: 10.1016/j.bcp.2017.05.008

Wind, M., Gogolou, A., Manipur, I., Granata, I., Butler, L., Andrews, P. W., et al. (2021). Defining the signaling determinants of a posterior ventral spinal cord identity in human neuromesodermal progenitor derivatives. *Development* 148:dev194415. doi: 10.1242/dev.194415

Xiong, M., Tao, Y., Gao, Q., Feng, B., Yan, W., Zhou, Y., et al. (2021). Human stem cell-derived neurons repair circuits and restore neural function. *Cell Stem Cell* 28, 112–126.e6. doi: 10.1016/j.stem.2020.08.014

Zavvarian, M.-M., Hong, J., and Fehlings, M. G. (2020). The functional role of spinal interneurons following traumatic spinal cord injury. *Front. Cell. Neurosci.* 14:127. doi: 10.3389/fncel.2020.00127

Conflict of Interest: The authors declare that the research was conducted in the absence of any commercial or financial relationships that could be construed as a potential conflict of interest.

Publisher's Note: All claims expressed in this article are solely those of the authors and do not necessarily represent those of their affiliated organizations, or those of the publisher, the editors and the reviewers. Any product that may be evaluated in this article, or claim that may be made by its manufacturer, is not guaranteed or endorsed by the publisher.

Copyright © 2022 Olmsted, Stigliano, Marzullo, Cibelli, Horner and Paluh. This is an open-access article distributed under the terms of the Creative Commons Attribution License (CC BY). The use, distribution or reproduction in other forums is permitted, provided the original author(s) and the copyright owner(s) are credited and that the original publication in this journal is cited, in accordance with accepted academic practice. No use, distribution or reproduction is permitted which does not comply with these terms.

frontiers in Cellular Neuroscience

ORIGINAL RESEARCH
published: 14 February 2022
doi: 10.3389/fncel.2021.817277

Vav3-Deficient Astrocytes Enhance the Dendritic Development of Hippocampal Neurons in an Indirect Co-culture System

*David Wegrzyn†, Josephine Zokol† and Andreas Faissner**

Department of Cell Morphology and Molecular Neurobiology, Ruhr-University Bochum, Bochum, Germany

Vav proteins belong to the class of guanine nucleotide exchange factors (GEFs) that catalyze the exchange of guanosine diphosphate (GDP) by guanosine triphosphate (GTP) on their target proteins. Here, especially the members of the small GTPase family, Ras homolog family member A (RhoA), Ras-related C3 botulinum toxin substrate 1 (Rac1) and cell division control protein 42 homolog (Cdc42) can be brought into an activated state by the catalytic activity of Vav-GEFs. In the central nervous system (CNS) of rodents Vav3 shows the strongest expression pattern in comparison to Vav2 and Vav1, which is restricted to the hematopoietic system. Several studies revealed an important role of Vav3 for the elongation and branching of neurites. However, little is known about the function of Vav3 for other cell types of the CNS, like astrocytes. Therefore, the following study analyzed the effects of a *Vav3* knockout on several astrocytic parameters as well as the influence of Vav3-deficient astrocytes on the dendritic development of cultured neurons. For this purpose, an indirect co-culture system of native hippocampal neurons and Vav3-deficient cortical astrocytes was used. Interestingly, neurons cultured in an indirect contact with Vav3-deficient astrocytes showed a significant increase in the dendritic complexity and length after 12 and 17 days *in vitro* (DIV). Furthermore, Vav3-deficient astrocytes showed an enhanced regeneration in the scratch wound heal assay as well as an altered profile of released cytokines with a complete lack of CXCL11, reduced levels of IL-6 and an increased release of CCL5. Based on these observations, we suppose that Vav3 plays an important role for the development of dendrites by regulating the expression and the release of neurotrophic factors and cytokines in astrocytes.

Keywords: Vav3, Rho-GTPases, guanine nucleotide exchange factor, astrocytes, hippocampal neurons, neuron-astrocyte interaction, cytokines, CCL5

OPEN ACCESS

Edited by:
Renato Socodato, Institute for Molecular and Cellular Biology (IBMC), Portugal

Reviewed by:
Cecilia Beatriz Conde, Medical Research Institute Mercedes and Martín Ferreyra (INIMEC), Argentina
Marta Zagrebelsky, Technische Universitat Braunschweig, Germany

***Correspondence:**
Andreas Faissner
andreas.faissner@rub.de

†These authors share first authorship

Specialty section:
This article was submitted to Non-Neuronal Cells, a section of the journal Frontiers in Cellular Neuroscience

Received: *17 November 2021*
Accepted: *29 December 2021*
Published: *14 February 2022*

Citation:
Wegrzyn D, Zokol J and Faissner A (2022) Vav3-Deficient Astrocytes Enhance the Dendritic Development of Hippocampal Neurons in an Indirect Co-culture System. Front. Cell. Neurosci. 15:817277. doi: 10.3389/fncel.2021.817277

INTRODUCTION

Vav3 belongs to the Dbl-family of guanine nucleotide exchange factors (GEFs) which includes further 68 members in humans (Rossman et al., 2005). It is characterized by the Dbl homology (DH) domain localized next to a regulatory pleckstrin homology (PH) domain and can be activated by the phosphorylation of a tyrosine residue (Tyr174) (Turner and Billadeau, 2002; Rossman et al., 2005).

The catalytic activity of Vav-GEFs is accomplished by an interaction between the DH domain and target proteins. Here, especially members of the Rho-GTPase family can be switched into an active state by Vav-GEFs. Vav3 can directly activate RhoA, RhoG and Rac-1 (Movilla and Bustelo, 1999; Movilla et al., 2001). Furthermore, a study described that Vav3 indirectly acts on Cdc42 by an accumulation of phosphatidylinositol 3,4,5-trisphosphate (PIP_3) (Aoki et al., 2005). Since RhoA, Rac-1 and Cdc42 are strong modulators of the cytoskeleton, Vav3 functions as a mediator of intracellular reorganizations of the cytoskeleton (Tapon and Hall, 1997). In this way, Vav3 regulates key events of CNS development like migration (Khodosevich et al., 2009), proliferation (Fujikawa et al., 2002), differentiation (Ulc et al., 2019) and axo-dendritic maturation (Quevedo et al., 2010; Sauzeau et al., 2010; Ulc et al., 2017; Wegrzyn et al., 2020).

Interestingly, several studies could show that a lack of Vav3 impacts the axonal and dendritic morphology of neurons in different brain areas. Purkinje and granule cells of *Vav3*-knockout animals showed a reduction of the dendritic complexity in the postnatal period of mice (Quevedo et al., 2010). This observation was accompanied by motoric deficiencies which, however, vanished in the adult stage. Furthermore, GABAergic neurons exhibited an impaired axon guidance in the brainstem when Vav3 was deficient (Sauzeau et al., 2010). The altered axon guidance of GABAergic neurons in the brainstem of mice was consequently linked to hypertension, tachycardia, and renocardiovascular dysfunctions (Sauzeau et al., 2010). Additionally, primary hippocampal neurons derived from Vav3-deficient embryonic animals displayed a significant raise in their axonal lengths and complexities as well as in their structural synapse numbers *in vitro* (Wegrzyn et al., 2020). In schizophrenia patients *VAV3* could be furthermore identified as a risk gene and polymorphisms were discussed to possibly be responsible for reduced volumes of the left superior and middle temporal *gyri* (Aleksic et al., 2013). Although, there are several studies with a focus of Vav3 on the neuronal development and differentiation, less is known about the function of Vav3 in astrocytes. Astrocytes are glial cells that highly support neurons in multiple ways (Ben Haim and Rowitch, 2017). With their protrusions, astrocytes form perisynaptic contacts and contribute to the tripartite synapse (Perea et al., 2009; Faissner et al., 2010; Bernardinelli et al., 2014). Furthermore, astrocytes are involved in the uptake and recycling of glutamate (Norenberg and Martinez-Hernandez, 1979), modulation of neuronal activity by the release of gliotransmitters (Zhang et al., 2003; Panatier et al., 2006; Jourdain et al., 2007; Henneberger et al., 2010), structure of the blood-brain barrier (Janzer and Raff, 1987) and metabolic support of neurons (Deitmer et al., 2019). There is a growing evidence that Rho-GTPases affect the stellation of astrocytes and modify neuron-astrocyte interactions (Zeug et al., 2018). Furthermore, different roles of RhoA, Rac-1 and Cdc42 could be observed for the morphological organization of astrocytes. RhoA has been identified to mainly act as a negative regulator of the astrocytic process outgrowth. The inhibition of RhoA by C3 derived from *Clostridium botulinum* enhanced the outgrowth and branching of astrocytic processes as well as the migratory activity in an *in vitro* scratch wound assay (Höltje et al., 2005). Similar results were obtained when the RhoA downstream target protein Rho-associated protein kinase (ROCK) was specifically inhibited via the selective inhibitor Y27632 (Höltje et al., 2005). Contrary effects could be seen for Rac-1. The transfection of primary astrocytes with Rac1-shRNA disrupted the formation of a stellate morphology when Y27632 was added to the culture medium (Racchetti et al., 2012). Additionally, studies with a dominant negative form of Rac1 could support this observation and furthermore show a reduced motility of astrocytic processes which went along with a reduced maturation of dendritic protrusions in organotypic slice cultures (Nishida and Okabe, 2007). The astrocytic migration is furthermore positively promoted by the activity of Rac1 (Liao et al., 2015). For Cdc42, especially an important role for the migration could be observed (Robel et al., 2011; Bardehle et al., 2013).

While there are several scientific publications about the individual impact of single Rho-GTPases on astrocytic properties, less is known about the role of regulatory upstream GEFs like Vav3. Here, we utilized an indirect co-culture system to investigate the impact of a *Vav3* knockout in astrocytes on the dendritic morphology of primary hippocampal neurons. Furthermore, we characterized the expression levels of several neurotrophic factors on mRNA level and the cytokine levels in the cell culture supernatant of native and Vav3-deficient astrocytes. A better understanding of Rho-GTPases and their upstream regulators might unravel novel aspects of neuron-astrocyte interactions and allow for new therapeutic strategies by the manipulation of Rho-GEFs.

MATERIALS AND METHODS

Animals

All experiments of this study were performed in accordance with the Society for Neuroscience and the European Council Directive of September 22, 2010 (2010/63/EU), for care of laboratory animals and approved by the animal care committee of North Rhine-Westphalia, Germany, based at the LANUV (Landesamt für Umweltschutz, Naturschutz und Verbraucherschutz, North Rhine-Westphalia, D-45659 Recklinghausen, Germany). Wildtype (WT) SV129 and *Vav3* knockout animals of both sexes were used and originated from the mouse colony of the Department for Cell Morphology and Molecular Neurobiology of the Ruhr-University Bochum (Luft et al., 2015; Wegrzyn et al., 2020). The animals were kept under standardized conditions with a regulated temperature (21°C), humidity (60–70%) and a 12 h dark/light circle. The animals were supplied with food and water *ad libitum*.

Cell Culture

Preparation of Mixed Glial Cultures

Primary mixed glial cultures derived from cerebellar tissue of SV129 and *Vav3*$^{-/-}$ animals and were performed as previously described, with slight modifications of the protocol (McCarthy and de Vellis, 1980; Gottschling et al., 2016). First, postnatal day 1–3 (P1-3) animals were decapitated, and six cortices were

transferred into 1 ml HBSS (Thermo Fisher Scientific Inc.; Cat. No.: 14170088). Afterward, the HBSS was replaced by 1 ml digestion solution composed of 30 U Papain (Worthington; Cat. No.: LS003126), 80 μg/ml (w/v) DNase I (Worthington; Cat. No.: LS002007), and 0.96 mg/ml (w/v) L-cysteine (Sigma-Aldrich; Cat. No.: C2529) in DMEM (Thermo Fisher Scientific Inc.; Cat. No.: 41966029) and incubated for 1 h at 37°C Contemporaneous, a T-75 culture flask (Sarstedt; Cat. No.: 83.3911.002) was coated with 10 μg/ml (w/v) poly-D-lysine (PDL, Sigma-Aldrich; Cat. No.: P0899) for 1 h at 37°C in the incubator. Afterward, the digestion solution was removed and replaced by freshly prepared astrocyte culture medium consisting of DMEM (Thermo Fisher Scientific Inc.; Cat. No.: 41966029) with 10% (v/v) horse serum (Sigma-Aldrich; Cat. No.: S9135) and 0.1% (v/v) gentamicin (Sigma-Aldrich; Cat. No.: S9135). After the digestion, the cortices were triturated and centrifuged at 1,000 rpm for 5 min. Next, the supernatant was discarded, and the pellet resuspended in 1 ml of astrocyte medium. Finally, the cell solution was added to 9 ml astrocyte medium in the T-75 culture flask, which was previously washed with PBS (1x) after the coating procedure. The cultures were kept at 37°C and 6% CO_2 with a first medium exchange after 7 days and the following medium exchanges were performed every second or third day.

Elimination of Microglia and Oligodendrocyte Precursor Cells

In order to receive pure astrocytic cultures, the T-75 culture flasks were placed on an orbital shaker for 1 h at 250 rpm and 37°C (New Brunswick Scientific) after an initial cultivation time of 7–8 days. In a second step, the flasks were shaken at 250 rpm and 37°C overnight after the lid of culture flask was covered with parafilm (Brand, Wertheim). This procedure accomplished a constant CO_2 level in the flasks. The following day, the culture medium was completely removed and replaced by fresh and pre-warmed astrocyte medium which additionally contained 20 mM of cytosine-1-β-D-arabinofuranoside (Ara-C, Sigma-Aldrich, Cat. No.: C1768). The treatment of the cells with Ara-C was maintained for 48–72 h and reduced the number of microglia and Oligodendrocyte Precursor Cells (OPCs). Finally, pure astrocyte cultures were kept at 37°C and 6% CO_2 with a complete medium exchange every second or third day until further experiments were performed.

Scratch Wound Healing Assay

For the scratch wound assay, 4-well plates (Thermo Fisher Scientific Inc.; Cat. No.: 176740) were used which were previously coated with 10 μg/ml (w/v) PDL. Wildtype or *Vav3*$^{-/-}$astrocytes were detached from the previously prepared T-75 flasks via an exchange of the astrocyte culture medium by 3 ml of 0.05% (v/v) trypsin/EDTA (T/E) (Thermo Fisher Scientific Inc.; Cat. No.: 25300054). The digestion solution was left on the astrocytic monolayer for 7 min at 37°C in the incubator. Then, the detached astrocytes were transferred into 7 ml of astrocyte medium and centrifuged at 1,000 rpm for 5 min. After the centrifugation, the supernatant was discarded, and the cell pellet resuspended in 1 ml astrocyte medium. A total number of 35,000 astrocytes in 500 μl culture medium (≙ 70,000 cells/ml) was plated out per well. The astrocytes were cultured at 37°C and 6% CO_2 with a total medium exchange every second or third day. After a cultivation time of 10 days, astrocytes were confluently grown and a scratch was carefully drawn across the cell layer with the tip of a 10 μl pipette, as previously described (Etienne-Manneville, 2006). Afterward, the wound closure was documented after 24, 48, and 72 h via phase contrast microscopy.

Culturing of Astrocytes in Transwells

In order to prepare different co-culture combinations, astrocytes of both conditions were plated out in transwells with a permeable membrane (pore size: 0.4 μm; Falcon by Thermo Fisher Scientific Inc.; Cat. No. 08-770). The membrane allowed for the diffusion of astrocytic secreted factors into the commonly shared medium (Geissler and Faissner, 2012). The detachment of wildtype and *Vav3*$^{-/-}$ astrocytes was performed as previously described in chapter 2.2.3. Here, the dissociated astrocytes were plated out in a density of 25,000 cells in 500 μl astrocyte medium (≙ 50,000 cells/ml) on PDL-coated transwells. Finally, the transwells were hang in 24-well dishes (Thermo Fisher Scientific Inc.; Cat. No.: 142475) and placed in the incubator at 37°C and 6% CO_2. After a cultivation time of approximately 4–5 days the transwells were used for the co-cultures.

Primary Hippocampal Neuronal Cultures

For the culturing of pure primary neurons, embryonic wildtype and *Vav3*$^{-/-}$ animals of the developmental stage E15.5 were used and the embryonic hippocampi dissected, as previously described (Gottschling et al., 2016). The embryonic day 15.5 was determined for the preparation in order to obtain pure neuronal cultures without astrocytes which begin to form at earliest at E17.5 and especially in the first postnatal week (Bond et al., 2020). The use of serum-free medium prevented the proliferation of any astrocyte progenitors. Isolated hippocampi were transferred and collected in dissection medium consisting of HBSS (Thermo Fisher Scientific Inc.; Cat. No.: 14170088), 0.6% (w/v) glucose (Serva Electrophoresis GmbH; Cat. No.: 22700), and 10 mM HEPES (Thermo Fisher Scientific Inc.; Cat. No.: 15630080). After the dissection, the tissue digestion was performed using 30 U Papain (Worthington; Cat. No.: LS003126) in MEM (Thermo Fisher Scientific Inc.; Cat. No.: 31095029) with 80 μg/ml (w/v) DNase I (Worthington; Cat. No.: LS002007) and 0.96 mg/ml (w/v) L-cysteine (Sigma-Aldrich; Cat. No.: C2529) for 15 min at 37°C. Next, the digestion solution was aspirated and replaced by fresh neuron medium composed of MEM (Thermo Fisher Scientific Inc.; Cat. No.: 31095029), 2% (v/v) B27 (Thermo Fisher Scientific Inc.; Cat. No.: 17504044), 0.1% (v/v) ovalbumin (Sigma-Aldrich; Cat. No.: A7641) 10 mM sodium pyruvate (Sigma-Aldrich; Cat. No.: S8636), and 0.1% (v/v) gentamicin (Sigma-Aldrich; Cat. No.: S9135). The hippocampi were washed three times by exchanging the neuron medium. After the final washing step, the tissue was carefully triturated to a single cell suspension which was subsequently used for the co-cultures.

Indirect Co-culturing of Neurons and Astrocytes

Primary hippocampal neurons were cultured on poly-L-ornithine (PLO) (15 μg/ml; Sigma-Aldrich; Cat. No.: P3655)

coated glass cover slips in special 24-well plates which were suitable for the astrocyte containing transwells (Falcon; Product No.: 353504). A total number of 35,000 wildtype or *Vav3*$^{-/-}$ neurons was plated out in 500 µl neuron medium per well (≙ 70,000 cells/ml). Afterward, the well plates were placed in the incubator for 1 h to allow the cells to attach to the cover slips. During this incubation time, the serum-containing astrocyte medium in the transwells was replaced by serum-free neuron medium. Then, the astrocyte containing transwells were carefully hung in the 24-well plates with the neurons. The co-cultures were kept in the incubator at 37°C and 6% CO_2 until further experiments were performed. After a cultivation time of 12 and 17 days *in vitro*, the transwells were removed and the neuronal networks were fixed with pre-warmed 4% (w/v) paraformaldehyde (Carl Roth GmbH & Co., KG; Cat. No.:4235.1) for 10 min. After three washing steps with PBS, the cells were kept at 4°C until the immunocytochemical visualization of the dendrites was performed.

Immunocytochemistry

Visualization of Dendritic Trees

After the fixation, neurons were incubated with primary antibodies diluted in PBT-1 (PBS with 0.1% v/v Triton X-100 (AppliChem GmbH; Cat. No.: A4975,0500; Sigma-Aldrich) and 1% w/v bovine serum albumin (BSA) (Carl Roth GmbH & Co., KG; Cat. No.:8076.2). Here, the following antibodies were used: anti-Map2 [1:300, rabbit, polyclonal, RRID: AB_1840999; Sigma-Aldrich (by Merck KGaA)], anti GAD65/76 antibody (1:300, mouse, monoclonal, RRID: AB_2039129, Enzo Life Sciences). Since interneurons form morphologically different dendritic trees compared to pyramidal neurons, GAD65/67 was used to distinguish between these two neuronal types. The incubation was carried out in a humid chamber for 1 h at room temperature. Then, the antibody solution was aspirated, and the coverslips were washed three times with PBS/A (PBS with 0.1% (w/v) BSA). Then, the cover slips were incubated with the secondary antibody solution containing the following antibodies: anti-rabbit (Cy3, polyclonal, goat, RRID: AB_2338003, Jackson ImmunoResearch Labs), anti-mouse (AF488, polyclonal, goat, RRID:AB_AB_2338844, Jackson ImmunoResearch Labs). Furthermore, bisbenzimide (Hoechst 33258, 1:100.000, Sigma-Aldrich) was used in a dilution of 1:1,00,000 in the secondary antibody solution for the visualization of nuclei. The secondary antibodies were left for 45–60 min on the coverslips at room temperature. Afterward, the coverslips were rinsed three times with PBS (1x) and once with purified Milli-Q water. In a final step, the coverslips were placed on microscope slides (Thermo Fisher Scientific Inc.; Cat. No.: 630-2012) and mounted with ImmuMount (Thermo Fisher Scientific Inc.; Cat. No.: 10662815).

Molecular Biology

Sample Collection and mRNA Isolation

Previously prepared wildtype and *Vav3*$^{-/-}$ astrocytes were detached from the T-75 flasks as described in chapter 2.2.3. Then, a total number of 200,000 astrocytes was plated out in 3 ml astrocyte medium (≙ 66,667 cells/ml) per well. Here, PDL-coated 6-well plates (Thermo Fisher Scientific Inc.; Cat. No.:140675) were used. After a cultivation time of 10 days *in vitro*, the cells were lysed following the manufacturers instruction. The GenElute Mammalian Total RNA Miniprep Kit (Sigma-Aldrich by Merck KGaA; Cat. No.: RTN350) was used for the isolation and purification of the mRNA. Furthermore, the lysates of two wells were pooled in order to obtain a sufficient amount of mRNA for further analysis.

cDNA Synthesis

The cDNA synthesis was performed with the First Strand cDNA Synthesis Kit from Thermo Fisher Scientific Inc. (Cat. No.: K1622). Here, 1 µg mRNA was utilized for the synthesis of cDNA which was subsequently stored at −20°C until the Polymerase chain reactions (PCR) were performed.

Reverse Transcriptase-PCR

The reverse transcriptase (RT) PCRs were performed with the primer pairs listed in **Table 1**. All primers were ordered and obtained from Sigma-Aldrich.

Medium Conditioning and Cytokine Array

For the analysis of the secreted cytokines in the supernatant of wildtype and *Vav3*$^{-/-}$ astrocytes, the Proteome Profiler Mouse Cytokine Array Panel A (R&D Systems, Cat. No.: ARY006) was used without changing the manufacturers protocol. Here, the astrocytes were cultured in T-25 flasks (Sarstedt; Cat. No.: 83.3911.002) which were previously coated with 10 µg/ml (w/v) PDL. After purifying the cultures from microglia and OPCs (10–11 days in culture) the astrocyte medium was replaced by serum-free neuron medium composed of MEM (Thermo Fisher Scientific Inc.; Cat. No.: 31095029), 2% (v/v) B27 (Thermo Fisher Scientific Inc.; Cat. No.: 17504044), 0.1% (v/v) ovalbumin (Sigma-Aldrich; Cat. No.: A7641) 10 mM sodium pyruvate (Sigma-Aldrich; Cat. No.: S8636), and 0.1% (v/v) gentamicin (Sigma-Aldrich; Cat. No.: S9135) and conditioned for 24 h. Then, the supernatant was collected and stored at −80°C until the cytokine array analysis was performed. For the cytokine array 1 ml of the astrocyte supernatant was used for every experimental repetition. The chemiluminescence signals were measured with a chemiluminescence reader from Biostep and an exposure time of 2 min was set. The quantification of the signals was performed via ImageJ and the signal intensities were normalized against the internal positive controls of the array.

Neurotrophin-3 ELISA

For the detection of NT-3 in the supernatant of wildtype and *Vav3*$^{-/-}$ astrocytes, serum-free neuronal medium was conditioned for 24 h, as previously mentioned under 2.5. Then, the Mouse Neurotrophin-3 ELISA Kit (ab213882) from Abcam was used without any changes of the manufacturers protocol.

Microscopy

The immunocytochemically stained neurons were recorded with the fluorescence microscope AxioPlan 2 from Zeiss with an affiliated digital camera (AxioCam MRm, Zeiss). Furthermore,

TABLE 1 | Primer sequences and PCR settings.

Gene	Primer sequence	Product length	Cycle number	Annealing temperature
Tsp1 for	5′ GCTGCCAATCATAACCAGCG 3′	415 bp	30	64°C
Tsp1 rev	5′ GGTTGTTTGGCGGTGAGTTC 3′			
Tsp2 for	5′ AGAGAGAGCCAGTCCGATGT 3′	732 bp	30	63°C
Tsp2 rev	5′ TCGATAAGATCGCAGCCCAC 3′			
NT-3 for	5′ ATCCAAGGCAACAGCATGGA 3′	474 bp	30	64°C
NT-3 rev	5′ CTGGTGTCCCCGAATGTCAA 3′			
NGFv1 for	5′ GGGAGCGCATCGAGTGAC 3′	264 bp	30	62°C
NGFv1 rev	5′ CCTCACTGCGGCCAGTATAG 3′			
NGFv2 for	5′ GGGAGCGCATCGAGTTTT 3′	341 bp	30	63°C
NGFv2 rev	5′ CTGTCACTCGGGCAGCTATT 3′			
TGF-β for	5′ ATGCTAAAGAGGTCACCCGC 3′	452 bp	30	64°C
TGF-β rev	5′ GTTCATGTCATGGATGGTGCC 3′			
BDNF for	5′ GACGACATCACTGGCTGACA 3′	372 bp	32	64°C
BDNF rev	5′ TGCTTCAGTTGGCCTTTGGA 3′			
CNTF for	5′ TTAGGGGATGGCTTTCGCAG 3′	317 bp	30	66°C
CNTF rev	5′ CACCTTCAGTCGGGGTGAAA 3′			
LIF for	5′ GAGAGCTAAGGGGACTGGGA 3′	559 bp	30	62°C
LIF rev	5′ AAGTACCTTTGCGACCTCCG 3′			
Vav3 for	5′ CAGTGGCTCATCCACAGCA 3′	237 bp	30	62°C
Vav3 rev	5′ TCCAAAGGIATCGCAGCAGG 3′			
Actin for	5′ TATGCCAACACAGTGCTGTCTGG 3′	247 bp	30	62°C
Actin rev	5′ AGAAGCACTTGCGGTGCACGATG 3′			

the associated AxioVision 4.5 software (Zeiss) was utilized for the data documentation. For the phase contrast images of the astrocytes and neuronal networks the light microscope AxioObserver A1 (Zeiss) was used.

Data Quantification

The dendritic arborization was analyzed using the "Sholl analysis v3.0" plugin for ImageJ which is freely available at https://imagej.net/plugins/sholl-analysis (Sholl, 1953; Ferreira et al., 2014). Here, the immunocytochemical recordings were first transformed into binary images and then skeletonized. Afterward, a region of interest (ROI) was defined, and the radius step size was set at 15 μm. The obtained data points were transferred to Microsoft Excel for further quantification. Additionally, the dendritic lengths and the number of dendrites were manually measured with the "Freehand line" tool and the "Multi-point" tool in ImageJ (v 1.53k). The morphological analysis of this study was limited to the dendritic compartment since the axons were extensively branched and highly wired with axons of other neurons, at this culturing stage. A quantification of single axons was consequently not possible in this culture system.

For the measurement of the scratch area in the astrocytic monolayer the "Freehand Selections" tool was utilized after defining a scale bar.

The results of the RT-PCRs were quantified with the "Rectangle" tool in ImageJ. Here, the mean gray value of every PCR band was measured. After subtracting the background, the values were set in relation to the intensity of the actin bands.

The signal intensities of the cytokine array were evaluated similarly. However, the "Oval" tool in ImageJ was used instead of the "Rectangle" tool. Here, also the mean gray values were measured and set in relation to the internal positive controls after subtracting the background noise.

Statistics

The statistical analysis of this study was carried out with GraphPad Prism (v. 8.2.1). For the Sholl analysis as well as for the dendrite lengths and branches the normality distribution of the data sets was tested with the Kolmogorov-Smirnov test. Afterward, the Kruskal-Wallis test with a Dunn's multiple comparison test was performed to determine the significance level between the groups. For a better and clearer overview the data were shown in a pairwise manner in individual graphs. A detailed description about the number of experimental repetitions as well as the total number of analyzed neurons can be found in the figure legends.

For the scratch wound assay the normality distribution of the data sets was also tested via the Kolmogorov-Smirnov test. Here, normally distributed data sets were statistically analyzed with the unpaired *t*-test. A detailed description about the number of analyzed recordings is also given in the associated figure legends.

The normality distribution of the PCR data sets was tested with the Shapiro-Wilk-test. Since all data sets were normally distributed, the unpaired *t*-test was performed to determine the significance levels. This was also the case for the data sets from the cytokine array analysis. The associated figure legends give a detailed description about the number of experimental repetitions and replicates.

RESULTS

Vav3$^{-/-}$ Astrocytes Enhance the Dendritic Development of Wildtype Neurons *in vitro*

In order to analyze the impact of *Vav3*$^{-/-}$ astrocytes on the development of primary hippocampal neurons, indirect co-cultures were used with varying combinations of wildtype/*Vav3*$^{-/-}$ neurons and wildtype/*Vav3*$^{-/-}$ astrocytes (**Figure 1A**). As the control condition, wildtype neurons were co-cultured with wildtype astrocytes. Furthermore, wildtype neurons were cultured in an indirect contact with *Vav3*$^{-/-}$ astrocytes. Finally, *Vav3*$^{-/-}$ neurons were kept in culture with wildtype astrocytes since it is known that a deficiency of *Vav3*$^{-/-}$ influences the early development of axons and dendrites *in vitro* (Wegrzyn et al., 2020). The neurons of all three culture combinations formed highly branched and complex networks after a cultivation time of 12 and 17 days *in vitro* (**Figures 1B–D,1B'–D'**). The phase contrast images did not show obvious differences between the culture combinations at both analyzed timepoints.

The analysis of the dendritic complexity was performed by an immunocytochemical staining against the microtubule associated protein Map2 which was subsequently combined with the Sholl analysis, as similarly performed in various studies (**Figures 2A–A",B–B",C–C"**, **3A–A",B–B",C–C"**; Huang et al., 2011; Bartelt-Kirbach et al., 2016; Jacobs et al., 2016; Czaniecki et al., 2019). The expression of Map2 is strictly limited to the dendritic compartment and occurs in the main stable dendrites (Caceres et al., 1984). In addition, neurons were co-stained with an antibody against GAD65/67 because interneurons highly differ in their morphology and might negatively affect the outcome of the analysis. In this way, a

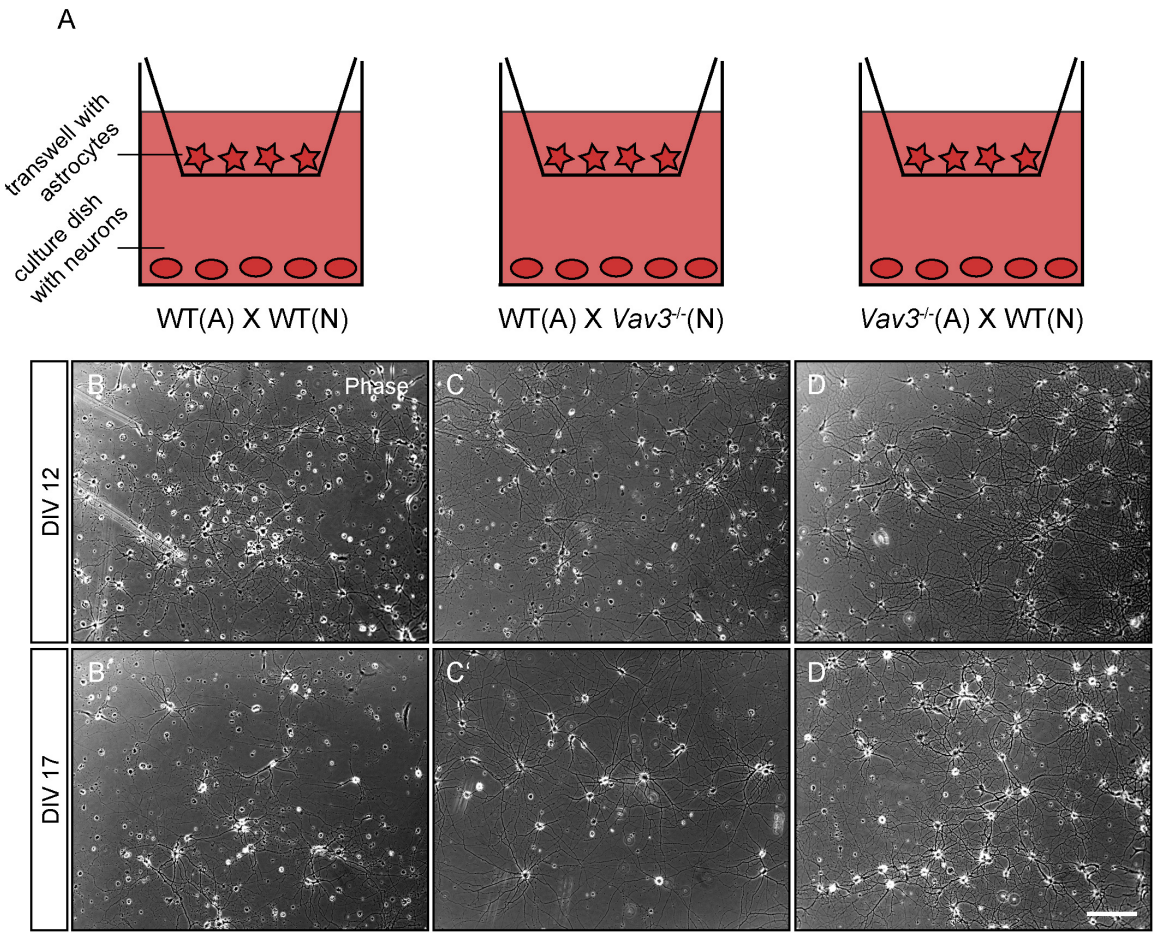

FIGURE 1 | (A) Primary hippocampal neurons were cultured in an indirect co-culture setup with cortical astrocytes. In order to analyze the influence of a Vav3 deficiency in neurons and astrocytes, different combinations of *Vav3* knockout neurons and astrocytes were used. First, wildtype neurons were cultured with wildtype astrocytes and served as the control condition. Furthermore, *Vav3*$^{-/-}$ neurons were combined with wildtype astrocytes for the analysis of neuron-specific effects induced by the *Vav3* knockout. Last, wildtype neurons were cultured with *Vav3*$^{-/-}$ astrocytes to investigate possible positive or negative effects for native neurons. **(B–D)** Neurons were kept in culture for 12 days in completely defined medium without serum and formed a highly complex network. Native neurons cultured with *Vav3*$^{-/-}$ astrocytes appeared slightly more complex in comparison to the other culture combinations. **(B'–D')** Additionally, neurons were cultured for a longer culturing time of 17 days since the dendrites become longer and more complex at this point in time. Scale bar: 200 μm.

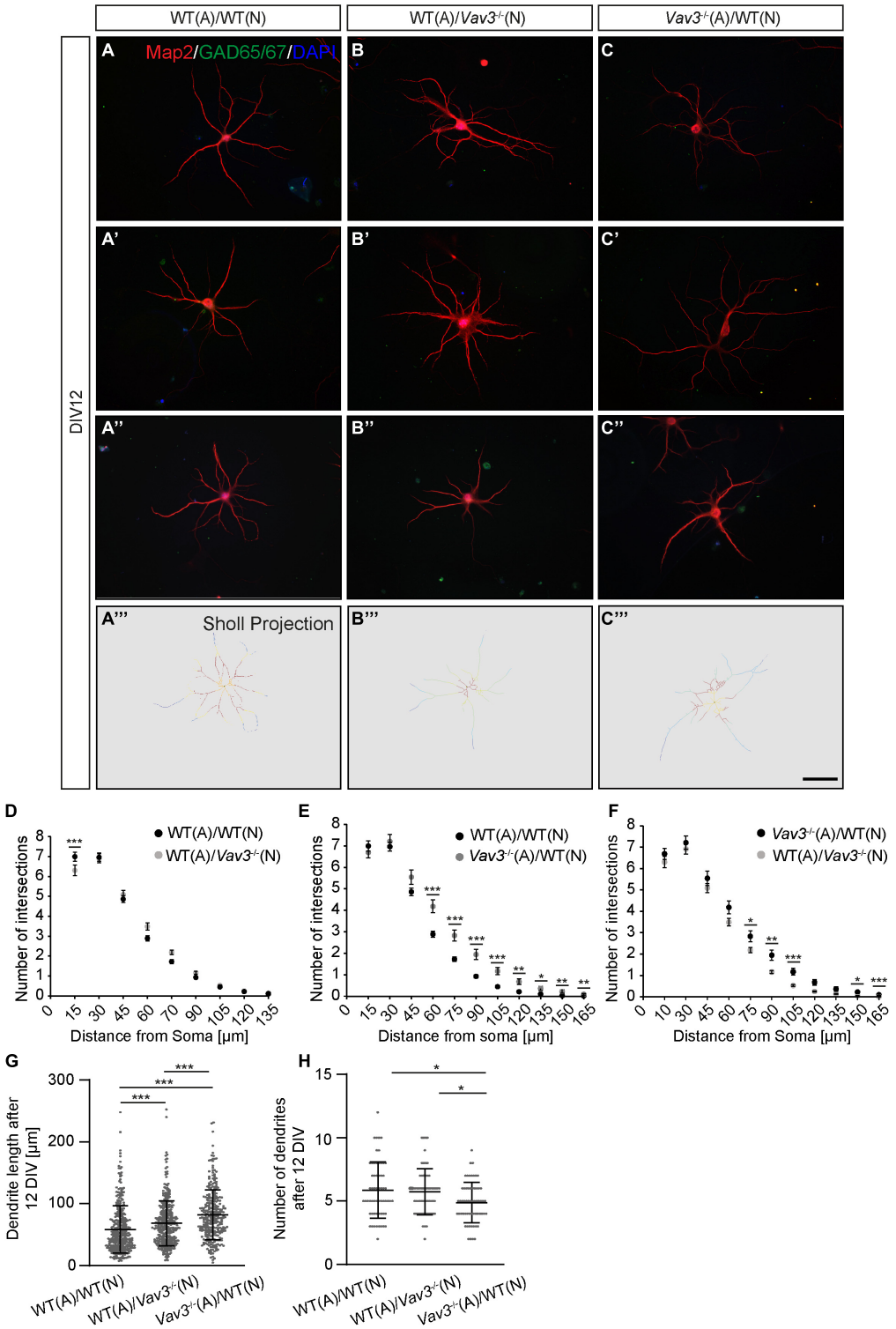

FIGURE 2 | (A–A", B–B", C–C") After a culturing time of 12 days neurons were immunocytochemically stained with specific antibodies against the dendritic marker Map2 and the interneuron marker GAD65/67. Furthermore DAPI was used for the visualization of nuclei. The GAD65/67 positive neurons were excluded from the analysis since interneurons have a highly differing morphology in comparison to pyramidal neurons and might falsify the experimental outcome. Three exemplary neurons are depicted per condition. **(A"'–C"')** A Sholl analysis was performed for determining the dendritic complexity. The projections depict the skeletonized dendrites and red areas represent a high number of intersections while blue regions represent a low number of intersections, **(D–F)** The quantification of the Sholl analysis could show that especially wildtype neurons cultured with *Vav3*$^{-/-}$ astrocytes developed more complex dendrites than neurons of both other conditions.

(Continued)

FIGURE 2 | (G) The quantification of the dendritic lengths revealed a significant increase in *Vav3*$^{-/-}$ neurons cultured with wildtype astrocytes and in native neurons cultured with *Vav3*$^{-/-}$ astrocytes in comparison to the controls. Dots are representing single analyzed dendrites. **(H)** In contrast, the number of dendrites was slightly reduced in the cultures consisting of wildtype neurons combined with *Vav3*$^{-/-}$ astrocytes. Dots are representing individual neurons analyzed regarding their number of dendrites. Statistics: For the Sholl analysis five experimental repetitions ($N = 5$) were performed for the culture combinations WT(N)/WT(A) and *Vav3*$^{-/-}$ (N)/WT(A) while three experimental repetitions ($N = 3$) were performed for the combination WT(N)/*Vav3*$^{-/-}$ (A). Furthermore, 40 neurons ($n = 40$) were recorded and analyzed per experimental repetition. For the dendritic lengths and numbers 3 experimental repetitions ($N = 3$) were performed with 20 quantified neurons ($n = 20$) per repetition. Kruskal-Wallis test with a following Dunn's multiple comparison test; $^{*}p \leq 0.05$, $^{**}p \leq 0.01$ and $^{***}p \leq 0.001$, data are represented as mean ± SEM. Scale bar: 50 μm.

differentiation between pyramidal neurons and interneurons was possible. The complexity of the dendritic trees was quantified using the Sholl analysis (**Figures 2A"'–C"'**, **3A"'–C"'**; Sholl, 1953). After a cultivation time of 12 days *in vitro*, *Vav3*$^{-/-}$ neurons cultured with wildtype astrocytes showed a mild but significantly decreased number of intersections in a region close to the cell soma compared to the control condition (**Figure 2D**). The number of intersections measured at all other distances from the soma revealed no significant changes between these two conditions. **Table 2** gives an overview about all values.

The most prominent difference could be seen when wildtype neurons cultured with *Vav3*$^{-/-}$ astrocytes were compared with the control condition (**Figure 2E**). Here, *Vav3*$^{-/-}$ astrocytes significantly increased the dendritic complexity of wildtype neurons between 60 and 165 μm distant from the soma compared to the control combination of wildtype neurons with wildtype astrocytes, as indicated in **Table 3**.

A comparison of wildtype neurons cultured with *Vav3*$^{-/-}$ astrocytes with *Vav3*$^{-/-}$ neurons cultured with wildtype astrocytes revealed only minor differences in a distance of 75, 90, and 105 μm (**Figure 2F**). The number of intersections and the *p*-values are listed in **Table 4**.

In addition to the Sholl analysis, the average number of dendrites per neuron and the dendritic lengths were analyzed (**Figures 2G,H**). Wildtype neurons which were co-cultured with wildtype astrocytes formed dendrites with an average length of 57.79 ± 2.03 μm after a cultivation time of 12 days. Interestingly, *Vav3*$^{-/-}$ neurons cultured with wildtype astrocytes formed significantly longer dendrites with an average length of 68.26 ± 4.71 μm when they were compared with the previously mentioned control condition ($p < 0.0001$). However, the longest dendrites could be observed when wildtype neurons were co-cultured with *Vav3*$^{-/-}$ astrocytes. In this combination, neurons formed dendrites with an average length of 82.02 ± 5.22 μm and were significantly longer in comparison to both other conditions ($p < 0.0001$) (**Figure 2G**). For the number of dendrites a slight but significant ($p = 0.014$) reduction could be seen when wildtype neurons were cultured with *Vav3*$^{-/-}$ astrocytes (4.88 ± 0.21) and compared with the control condition (5.82 ± 0.29) (**Figure 2H**).

The dendritic parameters were furthermore analyzed after a longer cultivation time of 17 days *in vitro* (**Figures 3A–A",B–B",C–C"**). Here, *Vav3*$^{-/-}$ neurons cultured with wildtype

TABLE 2 | Intersection numbers of *Vav3*$^{-/-}$ neurons compared to the control condition after a cultivation time of 12 days.

Distance from soma (μm)	Number of intersections WT(N) × WT(A)	Number of intersections *Vav3*$^{-/-}$(N) × WT(A)	*p*-value
15	6.99 ± 0.17	6.31 ± 0.22	0.0004
30	6.96 ± 0.23	6.92 ± 0.26	0.982
45	4.86 ± 0.21	5.09 ± 0.24	>0.999
60	2.89 ± 0.17	3.49 ± 0.22	0.253
75	1.72 ± 0.13	2.19 ± 0.17	0.312
90	0.93 ± 0.11	1.17 ± 0.12	0.253
105	0.46 ± 0.08	0.53 ± 0.07	0.813
120	0.22 ± 0.05	0.26 ± 0.04	0.492
135	0.11 ± 0.04	0.14 ± 0.03	0.739

TABLE 3 | Intersection numbers of wildtype neurons cultured with *Vav3*$^{-/-}$ astrocytes in comparison to the control condition after cultivation time of 12 days.

Distance from soma (μm)	Number of intersections WT(N) × WT(A)	Number of intersections WT (N) × *Vav3*$^{-/-}$(A)	*p*-value
15	6.99 ± 0.17	6.69 ± 0.26	0.534
30	6.96 ± 0.23	7.21 ± 0.31	>0.999
45	4.86 ± 0.21	5.55 ± 0.33	0.415
60	2.89 ± 0.17	4.18 ± 0.29	0.0005
75	1.72 ± 0.13	2.83 ± 0.25	0.0003
90	0.93 ± 0.11	1.95 ± 0.24	≤0.0001
105	0.46 ± 0.08	1.17 ± 0.16	≤0.0001
120	0.22 ± 0.05	0.68 ± 0.13	<0.0001
135	0.11 ± 0.04	0.37 ± 0.10	0.004
150	0.04 ± 0.02	0.27 ± 0.07	0.002
165	0.02 ± 0.01	0.10 ± 0.03	0.029

TABLE 4 | Intersection numbers of wildtype neurons cultured with *Vav3*$^{-/-}$ astrocytes in comparison to *Vav3*$^{-/-}$ neurons cultured with wildtype astrocytes after cultivation time of 12 days.

Distance from soma (μm)	Number of intersections *Vav3*$^{-/-}$ (N) × WT(A)	Number of intersections WT (N) × *Vav3*$^{-/-}$ (A)	*p*-value
15	6.31 ± 0.22	6.69 ± 0.26	0.147
30	6.92 ± 0.26	7.21 ± 0.31	0.566
45	5.09 ± 0.24	5.55 ± 0.33	0.558
60	3.49 ± 0.22	4.18 ± 0.29	0.068
75	2.19 ± 0.17	2.83 ± 0.25	0.042
90	1.17 ± 0.12	1.95 ± 0.24	0.008
105	0.53 ± 0.07	1.17 ± 0.16	0.0007
120	0.26 ± 0.04	0.68 ± 0.13	0.173
135	0.14 ± 0.03	0.37 ± 0.10	0.182
150	0.06 ± 0.02	0.27 ± 0.07	0.019
165	0.02 ± 0.02	0.10 ± 0.03	0.0005

astrocytes showed a mild increase in the number of intersections in 105–150 μm distant from the soma compared to the control condition (**Figure 3**). **Table 5** contains all values of the afore mentioned combinations.

In accordance with the previously described increase of the dendritic complexity when wildtype neurons were cultured with *Vav3*$^{-/-}$ astrocytes for 12 days *in vitro*, similar results were obtained after a longer cultivation time (**Figure 3E**). Here, the neurons formed dendrites with a clearly increased number of intersections at nearly all analyzed distances. The exact values are given in **Table 6**.

When wildtype neurons cultured with *Vav3*$^{-/-}$ astrocytes were compared with *Vav3*$^{-/-}$ neurons cultured with wildtype astrocytes only minor differences were seen after 17 DIV (**Figure 3F**). In a distance of 60 and 75 μm from the soma *Vav3*$^{-/-}$ neurons formed a higher number of intersections. However, all other analyzed distances revealed no significant alteration of the intersection number. The whole data set is listed in **Table 7**.

The dendritic lengths as well as the number of dendrites were also analyzed after 17 DIV (**Figures 3G,H**). Here, the increased dendrite lengths of wildtype neurons cultured with *Vav3*$^{-/-}$ astrocytes could not be observed anymore. Neurons of the control condition formed dendrites with an average length of 92.97 ± 2.65 μm. In comparison, wildtype neurons cultured with *Vav3*$^{-/-}$ astrocytes formed dendrites with a similar average dendritic length of 97.70 ± 7.07 μm. The statistical test revealed no significance for these two conditions ($p > 0.999$). Interestingly, *Vav3*$^{-/-}$ neurons co-cultured with wildtype astrocytes developed dendrites with an average length of 75.41 ± 5.21 μm and were significantly shorter compared to both other conditions ($p < 0.0001$) (**Figure 3G**). With regard to the number of dendrites no significant change could be seen when all three combinations were compared with each other (**Figure 3H**).

Vav3$^{-/-}$ Astrocytes Show Higher Expression Levels of *NT-3* and *TSP-1* *in vitro*

Since a higher arborization and length of dendrites were observed when wildtype neurons were co-cultured with Vav3 deficient astrocytes, the expression levels of different neurotrophins and neurotrophic cytokines were investigated via RT-PCR analysis (**Figures 4A,B**). Interestingly, *Vav3*$^{-/-}$ astrocytes showed a significantly raised expression of *NT-3* and *TSP-1* (**Figures 4C,D**). Here, wildtype neurons showed a relative expression of 0.13 ± 0.05 for *NT-3* and 0.71 ± 0.07 for *TSP-1*. In comparison, *Vav3*$^{-/-}$ astrocytes displayed significantly increased expression levels for *NT-3* (0.38 ± 0.07, $p = 0.0002$) and *TSP-1* (0.91 ± 0.15, $p = 0.0289$). Surprisingly, NT-3 could merely be detected in exceedingly low levels in the conditioned medium of wildtype and *Vav3*$^{-/-}$ astrocytes via ELISA (**Supplementary Figure 1**). A comparison of the OD_{450} values revealed similar signals intensities between both analyzed conditions. Furthermore, the expression of *thrombospondin-2* (*TSP-2*) was unchanged when both groups were compared with each other (WT: 0.68 ± 0.34, *Vav3*$^{-/-}$: 0.32 ± 0.21, $p = 0.868$) (**Figure 4E**). A significant downregulation of the transcript variant 1 of the *nerve growth factor* (*NGF*) could be seen in *Vav3*$^{-/-}$ astrocytes (0.25 ± 0.06) compared to wildtype astrocytes (0.47 ± 0.13, $p = 0.01$) (**Figure 4F**). A comparison of the expression levels of further neurotrophic factors revealed no significant alterations (**Figures 4G–K**). Here, the expression of the transcript variant 2 of *NGF* (WT: 0.74 ± 0.16, *Vav3*$^{-/-}$: 0.59 ± 0.06, $p = 0.082$), *transforming growth factor*β (*TGF*-β) (WT: 1.05 ± 0.19, *Vav3*$^{-/-}$: 0.99 ± 0.12, $p = 0.578$), *brain-derived neurotrophic factor* (*BDNF*) (WT: 0.80 ± 0.14, *Vav3*$^{-/-}$: 0.72 ± 0.08, $p = 0.283$), *ciliary neurotrophic factor* (*CNTF*) (WT: 0.59 ± 0.13, *Vav3*$^{-/-}$: 0.47 ± 0.15, $p = 0.176$) and *leukemia inhibitory factor* (*LIF*) (WT: 0.90 ± 0.32, *Vav3*$^{-/-}$: 0.96 ± 0.17, $p = 0.716$) was similar in wildtype and *Vav3*$^{-/-}$ astrocytes.

Vav3$^{-/-}$ Astrocytes Show an Altered Secretion Pattern of Chemokines and Cytokines

Because NT-3 could not be detected in the conditioned medium of wildtype as well as *Vav3*$^{-/-}$ astrocytes, a cytokine array analysis was performed in order to identify further secreted factors which might possibly be responsible for the enhanced dendrite growth and branching (**Figure 5A**). For this purpose, serum free medium with the same composition as the neuronal culture medium described under 2.2.5 was conditioned for 24 h by wildtype and *Vav3*$^{-/-}$ astrocytes. The cytokine array revealed similar values for most of the cytokines detected in the supernatants, as indicated in the heatmap (**Figure 5B**). However, the analysis of the conditioned medium of *Vav3*$^{-/-}$ astrocytes unraveled reduced levels of IL-6 and a complete lack of CXCL11 (**Figures 5A,B**). Furthermore, the conditioned medium of *Vav3*$^{-/-}$ astrocytes showed an increased concentration of CCL5. The statistical quantification of the data verified these observations (**Figures 5C–Q**). For CXCL11, a relative signal intensity of 0.19 ± 0.05 could be detected in the supernatant of wildtype astrocytes while the signal was nearly not detectable in the supernatant of *Vav3*$^{-/-}$ astrocytes [0.00004 ± 0.00002 ($p = 0.0049$)] (**Figures 5B,D**). Further members of the CXCL chemokine family could be observed but did not show significant alterations between both conditions (CXCL1: WT: 1.03 ± 0.064, *Vav3*$^{-/-}$: 1.14 ± 0.025, $p = 0.136$; CXCL2: WT: 0.25 ± 0.080, *Vav3*$^{-/-}$: 0.48 ± 0.06, $p = 0.093$; CXCL10: WT: 0.71 ± 0.10, *Vav3*$^{-/-}$: 0.71 ± 0.03, $p = 0.999$; CXCL12: WT: 0.015 ± 0.004, *Vav3*$^{-/-}$: 0.018 ± 0.004, $p = 0.818$) (**Figures 5B,C,H,N,Q**). Interestingly, the conditioned medium of *Vav3*$^{-/-}$ astrocytes showed a reduced signal intensity for IL-6 which was 0.09 ± 0.05 and hence significantly reduced in comparison to the signal intensity of IL-6 in the supernatant of wildtype astrocytes [0.56 ± 0.20 ($p = 0.0488$)] (**Figures 5B,I**). Beside IL-6, the cytokine TNF-α (WT: 0.86 ± 0.22, *Vav3*$^{-/-}$: 0.96 ± 0.07, $p = 0.650$) and IL-1ra (WT: 0.01 ± 0.006, *Vav3*$^{-/-}$: 0.02 ± 0.014, $p = 0.999$) could be detected without significant changes between wildtype and *Vav3*$^{-/-}$ astrocytes (**Figures 5B,G,P**). CCL5 was the only detected cytokine which showed a significantly increased signal intensity in the knockout condition. Here, an average signal intensity of 0.53 ± 0.11 could be seen in the

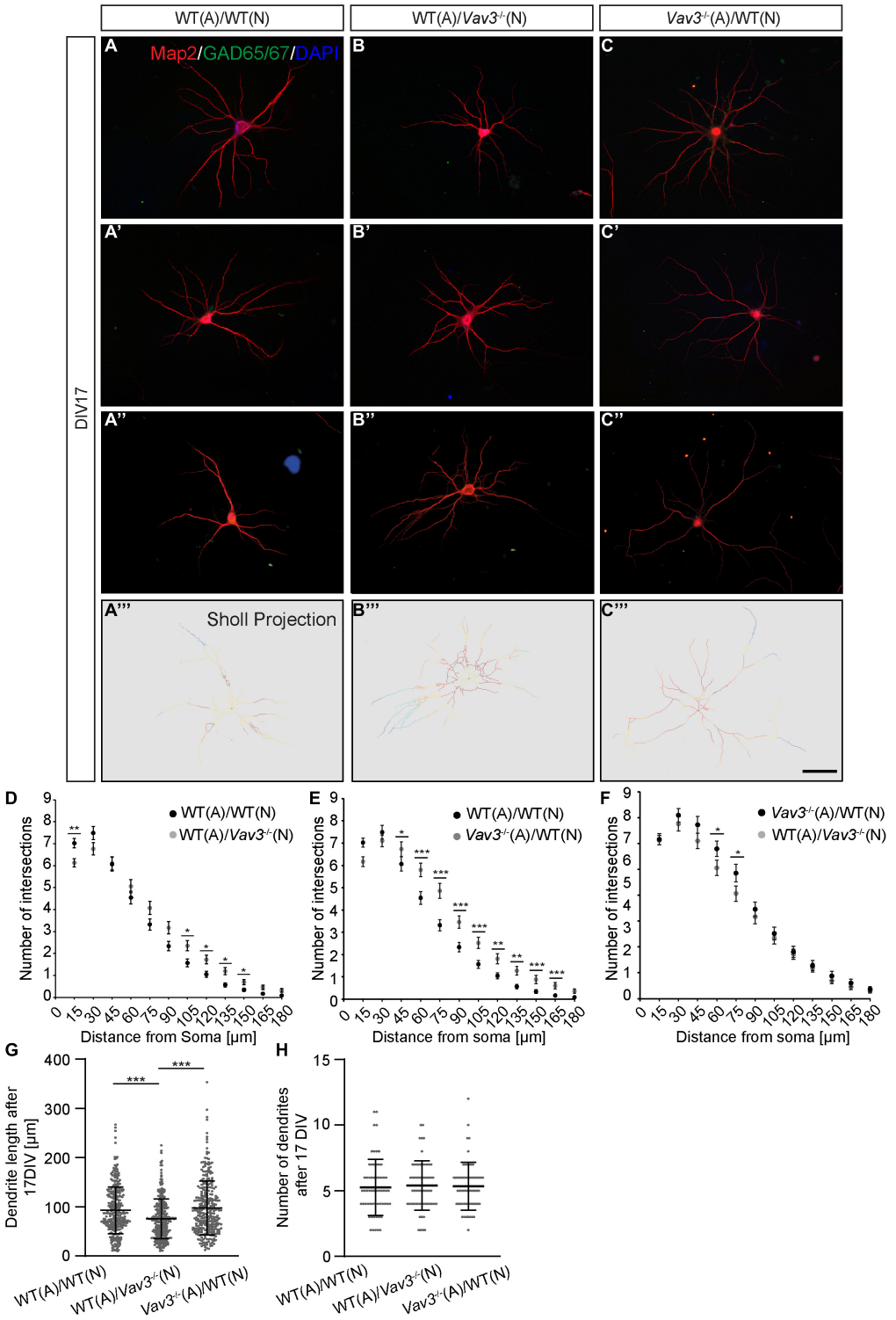

FIGURE 3 | (A–A",B–B",C–C") Neurons of the different combinations were fixed after a culturing time of 17 days and immunostained against Map2 and GAD65/67. As previously mentioned GAD65/67 positive neurons were excluded from the analysis since interneurons possess a strongly differing morphology compared to pyramidal neurons. DAPI was utilized for the visualization of nuclei. Three exemplary neurons are shown per condition. **(A"'–C"')** The Sholl projection represents the skeletonized dendrites and depicts highly branched regions with a red labeling while less branched regions are marked by a blue labeling. **(D–F)** After a culturing time of 17 days *in vitro* wildtype neurons which were kept in culture with *Vav3*$^{-/-}$ astrocytes showed a significantly increase in the number of intersections at nearly all analyzed distances from the soma. Furthermore, *Vav3*$^{-/-}$ neurons developed a higher number of intersections in the distal part of the dendrites. **(G)** *Vav3*$^{-/-}$ neurons

(Continued)

FIGURE 3 | cultured with wildtype astrocytes showed a significantly reduced dendritic length in comparison to both other conditions. Dots are representing single analyzed dendrites. **(H)** The quantification of the number of dendrites revealed no significant differences between all analyzed conditions. Dots are representing individual neurons analyzed for their number of dendrites. As already described in **Figure 2** five experimental repetitions ($N = 5$) were performed for the culture combinations WT(N)/WT(A) and *Vav3*$^{-/-}$(N)/WT(A) while three experimental repetitions ($N = 3$) were performed for the combination WT(N)/*Vav3*$^{-/-}$(A) for the Sholl analysis. Furthermore, 40 neurons ($n = 40$) were recorded and analyzed per experimental repetition. For the dendritic lengths and numbers 3 experimental repetitions ($N = 3$) were performed with 20 quantified neurons ($n = 20$) per repetition. Kruskal-Wallis test with a following Dunn's multiple comparison test; $^{*}p \leq 0.05$, $^{**}p \leq 0.01$ and $^{***}p \leq 0.001$, data are represented as mean ± SEM. Scale bar: 50 μm.

TABLE 5 | Intersection numbers of *Vav3*$^{-/-}$ neurons in comparison to the control condition after cultivation time of 17 days.

Distance from soma (μm)	Number of intersections WT(N) × WT(A)	Number of intersections *Vav3*$^{-/-}$ (N) × WT(A)	*p*-value
15	7.03 ± 0.21	6.13 ± 0.18	0.0049
30	7.49 ± 0.30	6.76 ± 0.28	0.240
45	6.07 ± 0.32	6.10 ± 0.29	> 0.999
60	4.55 ± 0.29	5.06 ± 0.29	0.490
75	3.32 ± 0.25	4.07 ± 0.30	0.161
90	2.34 ± 0.22	3.17 ± 0.27	0.057
105	1.57 ± 0.18	2.35 ± 0.23	0.047
120	1.05 ± 0.14	1.72 ± 0.20	0.022
135	0.57 ± 0.09	1.19 ± 0.16	0.043
150	0.34 ± 0.08	0.69 ± 0.12	0.021
165	0.17 ± 0.05	0.46 ± 0.10	0.061
180	0.09 ± 0.03	0.31 ± 0.09	0.099

TABLE 6 | Intersection numbers of wildtype neurons cultured with *Vav3*$^{-/-}$ astrocytes in comparison to the control condition after cultivation time of 17 days.

Distance from soma (μm)	Number of intersections WT(N) × WT(A)	Number of intersections WT (N) × *Vav3*$^{-/-}$ (A)	*p*-value
15	7.03 ± 0.21	6.17 ± 0.22	0.092
30	7.49 ± 0.30	7.10 ± 0.26	> 0.999
45	6.07 ± 0.32	6.73 ± 0.33	0.026
60	4.55 ± 0.29	5.80 ± 0.30	0.0002
75	3.32 ± 0.25	4.86 ± 0.39	< 0.0001
90	2.34 ± 0.22	3.46 ± 0.27	0.0001
105	1.57 ± 0.18	2.52 ± 0.25	0.0003
120	1.05 ± 0.14	1.81 ± 0.22	0.002
135	0.57 ± 0.09	1.28 ± 0.19	0.003
150	0.34 ± 0.08	0.88 ± 0.18	0.0004
165	0.17 ± 0.05	0.61 ± 0.14	0.0008
180	0.09 ± 0.03	0.36 ± 0.10	0.055

supernatant of wildtype astrocytes and 0.97 ± 0.029 in the supernatant of *Vav3*$^{-/-}$ astrocytes ($p = 0.003$) (**Figures 5B,O**). In addition, several other members of the CCL chemokine family were verified in similar levels between both conditions (CCL1: WT: 0.004 ± 0.002, *Vav3*$^{-/-}$: 0.003 ± 0.002, $p = 0.686$; CCL2: WT: 0.33 ± 0.09, *Vav3*$^{-/-}$: 0.30 ± 0.09, $p = 0.809$; CCL3: WT: 0.59 ± 0.20, *Vav3*$^{-/-}$: 0.67 ± 0.11, $p = 0.706$; CCL4: WT: 0.68 ± 0.23, *Vav3*$^{-/-}$: 0.61 ± 0.13, $p = 0.802$; CCL12: 0.006 ± 0.003, *Vav3*$^{-/-}$: 0.004 ± 0.002, $p = 0.700$) (**Figures 5B,J,L,M**). Different colony stimulating factors could be verified in the supernatant of both, wildtype and knockout astrocytes. However, their signal intensities were low, and no significant changes could be seen (G-CSF: WT: 0.04 ± 0.016, *Vav3*$^{-/-}$: 0.01 ± 0.005, $p = 0.115$; GM-CSF: WT: 0.088 ± 0.04, *Vav3*$^{-/-}$: 0.009 ± 0.005, $p = 0.080$; M-CSF: WT: 0.032 ± 0.017,

TABLE 7 | Intersection numbers of wildtype neurons cultured with *Vav3*$^{-/-}$ astrocytes in comparison to *Vav3*$^{-/-}$ neurons cultured with wildtype astrocytes after cultivation time of 17 days.

Distance from soma (μm)	Number of intersections *Vav3*$^{-/-}$ (N) × WT(A)	Number of intersections WT (N) × *Vav3*$^{-/-}$ (A)	*p*-value
15	6.13 ± 0.18	6.17 ± 0.22	> 0.999
30	6.76 ± 0.28	7.10 ± 0.26	0.174
45	6.10 ± 0.29	6.73 ± 0.33	0.070
60	5.06 ± 0.29	5.80 ± 0.30	0.016
75	4.07 ± 0.30	4.86 ± 0.39	0.022
90	3.17 ± 0.27	3.46 ± 0.27	0.103
105	2.35 ± 0.23	2.52 ± 0.25	0.218
120	1.72 ± 0.20	1.81 ± 0.22	0.850
135	1.19 ± 0.16	1.28 ± 0.19	0.685
150	0.69 ± 0.12	0.88 ± 0.18	0.400
165	0.46 ± 0.10	0.61 ± 0.14	0.312
180	0.31 ± 0.09	0.36 ± 0.10	> 0.999

Vav3$^{-/-}$: 0.020 ± 0.010, $p = 0.559$) (**Figures 5B,F**). Finally, Timp-1 (WT: 0.57 ± 0.122, *Vav3*$^{-/-}$: 0.61 ± 0.04, $p = 0.724$), sICAM-1 (WT: 0.33 ± 0.120, *Vav3*$^{-/-}$: 0.26 ± 0.097, $p = 0.670$) and TREM-1 (WT: 0.003 ± 0.002, *Vav3*$^{-/-}$: 0.03 ± 0.001, $p = 0.802$) were detected with similar mean values between both analyzed groups (**Figures 5B,E,K**).

Vav3$^{-/-}$ Astrocytes Show a Faster Regeneration in a Scratch Wound Healing Assay

Rho-GTPases are highly involved in the regulation of cytoskeletal reorganizations. This is necessary in cases of migration and proliferation. In order to examine if a lack of Vav3 has effects on the astrocytic migration, a scratch wound healing assay was performed (Etienne-Manneville, 2006; **Figures 6A–D,A'–D'**). Although the average size of the initial scratch was higher in the *Vav3*$^{-/-}$ astrocyte cultures (416987.73 ± 7963.12 μm^2) than in the wildtype cultures (380123.67 ± 14206.58 μm^2, $p = 0.028$), *Vav3*$^{-/-}$ astrocytes showed a significantly lower scratch area after 24 h (WT: 208997.23 ± 15449.84 μm^2, *Vav3*$^{-/-}$: 159452.72 ± 10843.95 μm^2, $p = 0.016$), 48 h (WT: 57346.53 ± 9698.27 μm^2, *Vav3*$^{-/-}$: 15674.60 ± 4302.31 μm^2, $p = 0.0002$) and 72 h (WT: 14496.64 ± 4273.20 μm^2, *Vav3*$^{-/-}$: 1872.90 ± 1325.65 μm^2, $p = 0.0065$) (**Figures 6F–H**). A lack of Vav3 in the knockout cultures was verified via RT-PCR analysis (**Figure 6I**). Interestingly, a scratch in the wildtype astrocyte monolayer induced the downregulation of Vav3 on mRNA level

as shown in **Figure 6J**. Before performing the scratch, native astrocytes showed a relative expression of 0.59 ± 0.15 for *Vav3*. However, 24 h after the scratch the astrocytes showed just a relative *Vav3* expression of 0.16 ± 0.03. Similar results were also obtained 48 h (0.14 ± 0.01) and 72 h (0.14 ± 0.01) after the scratch. The relative expression of Vav3 at all analyzed points in time after the scratch was significantly reduced ($p < 0.0001$).

DISCUSSION

Vav3 Deficiency Alters Dendrite Lengths of Hippocampal Neurons After 12 and 17 DIV

In the present study, we could observe that a knockout of the GEF Vav3 has merely mild effects on the dendritic complexity of primary hippocampal neurons *in vitro* (**Figures 2D**, **3D**). After a culturing time of 12 days nearly no difference was visible between wildtype and knockout neurons, while after 17 days a mild increase in the number of intersections could be detected. This was especially the case for the distal regions of *Vav3*$^{-/-}$ dendrites. Nevertheless, the lack of Vav3 showed a stronger impact on the average dendritic length. Here, a statistically significant increase of the dendrite lengths was observed after 12 days *in vitro* and a decrease after 17 days *in vitro* (**Figures 2G**, **3G**). These data suggest, that Vav3 rather acts as a regulator of the dendrite elongation than as a regulator of the dendritic branching, at least, in the here analyzed culture period of 17 days. In a previous study, we could already observe an increase of the dendrite lengths after a short culturing time of 3 and 5 days in primary hippocampal neurons lacking Vav3 (Wegrzyn et al., 2020). This indicates that Vav3 might have distinct regulatory roles for the early and later dendrite development. Interestingly, a previous study could prove an important function of Vav3 for the dendrite branching of Purkinje and granule cells in the cerebellum of mice (Quevedo et al., 2010). Here, significant branching deficits could be seen in the early postnatal period which vanished in adult animals. Furthermore, this study could detect varying expression levels of Vav3 in different developmental stages, supporting the previously mentioned aspect of an regulating function of Vav3 during early and late developmental stages or culturing periods (Quevedo et al., 2010). Other studies unraveled significant effects of a *Vav3* knockout on the axonal development in early culturing stages as well as *in vivo* (Sauzeau et al., 2010; Wegrzyn et al., 2020). Because of the highly complex wiring of individual axons with axons of other neurons, this neuronal compartment was not considered for this study. Nevertheless, it would be of great interest to investigate the impact of a Vav3 deletion on the axonal morphology in matured neurons in future studies. Here, cultures with a low cell density could be used to track individual axons. As indicated in the introduction, Vav3 acts as an activator of the Rho-GTPases RhoA, Rac-1 and Cdc42, which are modulators of the cytoskeleton (Movilla and Bustelo, 1999; Movilla et al., 2001; Scott et al., 2003; Aoki et al., 2005). Biochemical [^{3}H]GDP-releasing assays could verify that Vav3 strongly induces a nucleotide exchange on RhoA, to a lesser extent on Rac-1 and is nearly inactive on Cdc42 (Movilla and Bustelo, 1999). Therefore, most of the observed effects in this study might result from a lowered RhoA activity. However, this assumption must be proven by analyzing the activity of the different Rho-GTPases in *Vav3* knockout neurons in future studies. Unfortunately, the low cell number of the present culture system did not permit for the detection of individual Rho-GTPase activities. Nevertheless, previous studies could already show that a lack of RhoA in neurons of *Drosophila melanogaster* was responsible for the overextension of dendrites (Lee et al., 2000). Here, the authors discuss that RhoA is essential for a limitation of the dendrite growth. In accordance with this conclusion, studies that utilized dominant active forms of RhoA revealed a reduction of dendrite lengths and a simplification of dendritic trees in rodents via Rho-associated protein kinase (ROCK) activation (Nakayama et al., 2000; Ahnert-Hilger et al., 2004). This is in accordance with our observation of the increased dendrite lengths after 12 days *in vitro* but not with the reduced dendrite lengths after 17 days *in vitro*. A possible explanation might be that compensatory mechanisms intervene after a longer culturing time and that other GEFs like Vav2 prevent a persisting extension of dendrites. Here, it has been shown that Vav2 unfolds regulatory functions for the branching and elongation of neurites in *Xenopus laevis in vivo* as well as *in vitro* (Moon and Gomez, 2010). Interestingly, a previous study described the protein expression levels of Vav2 in whole brain lysates (without cerebellar tissue) at different developmental stages and observed a strong expression at E13.5-E18.5 which gradually decreased at postnatal stages and reached the lowest levels in adult animals (Cowan et al., 2005). Since this study showed a gradual decrease over time it might be possible that Vav2 merely compensates the effects of a *Vav3* knockout on the dendritic complexity at early culturing stages but not in advanced cultures. Here, the slight increase of the intersection number in regions farther away from the soma at DIV17 as well as the decreased dendritic lengths might be indications for this. However, Vav2 does not prevent an overextension of dendrites at DIV12. For this reason it is necessary to define the expression levels of Vav2 also *in vitro*. Furthermore, there is a great number of GEFs which could be upregulated and compensate the lack of Vav3 explaining the mild phenotype. Here members of the ArhGEF family could play an important role. Recent studies unraveled that especially ArhGEF1 and ArhGEF2 are highly involved in the regulation of the dendritic development as activators of RhoA (Xiang et al., 2016, 2017; Zhou et al., 2021). Other potential candidates are Ephexins as well as Trio which have important regulatory functions for the dendritogenesis (Wu et al., 2007; Iyer et al., 2012). In addition, lowered activities of Rac-1 or Cdc42 could be further explanations for the observed effects. Studies utilizing dominant negative forms of Rac-1 or knockdowns revealed only mild changes for the dendrite complexity but a progressive elimination of dendritic spines in hippocampal neurons (Nakayama et al., 2000; Gualdoni et al., 2007). Therefore, a lowered Rac-1 activity as consequence of the *Vav3* knockout might not primarily affect the dendritic complexity but rather the spine number and stability.

Furthermore, studies could show that a reduced or lacking Cdc42 activity induced the formation of more dendritic branches but impaired the stability of dendritic spines and synapses (Wegner et al., 2008; Schulz et al., 2016). Here, also a reduced Cdc42 activity induced by the lack of Vav3 might explain the slightly increased intersection number of Vav3-deficient neurons after 17 days *in vitro*. Since Rac1 and Cdc42 play an important role for the formation and stability of dendritic spines it would be of great interest to analyze the dendrite number and morphology in *Vav3*$^{-/-}$ neurons.

Vav3$^{-/-}$ Astrocytes Promote the Dendritic Development of Wildtype Neurons and Show an Altered Cytokine Profile With Increased CCL5 Levels, Reduced IL-6 Levels and a Lack of CXCL11

The most prominent effect could be observed when wildtype neurons were co-cultured with *Vav3*$^{-/-}$ astrocytes (**Figures 2E,G**, **3E,G**). Here, wildtype neurons developed significantly longer dendrites and higher branched dendritic trees than neurons cultured with wildtype astrocytes. To determine how *Vav3*$^{-/-}$ astrocytes enhance the elongation and branching of dendrites a RT-PCR analysis for different neurotrophic factors as well as a cytokine array with conditioned media of wildtype and knockout astrocytes was performed (**Figures 4**, **5**). It is well known that astrocytes secrete a variety of neurotrophic factors and promote therefore the neurite growth as well as the synaptogenesis (Müller et al., 1995; Clarke and Barres, 2013). NT-3 is one of these secreted factors and acts through the tropomyosin receptor kinase C (TrkC) promoting the outgrowth, branching and elongation of neurites (Rudge et al., 1992; Morfini et al., 1994; Labelle and Leclerc, 2000; Mele et al., 2010). The RT-PCR analysis revealed significantly raised expression levels of *NT-3* in *Vav3*$^{-/-}$ astrocytes (**Figure 4C**). For further analysis we focused on the NT-3 protein levels in the conditioned supernatants of wildtype and *Vav3*$^{-/-}$ astrocytes. Surprisingly, very low signal intensities could be observed for NT-3 when the ELISA was performed (**Supplementary Figure 1**). We suspect that the conditioning period of 24 h possibly was too short. A longer conditioning time might lead to a higher accumulation of NT-3 in the supernatant which should be better detectable. Nevertheless, if *Vav3*$^{-/-}$ astrocytes would secrete significantly higher amounts of NT-3 differences between wildtype and knockout astrocytes should be seen, also after a short conditioning time. Therefore, it is questionable if NT-3 is responsible for the enhanced dendrite development observed in our experiments. TSP-1 is another astrocytic factor which is highly involved in synapse formation via integrin α3β1 signaling (O'Shea et al., 1991; Osterhout et al., 1992; DeFreitas et al., 1995; Christopherson et al., 2005). The RT-PCR analysis revealed significantly raised expression levels of *TSP-1* in *Vav3*$^{-/-}$ astrocytes (**Figure 4D**). Since TSP-1 plays an important role for the synapse formation it would be interesting to analyze the influence of *Vav3*$^{-/-}$ astrocytes on native neurons rather in the context of structural synapse numbers than in the context of dendrite development. Future studies might utilize the indirect co-culture system for this purpose and focus on the expression of synaptic proteins. Surprisingly, the expression of the transcript variant 1 of *NGF* was reduced in the RT-PCR analysis (**Figure 4F**). NGF normally acts as a strong promoter of the neurite outgrowth by activating the tropomyosin receptor kinase A (TrkC). Therefore, a reduced expression level of NGF should impair the dendrite elongation. Since this was not the case in our morphological analysis, we assume that increased levels of other secreted factors might dominate the lowered NGF levels and shift the dendrites toward extensions and branching mechanisms.

In addition to neurotrophic factors, astrocytes are able to express and secrete different cytokines and chemokines as previously described for humans and rodents (Wiese et al., 2012; Choi et al., 2014). A comparison between the cytokine patterns of wildtype and *Vav3*$^{-/-}$ astrocytes revealed mainly three aberrances in the knockout condition: A complete lack of CXCL-11 which is also referred to as Interferon-inducible T-cell alpha chemoattractant (I-TAC), a significant reduction of IL-6 and a significant increase of CCL5 (**Figures 5A,B,D,I,O**). The most interesting candidate for the enhanced dendritic elongation and branching, is CCL5, also known as Regulated on Activation Normal T-cell Expressed and Secreted (RANTES). A recently published study could show that the treatment of hippocampal neurons with CCL5 activated the PI3K/Akt signaling pathway, which is an important pathway for the neurite outgrowth and elongation (Ajoy et al., 2021). Interestingly, this study could also show that an overexpression of CCL5 promotes the aerobic glucose metabolism, ATP synthesis, synapse formation, and enhances the memory in mice (Ajoy et al., 2021). Furthermore, in a Huntingtin model, the conditioned medium of primary astrocytes contained significantly lower levels of CCL5 and the treatment of cortical neurons induced a reduction of the neurite length and branching (Chou et al., 2008). Therefore, CCL5 is discussed to be a promising neurotrophic factor and could already show beneficial effects in a recently published optic nerve regeneration study (Xie et al., 2021). As previously mentioned, *Vav3*$^{-/-}$ astrocytes showed a lack of CXCL11. Since there are no data about the influence of CXCL11 on the dendritic development of neurons, it is difficult to speculate about the consequences of a CXCL11 lack in our co-cultures. A previously published study could observe that CXCL11 induces the death of dopaminergic neurons in midbrain neuron-glia mixed cultures but not in enriched neuronal cultures, indicating an indirect toxic effect on neurons (Chien et al., 2016). Furthermore, it is known that CXCL11 acts through the binding to CXCR3, a Gα-protein-coupled receptor. An activation of CXCR3 with CXCL10 which acts similarly as CXCL11 was associated with an influx of Ca^{2+}, the activation of caspases and apoptosis (Sui et al., 2006). Contrary, an inhibition of CXCR3 unraveled positive effects for the neuronal survival in different disease models (Zhang et al., 2010; van Weering et al., 2011). A lack of CXCL11 might therefore induce neuroprotective effects and enhance the development of neurites, however, further studies

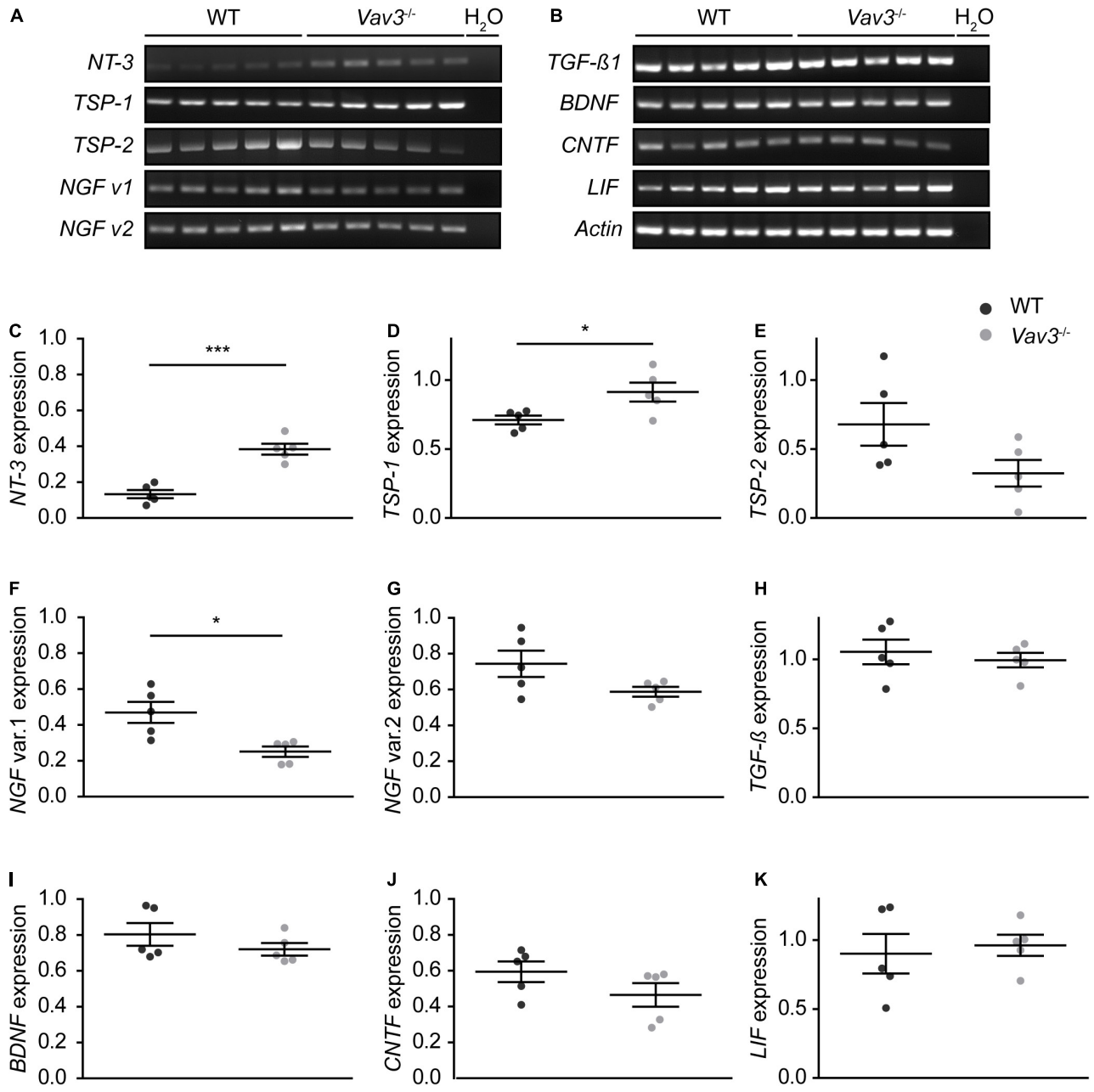

FIGURE 4 | (A,B) Wildtype and *Vav3*$^{-/-}$ astrocytes were lysed and a RT-PCR analysis with primers for different neurotrophic factors was performed. The signal intensity of *NT-3* appeared stronger in *Vav3*$^{-/-}$ astrocytes compared to wildtype astrocytes. Furthermore, there was a slightly reduced signal intensity of the transcript variant 1 of *NGF* in *Vav3*$^{-/-}$ astrocytes. **(C–K)** The signal intensity of the PCR bands was set in relation to the actin positive control and compared between both groups. The quantification revealed a significantly increased expression of *NT-3* and *TSP-1* while the transcript variant of *NGF* was reduced. The expression of all other analyzed neurotrophic factors was unchanged in the knockout condition. Individual dots are representing the signal intensity of every sample in relation to actin Statistics: in total, five independent experimental repetitions ($N = 5$) were performed and one lysed sample ($n = 1$) per repetition was used for the PCRs. Unpaired *t*-test; $^{*}p \leq 0.05$, $^{**}p \leq 0.01$ and $^{***}p \leq 0.001$, data are represented as mean ± SEM.

are necessary to shed light on the influence of CXCL11 on dendritic parameters. Last, the IL-6 levels were significantly lower in the conditioned medium of *Vav3*$^{-/-}$ astrocytes. Here, a study on cultured hippocampal neurons revealed that a treatment with increasing levels of IL-6 increased the length of secondary neurites (Sarder et al., 1996). However, the number of branch points of the primary dendrite per neuron remained unaltered and a detailed number about clearly defined dendritic branches is not given. Another study revealed that high levels IL-6 inhibit the dendrite growth and branching in primary cortical

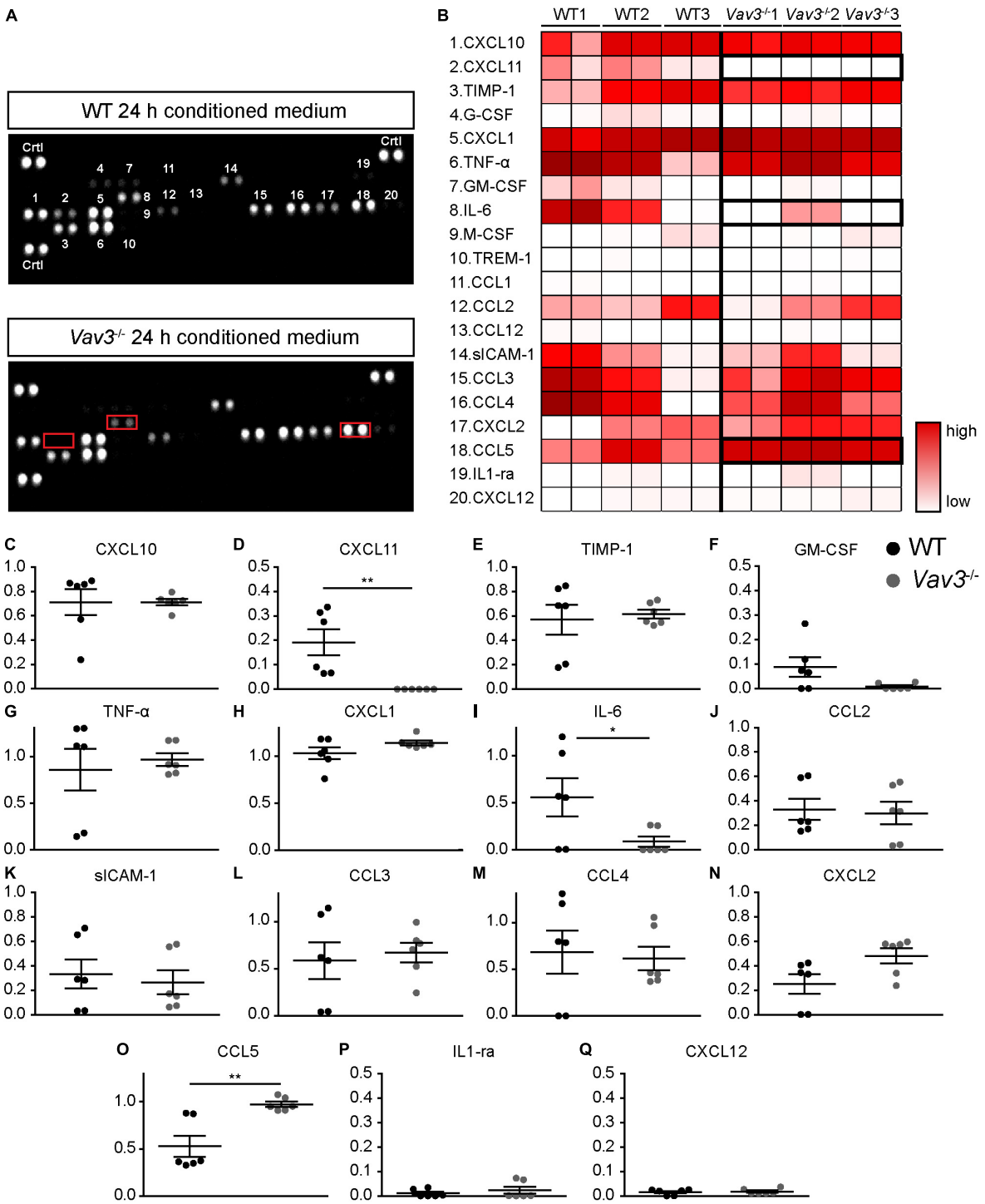

FIGURE 5 | (A) Serum-free neuronal medium was conditioned for 24 h with the secreted factors of wildtype and *Vav3*$^{-/-}$ astrocytes. Then, cytokine arrays were used in order to determine the cytokine and chemokine profiles of both groups. The conditioned medium of *Vav3*$^{-/-}$ astrocytes revealed an altered profile with a lack of CXCL11, reduced levels of IL-6 and increased levels of CCL5 (indicated by red boxes). **(B)** A total number of 20 cytokines and chemokines could be detected in the supernatants and are depicted in the heatmap. The individual numbers on the membranes are defined by the corresponding cytokine and chemokine names in the heatmap. A low cytokine level is represented by a white color while a strong level is represented by dark red colors. As indicated by the bold boxes, the conditioned medium of *Vav3*$^{-/-}$ astrocytes showed a lack of CXCL11, increased concentrations of CCL5 and reduced levels of IL-6. **(C–Q)** The statistical analysis of the cytokine array confirmed these observations. Since the concentrations of Trem1, CCL1, G-CSF, M-CSF, and CCL12 were exceedingly low in the supernatants they were shown in detail by diagrams. The exact values can be found in the result part 3.3. Statistics: Three experimental repetitions ($N = 3$) were performed, and two technical replicates ($n = 2$) were considered per repetition. Unpaired *t*-test, $^{*}p \leq 0.05$, $^{**}p \leq 0.01$ and $^{***}p \leq 0.001$, data are represented as mean ± SEM.

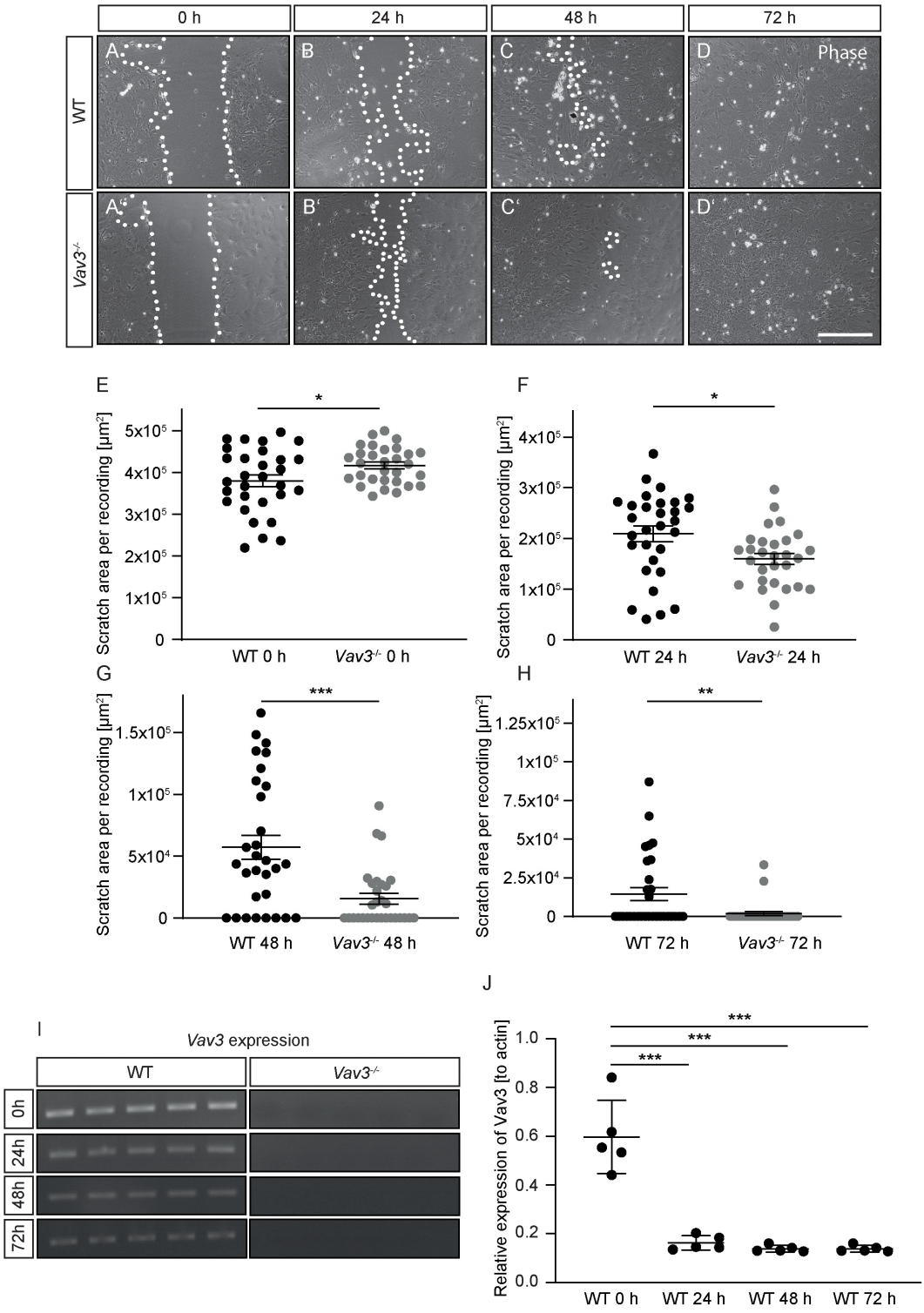

FIGURE 6 | (A–D,A'–D') Wildtype and *Vav3*$^{-/-}$ astrocytes were tested regarding their migration behavior in a scratch wound healing assay. Phase contrast images were taken immediately after performing the scratch (0 h) and after 24, 48, and 72 h. **(E–H)** The scratch area was visibly smaller in the *Vav3*$^{-/-}$ astrocyte cultures after 24 and 72 h, although the initially performed scratch was greater in these cultures. **(I)** RT-PCR analysis confirmed the absence of *Vav3*$^{-/-}$ in cultured astrocytes. **(J)** Furthermore, the expression of *Vav3* was significantly reduced in wildtype cultures after performing the scratch. Statistics: In total, five experimental repetitions ($N = 5$) were performed for the scratch wound healing assay. Here, 6 phase contrast images ($n = 6$) were recorded and quantified per experimental repetition. For the *Vav3* RT-PCR also five experimental repetitions ($N = 5$) and one sample per preparation ($n = 1$) were used. Unpaired *t*-test, $^{*}p \leq 0.05$, $^{**}p \leq 0.01$ and $^{***}p \leq 0.001$, data are represented as mean ± SEM. Scale bar: 200 µm.

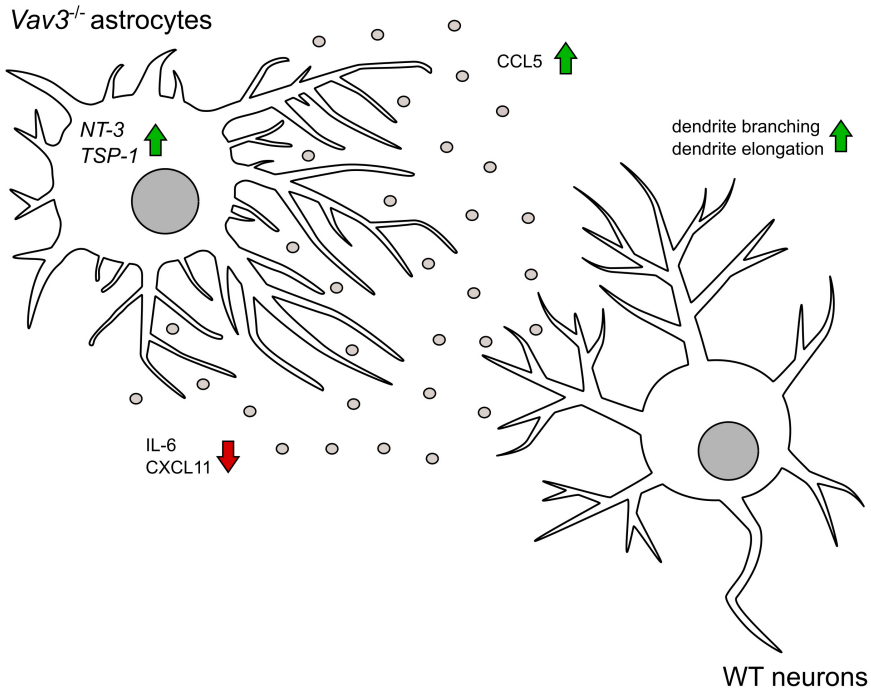

FIGURE 7 | The graphical abstract depicts that *Vav3*$^{-/-}$ astrocytes promote the branching and the elongation of dendrites on wildtype neurons in an indirect co-culture system. Knockout astrocytes show a higher secretion of the chemokine CCL5 which has a neurotropic potential. Contrary, the pro-inflammatory cytokine IL-6 is released in lower amounts. In contrast to wildtype astrocytes, *Vav3*$^{-/-}$ astrocytes do not release CXCL11. On mRNA level *Vav3*$^{-/-}$ astrocytes express more *NT-3* and *TSP-1*.

cultures (Gilmore et al., 2004). A reduced secretion of IL-6 might therefore rather enhance the dendritic development. The graphical abstract (**Figure 7**) summarizes a suggestion how the knockout of *Vav3* in astrocytes might affect dendritic parameters of neurons.

A Lack of Vav3 Promotes the Regeneration of Astrocytes in the Scratch Wound Healing Assay

One remaining question is how a deficiency of Vav3 induces an altered profile of released chemokines and cytokines. A possible explanation might be that a reduced activity of RhoA which is the main target of Vav3 alters the reactivity state of cultured astrocytes. Here, a previously published study could already show that a treatment of primary astrocytes with metallothionein induced a reactive state of astrocytes with a significantly reduced activity level of RhoA which, however, had beneficial effects for the neurite outgrowth of neurons (Leung et al., 2010). Another hint for an altered reactive state of *Vav3*$^{-/-}$ astrocytes is the enhanced wound closure observed in the scratch assay of this study (**Figures 6A–H**). Here, *Vav3*$^{-/-}$ astrocytes showed a faster closure of the scratch area in comparison to wildtype astrocytes. Interestingly, it has been shown that a conditional knockout of Stat3 induced a higher activity level of RhoA which consequently led to a reduced migration of cultured astrocytes (Renault-Mihara and Okano, 2017; Renault-Mihara et al., 2017). The authors of this publication argue that the raised RhoA activity increases the actomyosin tone and reduces focal adhesion dynamics leading to a reduced migration speed of cultured astrocytes (Renault-Mihara and Okano, 2017; Renault-Mihara et al., 2017). Similar observations were made when Thy-1 receptor interactions were prolonged and induced an inhibition of RhoA, FAK, PI3K and Rac1 was activated and led to a higher migration behavior of astrocytes (Kong et al., 2013). A lowered RhoA activity could therefore reduce the actomyosin tone and increase focal adhesions inducing a higher migration speed, as observed in the scratch wound healing assay. The alterations of RhoA and of the cytoskeleton might furthermore induce the secretion of an altered chemokine/cytokine pattern.

CONCLUSION

In conclusion, we could demonstrate as the first that a lack of the guanine nucleotide exchange factor Vav3 in astrocytes changes the pattern of released cytokines, chemokines and neurotrophic factors and enhance the outgrowth as well as the branching of dendrites in primary hippocampal neurons. The altered release of astrocytic factors is accompanied by a higher migration speed in a scratch wound healing assay. This observations might be used in order develop therapeutical strategies which target the astrocytic Vav3 and induce beneficial effects for neuroprotective or regenerative mechanisms in the CNS.

DATA AVAILABILITY STATEMENT

The raw data supporting the conclusions of this article will be made available by the authors, without undue reservation.

ETHICS STATEMENT

The animal study was reviewed and approved by the Landesamt für Umweltschutz, Naturschutz und Verbraucherschutz, North Rhine-Westphalia, D-45659 Recklinghausen, Germany.

AUTHOR CONTRIBUTIONS

AF designed the study and supervised the study. JZ and DW performed the experiments and quantified as well as interpreted the data. DW drafted the manuscript. AF and JZ revised the manuscript. All authors contributed to the article and approved the submitted version.

FUNDING

This work was funded by the German Research Foundation (DFG, FA 159/22-1 to AF) and the SFB 642/TPA24. We acknowledge support from the DFG Open Access Publication Funds of the Ruhr-Universität Bochum.

SUPPLEMENTARY MATERIAL

The Supplementary Material for this article can be found online at: https://www.frontiersin.org/articles/10.3389/fncel.2021.817277/full#supplementary-material

Supplementary Figure 1 | (A) ELISA standard curve for the determination of NT3 in the supernatant of wildtype and *Vav3*$^{-/-}$ astrocytes after a conditioning time of 24 h. **(B)** The mean OD_{450} values of the analyzed wildtype and knockout probes revealed exceedingly low levels of NT3 in the supernatants which, furthermore, did not differ between both analyzed conditions.

REFERENCES

Ahnert-Hilger, G., Höltje, M., Grosse, G., Pickert, G., Mucke, C., Nixdorf-Bergweiler, B., et al. (2004). Differential effects of Rho GTPases on axonal and dendritic development in hippocampal neurones. *J. Neurochem.* 90, 9–18. doi: 10.1111/j.1471-4159.2004.02475.x

Ajoy, R., Lo, Y.-C., Ho, M.-H., Chen, Y.-Y., Wang, Y., Chen, Y.-H., et al. (2021). CCL5 promotion of bioenergy metabolism is crucial for hippocampal synapse complex and memory formation. *Mol. Psychiatry* 26, 6451–6468. doi: 10.1038/s41380-021-01103-3

Aleksic, B., Kushima, I., Hashimoto, R., Ohi, K., Ikeda, M., Yoshimi, A., et al. (2013). Analysis of the VAV3 as candidate gene for schizophrenia: evidences from voxel-based morphometry and mutation screening. *Schizophr. Bull.* 39, 720–728. doi: 10.1093/schbul/sbs038

Aoki, K., Nakamura, T., Fujikawa, K., and Matsuda, M. (2005). Local phosphatidylinositol 3,4,5-trisphosphate accumulation recruits Vav2 and Vav3 to activate Rac1/Cdc42 and initiate neurite outgrowth in nerve growth factor-stimulated PC12 cells. *Mol. Biol. Cell* 16, 2207–2217. doi: 10.1091/mbc.e04-10-0904

Bardehle, S., Krüger, M., Buggenthin, F., Schwausch, J., Ninkovic, J., Clevers, H., et al. (2013). Live imaging of astrocyte responses to acute injury reveals selective juxtavascular proliferation. *Nat. Neurosci.* 16, 580–586. doi: 10.1038/nn.3371

Bartelt-Kirbach, B., Moron, M., Glomb, M., Beck, C.-M., Weller, M.-P., and Golenhofen, N. (2016). HspB5/αB-crystallin increases dendritic complexity and protects the dendritic arbor during heat shock in cultured rat hippocampal neurons. *Cell Mol. Life. Sci.* 73, 3761–3775. doi: 10.1007/s00018-016-2219-9

Ben Haim, L., and Rowitch, D. H. (2017). Functional diversity of astrocytes in neural circuit regulation. *Nat. Rev. Neurosci.* 18, 31–41. doi: 10.1038/nrn.2016.159

Bernardinelli, Y., Muller, D., and Nikonenko, I. (2014). Astrocyte-synapse structural plasticity. *Neural Plast.* 2014:232105. doi: 10.1155/2014/232105

Bond, A. M., Berg, D. A., Lee, S., Garcia-Epelboim, A. S., Adusumilli, V. S., Ming, G.-L., et al. (2020). Differential timing and coordination of neurogenesis and astrogenesis in developing mouse hippocampal subregions. *Brain Sci.* 10:909. doi: 10.3390/brainsci10120909

Caceres, A., Banker, G., Steward, O., Binder, L., and Payne, M. (1984). MAP2 is localized to the dendrites of hippocampal neurons which develop in culture. *Brain Res.* 315, 314–318. doi: 10.1016/0165-3806(84)90167-6

Chien, C.-H., Lee, M.-J., Liou, H.-C., Liou, H.-H., and Fu, W.-M. (2016). Microglia-Derived Cytokines/Chemokines are involved in the enhancement of LPS-Induced loss of nigrostriatal dopaminergic neurons in DJ-1 knockout mice. *PLoS One* 11:e0151569. doi: 10.1371/journal.pone.0151569

Choi, S. S., Lee, H. J., Lim, I., Satoh, J., and Kim, S. U. (2014). Human astrocytes: secretome profiles of cytokines and chemokines. *PLoS One* 9:e92325. doi: 10.1371/journal.pone.0092325

Chou, S.-Y., Weng, J.-Y., Lai, H.-L., Liao, F., Sun, S. H., Tu, P.-H., et al. (2008). Expanded-polyglutamine huntingtin protein suppresses the secretion and production of a chemokine (CCL5/RANTES) by astrocytes. *J. Neurosci.* 28, 3277–3290. doi: 10.1523/JNEUROSCI.0116-08.2008

Christopherson, K. S., Ullian, E. M., Stokes, C. C. A., Mullowney, C. E., Hell, J. W., Agah, A., et al. (2005). Thrombospondins are astrocyte-secreted proteins that promote CNS synaptogenesis. *Cell* 120, 421–433. doi: 10.1016/j.cell.2004.12.020

Clarke, L. E., and Barres, B. A. (2013). Emerging roles of astrocytes in neural circuit development. *Nat. Rev. Neurosci.* 14, 311–321. doi: 10.1038/nrn3484

Cowan, C. W., Shao, Y. R., Sahin, M., Shamah, S. M., Lin, M. Z., Greer, P. L., et al. (2005). Vav family GEFs link activated Ephs to endocytosis and axon guidance. *Neuron* 46, 205–217. doi: 10.1016/j.neuron.2005.03.019

Czaniecki, C., Ryan, T., Stykel, M. G., Drolet, J., Heide, J., Hallam, R., et al. (2019). Axonal pathology in hPSC-based models of Parkinson's disease results from loss of Nrf2 transcriptional activity at the Map1b gene locus. *Proc. Natl. Acad. Sci. U S A.* 116, 14280–14289. doi: 10.1073/pnas.1900576116

DeFreitas, M. F., Yoshida, C. K., Frazier, W. A., Mendrick, D. L., Kypta, R. M., and Reichardt, L. F. (1995). Identification of integrin alpha 3 beta 1 as a neuronal thrombospondin receptor mediating neurite outgrowth. *Neuron* 15, 333–343. doi: 10.1016/0896-6273(95)90038-1

Deitmer, J. W., Theparambil, S. M., Ruminot, I., Noor, S. I., and Becker, H. M. (2019). Energy dynamics in the brain: contributions of astrocytes to metabolism and pH homeostasis. *Front. Neurosci.* 13:1301. doi: 10.3389/fnins.2019.01301

Etienne-Manneville, S. (2006). *In vitro* assay of primary astrocyte migration as a tool to study Rho GTPase function in cell polarization. *Methods Enzymol.* 406, 565–578. doi: 10.1016/S0076-6879(06)06044-7

Faissner, A., Pyka, M., Geissler, M., Sobik, T., Frischknecht, R., Gundelfinger, E. D., et al. (2010). Contributions of astrocytes to synapse formation and maturation - potential functions of the perisynaptic extracellular matrix. *Brain Res. Rev.* 63, 26–38. doi: 10.1016/j.brainresrev.2010.01.001

Ferreira, T. A., Blackman, A. V., Oyrer, J., Jayabal, S., Chung, A. J., Watt, A. J., et al. (2014). Neuronal morphometry directly from bitmap images. *Nat. Methods* 11, 982–984. doi: 10.1038/nmeth.3125

Fujikawa, K., Inoue, Y., Sakai, M., Koyama, Y., Nishi, S., Funada, R., et al. (2002). Vav3 is regulated during the cell cycle and effects cell division. *Proc. Natl. Acad. Sci. U S A.* 99, 4313–4318. doi: 10.1073/pnas.052715699

Geissler, M., and Faissner, A. (2012). A new indirect co-culture set up of mouse hippocampal neurons and cortical astrocytes on microelectrode arrays. *J. Neurosci. Methods* 204, 262–272. doi: 10.1016/j.jneumeth.2011.11.030

Gilmore, J. H., Fredrik Jarskog, L., Vadlamudi, S., and Lauder, J. M. (2004). Prenatal infection and risk for schizophrenia: IL-1beta, IL-6, and TNFalpha inhibit cortical neuron dendrite development. *Neuropsychopharmacology* 29, 1221–1229. doi: 10.1038/sj.npp.1300446

Gottschling, C., Dzyubenko, E., Geissler, M., and Faissner, A. (2016). The indirect neuron-astrocyte coculture assay: an *in vitro* set-up for the detailed investigation of neuron-glia interactions. *J. Vis. Exp.* 14:54757. doi: 10.3791/54757

Gualdoni, S., Albertinazzi, C., Corbetta, S., Valtorta, F., and de Curtis, I. (2007). Normal levels of Rac1 are important for dendritic but not axonal development in hippocampal neurons. *Biol. Cell* 99, 455–464. doi: 10.1042/BC20060119

Henneberger, C., Papouin, T., Oliet, S. H. R., and Rusakov, D. A. (2010). Long-term potentiation depends on release of D-serine from astrocytes. *Nature* 463, 232–236. doi: 10.1038/nature08673

Höltje, M., Hoffmann, A., Hofmann, F., Mucke, C., Grosse, G., van Rooijen, N., et al. (2005). Role of Rho GTPase in astrocyte morphology and migratory response during *in vitro* wound healing. *J. Neurochem.* 95, 1237–1248. doi: 10.1111/j.1471-4159.2005.03443.x

Huang, W., Zhou, Z., Asrar, S., Henkelman, M., Xie, W., and Jia, Z. (2011). p21-Activated kinases 1 and 3 control brain size through coordinating neuronal complexity and synaptic properties. *Mol. Cell. Biol.* 31, 388–403. doi: 10.1128/MCB.00969-10

Iyer, S. C., Wang, D., Iyer, E. P. R., Trunnell, S. A., Meduri, R., Shinwari, R., et al. (2012). The RhoGEF trio functions in sculpting class specific dendrite morphogenesis in Drosophila sensory neurons. *PLoS One* 7:e33634. doi: 10.1371/journal.pone.0033634

Jacobs, S., Cheng, C., and Doering, L. C. (2016). Hippocampal neuronal subtypes develop abnormal dendritic arbors in the presence of Fragile X astrocytes. *Neuroscience* 324, 202–217. doi: 10.1016/j.neuroscience.2016.03.011

Janzer, R. C., and Raff, M. C. (1987). Astrocytes induce blood-brain barrier properties in endothelial cells. *Nature* 325, 253–257. doi: 10.1038/325253a0

Jourdain, P., Bergersen, L. H., Bhaukaurally, K., Bezzi, P., Santello, M., Domercq, M., et al. (2007). Glutamate exocytosis from astrocytes controls synaptic strength. *Nat. Neurosci.* 10, 331–339. doi: 10.1038/nn1849

Khodosevich, K., Seeburg, P. H., and Monyer, H. (2009). Major signaling pathways in migrating neuroblasts. *Front. Mol. Neurosci.* 2:7. doi: 10.3389/neuro.02.007

Kong, M., Muñoz, N., Valdivia, A., Alvarez, A., Herrera-Molina, R., Cárdenas, A., et al. (2013). Thy-1-mediated cell-cell contact induces astrocyte migration through the engagement of αVβ3 integrin and syndecan-4. *Biochim. Biophys. Acta* 1833, 1409–1420. doi: 10.1016/j.bbamcr.2013.02.013

Labelle, C., and Leclerc, N. (2000). Exogenous BDNF, NT-3 and NT-4 differentially regulate neurite outgrowth in cultured hippocampal neurons. *Brain Res. Dev. Brain Res.* 123, 1–11. doi: 10.1016/s0165-3806(00)00069-9

Lee, T., Winter, C., Marticke, S. S., Lee, A., and Luo, L. (2000). Essential roles of *Drosophila* RhoA in the regulation of neuroblast proliferation and dendritic but not axonal morphogenesis. *Neuron* 25, 307–316. doi: 10.1016/s0896-6273(00)80896-x

Leung, Y. K. J., Pankhurst, M., Dunlop, S. A., Ray, S., Dittmann, J., Eaton, E. D., et al. (2010). Metallothionein induces a regenerative reactive astrocyte phenotype via JAK/STAT and RhoA signalling pathways. *Exp. Neurol.* 221, 98–106. doi: 10.1016/j.expneurol.2009.10.006

Liao, R., Jiang, L., Wang, R., Zhao, H., Chen, Y., Li, Y., et al. (2015). Histidine provides long-term neuroprotection after cerebral ischemia through promoting astrocyte migration. *Sci. Rep.* 5:15356. doi: 10.1038/srep15356

Luft, V., Reinhard, J., Shibuya, M., Fischer, K. D., and Faissner, A. (2015). The guanine nucleotide exchange factor Vav3 regulates differentiation of progenitor cells in the developing mouse retina. *Cell Tissue Res.* 359, 423–440. doi: 10.1007/s00441-014-2050-2

McCarthy, K. D., and de Vellis, J. (1980). Preparation of separate astroglial and oligodendroglial cell cultures from rat cerebral tissue. *J. Cell Biol.* 85, 890–902. doi: 10.1083/jcb.85.3.890

Mele, T., Carman-Krzan, M., and Juric, D. M. (2010). Regulatory role of monoamine neurotransmitters in astrocytic NT-3 synthesis. *Int. J. Dev. Neurosci.* 28, 13–19. doi: 10.1016/j.ijdevneu.2009.10.003

Moon, M., and Gomez, T. M. (2010). Balanced Vav2 GEF activity regulates neurite outgrowth and branching *in vitro* and *in vivo*. *Mol. Cell. Neurosci.* 44, 118–128. doi: 10.1016/j.mcn.2010.03.001

Morfini, G., DiTella, M. C., Feiguin, F., Carri, N., and Cáceres, A. (1994). Neurotrophin-3 enhances neurite outgrowth in cultured hippocampal pyramidal neurons. *J. Neurosci. Res.* 39, 219–232. doi: 10.1002/jnr.490390212

Movilla, N., and Bustelo, X. R. (1999). Biological and regulatory properties of Vav-3, a new member of the Vav family of oncoproteins. *Mol. Cell. Biol.* 19, 7870–7885. doi: 10.1128/MCB.19.11.7870

Movilla, N., Dosil, M., Zheng, Y., and Bustelo, X. R. (2001). How Vav proteins discriminate the GTPases Rac1 and RhoA from Cdc42. *Oncogene* 20, 8057–8065. doi: 10.1038/sj.onc.1205000

Müller, H. W., Junghans, U., and Kappler, J. (1995). Astroglial neurotrophic and neurite-promoting factors. *Pharmacol. Ther.* 65, 1–18. doi: 10.1016/0163-7258(94)00047-7

Nakayama, A. Y., Harms, M. B., and Luo, L. (2000). Small GTPases Rac and Rho in the maintenance of dendritic spines and branches in hippocampal pyramidal neurons. *J. Neurosci.* 20, 5329–5338. doi: 10.1523/JNEUROSCI.20-14-05329.2000

Nishida, H., and Okabe, S. (2007). Direct astrocytic contacts regulate local maturation of dendritic spines. *J. Neurosci.* 27, 331–340. doi: 10.1523/JNEUROSCI.4466-06.2007

Norenberg, M. D., and Martinez-Hernandez, A. (1979). Fine structural localization of glutamine synthetase in astrocytes of rat brain. *Brain Res.* 161, 303–310. doi: 10.1016/0006-8993(79)90071-4

O'Shea, K. S., Liu, L. H., and Dixit, V. M. (1991). Thrombospondin and a 140 kd fragment promote adhesion and neurite outgrowth from embryonic central and peripheral neurons and from PC12 cells. *Neuron* 7, 231–237. doi: 10.1016/0896-6273(91)90261-w

Osterhout, D. J., Frazier, W. A., and Higgins, D. (1992). Thrombospondin promotes process outgrowth in neurons from the peripheral and central nervous systems. *Dev. Biol.* 150, 256–265. doi: 10.1016/0012-1606(92)90240-h

Panatier, A., Theodosis, D. T., Mothet, J.-P., Touquet, B., Pollegioni, L., Poulain, D. A., et al. (2006). Glia-derived D-serine controls NMDA receptor activity and synaptic memory. *Cell* 125, 775–784. doi: 10.1016/j.cell.2006.02.051

Perea, G., Navarrete, M., and Araque, A. (2009). Tripartite synapses: astrocytes process and control synaptic information. *Trends Neurosci.* 32, 421–431. doi: 10.1016/j.tins.2009.05.001

Quevedo, C., Sauzeau, V., Menacho-Márquez, M., Castro-Castro, A., and Bustelo, X. R. (2010). Vav3-deficient mice exhibit a transient delay in cerebellar development. *Mol. Biol. Cell* 21, 1125–1139. doi: 10.1091/mbc.e09-04-0292

Racchetti, G., D'Alessandro, R., and Meldolesi, J. (2012). Astrocyte stellation, a process dependent on Rac1 is sustained by the regulated exocytosis of enlargeosomes. *Glia* 60, 465–475. doi: 10.1002/glia.22280

Renault-Mihara, F., and Okano, H. (2017). STAT3-regulated RhoA drives reactive astrocyte dynamics. *Cell Cycle* 16, 1995–1996. doi: 10.1080/15384101.2017.1377032

Renault-Mihara, F., Mukaino, M., Shinozaki, M., Kumamaru, H., Kawase, S., Baudoux, M., et al. (2017). Regulation of RhoA by STAT3 coordinates glial scar formation. *J. Cell Biol.* 216, 2533–2550. doi: 10.1083/jcb.201610102

Robel, S., Bardehle, S., Lepier, A., Brakebusch, C., and Götz, M. (2011). Genetic deletion of cdc42 reveals a crucial role for astrocyte recruitment to the injury site *in vitro* and *in vivo*. *J. Neurosci.* 31, 12471–12482. doi: 10.1523/JNEUROSCI.2696-11.2011

Rossman, K. L., Der, C. J., and Sondek, J. (2005). GEF means go: turning on RHO GTPases with guanine nucleotide-exchange factors. *Nat. Rev. Mol. Cell Biol.* 6, 167–180. doi: 10.1038/nrm1587

Rudge, J. S., Alderson, R. F., Pasnikowski, E., McClain, J., Ip, N. Y., and Lindsay, R. M. (1992). Expression of ciliary neurotrophic factor and the neurotrophins-nerve growth factor, brain-derived neurotrophic factor and neurotrophin 3-in cultured rat hippocampal astrocytes. *Eur. J. Neurosci.* 4, 459–471. doi: 10.1111/j.1460-9568.1992.tb00896.x

Sarder, M., Abe, K., Saito, H., and Nishiyama, N. (1996). Comparative effect of IL-2 and IL-6 on morphology of cultured hippocampal neurons from fetal rat brain. *Brain Res.* 715, 9–16. doi: 10.1016/0006-8993(95)01291-5

Sauzeau, V., Horta-Junior, J. A. C., Riolobos, A. S., Fernández, G., Sevilla, M. A., López, D. E., et al. (2010). Vav3 is involved in GABAergic axon guidance events important for the proper function of brainstem neurons controlling cardiovascular, respiratory, and renal parameters. *Mol. Biol. Cell* 21, 4251–4263. doi: 10.1091/mbc.E10-07-0639

Schulz, J., Franke, K., Frick, M., and Schumacher, S. (2016). Different roles of the small GTPases Rac1, Cdc42, and RhoG in CALEB/NGC-induced dendritic tree complexity. *J. Neurochem.* 139, 26–39. doi: 10.1111/jnc.13735

Scott, E. K., Reuter, J. E., and Luo, L. (2003). Small GTPase Cdc42 is required for multiple aspects of dendritic morphogenesis. *J. Neurosci.* 23, 3118–3123. doi: 10.1523/JNEUROSCI.23-08-03118.2003

Sholl, D. A. (1953). Dendritic organization in the neurons of the visual and motor cortices of the cat. *J. Anat.* 87, 387–406.

Sui, Y., Stehno-Bittel, L., Li, S., Loganathan, R., Dhillon, N. K., Pinson, D., et al. (2006). CXCL10-induced cell death in neurons: role of calcium dysregulation. *Eur. J. Neurosci.* 23, 957–964. doi: 10.1111/j.1460-9568.2006.04631.x

Tapon, N., and Hall, A. (1997). Rho, Rac and Cdc42 GTPases regulate the organization of the actin cytoskeleton. *Curr. Opin. Cell Biol.* 9, 86–92. doi: 10.1016/s0955-0674(97)80156-1

Turner, M., and Billadeau, D. D. (2002). VAV proteins as signal integrators for multi-subunit immune-recognition receptors. *Nat. Rev. Immunol.* 2, 476–486. doi: 10.1038/nri840

Ulc, A., Gottschling, C., Schäfer, I., Wegrzyn, D., van Leeuwen, S., Luft, V., et al. (2017). Involvement of the guanine nucleotide exchange factor Vav3 in central nervous system development and plasticity. *Biol. Chem.* 398, 663–675. doi: 10.1515/hsz-2016-0275

Ulc, A., Zeug, A., Bauch, J., van Leeuwen, S., Kuhlmann, T., Ffrench-Constant, C., et al. (2019). The guanine nucleotide exchange factor Vav3 modulates oligodendrocyte precursor differentiation and supports remyelination in white matter lesions. *Glia* 67, 376–392. doi: 10.1002/glia.23548

van Weering, H. R. J., Boddeke, H. W. G. M., Vinet, J., Brouwer, N., Haas, A. H., de, et al. (2011). CXCL10/CXCR3 signaling in glia cells differentially affects NMDA-induced cell death in CA and DG neurons of the mouse hippocampus. *Hippocampus* 21, 220–232. doi: 10.1002/hipo.20742

Wegner, A. M., Nebhan, C. A., Hu, L., Majumdar, D., Meier, K. M., Weaver, A. M., et al. (2008). N-wasp and the arp2/3 complex are critical regulators of actin in the development of dendritic spines and synapses. *J. Biol. Chem.* 283, 15912–15920. doi: 10.1074/jbc.M801555200

Wegrzyn, D., Wegrzyn, C., Tedford, K., Fischer, K.-D., and Faissner, A. (2020). Deletion of the nucleotide exchange factor Vav3 enhances axonal complexity and synapse formation but tampers activity of hippocampal neuronal networks *in vitro*. *Int. J. Mol. Sci.* 21:856. doi: 10.3390/ijms21030856

Wiese, S., Karus, M., and Faissner, A. (2012). Astrocytes as a source for extracellular matrix molecules and cytokines. *Front. Pharmacol.* 3:120. doi: 10.3389/fphar.2012.00120

Wu, J. I., Lessard, J., Olave, I. A., Qiu, Z., Ghosh, A., Graef, I. A., et al. (2007). Regulation of dendritic development by neuron-specific chromatin remodeling complexes. *Neuron* 56, 94–108. doi: 10.1016/j.neuron.2007.08.021

Xiang, X., Li, S., Zhuang, X., and Shi, L. (2016). Arhgef1 negatively regulates neurite outgrowth through activation of RhoA signaling pathways. *FEBS Lett.* 590, 2940–2955. doi: 10.1002/1873-3468.12339

Xiang, X., Zhuang, X., Li, S., and Shi, L. (2017). Arhgef1 is expressed in cortical neural progenitor cells and regulates neurite outgrowth of newly differentiated neurons. *Neurosci. Lett.* 638, 27–34. doi: 10.1016/j.neulet.2016.11.067

Xie, L., Yin, Y., and Benowitz, L. (2021). Chemokine CCL5 promotes robust optic nerve regeneration and mediates many of the effects of CNTF gene therapy. *Proc. Natl. Acad. Sci. U S A.* 118, e2017282118. doi: 10.1073/pnas.2017282118

Zeug, A., Müller, F. E., Anders, S., Herde, M. K., Minge, D., Ponimaskin, E., et al. (2018). Control of astrocyte morphology by Rho GTPases. *Brain Res. Bull.* 136, 44–53. doi: 10.1016/j.brainresbull.2017.05.003

Zhang, B., Patel, J., Croyle, M., Diamond, M. S., and Klein, R. S. (2010). TNF-alpha-dependent regulation of CXCR3 expression modulates neuronal survival during West Nile virus encephalitis. *J. Neuroimmunol.* 224, 28–38. doi: 10.1016/j.jneuroim.2010.05.003

Zhang, J., Wang, H., Ye, C., Ge, W., Chen, Y., Jiang, Z., et al. (2003). ATP released by astrocytes mediates glutamatergic activity-dependent heterosynaptic suppression. *Neuron* 40, 971–982. doi: 10.1016/s0896-6273(03)00717-7

Zhou, P., Qi, Y., Fang, X., Yang, M., Zheng, S., Liao, C., et al. (2021). Arhgef2 regulates neural differentiation in the cerebral cortex through mRNA m6A-methylation of Npdc1 and Cend1. *iScience* 24:102645. doi: 10.1016/j.isci.2021.102645

Conflict of Interest: The authors declare that the research was conducted in the absence of any commercial or financial relationships that could be construed as a potential conflict of interest.

Publisher's Note: All claims expressed in this article are solely those of the authors and do not necessarily represent those of their affiliated organizations, or those of the publisher, the editors and the reviewers. Any product that may be evaluated in this article, or claim that may be made by its manufacturer, is not guaranteed or endorsed by the publisher.

Copyright © 2022 Wegrzyn, Zokol and Faissner. This is an open-access article distributed under the terms of the Creative Commons Attribution License (CC BY). The use, distribution or reproduction in other forums is permitted, provided the original author(s) and the copyright owner(s) are credited and that the original publication in this journal is cited, in accordance with accepted academic practice. No use, distribution or reproduction is permitted which does not comply with these terms.

frontiers in Cellular Neuroscience

ORIGINAL RESEARCH
published: 17 February 2022
doi: 10.3389/fncel.2022.792089

Hearing Recovery Induced by DNA Demethylation in a Chemically Deafened Adult Mouse Model

Xin Deng[1] *and Zhengqing Hu*[1,2]*

[1] Department of Otolaryngology-Head and Neck Surgery (HNS), Wayne State University School of Medicine, Detroit, MI, United States, [2] John D. Dingell VA Medical Center, Detroit, MI, United States

Functional hair cell regeneration in the adult mammalian inner ear remains challenging. This study aimed to study the function of new hair cells induced by a DNA demethylating agent 5-azacytidine. Adult mice were deafened chemically, followed by injection of 5-azacytidine or vehicle into the inner ear. Functionality of regenerated hair cells was evaluated by expression of hair cell proteins, auditory brainstem response (ABR), and distortion-product otoacoustic emission (DPOAE) tests for 6 weeks. In the vehicle-treated group, no cells expressed the hair cell-specific protein myosin VIIa in the cochlea, whereas numerous myosin VIIa-expressing cells were found in the 5-azacytidine-treated cochlea, suggesting the regeneration of auditory hair cells. Moreover, regenerated hair cells were co-labeled with functional proteins espin and prestin. Expression of ribbon synapse proteins suggested synapse formation between new hair cells and neurons. In hearing tests, progressive improvements in ABR [5–30 dB sound pressure level (SPL)] and DPOAE (5–20 dB) thresholds were observed in 5-azacytidine-treated mice. In vehicle-treated mice, there were <5 dB threshold changes in hearing tests. This study demonstrated the ability of 5-azacytidine to promote the functional regeneration of auditory hair cells in a mature mouse model *via* DNA demethylation, which may provide insights into hearing regeneration using an epigenetic approach.

Keywords: espin, otoacoustic emission, prestin, ribbon synapse, hair cell, auditory brainstem response (ABR), DNA demethylation

OPEN ACCESS

Edited by:
Arturo Ortega, Centro de Investigación y de Estudios Avanzados del Instituto Politécnico Nacional, Mexico

Reviewed by:
Daniel Hernández Sotelo, Autonomous University of Guerrero, Mexico
Liman Liu, University of Kentucky Medical Center, United States

***Correspondence:**
Zhengqing Hu
zh@med.wayne.edu

Specialty section:
This article was submitted to Non-Neuronal Cells, a section of the journal Frontiers in Cellular Neuroscience

Received: *09 October 2021*
Accepted: *04 January 2022*
Published: *17 February 2022*

Citation:
Deng X and Hu Z (2022) Hearing Recovery Induced by DNA Demethylation in a Chemically Deafened Adult Mouse Model. Front. Cell. Neurosci. 16:792089. doi: 10.3389/fncel.2022.792089

INTRODUCTION

According to the WHO, more than 1.5 billion people experience various extents of hearing disorders in the world (World Health Organization, 2021), which largely attribute to auditory hair cell loss and dysfunction. The mammalian cochlear hair cell epithelium has two types of hair cells: inner and outer hair cells. Inner hair cells transfer auditory information to spiral ganglion neurons *via* hair cell ribbon synapses. The neurotransmission between inner hair cells and spiral ganglion neurons involves C-terminal-binding proteins (CtBPs) family of transcriptional corepressor C-terminal-binding protein 2 (CtBP2) expressed at the presynaptic ribbon structure (Nouvian et al., 2006; Matthews and Fuchs, 2010; Uthaiah and Hudspeth, 2010; Liberman et al., 2011) and glutamate receptor 2 (GluR2) as one of the postsynaptic α-amino-3-hydroxy-5-methyl-4-isoxazolepropionic acid (AMPA)-type glutamate receptors (Nouvian et al., 2006; Uthaiah and Hudspeth, 2010; Liberman et al., 2011). Outer hair cells are able to detect weak sound vibrations that are attributed to cochlear amplification, likely *via* the endowed electromotility

(Hudspeth, 1989, 2008). Prestin is a motor protein that is robustly expressed in outer hair cells and acts as an amplifier of sound stimulations (Zheng et al., 2000a; Dallos, 2008). In the complex mammalian auditory system, the functionality of hair cells is carried out by the stereocilia of hair bundles, which consist of a variety of proteins, including actin cross-linking proteins, such as espin (Hudspeth, 1989, 2008; Bartles, 2000), as well as the abovementioned functional proteins to detect sound stimulation and transfer signals to spiral ganglion neurons. However, mammalian auditory system is vulnerable to a variety of insults, which causes irreversible degeneration of auditory hair cell functional proteins and loss of hair cells, leading to permanent sensorineural hearing loss (Hawkins et al., 1976; Bohne et al., 1987). Therefore, a successful hair cell regeneration includes not only the reconstitution of structure and morphology, but also the regeneration of hair cell functional proteins and synaptic connections.

In the past decades, research on hair cell regeneration has gained significant progress. Regenerated hair cells are observed in the *in vitro* system (White et al., 2006; Oshima et al., 2010; Chai et al., 2012; Chen et al., 2012; György et al., 2017; Koehler et al., 2017) and neonatal *in vivo* models (White et al., 2006; Chai et al., 2012; György et al., 2017; Isgrig et al., 2017). Gene therapy is shown to repair the function of hair cells in the neonatal mouse (Isgrig et al., 2017; Nist-Lund et al., 2019) and rescue the deafness phenotype in the postnatal mouse (György et al., 2017). In an *in vitro* study, the gerbil organ of Corti was cultured in the presence of a Notch signaling inhibitor. Supporting cell stereocilia formation and native hair cell supernumerary stereocilia were identified, which showed mechanotransduction currents following fluid jet stimulation (Li et al., 2018). In addition, Notch inhibition induced new hair cells to express prestin, a major characteristic protein of outer hair cells that mediates somatic mobility (Santos-Sacchi and Dilger, 1988; Zheng et al., 2000b; Liberman et al., 2002). *In vivo*, hair bundle-like structures and possible nerve connection adjacent to newly generated hair cell-like cells were induced by ectopic expression of Atonal homolog 1 (*Atoh1*), POU class 4 transcription factor 3 (*Pou4f3*), and GATA-binding protein 3 (*Gata3*) in the presence of $P27^{Kip1}$ inhibition. In the other *in vivo* study, new hair cell-like cells expressed prestin, CtBP2, and vesicular glutamate transporter 3 (VGluT3) and showed FM1-43 intake following *Atoh1*, *Pou4f3*, and growth factor independence-1 (*Gfi1*) overexpression (Chen et al., 2021). However, the overall hearing threshold was worsened, indicating the hearing function recovery is still challenging (Chen et al., 2021). These previous reports demonstrate promising, but limited progress on hair cell function regeneration, suggesting that regeneration of functional hair cells in adult mammals remains a major obstacle.

In this study, we attempted to investigate the functionality of newly generated hair cells induced by a previously established epigenetic approach in a deafened adult mouse model (Deng et al., 2019; Deng and Hu, 2020). The advantage of an epigenetic approach is that this approach does not change the DNA sequence (Jones and Takai, 2001; Layman and Zuo, 2015), which may be critical for future clinical application. In our previous report, a DNA demethylating agent 5-azacytidine (5-aza) was able to stimulate mouse utricle sensory epithelia-derived progenitor cells (MUCs) to differentiate into hair cell-like cells expressing *Atoh1*, myosin VIIa, myosin VI, espin, and Pou4f3 *in vitro* (Zhou and Hu, 2016). FM1-43 permeation assay revealed that the 5-aza-treated MUCs may possess functional mechanosensory transduction channels (Zhou and Hu, 2016). Later, 5-aza was injected into the inner ear of the deafened adult mouse to investigate whether 5-aza could promote hair cell regeneration *in vivo* (Deng et al., 2019). Two weeks following 5-aza treatment, regenerated hair cells were identified in the cochlear sections and basilar membrane surface preparations, which were confirmed by myosin VIIa immunostaining and fluorescent F-actin double-labeling (Deng et al., 2019). The regenerated hair cells were observed in all the three cochlear turns and were able to survive for at least 6 weeks (Deng et al., 2019). Moreover, the inner ear DNA methyltransferase 1 (Dnmt1) messenger RNA (mRNA) expression level of the 5-aza treatment group was significantly lower than that of the vehicle treatment group, suggesting that DNA demethylation and Dnmt1 inhibition may play a role in 5-aza-induced new hair cell generation (Deng et al., 2019). In order to determine the cell sources for the new hair cells, a transgenic mouse strain that the expression of enhanced green fluorescent protein (EGFP) is under control of the endogenous SRY-Box transcription factor 2 (Sox2) regulatory element (the Sox2-EGFP transgenic mouse) was applied. The results indicate that the new hair cells may be converted from Sox2-positive supporting cells 5–7 days post-5-aza injection (Deng and Hu, 2020). Further, CtBP2 expression observed in new hair cells suggests that these 5-aza-induced hair cells may have the potential to form hair cell ribbon synapses (Deng et al., 2019). These data motivated us to further the study to investigate the function of new hair cells generated by 5-aza treatment *in vivo*.

MATERIALS AND METHODS

Animals

Young adult (4–6 weeks old, either sex) wildtype Swiss Weber mice were included in this study. The care and use of animals have been approved by the Wayne State University Institutional Animal Care and Use Committee. A total of 48 animals were included in the surgery, 24 animals for the 5-aza and 24 animals for the vehicle groups. Six animals were assigned to the 1, 2, 4, and 6 weeks postsurgery groups for the 5-aza and vehicle groups, respectively. Additionally, six untreated normal hearing mice were included in the synapse study.

Hearing Test

Auditory brainstem response (ABR) and distortion-product otoacoustic emission (DPOAE) tests are two major methods used to determine the function of the auditory system and outer hair cells, respectively (Tadros et al., 2007a,b). The five waveforms of ABR test provide information about the auditory nerve and different cell types in the cochlear nucleus and superior olivary complex (Tadros et al., 2007a,b). DPOAE measures the amplification of cochlear vibration generated by outer hair cells

(Tadros et al., 2007a,b). Thus, a combination of ABR and DPOAE provides a functional status of the hair cells.

Baseline pure-tone ABR and DPOAE were used to evaluate the auditory and outer hair cell function using our published methods (Deng et al., 2019; Hu et al., 2021). ABR and DPOAE were measured using RP2.1 and RZ6 systems [Tucker-Davis Technology (TDT), Alachua, FL, United States]. The TDT System 3 software was utilized for signal generation and response collection. At 8, 16, 24, and 32 kHz, the ABR stimulation ranged from 10 to 90 dB sound pressure level (SPL) in 5 dB steps. The threshold was determined as the lowest stimulation dB SPL level that generated wave-I amplitude larger than 0.2 μV (microvolt). At 16 and 24 kHz, the configuration of DPOAE was F2/F1 at 1.2, L1 = L2 + 10 dB. L1 ranged from 10 to 90 dB SPL in 5 dB SPL steps. DPOAE threshold was determined as the lowest level with DPOAE responses (dp) of at least 10 dB above the noise floor.

Auditory brainstem response and DPOAE tests were performed prior to deafening to record the baseline, 3-day postdeafening to confirm deafness, and at each week following surgery for up to 6 weeks to determine hearing ability recovery. Since all the follow-up animals received weekly hearing tests after the surgery, 24, 18, 12, and 6 animals received hearing tests at 1, 2, 4, and 6 weeks following 5-aza treatment, respectively. Similarly, 24, 18, 12, and 6 animals received hearing tests at 1, 2, 4, and 6 weeks after surgery in the vehicle group, respectively.

Deafening

Baseline pure-tone ABR and DPOAE were performed on each mouse to assure normal hearing. The deafening was performed using our published methods (Deng et al., 2019). Briefly, kanamycin (1 g/kg body weight, sc) was injected, followed by furosemide treatment (300 mg/kg body weight, ip) after 25–30 min (Deng et al., 2019). Deafness was confirmed 3-day after kanamycin and furosemide injection. ABR threshold shift larger than 40 dB SPL was set as criteria of successful deafening.

Inner Ear Surgery

At 3 days postdeafening, 4 mM 5-aza was injected into deafened mouse inner ears after hearing tests using our published methods (Deng et al., 2019). The control group was injected with saline, which was the vehicle. Under deep anesthesia, the left temporal bone was exposed and opened to enable visuality of the basal cochlear turn and round window. A volume of 0.2 μl of 5-aza or saline was injected *via* a microsyringe (Hamilton, Reno, NV, United States), which was connected to a small catheter inserting into the round window. Mice were followed up for 6 weeks, with ABR and DPOAE tests weekly.

Immunofluorescence

At the end of the experiment, mice were euthanized and cochlear samples were harvested and fixed by 4% paraformaldehyde (Sigma-Aldrich, Burlington, MA, United States) using our published methods (Deng et al., 2019). Cochleae were decalcified by 0.1 M ethylenediaminetetraacetic acid (EDTA) (Sigma-Aldrich) for 1 week. After decalcification, cochleae were cryosectioned at 10 μm thickness. For immunostaining, cochlear samples were treated with phosphate-buffered saline (PBS) containing 5% normal donkey serum (Jackson ImmunoResearch, West Grove, PA, United States) and 0.2% Triton X-100 (Sigma-Aldrich) for 30 min. Cochlear sections were incubated in primary antibodies at 4°C overnight, followed by secondary antibody incubation at room temperature for 2 h. The primary antibodies included: anti-myosin VIIa [1:100; Developmental Studies Hybridoma Bank (DSHB), Iowa City, IA, United States and Proteus Biosciences, Ramona, CA, United States], anti-espin (1:50; gift of Dr. James Bartels), anti-prestin (1:50, Sigma-Aldrich), anti-CtBP2 (1:200, BD Biosciences, San Jose, CA, United States), and anti-GluR2 (1:200, Millipore, Burlington, MA, United States). Secondary antibodies included Dylight-488-, Cy3-, and Dylight-647-conjugated antibodies (1:500; Jackson ImmunoResearch, West Grove, PA, United States). 4,6-diamidino-2-phenylindole (DAPI) (Invitrogen, Waltham, MA, United States) was used to label all the nuclei. Leica confocal microscopy was used to capture images.

Data Analysis

The expressions of CtBP2 and GluR2 were quantified by counting the number of puncta per inner hair cell within the inner hair cell area. Data were sampled from the normal hearing mice and 5-aza-treated mice. Because no or very few inner hair cells were observed in the vehicle group, vehicle-treated mice were not included in the synapse study analysis. Statistical analysis was performed by Tukey's honestly significant difference (HSD) test. $p < 0.05$ was considered as statistically significant in this study.

To evaluate the hearing function of the 5-aza- or vehicle-treated mice, ABR and DPOAE threshold shifts were calculated by the thresholds measured postsurgery, subtracting those at 3 days postdeafening, which was just before the surgery. Data were shown by mean ± SEM. Lower thresholds indicated better hearing function and the negative threshold shifts suggested a decrease in the thresholds and improvement of hearing. Two-way ANOVA followed by Tukey's test was used to define the threshold shift difference between the vehicle- and 5-aza-treated mice among different follow-up points. $p < 0.05$ was considered as statistically significant in this study.

RESULTS

Hair Cell Functional Proteins Were Expressed Following 5-Aza Treatment

Administration of kanamycin and furosemide (see section "Materials and Methods") was consistently shown to deafen young adult mice (4–6 weeks old) (Deng et al., 2019; Deng and Hu, 2020). Pure-tone ABR and DPOAE were measured prior to and 3 days after deafening to confirm deafness, as shown in our previous reports (Deng et al., 2019; Deng and Hu, 2020). Two weeks after 5-aza or vehicle injection, cochlear section immunostaining was performed to observe the expression of hair cell functional proteins. Previous reports utilized expressions of espin in hair cell bundle stereocilia (Bartles, 2000) and prestin in the outer hair cells (Zheng et al., 2000a; Dallos, 2008) to evaluate the functionality of hair cells. In this study, no myosin VIIa-expressing cell was found in vehicle-treated mice

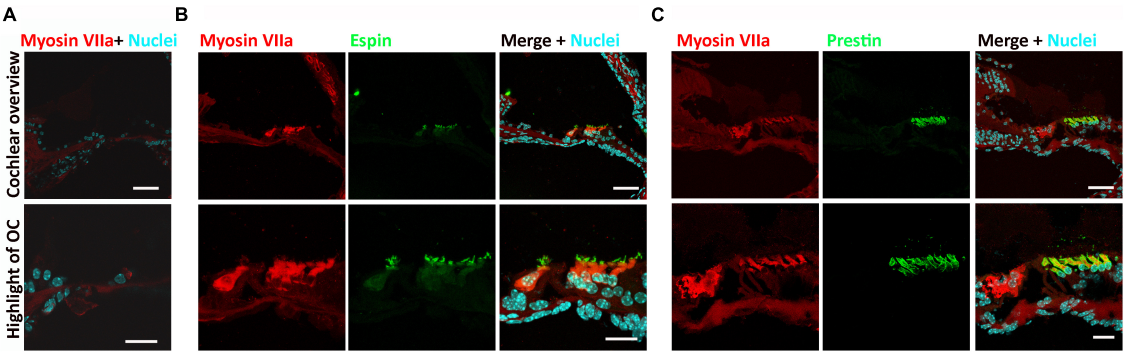

FIGURE 1 | Expression of espin and prestin was observed in the 5-azacytidine (5-aza)-treated mouse inner ear. **(A)** No hair cell was observed in the cochlear sections of the vehicle-treated mice. **(B)** Expression of espin was observed in the hair bundles of myosin VIIa-expressing regenerated hair cells in the 5-aza-treated mice. **(C)** Prestin expressed in the myosin VIIa-expressing outer hair cells in the cochlear sections of the 5-aza group mouse. All the figures were from the apical cochlear turn. OC, organ of Corti. Scale bar: 50 μm in cochlear overview and 20 μm in OC highlight.

(**Figure 1A**), suggesting no hair cell was regenerated in the vehicle group, which is consistent with our previous report (Deng et al., 2019). In contrast, myosin VIIa-expressing hair cells were observed in the 5-aza-treated mice (**Figures 1B,C**), confirming hair cells regeneration induced by 5-aza. All the myosin VIIa-expressing hair cells were colabeled with espin (**Figure 1B**), indicating the expression of hair bundle proteins in these new hair cells. Expression of prestin was also observed in myosin VIIa-expressing hair cells and all the myosin VIIa-positive cells in the outer hair cell region were prestin positive (**Figure 1C**), suggesting the recovery of outer hair cell functional proteins.

Hair Cell Ribbon Synapse Proteins Were Expressed Following 5-Aza Treatment

C-terminal-binding protein 2 (CtBP2) is the ribbon synapse vesicle protein of hair cell afferent synapses (Uthaiah and Hudspeth, 2010) and GluR2 is the postsynaptic AMPA-type glutamate receptors (Liberman et al., 2011). In this study, anti-CtBP2 and anti-GluR2 antibodies were applied to the basilar membrane to immunolabel these synaptic proteins to evaluate their expression in inner hair cell afferent ribbon synapses at 2 weeks after 5-aza treatment (**Figure 2**). CtBP2 and GluR2 puncta were observed in all the three cochlear turns in the 5-aza-treated mice. **Figure 2A** shows CtBP2 and GluR2 immunofluorescence labeling in the middle turn of normal hearing and the 5-aza treated mice. CtBP2 and adjacent GluR2 expression were observed in the inner hair cell region of both the 5-aza and normal hearing groups (**Figure 2A**). Merged figures revealed that some of CtBP2 and GluR2 signals were colocalized (**Figure 2A**). The quantitative study compared the expression of CtBP2 and GluR2 in the normal hearing and 5-aza groups (**Figure 2B**). In the quantification study, the average number of CtBP2 and GluR2 puncta per inner hair cell in the normal hearing group was normalized to 1.0 (**Figure 2B**). The average number of CtBP2 puncta per inner hair cell in the 5-aza group was 0.66 ± 0.09 (**Figure 2B**). Statistical analysis showed significant difference in the number of CtBP2 puncta between the normal hearing and 5-aza groups (p = 0.022; **Figure 2B**). After normalizing the GluR2 puncta in normal hearing mice, the number of GluR2 puncta per inner hair cell of the 5-aza group was 0.41 ± 0.12 (**Figure 2B**). Statistical analysis shows significant difference in GluR2 puncta between the normal and 5-aza groups (p = 0.001; **Figure 2B**). These data indicate that

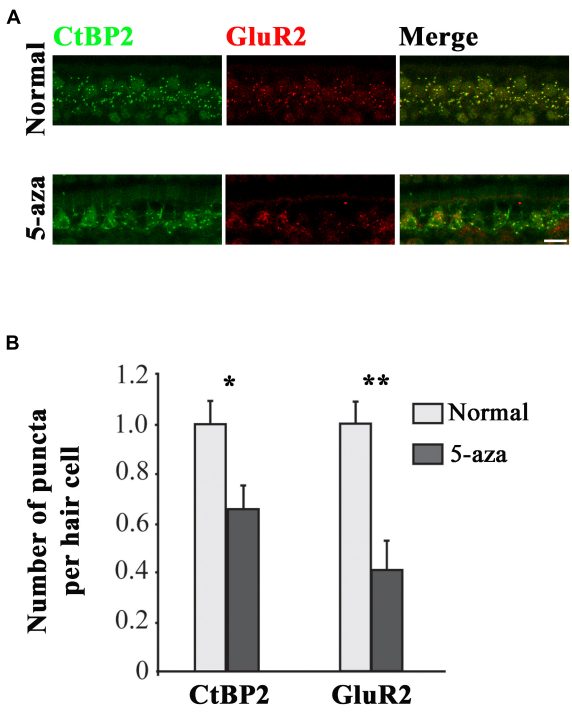

FIGURE 2 | Expression of C-terminal-binding protein 2 (CtBP2) and GluR2 was observed in the 5-aza-treated mice. **(A)** Expression of CtBP2 and GluR2 in the surface preparation of the basilar membrane of the normal hearing and 5-aza-treated mice. Scale bar: 50 μm. **(B)** Quantification of CtBP2 and GluR2 expression. The number of CtBP2 and GluR2 puncta per inner hair cell was normalized to 1 for the normal hearing mouse. Data are means ± SEM. Statistical analysis was performed by Tukey's honestly significant difference (HSD) test. * indicates $p < 0.05$; **indicates $p < 0.01$.

functional synaptic proteins have been regenerated in the 5-aza group. However, these 5-aza-induced synaptic protein expression has not been fully recovered to the normal hearing level.

Auditory Brainstem Response Thresholds Were Improved by 5-Aza Treatment

Auditory brainstem response was applied to acquire functional information on the cochlea and auditory pathway (Squires et al., 1978; Parham et al., 1999). Baselines pure-tone ABRs were measured to ascertain that all the animals included in this study showed normal hearing ability. The baseline pure-tone ABR thresholds in both the 5-aza and vehicle mice were approximately 10–40 dB SPL at 8, 16, 24, and 32 kHz (**Figures 3A,B**). Three days after kanamycin/furosemide treatment, ABR thresholds of the same mice were >70 dB SPL at 8, 16, 24, and 32 kHz (**Figure 3A**), indicating that mice were chemically deafened. Vehicle-treated animals did not show significant ABR threshold changes up to 6 weeks after vehicle injection into the cochleae (**Figures 3A,B**).

In contrast, mice treated with 4 mM 5-aza showed improved thresholds after surgery (**Figure 3C**), suggesting that 5-aza treatment may lead to hearing function improvement. To quantify hearing improvements, ABR thresholds were measured each week for up to 6 weeks after the 5-aza or vehicle treatment. The threshold shifts were calculated as threshold measured each week for up to 6 weeks subtracting the threshold prior to the 5-aza or vehicle treatment (see section "Materials and Methods"). **Table 1** shows ABR threshold shifts at different frequencies in 5-aza and vehicle mice from 1- to 6-week following treatment. In contrast to the vehicle-treated mice with overall ABR threshold changes around −2 to 5 dB SPL, the 5-aza-treated mice exhibited

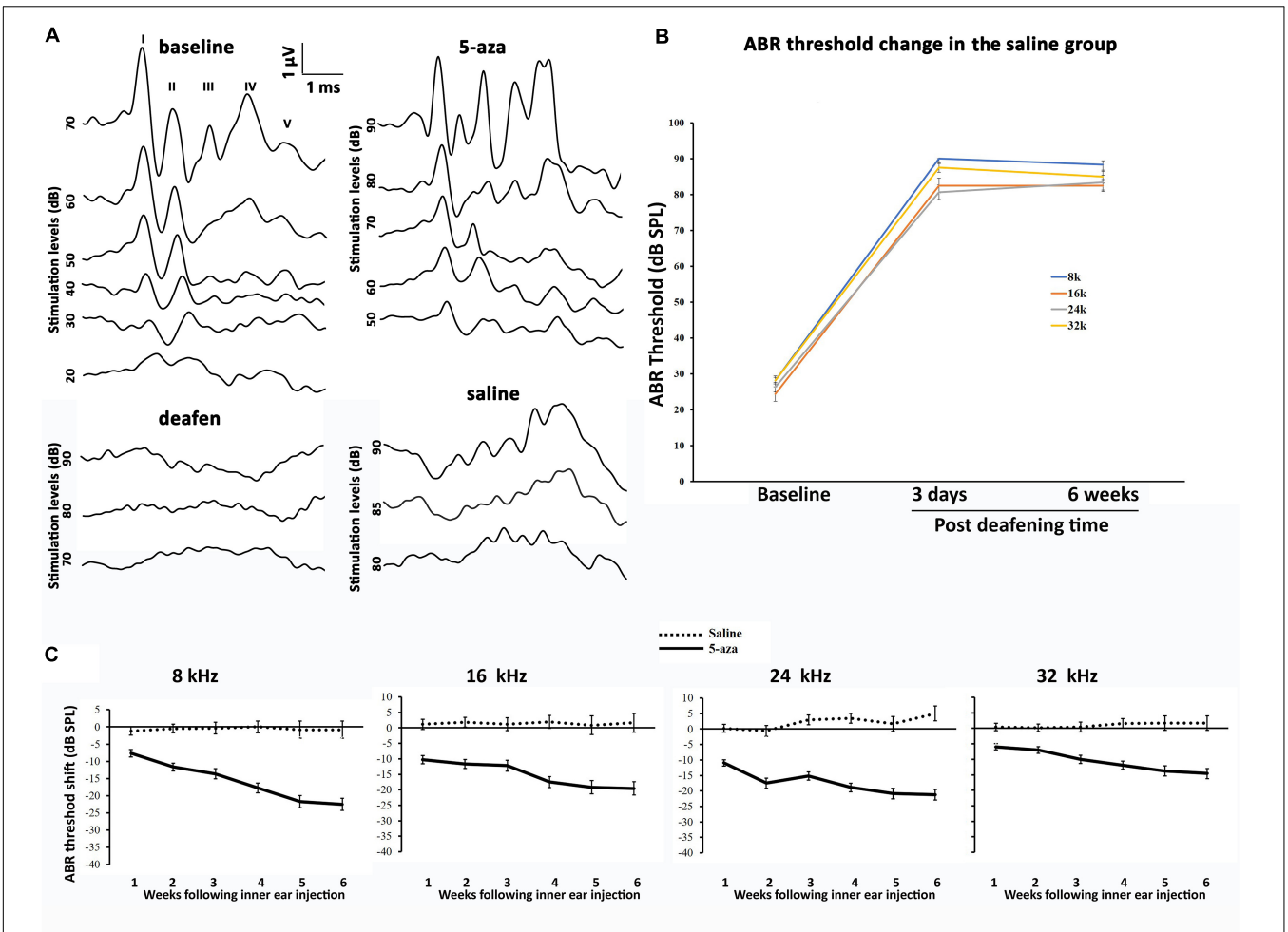

FIGURE 3 | Auditory brainstem response (ABR) thresholds in the 5-aza- and vehicle-treated mice. **(A)** Representative ABR waveforms of four groups of mice. ABR threshold was determined by the lowest stimulation dB sound pressure level (SPL) that generates the amplitude of wave I greater than 0.2 μV. The baseline threshold was about 30 dB in this figure. Three days after deafening, deafened mice showed no ABR response up to 90 dB SPL stimulation. Two weeks after 5-aza treatment, ABR trace showed a threshold of 50 dB SPL. In contrast, the vehicle-treated mouse showed messy traces without typical ABR waveform responses. **(B)** ABR threshold shifts were over 40 dB SPL 3 days after deafening in the saline group. The threshold shifts remained 6 weeks following deafening. **(C)** ABR threshold shifts trend for up to 6 weeks after surgery in the 5-aza and vehicle groups at 8, 16, 24, and 32 kHz. Negative values in the 5-aza group revealed hearing improvement. ABR threshold shifts in the vehicle group were close to zero, indicating that vehicle injection did not significantly change ABR threshold. Data are means ± SEM.

TABLE 1 | Auditory brainstem response (ABR) threshold shifts after 5-aza/vehicle treatment.

Frequency (kHz)	Group	1-week	2-week	3-week	4-week	5-week	6-week
8	5-aza	−8.125 ± 1.137	−12.222 ± 1.312	−13.75 ± 1.607	−16.25 ± 1.607	−24.167 ± 2.273	−30.833 ± 2.273
	Vehicle	−1.042 ± 1.137	−0.556 ± 1.312	−0.417 ± 1.607	−0.001 ± 1.607	−0.833 ± 2.273	−0.833 ± 2.273
16	5-aza	−10.625 ± 1.491	−11.944 ± 1.722	−11.25 ± 2.109	−17.083 ± 2.109	−20.833 ± 2.982	−24.167 ± 2.982
	Vehicle	1.042 ± 1.491	1.389 ± 1.722	0.417 ± 2.109	2.083 ± 2.109	0.833 ± 2.982	1.667 ± 2.982
24	5-aza	−11.875 ± 1.076	−16.389 ± 1.242	−17.083 ± 1.522	−20.417 ± 1.522	−22.5 ± 2.152	−22.5 ± 2.152
	Vehicle	0.417 ± 1.076	3.056 ± 1.242	1.25 ± 1.522	4.583 ± 1.522	1.667 ± 2.152	1.667 ± 2.152
32	5-aza	−5.833 ± 1.021	−8.611 ± 1.178	−11.25 ± 1.443	−12.5 ± 1.443	−17.5 ± 2.041	−22.5 ± 2.041
	Vehicle	0.208 ± 1.201	0.833 ± 1.178	0.001 ± 1.443	1.667 ± 1.443	1.667 ± 2.041	1.667 ± 2.041

Threshold shift (dB SPL) was calculated as ABR threshold measured after the treatment minus the threshold prior to the treatment (3 days after deafening). Data are means ± SEM.

progressive ABR threshold improvement for up to 30 dB SPL from 1 to 6-week following treatment in all the frequencies measured (**Table 1** and **Figure 3C**).

Statistical analysis revealed that ABR threshold improvements in 5-aza and vehicle mice were significantly different at all the follow-up points at all the frequencies using two-way ANOVA and *post-hoc* tests. The two factors are treatment type (5-aza and vehicle) and follow-up times (1–6 weeks). At 8 kHz, the overall effects were $F_{(5,\ 144)} = 10.82$ and $p < 0.0001$, whereas the effects of treatment type and follow-up time were $F_{(1,\ 144)} = 279.2/p < 0.0001$ and $F_{(5,\ 144)} = 10.31/p < 0.0001$, respectively. In *post-hoc* tests of comparing the 5-aza and vehicle groups, $p < 0.0001$ was observed from 1 to 6 weeks posttreatment. At 16 kHz, two-way ANOVA showed that the overall, treatment type, and follow-up time effects were significant, $F_{(5,\ 144)} = 3.003/p = 0.0131$, $F_{(1,\ 144)} = 189.5/p < 0.0001$, and $F_{(5,\ 144)} = 2.401/p = 0.0399$, respectively. In *post-hoc* tests, the 5-aza vs. vehicle groups comparison showed $p < 0.0001$ for the 1, 2, 4, 5, and 6 weeks measurements, whereas $p = 0.0004$ for the 3 weeks measurements. At 24 kHz, two-way ANOVA analysis revealed that the effects of overall, treatment type, and follow-up times were statistically significant: $F_{(5,\ 144)} = 9.840/p < 0.0001$, $F_{(1,\ 144)} = 534.8/p < 0.0001$, and $F_{(5,\ 144)} = 3.107/p = 0.0108$, respectively. In *post-hoc* comparison of the 5-aza and vehicle groups 1–6 weeks after the treatment, *p*-values were all < 0.0001. At 32 kHz, two-way ANOVA analysis revealed significant difference ($p < 0.0001$) in the overall, treatment type, and follow-up time effects: $F_{(5,\ 144)} = 8.756$, $F_{(1,\ 144)} = 237.6$, and $F_{(5,\ 144)} = 5.915$, respectively. In *post-hoc* comparison of the 5-aza and vehicle groups 1–6 weeks following treatment, $p = 0.0003$ for the 1-week follow-up and $p < 0.0001$ for the 2–6 weeks follow-ups.

To compare the 5-aza group threshold improvement among follow-up times, **Table 2** shows the statistical analysis of ABR threshold shift 1–6 weeks post-5-aza treatment. In all frequencies, ABR threshold improvements of the 5- and 6-week groups were significantly greater than the 1- and 2-week groups (**Table 2**). For the vehicle group, there was no significant difference in all the comparisons at all the frequencies.

Taken together, statistical analysis revealed that ABR threshold improvements in the 5-aza and vehicle groups were significantly different at all follow-up timepoints and all frequencies ($p < 0.001$ in all the comparisons), suggesting 5-aza-induced hearing improvement for at least 6 weeks compared to the vehicle group.

TABLE 2 | Statistical analysis of weekly auditory brainstem response (ABR) threshold shifts of the 5-aza group.

	8 kHz	16 kHz	24 kHz	32 kHz
6-week	vs. 1-week (***); vs. 2-week (***); vs. 3-week (***); vs. 4-week (***); vs. 5-week (0.301)	vs. 1-week (***); vs. 2-week (**); vs. 3-week (**); vs. 4-week (0.378); vs. 5-week (0.969)	vs. 1-week (***); vs. 2-week (**); vs. 3-week (**); vs. 4-week (0.969); vs. 5-week (1.000)	vs. 1-week (***); vs. 2-week (***); vs. 3-week (***); vs. 4-week (***); vs. 5-week (0.510)
5-week	vs. 1-week (***); vs. 2-week (***); vs. 3-week (**); vs. 4-week (0.051)	vs. 1-week (**); vs. 2-week (0.102); vs. 3-week (0.091); vs. 4-week (0.909)	vs. 1-week (***); vs. 2-week (0.136); vs. 3-week (0.311); vs. 4-week (0.969)	vs. 1-week (***); vs. 2-week (**); vs. 3-week (0.124); vs. 4-week (0.342)
4-week	vs. 1-week (***); vs. 2-week (0.377); vs. 3-week (0.882)	vs. 1-week (0.124); vs. 2-week (0.401); vs. 3-week (0.368)	vs. 1-week (***); vs. 2-week (0.314); vs. 3-week (0.632)	vs. 1-week (**); vs. 2-week (0.294); vs. 3-week (0.717)
3-week	vs. 1-week (*); vs. 2-week (0.977)	vs. 1-week (1.000); vs. 2-week (1.000)	vs. 1-week (0.058); vs. 2-week (0.999)	vs. 1-week (*); vs. 2-week (0.249)
2-week	vs. 1-week (0.17)	vs. 1-week (0.992)	vs. 1-week (0.066)	vs. 1-week (0.478)

*Pairwise comparison was performed by the Tukey test. P-values were stated in parentheses. *, **, and *** indicate $p < 0.05$, $p < 0.01$, and $p < 0.001$, respectively.*

Distortion-Product Otoacoustic Emission Thresholds Were Improved by 5-Aza Treatment

Distortion-product otoacoustic emissions at 16 and 24 kHz were applied to test the functionality of outer hair cells. In baseline tests, DPOAE thresholds were approximately 20–40 dB at 16 and 24 kHz (**Figures 4A,B**). Three days following kanamycin/furosemide treatment, DPOAE thresholds of the same mice went up to >50 dB (**Figures 4A,B**), indicating impairment of outer hair cells. After the treatment, the control group animals showed no significant DPOAE threshold changes up to 6 weeks after vehicle injection into the cochleae (**Figure 4B**).

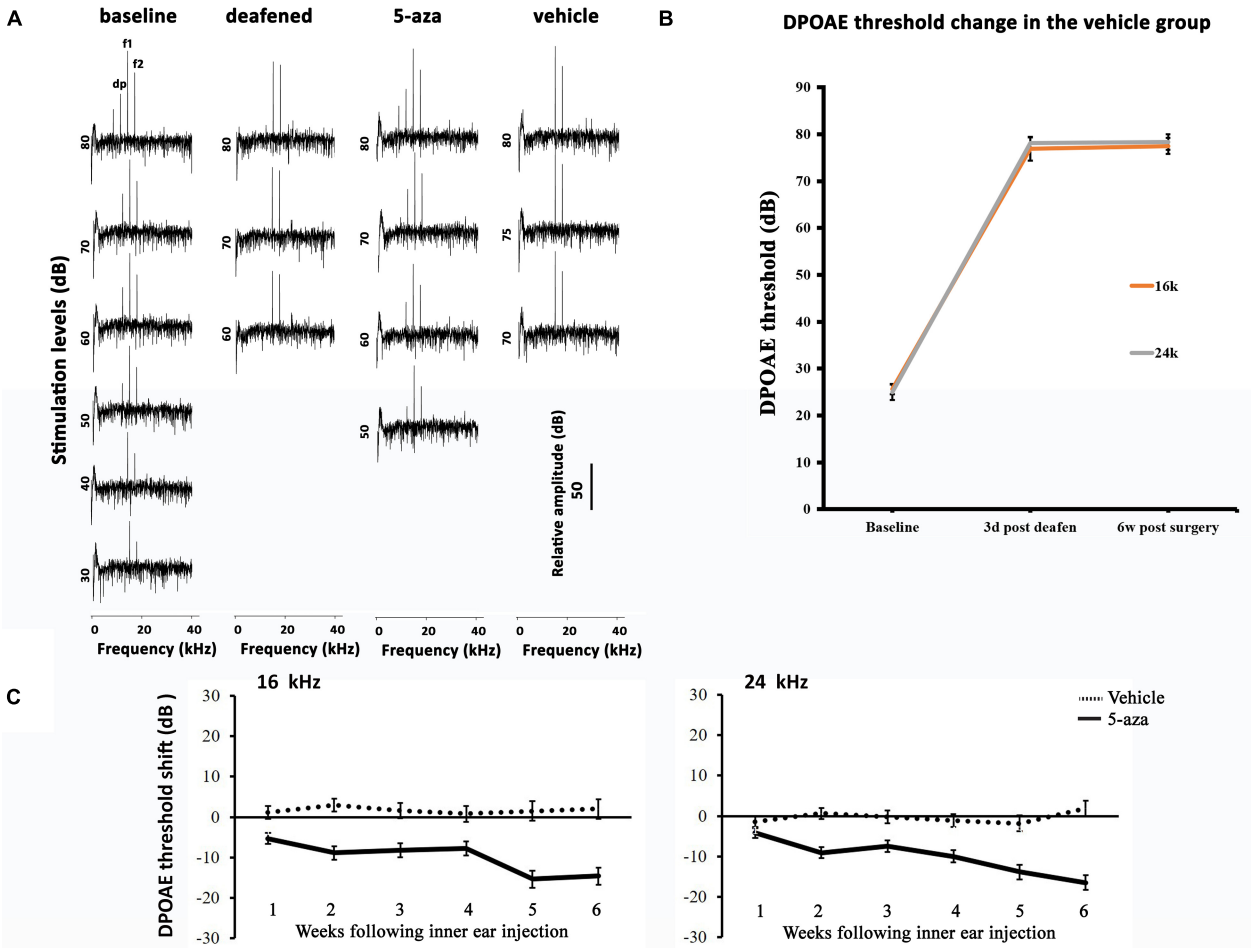

FIGURE 4 | Distortion-product otoacoustic emission (DPOAE) thresholds in the 5-aza- and vehicle-treated mice. **(A)** Representative DPOAE traces of 4 groups of mice. DPOAE threshold was determined by the lowest stimulation dB level that generates dp of at least 10 dB above the noise floor. The baseline threshold was 40 dB in this figure. Three days after deafening, DPOAE threshold was 80 dB. The 5-aza treated mouse showed 50 dB threshold 6 weeks after treatment, while the vehicle-treated mouse showed no DPOAE response 6 weeks after injection. **(B)** DPOAE threshold shifts were over 40 dB SPL 3 days after deafening in the saline group. The threshold shifts remained 6 weeks following deafening. **(C)** DPOAE threshold shifts trend for up to 6 weeks after surgery in the 5-aza and vehicle groups at 16 and 24 kHz. Negative values suggest hearing improvement. DPOAE threshold shifts in the vehicle group were close to zero, indicating that vehicle injection did not significantly change DPOAE threshold. Data are means ± SEM.

In contrast, mice treated with 4 mM 5-aza showed improved thresholds after the treatment (**Figures 4A,C**), suggesting that 5-aza treatment may lead to hearing function improvement. To evaluate outer hair cell function improvements, DPOAE thresholds of the 5-aza- and vehicle-treated mice were measured each week for up to 6 weeks following surgery and then compared against DPOAE thresholds right before the surgery (n = 6 mice per group; see section "Materials and Methods"). Similar to the analysis of ABR threshold shifts, DPOAE threshold improvements show a trend of 5–20 dB increase from 1 to 6 weeks after 5-aza injection (**Figure 4C**). In the vehicle-treated mice, limited DPOAE threshold shifts were observed after surgery in both frequencies (**Figure 4B**). **Table 3** shows DPOAE threshold shifts in the 5-aza and vehicle groups.

Two-way ANOVA analysis revealed significant difference at 16 kHz for the overall, treatment type (5-aza vs. vehicle), and follow-up period (1–6 weeks follow-up) effects: $F_{(5,\ 144)} = 2.828/p = 0.0182$, $F_{(1,\ 144)} = 125.6/p < 0.0001$, and $F_{(5,\ 144)} = 3.250/p = 0.0082$, respectively. These numbers became $F_{(5,\ 144)} = 2.648/p = 0.0254$, $F_{(1,\ 144)} = 93.14/p < 0.0001$, and $F_{(5,\ 144)} = 6.293/p < 0.0001$ for 24 kHz, respectively. In *post-hoc* comparison of the 5-aza and vehicle groups from 1 to 6 weeks follow-up at 16 kHz, p-values were 0.0011 and 0.0002 for 1- and 3-week posttreatment, whereas $p < 0.0001$ for 2-, 4-, 5-, and 6-week follow-ups. At 24 kHz, p-values were 0.0017, 0.0024, 0.0075, 0.0013, 0.0017, and <0.0001 for 1–6 weeks posttreatment in the comparison of the 5-aza and vehicle-treated groups, respectively.

To compare the 5-aza group threshold shift improvement among follow-up times, **Table 4** shows the significant difference in *post-hoc* analysis in both frequencies. DPOAE threshold improvements of the 5- and 6-week groups showed greater

TABLE 3 | Distortion-product otoacoustic emission (DPOAE) threshold shifts 1–6 weeks post-treatment.

Frequency (kHz)	Group	1-week	2-week	3-week	4-week	5-week	6-week
16	5-aza	−5.833 ± 1.346	−8.889 ± 1.554	−10 ± 1.904	−11.667 ± 1.904	−18.333 ± 2.692	−18.333 ± 2.692
	Vehicle	1.458 ± 1.346	1.667 ± 1.554	1.667 ± 1.904	0.417 ± 1.904	0.833 ± 2.692	1.667 ± 2.692
24	5-aza	−5.208 ± 1.267	−7.778 ± 1.463	−9.167 ± 1.792	−10.417 ± 1.792	−17.5 ± 2.534	−20 ± 2.534
	Vehicle	−0.833 ± 1.267	−0.278 ± 1.463	−0.833 ± 1.792	−0.833 ± 1.792	−4.167 ± 2.534	0.001 ± 2.534

Threshold shift (dB) was calculated as DPOAE threshold measured weekly after treatment minus DPOAE threshold prior to the treatment (3 days after deafening). Data are means ± SEM.

threshold improvements than the first 2 weeks groups (**Table 4**). No significant difference was observed in all the comparisons within the vehicle group in either frequency.

TABLE 4 | Statistical analysis of distortion-product otoacoustic emission (DPOAE) threshold shifts of the 5-aza group.

	16 kHz	24 kHz
6-week	vs. 1-week (***) vs. 2-week (*) vs. 3-week (0.116) vs. 4-week (0.330) vs. 5-week (1.000)	vs. 1-week (***) vs. 2-week (***) vs. 3-week (**) vs. 4-week (*) vs. 5-week (0.982)
5-week	vs. 1-week (***) vs. 2-week (*); vs. 3-week (0.116); vs. 4-week (0.330)	vs. 1-week (*); vs. 2-week (*); vs. 3-week (0.078); vs. 4-week (0.201)
4-week	vs. 1-week (0.123); vs. 2-week (0.869); vs. 3-week (0.990)	vs. 1-week (0.166); vs. 2-week (0.864); vs. 3-week (0.996)
3-week	vs. 1-week (0.474); vs. 2-week (0.998)	vs. 1-week (0.463); vs. 2-week (0.991)
2-week	vs. 1-week (0.673)	vs. 1-week (0.770)

*Pairwise comparison was performed by the Tukey test. P-values were stated in parentheses. *, **, and *** indicate $p < 0.05$, $p < 0.01$, and $p < 0.001$, respectively.*

DISCUSSION

In this study, DNA demethylating agent 5-aza was injected into chemically deafened mature mouse cochleae. Generation of new hair cells was observed in the 5-aza-treated mouse inner ear. The new hair cells expressed hair cell functional proteins, including espin and prestin. Expression of hair cell ribbon synaptic proteins CtBP2 and GluR2 was observed and analyzed. Functional evaluation by ABR and DPOAE assays revealed improved ABR and DPOAE thresholds in the 5-aza-treated mice, suggesting that these new hair cells may be functional. These data indicate that DNA demethylation facilitates the regeneration of functional hair cells in the young adult mouse.

The deafening method using the combination of kanamycin and furosemide in this study was shown to entirely damage outer hair cells at 3 days postdeafening (**Figure 1A**; Deng et al., 2019). In the 5-aza groups, outer hair cells were observed by the immunolabeling of myosin VIIa antibody 2–6 weeks after the treatment, indicating and confirming the regeneration of outer hair cells by the Dnmt1 inhibitor 5-aza (**Figures 1B,C**; Deng et al., 2019). The immunostaining of espin and prestin was both colabeled with myosin VIIa, indicating the functionality of hair bundles and outer hair cells by 5-aza treatment (**Figures 1B,C**). The irregular orientation observed from espin and prestin labeling is consistent with the previous results that the regenerated hair cell bundles were abnormal (Deng et al., 2019), suggesting recovered albeit compromised functionality of new hair cells.

Expression of CtBP2 and GluR2 puncta in myosin VIIa-expressing cells at 2 weeks following 5-aza treatment suggested the regeneration of hair cell ribbon synapse vesicles (**Figure 2A**). The numbers of CtBP2 and GluR2 puncta of the 5-aza-treated mice remained less than that of the normal hearing mice, suggesting that the synaptic connection of newly generated hair cells was not fully recovered. Notably, the 5-aza-treated mice showed the presence of hair cells in the inner hair cell region (**Figure 2A**). It has been found in our previous report that a few inner hair cells survived at 3 days after deafening and 5-aza was injected into the inner ear 3 days postdeafening (Deng et al., 2019). Therefore, in this and previous studies (Deng et al., 2019), hair cells observed at the inner hair cell region in the 5-aza-treated mice might be new hair cells or surviving/recovery of native inner hair cells, which deserves an independent study.

The hearing recovery was confirmed by ABR and DPOAE test. ABR assays showed the functional recovery of regenerated hair cells by 5-aza. Overall, the 5-aza-treated mice showed at least 5 dB SPL and no more than 30 dB SPL threshold improvements in pure-tone ABR measurements (**Figure 3C**). At all the studied frequencies ranging from 8 to 32 kHz, ABR thresholds exhibited a trend of increasing improvement from 1 to 6 weeks after 5-aza injection (**Figure 3C**), indicating that new hair cells with corresponding basilar membrane were able to respond to sound wave dispersion for their spatially separated frequencies selectivity. The greatest ABR threshold improvement was at 8 kHz and the smallest ABR threshold improvement was at 32 kHz (**Figure 3C**). These data were consistent with the previous report studying the outer hair cell regeneration in different cochlear turns (Deng et al., 2019), in which the majority of regenerated outer hair cells were in the apex and middle turns (Deng et al., 2019). Notably, in all investigated frequencies, significantly greater threshold improvements were usually observed 4–5 weeks post-5-aza treatment, suggesting that the functionality of regenerated hair cells became better over time, while during 1–3 weeks after 5-aza injection, the regeneration was progressing. It is noted that no significant difference in ABR threshold shifts was observed between the

5- and 6-week groups, which may indicate that the hair cell functionality regeneration reaches stability from 5 weeks after 5-aza injection.

DPOAE thresholds of the 5-aza mice at 16 and 24 kHz progressively improved from 5 to 16 dB from 1 to 6 weeks following surgery (**Figure 4C**). Furthermore, previous data revealed that the percentage of mice with regenerated hair cells increased from 1 to 2 weeks after the treatment and then decreased from 4 to 6 weeks following 5-aza treatment (Deng et al., 2019). Here, DPOAE thresholds in the 5-aza-treated mice exhibited continuous improvement from 1- to 6-week postsurgery in both frequencies. The reason for the inconsistency is obscure, but it may be because not all the regenerated outer hair cells are functional and that the functionality of new hair cells may not be linear with the number of new hair cells. Further experiments are required to understand the relationship between regenerated hair cells and their functionality. There are greater DPOAE threshold improvements at 24 kHz than 16 kHz by 6 weeks after 5-aza treatment (**Table 3**), which may indicate a better functionality of outer hair cells located in a relatively higher frequency area. Statistical analysis reveals that the 5-aza group showed significantly improved thresholds compared to the vehicle groups from 1 to 6 weeks after treatment in both frequencies. Within the 5-aza group, the threshold improvement of the 5- and 6-week groups was greater than the 1-week group (**Table 4**). These data may also suggest a continuously improved functionality of outer hair cells following 5-aza treatment.

In our previous study, the relative Dnmt1 mRNA expression levels were measured by quantitative real-time PCR in the 5-aza and vehicle treatment groups 2 weeks after the inner ear injection. The results showed that the Dnmt1 mRNA expression level of the 5-aza group was significantly lower than that of the vehicle group, suggesting that DNA demethylation and Dnmt1 inhibition may play a role in 5-aza-induced new hair cell generation (Deng et al., 2019). In this study, hearing function improvements were observed in the 5-aza group, but not in the vehicle treatment group. These data suggest that the hearing function improvement observed in this study may be related to 5-aza-induced DNA demethylation. Independent research is required to further detail the relationship between hearing function improvement and DNA demethylation.

This study aimed to determine the function of regenerated adult mammalian auditory hair cells stimulated by 5-aza, an epigenetic reprogramming approach. The results of this study suggest that the DNA demethylating agent 5-aza is capable of regenerating hair cells with recovered functionality, including expression of cell type-specific functional proteins, ribbon synapse proteins, and hearing functional improvement. This study may open avenues to develop novel methods to restore the function of mammalian hair cells to treat hearing loss. Outcomes of this study may be applied to other neurodegenerative diseases, which may provide insights into translation research to generate functional cells *via* epigenetics-based reprogramming.

DATA AVAILABILITY STATEMENT

The original contributions presented in the study are included in the article/supplementary material, further inquiries can be directed to the corresponding author.

ETHICS STATEMENT

The animal study was reviewed and approved by the Wayne State University Institutional Animal Care and Use Committee.

AUTHOR CONTRIBUTIONS

XD and ZH designed the project and wrote the manuscript, performed the experiment, and analyzed the data. Both authors have read the article and approved the final version of the manuscript.

FUNDING

This study was supported by the Veterans Affairs Merit Review Award (RX002100) and the Wayne State University Grants Plus Program (both to ZH).

ACKNOWLEDGMENTS

We thank Zhenjie Liu, Shuangshuang Lv, Li Tian, and Jingyun Sun for technical support, anti-myosin VIIa antibody from DSHB, anti-espin antibody from James Bartels, and valuable comments by Nathan Sim and Archana Singh to the manuscript.

REFERENCES

Bartles, J. R. (2000). Parallel actin bundles and their multiple actin-bundling proteins. *Curr. Opin. Cell Biol.* 12, 72–78. doi: 10.1016/s0955-0674(99)00059-9

Bohne, B. A., Yohman, L., and Gruner, M. M. (1987). Cochlear damage following interrupted exposure to high-frequency noise. *Hear. Res.* 29, 251–264. doi: 10.1016/0378-5955(87)90172-9

Chai, R., Kuo, B., Wang, T., Liaw, E. J., Xia, A., Jan, T. A., et al. (2012). Wnt signaling induces proliferation of sensory precursors in the postnatal mouse cochlea. *Proc. Natl. Acad. Sci. U. S. A.* 109, 8167–8172. doi: 10.1073/pnas.1202774109

Chen, W., Jongkamonwiwat, N., Abbas, L., Eshtan, S. J., Johnson, S. L., Kuhn, S., et al. (2012). Restoration of auditory evoked responses by human ES-cell-derived otic progenitors. *Nature* 490, 278–282. doi: 10.1038/nature11415

Chen, Y., Gu, Y., Li, Y., Li, G. L., Chai, R., Li, W., et al. (2021). Generation of mature and functional hair cells by co-expression of Gfi1, Pou4f3, and Atoh1 in the postnatal mouse cochlea. *Cell Rep.* 35:109016. doi: 10.1016/j.celrep.2021.109016

Dallos, P. (2008). Cochlear amplification, outer hair cells and prestin. *Curr. Opin. Neurobiol.* 18, 370–376. doi: 10.1016/j.conb.2008.08.016

Deng, X., and Hu, Z. (2020). Generation of cochlear hair cells from sox2 positive supporting cells via dna demethylation. *Int. J. Mol. Sci.* 21:8649. doi: 10.3390/ijms21228649

Deng, X., Liu, Z., Li, X., Zhou, Y., and Hu, Z. (2019). Generation of new hair cells by DNA methyltransferase (Dnmt) inhibitor 5-azacytidine in a chemically-deafened mouse model. *Sci. Rep.* 9:7997. doi: 10.1038/s41598-019-44313-0

György, B., Sage, C., Indzhykulian, A. A., Scheffer, D. I., Brisson, A. R., Tan, S., et al. (2017). Rescue of hearing by gene delivery to inner-ear hair cells using exosome-associated AAV. *Mol. Ther.* 25, 379–391. doi: 10.1016/j.ymthe.2016.12.010

Hawkins, J. E., Johnsson, L. G., Stebbins, W. C., Moody, D. B., and Coombs, S. L. (1976). Hearing loss and cochlear pathology in monkeys after noise exposure. *Acta Otolaryngol.* 81, 337–343. doi: 10.3109/00016487609119971

Hu, Z., Komal, F., Singh, A., and Meng, D. (2021). Generation of a spiral ganglion neuron degeneration mouse model. *Front. Cell Dev. Biol.* 9:761847. doi: 10.3389/fcell.2021.761847

Hudspeth, A. J. (1989). How the ear's works work. *Nature* 341, 397–404.

Hudspeth, A. J. (2008). Making an effort to listen: mechanical amplification in the Ear. *Neuron* 59, 530–545. doi: 10.1016/j.neuron.2008.07.012

Isgrig, K., Shteamer, J. W., Belyantseva, I. A., Drummond, M. C., Fitzgerald, T. S., Vijayakumar, S., et al. (2017). Gene therapy restores balance and auditory functions in a mouse model of usher syndrome. *Mol. Ther.* 25, 780–791. doi: 10.1016/j.ymthe.2017.01.007

Jones, P. A., and Takai, D. (2001). The role of DNA methylation in mammalian epigenetics. *Science* 293, 1068–1071. doi: 10.1126/science.1063852

Koehler, K. R., Nie, J., Longworth-Mills, E., Liu, X. P., Lee, J., Holt, J. R., et al. (2017). Generation of inner ear organoids containing functional hair cells from human pluripotent stem cells. *Nat. Biotechnol.* 35, 583–589. doi: 10.1038/nbt.3840

Layman, W. S., and Zuo, J. (2015). Epigenetic regulation in the inner ear and its potential roles in development, protection, and regeneration. *Front. Cell. Neurosci.* 8:446. doi: 10.3389/fncel.2014.00446

Li, Y., Jia, S., Liu, H., Tateya, T., Guo, W., Yang, S., et al. (2018). Characterization of hair cell-like cells converted from supporting cells after notch inhibition in cultures of the organ of corti from neonatal gerbils. *Front. Cell. Neurosci.* 12:73. doi: 10.3389/fncel.2018.00073

Liberman, L. D., Wang, H., and Liberman, M. C. (2011). Opposing gradients of ribbon size and AMPA receptor expression underlie sensitivity differences among cochlear-nerve/hair-cell synapses. *J. Neurosci.* 31, 801–808. doi: 10.1523/JNEUROSCI.3389-10.2011

Liberman, M. C., Gao, J., He, D. Z., Wu, X., Jia, S., and Zuo, J. (2002). Prestin is required for electromotility of the outer hair cell and for the cochlear amplifier. *Nature* 419, 300–304. doi: 10.1038/nature01059

Matthews, G., and Fuchs, P. (2010). The diverse roles of ribbon synapses in sensory neurotransmission. *Nat. Rev. Neurosci.* 11, 812–822. doi: 10.1038/nrn2924

Nist-Lund, C. A., Pan, B., Patterson, A., Asai, Y., Chen, T., Zhou, W., et al. (2019). Improved TMC1 gene therapy restores hearing and balance in mice with genetic inner ear disorders. *Nat. Commun.* 10:236.

Nouvian, R., Beutner, D., Parsons, T. D., and Moser, T. (2006). Structure and function of the hair cell ribbon synapse. *J. Membr. Biol.* 209, 153–165. doi: 10.1007/s00232-005-0854-4

Oshima, K., Shin, K., Diensthuber, M., Peng, A. W., Ricci, A. J., Heller, S., et al. (2010). Mechanosensitive hair cell-like cells from embryonic and induced pluripotent stem cells. *Cell* 141, 704–716. doi: 10.1016/j.cell.2010.03.035

Parham, K., Sun, X. M., and Kim, D. O. (1999). Distortion product otoacoustic emissions in the CBA/J mouse model of presbycusis. *Hear. Res.* 134, 29–38. doi: 10.1016/s0378-5955(99)00059-3

Santos-Sacchi, J., and Dilger, J. P. (1988). Whole cell currents and mechanical responses of isolated outer hair cells. *Hear. Res.* 35, 143–150. doi: 10.1016/0378-5955(88)90113-x

Squires, K. C., Chu, N. S., and Starr, A. (1978). Acute effects of alcohol on auditory brainstem potentials in humans. *Science* 201, 174–176. doi: 10.1126/science.208148

Tadros, S. F., D'Souza, M., Zettel, M. L., Zhu, X., and Frisina, R. D. (2007a). Glutamate-related gene expression changes with age in the mouse auditory midbrain. *Brain Res.* 1127, 1–9. doi: 10.1016/j.brainres.2006.09.081

Tadros, S. F., D'Souza, M., Zettel, M. L., Zhu, X., Lynch-Erhardt, M., Frisina, R. D., et al. (2007b). Serotonin 2B receptor: upregulated with age and hearing loss in mouse auditory system. *Neurobiol. Aging* 28, 1112–1123. doi: 10.1016/j.neurobiolaging.2006.05.021

Uthaiah, R. C., and Hudspeth, A. J. (2010). Molecular anatomy of the hair cell's ribbon synapse. *J. Neurosci.* 30, 12387–12399. doi: 10.1523/JNEUROSCI.1014-10.2010

White, P. M., Doetzlhofer, A., Lee, Y. S., Groves, A. K., and Segil, N. (2006). Mammalian cochlear supporting cells can divide and trans-differentiate into hair cells. *Nature* 441, 984–987. doi: 10.1038/nature04849

World Health Organization (2021). *World Report on Hearing. World Report on Hearing*. Geneva: WHO.

Zheng, J. L., Shou, J., Guillemot, F., Kageyama, R., and Gao, W. Q. (2000b). Hes1 is a negative regulator of inner ear hair cell differentiation. *Development* 127, 4551–4560.

Zheng, J., Shen, W., He, D. Z., Long, K. B., Madison, L. D., Dallos, P., et al. (2000a). Prestin is the motor protein of cochlear outer hair cells. *Nature* 405, 149–155.

Zhou, Y., and Hu, Z. (2016). Epigenetic DNA demethylation causes inner ear stem cell differentiation into hair cell-like cells. *Front. Cell. Neurosci.* 10:185. doi: 10.3389/fncel.2016.00185

Conflict of Interest: The authors declare that the research was conducted in the absence of any commercial or financial relationships that could be construed as a potential conflict of interest.

Publisher's Note: All claims expressed in this article are solely those of the authors and do not necessarily represent those of their affiliated organizations, or those of the publisher, the editors and the reviewers. Any product that may be evaluated in this article, or claim that may be made by its manufacturer, is not guaranteed or endorsed by the publisher.

Copyright © 2022 Deng and Hu. This is an open-access article distributed under the terms of the Creative Commons Attribution License (CC BY). The use, distribution or reproduction in other forums is permitted, provided the original author(s) and the copyright owner(s) are credited and that the original publication in this journal is cited, in accordance with accepted academic practice. No use, distribution or reproduction is permitted which does not comply with these terms.

frontiers in Cellular Neuroscience

ORIGINAL RESEARCH
published: 28 March 2022
doi: 10.3389/fncel.2022.812887

Metabolic Reprogramming in HIV-Associated Neurocognitive Disorders

*Charles N. S. Allen[1], Sterling P. Arjona[1], Maryline Santerre[1], Claudio De Lucia[2], Walter J. Koch[2] and Bassel E. Sawaya[1,3,4]**

[1] Molecular Studies of Neurodegenerative Diseases Lab, Fels Cancer Institute for Personalized Medicine, Lewis Katz School of Medicine, Temple University, Philadelphia, PA, United States, [2] Department of Cardiovascular Sciences, Lewis Katz School of Medicine, Temple University, Philadelphia, PA, United States, [3] Department of Cancer and Cellular Biology, Lewis Katz School of Medicine, Temple University, Philadelphia, PA, United States, [4] Department of Neural Sciences, Lewis Katz School of Medicine, Temple University, Philadelphia, PA, United States

A significant number of patients infected with HIV-1 suffer from HIV-associated neurocognitive disorders (HAND) such as spatial memory impairments and learning disabilities (SMI-LD). SMI-LD is also observed in patients using combination antiretroviral therapy (cART). Our lab has demonstrated that the HIV-1 protein, gp120, promotes SMI-LD by altering mitochondrial functions and energy production. We have investigated cellular processes upstream of the mitochondrial functions and discovered that gp120 causes metabolic reprogramming. Effectively, the addition of gp120 protein to neuronal cells disrupted the glycolysis pathway at the pyruvate level. Looking for the players involved, we found that gp120 promotes increased expression of polypyrimidine tract binding protein 1 (PTBP1), causing the splicing of pyruvate kinase M (PKM) into PKM1 and PKM2. We have also shown that these events lead to the accumulation of advanced glycation end products (AGEs) and prevent the cleavage of pro-brain-derived neurotrophic factor (pro-BDNF) protein into mature brain-derived neurotrophic factor (BDNF). The accumulation of proBDNF results in signaling that increases the expression of the inducible cAMP early repressor (ICER) protein which then occupies the cAMP response element (CRE)-binding sites within the BDNF promoters II and IV, thus altering normal synaptic plasticity. We reversed these events by adding Tepp-46, which stabilizes the tetrameric form of PKM2. Therefore, we concluded that gp120 reprograms cellular metabolism, causing changes linked to disrupted memory in HIV-infected patients and that preventing the disruption of the metabolism presents a potential cure against HAND progression.

Keywords: HIV gp120, glycolysis, memory, neurons, metabolic reprogramming, advanced glycation end-product

OPEN ACCESS

Edited by:
Fu-Chin Liu,
National Yang Ming Chiao Tung University, Taiwan

Reviewed by:
Prasun K. Datta,
Tulane University, United States
Howard Eliot Gendelman,
University of Nebraska Medical Center, United States

***Correspondence:**
Bassel E. Sawaya
sawaya@temple.edu

Specialty section:
This article was submitted to Cellular Neuropathology, a section of the journal Frontiers in Cellular Neuroscience

Received: *10 November 2021*
Accepted: *21 February 2022*
Published: *28 March 2022*

Citation:
Allen CNS, Arjona SP, Santerre M, De Lucia C, Koch WJ and Sawaya BE (2022) Metabolic Reprogramming in HIV-Associated Neurocognitive Disorders. Front. Cell. Neurosci. 16:812887. doi: 10.3389/fncel.2022.812887

INTRODUCTION

Patients infected with HIV-1 suffer from neurocognitive defects that persist even after the implementation of cART (Heaton et al., 2011). These defects range from asymptomatic conditions and mild disorders to more severe such as spatial memory impairment and learning difficulties (SMI-LD) (Woods et al., 2009). These symptoms result from released viral proteins shed from

infected cells or defective proviruses. Studies revealed the presence of viral proteins like gp120 in the cerebrospinal fluid (CSF) of infected patients (Desplats et al., 2013). Studies also described the neuronal damage caused by these viral proteins (Santerre et al., 2019, 2021; Speidell et al., 2020).

HIV-1 gp120 is the envelope protein that allows HIV-1 virions to associate with host receptors (CD4+) and co-receptors (CCR5 and CXCR4) (Chen, 2019). HIV-1 gp120 is released from infected cells and taken up by neurons contributing to neuronal dysfunction (Berth et al., 2015). Some described gp120 as toxic to neurons *via* the activation of the NMDA receptor, increased calcium uptake, induction of the oxidative stress (OS) pathway, and the release of lipids from cellular membranes (Fields et al., 2016). Gp120 can also alter mitochondrial functions and mitochondria-axonal transport, contributing to neurocognitive dysfunctions (Berth et al., 2015; Fields and Ellis, 2019). Further, the addition of gp120 to neurons results in increased mitochondrial fragmentation due to incomplete mitophagy. This damage alters mitochondrial dynamics and is associated with the development of HAND (Teodorof-Diedrich and Spector, 2018, 2020). The mechanisms remain unclear; however, it has been suggested that miRNA may be a critical player. Indeed, treatment of the cells with either gp120 or Tat proteins induces several miRNAs. Further, the presence of gp120 increases shuttling of miRNA between HIV infected macrophages and surrounding cells that can cause cellular changes (Yuan et al., 2019). We showed that neurons switch from reliance on mitochondrial-associated respiration to glycolysis, which is partly due to incomplete mitophagy. Finally, gp120 was reported to alter synaptic plasticity through cAMP response element-binding (CREB) protein signaling (Zhou et al., 2016).

Several labs, including ours, showed that HIV-1 proteins reprogram the metabolism. Through metabolic reprogramming, HIV-1 creates an environment conducive to replication through biochemical and structural changes in the host cell (Thaker et al., 2019). Other viruses use this pathway to change the host cell environment (Polcicova et al., 2020). Metabolic reprogramming is a mechanism observed in diseases like cancer, viral infections, and many neurodegenerative diseases (Medina, 2020; Polcicova et al., 2020; Han et al., 2021). This pathway remains to be elucidated in neurons affected by HIV-1 proteins.

Using LUHMES (behave as dopaminergic neurons) (Slanzi et al., 2020), we identified the pathway used by HIV gp120 protein leading to metabolic reprogramming. These results contribute to a therapeutic approach that inhibits metabolic reprogramming and ultimately prevents memory impairment associated with HIV-1 infections.

MATERIALS AND METHODS

Cell Culture and Treatments

Lund human mesencephalic cells (LUHMES) were received from ATCC (cat. No. CRL-2927) and cultured as previously described (Scholz et al., 2011). LUHMES are human embryonic neural precursor cells that are immortalized and proliferative due to a transgenic *v*-myc expressed under a tetracycline-regulated off (Tet-off) promoter (Lotharius et al., 2002). LUHMES can be differentiated into post-mitotic mature dopaminergic-like neurons and express markers of mature neurons after 5 days of treatment with tetracycline (Scholz et al., 2011).

Cell culture plates were coated with 50 μg/ml poly-L-ornithine (PLO) and 1 μg/ml fibronectin overnight at 37°C. LUHMES were then maintained in a growth medium containing DMEM/F12 supplemented with 2 mM L-glutamine, 1× N2-supplement, and 40 ng/ml recombinant human fibroblast growth factor (FGF). All cells were used under 20 passages and were differentiated using a medium that consisted of DMEM/F12 supplemented with 2 mM L-glutamine, 1× N2-supplement, 1 μg/ml doxycycline, and 2 ng/ml recombinant human glial neurotrophic factor (GDNF). After 1 day of differentiation, cells were split 1:2 and allowed to continue differentiating until day 6.

HIV-1 gp120 Treatments

Recombinant HIV-1IIIB gp120 (clade B) protein was kindly received from the NIH AIDS Reagent Program. Samples were treated for 8 h using 100 ng/ml concentration.

Chemical Reagents

Tepp-46 (ML-265) is a potent and selective pyruvate kinase M2 (PKM2) tetramer stabilizer. Echinomycin *Streptomyces* sp. (ES) and PX-12 are both HIF-1α inhibitors. LUHMES were treated with 10 nM of Tepp-46 (purchased from VWR), 10 μM of ES (purchased from Thomas Scientific), or 10 μM of PX-12 (purchased from Thomas Scientific). A dose-response curve was conducted to determine the working concentration of Tepp-46 in LUHMES by using a pyruvate assay. The dose curve was done using undifferentiated LUHMES since undifferentiated cells express more PKM2 over PKM1 to facilitate proliferation (Zheng et al., 2016).

Western Blot Assay

Proteins were extracted using radioimmunoprecipitation assay (RIPA) lysis buffer (25 mM Tris-HCl pH 7.6, 150 mM NaCl, 1% Triton x-100, 0.1% SDS, and 1× protease inhibitor cocktail). Protein concentrations were estimated using a bicinchoninic acid (BCA) assay (Thermo Fisher Scientific, Waltham, MA, United States). Western blot was performed using 20 μg of extracts per well. Antibodies used and the concentrations are as follows: PKM1 (1/1000; D30G6), PKM2 (1/1000; D78A4), CREB (1/1000; 48H2) (Cell Signaling, Danvers, MA, United States); PTBP1 (1/1000; 12582-1-Ap), Furin (1/500; 18413-1-Ap) (Proteintech, Rosemont, IL, United States); ICER (1 μg/ml; WH0001390M2), secondary anti-mouse (1/5000; 71045-3), secondary anti-rabbit (1/10000; AP187P) (Sigma-Aldrich, St. Louis, MO, United States); brain-derived neurotrophic factor (BDNF) (2 μg/ml; ab10505) (Abcam, Cambridge, United Kingdom); proBDNF (1/400; ant-006) (Allomone); and H3 (0.5 μg/ml; A01502) (GenScript, Piscataway, NJ, United States). The densitometry ratios of the

bands were determined using ImageJ and were normalized to loading control, H3.

Immunoprecipitation of Brain-Derived Neurotrophic Factor and Pro-brain-Derived Neurotrophic Factor

Differentiated LUHMES were treated with gp120, Tepp-46, or both gp120 and Tepp-46 for 8 h. The cell media was collected and concentrated using Advanced Centrifugal Devices with 1K MWCO (Pall Corporation, MAP001C36). The concentrated media was then added to either prepared anti-mouse IgG Dynabeads (Invitrogen, Waltham, MA, United States, 11201D) or anti-rabbit IgG Dynabeads (Invitrogen, Waltham, MA, United States, 11203D) and then rotated at 4°C overnight. Dynabeads were prepared following the manufacturer's protocol. Briefly, 50 μl of beads were used per 250 μg of sample media. The beads were washed in washing buffer, and then 4 μg of either anti-BDNF or anti-proBDNF antibodies were added to the beads, and samples were rotated at 4°C overnight. The next day the samples were washed and eluted in a 5× SDS loading buffer, and then eluted samples were used for a western blot analysis.

RNA Extraction

Total RNA was extracted from samples using a SurePrep TrueTotal RNA purification kit (Fisher Bioreagents, BP2800-50). A NanoDrop 2000 spectrophotometer (Thermo Scientific) was used to determine the purity and concentration of the RNA extracted.

qPCR Assay

cDNA was synthesized from collected RNA using the SuperScript IV VILO cDNA Master Mix with ezDNase (Invitrogen, Waltham, MA, United States, 11766050). The following primers (purchased from IDT) were used: HIF-1α: (F) 5′-gaacgtcgaaaagaaaagtctcg -3′; (R) 5′-ccttatcaagatgcgaactcaca-3′. ICER: (F) 5′-acagtacgcagcacaatcag-3′; (R) 5′-ctggtaagttggcatgtcacc-3′. PTBP1: (F) 5′-aatgacaagagccgtgactac-3′; (R) 5′-ggaaccagctcctgca tac-3′. PKM1: (F) 5′-cgagcctcaagtcactccac-3′; (R) 5′-acgacgtcaccccggtattagc-3′. PKM2: (F) 5′-attatttga ggaactccgccgcct-3′; (R) 5′-attccgggtcacagcaatgatgg-3′. BDNF: (F) 5′-caggggcatagacaaaag-3′; (R) 5′-cttcc ccttttaatgg tc-3′. GAPDH: (F) 5′-caaggctgagaacgggaag-3′; (R) 5′-tgaagacgccagtggactc-3′. All qPCR was performed using FastStart Universal SYBR Green (Roche, 04913914001) according to the manufacturer's instructions. The relative quantitation of mRNA was performed using the comparative ΔΔCt method, and all results are compared to that of the control group and GAPDH.

Chromatin Immunoprecipitation Assay

Differentiated LUHMES were treated with 100 ng/ml of recombinant gp120 protein for 8 h. Formaldehyde was then added to the cells at a final concentration of 0.75% and incubated for 10 min. Cross-linking was stopped by the addition of glycine (125 mM final concentration) and incubated for 5 min. Cells were then rinsed with cold PBS and collected in 5 ml of cold PBS. Samples were centrifuged (1,000 *g*) for 5 min at 4°C. The supernatant was removed, and the pellet was resuspended in ChIP lysis buffer (50 mM HEPES, 140 mM NaCl, 2 mM EDTA, 1% NP-40, 0.5% Sodium Deoxycholate, 0.1% SDS, and protease inhibitors) and incubated on ice for 10 min. Samples were then sonicated to achieve DNA fragmentation between 200 and 1,000 bp, centrifuged (8,000 *g*) for 10 min at 4°C. The supernatant was removed and used for immunoprecipitation (IP). 10 μg of CREB antibody were added to 25 μg of DNA, diluted 1:20 in RIPA buffer, then rotated at 4°C for 1 h. Next, Dynabeads were added to each sample and rotated at 4°C overnight. The following day, samples were washed in a low salt wash buffer (0.1% SDS, 1% Triton X-100, 2 mM EDTA, 20 mM Tris-HCl, 150 mM NaCl) and then eluted in 120 μl of elution buffer (1% SDS, 100 mM NaHCO3). 4.8 μl of 5 M NaCl and 2 μl of RNase A (10 mg/ml) were added to eluted samples and incubated at 65°C overnight. The following day, 2 μl of proteinase K (20 mg/ml) was added and incubated at 60°C for 1 h. DNA levels were measured by qPCR using the following primers: hBDNF promoter II: (F) 5′-gagtcccattcagcaccttgga-3′; (R) 5′-atctcagtg tgagccgaacct-3′, and hBDNF promoter IV: (F) 5′-agagtgtctatttcgaggcagc-3′; (R) 5′-aatgggaaagtgggtggg agt-3′.

Oxygen Consumption Rate Test

Changes in oxygen consumption after gp120 treatment were analyzed using the XFe96 Seahorse Analyzer from Agilent Technologies. LUHMES were differentiated for 5 days, then split onto a PLO/fibronectin-coated XFe96-well microplate and were cultured overnight. On the experiment day, the growth medium was replaced with an XF assay medium containing DMEM supplemented with 10 mM glucose, 4 mM L-glutamine, and 2 mM sodium pyruvate and allowed to incubate at 37°C in an incubator without the addition of carbon dioxide. Extracellular acidification rate (ECAR) and oxygen consumption rate (OCR) measurements were made at basal conditions and in response to 1 μM Oligomycin, 1.5 μM FCCP, and 1 μM rotenone/1 μM antimycin A (Delp et al., 2019).

Metabolomic Analysis

LUHMES cells were cultured in a differentiation medium for 5 days. Then the medium was switched to a glucose-free differentiation medium with the addition of D-Glucose-13C6 (Aldrich, 389374-250MG) for an additional 24 h. Eight hours before collection, 100 ng/ml of recombinant gp120 protein were added to the cells. Control untreated cells were also cultured in an unlabeled differentiation medium lacking D-Glucose-13C6. The polar metabolites were collected using an ice-cold extraction solution of 80% methanol and 20% water. As previously described, samples were analyzed at the Proteomics and Metabolomics Center at the Wistar Institute in Philadelphia (Di Marcantonio et al., 2021). Raw data were normalized to total protein recovered from the polar metabolites and analyzed using MetaboAnalyst 5.0 online software[1].

Pyruvate Assay

A fluorometric Pyruvate Assay Kit (Cayman Chemical, C789C04) was used to determine pyruvate production. Differentiated LUHMES cells were treated with gp120, Tepp-46, or gp120 and

[1] www.metaboanalyst.ca/

Tepp-46 for 8 h. Cells were collected, and the experiment was performed following the manufacturer's protocol. Values were normalized to the cell count of each sample.

Methylglyoxal Assay

Methylglyoxal concentration was determined using a PriceProbe^{TM} Methylglyoxal Assay Kit (Fluorometric) (K461-100, BioVision). Differentiated LUHMES cells were treated with gp120, Tepp-46, or gp120 and Tepp-46 for 8 h. The cells were collected, and the experiment was processed following the manufacturer's protocol.

ATP Concentration Assay

Following the manufacturer's protocol, ATP concentrations were determined using an ATP Determination Kit (a22066 Invitrogen, Waltham, MA, United States). Differentiated LUHMES cells were treated with gp120, Tepp-46, or gp120 and Tepp-46 for 8 h. The cells were collected, centrifuged (800 *g*) for 5 min, and the supernatant was removed. 500 μl of boiling dH2O was added to the pellet, and the samples were centrifuged again (12,000 *g*) for 10 min before collecting the supernatant. 10 μl of sample per 100 μl final volume was used. ATP concentration was determined and normalized to the cell count of each sample.

Human Advanced Glycation End-Products ELISA

Advanced glycation end-product (AGE) concentrations were measured using Immunotag Human AGEs ELISA kit (G biosciences, cat# IT1931) following the manufacturer's protocol. Differentiated LUHMES were treated with gp120, Tepp-46, or gp120 and Tepp-46 for 8 h. Cells were collected, centrifuged (800 g) for 5 min, and the supernatant was removed. 100 μl of RIPA buffer with protease inhibitors were added to the cells and rotated at 4°C for an hour. The ELISA plate was prepared and washed following the manufacturer's protocol. The samples were diluted in Sample Dilution buffer at a dilution of 1:5, and the diluted samples were added to the wells and incubated at 37°C for 90 min. After 90 min, the biotin detection antibody was added to the wells. The plate was then re-incubated for an additional 60 min at 37°C. Next, HRP-Streptavidin Conjugate was added and incubated at 37°C for 30 min. The TMB Substrate was then added and incubated at 37°C for 15 min in the dark. After the reaction achieved optimal levels determined by the color of the reaction in the standard curve wells, Stop Solution was added, and the plate was read at 450 nm. Concentrations were derived from the standard curve, and samples were normalized to dilution factor and cell count.

The BDNF IP samples were prepared as previously described (Wu et al., 2021). The samples were prepared following the above IP protocol; however, the beads were eluted in 100 μL of 0.1% trifluoroacetic acid (TFA) solution and incubated in a 37°C water bath for 30 min. Samples were then added to the ELISA plate undiluted, and the above ELISA protocol was followed.

Statistical Analysis

All the experiments were repeated at least in triplicate. Statistical analysis was performed using a one-way analysis of variance (ANOVA) or a student's *t*-test. Data are expressed as the mean with ±1 standard deviation (S.D.). Results were judged statistically significant if $p < 0.05$ by analysis of variance (marked in the figures as $^{*}p < 0.05$, $^{**}p < 0.01$, $^{***}p < 0.001$, $^{****}p < 0.0001$ where needed). Data were plotted using GraphPad Prism version 7.0.

RESULTS

gp120 Promotes a Decrease in Mitochondrial Oxygen Consumption

This study uses LUHMES as our cellular model since metabolic reprogramming is a significant driver of proliferation in cancer cells and is observed in other cell lines such as SH-SY5Y neuroblastoma cells commonly used to study neurodegeneration (Phan et al., 2014). Once LUHMES are differentiated, they no longer display the metabolic reprogramming needed to sustain growth; this allows us to observe any metabolic changes attributed to gp120 (Delp et al., 2019).

Previously, our lab and others have demonstrated that the addition of gp120 to neurons causes a decrease in ATP production and disruption in mitochondrial movement (Avdoshina et al., 2016). These alterations in mitochondrial functions suggest that mitochondrial metabolism is altered with gp120 treatment. To discover any changes in mitochondrial metabolism due to gp120, we measured the oxygen consumption rate (OCR) of differentiated LUHMES treated with 100 ng/ml of recombinant gp120 using a Seahorse Mito Stress Test. **Figure 1A** illustrates a typical Mito Stress Test and the results and interpretation of the oxygen consumption data.

The addition of gp120 decreases OCR associated with maximal respiration compared to the control untreated cells (**Figures 1B,C**). The maximal oxygen consumption measures the maximum capacity of the electron transport chain that the cells can achieve. Any decrease in maximum respiration rate is a sign of mitochondrial damage or decreased ability to progress through the electron transport chain (Gu et al., 2020).

The percentage of spare respiration capacity also decreases in the presence of gp120 (**Figure 1C**). The spare respiration capacity is a measurement of the difference between maximum respiratory capacity and basal respiratory capacity. The spare respiration capacity is crucial in cellular states where the energy demand exceeds the energy supply, for instance, in a state of increased neuronal activity (Pfleger et al., 2015). The decrease in spare respiration capacity, sometimes referred to as the reserve respiratory capacity (RRC), is associated with neuronal disease and cell death (Yadava and Nicholls, 2007). It has been discovered that one of the major factors in spare respiration capacity and maximum respiratory capacity is the availability of substrates to enter the TCA cycle (Sansbury et al., 2011).

These measurements suggest that gp120 causes a decrease in oxygen consumption associated with aerobic mitochondrial metabolism during a high energy-demanding state. In addition, they suggest that gp120 causes a decrease in mitochondrial oxidative phosphorylation (OXPHOS) and a decrease in ATP production associated with the mitochondria electron transport chain.

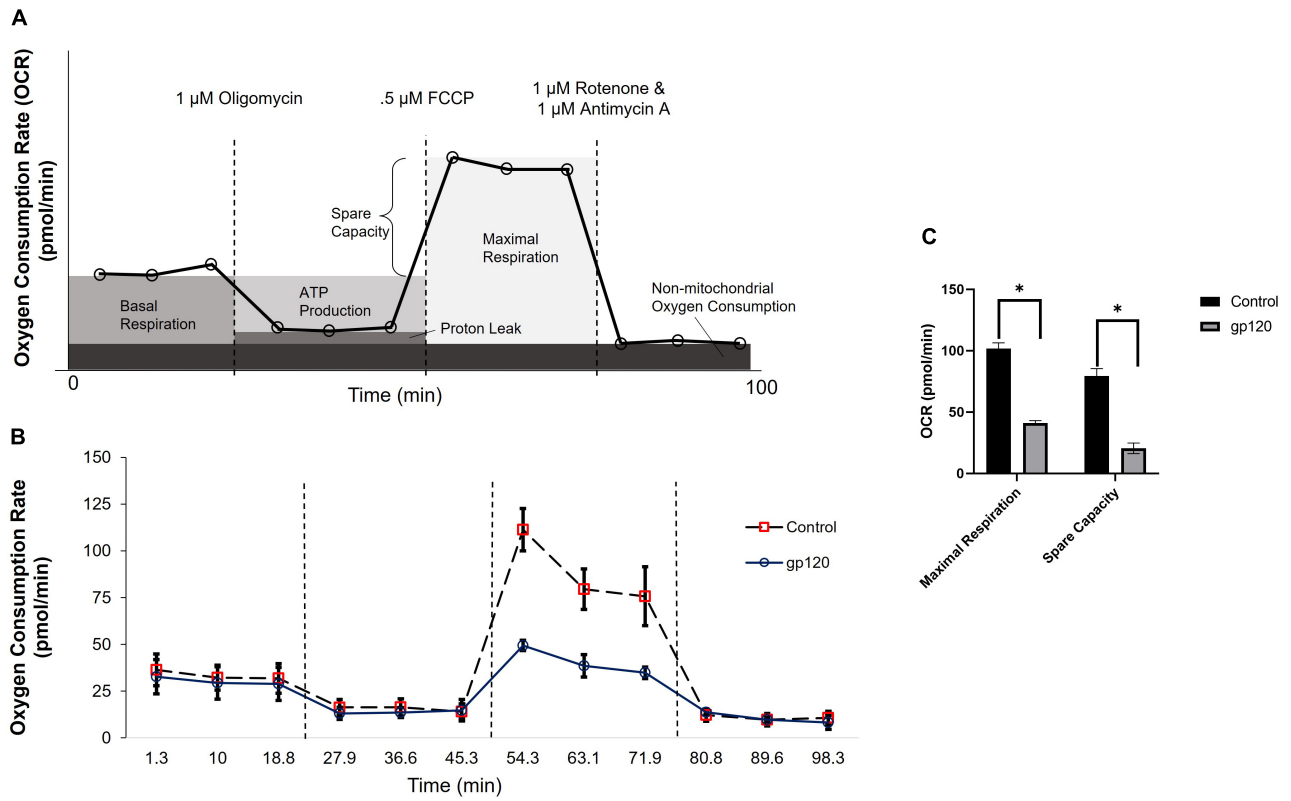

FIGURE 1 | gp120 alters mitochondrial maximal respiration. **(A)** A schematic of typical results from a Seahorse Mito Stress Test showing the interpretation of each measurement taken at different time points. **(B)** Measurement of oxygen consumption rate (OCR) in LUHMES cells untreated (dotted lane/red squares) or treated with 100 ng/ml of gp120 protein (solid lane/black circles) for 8 h using a Seahorse XFe96 analyzer and a Mito stress test kit from Seahorse. Oligomycin, FCCP, and rotenone/antimycin (dotted lines) were added at 23, 50, and 75 min, respectively. **(C)** Graph displaying the maximal respiration and spare capacity measured (pmol/min) in LUHMES untreated or treated with gp120. Values derived from the Seahorse analyzer and computed using Seahorse software were considered statistically significant (*$p < 0.05$).

gp120 Changes Metabolite Levels Indicative of Metabolic Reprogramming

It has been discovered that one of the major factors that regulate spare respiration capacity and maximum respiratory capacity is the availability of substrates to enter the TCA cycle (Sansbury et al., 2011). Pyruvate is the primary substrate for mitochondrial-associated respiration and is produced in the last step of glycolysis. Other than pyruvate, many other substrates can fuel mitochondrial respiration, for example, glutamate or malate.

To explore changes in TCA cycle substrates that could contribute to the decrease in mitochondrial OXPHOS observed in the Seahorse Mito Stress test, we performed a metabolomic mass spectrometry analysis on differentiated LUHMES treated with 100 ng/ml of recombinant gp120.

In the gp120 treated LUHMES, we observe an increase in glycolysis-associated metabolites and a decrease in TCA-associated metabolites compared to the untreated cells (**Figures 2A,B**). More specifically, we see an increase in glucose, glucose-6-phosphate (G6P), fructose-1,6-biphosphate (FBP), glyceraldehyde-3-phosphate (G3P), 3-phosphoglycerate (3PG), phosphoenolpyruvate (PEP), and lactate (**Figure 2B**). However, we do observe a decrease in Pyruvate (**Figure 2B**). Additionally, we observe a decrease in ATP and a corresponding increase in ADP (**Figures 2C,D**).

Besides the apparent increase in aerobic glycolysis, we also see TCA cycle rewiring, another hallmark of metabolic reprogramming in our gp120 treated LUHMES (**Figure 3**). We observed decreases in many TCA cycle-associated metabolites, including *cis*-aconitic acid, 2-oxoglutarate, and succinate, indicating decreased TCA cycle possible due to the decrease in pyruvate (**Figure 3**). The decrease in TCA metabolites and the decrease in pyruvate correlate with a reduction in OXPHOS and reduced mitochondrial respiration. Fumarate also decreases but the change is not significant.

However, we also see an increase in some TCA cycle metabolites, citrate, and a slight increase in malate, but it is not significant (**Figure 3**). Both citrate and malate are commonly upregulated metabolites in metabolic reprogramming (Williams and O'Neill, 2018). The increase in citrate and malate indicates a rewiring of the TCA cycle that allows for acetyl-CoA production to fuel fatty acid synthesis and to continue to fuel the TCA cycle when pyruvate production is altered (**Figure 3**) (Saggerson, 2008).

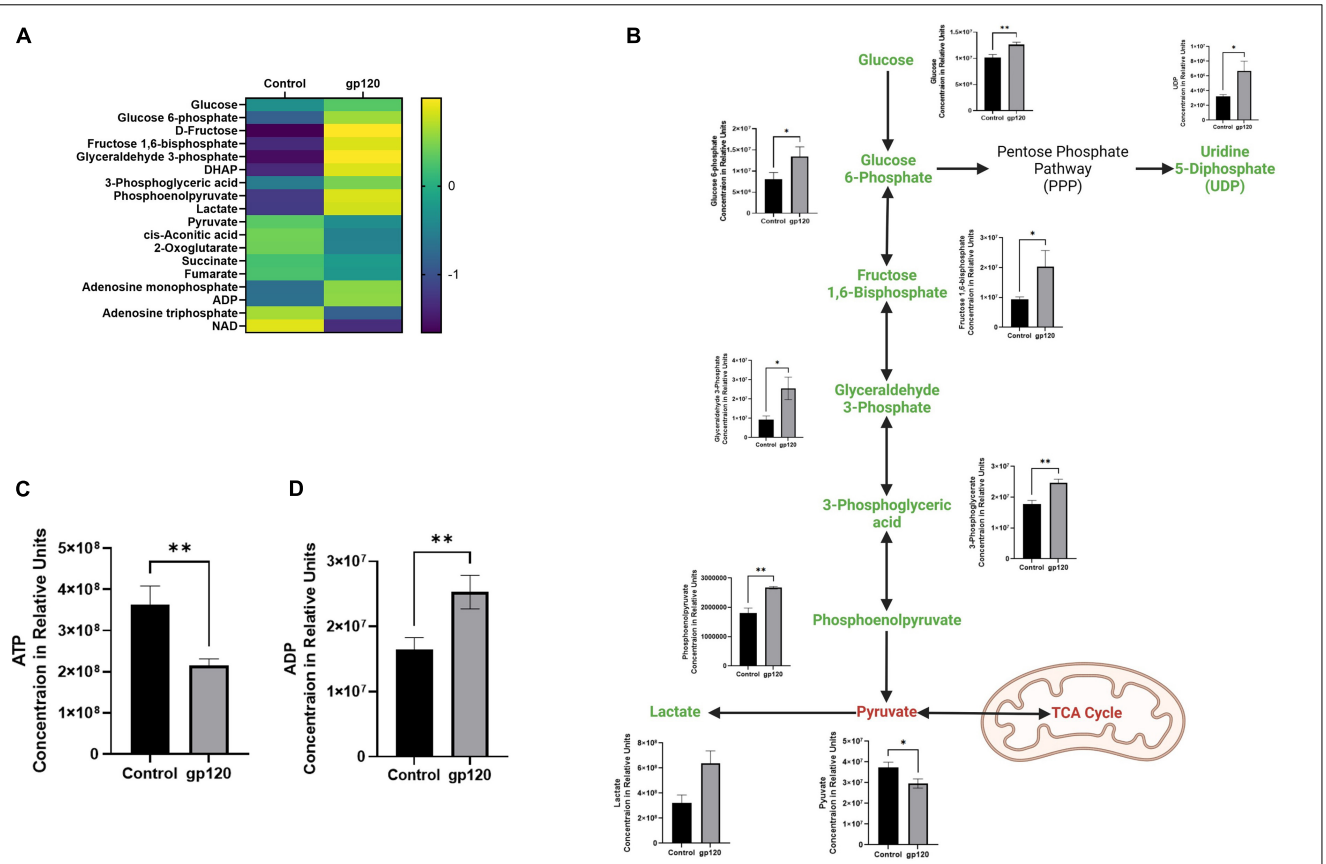

FIGURE 2 | Alterations in glycolysis after gp120 treatment. **(A)** Differential expression of metabolites measured in untreated and gp120-treated LUHMES cells in triplicate by metabolomic analysis. ($p < 0.05$). **(B)** Glycolysis pathway with metabolites that are upregulated (green) and downregulated (red) in LUHMES treated with gp120 compared to control cells. Graphs next to each metabolite show changes in associated metabolites between control and gp120 treated LUHMES. **(C)** ATP and **(D)** ADP concentrations in LUHMES treated with gp120 compared to control cells. Bar Graphs black bars are control samples, gray bars are gp120 treated samples (*$p < 0.05$, **$p < 0.01$).

The TCA cycle can also use glutamine as an anaplerotic molecule to continue the cycle's progression (Zhao et al., 2019). In our metabolomics study, we observe a decrease in glutamine and an increase in glutamate, the first step of glutaminolysis (**Figure 3**). Once glutamine is converted into glutamate, it can be further converted to α-ketoglutarate or citrate and then enter the TCA cycle (Udupa et al., 2019).

Glutamate can also be converted into other amino acids to fuel protein production, like proline and alanine, which are both elevated in our metabolomics study. This increase in glutamate, proline, and alanine, along with the decrease in glutamine, suggests that gp120 is inducing anaplerosis by way of glutaminolysis, thus implicating metabolic reprogramming (**Figure 3**).

We also observed a decrease in serine and an increase in glycine (**Figure 4**). Serine is an important regulator of glycolysis through its positive regulation of PKM2 enzymatic activity resulting in a higher conversion of PEP into pyruvate, but when serine is reduced, PKM2 enzymatic activity is also reduced (Chaneton et al., 2012). However, serine also is vital in one-carbon metabolism, where the conversion of serine into glycine fuels the folate cycle resulting in the biosynthesis of nucleotides and fatty acids (**Figure 4**) (Amelio et al., 2014). Further, our metabolomic analysis shows an increase in both purines produced in the folate cycle pathway, adenosine monophosphate (AMP) and guanosine monophosphate (GMP). We observed an increase in methionine and in methionine cycle metabolites, s-adenosylmethionine (SAM), and cystathionine, as well as a decrease in cysteine and glutathione (**Figure 4**). Upregulation of the methionine cycle intermediates and the decrease in cystine production suggests that the majority of homocysteine produced in the cycle gets recycled back to methionine to continue this cycle, so it continues to drive the folate cycle resulting in more conversion of serine into glycine to enter the one-carbon pathway fueling more purine production.

In addition to increased purines, we detected an increase in uridine 5-diphosphate (UDP), the primary precursor for pyrimidine synthesis (**Figure 2**). Upregulated UDP suggests that gp120 is causing an influx of G6P, a metabolite of glycolysis, to enter the pentose phosphate pathway (PPP) to be converted to ribose 5-phosphate and then undergo further conversion into UDP to be used in the synthesis of pyrimidines.

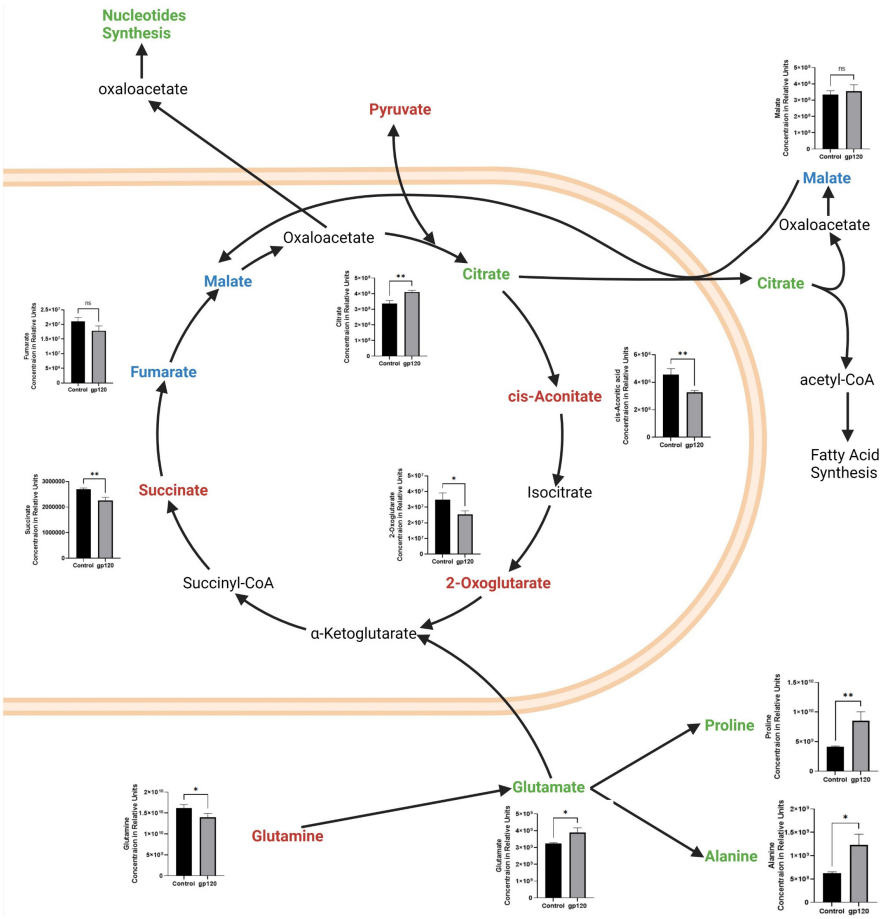

FIGURE 3 | Alterations in the TCA cycle and glutaminolysis pathway after gp120 treatment. TCA cycle and glutaminolysis pathway metabolites that are upregulated (green), downregulated (red), and not significantly changed (blue) in LUHMES treated with gp120 compared to control cells. Graphs show changes in the associated TCA cycle and glutaminolysis pathway metabolites in control and gp120 treated LUHMES. Bar Graphs black bars are control samples, gray bars are gp120 treated samples (*$p < 0.05$, **$p < 0.01$).

The metabolism of other amino acids is also disrupted in LUHMES treated with gp120 (**Figure 5A**). For instance, tryptophan is significantly reduced, suggesting an increase in tryptophan usage, most likely in the NAD *de novo* synthesis pathway as a way to replenish NAD levels to continue to fuel the increase in metabolic redox reactions (**Figure 5B**) (Stein and Imai, 2012). These results suggest that gp120 protein caused cellular changes that can fuel the production of lipids, proteins, and nucleotides needed for viral replication. These changes have been shown to contribute to neurocognitive defects, including alterations in memory and learning dysfunction making metabolic reprogramming an effector of HAND (Tang, 2020).

Impact of gp120 on Factors Involved in Warburg Effect and Metabolic Reprogramming

The last step of glycolysis, the conversion of PEP into pyruvate, is carried out by the enzyme pyruvate kinase enzyme (PK), which has four isoforms: pyruvate kinase liver (PKL), pyruvate kinase red blood cells (PKR), pyruvate kinase muscle isoform 1 (PKM1), and pyruvate kinase muscle isoform 2 (PKM2). PKM1 and PKM2 isoforms are found in most tissues, including neurons, and are a result of alternative splicing of the PK mRNA (Gupta and Bamezai, 2010).

The polypyrimidine tract-binding protein 1 (PTBP1) is the posttranscriptional regulator for the difference in splicing PKM into its isoforms PKM1 or PKM2 by way of exon skipping (Calabretta et al., 2016). PTBP1 promotes the expression of PKM2 and decreases the expression of PKM1 through PTBP1 inclusion of exon 10 and splicing out of exon 9.

We sought to determine whether the addition of gp120 increases the expression of PTBP1, resulting in the promotion of PKM2 over PKM1. In order to test this, we used differentiated LUHMES that were treated with 100 ng/ml of gp120 for 8 h. mRNA and protein were isolated, and qPCR and western blot analysis was conducted. The exposure to gp120 leads to an increase in the expression of PTBP1 mRNA and protein (**Figures 6A,B**), a decrease in the expression of PKM1 mRNA (**Figure 6C**), and an increase in PKM2 mRNA (**Figure 6D**).

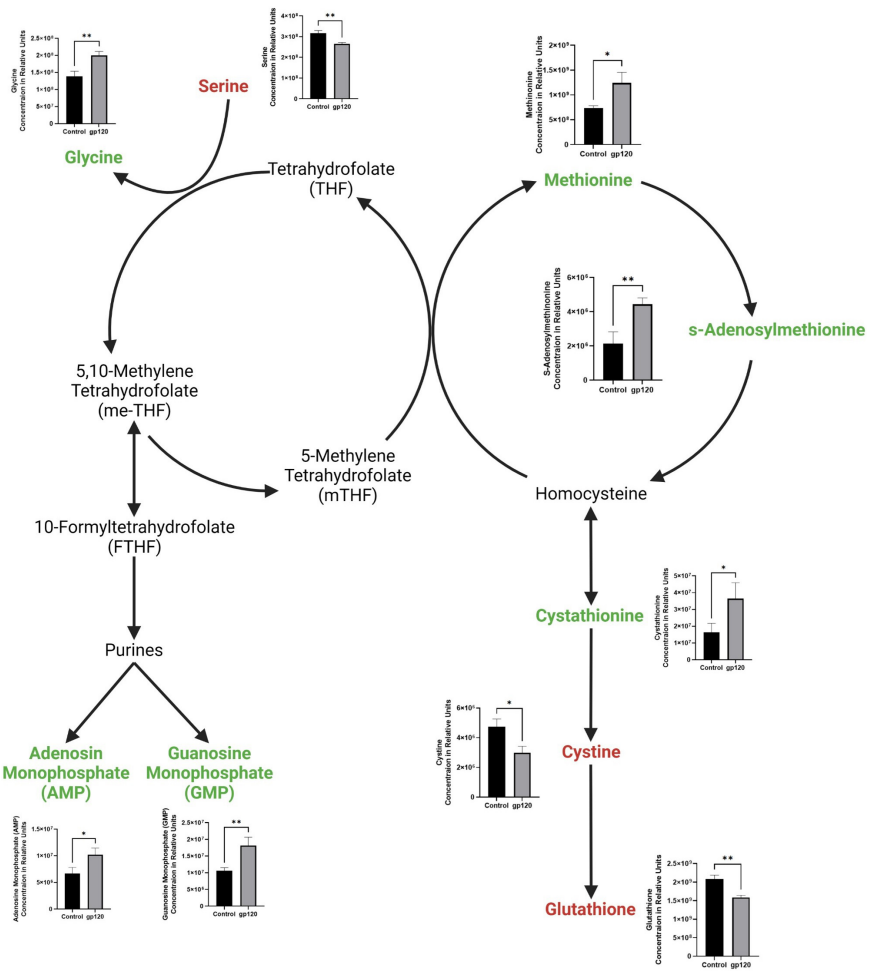

FIGURE 4 | Alterations in folate cycle and methionine cycle with gp120 treatment. Folate cycle and methionine cycle pathway with metabolites that are upregulated (green) and downregulated (red) in LUHMES treated with gp120 compared to control cells. Graphs show changes in folate and methionine cycle metabolites, as well as purine synthesis pathway metabolites in control and gp120-treated LUHMES. Bar graphs black bars are control samples, gray bars are gp120 treated samples (*$p < 0.05$, **$p < 0.01$).

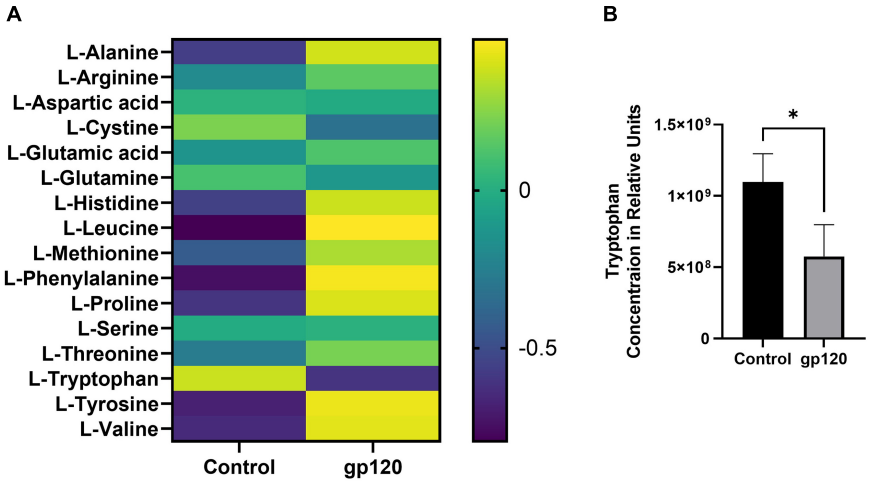

FIGURE 5 | Alterations in amino acids after gp120 treatment. **(A)** Differential expression of amino acids measured in untreated and gp120-treated LUHMES cells in triplicate by metabolomic analysis. **(B)** Graph showing a decrease in tryptophan levels in control and gp120 treated LUHMES (*$p < 0.05$).

We also see an increase in the expression of PKM2 protein (**Figure 6E**) and a decrease in PKM1 protein (**Figure 6F**). These results signify that gp120 exposure results in an increased expression of PTBP1, and through this increase, the cell favors the splicing of PKM2 over PKM1.

gp120 Prevents Phosphoenolpyruvate Conversion to Pyruvate

In mature neurons, PKM1 is the dominant isoform and is enzymatically constitutively active, while in immature neurons, PKM2 is the dominant isoform, and its enzymatic activity is allosterically controlled (Su et al., 2017; Nandi et al., 2020). The enzymatic activity of PKM2 depends on if PKM2 is a dimer or tetramer. When PKM2 is a tetramer, then it carries out the enzymatic conversion of PEP into pyruvate, much like PKM1. However, if PKM2 is a dimer, it cannot carry out the enzymatic conversion (Zahra et al., 2020). The loss of enzymatic activity of dimeric PKM2 has been shown to accumulate glycolytic metabolites. The increase in glycolytic intermediates or metabolites has been shown to increase biomass biosynthesis (Chhipa and Patel, 2021).

To explore the effect that gp120 has on pyruvate production, we treated LUHMES with Tepp-46 with and without gp120. Tepp-46 (ML-265) is a potent and selective PKM2 tetrameric stabilizer, returning the catalytic activity to PKM2, so PKM2 acts like PKM1 and converts PEP into pyruvate (**Figure 7A**) (Anastasiou et al., 2012). Tepp-46 is a small molecule activator that binds PKM2 and promotes the formation of tetramers through the promotion of tight protein binding and holds the four PKM2 monomers in the tetrameric form. By measuring intracellular pyruvate concentrations in response to varying molarities of Tepp-46, we determined that 10nM was the ideal concentration to increase pyruvate through increased PKM2 enzyme activity in LUHMES (**Figure 7B**).

Differentiated LUHMES were treated with gp120, Tepp-46, or both gp120 and Tepp-46 for 8 h. As expected, the addition of gp120 decreases the production and accumulation of internal and external pyruvate, while the addition of Tepp-46 on non-gp120 treated cells does not affect pyruvate production or accumulation. Interestingly, treatment of the cells with both gp120 and Tepp-46 resulted in a significant increase in internal and external pyruvate levels indicating that Tepp-46 rescued the pyruvate production through the formation of PKM2 tetramers (**Figures 7C,D**). These results suggest that exposure to gp120 is causing the dimerization of PKM2 and reduction of enzyme activity resulting in a reduced amount of pyruvate produced from glycolysis. These results also show that through Tepp-46, PKM2 tetramers can be formed, and the enzymatic activity of PKM2 can be returned, increasing the production of pyruvate. Together, these data suggest that PKM2 may be the critical enzyme altered with gp120, contributing to the metabolic reprogramming we show in gp120 treated LUHMES.

Tepp-46 Treatment Rescues ATP Levels in gp120-Treated Cells

ATP production from the TCA cycle is much greater than ATP produced through glycolysis alone (Zheng, 2012). In our LUHMES treated with gp120, we expect decreased ATP production due to the decrease in pyruvate, the primary TCA cycle substrate. We, therefore, measured ATP production using a luciferase ATP detection kit. We treated differentiated LUHMES with gp120, Tepp-46, or both gp120 and Tepp-46. In gp120 treated LUHMES, we saw a decrease in ATP levels which correlates with the reduced ATP levels in the metabolomics analysis (**Figure 7E**). We also discovered that the addition of Tepp-46 could return ATP levels to that of control cells even in the presence of gp120 (**Figure 7E**). This reduction in ATP would correlate with the previously seen reduction of ATP in the brains of people living with HIV using magnetic resonance spectroscopy (MRS) (Deicken et al., 1991). In addition, it has been shown that the addition of Tepp-46 can increase ATP production by returning enzyme activity to PKM2, resulting in increased pyruvate production to be used in the TCA cycle and to fuel OXPHOS (Qi et al., 2017).

These data further show that gp120 treatment leads to increased PKM2 and dimerization of PKM2, resulting in decreased pyruvate production and a decrease in ATP. The data also show that the treatment with Tepp-46 can restore enzymatic activity to PKM2 by creating PKM2 tetramers, thus increasing the amount of PEP converted to pyruvate and increasing the amount of pyruvate available to generate ATP.

gp120 Metabolic Reprogramming Results in Advanced Glycation End Products Accumulation

A significant result of reduced OXPHOS and decreased ATP production by PKM2 dimerization is increased glycolysis to compensate for the reduction in ATP (Zahra et al., 2020). A result of the increased glycolysis, by way of reduced PKM2 enzymatic activity, is the increase of glycolytic metabolites, which then can undergo other reactions (Wang et al., 2017). Some of the metabolites that accumulate due to reduced PKM2 activity can enter other biosynthesis pathways increasing biomass (Macintyre and Rathmell, 2011). At the same time, other glycolytic metabolites that are increased can contribute to the production and accumulation of advanced glycation end products (AGEs) (Khan et al., 2018). AGEs are produced through a non-enzymatic, spontaneous chemical reaction between a highly reactive dicarbonyl, in most cases methylglyoxal (MG), and an amino acid, usually an arginine or lysine (**Figure 8A**) (Lin et al., 2016).

Dihydroxyacetone phosphate (DHAP) and G3P are the primary glycolytic intermediates that are spontaneously degraded into MG, and in our metabolomic data, the analysis shows an increase in both G3P (**Figure 2B**) and DHAP (**Figure 8B**). We also examined the status of methylglyoxal (MG) in gp120-treated LUHMES. Following the same procedures as above, we observed that the expression of MG increases in gp120-treated cells but not when Tepp-46 is added as obtained using a fluorometric assay kit (**Figure 8C**). Therefore, we set out to determine whether gp120 treatment also results in increased AGE formation.

To explore this, we used differentiated LUHMES treated with gp120, Tepp-46, or both gp120 and Tepp-46 for 8 h. The cell lysates were then subjected to an ELISA to measure the concentration of AGEs. As expected, we observed an

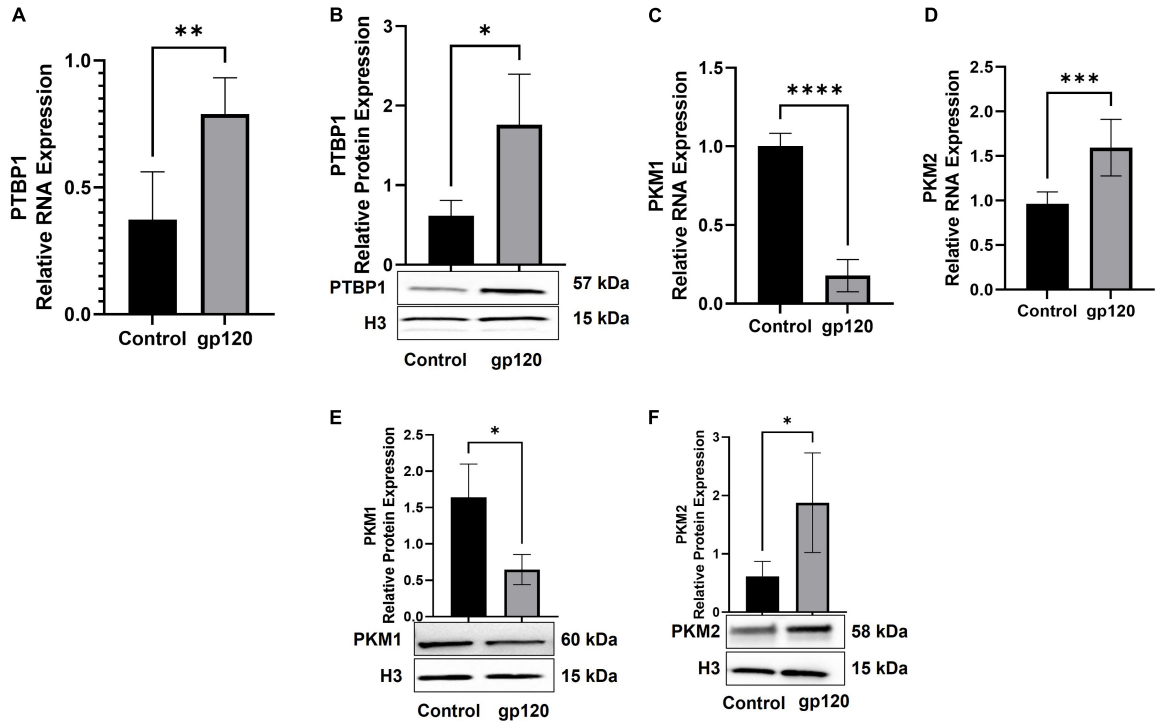

FIGURE 6 | Changes in proteins responsible for metabolic reprogramming. Expression of PTBP1 **(A,B)**, PKM1 **(C,E)**, and PKM2 **(D,F)** mRNA and protein isolated from untreated or gp120-treated LUHMES for 8 h as obtained by qPCR and normalized to GAPDH as an internal control **(A,C,D)** and Western blot **(B,E,F)**, respectively. Quantification of the relative protein levels was determined from the band intensity using ImageJ software and normalized relative to the H3. Bar graphs represent means ± S.D. Data represent the mean ± S.D. Results were judged statistically significant by ANOVA (*$p < 0.05$, **$p < 0.01$, ***$p < 0.001$, ****$p < 0.0001$).

increase in AGE concentration in the gp120-treated samples compared to the untreated control samples (**Figure 8D**). We also observed that the Tepp-46 treatment to gp120-exposed LUHMES decreased AGE concentration compared to the gp120 experimental samples (**Figure 8D**).

This decrease in AGE formation due to Tepp-46 could be due to the decrease in metabolites accumulating due to recovered tetrameric PKM2 activity and the decrease in glycolytic metabolites, including G3P and DHAP. Subsequently, the decrease in G3P and DHAP would lead to less spontaneous decay of these metabolites to MG resulting in less MG reacting with lysine or arginine and decreased AGE formation as observed in panel C. These results suggest that the gp120-associated increase in glycolytic metabolites through the decreased enzymatic activity of PKM2 results in an accumulation of MG, and the increase of MG results in a more significant amount of AGE formation. The pharmacological intervention of Tepp-46 to return enzymatic activity to PKM2 also results in decreased glycolytic intermediates and ultimately prevents AGE formation.

gp120 Prevents the Cleavage of Mature Brain-Derived Neurotrophic Factor

Brain-derived neurotrophic factor (BDNF) plays an essential role in neuron survival, morphology, and synaptic activity (Miranda et al., 2019). BDNF also plays an essential role in long-term potentiation (LTP), and it has been suggested that BDNF plays a crucial role in supporting memory formation and maintenance through the control of synaptic consolidation (Bramham and Messaoudi, 2005). In mice, it has been shown that the deletion of BDNF results in impaired spatial memory and memory recall (Heldt et al., 2007).

The BDNF is first transcribed as proBDNF and is cleaved to form the pro-peptide and the mature BDNF (mBDNF) (Borodinova and Salozhin, 2017). Mature BDNF and proBDNF are both biologically active; however, they have opposing cellular actions. mBDNF signals through its receptor, tropomyosin receptor kinase B (TrkB), and is associated with neuron survival, differentiation, neurite outgrowth, and long-term potentiation. However, proBDNF signals through its receptor, sortilin/p75 neurotrophin receptor ($p75^{NTR}$), and is associated with apoptosis, neurite retraction, and long-term depression (LTD) (Deinhardt and Chao, 2014). It has been shown that increases in the un-cleaved proBDNF in the hippocampus of mice can contribute to memory impairments (Buhusi et al., 2017). In Alzheimer's, it has been shown that there is an increase in $p75^{NTR}$ signaling through proBDNF. The decrease in cleavage of proBDNF is a result of AGEs binding to lysine in the cleavage site-blocking enzymatic cleavage (Fleitas et al., 2018).

To determine if this phenomenon is also occurring in neurons exposed to gp120, we first set out to determine if there were any changes in mBDNF and proBDNF levels. To do this, we

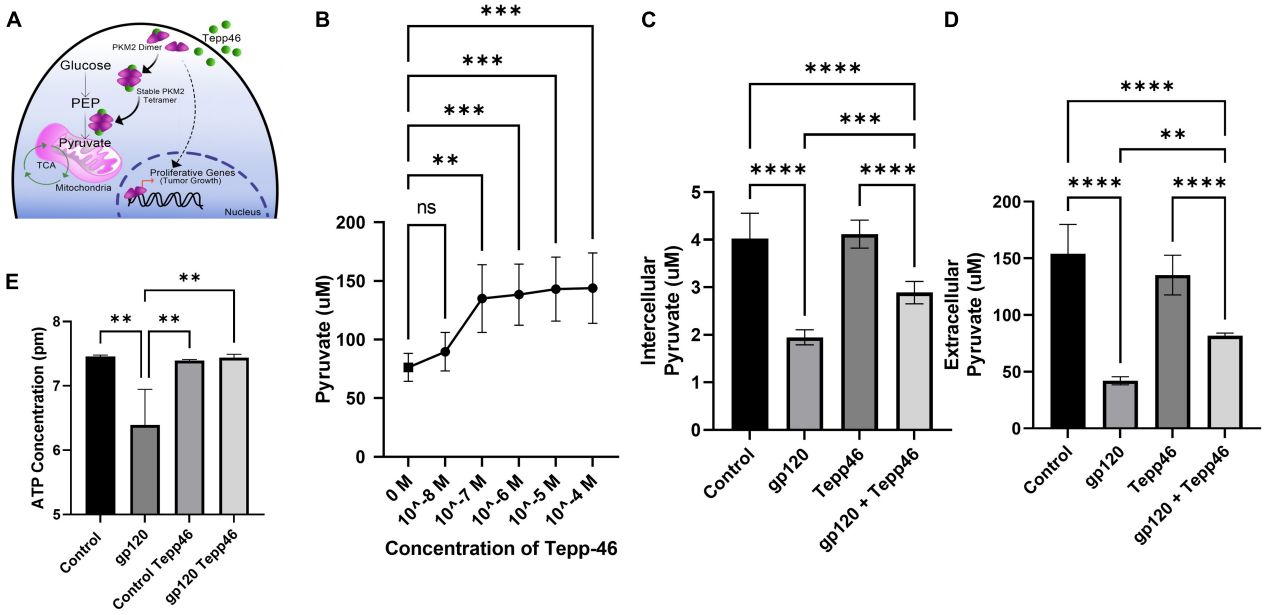

FIGURE 7 | Tepp-46 and its effect on pyruvate production. **(A)** A schematic illustration of the mechanism of action of Tepp-46 has on PKM2 and its correlation to pyruvate production and the effect on mitochondrial metabolism. **(B)** Concentrations of intercellular pyruvate in undifferentiated LUHMES cells treated with increasing concentration of Tepp-46 as indicated. **(C,D)** Differentiated LUHMES cells untreated or treated with 100 ng/ml of gp120 and/or 10 nM of Tepp-46. The concentration of intracellular **(C)** and extracellular **(D)** pyruvate were measured. Bar graphs represent means ± SD. **(E)** Measurement of ATP concentration in LUHMES cells untreated or treated with 100 ng/ml of gp120 and/or 10 nM of Tepp-46. Data represent the mean ± S.D. Results were judged statistically significant by the ANOVA test (**$p < 0.01$, ***$p < 0.001$, ****$p < 0.0001$).

performed immunoprecipitation (IP) followed by a western blot on the cellular media from cells treated with gp120, Tepp-46, or both gp120 and Tepp-46 for 8 h. We discovered that the addition of gp120 results in an increase in proBDNF and a correlating decrease in mBDNF, suggesting that cleavage is prevented (**Figures 8E–G**). However, treatment with Tepp-46 and gp120 shows no decrease in BDNF mRNA and does not display an increase in proBDNF (**Figures 8E–G**). The prevention of decreased cleavage by Tepp-46 suggests that the blockage of proBDNF cleavage is related to the increase in glycolysis caused by the reduced enzymatic activity of PKM2.

We next examined whether gp120 alters furin, the protease mainly responsible for the cleavage of proBDNF into mBDNF (Pang et al., 2016). Differentiated LUHMES were treated with gp120 for 8 h, and furin protein level was analyzed by a western blot. We observed no significant change in furin protein expression in gp120-treated cells compared to untreated cells (**Figure 8H**). The lack of change in furin expression suggests that the lack of proBDNF cleavage seen with gp120 treatment is not a result of a reduction in furin levels but rather a blockage of the cleavage site.

To determine if the decrease in cleavage of proBDNF to mBDNF is a result of AGE modification to proBDNF resulting in the blockage of normal cleavage, we collected cell culture media from cells treated with gp120, Tepp-46, or both gp120 and Tepp-46 for 8 h, Afterwards, the media was condensed, and an IP using anti-BDNF antibody was conducted. The isolated BDNF protein from the samples was then subjected to an ELISA to measure the level of AGEs in the isolated BDNF. We observed that gp120 increases the amount of AGE modification on BDNF compared to the control and that Tepp-46 prevents the gp120-associated increase in AGE modifications (**Figure 8I**).

These results suggest that decreased cleavage of proBDNF to mBDNF is contributed to the formation of AGE modifications to BDNF. These results also suggest that Tepp-46, through the stabilization and formation of PKM2 tetramers, decreases the accumulation of AGEs and consequently reduces AGEs associated with BDNF. It also confirms that AGE modification of the cleavage site of proBDNF prevents the cleavage into mBDNF in the presence of gp120.

gp120 Favors Inducible cAMP Early Repressor -cAMP Responsive-Element Binding

Pro-brain-derived neurotrophic factor has been shown to signal through the sortilin/$p75^{NTR}$ receptor and ultimately results in the induction of the inducible cAMP early repressor (ICER) protein (Riffault et al., 2014). ICER binds to CRE sites within promoter sequences and thus blocks cAMP responsive-element binding (CREB) protein binding and leads to decreased gene expression (Porcher et al., 2018). CREB has been identified as an essential transcription factor in long-term memory and synaptic plasticity and plays a role in neuronal protection and prevention of neurodegeneration (Sakamoto et al., 2011). It has also been shown that disruption of CREB binding can lead

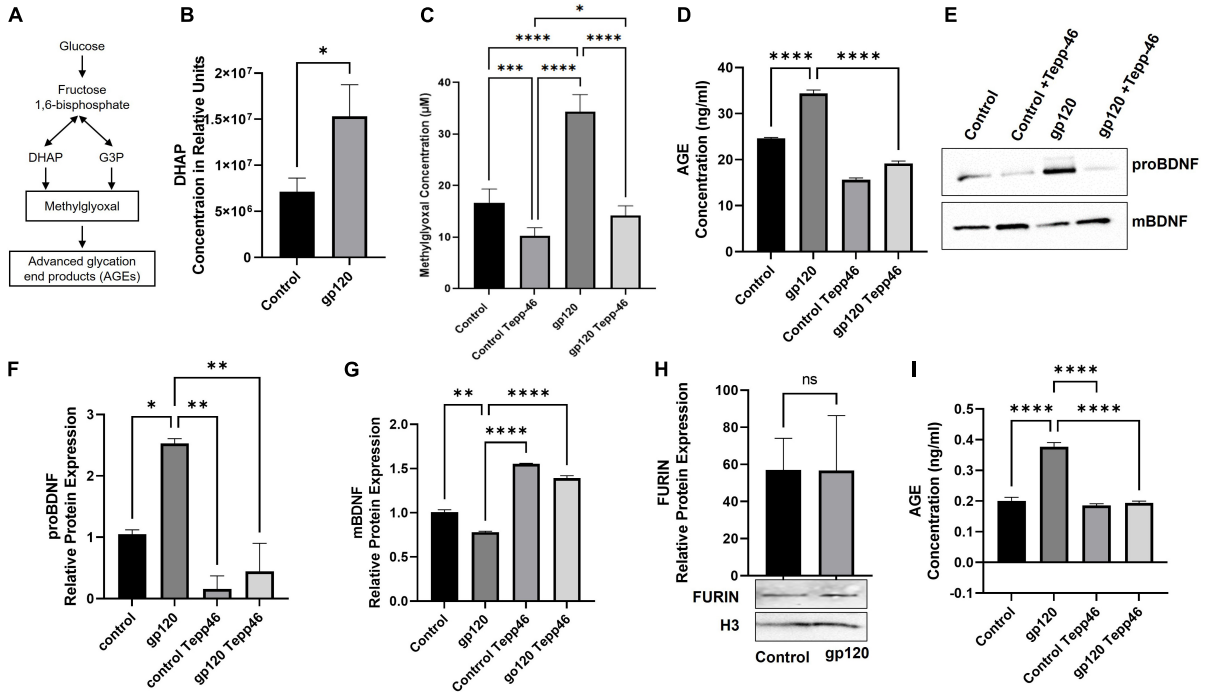

FIGURE 8 | Altered expression of proBDNF, BDNF, and AGE in gp120-treated cells. **(A)** Schematic representation of advanced glycation end products (AGEs) pathway activation. **(B)** Dihydroxyacetone phosphate (DHAP) relative concentration as obtained by MetaboAnalyst 5.0 online software (*$p < 0.05$). **(C,D)** Differentiated LUHMES cells untreated or treated with 100 ng/ml of gp120 and/or 10 nM of Tepp-46. The cellular concentration of methylglyoxal (MG) (μM) and AGEs (ng/ml) were measured by ELISA, samples were normalized to dilution factor and cell count. **(E)** Differentiated LUHMES cells untreated or treated with 100 ng/ml of gp120 and/or 10 nM of Tepp-46. 250 μg of cell extracts were used for immunoprecipitation using anti-proBDNF or -BDNF antibodies followed by Western analysis as shown. **(F,G)** Quantification of the relative protein levels was determined from the band intensity using ImageJ software. Bar graphs represent means ± S.D. **(H)** Expression of furin protein isolated from untreated or gp120-treated LUHMES for 8 h as obtained by Western blot. Quantification of the relative protein levels was determined from the band intensity using ImageJ software and normalized relative to the H3. **(I)** AGEs concentration was measured *via* ELISA on IP pull-down of BDNF from these samples. Data represent the mean ± S.D. **(I)** Data represent the mean ± S.D. Results were judged statistically significant by ANOVA (*$p < 0.05$, **$p < 0.01$, ***$p < 0.001$, ***$p < 0.0001$).

to neurodegeneration in mice (Mantamadiotis et al., 2002). Furthermore, overexpression of ICER in mice has been shown to result in memory impairment, while knocking out ICER results in enhanced long-term memory (Borlikova and Endo, 2009). It has also been demonstrated in elderly rats that the increase of ICER binding to CRE sites contributes to memory impairments seen with aging (Mouravlev et al., 2006).

Because we see an increase in proBDNF expression in gp120-treated cells, we sought to determine if the expression of ICER is changed as well. To measure ICER levels, differentiated LUHMES were treated with gp120 for 8 h, after which mRNA and protein were isolated and subjected to qPCR and western blot analysis, respectively. Here, the addition of gp120 leads to an increase in the expression of ICER mRNA (**Figure 9A**) and ICER protein (**Figure 9B**). The increase in ICER suggests that, along with the increase in un-cleaved proBDNF due to AGE modification, there is also an increase in sortilin/p75 signaling.

Next, to determine if the increase in ICER resulted in altered CREB binding and transcriptional promotion, we looked at the ability of ICER and CREB to bind to CRE sites. We looked at specifically *Bdnf* promoters II and IV, which contain CRE sites, using chromatin immunoprecipitation assay (ChIP). Both BDNF promoter II and BDNF promoter IV have been identified as having CRE sites important for CREB binding and controlling the transcription of BDNF in relation to neuronal health and memory (Esvald et al., 2020).

Differentiated LUHMES were treated with gp120 for 8 h, then were fixed with formaldehyde and subjected to ChIP assay using CREB and ICER antibodies along with primers for BDNF exon II and exon IV promoters. Here we see that in cells treated with gp120, ICER is the dominant interacting transcription factor in both BDNF promoter II and promoter IV while CREB binding to these promoters is reduced (**Figures 9C,D**). In cells not treated with gp120, CREB is the dominant transcription factor binding to BDNF promoter II and promoter IV (**Figures 9C,D**). The increase of ICER and decrease of CREB in the promoter regions implies that gp120 is decreased CREB-associated transcription through the inhibition of CREB binding by ICER.

Next, we sought to determine if the dimerization of PKM2 contributes to the increase in ICER through a qPCR using LUHMES treated with gp120, Tepp-46, or both gp120 and Tepp-46. We detected that the addition of gp120 failed to increase ICER mRNA expression in the presence of Tepp-46 when compared to gp120 treatment alone. Correspondingly

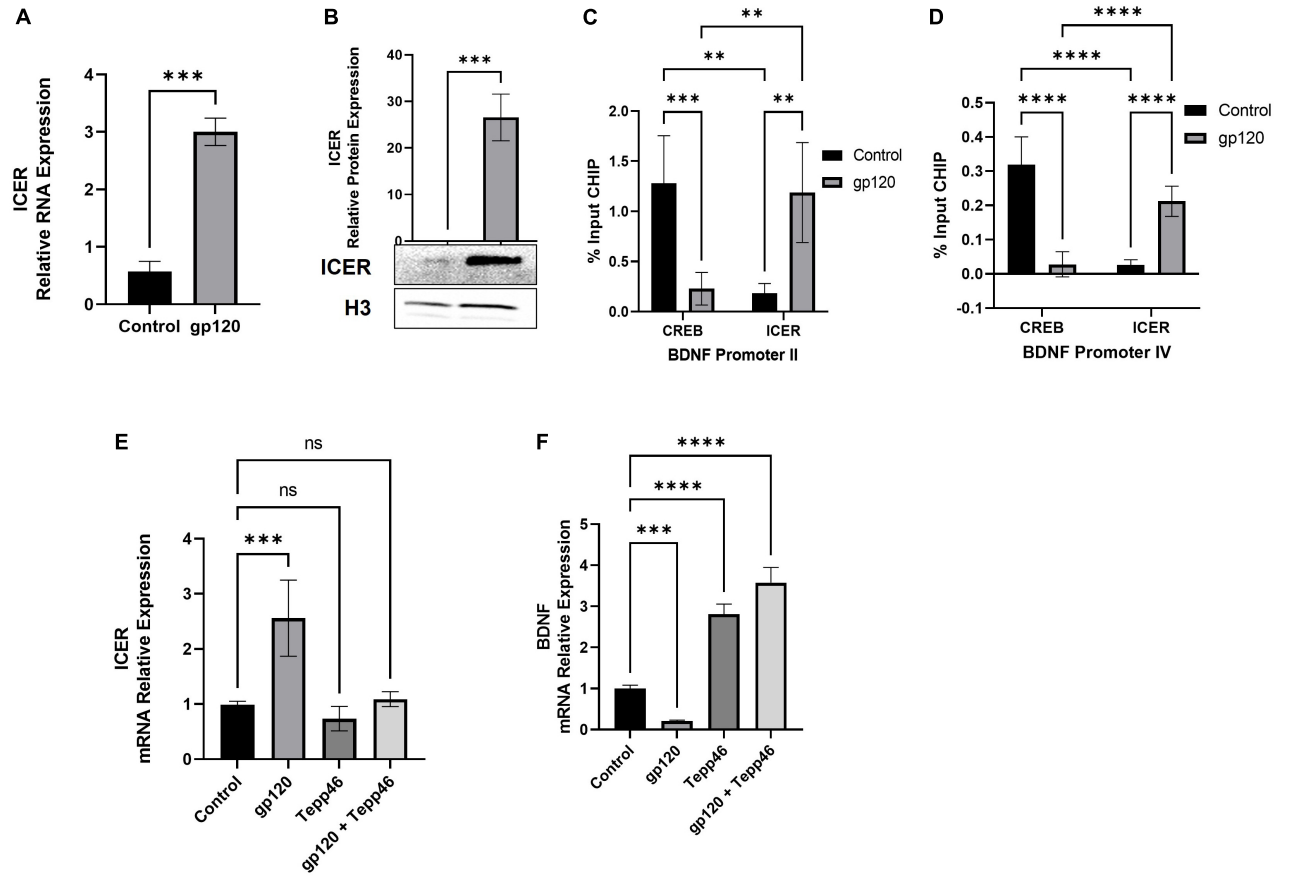

FIGURE 9 | Effect of gp120 on CREB/ICER signaling and HIF-1α expression. **(A)** Expression of ICER mRNA isolated from untreated or HIV-1 gp120-treated LUHMES for 8 h as obtained by qPCR and normalized to GAPDH as an internal control. **(B)** Expression of ICER protein isolated from untreated or HIV-1 gp120-treated LUHMES for 8 h as obtained by western blot and normalized to H3 as an internal control. Quantification of the relative protein levels was determined from the band intensity using ImageJ software and normalized relative to the H3. **(C,D)** Interaction of ICER and CREB with BDNF promotors II **(C)** and IV **(D)** as obtained by ChIP in untreated and gp120-treated LUHMES cells. **(E)** Differentiated LUHMES cells untreated or treated with 100 ng/ml of gp120 and/or 10 nM of Tepp-46. Expression of ICER mRNA as obtained by qPCR and normalized to GAPDH. **(F)** Differentiated LUHMES cells untreated or treated with 100 ng/ml of gp120 and/or 10 nM of Tepp-46. The expression of BDNF mRNA is obtained by qPCR and normalized to GAPDH as an internal control Data represent the mean ± S.D. Results were judged statistically significant by ANOVA or students *T*-test (**$p < 0.01$, ***$p < 0.001$, ****$p < 0.0001$).

gp120 treatment without Tepp-46 results in the increase of ICER mRNA (**Figure 9E**).

Next, we wanted to see if the increase in ICER and decrease in CREB binding to the BDNF promoter decreased BDNF transcription. We also wanted to explore if Tepp-46 could increase BDNF transcription through the Tepp-46 associated decrease in ICER that we previously observed. To achieve this, we collected RNA from cells treated with gp120, Tepp-46, or both gp120 and Tepp-46 for 8 h. The RNA collected was subjected to qPCR to determine BDNF mRNA expression (**Figure 9F**). The addition of gp120 decreases BDNF mRNA expression, while Tepp-46 and gp120 treated cells showed no decrease in BDNF mRNA. The decrease in BDNF mRNA suggests there is less CREB associated transcription through the increased binding of ICER to the CRE sites of the BDNF promoter. The increase in BDNF transcription with the addition of Tepp-46 suggests that returning enzymatic activity to PKM2 and the subsequent reduction in glycolytic metabolites contributes to the lack of AGE modified proBDNF reducing the switch from Sortilin/p75^{NTR} receptor signaling from TrkB receptor resulting in increased CREB binding to BDNF CRE promoter sites.

These results support our model that the decrease in PEP to pyruvate conversion by PKM2 dimerization led to an increase in AGEs, causing a reduction in mBDNF cleavage and increased proBDNF signaling through the sortilin/p75^{NTR} receptor. The increase in proBDNF signaling increases ICER expression and a subsequent reduction in CREB-associated transcription. Interestingly, Tepp-46, through the stabilization of the PKM2 tetramer, appears to inhibit the gp120-associated increase of ICER.

gp120 Promotes Metabolic Reprogramming Through HIF-1α

We have shown that gp120 increases PTBP1-mediated splicing of PKM into the PKM2 isoform over the PKM1 isoform. The

expression of PTBP1 has been shown to be negatively regulated by miR-124 (Caruso et al., 2017). In addition, it has been shown that hypoxia-inducible factor 1 alpha (HIF-1α) can also mediate the switch from PKM1 to PKM2 by binding PKM exon 10 and aiding in the inclusion of this exon during splicing resulting in PKM2 translation (Williams et al., 2018). Furthermore, dimerized PKM2 can translocate to the nucleus where it can interact with HIF-1α and stimulates HIF-1α promotion of key genes associated with glycolysis (Palsson-McDermott et al., 2017). It has also been shown that the activation of HIF-1α can decrease the expression of miR-124 (Wang et al., 2020). This HIF-1α mediated decrease in miR-124 could be responsible for the increase in PTBP1 we see in our gp120 treated LUHMES.

Therefore, we sought to determine whether the addition of gp120 increases PTBP1 levels by affecting miR-124 and if the promotion of PKM2 splicing over PKM1 is attributed to HIFα expression. To do this, we used differentiated LUHMES that were treated with gp120 for 8 h. RNA was collected and then subjected to qPCR. We determined that the addition of gp120 led to a decrease in the expression of miR-124 (**Figure 10A**). This decrease in miR-124 would account for the increase in PTBP1 that we observe with gp120 treatment.

Next, we examined the expression levels of HIF-1α mRNA after cells were treated with gp120 for 8 h. We observed that the addition of gp120 increases HIF-1α mRNA expression (**Figure 10B**). However, cells treated with Tepp-46 and gp120 did not result in a decrease in HIF-1α indicating that the increase in HIF-1α is not contributed to the increase in glycolysis but suggests that HIF-1α increase is upstream and a possible cause of the metabolic reprogramming (**Figure 10B**). The increase of HIF-1α expression, along with the previously shown increase in oxidative stress, would contribute to the increased splicing of PKM2 over PKM1 (Agrawal et al., 2010).

Since we see an increase in HIF-1α expression, we wanted to see if inhibiting HIF-1α would decrease PTBP1 levels in gp120-treated cells. Therefore, we treated differentiated LUHMES with two HIF-1α inhibitors, E.S and the antitumor agent PX-12. Both chemicals have been described to inhibit HIF-1α protein function (Kong et al., 2005; Kim et al., 2011).

Differentiated LUHMES were treated with E.S, PX-12, gp120, gp120, and E.S, or gp120 and PX-12. RNA was then isolated and subjected to a qPCR. In LUHMES treated with either HIF-1α inhibitor, gp120 treatment failed to increase the expression of PTBP1 (**Figure 10C**). The lack of increase in PTBP1 with the inhibition of HIF-1α indicates that HIF-1α signaling contributes to the increase of PTBP1 seen after treatment with gp120.

To determine if the HIF-1α regulation of PTBP1 could also account for the downstream induction of ICER through the increased sortilin/$p75^{NTR}$ signaling by AGE modified proBDNF, we analyzed the mRNA expression of ICER following HIF-1α inhibition and gp120 treatment. Interestingly we observed that cells treated with HIF-1α inhibitors and gp120 failed to result in the increased ICER expression that we show in gp120 treated LUHMES without HIF-1α inhibitors (**Figure 10D**). The lack of increase in PTBP1 in cells treated with the HIF-1α inhibitor suggests HIF-1α may play an essential role in gp120-mediated metabolic reprogramming, specifically by the upregulation of PTBP1 and subsequent PKM2 dimerization, thus decreasing the conversion of PEP to pyruvate.

DISCUSSION

Metabolic reprogramming is a common phenomenon observed in several diseases, including cancer and viral infections (Sanchez and Lagunoff, 2015; Medina, 2020; Polcicova et al., 2020). Metabolic reprogramming is also observed in many neurodegenerative diseases like Alzheimer's disease, Amyotrophic Lateral Sclerosis (ALS), and Parkinson's disease (Han et al., 2021; Lu et al., 2021). However, little is known about metabolic reprogramming in neurons affected by HIV-1 and the role metabolic reprogramming plays in the progression of HAND.

This study demonstrated that HIV-1 gp120 reduces the OCR associated with maximal respiration and the RRC in LUHMES using the Seahorse Mito Stress Test. Therefore, we see that HIV-1 gp120 diminishes the mitochondrial respiration associated with a high energy-demanding state. This decrease in mitochondrial respiration may be associated with decreased production of acetyl-CoA or pyruvate that can enter the TCA cycle as substrate availability is the main contributor to decreased maximum respiratory capacity and RRC (Gu et al., 2020).

The induction of the Warburg effect has been demonstrated in other viral infections and in T cells infected with HIV; however, to our knowledge, it has never been shown to occur in neurons in response to gp120 (Prusinkiewicz and Mymryk, 2019; Kang and Tang, 2020). The induction of the Warburg effect has been linked to the progression of neurocognitive diseases like Alzheimer's and Parkinson's (Requejo-Aguilar and Bolaños, 2016; Atlante et al., 2017). Thus, our metabolomic results demonstrate that gp120 affects the final step of glycolysis. This reduced enzymatic conversion of PEP to pyruvate and subsequent increased production of lactate increases glycolytic metabolites while reducing TCA cycle-associated metabolites. The increase in glycolysis and lactate production represents induction of the Warburg effect and indicates that at least one cellular hallmark of metabolic reprogramming occurs in neurons exposed to gp120. The onset of the Warburg effect also leads us to believe this may be a contributing factor to the progression of HAND since the Warburg effect has been associated with other neurocognitive disorders.

Also, in our metabolomic study, we show that tryptophan is reduced in HIV-1 gp120-treated cells. Interestingly, the increase in tryptophan metabolites that result from the breakdown of tryptophan has been shown to contribute to the progression of Alzheimer's disease (Bonda et al., 2010). Another amino acid pathway that is seen to be disrupted in our gp120-treated cells is the methionine cycle, in which methionine, through regulated steps, is converted to homocysteine, then cysteine, and ultimately glutathione (Sanderson et al., 2019). Glutathione is an essential cellular ROS scavenger and protects proteins from oxidative damage, and the decrease in glutathione has been linked to neurodegenerative diseases (Schulz et al., 2000).

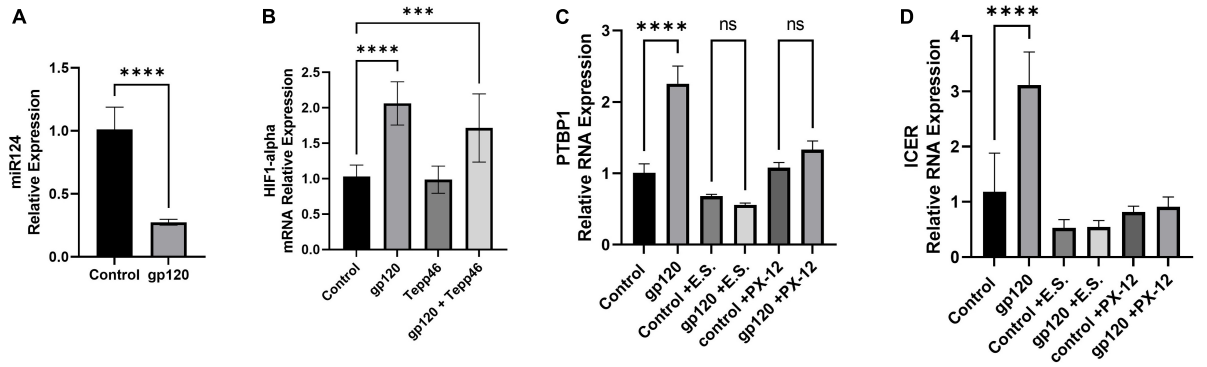

FIGURE 10 | Effects of gp120 on miR-124 and HIF-1α and HIF-1α inhibition on metabolic reprogramming. **(A)** Fold changes of miRNA-124 expression in gp120-treated LUHMES cells compared to control untreated cells obtained by qPCR. **(B)** Expression of HIF-1α mRNA in gp120-treated LUHMES cells compared to control untreated cells obtained by qPCR. **(C)** Differentiated LUHMES cells untreated or treated with HIF-1α inhibitors, E.S. or XP-12 as indicated. Expression of PTBP1 as obtained by qPCR. **(D)** Differentiated LUHMES cells untreated or treated with HIF-1α inhibitors, E.S. or XP-12 as indicated. Expression of ICER mRNA as obtained by qPCR (***$p < 0.001$, ****$p < 0.0001$).

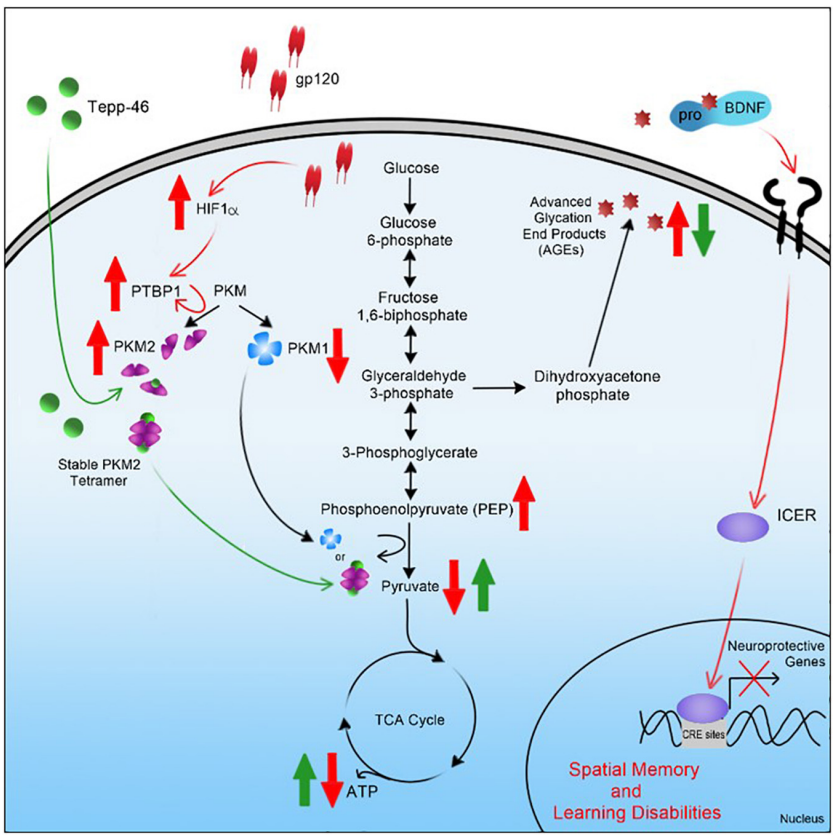

FIGURE 11 | Graphical summary of project. A schematic representation of the pathway used by HIV-1 gp120 is elucidated here leading to metabolic reprogramming in neurons and contributing to cellular changes associated with HAND.

Increased expression of PTBP1 has also been associated with the induction of the Warburg effect and plays a role in the growth and differentiation of neuronal cells (Linares et al., 2015). The increase in PKM2 over PKM1 has been linked to cancer progression and increased proliferation (Calabretta et al., 2016). In this study, we see increased PTBP1 expression, increased expression of PKM2, and decreased expression of PKM1 with gp120-treatment, as well as signaling events associated with the PKM2 dimeric form. The prevention of tetramer formation resulting in the dimeric form is

controlled by many post-translational modifications (PTM). These modifications include tyrosine phosphorylation, serine phosphorylation, threonine phosphorylation, lysine acetylation, proline hydroxylation, cysteine oxidation, ubiquitination, and glycosylation (Prakasam et al., 2018). This phenomenon is widely used by many tumor cells to promote the accumulation of materials for biosynthesis, which is needed to drive proliferation (Zahra et al., 2020). In other viral infections, it has been shown that there is an increase in tyrosine 105 phosphorylation of PKM2 (McElvaney et al., 2020). This phosphorylation is a leading contributor to the dimerization of PKM2 and is associated with increased glycolysis and biomass accumulation.

It has been shown previously that HIV-1 infections can prevent the conversion of glucose into pyruvate in T-cells (Kang and Tang, 2020). In addition, it has been previously shown that the viral protein alone is sufficient to cause metabolic reprogramming in glioma cells (Valentín-Guillama et al., 2018). However, this is the first study linking gp120 to metabolic reprogramming in mature neurons and, since previous work has been observed in cancer cells, the effect of metabolic reprogramming in non-proliferating cells has yet to be explored.

Here we show that gp120 can cause metabolic reprogramming through the increase in HIF-1α followed by a reduction in miR-124, leading to the expression of PTBP1. The increase in HIF-1α in conjunction with gp120 has previously been shown to be in part due to increased ROS (Agrawal et al., 2010). This increase of ROS in response to gp120 has been shown to occur due to two different sources; however, both sources of ROS are triggered by increased calcium uptake. ROS also plays a critical role in gp120-induced pain in patients using opioids (Shi et al., 2021). Increased cytosolic calcium due to gp120 has been shown previously by our lab and others and has been shown to occur in neurons *via* gp120's interaction with chemokine receptors CXCR4 and CCR5 and through gp120's direct interaction with NMDA receptors (Zheng et al., 1999). In addition, gp120 has also been shown to increase mitochondrial uptake of calcium through the phosphorylation of the MCU by Pyk2 (Zhang et al., 2018).

The increase in cytosolic and mitochondrial calcium increases ROS production. Increases in mitochondrial calcium have increased superoxide production, resulting in increased hydrogen peroxide formation (Starkov et al., 2002). Cytosolic increase in calcium has been shown to contribute to ROS accumulation through the activation of NOX5, causing the transfer of an electron from NADPH to oxygen, resulting in superoxides (Panday et al., 2015). An increase in NOX5 activity and the resulting ROS increase has been shown to take place after gp120 treatment (Smith et al., 2021). This increase in ROS has been linked to gp120 induction of endolysosome de-acidification, which results in increased mitochondrial iron content and directly contributes to the accumulation of cellular ROS (Halcrow et al., 2021). Increased ROS plays a critical role in the formation and accumulation of AGEs.

We observed increases in glycolytic metabolites, including G3P and DHAP, which can undergo spontaneous degradation to form reactive MG, which then can covalently bond to lysine and arginine residues creating AGEs. Our data also show that there is an increase in AGE formation when LUHMES are treated with gp120. Accumulation of AGEs has been described to be involved in neurodegenerative diseases such as Alzheimer's disease and Parkinson's Disease, as well as diabetes, vascular diseases, and inflammation (Li et al., 2012; Kennon and Stewart, 2021; Lotan et al., 2021). Specifically, in Alzheimer's patients, it has been shown that AGEs may accelerate beta-amyloid aggregate formation (Vitek et al., 1994).

The AGEs can act as ligands and bind to receptors for AGEs (RAGE). AGEs binding to RAGE have been shown to contribute to many diseases, including diabetes, Alzheimer's disease, cancer, and inflammatory diseases (Alexiou et al., 2010). RAGE signaling triggers many cellular pathways, including the activation of the transcription factor NF-κB, which results in a positive feedback loop increasing RAGE expression (Li and Schmidt, 1997). A significant result of AGE binding to RAGE is the activation of cell signaling pathways that result in the expression of pro-inflammatory proteins (Kislinger et al., 1999). The induction of pro-inflammatory proteins leads to increased cellular ROS, which further fuels the production of AGEs and subsequently increases the signaling through RAGE and further increases inflammation (Younessi and Yoonessi, 2011; Qosa et al., 2014).

Inflammation plays a significant role in many neurodegenerative diseases, including HAND (Saylor et al., 2016). Increased neuroinflammation has been linked to the production of cytokines that are linked with RAGE signaling. Furthermore, when RAGE expression is reduced by siRNA suppression, the induction of pro-inflammatory cytokines is inhibited (Saha et al., 2008). The increase of inflammation through AGE binding to RAGE could contribute to the progression of HAND, and in this study, we show that AGE production is reduced in LUHMES treated with the PKM2 tetramer stabilizer Tepp-46. This reduction in AGE production might serve as a potential target for reducing AGE-RAGE-associated inflammation in neurodegenerative diseases. In addition to increased inflammation, AGEs can also induce cellular senescence in nearby cells (Liu et al., 2014). The induction of senescence has been linked to the increase in AGE signaling through RAGE, which induces p21, an essential regulator of senescence (Brizzi et al., 2004). Increased senescence has been linked with the acceleration of many age-related diseases observed with HIV infections, including HAND (Cohen and Torres, 2017). While neurons do not undergo senescence, the release of AGEs from metabolic reprogrammed neurons, along with other HIV-infected cells, can bind to RAGE receptors nearby and cause other cells to undergo senescence (Shi et al., 2019). One of these neighboring cell types that can be influenced by secreted AGEs and undergo premature senescence is astrocytes. In addition, it has been shown that senescence in astrocytes is a component of neurodegenerative diseases like Alzheimer's disease (Bhat et al., 2012).

The AGEs have been shown to play another role in disease progression by creating cross-linked protein aggregates and protein adducts that modify the proteins' function (Rungratanawanich et al., 2021). In Alzheimer's disease, increased AGEs have been shown to modify tau proteins resulting in increased tauopathies and contributing to the

neurodegenerative pathologies of Alzheimer's disease (Kontaxi et al., 2017). In addition, protein cross-linking from AGE modifications results in changes in protein structure and function. These changes can result in a reduction of enzymatic activity, formation of protein aggregation, and changes in protein-protein interactions, all contributing to the progression of neurodegenerative diseases (Lannuzzi et al., 2014). AGEs can also create non-crosslinking protein abducts; these can change receptor ligands, block the binding to receptors, block cleavage sites, induce protein misfolding, and inhibit the expected degradation of proteins (Kichev et al., 2009).

In this study, we demonstrate that the addition of gp120 protein prevents the cleavage of proBDNF into mature BDNF through AGE modification of proBDNF. Further, we showed that the addition of gp120 protein increases the expression of un-cleaved proBDNF. Overexpression of un-cleaved proBDNF has been shown to decrease the dendritic arborization and spine density in hippocampal neurons causing altered synaptic transmission (Yang et al., 2014). In addition, proBDNF expression is shown to increase in the hippocampus of patients infected with HIV-1 and in gp120-tg mice (Speidell et al., 2020). In addition, upregulation of $p75^{NTR}$ in gp120-treated cells and gp120-tg mice has been shown to cause a synaptic loss in the striatum. Moreover, using small molecules to block proBDNF from binding to $p75^{NTR}$ has been shown to lower the neurodegeneration events observed in gp120-tg mice (Xie et al., 2021). Interestingly, $p75^{NTR}$ is shown to induce ICER in cultured hippocampal neurons, and ICER can heterodimerize with CREB and block CREB-induced transcription of several genes, including BDNF (Thomas et al., 2016). ICER itself, a short RNA transcript from the CREM gene, can bind to CRE sites in the promoters and block CREB binding, causing inhibition of CREB-associated transcription (Krueger et al., 1999).

While any promoter containing CRE sites would be targeted for ICER-associated inhibition of CREB promoted transcription, we chose BDNF promoters II and IV to study due to the connection between BDNF and neurodegenerative diseases. Several transcription factors regulate the BDNF promoter; however, its activity depends on phosphorylated CREB to bind to the CRE domain within the BDNF promoters (Zhu et al., 2012). ICER binding to the BDNF promoter in hippocampal neurons has been shown to contribute to BDNF loss of function, altered synaptic plasticity, and episodic memory impairments (Zhu et al., 2012). The loss of BDNF function has been implicated in many neurodegenerative diseases (Zuccato and Cattaneo, 2009). Reductions in BDNF promoter II and BDNF promoter IV transcriptions have been linked to Huntington's disease. Alzheimer's disease is also marked by reductions in BDNF expression caused by decreased CREB-associated transcription of exon IV (Aarons et al., 2019). In patients with HAND, studies have shown that decreased BDNF levels correlate with cognitive defects (Michael et al., 2020).

In summary, the results of this study suggest that gp120 causes activation of HIF-1α, which, through a decrease of miR-124, increased PTBP1, and subsequent increase in PKM2, leads to a decrease in PEP to pyruvate conversion (**Figure 11**). An increase in PKM2 dimerization, leading to an increase in AGEs that caused a reduction in mBDNF cleavage and increased proBDNF signaling through the sortilin/$p75^{NTR}$ receptor, increases ICER expression and subsequent reduction in CREB-associated transcription (**Figure 11**). Interestingly, Tepp-46, through the stabilization of the PKM2 tetramer, appears to inhibit the gp120-associated increase of ICER by decreasing metabolic metabolite build-up linked to increased pyruvate production and subsequently increasing ATP output through OXPHOS.

DATA AVAILABILITY STATEMENT

The original contributions presented in the study are included in the article/supplementary material, further inquiries can be directed to the corresponding author.

AUTHOR CONTRIBUTIONS

CA designed, performed the studies, and wrote the manuscript. SA helped with the experiments and made the figures. MS provided reagents and helped to edit the manuscript. CD and WK provided a seahorse analyzer. BS directed, supervised, designed, and wrote the manuscript. All authors contributed to the article and approved the submitted version.

FUNDING

This work was supported by an NIH-NIA grant AG054411 and by previous NIH grants NS076402 and MH093331 awarded to BS.

ACKNOWLEDGMENTS

The authors would like to thank the Wistar Institute in Philadelphia and Aaron Goldman for the metabolomic experiment. The following reagents were obtained through the NIH AIDS Reagent Program, Division of AIDS, NIAID, NIH: HIV-1 IIIB gp120 Recombinant Protein from ImmunoDX, LLC; HIV-1 JR-CSF Fcgp120 Recombinant Protein (Cat#11556) from Aymeric de Parseval and John H. Elder.

REFERENCES

Aarons, T., Bradburn, S., Robinson, A., Payton, A., Pendleton, N., and Murgatroyd, C. (2019). Dysregulation of BDNF in Prefrontal Cortex in Alzheimer's Disease. *J. Alzheimers. Dis.* 69, 1089–1097. doi: 10.3233/JAD-190049

Agrawal, L., Louboutin, J. P., Marusich, E., Reyes, B. A., Van Bockstaele, E. J., and Strayer, D. S. (2010). Dopaminergic neurotoxicity of HIV-1 gp120: reactive oxygen species as signaling intermediates. *Brain Res.* 1306, 116–130.

Alexiou, P., Chatzopoulou, M., Pegklidou, K., and Demopoulos, V. J. (2010). RAGE: a multi-ligand receptor unveiling novel insights in health and

disease. *Curr. Med. Chem.* 17, 2232–2252. doi: 10.2174/09298671079133 1086

Amelio, I., Cutruzzolá, F., Antonov, A., Agostini, M., and Melino, G. (2014). Serine and glycine metabolism in cancer. *Trends Biochem. Sci.* 39, 191–198.

Anastasiou, D., Yu, Y., Israelsen, W. J., Jiang, J. K., Boxer, M. B., Hong, B. S., et al. (2012). Pyruvate kinase M2 activators promote tetramer formation and suppress tumorigenesis. *Nat. Chem. Biol.* 8, 839–847. doi: 10.1038/nchembio. 1060

Atlante, A., de Bari, L., Bobba, A., and Amadoro, G. (2017). A disease with a sweet tooth: exploring the Warburg effect in Alzheimer's disease. *Biogerontology* 18, 301–319. doi: 10.1007/s10522-017-9692-x

Avdoshina, V., Fields, J. A., Castellano, P., Dedoni, S., Palchik, G., Trejo, M., et al. (2016). The HIV Protein gp120 Alters Mitochondrial Dynamics in Neurons. *Neurotox. Res.* 29, 583–593. doi: 10.1007/s12640-016-9608-6

Berth, S., Caicedo, H. H., Sarma, T., Morfini, G., and Brady, S. T. (2015). Internalization and axonal transport of the HIV glycoprotein gp120. *ASN Neuro*. 7:1759091414568186. doi: 10.1177/1759091414568186

Bhat, R., Crowe, E. P., Bitto, A., Moh, M., Katsetos, C. D., Garcia, F. U., et al. (2012). Astrocyte senescence as a component of Alzheimer's disease. *PLoS One* 7:e45069. doi: 10.1111/acel.12937

Bonda, D. J., Mailankot, M., Stone, J. G., Garrett, M. R., Staniszewska, M., Castellani, R. J., et al. (2010). Indoleamine 2,3-dioxygenase and 3-hydroxykynurenine modifications are found in the neuropathology of Alzheimer's disease. *Redox Rep.* 15, 161–168. doi: 10.1179/ 174329210X12650506623645

Borlikova, G., and Endo, S. (2009). Inducible cAMP early repressor (ICER) and brain functions. *Mol. Neurobiol.* 40, 73–86. doi: 10.1007/s12035-009-8072-1

Borodinova, A. A., and Salozhin, S. V. (2017). Differences in the Biological Functions of BDNF and proBDNF in the Central Nervous System. *Neurosci. Behav. Physiol.* 47, 251–265.

Bramham, C. R., and Messaoudi, E. (2005). BDNF function in adult synaptic plasticity: the synaptic consolidation hypothesis. *Prog. Neurobiol.* 76, 99–125. doi: 10.1016/j.pneurobio.2005.06.003

Brizzi, M. F., Dentelli, P., Rosso, A., Calvi, C., Gambino, R., Cassader, M., et al. (2004). RAGE- and TGF-beta receptor-mediated signals converge on STAT5 and p21waf to control cell-cycle progression of mesangial cells: a possible role in the development and progression of diabetic nephropathy. *FASEB J.* 18, 1249–1251. doi: 10.1096/fj.03-1053fje

Buhusi, M., Etheredge, C., Granholm, A. C., and Buhusi, C. V. (2017). Increased Hippocampal ProBDNF Contributes to Memory Impairments in Aged Mice. *Front. Aging Neurosci.* 9:284. doi: 10.3389/fnagi.2017.00284

Calabretta, S., Bielli, P., Passacantilli, I., Pilozzi, E., Fendrich, V., Capurso, G., et al. (2016). Modulation of PKM alternative splicing by PTBP1 promotes gemcitabine resistance in pancreatic cancer cells. *Oncogene* 35, 2031–2039. doi: 10.1038/onc.2015.270

Caruso, P., Dunmore, B. J., Schlosser, K., Schoors, S., Dos Santos, C., Perez-Iratxeta, C., et al. (2017). Identification of MicroRNA-124 as a Major Regulator of Enhanced Endothelial Cell Glycolysis in Pulmonary Arterial Hypertension via PTBP1 (Polypyrimidine Tract Binding Protein) and Pyruvate Kinase M2. *Circulation* 136, 2451–2467. doi: 10.1161/CIRCULATIONAHA.117.028034

Chaneton, B., Hillmann, P., Zheng, L., Martin, A., Maddocks, O., Chokkathukalam, A., et al. (2012). Serine is a natural ligand and allosteric activator of pyruvate kinase M2. *Nature* 491, 458–462. doi: 10.1038/nature11540

Chen, B. (2019). Molecular Mechanism of HIV-1 Entry. *Trends Microbiol.* 27, 878–891.

Chhipa, A. S., and Patel, S. (2021). Targeting pyruvate kinase muscle isoform 2 (PKM2) in cancer: what do we know so far? *Life Sci.* 280:119694. doi: 10.1016/j. lfs.2021.119694

Cohen, J., and Torres, C. (2017). HIV-associated cellular senescence: a contributor to accelerated aging. *Ageing Res. Rev.* 36, 117–124. doi: 10.1016/j.arr.2016.12. 004

Deicken, R. F., Hubesch, B., Jensen, P. C., Sappey-Marinier, D., Krell, P., Wisniewski, A., et al. (1991). Alterations in brain phosphate metabolite concentrations in patients with human immunodeficiency virus infection. *Arch. Neurol.* 48, 203–209. doi: 10.1001/archneur.1991.00530140099022

Deinhardt, K., and Chao, M. V. (2014). Shaping neurons: long and short range effects of mature and proBDNF signalling upon neuronal structure. *Neuropharmacology* 76, 603–609. doi: 10.1016/j.neuropharm.2013.04.054

Delp, J., Funke, M., Rudolf, F., Cediel, A., Bennekou, S. H., van der Stel, W., et al. (2019). Development of a neurotoxicity assay that is tuned to detect mitochondrial toxicants. *Arch. Toxicol.* 93, 1585–1608. doi: 10.1007/s00204-019-02473-y

Desplats, P., Dumaop, W., Smith, D., Adame, A., Everall, I., Letendre, S., et al. (2013). Molecular and pathologic insights from latent HIV-1 infection in the human brain. *Neurology* 80, 1415–1423. doi: 10.1212/WNL.0b013e31828c2e9e

Di Marcantonio, D., Martinez, E., Kanefsky, J. S., Huhn, J. M., Gabbasov, R., Gupta, A., et al. (2021). ATF3 coordinates serine and nucleotide metabolism to drive cell cycle progression in acute myeloid leukemia. *Mol. cell* 81, 2752.e–2764.e. doi: 10.1016/j.molcel.2021.05.008

Esvald, E. E., Tuvikene, J., Sirp, A., Patil, S., Bramham, C. R., and Timmusk, T. (2020). CREB Family Transcription Factors Are Major Mediators of BDNF Transcriptional Autoregulation in Cortical Neurons. *J. Neurosci.* 40, 1405–1426. doi: 10.1523/JNEUROSCI.0367-19.2019

Fields, J. A., and Ellis, R. J. (2019). HIV in the cART era and the mitochondrial: immune interface in the CNS. *Int. Rev. Neurobiol.* 145, 29–65. doi: 10.1016/bs. irn.2019.04.003

Fields, J. A., Overk, C., Adame, A., Florio, J., Mante, M., Pineda, A., et al. (2016). Neuroprotective effects of the immunomodulatory drug FK506 in a model of HIV1-gp120 neurotoxicity. *J. Neuroinflammation* 13:120. doi: 10.1186/s12974-016-0585-8

Fleitas, C., Piñol-Ripoll, G., Marfull, P., Rocandio, D., Ferrer, I., Rampon, C., et al. (2018). proBDNF is modified by advanced glycation end products in Alzheimer's disease and causes neuronal apoptosis by inducing p75 neurotrophin receptor processing. *Mol. Brain* 11:68. doi: 10.1186/s13041-018-0411-6

Gu, X., Ma, Y., Liu, Y., and Wan, Q. (2020). Measurement of mitochondrial respiration in adherent cells by Seahorse XF96 Cell Mito Stress Test. *STAR Protoc.* 2:100245. doi: 10.1016/j.xpro.2020.100245

Gupta, V., and Bamezai, R. N. (2010). Human pyruvate kinase M2: a multifunctional protein. *Protein Sci.* 19, 2031–2044. doi: 10.1002/pro.505

Halcrow, P. W., Lakpa, K. L., Khan, N., Afghah, Z., Miller, N., Datta, G., et al. (2021). HIV-1 gp120-induced endolysosome de-acidification leads to efflux of endolysosome iron, and increases in mitochondrial iron and reactive oxygen species. *J. Neuroimmune. Pharmacol.* .[Epub online ahead of print]. doi: 10. 1007/s11481-021-09995-2

Han, R., Liang, J., and Zhou, B. (2021). Glucose Metabolic Dysfunction in Neurodegenerative Diseases-New Mechanistic Insights and the Potential of Hypoxia as a Prospective Therapy Targeting Metabolic Reprogramming. *Int. J. Mol. Sci.* 22:5887. doi: 10.3390/ijms22115887

Heaton, R. K., Franklin, D. R., Ellis, R. J., McCutchan, J. A., Letendre, S. L., Leblanc, S., et al. (2011). HIV-associated neurocognitive disorders before and during the era of combination antiretroviral therapy: differences in rates, nature, and predictors. *J. Neurovirol.* 17, 3–16. doi: 10.1007/s13365-010-0006-1

Heldt, S. A., Stanek, L., Chhatwal, J. P., and Ressler, K. J. (2007). Hippocampus-specific deletion of BDNF in adult mice impairs spatial memory and extinction of aversive memories. *Psychiatry* 12, 656–670. doi: 10.1038/sj.mp.4001957

Lannuzzi, C., Irace, G., and Sirangelo, I. (2014). Differential effects of glycation on protein aggregation and amyloid formation. *Front. Mol. Biosci.* 1:9. doi: 10.3389/fmolb.2014.00009

Kang, S., and Tang, H. (2020). HIV-1 Infection and Glucose Metabolism Reprogramming of T Cells: another Approach Toward Functional Cure and Reservoir Eradication. *Front Immunol.* 11:572677. doi: 10.3389/fimmu.2020. 572677

Kennon, A. M., and Stewart, J. A. Jr. (2021). RAGE Differentially Altered in vitro Responses in Vascular Smooth Muscle Cells and Adventitial Fibroblasts in Diabetes-Induced Vascular Calcification. *Front. Physiol.* 12:676727. doi: 10. 3389/fphys.2021.676727

Khan, M. I., Rath, S., Adhami, V. M., and Mukhtar, H. (2018). Hypoxia driven glycation: mechanisms and therapeutic opportunities. *Semin. Cancer Biol.* 49, 75–82. doi: 10.1016/j.semcancer.2017.05.008

Kichev, A., Ilieva, E. V., Piñol-Ripoll, G., Podlesniy, P., Ferrer, I., Portero-Otín, M., et al. (2009). Cell death and learning impairment in mice caused by in vitro modified pro-NGF can be related to its increased oxidative modifications in Alzheimer disease. *Am. J. Pathol.* 175, 2574–2585. doi: 10.2353/ajpath.2009. 090018

Kim, Y. H., Coon, A., Baker, A. F., and Powis, G. (2011). Antitumor agent PX-12 inhibits HIF-1α protein levels through an Nrf2/PMF-1-mediated increase in spermidine/spermine acetyl transferase. *Cancer Chemother. Pharmacol.* 68, 405–413. doi: 10.1007/s00280-010-1500-0

Kislinger, T., Fu, C., Huber, B., Qu, W., Taguchi, A., Du Yan, S., et al. (1999). N(epsilon)-(carboxymethyl)lysine adducts of proteins are ligands for receptor for advanced glycation end products that activate cell signaling pathways and modulate gene expression. *J. Biol. Chem.* 274, 31740–31749. doi: 10.1074/jbc.274.44.31740

Kong, D., Park, E. J., Stephen, A. G., Calvani, M., Cardellina, J. H., Monks, A., et al. (2005). Echinomycin, a small-molecule inhibitor of hypoxia-inducible factor-1 DNA-binding activity. *Cancer Res.* 65, 9047–9055. doi: 10.1158/0008-5472.CAN-05-1235

Kontaxi, C., Piccardo, P., and Gill, A. C. (2017). Lysine-Directed Post-translational Modifications of Tau Protein in Alzheimer's Disease and Related Tauopathies. *Front. Mol. Biosci.* 4:56. doi: 10.3389/fmolb.2017.00056

Krueger, D. A., Mao, D., Warner, E. A., and Dowd, D. R. (1999). Functional analysis of the mouse ICER (Inducible cAMP Early Repressor) promoter: evidence for a protein that blocks calcium responsiveness of the CAREs (cAMP autoregulatory elements). *Mol. Endocrinol.* 13, 1207–1217. doi: 10.1210/mend.13.7.0319

Li, J., Liu, D., Sun, L., Lu, Y., and Zhang, Z. (2012). Advanced glycation end products and neurodegenerative diseases: mechanisms and perspective. *J. Neurol. Sci.* 317, 1–5. doi: 10.1016/j.jns.2012.02.018

Li, J., and Schmidt, A. M. (1997). Characterization and functional analysis of the promoter of RAGE, the receptor for advanced glycation end products. *J. Biol. Chem.* 272, 16498–16506. doi: 10.1074/jbc.272.26.16498

Lin, J. A., Wu, C. H., Lu, C. C., Hsia, S. M., and Yen, G. C. (2016). Glycative stress from advanced glycation end products (AGEs) and dicarbonyls: an emerging biological factor in cancer onset and progression. *Mol. Nutr. Food Res.* 60, 1850–1864. doi: 10.1002/mnfr.201500759

Linares, A. J., Lin, C. H., Damianov, A., Adams, K. L., Novitch, B. G., and Black, D. L. (2015). The splicing regulator PTBP1 controls the activity of the transcription factor Pbx1 during neuronal differentiation. *ELife* 4:e09268. doi: 10.7554/eLife.09268

Liu, J., Huang, K., Cai, G. Y., Chen, X. M., Yang, J. R., Lin, L. R., et al. (2014). Receptor for advanced glycation end-products promotes premature senescence of proximal tubular epithelial cells via activation of endoplasmic reticulum stress-dependent p21 signaling. *Cell. Signal* 26, 110–121. doi: 10.1016/j.cellsig.2013.10.002

Lotan, R., Ganmore, I., Livny, A., Itzhaki, N., Waserman, M., Shelly, S., et al. (2021). Effect of Advanced Glycation End Products on Cognition in Older Adults with Type 2 Diabetes: results from a Pilot Clinical Trial. *J. Alzheimers Dis.* 82, 1785–1795. doi: 10.3233/JAD-210131

Lotharius, J., Barg, S., Wiekop, P., Lundberg, C., Raymon, H. K., and Brundin, P. (2002). Effect of mutant alpha-synuclein on dopamine homeostasis in a new human mesencephalic cell line. *J. Biol. Chem.* 277, 38884–38894. doi: 10.1074/jbc.M205518200

Lu, J., Zhou, W., Dou, F., Wang, C., and Yu, Z. (2021). TRPV1 sustains microglial metabolic reprogramming in Alzheimer's disease. *EMBO Rep.* 22:e52013. doi: 10.15252/embr.202052013

Macintyre, A. N., and Rathmell, J. C. (2011). PKM2 and the tricky balance of growth and energy in cancer. *Mol. Cell* 42, 713–714. doi: 10.1016/j.molcel.2011.06.003

Mantamadiotis, T., Lemberger, T., Bleckmann, S. C., Kern, H., Kretz, O., Martin Villalba, A., et al. (2002). Disruption of CREB function in brain leads to neurodegeneration. *Nat. Genet.* 31, 47–54. doi: 10.1038/ng882

McElvaney, O. J., McEvoy, N. L., McElvaney, O. F., Carroll, T. P., Murphy, M. P., Dunlea, D. M., et al. (2020). Characterization of the Inflammatory Response to Severe COVID-19 Illness. *Am. J. Respir. Crit. Care Med.* 202, 812–821. doi: 10.1164/rccm.202005-1583OC

Medina, M. Á (2020). Metabolic Reprogramming is a Hallmark of Metabolism Itself. *Bioessays* 42, e2000058. doi: 10.1002/bies.202000058

Michael, H., Mpofana, T., Ramlall, S., and Oosthuizen, F. (2020). The Role of Brain Derived Neurotrophic Factor in HIV-Associated Neurocognitive Disorder: from the Bench-Top to the Bedside. *Neuropsychiatr. Dis. Treat.* 16, 355–367. doi: 10.2147/NDT.S232836

Miranda, M., Morici, J. F., Zanoni, M. B., and Bekinschtein, P. (2019). Brain-Derived Neurotrophic Factor: a Key Molecule for Memory in the Healthy and the Pathological Brain. *Front. Cell Neurosci.* 13:363. doi: 10.3389/fncel.2019.00363

Mouravlev, A., Dunning, J., Young, D., and During, M. J. (2006). Somatic gene transfer of cAMP response element-binding protein attenuates memory impairment in aging rats. *Proc. Natl. Acad. Sci. USA.* 103, 4705–4710. doi: 10.1073/pnas.0506137103

Nandi, S., Razzaghi, M., Srivastava, D., and Dey, M. (2020). Structural basis for allosteric regulation of pyruvate kinase M2 by phosphorylation and acetylation. *J. Biol. Chem.* 295, 17425–17440. doi: 10.1074/jbc.RA120.015800

Palsson-McDermott, E. M., Dyck, L., Zasłona, Z., Menon, D., McGettrick, A. F., Mills, K., et al. (2017). Pyruvate Kinase M2 Is Required for the Expression of the Immune Checkpoint PD-L1 in Immune Cells and Tumors. *Front. Immunol.* 8:1300. doi: 10.3389/fimmu.2017.01300

Panday, A., Sahoo, M. K., Osorio, D., and Batra, S. (2015). NADPH oxidases: an overview from structure to innate immunity-associated pathologies. *Cell Mol. Immunol.* 12, 5–23. doi: 10.1038/cmi.2014.89

Pang, P. T., Nagappan, G., Guo, W., and Lu, B. (2016). Extracellular and intracellular cleavages of proBDNF required at two distinct stages of late-phase LTP. *NPJ Sci. Learn.* 1:16003. doi: 10.1038/npjscilearn.2016.3

Pfleger, J., He, M., and Abdellatif, M. (2015). Mitochondrial complex II is a source of the reserve respiratory capacity that is regulated by metabolic sensors and promotes cell survival. *Cell Death Dis.* 6:e1835. doi: 10.1038/cddis.2015.202

Phan, L. M., Yeung, S. C., and Lee, M. H. (2014). Cancer metabolic reprogramming: importance, main features, and potentials for precise targeted anti-cancer therapies. *Cancer Biol. Med.* 11, 1–19. doi: 10.7497/j.issn.2095-3941.2014.01.001

Polcicova, K., Badurova, L., and Tomaskova, J. (2020). Metabolic reprogramming as a feast for virus replication. *Acta Virol.* 64, 201–215. doi: 10.4149/av_2020_210

Porcher, C., Medina, I., and Gaiarsa, J. L. (2018). Mechanism of BDNF Modulation in GABAergic Synaptic Transmission in Healthy and Disease Brains. *Front. Cell. Neurosci.* 12:273. doi: 10.3389/fncel.2018.00273

Prakasam, G., Iqbal, M. A., Bamezai, R., and Mazurek, S. (2018). Posttranslational Modifications of Pyruvate Kinase M2: tweaks that Benefit Cancer. *Front. Oncol.* 8:22. doi: 10.3389/fonc.2018.00022

Prusinkiewicz, M. A., and Mymryk, J. S. (2019). Metabolic Reprogramming of the Host Cell by Human Adenovirus Infection. *Viruses* 11:141. doi: 10.3390/v11020141

Qi, W., Keenan, H. A., Li, Q., Ishikado, A., Kannt, A., Sadowski, T., et al. (2017). Pyruvate kinase M2 activation may protect against the progression of diabetic glomerular pathology and mitochondrial dysfunction. *Nat. Med.* 23, 753–762. doi: 10.1038/nm.4328

Qosa, H., LeVine, H. III, Keller, J. N., and Kaddoumi, A. (2014). Mixed oligomers and monomeric amyloid-β disrupts endothelial cells integrity and reduces monomeric amyloid-β transport across hCMEC/D3 cell line as an in vitro blood-brain barrier model. *Biochim. Biophys. Acta.* 1842, 1806–1815. doi: 10.1016/j.bbadis.2014.06.029

Requejo-Aguilar, R., and Bolaños, J. P. (2016). Mitochondrial control of cell bioenergetics in Parkinson's disease. *Free Radic. Biol. Med.* 100, 123–137. doi: 10.1016/j.freeradbiomed.2016.04.012

Riffault, B., Medina, I., Dumon, C., Thalman, C., Ferrand, N., Friedel, P., et al. (2014). Pro-brain-derived neurotrophic factor inhibits GABAergic neurotransmission by activating endocytosis and repression of GABAA receptors. *J. Neurosci.* 34, 13516–13534. doi: 10.1523/JNEUROSCI.2069-14.2014

Rungratanawanich, W., Qu, Y., Wang, X., Essa, M. M., and Song, B. J. (2021). Advanced glycation end products (AGEs) and other adducts in aging-related diseases and alcohol-mediated tissue injury. *Exp. Mol. Med.* 53, 168–188. doi: 10.1038/s12276-021-00561-7

Saggerson, D. (2008). Malonyl-CoA, a key signaling molecule in mammalian cells. *Annu. Rev. Nutr.* 28, 253–272. doi: 10.1146/annurev.nutr.28.061807.155434

Saha, A., Kim, S. J., Zhang, Z., Lee, Y. C., Sarkar, C., Tsai, P. C., et al. (2008). RAGE signaling contributes to neuroinflammation in infantile neuronal ceroid lipofuscinosis. *FEBS Lett.* 582, 3823–3831. doi: 10.1016/j.febslet.2008.10.015

Sakamoto, K., Karelina, K., and Obrietan, K. (2011). CREB: a multifaceted regulator of neuronal plasticity and protection. *J Neurochem.* 116, 1–9. doi: 10.1111/j.1471-4159.2010.07080.x

Sanchez, E.L., and Lagunoff, M. (2015). Viral activation of cellular metabolism. *Virology*. 479–480, 609–618. doi: 10.1016/j.virol.2015.02.038

Sanderson, S. M., Gao, X., Dai, Z., and Locasale, J. W. (2019). Methionine metabolism in health and cancer: a nexus of diet and precision medicine. *Nat. Rev. Cancer* 19, 625–637. doi: 10.1038/s41568-019-0187-8

Sansbury, B. E., Jones, S. P., Riggs, D. W., Darley-Usmar, V. M., and Hill, B. G. (2011). Bioenergetic function in cardiovascular cells: the importance of the reserve capacity and its biological regulation. *Chem. Biol. Interact.* 191, 288–295. doi: 10.1016/j.cbi.2010.12.002

Santerre, M., Arjona, S. P., Allen, C. N., Callen, S., Buch, S., and Sawaya, B. E. (2021). HIV-1 Vpr protein impairs lysosome clearance causing SNCA/alpha-synuclein accumulation in neurons. *Autophagy* 17, 1768–1782. doi: 10.1080/15548627.2021.1915641

Santerre, M., Bagashev, A., Gorecki, L., Lysek, K. Z., Wang, Y., Shrestha, J., et al. (2019). HIV-1 Tat protein promotes neuronal dysregulation by inhibiting E2F transcription factor 3 (E2F3). *J. Biol. Chem.* 294, 3618–3633. doi: 10.1074/jbc.RA118.003744

Saylor, D., Dickens, A. M., Sacktor, N., Haughey, N., Slusher, B., Pletnikov, M., et al. (2016). HIV-associated neurocognitive disorder–pathogenesis and prospects for treatment. *Nat. Rev. Nat. Rev. Neurol.* 12, 234–248.

Scholz, D., Pöltl, D., Genewsky, A., Weng, M., Waldmann, T., Schildknecht, S., et al. (2011). Rapid, complete and large-scale generation of post-mitotic neurons from the human LUHMES cell line. *J. Neurochem.* 119, 957–971. doi: 10.1111/j.1471-4159.2011.07255.x

Schulz, J. B., Lindenau, J., Seyfried, J., and Dichgans, J. (2000). Glutathione, oxidative stress and neurodegeneration. *Eur. J. Biochem.* 267, 4904–4911. doi: 10.1046/j.1432-1327.2000.01595.x

Shi, M., Yang, S., Zhu, X., Sun, D., Sun, D., Jiang, X., et al. (2019). The RAGE/STAT5/autophagy axis regulates senescence in mesangial cells. *Cell Signal* 62:109334. doi: 10.1016/j.cellsig.2019.05.019

Shi, Y., Yuan, S., and Tang, S.-J. (2021). Reactive oxygen species (ROS) are critical for morphine exacerbation of HIV-1 gp120-induced pain. *J. Neuroimmun. Pharmacol.* 16, 581–591. doi: 10.1007/s11481-020-09951-6

Slanzi, A., Iannoto, G., Rossi, B., Zenaro, E., and Constantin, G. (2020). In vitro models of neurodegenerative diseases. *Front. Cell Dev. Biol.* 8:328. doi: 10.3389/fcell.2020.00328

Smith, L. K., Babcock, I. W., Minamide, L. S., Shaw, A. E., Bamburg, J. R., and Kuhn, T. B. (2021). Direct interaction of HIV gp120 with neuronal CXCR4 and CCR5 receptors induces cofilin-actin rod pathology via a cellular prion protein- and NOX-dependent mechanism. *PloS One* 16:e0248309. doi: 10.1371/journal.pone.0248309

Speidell, A., Asuni, G. P., Wakulski, R., and Mocchetti, I. (2020). Up-regulation of the p75 neurotrophin receptor is an essential mechanism for HIV-gp120 mediated synaptic loss in the striatum. *Brain Behav. Immun.* 89, 371–379. doi: 10.1016/j.bbi.2020.07.023

Starkov, A. A., Polster, B. M., and Fiskum, G. (2002). Regulation of hydrogen peroxide production by brain mitochondria by calcium and Bax. *J. Neurochem.* 83, 220–228. doi: 10.1046/j.1471-4159.2002.01153.x

Stein, L. R., and Imai, S. (2012). The dynamic regulation of NAD metabolism in mitochondria. *Trends Endocrinol. Metab.* 23, 420–428. doi: 10.1016/j.tem.2012.06.005

Su, C. H., Hung, K. Y., Hung, S. C., and Tarn, W. Y. (2017). RBM4 Regulates Neuronal Differentiation of Mesenchymal Stem Cells by Modulating Alternative Splicing of Pyruvate Kinase M. *Mol Cell Biol.* 37, e466–e416. doi: 10.1128/MCB.00466-16

Tang, B. L. (2020). Glucose, glycolysis, and neurodegenerative diseases. *J. Cell. Physiol.* 235, 7653–7662. doi: 10.1002/jcp.29682

Teodorof-Diedrich, C., and Spector, S. A. (2018). Human immunodeficiency virus type 1 gp120 and TAT induce mitochondrial fragmentation and incomplete mitophagy in human neurons. *J. Virol.* 92, 993–918. doi: 10.1128/JVI.00993-18

Teodorof-Diedrich, C., and Spector, S. A. (2020). Human immunodeficiency virus type 1 and methamphetamine-mediated mitochondrial damage and neuronal degeneration in human neurons. *J. Virol.* 94, 924–920. doi: 10.1128/JVI.00924-20

Thaker, S. K., Ch'ng, J., and Christofk, H. R. (2019). Viral hijacking of cellular metabolism. *BMC Biol.* 17:59. doi: 10.1186/s12915-019-0678-9

Thomas, A. X., Cruz Del, Angel, Y., Gonzalez, M. I., Carrel, A. J., Carlsen, J., et al. (2016). Rapid Increases in proBDNF after Pilocarpine-Induced Status Epilepticus in Mice Are Associated with Reduced proBDNF Cleavage Machinery. *eNeuro* 3:ENEURO.20–ENEURO.15. doi: 10.1523/ENEURO.0020-15.2016

Udupa, S., Nguyen, S., Hoang, G., Nguyen, T., Quinones, A., Pham, K., et al. (2019). Upregulation of the Glutaminase II Pathway Contributes to Glutamate Production upon Glutaminase 1 Inhibition in Pancreatic Cancer. *Proteomics* 19:e1800451. doi: 10.1002/pmic.201800451

Valentín-Guillama, G., López, S., Kucheryavykh, Y. V., Chorna, N. E., Pérez, J., Ortiz-Rivera, J., et al. (2018). HIV-1 Envelope Protein gp120 Promotes Proliferation and the Activation of Glycolysis in Glioma Cell. *Cancers* 10:301. doi: 10.3390/cancers10090301

Vitek, M. P., Bhattacharya, K., Glendening, J. M., Stopa, E., Vlassara, H., Bucala, R., et al. (1994). Advanced glycation end products contribute to amyloidosis in Alzheimer disease. *Proc. Natl. Acad. Sci. U.S.A* 91, 4766–4770. doi: 10.1073/pnas.91.11.4766

Wang, S., Qi, Y., Gao, X., Qiu, W., Liu, Q., Guo, X., et al. (2020). Hypoxia-induced lncRNA PDIA3P1 promotes mesenchymal transition via sponging of miR-124-3p in glioma. *Cell Death Dis.* 11:168. doi: 10.1038/s41419-020-2345-z

Wang, Y., Liu, J., Jin, X., Zhang, D., Li, D., Hao, F., et al. (2017). O-GlcNAcylation destabilizes the active tetrameric PKM2 to promote the Warburg effect. *Proc. Natl. Acad. Sci. U.S.A* 114, 13732–13737. doi: 10.1073/pnas.1704145115

Williams, A. L., Khadka, V., Tang, M., Avelar, A., Schunke, K. J., Menor, M., et al. (2018). HIF1 mediates a switch in pyruvate kinase isoforms after myocardial infarction. *Physiol. Genom.* 50, 479–494. doi: 10.1152/physiolgenomics.00130.2017

Williams, N. C., and O'Neill, L. (2018). A Role for the Krebs Cycle Intermediate Citrate in Metabolic Reprogramming in Innate Immunity and Inflammation. *Front. Immunol.* 9:141. doi: 10.3389/fimmu.2018.00141

Woods, S. P., Moore, D. J., Weber, E., and Grant, I. (2009). Cognitive neuropsychology of HIV-associated neurocognitive disorders. *Neuropsychol. Rev.* 19, 152–168. doi: 10.1007/s11065-009-9102-5

Wu, G., Cheney, C., Huang, Q., Hazuda, D. J., Howell, B. J., and Zuck, P. (2021). Improved Detection of HIV Gag p24 Protein Using a Combined Immunoprecipitation and Digital ELISA Method. *Front Microbiol.* 12:636703. doi: 10.3389/fmicb.2021.636703

Xie, Y., Seawell, J., Boesch, E., Allen, L., Suchy, A., Longo, F. M., et al. (2021). Small molecule modulation of the p75 neurotrophin receptor suppresses age- and genotype-associated neurodegeneration in HIV gp120 transgenic mice. *Exp. Neurol.* 335:113489. doi: 10.1016/j.expneurol.2020.113489

Yadava, N., and Nicholls, D. G. (2007). Spare respiratory capacity rather than oxidative stress regulates glutamate excitotoxicity after partial respiratory inhibition of mitochondrial complex I with rotenone. *J. Neurosci.* 27, 7310–7317. doi: 10.1523/JNEUROSCI.0212-07.2007

Yang, J., Harte-Hargrove, L. C., Siao, C. J., Marinic, T., Clarke, R., Ma, Q., et al. (2014). proBDNF negatively regulates neuronal remodeling, synaptic transmission, and synaptic plasticity in hippocampus. *Cell Rep.* 7, 796–806. doi: 10.1016/j.celrep.2014.03.040

Younessi, P., and Yoonessi, A. (2011). Advanced glycation end-products and their receptor-mediated roles: inflammation and oxidative stress. *Iran J. Med. Sci.* 36, 154–166.

Yuan, Z., Petree, J. R., Lee, F. E.-H., Fan, X., Salaita, K., Guidot, D. M., et al. (2019). Macrophages exposed to HIV viral protein disrupt lung epithelial cell integrity and mitochondrial bioenergetics via exosomal microrna shuttling. *Cell Death Dis.* 10:580. doi: 10.1038/s41419-019-1803-y

Zahra, K., Dey, T., Ashish, Mishra, S. P., and Pandey, U. (2020). Pyruvate Kinase M2 and Cancer: The Role of PKM2 in Promoting Tumorigenesis. *Front. Oncol.* 10:159. doi: 10.3389/fonc.2020.00159

Zhang, K., Yan, J., Wang, L., Tian, X., Zhang, T., Guo, L., et al. (2018). The Pyk2/MCU pathway in the rat middle cerebral artery occlusion model of ischemic stroke. *Neurosci. Res.* 131, 52–62. doi: 10.1016/j.neures.2017.09.002

Zhao, Y., Zhao, X., Chen, V., Feng, Y., Wang, L., Croniger, C., et al. (2019). Colorectal cancers utilize glutamine as an anaplerotic substrate of the TCA cycle in vivo. *Sci. Rep.* 9:19180. doi: 10.1038/s41598-019-55718-2

Zheng, J. (2012). Energy metabolism of cancer: glycolysis versus oxidative phosphorylation (Review). *Oncol Lett.* 4, 1151–1157. doi: 10.3892/ol.2012.928

Zheng, J., Thylin, M. R., Ghorpade, A., Xiong, H., Persidsky, Y., Cotter, R., et al. (1999). Intracellular CXCR4 signaling, neuronal apoptosis and neuropathogenic mechanisms of HIV-1-associated dementia. *J. Neuroimmunol.* 98, 185–200. doi: 10.1016/s0165-5728(99)00049-1

Zheng, X., Boyer, L., Jin, M., Mertens, J., Kim, Y., Ma, L., et al. (2016). Metabolic reprogramming during neuronal differentiation from aerobic glycolysis to neuronal oxidative phosphorylation. *eLife* 5:e13374. doi: 10.7554/eLife.13374

Zhou, M., Greenhill, S., Huang, S., Silva, T. K., Sano, Y., Wu, S., et al. (2016). CCR5 is a suppressor for cortical plasticity and hippocampal learning and memory. *eLife* 5:e20985. doi: 10.7554/eLife.20985

Zhu, X., Han, X., Blendy, J. A., and Porter, B. E. (2012). Decreased CREB levels suppress epilepsy. *Neurobiol. Dis.* 45, 253–263. doi: 10.1016/j.nbd.2011.08.009

Zuccato, C., and Cattaneo, E. (2009). Brain-derived neurotrophic factor in neurodegenerative diseases. *Nat. Rev. Neurol.* 5, 311–322. doi: 10.1038/nrneurol.2009.54

Conflict of Interest: The authors declare that the research was conducted in the absence of any commercial or financial relationships that could be construed as a potential conflict of interest.

Publisher's Note: All claims expressed in this article are solely those of the authors and do not necessarily represent those of their affiliated organizations, or those of the publisher, the editors and the reviewers. Any product that may be evaluated in this article, or claim that may be made by its manufacturer, is not guaranteed or endorsed by the publisher.

Copyright © 2022 Allen, Arjona, Santerre, De Lucia, Koch and Sawaya. This is an open-access article distributed under the terms of the Creative Commons Attribution License (CC BY). The use, distribution or reproduction in other forums is permitted, provided the original author(s) and the copyright owner(s) are credited and that the original publication in this journal is cited, in accordance with accepted academic practice. No use, distribution or reproduction is permitted which does not comply with these terms.

frontiers | Frontiers in Cellular Neuroscience

ORIGINAL RESEARCH
published: 15 April 2022
doi: 10.3389/fncel.2022.797588

Plasticity-Related Gene 5 Is Expressed in a Late Phase of Neurodifferentiation After Neuronal Cell-Fate Determination

*Isabel Gross[1,2], Nicola Brandt[1,2], Danara Vonk[1,2,3], Franziska Köper[1,2,4], Lars Wöhlbrand[5], Ralf Rabus[5], Martin Witt[6], Axel Heep[2,4,7], Torsten Plösch[2,4,7], Mark S. Hipp[2,3] and Anja U. Bräuer[1,2,7]**

[1] Research Group Anatomy, School of Medicine and Health Sciences, Carl von Ossietzky University of Oldenburg, Oldenburg, Germany, [2] School of Medicine and Health Sciences, Carl von Ossietzky University of Oldenburg, Oldenburg, Germany, [3] Department of Biomedical Sciences of Cells and Systems, University Medical Center Groningen, University of Groningen, Groningen, Netherlands, [4] Perinatal Neurobiology Research Group, School of Medicine and Health Sciences, Carl von Ossietzky University of Oldenburg, Oldenburg, Germany, [5] General and Molecular Microbiology, Institute for Chemistry and Biology of the Marine Environment (ICBM), Carl von Ossietzky University of Oldenburg, Oldenburg, Germany, [6] Department of Anatomy, University Medical Center Rostock, Rostock, Germany, [7] Research Center Neurosensory Science, Carl von Ossietzky University of Oldenburg, Oldenburg, Germany

OPEN ACCESS

Edited by:
Clive R. Bramham, University of Bergen, Norway

Reviewed by:
Pirta Elina Hotulainen, Minerva Foundation Institute for Medical Research, Finland
Jocelyn Widagdo, The University of Queensland, Australia

***Correspondence:**
Anja U. Bräuer
anja.braeuer@uni-oldenburg.de

Specialty section:
This article was submitted to Cellular Neurophysiology, a section of the journal Frontiers in Cellular Neuroscience

Received: *18 October 2021*
Accepted: *17 March 2022*
Published: *15 April 2022*

Citation:
Gross I, Brandt N, Vonk D, Köper F, Wöhlbrand L, Rabus R, Witt M, Heep A, Plösch T, Hipp MS and Bräuer AU (2022) Plasticity-Related Gene 5 Is Expressed in a Late Phase of Neurodifferentiation After Neuronal Cell-Fate Determination. Front. Cell. Neurosci. 16:797588. doi: 10.3389/fncel.2022.797588

During adult neurogenesis, neuronal stem cells differentiate into mature neurons that are functionally integrated into the existing network. One hallmark during the late phase of this neurodifferentiation process is the formation of dendritic spines. These morphological specialized structures form the basis of most excitatory synapses in the brain, and are essential for neuronal communication. Additionally, dendritic spines are affected in neurological disorders, such as Alzheimer's disease or schizophrenia. However, the mechanisms underlying spinogenesis, as well as spine pathologies, are poorly understood. Plasticity-related Gene 5 (PRG5), a neuronal transmembrane protein, has previously been linked to spinogenesis *in vitro*. Here, we analyze endogenous expression of the PRG5 protein in different mouse brain areas, as well as on a subcellular level. We found that native PRG5 is expressed dendritically, and in high abundance in areas characterized by their regenerative capacity, such as the hippocampus and the olfactory bulb. During adult neurogenesis, PRG5 is specifically expressed in a late phase after neuronal cell-fate determination associated with dendritic spine formation. On a subcellular level, we found PRG5 not to be localized at the postsynaptic density, but at the base of the synapse. In addition, we showed that PRG5-induced formation of membrane protrusions is independent from neuronal activity, supporting a possible role in the morphology and stabilization of spines.

Keywords: neurogenesis, PRGs, dendritic spines, neurodifferentiation, brain development

INTRODUCTION

Complex molecular processes during the development of the central nervous system (CNS) lead to an intricate network of highly specialized cells that communicate via synaptic activity. This development is established by a well-organized progression of events that are still poorly understood. Research has often focused on early embryonic stages of CNS development, but important steps of neuro-differentiation also continue after birth. Postnatal development involves axonal pathfinding and dendrite outgrowth, as well as establishing cell-cell contacts during spinogenesis and synaptogenesis (Lewis et al., 2013; Elston and Fujita, 2014). Even in adulthood, after development is completed, there are areas of the brain, retaining their capacity to generate new neurons, that then differentiate and are integrated into the existing network (Altman and Das, 1965; Paton and Nottebohm, 1984; Zhao et al., 2008; Ming and Song, 2011). In the mouse, this adult neurogenesis appears to occur only in the subventricular zone (svz) of the lateral ventricle and the subgranular zone (sgz) of the hippocampal dentate gyrus. Proliferating radial or non-radial precursor cells develop into transient amplifying cells in the svz, or into intermediate progenitor cells in the sgz, which can then both turn into neuroblasts. In the svz, doublecortin (DCX)-expressing neuroblasts migrate toward the olfactory bulb by forming a chain through a glial tube, called the rostral migratory stream (RMS). Upon arrival, they detach from the RMS by radial migration to the glomerular layer, where they differentiate and synaptic integration occurs (Lois et al., 1996; Lledo et al., 2006). In the second region of adult neurogenesis, the sgz in the hippocampus, the neuroblasts develop into immature neurons that start to migrate into the granule-cell layer and concurrently start to differentiate into dentate granule cells, including their synaptic integration into the hippocampal network (Lledo et al., 2006; Zhao et al., 2006; Ming and Song, 2011).

In both postnatal development and adult neurogenesis, late neurodifferentiation is characterized by the formation of dendritic spines (Stiles and Jernigan, 2010; Chen et al., 2014). These morphologically specialized structures extend from the dendrites and form the basis of most excitatory synapses in the brain. They exist in different sizes and shapes, and maintain a high capacity for plastic changes (Hering and Sheng, 2001; Tashiro and Yuste, 2003; Yuste and Bonhoeffer, 2004). Extensive research on dendritic spines reveals their importance for neuronal information processing, but the mechanisms of spine generation are still not well understood. Due to their central role in the functionality of the CNS, dendritic spines have been linked to several neurodegenerative pathologies, for example Alzheimer's or Huntington's disease. Additionally, proper spine development is impaired in neurodevelopmental disorders that are marked by intellectual disabilities, as in schizophrenia or autism-spectrum disorders (Herms and Dorostkar, 2016; Martinez-Cerdeno, 2017).

So far, several molecules involved in spinogenesis have been identified (Zhang and Benson, 2000; Sala et al., 2008). One of them is Plasticity-related Gene 5 (PRG5) a member of the lipid-phosphate phosphatase (LPP) superfamily (Coiro et al., 2014). LPPs are integral membrane proteins that consist of six transmembrane domains with three extracellular loops, containing one conserved ecto-phosphatase site (Brindley, 2004; Pyne et al., 2004; Sigal et al., 2005). By modifying their extracellular concentration or receptor affinity, they can modulate the signal transduction of lipid phosphate esters such as lysophosphatidic acid (LPA) or sphingosine-1-phosphate (S1P) (Brindley and Waggoner, 1998). In the LPP subfamily of PRGs, also called lipid-phosphate phosphatase related proteins (LPPRs), the conserved amino acids for the ecto-phosphatase activity have been modified. They therefore lack the enzymatic activity, but are still capable of modifying bioactive lipid signaling. The underlying mechanisms are still under investigation (Zhang et al., 2000; Brindley, 2004; Bräuer and Nitsch, 2008).

Another notable difference to the rest of the LPP family members is their vertebrate-specific and predominant neuronal expression (Bräuer et al., 2003). PRG5 (synonyms: LPPR5, PAP2D) mRNA is strongly expressed during mouse brain development, where it peaks around birth and slightly decreases toward adult stages. Only in areas of high synaptic plasticity and adult neurogenesis does PRG5 expression remain elevated (Coiro et al., 2014; Gross et al., 2021). *In vitro* analysis of developing hippocampal neurons showed a shift in expression, from an equal distribution along all neurites toward increased localization only along dendrites (Broggini et al., 2010; Coiro et al., 2014). The overexpression of PRG5 in immature primary hippocampal neurons led to an early increase in the formation of spine-like membrane protrusions. In mature neurons, PRG5 overexpression increased the number of homer-positive spines, as well as their spine-head diameters (Coiro et al., 2014). These results strongly support a functional role of PRG5 in dendritic spine development that should be analyzed during neuronal development.

Because previous PRG5 studies focused almost exclusively on *in vitro* experiments, the first aim of this study was to analyze endogenous PRG5 expression in mouse brain tissue. Therefore, we validated a specific PRG5 antibody and analyzed its protein detection in western blot experiments and with mass spectrometry. We performed immunofluorescence of different mouse brain regions and developmental stages. We found PRG5 to be ubiquitously expressed in the mouse brain, with high protein expression in regions of adult neurogenesis, such as the hippocampus and the olfactory bulb. However, we found PRG5 not to be involved in early processes of adult neurogenesis but associated with late post-mitotic neurodifferentiation. On a subcellular level, we found the PRG5 protein not to be located at the postsynaptic density and therefore postulate an important role of PRG5 in the formation and stabilization of dendritic spine morphology.

RESULTS

Plasticity-Related Gene 5 Is a Glycosylated Membrane Protein in Mouse Brain Tissue

Existing studies of PRG5 expression were predominantly based on mRNA analysis, and protein studies so far focused primarily on *in vitro* experiments (Broggini et al., 2010; Coiro et al., 2014;

Yu et al., 2015). To further investigate the role of PRG5 in the mouse brain, we identified a previously used PRG5 polyclonal antibody to be suitable for western blot and immunofluorescence in mouse brain tissue samples (Coiro et al., 2014). Antibody specificity to PRG5, compared to other PRG family members, was verified by western blotting of isolated eGFP constructs from HEK293H cells overexpressing all PRGs, and the respective detection of antibodies (**Figure 1A**). The antibody specifically detected the isolated PRG5-eGFP protein construct in bands at 60 kDa, equivalent to the predicted molecular weight of PRG5 and eGFP protein combined, but also in a band above 150 kDa. These bands were additionally analyzed by mass spectrometry (MS), and both contained PRG5 peptides (**Figure 1A**, bands marked with asterisks, for MS data see **Supplementary Table 1**). In a previous study, quantitative real-time PCR of different mouse tissue samples revealed highest PRG5 mRNA expression in the brain. Additionally, low mRNA expression in heart, lung, and testes was found, whereas no mRNA expression was detected in thymus, liver, spleen, and kidney (Coiro et al., 2014). We therefore used liver and spleen protein lysates as negative controls and cerebellum protein lysate as positive control for the anti-PRG5 antibody in western blot analysis. We found a strong PRG5 signal around 150 kDa and a weak signal around 37 kDa in cerebellum lysates. No PRG5 signal was detected in liver and spleen protein lysates (**Figure 1B** and **Supplementary Figure 1**).

Like its PRG family members, PRG5 is a six-transmembrane protein with intracellular N- and C-termini (**Figure 1C**; Brindley, 2004; Bräuer and Nitsch, 2008; Strauss and Bräuer, 2013). The antibody binding site in the first extracellular loop is indicated in **Figure 1C**. We previously demonstrated membranous protein expression of PRG5 in protein lysates of cultured primary hippocampal neurons (Coiro et al., 2014). Here, we confirm this membrane localization of PRG5 for brain tissue by analyzing postnatal day 15 (P15) mouse cortex lysates (**Figure 1C**). We also demonstrated N-glycosylation of the native PRG5 protein in mouse cortex lysate by a band shift after hydrolyzation of N-linked glycan chains using N-glycosidase F (**Figure 1C**).

The Plasticity-Related Gene 5 Protein Is Developmentally Regulated in the Mouse Cortex

We previously analyzed PRG1-5 expression on the mRNA level during mouse brain development via quantitative RT-PCR and found expression patterns to be dynamic (Velmans et al., 2013; Coiro et al., 2014; Gross et al., 2021). Here, we confirm a developmental regulation also for the PRG5 protein in cortex lysates from developmental stages E14 to P60 (**Figure 2A**). A protein band around 150 kDa was observable from embryonic stages on, and increased toward adulthood. On the other hand, a 37 kDa band, equivalent to the predicted molecular weight of PRG5, was clearly detectable at P10 and its intensity remained stable in adult stages. At younger stages, this band showed weaker intensity. Changes of PRG5 protein level during development were also found in hippocampus, olfactory bulb, and cerebellum (**Supplementary Figure 2A**).

For the first time, we were able to analyze PRG5 protein localization in sagittal mouse brain sections using immunohistochemistry. Staining of adult cortex sections supported the western blot results, as we found strong PRG5 signal throughout all cortical layers. There, PRG5 was localized to the soma and to dendritic structures of cortical neurons (**Figure 2B**).

Plasticity-Related Gene 5 Protein Is Mainly Dendritically Expressed in the Mouse Brain

After we demonstrated the presence of PRG5 protein in cortex lysates and sections, we aimed to analyze its specific localization in other brain areas. For this purpose, we performed immunohistochemical staining of adult (P30 and older) mouse-brain sagittal and coronal sections. We detected PRG5 immunofluorescence throughout the brain, but enriched in the hippocampal formation (HPF), cerebellum (CB), and the olfactory bulb (OB) (**Figure 3A** and **Supplementary Figures 2B–D**). Fluorescent signals of PRG5 were very prominent in dendritic regions of the hippocampus, such as the stratum radiale (sr) and the stratum lacunosum-moleculare (slm) of Ammon's horn (CA). Dendritic expression of PRG5 was verified by co-localization with the dendritic cytoskeletal protein microtubule-associated protein 2 (MAP2). Additionally, somata of pyramidal cells of the stratum pyramidale (sp) showed PRG5 positive staining (**Figure 3B**). Axonal regions of the hippocampus on the other hand, were marked by neurofilament-M (NF-M) staining and showed only weak or no PRG5 signal. Somata of granule cells in the stratum granulosum (sg) of the DG showed a strong expression of PRG5 that extended into the basal dendrites of the molecular layer (mo) (**Figure 3C** and **Supplementary Figure 2B**). However, neuronal stem cells in the sgz lacked PRG5 expression and were only marked by DAPI staining (**Figure 3C** and **Supplementary Figure 2B**).

In the cerebellum, (CB) we found that Purkinje cells (pu), marked by parvalbumin (PV), strongly expressed PRG5 in their soma and in their intricately branched dendritic arbors in the molecular layer (mo) (**Figure 3D** and **Supplementary Figure 2D**). However, NeuN-positive granule cells in the granule layer (gr) of the CB showed no PRG5 signal (**Figure 3E**).

Plasticity-Related Gene 5 Is Expressed in Inhibitory and Excitatory Neurons and in an Oligodendrocyte Subtype, but Not in Astrocytes

Tyrosine hydroxylase (TH) -positive dopaminergic neurons in the MOB expressed PRG5, as shown by an overlay of fluorescent signals (**Figure 4A**, white arrow heads). Co-staining against parvalbumin (PV) revealed PRG5 expression in inhibitory GABAergic interneurons, here shown in the CA1 region of the hippocampus (**Figure 4B**).

In line with previous *in vitro* results, where PRG5 mRNA expression was restricted to primary cultured neurons and was not found in primary cultured astrocytes (Coiro et al., 2014), we did not detect PRG5 in GFAP-positive astrocytes

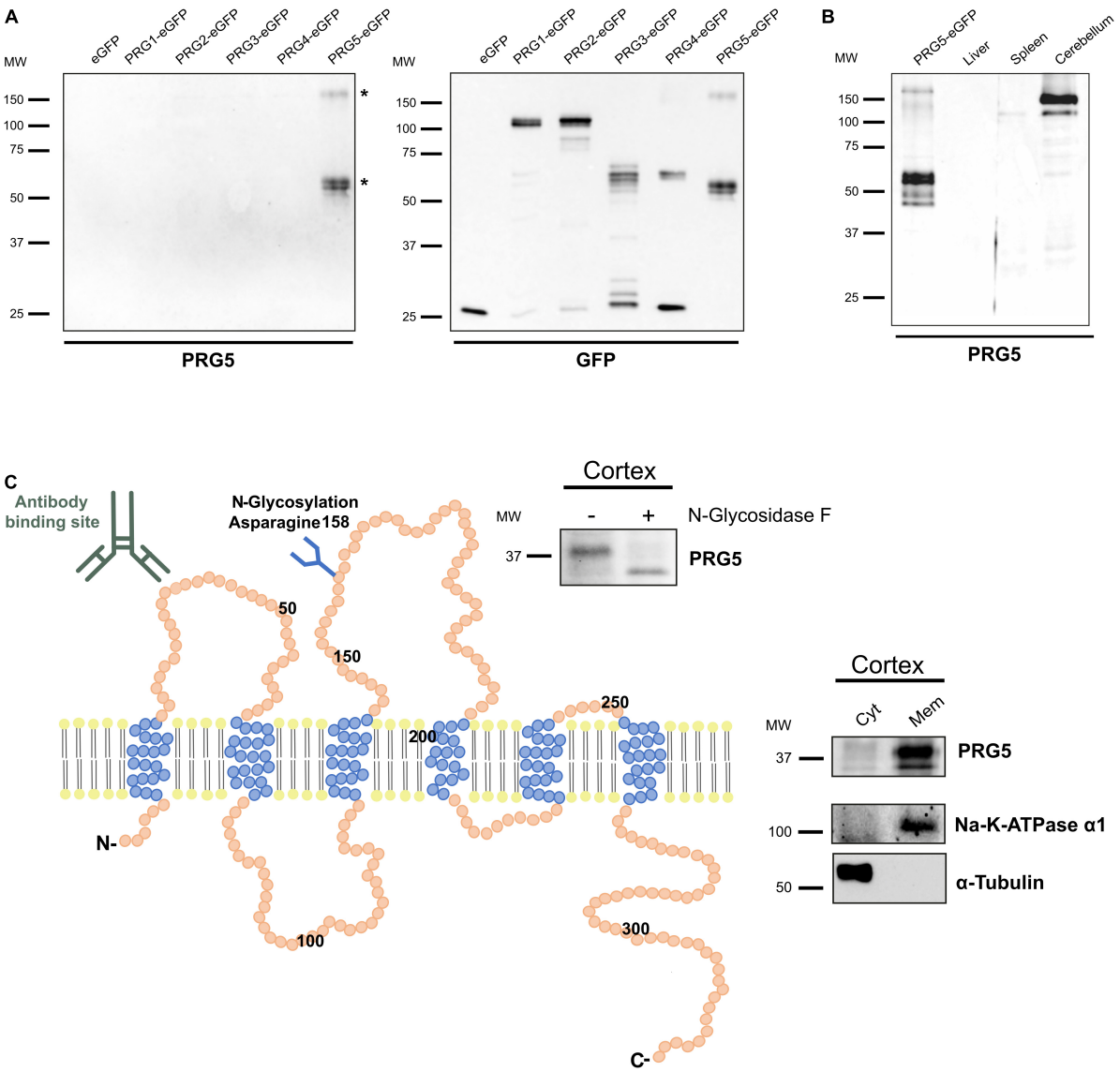

FIGURE 1 | PRG5 is a glycosylated membrane protein in brain tissue. **(A)** Specificity analysis of a polyclonal PRG5 antibody shows specific binding only to PRG5 and no cross-reactivity to other PRG family members. Fusion proteins of PRG1-5 with eGFP were used for western blotting. The PRG5 antibody detected bands around 50 kDa and above 150 kDa. Bands marked with asterisks (*) were analyzed by MS and contained PRG5 peptides. **(B)** Western Blot analysis of protein lysates of adult mouse tissue shows strong PRG5 signal in the cerebellum, but not in liver or spleen (probed with anti-PRG5 antibody). Loading control is shown in **Supplementary Figure 1**. **(C)** Schematic depiction of the murine PRG5 protein and its orientation in the plasma membrane based on its amino acid sequence (primary accession number Q8BJ52). The six transmembrane regions are illustrated in blue, N- and C-termini are located intracellularly. The antibody-binding site in the first extracellular loop is indicated. An N-glycosylation site at asparagine 158 in the second extracellular loop is indicated, and was supported by western blot of P15 mouse cortex lysate treated with (+) and without (–) N-glycosidase F, and a subsequent shift of the PRG5 band to a lower molecular weight after treatment (blot above). Endogenous membrane localization of PRG5 was validated by western blot of cytosolic (Cyt) and membrane (Mem) protein fractions of P15 mouse cortex lysates (blot on the right). α-tubulin was used as a cytosolic marker, Na-K-ATPase α1 as a membrane marker. MW, molecular weight.

in the brain (**Figure 4C**, white arrow heads). On the other hand, we had previously demonstrated PRG5 mRNA expression in primary immature and mature cultured oligodendrocytes (Gross et al., 2021). In immunostaining of brain sections, we found PRG5 protein in a subtype of oligodendrocytes in the corpus callosum (cc), but we could not detect a PRG5 signal in axonal fibers of the cc, marked by NF-M (**Figure 4D**, white arrow heads).

Plasticity-Related Gene 5 Is Widely Distributed in the Brain of Neonatal Mice (P0) but Not in Nestin-Positive Precursor Cells

After we identified a developmental regulation of PRG5 protein expression in the mouse brain, we analyzed neonatal mice brain (P0) sections for PRG5 expression, by immunostaining

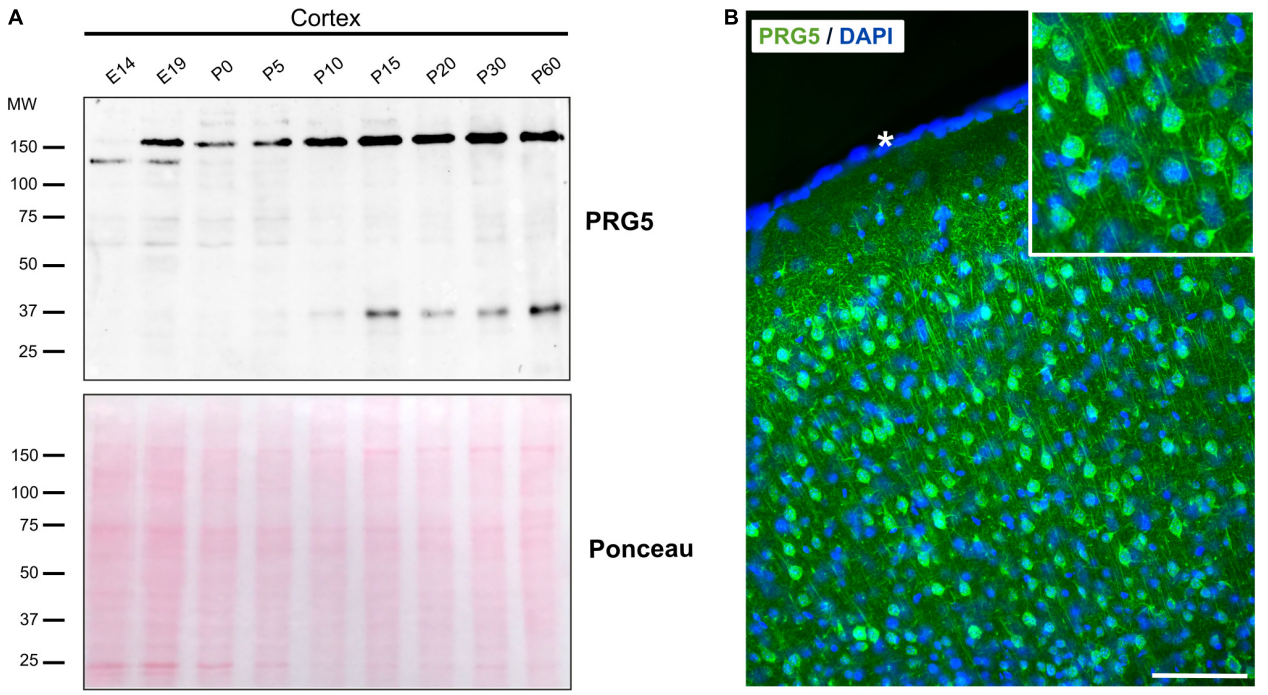

FIGURE 2 | PRG5 protein expression in the mouse cortex increases during maturation. **(A)** Representative western blot analysis of total protein lysates of mouse cortex tissue between E14 and P60, probed with an anti-PRG5 antibody. The 150 kDa band was detected from E19 and increased toward adult stages. The 37 kDa band was detectable from P10. Only a very weak band was detectable in younger stages. Ponceau-S staining of total proteins is shown as a loading control. A representative blot of three technical repeats for each of three tissue preparations is shown. MW, molecular weight. **(B)** Immunostaining of PRG5 (green) and DAPI (blue) in a sagittal section of P15 mouse cortex. PRG5 expression was detected in neurons of all cortical layers. Asterisk (*) indicates pial surface. Scale bar = 100 μm.

with the PRG5 antibody. We found a wide distribution of the PRG5 protein throughout all brain areas, with particularly high abundance in the medial pallidum (MPall), the developing hippocampus (**Figure 5A**). Neuronal and glial precursor cells, marked by a nestin antibody, did not show PRG5-positive staining (**Figure 5A**), indicating that the PRG5 protein is first expressed after neuronal cell fate has been determined.

Plasticity-Related Gene 5 Protein Expression Is a Marker for Late Neurodifferentiation During Adult Neurogenesis

To gain further insight into the time point of PRG5 expression during neurodifferentiation, we analyzed its expression during adult neurogenesis. In **Figure 5B**, marker proteins of different developmental stages were used, together with PRG5 staining in the sgz of the dentate gyrus (DG) of the hippocampus. Early neurogenesis is marked by nestin and later by doublecortin (DCX) expression of mitotic immature neurons (Gleeson et al., 1999; Michalczyk and Ziman, 2005). Cells that are positive for either nestin or DCX, do not express the PRG5 protein (**Figure 5B**). During neuronal maturation, neurons downregulate DCX and increase their expression of NeuN, which is a marker for postmitotic neurons (Mullen et al., 1992; Gleeson et al., 1999). We found PRG5 protein abundance only in postmitotic NeuN-expressing neurons that had migrated from the sgz into the sg and the mo of the DG, indicating an involvement of PRG5 in late postmitotic neurodifferentiation processes (**Figure 5B**).

PRG5 protein abundance was not found during RMS migration of neuroblasts, but was first detected when they entered the olfactory bulb; it increased in radial migrating cells in the olfactory bulb (**Figure 6**). These findings suggest a specific role for PRG5 in late neuro-differentiation processes, rather than in neurogenesis itself.

Plasticity-Related Gene 5 Is Not Localized at the Postsynaptic Density, but at the Base of the Synapse

Another dendritically expressed PRG family member, PRG1, has been shown to be located at the postsynaptic density and to be involved in excitatory synaptic transmission (Trimbuch et al., 2009; Unichenko et al., 2016). As synaptic activity is only established during late neurodifferentiation, we asked whether PRG5 is also a postsynaptic density protein, and thus analyzed its subcellular localization. To this end, we performed further subfractionation of mouse neocortex protein lysates, followed by western blot analysis (Cotman and Taylor, 1972; Carlin et al., 1980; Trimbuch et al., 2009). We found PRG5 37 and 150 kDa bands in the myelin-enriched fraction, in the

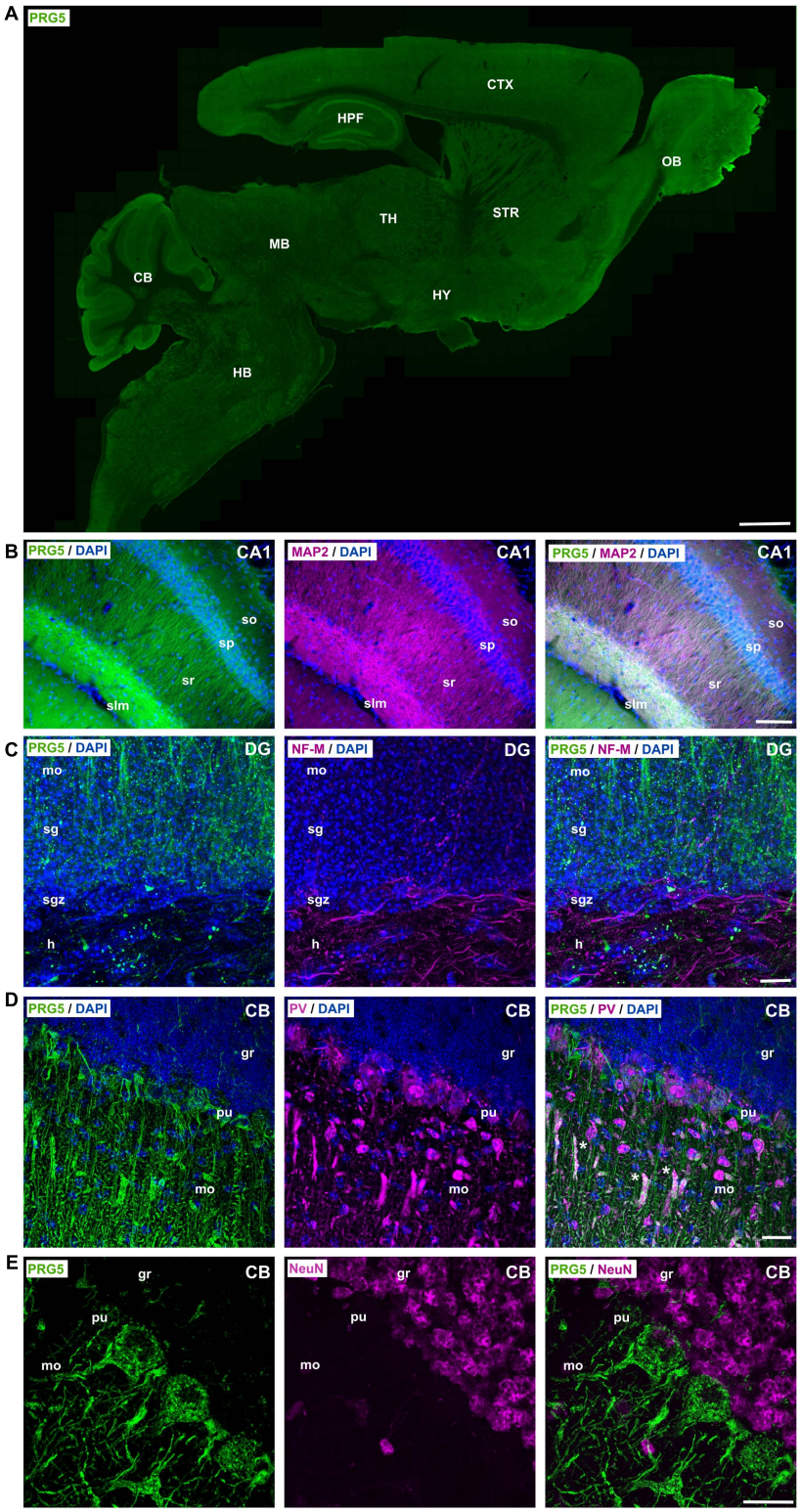

FIGURE 3 | PRG5 is enriched in dendritic areas of the mouse hippocampus, olfactory bulb, and cerebellum. **(A)** Montage of a sagittal adult mouse brain section labeled with PRG5 (green) shows highest PRG5 expression in the cerebellum, hippocampus, and the olfactory bulb. Mosaic stitched from 635 tiles. Scale bar = 1 mm. **(B)** Dendritic expression of PRG5 (green) in the hippocampal CA1 region shown by co-immunostaining with MAP2 (magenta). PRG5 expression was found in the soma of pyramidal cells of the sp and increased in their dendritic arbors in the sr and slm. Scale bar = 100 μm. **(C)** Low axonal expression of PRG5

(Continued)

FIGURE 3 | (green) in the DG of the hippocampus is shown by co-immunostaining with axonal marker NF-M (magenta). Strong PRG5 expression was found in granule cells in the sg and their dendritic arbors in the mo, whereas there was only low expression in their mossy fibers in the hilum. Scale bar = 10 μm. **(D)** Purkinje cells of the CB showed strong PRG5 signal in their soma and in their dendritic arbors in the mo. Unspecific overlapping staining of blood vessels is marked with asterisks. Scale bar = 20 μm. **(E)** NeuN positive granule cells of the granule layer of the CB show no PRG5 expression. Scale bar = 20 μm. DAPI visualizes cell nuclei (blue). CA, cornu ammonis; CB, cerebellum; CTX, cerebral cortex; DG, dentate gyrus; gl, glomerular layer; gr, granule layer; h, hilus; HB, hindbrain; HPF, hippocampus formation; HY, hypothalamus; ipl, inner plexiform layer; MB, midbrain; mi, mitral layer; mo, molecular layer; MOB, main olfactory bulb; opl, outer plexiform layer; pu, Purkinje layer; sg, stratum granulosum; sgz, subgranular zone; slm, stratum lacunosum-moleculare; so, stratum oriens; sp, stratum pyramidale; sr, stratum radiale; STR, striatum; TH, thalamus. Representative images; Stainings of brain sections from at least three different animals were analyzed and revealed similar results.

endoplasmic reticulum (ER), in the Golgi-enriched fraction, and in the synaptosomal fraction. In the synaptic cytoplasm and crude synaptic-vesicle fraction, we detected a weak signal for the 150 kDa band, but not for the 37 kDa band. The crude synaptic plasma membrane fraction revealed a strong signal for the 37 kDa band and only a weak signal for the 150 kDa band. Interestingly, we could not detect any PRG5 protein bands in the postsynaptic density (PSD) fraction (**Figure 7A**).

To further analyze the localization of PRG5 at the synapse, we conducted immunostaining of murine primary hippocampal neurons. We found PRG5 not to be co-localized to marker proteins of the pre- and postsynaptic transmission sites, bassoon and homer1 (**Figure 7B**, top). Instead, we detected the PRG5 signal between the homer1 signal at the postsynaptic density and MAP2-positive cytoskeletal structures in the dendritic shaft (**Figure 7B**, bottom). Our results show that PRG5 is located at the neck of dendritic spines, rather than at the actual spine head.

Plasticity-Related Gene 5 Stimulates the Formation of Dendritic Protrusions Independent From Neuronal Activity

Coiro et al. (2014) showed that down-regulation of PRG5 expression reduces the number of functional synapses in mature hippocampal neurons. To analyze if the PRG5-induced formation of dendritic protrusions in primary hippocampal neurons is depending on synaptic activity, we applied an activity inhibitor cocktail along with PRG5 overexpression. Activity inhibition significantly reduced the number of overall dendritic protrusions, as well as of homer1-positive spines in CFP-MEM transfected control cells (**Figure 7C** and **Supplementary Table 2**, line 2). Protrusions between 0.2 and 7 μm lengths were counted and defined as dendritic protrusions, homer1-positive protrusions were defined as spines (Yuste and Denk, 1995; Ruszczycki et al., 2012).

In PRG5 overexpressing neurons, activity inhibition reduced the number of overall protrusions (**Figure 7C** and **Supplementary Table 2**, Line 24). Nevertheless, significantly higher numbers of overall protrusions compared to CFP-MEM expressing control cells were found, even in the presence of inhibitors (**Figure 7C** and **Supplementary Table 2**, Line 17). A comparable pattern was observed for homer1-positive spines, although the differences were not significant (**Figure 7C** and **Supplementary Table 2**, Lines 11, 22, 27). As homer1-positive spines are more likely associated to active synapses, our results indicate activity independent induction of dendritic membrane protrusions and spines by PRG5 overexpression (**Figure 7C** and **Supplementary Table 2**).

DISCUSSION

In this study, we analyzed for the first time the expression and localization of the endogenous PRG5 protein in mouse brain tissue. We identified a PRG5 antibody that specifically detects PRG5 protein in mouse brain tissue samples, in both western blot and immunofluorescence experiments. We confirmed a membranous localization of the endogenous PRG5 in the brain, as well as its N-glycosylation, most likely at the predicted glycosylation site at asparagine 158 (Coiro et al., 2014). In western blot experiments, we identified a band fitting the predicted size of PRG5, with a molecular weight of 37 kDa, but also one very prominent band above 150 kDa. In MS analyses of these bands, isolated from PRG5-eGFP-overexpressing HEK293H cells, we found PRG5 peptides in both bands. Yu et al. (2015) proposed cooperative interactions of PRG family members, including the formation of hetero- and homodimers. Endogenous expression of the neuronal PRGs in HEK293H cells is unlikely, and we did not identify other PRG peptides in our MS analysis. Therefore, we postulate a possible homo-oligomerization of the PRG5 construct, resulting in a 150 kDa protein band. We additionally found this band in mouse brain-tissue samples, but not in liver or spleen samples. Our results indicate a potential homo-oligomerization of the native PRG5 protein in the brain; this needs to be evaluated further.

Using qRT-PCR, PRGs have been shown to be developmentally regulated on the mRNA level (Bräuer et al., 2003; Velmans et al., 2013; Coiro et al., 2014; Gross et al., 2021). We analyzed PRG5-protein expression during cortex development and found a developmental regulation, with increasing expression from late embryonic stages onward. Interestingly, we found an earlier appearance of the band around 150 kDa, whereas the 37 kDa band was only detectable in postnatal stages. This hints at different functional roles for monomeric and oligomeric states of PRGs, which should be considered when analyzing PRG functions.

By immunostaining of adult mouse-brain sections, we found PRG5 protein to be ubiquitously expressed in the brain, but enriched in brain areas that have high plasticity and regeneration capacity, such as the hippocampus or the olfactory bulb. Additionally, we found PRG5 to be predominantly localized to dendritic structures. Previous *in vitro*

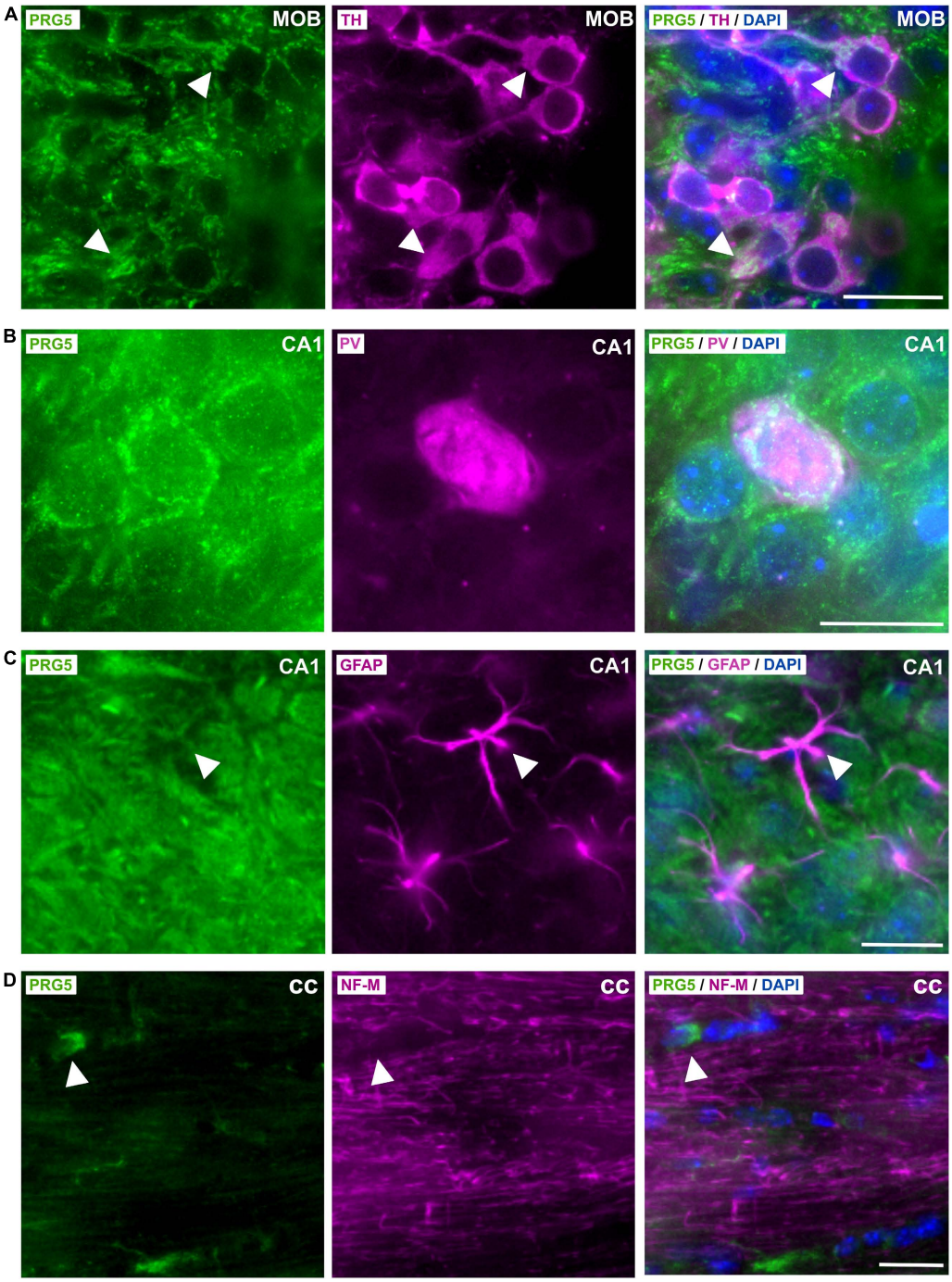

FIGURE 4 | Cell-type specific expression of PRG5 in the brain. **(A)** TH-positive (magenta) dopaminergic neurons in the gl of the MOB expressed PRG5 (green). Scale bar = 20 μm. **(B)** PV (magenta)-positive inhibitory GABAergic interneurons in the hippocampus also expressed PRG5 (green). Scale bar = 20 μm. **(C)** PRG5 (green) was not expressed by GFAP-positive (magenta) astrocytes. Scale bar = 20 μm. **(D)** NF-M-expressing (magenta) axonal fibers in the cc did not show PRG5 (green) positive staining, but a PRG5-expressing subtype of oligodendrocytes was detected. Scale bar = 20 μm. DAPI was used to visualize cell nuclei (blue). CA, cornu ammonis; cc, corpus callosum; MOB, main olfactory bulb. Representative images; Stainings of brain sections from at least three different animals were analyzed and revealed similar results.

overexpression studies demonstrated a participation of PRG5 in the formation, morphology, and stabilization of dendritic spines (Coiro et al., 2014). These processes occur in the adult brain in regions in which we found high PRG5 abundance, supporting a similar function for the endogenous PRG5 protein in the brain.

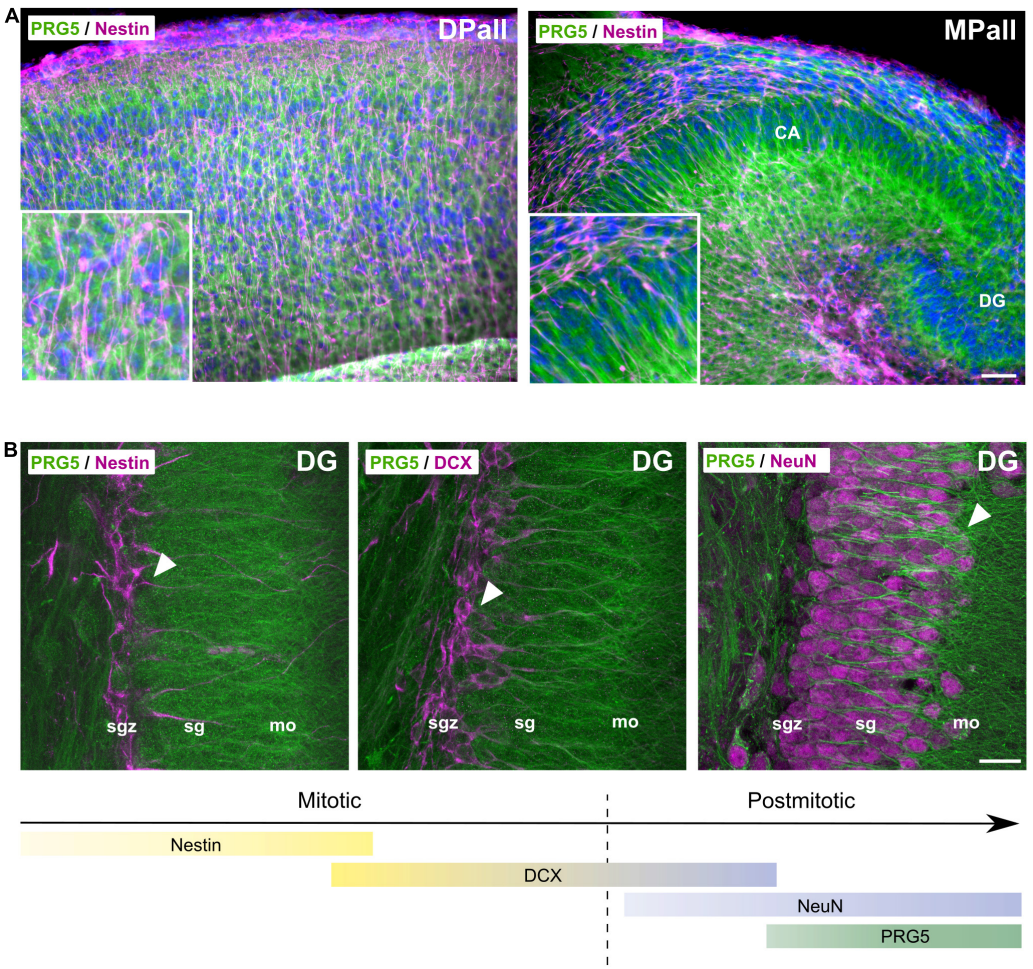

FIGURE 5 | PRG5 protein is expressed after neuronal cell fate determination. **(A)** Representative sagittal sections of P0 mice brain, stained with antibodies against PRG5 (green) and nestin (magenta), revealed PRG5 expression in the developing isocortex (dorsal pallium, DPall) and the developing hippocampus (medial pallium, MPall) that was not colocalized to nestin-positive progenitor cells. Scale bar = 50 μm. **(B)** During adult neurogenesis in the sgz of the dentate gyrus in the hippocampus, PRG5 (green) expression was detected in a late postmitotic phase, together with NeuN (magenta, right image) expression, but not with mitotic neurodifferentiation markers nestin (magenta, left image) and DCX (magenta, middle image). Scale bar = 20 μm. CA, cornu ammonis; DG, dentate gyrus; DPall, dorsal pallium; mo, molecular layer, MPall, medial pallium; sg, stratum granulosum; sgz, subgranular zone. Representative images; Stainings of brain sections from at least three different animals were analyzed and revealed similar results.

Consistent with previous mRNA-expression analysis in primary cultured brain cells, we found PRG5 protein to be primarily expressed in neurons and in an oligodendrocyte subtype, but not in astrocytes (Coiro et al., 2014; Gross et al., 2021). In neurons, we found PRG5 in both excitatory and inhibitory cells. Another mainly dendritically expressed PRG, PRG1, was shown to be solely expressed by excitatory glutamatergic neurons and to be an important player in LPA-dependent regulation of glutamatergic transmission (Trimbuch et al., 2009; Unichenko et al., 2016). Our mRNA-expression analysis showed high PRG1 expression in adulthood, whereas PRG5 expression increased toward adult stages. Furthermore, we analyzed the subcellular localization of the PRG5 protein and, unlike PRG1, it is not localized at the postsynaptic density, and we could not detect any co-localization with pre- and postsynaptic active-zone proteins at the synapse. In immunostaining, we found PRG5 to be localized at the base of the synapses between the postsynaptic density and the dendritic shaft. Our results suggest that endogenous PRG5 is more likely to play a role in spinogenesis and spine stabilization, than in synaptic transmission processes at the postsynaptic density.

To gain further insight into the time point of PRG5 expression during neurodifferentiation, we used adult neurogenesis as a model system. New-born neurons of the sgz in the hippocampus and the svz pass through distinct developmental stages, as during brain development, and are subsequently integrated into the existing neuronal network (Zhao et al., 2006, 2008). In both areas of adult neurogenesis, we found PRG5 to be only expressed in the postmitotic maturation phase. Stem cells, radial glia, and early neuroblasts did not express the PRG5 protein. Dendritic spine formation and maturation occur during late neurodifferentiation and are associated with a downregulation of DCX, accompanied

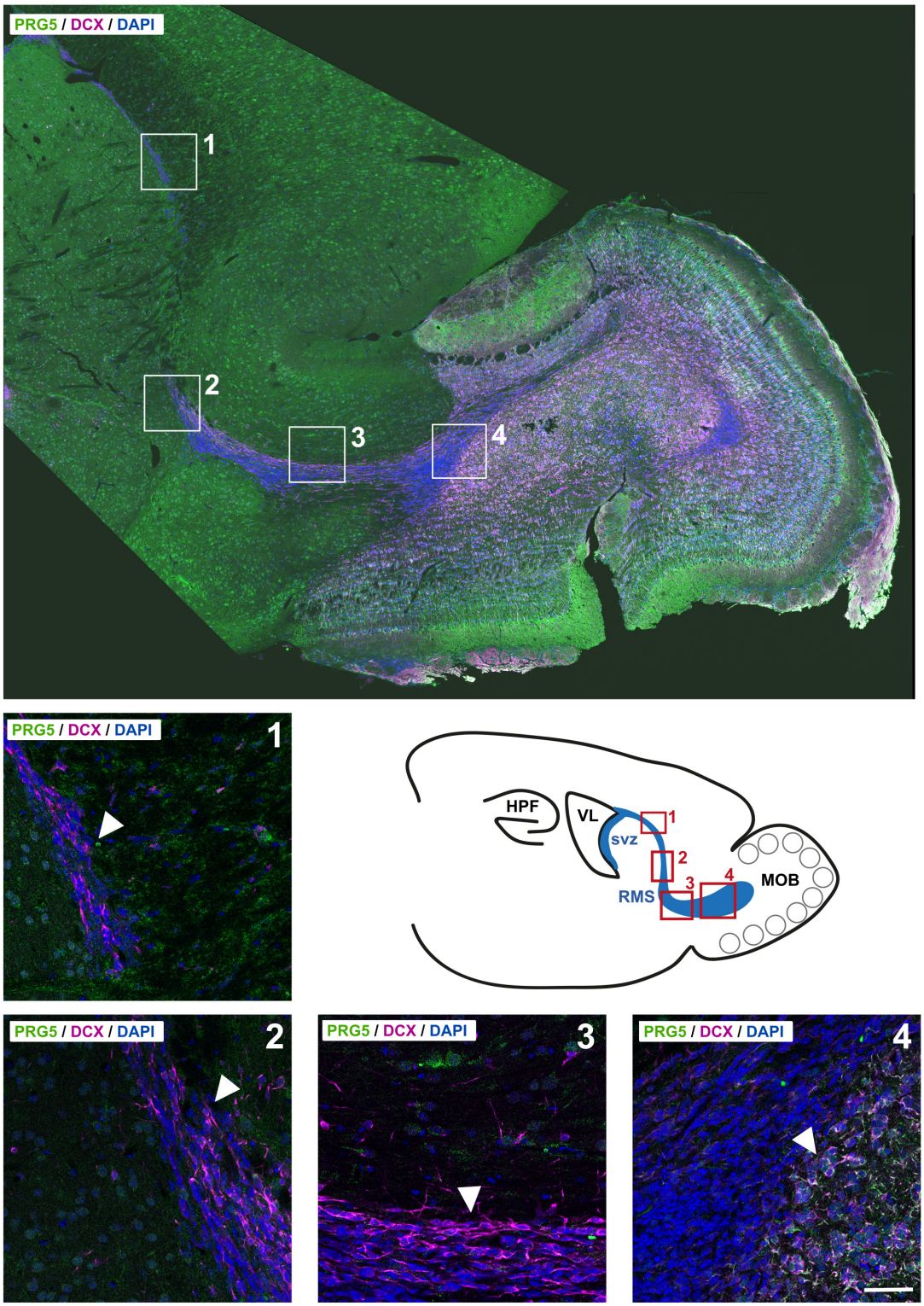

FIGURE 6 | PRG5 protein expression is present in a late phase of neurodifferentiation in adult neurogenesis of the rostral migratory stream (RMS). Top: Montage of a sagittal adult mouse brain section labeled with PRG5 (green), DCX (magenta) and DAPI (cell nuclei, blue). Mosaic stitched from 234 tiles. Bottom: Full-resolution views of representative stages of migration in the RMS and schematic drawing of the svz, RMS, and the olfactory bulb in sagittal view. PRG5 protein abundance was only present at a late stage of neurodifferentiation, when neuroblasts entered the olfactory bulb and started differentiating. HPF, hippocampal formation; MOB, main olfactory bulb; RMS, rostral migratory stream, svz, subventricular zone; VL, lateral ventricle. Scale bar = 50 μm. Representative images; Stainings of brain sections from at least three different animals were analyzed and revealed similar results.

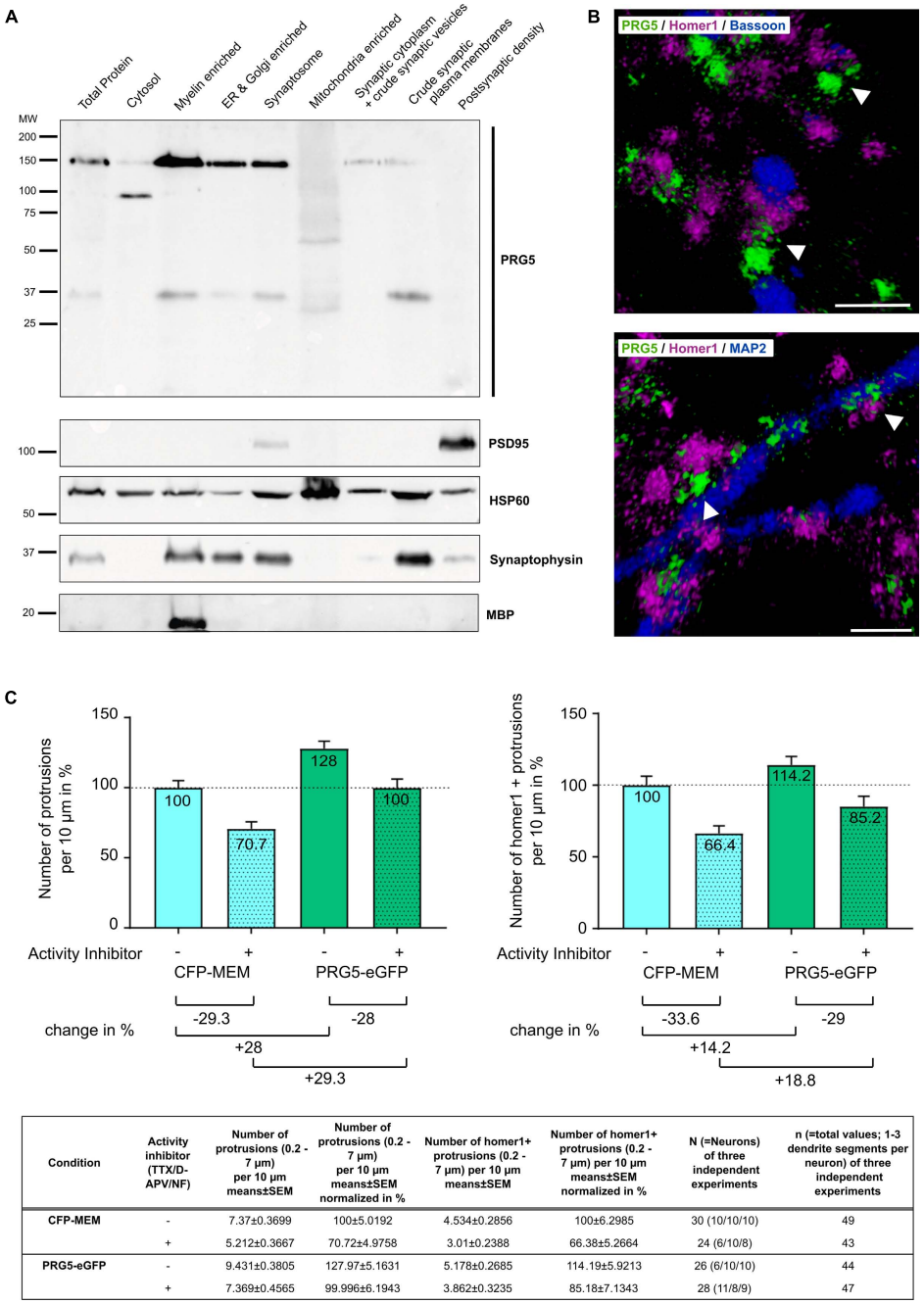

Condition	Activity inhibitor (TTX/D-APV/NF)	Number of protrusions (0.2 - 7 µm) per 10 µm means±SEM	Number of protrusions (0.2 - 7 µm) per 10 µm means±SEM normalized in %	Number of homer1+ protrusions (0.2 - 7 µm) per 10 µm means±SEM	Number of homer1+ protrusions (0.2 - 7 µm) per 10 µm means±SEM normalized in %	N (=Neurons) of three independent experiments	n (=total values; 1-3 dendrite segments per neuron) of three independent experiments
CFP-MEM	-	7.37±0.3699	100±5.0192	4.534±0.2856	100±6.2985	30 (10/10/10)	49
	+	5.212±0.3667	70.72±4.9758	3.01±0.2388	66.38±5.2664	24 (6/10/8)	43
PRG5-eGFP	-	9.431±0.3805	127.97±5.1631	5.178±0.2685	114.19±5.9213	26 (6/10/10)	44
	+	7.369±0.4565	99.996±6.1943	3.862±0.3235	85.18±7.1343	28 (11/8/9)	47

FIGURE 7 | PRG5 stimulates formation of dendritic protrusions, independent of neuronal activity. **(A)** Representative western blot after subcellular fractionation of adult mouse cerebral cortex, probed with PRG5, with PSD95 as a postsynaptic density marker, HSP60 as a mitochondrial marker, synaptophysin as a synaptic marker, and MBP as a myelin marker. PRG5 was detected in myelin-, ER-, Golgi-enriched, and in synaptosomal fractions, predominantly around 150 kDa. The 37 kDa PRG5 band was mainly detected in the myelin-enriched and the crude synaptic plasma-membrane fractions. No PRG5 signal was found in the postsynaptic density fraction. A representative blot of three technical repeats for each of three tissue preparations is shown. MW, molecular weight. **(B)** Representative volume-rendered 3D projections of z-stack images of murine primary neurons cultured 15 days *in vitro* and stained for PRG5 (green), homer1 (magenta), and bassoon (top, blue) or MAP2 (bottom, blue). Stainings were analyzed for three independent neuron preparations. PRG5 protein was not localized to pre- and postsynaptic transmission sites, as shown by a lack of signal overlap to homer1 or bassoon proteins (top, white arrow heads). PRG5 was localized at the bases of postsynaptic spines, between postsynaptic density protein homer1 and dendritic-cytoskeletal protein MAP2 (bottom, white arrow heads). Scale bars = 1 µm. **(C)** Quantification of protrusions of mature primary neurons transfected either with CFP-MEM (control) or PRG5-eGFP with (+) and without (–) activity inhibition (1 µM TTX, 50 µM D-APV and 10 µM nifedipine). PRG5- overexpressing neurons showed elevated number of overall protrusions and of homer-positive protrusions compared to control cells after inhibition of neuronal activity. Number of protrusions was normalized to control (CFP-MEM) without activity inhibition (100%) and are shown as mean in% + SEM. Counted numbers and *n*-values are listed in the table below graphs. Statistical data is shown in **Supplementary Table 2**.

TABLE 1 | Primary antibodies and concentrations used for immunochemistry and western blot experiments.

Antibody	Dilution for western blot	Dilution for immunochemistry	Source	Identifier
Anti-bassoon	–	1:100	Synaptic Systems	Cat# 141011, RRID: AB_2619827
Anti-doublecortin	–	1:2,000	Merck Millipore	Cat# AB2253, RRID: AB_1586992
Anti-GFAP	–	1:500	Merck Millipore	Cat# MAB360, RRID: AB_11212597
Anti-GFP (JL-8)	1:2,500	–	Clontech Laboratories	Cat# 632380, RRID: AB_10013427
Anti-GFP		1:1,000	Abcam	Cat# ab6556, RRID:AB_305564
Anti-homer 1	–	1:200	Synaptic Systems	Cat# 160 004, RRID: AB_10549720
Anti-HSP60 (LK-2)	1:2,000	–	Enzo Life Science	Cat# ADI-SPA-807-E, RRID: AB_2039242
Anti-MAP2 (HM-2)	–	1:1,000	Sigma-Aldrich	Cat# M4403, RRID: AB_477193
Anti-MAP2	–	1:1,000	Synaptic Systems	Cat# 188 004, RRID: AB_2138181
Anti-MBP (12)	1:500	–	Merck Millipore	Cat# MAB386, RRID: AB_94975
Anti-Nestin (rat-401)	–	1:100	Merck Millipore	Cat# MAB353, RRID: AB_94911
Anti-NeuN (1B7)	–	1:1,000	Abcam	Cat# ab104224, RRID: AB_10711040
Anti-Neurofilament M (NN18)	–	1:200	Merck Millipore	Cat# MAB5254, RRID: AB_2150076
Anti-Parvalbumin	–	1:1,000	Sigma-Aldrich	Cat# P3088, RRID: AB_477329
Anti-PRG5	1:500	1:300	Abcam	Cat# ab84659, RRID: AB_1925293
Anti-PSD95 (7E3-1B8)	1:1,000	1:500	Thermo Fisher Scientific	Cat# MA1-046, RRID: AB_2092361
Anti-sodium potassium ATPase (464.6)	1:200	–	Abcam	Cat# ab7671, RRID: AB_306023
Anti-synaptophysin 1	1:500	–	Synaptic Systems	Cat# 101 011, RRID: AB_887824
Anti-TH (Inc1)	–	1:200	Merck Millipore	Cat# MAB318, RRID: AB_2201528
Anti-α-tubulin	1:3,000	–	Synaptic Systems	Cat# 302 211, RRID: AB_887862

by an increase of the neuronal marker NeuN (Zhao et al., 2008). We found co-expression of PRG5 and DCX in the MOB, but not in the dentate gyrus. However, co-expression of PRG5 and DCX in the MOB was limited to the late migration phase, where neurodifferentiation proceeds and integration into the neuronal network begins. In both areas, PRG5 was localized to NeuN-expressing neurons. Our results identify PRG5 as a marker for late neurodifferentiation after neuronal fate determination. In a previous study, we demonstrated that knockdown of PRG5 in mature primary hippocampal neurons significantly reduced the number of functional synapses *in vitro* (Coiro et al., 2014). Together with our recent data, this strongly supports a functional role of endogenous PRG5 protein in spinogenesis.

During dendritic differentiation, the shape of dendritic protrusions changes, from thin, elongated filopodia in immature neurons to mature dendritic spines with an enlarged spine head. PRG5 has been shown to induce filopodial outgrowth in non-neuronal cell lines (Broggini et al., 2010; Yu et al., 2015). Our data imply a possible role for PRG5 in shaping dendritic spine morphology. Considering its high expression in mature neurons, and its localization at the bases of synapses, an additional role in dendritic spine stabilization is likely.

Various studies have shown a correlation between neuronal activity and rapid structural as well as functional modifications of dendritic spines (Maletic-Savatic et al., 1999; Chen et al., 2007; Nakahata and Yasuda, 2018). We found PRG5 expressed in areas of the brain characterized by their capability for synaptic plasticity. On a subcellular level, we showed that PRG5 is not associated with the synaptic active zone. Additionally, we showed, that PRG5 significantly induces the formation of dendritic protrusions and tends to induce the formation of homer1-positive spines, when compared to CFP-MEM transfected mature primary cultured neurons. Interestingly, neuronal activity inhibition did not prevent the formation of dendritic membrane protrusions by PRG5 overexpression. Taken together, these data suggest involvement of PRG5 in dendritic spine morphogenesis rather than in synaptic activity.

Many neurological disorders include dendritic spine defects that can affect both spine distribution and spine ultrastructure. The spine pathologies include aberrant number, shape, or localization of spines, as well as subcellular changes of, for example, organelles within the spine (Fiala et al., 2002; Lee et al., 2015). In schizophrenia-spectrum disorders, a reduction of spine number in, for example, the prefrontal cortex or in pyramidal neurons of the hippocampus was seen, whereas an increased number of spines was found in the putamen patch and the caudate matrix (Roberts et al., 1996, 2005; Garey et al., 1998; Glantz and Lewis, 2000; Kolomeets et al., 2005; Sweet et al., 2009). Genes and proteins that have been linked to the regulation of spine morphology and development, such as Neuregulin-1 and ErbB4 or Cdc42, show aberrant expression or signaling in schizophrenia patients (Stefansson et al., 2002; Hashimoto et al., 2004; Hill et al., 2006; Pan et al., 2011). Functional analysis suggests that PRG5 acts through a Cdc42-independent pathway to promote the formation of membrane protrusions (Broggini et al., 2010). Understanding the complex mechanisms of initial spine formation and their stabilization and regulation mechanisms is of vital importance, including for therapeutic research on neurological disorders. Considering its high expression during late neurodifferentiation, PRG5 is likely to be an important player in these processes, acting via an unidentified signaling pathway that could be of interest in therapeutic approaches to spine pathologies.

CONCLUSION

We found the endogenous PRG5 protein in mouse brain tissues in its monomeric 37 kDa state, as well as in a larger 150 kDa state, most likely in a homo-oligomeric structure. In mouse brain slices, we found ubiquitous expression of PRG5 in soma and dendrites of neurons, with high abundance in the hippocampus, cerebellum, and the olfactory bulb. PRG5 expression in neurons is independent of their neurotransmitters, and we found PRG5 in an oligodendrocyte subtype, but not in astrocytes. In adult neurogenesis, PRG5 is only expressed during a late phase of neurodifferentiation, associated with spinogenesis. On a subcellular level, we localized PRG5 to the bases of dendritic spines, rather than to the postsynaptic density. Additionally, PRG5-induced formation of dendritic protrusions is independent from neuronal activity. Therefore, our results support an important participation of PRG5 in dendritic spine morphogenesis.

EXPERIMENTAL PROCEDURES

Animals

Time-pregnant, postnatal, and adult wild-type C57BL/6J mice were procured from the central animal facility of the University Medical Center Rostock or the central animal facility of the Carl von Ossietzky University of Oldenburg. They were kept under standard laboratory conditions in accordance with German and European guidelines for the use of laboratory animals (2010/63/EU; 12 h light/dark cycle; 55% ± 15% humidity; 22°C ± 2°C room temperature (RT) and water *ad libitum*, enriched and grouped). All protocols were in accordance with the German Animal Protection Law and were approved by the local ethics body of Mecklenburg-Western Pomerania (LALLF) and Lower Saxony (LAVES; TV 33.19-42502-04-18/2759 and 33.19-42502-04-18/2766). For determining embryonic stages, the day of the vaginal plug following mating was assigned as embryonic day 0.5 (E0.5). Mice of both sexes were used for protein lysis and immunostaining.

HEK293H Cell Culture and Transfection

HEK293H cells (Thermo Fisher Scientific, Waltham, MA, United States; Catalog ID 11631017) were routinely maintained in Dulbecco's Modified Eagle Medium (DMEM; Thermo Fisher Scientific) supplemented with 10% fetal bovine serum (FBS; PAN-Biotech, Aidenbach, Germany), 2 mM L-glutamine (Merck Millipore, Darmstadt, Germany), 100 units/ml penicillin, and 100 μg/ml streptomycin (PAN-Biotech) under standard conditions of 5% (v/v) CO_2 and 37°C. Cells were passaged every 3–4 days at around 90% confluency. For transfection, cells were seeded in 100 mm petri dishes with 1.5×10^6 cells per dish and transfected after 24 h with calcium-phosphate precipitation. For this purpose, 22 μg DNA in 337.5 μl sterile H_2O and 37.5 μl 2.5 M $CaCl_2$, was precipitated by slow drop-by-drop addition of 337 μl HEPES-buffered saline pH 7.05 (42 mM HEPES, 10 mM KCl, 1.5 mM Na_2HPO_4, 1.1 mM glucose), then incubated for 30 min at RT and added to the cells. Cells were lysed after 24–48 h. The following expression plasmids were used for transfection: peGFP-N1-mPRG1, peGFP-N1-rPRG2, peGFP-N1-mPRG3, peGFP-C1-mPRG4, peGFP-N1-rPRG5 (Savaskan et al., 2004; Broggini et al., 2010; Velmans et al., 2013; Coiro et al., 2014).

Tissue and Cell Protein Lysis, Purification, and Deglycosylation

For obtaining protein lysates of different organs and brain areas, mice of varied developmental stages were sacrificed by cervical dislocation, individual organs were removed, and specific brain areas dissected on ice. For embryonic stages, tissue samples of all embryos of one litter (seven to ten embryos; sex not specified) were pooled. Postnatal tissue samples were pooled from four to eight mice of both sexes. For cortex samples, three pooled samples from three independent preparations were used. For other brain areas, one pooled sample of one preparation was used (**Supplementary Figure 2A**). Liver and spleen samples for antibody verification were obtained from a single adult female mouse.

Cortex tissue was then homogenized with a syringe and cannula in lysis buffer containing 20 mM Tris-HCl pH 7.5, 250 mM sucrose, 1 mM EGTA, 5 mM EDTA, 1x cOmplete mini protease inhibitor cocktail (Sigma-Aldrich, St. Louis, MO, United States) and 1x PhosSTOP phosphatase inhibitor (Sigma-Aldrich). Cultured cells were washed twice with ice-cold 1x PBS, lysis buffer was added, and cells were scraped off the culture plates with a cell scraper. All samples were sonicated for 3 × 3 s and then incubated on ice for 30 min. Cell debris was pelleted by centrifugation at 10,000–12,000 × g for 10–15 min at 4°C and total protein lysates were stored for the short term at –20°C or the long term at –80°C. For separation of cytosolic and membrane protein fractions, total protein lysates were further centrifuged at 200,000 × g for 30 min at 4°C. The supernatant was collected as the cytosolic protein fraction, while the pellet was re-suspended in lysis buffer additionally containing 1% (v/v) Triton X-100, and incubated for 10 min on ice. Samples were again centrifuged for 10 min at 4°C and 100,000 × g; the resulting supernatant contained fractions of membrane proteins. Protein concentrations were determined by BCA protein assay (Thermo Fisher Scientific) with BSA standards, following the manufacturer's protocol.

For purification of eGFP fusion proteins, lysates of transfected HEK293H cells were processed with the μMACS GFP Isolation Kit (Miltenyi Biotec, Bergisch Gladbach, Germany) according to the manufacturer's instructions.

For the deglycosylation assay, P15-cortex protein lysates were treated with Peptide-N-glycosidase F (PNGase F, Roche, Basel, Switzerland) as recommended by the manufacturer, run over night at 37°C. Negative controls were incubated without PNGase F.

Western Blot

Protein lysates were diluted in 5 × Laemmli buffer containing 1% (v/v) 2-mercaptoethanol or, for PRG5 detection, without 2-mercaptoethanol but with the addition of 8 M urea. Proteins were

separated by SDS-PAGE and transferred on nitrocellulose (NC) membranes with tank-blotting procedure for 70 min at 100 V and 4°C. To establish the total protein content, blotted membranes were briefly stained with 0.1% (w/v) Ponceau-S in 5% (v/v) acetic acid. Non-specific antibody binding was blocked with 5% (w/v) bovine serum albumin (BSA; Carl Roth, Karlsruhe, Germany) or 2.5–5% milk (Carl Roth) in PBS or TBST. Primary antibody incubation was carried out in blocking solution overnight at 4°C (for antibodies and concentrations, see **Table 1**).

Membranes were washed three to six times at RT with PBST or TBST, and subsequently incubated with horseradish peroxidase-conjugated secondary antibodies (GE Healthcare, Boston, MA, United States) 1: 10,000 in 2.5% (w/v) BSA in PBST or TBST for 1.5 h at RT. Membranes were again washed 3 times at RT with PBST, TBS or TBST, and any immunoreaction was detected with Clarity or Clarity Max ECL substrate (Bio-Rad Laboratories, Hercules, CA, United States) according to the manufacturer's protocol.

Immunohistochemistry

Adult mice were deeply anesthetized with sodium pentobarbital (Narcoren; Boehringer Ingelheim, Germany), then transcardially perfused with cold 1x PB, followed by cold 4% (w/v) paraformaldehyde (PFA; Merck Millipore) in 1x PB fixation solution. P0 mice were sacrificed by cervical dislocation. Brains were removed and additionally immersion-fixed in 4% (w/v) PFA in 1x PB for 24–48 h at 4°C. Coronal or sagittal 35–40 μm brain sections were prepared on a Leica VT1000S vibratome (Leica Microsystems, Wetzlar, Germany). To reduce autofluorescence, slices were treated with 1% (v/v) $NaBH_4$ in 0.1 M PB pH 7.2 for 15–60 min at RT, with mild agitation. Slices were washed four times for 5 min with PB, followed by blocking of non-specific antibody binding overnight at 4°C with 10% (v/v) FBS or 1% BSA, 1% (v/v) normal goat serum (NGS; Vector laboratories, Burlingame, CA, United States), and 0.2% (w/v) saponin in PB. Primary antibodies were diluted in 5% (v/v) FBS or 0.5% BSA, 1% (v/v) NGS and 0.2% (w/v) saponin, and slices were incubated for 48 h at 4°C, with gentle agitation. Primary antibodies and concentrations are listed in **Table 1**. Slices were washed three times with PB with 0.2% (w/v) saponin for 10, 20, and 30 min at RT. Secondary-antibody and DAPI incubation was performed overnight at 4°C in the same solution as primary-antibody incubation. The following secondary antibodies were used: goat-anti-mouse IgG Alexa Fluor 568 (1:1,500; Thermo Fisher Scientific), goat-anti-rabbit IgG Alexa Fluor 488 (1:1,500; Thermo Fisher Scientific) and goat-anti-guinea pig Cy3 (1:400; Jackson Immuno Research, West Grove, PA, United States). DAPI (Carl Roth) was used at 0.5 μg/ml, and added to the secondary-antibody solution. Slices were again washed three times at RT with 0.1 M PB, mounted on microscopy glass slides, and dried for 20 min at RT. For further microscopic analysis, slices were cover-slipped with Mowiol/DABCO (Carl Roth) or Immumount (Thermo Fisher Scientific). Nomenclature of brain regions was taken from The Allen Mouse Brain Atlas (RRID:SCR_002978) and The Allen Developing Mouse Brain Atlas (RRID:SCR_002990). All immunostainings were performed at least three times with sections from at least three different animals with different sexes. Stainings revealed similar results for all animals and sexes and representative images were chosen for this publication.

Primary Mouse Hippocampal Neuron Culture

Hippocampi of all E18 (± 0.5 days) mouse embryos from one pregnant mouse were dissected and primary neuron cultures prepared as previously described by Brewer et al. (1993). Neurons were plated onto poly-l-lysine-coated glass coverslips (Sigma-Aldrich) at a density of 2.1 × 104 cells/cm^2 in Minimal Essential Medium (Thermo Fisher Scientific) supplemented with 0.6% glucose, 10% (v/v) horse serum, and 100 U/ml penicillin/streptomycin (PAN-Biotech). Media were changed after 3–4 h to Neurobasal A media, supplemented with 2% (v/v) B27, 0.5 mM glutamine (all from Gibco, Thermo Fisher Scientific) and 100 U/ml penicillin/streptomycin.

Primary cultured neurons were transfected at DIV 14 with Effectene (Qiagen, Hilden, Germany) according to manufacturer's instructions. Media was changed 3 h after transfection. The following expression plasmids were used for transfection: pEGFP-N1-rPRG5 (Coiro et al., 2014) and pECFP-MEM (Takara Bio Inc., Clontech, Kusatsu, Japan).

Primary neurons were treated with an activity inhibitor cocktail or solvents 3 h after transfection along with change of media after transfection. Cells were incubated for 20 h. Activity inhibitor cocktail contained 50 μm D(–)-2-amino-5-phosphonopentanoic acid (D-APV) (in ddH_2O; Sigma-Aldrich, A8054), 10 μM nifedipine (in DMSO; Research Biochemicals International, N-114, Natick, MA, United States) and 1 μM tetrodotoxin (TTX) (in ddH_2O; Alomone Labs, T-550, Jerusalem, Israel) (Yu and Malenka, 2003; Brandt et al., 2007; Xie et al., 2007).

For immunocytochemical staining, neurons on coverslips were fixed with 4% (w/v) PFA and 15% (w/v) sucrose in PBS for 15 min at RT. For stainings including the PRG5 antibody, coverslips were washed three times with PBS and cells were blocked with 5% (v/v) NGS and 0.2% (w/v) saponin in PBS for 1 h at RT. Primary antibody incubation was carried out overnight at 4°C in 1% (v/v) NGS and 0.2% (w/v) saponin in PBS; primary antibodies and concentrations are listed in **Table 1**. Cells were washed three times for 10 min with PBS at RT. Secondary antibodies were incubated for 90 min at RT in the same solution as primary antibodies. For stainings after activity inhibition, cells were fixed as described. Permeabilization was carried out 20 min at RT with 0.5% Triton-X-100 and 0.1% sodium-citrate in PBS. Cells were wahsed three times with PBS and blocked for 1 h at RT with 10% FBS and 1% NGS in PBS. Antibody incubation was carried out in 5% FBS and 1% NGS overnight at 4°C for primary and for 90 min at RT for secondary antibodies. The following secondary antibodies were used: goat-anti-rabbit IgG Alexa Fluor 488 (1:1,500; Thermo Fisher Scientific), goat-anti-guinea pig Cy3 (1:400; Jackson Immuno Research), goat-anti-mouse IgG Alexa Fluor 647 (1:1,500; Thermo Fisher Scientific) and DAPI (0.5 μm/μl). Coverslips were washed three times with PBS and mounted on microscope slides with Mowiol/DABCO.

Microscopy

Fluorescent images of brain slices were obtained using an IX83 inverted-imaging system with a DP80 camera and 10x, 20x, or 40x UPlanSApo (0.75 NA) and 60x UPlanSApo oil-immersion (1.35 NA) objectives (Olympus, Shinjuku, Japan).

For confocal-image acquisition, either an upright TCS SP8 Laser microscope equipped with a 63x objective (oil-immersion, 1.2 NA) using sequential scanning with the 488 nm line of an argon-ion laser and the 543 nm line from helium–neon lasers (for Alexa 488 and Alexa 568, respectively) (Leica Microsystems) or an inverted confocal laser scanning FV3000 microscope equipped with 10x (0.75 NA), 20x (0.8 NA), and 40x (oil-immersed, 1.4 NA) objectives using sequential scanning with 405 nm, 488 nm, 561 nm cw diode lasers (for DAPI, Alexa488, Cy3 or Alexa 568, respectively) (Olympus) was used. Background correction and adjustment of brightness and contrast were performed using either LasX confocal software version 3.5.7 (Leica Microsystems, RRID:SCR_013673), cellSens Dimension version 1.18 (Olympus) or Fiji (NIH, Bethesda, MD, RRID:SCR_002285). Image analysis of protrusions was performed using cellSens Software (Olympus).

Subcellular Fractionation of Mouse Total-Brain Protein Lysates

Subcellular fractionation was adapted from previously described protocols (Cotman and Taylor, 1972; Mizoguchi et al., 1989; Trimbuch et al., 2009). Adult mice were sacrificed and brains dissected as described. Brains were homogenized in 0.32 M sucrose, 1 mM $NaHCO_3$ in H_2O with a syringe and cannula. Homogenate was layered on top of a sucrose gradient consisting of 0.85, 1, and 1.2 M sucrose solutions and ultra-centrifuged at 82,000 × g, at 4°C for 2 h (Beckmann Coulter, Brea, CA, United States). After centrifugation, the topmost layer of 0.32 M sucrose contained the cytosolic fraction, the band between 0.32 and 0.85 M sucrose contained the myelin-enriched fraction, the band between 0.85 and 1 M sucrose contained the Golgi- and ER-enriched fraction, the band between 1 and 1.2 M sucrose contained the synaptosomal fraction, and the pellet consisted of the mitochondria-enriched fraction. The synaptosomal fraction was further centrifuged at 33,000 × g at 4°C for 20 min and the resulting pellet was re-suspended in 6 mM Tris/HCl pH 8.0 for hypo-osmotic shock. The solution was again centrifuged at 33,000 × g at 4°C for 20 min. The resulting supernatant contained synaptic cytoplasm and the crude synaptic-vesicle fraction. The crude synaptic-plasma membrane fraction was extracted by re-suspending the pellet with 6 mM Tris/HCl pH 8 and 1% (v/v) Triton X-100. The crude synaptic plasma membrane fraction was then centrifuged a 33,000 × g at 4°C for 10 min; the resulting pellet contained the postsynaptic density fraction.

Proteomic Analysis

Following electrophoresis, gels were stained with Coomassie Brilliant Blue (Neuhoff et al., 1988) and slices of interest excised from the gels. Each slice was cut into small pieces (∼1 mm^2) prior to washing, reduction, alkylation and tryptic digestion (Kossmehl et al., 2013). The resulting peptides were separated applying nano-liquid chromatography using a trap column (2 cm, C18, 5 μm bead size, 75 μm inner diameter; Thermo Fisher Scientific) coupled to a 25 cm analytical column (C18, 2 μm bead size, 75 μm inner diameter; Thermo Fisher Scientific) using a 180 min linear gradient (Wöhlbrand et al., 2016). Eluting peptides were ionized online (captive spray ion source, Bruker Daltonik GmbH, Bremen, Germany) and mass analyzed by an ion-trap mass spectrometer (amaZon speed ETD, Bruker Daltonik). Positive ions were analyzed with a capillary current of 1.3 kV and dry-gas flow of 3 l/min nitrogen at 150°C. Active precursor exclusion was set for 0.2 min and 20 MS/MS spectra per full scan MS acquired. Protein identification was performed by Mascot (version 2.3, Matrix Science Ltd., London, United Kingdom) operated via the ProteinScape platform (Version 4.2, Bruker Daltonik GmbH) searching against the translated genome sequences of *Mus musculus*. Search settings were as follows: significance threshold $p < 0.05$; mass tolerance MS 0.3 Da, MS/MS 0.4 Da; false discovery rate 1.0% (applying target decoy); 1 missed cleavage site allowed; oxidation M variable modification; carbamidomethyl C fixed modification. A summary of identified proteins is provided in **Supplementary Table 1**.

Data Analysis

Data analysis was performed using GraphPad Prism 7.05 (GraphPad Software Inc., La Jolla, CA, United States). All data are presented as mean + SEM. A level of confidence of $p \leq 0.05$ was adopted [$^{*}p \leq 0.05$, $^{**}p \leq 0.01$, $^{***}p \leq 0.001$, ns = not significant ($p > 0.05$)]. Values were analyzed for normal distribution using the D'Agostino and Pearson test. Statistical analysis was performed using the 1 way ANOVA (robust against violation of normal distribution; Schmider et al., 2010).

DATA AVAILABILITY STATEMENT

The original contributions presented in the study are included in the article/**Supplementary Material**, further inquiries can be directed to the corresponding author/s.

ETHICS STATEMENT

The animal study was reviewed and approved by the Landesamt für Landwirtschaft, Lebensmittelsicherheit und Fischerei Mecklenburg-Vorpommern (LALLF) and Niedersächsisches Landesamt für Verbraucherschutz und Lebensmittelsicherheit (LAVES).

AUTHOR CONTRIBUTIONS

AB, IG, and NB designed the study. AB and IG wrote the manuscript, with contribution from all co-authors. IG performed western blot experiments and immunostainings and analyzed the results. DV performed primary neuron transfection and immunostainings. FK performed western blot experiments. NB performed and analyzed activity inhibitor

experiments. LW and RR performed the proteomic analysis. MW helped with RMS analysis. AH, TP, and MH revised the manuscript. Data from this work was part of the Ph.D. theses of IG, DV, and FK. All authors read and approved the final manuscript.

FUNDING

This work was supported by the FAZIT Stiftung, funding IG's work. Further funding was provided to AH and AB, by the research pool of the Carl von Ossietzky Universität Oldenburg, Special Topic "Rare Disease" (FP 2020-009). Parts of this study were supported by the Verbund Norddeutscher Universitäten to AB and MH.

ACKNOWLEDGMENTS

We thank Robin Piecha, Jennifer Sevecke-Rave, and Beate Bous for excellent technical assistance. Support by the Core Facility Fluorescence Microscopy (University of Oldenburg, Germany) with confocal imaging for this publication is gratefully acknowledged. English-language support was provided by stels-ol.de.

SUPPLEMENTARY MATERIAL

The Supplementary Material for this article can be found online at: https://www.frontiersin.org/articles/10.3389/fncel.2022.797588/full#supplementary-material

REFERENCES

Altman, J., and Das, G. D. (1965). Autoradiographic and histological evidence of postnatal hippocampal neurogenesis in rats. *J. Comp. Neurol.* 124, 319–335. doi: 10.1002/cne.901240303

Brandt, N., Franke, K., Rasin, M. R., Baumgart, J., Vogt, J., Khrulev, S., et al. (2007). The neural EGF family member CALEB/NGC mediates dendritic tree and spine complexity. *Embo J.* 26, 2371–2386. doi: 10.1038/sj.emboj.7601680

Bräuer, A. U., and Nitsch, R. (2008). Plasticity-related genes (PRGs/LRPs): a brain-specific class of lysophospholipid-modifying proteins. *Biochim. Biophys. Acta* 1781, 595–600. doi: 10.1016/j.bbalip.2008.04.004

Bräuer, A. U., Savaskan, N. E., Kuhn, H., Prehn, S., Ninnemann, O., and Nitsch, R. (2003). A new phospholipid phosphatase, PRG-1, is involved in axon growth and regenerative sprouting. *Nat. Neurosci.* 6, 572–578. doi: 10.1038/nn1052

Brewer, G. J., Torricelli, J. R., Evege, E. K., and Price, P. J. (1993). Optimized survival of hippocampal neurons in B27-supplemented Neurobasal, a new serum-free medium combination. *J. Neurosci. Res.* 35, 567–576. doi: 10.1002/jnr.490350513

Brindley, D. N. (2004). Lipid phosphate phosphatases and related proteins: signaling functions in development, cell division, and cancer. *J. Cell Biochem.* 92, 900–912. doi: 10.1002/jcb.20126

Brindley, D. N., and Waggoner, D. W. (1998). Mammalian lipid phosphate phosphohydrolases. *J. Biol. Chem.* 273, 24281–24284. doi: 10.1074/jbc.273.38.24281

Broggini, T., Nitsch, R., and Savaskan, N. E. (2010). Plasticity-related gene 5 (PRG5) induces filopodia and neurite growth and impedes lysophosphatidic acid- and nogo-A-mediated axonal retraction. *Mol. Biol. Cell.* 21, 521–537. doi: 10.1091/mbc.E09-06-0506

Carlin, R. K., Grab, D. J., Cohen, R. S., and Siekevitz, P. (1980). Isolation and characterization of postsynaptic densities from various brain regions: enrichment of different types of postsynaptic densities. *J. Cell. Biol.* 86, 831–845. doi: 10.1083/jcb.86.3.831

Chen, C. C., Lu, J., and Zuo, Y. (2014). Spatiotemporal dynamics of dendritic spines in the living brain. *Front. Neuroanat.* 8:28. doi: 10.3389/fnana.2014.00028

Chen, L. Y., Rex, C. S., Casale, M. S., Gall, C. M., and Lynch, G. (2007). Changes in synaptic morphology accompany actin signaling during LTP. *J. Neurosci.* 27, 5363–5372. doi: 10.1523/JNEUROSCI.0164-07.2007

Coiro, P., Stoenica, L., Strauss, U., and Bräuer, A. U. (2014). Plasticity-related gene 5 promotes spine formation in murine hippocampal neurons. *J. Biol. Chem.* 289, 24956–24970. doi: 10.1074/jbc.M114.597880

Cotman, C. W., and Taylor, D. (1972). Isolation and structural studies on synaptic complexes from rat brain. *J. Cell. Biol.* 55, 696–711. doi: 10.1083/jcb.55.3.696

Elston, G. N., and Fujita, I. (2014). Pyramidal cell development: postnatal spinogenesis, dendritic growth, axon growth, and electrophysiology. *Front. Neuroanat.* 8:78. doi: 10.3389/fnana.2014.00078

Fiala, J. C., Spacek, J., and Harris, K. M. (2002). Dendritic spine pathology: cause or consequence of neurological disorders? *Brain Res. Brain Res. Rev.* 39, 29–54. doi: 10.1016/s0165-0173(02)00158-3

Garey, L. J., Ong, W. Y., Patel, T. S., Kanani, M., Davis, A., Mortimer, A. M., et al. (1998). Reduced dendritic spine density on cerebral cortical pyramidal neurons in schizophrenia. *J. Neurol. Neurosurg. Psychiatry* 65, 446–453. doi: 10.1136/jnnp.65.4.446

Glantz, L. A., and Lewis, D. A. (2000). Decreased dendritic spine density on prefrontal cortical pyramidal neurons in schizophrenia. *Arch. Gen. Psychiatry* 57, 65–73. doi: 10.1001/archpsyc.57.1.65

Gleeson, J. G., Lin, P. T., Flanagan, L. A., and Walsh, C. A. (1999). Doublecortin is a microtubule-associated protein and is expressed widely by migrating neurons. *Neuron* 23, 257–271. doi: 10.1016/s0896-6273(00)80778-3

Gross, I., Tschigor, T., Salman, A. L., Yang, F., Luo, J., Vonk, D., et al. (2021). A systematic expression analysis of Plasticity-Related Genes in mouse brain development brings PRG4 into play. *Dev. Dyn.* [Online ahead of print], doi: 10.1002/dvdy.428

Hashimoto, R., Straub, R. E., Weickert, C. S., Hyde, T. M., Kleinman, J. E., and Weinberger, D. R. (2004). Expression analysis of neuregulin-1 in the dorsolateral prefrontal cortex in schizophrenia. *Mol. Psychiatry* 9, 299–307. doi: 10.1038/sj.mp.4001434

Hering, H., and Sheng, M. (2001). Dendritic spines: structure, dynamics and regulation. *Nat. Rev. Neurosci.* 2, 880–888. doi: 10.1038/35104061

Herms, J., and Dorostkar, M. M. (2016). Dendritic spine pathology in neurodegenerative diseases. *Annu. Rev. Pathol.* 11, 221–250. doi: 10.1146/annurev-pathol-012615-044216

Hill, J. J., Hashimoto, T., and Lewis, D. A. (2006). Molecular mechanisms contributing to dendritic spine alterations in the prefrontal cortex of subjects with schizophrenia. *Mol. Psychiatry* 11, 557–566. doi: 10.1038/sj.mp.4001792

Kolomeets, N. S., Orlovskaya, D. D., Rachmanova, V. I., and Uranova, N. A. (2005). Ultrastructural alterations in hippocampal mossy fiber synapses in schizophrenia: a postmortem morphometric study. *Synapse* 57, 47–55. doi: 10.1002/syn.20153

Kossmehl, S., Wöhlbrand, L., Druppel, K., Feenders, C., Blasius, B., and Rabus, R. (2013). Subcellular protein localization (cell envelope) in *Phaeobacter inhibens* DSM 17395. *Proteomics* 13, 2743–2760. doi: 10.1002/pmic.201300112

Lee, S., Zhang, H. Y., and Webb, D. J. (2015). Dendritic spine morphology and dynamics in health and disease. *Cell Health Cytoskeleton* 7, 121–131. doi: 10.2147/Chc.S82214

Lewis, T. L. Jr., Courchet, J., and Polleux, F. (2013). Cell biology in neuroscience: cellular and molecular mechanisms underlying axon formation, growth, and branching. *J. Cell Biol.* 202, 837–848. doi: 10.1083/jcb.201305098

Lledo, P. M., Alonso, M., and Grubb, M. S. (2006). Adult neurogenesis and functional plasticity in neuronal circuits. *Nat. Rev. Neurosci.* 7, 179–193. doi: 10.1038/nrn1867

Lois, C., Garcia-Verdugo, J. M., and Alvarez-Buylla, A. (1996). Chain migration of neuronal precursors. *Science* 271, 978–981. doi: 10.1126/science.271.5251.978

Maletic-Savatic, M., Malinow, R., and Svoboda, K. (1999). Rapid dendritic morphogenesis in CA1 hippocampal dendrites induced by synaptic activity. *Science* 283, 1923–1927. doi: 10.1126/science.283.5409.1923

Martinez-Cerdeno, V. (2017). Dendrite and spine modifications in autism and related neurodevelopmental disorders in patients and animal models. *Dev. Neurobiol.* 77, 393–404. doi: 10.1002/dneu.22417

Michalczyk, K., and Ziman, M. (2005). Nestin structure and predicted function in cellular cytoskeletal organisation. *Histol. Histopathol.* 20, 665–671. doi: 10.14670/HH-20.665

Ming, G. L., and Song, H. (2011). Adult neurogenesis in the mammalian brain: significant answers and significant questions. *Neuron* 70, 687–702. doi: 10.1016/j.neuron.2011.05.001

Mizoguchi, A., Ueda, T., Ikeda, K., Shiku, H., Mizoguti, H., and Takai, Y. (1989). Localization and subcellular distribution of cellular ras gene products in rat brain. *Brain Res. Mol. Brain Res.* 5, 31–44. doi: 10.1016/0169-328x(89)90015-6

Mullen, R. J., Buck, C. R., and Smith, A. M. (1992). NeuN, a neuronal specific nuclear protein in vertebrates. *Development* 116, 201–211. doi: 10.1242/dev.116.1.201

Nakahata, Y., and Yasuda, R. (2018). Plasticity of spine structure: local signaling, translation and cytoskeletal reorganization. *Front. Synaptic. Neurosci.* 10:29. doi: 10.3389/fnsyn.2018.00029

Neuhoff, V., Arold, N., Taube, D., and Ehrhardt, W. (1988). Improved staining of proteins in polyacrylamide gels including isoelectric focusing gels with clear background at nanogram sensitivity using Coomassie Brilliant Blue G-250 and R-250. *Electrophoresis* 9, 255–262. doi: 10.1002/elps.1150090603

Pan, B., Huang, X. F., and Deng, C. (2011). Antipsychotic treatment and neuregulin 1-ErbB4 signalling in schizophrenia. *Progr. Neuro-Psychopharmacol. Biol. Psychiatry* 35, 924–930. doi: 10.1016/j.pnpbp.2011.04.002

Paton, J. A., and Nottebohm, F. N. (1984). Neurons generated in the adult brain are recruited into functional circuits. *Science* 225, 1046–1048. doi: 10.1126/science.6474166

Pyne, S., Kong, K. C., and Darroch, P. I. (2004). Lysophosphatidic acid and sphingosine 1-phosphate biology: the role of lipid phosphate phosphatases. *Semin. Cell. Dev. Biol.* 15, 491–501. doi: 10.1016/j.semcdb.2004.05.007

Roberts, R. C., Conley, R., Kung, L., Peretti, F. J., and Chute, D. J. (1996). Reduced striatal spine size in schizophrenia: a postmortem ultrastructural study. *Neuroreport* 7, 1214–1218. doi: 10.1097/00001756-199604260-00024

Roberts, R. C., Roche, J. K., and Conley, R. R. (2005). Synaptic differences in the patch matrix compartments of subjects with schizophrenia: a postmortem ultrastructural study of the striatum. *Neurobiol. Dis.* 20, 324–335. doi: 10.1016/j.nbd.2005.03.015

Ruszczycki, B., Szepesi, Z., Wilczynski, G. M., Bijata, M., Kalita, K., Kaczmarek, L., et al. (2012). Sampling issues in quantitative analysis of dendritic spines morphology. *BMC Bioinform.* 13:213. doi: 10.1186/1471-2105-13-213

Sala, C., Cambianica, I., and Rossi, F. (2008). Molecular mechanisms of dendritic spine development and maintenance. *Acta Neurobiol. Exp. (Wars)* 68, 289–304.

Savaskan, N. E., Bräuer, A. U., and Nitsch, R. (2004). Molecular cloning and expression regulation of PRG-3, a new member of the plasticity-related gene family. *Eur. J. Neurosci.* 19, 212–220. doi: 10.1046/j.1460-9568.2003.03078.x

Schmider, E., Ziegler, M., Danay, E., Beyer, L., and Buhner, M. (2010). Is it really robust? Reinvestigating the robustness of ANOVA against violations of the normal distribution assumption. *Methodol.-Eur. J. Res. Methods Behav. Soc. Sci.* 6, 147–151. doi: 10.1027/1614-2241/a000016

Sigal, Y. J., McDermott, M. I., and Morris, A. J. (2005). Integral membrane lipid phosphatases/phosphotransferases: common structure and diverse functions. *Biochem. J.* 387(Pt 2), 281–293. doi: 10.1042/BJ20041771

Stefansson, H., Sigurdsson, E., Steinthorsdottir, V., Bjornsdottir, S., Sigmundsson, T., Ghosh, S., et al. (2002). Neuregulin 1 and susceptibility to schizophrenia. *Am. J. Med. Genet.* 114, 747–747.

Stiles, J., and Jernigan, T. L. (2010). The basics of brain development. *Neuropsychol. Rev.* 20, 327–348. doi: 10.1007/s11065-010-9148-4

Strauss, U., and Bräuer, A. U. (2013). Current views on regulation and function of plasticity-related genes (PRGs/LPPRs) in the brain. *Biochim. Biophys. Acta* 1831, 133–138. doi: 10.1016/j.bbalip.2012.08.010

Sweet, R. A., Henteleff, R. A., Zhang, W., Sampson, A. R., and Lewis, D. A. (2009). Reduced dendritic spine density in auditory cortex of subjects with schizophrenia. *Neuropsychopharmacology* 34, 374–389. doi: 10.1038/npp.2008.67

Tashiro, A., and Yuste, R. (2003). Structure and molecular organization of dendritic spines. *Histol. Histopathol.* 18, 617–634. doi: 10.14670/HH-18.617

Trimbuch, T., Beed, P., Vogt, J., Schuchmann, S., Maier, N., Kintscher, M., et al. (2009). Synaptic PRG-1 modulates excitatory transmission via lipid phosphate-mediated signaling. *Cell* 138, 1222–1235. doi: 10.1016/j.cell.2009.06.050

Unichenko, P., Kirischuk, S., Yang, J. W., Baumgart, J., Roskoden, T., Schneider, P., et al. (2016). Plasticity-Related Gene 1 affects mouse barrel cortex function via strengthening of glutamatergic thalamocortical transmission. *Cereb. Cortex* 26, 3260–3272. doi: 10.1093/cercor/bhw066

Velmans, T., Battefeld, A., Geist, B., Farres, A. S., Strauss, U., and Bräuer, A. U. (2013). Plasticity-related gene 3 promotes neurite shaft protrusion. *BMC Neurosci.* 14:36. doi: 10.1186/1471-2202-14-36

Wöhlbrand, L., Ruppersberg, H. S., Feenders, C., Blasius, B., Braun, H. P., and Rabus, R. (2016). Analysis of membrane-protein complexes of the marine sulfate reducer *Desulfobacula toluolica* Tol2 by 1D blue native-PAGE complexome profiling and 2D blue native-/SDS-PAGE. *Proteomics* 16, 973–988. doi: 10.1002/pmic.201500360

Xie, Z., Srivastava, D. P., Photowala, H., Kai, L., Cahill, M. E., Woolfrey, K. M., et al. (2007). Kalirin-7 controls activity-dependent structural and functional plasticity of dendritic spines. *Neuron* 56, 640–656. doi: 10.1016/j.neuron.2007.10.005

Yu, P., Agbaegbu, C., Malide, D. A., Wu, X., Katagiri, Y., Hammer, J. A., et al. (2015). Cooperative interactions of LPPR family members in membrane localization and alteration of cellular morphology. *J. Cell Sci.* 128, 3210–3222. doi: 10.1242/jcs.169789

Yu, X., and Malenka, R. C. (2003). beta-catenin is critical for dendritic morphogenesis. *Nat. Neurosci.* 6, 1169–1177. doi: 10.1038/nn1132

Yuste, R., and Bonhoeffer, T. (2004). Genesis of dendritic spines: insights from ultrastructural and imaging studies. *Nat. Rev. Neurosci.* 5, 24–34. doi: 10.1038/nrn1300

Yuste, R., and Denk, W. (1995). Dendritic spines as basic functional units of neuronal integration. *Nature* 375, 682–684. doi: 10.1038/375682a0

Zhang, Q. X., Pilquil, C. S., Dewald, J., Berthiaume, L. G., and Brindley, D. N. (2000). Identification of structurally important domains of lipid phosphate phosphatase-1: implications for its sites of action. *Biochem. J.* 345(Pt 2), 181–184. doi: 10.1042/bj3450181

Zhang, W., and Benson, D. L. (2000). Development and molecular organization of dendritic spines and their synapses. *Hippocampus* 10, 512–526. doi: 10.1002/1098-1063200010:5<512::AID-HIPO2<3.0.CO;2-M

Zhao, C., Deng, W., and Gage, F. H. (2008). Mechanisms and functional implications of adult neurogenesis. *Cell* 132, 645–660. doi: 10.1016/j.cell.2008.01.033

Zhao, C., Teng, E. M., Summers, R. G. Jr., Ming, G. L., and Gage, F. H. (2006). Distinct morphological stages of dentate granule neuron maturation in the adult mouse hippocampus. *J. Neurosci.* 26, 3–11. doi: 10.1523/JNEUROSCI.3648-05.2006

Conflict of Interest: The authors declare that the research was conducted in the absence of any commercial or financial relationships that could be construed as a potential conflict of interest.

Publisher's Note: All claims expressed in this article are solely those of the authors and do not necessarily represent those of their affiliated organizations, or those of the publisher, the editors and the reviewers. Any product that may be evaluated in this article, or claim that may be made by its manufacturer, is not guaranteed or endorsed by the publisher.

Copyright © 2022 Gross, Brandt, Vonk, Köper, Wöhlbrand, Rabus, Witt, Heep, Plösch, Hipp and Bräuer. This is an open-access article distributed under the terms of the Creative Commons Attribution License (CC BY). The use, distribution or reproduction in other forums is permitted, provided the original author(s) and the copyright owner(s) are credited and that the original publication in this journal is cited, in accordance with accepted academic practice. No use, distribution or reproduction is permitted which does not comply with these terms.

frontiers | Frontiers in Cellular Neuroscience

REVIEW
published: 22 April 2022
doi: 10.3389/fncel.2022.869779

Astroglia in the Vulnerability to and Maintenance of Stress-Mediated Neuropathology and Depression

*José Javier Miguel-Hidalgo**

Department of Psychiatry and Human Behavior, University of Mississippi Medical Center, Jackson, MS, United States

Significant stress exposure and psychiatric depression are associated with morphological, biochemical, and physiological disturbances of astrocytes in specific brain regions relevant to the pathophysiology of those disorders, suggesting that astrocytes are involved in the mechanisms underlying the vulnerability to or maintenance of stress-related neuropathology and depression. To understand those mechanisms a variety of studies have probed the effect of various modalities of stress exposure on the metabolism, gene expression and plasticity of astrocytes. These studies have uncovered the participation of various cellular pathways, such as those for intracellular calcium regulation, neuroimmune responses, extracellular ionic regulation, gap junctions-based cellular communication, and regulation of neurotransmitter and gliotransmitter release and uptake. More recently epigenetic modifications resulting from exposure to chronic forms of stress or to early life adversity have been suggested to affect not only neuronal mechanisms but also gene expression and physiology of astrocytes and other glial cells. However, much remains to be learned to understand the specific role of those and other modifications in the astroglial contribution to the vulnerability to and maintenance of stress-related disorders and depression, and for leveraging that knowledge to achieve more effective psychiatric therapies.

Keywords: astrocytes, stress, depression, pathology, epigenetics, glutamate

OPEN ACCESS

Edited by:
Yuriy Pankratov,
University of Warwick,
United Kingdom

Reviewed by:
Andrea Rivera,
University of Padua, Italy
Arthur Morgan Butt,
University of Portsmouth,
United Kingdom
Yuriy Pankratov,
University of Warwick,
United Kingdom

***Correspondence:**
José Javier Miguel-Hidalgo
jmiguel-hidalgo@umc.edu

Specialty section:
This article was submitted to Cellular Neurophysiology, a section of the journal Frontiers in Cellular Neuroscience

Received: *05 February 2022*
Accepted: *01 April 2022*
Published: *22 April 2022*

Citation:
Miguel-Hidalgo JJ (2022) Astroglia in the Vulnerability to and Maintenance of Stress-Mediated Neuropathology and Depression. Front. Cell. Neurosci. 16:869779. doi: 10.3389/fncel.2022.869779

INTRODUCTION

Stress and the systemic and neurophysiological responses it triggers are major risk factors for depression and other psychiatric disorders. In these disorders as well as in animal models for the effects of stress, astrocytes in several brain regions display morphological and molecular alterations (Bender et al., 2016; Murphy-Royal et al., 2019) that may result in grave consequences for the physiology and connectivity of brain circuits (Fields et al., 2015). A variety of chronic stress-inducing procedures in animals, such as chronic unpredictable stress, repeated fearful social interactions or recurrent restraint in rodents result in reductions in the numbers of astrocyte labeled for specific markers such as glial fibrillary acidic proteins (GFAP), in the levels the mRNA expression of the markers, and in the extent of the labeled processes that stem from their cell bodies in prefrontal cortical areas, the hippocampus or other brain regions (Banasr and Duman, 2008; Liu et al., 2009; Banasr et al., 2010; Araya-Callis et al., 2012; Imbe et al., 2012, 2013; Li L. F. et al., 2013; Li Y. S. et al., 2013; Tynan et al., 2013; Codeluppi et al., 2021). Interestingly, laboratory rats of the Wistar Kyoto strain, known to display spontaneously some depression-like behaviors, show comparable

lower levels of GFAP astrocyte immunostaining (Gosselin et al., 2009). Social defeat stress in a different species, the tree shrew, a marsupial mammal, leads to significant decrease in GFAP positive astrocyte and their cell body size in the hippocampus (Czeh et al., 2006).

Although most examples of chronic stress result in reduction of astrocytes' cell size or their GFAP expression as well as reduced levels of glutamate transporters, acute or short exposures to various stress procedures appear to augment rather than decrease markers of astrocytes (Bender et al., 2016; Yoshino et al., 2020). For example, two exposures in two consecutive days to electric shocks produced learned hopelessness in rats, but they increased the expression of glutamate transporter 1 (GLT-1) and glutamine synthetase (Yoshino et al., 2020). Similar results in other studies of the effects of short exposure to stress or adversity, have led some researchers to suggest that moderate or short stress [with the exception perhaps of post-traumatic stress disorder (PTSD)] rather than contributing to eventual depression would increase resilience and that astrocytes alterations may also be involved in positive effects of short-term stresses (Franklin et al., 2012; Menard et al., 2017). Nonetheless, most of the examples of astrocyte involvement in stress effects and depression-related behaviors discussed below are mostly related to chronic stress or stress undergone in early life stages.

It must also be pointed out that repeated exposure to altered concentrations of glucocorticoids in chronic stress may be a major factor determining the pathological changes in astrocytes that contribute to depression-like behavior. For instance, chronic treatment with corticosterone in mice results in reduced numbers of GFAP-positive astrocytes, smaller volume of their cells bodies and shorter process length and induces hippocampal atrophy in mice (Zhang et al., 2015). More recently, exposure to chronic social defeat stress, lipopolysaccharide or corticosteroid analog dexamethasone (DEX) have been shown to result in marked downregulation of glucocorticoid receptor (GR) expression in astrocytes and much less so in neurons in mice (Lu et al., 2021). Absence of those receptors in astrocytes results in depression-like behaviors while astrocyte-specific restoration of the receptors in the medial prefrontal cortex greatly mitigated the depression-like behavior (Lu et al., 2021). Thus, depletion of GR expression in astrocytes of the prefrontal cortex and other brain regions may be a major factor in the various astrocyte-specific molecular changes and the mechanism by which they contribute to long lasting behavioral and emotional effects of stress.

ASTROCYTES AND GLUTAMATE NEUROTRANMISSION AND REUPTAKE

Stress and the Role of NMDA-Type Glutamate Receptors

In animal models, stress that results in depression- and anxiety-like behaviors induces profound changes in various components of glutamate- and gamma-aminobutyric acid (GABA)-driven neurotransmission (Choudary et al., 2005; Kendell et al., 2005; Karolewicz et al., 2010; McKlveen et al., 2016; Réus et al., 2016). At the neuronal level, chronic stress and excess glucocorticoids lead to decreased expression of glutamate receptors in the prefrontal cortex, an effect that is dependent on the activation of glucocorticoid receptors (Yuen et al., 2012). In human subjects, elevated levels for N-methyl-D-aspartate-type (NMDA) and metabotropic glutamate receptor subunits were measured in the locus coeruleus of depressed subjects but not in pyramidal cells of the prefrontal cortex (Chandley et al., 2014), although a study found increases of metabotropic glutamate receptor 2/3 in Brodmann's area 10 of the prefrontal cortex (Feyissa et al., 2010). However, the regulation of glutamatergic neurotransmission is also critically dependent on the ability to reuptake released glutamate and recycle it to glutamine by astrocyte processes surrounding synapses, glutamine then being returned to the presynaptic element for further generation and release of glutamate. Thus, astrocytes have a critical role not only in terminating synaptic actions of glutamate but also in ensuring the continuous supply of releasable glutamate (Had-Aissouni et al., 2002).

Astrocytic Glutamate Transporters and Glutamine Synthetase in the Vulnerability to Stress and Depression

Regulation of the extracellular content of glutamate at synaptic and extra-synaptic sites is highly dependent on the activity of glutamate transporters EAAT1 and EAAT2 in the membranes of astrocytes processes, while the recycling of glutamate to glutamine within astrocytes is also performed in astrocytes by the action of glutamine synthetase. In human subjects with depression there are lower levels of glutamate transporters in the prefrontal cortex (Miguel-Hidalgo et al., 2010; Nagy et al., 2015). Similarly, in rodents subjected to chronic stress and in other animal models exhibiting depressive behaviors there is also a decrease in the expression of astrocytic glutamate transporters (Zink et al., 2010; Gomez-Galan et al., 2013; Piao et al., 2019) or glutamate reuptake (Almeida et al., 2010; de Vasconcellos-Bittencourt et al., 2011) in the cortex and hippocampus as compared to non-stressed controls.

Reduction in astrocytic transport relevant to the manifestation of depressive behaviors is not limited to cortical regions of the brain but extends as well to subcortical structures that have been long known to substantially contribute to the pathophysiology of stress effects and depression. In mice with depression-like behaviors caused by early life stress, the immunostaining of GLT1 astrocyte transporters and the thickness of astrocyte processes are reduced in the corticotrophin-releasing factor (CRF)-expressing dorsal-medial (MPD) neurons of the hypothalamus, effects which are concomitant with increased excitability of the surrounding neurons (Gunn et al., 2013). Also in mice, decreased activity of GLT1 transporters in the habenula promotes depression-like behaviors and increases the behavioral vulnerability to depression-like behavioral effects of chronic stress (Cui et al., 2014). Loss of astrocyte glutamate transporter GLT-1 was observed also in the periaqueductal gray matter of rats subjected to chronic restraint stress (Imbe et al., 2012). Thus, the available evidence strongly suggests that

prolonged or repetitive stress results in a generalized or, at least, amply extensive decrease in the astrocytic cellular systems for glutamate reuptake, and that behavioral effects may be greatly influenced by the corresponding disturbances in neuronal excitability. This involvement of glutamate reuptake dysfunction in the depression-like behavioral effects of stress is supported also by the demonstration that administration of riluzole, a compound that stimulates the reuptake of glutamate by astrocytes, and also reduces its release, mitigates depression-like behaviors and prevents alterations of astrocyte metabolism and GFAP mRNA expression in rodent models of stress (Banasr et al., 2010). Likewise, ceftriaxone, a beta-lactam antibiotic that favors glutamate uptake, results in antidepressant-like effects across models of stress in mice (Mineur et al., 2007).

Gap Junctions of Astrocytes in Stress and Depression

In animals under chronic stress and in humans with major depression) there are drastically low levels of astrocytic gap junction proteins connexin 43 (Cx43) and connexin 30 (Cx30) in the prefrontal cortex (PFC) as compared to controls (Ernst et al., 2011; Sun et al., 2012; Miguel-Hidalgo et al., 2014, 2018; Nagy et al., 2016). Likewise, some animal models of stress leading to depression-like behaviors have demonstrated a region-specific decrease in myelination markers after prolonged stress, partially reversible with antidepressant treatments or myelin-promoting agents (Liu et al., 2012, 2016). This is consistent with findings in the PFC of human subjects with depression, where there is reduced expression of myelin- and astrocyte-related mRNAs (Liu et al., 2012, 2016; Rajkowska et al., 2015; Miguel-Hidalgo et al., 2017, 2018). More recently, highly suggestive evidence of reduced gap junction coupling between astrocytes and oligodendrocytes has been also observed in the anterior cingulate cortex of subjects with depression (Tanti et al., 2019). Gap junctions formed by astrocyte connexons (made of Cx43 or Cx30 subunits) interacting with the corresponding connexons from oligodendrocytes (made of Cx47 or C32) (Giaume and McCarthy, 1996) have proven crucial for the maintenance of myelin, as mice with KO for different combinations of astrocyte and oligodendrocyte connexins demonstrate variable degrees of myelin vacuolization and degradation, and profound behavioral deficits (Lutz et al., 2009; Magnotti et al., 2011; Li et al., 2014; Basu and Sarma, 2018). Whether chronic stress or sustained high corticosteroids in the blood circulation or the brain results in deficient myelin formation or maintenance mediated by reduced astrocyte connexins is less well established, although recently published evidence from our laboratory, has provided the first proof-of-concept evidence that stress, or high corticosterone during myelination, results in concomitant myelin and Cx43/Cx30 alterations that involve lower immunoreactivity for myelin basic protein and those connexins *in vivo* (Miguel-Hidalgo et al., 2018) and *in vitro* (Miguel-Hidalgo et al., 2019), and decreased morphological indices of myelination *in vitro*. We also have observed that concurrent reductions of connexins and myelin proteins in cortical primary cell cultures *in vitro* can both be prevented by the glucocorticoid receptor antagonist mifepristone (Miguel-Hidalgo et al., 2019).

Mechanisms by which glucocorticoids regulate the expression, turnover or function of Cx43-containing gap junctions have been partially characterized in cells from tissues outside of nervous system. In cells from these tissues corticosterone (CORT) causes Cx43 degradation through autophagy mechanisms (Gao et al., 2016) or the activation of the Akt/mTOR signaling pathway (Shen et al., 2016). Activation of GC receptors is involved in those mechanisms because antagonism with mifepristone blocks CORT effects. In addition, some *in vitro* studies with primary cortical astrocytes, and *in vivo* research in the cerebral cortex, have found that high CORT levels cause reduction in Cx43 protein (Xia et al., 2017, 2018) or mRNA (Samarasinghe et al., 2012; Carter et al., 2013) and that inactivation of p38 and c-fos/AP1 pathways (Morioka et al., 2014) may also lead to reduced Cx43. Also *in vivo*, some antidepressants, or GC receptor antagonists such as mifepristone mitigate the reduction of Cx43 caused by chronic unpredictable stress in animals (Sun et al., 2012; Xia et al., 2017). However, the mechanisms by which glucocorticoid receptor activation leads to Cx43 reductions in the CNS, and particularly in the PFC in stress or in postmortem brains from subjects with depression, remain to be ascertained. Neurodevelopmental research in prenatal neural progenitors has also indicated that the inactivation and reduction Cx43 gap junctions can be mediated by non-genomic actions of caveolin-1-attached GC receptors through the activation of the Raf-RAS-ERK1/2 pathway (Pedram et al., 2006; Hammes and Levin, 2007; Samarasinghe et al., 2012), although other effects on astrocytes may depend on the genomic pathway of GR activation (Kumar et al., 1986). Furthermore caveolin-1 is strongly expressed in astrocytes (Yun et al., 2011). Excess CORT-related decreases of brain-derived neurotrophic factor (BDNF) may also contribute to the reduction of Cx43, as shown in hippocampal astrocytes although this mechanism might not operate in the PFC (Schaaf et al., 1998). Thus, increased autophagy, AKt/mTOR activation, ERK-activation/Cx43-reduction by non-genomic GR mechanisms, or excess GC-induced BDNF decrease may also lead to alterations in the structure and function of astrocyte gap junctions. However, it is unknown whether and which of those mechanisms operates in the effects of stress (or high CORT) on astrocyte connexins or their companion oligodendrocyte connexins in the PFC. Interestingly, in our recent *in vitro* studies of mixed rat cortical primary cell cultures, we observed that reduction of Cx43 with a high dose of CORT analog DEX, which has a very high effectivity for genomic GR actions, was noticeably smaller than with high CORT (Miguel-Hidalgo et al., 2019), suggesting that, besides the genome-acting GC receptors, reductions of Cx43 with stress may be substantially due to non-genomic effects of GR activation.

An important contribution of astrocyte Cx43 and Cx30 to the maintenance of myelin integrity has been established in rodent models with KO of Cx43 and Cx30 expression alone or in combination with their KO of Cx47 and Cx32 oligodendrocyte partners, where the KO leads in many instances to patent myelin disorganization (Lutz et al., 2009; Magnotti et al., 2011; Tress et al., 2012; Li et al., 2014). However, it is yet unknown whether

connexin decreases caused by high glucocorticoids or stress is part of mechanisms that would lead to reduced expression of myelin proteins or to anomalous myelination in the PFC and its connections. Clearly, the magnitude and extent of Cx43 and myelin changes detected after stress, though significant, are smaller than in connexin KO animals. However, during the last decade it has become clear that plasticity of myelin leading to significant, but not necessarily catastrophic, changes in the morphology or extent of myelin results in meaningful variations in function and connectivity (Nave, 2010; Nave and Ehrenreich, 2014; Fields, 2015; Fields et al., 2015).

Involvement of Astrocytes in Neuroimmune Activation Elicited by Stress-Responses

Depression and stress responses are closely accompanied by dysregulation of immune activation and by expression of neuroimmune mediators produced by microglia and astrocytes (Hodes et al., 2015; Miller and Raison, 2016). Astrocytes carry receptors for various cytokines and chemokines and can thus respond to some of those mediators released by surrounding microglial cells or provided in the blood circulation (Maeng and Hong, 2019). Some of these responses involve chemokine expression that would in turn increase the ability to attract peripheral immune cells to the brain (Hennessy et al., 2015). Importantly, the actions of immune mediators on astrocytes directly influence their ability to perform essential functions (Sofroniew, 2014) in the support of neuronal activity, such as neurotransmitter metabolism (Muller and Schwarz, 2007), glutamate transport (Haroon et al., 2017, 2018; Piao et al., 2019), expression of aquaporins, maintenance of gap junctions (John et al., 1999; Karpuk et al., 2011) or expression of connexin 43 in a nuclear factor-kB (NF-kB)-dependent manner (Zhao et al., 2006). Conversely, connexin 43, which is present in astrocyte gap junctions interacting with the blood brain barrier (BBB), works as a main factor in regulating immune cell recruitment and antigen presentation at the BBB (Boulay et al., 2015). Thus, the sensitivity of astrocytes to inflammatory and other immune system-derived factors and the feedback they may exert to further regulate immune responses may be major contributors to neuronal metabolism and connectivity deficits that are thought to underpin the emotional and behavioral pathology caused by stress and other depressogenic neural mechanisms.

The intracellular molecular pathways involved in stress-induced activation of immune responses by astrocytes may involve the regulation of NF-kB by menin, because in non-stressed conditions this protein keeps in check the content of nervous system pro-inflammatory transcriptional activator NF-kB and the consequent downstream stimulation of interleukin 1ß (IL-1ß), while chronic stress results in menin reduction and subsequent activation of NF-kB and IL-1ß increase. Depression-like behaviors in the same animal model were prevented by the use of NF-kB inhibitors or IL1ß antagonists (Leng et al., 2018; Zhuang et al., 2018). Likewise, a polymorphism of gene *MEN1* (which encodes menin) was found to be significantly linked to higher risk for the onset of depression (Leng et al., 2018). In fact, the polymorphism reduces the binding of menin to NF-kB component p65, effectively enhancing the activation of Nf-kB and thus the production of IL1ß by astrocytes.

Astrocyte Thrombospondin in Depression and Stress-Related Synaptic Alterations

Release of extracellular matrix proteins thrombospondin-1 and -2 by astrocytes is a strong promoter of synapse formation *in vitro* and *in vivo* (Christopherson et al., 2005; Jayakumar et al., 2014). Since changes of synaptic plasticity are involved in the pathophysiology of stress responses, depression, and other psychiatric disorders (Duman and Aghajanian, 2012; Yuen et al., 2012; Treccani et al., 2014; Csabai et al., 2018), some researchers have targeted the putative involvement of astrocyte-expressed thrombospondins 1 (TSP1) and 2 in the consequences of stress, including the generation of depression-like behaviors, as well as in the synaptic effects of antidepressant treatments. For instance, TSP-1 synthesis and mRNA expression are increased in the hippocampus after repeated electroconvulsive therapy, one of the most effective antidepressant treatments, although pharmacological antidepressants are apparently ineffective (Okada-Tsuchioka et al., 2014, 2017). In human subjects, plasma levels of TSP-1 levels were also found to be decreased in depression, at least in females (Okada-Tsuchioka et al., 2020).

Astrocyte Processes and Aquaporin at the Blood Brain Barrier in Stress-Related Neuropathology

In the prefrontal cortex of human subjects with depression, the coverage of vessels by the aquaporin 4 (AQP-4)-immunoreactive endfeet of astrocytes is significantly reduced, even if the extent of those feet is not changed when labeled for the cytoskeletal protein GFAP (Rajkowska et al., 2013). Interestingly, in a genetic rat model for depression-like behaviors (Arauchi et al., 2018), AQP-4-positive astrocyte endfeet were also found to be reduced when compared with Wistar rats. Remarkably, electroconvulsive therapy was able to suppress depression-like behaviors and increased the extent of AQP-4 immunoreactive processes around blood vessels in the rat genetic model (Azis et al., 2019). In fact, the functions of astrocytes' processes abutting at the basal lamina of arterioles are not limited to the control of BBB exchanges, but also include the regulation of the neurovascular coupling that depends on arteriole smooth muscle responses to extracellular potassium ions (Longden et al., 2014). This regulation may be significantly affected by elevated glucocorticoids in stress because corticoids, besides affecting smooth muscle potassium channels, would also alter coverage of arterioles by astrocytes processes, thus adding another risk factor for astrocyte-induced blood flow dysregulation upon the stress response.

Chronic stress can also cause astrocyte mediated alterations of cerebrovascular regulation through increases in oxidative damage elicited by neuroinflammation and oxidative stress. These processes are increased in the brain of subjects with depression, involving decreased levels of antioxidants and

higher levels of products of lipid peroxidation or, in serum, accompanied by augmented amounts of malondialdehyde, decreased antioxidant enzymes such as glutathione peroxidase and catalase, and increased superoxide and nNOS (Burrage et al., 2018). Decreases in eNOS in astrocytes and endothelial cells after stress may displace the equilibrium between oxidative and antioxidant processes to favor excess generation of deleterious superoxide.

Astrocyte Epigenetic Markers in Stress and Depression

As presented above, there are major effects of stress and probably other depressogenic mechanisms on the expression of astrocytes' connexins 43 and 30 in brain cortical areas (Sun et al., 2012; Miguel-Hidalgo et al., 2014, 2018, 2019). These reductions also affect their corresponding mRNAs both in animal models of stress (Sun et al., 2012) and in humans subjects with depression (Nagy et al., 2016) and have been convincingly attributed to epigenetic marker alterations such as methylation of histone 3 at Cx43 and Cx30 genes in the prefrontal cortex using chromatin immunoprecipitation (Nagy et al., 2016). The epigenetic differences between subjects with depression and controls also extend to the pattern of DNA methylation for genes expressed at a high level in astrocytes as compared to other cell types (Nagy et al., 2015) including *GFAP, ALDHL1*, *SLC1A3, GJA1, GJB6*, *GLUL* and *SOX9,* all of which are found to be reduced in the dorsolateral prefrontal cortex of subjects with depression (Nagy et al., 2015). Depression-linked histone methylation modifications in astrocytes also have been detected for genes involved in the signaling of trophic factors such as *BDNF*, which is altered in some subjects with depression and in stress models. The levels of a BDNF receptor variant expressed in astrocytes, TrkB.T1, were found to be decreased in the prefrontal cortex of depressed suicide completers and inversely correlated with the levels of Hiistone 3 methylation at lysine 27 (Ernst et al., 2009a,b). It has been suggested that vulnerability to the effects of stress, at least of a social nature, could be related to the expression of the Trkb.T1 variant in astrocytes, because mice with higher expression levels of that variant express avoidance behaviors to a higher extent than control mice, behavior that would be related to the increased probability of epigenetic modifications at Trkb.T1 in astrocytes (Razzoli et al., 2011; Hodes et al., 2017).

Further research into the regulation of astrocyte glutamate uptake has also indicated that epigenetic alterations of glutamate transporter genes *EAAT1* and *EAAT2* (*GLAST* and *GLT-1* respectively in rats) may confer vulnerability to the effects of stress or the manifestation of depression.

Specificity of epigenetic changes in astrocytes as compared to changes in neurons is underscored by astrocyte-specific higher or lower expression of some of the enzymes that are in charge of executing epigenetic modifications, astrocytes featuring higher mRNA expression of histone deacetylase Hdac8, sirtuin Sirt8, histone methyl-transferase Mll3 or histone demethylase Kdm5d, while underexpressing histone deacetylase Hdac5, Hdac11 or histone demethylase Kdm2b (Zhang et al., 2014; Jakovcevski et al., 2016). This capability of astrocytes to differentially contribute to epigenetic changes may be of great relevance to the vulnerability to stress-related disorders and depression since disturbances in the expression of epigenetic enzymes and in the epigenetic changes themselves have been found to distinguish specific brain regions of subjects with depression as compared to non-psychiatric human subjects (Lopizzo et al., 2015; Jakovcevski et al., 2016). Other studies have pointed to factors involved in regulating the transcription of glutamate transporters such as the astrocyte-elevated gene which acts as corepressor of factor YY1 to repress the transcription of *GLT-1* and diminish glutamate uptake by astrocytes. YY1 also mediates repression of *GLAST* and *GLT-1* expression after exposure to inflammatory cytokine tumor necrosis factor α (TNF-α) by recruiting histone deacetylases to the promoter of glutamate transporter genes (Pajarillo et al., 2019). Some of the changes in epigenetic regulation of glutamate transporter expression may also be involved in depression-like behaviors and cognitive alterations secondary to neurological conditions, such as subarachnoid hemorrhage, in which astrocyte histone deacetylase 2 negatively regulates the expression of *GLT-1* (Tao et al., 2020).

Effects of Early Stress Exposure on Astrocytes and Their Role in the Development of Depression

Paramount among the studies addressing the vulnerability to depressive and anxiety symptoms are those focusing on the effects of early life adversity and stress on the probability of developing depressive and other psychiatric illnesses during and adolescence and adulthood (Chen and Baram, 2016). Various of these studies have been based on different forms of early adversity, including maternal separation/deprivation, malnutrition, overnutrition or immune challenges. A recent review has stressed the importance of early adversity in the responses of astrocytes to immune challenges later in life, as well the effects of disturbed astrocyte metabolism due to malnutrition, which could set the stage for astrocyte priming as a factor for the level of vulnerability to affective and other psychiatric disorders (Abbink et al., 2019). In the hippocampus, the multifaceted physiological roles of astrocytes and their involvement in functional plasticity such as long-term potentiation have been recently reviewed by Çalişkan et al. (2020), also indicating that early or juvenile stress results in reduced GFAP expression and diminished complexity of morphological features in astrocytes as well as reduced uptake of glutamate and GABA, and impaired conversion of glutamate to glutamine (Çalişkan et al., 2020). Repeated or chronic maternal separation in infant rats during the lactating period was also found to cause drastic reductions in the number of GFAP-immunoreactive astrocytes in the prefrontal cortex, hippocampus and striatum (Banqueri et al., 2019). For instance, maternal separation stress results in depletion of GFAP and S100b immunoreactive astrocytes in the medial precentral cortex of the Wistar rat strain (Musholt et al., 2009). Similarly, in Fischer rats, which are constitutively highly responsive to stress, 14 days of early maternal deprivation leads to reduced density of GFAP-immunoreactive astrocytes in the prefrontal cortex, hippocampal regions and the amygdala (Leventopoulos et al., 2007) in adult

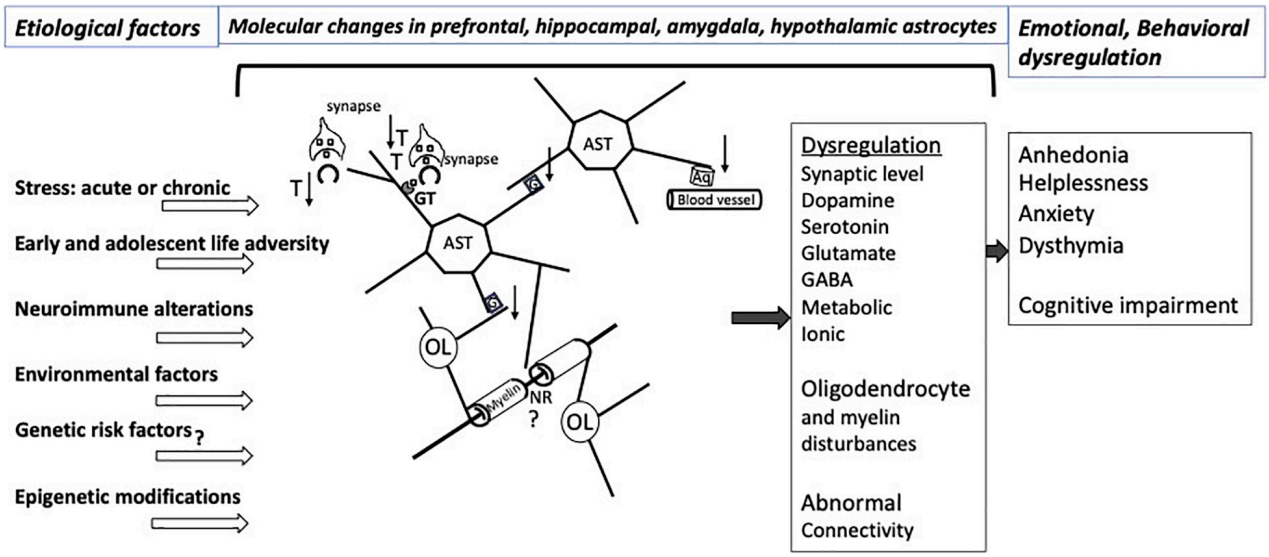

FIGURE 1 | Illustration of relevant interactions involving CNS astrocytes that would be affected by various types of stress and other factors predisposing to affective disorders. The pathological interactions with astrocytes result in a variety of molecular and neurotransmitters alterations in the prefrontal cortex, hippocampus, amygdala, striatum, hypothalamus involving dysregulation of at least dopamine, serotonin, glutamate and GABA neurotransmission, with varying degrees of regional specificity. Stress exposure and other risk factors for neuropathology itself also may lead to pathological disturbances of astrocyte-contributions to BBB regulation and to the extracellular matrix NRs and other parts of the white matter. More recent research work has revealed epigenetic abnormalities or changed levels of specific miRNAs and other non-coding RNAs in affective disorders that may contribute to specific emotional and cognitive symptoms in particular brain regions. Nonetheless, substantial additional research is required to improve our understanding of mechanisms underpinning the relationship of cellular and molecular pathology to epigenetic and non-coding RNA markers that result in dysfunctional astrocyte contacts with neurons and oligodendrocytes, eventually leading to abnormal brain connectivity in affective disorders. Aq, aquaporin 4; AST, astrocytes; G, gap junctions; GT, glutamate and GABA transporters; NR, node of Ranvier; OL, oligodendrocyte; T, thrombospondin; ↑, up-regulation; ↓, down-regulation. At the synapse, squares represent neurotransmitters.

animals. In guinea pigs, antenatal stress of dams results as well in reduced GFAP immunostaining of CA1 hippocampal astrocytes when examined in 21-days old offspring (Bennett et al., 2015). In view of the lower immunoreactivity of GFAP immunoreactive astrocytes and the lower levels of GFAP observed in the prefrontal cortex in postmortem human brains from younger subjects with major depression (as compared to older subjects or to non-psychiatric controls) (Miguel-Hidalgo et al., 2000; Si et al., 2004), early stress, adversity or excessive immune activation may prime astrocytes to facilitate, at least in some human subjects, manifestations of depression in late-adolescence and adulthood.

Since early life stress (ELS) also involves the activation of hormonal responses regulated by the hypothalamic-pituitary-adrenal axis, some research has addressed cellular and neurotransmitter dysfunction in the hypothalamus and a putative involvement of astrocytes. In mature hypothalamic neurons, the ability of neurosteroids to reduce overactivation was found to be curtailed by ELS. This effect is dependent on an excessive glutamatergic activation that derives in part from impaired astrocytic regulation of extracellular glutamate levels (Gunn et al., 2013). This alteration was concomitant with morphological changes of GFAP-immunoreactive astrocyte processes and a reduction of the immunoreactivity of astrocytic glutamate transporters (Gunn et al., 2013).

Long-lasting astrocyte glutamate transport deficits may lead to dysfunction of specific circuits known to be involved in the pathophysiology of affective and psychiatric disorders. For instance, in the medial prefrontal cortex of rodents, astrocytic glutamate transport activity plays a major role in modulating the connections between the prefrontal cortex and the serotonergic neurons of the raphe nucleus (Fullana et al., 2020). Accordingly, prolonged suppression of the astrocyte-dependent glutamate transport capacity in the prefrontal cortex of mice results in depression-like behaviors (Fullana et al., 2019a,b), although the effects of acute vs chronic stress on the connections between the various subdivisions of the PFC and the serotonergic raphe neurons remain to be fully elucidated (Fullana et al., 2020).

CONCLUSION

Astrocytes' multifaceted involvement in various aspects of neuronal metabolism, support of neurotransmission, supply of neurotrophic factors, neuroimmune reactivity, myelin maintenance, and regulation of signal propagation as well as their capacity to directly respond to hormonal and other molecular adaptations caused by stress sets them to be major players in determining the behavioral and emotional vulnerability to the effects of stress (**Figure 1**). These effects may be long lasting because at different stages of development and in adulthood there is substantial epigenetic regulation of gene expression in astrocytes, and the astrocytes themselves are crucial

in supporting the development of other neural cells, synaptic connections, and axonal pathways in the central nervous system. Some of the epigenetic and molecular mechanisms regarding glutamate transport, gap junction communication and neuroimmune regulation that are related to stress effects are starting to be ascertained. However, much remains to be learned to understand the specific role of those and other modifications in the astroglial contribution to the vulnerability to and maintenance of stress-related disorders and depression, and for leveraging that knowledge to achieve more effective psychiatric therapies.

AUTHOR CONTRIBUTIONS

The author confirms being the sole contributor of this work and approved it for publication.

FUNDING

This work was supported by IRSP of the University of Mississippi Medical Center and by the National Institute of Mental Health, grant MH118675.

REFERENCES

Abbink, M. R., Van Deijk, A. F., Heine, V. M., Verheijen, M. H., and Korosi, A. (2019). The involvement of astrocytes in early-life adversity induced programming of the brain. *Glia* 67, 1637–1653. doi: 10.1002/glia.23625

Almeida, R. F., Thomazi, A. P., Godinho, G. F., Saute, J. A., Wofchuk, S. T., Souza, D. O., et al. (2010). Effects of depressive-like behavior of rats on brain glutamate uptake. *Neurochem. Res.* 35, 1164–1171. doi: 10.1007/s11064-010-0169-4

Arauchi, R., Hashioka, S., Tsuchie, K., Miyaoka, T., Tsumori, T., Limoa, E., et al. (2018). Gunn rats with glial activation in the hippocampus show prolonged immobility time in the forced swimming test and tail suspension test. *Brain Behav.* 8:e01028. doi: 10.1002/brb3.1028

Araya-Callis, C., Hiemke, C., Abumaria, N., and Flugge, G. (2012). Chronic psychosocial stress and citalopram modulate the expression of the glial proteins GFAP and NDRG2 in the hippocampus. *Psychopharmacology (Berl.)* 224, 209–222. doi: 10.1007/s00213-012-2741-x

Azis, I. A., Hashioka, S., Tsuchie, K., Miyaoka, T., Abdullah, R. A., Limoa, E., et al. (2019). Electroconvulsive shock restores the decreased coverage of brain blood vessels by astrocytic endfeet and ameliorates depressive-like behavior. *J. Affect. Disord.* 257, 331–339. doi: 10.1016/j.jad.2019.07.008

Banasr, M., Chowdhury, G. M., Terwilliger, R., Newton, S. S., Duman, R. S., Behar, K. L., et al. (2010). Glial pathology in an animal model of depression: reversal of stress-induced cellular, metabolic and behavioral deficits by the glutamate-modulating drug riluzole. *Mol. Psychiatry* 15, 501–511. doi: 10.1038/mp.2008.106

Banasr, M., and Duman, R. S. (2008). Glial loss in the prefrontal cortex is sufficient to induce depressive-like behaviors. *Biol. Psychiatry* 64, 863–870. doi: 10.1016/j.biopsych.2008.06.008

Banqueri, M., Mendez, M., Gomez-Lazaro, E., and Arias, J. L. (2019). Early life stress by repeated maternal separation induces long-term neuroinflammatory response in glial cells of male rats. *Stress* 22, 563–570. doi: 10.1080/10253890.2019.1604666

Basu, R., and Sarma, J. D. (2018). Connexin 43/47 channels are important for astrocyte/ oligodendrocyte cross-talk in myelination and demyelination. *J. Biosci.* 43, 1055–1068. doi: 10.1007/s12038-018-9811-0

Bender, C. L., Calfa, G. D., and Molina, V. A. (2016). Astrocyte plasticity induced by emotional stress: a new partner in psychiatric physiopathology? *Prog. Neuropsychopharmacol. Biol. Psychiatry* 65, 68–77. doi: 10.1016/j.pnpbp.2015.08.005

Bennett, G. A., Palliser, H. K., Shaw, J. C., Walker, D., and Hirst, J. J. (2015). Prenatal stress alters hippocampal neuroglia and increases anxiety in childhood. *Dev. Neurosci.* 37, 533–545. doi: 10.1159/000437302

Boulay, A. C., Mazeraud, A., Cisternino, S., Saubamea, B., Mailly, P., Jourdren, L., et al. (2015). Immune quiescence of the brain is set by astroglial connexin 43. *J. Neurosci.* 35, 4427–4439. doi: 10.1523/JNEUROSCI.2575-14.2015

Burrage, E., Marshall, K. L., Santanam, N., and Chantler, P. D. (2018). Cerebrovascular dysfunction with stress and depression. *Brain Circ.* 4, 43–53. doi: 10.4103/bc.bc_6_18

Çalişkan, G., Muller, A., and Albrecht, A. (2020). Long-term impact of early-life stress on hippocampal plasticity: spotlight on astrocytes. *Int. J. Mol. Sci.* 21:4999. doi: 10.3390/ijms21144999

Carter, B. S., Hamilton, D. E., and Thompson, R. C. (2013). Acute and chronic glucocorticoid treatments regulate astrocyte-enriched mRNAs in multiple brain regions in vivo. *Front. Neurosci.* 7:139. doi: 10.3389/fnins.2013.00139

Chandley, M. J., Szebeni, A., Szebeni, K., Crawford, J. D., Stockmeier, C. A., Turecki, G., et al. (2014). Elevated gene expression of glutamate receptors in noradrenergic neurons from the locus coeruleus in major depression. *Int. J. Neuropsychopharmacol.* 17, 1569–1578. doi: 10.1017/S1461145714000662

Chen, Y., and Baram, T. Z. (2016). Toward understanding how early-life stress reprograms cognitive and emotional brain networks. *Neuropsychopharmacology* 41, 197–206. doi: 10.1038/npp.2015.181

Choudary, P. V., Molnar, M., Evans, S. J., Tomita, H., Li, J. Z., Vawter, M. P., et al. (2005). Altered cortical glutamatergic and GABAergic signal transmission with glial involvement in depression. *Proc. Natl. Acad. Sci. U.S.A.* 102, 15653–15658. doi: 10.1073/pnas.0507901102

Christopherson, K. S., Ullian, E. M., Stokes, C. C., Mullowney, C. E., Hell, J. W., Agah, A., et al. (2005). Thrombospondins are astrocyte-secreted proteins that promote CNS synaptogenesis. *Cell* 120, 421–433. doi: 10.1016/j.cell.2004.12.020

Codeluppi, S. A., Chatterjee, D., Prevot, T. D., Bansal, Y., Misquitta, K. A., Sibille, E., et al. (2021). Chronic stress alters astrocyte morphology in mouse prefrontal cortex. *Int. J. Neuropsychopharmacol.* 24, 842–853. doi: 10.1093/ijnp/pyab052

Csabai, D., Wiborg, O., and Czeh, B. (2018). Reduced synapse and axon numbers in the prefrontal cortex of rats subjected to a chronic stress model for depression. *Front. Cell. Neurosci.* 12:24. doi: 10.3389/fncel.2018.00024

Cui, W., Mizukami, H., Yanagisawa, M., Aida, T., Nomura, M., Isomura, Y., et al. (2014). Glial dysfunction in the mouse habenula causes depressive-like behaviors and sleep disturbance. *J. Neurosci.* 34, 16273–16285. doi: 10.1523/JNEUROSCI.1465-14.2014

Czeh, B., Simon, M., Schmelting, B., Hiemke, C., and Fuchs, E. (2006). Astroglial plasticity in the hippocampus is affected by chronic psychosocial stress and concomitant fluoxetine treatment. *Neuropsychopharmacology* 31, 1616–1626. doi: 10.1038/sj.npp.1300982

de Vasconcellos-Bittencourt, A. P., Vendite, D. A., Nassif, M., Crema, L. M., Frozza, R., Thomazi, A. P., et al. (2011). Chronic stress and lithium treatments alter hippocampal glutamate uptake and release in the rat and potentiate necrotic cellular death after oxygen and glucose deprivation. *Neurochem. Res.* 36, 793–800. doi: 10.1007/s11064-011-0404-7

Duman, R. S., and Aghajanian, G. K. (2012). Synaptic dysfunction in depression: potential therapeutic targets. *Science* 338, 68–72. doi: 10.1126/science.1222939

Ernst, C., Chen, E. S., and Turecki, G. (2009a). Histone methylation and decreased expression of TrkB.T1 in orbital frontal cortex of suicide completers. *Mol. Psychiatry* 14, 830–832. doi: 10.1038/mp.2009.35

Ernst, C., Deleva, V., Deng, X., Sequeira, A., Pomarenski, A., Klempan, T., et al. (2009b). Alternative splicing, methylation state, and expression profile of tropomyosin-related kinase B in the frontal cortex of suicide completers. *Arch. Gen. Psychiatry* 66, 22–32. doi: 10.1001/archpsyc.66.1.22

Ernst, C., Nagy, C., Kim, S., Yang, J. P., Deng, X., Hellstrom, I. C., et al. (2011). Dysfunction of astrocyte connexins 30 and 43 in dorsal lateral prefrontal cortex of suicide completers. *Biol. Psychiatry* 70, 312–319. doi: 10.1016/j.biopsych.2011.03.038

Feyissa, A. M., Woolverton, W. L., Miguel-Hidalgo, J. J., Wang, Z., Kyle, P. B., Hasler, G., et al. (2010). Elevated level of metabotropic glutamate receptor 2/3

in the prefrontal cortex in major depression. *Prog. Neuropsychopharmacol. Biol. Psychiatry* 34, 279–283. doi: 10.1016/j.pnpbp.2009.11.018

Fields, R. D. (2015). A new mechanism of nervous system plasticity: activity-dependent myelination. *Nat. Rev. Neurosci.* 16, 756–767. doi: 10.1038/nrn4023

Fields, R. D., Woo, D. H., and Basser, P. J. (2015). Glial regulation of the neuronal connectome through local and long-distant communication. *Neuron* 86, 374–386. doi: 10.1016/j.neuron.2015.01.014

Franklin, T. B., Saab, B. J., and Mansuy, I. M. (2012). Neural mechanisms of stress resilience and vulnerability. *Neuron* 75, 747–761. doi: 10.1016/j.neuron.2012.08.016

Fullana, M. N., Covelo, A., Bortolozzi, A., Araque, A., and Artigas, F. (2019a). In vivo knockdown of astroglial glutamate transporters GLT-1 and GLAST increases excitatory neurotransmission in mouse infralimbic cortex: relevance for depressive-like phenotypes. *Eur. Neuropsychopharmacol.* 29, 1288–1294. doi: 10.1016/j.euroneuro.2019.09.004

Fullana, M. N., Ruiz-Bronchal, E., Ferres-Coy, A., Juarez-Escoto, E., Artigas, F., and Bortolozzi, A. (2019b). Regionally selective knockdown of astroglial glutamate transporters in infralimbic cortex induces a depressive phenotype in mice. *Glia* 67, 1122–1137. doi: 10.1002/glia.23593

Fullana, N., Gasull-Camos, J., Tarres-Gatius, M., Castane, A., Bortolozzi, A., and Artigas, F. (2020). Astrocyte control of glutamatergic activity: downstream effects on serotonergic function and emotional behavior. *Neuropharmacology* 166:107914. doi: 10.1016/j.neuropharm.2019.107914

Gao, J., Cheng, T. S., Qin, A., Pavlos, N. J., Wang, T., Song, K., et al. (2016). Glucocorticoid impairs cell-cell communication by autophagy-mediated degradation of connexin 43 in osteocytes. *Oncotarget* 7, 26966–26978. doi: 10.18632/oncotarget.9034

Giaume, C., and McCarthy, K. D. (1996). Control of gap-junctional communication in astrocytic networks. *Trends Neurosci.* 19, 319–325. doi: 10.1016/0166-2236(96)10046-1

Gomez-Galan, M., De Bundel, D., Van Eeckhaut, A., Smolders, I., and Lindskog, M. (2013). Dysfunctional astrocytic regulation of glutamate transmission in a rat model of depression. *Mol. Psychiatry* 18, 582–594. doi: 10.1038/mp.2012.10

Gosselin, R. D., Gibney, S., O'malley, D., Dinan, T. G., and Cryan, J. F. (2009). Region specific decrease in glial fibrillary acidic protein immunoreactivity in the brain of a rat model of depression. *Neuroscience* 159, 915–925. doi: 10.1016/j.neuroscience.2008.10.018

Gunn, B. G., Cunningham, L., Cooper, M. A., Corteen, N. L., Seifi, M., Swinny, J. D., et al. (2013). Dysfunctional astrocytic and synaptic regulation of hypothalamic glutamatergic transmission in a mouse model of early-life adversity: relevance to neurosteroids and programming of the stress response. *J. Neurosci.* 33, 19534–19554. doi: 10.1523/JNEUROSCI.1337-13.2013

Had-Aissouni, L., Re, D. B., Nieoullon, A., and Kerkerian-Le Goff, L. (2002). Importance of astrocytic inactivation of synaptically released glutamate for cell survival in the central nervous system–are astrocytes vulnerable to low intracellular glutamate concentrations? *J. Physiol. Paris* 96, 317–322. doi: 10.1016/s0928-4257(02)00022-0

Hammes, S. R., and Levin, E. R. (2007). Extranuclear steroid receptors: nature and actions. *Endocr. Rev.* 28, 726–741. doi: 10.1210/er.2007-0022

Haroon, E., Chen, X., Li, Z., Patel, T., Woolwine, B. J., Hu, X. P., et al. (2018). Increased inflammation and brain glutamate define a subtype of depression with decreased regional homogeneity, impaired network integrity, and anhedonia. *Transl. Psychiatry* 8:189. doi: 10.1038/s41398-018-0241-4

Haroon, E., Miller, A. H., and Sanacora, G. (2017). Inflammation, glutamate, and glia: a trio of trouble in mood disorders. *Neuropsychopharmacology* 42, 193–215. doi: 10.1038/npp.2016.199

Hennessy, E., Griffin, E. W., and Cunningham, C. (2015). Astrocytes are primed by chronic neurodegeneration to produce exaggerated chemokine and cell infiltration responses to acute stimulation with the cytokines IL-1beta and TNF-alpha. *J. Neurosci.* 35, 8411–8422. doi: 10.1523/JNEUROSCI.2745-14.2015

Hodes, G. E., Kana, V., Menard, C., Merad, M., and Russo, S. J. (2015). Neuroimmune mechanisms of depression. *Nat. Neurosci.* 18, 1386–1393. doi: 10.1038/nn.4113

Hodes, G. E., Walker, D. M., Labonte, B., Nestler, E. J., and Russo, S. J. (2017). Understanding the epigenetic basis of sex differences in depression. *J. Neurosci. Res.* 95, 692–702. doi: 10.1002/jnr.23876

Imbe, H., Kimura, A., Donishi, T., and Kaneoke, Y. (2012). Chronic restraint stress decreases glial fibrillary acidic protein and glutamate transporter in the periaqueductal gray matter. *Neuroscience* 223, 209–218. doi: 10.1016/j.neuroscience.2012.08.007

Imbe, H., Kimura, A., Donishi, T., and Kaneoke, Y. (2013). Effects of restraint stress on glial activity in the rostral ventromedial medulla. *Neuroscience* 241, 10–21. doi: 10.1016/j.neuroscience.2013.03.008

Jakovcevski, M., Akbarian, S., and Di Benedetto, B. (2016). Pharmacological modulation of astrocytes and the role of cell type-specific histone modifications for the treatment of mood disorders. *Curr. Opin. Pharmacol.* 26, 61–66. doi: 10.1016/j.coph.2015.10.002

Jayakumar, A. R., Tong, X. Y., Curtis, K. M., Ruiz-Cordero, R., Shamaladevi, N., Abuzamel, M., et al. (2014). Decreased astrocytic thrombospondin-1 secretion after chronic ammonia treatment reduces the level of synaptic proteins: in vitro and in vivo studies. *J. Neurochem.* 131, 333–347. doi: 10.1111/jnc.12810

John, G. R., Scemes, E., Suadicani, S. O., Liu, J. S., Charles, P. C., Lee, S. C., et al. (1999). IL-1beta differentially regulates calcium wave propagation between primary human fetal astrocytes via pathways involving P2 receptors and gap junction channels. *Proc. Natl. Acad. Sci. U.S.A.* 96, 11613–11618. doi: 10.1073/pnas.96.20.11613

Karolewicz, B., Maciag, D., O'dwyer, G., Stockmeier, C. A., Feyissa, A. M., and Rajkowska, G. (2010). Reduced level of glutamic acid decarboxylase-67 kDa in the prefrontal cortex in major depression. *Int. J. Neuropsychopharmacol.* 13, 411–420. doi: 10.1017/S1461145709990587

Karpuk, N., Burkovetskaya, M., Fritz, T., Angle, A., and Kielian, T. (2011). Neuroinflammation leads to region-dependent alterations in astrocyte gap junction communication and hemichannel activity. *J. Neurosci.* 31, 414–425. doi: 10.1523/JNEUROSCI.5247-10.2011

Kendell, S. F., Krystal, J. H., and Sanacora, G. (2005). GABA and glutamate systems as therapeutic targets in depression and mood disorders. *Expert Opin. Ther. Targets* 9, 153–168. doi: 10.1517/14728222.9.1.153

Kumar, S., Holmes, E., Scully, S., Birren, B. W., Wilson, R. H., and De Vellis, J. (1986). The hormonal regulation of gene expression of glial markers: glutamine synthetase and glycerol phosphate dehydrogenase in primary cultures of rat brain and in C6 cell line. *J. Neurosci. Res.* 16, 251–264. doi: 10.1002/jnr.490160122

Leng, L., Zhuang, K., Liu, Z., Huang, C., Gao, Y., Chen, G., et al. (2018). Menin deficiency leads to depressive-like behaviors in mice by modulating astrocyte-mediated neuroinflammation. *Neuron* 100, 551–563.e7. doi: 10.1016/j.neuron.2018.08.031

Leventopoulos, M., Ruedi-Bettschen, D., Knuesel, I., Feldon, J., Pryce, C. R., and Opacka-Juffry, J. (2007). Long-term effects of early life deprivation on brain glia in Fischer rats. *Brain Res.* 1142, 119–126. doi: 10.1016/j.brainres.2007.01.039

Li, L. F., Yang, J., Ma, S. P., and Qu, R. (2013). Magnolol treatment reversed the glial pathology in an unpredictable chronic mild stress-induced rat model of depression. *Eur. J. Pharmacol.* 711, 42–49. doi: 10.1016/j.ejphar.2013.04.008

Li, T., Giaume, C., and Xiao, L. (2014). Connexins-mediated glia networking impacts myelination and remyelination in the central nervous system. *Mol. Neurobiol.* 49, 1460–1471. doi: 10.1007/s12035-013-8625-1

Li, Y. S., Hong, Y. F., He, J., Lin, J. X., Shan, Y. L., Fu, D. Y., et al. (2013). Effects of magnolol on impairment of learning and memory abilities induced by scopolamine in mice. *Biol. Pharm. Bull.* 36, 764–771. doi: 10.1248/bpb.b12-00880

Liu, J., Dietz, K., Deloyht, J. M., Pedre, X., Kelkar, D., Kaur, J., et al. (2012). Impaired adult myelination in the prefrontal cortex of socially isolated mice. *Nat. Neurosci.* 15, 1621–1623. doi: 10.1038/nn.3263

Liu, J., Dupree, J. L., Gacias, M., Frawley, R., Sikder, T., Naik, P., et al. (2016). Clemastine enhances myelination in the prefrontal cortex and rescues behavioral changes in socially isolated mice. *J. Neurosci.* 36, 957–962. doi: 10.1523/JNEUROSCI.3608-15.2016

Liu, Q., Li, B., Zhu, H. Y., Wang, Y. Q., Yu, J., and Wu, G. C. (2009). Clomipramine treatment reversed the glial pathology in a chronic unpredictable stress-induced rat model of depression. *Eur. Neuropsychopharmacol.* 19, 796–805. doi: 10.1016/j.euroneuro.2009.06.010

Longden, T. A., Dabertrand, F., Hill-Eubanks, D. C., Hammack, S. E., and Nelson, M. T. (2014). Stress-induced glucocorticoid signaling remodels neurovascular coupling through impairment of cerebrovascular inwardly rectifying K+

channel function. *Proc. Natl. Acad. Sci. U.S.A.* 111, 7462–7467. doi: 10.1073/pnas.1401811111

Lopizzo, N., Bocchio Chiavetto, L., Cattane, N., Plazzotta, G., Tarazi, F. I., Pariante, C. M., et al. (2015). Gene-environment interaction in major depression: focus on experience-dependent biological systems. *Front. Psychiatry* 6:68. doi: 10.3389/fpsyt.2015.00068

Lu, C.-L., Ren, J., Mo, J.-W., Fan, J., Guo, F., Chen, L.-Y., et al. (2021). Glucocorticoid receptor-dependent astrocytes mediate stress vulnerability. *Biol. Psychiatry*. doi: 10.1016/j.biopsych.2021.11.022

Lutz, S. E., Zhao, Y., Gulinello, M., Lee, S. C., Raine, C. S., and Brosnan, C. F. (2009). Deletion of astrocyte connexins 43 and 30 leads to a dysmyelinating phenotype and hippocampal CA1 vacuolation. *J. Neurosci.* 29, 7743–7752. doi: 10.1523/JNEUROSCI.0341-09.2009

Maeng, S. H., and Hong, H. (2019). Inflammation as the potential basis in depression. *Int. Neurourol. J.* 23, S63–S71. doi: 10.5213/inj.1938226.113

Magnotti, L. M., Goodenough, D. A., and Paul, D. L. (2011). Deletion of oligodendrocyte Cx32 and astrocyte Cx43 causes white matter vacuolation, astrocyte loss and early mortality. *Glia* 59, 1064–1074. doi: 10.1002/glia.21179

McKlveen, J. M., Morano, R. L., Fitzgerald, M., Zoubovsky, S., Cassella, S. N., Scheimann, J. R., et al. (2016). Chronic stress increases prefrontal inhibition: a mechanism for stress-induced prefrontal dysfunction. *Biol. Psychiatry* 80, 754–764. doi: 10.1016/j.biopsych.2016.03.2101

Menard, C., Pfau, M. L., Hodes, G. E., and Russo, S. J. (2017). Immune and neuroendocrine mechanisms of stress vulnerability and resilience. *Neuropsychopharmacology* 42, 62–80. doi: 10.1038/npp.2016.90

Miguel-Hidalgo, J. J., Baucom, C., Dilley, G., Overholser, J. C., Meltzer, H. Y., Stockmeier, C. A., et al. (2000). Glial fibrillary acidic protein immunoreactivity in the prefrontal cortex distinguishes younger from older adults in major depressive disorder. *Biol. Psychiatry* 48, 861–873. doi: 10.1016/s0006-3223(00)00999-9

Miguel-Hidalgo, J. J., Carter, K., Deloach, P. H., Sanders, L., and Pang, Y. (2019). Glucocorticoid-induced reductions of myelination and connexin 43 in mixed central nervous system cell cultures are prevented by mifepristone. *Neuroscience* 411, 255–269. doi: 10.1016/j.neuroscience.2019.05.050

Miguel-Hidalgo, J. J., Hall, K. O., Bonner, H., Roller, A. M., Syed, M., Park, C. J., et al. (2017). MicroRNA-21: expression in oligodendrocytes and correlation with low myelin mRNAs in depression and alcoholism. *Prog. Neuropsychopharmacol. Biol. Psychiatry* 79, 503–514. doi: 10.1016/j.pnpbp.2017.08.009

Miguel-Hidalgo, J. J., Moulana, M., Deloach, P. H., and Rajkowska, G. (2018). Chronic unpredictable stress reduces immunostaining for connexins 43 and 30 and myelin basic protein in the rat prelimbic and orbitofrontal cortices. *Chronic Stress* 2, 1–12. doi: 10.1177/2470547018814186

Miguel-Hidalgo, J. J., Waltzer, R., Whittom, A. A., Austin, M. C., Rajkowska, G., and Stockmeier, C. A. (2010). Glial and glutamatergic markers in depression, alcoholism, and their comorbidity. *J. Affect. Disord.* 127, 230–240. doi: 10.1016/j.jad.2010.06.003

Miguel-Hidalgo, J. J., Wilson, B. A., Hussain, S., Meshram, A., Rajkowska, G., and Stockmeier, C. A. (2014). Reduced connexin 43 immunolabeling in the orbitofrontal cortex in alcohol dependence and depression. *J. Psychiatr. Res.* 55, 101–109. doi: 10.1016/j.jpsychires.2014.04.007

Miller, A. H., and Raison, C. L. (2016). The role of inflammation in depression: from evolutionary imperative to modern treatment target. *Nat. Rev. Immunol.* 16, 22–34. doi: 10.1038/nri.2015.5

Mineur, Y. S., Picciotto, M. R., and Sanacora, G. (2007). Antidepressant-like effects of ceftriaxone in male C57BL/6J mice. *Biol. Psychiatry* 61, 250–252. doi: 10.1016/j.biopsych.2006.04.037

Morioka, N., Suekama, K., Zhang, F. F., Kajitani, N., Hisaoka-Nakashima, K., Takebayashi, M., et al. (2014). Amitriptyline up-regulates connexin43-gap junction in rat cultured cortical astrocytes via activation of the p38 and c-Fos/AP-1 signalling pathway. *Br. J. Pharmacol.* 171, 2854–2867. doi: 10.1111/bph.12614

Muller, N., and Schwarz, M. J. (2007). The immune-mediated alteration of serotonin and glutamate: towards an integrated view of depression. *Mol. Psychiatry* 12, 988–1000. doi: 10.1038/sj.mp.4002006

Murphy-Royal, C., Gordon, G. R., and Bains, J. S. (2019). Stress-induced structural and functional modifications of astrocytes-further implicating glia in the central response to stress. *Glia* 67, 1806–1820. doi: 10.1002/glia.23610

Musholt, K., Cirillo, G., Cavaliere, C., Rosaria Bianco, M., Bock, J., Helmeke, C., et al. (2009). Neonatal separation stress reduces glial fibrillary acidic protein- and S100beta-immunoreactive astrocytes in the rat medial precentral cortex. *Dev. Neurobiol.* 69, 203–211. doi: 10.1002/dneu.20694

Nagy, C., Suderman, M., Yang, J., Szyf, M., Mechawar, N., Ernst, C., et al. (2015). Astrocytic abnormalities and global DNA methylation patterns in depression and suicide. *Mol. Psychiatry* 20, 320–328. doi: 10.1038/mp.2014.21

Nagy, C., Torres-Platas, S. G., Mechawar, N., and Turecki, G. (2016). Repression of astrocytic connexins in cortical and subcortical brain regions and prefrontal enrichment of H3K9me3 in depression and suicide. *Int. J. Neuropsychopharmacol.* 20, 50–57. doi: 10.1093/ijnp/pyw071

Nave, K. A. (2010). Myelination and the trophic support of long axons. *Nat. Rev. Neurosci.* 11, 275–283. doi: 10.1038/nrn2797

Nave, K. A., and Ehrenreich, H. (2014). Myelination and oligodendrocyte functions in psychiatric diseases. *JAMA Psychiatry* 71, 582–584. doi: 10.1001/jamapsychiatry.2014.189

Okada-Tsuchioka, M., Omori, W., Kajitani, N., Shibasaki, C., Itagaki, K., and Takebayashi, M. (2020). Decreased serum levels of thrombospondin-1 in female depressed patients. *Neuropsychopharmacol. Rep.* 40, 39–45. doi: 10.1002/npr2.12088

Okada-Tsuchioka, M., Segawa, M., Kajitani, N., Hisaoka-Nakashima, K., Shibasaki, C., Morinobu, S., et al. (2014). Electroconvulsive seizure induces thrombospondin-1 in the adult rat hippocampus. *Prog. Neuropsychopharmacol. Biol. Psychiatry* 48, 236–244. doi: 10.1016/j.pnpbp.2013.10.001

Okada-Tsuchioka, M., Shibasaki, C., and Takebayashi, M. (2017). "How does electroconvulsive therapy work in the brain?–Involvement of the astrocyte-derived synaptogenic factor, Thrombospondin-1," in *Advances in Modern Medicine*, Vol. 242, eds K. Taniyama and W. Kamiike (Sharjah: Bentham Science Publishers), 242–250. doi: 10.2174/9781681080239117010028

Pajarillo, E., Rizor, A., Lee, J., Aschner, M., and Lee, E. (2019). The role of astrocytic glutamate transporters GLT-1 and GLAST in neurological disorders: potential targets for neurotherapeutics. *Neuropharmacology* 161:107559. doi: 10.1016/j.neuropharm.2019.03.002

Pedram, A., Razandi, M., and Levin, E. R. (2006). Nature of functional estrogen receptors at the plasma membrane. *Mol. Endocrinol.* 20, 1996–2009. doi: 10.1210/me.2005-0525

Piao, C. S., Holloway, A. L., Hong-Routson, S., and Wainwright, M. S. (2019). Depression following traumatic brain injury in mice is associated with down-regulation of hippocampal astrocyte glutamate transporters by thrombin. *J. Cereb. Blood Flow Metab.* 39, 58–73. doi: 10.1177/0271678X17742792

Rajkowska, G., Hughes, J., Stockmeier, C. A., Javier Miguel-Hidalgo, J., and Maciag, D. (2013). Coverage of blood vessels by astrocytic endfeet is reduced in major depressive disorder. *Biol. Psychiatry* 73, 613–621. doi: 10.1016/j.biopsych.2012.09.024

Rajkowska, G., Mahajan, G., Maciag, D., Sathyanesan, M., Iyo, A. H., Moulana, M., et al. (2015). Oligodendrocyte morphometry and expression of myelin-related mRNA in ventral prefrontal white matter in major depressive disorder. *J. Psychiatr. Res.* 65, 53–62. doi: 10.1016/j.jpsychires.2015.04.010

Razzoli, M., Domenici, E., Carboni, L., Rantamaki, T., Lindholm, J., Castren, E., et al. (2011). A role for BDNF/TrkB signaling in behavioral and physiological consequences of social defeat stress. *Genes Brain Behav.* 10, 424–433. doi: 10.1111/j.1601-183X.2011.00681.x

Réus, G. Z., Abelaira, H. M., Tuon, T., Titus, S. E., Ignácio, Z. M., Rodrigues, A. L. S., et al. (2016). "Chapter five – glutamatergic NMDA receptor as therapeutic target for depression," in *Advances in Protein Chemistry and Structural Biology*, ed. R. Donev (Cambridge, MA: Academic Press), 169–202. doi: 10.1016/bs.apcsb.2015.10.003

Samarasinghe, R. A., Witchell, S. F., and Defranco, D. B. (2012). Cooperativity and complementarity: synergies in non-classical and classical glucocorticoid signaling. *Cell Cycle* 11, 2819–2827. doi: 10.4161/cc.21018

Schaaf, M. J., De Jong, J., De Kloet, E. R., and Vreugdenhil, E. (1998). Downregulation of BDNF mRNA and protein in the rat hippocampus by corticosterone. *Brain Res.* 813, 112–120. doi: 10.1016/s0006-8993(98)01010-5

Shen, C., Kim, M. R., Noh, J. M., Kim, S. J., Ka, S. O., Kim, J. H., et al. (2016). Glucocorticoid suppresses Connexin 43 expression by inhibiting the Akt/mTOR signaling pathway in osteoblasts. *Calcif. Tissue Int.* 99, 88–97. doi: 10.1007/s00223-016-0121-y

Si, X. H., Miguel-Hidalgo, J. J., O'dwyer, G., Stockmeier, C. A., and Rajkowska, G. (2004). Age-dependent reductions in the level of glial fibrillary acidic protein in the prefrontal cortex in major depression. *Neuropsychopharmacology* 29, 2088–2096. doi: 10.1038/Sj.Npp.1300525

Sofroniew, M. V. (2014). Multiple roles for astrocytes as effectors of cytokines and inflammatory mediators. *Neuroscientist* 20, 160–172. doi: 10.1177/1073858413504466

Sun, J. D., Liu, Y., Yuan, Y. H., Li, J., and Chen, N. H. (2012). Gap junction dysfunction in the prefrontal cortex induces depressive-like behaviors in rats. *Neuropsychopharmacology* 37, 1305–1320. doi: 10.1038/npp.2011.319

Tanti, A., Lutz, P. E., Kim, J., O'leary, L., Theroux, J. F., Turecki, G., et al. (2019). Evidence of decreased gap junction coupling between astrocytes and oligodendrocytes in the anterior cingulate cortex of depressed suicides. *Neuropsychopharmacology* 44, 2099–2111. doi: 10.1038/s41386-019-0471-z

Tao, K., Cai, Q., Zhang, X., Zhu, L., Liu, Z., Li, F., et al. (2020). Astrocytic histone deacetylase 2 facilitates delayed depression and memory impairment after subarachnoid hemorrhage by negatively regulating glutamate transporter-1. *Ann. Transl. Med.* 8:691. doi: 10.21037/atm-20-4330

Treccani, G., Musazzi, L., Perego, C., Milanese, M., Nava, N., Bonifacino, T., et al. (2014). Stress and corticosterone increase the readily releasable pool of glutamate vesicles in synaptic terminals of prefrontal and frontal cortex. *Mol. Psychiatry* 19, 433–443. doi: 10.1038/mp.2014.5

Tress, O., Maglione, M., May, D., Pivneva, T., Richter, N., Seyfarth, J., et al. (2012). Panglial gap junctional communication is essential for maintenance of myelin in the CNS. *J. Neurosci.* 32, 7499–7518. doi: 10.1523/JNEUROSCI.0392-12.2012

Tynan, R. J., Beynon, S. B., Hinwood, M., Johnson, S. J., Nilsson, M., Woods, J. J., et al. (2013). Chronic stress-induced disruption of the astrocyte network is driven by structural atrophy and not loss of astrocytes. *Acta Neuropathol.* 126, 75–91. doi: 10.1007/s00401-013-1102-0

Xia, C. Y., Chu, S. F., Zhang, S., Gao, Y., Ren, Q., Lou, Y. X., et al. (2017). Ginsenoside Rg1 alleviates corticosterone-induced dysfunction of gap junctions in astrocytes. *J. Ethnopharmacol.* 208, 207–213. doi: 10.1016/j.jep.2017.06.031

Xia, C. Y., Wang, Z. Z., Zhang, Z., Chen, J., Wang, Y. Y., Lou, Y. X., et al. (2018). Corticosterone impairs gap junctions in the prefrontal cortical and hippocampal astrocytes via different mechanisms. *Neuropharmacology* 131, 20–30. doi: 10.1016/j.neuropharm.2017.12.003

Yoshino, K., Oda, Y., Kimura, M., Kimura, H., Nangaku, M., Shirayama, Y., et al. (2020). The alterations of glutamate transporter 1 and glutamine synthetase in the rat brain of a learned helplessness model of depression. *Psychopharmacology (Berl.)* 237, 2547–2553. doi: 10.1007/s00213-020-05555-3

Yuen, E. Y., Wei, J., Liu, W., Zhong, P., Li, X., and Yan, Z. (2012). Repeated stress causes cognitive impairment by suppressing glutamate receptor expression and function in prefrontal cortex. *Neuron* 73, 962–977. doi: 10.1016/j.neuron.2011.12.033

Yun, J. H., Park, S. J., Jo, A., Kang, J. L., Jou, I., Park, J. S., et al. (2011). Caveolin-1 is involved in reactive oxygen species-induced SHP-2 activation in astrocytes. *Exp. Mol. Med.* 43, 660–668. doi: 10.3858/emm.2011.43.12.075

Zhang, H., Zhao, Y., and Wang, Z. (2015). Chronic corticosterone exposure reduces hippocampal astrocyte structural plasticity and induces hippocampal atrophy in mice. *Neurosci. Lett.* 592, 76–81. doi: 10.1016/j.neulet.2015.03.006

Zhang, Y., Chen, K., Sloan, S. A., Bennett, M. L., Scholze, A. R., O'Keeffe, S., et al. (2014). An RNA-sequencing transcriptome and splicing database of glia, neurons, and vascular cells of the cerebral cortex. *J. Neurosci.* 34, 11929–11947. doi: 10.1523/JNEUROSCI.1860-14.2014

Zhao, Y., Rivieccio, M. A., Lutz, S., Scemes, E., and Brosnan, C. F. (2006). The TLR3 ligand polyI: C downregulates connexin 43 expression and function in astrocytes by a mechanism involving the NF-kappaB and PI3 kinase pathways. *Glia* 54, 775–785. doi: 10.1002/glia.20418

Zhuang, K., Huang, C., Leng, L., Zheng, H., Gao, Y., Chen, G., et al. (2018). Neuron-specific menin deletion leads to synaptic dysfunction and cognitive impairment by modulating p35 expression. *Cell Rep.* 24, 701–712. doi: 10.1016/j.celrep.2018.06.055

Zink, M., Vollmayr, B., Gebicke-Haerter, P. J., and Henn, F. A. (2010). Reduced expression of glutamate transporters vGluT1, EAAT2 and EAAT4 in learned helpless rats, an animal model of depression. *Neuropharmacology* 58, 465–473. doi: 10.1016/j.neuropharm.2009.09.005

Conflict of Interest: The author declares that the research was conducted in the absence of any commercial or financial relationships that could be construed as a potential conflict of interest.

Publisher's Note: All claims expressed in this article are solely those of the authors and do not necessarily represent those of their affiliated organizations, or those of the publisher, the editors and the reviewers. Any product that may be evaluated in this article, or claim that may be made by its manufacturer, is not guaranteed or endorsed by the publisher.

Copyright © 2022 Miguel-Hidalgo. This is an open-access article distributed under the terms of the Creative Commons Attribution License (CC BY). The use, distribution or reproduction in other forums is permitted, provided the original author(s) and the copyright owner(s) are credited and that the original publication in this journal is cited, in accordance with accepted academic practice. No use, distribution or reproduction is permitted which does not comply with these terms.

frontiers | Frontiers in Cellular Neuroscience

REVIEW
published: 22 April 2022
doi: 10.3389/fncel.2022.872501

Neuronal Redevelopment and the Regeneration of Neuromodulatory Axons in the Adult Mammalian Central Nervous System

Patrick Cooke, Haley Janowitz and Sarah E. Dougherty*

Linden Lab, Solomon H. Snyder Department of Neuroscience, Johns Hopkins University School of Medicine, Baltimore, MD, United States

One reason that many central nervous system injuries, including those arising from traumatic brain injury, spinal cord injury, and stroke, have limited recovery of function is that neurons within the adult mammalian CNS lack the ability to regenerate their axons following trauma. This stands in contrast to neurons of the adult mammalian peripheral nervous system (PNS). New evidence, provided by single-cell expression profiling, suggests that, following injury, both mammalian central and peripheral neurons can revert to an embryonic-like growth state which is permissive for axon regeneration. This "redevelopment" strategy could both facilitate a damage response necessary to isolate and repair the acute damage from injury and provide the intracellular machinery necessary for axon regrowth. Interestingly, serotonin neurons of the rostral group of raphe nuclei, which project their axons into the forebrain, display a robust ability to regenerate their axons unaided, counter to the widely held view that CNS axons cannot regenerate without experimental intervention after injury. Furthermore, initial evidence suggests that norepinephrine neurons within the locus coeruleus possess similar regenerative abilities. Several morphological characteristics of serotonin axon regeneration in adult mammals, observable using longitudinal *in vivo* imaging, are distinct from the known characteristics of unaided peripheral nerve regeneration, or of the regeneration seen in the spinal cord and optic nerve that occurs with experimental intervention. These results suggest that there is an alternative CNS program for axon regeneration that likely differs from that displayed by the PNS.

Keywords: axon regeneration, spinal cord injury, neuronal injury and repair, serotonin, redevelopment, glial scar, neuromodulatory neuron

OPEN ACCESS

Edited by:
Claudio Rivera,
Aix-Marseille Université, France

Reviewed by:
Saijilafu,
Soochow University Medical College, China
Kai Liu,
Hong Kong University of Science and Technology, Hong Kong SAR, China

****Correspondence:***
Patrick Cooke
pcooke2@jhmi.edu

Specialty section:
This article was submitted to Cellular Neuropathology, a section of the journal Frontiers in Cellular Neuroscience

Received: *09 February 2022*
Accepted: *24 March 2022*
Published: *22 April 2022*

Citation:
Cooke P, Janowitz H and Dougherty SE (2022) Neuronal Redevelopment and the Regeneration of Neuromodulatory Axons in the Adult Mammalian Central Nervous System. Front. Cell. Neurosci. 16:872501. doi: 10.3389/fncel.2022.872501

INTRODUCTION

A general view in the field of neuronal regeneration is that axons in the central nervous system (CNS) do not regenerate following injury. This appears to hold true for the axons of almost all neurons within the CNS, which do indeed have a very limited capacity to regrow after injury (Huebner and Strittmatter, 2009; Canty et al., 2013; Akassoglou et al., 2017). Traumatic brain injury, spinal cord injury, and stroke can often lead to severe lifelong physical, mental, and emotional symptoms, including paralysis, depression, attention deficits, and memory loss. Axon damage

accompanies the general tissue damage to the injured area, and the lack of axon regeneration within the CNS is believed to be a major underlying reason behind the persistence of symptoms following these CNS injuries. Even when the tissue is stabilized, irreparable damage to neuronal circuitry remains. Unlike CNS neurons, those with cell bodies located within the peripheral nervous system (PNS) are able to regenerate their axons and reconstruct the lost circuitry with varying degrees of success depending on the severity of damage.

Over the past 30 years, the axon regeneration field has been seeking to uncover the mechanisms underlying peripheral axon regeneration. With these results in mind, researchers then approach the CNS with two questions: (1) Why is this regeneration not occurring within the CNS and (2) If we ectopically induce these mechanisms, will we see improved regeneration? This approach has led to the theory that CNS neurons would be able to regenerate their axons if they existed within a permissive environment. However, the CNS is not an environment permissive to axon regeneration (Pasterkamp and Verhaagen, 2006; Canty et al., 2013; Sami et al., 2020). CNS injury leads to the formation of the glial scar, which includes several inhibitory molecules and secreted proteins that prevent axon regeneration (Fitch and Silver, 2008; Bradbury and Burnside, 2019). Aside from the glial scar, other factors, such as semaphorins and myelin associated glycoproteins also act as barriers to regeneration and are expressed within healthy tissue. These inhibitory factors bind receptors expressed on extending neurites and signal growth cone collapse and the cessation of axon regrowth (Schwab, 2004; Pasterkamp and Verhaagen, 2006). In this context, scientists have attempted to stimulate CNS axon regeneration in three main ways. The first avenue of treatment is to block the inhibitory signaling, either through removal of the inhibitory extracellular signal itself or blockade of its relevant receptor (Schwab, 2004; Yiu and He, 2006; Dyck and Karimi-Abdolrezaee, 2015). Second, researchers have attempted to jumpstart CNS axon regeneration by inducing the expression of pro-regenerative genes, some of which were identified within the PNS (Ma and Willis, 2015). The final approach has been to graft permissive tissues such as peripheral nerve or neuronal progenitor cells into the lesioned area in an attempt to replace the inhibitory environment with a permissive one (Richardson et al., 1980; Fischer et al., 2020). Unfortunately, each of these treatment approaches have shown only limited success, even when used in combination (Fischer et al., 2020).

Recent discoveries offer exciting new avenues of research for the field of axon regeneration within the CNS. Over the past 30 years, various grafts have been applied to the lesion site of a spinal cord injury to promote local regeneration. The most successful of these has been the neural progenitor cell (NPC) graft, which was the first treatment that succeeded in promoting some regeneration of corticospinal tract (CST) axons (Kadoya et al., 2016). Single-cell expression profiling techniques show that this regeneration is enabled through transcriptional reversion to an embryonic-like phenotype (Poplawski et al., 2020). A similar study in the PNS aligns with these results, indicating that, following injury, both PNS and CNS neurons revert to a developmental phenotype in order to promote axon regeneration (Renthal et al., 2020). While this redevelopment strategy has been hinted at in the past, these studies provide compelling evidence at a cellular resolution that inducing the reversion to a developmental-like state in adult neurons may be the key to developing new therapies to treat CNS injury.

Interestingly, serotonin and norepinephrine expressing neurons within the CNS are able to regenerate their cranial projecting axons unaided. This unprecedented phenomenon stands in contrast to the view that the CNS is an environment non-permissive to all axon regeneration. This regeneration has been widely overlooked within the field and further investigation into this regeneration promises to shed light onto many of the outstanding questions in the field, including the role of the CNS environment in inhibiting axon regeneration and potential genetic programs that could be successful in promoting axon regeneration. What is different about these neuromodulatory neurons that affords them the capacity to regenerate their axons unaided while all other neuronal subtypes are unable to do so? Are these neurons somehow able to revert more successfully to a developmental phenotype or are they employing a different pathway for regeneration than that seen within the CNS? Answering these questions and more promises to unravel many of the long outstanding mysteries within the field of CNS axon regeneration more broadly.

AXONS IN THE ADULT MAMMALIAN CENTRAL NERVOUS SYSTEM DO NOT REGENERATE FOLLOWING INJURY

Intrinsic Barriers to Central Nervous System Axon Regeneration

The disparity in regenerative potential seen by the PNS as compared to the CNS was first described by Ramon y Cajal in the early twentieth century (Cajal, 1928) and has been replicated many times since. Here, regeneration is defined as the regrowth of a severed axon, either from the severed end itself or from a new branch of the same axon generated proximal to the injured end that extends past the site of injury (**Figure 1**; Tuszynski and Steward, 2012). Following nerve crush injury in the PNS, the distal portion of an axon degenerates and is cleared by macrophages. The proximal end initially retracts from the lesion site back to the first Node of Ranvier and then begins a process of regeneration (Menorca et al., 2013; Sulaiman and Gordon, 2013). Initially, this regeneration consists of arborization of the axon to generate multiple outgrowing neurite branches that allow the axon to interact with the extracellular environment more broadly. Eventually a single branch will stabilize due to interactions with extracellular signaling molecules and regrow along the path left by the degenerated axon to reinnervate its target. The other neurites are then pruned (**Figure 2**; Cajal, 1928; Nguyen et al., 2002; Witzel et al., 2005). If the peripheral nerve is cut, rather than crushed, reinnervation of target tissue is delayed and less extensive, but still occurs in a similar manner.

The process required for regeneration is broad and multifaceted. Prior to regeneration, the neuron first undergoes a

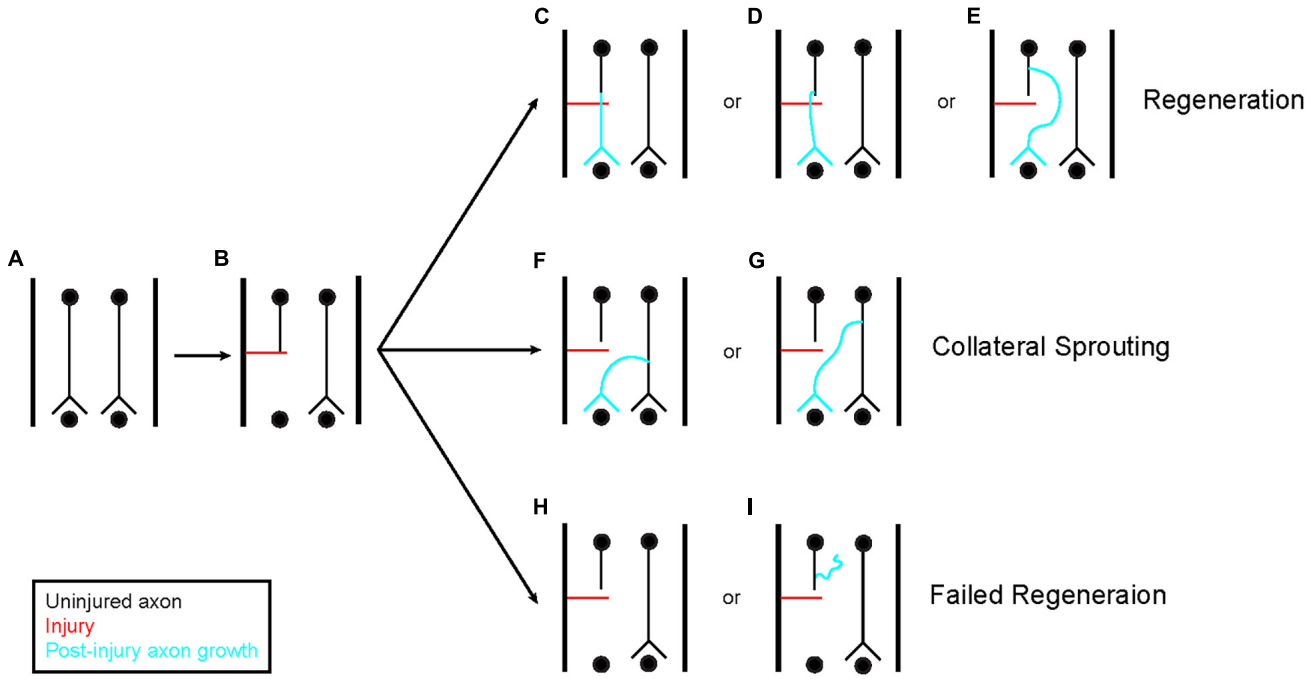

FIGURE 1 | Axon regeneration and collateral sprouting. A few different classes of response can occur following axon injury **(A,B)**. First, the injured axon can regenerate **(C–E)**. This regeneration can originate directly from the transected tip **(C)** or from the axon shaft **(D,E)**. Regeneration from the axon shaft can occur close to the injured end **(D)** or from a region more remote to the injury site **(E)**. The regenerating axon does not have to pass through the injured tissue, it can also navigate around the tissue as shown in **(E)**. In addition to regeneration, axons that were spared from injury can sprout collaterals to reinnervate the denervated tissue and compensate for the damage **(F,G)**. This is a distinct process from regeneration. These collaterals can originate anywhere on the intact axon. Finally, the axon can fail to regenerate **(H,I)**. This can be observed through a complete failure to generate new growth **(H)** or new growth that fails to navigate distal to the site of injury **(I)**. These three classes of response are not mutually exclusive, each one can occur simultaneously at the same injury site across the population of injured axons.

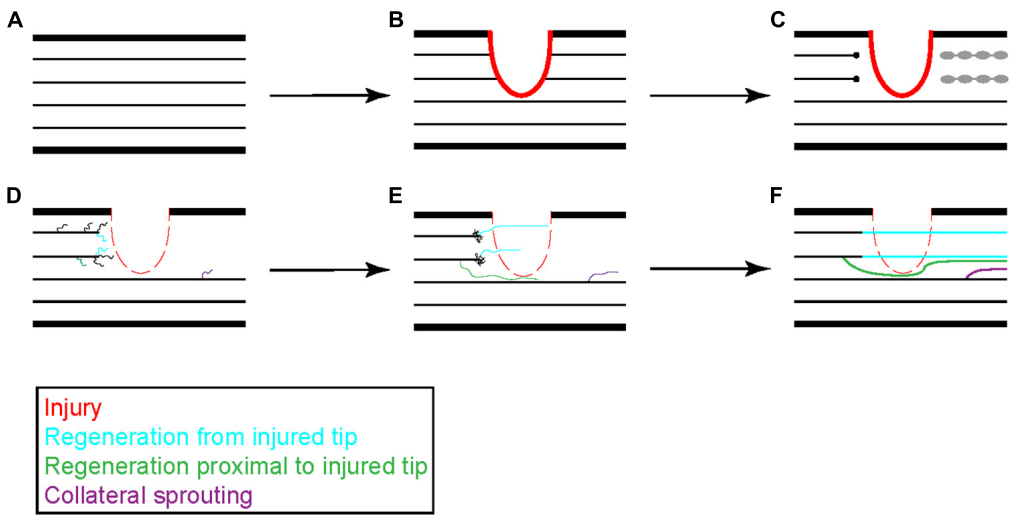

FIGURE 2 | Progression of peripheral axon regeneration following injury. Following peripheral nerve injury **(A,B)**, the distal portion of an injured peripheral axon undergoes Wallerian degeneration and is cleared by invading macrophages while the proximal end retracts a short distance from the site of injury **(C)**. The proximal end of the injured axon will stabilize and form a growth cone that generates new neurites to sample the surrounding environment. These neurites can originate from the injured tip, as shown in blue, or from the axon shaft, as shown in green. Surviving axons can also undergo collateral sprouting, shown in purple, to help reinnervate distal tissues **(D)**. Neurites that receive sufficient growth factor signaling stabilize and elongate while the others retract back to the main axon shaft **(E)**. Occasionally two neurites from a single damaged axon can stabilize leading to growth from two branches. These new growths can navigate through the injured tissue or around the injured tissue to reestablish pre-injury synaptic connections **(F)**.

complex damage response triggered by dramatic depolarization and Ca^{2+} influx that occurs due to unregulated exposure to the extracellular environment at the lesion site. The first stage of this damage response includes resealing of the plasma membrane, often leading to the formation of a swollen dystrophic end bulb, and withdrawal from the wounded area. Following this stabilization, the axon can generate a new growth cone at its tip that will elongate and navigate to reinnervate its target (Bradke et al., 2012). Such a response requires chromatin modifications, the activation of nested transcription factor networks to induce widespread transcriptional programs, and massive cytoskeletal rearrangement reviewed in Bradke et al. (2012).

Axons within the CNS do not regenerate after injury, although some damaged axons may generate branches and extend neurites toward the lesion in a process resembling the initial stages of PNS axon regeneration. Unfortunately, this branching and outgrowth stalls before reaching the lesion site and thus does not result in regeneration following spinal cord or traumatic brain injury (Guth, 1975; Huebner and Strittmatter, 2009; Canty et al., 2013).

PNS neurons undergo dramatic transcriptional changes which are different from those seen in CNS neurons following injury. Notably, injury-evoked activation of adenylyl cyclase together with Ca^{2+} influx leads to the elevation of cyclic adenosine monophosphate (cAMP). Among other targets, cAMP activates protein kinase A (PKA), a positive regulator of two transcription factors: cAMP response element binding protein (CREB) and Activator Protein 1 (AP1). Within the vast array of genes whose transcription is altered in this response are regeneration associated genes (RAGs) (**Figure 3**). RAGs are genes that contribute to PNS axon regeneration, many of which can also promote partial CNS axon regrowth (Neumann et al., 2002; Qiu et al., 2002; Huebner and Strittmatter, 2009; Knott et al., 2014; Ma and Willis, 2015).

Over the years, a number of genes have been identified as contributors to PNS axon regeneration. These experiments used mutant mice or RNAi loss-of-function (LOF) strategies to knockdown expression of specific proteins in order to assess their involvement in axon regenerations. Many of these genes have subsequently been experimentally expressed within CNS neurons in an attempt to promote axon regeneration. The most successful genetic manipulations aimed at improving CNS axon regeneration are the overexpression of transcription factors that are able to modulate the expression of yet other transcription factors involved in regenerative programs, termed "hubs." These hubs include ATF3, AP1 (c-Jun and c-Fos), C/EBPβ, KLF family members, CREB, SMAD1, SOX11, STAT3, and several others (Jenkins and Hunt, 1991; Schwaiger et al., 2000; Tsujino et al., 2000; Gao et al., 2004; Nadeau et al., 2005; Okuyama et al., 2007;

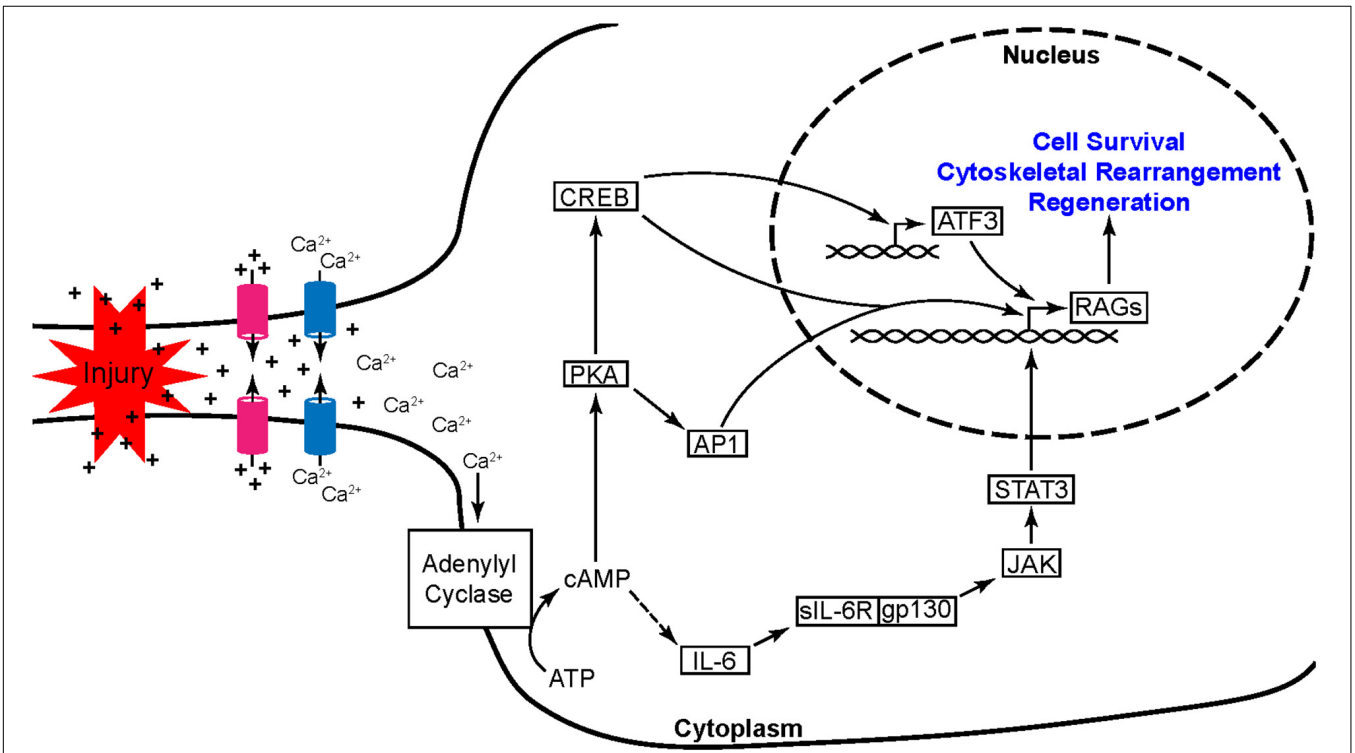

FIGURE 3 | Peripheral nerve injury induces the activation of nested transcription factor networks. Axonal injury leads to the unregulated flow of ions at the breach resulting in a propagating wave of depolarization and the opening of voltage gated Ca^{2+} channels. The rise in Ca^{2+} is further potentiated by Ca^{2+} induced Ca^{2+} release from internal stores (not shown). Ca^{2+} then activates adenylyl cyclase leading to a dramatic increase in cAMP production. This rise in cAMP promotes axon regeneration through two pathways, one initiated by PKA and the other through activation of IL-6. PKA leads to the activation of transcription factor hubs AP1 and CREB while the IL-6 pathway leads to the activation of STAT3. These three transcription factor hubs induce the expression of other regeneration associated genes (RAGs) including ATF3, another transcription factor hub crucial to the early injury and regeneration response.

Moore et al., 2009; Zou et al., 2009; Knott et al., 2014; Ma and Willis, 2015).

Inducing ectopic expression, primarily through the use of AAV transfection, of any individual hub gene in CST neurons *in vivo* does not yield impressive results for central axon regeneration following spinal cord injury- they increase initial axon arborization and can promote some process extension that is not able to cross the lesion site (Ma and Willis, 2015). Induction of multiple hubs concurrently has been shown to improve neurite outgrowth from the injured axon and increase the distance these neurites are able to regrow. One of the most successful molecular manipulations shown to improve regeneration of CNS axons *in vivo* is the injection of cAMP into neurons following injury. Injection of cAMP, or its synthetic analog, dibutyryl cAMP, into the cell bodies of injured neurons has been shown to improve axon regeneration across the lesion site following multiple injury models in several different neuronal subtypes within the CNS (Hannila and Filbin, 2008). cAMP elevation leads to the activation of CREB and AP-1, both important transcription factor hubs that promote regenerative programs (Knott et al., 2014; Ma et al., 2014). Furthermore, the results from these studies support the hypothesis that CNS neurons would be able to functionally regenerate their axons following injury if they were able to activate regenerative gene programs, as seen in the PNS.

Another strategy for promoting axon regeneration is to induce the activity of downstream pathways that directly affect axon growth. The most promising attempt has involved inhibiting phosphatase and tensin homolog (PTEN), a phosphatase which serves as a negative regulator of the mammalian target of rapamycin (mTOR) pathway. Deleting or inhibiting PTEN removes the brakes from the mTOR pathway which is involved in cell growth and proliferation and, during neuronal development, in axon extension (Ménager et al., 2004; Zhou et al., 2004; Cosker and Eickholt, 2007; Nieuwenhuis and Eva, 2022). PTEN deletion promotes regeneration through the lesion site of optic nerve and spinal cord injuries, albeit in an age-dependent manner. PTEN knock-out mice injured at 6 weeks old show impressive regeneration following both optic nerve and spinal cord injury. However, this regeneration is reduced if the mice are instead injured at 8 weeks old and further reduced if injured between 10 and 14 weeks of age (Park et al., 2008; Liu et al., 2010; Du et al., 2015; Geoffroy et al., 2016; Leibinger et al., 2016; Nieuwenhuis and Eva, 2022). Much like the studies which promoted axon regeneration through the activation of transcription factor hubs, PTEN deletion did not improve functional recovery following spinal cord injury in adult mice following T8 dorsal hemisection injury as assessed by monitoring hindlimb function Geoffroy et al., 2015; reviewed in Nieuwenhuis and Eva (2022).

While limited, inducing the expression of transcription factor hubs or the activity of downstream pathways successfully promotes partial axon regeneration in the adult mammalian CNS. This partial success indicates that these neurons harbor the required programs for axon regeneration, however, these programs are failing for some reason. These results suggest the following questions: what is preventing CNS axons from activating regenerative programs? When induced experimentally, why do these programs show some initial success before failing, is something actively inhibiting them? Do epigenetic changes following neuronal development permanently lock these genes in heterochromatin or do extrinsic signals suppress regenerative gene expression programs in CNS neurons?

Extrinsic Barriers to Central Nervous System Axon Regeneration and Molecular Components of the Glial Scar

Following CNS injury, microglia, oligodendrocyte precursor cells, meningeal cells, and astrocytes are recruited to the injury site to form a glial scar. Astrocytes activate and secrete tenascin, semaphorin3, ephrin-B2, and chondroitin sulfate proteoglycans (CSPGs) to isolate the injury in order localize the damage and inflammation as well as to facilitate healing (Fitch and Silver, 2008; Bradbury and Burnside, 2019). Conditional deletion of STAT3 or SOCS3 within the astrocytes of adult mice, to prevent their activation, is associated with increased tissue disruption, demyelination, cell death, and a failure to repair the blood brain barrier (Okada et al., 2006; Herrmann et al., 2008; Dyck and Karimi-Abdolrezaee, 2015). Though scar formation is crucial for the acute damage response, it also may create a barrier through which axons are unable to regrow.

The formation of the glial scar is believed to be a major factor preventing axon regeneration within the CNS. While each of the astrocyte secreted factors previously mentioned are associated with extrinsic inhibition of regeneration, CSPGs have been the dominant focus within the field. CSPGs are a family of proteoglycans that constitute part of the extracellular matrix of the glial scar and include aggrecan, brevican, neurocan, versican, phosphocan, and NG2 (Silver and Miller, 2004; Yiu and He, 2006). In the developing nervous system, CSPGs help mark glial boundaries such as the spinal cord roof plate, optic tectum, and dorsal root entry zone to prevent ectopic growth of axons in the adult nervous system (Kubota et al., 1999; Dyck and Karimi-Abdolrezaee, 2015). CSPGs may inhibit axon regeneration by various mechanisms. The core protein of NG2 has been shown to act as an inhibitory signaling molecule, preventing axon regrowth (Ughrin et al., 2003). Additionally, the glycosaminoglycan (GAG) side chains of CSPGs have been heavily implicated in this inhibitory process. GAG side chain binding to receptor protein tyrosine phosphatase σ (PTPσ) or its subfamily member leukocyte common antigen related phosphatase (LAR) inhibits growth cone extension by activating the Rho/ROCK pathway at the growth cone and inhibiting Erk1/2 signaling in the cell body (**Figure 4**; Shen et al., 2009; Fisher et al., 2011; Sami et al., 2020). Additionally, GAG side chains create a dense network that can block growth by sterically hindering pro-growth adhesion molecules such as laminins and integrins, thus depriving the growth cone of the signals required for extension (Sami et al., 2020).

Treatment with Chondroitinase ABC degrades CSPG GAG chains by enzymatic digestion into smaller disaccharides, removing their growth inhibitory capability. Within the glial scar, chondrointinase treatment has been one of the most promising strategies for improving axonal regeneration following injury to both the spinal cord and optic nerve in rodents

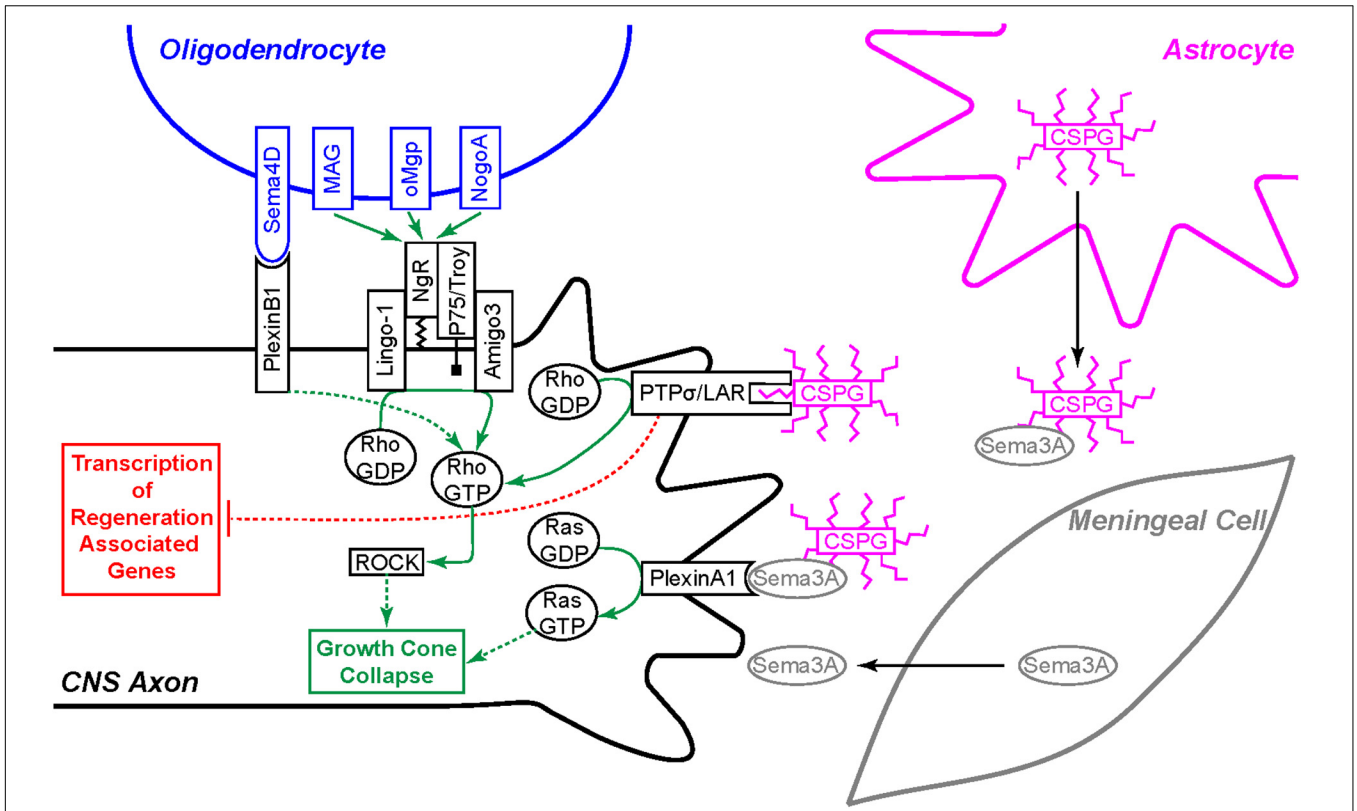

FIGURE 4 | Extrinsic inhibition of CNS axon regeneration. Oligodendrocytes express four membrane bound regeneration inhibitors: Sema4D, MAG, oMgp, and NogoA. Sema4D binds to the PlexinB1 receptor and the others bind to the Nogo-66 Receptor (NgR) complex expressed on the CNS axon. Each of these receptors signal growth cone collapse through the Rho/ROCK pathway. Invading meningeal cells in the glial scar secrete Sema3A molecules which associate with chondroitin sulfate proteoglycan (CSGP) glycosaminoglycan (GAG) side-chains and bind the PlexinA1 receptor to signal growth cone collapse through the activation of Ras. CSPG GAG chains, secreted by astrocytes and other cells, bind the PTPσ or the LAR receptor to signal growth cone collapse through the same Rho/ROCK pathway. Furthermore, the PTPσ and LAR receptors also signal back to the cell body to inhibit pro-regeneration signaling cascades.

and in non-human primate models of spinal cord injury (Lemons et al., 1999; Bradbury et al., 2002; Yiu and He, 2006; Dyck and Karimi-Abdolrezaee, 2015; Rosenzweig et al., 2019). While chondroitinase ABC treatment is able to improve regeneration and some functional recovery following injury, complete recovery remains elusive. The studies mentioned here present a simplified role for CSPGs in axon regeneration. The true role of CSPGs is much more nuanced, the details of which are beyond the scope of this review (reviewed in Dyck and Karimi-Abdolrezaee, 2015; Sami et al., 2020). In short, CSPG GAG chains have pro-regeneration factors associated with them as well as those involved with inhibition. Furthermore, there appear to be differences in the molecules that associate with CSPG GAG chains based upon the cell type that secreted them. These factors likely explain why chondroitinase ABC treatment has not been able to promote axon regeneration as effectively as many had predicted.

Recent evidence suggests that the reactive astrocytic component of the glial scar may not always inhibit regeneration, as previously believed. For example, researchers can experimentally promote regeneration of a DRG sensory neuron's central ascending branch by first applying a "conditioning lesion" to its peripheral branch. Combining a conditioning lesion with locally applied brain-derived neurotrophic factor (BDNF) and neurotrophin-3 (NT-3) stimulates regeneration of ascending sensory axons through the glial scar without any direct manipulations to degrade the scar itself (Anderson et al., 2016). When astrocyte activation was blocked in mice, using conditional knock-out of the STAT3 gene, spinal cord axons did not display increased branching or regrowth following severe spinal crush injury. On the contrary, both descending CST and ascending sensory tract axons retracted further from the lesion site than those of WT control mice. According to the glial scar hypothesis, preventing astrocyte activation should increase axon arborization and regeneration, a result not seen in this set of experiments. Interestingly, in these STAT3 conditional knock-out mice, CSPG levels remained elevated, indicating that other cells involved in the injury response may be responsible for the bulk of CSPG production. When this group examined gene expression profiles before and after spinal cord injury in STAT3 conditional knock-out mice compared to WT, they found a wide range of injury-induced changes to WT astrocytes, some known to be beneficial to regrowth. Astrocytes from injured animals harboring the conditional STAT3 knock-out remained transcriptionally similar to uninjured WT astrocytes (Anderson et al., 2016). While this set of experiments casts doubt onto the

role that activated astrocytes play in obstructing regeneration, further experiments are required to address the roles of the other scar components before dismissing the glial scar hypothesis. In these experiments, CSPG levels remained elevated at the lesion site independent of astrocyte activation. Furthermore, the success that other groups have achieved in promoting neurite outgrowth following spinal cord injury using chondroitinase ABC, indicates that scar formation and the CSPGs inherent to it are likely a major barrier to regeneration. Rather it seems that astrocyte activation is not as crucial to the inhibition of axon regeneration as previously believed, and it could actually be beneficial for promoting healing and regrowth, at least in some circumstances.

Supporting the idea that the injury induced glial scar is an important barrier to regeneration, Silver and colleagues used a model of minimal injury at the dorsal root entry zone to sever the central branch of sensory axons without inducing a glial scar. These axons showed impressive regeneration into the spinal cord following injury (Davies et al., 1997). A follow up study found that the donor sensory axons grew when transplanted rostral to the lesion site of a spinal cord injury, indicating that the glial scar is indeed a major barrier to axon growth (Davies et al., 1999).

The glial scar is not the only extrinsic barrier an injured neuron faces. Canty et al. (2013) used a laser to cause microlesions that sever either a single or a small number of axons without inducing an inflammatory response or glial scar. Interestingly, following these laser-induced axotomies in the adult mouse cerebral cortex, neurons showed very limited regrowth even without having to overcome the obstacle of a glial scar. These results indicate that a non-permissive environment exists within healthy CNS tissue (Canty et al., 2013). One possible caveat is that the damage caused by laser-induced axotomy, which is not extensive enough to activate glial scarring, does not damage tissue enough to extensively activate regenerative gene programs necessary for regrowth. Additionally, a laser microlesion may create a unique barrier that has yet to be characterized.

As demonstrated by Canty and colleagues, the environment of the adult mammalian CNS is not permissive to axon regeneration even in the absence of glial scarring. One contributor to this non-permissive environment is CNS myelin. The oligodendrocytes that form myelin sheaths within the CNS express myelin-associated proteins that directly inhibit axon regeneration. The most well-known of these inhibitors are Nogo-A, myelin-associated glycoprotein (MAG), and oligodendrocyte-myelin glycoprotein (OMgp). These three myelin-associated axon regeneration inhibitors all bind with high affinity to the Nogo-66 receptor (NgR), triggering an intracellular signaling cascade that leads to the activation of RhoA, eventual stabilization of actin filaments within the growth cone, and thereby halting further elongation (Fournier et al., 2001; Domeniconi et al., 2002; Liu et al., 2002; Wang et al., 2002; Schwab, 2004). Blocking the inhibitory action of the Nogo-66 receptor is associated with improved recovery following CNS injury in both rodent and non-human primate models (Simonen et al., 2003; Schwab, 2004; Wang et al., 2020). CSPG inhibitory effects on axon regeneration converge on this same pathway through activation of RhoA (Monnier et al., 2003; Schwab, 2010; Sami et al., 2020). Unlike CSPGs from astrocytes, myelin-associated inhibitors are constitutively expressed within oligodendrocytes in the absence of injury (Pasterkamp and Verhaagen, 2006). While myelin-associated inhibitors and Nogo-66 receptor expression remains constant, molecules involved in the signaling cascade downstream of the Nogo-66 receptor are differentially regulated following CNS injury making neurons more sensitive to myelin-associated inhibition. Examples of such downstream proteins include AMIGO-3 and LINGO-1, both integral components of the Nogo-66 receptor signaling complex (**Figure 4**; Mi et al., 2004; Ahmed et al., 2013).

In addition to myelin-associated inhibitors, certain semaphorins (Semas) also contribute to the general inhibitory environment within the CNS. Semaphorins comprise a large gene family of both secreted and membrane-associated proteins that act as guidance cues within the developing CNS. All neurons and some glial cells within the CNS express semaphorins during development. In the adult mouse, semaphorin expression becomes restricted to a specific population of neurons. The membrane bound Sema4D is expressed on oligodendrocytes and plays a similar role to myelin associated inhibitors, contributing to the general non-permissive environment of the CNS (Pasterkamp and Verhaagen, 2006). Sema4D binding to its receptor, plexinB1, initiates a signaling pathway that leads to cytoskeletal changes and growth cone collapse through the Rho/ROCK pathway, similar to the Nogo-66 receptor (Oinuma et al., 2004). The most studied semaphorins affecting axon regeneration in the adult CNS are the secreted Sema3s (Pasterkamp and Verhaagen, 2006; Mecollari et al., 2014). In contrast to Sema4D, the Sema3s are specifically upregulated following CNS injury (Pasterkamp et al., 1999). Sema3A is the best studied of the Sema3s and colocalizes with fibrotic expression indicating that meningeal cells invading the neuronal scar are their main source. Neurons themselves may also contribute to Sema3A levels as they are known to secrete Sema3A under hypoxic conditions following ischemic events (Joyal et al., 2011). Once secreted, Sema3A molecules associate with CSPGs and signal through a holoreceptor complex made up of neuropilin and plexinA1 subunits. Like Sema4D, Sema3A binding to its neuropilin/plexin holoreceptor induces growth cone collapse, directly preventing axon regeneration through the scar (**Figure 4**; Pasterkamp and Verhaagen, 2006; Mecollari et al., 2014; Sami et al., 2020).

Finally, the CNS inhibitory environment is inflammation. The microglia and astrocytes recruited to the site of injury not only contribute to glial scar formation, but they also secrete cytokines which recruit non-resident immune cells like macrophages (Gaudet and Fonken, 2018). The result of this inflammatory response is complex, with evidence suggesting inflammation creates a barrier for axon regeneration (Gaudet et al., 2016; Gaudet and Fonken, 2018) but also that inflammation is sometimes necessary for axon regrowth (Kigerl et al., 2009; Harrison et al., 2017; Wang et al., 2019). The role of inflammation in regeneration is an ever-broadening field which has been extensively review elsewhere (Fitch and Silver, 2008;

Benowitz and Popovich, 2011; Orr and Gensel, 2018; Estera et al., 2021; Kwiecien, 2022).

GRAFT TRANSPLANTS PROMOTE AXON REGENERATION FOLLOWING SPINAL CORD INJURY

Neurite outgrowth and regeneration following spinal cord injury can be promoted through the application of various tissue grafts to the site of injury. The first studies of this type, by Aguayo and colleagues in the 1970s, used peripheral nerve and Schwann cell grafts. In a series of experiments, the group cut out tissue around the optic nerve and grafted it in multiple places throughout the PNS. Upon later examination, they found regenerated PNS axons distal to the injury site. However, the axons did not regrow through the graft but rather around it. In contrast, they found that if a PNS graft was placed in the lesion site following spinal cord injury, axons from various brainstem nuclei were able to regrow into the PNS graft, although none were seen to extend beyond the grafted tissue (Aguayo et al., 1978; Richardson et al., 1980, 1984; David and Aguayo, 1981). Somehow, the PNS environment was able to partially stimulate a regenerative state in CNS neurons whose axons were injured, despite the general inhibitory environment comprising the distance between the graft and neuronal cell bodies. These studies helped to establish the hypothesis that adult mammalian CNS neurons are able to regenerate their axons following injury if they can enter the correct regenerative state. Such a state can be achieved within the right environment, as exists in the PNS.

By the late 1980s, other groups had identified Schwann cells as a key component in the PNS graft's ability to promote regeneration of CNS neurons following spinal cord injury (Kromer and Cornbrooks, 1985; Guénard et al., 1992). While PNS grafts were able to stimulate axon regeneration into the graft itself, axons were unable to reinnervate the region distal to the graft to any significant extent–significant reinnervation and reformation of synapses in target tissues was never seen with PNS grafts alone. Furthermore, these studies never showed axon regrowth from neurons with somata residing in the brain. Rather, the regenerating axons were all from propriospinal neurons within the spinal cord. In 1995, Xu and colleagues hypothesized that Schwann cell expression of BDNF and NT-3 was partially responsible for this regeneration. When they treated with both BDNF and NT-3 in addition to a Schwann cell graft, they not only showed a significant increase in the number of fibers that were able to extend into the grafted tissue but also identified serotonergic fibers from the raphe nuclei extending past the lesion site, marking the first observation of axon regeneration in the spinal cord from a CNS neuron situated within the brain (Xu et al., 1995). Later studies replaced Schwann cells with cultured fibroblasts genetically modified to express BDNF, suggesting that the growth factors, rather than the Schwann cells themselves, were stimulating axon regeneration (Liu et al., 1999). This approach was then further improved by combining bone marrow stromal cell grafts and the injection of growth factor expressing Lentivirus into target regions for axon regrowth. Initially, it was hoped that these bone marrow stromal cells would develop into new neurons to repopulate the injured area. While these cells did not transition into a neuronal fate, this graft helped promote tissue healing through the expression of growth factors and cytokines to support revascularization of the injured region (Parr et al., 2007). The important aspect of this method is the injection of growth factor expressing Lentivirus into the denervated tissue. The growth factors produced by injected Lentivirus diffuse, creating a concentration gradient originating from the target tissue and thus providing an instructional environment to guide the new growth cones. This approach facilitated increased axon regeneration, partial reinnervation of target tissues, and some reformation of synapses following spinal cord injury (Alto et al., 2009; Lee et al., 2013). Other experiments have paired the application of a graft with blockade of CSPG signaling (Bradbury et al., 2002; Vavrek et al., 2007; Shen et al., 2009; Lee et al., 2013). The benefits provided by these growth factors show that a permissive environment lacking extrinsic inhibitors might not be sufficient for axon regrowth. Instead, the environment may have to provide signals to promote regeneration. Growth factors gradients originating from denervated tissue could provide guidance to promote productive axon regrowth beyond that seen following interventions that only address inhibitory factors such as Chontroitinase ABC treatment or blockade of the Nogo-66 receptor intended to merely remove non-permissive signals from the environment.

These studies, and others, support the hypothesis that CNS neurons maintain the capacity to regenerate when provided with not only permissive substrates but also an environment that promotes a growth state. By adding chondroitinase to cleave CSPGs within the path of regrowing axons, inhibitory signals are removed from the environment. Adding growth factors then provides the positive, perhaps at times instructive, signals for regrowth. This favorable environment is completed by applying a bone marrow stromal cell graft or a Schwann cell graft to the lesion site providing tissue the axon can regrow through. However, a few caveats must be mentioned. First, while these methods are able to promote axon regeneration and partial behavioral recovery, full behavioral recovery as assessed by various motor related tasks following a complete spinal cord transection was not shown. These studies examined either partial transection or crush (contusion) injuries (Cheriyan et al., 2014). Furthermore, the regenerating axons do not reach target tissues and reform synapses at densities seen prior to injury. Finally, axon regeneration occurred to varying extents depending on neuronal subtype. Neurons that displayed some increased sprouting and regrowth were located within the spinal cord, reticular nucleus, raphe nucleus, locus coeruleus, and other brain stem nuclei (Jin et al., 2002; Vavrek et al., 2007; Lu et al., 2012; Lee et al., 2013). No study was able to provide definitive evidence of functional CST axon regeneration, regardless of intervention strategy. Zhigang He's group found that CST axons extended caudal to a spinal cord hemisection, in which half the spinal cord is transected, or complete crush injury following mTOR stimulation through PTEN deletion or the enforced overexpression of insulin-like growth factor 1 in CST neurons. This regrowth was accompanied by some synaptic reformation,

as observed by BDA/vGlut1 immunostaining and, following dorsal hemisection, minor improvement in hindlimb function (Liu et al., 2010, 2017; Zukor et al., 2013). While these results are promising, the incomplete nature of the hemisection injury leaves open the possibility that axon reappearance occurred due to collateral sprouting and the improvement in hindlimb function could be a result of reinforcement of surviving circuits due to repeated behavioral testing as was noted by the same group in a later study (Chen et al., 2018).

The findings discussed thus far indicate that there is more to CNS axon regrowth than just the presence of inhibitory factors and the lack of a pro-growth environment preventing the activation of the regenerative program in CNS neurons. One possibility is that these studies had not identified the correct milieu required to promote effective regrowth. However, the difference in regenerative capacity seen across neuronal subtypes indicates that there are neuron-specific considerations as well. Similar cell-type specific differences were observed examining the regeneration of retinal ganglion cell subtypes following optic nerve crush in PTEN knock down mice. PTEN knock-down to stimulate mTOR activity has been shown to be one of the most effective methods at promoting axon regeneration of RGCs, however, this regeneration seems to be dominated by α and M1 RGCs with very limited success in other subtypes (Duan et al., 2015). The disparity seen between different cell types indicates that these populations may have different requirements for activating this regenerative gene program or perhaps different regeneration programs entirely.

While the studies discussed thus far successfully demonstrated regeneration of CNS neurons, no experiment had shown direct evidence of CST axon regeneration. Previous studies had recorded motor recovery following incomplete spinal cord injuries, in which only half the spine is damaged, using behavioral tests or extracellular recordings in the spinal cord following stimulation in the motor cortex (Bregman et al., 1995; Bradbury et al., 2002). Bregman and colleagues went as far as removing the sensorimotor cortex to indicate that behavioral recovery was reliant upon regeneration of CST axons. Each of these methods indicates that these CST axons may be regenerating; however, they do not rule out the possibility that the behavioral recovery is a result of collateral sprouting from surviving axons on the undamaged side. One method to definitively show axon regeneration would be to perform a complete spinal cord transection.

The first study that showed CST axon regeneration following complete transection of the spinal cord was performed using a combined treatment of cAMP injections to the neuronal cell bodies, a bone marrow stromal cell graft to the lesion site, and the careful construction of a BDNF gradient distal to the lesion (Lu et al., 2012). What set this study apart from others was the careful construction of a BDNF gradient distal to the lesion site. Here, the authors showed that using growth factor guidance cues to create a spatially instructive environment in tandem with the permissive graft is much more effective at promoting regeneration than the graft-facilitated permissive environment alone.

To date, the most successful intervention in promoting recovery following a spinal cord injury is the application of a multipotent neural progenitor cell (NPC) graft. These grafts improve tissue reconstitution within the lesion site and are able to replace lost adult neural cell tissue with cells homologous to those in the pre-injured state. When a severed axon regrows into an NPC graft, it forms synapses on these developing progenitor cells. These NPCs then project axons that synapse onto other NPCs, eventually leading to circuit extension distal to the lesion site and improved functional recovery when compared to other treatments, although recovery of axon density caudal to the lesion site is still sparse (Kadoya et al., 2016; Fischer et al., 2020). Unfortunately, even with this new discovery that NPCs act as better graft that no longer requires experimental cAMP application (Kadoya et al., 2016.), full functional recovery is still unattainable following spinal cord injury (Fischer et al., 2020). In addition to the decreased axon density caudal to the graft, complete functional recovery is complicated by the "bridging" required for this regrowth. This "bridging" process takes a circuit that was once monosynaptic and creates a polysynaptic circuit reducing the speed and specificity at which signals from the motor cortex can reach their targets. In support of this bridging strategy, another group found that treatment with CLP290 to hyperpolarize lumbar inhibitory interneurons significantly improved hindlimb weight bearing stepping capacity through the revival of spared polysynaptic circuits following a bilateral double hemisection spinal cord injury at the T7 and T10 vertebrae (Chen et al., 2018). While this treatment did not induce any axon regeneration it demonstrates the potential for functional recovery through the creation of alternative circuits. There are many additional tissue grafts and experimental cell therapies for improving axon regeneration following SCI, for a comprehensive list (see Huang et al., 2021).

All neurons examined that project axons into the spinal cord have been shown to possess some regenerative potential in adult murine models. Yet, to date, no therapeutic approach has been able to produce full functional restoration of the deficits associated with CNS injury. The local milieu of the CNS is credited as a major factor dictating the dramatic shortcomings of CNS regeneration compared to that seen within the PNS, and yet, even in the context of modern treatment advancements, we still see differences between neuronal subtypes in both the rate and extent of regrowth. Is this extrinsic obstacle as critical as previously believed given the disparity in regeneration potential displayed across various CNS neuronal subtypes through an inhibitory environment that is consistent?

MAMMALIAN NEURONS REVERT TO A DEVELOPING PHENOTYPE FOLLOWING INJURY

Transcriptomic profiling using RNA sequencing techniques offers a new avenue to elucidate many of the genetic mechanisms underlying neuronal subtype-specific axon regeneration. By examining the transcriptome of individual neurons before injury and then at multiple timepoints following injury, we should be able to understand the gene expression events underlying axon regeneration. Furthermore, by comparing the results

from different neuronal subpopulations, we should gain a greater understanding of why these populations display different propensities for regeneration.

An early study examining the transcriptome of regenerating DRG neurons in comparison to non-regenerating CNS neurons showed differences in the expression of various genes known to be associated with axon regeneration (Lerch et al., 2012; Dulin et al., 2015). This discovery provides potential insight to understanding the differences in regenerative potential shown by various neuronal subpopulations. Further studies used RNA-seq to examine specific pathways in detail. For example, Ma and colleagues found that CREB activated genes work in concert with AP-1 controlled genes to promote axon regeneration of cortical CNS neurons *in vitro* (Ma et al., 2014; Dulin et al., 2015). Studies such as these seek to understand axon regeneration at a pathway specific level in the hopes of identifying molecular targets for therapies.

Poplawski and colleagues recently published a study in which they used single-cell RNA-sequencing to examine the expression profile of individual CST neurons following spinal cord injury in mice at multiple timepoints throughout the regeneration process. They compared these profiles from mice that received NPC graft treatment to mice that had received only sham graft surgery after spinal cord injury. Surprisingly, both the NPC graft-treated animals and the lesion-only animals displayed the same initial transcriptional changes following injury, termed the "regeneration transcriptome." The major difference seen between each group was the duration that the cell was able to maintain the regeneration transcriptome following injury. While some of the pathways activated were expected, such as those involved in axon guidance, others were surprising. Gene ontology analysis of the regeneration transcriptome revealed activation of proliferation, differentiation, and cell-cycle progression-related functions. These regenerating neurons had a transcriptome that was most highly similar to embryonic day 18 CST neurons, appearing that the injury was inducing "terminally differentiated" neurons to revert to an embryonic state (Poplawski et al., 2020).

Another key study using single-cell RNA-sequencing examined DRG neuron axon regeneration following a crush injury in the PNS (Renthal et al., 2020). Following injury application, the authors monitored the expression profiles of individual DRG neuronal subtypes to determine if they differ in their injury response. They were initially unable to identify the neuronal subpopulations after injury since the cells were downregulating genes classically used to distinguish those subtypes. While CST neurons reverted to a cell state closely resembling embryonic CST neurons, DRG neurons did not revert to this extent. Rather, DRG neurons increased the expression of transcription factors expressed during development which promote pluripotency. This increase was accompanied by the loss of cell identity indicative of reversion to a less differentiated state. Here in the periphery, we still see transcriptional reprogramming to a cell state resembling developmental neurons; however, the overlap between gene expression programs active during a specific developmental timepoint and those active during regeneration did not achieve statistical significance. Glial cells within the DRG did not experience a similar loss of identity, demonstrating that this is not a general cellular response to injury and is neuron-specific (Renthal et al., 2020). The findings from these two studies have the potential to alter the field's approach to investigating axon regeneration, which has often focused on addressing individual barriers to regeneration. Rather than attempting to address specific extrinsic or intrinsic barriers, efforts can be redirected to initiating and prolonging neuronal reversion to a developmental state that would presumably lack intrinsic barriers.

Many studies in the past focused on identifying genes that are known to play a role in neuronal development and axon elongation with the hope of using those programs to promote regeneration. Such attempts have yielded only limited success over the course of decades. The dominant view has been that CNS neurons in adult mammals terminally differentiate following development and are incapable of fundamentally altering their transcriptional identity. With terminal differentiation in mind, researchers have been attempting to promote regeneration by blocking inhibition or activating regeneration-associated signaling pathways in the context of an adult neuron. The new findings by Poplawski et al. (2020) and Renthal et al. (2020) are some of the first to contradict this framework. It is important to note that while these redeveloping neurons may have overcome the intrinsic barriers to regeneration discussed above, they still face the same adult extracellular environment complete with an array of molecules inhibitory to axon regeneration. Still, results from these two studies could shift a major aim within the field from identifying specific RAGs that promote a slight increase in neurite outgrowth to identifying transcription factor hubs that promote or sustain neuronal reversion to an embryonic-like cell state.

If we were to assume that all neurons attempt a similar reversion following injury, we would be left with many of the same questions previously held in the field as well as some new ones. We still observe differences in the capacity of neuronal subpopulations to regenerate following injury, why is this? Perhaps certain neurons are able revert more quickly in response to injury or perhaps they are able to maintain this reverted state for longer. How do regeneration inhibitors affect this reverted state, are they promoting redifferentiation in some way? If all neurons undergo a process of redevelopment in order to respond to damage and facilitate recovery, it seems reasonable to assume that the local milieu of the PNS provides a better environment for neurons to maintain this reverted state. Does this warrant reexamination of factors previously identified to promote axon regeneration within this new context? Fitting these unanswered questions into a context of redevelopment may be the key to solving the puzzle of axon regeneration in the mammalian CNS.

SOME CENTRAL NERVOUS SYSTEM NEUROMODULATORY NEURONS CAN REGENERATE THEIR AXONS UNAIDED FOLLOWING BRAIN INJURY IN ADULT MAMMALS

There is increasing evidence for spontaneous serotonergic neuron axon regrowth within the CNS following chemical or

physical insults. Initial fixed tissue studies in the mammalian forebrain showed robust recovery of serotonin axon density following chemical lesioning with amphetamines as assessed using antibody staining against serotonin (O'Hearn et al., 1988; Molliver et al., 1990; Wilson and Molliver, 1994; Mamounas et al., 2000). A later investigation also used antibody staining against serotonin to demonstrate regrowth of serotonin axons in otherwise non-permissive environments including the subventricular zone and areas adjacent to a glial scar following a thermal injury—a feat not replicated by callosal fibers within the same cortical region (Hawthorne et al., 2011). Other studies examining recovery from spinal cord injury in rodents found that surviving serotonin axons exhibit significant compensatory sprouting rostral to the site of injury (Inman and Steward, 2003; Camand et al., 2004; Holmes et al., 2005; Hayashi et al., 2010). However, these experiments were unable to determine whether the recovery seen was truly due to regeneration. First, while the loss and subsequent recovery of serotonin immunoreactivity could indicate the retraction and regrowth of serotonin axons, this same effect could be observed if amphetamine treatment merely induced a long pause on the production of serotonin, effectively emptying the axons of serotonin for a period of time. Furthermore, because fixed tissue only displays a single moment in time, the recovery seen in these experiments may not be a result of bona fide regeneration, defined as growth originating from damaged axons, but rather the collateral sprouting of surviving axons (see **Figure 1**).

To directly address the issues inherent in examining axon regeneration using serotonin immunoreactivity as a measure, Linden and colleagues used long-term *in vivo* imaging in transgenic mice expressing eGFP selectively in serotonin neurons (Jin et al., 2016). Directly expressing eGFP within neurons, rather than staining the tissue with antibodies raised against serotonin, removes the concern that these axons may be emptying and refilling with serotonin following injury rather than retracting and regenerating. Furthermore, by examining regeneration *in vivo* using two-photon microscopy, directly monitoring the origin of axon recovery following parachloroamphetamine (PCA) treatment in individual damaged serotonin axons is possible. PCA treatment leads to the degeneration of serotonin axons back to the first presynaptic active zone (Molliver et al., 1990; Fuller, 1992). One week following PCA treatment there was a significant loss of serotonin axons within the neocortex; however, substantial recovery of serotonin axons was observed at both 3 and 6 months following PCA treatment. The rate of collateral axon sprouting in injured animals was the same as in controls, indicating that regeneration is indeed responsible for the recovery of axon density (Jin et al., 2016). The extent to which serotonin axons regenerated following PCA-induced serotonin degeneration is unprecedented compared to other studies examining recovery following CNS injury in wild-type animals. However, direct comparisons between recovery following a physical injury to that observed following a chemically induced serotonin axon-selective injury may not be appropriate. Physical injury not only affects all cells within the area, but also causes secondary injury cascades and glial scarring not seen following PCA treatment.

Though chemically induced neurodegeneration can occur in patients with long term amphetamine abuse (Halpin et al., 2014), this is not the most clinically relevant form of CNS injury. To address a more typical form of injury, Jin et al. (2016) further investigated this regrowth phenomenon of serotonin axons in physical injury models using transgenic mice expressing eGFP selectively within serotonin neurons. These mice received a stab wound to the somatosensory cortex in which a scalpel, oriented in the coronal plane, was inserted to transect serotonin axons running along their anterior to posterior trajectory. Unlike the amphetamine-induced injury, which selectively targets serotonin neurons leading to widespread axon degeneration back to the first presynaptic active zone, a physical stab injury damages all cell types in the area while only causing the proximal portions of serotonin axons to retract for tens of microns. Over the course of 12 weeks following injury, serotonergic axons traversed the glial scar and recovered regional axon density identical to mice that received a sham surgery. Using longitudinal *in vivo* imaging following stab injuries, axon regrowth directly from the severed ends of cut-injured axons was observed, providing direct evidence for axon regeneration (Jin et al., 2016). The same transgenic mouse model was also used to examine regeneration of serotonin axons following a controlled cortical impact (CCI) to induce traumatic brain injury (Kajstura et al., 2018). These mice received standardized impacts to the surface of the cortex, resulting in visible damage to cortical layers 1 through 4. Due to the extensive nature of the injury, axon regeneration was measured in the fixed tissue both anterior and posterior to the site. A week after injury, serotonin axon density is decreased only posterior to the CCI injury. However, a month after injury, the density of serotonin axons posterior to the injury is largely recovered despite the large crater created by the impact injury, which remains devoid of axons. This experiment indicates robust axon regeneration by serotoninergic neurons in the context of a more extensive injury is indeed possible (Kajstura et al., 2018).

When contemplating why serotonin axons seem to harbor an unusual ability to regrow without aid, we must consider how serotonin neurons are unique in their axonal structure, extensive neocortical innervation, and downstream neurotransmission. Serotonergic axons in the neocortex originate from cell bodies located in the rostral group of brainstem raphe nuclei. Their trajectory follows a C-shaped pattern from the brain stem along the base of the hypothalamus, through the medial forebrain bundle, up and around the anterior pole of the frontal lobe, and then anterior to posterior through cortical layers one and six as well as the underlying white matter; this trajectory defines these axons as some of the longest in the brain. Serotonergic axons running through these neocortical layers then branch off and dive to inferior locations, or climb to superior locations, to innervate all cortical layers (Jacobs and Azmitia, 1992). The inherent ability of serotonergic neurons to support these extremely long axons may provide them with the mechanistic framework to rebuild and repair them following axonal damage. However, simple mechanics might not entirely explain this phenomenon, since shorter projecting serotonergic axons are also capable of regrowth while other very long axons, such as CST axons, are unable to regrow following injury.

Another distinguishing quality of serotonergic neurons is that they mainly employ volume transmission, rather than conventional point-to-point synaptic transmission, as their primary method of signaling. In synaptic transmission, neurotransmitters such as glutamate, GABA, or glycine are released and activate receptors at classical synapses in which the presynaptic active zone faces a receptor-laden postsynaptic density lying across the narrow synaptic cleft. This form of point-to-point neurotransmission is built to convey information quickly (on a time scale of milliseconds to tens of milliseconds) and in a spatially restricted manner, with transmitter spillover usually restricted to only a few adjacent synapses. In volumetric transmission, there is no postsynaptic density bearing a high concentration of receptors facing the presynaptic active zone. Therefore, released serotonin diffuses in the extracellular space for a much greater distance in order to encounter dispersed receptors present on many cells within a larger volume (Séguéla et al., 1989; Bunin and Wightman, 1998, 1999; Fuxe et al., 2007; Kaushalya et al., 2008; Colgan et al., 2012). Due to the precision required for synapse-based signaling, if a damaged glutamate axon regrows, it must reinnervate its postsynaptic targets with great accuracy to reconstitute pre-injury function. By contrast, volume transmitting axons that regrow need only target the general area that was denervated, since their signaling is not so spatially or temporally constrained. Perhaps volume transmitting axons, like those that release serotonin, have the capacity to regrow after injury within the adult brain because such regrowth restores pre-lesion function without having to reform each of the precise connections of the previously injured axon.

The characteristics that may afford serotonin fibers the capability to regenerate unaided following injury—very long-distance axon projections and the use of volume transmission—are also shared by other neuromodulatory neurons, specifically norepinephrine- (also referred to as noradrenaline) expressing neurons. Like serotonin axons in the neocortex, norepinephrine axons also originate from cell bodies located in the brainstem in a region called the locus coeruleus, and they follow a similar C-shaped trajectory through the brain while also sending projections into the cerebellum and hindbrain (Beaudet and Descarries, 1978; Papadopoulos and Parnavelas, 1991; Berridge and Waterhouse, 2003; Sara, 2009; Shnitko and Robinson, 2014). Additionally, they also employ volume transmission to modulate target cells (Séguéla et al., 1990; Umbriaco et al., 1995; Fuxe et al., 2007). Previous studies show that lesions to the superior peduncle of the rat cerebellar cortex results in increased arborization of terminal norepinephrine fibers visualized *via* formaldehyde-induced fluorescence of catecholamines (Pickel et al., 1973). Chemical lesioning with the neurotoxin 6-hydroxydopamine (6-OHDA) led to a cortical decrease of norepinephrine, measured using a tritiated norepinephrine reuptake assay, in rats; these levels returned to normal after 3 months, suggesting regeneration or compensatory sprouting (Levin, 1983). Additionally, analysis of fixed tissue following 6-OHDA lesioning of the adult cat occipital cortex revealed degeneration and successive recovery of norepinephrine fibers over the course of 52 weeks, measured *via* antibodies against dopamine beta hydroxylase, the last enzyme in the norepinephrine metabolic pathway (Nakai et al., 1994). Following chemical damage with a selective norepinephrine neurotoxin (N-(2-chloroethyl)-N-ethyl-2-bromobenzylamine, known as DSP-4), norepinephrine immunoreactivity is first lost and then subsequently recovered by 12 months post-damage (Fritschy and Grzanna, 1992).

A recent study showed reduction of norepinephrine axon density following CCI or the application of a cortical stab wound at 1 week and 1 month following injury. Much like serotonin axons, axon density slowly returned over the course of several months to levels indistinguishable from the cortical innervation observed in control mice (Dougherty et al., 2020). As with the initial evidence of serotonergic regeneration, these fixed tissue studies are unable to provide definitive evidence of regeneration vs. collateral sprouting, and so long-term *in vivo* imaging is still required.

Together these results suggest that both serotonin and norepinephrine neurons in the CNS possess the intrinsic ability to regrow their axons in the adult brain. It is not known whether this phenomenon is shared by any other class of neuron, or if this ability is a result of their unique characteristics. Further studies need to be conducted to determine if other neuromodulatory axons can regrow after injury, or if CNS regeneration is exclusive to serotonin and norepinephrine-expressing neurons.

CONCLUSION: IMPLICATIONS OF REDEVELOPMENT AND REGENERATION OF NEUROMODULATORY AXONS

The discovery that serotonin and norepinephrine neurons can regenerate axons projecting throughout the cerebrum raises several interesting questions. Over the past several decades, extensive work has shown that the PNS offers a much more effective environment for regeneration than the CNS. Indeed, limitations of PNS axon regeneration through a CNS graft and the effectiveness of promoting CNS axon regeneration through the application of a PNS graft clearly demonstrates this difference (Aguayo et al., 1978; Richardson et al., 1980; David and Aguayo, 1981; Richardson et al., 1984). Subsequent work showing the increased effectiveness of both bone marrow stromal cell and also NPC-based grafts improve upon the pro-growth effects observed following application of PNS grafts (Jin et al., 2002; Vavrek et al., 2007; Lu et al., 2012; Lee et al., 2013; Kadoya et al., 2016; Fischer et al., 2020). The recent findings that axon regeneration may be facilitated by the reversion to an embryonic-like cell state that can be maintained for longer periods by the addition of an NPC graft also fits within this narrative. These studies show that CNS neurons maintain an ability to regenerate following axonal injury given the right environment to promote an internal growth state. This permissive environment is present within axon tracts of the PNS but not the CNS.

The regenerative capabilities of serotonin axons from the dorsal/median raphe and norepinephrine axons from the locus coeruleus into the cerebral cortex show that adult mammalian CNS neurons are indeed able to regenerate axons following

injury through an environment that has traditionally been considered non-permissive. Several groups have observed the ability of axons from serotonin and norepinephrine-expressing neurons to regenerate over long distances following traumatic brain injury, a cortical stab wound, or selective chemical lesions (O'Hearn et al., 1988; Molliver et al., 1990; Fritschy and Grzanna, 1992; Nakai et al., 1994; Wilson and Molliver, 1994; Mamounas et al., 2000; Inman and Steward, 2003; Camand et al., 2004; Holmes et al., 2005; Hayashi et al., 2010; Jin et al., 2016; Kajstura et al., 2018; Dougherty et al., 2020). The magnitude of regeneration observed within these studies is beyond that of any other CNS axon regeneration observed to date and requires no experimental intervention. These regenerated serotonergic and noradrenergic axons are present in densities equivalent to what is observed in uninjured tissue. Further, these regenerated axons are capable of neurotransmitter release by 6 months following injury, as detected by fast-scan cyclic voltammetry, albeit evoked by pulse trains far beyond those which occur physiologically. Remarkably, this regeneration results in mice that are indistinguishable from their littermate controls in several behavioral tasks (Jin et al., 2016).

Multiple approaches have been shown to improve behavioral recovery following spinal cord injury, neural progenitor cell grafting being the most successful; however, full recovery including the more complicated movements has yet to be observed. It should be noted that the role these modulatory neurotransmitters play in behavior is much more subtle than the role that CST neurons play in movement. Nevertheless, regeneration on this scale has yet to be seen under any circumstance in the spinal cord or the optic nerve.

Serotonin and norepinephrine axon regeneration through the cerebral cortex shows several distinct features from axon regeneration induced in the spinal cord, optic nerve, or that seen in the PNS. First, cortical serotonergic and noradrenergic axons are able to regenerate through the glial scar created by a cortical stab wound (Jin et al., 2016; Dougherty et al., 2020). Following spinal cord injury, no axon is able to pass through the glial scar unaided. Furthermore, when glial scar tissue is grafted into a PNS lesion, DRG axons are unable able to regrow through the graft (Davies et al., 1997; Davies et al., 1999). Interestingly, serotonin and norepinephrine axons are unable to pass through the glial scar of a spinal cord transection unaided but are able to do so in the cerebral cortex (Lee et al., 2010). Somehow, these neuromodulatory axons within the brain are able to ignore the inhibitory cues inherent to the CNS. Are there intrinsic differences between the subpopulations of neuromodulatory neurons that project into the spinal cord and those that project cranially? For example, the cranial projecting neurons may display variation in key signal transduction pathways that inhibit regeneration which eliminates the potential for that signaling. It is also possible that the environment within the adult mammalian brain is more permissive for axon regeneration than previously believed, at least for neuromodulatory neurons.

Another difference between DRG and serotonergic axon regeneration is that serotonergic axons do not regrow along the exact path from which they retracted, as is observed for regenerating PNS axons, indicating that these neurons use different axon guidance mechanisms. Finally, following spinal cord or PNS injury, there are many more branches that extend from damaged axons than the final number that will eventually innervate their targets. Axon branches that do not receive growth factor signaling from that target organ, or from a graft following spinal cord injury, are eliminated. This resembles the overgrowth and pruning process seen in the developing nervous system. Monitoring regrowth using *in vivo* 2-photon imaging of serotonergic axons during regeneration through the cerebral cortex did not reveal similar overgrowth and pruning.

Given the observed differences between serotonergic axon regeneration and DRG axon regeneration, it is possible that serotonergic and norepinephrine neurons regrow using different regeneration programs than PNS neurons. The experiments conducted by Poplawski et al. (2020) and Renthal et al. (2020) indicate that CST neurons following spinal cord injury and implementation of an NPC graft, as well as DRG neurons following peripheral crush injury, undergo reversion to a developmental-like phenotype to promote recovery and axon regeneration. This hypothesis is further supported by the overgrowth and pruning of axonal branches following these injuries as well as the success many labs have found in promoting regeneration through mTOR, a pathway highly active during development (Nieuwenhuis and Eva, 2022). Developing cells are much more resilient to damage than adult cells and thus this reversion to a developmental phenotype may be part of the common neuronal injury response.

One characteristic of developing neurons is increased neurite sprouting, which would explain the arborization and pruning observed during PNS regeneration. The increased expression of growth factors such as BDNF seen in the periphery likely provides signaling necessary for DRG neurons to maintain a reverted developmental phenotype long enough to reestablish synaptic connection to the target organs. Graft implementation following a spinal cord injury approximates this same process, adding developmental tissue to the injured neurons providing the molecular signaling sufficient to maintain this reverted state for longer. The observed differences described above indicate that serotonergic neurons may not undergo this same process of "redevelopment," raising the possibility that they may be using regenerative programs distinct from that of the PNS. If this is the case, new avenues of research for the field in CNS axon regeneration present the opportunities to identify and exploit these novel regenerative programs. Perhaps attempting to recapitulate the PNS is not the only, or best, approach to achieve clinically relevant regeneration within the CNS.

Single cell expression profiling experiments should begin to answer some of these questions. Okaty et al. (2020) recently published an in-depth single cell transcriptomic atlas of serotonin neurons within the dorsal raphe of young adult mice aged 6–10 weeks. They identified up to 14 distinct neuronal subtypes within the region, all expressing serotonin. Broadly, these subtypes can be split into two groups, those that co-express GABA and those that co-express glutamate (Okaty et al., 2020). This discovery calls into question the regeneration of "serotonin" neurons as a broad definition. Do

all of these subtypes possess the same capacity for regeneration or are only a few competent to regenerate? If these different subtypes of serotonin neurons are all competent to regenerate, will they regress to a developing phenotype? If so, to what extent will this regression occur, will they lose their individual identities as seen within different subtypes of DRG neurons? Expression profiling before and at multiple time points after axon injury will reveal the "regeneration transcriptome" of serotonin and norepinephrine neurons which can be compared to the transcriptomes of developing serotonin (Wyler et al., 2016) and norepinephrine neurons.

Comparing the transcriptome of regenerating neuromodulatory neurons to those of DRG and CST neurons at equivalent timepoints will determine whether serotonin and norepinephrine neurons undergo a similar reversion process in order to facilitate recovery. Results from these experiments could change our view of how to search treatments directed toward traumatic brain and spinal cord injuries. Rather than attempting to induce expression of the ideal transcriptional programs in CNS associated with peripheral nerve regeneration, efforts designed to maintain a "redevelopment" phenotype specific to CNS neurons, or perhaps a program unique to nerumodulatory neurons will be most productive. How does the unprecedented regenerative capacity of neuromodulatory axons in the brain fit into the overall narrative of redevelopment? If neuromodulatory neurons facilitate regeneration through redevelopment, then extending this period of redevelopment should be a central focus of research in the search for therapies. If, however, neuromodulatory neurons use alternative mechanisms, then these hold the promise for recapitulating regenerative programs proven to work within the CNS. It is important to note that neuromodulatory neurons are quite different from other neurons in both structure and function and thus a deep understanding of their regenerative states is required in order to determine whether their regenerative programs may be utilized in other systems.

AUTHOR CONTRIBUTIONS

PC conceived the review and wrote sections "Axons in the Adult Mammalian Central Nervous System Do Not Regenerate Following Injury," "Graft Transplants Promote Axon Regeneration Following Spinal Cord Injury", "Mammalian Neurons Revert to a Developing Phenotype Following Injury", and "Conclusion: Implications of Redevelopment and Regeneration of Neuromodulatory Axons" and conceptualized the figures. HJ wrote sections "Axons in the Adult Mammalian Central Nervous System Do Not Regenerate Following Injury" and "Some Central Nervous System Neuromodulatory Neurons Can Regenerate Their Axons Unaided Following Brain Injury in Adult Mammals". SD wrote section "Some Central Nervous System Neuromodulatory Neurons Can Regenerate Their Axons Unaided Following Brain Injury in Adult Mammals". HJ created the figures. PC, HJ, and SD edited the manuscript. All authors contributed to the article and approved the submitted version.

ACKNOWLEDGMENTS

David Linden provided guidance in the research and writing process and edited the manuscript. Alex Kolodkin provided guidance in the research and edited the manuscript.

REFERENCES

Aguayo, A. J., Dickson, R., Trecarten, J., Attiwell, M., Bray, G. M., and Richardson, P. (1978). Ensheathment and myelination of regenerating PNS fibres by transplanted optic nerve glia. *Neurosci. Lett.* 9, 97–104. doi: 10.1016/0304-3940(78)90055-1

Ahmed, Z., Douglas, M. R., John, G., Berry, M., and Logan, A. (2013). AMIGO3 is an NgR1/p75 co-receptor signalling axon growth inhibition in the acute phase of adult central nervous system injury. *PLoS One* 8:e61878. doi: 10.1371/journal.pone.0061878

Akassoglou, K., Merlini, M., Rafalski, V. A., Real, R., Liang, L., Jin, Y., et al. (2017). *In Vivo* Imaging of CNS Injury and Disease. *J. Neurosci.* 37, 10808–10816. doi: 10.1523/JNEUROSCI.1826-17.2017

Alto, L. T., Havton, L. A., Conner, J. M., Hollis, E. R. II, Blesch, A., and Tuszynski, M. H. (2009). Chemotropic guidance facilitates axonal regeneration and synapse formation after spinal cord injury. *Nat. Neurosci.* 12, 1106–1113. doi: 10.1038/nn.2365

Anderson, M. A., Burda, J. E., Ren, Y., Ao, Y., O'Shea, T. M., Kawaguchi, R., et al. (2016). Astrocyte scar formation aids central nervous system axon regeneration. *Nature* 532, 195–200. doi: 10.1038/nature17623

Beaudet, A., and Descarries, L. (1978). The monoamine innervation of rat cerebral cortex: synaptic and nonsynaptic axon terminals. *Neuroscience* 3, 851–860. doi: 10.1016/0306-4522(78)90115-x

Benowitz, L. I., and Popovich, P. G. (2011). Inflammation and axon regeneration. *Curr. Opin. Neurol.* 24, 577–583. doi: 10.1097/WCO.0b013e32834c208d

Berridge, C. W., and Waterhouse, B. D. (2003). The locus coeruleus-noradrenergic system: modulation of behavioral state and state-dependent cognitive processes. *Brain Res. Brain Res. Rev.* 42, 33–84. doi: 10.1016/s0165-0173(03)00143-7

Bradbury, E. J., and Burnside, E. R. (2019). Moving beyond the glial scar for spinal cord repair. *Nat. Comm.* 10:3879. doi: 10.1038/s41467-019-11707-7

Bradbury, E. J., Moon, L. D., Popat, R. J., King, V. R., Bennett, G. S., Patel, P. N., et al. (2002). Chondroitinase ABC promotes functional recovery after spinal cord injury. *Nature* 416, 636–640. doi: 10.1038/416636a

Bradke, F., Fawcett, J. W., and Spira, M. E. (2012). Assembly of a new growth cone after axotomy: the precursor to axon regeneration. *Nat. Rev. Neurosci.* 13, 183–193. doi: 10.1038/nrn3176

Bregman, B. S., Kunkel-Bagden, E., Schnell, L., Dai, H. N., Gao, D., and Schwab, M. E. (1995). Recovery from spinal cord injury mediated by antibodies to neurite growth inhibitors. *Nature* 378, 498–501. doi: 10.1038/378498a0

Bunin, M. A., and Wightman, R. M. (1998). Quantitative evaluation of 5-hydroxytryptamine (serotonin) neuronal release and uptake: an investigation of extrasynaptic transmission. *J. Neurosci.* 18, 4854–4860. doi: 10.1523/JNEUROSCI.18-13-04854.1998

Bunin, M. A., and Wightman, R. M. (1999). Paracrine neurotransmission in the CNS: involvement of 5-HT. *Trends Neurosci.* 22, 377–382. doi: 10.1016/s0166-2236(99)01410-1

Cajal, S. R. (1928). *Degeneration & regeneration of the nervous system*. Oxford: Oxford University Press.

Camand, E., Morel, M. P., Faissner, A., Sotelo, C., and Dusart, I. (2004). Long-term changes in the molecular composition of the glial scar and progressive increase of serotoninergic fibre sprouting after hemisection of the mouse spinal cord. *Eur. J. Neurosci.* 20, 1161–1176. doi: 10.1111/j.1460-9568.2004.03558.x

Canty, A. J., Huang, L., Jackson, J. S., Little, G. E., Knott, G., Maco, B., et al. (2013). In-vivo single neuron axotomy triggers axon regeneration to restore synaptic density in specific cortical circuits. *Nat. Comm.* 4:2038. doi: 10.1038/ncomms3038

Chen, B., Li, Y., Yu, B., Zhang, Z., Brommer, B., Williams, P. R., et al. (2018). Reactivation of Dormant Relay Pathways in Injured Spinal Cord by KCC2 Manipulations. *Cell* 174, 521.e–535.e. doi: 10.1016/j.cell.2018.06.005

Cheriyan, T., Ryan, D. J., Weinreb, J. H., Cheriyan, J., Paul, J. C., Lafage, V., et al. (2014). Spinal cord injury models: a review. *Spinal Cord* 52, 588–595. doi: 10.1038/sc.2014.91

Colgan, L. A., Cavolo, S. L., Commons, K. G., and Levitan, E. S. (2012). Action potential-independent and pharmacologically unique vesicular serotonin release from dendrites. *J. Neurosci.* 32, 15737–15746. doi: 10.1523/JNEUROSCI.0020-12.2012

Cosker, K. E., and Eickholt, B. J. (2007). Phosphoinositide 3-kinase signalling events controlling axonal morphogenesis. *Biochem. Soc. Trans.* 35(Pt 2), 207–210. doi: 10.1042/BST0350207

David, S., and Aguayo, A. J. (1981). Axonal elongation into peripheral nervous system "bridges" after central nervous system injury in adult rats. *Science* 214, 931–933. doi: 10.1126/science.6171034

Davies, S. J., Fitch, M. T., Memberg, S. P., Hall, A. K., Raisman, G., and Silver, J. (1997). Regeneration of adult axons in white matter tracts of the central nervous system. *Nature* 390, 680–683. doi: 10.1038/37776

Davies, S. J., Goucher, D. R., Doller, C., and Silver, J. (1999). Robust regeneration of adult sensory axons in degenerating white matter of the adult rat spinal cord. *J. Neurosci.* 19, 5810–5822. doi: 10.1523/JNEUROSCI.19-14-05810.1999

Domeniconi, M., Cao, Z., Spencer, T., Sivasankaran, R., Wang, K., Nikulina, E., et al. (2002). Myelin-associated glycoprotein interacts with the Nogo66 receptor to inhibit neurite outgrowth. *Neuron* 35, 283–290. doi: 10.1016/s0896-6273(02)00770-5

Dougherty, S. E., Kajstura, T. J., Jin, Y., Chan-Cortés, M. H., Kota, A., and Linden, D. J. (2020). Catecholaminergic axons in the neocortex of adult mice regrow following brain injury. *Exp. Neurol.* 323:113089. doi: 10.1016/j.expneurol.2019.113089

Du, K., Zheng, S., Zhang, Q., Li, S., Gao, X., Wang, J., et al. (2015). Pten Deletion Promotes Regrowth of Corticospinal Tract Axons 1 Year after Spinal Cord Injury. *J. Neurosci.* 35, 9754–9763. doi: 10.1523/JNEUROSCI.3637-14.2015

Duan, X., Qiao, M., Bei, F., Kim, I. J., He, Z., and Sanes, J. R. (2015). Subtype-specific regeneration of retinal ganglion cells following axotomy: effects of osteopontin and mTOR signaling. *Neuron* 85, 1244–1256. doi: 10.1016/j.neuron.2015.02.017

Dulin, J. N., Antunes-Martins, A., Chandran, V., Costigan, M., Lerch, J. K., Willis, D. E., et al. (2015). Transcriptomic Approaches to Neural Repair. *J. Neurosci.* 35, 13860–13867. doi: 10.1523/JNEUROSCI.2599-15.2015

Dyck, S. M., and Karimi-Abdolrezaee, S. (2015). Chondroitin sulfate proteoglycans: key modulators in the developing and pathologic central nervous system. *Exp. Neurol.* 269, 169–187. doi: 10.1016/j.expneurol.2015.04.006

Estera, L. A., Walsh, S. P., Headen, J. A., Williamson, R. E., and Kalinski, A. L. (2021). Neuroinflammation: breaking barriers and bridging gaps. *Neurosci. Res.* 2021:001. doi: 10.1016/j.neures.2021.11.001

Fischer, I., Dulin, J. N., and Lane, M. A. (2020). Transplanting neural progenitor cells to restore connectivity after spinal cord injury. *Nat. Rev. Neurosci.* 21, 366–383. doi: 10.1038/s41583-020-0314-2

Fisher, D., Xing, B., Dill, J., Li, H., Hoang, H. H., Zhao, Z., et al. (2011). Leukocyte common antigen-related phosphatase is a functional receptor for chondroitin sulfate proteoglycan axon growth inhibitors. *J. Neurosci.* 31, 14051–14066. doi: 10.1523/JNEUROSCI.1737-11.2011

Fitch, M. T., and Silver, J. (2008). CNS injury, glial scars, and inflammation: Inhibitory extracellular matrices and regeneration failure. *Exp. Neurol.* 209, 294–301. doi: 10.1016/j.expneurol.2007.05.014

Fournier, A. E., GrandPre, T., and Strittmatter, S. M. (2001). Identification of a receptor mediating Nogo-66 inhibition of axonal regeneration. *Nature* 409, 341–346. doi: 10.1038/35053072

Fritschy, J. M., and Grzanna, R. (1992). Restoration of ascending noradrenergic projections by residual locus coeruleus neurons: compensatory response to neurotoxin-induced cell death in the adult rat brain. *J. Comp. Neurol.* 321, 421–441. doi: 10.1002/cne.903210309

Fuller, R. W. (1992). Effects of p-chloroamphetamine on brain serotonin neurons. *Neurochem. Res.* 17, 449–456. doi: 10.1007/BF00969891

Fuxe, K., Dahlström, A., Höistad, M., Marcellino, D., Jansson, A., Rivera, A., et al. (2007). From the Golgi-Cajal mapping to the transmitter-based characterization of the neuronal networks leading to two modes of brain communication: wiring and volume transmission. *Brain Res. Rev.* 55, 17–54. doi: 10.1016/j.brainresrev.2007.02.009

Gao, Y., Deng, K., Hou, J., Bryson, J. B., Barco, A., Nikulina, E., et al. (2004). Activated CREB is sufficient to overcome inhibitors in myelin and promote spinal axon regeneration in vivo. *Neuron* 44, 609–621. doi: 10.1016/j.neuron.2004.10.030

Gaudet, A. D., and Fonken, L. K. (2018). Glial Cells Shape Pathology and Repair After Spinal Cord Injury. *Neurotherapeutics* 15, 554–577. doi: 10.1007/s13311-018-0630-7

Gaudet, A. D., Mandrekar-Colucci, S., Hall, J. C., Sweet, D. R., Schmitt, P. J., Xu, X., et al. (2016). miR-155 Deletion in Mice Overcomes Neuron-Intrinsic and Neuron-Extrinsic Barriers to Spinal Cord Repair. *J. Neurosci.* 36, 8516–8532. doi: 10.1523/JNEUROSCI.0735-16.2016

Geoffroy, C. G., Hilton, B. J., Tetzlaff, W., and Zheng, B. (2016). Evidence for an Age-Dependent Decline in Axon Regeneration in the Adult Mammalian Central Nervous System. *Cell Rep.* 15, 238–246. doi: 10.1016/j.celrep.2016.03.028

Geoffroy, C. G., Lorenzana, A. O., Kwan, J. P., Lin, K., Ghassemi, O., Ma, A., et al. (2015). Effects of PTEN and Nogo Codeletion on Corticospinal Axon Sprouting and Regeneration in Mice. *J. Neurosci.* 35, 6413–6428. doi: 10.1523/JNEUROSCI.4013-14.2015

Guénard, V., Kleitman, N., Morrissey, T. K., Bunge, R. P., and Aebischer, P. (1992). Syngeneic Schwann cells derived from adult nerves seeded in semipermeable guidance channels enhance peripheral nerve regeneration. *J. Neurosci.* 12, 3310–3320. doi: 10.1523/JNEUROSCI.12-09-03310.1992

Guth, L. (1975). History of central nervous system regeneration research. *Exp. Neurol.* 48(3 pt. 2), 3–15. doi: 10.1016/0014-4886(75)90168-5

Halpin, L. E., Collins, S. A., and Yamamoto, B. K. (2014). Neurotoxicity of methamphetamine and 3,4-methylenedioxymethamphetamine. *Life Sci.* 97, 37–44. doi: 10.1016/j.lfs.2013.07.014

Hannila, S. S., and Filbin, M. T. (2008). The role of cyclic AMP signaling in promoting axonal regeneration after spinal cord injury. *Exp. Neurol.* 209, 321–332. doi: 10.1016/j.expneurol.2007.06.020

Harrison, E. B., Emanuel, K., Lamberty, B. G., Morsey, B. M., Li, M., Kelso, M. L., et al. (2017). Induction of miR-155 after Brain Injury Promotes Type 1 Interferon and has a Neuroprotective Effect. *Front. Mole. Neurosci.* 10:228. doi: 10.3389/fnmol.2017.00228

Hawthorne, A. L., Hu, H., Kundu, B., Steinmetz, M. P., Wylie, C. J., Deneris, E. S., et al. (2011). The unusual response of serotonergic neurons after CNS Injury: lack of axonal dieback and enhanced sprouting within the inhibitory environment of the glial scar. *J. Neurosci.* 31, 5605–5616. doi: 10.1523/JNEUROSCI.6663-10.2011

Hayashi, Y., Jacob-Vadakot, S., Dugan, E. A., McBride, S., Olexa, R., Simansky, K., et al. (2010). 5-HT precursor loading, but not 5-HT receptor agonists, increases motor function after spinal cord contusion in adult rats. *Exp. Neurol.* 221, 68–78. doi: 10.1016/j.expneurol.2009.10.003

Herrmann, J. E., Imura, T., Song, B., Qi, J., Ao, Y., Nguyen, T. K., et al. (2008). STAT3 is a critical regulator of astrogliosis and scar formation after spinal cord injury. *J. Neurosci.* 28, 7231–7243. doi: 10.1523/JNEUROSCI.1709-08.2008

Holmes, G. M., Van Meter, M. J., Beattie, M. S., and Bresnahan, J. C. (2005). Serotonergic fiber sprouting to external anal sphincter motoneurons after spinal cord contusion. *Exp. Neurol.* 193, 29–42. doi: 10.1016/j.expneurol.2005.01.002

Huang, L., Fu, C., Xiong, F., He, C., and Wei, Q. (2021). Stem Cell Therapy for Spinal Cord Injury. *Cell Transpl.* 30:963689721989266. doi: 10.1177/0963689721989266

Huebner, E. A., and Strittmatter, S. M. (2009). Axon regeneration in the peripheral and central nervous systems. *Results Prob. Cell Diff.* 48, 339–351. doi: 10.1007/400_2009_19

Inman, D. M., and Steward, O. (2003). Ascending sensory, but not other long-tract axons, regenerate into the connective tissue matrix that forms at the site of a spinal cord injury in mice. *J. Comp. Neurol.* 462, 431–449. doi: 10.1002/cne.10768

Jacobs, B. L., and Azmitia, E. C. (1992). Structure and function of the brain serotonin system. *Physiol. Rev.* 72, 165–229. doi: 10.1152/physrev.1992.72.1.165

Jenkins, R., and Hunt, S. P. (1991). Long-term increase in the levels of c-jun mRNA and jun protein-like immunoreactivity in motor and sensory neurons following axon damage. *Neurosci. Lett.* 129, 107–110. doi: 10.1016/0304-3940(91)90731-8

Jin, Y., Dougherty, S. E., Wood, K., Sun, L., Cudmore, R. H., Abdalla, A., et al. (2016). Regrowth of Serotonin Axons in the Adult Mouse Brain Following Injury. *Neuron* 91, 748–762. doi: 10.1016/j.neuron.2016.07.024

Jin, Y., Fischer, I., Tessler, A., and Houle, J. D. (2002). Transplants of fibroblasts genetically modified to express BDNF promote axonal regeneration from supraspinal neurons following chronic spinal cord injury. *Exp. Neurol.* 177, 265–275. doi: 10.1006/exnr.2002.7980

Joyal, J. S., Sitaras, N., Binet, F., Rivera, J. C., Stahl, A., Zaniolo, K., et al. (2011). Ischemic neurons prevent vascular regeneration of neural tissue by secreting semaphorin 3A. *Blood* 117, 6024–6035. doi: 10.1182/blood-2010-10-311589

Kadoya, K., Lu, P., Nguyen, K., Lee-Kubli, C., Kumamaru, H., Yao, L., et al. (2016). Spinal cord reconstitution with homologous neural grafts enables robust corticospinal regeneration. *Nat. Med.* 22, 479–487. doi: 10.1038/nm.4066

Kajstura, T. J., Dougherty, S. E., and Linden, D. J. (2018). Serotonin axons in the neocortex of the adult female mouse regrow after traumatic brain injury. *J. Neurosci. Res.* 96, 512–526. doi: 10.1002/jnr.24059

Kaushalya, S. K., Nag, S., Balaji, J., and Maiti, S. (2008). Serotonin multiphoton imaging and relevant spectral data. *Proc. Spie.* 6860:68601C.

Kigerl, K. A., Gensel, J. C., Ankeny, D. P., Alexander, J. K., Donnelly, D. J., and Popovich, P. G. (2009). Identification of two distinct macrophage subsets with divergent effects causing either neurotoxicity or regeneration in the injured mouse spinal cord. *J. Neurosci.* 29, 13435–13444. doi: 10.1523/JNEUROSCI.3257-09.2009

Knott, E. P., Assi, M., and Pearse, D. D. (2014). Cyclic AMP signaling: a molecular determinant of peripheral nerve regeneration. *Biomed. Res. Int*. 2014:651625. doi: 10.1155/2014/651625

Kromer, L. F., and Cornbrooks, C. J. (1985). Transplants of Schwann cell cultures promote axonal regeneration in the adult mammalian brain. *Proc. Natl. Acad. Sci. U S A* 82, 6330–6334. doi: 10.1073/pnas.82.18.6330

Kubota, Y., Morita, T., Kusakabe, M., Sakakura, T., and Ito, K. (1999). Spatial and temporal changes in chondroitin sulfate distribution in the sclerotome play an essential role in the formation of migration patterns of mouse neural crest cells. *Dev. Dyn.* 214, 55–65. doi: 10.1002/(SICI)1097-0177(199901)214:1<55::AID-DVDY6<3.0.CO;2-E

Kwiecien, J. M. (2022). Barriers to axonal regeneration after spinal cord injury: a current perspective. *Neur. Regen. Res.* 17, 85–86. doi: 10.4103/1673-5374.314299

Lee, J. K., Chow, R., Xie, F., Chow, S. Y., Tolentino, K. E., and Zheng, B. (2010). Combined genetic attenuation of myelin and semaphorin-mediated growth inhibition is insufficient to promote serotonergic axon regeneration. *J. Neurosci.* 30, 10899–10904. doi: 10.1523/JNEUROSCI.2269-10.2010

Lee, Y. S., Lin, C. Y., Jiang, H. H., Depaul, M., Lin, V. W., and Silver, J. (2013). Nerve regeneration restores supraspinal control of bladder function after complete spinal cord injury. *J. Neurosci.* 33, 10591–10606. doi: 10.1523/JNEUROSCI.1116-12.2013

Leibinger, M., Andreadaki, A., Gobrecht, P., Levin, E., Diekmann, H., and Fischer, D. (2016). Boosting Central Nervous System Axon Regeneration by Circumventing Limitations of Natural Cytokine Signaling. *Mole. Ther.* 24, 1712–1725. doi: 10.1038/mt.2016.102

Lemons, M. L., Howland, D. R., and Anderson, D. K. (1999). Chondroitin sulfate proteoglycan immunoreactivity increases following spinal cord injury and transplantation. *Exp. Neurol.* 160, 51–65. doi: 10.1006/exnr.1999.7184

Lerch, J. K., Kuo, F., Motti, D., Morris, R., Bixby, J. L., and Lemmon, V. P. (2012). Isoform diversity and regulation in peripheral and central neurons revealed through RNA-Seq. *PLoS One* 7:e30417. doi: 10.1371/journal.pone.0030417

Levin, B. E. (1983). Alterations of norepinephrine metabolism in rat locus coeruleus neurons in response to axonal injury. *Brain Res.* 289, 205–214. doi: 10.1016/0006-8993(83)90021-5

Liu, B. P., Fournier, A., GrandPré, T., and Strittmatter, S. M. (2002). Myelin-associated glycoprotein as a functional ligand for the Nogo-66 receptor. *Science* 297, 1190–1193. doi: 10.1126/science.1073031

Liu, K., Lu, Y., Lee, J. K., Samara, R., Willenberg, R., Sears-Kraxberger, I., et al. (2010). PTEN deletion enhances the regenerative ability of adult corticospinal neurons. *Nat. Neurosci.* 13, 1075–1081. doi: 10.1038/nn.2603

Liu, Y., Kim, D., Himes, B. T., Chow, S. Y., Schallert, T., Murray, M., et al. (1999). Transplants of fibroblasts genetically modified to express BDNF promote regeneration of adult rat rubrospinal axons and recovery of forelimb function. *J. Neurosci.* 19, 4370–4387. doi: 10.1523/JNEUROSCI.19-11-04370.1999

Liu, Y., Wang, X., Li, W., Zhang, Q., Li, Y., Zhang, Z., et al. (2017). A Sensitized IGF1 Treatment Restores Corticospinal Axon-Dependent Functions. *Neuron* 95, 817.e–833.e. doi: 10.1016/j.neuron.2017.07.037

Lu, P., Blesch, A., Graham, L., Wang, Y., Samara, R., Banos, K., et al. (2012). Motor axonal regeneration after partial and complete spinal cord transection. *J. Neurosci.* 32, 8208–8218. doi: 10.1523/JNEUROSCI.0308-12.2012

Ma, T. C., Barco, A., Ratan, R. R., and Willis, D. E. (2014). cAMP-responsive element-binding protein (CREB) and cAMP co-regulate activator protein 1 (AP1)-dependent regeneration-associated gene expression and neurite growth. *J. Biol. Chem.* 289, 32914–32925. doi: 10.1074/jbc.M114.582460

Ma, T. C., and Willis, D. E. (2015). What makes a RAG regeneration associated? *Front. Mole. Neurosci.* 8:43. doi: 10.3389/fnmol.2015.00043

Mamounas, L. A., Altar, C. A., Blue, M. E., Kaplan, D. R., Tessarollo, L., and Lyons, W. E. (2000). BDNF promotes the regenerative sprouting, but not survival, of injured serotonergic axons in the adult rat brain. *J. Neurosci.* 20, 771–782. doi: 10.1523/JNEUROSCI.20-02-00771.2000

Mecollari, V., Nieuwenhuis, B., and Verhaagen, J. (2014). A perspective on the role of class III semaphorin signaling in central nervous system trauma. *Front. Cell. Neurosci.* 8:328. doi: 10.3389/fncel.2014.00328

Ménager, C., Arimura, N., Fukata, Y., and Kaibuchi, K. (2004). PIP3 is involved in neuronal polarization and axon formation. *J. Neurochem.* 89, 109–118. doi: 10.1046/j.1471-4159.2004.02302.x

Menorca, R. M., Fussell, T. S., and Elfar, J. C. (2013). Nerve physiology: mechanisms of injury and recovery. *Hand Clin.* 29, 317–330. doi: 10.1016/j.hcl.2013.04.002

Mi, S., Lee, X., Shao, Z., Thill, G., Ji, B., Relton, J., et al. (2004). LINGO-1 is a component of the Nogo-66 receptor/p75 signaling complex. *Nat. Neurosci.* 7, 221–228. doi: 10.1038/nn1188

Molliver, M. E., Berger, U. V., Mamounas, L. A., Molliver, D. C., O'Hearn, E., and Wilson, M. A. (1990). Neurotoxicity of MDMA and related compounds: anatomic studies. *Ann. N Y Acad. Sci.* 600, 649–664. doi: 10.1111/j.1749-6632.1990.tb16916.x

Monnier, P. P., Sierra, A., Schwab, J. M., Henke-Fahle, S., and Mueller, B. K. (2003). The Rho/ROCK pathway mediates neurite growth-inhibitory activity associated with the chondroitin sulfate proteoglycans of the CNS glial scar. *Mole. Cell. Neurosci.* 22, 319–330. doi: 10.1016/s1044-7431(02)00035-0

Moore, D. L., Blackmore, M. G., Hu, Y., Kaestner, K. H., Bixby, J. L., Lemmon, V. P., et al. (2009). KLF family members regulate intrinsic axon regeneration ability. *Science* 326, 298–301. doi: 10.1126/science.1175737

Nadeau, S., Hein, P., Fernandes, K. J., Peterson, A. C., and Miller, F. D. (2005). A transcriptional role for C/EBP beta in the neuronal response to axonal injury. *Mole. Cell. Neurosci.* 29, 525–535. doi: 10.1016/j.mcn.2005.04.004

Nakai, K., Niiyama, K., Kasamatsu, T., Naka, Y., Itakura, T., and Komai, N. (1994). Regeneration of norepinephrine-containing fibers in occipital cortex of adult cats. *Brain Res. Bull.* 35, 409–412. doi: 10.1016/0361-9230(94)90152-x

Neumann, S., Bradke, F., Tessier-Lavigne, M., and Basbaum, A. I. (2002). Regeneration of sensory axons within the injured spinal cord induced by intraganglionic cAMP elevation. *Neuron* 34, 885–893. doi: 10.1016/s0896-6273(02)00702-x

Nguyen, Q. T., Sanes, J. R., and Lichtman, J. W. (2002). Pre-existing pathways promote precise projection patterns. *Nat. Neurosci.* 5, 861–867. doi: 10.1038/nn905

Nieuwenhuis, B., and Eva, R. (2022). Promoting axon regeneration in the central nervous system by increasing PI3-kinase signaling. *Neur. Regenerat. Res.* 17, 1172–1182. doi: 10.4103/1673-5374.327324

O'Hearn, E., Battaglia, G., De Souza, E. B., Kuhar, M. J., and Molliver, M. E. (1988). Methylenedioxyamphetamine (MDA) and methylenedioxymethamphetamine (MDMA) cause selective ablation of serotonergic axon terminals in forebrain: immunocytochemical evidence for neurotoxicity. *J. Neurosci.* 8, 2788–2803. doi: 10.1523/JNEUROSCI.08-08-02788.1988

Oinuma, I., Ishikawa, Y., Katoh, H., and Negishi, M. (2004). The Semaphorin 4D receptor Plexin-B1 is a GTPase activating protein for R-Ras. *Science* 305, 862–865. doi: 10.1126/science.1097545

Okada, S., Nakamura, M., Katoh, H., Miyao, T., Shimazaki, T., Ishii, K., et al. (2006). Conditional ablation of Stat3 or Socs3 discloses a dual role for reactive astrocytes after spinal cord injury. *Nat. Med.* 12, 829–834. doi: 10.1038/nm1425

Okaty, B. W., Sturrock, N., Escobedo Lozoya, Y., Chang, Y., Senft, R. A., Lyon, K. A., et al. (2020). A single-cell transcriptomic and anatomic atlas of mouse dorsal raphe *Pet1* neurons. *eLife* 9:e55523. doi: 10.7554/eLife.55523

Okuyama, N., Kiryu-Seo, S., and Kiyama, H. (2007). Altered expression of Smad family members in injured motor neurons of rat. *Brain Res.* 1132, 36–41. doi: 10.1016/j.brainres.2006.11.019

Orr, M. B., and Gensel, J. C. (2018). Spinal Cord Injury Scarring and Inflammation: Therapies Targeting Glial and Inflammatory Responses. *Neurotherapeutics* 15, 541–553. doi: 10.1007/s13311-018-0631-6

Papadopoulos, G. C., and Parnavelas, J. G. (1991). Monoamine systems in the cerebral cortex: evidence for anatomical specificity. *Prog. Neurob.* 36, 195–200. doi: 10.1016/0301-0082(91)90030-5

Park, K. K., Liu, K., Hu, Y., Smith, P. D., Wang, C., Cai, B., et al. (2008). Promoting axon regeneration in the adult CNS by modulation of the PTEN/mTOR pathway. *Science* 322, 963–966. doi: 10.1126/science.1161566

Parr, A. M., Tator, C. H., and Keating, A. (2007). Bone marrow-derived mesenchymal stromal cells for the repair of central nervous system injury. *Bone Marr. Transpl.* 40, 609–619. doi: 10.1038/sj.bmt.1705757

Pasterkamp, R. J., Giger, R. J., Ruitenberg, M. J., Holtmaat, A. J., De Wit, J., De Winter, F., et al. (1999). Expression of the gene encoding the chemorepellent semaphorin III is induced in the fibroblast component of neural scar tissue formed following injuries of adult but not neonatal CNS. *Mole. Cell. Neurosci.* 13, 143–166. doi: 10.1006/mcne.1999.0738

Pasterkamp, R. J., and Verhaagen, J. (2006). Semaphorins in axon regeneration: developmental guidance molecules gone wrong? *Philosoph. Trans. R. Soc. Lond. Ser. B Biol. Sci.* 361, 1499–1511. doi: 10.1098/rstb.2006.1892

Pickel, V. M., Krebs, H., and Bloom, F. E. (1973). Proliferation of norepinephrine-containing axons in rat cerebellar cortex after peduncle lesions. *Brain Res.* 59, 169–179. doi: 10.1016/0006-8993(73)90258-8

Poplawski, G., Kawaguchi, R., Van Niekerk, E., Lu, P., Mehta, N., Canete, P., et al. (2020). Injured adult neurons regress to an embryonic transcriptional growth state. *Nature* 581, 77–82. doi: 10.1038/s41586-020-2200-5

Qiu, J., Cai, D., Dai, H., McAtee, M., Hoffman, P. N., Bregman, B. S., et al. (2002). Spinal axon regeneration induced by elevation of cyclic AMP. *Neuron* 34, 895–903. doi: 10.1016/s0896-6273(02)00730-4

Renthal, W., Tochitsky, I., Yang, L., Cheng, Y. C., Li, E., Kawaguchi, R., et al. (2020). Transcriptional Reprogramming of Distinct Peripheral Sensory Neuron Subtypes after Axonal Injury. *Neuron* 108, 128.e–144.e. doi: 10.1016/j.neuron.2020.07.026

Richardson, P. M., Issa, V. M., and Aguayo, A. J. (1984). Regeneration of long spinal axons in the rat. *J. Neurocyt.* 13, 165–182. doi: 10.1007/BF01148324

Richardson, P. M., McGuinness, U. M., and Aguayo, A. J. (1980). Axons from CNS neurons regenerate into PNS grafts. *Nature* 284, 264–265. doi: 10.1038/284264a0

Rosenzweig, E. S., Salegio, E. A., Liang, J. J., Weber, J. L., Weinholtz, C. A., Brock, J. H., et al. (2019). Chondroitinase improves anatomical and functional outcomes after primate spinal cord injury. *Nat. Neurosci.* 22, 1269–1275. doi: 10.1038/s41593-019-0424-1

Sami, A., Selzer, M. E., and Li, S. (2020). Advances in the Signaling Pathways Downstream of Glial-Scar Axon Growth Inhibitors. *Front. Cell. Neurosci.* 14:174. doi: 10.3389/fncel.2020.00174

Sara, S. J. (2009). The locus coeruleus and noradrenergic modulation of cognition. *Nat. Rev. Neurosci.* 10, 211–223. doi: 10.1038/nrn2573

Schwab, M. E. (2004). Nogo and axon regeneration. *Curr. Opin. Neurob.* 14, 118–124. doi: 10.1016/j.conb.2004.01.004

Schwab, M. E. (2010). Functions of Nogo proteins and their receptors in the nervous system. *Nat. Rev.* 11, 799–811. doi: 10.1038/nrn2936

Schwaiger, F. W., Hager, G., Schmitt, A. B., Horvat, A., Hager, G., Streif, R., et al. (2000). Peripheral but not central axotomy induces changes in Janus kinases (JAK) and signal transducers and activators of transcription (STAT). *Eur. J. Neurosci.* 12, 1165–1176. doi: 10.1046/j.1460-9568.2000.00005.x

Séguéla, P., Watkins, K. C., and Descarries, L. (1989). Ultrastructural relationships of serotonin axon terminals in the cerebral cortex of the adult rat. *J. Comp. Neurol.* 289, 129–142. doi: 10.1002/cne.902890111

Séguéla, P., Watkins, K. C., Geffard, M., and Descarries, L. (1990). Noradrenaline axon terminals in adult rat neocortex: an immunocytochemical analysis in serial thin sections. *Neuroscience* 35, 249–264. doi: 10.1016/0306-4522(90)90079-j

Shen, Y., Tenney, A. P., Busch, S. A., Horn, K. P., Cuascut, F. X., Liu, K., et al. (2009). PTPsigma is a receptor for chondroitin sulfate proteoglycan, an inhibitor of neural regeneration. *Science* 326, 592–596. doi: 10.1126/science.1178310

Shnitko, T. A., and Robinson, D. L. (2014). Anatomical and pharmacological characterization of catecholamine transients in the medial prefrontal cortex evoked by ventral tegmental area stimulation. *Synapse* 68, 131–143. doi: 10.1002/syn.21723

Silver, J., and Miller, J. H. (2004). Regeneration beyond the glial scar. *Nat. Rev. Neurosci.* 5, 146–156. doi: 10.1038/nrn1326

Simonen, M., Pedersen, V., Weinmann, O., Schnell, L., Buss, A., Ledermann, B., et al. (2003). Systemic deletion of the myelin-associated outgrowth inhibitor Nogo-A improves regenerative and plastic responses after spinal cord injury. *Neuron* 38, 201–211. doi: 10.1016/s0896-6273(03)00226-5

Sulaiman, W., and Gordon, T. (2013). Neurobiology of peripheral nerve injury, regeneration, and functional recovery: from bench top research to bedside application. *Ochsner J.* 13, 100–108.

Tsujino, H., Kondo, E., Fukuoka, T., Dai, Y., Tokunaga, A., Miki, K., et al. (2000). Activating transcription factor 3 (ATF3) induction by axotomy in sensory and motoneurons: a novel neuronal marker of nerve injury. *Mole. Cell. Neurosci.* 15, 170–182. doi: 10.1006/mcne.1999.0814

Tuszynski, M. H., and Steward, O. (2012). Concepts and methods for the study of axonal regeneration in the CNS. *Neuron* 74, 777–791. doi: 10.1016/j.neuron.2012.05.006

Ughrin, Y. M., Chen, Z. J., and Levine, J. M. (2003). Multiple regions of the NG2 proteoglycan inhibit neurite growth and induce growth cone collapse. *J. Neurosci.* 23, 175–186. doi: 10.1523/JNEUROSCI.23-01-00175.2003

Umbriaco, D., Garcia, S., Beaulieu, C., and Descarries, L. (1995). Relational features of acetylcholine, noradrenaline, serotonin and GABA axon terminals in the stratum radiatum of adult rat hippocampus (CA1). *Hippocampus* 5, 605–620. doi: 10.1002/hipo.450050611

Vavrek, R., Pearse, D. D., and Fouad, K. (2007). Neuronal populations capable of regeneration following a combined treatment in rats with spinal cord transection. *J. Neurotr.* 24, 1667–1673. doi: 10.1089/neu.2007.0290

Wang, K. C., Koprivica, V., Kim, J. A., Sivasankaran, R., Guo, Y., Neve, R. L., et al. (2002). Oligodendrocyte-myelin glycoprotein is a Nogo receptor ligand that inhibits neurite outgrowth. *Nature* 417, 941–944. doi: 10.1038/nature00867

Wang, T., Li, B., Wang, Z., Yuan, X., Chen, C., Zhang, Y., et al. (2019). miR-155-5p Promotes Dorsal Root Ganglion Neuron Axonal Growth in an Inhibitory Microenvironment via the cAMP/PKA Pathway. *Intern. J. Biol. Sci.* 15, 1557–1570. doi: 10.7150/ijbs.31904

Wang, X., Zhou, T., Maynard, G. D., Terse, P. S., Cafferty, W. B., Kocsis, J. D., et al. (2020). Nogo receptor decoy promotes recovery and corticospinal growth in non-human primate spinal cord injury. *Brain* 143, 1697–1713. doi: 10.1093/brain/awaa116

Wilson, M. A., and Molliver, M. E. (1994). Microglial response to degeneration of serotonergic axon terminals. *Glia* 11, 18–34. doi: 10.1002/glia.440110105

Witzel, C., Rohde, C., and Brushart, T. M. (2005). Pathway sampling by regenerating peripheral axons. *J. Comp. Neurol.* 485, 183–190. doi: 10.1002/cne.20436

Wyler, S. C., Spencer, W. C., Green, N. H., Rood, B. D., Crawford, L., Craige, C., et al. (2016). Pet-1 Switches Transcriptional Targets Postnatally to Regulate Maturation of Serotonin Neuron Excitability. *J. Neurosci.* 36, 1758–1774. doi: 10.1523/JNEUROSCI.3798-15.2016

Xu, X. M., Guénard, V., Kleitman, N., Aebischer, P., and Bunge, M. B. (1995). A combination of BDNF and NT-3 promotes supraspinal axonal regeneration into Schwann cell grafts in adult rat thoracic spinal cord. *Exp. Neurol.* 134, 261–272. doi: 10.1006/exnr.1995.1056

Yiu, G., and He, Z. (2006). Glial inhibition of CNS axon regeneration. *Nat. Rev. Neurosci.* 7, 617–627. doi: 10.1038/nrn1956

Zhou, F. Q., Zhou, J., Dedhar, S., Wu, Y. H., and Snider, W. D. (2004). NGF-induced axon growth is mediated by localized inactivation of GSK-3beta and functions of the microtubule plus end binding protein APC. *Neuron* 42, 897–912. doi: 10.1016/j.neuron.2004.05.011

Zou, H., Ho, C., Wong, K., and Tessier-Lavigne, M. (2009). Axotomy-induced Smad1 activation promotes axonal growth in adult sensory neurons. *J. Neurosci.* 29, 7116–7123. doi: 10.1523/JNEUROSCI.5397-08.2009

Zukor, K., Belin, S., Wang, C., Keelan, N., Wang, X., and He, Z. (2013). Short hairpin RNA against PTEN enhances regenerative growth of corticospinal tract axons after spinal cord injury. *J. Neurosci.* 33, 15350–15361. doi: 10.1523/JNEUROSCI.2510-13.2013

Conflict of Interest: The authors declare that the research was conducted in the absence of any commercial or financial relationships that could be construed as a potential conflict of interest.

Publisher's Note: All claims expressed in this article are solely those of the authors and do not necessarily represent those of their affiliated organizations, or those of the publisher, the editors and the reviewers. Any product that may be evaluated in this article, or claim that may be made by its manufacturer, is not guaranteed or endorsed by the publisher.

Copyright © 2022 Cooke, Janowitz and Dougherty. This is an open-access article distributed under the terms of the Creative Commons Attribution License (CC BY). The use, distribution or reproduction in other forums is permitted, provided the original author(s) and the copyright owner(s) are credited and that the original publication in this journal is cited, in accordance with accepted academic practice. No use, distribution or reproduction is permitted which does not comply with these terms.

frontiers | Frontiers in Cellular Neuroscience

REVIEW
published: 28 April 2022
doi: 10.3389/fncel.2022.876342

Targeting C–C Chemokine Receptor 5: Key to Opening the Neurorehabilitation Window After Ischemic Stroke

*Yi-Qi Feng, Zhen-Zhen Xu, Yan-Ting Wang, Yue Xiong, Wanli Xie, Yu-Yao He, Lu Chen, Guo-Yang Liu, Xia Li, Jie Liu and Qingping Wu**

Department of Anesthesiology, Union Hospital, Tongji Medical College, Huazhong University of Science and Technology, Wuhan, China

Stroke is the world's second major cause of adult death and disability, resulting in the destruction of brain tissue and long-term neurological impairment; induction of neuronal plasticity can promote recovery after stroke. C–C chemokine receptor 5 (CCR5) can direct leukocyte migration and localization and is a co-receptor that can mediate human immunodeficiency virus (HIV) entry into cells. Its role in HIV infection and immune response has been extensively studied. Furthermore, CCR5 is widely expressed in the central nervous system (CNS), is engaged in various physiological activities such as brain development, neuronal differentiation, communication, survival, and learning and memory capabilities, and is also involved in the development of numerous neurological diseases. CCR5 is differentially upregulated in neurons after stroke, and the inhibition of CCR5 in specific regions of the brain promotes motor and cognitive recovery. The mechanism by which CCR5 acts as a therapeutic target to promote neurorehabilitation after stroke has rarely been systematically reported yet. Thus, this review aims to discuss the function of CCR5 in the CNS and the mechanism of its effect on post-stroke recovery by regulating neuroplasticity and the inflammatory response to provide an effective basis for clinical rehabilitation after stroke.

Keywords: stroke, CCR5, chemokines, immune response, neuronal plasticity, neurorehabilitation

OPEN ACCESS

Edited by:
Marc J. Ruitenberg, The University of Queensland, Australia

Reviewed by:
Shan Huang, University of California, Los Angeles, United States
Renée Jade Turner, University of Adelaide, Australia

***Correspondence:**
Qingping Wu
wqp1968@163.com

Specialty section:
This article was submitted to Cellular Neuropathology, a section of the journal Frontiers in Cellular Neuroscience

Received: *16 February 2022*
Accepted: *05 April 2022*
Published: *28 April 2022*

Citation:
Feng Y-Q, Xu Z-Z, Wang Y-T, Xiong Y, Xie WL, He Y-Y, Chen L, Liu G-Y, Li X, Liu J and Wu QP (2022) Targeting C–C Chemokine Receptor 5: Key to Opening the Neurorehabilitation Window After Ischemic Stroke. Front. Cell. Neurosci. 16:876342. doi: 10.3389/fncel.2022.876342

INTRODUCTION

The limited recovery following acute brain damage leading to stroke is among the most common causes of adult physical disability worldwide (Benjamin et al., 2019), with ischemic stroke accounting for 71% of all strokes (Collaborators et al., 2018). Most ischemic strokes are thromboembolic in origin, and regions without adequate blood flow lead to energy depletion, metabolic disorders, and abnormal electrical activity, which become irreversibly injured and contribute to the clinical deficit over time (Campbell et al., 2019). Progress has been made in facilitating individuals' recovery from ischemic stroke following advancements in pharmaceutical mechanic and thrombolysis (Paul and Candelario-Jalil, 2021). However, because of the limited window for reperfusion therapies and irreversible neuron death, approximately 50–60% of patients still suffer from motor impairments after successful endovascular clot removal (Schaechter, 2004; Leng and Xiong, 2019). Hence, apart from therapies that promote cerebral blood vessel reperfusion, medical treatments developed to enhance recovery after

stroke have wide prospects for clinical application. The process of neuronal recovery in brain traumas, including stroke, includes upregulation of growth-promoting genes (Cramer and Procaccio, 2012), axonal sprouting (Li et al., 2010), and alterations in tonic gamma-aminobutyric acid and α-amino-3-hydroxy-5methyl-4-isoxazole propionic acid (AMPA) receptor signaling (Clarkson et al., 2010, 2011). Accumulating evidence indicates that enhancing plasticity processes in brain circuits plays a significant role in neurorehabilitation therapies after stroke (Joy and Carmichael, 2021).

C–C chemokine receptor 5 (CCR5) is a seven-membrane G protein-coupled receptor (GPCR) composed of 352 amino acids. CCR5 contains multiple ligands, including CCL3 (MIP-1α), CCL4 (MIP-1β), CCL5 (RANTES), CCL8 (MCP-2), CCL3L1 (LD78), and CCL11 (eotaxin; Chen et al., 2018; Jiao et al., 2019). Regulation of leukocyte migration is tightly linked to CCR5 expression and activation. In 1996, it was shown that CCR5 is key co-receptor that allows human immunodeficiency virus (HIV) to enter target cells (Alkhatib et al., 1996). Chemokine receptors, furthermore, play a role in a wide range of physiological and pathological processes in the central nervous system (CNS), as demonstrated by mounting evidence (Babcock et al., 2003; Rostène et al., 2007). In 2019, CCR5 was shown to be an effective therapeutic target for recovery from traumatic brain injury (TBI) and stroke, and became the first reported gene associated with enhanced recovery in human stroke (Joy et al., 2019). However, the mechanism by which CCR5 acts as a therapeutic target to promote neurorehabilitation after stroke has rarely been systematically reported. We have consequently reviewed the current knowledge of CCR5 distribution and function, as well as its mechanism and research development, as a target for ischemic stroke rehabilitation.

C–C CHEMOKINE RECEPTOR 5 IN THE BODY: DISTRIBUTION AND FUNCTIONS

C–C Chemokine Receptor 5 Expression and Localization

Chemokine receptors are critical for immune cell recruitment and development and play important roles in a wide range of inflammatory responses, both protective and destructive. CCR5 expression has been demonstrated in various immune cells, including dendritic cells, NK cells, macrophages, T-lymphocytes, and B-lymphocytes (Griffith et al., 2014; Hughes and Nibbs, 2018). In addition, microglia, astrocytes, and neurons in the CNS also express CCR5 (Klein et al., 1999; Mennicken et al., 2002; Westmoreland et al., 2002; Flynn et al., 2003). The presence of CCR5 in vascular smooth muscle cells and capillary endothelial cells has also been reported, but its function is still poorly defined (Rottman et al., 1997; Murphy et al., 2000; Jones et al., 2011). **Table 1** shows the expression of CCR5 gene in cells.

Abbreviations: AC, adenylyl cyclase; AD, Alzheimer's disease; AMPA, α-amino-3-hydroxy-5methyl-4-isoxazole propionic acid; BBB, blood-brain barrier; BDNF, brain-derived neurotrophic factor; cAMP, cyclic adenosine monophosphate; CCR5, C–C chemokine receptor 5; CNS, central nervous system; CREB, cAMP-response-element binding protein; DAG, diacylglycerol; DC, dendritic cells; DLK, dual-leucine zipper kinase; ERK1/2, extracellular signal-regulated kinase; GABA, gamma-aminobutyric acid; GPCR, G protein-coupled receptor; HIV, human immunodeficiency virus; ICAM-1, intercellular adhesion molecule-1; IP3, inositol 1,4,5-trisphosphate; JAK2, Janus kinases; JNK, C-Jun N-terminal kinases; LPS, lipopolysaccharide; MAP, mitogen-activated protein; MAPK, mitogen-activated protein kinase; MMPs, matrix metalloproteinases; NMDAR-1, N-Methyl D-Aspartate Receptor 1; NK, natural killer cell; pCREB, phosphorylated cAMP-response-element binding protein; PIP2, phosphatidylinositol 4,5-bisphosphate; PMCA, plasma membrane Ca^{2+}-ATPase; PI-3K, phosphatidylinositol 3-kinases; PKB, protein kinase B; PLC, phospholipase C; PYK2, proline-rich tyrosine kinase 2; STAT, signal transducer and activator of transcription; TBI, traumatic brain injury; VCAM-1, vascular cell adhesion molecule 1.

Signaling Pathways in C–C Chemokine Receptor 5 Functions

C–C chemokine receptor 5 belongs to the GPCR family and, contains multiple ligands, including CCL3, CCL4, and CCL5. Other inflammatory chemokines that act as CCR5 agonists include CCL8, CCL3L1, and CCL11 (Zlotnik and Yoshie, 2012; Bredesen, 2014; Brelot and Chakrabarti, 2018). Binding of ligands to CCR5 leads to the dissociation of the G protein heterotrimer into α and βγ subunits, and the α subunits include two types: $G\alpha_q$ and $G\alpha_i$ (**Figure 1**). When $G\alpha_q$ is activated, PLC, which splits PIP2 into IP3 and DAG, is activated. Calcium levels are raised by IP3, which triggers PKC with DAG. The release of intracellular Ca^{2+} activates the mitogen-activated protein (MAP) kinases ERK1/2 (extracellular signal-regulated kinase), p38, and JNK, which paly essential roles in cell migration and immune response, as well as proline-rich tyrosine kinase 2, which is important for cell motility (Dairaghi et al., 1998; Ganju et al., 1998; Del Corno et al., 2001; Kraft et al., 2001; Missé et al., 2001; Wong et al., 2001; Brelot and Chakrabarti, 2018). In addition, the $G\alpha_i$ pathway inhibits adenylyl cyclase, resulting in decreased cAMP and pCREB levels. As a result, plasticity-related protein transcription and synaptic plasticity are reduced, leading to poorer learning and memory function, as well as a worsened recovery from neuronal damage. Neuronal plasticity and memory problems have been linked to stroke, Huntington's disease, Alzheimer's disease, and other neurocognitive disorders (Zhou et al., 2009; Sano et al., 2014; Lorenzen et al., 2018). Rho GTPase and protein kinase B (PKB/Akt) are stimulated when βγ subunits activate PI-3K. The former is associated with cell survival, whereas the latter regulates cell adhesion and motility (Burgering and Coffer, 1995; Neptune and Bourne, 1997; Downward, 2004; Oppermann, 2004). CCR5 activation also results in phosphorylation of Janus kinases (JAK2) and subsequent activation of the JAK/STAT pathway, which is unaffected by $G\alpha_q$ or $G\alpha_i$ (Mueller and Strange, 2004). CCR5 is involved in a variety of cellular biological changes through complex signaling processes, including cell migration, adhesion, survival, and neuronal plasticity.

Physiological Function of C–C Chemokine Receptor 5

Functions of C–C Chemokine Receptor 5 in Immune System

C–C Chemokine Receptor 5 Induces Immune Cell Migration

Leukocyte motility plays a critical role in inflammatory responses, as it is essential to rapidly recruit innate immune cells to

TABLE 1 | Expression of CCR5 genes in cells.

System	Cell type	Species	Author and year
The cardio-vascular system	Vascular endothelial cells (coronary endothelia, brain endothelia)	Human	Berger et al., 1999
	Vascular smooth muscle cells (aorta, coronary artery and saphenous vein)	Human, Macaques	Rottman et al., 1997
The central nervous system	Neurons (CA1–4 pyramidal hippocampal, dentate gyrus, cortical white matter, brain stem neurons)	Human, Macaques	Westmoreland et al., 2002
	Astrocytes	Human	Flynn et al., 2003
	Microglia		
The immune system	**Innate lymphocytes**	Human	Hughes and Nibbs, 2018
	Innate lymphoid		
	Natural killer cells		
	Myeloid cells		
	Mactophages (spleen, lung, body cavity, intestine, liver) classical/non-classical monocytes (bone marrow, blood)		
	Dendritic cells (DCs)		
	Skin DCs/Langerhans cells		
	DCs (thymus, spleen, lymph node, skin, lung)		
	DC precursors		
	B/T-lymphocytes		
	Natural killer T cells		
	Marginal Zone B cells		
	B cell precursors (bone marrow)		
	Memory $CD4^+/CD8^+$ T cells		
	Activated $CD8^+$ T cells		
	B1 cells		
	γσ T cells (thymus, periphery)		

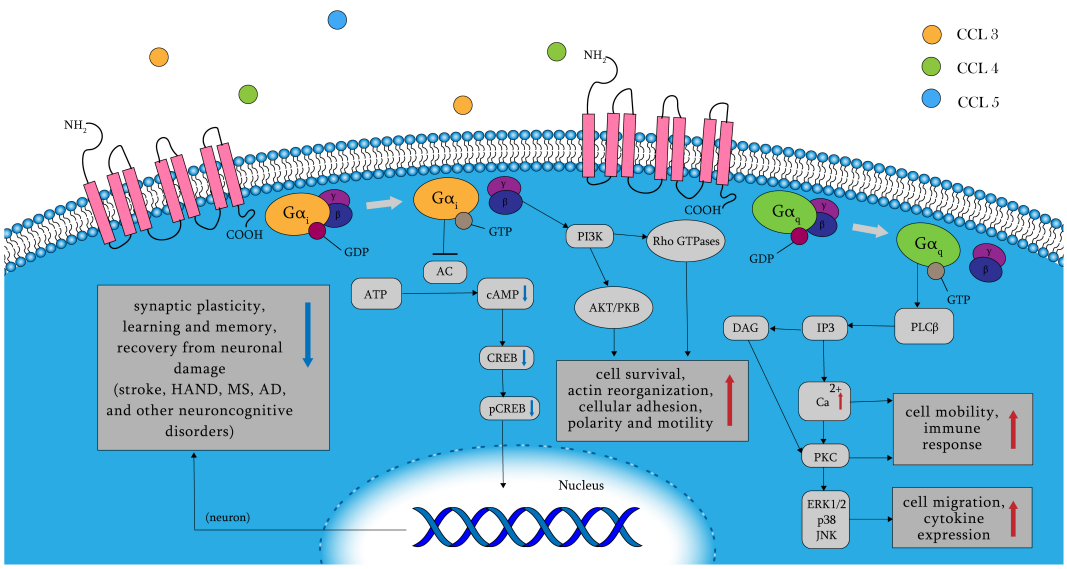

FIGURE 1 | CCR5 receptor signaling pathways. When the amino terminus of CCR5 binds to its ligand, its following signaling pathway is mainly controlled by $G\alpha_q$, $G\alpha_i$, and $\beta\gamma$ subunits. The $G\alpha_i$ pathway results in the release of intracellular Ca^{2+} and decreased learning and memory function, as well as worsened recovery from neuronal damage by reduced cAMP and pCREB. Activation of $G\alpha_q$ results in cell migration and cytokine expression in immune response. And the $\beta\gamma$ subunits leads to cell survival, adhesion and motility through multiple following signaling pathways such as AKT/PKB and Rho GTPase. AC, adenylyl cyclase; AD, Alzheimer's disease; AKT/PKB, protein kinase B; cAMP, cyclic adenosine monophosphate; CCR5, C–C chemokine receptor 5; CREB, cAMP-response-element binding protein; DAG, diacylglycerol; HAND, HIV-related neurocognitive disorders; IP3, inositol 1,4,5-trisphosphate; JNK, C-Jun N-terminal kinases; MS, multiple sclerosis; pCREB, phosphorylated cAMP-response-element binding protein; PKB/Akt, protein kinase B; PKC, protein kinase C; PLC, phospholipase C.

kill pathogens, prevent the spread of microorganisms, trigger inflammation, and repair damage. The classical function of chemokines is to regulate inflammation and drive immune cells through the blood and lymphatic vessels, directing their migration and localization by forming soluble concentration gradients in an autocrine or paracrine manner (Hughes and Nibbs, 2018; Lau et al., 2020). In some contexts, chemokines are also selectively recruited to the cell surface by glycosaminoglycans polysaccharides present within extracellular matrices and at the cell surface which can form fixed concentration gradients and fine-tune the immune response (Paul and Candelario-Jalil, 2021). In NK cells and mast cell precursors, CCR5 binds to locally generated chemokines and inflammatory mediators and causes these innate immune cells to cross the endothelium into peripheral tissues during acute inflammation. Chemokines can regulate immunological responses by guiding regulatory T cell (Treg) migration, and CCR5 may influence the antibody response in the lymph nodes by enhancing the contact of Tregs with B cells and antigen presenting cells (APCs; Maurer and von Stebut, 2004; Khan et al., 2006; Maghazachi, 2010; Griffith et al., 2014). In addition, CCL3/CCR5 was shown to be very effective in augmenting the adhesion of the monocytes to intercellular adhesion molecule-1 during monocyte–endothelial cell interactions, and CCL4/CCR5 can enhance the adhesion of T lymphocytes to vascular cell adhesion molecule 1, which drives immune cell migration from the blood to local tissues across the endothelium (Menten et al., 2002).

C–C Chemokine Receptor 5 Affects Immune Cell Differentiation

Chemokines can induce T cells to differentiate into different subsets and mediate different types of immune responses. Interferon production and macrophage activation are associated with the T helper (Th)1 response; whereas antibody response, B cell assistance, and IL-4 and IL-5 production are associated Th2 response. CCL3, CCL4, and CCL5, which are ligands of CCR5, are chemotactic on Th1 cells, but not on Th2 cells; Th2 cells mainly express CCR2 and CCR4 (Rossi and Zlotnik, 2000; Wong and Fish, 2003). There was a skewed Th2 cytokine profile in mice lacking CCR5, indicating that CCL3/CCR5 and CCL4/CCR5 can influence the immune response by regulating the differentiation of Th to Th1 (Andres et al., 2000; Luther and Cyster, 2001).

C–C Chemokine Receptor 5 Promotes Immune Cell Activation

Binding of CCR5 to ligands causes the $CD8^+$ subset of DC to produce IL-12, which is regarded as a critical step in initiating cell-mediated immunity against intracellular infections (Aliberti et al., 2000). CCR5 is activated when T cells come into contact with APCs and is induced by IL-2 into positive feedback expression on T cells. Simultaneously, CCR5 is recruited to the immunological synapse to reduce T cell responsiveness to other chemotactic substances, through which the stability of T cell-APC interactions is increased and T cell activation is enhanced (Molon et al., 2005). When $CD4^+$ T cells interact with DCs, both $CD4^+$ T cells and the DC generate CCL3 and CCL4. At the same time, CCR5 is upregulated on naive $CD8^+$ T cells entering the lymph node and binds to these chemokines, promoting their migration to $CD4^+$ T cell/DC clusters, which finally leads to improved interactions between naive $CD8^+$ T cells and DCs licensed by $CD4^+$ T helper cells and increased quality and quantity of the $CD8^+$ T cell memory response (Del Corno et al., 2001; Griffith et al., 2014). Bystander T cells in the immune system can rapidly respond and secrete cytokines even without antigenic stimulation. CCL5/CCR5 may promote cytokine production and proliferation of bystander T cells, which is important for autoimmunity (Wong and Fish, 2003).

C–C Chemokine Receptor 5 Regulates Immune Cell Survival and Apoptosis

The goal of the host's reaction to intracellular infections is to eliminate the infected cells as quickly as possible. In addition, it is crucial to remove infected, apoptotic cells from the tissue. Pathogens, activated macrophages, and residual apoptotic cells through proinflammatory proteinases and cytokines cause further tissue damage if the clearance process is disrupted. CCL5-CCR5 interaction can activate MEK-ERK and PI3K-AKT anti-apoptotic signals, which mediate cell growth and survival (Tyner et al., 2005). CCR5 may stimulate T-cell proliferation by triggering STATs (signal transducers and activators of transcription) activation, as chemokine receptors can regulate many transcription factors (López-Cotarelo et al., 2017). By binding to and activating CCR5, CCL5 generated by melanoma tumor cells may trigger the death of tumor-infiltrating T lymphocytes. This process is dependent on the release of cytochrome c into the cytoplasm, rather than on the Fas/Fas ligand. Continued activation of CCR5 by CCL5 following T-cell activation has been shown to cause T-cell death in other studies, indicating that it is a chemokine-dependent late regulation mechanism at an inflammatory site (Wong and Fish, 2003).

Functions of C–C Chemokine Receptor 5 in Central Nervous System

Chemokines, including astrocytes, microglia, and neurons, are expressed in the human CNS from the embryonic stage to adult stage (Westmoreland et al., 2002). CCR5 is mainly distributed in microglia, with lower expression levels in astrocytes and neurons, although all are upregulated in disease states (Xia et al., 1998; Cartier et al., 2005). Numerous experiments have demonstrated that chemokines in the brain function beyond directing immune cell migration, including brain development, neuronal differentiation, neuronal communication, neuron survival, and learning and memory capabilities, directly by affecting neurons, or indirectly through glial cells (Song et al., 2002; Sorce et al., 2011; Wang et al., 2016).

C–C Chemokine Receptor 5 Is Involved in Brain Development and Neuronal Differentiation

Neural progenitor cells express CCR5 and are significantly induced to migrate by CCL5 from activated microglia and astrocytes during human brain development; this migration can be suppressed by antibodies against CCR5 (Park et al., 2009). Mutant CCR5 mice showed fewer and later differentiation of neuronal cells with instant motor deficits, and lacked nociceptive responses, this supports the idea that CCR5 participates in the

development of the CNS by inducing neural progenitor cells to migrate to their target destination and promoting neuronal differentiation (Aarum et al., 2003; Tran et al., 2007; Park et al., 2009). CCR5 KO mice have fewer nigral dopaminergic neurons than normal mice, suggesting that CCR5 may play an important role in promoting maturation or development of the nigral dopaminergic system (Park et al., 2009; Choi et al., 2013). Furthermore, the recruitment function of CCR5 promotes monocyte migration along the hippocampal sulcus during brain development and facilitates microglial colonization of the nervous system. Under normal conditions, attracting microglia by chemokines produced by neural progenitor cells may play an essential role in normal brain function, including nutritional support, regulation of neuronal development, and removal of toxic debris (Polazzi and Contestabile, 2002; Ji et al., 2004; Simard et al., 2006; Hahn et al., 2010). Simultaneously, CCR5 ligands from progenitors, microglia, and astrocytes can attract CCR5-expressing dendritic cells, lymphocytes, and monocytes across the immature blood-brain barrier (BBB) into the CNS to inspect the newly generated cells (Cowell et al., 2006; Whitney et al., 2009). CCR5 activation can regulate many transcription factors including cAMP-response-element binding protein (CREB), which participates in a variety of cellular activities and plays an essential role in the CNS, such as neuronal development, neuroprotection, and disease processes (Finkbeiner, 2000; Lonze and Ginty, 2002; Kuipers et al., 2008). These findings may partially explain the function of CCR5 in brain development and neuronal differentiation; however, the implications of these findings remain unclear.

C–C Chemokine Receptor 5 Affects Signaling Between Neuronal Cells

By sensing chemokines in the blood generated by immune cells, area postrema (AP)/nucleus tractus solitarius neurons in the CNS may deliver signals from the active immune system to the CNS. Through voltage-dependent Ca^{2+} channels, chemokine receptors can reduce Ca^{2+} influx so that Ca^{2+}-dependent K^{+} currents might be inhibited, thereby regulating neuronal excitability and neurotransmitter release (Oh et al., 2002). However, the activation of presynaptic chemokine receptors on hippocampal neurons can regulate the release of glutamate at these synapses and reduce the frequency by voltage-dependent Ca^{2+} channels; this may produce presynaptic inhibition (Meucci et al., 1998). The current study shows that because of PLC/IP3-induced Ca^{2+} mobilization following G protein activation, CCL5/CCR5 plays a dual role in glutamate transmission: the chemokine inhibits the depolarization-evoked glutamate release, but potentiates the basal release of glutamate (Musante et al., 2008).

C–C Chemokine Receptor 5 Regulates Neuronal Survival and Apoptosis

C–C chemokine receptor 5 regulates a variety of transcription factors involved in cell survival such as STAT and CREB. Furthermore, because CCR5 mediates crosstalk between glia and neurons, it is critical for neuronal survival in both normal and pathological situations (Choi et al., 2013). Various stimuli may induce the expression of CCR5, such as proinflammatory cytokines TNF-α and INF-γ, lipopolysaccharide (LPS), and hypoxic-ischemic brain injury; these can lead to neuronal death through the release of excitatory amino acids and reactive oxygen species (Hagberg and Mallard, 2005; Kaul et al., 2005; Cowell et al., 2006). During brain aging and neurodegeneration, the function of plasma membrane Ca^{2+}-ATPase gradually declines, and a large amount of cytosolic Ca^{2+} released via the CCL5/CCR5 and PLC/IP3 pathways cannot be effectively removed. Inflammatory CCL5 activity and long-lasting Ca^{2+} dyshomeostasis can lead to neuronal apoptosis (Radzik et al., 2019). In addition, chemokines regulate the production of matrix metalloproteinases (MMPs), suggesting that they may contribute to MMP activity-mediated neuronal cell survival and death (Rostène et al., 2007).

C–C Chemokine Receptor 5 Inhibits Learning and Memory Processes

As a strong inhibitor of hippocampal and cortical plasticity, CCR5 affects the MAPK/CREB signaling pathway to influence learning and memory. During learning, MAPK and CREB levels are enhanced after CCR5 antagonist use, region-specific viral knockdown, or CCR5 knockout, whereas transgenic mice that overexpress CCR5 in excitatory neurons display learning and memory deficits (Zhou et al., 2016; Merino et al., 2020). The transcription factor CREB in neurons promotes long-term potentiation and enhances synaptic plasticity. Simultaneously, neurons with higher CREB levels are more excitable; consequently, they are more likely to be recruited to participate in the process of learning and memory (Zhou et al., 2009). N-methyl D-aspartate receptor 1 (NMDAR-1) plays an important role in social recognition behavior, as demonstrated by the impaired social recognition of mice with inactive NMDAR-1 receptors. The expression of NMDAR-1 is higher in the brains of $CCR5^{-/-}$ mice than in those of WT mice; additionally $CCR5^{-/-}$ mice show a significant improvement in social identification (Kalkonde et al., 2011). Dendritic spine turnover and spine clustering associated with learning and memory depend on NMDAR. In mammals, higher pre-learning spine turnover rates are closely linked to increased levels of learning and memory, which occur during important developmental periods as well as maturity. After CCR5 knockout, increased dendritic spine turnover rates may allow neurons to explore this space more frequently, enhancing connections with appropriate presynaptic neurons and consolidating new synapses through clustering during learning (Frank et al., 2018). CCR5 activation can lead to impaired AMPA-dependent synaptic transmission and significantly reduced excitatory postsynaptic potential, thereby impairing long-term memory and cognitive deficits (Marciniak et al., 2015).

Additionally, astrocytes involved in learning and memory processes can secrete chemokines to mediate synaptic transmission and plasticity after binding to CCR5 via various mechanisms; these including prevention of extrasynaptic neurotransmitter diffusion and removal to modulate synaptic release (De Pitta et al., 2016; Necula et al., 2021).

C–C Chemokine Receptor 5 Mediates Neuroinflammation

C–C chemokine receptor 5 participates in the inflammatory response in the CNS not only by mediating immune cell migration but also by affecting the permeability of the BBB and activating microglia (Necula et al., 2021). DCs can acquire essential maturation signals from invading T cells when inflammation occurs around CNS blood arteries. They then operate locally to boost immunological responses or trigger additional waves of autoreactive T cells after traveling to draining lymph nodes (Ambrosini et al., 2005). In the early stages of inflammation, the chemokine CCL5 released from endothelial cells induces resident brain microglia expressing CCR5 to migrate to cerebral vessels, causing microglial cells to infiltrate through the neurovascular unit and express CLDN5. Thus brain microglia initially contact endothelial cells and develop tight junctions to maintain the integrity of BBB. However, prolonged inflammation may cause brain microglia to evolve into a phagocytic phenotype that includes morphological alterations, astrocytic fragment engulfment, and leakage across the BBB. Therefore, CCR5-positive microglia play a dual role in inflammation-induced BBB permeability (Haruwaka et al., 2019). The migration of CCL5-driven peripheral blood mononuclear cells across the BBB is dependent on ligand interactions with CCR1 and CCR5: CCR1 is involved in the arrest, while CCR5 is involved in spreading. These interactions can directly affect the development of certain neuroinflammatory diseases (Ubogu et al., 2006). At the same time, CCR5 activation and Ca^{2+} increase can affect gene expression and microglia activation, which can promote microglial cell activation and proliferation. Therapeutic targeting of CCR5 may decrease BBB leakage, increase neurogenesis stimulated by the excitotoxin kainic acid (KA), and promote migration of bone marrow-derived cells to the brain to become neurons, thereby promoting the repair of nervous system damage (Louboutin and Strayer, 2013).

C–C Chemokine Receptor 5 Mediates the Interaction Between Neurons and Glial Cells

UsingCCR5 and its ligands, bidirectional interactions between neurons and between neurons and glial cells play a critical role in maintaining normal neuronal activity (Choi et al., 2013). The CCR5/CREB pathway affects plasticity in neurons in a unique way, whereas CCR5 activation in glial cells is intimately linked to elevated Ca^{2+} (Louboutin and Strayer, 2013). Microglia can communicate with immune cells and neurons through a variety of signaling pathways. Microglial cells undergo a complex, multistage activation process, when evidence of brain lesions or nervous system dysfunction is detected, which allows them to migrate to the injury site, phagocytose cells, proliferate, and lead to protective or neurotoxic effects by releasing active substances (Gebicke-Haerter, 2001; Streit, 2002). CCR5 participates in the migration and activation of microglia through Ca^{2+} signaling, which may damage vascular epithelial cells and neurons (Shideman et al., 2006). Furthermore, a GPCR screen showed the role of CCR5 in microglial neurotoxicity suppression; it is activated by RANTES, as a signal mediator between microglia and neurons, and decreases the expression of toxic iNOS and inflammatory cytokines (Gamo et al., 2008). Beyond being a component of the immune response, microglia also can rebuild dendritic spines and synaptic adhesion and transmission after CCR5-mediated migration to ligand-directed chemotactic gradients, which leads to network-level effects (Ekdahl, 2012; Louboutin and Strayer, 2013; Posfai et al., 2019). Astrocytes also respond to a variety of stimuli via CCR5 mediated calcium signals, supporting and modulating particular neuronal networks in different ways after activation by ligands (Ben Haim and Rowitch, 2017). Additionally, astrocytes, which are involved in learning and memory processes, can secrete chemokines to mediate synaptic transmission and plasticity after binding to CCR5 via various mechanisms; these include the prevention of extrasynaptic neurotransmitter diffusion and removal to modulate synaptic release (De Pitta et al., 2016; Adamsky et al., 2018; Allen and Lyons, 2018).

C–C CHEMOKINE RECEPTOR 5 AND STROKE

Effects of C–C Chemokine Receptor 5 Inhibition on Neurological Rehabilitation After Stroke

After a stroke, multiple biochemical and molecular mechanisms can cause brain damage. The activation and interaction of different signaling pathways following ischemia have different effects on the final extent of the infarct. Inducible upregulation of CCR5 and its ligands after stroke is particularly pronounced in neurons. There are many relevant studies on the effect of CCR5 inhibition after stroke, but owing to the redundant manner in which chemokine families act, complex cellular and molecular changes after stroke, and differences in experimental methods and genetic backgrounds, the results of these studies vary to some extent. In conclusion, mice knocked out for the CCR5 gene showed increased neuronal apoptosis and increased infarct size in histological analysis within 1 week after cerebral ischemia. These results may be explained by the increased expression of CCR2 caused by the loss of CCR5, which activates inflammatory response and increases neuronal degeneration and apoptosis (Zhou et al., 2009; Sorce et al., 2010). CCR5 activation is also required for adoptively the adoptive transfer of Tregs to the ischemia-damaged endothelium. Tregs can prevent proteolytic damage to the BBB by inhibiting the production of matrix metallopeptidase 9. Therefore, CCR5 deficiency may contribute to BBB damage and increased inflammation after stroke (Li et al., 2017). However, it is clear that CCR5 has important effects on neurological recovery in the subacute phase after stroke, because mice injected with shCCR5 adeno-associated virus into the pre-motor cortex showed a significant and sustained improvement in motor control and cognitive function 1 week after stroke (Joy et al., 2019). This improvement does not occur through neuronal protection, and it mechanism is elaborated below. Furthermore, 2 months after cortical ischemia, brain-derived CCR5 deficiency causes an increase in infarction size, dendritic loss in the peri-infarct cortex, and less long-term inflammatory cell accumulation. This discrepancy shows that

the role of brain-derived CCR5 in preserving and regulating neurostructural connections after stroke may be cell dependent (Ping et al., 2021).

A 32-bp deletion in CCR5 causes the receptor to be non-functional. Furthermore, the homozygous CCR5 delta32 deletion confers inherent resistance to HIV infection, which is found in approxiamately 1% of Caucasians (Hutter et al., 2009). The CCR5-Δ32 mutation is the first report of a human genetic variable linked to enhanced stroke recovery. Patients with loss-of-function CCR5 were found to have enhanced stroke recovery on multiple measures of motor, cognitive, and sensory function in a large patient cohort, which included verbal functioning, memory, and attention (Ben Assayag et al., 2012). Post-stroke depression is a common neuropsychiatric comorbidity, it may negatively affect outcomes by increasing the rates of disability and mortality (Wu et al., 2018). A clinical study showed that, compared with non-carriers, depressive symptoms tend to improve over time after stroke in CCR5-Δ32 carriers, which provides further evidence that inhibition of CCR5 function is a protective factor for neurorehabilitation after stroke (Tene et al., 2021).

Changes of Cell Biology After C–C Chemokine Receptor 5 Inhibition

Inflammatory Response in Central Nervous System Is Reduced

In addition to adhesion molecules and inflammatory cytokines, chemokines and their receptors play critical roles in the accumulation of leukocytes around the infarct tissues (Feuerstein et al., 1998). Local and peripheral immune cells, including astrocytes, microglia, neutrophils, macrophages, and monocytes, are recruited after a stroke (Iadecola and Anrather, 2011; Chen et al., 2020). Inhibition of CCR5 expression in premotor cortical neurons after stroke can modulate astrogliosis, reduce astrocyte reactivity, and dampen macrophage recruitment; this inhibition as an intervention can help create a conducive environment for neural repair (Adelson et al., 2012; Barreto et al., 2012; Liraz-Zaltsman et al., 2021). CCR5 inhibition of premotor cortical neurons has no significant effect on microglia responsiveness, but 2 months after ischemia, mice with complete CCR5 deletion in the brain have fewer long-term inflammatory cells, such as $Iba1^+$ cell infiltration around the peri-infarct tissues (Sorce et al., 2010; Ping et al., 2021).

Neuronal Excitability Is Increased

Neuronal excitability and plasticity are similar mechanisms between normal memory formation and recovery after stroke, which can strengthen the connections underlying memory formation and restore lost motor function after stroke. CCR5 inhibition increases neuronal CREB and pCREB expression after stroke, thereby enhancing cellular excitability (Kandel, 2012; Joy et al., 2019). After stroke, there were four separate time epochs: hyperacute, acute, subacute, and chronic (Bernhardt et al., 2017). In the hyperacute phase of stroke, extensive cell death occurs, followed by an acute phase of delayed neuronal apoptosis 1 week later, during which increased neuronal excitability can exacerbate brain damage due to enhanced excitotoxic signaling pathways (Joy and Carmichael, 2021). The subacute period of stroke lasts approximately a month in rodents and up to 3 months in humans, and increased neuronal excitability during this phase can promote motor recovery (Cheng et al., 2014), which partly explains the differential effect on brain injury after CCR5 inhibition. Furthermore, activation of CCR5 affects glutamate release and may affect neuronal signaling through AMPA receptors. Although there are no clear related studies, inhibition of CCR5 may alter neuronal excitability by modulating excitatory neurotransmitters and signaling (Musante et al., 2008; Marciniak et al., 2015). Similar to CCR5, the AMPA receptor is important in the pathophysiology of stroke, but is functionally contradictory. Binding of glutamate to AMPA receptors results in cation influx, depolarization, and the expression of downstream genes, such as brain-derived neurotrophic factor (BDNF). Early potentiation of AMPAR signaling exacerbates stroke damage, while delayed enhancement of the same system may enhance functional recovery (Jourdi et al., 2009; Clarkson et al., 2011). Because both initial cell death and delayed restorations of function are caused by excitatory pathways in neurons, CCR5-targeted treatment must be administered at specified time intervals after the beginning of the stroke.

Neuronal Plasticity Is Increased

In the subacute phase of stroke, the brain is in a plastic state called the sensitive period in stroke recovery, similar to the critical period of enhanced plasticity during development (Carmichael, 2016; Zeiler et al., 2016). Increased plasticity during this period leads to axonal sprouting, dendritic spine morphogenesis, and the remapping of movement representations, which are extremely important for the recovery of adult brain injury (Li et al., 2010; Cirillo et al., 2020). During the sensitive period of stroke recovery and learning and memory, common mechanisms include neuronal distribution, competitiveness controlled by the excitability state, morphogenesis of dendritic spine in engram generation, and compensation for disrupted engrams. After CCR5 inhibition in cortical neurons, enhanced CREB signaling increases neuronal excitability. Furthermore, neurons with higher excitability are more likely to synergize with other neurons after the arrival of a stimulus, forming an engram that will be stored (Yiu et al., 2014). Specifically, because of increased CREB function, neurons with CCR5 knockdown are specifically incorporated into the same motor circuit. CCR5 knockdown induces upregulation of CREB and downstream proteins, such as dual-leucine zipper kinase proteins, in the premotor cortex, which may help preserve the dendritic spine in the early stages of stroke, induce axonal sprouting in the contralateral cortex, improve remapping of damaged sensory and injured motor circuits, and stimulate the creation of new links in these circuits (Joy et al., 2019). Furthermore, CREB induction can also adaptive or compensatory if nearby areas of the brain are injured because of the compensation of memory engrams for brain regions that are dysfunctional or inactivated (Caracciolo et al., 2018). In addition, CCR5 may indirectly affect the plasticity of the CNS after stroke by affecting the reactivity of astrocytes. Activated astrocytes can form glial scars after ischemic injury, which sequesters the injury site and protects cells against the release of harmful substances during the acute phase (Liu and Chopp,

2016). However, persistent glial scars hinder axonal regeneration and inhibit neural plasticity (Pekny et al., 2016). Thus, decreased astrocyte reactivity after CCR5 inhibition may be beneficial to functional outcomes.

Clinical Significance of Targeting C–C Chemokine Receptor 5 After Ischemic Stroke

Additionally, treatment with Maraviroc (Pfizer, New York, United States), a CCR5 antagonist approved by the FDA, improves motor recovery in rodent models of stroke and TBI by enhancing tissue preservation in the brain, attenuating inflammatory responses, and upregulating the levels of cognition-related signaling molecules to promote neural plasticity (Villanueva, 2019; Friedman-Levi et al., 2021). However, using antagonists to inhibit the function of CCR5 requires improved consideration of its potential negative effects. In other studies, CCR5-deficient mice showed increased damage after stroke, which is mainly related to differences in animal models and time of intervention (Sorce et al., 2010). Knockout of the CCR5 gene, compared with using Maraviroc and other antagonists, or small interfering RNA, may cause dramatic effects on cell signaling pathways and lead to a worse prognosis, while reducing CCR5 expression in specific cell types may be more beneficial for neurorehabilitation (Joy et al., 2019; Ping et al., 2021). Furthermore, the enhancement of neuronal excitability after inhibition of CCR5 increases neuronal death in the acute phase; therefore, CCR5-targeted treatment at a specified time in the late subacute phase may be more beneficial for ischemic stroke (Clarkson et al., 2011; Joy and Carmichael, 2021). Although it plays multiple roles represented by immunology in the CNS, inhibition of CCR5 during pathological injury does not reduce immune microglial migration, which notes the loss of CCR5 may be compensated by increased expression of CCR3 and CCR2 (Bauss et al., 2021). Therefore, due to the complexity and interactions of the chemokine receptor family, the benefits of CCR5-targeted therapy after stroke require further investigation and confirmation. Maraviroc is currently being tested in clinical trials for stroke recovery (NCT03172026; Medicine, 2019).

In addition to promoting neurorehabilitation, recent studies have suggested other clinical implications of CCR5 in the context of stroke, including identification of stroke type and prognosis. Transient ischemic attack and ischemic stroke together constitute ischemic cerebrovascular disease, which has four subtypes: cardioembolism, large artery atherosclerosis, cryptogenic disease, and small artery occlusion. A study showed that in cardioembolism but not in other subtypes, the Δ32 allele frequency was lower, which suggests that CCR5 Δ32 plays a protective role in the cardioembolism, and Δ32 polymorphism helps identify stroke type (Kostulas et al., 2009). $CCR5^+$ Tregs combined with Tregs may function as biomarkers for predicting the prognosis of ischemic stroke. CCR5 chemotactic Tregs can reduce inflammation after stroke and protect the BBB. Higher expression of Tregs often appears in severe stroke patients and large infarction groups, and high expression of $CCR5^+$ Tregs may indicate mild stroke and smaller infarct area (Zhang et al., 2020).

C–C CHEMOKINE RECEPTOR 5 AND OTHER DISEASES

C–C chemokine receptor 5 is involved in the pathophysiological process of a wide range of human diseases through its complex signaling pathways, ranging from infectious diseases, tumors to various neurological diseases, and its mechanism in different diseases may also provide clues for targeted rehabilitation therapy after stroke. **Table 2** summaries CCR5's different roles in CNS during normal and disordered conditions.

C–C Chemokine Receptor 5 and Infectious Diseases

C–C chemokine receptor 5 plays an important role in the immune processes of various infectious diseases, such as pathogen removal and inflammatory response regulation. These effects can limit the development of infectious diseases and maintain the stability of the body's internal environment but can also cause pathological damage under certain conditions. Multiple studies on CCR5 and HIV were published in 1996, identifying CCR5 as an essential co-receptor for HIV entrance. After the envelope glycoprotein attaches to CCR5, the envelope is embedded in the host cell membrane (Alkhatib et al., 1996; Kwong et al., 1998). Neuronal damage caused by HIV infection leads about half of the infected people to acquire HIV-related neurocognitive disorders (Ru and Tang, 2017). Microglial activation and subsequent neuronal injury are prevented by the genetic deletion of CCR5, which in a transgenic model also rescues spatial learning and memory. Cognitive performance is also improved in chronic HIV patients after dual CCR2 and CCR5 antagonism (Maung et al., 2014; D'Antoni et al., 2018). CCR5 is crucial in West Nile virus (WNV) infection as an antiviral and survival factor, as evidenced by the enhanced leukocyte accumulation in the CNS and increased survival of up to 60% after splenocytes from WNV-infected WT mice were transferred into WNV-infected $CCR5^{-/-}$ mice (Glass et al., 2005). Endothelial cells of the cerebral microvasculature produce CCL3, CCL4, and CCL5 after cerebral malaria infection, which could attract CCR5-positive leukocytes toward the brain, where they would eliminate parasites. Nevertheless, brain-recruited effector $CD8^+$ T cells destroy ECs, causing the BBB to break (Belnoue et al., 2003).

C–C Chemokine Receptor 5 and Cancers

C–C chemokine receptor 5 has anti-cancer and pro-cancer effects. Anti-cancer properties include recruitment of tumor-infiltrating lymphocytes and destruction of cancer cells. In contrast, chemokines exhibit pro-cancer properties by promoting angiogenesis and lymphangiogenesis, as well as enhancing cancer cell migration, invasion, and proliferation and recruiting cells that promote tumor development (Korbecki et al., 2020).

TABLE 2 | Various roles of CCR5 in the CNS during healthy and diseased states.

Condition	Cell type	Role of CCR5 in CNS	References
Normal	Neural progenitor cells	Induces neural progenitor cells to migrate and promotes neuronal differentiation	Ji et al., 2004; Park et al., 2009
	Neuron	Promotes neuronal growth and differentiation during embryonic development	Bolin et al., 1998; Park et al., 2009
		Modulates neuronal excitability and neurotransmitter release	Oh et al., 2002; Musante et al., 2008
		Regulates neuronal survival or apoptosis	Choi et al., 2013; Radzik et al., 2019
		Inhibits hippocampus and cortical plasticity, impairs learning and memory processes	Zhou et al., 2016; Necula et al., 2021
	Microglia	Mediates microglia migration and colonization, which may provide nutritional support, regulation of neuronal development, and removal of toxic debris	Polazzi and Contestabile, 2002; Cowell et al., 2006
	Astrocytes	Regulates the proliferation, survival and differentiation of astrocyte progenitors during embryonic development	Bakhiet et al., 2001; Cartier et al., 2005; Necula et al., 2021
Ischemic stroke	Neuron	Inhibits neuronal plasticity and recovery	Joy et al., 2019; Joy and Carmichael, 2021
	Astrocytes	Promotes astrocytes proliferation and activation	Liraz-Zaltsman et al., 2021
	Monocytes	Recruites monocytes and modulates the immune response	Cartier et al., 2005
	Treg cells	Mediates the docking of transferred Tregs to relieve neutrophil accumulation and protect BBB	Sorce et al., 2010; Li et al., 2017
	Neutrophils	Induces neutrophils migration toward the injured area and leads to deteriorated brain injury	Chen et al., 2020
Intracerebral hemorrhage	Neuron	Mediates neurological deficits and neuronal pyroptosis via CCR5/PKA/CREB pathway	Yan et al., 2021
Neuroinflammation	Microglia	Induces microglia proliferation and activation	Louboutin and Strayer, 2013
	Monocytes	Mediates monocyte migration and affects the leakage of BBB	Ubogu et al., 2006; Louboutin et al., 2011
Infectious disease			
West Nile virus infection	Monocytes, Macrophages, NK cells, and T lymphocytes	Regulates trafficking of leukocytes to CNS to contain and clear the virus	Glass et al., 2005
Mouse Hepatitis Virus intracranial infection	Macrophages	Mediates macrophage trafficking into CNS and leads to demyelination	Glass et al., 2001
HIV-Associated Neurocognitive Disease (HAND)	$CD4^+$ T lymphocytes	Mediates HIV-1 entry into $CD4^+$ cells as a fusion cofactor	Kwong et al., 1998
	Microglia	Promotes microglial activation and neuronal damage, thereby improved cognition	Maung et al., 2014; D'Antoni et al., 2018
	Monocytes	Recruits HIV-infected monocytes to CNS and leads to intracranial infection and inflammation.	Hahn et al., 2010
Cerebral malaria	$CD8^+$ T lymphocytes	Regulates trafficking of $CD8^+$ T lymphocytes to destroy brain endothelial cells and BBB	Belnoue et al., 2003
Cancer			
Primary central nervous system lymphomas	Malignant B lymphocytes	Induces B lymphocytes homing to the brain and spreading within CNS	Brunn et al., 2007
Glioblastoma	Glioma-associated microglia/macrophages (GAMs)	Induces glioma invasive process	Yu-Ju Wu et al., 2020
		Regulates M1/M2 microglia phenotype	Laudati et al., 2017
	Treg cells, Monocyte	Recruits immunosuppressive cells to induce immune tolerance	Jiao et al., 2019
	Tumor cell	Promotes tumor cell proliferation and migration	Aldinucci and Colombatti, 2014
Pathological pain	Neuron	Activates neuron ERK to create and maintain pathological pain	Piotrowska et al., 2016; Hang et al., 2017; Lu et al., 2017
		Reduces the antinociceptive action of opioid receptor agonists	Szabo et al., 2002; Chen et al., 2007

(Continued)

TABLE 2 | (Continued)

Condition	Cell type	Role of CCR5 in CNS	References
Multiple sclerosis (MS)	T lymphocytes	Regulates trafficking of inflammatory T cells into CNS to induce self-destructive inflammatory process	Zang et al., 2000; Menten et al., 2002; Schlager et al., 2016
Neurodegenerative disease			
Alzheimer's disease (AD)	Microglia, Astrocytes	Recruits and activates astrocytes and microglia to affect amyloid deposition and memory function with CCR2	Cartier et al., 2005; Lee et al., 2009; Goldeck et al., 2013
Parkinson's disease (PD)	neuron	Promotes maturation of nigral dopaminergic neurons	Choi et al., 2013

CCR5 plays a role in tumor development or progression in multiple myeloma, classical Hodgkin lymphoma, prostate, breast, gastric, colon, and ovarian cancer, glioblastoma, and melanoma (Brunn et al., 2007; Yu-Ju Wu et al., 2020). Notably, CCR5 promotes tumor cell proliferation mechanisms, including the Jak-STAT or the MAPK/ERK signaling pathway leading to upregulation of cyclin expression and the PI-3K pathway resulting in the proliferation of progenitor and stem cells when the serine/threonine kinase protein kinase B (AKT) and PDK1 increase. Furthermore, via Akt phosphorylation, which stimulates the uptake of glucose, glutamine metabolism, fatty acid synthesis and the pentose phosphate pathway, CCR5 enables tumor cells to utilize glucose and catabolites more efficiently (Aldinucci and Colombatti, 2014; Jiao et al., 2019). CCR5 induces the expression and activity of DNA repair genes, resulting in aberrant cell survival and resistance to agents that cause DNA damage. The CCR5 antagonists Maraviroc and Vicriviroc dramatically enhance cell destruction mediated by DNA-damaging chemotherapeutic agents (Jiao et al., 2018).

C–C Chemokine Receptor 5 and Pain

Spinal CCR5 is involved in the development and maintenance of pathological pain, including visceral hyperalgesia, cancer-induced bone pain, and neuropathic pain induced by spinal nerve injury. A novel medication for pathological pain that targets the CCL8/CCR5/ERK pathway in the spinal cord can be developed (Piotrowska et al., 2016; Hang et al., 2017; Lu et al., 2017). Activation of CCR5 in the brain significantly reduce the antinociceptive action of opioid receptor agonists, which is based on heterologous desensitization of μ-opioid receptors. These results shed light on the treatment of hyperalgesia related to inflammatory reactions and also suggest that the chemokine system, joins neurotransmitters and neuropeptides (Szabo et al., 2002).

C–C Chemokine Receptor 5 and Other Central Nervous System Diseases

Alzheimer's disease (AD) is a neurodegenerative disease that is characterized by a neuroinflammatory component. CCR5 and its ligands are overexpressed in both the periphery and brain of AD patients, which activates astrocytes and microglia, leading to amyloid deposits and memory dysfunction. However, some studies have also shown that CCR5 deletion can lead to worsening of AD, which may be due to a compensatory increase in CCR2 (Cartier et al., 2005; Goldeck et al., 2013). The autoimmune disease multiple sclerosis (MS) is a CNS disease with chronic inflammation caused by T cells. T cells from patients with MS had a considerably higher migratory rate than healthy cells that selectively migrated toward CCL3. In addition, CCR5 is involved in myelin degradation and, hence, plays a crucial role in the progression of MS (Zang et al., 2000; Janssen et al., 2016).

This review focuses on the research progress of CCR5 in ischemic stroke, but there are numerous functions of CCR5 in stroke and other diseases in CNS waiting for exploration. A recent study found CCR5 activation after intracerebral hemorrhage, partially through the CCR5/PKA/CREB/NLRP1 (nucleotide-binding domain leucine-rich repeat pyrin domain containing 1) signaling pathway, promoted neuronal pyroptosis, and neurological deficits (Yan et al., 2021).

CONCLUSION

The broader biological role of CCR5 has been confirmed as scientific research progresses. CCR5 was once thought to be involved exclusively in immune responses, such as leukocyte migration and pathogen clearance, but new data have revealed that it also modulates cell signaling and neural plasticity, which play a role in the control of learning and memory. The therapeutic effect of promoting cerebral reperfusion after stroke is strictly limited by the therapeutic time window, and limited recovery after acute brain injury leads to the prevalence of disability after stroke; therefore, neurorehabilitative therapies have broad therapeutic prospects. Numerous molecular, cellular, and behavioral studies have been conducted on neural recovery after brain injury, and recent studies have demonstrated that the function of CCR5 signaling is essential in human stroke recovery. CCR5 activation reduces neuroplasticity and inhibits the recovery process after stroke through CREB/MAPK inactivation, impaired axonal regeneration, and decreased synaptic plasticity, whereas inhibition of CCR5 function promotes neurorehabilitation after stroke. CCR5, the first reported gene linked to improved neurological recovery after

stroke in humans, reopens the recovery window after stroke (Zhou et al., 2016; Joy et al., 2019; Servick, 2019). There are common mechanisms between memory formation and brain repair, and the induction of neuronal plasticity provides a new therapeutic direction for promoting the recovery of motor and cognitive functions in patients with stroke.

AUTHOR CONTRIBUTIONS

Y-QF, Z-ZX, Y-TW, and YX contributed to the conceptual design, writing, and editing for this manuscript. Y-YH, LC, WLX, and G-YL conceived the tables. XL and JL provided critical input. QPW revised the manuscript and commented on previous versions of the manuscript. All authors contributed to the article and approved the submitted version.

FUNDING

This work was supported by the National Key Research and Development Program of China (Grant No. 2018YFC2001903), the National Natural Science Foundation of China (Grant No. 81873952), and the National Natural Science Foundation of China (Grant No. 81901948).

REFERENCES

Aarum, J., Sandberg, K., Haeberlein, S. L. B., and Persson, M. A. A. (2003). Migration and differentiation of neural precursor cells can be directed by microglia. *Proc. Natl. Acad. Sci. U.S.A.* 100, 15983–15988. doi: 10.1073/pnas.2237050100

Adamsky, A., Kol, A., Kreisel, T., Doron, A., Ozeri-Engelhard, N., Melcer, T., et al. (2018). Astrocytic Activation Generates De Novo Neuronal Potentiation and Memory Enhancement. *Cell* 174:e14. doi: 10.1016/j.cell.2018.05.002

Adelson, J. D., Barreto, G. E., Xu, L., Kim, T., Brott, B. K., Ouyang, Y. B., et al. (2012). Neuroprotection from stroke in the absence of MHCI or PirB. *Neuron* 73, 1100–1107. doi: 10.1016/j.neuron.2012.01.020

Aldinucci, D., and Colombatti, A. (2014). The inflammatory chemokine CCL5 and cancer progression. *Med. Inflamm.* 2014:292376. doi: 10.1155/2014/292376

Aliberti, J., E Sousa, C., Schito, M., Hieny, S., Wells, T., Huffnagle, G. B., et al. (2000). CCR5 provides a signal for microbial induced production of IL-12 by CD8 alpha+ dendritic cells. *Nat. immunol.* 1, 83–87. doi: 10.1038/76957

Alkhatib, G., Combadiere, C., Broder, C. C., Feng, Y., Kennedy, P. E., Murphy, P. M., et al. (1996). CC CKR5: a RANTES, MIP-1alpha, MIP-1beta receptor as a fusion cofactor for macrophage-tropic HIV-1. *Science* 272, 1955–1958. doi: 10.1126/science.272.5270.1955

Allen, N. J., and Lyons, D. A. (2018). Glia as architects of central nervous system formation and function. *Science* 362, 181–185. doi: 10.1126/science.aat0473

Ambrosini, E., Remoli, M. E., Giacomini, E., Rosicarelli, B., Serafini, B., Lande, R., et al. (2005). Astrocytes produce dendritic cell-attracting chemokines *in vitro* and in multiple sclerosis lesions. *J. Neuropathol. Exp. Neurol.* 64, 706–715. doi: 10.1097/01.jnen.0000173893.01929.fc

Andres, P. G., Beck, P. L., Mizoguchi, E., Mizoguchi, A., Bhan, A. K., Dawson, T., et al. (2000). Mice with a selective deletion of the CC chemokine receptors 5 or 2 are protected from dextran sodium sulfate-mediated colitis: lack of CC chemokine receptor 5 expression results in a NK1.1+ lymphocyte-associated Th2-type immune response in the intestine. *J. Immunol.* 164, 6303–6312. doi: 10.4049/jimmunol.164.12.6303

Babcock, A. A., Kuziel, W. A., Rivest, S., and Owens, T. (2003). Chemokine expression by glial cells directs leukocytes to sites of axonal injury in the CNS. *J. Neurosci.* 23, 7922–7930. doi: 10.1523/JNEUROSCI.23-21-07922.2003

Bakhiet, M., Tjernlund, A., Mousa, A., Gad, A., Stromblad, S., Kuziel, W. A., et al. (2001). RANTES promotes growth and survival of human first-trimester forebrain astrocytes. *Nat. Cell Biol.* 3, 150–157. doi: 10.1038/35055057

Barreto, G. E., White, R. E., Xu, L., Palm, C. J., and Giffard, R. G. (2012). Effects of heat shock protein 72 (Hsp72) on evolution of astrocyte activation following stroke in the mouse. *Exp. Neurol.* 238, 284–296. doi: 10.1016/j.expneurol.2012.08.015

Bauss, J., Morris, M., Shankar, R., Olivero, R., Buck, L. N., Stenger, C. L., et al. (2021). CCR5 and Biological Complexity: The Need for Data Integration and Educational Materials to Address Genetic/Biological Reductionism at the Interface of Ethical. Legal, and Social Implications. *Front. Immunol.* 12:790041. doi: 10.3389/fimmu.2021.790041

Belnoue, E., Kayibanda, M., Deschemin, J. C., Viguier, M., Mack, M., Kuziel, W. A., et al. (2003). CCR5 deficiency decreases susceptibility to experimental cerebral malaria. *Blood* 101, 4253–4259. doi: 10.1182/blood-2002-05-1493

Ben Assayag, E., Korczyn, A. D., Giladi, N., Goldbourt, U., Berliner, A. S., Shenhar-Tsarfaty, S., et al. (2012). Predictors for poststroke outcomes: the Tel Aviv Brain Acute Stroke Cohort (TABASCO) study protocol. *Int. J. Stroke* 7, 341–347. doi: 10.1111/j.1747-4949.2011.00652.x

Ben Haim, L., and Rowitch, D. H. (2017). Functional diversity of astrocytes in neural circuit regulation. *Nat. Rev. Neurosci.* 18, 31–41. doi: 10.1038/nrn.2016.159

Benjamin, E. J., Muntner, P., Alonso, A., Bittencourt, M. S., Callaway, C. W., and Carson, A. P. (2019). Heart Disease and Stroke Statistics-2019 Update: A Report From the American Heart Association. *Circulation* 139, e56–e528.

Berger, O., Gan, X., Gujuluva, C., Burns, A. R., Sulur, G., Stins, M., et al. (1999). CXC and CC chemokine receptors on coronary and brain endothelia. *Mol. Med.* 5, 795–805. doi: 10.1007/bf03401992

Bernhardt, J., Hayward, K. S., Kwakkel, G., Ward, N. S., Wolf, S. L., Borschmann, K., et al. (2017). Agreed Definitions and a Shared Vision for New Standards in Stroke Recovery Research: The Stroke Recovery and Rehabilitation Roundtable Taskforce. *Neurorehabil. Neural. Repair* 31, 793–799. doi: 10.1177/1545968317732668

Bolin, L. M., Murray, R., Lukacs, N. W., Strieter, R. M., Kunkel, S. L., Schall, T. J., et al. (1998). Primary sensory neurons migrate in response to the chemokine RANTES. *J. Neuroimmunol.* 81, 49–57. doi: 10.1016/s0165-5728(97)00158-6

Bredesen, D. E. (2014). Reversal of cognitive decline: a novel therapeutic program. *Aging* 6, 707–717. doi: 10.18632/aging.100690

Brelot, A., and Chakrabarti, L. A. (2018). CCR5 Revisited: How Mechanisms of HIV Entry Govern AIDS Pathogenesis. *J. Mol. Biol.* 430, 2557–2589. doi: 10.1016/j.jmb.2018.06.027

Brunn, A., Montesinos-Rongen, M., Strack, A., Reifenberger, G., Mawrin, C., Schaller, C., et al. (2007). Expression pattern and cellular sources of chemokines in primary central nervous system lymphoma. *Acta Neuropathol.* 114, 271–276. doi: 10.1007/s00401-007-0258-x

Burgering, B. M., and Coffer, P. J. (1995). Protein kinase B (c-Akt) in phosphatidylinositol-3-OH kinase signal transduction. *Nature* 376, 599–602. doi: 10.1038/376599a0

Campbell, B. C. V., De Silva, D. A., Macleod, M. R., Coutts, S. B., Schwamm, L. H., Davis, S. M., et al. (2019). Ischaemic stroke. *Nat. Rev. Dis. Primers* 5:70.

Caracciolo, L., Marosi, M., Mazzitelli, J., Latifi, S., Sano, Y., Galvan, L., et al. (2018). CREB controls cortical circuit plasticity and functional recovery after stroke. *Nat. Commun.* 9:2250. doi: 10.1038/s41467-018-04445-9

Carmichael, S. T. (2016). The 3 Rs of Stroke Biology: Radial. Relayed, and Regenerative. *Neurotherapeutics* 13, 348–359. doi: 10.1007/s13311-015-0408-0

Cartier, L., Hartley, O., Dubois-Dauphin, M., and Krause, K. H. (2005). Chemokine receptors in the central nervous system: role in brain inflammation and neurodegenerative diseases. *Brain Res. Brain Res. Rev.* 48, 16–42. doi: 10.1016/j.brainresrev.2004.07.021

Chen, C., Chu, S. F., Ai, Q. D., Zhang, Z., and Chen, N. H. (2020). CKLF1/CCR5 axis is involved in neutrophils migration of rats with transient cerebral ischemia. *Int. Immunopharmacol.* 85:106577. doi: 10.1016/j.intimp.2020.106577

Chen, C., Chu, S. F., Liu, D. D., Zhang, Z., Kong, L. L., Zhou, X., et al. (2018). Chemokines play complex roles in cerebral ischemia. *Neurochem. Int.* 112, 146–158. doi: 10.1016/j.neuint.2017.06.008

Chen, X., Geller, E. B., Rogers, T. J., and Adler, M. W. (2007). Rapid heterologous desensitization of antinociceptive activity between mu or delta opioid receptors and chemokine receptors in rats. *Drug Alcohol Depend* 88, 36–41. doi: 10.1016/j.drugalcdep.2006.09.010

Cheng, M. Y., Wang, E. H., Woodson, W. J., Wang, S., Sun, G., Lee, A. G., et al. (2014). Optogenetic neuronal stimulation promotes functional recovery after stroke. *Proc. Natl. Acad. Sci. U.S.A.* 111, 12913–12918. doi: 10.1073/pnas.1404109111

Choi, D. Y., Lee, M. K., and Hong, J. T. (2013). Lack of CCR5 modifies glial phenotypes and population of the nigral dopaminergic neurons, but not MPTP-induced dopaminergic neurodegeneration. *Neurobiol. Dis.* 49, 159–168. doi: 10.1016/j.nbd.2012.08.001

Cirillo, C., Brihmat, N., Castel-Lacanal, E., Le Friec, A., Barbieux-Guillot, M., and Raposo, N. (2020). Post-stroke remodeling processes in animal models and humans. *J. Cereb. Blood Flow Metab.* 40, 3–22. doi: 10.1177/0271678X19882788

Clarkson, A. N., Huang, B. S., Macisaac, S. E., Mody, I., and Carmichael, S. T. (2010). Reducing excessive GABA-mediated tonic inhibition promotes functional recovery after stroke. *Nature* 468, 305–309. doi: 10.1038/nature09511

Clarkson, A. N., Overman, J. J., Zhong, S., Mueller, R., Lynch, G., and Carmichael, S. T. (2011). AMPA receptor-induced local brain-derived neurotrophic factor signaling mediates motor recovery after stroke. *J. Neurosci.* 31, 3766–3775. doi: 10.1523/jneurosci.5780-10.2011

Collaborators, G. B. D. L. R. O. S., Feigin, V. L., Nguyen, G., Cercy, K., Johnson, C. O., Alam, T., et al. (2018). Global, Regional, and Country-Specific Lifetime Risks of Stroke, 1990 and 2016. *N. Engl. J. Med.* 379, 2429–2437. doi: 10.1056/NEJMoa1804492

Cowell, R. M., Xu, H., Parent, J. M., and Silverstein, F. S. (2006). Microglial expression of chemokine receptor CCR5 during rat forebrain development and after perinatal hypoxia-ischemia. *J. Neuroimmunol.* 173, 155–165. doi: 10.1016/j.jneuroim.2006.01.005

Cramer, S. C., and Procaccio, V. (2012). Correlation between genetic polymorphisms and stroke recovery: analysis of the GAIN Americas and GAIN International Studies. *Eur. J. Neurol.* 19, 718–724. doi: 10.1111/j.1468-1331.2011.03615.x

Dairaghi, D. J., Franz-Bacon, K., Callas, E., Cupp, J., Schall, T. J., Tamraz, S. A., et al. (1998). Macrophage inflammatory protein-1beta induces migration and activation of human thymocytes. *Blood* 91, 2905–2913. doi: 10.1182/blood.v91.8.2905.2905_2905_2913

D'Antoni, M. L., Paul, R. H., Mitchell, B. I., Kohorn, L., Fischer, L., and Lefebvre, E. (2018). Improved Cognitive Performance and Reduced Monocyte Activation in Virally Suppressed Chronic HIV After Dual CCR2 and CCR5 Antagonism. *J. Acquir. Immune. Defic. Syndr.* 79, 108–116. doi: 10.1097/QAI.0000000000001752

De Pitta, M., Brunel, N., and Volterra, A. (2016). Astrocytes: Orchestrating synaptic plasticity? *Neuroscience* 323, 43–61. doi: 10.1016/j.neuroscience.2015.04.001

Del Corno, M., Liu, Q. H., Schols, D., De Clercq, E., Gessani, S., Freedman, B. D., et al. (2001). HIV-1 gp120 and chemokine activation of Pyk2 and mitogen-activated protein kinases in primary macrophages mediated by calcium-dependent, pertussis toxin-insensitive chemokine receptor signaling. *Blood* 98, 2909–2916. doi: 10.1182/blood.v98.10.2909

Downward, J. (2004). PI 3-kinase, Akt and cell survival. *Semin. Cell Dev. Biol.* 15, 177–182. doi: 10.1016/j.semcdb.2004.01.002

Ekdahl, C. T. (2012). Microglial activation - tuning and pruning adult neurogenesis. *Front. Pharmacol.* 3:41. doi: 10.3389/fphar.2012.00041

Feuerstein, G. Z., Wang, X., and Barone, F. C. (1998). The role of cytokines in the neuropathology of stroke and neurotrauma. *Neuroimmunomodulation* 5, 143–159. doi: 10.1159/000026331

Finkbeiner, S. (2000). CREB couples neurotrophin signals to survival messages. *Neuron* 25, 11–14. doi: 10.1016/s0896-6273(00)80866-1

Flynn, G., Maru, S., Loughlin, J., Romero, I. A., and Male, D. (2003). Regulation of chemokine receptor expression in human microglia and astrocytes. *J. Neuroimmunol.* 136, 84–93. doi: 10.1016/s0165-5728(03)00009-2

Frank, A. C., Huang, S., Zhou, M., Gdalyahu, A., Kastellakis, G., Silva, T. K., et al. (2018). Hotspots of dendritic spine turnover facilitate clustered spine addition and learning and memory. *Nat. Commun.* 9:422. doi: 10.1038/s41467-017-02751-2

Friedman-Levi, Y., Liraz-Zaltsman, S., Shemesh, C., Rosenblatt, K., Kesner, E. L., Gincberg, G., et al. (2021). Pharmacological blockers of CCR5 and CXCR4 improve recovery after traumatic brain injury. *Exp. Neurol.* 338:113604. doi: 10.1016/j.expneurol.2021.113604

Gamo, K., Kiryu-Seo, S., Konishi, H., Aoki, S., Matsushima, K., Wada, K., et al. (2008). G-protein-coupled receptor screen reveals a role for chemokine receptor CCR5 in suppressing microglial neurotoxicity. *J. Neurosci.* 28, 11980–11988. doi: 10.1523/JNEUROSCI.2920-08.2008

Ganju, R. K., Dutt, P., Wu, L., Newman, W., Avraham, H., Avraham, S., et al. (1998). Beta-chemokine receptor CCR5 signals via the novel tyrosine kinase RAFTK. *Blood* 91, 791–797. doi: 10.1182/blood.v91.3.791

Gebicke-Haerter, P. J. (2001). Microglia in neurodegeneration: molecular aspects. *Microsc. Res. Tech.* 54, 47–58. doi: 10.1002/jemt.1120

Glass, W. G., Lim, J. K., Cholera, R., Pletnev, A. G., Gao, J. L., and Murphy, P. M. (2005). Chemokine receptor CCR5 promotes leukocyte trafficking to the brain and survival in West Nile virus infection. *J. Exp. Med.* 202, 1087–1098. doi: 10.1084/jem.20042530

Glass, W. G., Liu, M. T., Kuziel, W. A., and Lane, T. E. (2001). Reduced macrophage infiltration and demyelination in mice lacking the chemokine receptor CCR5 following infection with a neurotropic coronavirus. *Virology* 288, 8–17. doi: 10.1006/viro.2001.1050

Goldeck, D., Larbi, A., Pellicano, M., Alam, I., Zerr, I., Schmidt, C., et al. (2013). Enhanced Chemokine Receptor Expression on Leukocytes of Patients with Alzheimer's Disease. *PLoS One* 8:e66664. doi: 10.1371/journal.pone.0066664

Griffith, J. W., Sokol, C. L., and Luster, A. D. (2014). Chemokines and chemokine receptors: positioning cells for host defense and immunity. *Ann. Rev. Immunol.* 32, 659–702. doi: 10.1146/annurev-immunol-032713-120145

Hagberg, H., and Mallard, C. (2005). Effect of inflammation on central nervous system development and vulnerability. *Curr. Opin. Neurol.* 18, 117–123. doi: 10.1097/01.wco.0000162851.44897.8f

Hahn, Y. K., Vo, P., Fitting, S., Block, M. L., Hauser, K. F., and Knapp, P. E. (2010). beta-Chemokine production by neural and glial progenitor cells is enhanced by HIV-1 Tat: effects on microglial migration. *J. Neurochem.* 114, 97–109. doi: 10.1111/j.1471-4159.2010.06744.x

Hang, L. H., Li, S. N., Dan, X., Shu, W. W., Luo, H., and Shao, D. H. (2017). Involvement of Spinal CCR5/PKCgamma Signaling Pathway in the Maintenance of Cancer-Induced Bone Pain. *Neurochem. Res.* 42, 563–571. doi: 10.1007/s11064-016-2108-5

Haruwaka, K., Ikegami, A., Tachibana, Y., Ohno, N., Konishi, H., and Hashimoto, A. (2019). Dual microglia effects on blood brain barrier permeability induced by systemic inflammation. *Nat. Commun.* 10:5816. doi: 10.1038/s41467-019-13812-z

Hughes, C. E., and Nibbs, R. J. B. (2018). A guide to chemokines and their receptors. *FEBS J.* 285, 2944–2971. doi: 10.1111/febs.14466

Hutter, G., Nowak, D., Mossner, M., Ganepola, S., Mussig, A., Allers, K., et al. (2009). Long-term control of HIV by CCR5 Delta32/Delta32 stem-cell transplantation. *N. Engl. J. Med.* 360, 692–698. doi: 10.1056/NEJMoa0802905

Iadecola, C., and Anrather, J. (2011). The immunology of stroke: from mechanisms to translation. *Nat. Med.* 17, 796–808. doi: 10.1038/nm.2399

Janssen, K., Rickert, M., Clarner, T., Beyer, C., and Kipp, M. (2016). Absence of CCL2 and CCL3 Ameliorates Central Nervous System Grey Matter But Not White Matter Demyelination in the Presence of an Intact Blood-Brain Barrier. *Mol. Neurobiol.* 53, 1551–1564. doi: 10.1007/s12035-015-9113-6

Ji, J. F., He, B. P., Dheen, S. T., and Tay, S. S. (2004). Expression of chemokine receptors CXCR4. CCR2, CCR5 and CX3CR1 in neural progenitor cells isolated from the subventricular zone of the adult rat brain. *Neurosci. Lett.* 355, 236–240. doi: 10.1016/j.neulet.2003.11.024

Jiao, X., Nawab, O., Patel, T., Kossenkov, A. V., Halama, N., Jaeger, D., et al. (2019). Recent Advances Targeting CCR5 for Cancer and Its Role in Immuno-Oncology. *Cancer Res.* 79, 4801–4807. doi: 10.1158/0008-5472.CAN-19-1167

Jiao, X., Velasco-Velazquez, M. A., Wang, M., Li, Z., Rui, H., Peck, A. R., et al. (2018). CCR5 Governs DNA Damage Repair and Breast Cancer Stem Cell Expansion. *Cancer Res.* 78, 1657–1671. doi: 10.1158/0008-5472.CAN-17-0915

Jones, K. L., Maguire, J. J., and Davenport, A. P. (2011). Chemokine receptor CCR5: from AIDS to atherosclerosis. *Br. J. Pharmacol.* 162, 1453–1469. doi: 10.1111/j.1476-5381.2010.01147.x

Jourdi, H., Hsu, Y. T., Zhou, M., Qin, Q., Bi, X., and Baudry, M. (2009). Positive AMPA receptor modulation rapidly stimulates BDNF release and

increases dendritic mRNA translation. *J. Neurosci.* 29, 8688–8697. doi: 10.1523/JNEUROSCI.6078-08.2009

Joy, M. T., Ben Assayag, E., Shabashov-Stone, D., Liraz-Zaltsman, S., Mazzitelli, J., and Arenas, M. (2019). CCR5 Is a Therapeutic Target for Recovery after Stroke and Traumatic Brain Injury. *Cell* 176, 1143–1157e13. doi: 10.1016/j.cell.2019.01.044

Joy, M. T., and Carmichael, S. T. (2021). Encouraging an excitable brain state: mechanisms of brain repair in stroke. *Nat. Rev. Neurosci.* 22, 38–53. doi: 10.1038/s41583-020-00396-7

Kalkonde, Y. V., Shelton, R., Villarreal, M., Sigala, J., Mishra, P. K., Ahuja, S. S., et al. (2011). The CC chemokine receptor 5 regulates olfactory and social recognition in mice. *Neuroscience* 197, 153–161. doi: 10.1016/j.neuroscience.2011.09.039

Kandel, E. R. (2012). The molecular biology of memory: cAMP. PKA, CRE, CREB-1, CREB-2, and CPEB. *Mol. Brain* 5:14. doi: 10.1186/1756-6606-5-14

Kaul, M., Zheng, J., Okamoto, S., Gendelman, H. E., and Lipton, S. A. (2005). HIV-1 infection and AIDS: consequences for the central nervous system. *Cell Death Differ.* 12, 878–892. doi: 10.1038/sj.cdd.4401623

Khan, I. A., Thomas, S. Y., Moretto, M. M., Lee, F. S., Islam, S. A., Combe, C., et al. (2006). CCR5 is essential for NK cell trafficking and host survival following Toxoplasma gondii infection. *PLoS Pathogens* 2:e49. doi: 10.1371/journal.ppat.0020049

Klein, R. S., Williams, K. C., Alvarez-Hernandez, X., Westmoreland, S., Force, T., Lackner, A. A., et al. (1999). Chemokine receptor expression and signaling in macaque and human fetal neurons and astrocytes: implications for the neuropathogenesis of AIDS. *J. Immunol.* 163, 1636–1646.

Korbecki, J., Grochans, S., Gutowska, I., Barczak, K., and Baranowska-Bosiacka, I. (2020). CC Chemokines in a Tumor: A Review of Pro-Cancer and Anti-Cancer Properties of Receptors CCR5, CCR6, CCR7, CCR8, CCR9, and CCR10 Ligands. *Int. J. Mol. Sci.* 21:7619 doi: 10.3390/ijms21207619

Kostulas, N., Markaki, I., Kostulas, V., Hillert, J., and Kostulas, K. (2009). Common CCR 5 polymorphism in stroke: the CCR 5 delta32 polymorphism differentiates cardioembolism from other aetiologies of ischaemic cerebrovascular diseases. *Scand. J. Immunol.* 70, 475–480. doi: 10.1111/j.1365-3083.2009.02323.x

Kraft, K., Olbrich, H., Majoul, I., Mack, M., Proudfoot, A., and Oppermann, M. (2001). Characterization of sequence determinants within the carboxyl-terminal domain of chemokine receptor CCR5 that regulate signaling and receptor internalization. *J. Biol. Chem.* 276, 34408–34418. doi: 10.1074/jbc.M102782200

Kuipers, H. F., Biesta, P. J., Montagne, L. J., Van Haastert, E. S., Van Der Valk, P., and Van Den Elsen, P. J. (2008). CC chemokine receptor 5 gene promoter activation by the cyclic AMP response element binding transcription factor. *Blood* 112, 1610–1619. doi: 10.1182/blood-2008-01-135111

Kwong, P. D., Wyatt, R., Robinson, J., Sweet, R. W., Sodroski, J., and Hendrickson, W. A. (1998). Structure of an HIV gp120 envelope glycoprotein in complex with the CD4 receptor and a neutralizing human antibody. *Nature* 393, 648–659. doi: 10.1038/31405

Lau, S., Feitzinger, A., Venkiteswaran, G., Wang, J., Lewellis, S. W., Koplinski, C. A., et al. (2020). A negative-feedback loop maintains optimal chemokine concentrations for directional cell migration. *Nat. Cell Biol.* 22, 266–273. doi: 10.1038/s41556-020-0465-4

Laudati, E., Curro, D., Navarra, P., and Lisi, L. (2017). Blockade of CCR5 receptor prevents M2 microglia phenotype in a microglia-glioma paradigm. *Neurochem. Int.* 108, 100–108. doi: 10.1016/j.neuint.2017.03.002

Lee, Y. K., Kwak, D. H., Oh, K. W., Nam, S. Y., Lee, B. J., Yun, Y. W., et al. (2009). CCR5 deficiency induces astrocyte. *Neurobiol. Learn. Mem.* 92, 356–363. doi: 10.1016/j.nlm.2009.04.003

Leng, T., and Xiong, Z.-G. (2019). Treatment for ischemic stroke: From thrombolysis to thrombectomy and remaining challenges. *Brain Circ.* 5:8–11. doi: 10.4103/bc.bc_36_18

Li, P., Wang, L., Zhou, Y., Gan, Y., Zhu, W., and Xia, Y. (2017). C-C Chemokine Receptor Type 5 (CCR5)-Mediated Docking of Transferred Tregs Protects Against Early Blood-Brain Barrier Disruption After Stroke. *J. Am. Heart Assoc.* 6:e006387 doi: 10.1161/JAHA.117.006387

Li, S., Overman, J. J., Katsman, D., Kozlov, S. V., Donnelly, C. J., Twiss, J. L., et al. (2010). An age-related sprouting transcriptome provides molecular control of axonal sprouting after stroke. *Nat. Neurosci.* 13, 1496–1504. doi: 10.1038/nn.2674

Liraz-Zaltsman, S., Friedman-Levi, Y., Shabashov-Stone, D., Gincberg, G., and Atrakcy-Baranes, D. (2021). Chemokine Receptors CC Chemokine Receptor 5 and C-X-C Motif Chemokine Receptor 4 Are New Therapeutic Targets for Brain Recovery after Traumatic Brain Injury. *J. Neurotrauma.* 38, 2003–2017. doi: 10.1089/neu.2020.7015

Liu, Z., and Chopp, M. (2016). Astrocytes, therapeutic targets for neuroprotection and neurorestoration in ischemic stroke. *Prog. Neurobiol.* 144, 103–120. doi: 10.1016/j.pneurobio.2015.09.008

Lonze, B. E., and Ginty, D. D. (2002). Function and regulation of CREB family transcription factors in the nervous system. *Neuron* 35, 605–623. doi: 10.1016/s0896-6273(02)00828-0

López-Cotarelo, P., Gómez-Moreira, C., Criado-García, O., Sánchez, L., and Rodríguez-Fernández, J. L. (2017). Beyond Chemoattraction: Multifunctionality of Chemokine Receptors in Leukocytes. *Trends Immunol.* 38, 927–941. doi: 10.1016/j.it.2017.08.004

Lorenzen, E., Ceraudo, E., Berchiche, Y. A., Rico, C. A., Fürstenberg, A., Sakmar, T. P., et al. (2018). G protein subtype-specific signaling bias in a series of CCR5 chemokine analogs. *Sci. Signal.* 11:eaao6152 doi: 10.1126/scisignal.aao6152

Louboutin, J. P., Chekmasova, A., Marusich, E., Agrawal, L., and Strayer, D. S. (2011). Role of CCR5 and its ligands in the control of vascular inflammation and leukocyte recruitment required for acute excitotoxic seizure induction and neural damage. *FASEB J.* 25, 737–753. doi: 10.1096/fj.10-161851

Louboutin, J. P., and Strayer, D. S. (2013). Relationship between the chemokine receptor CCR5 and microglia in neurological disorders: consequences of targeting CCR5 on neuroinflammation, neuronal death and regeneration in a model of epilepsy. *CNS Neurol. Dis. Drug Targets* 12, 815–829. doi: 10.2174/18715273113126660173

Lu, Y., Jiang, B. C., Cao, D. L., Zhao, L. X., and Zhang, Y. L. (2017). Chemokine CCL8 and its receptor CCR5 in the spinal cord are involved in visceral pain induced by experimental colitis in mice. *Brain Res. Bull.* 135, 170–178. doi: 10.1016/j.brainresbull.2017.10.009

Luther, S. A., and Cyster, J. G. (2001). Chemokines as regulators of T cell differentiation. *Nat. Immunol.* 2, 102–107. doi: 10.1038/84205

Maghazachi, A. A. (2010). Role of chemokines in the biology of natural killer cells. *Curr. Top. Microbiol. Immunol.* 341, 37–58. doi: 10.1007/82_2010_20

Marciniak, E., Faivre, E., Dutar, P., pires, C., Demeyer, D., Caillierez, R., et al. (2015). The Chemokine MIP-1alpha/CCL3 impairs mouse hippocampal synaptic transmission, plasticity and memory. *Sci. Rep.* 5:15862. doi: 10.1038/srep15862

Maung, R., Hoefer, M. M., Sanchez, A. B., Sejbuk, N. E., Medders, K. E., and Desai, M. K. (2014). CCR5 knockout prevents neuronal injury and behavioral impairment induced in a transgenic mouse model by a CXCR4-using HIV-1 glycoprotein 120. *J. Immunol.* 193, 1895–1910. doi: 10.4049/jimmunol.1302915

Maurer, M., and von Stebut, E. (2004). Macrophage inflammatory protein-1. *Int. J. Biochem. Cell Biol.* 36, 1882–1886.

Medicine, U. N. L. O. (2019). *CinicalTrials.gov*. Available online at: https://clinicaltrials.gov/ct2/show/study/NCT03172026 (accessed April 13, 2022).

Mennicken, F., Chabot, J.-G., and Quirion, R. (2002). Systemic administration of kainic acid in adult rat stimulates expression of the chemokine receptor CCR5 in the forebrain. *Glia* 37, 124–138. doi: 10.1002/glia.10021

Menten, P., Wuyts, A., and Van damme, J. (2002). Macrophage inflammatory protein-1. *Cytokine Grow. Fact. Rev.* 13, 455–481.

Merino, J. J., Muneton-Gomez, V., Muneton-Gomez, C., Perez-Izquierdo, M. A., Loscertales, M., and Toledano Gasca, A. (2020). Hippocampal CCR5/RANTES Elevations in a Rodent Model of Post-Traumatic Stress Disorder: Maraviroc (a CCR5 Antagonist) Increases Corticosterone Levels and Enhances Fear Memory Consolidation. *Biomolecules* 10:212 doi: 10.3390/biom10020212

Meucci, O., Fatatis, A., Simen, A. A., Bushell, T. J., Gray, P. W., and Miller, R. J. (1998). Chemokines regulate hippocampal neuronal signaling and gp120 neurotoxicity. *Proc. Natl. Acad. Sci. U.S.A.* 95, 14500–14505. doi: 10.1073/pnas.95.24.14500

Missé, D., Esteve, P. O., Renneboog, B., Vidal, M., Cerutti, M., St Pierre, Y., et al. (2001). HIV-1 glycoprotein 120 induces the MMP-9 cytopathogenic factor production that is abolished by inhibition of the p38 mitogen-activated protein kinase signaling pathway. *Blood* 98, 541–547. doi: 10.1182/blood.v98.3.541

Molon, B., Gri, G., Bettella, M., Gómez-Moutón, C., Lanzavecchia, A., Martínez-A, C., et al. (2005). T cell costimulation by chemokine receptors. *Nat. Immunol.* 6, 465–471. doi: 10.1038/ni1191

Mueller, A., and Strange, P. G. (2004). CCL3, acting via the chemokine receptor CCR5, leads to independent activation of Janus kinase 2 (JAK2) and Gi proteins. *FEBS Lett.* 570, 126–132. doi: 10.1016/j.febslet.2004.04.100

Murphy, P. M., Baggiolini, M., Charo, I. F., Hébert, C. A., Horuk, R., Matsushima, K., et al. (2000). International union of pharmacology. XXII. Nomenclature for chemokine receptors. *Pharmacol. Rev.* 52, 145–176.

Musante, V., Longordo, F., Neri, E., Pedrazzi, M., Kalfas, F., Severi, P., et al. (2008). RANTES modulates the release of glutamate in human neocortex. *J. Neurosci.* 28, 12231–12240. doi: 10.1523/JNEUROSCI.3212-08.2008

Necula, D., Riviere-Cazaux, C., Shen, Y., and Zhou, M. (2021). Insight into the roles of CCR5 in learning and memory in normal and disordered states. *Brain Behav. Immun.* 92, 1–9. doi: 10.1016/j.bbi.2020.11.037

Neptune, E. R., and Bourne, H. R. (1997). Receptors induce chemotaxis by releasing the betagamma subunit of Gi, not by activating Gq or Gs. *Proc.Natl. Acad. Sci.U.S.A.* 94, 14489–14494. doi: 10.1073/pnas.94.26.14489

Oh, S. B., Endoh, T., Simen, A. A., Ren, D., and Miller, R. J. (2002). Regulation of calcium currents by chemokines and their receptors. *J. Neuroimmunol.* 123, 66–75. doi: 10.1016/s0165-5728(01)00485-4

Oppermann, M. (2004). Chemokine receptor CCR5: insights into structure, function, and regulation. *Cell. Signal.* 16, 1201–1210. doi: 10.1016/j.cellsig.2004.04.007

Park, M. H., Lee, Y. K., Lee, Y. H., Kim, Y. B., Yun, Y. W., Nam, S. Y., et al. (2009). Chemokines released from astrocytes promote chemokine receptor 5-mediated neuronal cell differentiation. *Exp. Cell Res.* 315, 2715–2726. doi: 10.1016/j.yexcr.2009.06.017

Paul, S., and Candelario-Jalil, E. (2021). Emerging neuroprotective strategies for the treatment of ischemic stroke: An overview of clinical and preclinical studies. *Exp. Neurol.* 335:113518. doi: 10.1016/j.expneurol.2020.113518

Pekny, M., Pekna, M., Messing, A., Steinhauser, C., Lee, J. M., Parpura, V., et al. (2016). Astrocytes: a central element in neurological diseases. *Acta Neuropathol.* 131, 323–345. doi: 10.1007/s00401-015-1513-1

Ping, S., Qiu, X., Kyle, M., and Zhao, L. R. (2021). Brain-derived CCR5 Contributes to Neuroprotection and Brain Repair after Experimental Stroke. *Aging Dis.* 12, 72–92. doi: 10.14336/AD.2020.0406

Piotrowska, A., Kwiatkowski, K., Rojewska, E., Makuch, W., and Mika, J. (2016). Maraviroc reduces neuropathic pain through polarization of microglia and astroglia - Evidence from *in vivo* and *in vitro* studies. *Neuropharmacology* 108, 207–219. doi: 10.1016/j.neuropharm.2016.04.024

Polazzi, E., and Contestabile, A. (2002). Reciprocal interactions between microglia and neurons: from survival to neuropathology. *Rev. Neurosci.* 13, 221–242. doi: 10.1515/revneuro.2002.13.3.221

Posfai, B., Cserep, C., Orsolits, B., and Denes, A. (2019). New Insights into Microglia-Neuron Interactions: A Neuron's Perspective. *Neuroscience* 405, 103–117. doi: 10.1016/j.neuroscience.2018.04.046

Radzik, T., Boczek, T., Ferenc, B., Studzian, M., Pulaski, L., and Zylinska, L. (2019). Calcium Dyshomeostasis Alters CCL5 Signaling in Differentiated PC12 Cells. *Biomed. Res. Int.* 2019, 9616248. doi: 10.1155/2019/9616248

Rossi, D., and Zlotnik, A. (2000). The biology of chemokines and their receptors. *Annu. Rev. Immunol.* 18, 217–242.

Rostène, W., Kitabgi, P., and Parsadaniantz, S. M. (2007). Chemokines: a new class of neuromodulator? Nature reviews. *Neuroscience* 8, 895–903. doi: 10.1038/nrn2255

Rottman, J. B., Ganley, K. P., Williams, K., Wu, L., Mackay, C. R., and Ringler, D. J. (1997). Cellular localization of the chemokine receptor CCR5. Correlation to cellular targets of HIV-1 infection. *Am. J. Pathol.* 151, 1341–1351.

Ru, W., and Tang, S. J. (2017). HIV-associated synaptic degeneration. *Mol. Brain* 10:40.

Sano, Y., Shobe, J. L., Zhou, M., Huang, S., Shuman, T., Cai, D. J., et al. (2014). CREB regulates memory allocation in the insular cortex. *Curr. Biol.*24, 2833–2837. doi: 10.1016/j.cub.2014.10.018

Schaechter, J. D. (2004). Motor rehabilitation and brain plasticity after hemiparetic stroke. *Prog. Neurobiol.* 73, 61–72. doi: 10.1016/j.pneurobio.2004.04.001

Schlager, C., Korner, H., Krueger, M., Vidoli, S., Haberl, M., and Mielke, D. (2016). Effector T-cell trafficking between the leptomeninges and the cerebrospinal fluid. *Nature* 530, 349–353. doi: 10.1038/nature16939

Servick, K. (2019). Unexpected drug emerges for stroke recovery. *Science* 363:805. doi: 10.1126/science.363.6429.805

Shideman, C. R., Hu, S., Peterson, P. K., and Thayer, S. A. (2006). CCL5 evokes calcium signals in microglia through a kinase-, phosphoinositide-, and nucleotide-dependent mechanism. *J. Neurosci. Res.* 83, 1471–1484. doi: 10.1002/jnr.20839

Simard, A. R., Soulet, D., Gowing, G., Julien, J. P., and Rivest, S. (2006). Bone marrow-derived microglia play a critical role in restricting senile plaque formation in Alzheimer's disease. *Neuron* 49, 489–502. doi: 10.1016/j.neuron.2006.01.022

Song, H., Stevens, C. F., and Gage, F. H. (2002). Astroglia induce neurogenesis from adult neural stem cells. *Nature* 417, 39–44. doi: 10.1038/417039a

Sorce, S., Bonnefont, J., Julien, S., Marq-Lin, N., Rodriguez, I., Dubois-Dauphin, M., et al. (2010). Increased brain damage after ischaemic stroke in mice lacking the chemokine receptor CCR5. *Br. J. Pharmacol.* 160, 311–321. doi: 10.1111/j.1476-5381.2010.00697.x

Sorce, S., Myburgh, R., and Krause, K.-H. (2011). The chemokine receptor CCR5 in the central nervous system. *Prog. Neurobiol.* 93, 297–311. doi: 10.1016/j.pneurobio.2010.12.003

Streit, W. J. (2002). Microglia as neuroprotective, immunocompetent cells of the CNS. *Glia* 40, 133–139. doi: 10.1002/glia.10154

Szabo, I., Chen, X. H., Xin, L., Adler, M. W., Howard, O. M., Oppenheim, J. J., et al. (2002). Heterologous desensitization of opioid receptors by chemokines inhibits chemotaxis and enhances the perception of pain. *Proc. Natl. Acad. Sci. U.S.A.* 99, 10276–10281. doi: 10.1073/pnas.102327699

Tene, O., Hallevi, H., Molad, J., Usher, S., Seyman, E., Bornstein, N. M., et al. (2021). CCR5-Delta32 polymorphism: a possible protective factor for post-stroke depressive symptoms. *J. Psychiatry Neurosci.* 46, E431–E440. doi: 10.1503/jpn.200197

Tran, P. B., Banisadr, G., Ren, D., Chenn, A., and Miller, R. J. (2007). Chemokine receptor expression by neural progenitor cells in neurogenic regions of mouse brain. *J. Comp. Neurol.* 500, 1007–1033. doi: 10.1002/cne.21229

Tyner, J. W., Uchida, O., Kajiwara, N., Kim, E. Y., Patel, A. C., O'sullivan, M. P., et al. (2005). CCL5-CCR5 interaction provides antiapoptotic signals for macrophage survival during viral infection. *Nat. Med.* 11, 1180–1187. doi: 10.1038/nm1303

Ubogu, E. E., Callahan, M. K., Tucky, B. H., and Ransohoff, R. M. (2006). Determinants of CCL5-driven mononuclear cell migration across the blood-brain barrier. Implications for therapeutically modulating neuroinflammation. *J. Neuroimmunol.* 179, 132–144. doi: 10.1016/j.jneuroim.2006.06.004

Villanueva, M. T. (2019). Repurposing CCR5 inhibitors for stroke recovery. *Nat. Rev. Drug Discov*. [Epub Online ahead of print]. doi: 10.1038/d41573-019-00038-3.

Wang, L., Conner, J. M., Nagahara, A. H., and Tuszynski, M. H. (2016). Rehabilitation drives enhancement of neuronal structure in functionally relevant neuronal subsets. *Proc. Natl. Acad. Sci. U.S.A.* 113, 2750–2755. doi: 10.1073/pnas.1514682113

Westmoreland, S. V., Alvarez, X., Debakker, C., Aye, P., Wilson, M. L., Williams, K. C., et al. (2002). Developmental expression patterns of CCR5 and CXCR4 in the rhesus macaque brain. *J. Neuroimmunol.* 122, 146–158. doi: 10.1016/s0165-5728(01)00457-x

Whitney, N. P., Eidem, T. M., Peng, H., Huang, Y., and Zheng, J. C. (2009). Inflammation mediates varying effects in neurogenesis: relevance to the pathogenesis of brain injury and neurodegenerative disorders. *J. Neurochem.* 108, 1343–1359. doi: 10.1111/j.1471-4159.2009.05886.x

Wong, M., Uddin, S., Majchrzak, B., Huynh, T., Proudfoot, A. E., Platanias, L. C., et al. (2001). Rantes activates Jak2 and Jak3 to regulate engagement of multiple signaling pathways in T cells. *J. Biol. Chem.* 276, 11427–11431. doi: 10.1074/jbc.M010750200

Wong, M. M., and Fish, E. N. (2003). Chemokines: attractive mediators of the immune response. *Semin. Immunol.*5, 5–14 doi: 10.1016/s1044-5323(02)00123-9

Wu, Y., Wang, L., Hu, K., Yu, C., Zhu, Y., Zhang, S., et al. (2018). Mechanisms and Therapeutic Targets of Depression After Intracerebral Hemorrhage. *Front. Psychiatry* 9:682. doi: 10.3389/fpsyt.2018.00682

Xia, M. Q., Qin, S. X., Wu, L. J., Mackay, C. R., and Hyman, B. T. (1998). Immunohistochemical study of the beta-chemokine receptors CCR3 and CCR5 and their ligands in normal and Alzheimer's disease brains. *Am. J. Pathol.* 153, 31–37. doi: 10.1016/s0002-9440(10)65542-3

Yan, J., Xu, W., Lenahan, C., Huang, L., Wen, J., Li, G., et al. (2021). CCR5 Activation Promotes NLRP1-Dependent Neuronal Pyroptosis via

CCR5/PKA/CREB Pathway After Intracerebral Hemorrhage. *Stroke* 52, 4021–4032. doi: 10.1161/STROKEAHA.120.033285

Yiu, A. P., Mercaldo, V., Yan, C., Richards, B., Rashid, A. J., Hsiang, H. L., et al. (2014). Neurons are recruited to a memory trace based on relative neuronal excitability immediately before training. *Neuron* 83, 722–735. doi: 10.1016/j.neuron.2014.07.017

Yu-Ju Wu, C., Chen, C. H., Lin, C. Y., Feng, L. Y., Lin, Y. C., Wei, K. C., et al. (2020). CCL5 of glioma-associated microglia/macrophages regulates glioma migration and invasion via calcium-dependent matrix metalloproteinase 2. *Neuro. Oncol.* 22, 253–266. doi: 10.1093/neuonc/noz189

Zang, Y. C., Samanta, A. K., Halder, J. B., Hong, J., Tejada-Simon, M. V., Rivera, V. M., et al. (2000). Aberrant T cell migration toward RANTES and MIP-1 alpha in patients with multiple sclerosis. Overexpression of chemokine receptor CCR5. *Brain* 123, 1874–1882. doi: 10.1093/brain/123.9.1874

Zeiler, S. R., Hubbard, R., Gibson, E. M., Zheng, T., Ng, K., O'brien, R., et al. (2016). Paradoxical Motor Recovery From a First Stroke After Induction of a Second Stroke: Reopening a Postischemic Sensitive Period. *Neurorehabil. Neural. Repair* 30, 794–800. doi: 10.1177/1545968315624783

Zhang, J., Liu, G., Chen, D., Wang, Z., Chen, D., Liu, Y., et al. (2020). The combination of CC chemokine receptor type 5(CCR5) and Treg cells predicts prognosis in patients with ischemic stroke. *J. Neuroimmunol.* 349:577404. doi: 10.1016/j.jneuroim.2020.577404

Zhou, M., Greenhill, S., Huang, S., Silva, T. K., Sano, Y., and Wu, S. (2016). CCR5 is a suppressor for cortical plasticity and hippocampal learning and memory. *Elife* 5:e20985 doi: 10.7554/eLife.20985

Zhou, Y., Won, J., Karlsson, M. G., Zhou, M., Rogerson, T., and Balaji, J. (2009). CREB regulates excitability and the allocation of memory to subsets of neurons in the amygdala. *Nat. Neurosci.* 12, 1438–1443. doi: 10.1038/nn.2405

Zlotnik, A., and Yoshie, O. (2012). The chemokine superfamily revisited. *Immunity* 36, 705–716. doi: 10.1016/j.immuni.2012.05.008

Conflict of Interest: The authors declare that the research was conducted in the absence of any commercial or financial relationships that could be construed as a potential conflict of interest.

Publisher's Note: All claims expressed in this article are solely those of the authors and do not necessarily represent those of their affiliated organizations, or those of the publisher, the editors and the reviewers. Any product that may be evaluated in this article, or claim that may be made by its manufacturer, is not guaranteed or endorsed by the publisher.

Copyright © 2022 Feng, Xu, Wang, Xiong, Xie, He, Chen, Liu, Li, Liu and Wu. This is an open-access article distributed under the terms of the Creative Commons Attribution License (CC BY). The use, distribution or reproduction in other forums is permitted, provided the original author(s) and the copyright owner(s) are credited and that the original publication in this journal is cited, in accordance with accepted academic practice. No use, distribution or reproduction is permitted which does not comply with these terms.

frontiers | Frontiers in Cellular Neuroscience

ORIGINAL RESEARCH
published: 20 May 2022
doi: 10.3389/fncel.2022.915969

Ablation of GSDMD Attenuates Neurological Deficits and Neuropathological Alterations After Traumatic Brain Injury

*Hao Du[1], Chang-Hong Li[1], Ruo-Bing Gao[1], Xiao-Qing Cen[1,2] and Ping Li[1,3]**

[1]Department of Army Occupational Disease, State Key Laboratory of Trauma, Burns and Combined Injury, Research Institute of Surgery and Daping Hospital, Army Medical University (Third Military Medical University), Chongqing, China, [2]College of Bioengineering, Chongqing University, Chongqing, China, [3]Institute of Brain and Intelligence, Army Medical University (Third Military Medical University), Chongqing, China

Pyroptosis plays a significant role in neuroinflammation after traumatic brain injury (TBI). However, the role of pyroptosis executor Gasdermin D (GSDMD) in neurological deficits and neuropathological alterations after TBI have not been elucidated. Our results demonstrated that GSDMD-KO exerted striking neuroprotective effects on motor dysfunction and neuropathological alterations (loss of synaptic proteins, microglia activation, astrogliosis, dendrite injury, and neuron death) at 3 days after TBI. GSDMD-KO inhibited the expression and release of pro-inflammatory cytokine releases (IL-1β and TNF-α) while promoting those of anti-inflammatory cytokines (IL-10 and TGF-β1). The temporal pattern of diverse inflammasome signals showed long-lasting elevations of NLRP3, caspase 1, and caspase 1 p20 after TBI, rather than NLRP1, NLRC4 or AIM2, similar to the change in GSDMD postinjury; and NLRP3-KO not only inhibited the expression and cleavage of GSDMD but also attenuated the loss of synaptic proteins and neurological deficits. Notably, RNA sequencing showed both GSDMD-KO and NLRP3-KO reversed the global expression of neuroinflammation- and neuropathology-related genes after TBI. Our findings proved that the inhibition of GSDMD exerts neuroprotective effects after TBI and is mainly driven by the NLRP3 inflammasome. GSDMD serves as a potent therapeutic target for the treatment of TBI.

Keywords: GSDMD, NLRP3 inflammasome, traumatic brain injury, neuroinflammation, neuropathology

OPEN ACCESS

Edited by:
Anwen Shao,
Zhejiang University, China

Reviewed by:
Di Hu,
Case Western Reserve University, United States
Tian Weidong,
Shihezi University, China
Xintong Ge,
Tianjin Medical University General Hospital, China

****Correspondence:***
Ping Li
ping_ping0074@sina.com

Specialty section:
This article was submitted to Cellular Neuropathology, a section of the journal Frontiers in Cellular Neuroscience

Received: *08 April 2022*
Accepted: *02 May 2022*
Published: *20 May 2022*

Citation:
Du H, Li C-H, Gao R-B, Cen X-Q and Li P (2022) Ablation of GSDMD Attenuates Neurological Deficits and Neuropathological Alterations After Traumatic Brain Injury. Front. Cell. Neurosci. 16:915969. doi: 10.3389/fncel.2022.915969

INTRODUCTION

Traumatic brain injury (TBI) is a great challenge that imposes heavy social and economic burdens worldwide and affects more than 50 million people each year (Jiang et al., 2019). TBI is considered a double-phase injury characterized by a primary injury caused by external forces and a delayed secondary injury (O Brien et al., 2020). The long-term outcomes of TBI are mainly determined by secondary injury, which has drawn extensive attention from researchers. It has been demonstrated that diverse mechanisms contribute to the progression of secondary injury after TBI, including reactive oxygen species, mitochondrial dysfunction, blood brain barrier dysfunction, and

neuroinflammation, while long-lasting neuroinflammation is considered the main contributor to the development of secondary injury (Corps et al., 2015; Morganti-Kossmann et al., 2019). Neuroinflammation development is implicated in numerous processes, including inflammatory cell infiltration and the release of inflammatory cytokines. The overactivation of neuroinflammation is considered the main reason for many of the complications that occur after TBI, such as motor dysfunction and cognitive deficits (Corps et al., 2015; Wilson et al., 2017). Therefore, the regulation of neuroinflammation after TBI has drawn extensive attention for TBI treatment.

Inflammasome signals have been implicated in the modulation of neuroinflammation in many central nervous system (CNS) diseases including Alzheimer's disease (AD), Parkinson's disease (PD), depression, and TBI (Ismael et al., 2021; Li et al., 2021). However, most of these studies focused on the most well-known NLRP3 inflammasome or the inflammasome signaling effector caspase 1 (Irrera et al., 2017; Liu et al., 2018), while they rarely paid attention to the pyroptosis executor gasdermin D (GSDMD).

GSDMD is a member of gasdermin family and has membrane pore-forming activity (Shi et al., 2017). The activation of inflammatory caspases (caspase 1/11 in mice or caspase 4/5 in humans) leads to the cleavage of full-length GSDMD at the Asp276 or Asp275 site in mice and humans, respectively, which then breaks the link between the two domains and releases the N-terminal domain (N-GSDMD) and C-terminal domain (C-GSDMD). The cleavage of this link abolishes the autoinhibition of the C-GSDMD domain on the N-GSDMD domain, and the latter then oligomerizes and binds to the cell membrane to form pores (Pandeya et al., 2019). It was newly found that the cleavage of GSDMD by inflammatory caspases (mainly caspase 1) is essential for pyroptosis and IL-1β secretion in mouse macrophages (He et al., 2015; Shi et al., 2015). Although it has been proven that GSDMD plays a crucial role in the ischemic stroke and experimental autoimmune encephalomyelitis mouse models (Li et al., 2019; Wang et al., 2020), the role of GSDMD in neuroinflammation progression after TBI has not been investigated.

The cleavage of GSDMD is driven by diverse inflammasome signals, which share the same downstream effector caspase 1 in the canonical pathway (Shi et al., 2017; Burdette et al., 2021). Moreover, it has been reported that multiple inflammasomes, including NLRP1, AIM2, NLRP3, and NLRC4, participate in the progression of neuroinflammation after TBI and that directly or indirectly targeting inflammasome signaling could mitigate neuroinflammation and contribute to better outcomes (de Rivero Vaccari et al., 2009; Ge et al., 2018; Sun et al., 2020). Nevertheless, these studies have not shown a temporal alteration of diverse inflammasomes after TBI or determined the main contributor among them. Because GSDMD is activated by many inflammasome signals, inhibition of a single inflammasome pathway may not be sufficiently effective. Therefore, we aim to explore the temporal changes in different inflammasomes after TBI and determine the dominant inflammasome pathway involved in neuroinflammation progression after TBI, which will enhance our understanding of the mechanisms of GSDMD-mediated neuroinflammation.

In this study, we investigated the temporal pattern of GSDMD and its localization after TBI. As the levels of GSDMD increased rapidly and dramatically postinjury, we aimed to investigate the neurobehavioral and neuropathological alterations in the early stage after TBI. Our results showed that GSDMD knockout (GSDMD-KO) attenuated neurological deficits and neuropathological alterations mainly by regulating inflammatory cytokine release at 3 days after TBI. Further studies confirmed that the NLRP3 inflammasome was the main contributor to the cleavage of GSDMD rather than other inflammasomes; and NLRP3 knockout (NLRP3-KO) also exerted neuroprotective effects similar to those of GSDMD-KO. Moreover, transcriptome RNA sequencing (RNA-seq) showed that both GSDMD-KO and NLRP3-KO reversed the global expression of neuroinflammation- and neuropathology-related genes. These results demonstrated GSDMD is a potent therapeutic target for TBI that is mainly driven by the NLRP3 inflammasome.

MATERIALS AND METHODS

Animals

GSDMD$^{-/-}$ mice (C57BL/6J background) were generated using CRISPR/Cas9 technique by the Cyagen Model Organisms company. Male and female heterozygous GSDMD$^{+/-}$ mice were mated to obtain homozygous and littermate WT control mice. The genotype was identified using PCR, and the primers are shown in the **Supplementary Tables S1**, **S2**. The knockout out efficiency were verified by WB. Mice were housed in the animal center of Daping Hospital, Army Medical University [Certificate SCXK (Yu) 2002-0002, Chongqing, China]. All animal experiments were approved by the Laboratory Animal Welfare and Ethics Committee of the Army Medical University (AMUWEC20191822) and complied with the NIH Guide for the Care and Use of Laboratory Animals.

TBI Model

The controlled cortical impact method was used to produce moderate TBI models with methods described previously (Li et al., 2008). Briefly, mice were anesthetized with intraperitoneal injection of 250 μl 2.5% Tribromoethanol (Sigma, T48402) and then subjected to a 5-mm-diameter craniotomy in the left parietal cortex. The center was placed between bregma and the lambdoid suture. An aerodynamic impact device (PSI, USA) with a 3-mm-diameter metal tip was used to produce the controlled cortical impact (2 mm below the dura, 3.5 m/s impact speed). Sham animals underwent the same procedure as TBI mice except for the impact.

Western Blot (WB)

WB was performed as previously reported (Du et al., 2022). Briefly, brain tissues were lysed using RIPA buffer containing protease inhibitor cocktail (Thermo Scientific). The protein concentration was measured using a BCA kit (Solarbio). Proteins were denatured and electrophoresed with 10% stain-free

SDS-PAGE gels (Bio-Rad). Total protein was visualized with Bio-Rad stain-free technology using a ChemiDoc imaging system (Bio-Rad). Then, the proteins were transferred to PVDF membranes and blocked for 1 h using quick-block solutions (Beyotime). Membranes were incubated with specific primary antibodies overnight at 4°C with gentle shaking. The antibodies used in the article and the dilutions were as follows: GSDMD (Abcam, ab219800), 1:1,000; N-GSDMD (CST, 10137), 1:1,000; PSD95 (Abcam, ab192757), 1:1,000; SYN1 (Abcam, ab254349), 1:1,000; SNAP25 (Abcam, ab109105), 1:1,000; VAMP1 (Abcam, ab151712), 1:1,000; NLRP1 (Santa Cruz, sc-390133), 1:200; NLRP3 (Adipogen, AG-20B-0014), 1:1,000; NLRC4 (Abcam, ab201792), 1:1,000; AIM2 (CST, 63660), 1:1,000; caspase 1 (Adipogen, AG-20B-0042), 1:1,000; caspase 1 p20 (CST, 89332), 1:1,000. The next day, the membranes were washed five times with TBST and incubated with specific horseradish peroxidase-conjugated secondary antibodies at 37°C for 1 h. Finally, the membranes were washed again and imaged by a ChemiDoc image system (Bio-Rad). Data were analyzed using ImageLab software (Bio-Rad).

Immunofluorescence

Immunofluorescence was carried out as previously reported (Zhang et al., 2020). Coronal brain sections (30 μm) were made using a cryotome (Leica). The brain slices were washed with PBS and permeabilized using 0.3% Triton X-100. After that, 10% goat serum was used for slice blocking. Primary antibody solutions were made according to the dilution rate provided by manufacturers and applied to the slice incubations at 4°C overnight with gentle shaking. The primary antibodies and dilutions used in the article were as follows: GSDMD (Abcam, ab219800), 1:100; Iba-1 (Sigma, SAB2702364), 1:100; GFAP (CST, 3670), 1:200; NeuN (Millipore, MAB377), 1:100; CD68 (Abcam, ab125212), 1:500; GFAP (Abcam, ab7260), 1:300; MAP2 (Abcam, ab32454), 1:500. The next day, the slices were rewarmed at 37°C for 1 h and washed three times with PBS. Corresponding secondary antibodies (Abcam) were diluted and used for staining following by nuclear labeling using DAPI (10 μg/ml, Sigma). Finally, the slices were washed and mounted using antifade mounting medium (Santa). Then, the slices were imaged with confocal microscopy (Leica) and analyzed using ImageJ software (NIH).

Behavioral Tests

As we aimed to explore neurofunctions at the early stage of TBI, we mainly examined changes in motor functions rather than cognition and learning memories, as they are affected by imbalanced motor functions. GSDMD-KO and NLRP3-KO mice as well as their littermate control mice were used for behavioral tests. All mice were chosen randomly and behavioral tests were performed by lab technicians who were blinded to the genotype and treatment of mice.

Neurological Severity Score (NSS) Test

Mice were scored for neurological severity at 3 days after TBI using the method reported before (Zeng et al., 2018). Neuromuscular function, performance on an inclined board, mobility, vestibulomotor function, and complex neuromotor functions were evaluated. The range of scores was from 0 to 20, with 0 for normal and 20 for the severest injury.

Beam Walk Test

The fine motor coordination of TBI mice was assessed by a beam walk test as described previously (Henry et al., 2020). Briefly, mice were placed on a 1-cm-width wooden beam, and the number of foot faults of the right hindlimb was recorded over 50 steps. Mice were trained for 3 days before sham or TBI and tested at 3 days after TBI.

Accelerating Rotarod Test

Gross motor function and balance were assessed on the accelerating rotarod as reported previously (Henry et al., 2020). Mice were placed on the rod, which accelerated from 4 to 40 RPM within 300 s. The latency to fall from the rod (or cling to and rotate with the rod) was recorded. Each mouse was given three trials at 3 days after TBI, and the latency times were averaged. A 10 min rest period with access to food and water was allowed between each trial.

Open Field Test

Spontaneous locomotor activity was assessed using the open field test as reported (Fan et al., 2017). The total distance traveled, and the times spent in the center area and in the perimeter were recorded across a 5-min recording period.

Quantitative PCR (qPCR)

qPCR was performed as reported before (Du et al., 2022). Briefly, total RNA was extracted with an RNA isolation kit (Promega). The RNA purity and concentration were detected by a NanoDrop One UV spectrophotometer. Reverse transcription was conducted using a GoScript Reverse Transcription kit (Promega) according to the manufacturer's instructions. cDNA was amplified using GoTaq qPCR mix (Promega) and the corresponding primers (**Supplementary Table S3**). The qPCR was performed for 40 cycles at 95°C for 15 s and 60°C for 1 min after an initial 10 min incubation at 95°C.

Enzyme-Linked Immunosorbent Assay (ELISA)

Mouse IL-1β, TNF-α, IL-10, and TGF-β1 ELISA kits (Novus, Valukine VAL601, VAL609, VAL605, and VAL611) were used for the detection of IL-1β, TNF-α, IL-10, and TGF-β1 in the cortex lysates according to manufacturer's instructions.

RNA-Seq Data Analysis

Samples from the peri-injury and sham cortex of GSDMD-KO, NLRP3-KO, and WT mice were obtained and flash frozen in liquid nitrogen. Then, the samples were processed for RNA sequencing analysis at Shanghai Majorbio Biopharm Technology Company. Total RNA was extracted from the tissue using TRIzol Reagent and genomic DNA was removed using Dnase I (TaKara). The RNA quality was determined and only high-quality RNA sample (OD260/280 = 1.8–2.2, OD260/230≥2.0, RIN≥6.5, 28S: 18S≥1.0, >1 μg) was used for sequencing library construction. The RNA-seq transcriptome library was constructed using Truseq^{TM} RNA Sample Prep Kit (Illumina, FC-122-1002) and paired-end RNA-seq sequencing

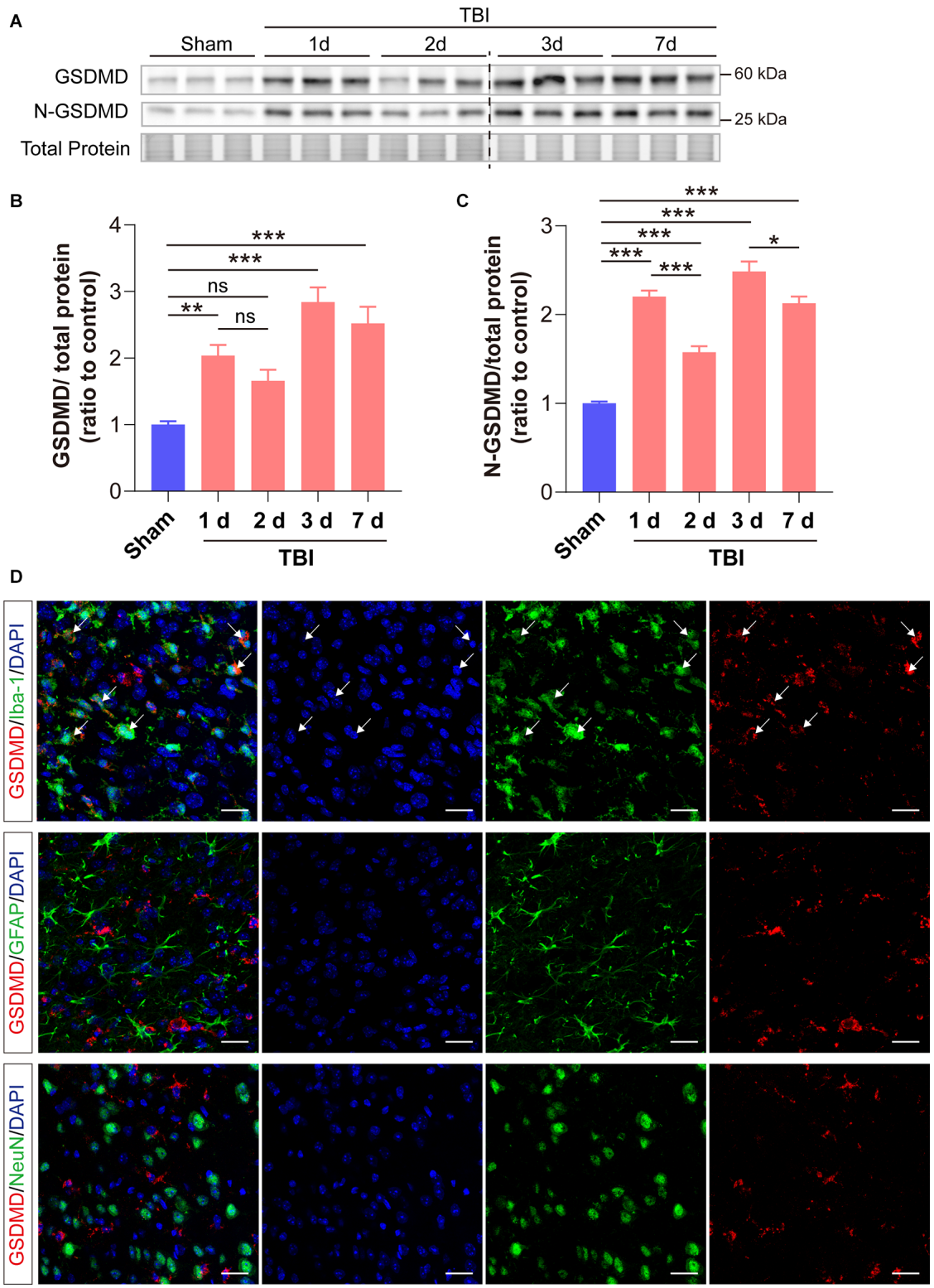

FIGURE 1 | GSDMD increased significantly in the peri-injury cortex after TBI and was mainly localized in microglia. **(A)** Representative images of immunoblots for GSDMD, N-GSDMD, and total protein. **(B,C)** Quantitative analysis of GSDMD and N-GSDMD protein levels ($n = 6$). **(D)** Representative immunofluorescence showed the localization of GSDMD (green) with Iba-1, GFAP, and NeuN (red), in the peri-injury cortex at 3 days after TBI. Scale bar = 20 μm. White arrows indicate GSDMD$^+$ and Iba-1$^+$ cells. All data are presented as the mean ± SEM and were analyzed using one-way ANOVA followed by Tukey's multiple comparisons test for significance. ns $p > 0.05$, $^*p < 0.05$, $^{**}p < 0.01$, and $^{***}p < 0.001$.

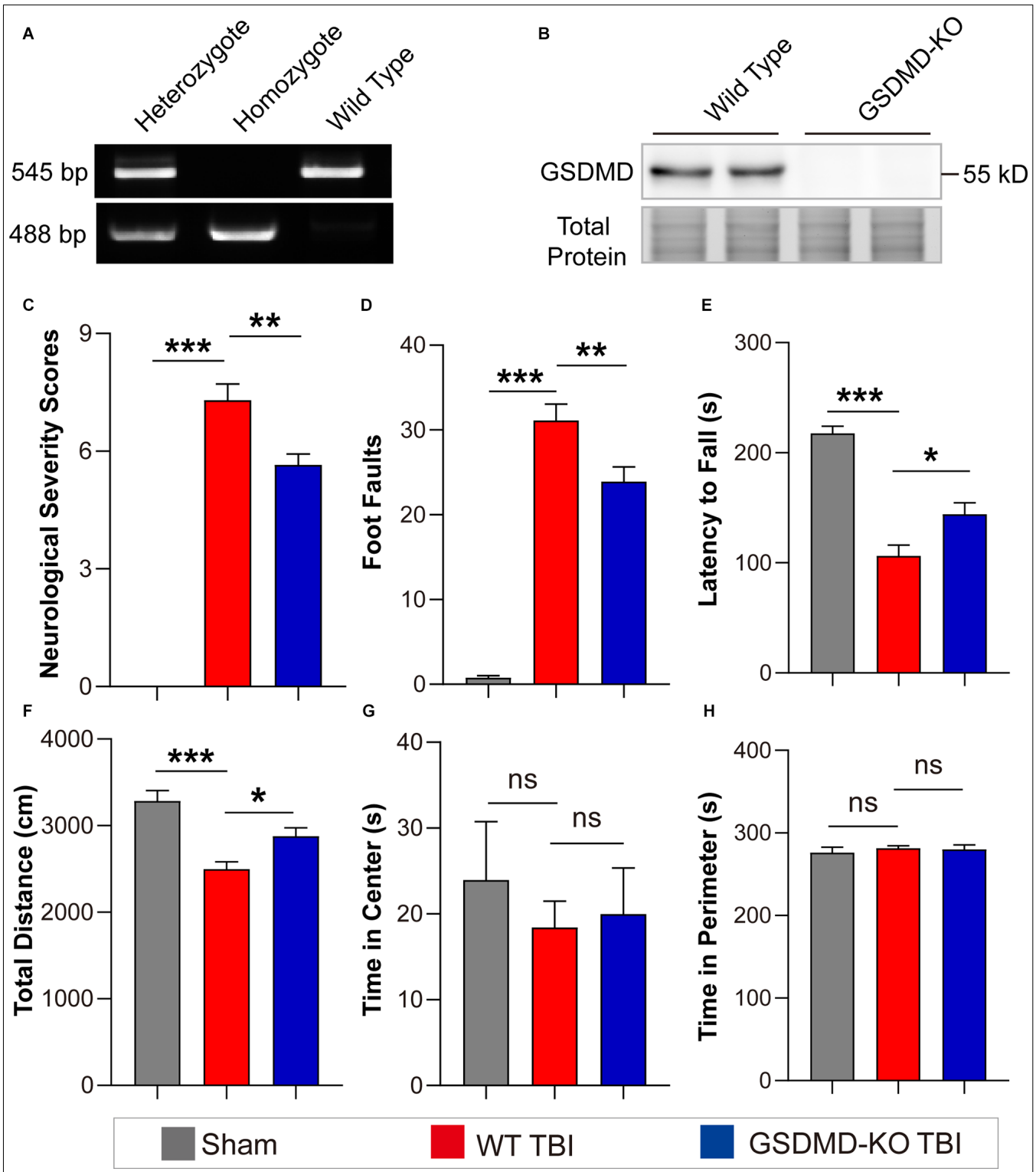

FIGURE 2 | GSDMD-KO attenuated neurological deficits at 3 days after TBI. **(A)** Representative images of agarose gel electrophoresis for GSDMD-KO mouse genotyping. **(B)** Representative images of immunoblots for GSDMD using brain samples from WT mice and GSDMD-KO mice. **(C–E)** Quantitative analysis of NSS scores, foot faults, and latency to fall (s) from NSS test, beam walk test, and accelerating rotarod test at 3 days after TBI (n = 9–10). **(F–H)** Quantitative analysis of total distance (cm), time in center (s), and time in perimeter (s) in the open field test at 3 days after TBI (n = 9–10). All data are presented as the mean ± SEM and were analyzed using one-way ANOVA followed by Tukey's multiple comparisons test for significance. ns $p > 0.05$, *$p < 0.05$, **$p < 0.01$, and ***$p < 0.001$.

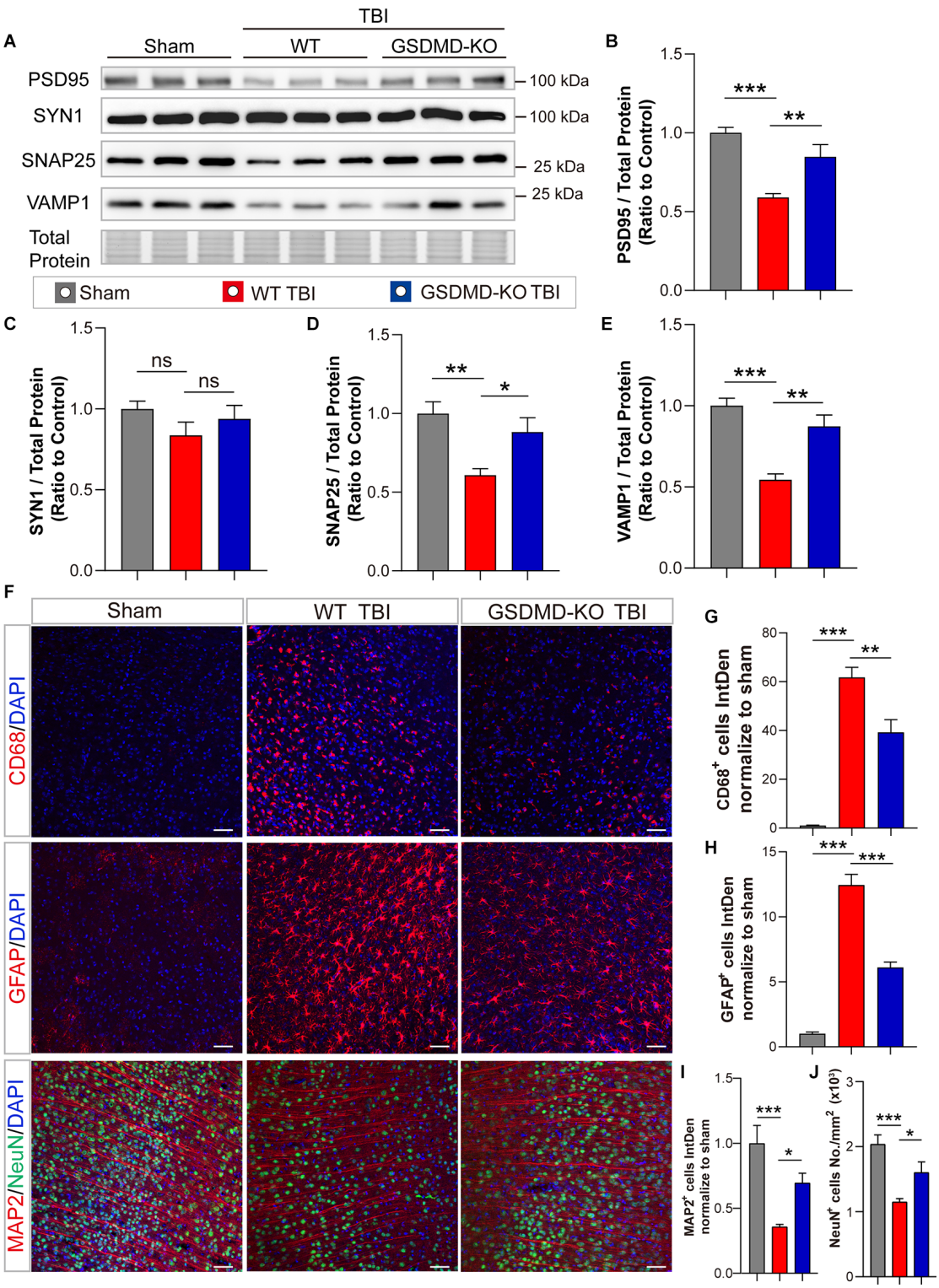

FIGURE 3 | GSDMD-KO mitigated neuropathological alterations in the peri-injury cortex at 3 days after TBI. **(A)** Representative images of immunoblots for synaptic proteins (PSD95, SYN1, SNAP25, and VAMP1) and total protein. **(B–E)** Quantitative analysis of synaptic proteins (n = 6). **(F)** Representative immunofluorescence images of CD68, GFAP, MAP2, and NeuN in the peri-injury cortex after TBI or in the paired sham cortex. Scale bar = 50 μm. **(G–J)** Quantitative analysis of integrated intensity of $CD68^+$, $GFAP^+$, and $MAP2^+$ cells and $NeuN^+$ cell number/mm^2 in the cortex (three slices from each brain and three brains were used for calculation). All data are presented as the mean ± SEM and were analyzed using one-way ANOVA followed by Tukey's multiple comparisons test for significance. ns $p > 0.05$, $^*p < 0.05$, $^{**}p < 0.01$, and $^{***}p < 0.001$.

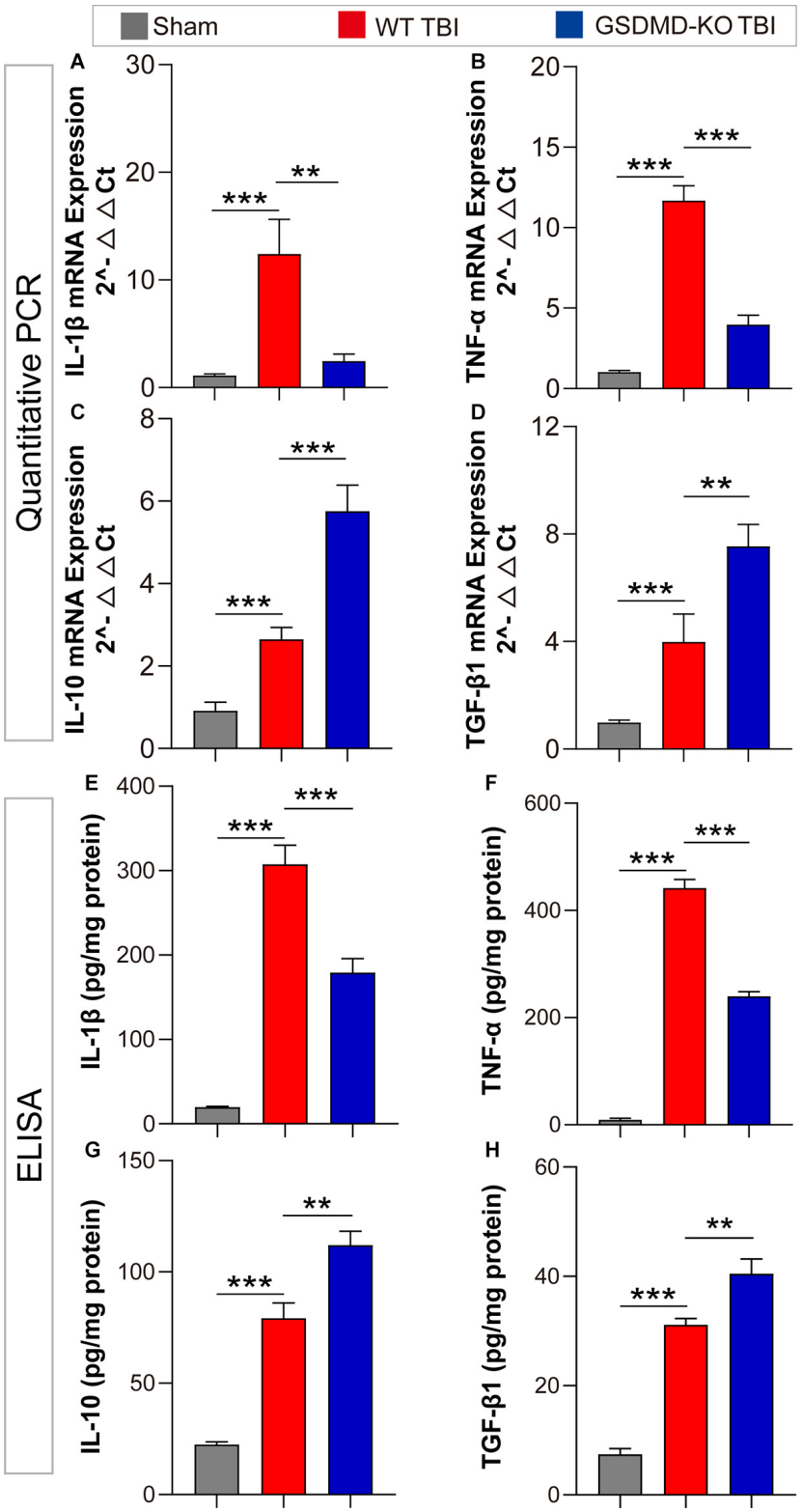

FIGURE 4 | GSDMD-KO diminished pro-inflammatory cytokine release but enhanced anti-inflammatory cytokine release at 3 days after TBI. **(A–D)** Quantitative analysis of IL-1β, TNF-α, IL-10, and TGF-β1 mRNA levels detected by qPCR (n = 7–8). **(E–H)** Quantitative analysis of IL-1β, TNF-α, IL-10, and TGF-β1 levels in the cortex lysates detected by ELISA (n = 6). All data are presented as the mean ± SEM and were analyzed using one-way ANOVA followed by Tukey's multiple comparisons test for significance. $^{**}p < 0.01$ and $^{***}p < 0.001$.

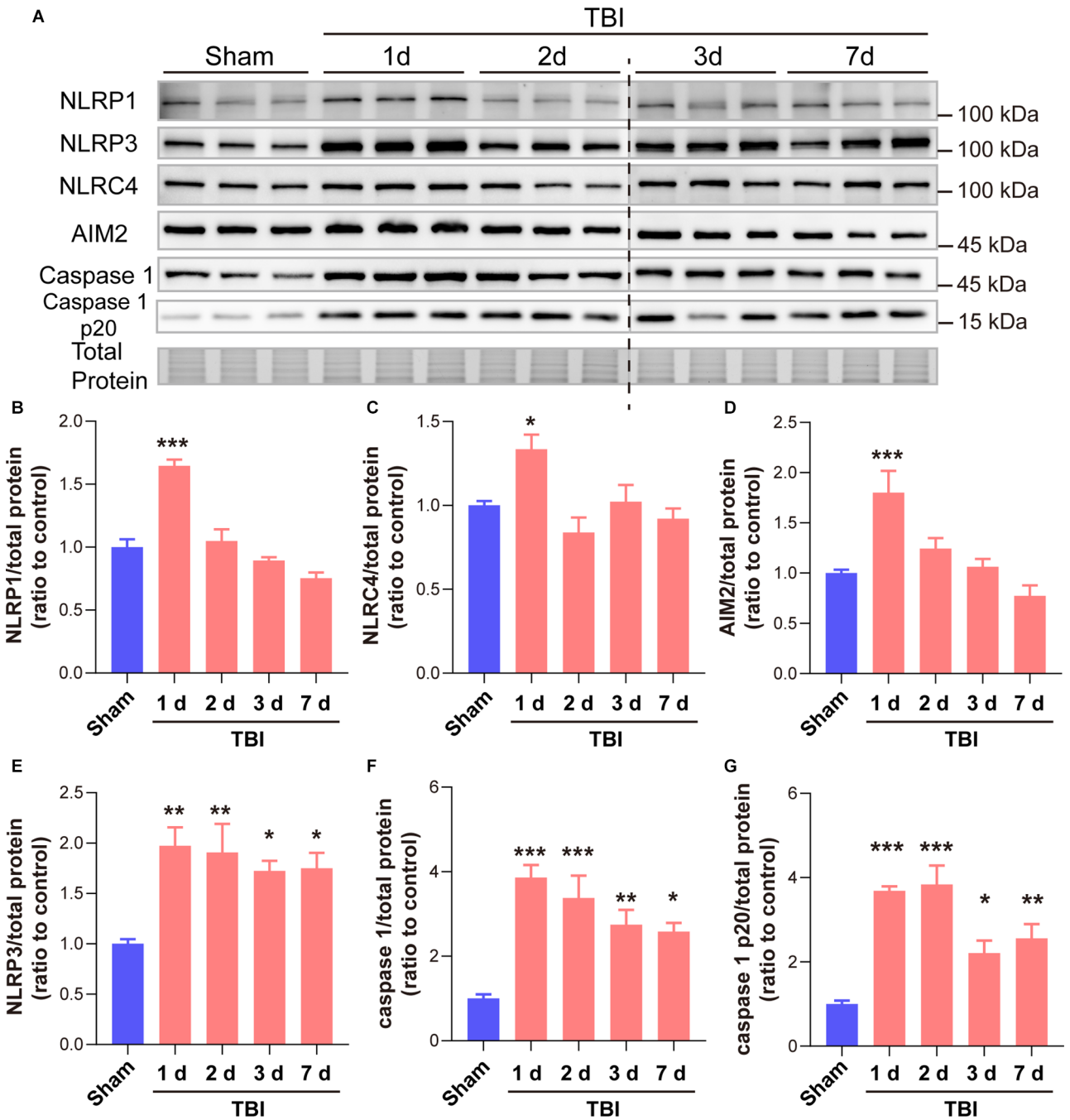

FIGURE 5 | GSDMD cleavage after TBI was mainly driven by the NLRP3 inflammasome rather than the NLRP1, NLRC4, and AIM2 inflammasomes. **(A)** Representative immunoblots images of NLRP1, NLRP3, NLRC4, AIM2, caspase 1, caspase 1 p20, and total protein. **(B–G)** Quantitative analysis of NLRP1, NLRC4, AIM2, NLRP3 caspase 1, and caspase 1 p20 levels ($n = 6$). All data are presented as the mean ± SEM and were analyzed using one-way ANOVA followed by Tukey's multiple comparisons test for significance. $^{*}p < 0.05$, $^{**}p < 0.01$, and $^{***}p < 0.001$.

library was sequenced with Illumina HiSeq xten/NovaSeq 6000 sequencer (2 × 150 bp read length). The raw paired end reads were trimmed and quality controlled by SeqPrep[1] and Sickle[2] with default parameters. Then clean reads were separately aligned to reference genome (GRCm39) with orientation mode using HISAT2 software (Kim et al., 2015). The mapped

[1]https://github.com/jstjohn/SeqPrep

[2]https://github.com/najoshi/sickle

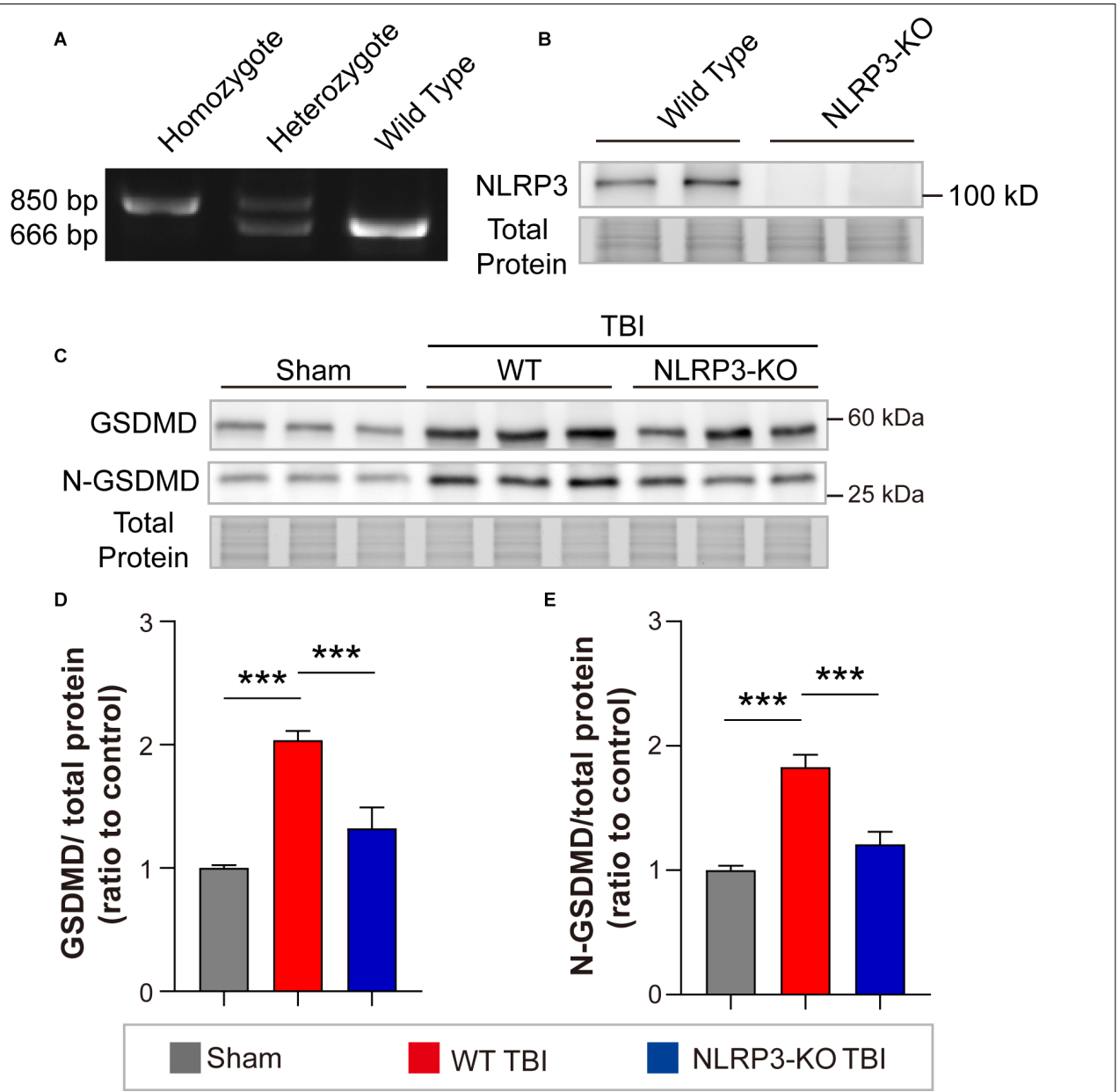

FIGURE 6 | NLRP3-KO inhibited the expression and cleavage of GSDMD at 3 days after TBI. **(A)** Representative images of agarose gel electrophoresis for NLRP3-KO mouse genotyping. **(B)** Representative images of immunoblots for NLRP3 using brain samples from WT mice and NLRP3-KO mice. **(C)** Representative images of immunoblots for GSDMD, N-GSDMD, and total protein. **(D,E)** Quantitative analysis of GSDMD and N-GSDMD levels ($n = 6$). All data are presented as the mean ± SEM and were analyzed using one-way ANOVA followed by Tukey's multiple comparisons test for significance. ***$p < 0.001$.

reads of each sample were assembled by StringTie (Pertea et al., 2015). PCA were performed using the online Majorbio Cloud Platform[3]. Neuroinflammation- and neuropathology-related gene lists were downloaded from Nanostring.com, as they are widely used in the transcriptome analysis of CNS diseases and are well elucidated (Ising et al., 2019; Tsai et al., 2021). The neuroinflammation- (685 genes) and neuropathology- (703 genes) related genes were extracted from the total expression matrix and analyzed with R language (version 4.1.2; **Supplementary File 2**). The heatmaps were visualized using the pheatmap package[4]. The raw data have been uploaded to the SRA database under the accession number PRJNA820566.

Statistics

Quantitative data are presented as the mean ± SEM. All data passed the normality test (Kolmogorov–Smirnov test) and were

[3]www.majorbio.com

[4]https://cran.r-project.org/web/packages/pheatmap/index.html

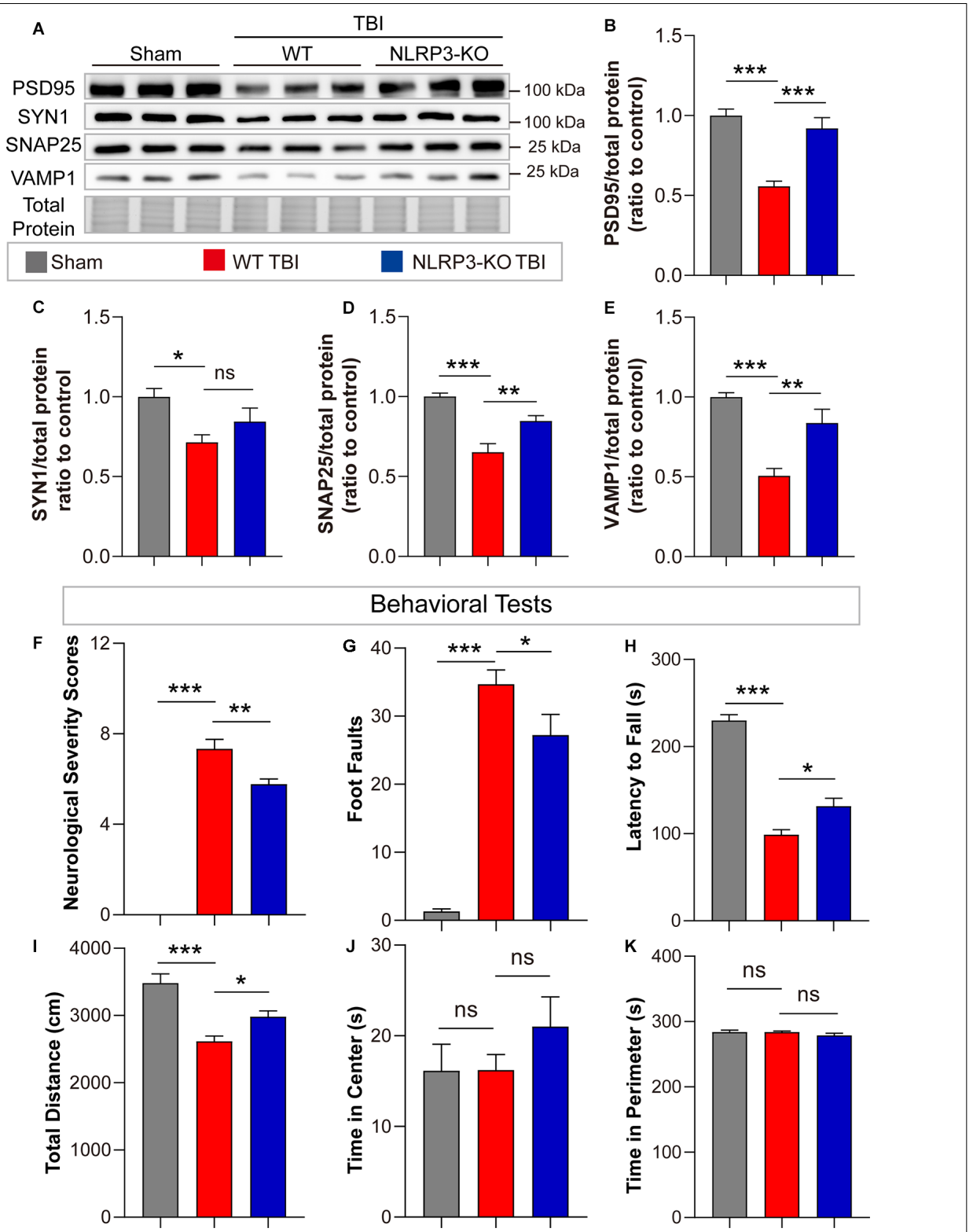

FIGURE 7 | NLRP3-KO attenuated synaptic protein loss and neurological deficits at 3 days after TBI. **(A)** Representative images of immunoblots for synaptic proteins (PSD95, SYN1, SNAP25, and VAMP1) and total protein. **(B–E)** Quantitative analysis of synaptic proteins ($n = 6$). **(F–H)** Quantitative analysis of NSS scores, foot faults and latency to fall (s) from the NSS test, beam walk test, and accelerating rotarod test ($n = 9–10$). **(I–K)** Quantitative analysis of total distance (cm), time in center (s) and time in perimeter (s) in the open field test ($n = 9–10$). All data are presented as the mean ± SEM and were analyzed using one-way ANOVA followed by Tukey's multiple comparisons test for significance. ns $p > 0.05$, $^{*}p < 0.05$, $^{**}p < 0.01$, and $^{***}p < 0.001$.

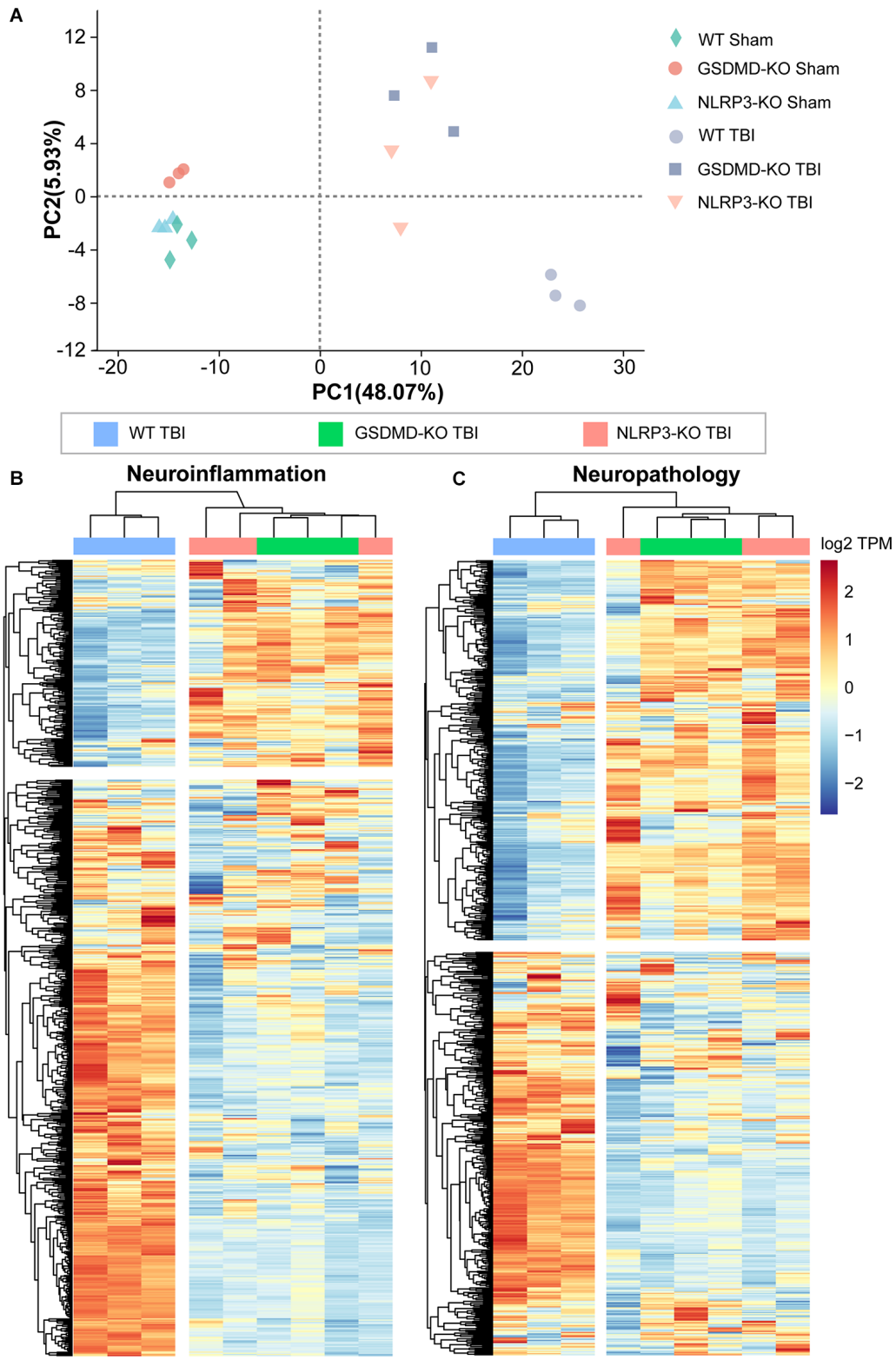

FIGURE 8 | Both GSDMD-KO and NLRP3-KO reversed the global expression of neuroinflammation- and neuropathology-related genes at 3 days after TBI. **(A)** PCA analysis of RNA-seq data from WT, GSDMD-KO, and NLRP3-KO mice at 3 days after sham or TBI treatment (n = 3). **(B,C)** Heatmap analysis of neuroinflammation- and neuropathology-related gene expression patterns from WT, NLRP3-KO, and GSDMD-KO mice at 3 days after TBI.

analyzed using one-way ANOVA followed by Tukey's multiple comparisons test for three or more groups *via* GraphPad Prism 8. The p value < 0.05 was considered statistically significant.

RESULTS

GSDMD Increased Significantly in the Peri-injury Cortex After TBI and Was Mainly Localized in Microglia

We first investigated the changes of GSDMD protein levels and its localization after TBI. Our results showed that the levels of GSDMD and N-GSDMD increased from 1 to 7 days after TBI and peaked at 3 days, while there was a small decrease at 2 days after TBI (**Figures 1A–C**). Moreover, immunofluorescence demonstrated that GSDMD was mainly localized in microglia (**Figure 1D**). These data suggested that microglial GSDMD participated in the neuroinflammation progression in the early stage of TBI; therefore, we aimed to explore the neurobehavioral and neuropathological changes during this stage postinjury.

GSDMD-KO Attenuated Neurological Deficits and Neuropathological Alterations in the Peri-injury Cortex at 3 Days After TBI

As the levels of GSDMD and N-GSDMD peaked at 3 days after TBI, neurobehavioral tests were performed at this timepoint. GSDMD-KO was verified by PCR and WB (**Figures 2A,B**). The neurofunctions of GSDMD-KO and wild-type (WT) mice were examined with neurobehavioral tests used in this study to exclude differences caused by gene knockout. The results showed that NSS scores were 0 and foot faults were fewer than 3 for all mice, and there were also no significant differences in the accelerating rotarod test and the open field test (**Supplementary Figures S1A–D**). Then, neurobehavioral tests were performed on mice after TBI or sham treatment. The results proved that GSDMD-KO mice had lower NSS scores and foot faults than WT mice after TBI in the NSS test and the beam walk test (**Figures 2C,D**). GSDMD-KO mice exhibited a higher latency to fall and total distance, while no significant differences in the time spent in the center or perimeter during the accelerating rotarod test and the open field test (**Figures 2E–H**). These results confirmed that GSDMD-KO alleviated neurological deficits at 3 days after TBI.

In addition, levels of synaptic proteins (PSD95, SNAP25, and VAMP1) from the peri-injury cortex were remarkably increased in GSDMD-KO mice compared to WT mice at 3 days after TBI, while there was no significant difference in the SYN1 protein level (**Figures 3A–E**). Moreover, as shown by immunofluorescence, GSDMD-KO reduced the levels of $CD68^+$ cells and $GFAP^+$ cells (**Figures 3F–H**) and enhanced the densities of $MAP2^+$ cells and $NeuN^+$ cells in the peri-injury cortex at 3 days postinjury (**Figures 3F,I,J**). These data demonstrated that GSDMD-KO could mitigate neuropathological alterations at 3 days after TBI.

GSDMD-KO Diminished Pro-inflammatory Cytokine Release but Enhanced Anti-inflammatory Cytokine Release at 3 Days After TBI

As GSDMD plays an important role in the release of inflammatory cytokines, we investigated the effects of GSDMD-KO on the expression and release of pro-inflammatory (IL-1β and TNF-α) and anti-inflammatory (IL-10 and TGF-β1) cytokines. Our results showed that GSDMD-KO significantly reduced the expression and release of IL-1β and TNF-α while enhancing those of IL-10 and TGF-β1 in the peri-injury cortex at 3 days after TBI (**Figures 4A–H**). These findings confirmed that GSDMD exerts neuroprotective effects by regulating inflammatory cytokines.

GSDMD Cleavage After TBI Was Mainly Driven by the NLRP3 Inflammasome Rather Than the NLRP1, NLRC4, and AIM2 Inflammasomes

As many types of inflammasomes participate in the activation and cleavage of GSDMD, we then tested the temporal patterns of diverse inflammasome proteins, including NLRP1, NLRP3, NLRC4, and AIM2, as well as the downstream co-effector caspase 1 and caspase 1 p20. Our results showed that NLRP1, NLRC4, and AIM2 only increased at 1 day after TBI while no significant differences at 2 days to 7 days after TBI (**Figures 5A–D**). However, long-term elevations in NLRP3, caspase 1, and caspase 1 p20 were found from 1 day to 7 days after TBI (**Figures 5E–G**). These data demonstrated that the temporal expression patterns of NLRP3, caspase 1, and caspase 1 p20 were similar to those of GSDMD and N-GSDMD after TBI, rather than NLRP1, AIM2, and NLRC4, suggesting that the NLRP3 inflammasome pathway mainly contributes to the activation of GSDMD after TBI.

NLRP3-KO Inhibited the Expression and Cleavage of GSDMD and Attenuated Synaptic Protein Loss and Neurological Deficits at 3 Days After TBI

To interrogate whether NLRP3 regulates GSDMD after TBI and its contributions to outcomes postinjury, we further investigated the effects of NLRP3-KO on the expression and cleavage of GSDMD, loss of synaptic proteins (PSD95, SYN1, SNAP25, and VAMP1) and neurological functions after TBI. The NLRP3-KO efficiency was verified by PCR and WB (**Figures 6A,B**). Our results showed that NLRP3-KO reduced the levels of GSDMD and N-GSDMD at 3 days after TBI (**Figures 6C–E**).

In addition, remarkable increases in synaptic proteins (PSD95, SNAP25, and VAMP1) were found in NLRP3-KO mice compared to WT mice after TBI, but there was no significant difference in SYN1 protein levels (**Figures 7A–E**). The neurofunctions of NLRP3-KO and wild-type (WT) mice were examined and the results showed no significant differences between them (**Supplementary Figures S1E–H**). Then neurobehavioral tests were performed on mice after TBI or sham treatment. The results demonstrated NLRP3-KO TBI

group showed lower NSS scores and foot faults than the WT TBI group (**Figures 7F,G**). Increasing latency to fall and total distance were observed in NLRP3-KO mice compared to WT mice after TBI, while there were no differences in the time spent in center or perimeter (**Figures 7H–K**). These results showed that NLRP3-KO exerts neuroprotective effects similar to those of GSDMD-KO by mitigating the expression and cleavage of GSDMD, which further confirmed that GSDMD cleavage is mainly driven by the NLRP3 inflammasome after TBI.

Both GSDMD-KO and NLRP3-KO Reversed the Global Expression of Neuroinflammation- and Neuropathology-Related Genes at 3 Days After TBI

We performed transcriptome RNA-seq to investigate the effects of GSDMD-KO and NLRP3-KO on the global expression of neuroinflammation- and neuropathology-related genes at 3 days after TBI. Principal component analysis (PCA) showed that the gene expression patterns of GSDMD-KO and NLRP3-KO mice were similar to those of WT mice before TBI but were strikingly different after TBI (**Figure 8A**). Moreover, heatmaps of neuroinflammation- and neuropathology-related gene expression showed similar expression patterns among GSDMD-KO, NLRP3-KO, and WT mice before TBI (**Supplementary Figure S2**) but remarkable different patterns were showed in GSDMD-KO and NLRP3-KO mice compared with WT mice (**Figures 8B,C**). In addition, expression patterns of neuroinflammation- and neuropathology-related genes in GSDMD-KO and NLRP3-KO groups were clustered together, which proved the similar roles of them at this timepoint after TBI (**Figures 8B,C**). Our results demonstrated GSDMD-KO and NLRP3-KO could globally reverse the expressions of neuroinflammation- and neuropathology-related genes at 3 days after TBI and the two groups are clustered together, which suggested both of them are in the same pathway.

DISCUSSION

In this study, we demonstrated the crucial role of GSDMD in early stage after TBI. The expression and cleavage of GSDMD increased at 1 day after TBI and lasted until 7 days. However, there was a small decrease at 2 days after TBI, which might be due to the subsidence of mechanical damage-induced acute inflammation; and it is also found that in the cerebrospinal fluid from infants and children with severe TBI, NLRP3 protein levels peaked within 24 h after TBI and then decreased at 25–48 h while increasing again from 48 h (Wallisch et al., 2017). This quadratic trend suggests that inflammasome signaling participates in both primary and secondary injury after TBI. Moreover, we found that levels of GSDMD and N-GSDMD peaked at 3 days after TBI, similar to the levels of NLRP3 inflammasome as reported previously (Xu et al., 2018). A previous study showed that many markers of M1 and M2 phenotype microglia/macrophage peaked at 3–5 days after TBI (Wang et al., 2013). Meanwhile, we also found that GSDMD mainly localized in microglia after TBI in the peri-injury cortex, which suggests that microglial GSDMD might be involved in microglial polarization. In general, our results illustrated the temporal pattern of GSDMD expression and cleavage as well as its localization, contributing to a better understanding of the crucial role of GSDMD in neuroinflammation progression after TBI.

GSDMD-KO showed striking neuroprotective effects on motor dysfunction at 3 days after TBI. It's also reported that GSDMD-KO mice showed lower modified NSS scores than WT mice in an ischemic stroke animal model (Wang et al., 2020). A previous study showed that GSDMD-KO mice had lower clinical scores than their WT counterparts in an experimental autoimmune encephalomyelitis model (Li et al., 2019). These results proved that GSDMD plays an essential role in the neurofunctional impairment of CNS diseases and that its inhibition contributes to better outcomes. Moreover, abundant studies have reported that the inhibition of inflammasome signals protects against neurological deficits in TBI, PD, AD, subarachnoid hemorrhage, vascular dementia, etc. (Irrera et al., 2017; Ising et al., 2019; Poh et al., 2020; Rui et al., 2020; Hu et al., 2021). However, these studies usually reported one of the inflammasome signals. GSDMD is activated by diverse inflammasome signals and serves as the executor of pyroptosis, so the inhibition to GSDMD might result in better neurofunctional outcomes than single pathway inhibition.

The neuropathological alterations caused by TBI, including synaptic protein loss, microglial activation, astrogliosis, dendritic injury, and neuronal death were remarkably mitigated by GSDMD-KO. Some studies have reported that levels of synaptic proteins decreased after TBI at acute stage (1–7 days), which reflects the severity of injury (Feng et al., 2016; Rehman et al., 2018; Rosa et al., 2021); and pharmacological treatments that attenuated the loss of synaptic proteins protects against motor dysfunction post TBI (Rehman et al., 2018), which is also found in our study. Therefore, the change of synaptic proteins could reflect the motor dysfunction severity at acute stage post TBI. Moreover, the neuron death was mitigated by GSDMD-KO in our manuscript. There might be two reasons for this neuroprotective effect. First, GSDMD-KO attenuated neuroinflammation after TBI and therefore reduced the inflammation-induced neural apoptosis. Apoptosis also affects the development of neuroinflammation. So the inhibition of inflammasome signals also contribute to apoptosis attenuation. Second, NLRP3 is also expressed in neurons after TBI as reported before (Liu et al., 2013). Therefore, neuronal NLRP3 inflammasome activation might result in neuron pyroptosis directly. The attenuation of microglial activation, astrogliosis, and dendritic injury by GSDMD-KO also contribute to better neurofunction postinjury. Moreover, GSDMD-KO also regulated inflammatory cytokine release after TBI by diminishing pro-inflammatory cytokine release and promoting anti-inflammatory cytokine release. As it has been proven that the membrane pore-forming effects of GSDMD is essential for IL-1β secretion in macrophages (He et al., 2015), GSDMD also plays a pivotal role in the

inflammatory cytokines release in CNS diseases, including TBI. The effects of GSDMD on inflammatory cytokine release regulation might be the main reason for reduced neuropathological changes after TBI in the GSDMD-KO mice.

We further investigated the temporal pattern of diverse inflammasome signals, the effects of NLRP3-KO on GSDMD activation and neurofunctional alterations. We finally confirmed that NLRP3 played a dominant role in the development of neuroinflammation after TBI rather than NLRP1, AIM2 or NLRC4 inflammasomes. It has been reported that NLRP1 knockout mice had no significant better outcomes than WT mice after TBI (Brickler et al., 2016). Some studies have shown that different inflammasomes increased after TBI and that targeting inflammasome signals *via* inhibiting the NLRP3 inflammasome pharmacologically or genetically, using caspase 1 inhibitors or anti-ASC antibodies, could attenuate neuroinflammation postinjury (de Rivero Vaccari et al., 2009; Irrera et al., 2017; Ge et al., 2018; Xu et al., 2018; Kuwar et al., 2019; Sun et al., 2020). However, a comprehensive understanding to the temporal pattern of diverse inflammasome signal activation after TBI is still needed to better understanding the role of inflammasome signals in neuroinflammation. We confirmed the expressions of NLRP3, caspase 1, and caspase 1 p20 elevated from 1 to 7 days after TBI and further proved the neuroprotective effects of NLRP3-KO postinjury. Moreover, RNA-seq analysis showed that expression patterns of neuroinflammation- and neuropathology-related genes in the GSDMD-KO TBI and the NLRP3-KO TBI groups were clustered together and both of them showed remarkable reversals to the global expression of neuroinflammation- and neuropathology-related genes. Our results demonstrated that the NLRP3-GSDMD pathway is the dominant inflammasome signal for neuroinflammation and neuropathology regulation after TBI.

In terms of the clinical translation of pyroptosis inhibition, more researches are still needed. First, the inhibition to NLRP3 protein directly usually aims to block the NACHT domain of NLRP3, including CY-09, Tranilast, Bay 11-7082, and MCC950 (Swanson et al., 2019; Li et al., 2021). This strategy is considered as the most efficient and specific way to control pyroptosis. However, as many of these chemical compounds are newly found so the clinical safety and side-effects in clinical translation should be considered. The clinical trial of the most well-known NLRP3 inhibitor MCC950 was suspended owing to hepatic toxicity (Swanson et al., 2019). In addition, other researchers aimed to develop caspase 1 inhibitors for the attenuation of inflammasome activation. Although the role of caspase 1 in cell death and inflammation have been demonstrated, emerging researches showed alternative caspase-independent pathway activated when performing caspase inhibition, which resulted in inadequate efficacy (Dhani et al., 2021); and the poor target specificity also limits the clinical application of caspase inhibitors (Kesavardhana et al., 2020). GSDMD was newly found as a pyroptosis executor and serves as a potent target for pyroptosis related diseases (Shi et al., 2015); and it is found that disulfiram, a drug used to treat alcohol addiction, could inhibit pyroptosis by blocking GSDMD pore formation (Hu et al., 2020). As this drug is almost approved by FDA and used in clinical practice, so the toxicity and side-effects are acceptable compared with other pyroptosis inhibitors. Other GSDMD inhibitors including necrosulfonamide and LDC7559 were also screened out, but there is a long way to develop them into clinical applications (Shi et al., 2017; Pandeya et al., 2019).

However, there are also limitations of our work. Although we aimed to investigate the effects of GSDMD on TBI-induced neurological deficits and neuropathological alterations in the early stage due to the high level of GSDMD at this time, the expression and cleavage of GSDMD is still higher at 7 days post TBI, so the long-term effects of GSDMD on TBI-induced brain damage including dementia and tauopathy should be investigated. It has been reported that the inflammasome activation and downstream IL-1β processing were found at 14 months post repetitive mild TBI and IL-1 receptor 1 knockout attenuated accumulation of pro-IL-1β and misfolded tau, thus protected against cognitive deficits post TBI (Wu et al., 2022). But the role of pyroptosis executor GSDMD on TBI-induced damage in the chronic stage remains elucidated. In our work, we only investigated the neuroprotective effects of GSDMD on TBI in the early stage, the long-term effects should be explored in the future.

CONCLUSIONS

In this study, we investigated the temporal patterns of GSDMD expression and activation, which implicated that GSDMD participates in neuroinflammation progression in the early stage after TBI. Moreover, GSDMD-KO attenuated neurological deficits and neuropathological alterations after TBI and was mainly driven by the NLRP3 inflammasome pathway. Transcriptome RNA-seq showed that both GSDMD-KO and NLRP3-KO reversed the global expression patterns of neuroinflammation- and neuropathology-related genes at 3 days after TBI and their expression patterns were clustered together. Our studies shed new light on understanding the role of GSDMD in neuroinflammation regulation after TBI and provide a potent target for TBI therapy.

DATA AVAILABILITY STATEMENT

The datasets presented in this study can be found in online repositories. The names of the repository/repositories and accession number(s) can be found below: https://www.ncbi.nlm.nih.gov/, PRJNA820566.

ETHICS STATEMENT

The animal study was reviewed and approved by the Laboratory Animal Welfare and Ethics Committee of the Army Medical University.

AUTHOR CONTRIBUTIONS

HD performed the construction of TBI mice model, western blots, immunofluorescence, quantitative analysis, RNA-seq data analysis, interpreted results, and wrote the manuscript. C-HL and R-BG performed mice genotyping, behavioral tests, and immunofluorescence. X-QC sampled mice, performed ELISA, and qPCR. PL conceived, designed, and supervised the study, interpreted results, and wrote the manuscript. All authors contributed to the article and approved the submitted version.

FUNDING

This research was funded by the Talent Pool of Army Medical University.

SUPPLEMENTARY MATERIAL

The Supplementary Material for this article can be found online at: https://www.frontiersin.org/articles/10.3389/fncel.2022.915969/full#supplementary-material.

REFERENCES

Brickler, T., Gresham, K., Meza, A., Coutermarsh-Ott, S., Williams, T. M., Rothschild, D. E., et al. (2016). Nonessential role for the NLRP1 inflammasome complex in a murine model of traumatic brain injury. *Mediators Inflamm.* 2016, 1–11. doi: 10.1155/2016/6373506

Burdette, B. E., Esparza, A. N., Zhu, H., and Wang, S. (2021). Gasdermin d in pyroptosis. *Acta Pharm. Sin. B.* 11, 2768–2782. doi: 10.1016/j.apsb.2021.02.006

Corps, K. N., Roth, T. L., and McGavern, D. B. (2015). Inflammation and neuroprotection in traumatic brain injury. *JAMA Neurol.* 72:355. doi: 10.1001/jamaneurol.2014.3558

de Rivero Vaccari, J. P., Lotocki, G., Alonso, O. F., Bramlett, H. M., Dietrich, W. D., Keane, R. W., et al. (2009). Therapeutic neutralization of the NLRP1 inflammasome reduces the innate immune response and improves histopathology after traumatic brain injury. *J. Cereb. Blood Flow Metab.* 29, 1251–1261. doi: 10.1038/jcbfm.2009.46

Dhani, S., Zhao, Y., and Zhivotovsky, B. (2021). A long way to go: caspase inhibitors in clinical use. *Cell Death Dis.* 12:949. doi: 10.1038/s41419-021-04240-3

Du, H., Tan, Y., Li, C., Zhao, Y., Li, P., Ning, Y., et al. (2022). High glutamate concentration reverses the inhibitory effect of microglial adenosine 2A receptor on NLRP3 inflammasome assembly and activation. *Neurosci. Lett.* 769:136431. doi: 10.1016/j.neulet.2021.136431

Fan, Z., Liang, Z., Yang, H., Pan, Y., Zheng, Y., Wang, X., et al. (2017). Tenuigenin protects dopaminergic neurons from inflammation via suppressing NLRP3 inflammasome activation in microglia. *J. Neuroinflamm.* 14:256. doi: 10.1186/s12974-017-1036-x

Feng, Y., Cui, Y., Gao, J., Li, R., Jiang, X., Tian, Y., et al. (2016). Neuroprotective effects of resveratrol against traumatic brain injury in rats: involvement of synaptic proteins and neuronal autophagy. *Mol. Med. Rep.* 13, 5248–5254. doi: 10.3892/mmr.2016.5201

Ge, X., Li, W., Huang, S., Yin, Z., Xu, X., Chen, F., et al. (2018). The pathological role of NLRs and AIM2 inflammasome-mediated pyroptosis in damaged blood-brain barrier after traumatic brain injury. *Brain Res.* 1697, 10–20. doi: 10.1016/j.brainres.2018.06.008

He, W. T., Wan, H., Hu, L., Chen, P., Wang, X., Huang, Z., et al. (2015). Gasdermin D is an executor of pyroptosis and required for interleukin-1beta secretion. *Cell Res.* 25, 1285–1298. doi: 10.1038/cr.2015.139

Henry, R. J., Ritzel, R. M., Barrett, J. P., Doran, S. J., Jiao, Y., Leach, J. B., et al. (2020). Microglial depletion with CSF1R inhibitor during chronic phase of experimental traumatic brain injury reduces neurodegeneration and neurological deficits. *J. Neurosci.* 40, 2960–2974. doi: 10.1523/JNEUROSCI.2402-19.2020

Hu, J. J., Liu, X., Xia, S., Zhang, Z., Zhang, Y., Zhao, J., et al. (2020). FDA-approved disulfiram inhibits pyroptosis by blocking gasdermin D pore formation. *Nat. Immunol.* 21, 736–745. doi: 10.1038/s41590-020-0669-6

Hu, X., Yan, J., Huang, L., Araujo, C., Peng, J., Gao, L., et al. (2021). INT-777 attenuates NLRP3-ASC inflammasome-mediated neuroinflammation via TGR5/cAMP/PKA signaling pathway after subarachnoid hemorrhage in rats. *Brain Behav. Immun.* 91, 587–600. doi: 10.1016/j.bbi.2020.09.016

Irrera, N., Pizzino, G., Calò, M., Pallio, G., Mannino, F., Famà, F., et al. (2017). Lack of the nlrp3 inflammasome improves mice recovery following traumatic brain injury. *Front. Pharmacol.* 8:459. doi: 10.3389/fphar.2017.00459

Ising, C., Venegas, C., Zhang, S., Scheiblich, H., Schmidt, S. V., Vieira-Saecker, A., et al. (2019). NLRP3 inflammasome activation drives tau pathology. *Nature* 575, 669–673. doi: 10.1038/s41586-019-1769-z

Ismael, S., Ahmed, H., Adris, T., Parveen, K., Thakor, P., and Ishrat, T. (2021). The NLRP3 inflammasome: a potential therapeutic target for traumatic brain injury. *Neural Regen. Res.* 16:49. doi: 10.4103/1673-5374.286951

Jiang, J. Y., Gao, G. Y., Feng, J. F., Mao, Q., Chen, L. G., Yang, X. F., et al. (2019). Traumatic brain injury in China. *Lancet Neurol.* 18, 286–295. doi: 10.1016/S1474-4422(18)30469-1

Kesavardhana, S., Malireddi, R., and Kanneganti, T. D. (2020). Caspases in cell death, inflammation and pyroptosis. *Annu. Rev. Immunol.* 38, 567–595. doi: 10.1146/annurev-immunol-073119-095439

Kim, D., Langmead, B., and Salzberg, S. L. (2015). HISAT: a fast spliced aligner with low memory requirements. *Nat. Methods* 12, 357–360. doi: 10.1038/nmeth.3317

Kuwar, R., Rolfe, A., Di, L., Xu, H., He, L., Jiang, Y., et al. (2019). A novel small molecular NLRP3 inflammasome inhibitor alleviates neuroinflammatory response following traumatic brain injury. *J. Neuroinflamm.* 16:81. doi: 10.1186/s12974-019-1471-y

Li, W., Dai, S., An, J., Li, P., Chen, X., Xiong, R., et al. (2008). Chronic but not acute treatment with caffeine attenuates traumatic brain injury in the mouse cortical impact model. *Neuroscience* 151, 1198–1207. doi: 10.1016/j.neuroscience.2007.11.020

Li, Y., Huang, H., Liu, B., Zhang, Y., Pan, X., Yu, X., et al. (2021). Inflammasomes as therapeutic targets in human diseases. *Signal Transduct. Target Ther.* 6:247. doi: 10.1038/s41392-021-00650-z

Li, S., Wu, Y., Yang, D., Wu, C., Ma, C., Liu, X., et al. (2019). Gasdermin d in peripheral myeloid cells drives neuroinflammation in experimental autoimmune encephalomyelitis. *J. Exp. Med.* 216, 2562–2581. doi: 10.1084/jem.20190377

Liu, W., Chen, Y., Meng, J., Wu, M., Bi, F., Chang, C., et al. (2018). Ablation of caspase-1 protects against TBI-induced pyroptosis *in vitro* and *in vivo*. *J. Neuroinflamm.* 15:48. doi: 10.1186/s12974-018-1083-y

Liu, H., Li, W., Chen, Z., Hu, Y., Zhang, D., Shen, W., et al. (2013). Expression of the NLRP3 inflammasome in cerebral cortex after traumatic brain injury in a rat model. *Neurochem. Res.* 38, 2072–2083. doi: 10.1007/s11064-013-1115-z

Morganti-Kossmann, M. C., Semple, B. D., Hellewell, S. C., Bye, N., and Ziebell, J. M. (2019). The complexity of neuroinflammation consequent to traumatic brain injury: from research evidence to potential treatments. *Acta Neuropathol.* 137, 731–755. doi: 10.1007/s00401-018-1944-6

O Brien, W. T., Pham, L., Symons, G. F., Monif, M., Shultz, S. R., and McDonald, S. J. (2020). The NLRP3 inflammasome in traumatic brain injury: potential as a biomarker and therapeutic target. *J. Neuroinflamm.* 17:104. doi: 10.1186/s12974-020-01778-5

Pandeya, A., Li, L., Li, Z., and Wei, Y. (2019). Gasdermin D (GSDMD) as a new target for the treatment of infection. *MedChemComm* 1, 66–667. doi: 10.1039/c9md00059c

Pertea, M., Pertea, G. M., Antonescu, C. M., Chang, T. C., Mendell, J. T., Salzberg, S. L., et al. (2015). StringTie enables improved reconstruction

of a transcriptome from RNA-seq reads. *Nat. Biotechnol.* 33, 290–295. doi: 10.1038/nbt.3122

Poh, L., Fann, D. Y., Wong, P., Lim, H. M., Foo, S. L., Kang, S., et al. (2020). AIM2 inflammasome mediates hallmark neuropathological alterations and cognitive impairment in a mouse model of vascular dementia. *Mol. Psychiatr.* 26, 4544–4560. doi: 10.1038/s41380-020-00971-5

Rehman, S. U., Ahmad, A., Yoon, G., Khan, M., Abid, M. N., Kim, M. O., et al. (2018). Inhibition of c-Jun N-Terminal kinase protects against brain damage and improves learning and memory after traumatic brain injury in adult mice. *Cereb. Cortex* 28, 2854–2872. doi: 10.1093/cercor/bhx164

Rosa, J. M., Farré Alins, V., Ortega, M. C., Navarrete, M., Lopez Rodriguez, A. B., Palomino Antolín, A., et al. (2021). TLR4 pathway impairs synaptic number and cerebrovascular functions through astrocyte activation following traumatic brain injury. *Br. J. Pharmacol.* 178, 3395–3413. doi: 10.1111/bph.15488

Rui, W., Li, S., Xiao, H., Xiao, M., and Shi, J. (2020). Baicalein attenuates neuroinflammation by inhibiting NLRP3/caspase-1/GSDMD pathway in MPTP induced mice model of Parkinson's disease. *Int. J. Neuropsychopharmacol.* 23, 762–773. doi: 10.1093/ijnp/pyaa060

Shi, J., Gao, W., and Shao, F. (2017). Pyroptosis: Gasdermin-Mediated programmed necrotic cell death. *Trends Biochem. Sci.* 42, 245–254. doi: 10.1016/j.tibs.2016.10.004

Shi, J., Zhao, Y., Wang, K., Shi, X., Wang, Y., Huang, H., et al. (2015). Cleavage of GSDMD by inflammatory caspases determines pyroptotic cell death. *Nature* 526, 660–665. doi: 10.1038/nature15514

Sun, Z., Nyanzu, M., Yang, S., Zhu, X., Wang, K., Ru, J., et al. (2020). VX765 attenuates pyroptosis and HMGB1/TLR4/NF-κB pathways to improve functional outcomes in TBI mice. *Oxid. Med. Cell. Longev.* 2020, 1–21. doi: 10.1155/2020/7879629

Swanson, K. V., Deng, M., and Ting, J. P. (2019). The NLRP3 inflammasome: Molecular activation and regulation to therapeutics. *Nat. Rev. Immunol.* 19, 477–489. doi: 10.1038/s41577-019-0165-0

Tsai, S. C., Yang, K. D., Chang, K. H., Lin, F. C., Chou, R. H., Li, M. C., et al. (2021). Umbilical cord mesenchymal stromal Cell-Derived exosomes rescue the loss of outer hair cells and repair cochlear damage in Cisplatin-Injected mice. *Int. J. Mol. Sci.* 22:6664. doi: 10.3390/ijms22136664

Wallisch, J. S., Simon, D. W., Bayir, H., Bell, M. J., Kochanek, P. M., and Clark, R. (2017). Cerebrospinal fluid NLRP3 is increased after severe traumatic brain injury in infants and children. *Neurocrit. Care* 27, 44–50. doi: 10.1007/s12028-017-0378-7

Wang, G., Zhang, J., Hu, X., Zhang, L., Mao, L., Jiang, X., et al. (2013). Microglia/macrophage polarization dynamics in white matter after traumatic brain injury. *J. Cereb. Blood Flow Metab.* 33, 1864–1874. doi: 10.1038/jcbfm.2013.146

Wang, K., Sun, Z., Ru, J., Wang, S., Huang, L., Ruan, L., et al. (2020). Ablation of GSDMD improves outcome of ischemic stroke through blocking canonical and non-canonical inflammasomes dependent pyroptosis in microglia. *Front. Neurol.* 11:577927. doi: 10.3389/fneur.2020.577927

Wilson, L., Stewart, W., Dams-O'Connor, K., Diaz-Arrastia, R., Horton, L., Menon, D. K., et al. (2017). The chronic and evolving neurological consequences of traumatic brain injury. *Lancet Neurol.* 16, 813–825. doi: 10.1016/S1474-4422(17)30279-X

Wu, L., Kalish, B. T., Finander, B., Cao, T., Jin, G., Yahya, T., et al. (2022). Repetitive mild closed head injury in adolescent mice is associated with impaired proteostasis, neuroinflammation and tauopathy. *J. Neurosci.* 42, 2418–2432. doi: 10.1523/JNEUROSCI.0682-21.2021

Xu, X., Yin, D., Ren, H., Gao, W., Li, F., Sun, D., et al. (2018). Selective NLRP3 inflammasome inhibitor reduces neuroinflammation and improves long-term neurological outcomes in a murine model of traumatic brain injury. *Neurobiol. Dis.* 117, 15–27. doi: 10.1016/j.nbd.2018.05.016

Zeng, X., Li, P., Ning, Y., Zhao, Y., Peng, Y., Yang, N., et al. (2018). Impaired autophagic flux is associated with the severity of trauma and the role of A2AR in brain cells after traumatic brain injury. *Cell Death Dis.* 9:252. doi: 10.1038/s41419-018-0316-4

Zhang, Z., Xu, Y., Peng, Y., Chen, X., Li, P., Zhou, Y., et al. (2020). Expression of a short antibody heavy chain peptide effectively antagonizes adenosine 2A receptor *in vitro* and *in vivo*. *Expert Opin. Ther. Targets* 24, 707–717. doi: 10.1080/14728222.2020.1758667

Conflict of Interest: The authors declare that the research was conducted in the absence of any commercial or financial relationships that could be construed as a potential conflict of interest.

Publisher's Note: All claims expressed in this article are solely those of the authors and do not necessarily represent those of their affiliated organizations, or those of the publisher, the editors and the reviewers. Any product that may be evaluated in this article, or claim that may be made by its manufacturer, is not guaranteed or endorsed by the publisher.

Copyright © 2022 Du, Li, Gao, Cen and Li. This is an open-access article distributed under the terms of the Creative Commons Attribution License (CC BY). The use, distribution or reproduction in other forums is permitted, provided the original author(s) and the copyright owner(s) are credited and that the original publication in this journal is cited, in accordance with accepted academic practice. No use, distribution or reproduction is permitted which does not comply with these terms.

frontiers | Frontiers in Cellular Neuroscience

REVIEW
published: 10 June 2022
doi: 10.3389/fncel.2022.916719

Immune Cells in Subretinal Wound Healing and Fibrosis

Manon Szczepan[1], María Llorián-Salvador[1†], Mei Chen[1] and Heping Xu[1,2]*

[1] The Wellcome-Wolfson Institute for Experimental Medicine, School of Medicine, Dentistry & Biomedical Sciences, Queen's University Belfast, Belfast, United Kingdom, [2] Aier Institute of Optometry and Vision Science, Changsha, China

The subretinal space is devoid of any immune cells under normal conditions and is an immune privileged site. When photoreceptors and/or retinal pigment epithelial cells suffer from an injury, a wound healing process will be initiated. Retinal microglia and the complement system, as the first line of retinal defense, are activated to participate in the wound healing process. If the injury is severe or persists for a prolonged period, they may fail to heal the damage and circulating immune cells will be summoned leading to chronic inflammation and abnormal wound healing, i.e., subretinal or intraretinal fibrosis, a sight-threatening condition frequently observed in rhematogenous retinal detachment, age-related macular degeneration and recurrent uveoretinitis. Here, we discussed the principles of subretinal wound healing with a strong focus on the conditions whereby the damage is beyond the healing capacity of the retinal defense system and highlighted the roles of circulating immune cells in subretinal wound healing and fibrosis.

Keywords: retina, inflammation, innate immunity, adaptive immunity, age-related macular degeneration, macular fibrosis, proliferative vitroretinopathy

OPEN ACCESS

Edited by:
Ulrich Bogdahn,
University of Regensburg, Germany

Reviewed by:
Daisy Y. Shu,
Schepens Eye Research Institute and Harvard Medical School, United States
Suneel Gupta,
University of Missouri, United States

****Correspondence:***
Heping Xu
heping.xu@qub.ac.uk

†Present address:
María Llorián-Salvador,
Diabetes and Metabolism Research Unit, Vall d'Hebron Research Institute, Universitat Autònoma de Barcelona, Barcelona, Spain

Specialty section:
This article was submitted to Cellular Neuropathology, a section of the journal Frontiers in Cellular Neuroscience

Received: *09 April 2022*
Accepted: *16 May 2022*
Published: *10 June 2022*

Citation:
Szczepan M, Llorián-Salvador M, Chen M and Xu H (2022) Immune Cells in Subretinal Wound Healing and Fibrosis. Front. Cell. Neurosci. 16:916719. doi: 10.3389/fncel.2022.916719

INTRODUCTION

Fibrosis is the formation of an abnormal amount of fibrous tissue in an organ as the result of dysregulated inflammation or wound healing. A variety of stimuli such as tissue injury, infection, autoimmune and allergic responses or radiation can trigger fibrosis (Wynn, 2008). Despite the large diversity of noxious signals, studies have reported that ischemia, abnormal angiogenesis, and chronic inflammation play an important role in the development and progression of fibrosis. When tissue suffers from injuries, the damaged cells release alarmins which recruit innate immune cells to remove the dead cells and repair the damage. However, if the injury is severe or persists, the wound healing process fails, and the tissue-educated innate immune cells summon adaptive immune cells for assistance (Matzinger and Kamala, 2011). The innate and adaptive immune systems may remove threats and tissue heals without fibrosis or scarring; they may also fail to solve the problem and the

Abbreviations: AMD, age-related macular degeneration; BRB, blood retinal barrier; CFB, complement factor B; CFH, complement factor H; CNV, choroidal neovascularization; COVID-19, Coronavirus disease 2019, DCs, dendritic cells; EAU, experimental autoimmune uveitis; ECM, extracellular matrix; EndoMT, endothelial-to-mesenchymal transitions; EMT, epithelial-to-mesenchymal transition; FFG-2, fibroblast growth factor-2; iBRB, inner blood retinal barrier; IL, interleukin; IP, immune privilege; MMT, macrophage-to-myofibroblast transition; nAMD, neovascular AMD; oBRB, outer blood retinal barrier; OIR, oxygen-induced retinopathy; PEDF, pigment epithelium derived factor; PDGF, platelet-derived growth factor; PDR, proliferative diabetic retinopathy; PVR, proliferative vitroretinopathy; RPE, retinal pigment epithelium; RRD, rhematogenous retinal detachment; SARS-CoV-2, severe acute respiratory syndrome coronavirus 2; TGF-β, transforming growth factor-ß; TNF-α, tumor necrosis factor-α; VEGF, vascular endothelial growth factor.

tissue is filled with, or even replaced by inflammatory fibrovascular membrane characterized by accumulation of various immune cells, new blood vessels, myofibroblasts and extensive deposition of Extracellular Matrix (ECM) proteins. During this process, the type of immune cells that infiltrate the tissue and their functions will determine the fate of the affected tissue. However, tissues are not simply passive recipients of immune protection but are active participants in their own defense (Matzinger and Kamala, 2011). Therefore, when tissues suffer from an insult, first, they must decide whether or not to call for assistance from the circulating immune system. They will then decide which immune cells should be summoned and what functions the immune cells will do. The type of immune cells and their released mediators vary in different tissues and under different conditions. The retina, particularly the subretinal space, is an immune privileged (IP) site. When damage occurs, such as in age-related macular degeneration (AMD), rhegmatogenous retinal detachment (RRD), or retinal penetrating injury, healing and repair can be very different from other tissues.

Here, we discuss the principles of the immune response to severe and/or persistent damages in the subretinal space, with a particular focus on the innate and adaptive immune cells and the mediators that may lead to the development of subretinal fibrosis. The majority of subretinal fibrosis develops secondary to neovascularization in AMD (nAMD) and RRD. In nAMD, the fibrotic lesion is located in the macula, therefore, is often called macular fibrosis. However, clinically, macular fibrosis includes pre-retinal macular fibrosis (also known as epiretinal membrane, retinal pucker) and subretinal macular fibrosis. The aetiologies of pre-retinal and subretinal macular fibrosis are different. To avoid any confusion, this article only discusses subretinal/intraretinal wound healing and fibrosis.

WOUND HEALING AND FIBROSIS IN THE SUBRETINAL SPACE

Subretinal Space – An Immune Privileged Site

The subretinal space refers to the interface between the neuroretina and RPE/choroid where the adherence between neuroretina and RPE cells is relatively weak. It is considered an IP site and is devoid of any immune cells under normal physiological conditions. The IP is achieved by the physical barrier (i.e., the blood-retina-barrier, BRB), the lack of lymphatic system, and the immunological barrier i.e., the immune suppressive properties of retinal neurons and RPE cells (Forrester et al., 2008). The physical barrier includes the inner BRB (iBRB) formed by tight junctions between retinal endothelial cells and the outer BRB (oBRB) formed by tight junctions between RPE cells. The oBRB regulates the passage of solutes and nutrients from the choroid to the retina and prevents the leakage of macromolecules and harmful agents into the retina (Cunha-Vaz et al., 2011). Subretinal injury often leads to oBRB damage and the development of inflammatory or degenerative conditions, such as nAMD, RRD, or diabetic retinopathy (Smith et al., 1992; Cunha-Vaz et al., 2011). The iBRB may also be affected during subretinal injury likely due to injury-mediated oxidative stress and inflammation (Toris and Pederson, 1985).

The immunological barrier in the subretinal space is achieved by RPE and photoreceptor cells. RPE cells contribute to the establishment of IP state in the subretinal space due to their constitutive expression of CD95 ligand, known to be expressed in immune privilege tissues (Wenkel and Streilein, 2000). In addition, RPE cells produce various immune regulators that can induce effector T cells apoptosis (Lau and Taylor, 2009) or convert them into regulatory T cells (Kawazoe et al., 2012). RPE cells can also modulate macrophage complement expression at the retina-choroidal interface. For example, they can upregulate the expression of C1 inhibitor (C1INH) in infiltrating macrophages (Luo et al., 2018). Under disease conditions, activated RPE cells can release a range of pro- and anti-inflammatory factors (Zamiri et al., 2006). Photoreceptors also express various immune regulators such as CD47 and CD59 (Liu et al., 2020). Thus, RPE cells together with photoreceptors tightly regulate the microenvironment of subretinal space and maintain its IP state. When damage occurs, they will decide which immune cells to recruit and guide them to do what they are supposed to do in the subretinal space. However, if the damage is severe, photoreceptors may die and RPE cells may undergo epithelial-to-mesenchymal transition (EMT) leading to the loss of IP.

Wound Healing in the Subretinal Space

A wound healing response in the subretinal space can be triggered by photoreceptor or RPE damage caused by multiple factors such as a breach in the oBRB, oxidative stress, post-infection and autoimmune response (e.g., autoimmune chorioretinitis), retinal detachment of rhegmatogenous origin (Idrees et al., 2019) or following administration of gene or cell therapy reagents into the subretinal space, etc. (Planul and Dalkara, 2017; Jin et al., 2019). The stressed RPE cells and/or photoreceptors will summon innate immune cells (i.e., microglia and macrophages) to clear the damage through phagocytosis as well as by releasing various inflammatory mediators (e.g., chemokines and cytokines) (Tonade et al., 2017; Detrick and Hooks, 2019). The complement system may be activated to promote the clearance of apoptotic cells through C3b-mediated opsonization. Retinal cells, including photoreceptors and RPE, are known to express complement components (Anderson et al., 2010; Xu and Chen, 2016; Liu et al., 2020). Subretinal microglia and macrophage accumulation and complement activation have been observed in normal aging (Xu et al., 2008; Ma et al., 2013), light-induced retinal degeneration (Rutar et al., 2011; Sennlaub et al., 2013) and various models of AMD (Combadière et al., 2007; Little et al., 2020b). In addition, RPE cells can act as a scavenger alongside the macrophages/microglia by phagocytosing debris (Friedlander, 2007). Müller cells may also be activated to participate in retinal repair. If the initial insult is cleared and the dead cells are removed, the innate immune response may heal the injury and the subretinal space returns to homeostasis (**Figure 1A**). However, if the injury causes a significant number of photoreceptor loss, active Müller cells along with ECM proteins produced by them will fill the space left by dead cells

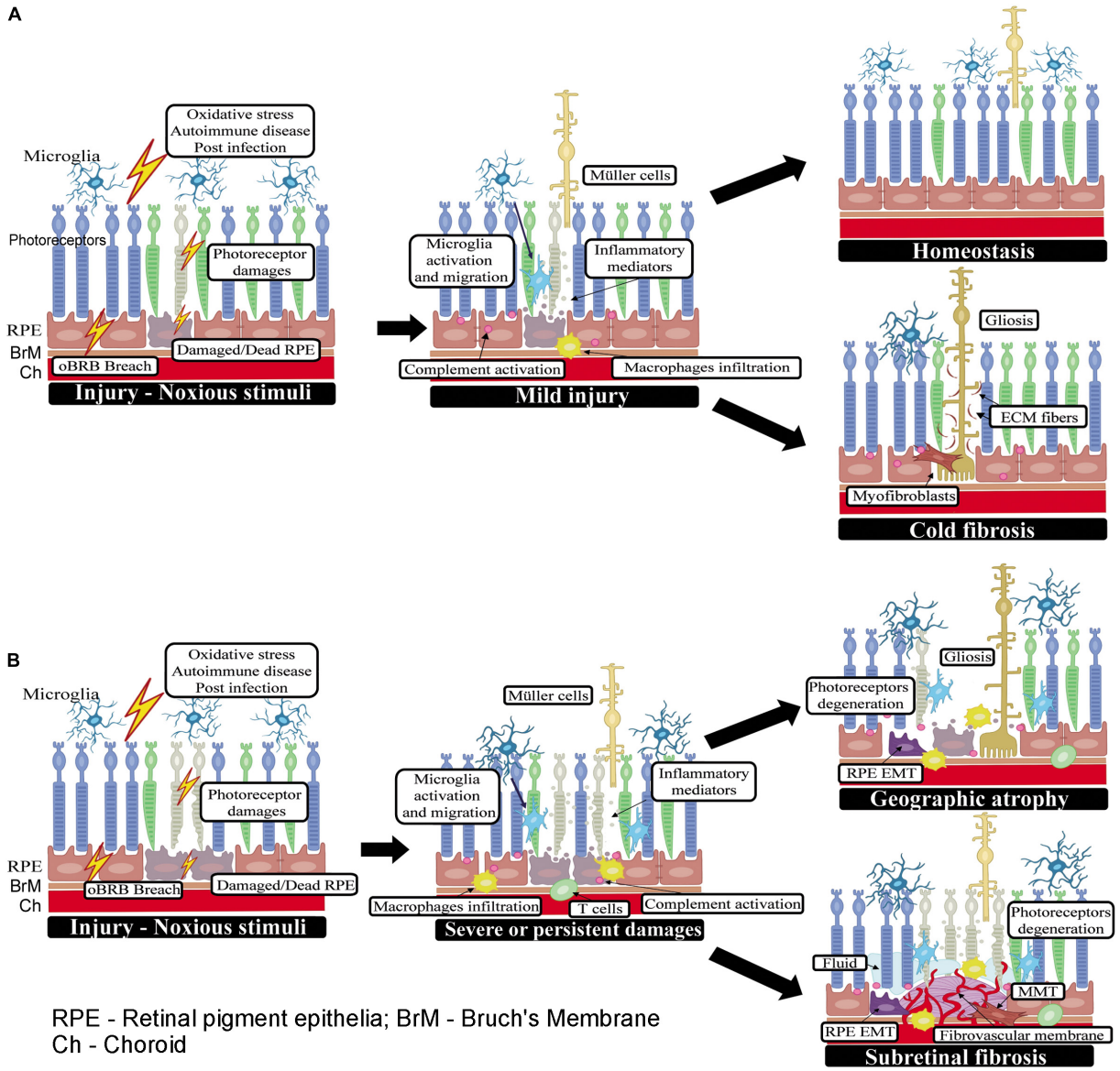

FIGURE 1 | Wound healing in the subretinal space. **(A)** When the initial insult is mild or one-off, the injury can be promptly rectified by retinal innate immune system (may also be assisted by infiltrating innate immune cells) and the subretinal space returns to homeostasis. If the injury causes a significant number of photoreceptor loss, Müller cells will be activated (may also be transdifferentiated into myofibroblast). Muller cells, myofibroblasts along with ECM proteins produced by them will fill the space left by dead cells forming gliosis without ongoing inflammation (or cold fibrosis). **(B)** When the insult to photoreceptors or RPE cells persists or is severe, retinal immune system, circulating innate and adaptive immune cells may all participate in the healing process. If the subretinal damage does not involve the ingrowth of new blood vessels, such as in GA and RRD, the damaged photoreceptor/RPE cells may be replaced by active Müller glia (i.e., gliosis) or myofibroblasts transdifferentiated from other cells such as RPE cells or macrophages. In RRD-induced PVR, the wound healing response leads to excessive ECM deposition and the development of subretinal fibrotic membrane; whereas, in GA, the wound is filled with active Muller glia and infiltrating immune cells without excessive ECM deposition and damage area becomes atrophic. In nAMD, new blood vessels are a part of the pathology, and the healing process is accompanied by continued immune cell infiltration and excessive deposition of ECM around the diseased blood vessels and eventually, the development of fibro-vascular membrane.

forming gliosis without ongoing inflammation (or cold fibrosis, see definition below) (**Figure 1A**).

If the insult to photoreceptors or RPE cells is severe or persists, adaptive immune cells may be recruited to the subretinal space. For example, aged Nrf2 knockout mice fed with high-fat diet developed RPE degeneration akin to dry AMD, which was accompanied by subretinal accumulation of MHC-II^{+} microglia, γδT cells and FoxP3^{+} regulatory T cells (Zhao et al., 2014b). In the meantime, Müller cells, particularly, those right on top of or near the damaged photoreceptor/RPE area may also be activated. In addition to their roles in maintaining retinal structure, neuroprotection and detoxification (Bringmann et al., 2006), Müller cells are critically involved in retinal wound healing and repair (Bringmann et al.,

2009; Bringmann and Wiedemann, 2012). They can participate in retinal wound healing by secreting pro-/anti-angiogenic cytokines such as VEGF, Fibroblast Growth Factor-2 (FGF-2), Tumor Necrosis Factor-α (TNF-α) (Bringmann et al., 2006), Pigment Epithelium Derived Factor (PEDF), Transforming Growth Factor-ß (TGF-ß), and thrombospondin-1 (Eichler et al., 2004) and be an important source of collagen I-VII, IX, and XI (Ponsioen et al., 2008). Müller cells are also believed to be dormant resident progenitor cells that can repair retinal neurons (Karl and Reh, 2010; Liu et al., 2013a).

During subretinal would healing, RPE cells can undergo EMT and acquire macrophage- or fibroblast-like phenotype depending on the microenvironment that they are exposed to. Specifically, RPE cells tend to adopt fibroblast properties when the environment is rich in collagen and fibronectin but can switch to a macrophage-like phenotype in the presence of vitreous or photoreceptor debris (Grierson et al., 1994). Multiple pathways (e.g., TGF-β, Wnt, miRNA, oxidative stress/Nrf2, etc.) are known to play a role in EMT by RPE and this topic has been reviewed extensively recently by others (Yang et al., 2015; Shu et al., 2020; Zhou et al., 2020; Blasiak et al., 2021). However, the molecular cues that guide RPE cells transdifferentiating into macrophage- or fibroblast-like phenotypes remain to be fully elucidated. A classical wound healing has three phases: inflammation, proliferation, and remodeling, with the aim to clear dead cells/debris, heal and stabilize the wound. But if the damage is severe or persists for a prolonged period, wound healing and cell death may co-exist in the subretinal space leading to significant overlaps in the three phases. Infiltrating innate and adaptive immune cells, the complement system and retinal resident cells (e.g., Müller cells, RPE cells etc.) all participate in the healing process. When there is an increasing demand for the removal of dead cells and debris in the subretinal space, RPE cells may adapt to a macrophage-like phenotype through EMT. During the proliferation and healing stages, RPE cells may transdifferentiate into fibroblast-like cells to fill the space left by dead cells and participate in retinal remodeling.

The subretinal space is devoid of blood vessels. If the subretinal damage does not involve the ingrowth of new blood vessels, such as in RRD, the damaged photoreceptor/RPE cells may be replaced by active Müller cells (i.e., gliosis) or myofibroblasts transdifferentiated from Müller glia, RPE cells or macrophages. The subretinal membranes in PVR are reported to constitute multiple types of cells, including fibroblasts, RPE cells, Müller cells, infiltrating macrophages, $CD4^+$ and $CD8^+$ T cells (Charteris et al., 1993). In nAMD, new blood vessels are a part of the pathology, and the healing process is accompanied by continued immune cell infiltration and excessive deposition of ECM around the diseased blood vessels and eventually, the development of fibro-vascular membrane (**Figure 1B**). Immunohistochemistry studies revealed complement deposition and immune cell infiltrations in subretinal fibro-vascular membrane from nAMD patients (Grossniklaus et al., 2005; Little et al., 2020a). To differentiate the scars that are well-settled and contain only fibroblasts from the ones with active inflammation and contain both myofibroblasts and immune cells, Adler et al. (2020) defined the former as "cold fibrosis" and the later as "hot fibrosis".

Subretinal Fibrosis

Subretinal fibrosis is the end stage of various eye diseases including RRD (Pastor et al., 2016) and nAMD (Daniel et al., 2014), recurrent uveoretinitis (Kim et al., 1987), proliferative diabetic retinopathy (Roy et al., 2016), or subretinal neovascularization secondary to high myopia (Montero and Ruiz-Moreno, 2010). When the lesion is located in the macula, it is often called "macular fibrosis." PVR is a major cause of retinal detachment surgery failure in RRD patients. Vitreous hemorrhage is known to be a risk factor for PVR (Duquesne et al., 1996). In nAMD, macular fibrosis stabilizes the neovascular membrane leading to non-responsiveness to the anti-VEGF treatment (Daniel et al., 2014; Ishikawa et al., 2016). Risk factors of nAMD-related macular fibrosis include initial worse visual acuity, persistent damage to RPE and the outer layers of the neuronal retina, a longer duration between disease onset and treatment and hemorrhage (Little et al., 2018; Teo et al., 2020). In addition to nAMD, choroidal neovascularization (CNV) also occurs in pathologic myopia (Ohno-Matsui et al., 2021) and recurrent uveoretinitis (Kim et al., 1987) and these patients are normally younger than nAMD patients. Interestingly, the CNVs in child and adolescent myopic patients are less likely to progress into macular fibrosis compared to those in nAMD. In fact, their CNV can regress spontaneously, and the regression is often accompanied by macular and choroidal atrophy but not fibrosis (Hayashi et al., 2010; Rishi et al., 2013). This suggests that old age increases the risk of subretinal fibrosis. RPE cells in the aging eye undergo significant cytoskeleton reorganization (Tarau et al., 2019) and are multinucleated and have impaired wound healing capacity (Chen et al., 2016b). The increased risk of subretinal fibrosis in the elderly may be related to RPE senescence and impaired wound healing.

The underlying mechanism of subretinal fibrosis is poorly defined although inflammation is believed to play an important role (Chen and Xu, 2015). A low-grade inflammation (para-inflammation) exists in the aging retina and RPE/choroid (Xu et al., 2009), which may favor a profibrotic response during subretinal wound healing. The risk factors of PVR and macular fibrosis in nAMD are indicatives of either severe insults to the macula or prolonged/sustained tissue damage, which will likely induce an inflammatory response that constitutes a variety of innate and adaptive immune cells. Activation of these immune cells creates a microenvironment that recruits and activates fibroblasts in the subretinal space, particularly when the oBRB is damaged such as in nAMD.

IMMUNE CELLS IN SUBRETINAL FIBROSIS

After injury, a timely inflammation is essential to eliminate harmful stimuli and initiate wound healing. The initial inflammatory response is dominated by innate immune cells such as neutrophil, monocytes, and macrophages (Oberyszyn, 2007). Prompt resolution of the inflammation will facilitate tissue repair and the wound heals with "cold fibrosis." However, if the inflammation fails to resolve, chronic inflammation will follow leading to further tissue damage and progressive fibrosis. Both

the innate and adaptive immune cells participate in chronic inflammation. In this section, we discuss the role of innate cells and adaptive immune cells in subretinal wound healing and fibrosis (**Figure 2**).

Innate Immune Cells

Macrophages

Subretinal phagocyte accumulation has been observed in the normal aging retina (Xu et al., 2008; Lad et al., 2015), after light damage (Sennlaub et al., 2013; Karlen et al., 2018) and is related to defective RPE immunomodulation (Xu et al., 2009). Although the source of subretinal phagocytes in various models of retinal degeneration (i.e., macrophages vs. microglia) differs (Karlen et al., 2018; Yu et al., 2020), infiltrating macrophages are believed to play a critical role in the laser-induced CNV and its related subretinal fibrosis (Sakurai et al., 2003; Tsutsumi et al., 2003; Little et al., 2020a). Both pro-inflammatory monocytes and pro-fibrotic and alternatively activated macrophages are reported to be involved in organ fibrosis including in severe COVID-19 patients (Page et al., 2012; Wendisch et al., 2021).

Upon the damage of the RPE/Bruch's membrane complex in laser-induced CNV, microglia and choroidal macrophages are parts of the first wave of infiltrating immune cells (Huang et al., 2013; Liu et al., 2013b). More recently, using single-cell

Innate Immune Cells

Immune cells	Wound healing	Subretinal fibrosis	Other organ fibrosis
Macrophages	**Inflammation** • Debris clearance • Promote complement activation • Recruit immune cells **Proliferation & remodeling** • Recruit and activate fibroblasts • Produce MMPs, TIMPs	○ Pro-angiogenic and fibrotic mediators ○ MMT ○ Induce EMT from RPE and EndoMT ○ Promote subretinal inflammation ○ Recruit choroidal fibroblasts and circulating fibrocytes	▪ Both pro-inflammatory monocytes and pro-fibrotic macrophages are involved in organ fibrosis ▪ Produce pro-angiogenic and fibrotic mediators ▪ Recruit and activate fibroblasts ▪ MMT
Dendritic cells	**Inflammation** • Modulation of immune response **Proliferation & remodeling** • Produce MMPs and TIMPs	○ Critically involved in retinal wound healing ○ MHC-II+ cells present in fibrotic lesions ○ Role in subretinal fibrosis - unknown	▪ Critical role in inflammation-driven fibrosis ▪ Impaired DC maturation leads to inadequate T-cell response and organ fibrosis
Neutrophils	**Inflammation** • First line of defense, acute inflammation • Release ROS, proteases and pro-inflammatory cytokines • NETs formation	○ Reduced retinal fibrosis in neutrophil-dominated inflammation (CCL2 KO mice) ○ Dysregulated neutrophil activation in macular fibrosis ○ Gr-1+ cells present in subretinal fibrosis	▪ Participated in chronic inflammation ▪ Promote organ fibrosis through the release of neutrophil elastase and neutrophil extracellular traps (NETs)
NK cells	Participate in **inflammatory** stages of wound healing	○ Detected in subretinal fibrotic lesion ○ Can produce VEGF in the presence of RPE ○ Role in subretinal fibrosis – unknown	▪ Promote angiogenesis and ameliorate fibrosis in the liver and heart
Mast cells	**Inflammation – Proliferation - Remodeling** • Vasodilators and proinflammatory mediators	○ Contribute to pathological angiogenesis ○ Involved in the development of epiretinal membrane ○ Role in subretinal fibrosis – unknown	▪ Participate in liver, kidney, lung and skin fibrosis ▪ Produce bFGF, PDGF, TGF-β, etc. ▪ Activate fibroblasts
Eosinophils	**Inflammation and Remodeling**	○ Not reported in human CNV ○ Role in subretinal fibrosis – unknown	▪ Involved in organ fibrosis ▪ Produce TGF-ß, IL13, CCL18, FGF9, VEGF, VCAM-1, etc.

Adaptive Immune Cells

Immune cells	Wound healing	Subretinal fibrosis	Other organ fibrosis
Th1/17 cells	**Chronic inflammation and Autoimmunity** • Delay wound healing	○ Higher levels of IL-17 in intraretinal fibrovascular membrane ○ Role in subretinal fibrosis – unknown	▪ Involved in idiopathic pulmonary fibrosis ▪ Contribute to lung injury in COVID-19
Th2 cells	**Autoimmunity, allergic inflammation** • Improve wound healing	○ Higher levels of IL-4 in nAMD ○ Role in subretinal fibrosis – unknown	▪ Promote ECM protein deposition ▪ Promote the release of fibrotic factors IL-13 and TGF-ß
CD8 T cells	**Inflammation** • Downregulating wound healing	○ No change in circulating CD8 T cells in nAMD ○ Role in subretinal fibrosis – unknown	▪ Involved in pulmonary fibrosis in COVID-19 patients and idiopathic pulmonary fibrosis
T-reg	**Inflammation** • Resolve inflammation • Facilitate wound healing	○ Subretinal accumulation of FoxP3+ regulatory T cells ○ Role in subretinal fibrosis – unknown	▪ Limit organ fibrosis in liver, lung, kidney, etc. ▪ Promote fibrosis via PDGF and TGF-ß
B cells	**Inflammation** • Antibodies to clear pathogens • Activate complement system • Facilitate wound healing	○ Detected in the subretinal membrane ○ Retinal autoantibodies have been detected in AMD patients ○ Role in subretinal fibrosis – unknown	▪ Altered B cell function in pulmonary fibrosis, skin and liver fibrosis ▪ Can produce TNF-α, IL-19 and CCL7 that shift pro-fibrotic immune response

FIGURE 2 | The role of innate and adaptive immune cells in wound healing, organ and subretinal fibrosis. Cells were adopted from BioRender.com.

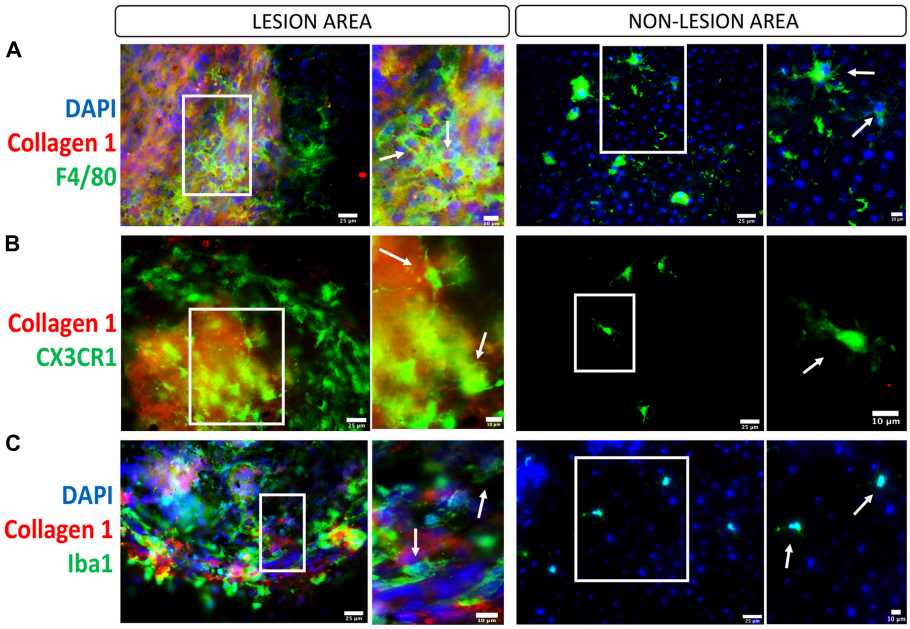

FIGURE 3 | Macrophages/microglia in the subretinal fibrotic lesion. Representative images, and their zoom-in images, of the lesion (left panel) and non-lesion (right panel) area of RPE flat mounts stained for collagen-1, DAPI and F4/80 (**A**, macrophage marker), CX3CR1 (**B**, microglial marker), and Iba1 (**C**, marker for activated microglia and macrophages). Scale bars = 25 μm; Zoom images Scale bars = 10 μm.

RNA sequencing analysis, Wieghofer et al. (2021) discovered that retinal microglia were the dominant cell subset present in CNV, suggesting an important contribution to CNV progression. However, their role in the development of subretinal fibrosis remains unknown. In the two-stage laser-induced subretinal fibrosis, we detected a large number of F4/80$^+$, CX3CR1$^+$, IBA-1$^+$ cells both inside and around the collagen-1$^+$ or fibronectin$^+$ fibrotic lesion (Little et al., 2020b; **Figure 3**). The primary role of infiltrating macrophages is undoubtedly to remove debris and initiate retinal repair, but they can promote subretinal fibrosis during chronic inflammation through multiple mechanisms (**Figure 2**).

First, macrophages can directly transdifferentiate into myofibroblasts, a process called macrophage-to-myofibroblast transition (MMT). MMT has been shown to contribute to renal fibrosis (Meng et al., 2016). It has been reported that M2, especially CD206$^+$ macrophages, rather than M1, undergo the transition (Wang et al., 2017). More recently, a study from our group demonstrated the existence of MMT in subretinal fibrosis (Little et al., 2020b) and further showed that, in addition to TGF-β, the anaphylatoxin C3a could induce MMT (Little et al., 2020a).

Second, macrophages can release pro-angiogenic and pro-fibrotic mediators that can either recruit and activate fibroblasts or induce mesenchymal transition from endothelial or epithelial cells (Wynn and Vannella, 2016; Zhu et al., 2017b). In the case of subretinal fibrosis, infiltrating macrophages may recruit choroidal fibroblasts or circulating fibrocytes to the site of CNV. They may also release pro-fibrotic mediators to induce EMT in RPE cells or endothelial-to-mesenchymal transitions (EndoMT) from choroidal vessels or CNV (Shu et al., 2020; Song et al., 2021).

Third, in response to prolonged tissue damage, macrophages can further promote subretinal inflammation, including the recruitment of other immune cells and complement activation. Macrophages can synthesize various complement components and directly contribute to subretinal complement activation (Luo et al., 2012). Uncontrolled complement activation is believed to drive AMD pathology (Xu and Chen, 2016; Armento et al., 2021). We reported that RPE cells could enhance the expression of complement C3 and complement factor B (CFB) and downregulate complement factor H (CFH) and CD59a expression in macrophages under inflammatory conditions (Luo et al., 2013). Higher plasma level of C3a, C4a, and C5a is related to subretinal fibrosis in nAMD (Lechner et al., 2016), indicative of the involvement of the complement system in subretinal fibrosis.

In humans, there are three functional monocytes subsets (i.e., precursors of macrophages), classical (CD14$^+$CD16$^-$), non-classical (CD14$^-$CD16$^+$), and intermediate (CD14$^+$CD16$^+$) (Wong et al., 2012). We reported that intermediate monocytes in nAMD patients expressed higher levels of HLA-DR (Chen et al., 2016a) and that monocytes from nAMD patients without macular fibrosis, produced higher levels of interleukine-8 (IL-8) and CCL2 (Lechner et al., 2017). The exact subsets of monocytes giving rise to pro-fibrotic macrophages in nAMD remain to be elucidated.

Dendritic Cells

Dendritic cells (DCs) are professional antigen-presenting cells involved in tissue homeostasis. Several populations of DCs are present in the eye but the majority of them reside in connective tissues (e.g., cornea, sclera, choroid) with only few in neurons (Forrester et al., 2010). A small number of DCs were reported to

be in the peripapillary and peripheral marginal retina in mice (Xu et al., 2007). DC are early responders to retinal injury. Lehmann et al. (2010) reported that $CD11c^{+}CD11b^{+}$ DCs responded rapidly to optic nerve injury and light-induced photoreceptor injury. They increased in number and accumulated at the injury site and became MHC-II^{+} (Lehmann et al., 2010), suggesting that DCs are key players in retinal injury and wound healing.

Dendritic cells are known to play a critical role in inflammation-driven fibrosis in multiple organs (Rahman and Aloman, 2013; Bocchino et al., 2021). Ahadome et al. (2016) showed that classical DC contributed to ocular mucosal fibrosis through the retinoic acid pathway in a model of allergic eye disease. Impaired DC maturation can lead to inadequate T-cell response and contribute to organ fibrosis as observed in COVID-19 patients (Borcherding et al., 2021). It has been reported that DCs contribute to scar formation in liver fibrosis and multiple sclerosis directly through secreting metalloproteinase and their inhibitors (Rahman and Aloman, 2013).

The critical role of DC in retinal inflammation has been documented by many studies (Xu et al., 2007; Forrester et al., 2010). In our two-stage laser-induced subretinal fibrosis, a large number of MHC-II^{+} cells were detected inside the lesion (**Figure 4A**) but their DC identity is unknown. The role of DC in subretinal fibrosis thus remains to be elucidated (**Figure 2**).

Neutrophils

Neutrophils are known to be associated with acute inflammation and are one of the first immune cells recruited to the site of injury or infection. Neutrophil respiratory burst through the NADH oxidase system is essential for efficient pathogen elimination. In addition, neutrophil granules contain various enzymes [e.g., lactoferrin, neutrophil gelatinase-associated lipocalin (lipocalin-2), gelatinase, etc.], which can participate in bacterial killing (Segal, 2005). Although the number of neutrophils declines rapidly after the initial phase of acute inflammation, neutrophil elastase and neutrophil extracellular traps (NETs) are known to critically contribute to inflammation-mediated organ fibrosis (Martínez-Alemán et al., 2017) including lung inflammation and fibrosis in COVID-19 patients (Wang et al., 2020; **Figure 2**).

The role of neutrophils in inflammation-mediated retinal fibrosis has not been systemically investigated. We and others have shown that retinal inflammation in the CCL2 or CCR2 deficient experimental autoimmune uveitis (EAU) mice is dominated by neutrophils (Sonoda et al., 2011; Chen et al., 2012). Interestingly, inflammation-induced intraretinal fibrovascular membrane is reduced in CCR2 KO (Chen et al., 2012) and CCL2/CX3CR1 double knockout mice (Zhao et al., 2014a). In oxygen-induced retinopathy (OIR), vascular remodeling is associated with neutrophil infiltrating and NETs can remove diseased endothelial cells and remodel unhealthy vessels (Binet et al., 2020). Data from the EAU and OIR studies appear to suggest that neutrophils may promote retinal vascular repair and reduce pathological fibrosis. In nAMD, the circulating level of neutrophils is higher compared to age-matched healthy controls (Niazi et al., 2019). We found that the plasma level of lipocalin-2 is increased in nAMD patients with macular fibrosis (Chen et al., 2020), suggesting a link between dysregulated neutrophil activation and macular fibrosis. In the two-stage laser-induced mouse model of subretinal fibrosis, we detected GR-1^{+} cells around and inside the lesion (**Figure 4B**). Further studies will be needed to understand the role of neutrophils in inflammation-induced retinal fibrosis.

Natural Killer Cells

Natural Killer (NK) cells are cytotoxic lymphocytes critically involved in innate immunity. It has been suggested that NK

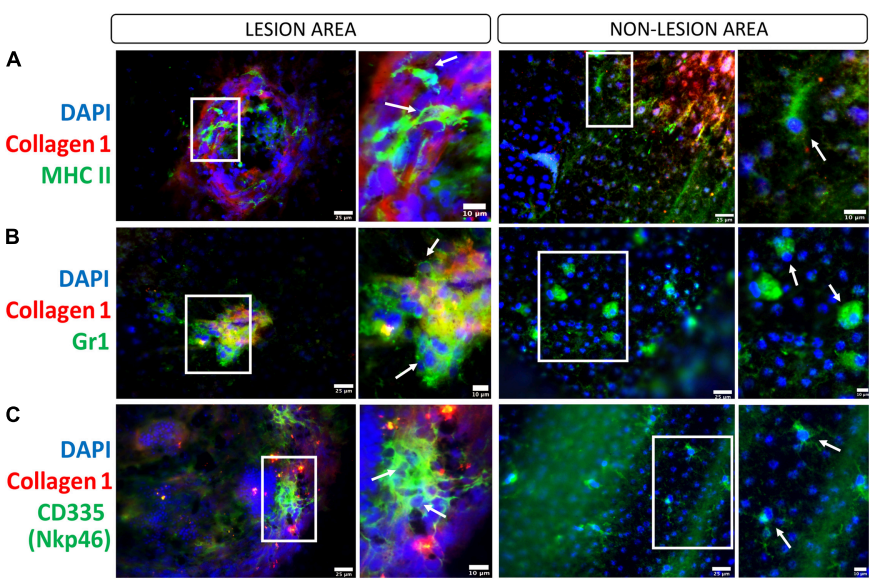

FIGURE 4 | Innate immune cells in the subretinal fibrotic lesion. Representative images, and their zoom in images, of the lesion (left panel) and non-lesion (right panel) areas of RPE flatmounts stained for collagen-1, DAPI and MHCII **(A)**, Gr-1 **(B)**, CD335/Nkp46 **(C)**. Scale bars = 25 μm; Zoom images Scale bars = 10 μm.

cells promote angiogenesis and ameliorate fibrosis in the liver and heart (Radaeva et al., 2006). On the other hand, NK cell accumulation could promote chronic kidney inflammation (Turner, 2017) and this has also been seen in severe COVID-19 patients with pulmonary fibrosis (Bi, 2022).

In the eye, infiltration and malfunction of NK cells have been reported in patients with non-infectious uveitis such as Behcet's disease (Kucuksezer et al., 2015), Vogt-Koyanagi-Harada disease (Levinson et al., 2016), and in viral uveitis (Hamzaoui et al., 1990). CNV is a serious complication of chorioretinitis/posterior uveitis, particularly in the forms affecting the outer retina-RPE-choroid interface (Baxter et al., 2013). The inflammation-induced CNV can become a fibrovascular membrane if remains untreated (Kim et al., 1987; Chen et al., 2012) but the role of NK cells in the development of uveitis-related retinal fibrovascular membrane remains to be investigated. In patients with proliferative DR (Obasanmi et al., 2020) and nAMD (Lechner et al., 2015), the percentage of $CD56^+$ NK cells was not altered compared to that in healthy controls. In our two-stage laser-induced subretinal fibrosis, we detected $Nkp46^+$ NK cells in the fibrotic lesion site (**Figure 4C**). A previous study showed that NK cells could produce VEGF when co-cultured with RPE (Hijioka et al., 2008). However, another study showed that human iPS-derived RPE greatly suppressed NK cell activation (Sugita et al., 2018). Further studies are required to understand the role of NK cells in subretinal fibrosis.

Mast Cells

Mast cells (MCs) are granulocytes involved, at different levels, in immune responses such as allergy responses, wound healing, angiogenesis, and immune tolerance (Krystel-Whittemore et al., 2016). MCs are particularly abundant within the mucosal and connective tissues of the skin, lungs, guts and are in proximity to small venules and capillaries. Their activation leads to the release of various mediators (e.g., histamine, tryptase, chymase), cytokines and chemokines (Krishnaswamy et al., 2005). MCs have been implicated in the pathogenesis of fibrotic conditions in the liver, kidney, skin, and lung (Overed-Sayer et al., 2014). Mechanistically, MCs can promote inflammation by releasing various vasodilators and proinflammatory mediators, and producing profibrotic factors such as bFGF, PDGF, and TGF-β (Monument et al., 2015). MCs can also activate fibroblasts through cell-to-cell communication *via* gap junction (Yamamoto et al., 2000). MC activation has been observed in COVID-19 patients and is believed to contribute to cytokine storm and related organ damage and fibrosis (Conti et al., 2020).

In the eye, MCs are primarily found in the choroid but absent in the retina (McMenamin, 1997). Elegant studies from Gerard A. Lutty's group demonstrated that the number and degradation of MC are increased in all forms of AMD including early AMD, GA, and nAMD (Bhutto et al., 2016). They further showed that mast cell-derived tryptase plays a critical role in the development and progression of the GA (McLeod et al., 2017). MC activation and degradation are also reported to contribute to pathological angiogenesis in OIR (Matsuda et al., 2017). In patients with idiopathic epiretinal membrane and idiopathic macular hole, MCs were detected in the *bursa premacularis* (Sato et al., 2019) suggesting that they may be involved in the development of epiretinal membrane. The implication of MCs in subretinal wound healing and fibrosis remains elusive (**Figure 2**).

Eosinophils

Eosinophils are major effectors of the innate immune system and are involved in a range of inflammatory conditions such as hypereosinophilic syndrome or asthma and eosinophilic esophagitis. Activated eosinophils are an important source of pro-fibrotic and proangiogenic factors like TGF-ß, IL-13, CCL-18, FGF-9, VEGF, and VCAM-1 (Wynn, 2008; Aceves, 2014). They are known to play a role in endomyocardial fibrosis (Spry, 1989) and pulmonary fibrosis, including SARS-CoV-2-induced respiratory inflammation and fibrosis (Kim et al., 2021, 19).

In the eye, eosinophils are known to play a role in allergic conjunctivitis (Trocme and Aldave, 1994), and Wegner's granulomatosis (Trocme, 1991), although little is known about their involvement in ocular fibrosis. Intraocular eosinophils were detected in *Toxocara canis* and *Ascaris suum* infected eyes (Rockey et al., 1979) but not in human CNV (Grossniklaus et al., 2005, 7). Since eosinophils are one of the major sources of pro-fibrotic mediators, further studies will be needed to elucidate their role in retinal fibrosis (**Figure 2**).

Adaptive Immunity

T Lymphocytes

During inflammation, infiltrating lymphocytes, in particular, T helper cells can influence the healing and scarring process (Zhang and Zhang, 2020). A previous study reported that CD4 T cell depletion decreased wound strength, resilience and toughness; whereas CD8 T cell depletion increased wound strength, resilience and toughness (Davis et al., 2001). The tissue-educated different subsets of T cells can secrete various mediators and growth factors that influence the microenvironment and directly affect the activity of macrophages and myofibroblasts, key cells for wound healing and fibrosis. It is believed that wound healing and fibrosis are orchestrated by Th2 cells, which secrete anti-inflammatory and pro-fibrotic factors such as IL-4, IL-5, and IL-13. These type 2 cytokines induce excessive deposition of proteins crucial for ECM remodeling, including pro-collagens, matrix metalloproteinase, etc. (Kryczka and Boncela, 2015). Th2 cytokines can induce pro-healing M2 macrophage differentiation. The cytokine IL-5 can activate eosinophils to release fibrotic factors IL-13 and TGF-ß (Le Moine et al., 1999). Regulatory T cells can also facilitate wound healing through upregulation of epidermal growth factor receptor expression (Nosbaum et al., 2016). Other T helper cells, including Th22, Th9, Th17, and T regulatory cells are all known to play a role in organ fibrosis (Zhang and Zhang, 2020). For example, CD4 and CD8 T cell accumulation and elevated levels of IL-17 and type 1 cytokines have been observed in severe COVID-19 patients, similar to idiopathic pulmonary fibrosis patients (Wu et al., 2020).

In the chronic phase of EAU, the development of intraretinal fibrovascular membrane is related to higher levels of IL-17 production, CD4 T cell and $arginase\text{-}1^+$ macrophage

accumulation (Chen et al., 2012), suggesting that both Th17 response and M2-type macrophages may play a role (**Figure 2**).

Previously, we reported that the percentage of CD4, but not CD8 T cells was significantly higher in nAMD patients with macular fibrosis compared to those without macular fibrosis (Lechner et al., 2015). Moreover, the levels of IL-4 were higher in nAMD patients suggesting an activated Th2 response (Yu et al., 2016) although direct evidence supporting the role of Th2 response in macular fibrosis secondary to nAMD is lacking (**Figure 2**).

B Lymphocytes

B cells are mainly involved in humoral immunity by producing antibodies. Compelling evidence suggests that B cells play an important role in inflammation-mediated fibrosis through antibody-independent mechanisms (Shen and Fillatreau, 2015). B cell deficient mice are resistant to silica-induced lung fibrosis (Arras et al., 2006), and carbon tetrachloride-induced liver fibrosis (Thapa et al., 2015). Mechanistically, active B cells can produce cytokines (e.g., TNF-α, IL-9) and chemokines (e.g., CCL7) that shift pro-fibrotic immune response; they can also interact with T cells, macrophages and myofibroblasts promoting fibrosis (Zhu et al., 2017a).

The role of B cells in non-infectious uveitis is well recognized (Smith et al., 2016). B cells have been shown to infiltrate the retina/choroid in choroiditis-related subretinal fibrosis (Kim et al., 1987). B cells were detected in the epiretinal membranes from proliferative DR (Tang et al., 1993). Retinal autoantibodies have been detected in AMD patients (Adamus et al., 2014). In our previous study, we did not observe any significant difference in circulating B cell population between nAMD patients and healthy controls. The number of circulating B cells in nAMD patients with and without macular fibrosis also did not differ (Lechner et al., 2015). The role of B cells in retinal fibrosis remains elusive (**Figure 2**).

CONCLUSION

When the retina or subretinal space suffers from a one-off mild injury, retinal glial cells and the complement system can heal and repair the damage to restore homeostasis. Once the injury is removed, inflammation will resolve, and the damages will be healed by gliosis without significant immune cell infiltration ("cold fibrosis"). However, when subretinal insult persists, circulating immune cells will be summoned leading to chronic inflammation that is executed by active microglia, the complement system, and various infiltrating immune cells (e.g., macrophages, neutrophils, T cells, etc.). The initial phase of immune cell infiltration is dominated by innate immune cells such as neutrophils and monocytes. As the disease progresses to chronic stages, retina-exposed innate immune cells will educate T and B cells in the regional lymph nodes. These educated T and B cells may migrate to the damaged retina and participate in wound healing. Within the retina, they will be further activated by alarmins released from damaged cells with the aim to clean the dead cells, remove debris and promote repair, although their activation will be regulated by remaining neurons and RPE cells. The wound will be filled with myofibroblasts (recruited or transdifferentiated through EMT, EndoMT, and MMT), EMC deposition and infiltrating innate and adaptive immune cells ("hot fibrosis"). Improved knowledge of how the immune cells orchestrate retinal/subretinal wound healing response, in particular, why and how the response is disrupted and/or dysregulated, could lead to the development of new therapeutic strategies to prevent or treat retinal fibrosis.

Future studies should aim to understand the cellular and molecular pathways involved in retinal wound healing, in particular the crosstalk between neurons and the immune system in the healthy and the damaged retina. knowledge of how chronic insult (e.g., oxidative stress in RRD and AMD) breaches the retinal IP, and how it affects the crosstalk between neurons and the immune system will be critical to uncovering molecular pathways underlying dysregulated retinal inflammation during wound healing.

The outstanding questions for developing preventive or therapeutic strategies for subretinal or intraretinal fibrosis include: (1) what are the signals that recruit and retain circulating immune cells in different stages of retinal wound healing? (2) how are the phenotype and function of infiltrating immune cells regulated by the retinal microenvironment at different stages of wound healing? (3) which immune cells are the key drivers of retinal fibrosis and what pro-fibrotic molecules that they produce?

ETHICS STATEMENT

All experiments using mice were performed under the regulation of the United Kingdom Home Office Animals (Scientific Procedures) Act 1986 and the protocols were approved by the Animal Welfare Ethical Review Body of Queen's University Belfast (PPL2876).

AUTHOR CONTRIBUTIONS

MS and HX did the literature search for this review and wrote the manuscript. MS drew **Figures 1**, **2** with conceptual input from HX. ML-S and MC supervised immunostaining, reviewed, edited, and provided counsel on the manuscript. All authors have read and approved the final version of the manuscript.

FUNDING

This work was supported by Fight for Sight (5057/5058, 5105/5106) and Medical Research Council (United Kingdom)(MR/W004681/1).

ACKNOWLEDGMENTS

We would like to thank Dr. Eimear Byrne for the valuable discussions.

REFERENCES

Aceves, S. S. (2014). Remodeling and fibrosis in chronic eosinophil inflammation. *Dig. Dis.* 32, 15–21. doi: 10.1159/000357004

Adamus, G., Chew, E. Y., Ferris, F. L., and Klein, M. L. (2014). Prevalence of anti-retinal autoantibodies in different stages of age-related macular degeneration. *BMC Ophthalmol.* 14:154. doi: 10.1186/1471-2415-14-154

Adler, M., Mayo, A., Zhou, X., Franklin, R. A., Meizlish, M. L., Medzhitov, R., et al. (2020). Principles of cell circuits for tissue repair and fibrosis. *iScience* 23:100841. doi: 10.1016/j.isci.2020.100841

Ahadome, S. D., Mathew, R., Reyes, N. J., Mettu, P. S., Cousins, S. W., Calder, V. L., et al. (2016). Classical dendritic cells mediate fibrosis directly via the retinoic acid pathway in severe eye allergy. *JCI Insight* 1:e87012. doi: 10.1172/jci.insight.87012

Anderson, D. H., Radeke, M. J., Gallo, N. B., Chapin, E. A., Johnson, P. T., Curletti, C. R., et al. (2010). The pivotal role of the complement system in aging and age-related macular degeneration: hypothesis re-visited. *Prog. Retin. Eye Res.* 29, 95–112. doi: 10.1016/j.preteyeres.2009.11.003

Armento, A., Ueffing, M., and Clark, S. J. (2021). The complement system in age-related macular degeneration. *Cell. Mol. Life Sci.* 78, 4487–4505. doi: 10.1007/s00018-021-03796-9

Arras, M., Louahed, J., Simoen, V., Barbarin, V., Misson, P., van den Brûle, S., et al. (2006). B Lymphocytes are critical for lung fibrosis control and prostaglandin E2 Regulation in IL-9 Transgenic Mice. *Am. J. Respir. Cell Mol. Biol.* 34, 573–580. doi: 10.1165/rcmb.2004-0383OC

Baxter, S. L., Pistilli, M., Pujari, S. S., Liesegang, T. L., Suhler, E. B., Thorne, J. E., et al. (2013). Risk of choroidal neovascularization among the uveitides. *Am. J. Ophthalmol.* 156, 468.e–477.e. doi: 10.1016/j.ajo.2013.04.040

Bhutto, I. A., McLeod, D. S., Jing, T., Sunness, J. S., Seddon, J. M., and Lutty, G. A. (2016). Increased choroidal mast cells and their degranulation in age-related macular degeneration. *Br. J. Ophthalmol.* 100, 720–726. doi: 10.1136/bjophthalmol-2015-308290

Bi, J. (2022). NK cell dysfunction in patients with COVID-19. *Cell. Mol. Immunol.* 19, 127–129. doi: 10.1038/s41423-021-00825-2

Binet, F., Cagnone, G., Crespo-Garcia, S., Hata, M., Neault, M., Dejda, A., et al. (2020). Neutrophil extracellular traps target senescent vasculature for tissue remodeling in retinopathy. *Science* 369:eaay5356. doi: 10.1126/science.aay5356

Blasiak, J., Koskela, A., Pawlowska, E., Liukkonen, M., Ruuth, J., Toropainen, E., et al. (2021). Epithelial-Mesenchymal transition and senescence in the retinal pigment epithelium of NFE2L2/PGC-1α double knock-out mice. *Int. J. Mol. Sci.* 22:1684. doi: 10.3390/ijms22041684

Bocchino, M., Zanotta, S., Capitelli, L., and Galati, D. (2021). Dendritic cells are the intriguing players in the puzzle of idiopathic pulmonary fibrosis pathogenesis. *Front. Immunol.* 12:664109. doi: 10.3389/fimmu.2021.664109

Borcherding, L., Teksen, A. S., Grosser, B., Schaller, T., Hirschbühl, K., Claus, R., et al. (2021). Impaired dendritic cell homing in COVID-19. *Front. Med.* 8:761372. doi: 10.3389/fmed.2021.761372

Bringmann, A., and Wiedemann, P. (2012). Müller glial cells in retinal disease. *Ophthalmologica* 227, 1–19. doi: 10.1159/000328979

Bringmann, A., Iandiev, I., Pannicke, T., Wurm, A., Hollborn, M., Wiedemann, P., et al. (2009). Cellular signaling and factors involved in Müller cell gliosis: neuroprotective and detrimental effects. *Prog. Retin. Eye Res.* 28, 423–451. doi: 10.1016/j.preteyeres.2009.07.001

Bringmann, A., Pannicke, T., Grosche, J., Francke, M., Wiedemann, P., Skatchkov, S., et al. (2006). Müller cells in the healthy and diseased retina. *Prog. Retin. Eye Res.* 25, 397–424. doi: 10.1016/j.preteyeres.2006.05.003

Charteris, D. G., Hiscott, P., Robey, H. L., Gregor, Z. J., Lightman, S. L., and Grierson, I. (1993). Inflammatory cells in proliferative vitreoretinopathy subretinal membranes. *Ophthalmology* 100, 43–46. doi: 10.1016/s0161-6420(93)31711-2

Chen, M., and Xu, H. (2015). Parainflammation, chronic inflammation, and age-related macular degeneration. *J. Leukocyte Biol.* 98, 713–725. doi: 10.1189/jlb.3RI0615-239R

Chen, M., Copland, D. A., Zhao, J., Liu, J., Forrester, J. V., Dick, A. D., et al. (2012). Persistent inflammation subverts thrombospondin-1–induced regulation of retinal angiogenesis and is driven by CCR2 Ligation. *Am. J. Pathol.* 180, 235–245. doi: 10.1016/j.ajpath.2011.09.020

Chen, M., Rajapakse, D., Fraczek, M., Luo, C., Forrester, J. V., and Xu, H. (2016b). Retinal pigment epithelial cell multinucleation in the aging eye – a mechanism to repair damage and maintain homoeostasis. *Aging Cell* 15, 436–445. doi: 10.1111/acel.12447

Chen, M., Lechner, J., Zhao, J., Toth, L., Hogg, R., Silvestri, G., et al. (2016a). STAT3 Activation in circulating monocytes contributes to neovascular age-related macular degeneration. *Curr. Mol. Med.* 16, 412–423. doi: 10.2174/1566524016666160324130031

Chen, M., Yang, N., Lechner, J., Toth, L., Hogg, R., Silvestri, G., et al. (2020). Plasma level of lipocalin 2 is increased in neovascular age-related macular degeneration patients, particularly those with macular fibrosis. *Immun. Ageing* 17:35. doi: 10.1186/s12979-020-00205-w

Combadière, C., Feumi, C., Raoul, W., Keller, N., Rodéro, M., Pézard, A., et al. (2007). CX3CR1-dependent subretinal microglia cell accumulation is associated with cardinal features of age-related macular degeneration. *J. Clin. Invest.* 117, 2920–2928. doi: 10.1172/JCI31692

Conti, P., Caraffa, A., Tetè, G., Gallenga, C. E., Ross, R., Kritas, S. K., et al. (2020). Mast cells activated by SARS-CoV-2 release histamine which increases IL-1 levels causing cytokine storm and inflammatory reaction in COVID-19. *J. Biol. Regul. Homeost. Agents* 34, 1629–1632. doi: 10.23812/20-2EDIT

Cunha-Vaz, J., Bernardes, R., and Lobo, C. (2011). Blood-Retinal Barrier. *Eur. J. Ophthalmol.* 21, 3–9. doi: 10.5301/EJO.2010.6049

Daniel, E., Toth, C. A., Grunwald, J. E., Jaffe, G. J., Martin, D. F., Fine, S. L., et al. (2014). Risk of scar in the comparison of age-related macular degeneration treatments trials. *Ophthalmology* 121, 656–666. doi: 10.1016/j.ophtha.2013.10.019

Davis, P. A., Corless, D. J., Aspinall, R., and Wastell, C. (2001). Effect of CD4(+) and CD8(+) cell depletion on wound healing. *Br. J. Surg.* 88, 298–304. doi: 10.1046/j.1365-2168.2001.01665.x

Detrick, B., and Hooks, J. J. (2019). "The RPE cell and the immune system," in *Retinal Pigment Epithelium in Health and Disease*, eds A. Klettner and S. Dithmar (Cham: Springer). 101–114. doi: 10.1007/978-3-030-28384-1_6

Duquesne, N., Bonnet, M., and Adeleine, P. (1996). Preoperative vitreous hemorrhage associated with rhegmatogenous retinal detachment: a risk factor for postoperative proliferative vitreoretinopathy? *Graefe's Arch. Clin. Exp. Ophthalmol.* 234, 677–682. doi: 10.1007/BF00292353

Eichler, W., Yafai, Y., Wiedemann, P., and Reichenbach, A. (2004). Angiogenesis-related factors derived from retinal glial (Müller) cells in hypoxia. *NeuroReport* 15, 1633–1637. doi: 10.1097/01.wnr.0000133071.00786.a4

Forrester, J. V., Xu, H., Kuffová, L., Dick, A. D., and McMenamin, P. G. (2010). Dendritic cell physiology and function in the eye. *Immunol. Rev.* 234, 282–304. doi: 10.1111/j.0105-2896.2009.00873.x

Forrester, J. V., Xu, H., Lambe, T., and Cornall, R. (2008). Immune privilege or privileged immunity? *Mucosal Immunol.* 1, 372–381. doi: 10.1038/mi.2008.27

Friedlander, M. (2007). Fibrosis and diseases of the eye. *J. Clin. Invest.* 117, 576–586. doi: 10.1172/JCI31030

Grierson, I., Hiscott, P., Hogg, P., Robey, H., Mazure, A., and Larkin, G. (1994). Development, repair and regeneration of the retinal pigment epithelium. *Eye* 8, 255–262. doi: 10.1038/eye.1994.54

Grossniklaus, H. E., Miskala, P. H., Green, W. R., Bressler, S. B., Hawkins, B. S., Toth, C., et al. (2005). Histopathologic and ultrastructural features of surgically excised subfoveal choroidal neovascular lesions: submacular surgery trials report No. 7. *Arch. Ophthalmol.* 123:914. doi: 10.1001/archopht.123.7.914

Hamzaoui, K., Ayed, K., Slim, A., Hamza, M., and Touraine, J. (1990). Natural killer cell activity, interferon-gamma and antibodies to herpes viruses in patients with Behçet's disease. *Clin. Exp. Immunol.* 79, 28–34. doi: 10.1111/j.1365-2249.1990.tb05122.x

Hayashi, K., Ohno-Matsui, K., Shimada, N., Moriyama, M., Kojima, A., Hayashi, W., et al. (2010). Long-term pattern of progression of myopic maculopathy: a natural history study. *Ophthalmology* 117, 1595–1611. doi: 10.1016/j.ophtha.2009.11.003

Hijioka, K., Sonoda, K.-H., Tsutsumi-Miyahara, C., Fujimoto, T., Oshima, Y., Taniguchi, M., et al. (2008). Investigation of the role of CD1d-restricted invariant NKT cells in experimental choroidal neovascularization. *Biochem. Biophys. Res. Commun.* 374, 38–43. doi: 10.1016/j.bbrc.2008.06.080

Huang, H., Parlier, R., Shen, J., Lutty, G. A., and Vinores, S. A. (2013). VEGF Receptor blockade markedly reduces retinal microglia/macrophage infiltration

into laser-induced CNV. *PLoS One* 8:e71808. doi: 10.1371/journal.pone.0071808

Idrees, S., Sridhar, J., and Kuriyan, A. E. (2019). Proliferative vitreoretinopathy: a review. *Int. Ophthalmol. Clin.* 59, 221–240. doi: 10.1097/IIO.0000000000000258

Ishikawa, K., Kannan, R., and Hinton, D. R. (2016). Molecular mechanisms of subretinal fibrosis in age-related macular degeneration. *Exp. Eye Res.* 142, 19–25. doi: 10.1016/j.exer.2015.03.009

Jin, Z. B., Gao, M. L., Deng, W. L., Wu, K. C., Sugita, S., Mandai, M., et al. (2019). Stemming retinal regeneration with pluripotent stem cells. *Prog. Retin. Eye Res.* 69, 38–56. doi: 10.1016/j.preteyeres.2018.11.003

Karl, M. O., and Reh, T. A. (2010). Regenerative medicine for retinal diseases: activating endogenous repair mechanisms. *Trends Mol. Med.* 16, 193–202. doi: 10.1016/j.molmed.2010.02.003

Karlen, S. J., Miller, E. B., Wang, X., Levine, E. S., Zawadzki, R. J., and Burns, M. E. (2018). Monocyte infiltration rather than microglia proliferation dominates the early immune response to rapid photoreceptor degeneration. *J. Neuroinflammation* 15:344. doi: 10.1186/s12974-018-1365-4

Kawazoe, Y., Sugita, S., Keino, H., Yamada, Y., Imai, A., Horie, S., et al. (2012). Retinoic acid from retinal pigment epithelium induces T regulatory cells. *Exp. Eye Res.* 94, 32–40. doi: 10.1016/j.exer.2011.11.002

Kim, D. M., Kim, Y., Seo, J. W., Lee, J., Park, U., Ha, N. Y., et al. (2021). Enhanced eosinophil-mediated inflammation associated with antibody and complement-dependent pneumonic insults in critical COVID-19. *Cell Rep.* 37:109798. doi: 10.1016/j.celrep.2021.109798

Kim, M. K., Chan, C.-C., Belfort, R., Farah, M., Burnier, M. P., Nussenblatt, R. B., et al. (1987). Histopathologic and immunohistopathologic features of subretinal fibrosis and uveitis syndrome. *Am. J. Ophthalmol.* 104, 15–23. doi: 10.1016/0002-9394(87)90287-X

Krishnaswamy, G., Ajitawi, O., and Chi, D. S. (2005). "The human mast cell," in *Mast Cells: Methods and Protocols*, eds G. Krishnaswamy and D. S. Chi (Totowa, NJ: Humana Press). 13–34. doi: 10.1385/1-59259-967-2:013

Kryczka, J., and Boncela, J. (2015). Leukocytes: the double-edged sword in fibrosis. *Mediators Inflamm.* 2015:652035. doi: 10.1155/2015/652035

Krystel-Whittemore, M., Dileepan, K. N., and Wood, J. G. (2016). Mast cell: a multi-functional master cell. *Front. Immunol.* 6:620. doi: 10.3389/fimmu.2015.00620

Kucuksezer, U. C., Aktas-Cetin, E., Bilgic-Gazioglu, S., Tugal-Tutkun, I., Gül, A., and Deniz, G. (2015). Natural killer cells dominate a Th-1 polarised response in Behçet's disease patients with uveitis. *Clin. Exp. Rheumatol.* 33, S24–S29.

Lad, E. M., Cousins, S. W., Van Arnam, J. S., and Proia, A. D. (2015). Abundance of infiltrating CD163+ cells in the retina of postmortem eyes with dry and neovascular age-related macular degeneration. *Graefes Arch Clin. Exp. Ophthalmol.* 253, 1941–1945. doi: 10.1007/s00417-015-3094-z

Lau, C. H., and Taylor, A. W. (2009). The Immune privileged retina mediates an alternative activation of J774A.1 cells. *Ocul. Immunol. Inflamm.* 17, 380–389. doi: 10.3109/09273940903118642

Le Moine, A., Flamand, V., Demoor, F.-X., Noël, J.-C., Surquin, M., Kiss, R., et al. (1999). Critical roles for IL-4, IL-5, and eosinophils in chronic skin allograft rejection. *J. Clin. Invest.* 103, 1659–1667. doi: 10.1172/JCI5504

Lechner, J., Chen, M., Hogg, R. E., Toth, L., Silvestri, G., Chakravarthy, U., et al. (2015). Alterations in circulating immune cells in neovascular age-related macular degeneration. *Sci. Rep.* 5:16754. doi: 10.1038/srep16754

Lechner, J., Chen, M., Hogg, R. E., Toth, L., Silvestri, G., Chakravarthy, U., et al. (2016). Higher plasma levels of complement C3a, C4a and C5a increase the risk of subretinal fibrosis in neovascular age-related macular degeneration: complement activation in AMD. *Immun. Ageing* 13:4. doi: 10.1186/s12979-016-0060-5

Lechner, J., Chen, M., Hogg, R. E., Toth, L., Silvestri, G., Chakravarthy, U., et al. (2017). Peripheral blood mononuclear cells from neovascular age-related macular degeneration patients produce higher levels of chemokines CCL2 (MCP-1) and CXCL8 (IL-8). *J. Neuroinflammation* 14:42. doi: 10.1186/s12974-017-0820-y

Lehmann, U., Heuss, N. D., McPherson, S. W., Roehrich, H., and Gregerson, D. S. (2010). Dendritic cells are early responders to retinal injury. *Neurobiol. Dis.* 40, 177–184. doi: 10.1016/j.nbd.2010.05.022

Levinson, R. D., Yung, M., Meguro, A., Ashouri, E., Yu, F., Mizuki, N., et al. (2016). KIR and HLA genotypes implicated in reduced killer lymphocytes immunity are associated with vogt-koyanagi-harada disease. *PLoS One* 11:e0160392. doi: 10.1371/journal.pone.0160392

Little, K., Llorián-Salvador, M., Tang, M., Du, X., O'Shaughnessy, Ó, McIlwaine, G., et al. (2020b). A Two-Stage laser-induced mouse model of subretinal fibrosis secondary to choroidal neovascularization. *Trans. Vis. Sci. Tech.* 9:3. doi: 10.1167/tvst.9.4.3

Little, K., Llorián-Salvador, M., Tang, M., Du, X., Marry, S., Chen, M., et al. (2020a). Macrophage to myofibroblast transition contributes to subretinal fibrosis secondary to neovascular age-related macular degeneration. *J. Neuroinflammation* 17:355. doi: 10.1186/s12974-020-02033-7

Little, K., Ma, J. H., Yang, N., Chen, M., and Xu, H. (2018). Myofibroblasts in macular fibrosis secondary to neovascular age-related macular degeneration – the potential sources and molecular cues for their recruitment and activation. *EBioMedicine* 38, 283–291. doi: 10.1016/j.ebiom.2018.11.029

Liu, B., Hunter, D. J., Rooker, S., Chan, A., Paulus, Y. M., Leucht, P., et al. (2013a). Wnt signaling promotes müller cell proliferation and survival after injury. *Invest. Ophthalmol. Vis. Sci.* 54:444. doi: 10.1167/iovs.12-10774

Liu, J., Copland, D. A., Horie, S., Wu, W.-K., Chen, M., Xu, Y., et al. (2013b). Myeloid cells expressing vegf and arginase-1 following uptake of damaged retinal pigment epithelium suggests potential mechanism that drives the onset of choroidal angiogenesis in mice. *PLoS One* 8:e72935. doi: 10.1371/journal.pone.0072935

Liu, J., Tang, M., Harkin, K., Du, X., Luo, C., Chen, M., et al. (2020). Single-cell RNA sequencing study of retinal immune regulators identified CD47 and CD59a expression in photoreceptors—Implications in subretinal immune regulation. *J. Neurosci. Res.* 98, 1498–1513. doi: 10.1002/jnr.24618

Luo, C., Chen, M., Madden, A., and Xu, H. (2012). Expression of complement components and regulators by different subtypes of bone marrow-derived macrophages. *Inflammation* 35, 1448–1461. doi: 10.1007/s10753-012-9458-1

Luo, C., Zhao, J., Chen, M., and Xu, H. (2018). The expression of C1 inhibitor (C1INH) in macrophages is upregulated by retinal pigment epithelial cells – implication in subretinal immune privilege in the aging eye. *Aging* 10, 1380–1389. doi: 10.18632/aging.101474

Luo, C., Zhao, J., Madden, A., Chen, M., and Xu, H. (2013). Complement expression in retinal pigment epithelial cells is modulated by activated macrophages. *Exp. Eye Res.* 112, 93–101. doi: 10.1016/j.exer.2013.04.016

Ma, W., Cojocaru, R., Gotoh, N., Gieser, L., Villasmil, R., Cogliati, T., et al. (2013). Gene expression changes in aging retinal microglia: relationship to microglial support functions and regulation of activation. *Neurobiol. Aging* 34, 2310–2321. doi: 10.1016/j.neurobiolaging.2013.03.022

Martínez-Alemán, S. R., Campos-García, L., Palma-Nicolas, J. P., Hernández-Bello, R., González, G. M., and Sánchez-González, A. (2017). Understanding the entanglement: neutrophil extracellular traps (NETs) in cystic fibrosis. *Front. Cell. Infect. Microbiol.* 7:104. doi: 10.3389/fcimb.2017.00104

Matsuda, K., Okamoto, N., Kondo, M., Arkwright, P. D., Karasawa, K., Ishizaka, S., et al. (2017). Mast cell hyperactivity underpins the development of oxygen-induced retinopathy. *J. Clin. Invest.* 127, 3987–4000. doi: 10.1172/JCI89893

Matzinger, P., and Kamala, T. (2011). Tissue-based class control: the other side of tolerance. *Nat. Rev. Immunol.* 11, 221–230. doi: 10.1038/nri2940

McLeod, D. S., Bhutto, I., Edwards, M. M., Gedam, M., Baldeosingh, R., and Lutty, G. A. (2017). Mast cell-derived tryptase in geographic atrophy. *Invest. Ophthalmol. Vis. Sci.* 58:5887. doi: 10.1167/iovs.17-22989

McMenamin, P. G. (1997). The distribution of immune cells in the uveal tract of the normal eye. *Eye* 11, 183–193. doi: 10.1038/eye.1997.49

Meng, X.-M., Wang, S., Huang, X.-R., Yang, C., Xiao, J., Zhang, Y., et al. (2016). Inflammatory macrophages can transdifferentiate into myofibroblasts during renal fibrosis. *Cell Death Dis.* 7, e2495–e2495. doi: 10.1038/cddis.2016.402

Montero, J.A, and Ruiz-Moreno, J. M. (2010). Treatment of choroidal neovascularization in high myopia. *Curr. Drug Targets* 11, 630–644. doi: 10.2174/138945010791011929

Monument, M. J., Hart, D. A., Salo, P. T., Befus, A. D., and Hildebrand, K. A. (2015). Neuroinflammatory mechanisms of connective tissue fibrosis: targeting neurogenic and mast cell contributions. *Adv. Wound Care* 4, 137–151. doi: 10.1089/wound.2013.0509

Niazi, S., Krogh Nielsen, M., Sørensen, T. L., and Subhi, Y. (2019). Neutrophil-to-lymphocyte ratio in age-related macular degeneration: a systematic review and meta-analysis. *Acta Ophthalmol.* 97, 558–566. doi: 10.1111/aos.14072

Nosbaum, A., Prevel, N., Truong, H. A., Mehta, P., Ettinger, M., Scharschmidt, T. C., et al. (2016). Cutting edge: regulatory t cells facilitate cutaneous wound healing. *J. Immunol.* 196, 2010–2014. doi: 10.4049/jimmunol.1502139

Obasanmi, G., Lois, N., Armstrong, D., Lavery, N.-J., Hombrebueno, J. R., Lynch, A., et al. (2020). Circulating leukocyte alterations and the development/progression of diabetic retinopathy in type 1 diabetic patients – a pilot study. *Curr. Eye Res.* 45, 1144–1154. doi: 10.1080/02713683.2020.1718165

Oberyszyn, T. M. (2007). Inflammation and wound healing. *Front. Biosci.* 12:2993–2999. doi: 10.2741/2289

Ohno-Matsui, K., Wu, P.-C., Yamashiro, K., Vutipongsatorn, K., Fang, Y., Cheung, C. M. G., et al. (2021). IMI pathologic myopia. *Invest. Ophthalmol. Vis. Sci.* 62:5. doi: 10.1167/iovs.62.5.5

Overed-Sayer, C., Rapley, L., Mustelin, T., and Clarke, D. L. (2014). Are mast cells instrumental for fibrotic diseases? *Front. Pharmacol.* 4:174. doi: 10.3389/fphar.2013.00174

Page, C., Goicochea, L., Matthews, K., Zhang, Y., Klover, P., Holtzman, M. J., et al. (2012). Induction of alternatively activated macrophages enhances pathogenesis during severe acute respiratory syndrome coronavirus infection. *J. Virol.* 86, 13334–13349. doi: 10.1128/JVI.01689-12

Pastor, J. C., Rojas, J., Pastor-Idoate, S., Di Lauro, S., Gonzalez-Buendia, L., and Delgado-Tirado, S. (2016). Proliferative vitreoretinopathy: a new concept of disease pathogenesis and practical consequences. *Prog. Retin. Eye Res.* 51, 125–155. doi: 10.1016/j.preteyeres.2015.07.005

Planul, A., and Dalkara, D. (2017). Vectors and gene delivery to the retina. *Annu. Rev. Vis. Sci.* 3, 121–140. doi: 10.1146/annurev-vision-102016-061413

Ponsioen, T. L., van Luyn, M. J. A., van der Worp, R. J., Pas, H. H., Hooymans, J. M. M., and Los, L. I. (2008). Human retinal Müller cells synthesize collagens of the vitreous and vitreoretinal interface in vitro. *Mol. Vis.* 14, 652–660.

Radaeva, S., Sun, R., Jaruga, B., Nguyen, V. T., Tian, Z., and Gao, B. (2006). Natural killer cells ameliorate liver fibrosis by killing activated stellate cells in NKG2D-dependent and tumor necrosis factor–related apoptosis-inducing ligand–dependent manners. *Gastroenterology* 130, 435–452. doi: 10.1053/j.gastro.2005.10.055

Rahman, A. H., and Aloman, C. (2013). Dendritic cells and liver fibrosis. *Biochim. Biophys. Acta* 1832, 998–1004. doi: 10.1016/j.bbadis.2013.01.005

Rishi, P., Gupta, A., Rishi, E., and Shah, B. J. (2013). Choroidal neovascularization in 36 eyes of children and adolescents. *Eye* 27, 1158–1168. doi: 10.1038/eye.2013.155

Rockey, J. H., Donnelly, J. J., Stromberg, B. E., and Soulsby, E. J. L. (1979). Immunopathology of toxocara canis and ascaris suum infections of the eye: the role of the eosinophil. *Invest. Ophthalmol. Vis. Sci.* 18, 1172–1184.

Roy, S., Amin, S., and Roy, S. (2016). Retinal fibrosis in diabetic retinopathy. *Exp. Eye Res.* 142, 71–75. doi: 10.1016/j.exer.2015.04.004

Rutar, M., Natoli, R., Kozulin, P., Valter, K., Gatenby, P., and Provis, J. M. (2011). Analysis of complement expression in light-induced retinal degeneration: synthesis and deposition of C3 by microglia/macrophages is associated with focal photoreceptor degeneration. *Invest. Opthalmol. Vis. Sci.* 52:5347. doi: 10.1167/iovs.10-7119

Sakurai, E., Anand, A., Ambati, B. K., van Rooijen, N., and Ambati, J. (2003). Macrophage depletion inhibits experimental choroidal neovascularization. *Invest. Ophthalmol. Vis. Sci.* 44:3578. doi: 10.1167/iovs.03-0097

Sato, T., Morishita, S., Horie, T., Fukumoto, M., Kida, T., Oku, H., et al. (2019). Involvement of premacular mast cells in the pathogenesis of macular diseases. *PLoS One* 14:e0211438. doi: 10.1371/journal.pone.0211438

Segal, A. W. (2005). How neutrophils kill microbes. *Annu. Rev. Immunol.* 23, 197–223. doi: 10.1146/annurev.immunol.23.021704.115653

Sennlaub, F., Auvynet, C., Calippe, B., Lavalette, S., Poupel, L., Hu, S. J., et al. (2013). CCR2+ monocytes infiltrate atrophic lesions in age-related macular disease and mediate photoreceptor degeneration in experimental subretinal inflammation in Cx3cr1 deficient mice. *EMBO Mol. Med.* 5, 1775–1793. doi: 10.1002/emmm.201302692

Shen, P., and Fillatreau, S. (2015). Antibody-independent functions of B cells: a focus on cytokines. *Nat. Rev. Immunol.* 15, 441–451. doi: 10.1038/nri3857

Shu, D. Y., Butcher, E., and Saint-Geniez, M. (2020). EMT and EndMT: emerging roles in age-related macular degeneration. *Int. J. Mol. Sci.* 21:4271. doi: 10.3390/ijms21124271

Smith, C. W., Guyer, D. R., and D'Amico, D. J. (1992). Subretinal fibrosis after laser photocoagulation for diabetic macular edema. *Am. J. Ophthalmol.* 113, 652–656. doi: 10.1016/S0002-9394(14)74789-0

Smith, J. R., Stempel, A. J., Bharadwaj, A., and Appukuttan, B. (2016). Involvement of B cells in non-infectious uveitis. *Clin. Trans. Immunol.* 5:e63. doi: 10.1038/cti.2016.2

Song, Y., Liao, M., Zhao, X., Han, H., Dong, X., Wang, X., et al. (2021). Vitreous M2 macrophage-derived microparticles promote RPE cell proliferation and migration in traumatic proliferative vitreoretinopathy. *Invest. Ophthalmol. Vis. Sci.* 62:26. doi: 10.1167/iovs.62.12.26

Sonoda, K.-H., Yoshimura, T., Egashira, K., Charo, I. F., and Ishibashi, T. (2011). Neutrophil-dominant experimental autoimmune uveitis in CC-chemokine receptor 2 knockout mice. *Acta Ophthalmol.* 89, e180–e188. doi: 10.1111/j.1755-3768.2010.01953.x

Spry, C. J. (1989). The pathogenesis of endomyocardial fibrosis: the role of the eosinophil. *Springer Semin Immunopathol.* 11, 471–477. doi: 10.1007/BF00201883

Sugita, S., Makabe, K., Iwasaki, Y., Fujii, S., and Takahashi, M. (2018). Natural killer cell inhibition by HLA-E molecules on induced pluripotent stem cell–derived retinal pigment epithelial cells. *Invest. Ophthalmol. Vis. Sci.* 59:1719. doi: 10.1167/iovs.17-22703

Tang, S., Scheiffarth†, O. F., Thurau, S. R., and Wildner, G. (1993). Cells of the immune system and their cytokines in epiretinal membranes and in the vitreous of patients with proliferative diabetic retinopathy. *Ophthal. Res.* 25, 177–185. doi: 10.1159/000267287

Tarau, I.-S., Berlin, A., Curcio, C. A., and Ach, T. (2019). The Cytoskeleton of the retinal pigment epithelium: from normal aging to age-related macular degeneration. *Int. J. Mol. Sci.* 20:3578. doi: 10.3390/ijms20143578

Teo, K. Y. C., Joe, A. W., Nguyen, V., Invernizzi, A., Arnold, J. J., Barthelmes, D., et al. (2020). PREVALENCE AND RISK FACTORS FOR THE DEVELOPMENT OF PHYSICIAN-GRADED SUBRETINAL FIBROSIS IN EYES TREATED FOR NEOVASCULAR AGE-RELATED MACULAR DEGENERATION. *Retina* 40, 2285–2295. doi: 10.1097/IAE.0000000000002779

Thapa, M., Chinnadurai, R., Velazquez, V. M., Tedesco, D., Elrod, E., Han, J.-H., et al. (2015). Liver fibrosis occurs through dysregulation of MyD88-dependent innate B-cell activity: liver biology/pathobiology. *Hepatology* 61, 2067–2079. doi: 10.1002/hep.27761

Tonade, D., Liu, H., Palczewski, K., and Kern, T. S. (2017). Photoreceptor cells produce inflammatory products that contribute to retinal vascular permeability in a mouse model of diabetes. *Diabetologia* 60, 2111–2120. doi: 10.1007/s00125-017-4381-5

Toris, C. B., and Pederson, J. E. (1985). Experimental retinal detachment. VIII. retinochoroidal horseradish peroxidase diffusion across the blood-retinal barrier. *Arch. Ophthalmol.* 103, 266–269. doi: 10.1001/archopht.1985.01050020118033

Trocme, S. D. (1991). Eosinophil and neutrophil degranulation in ophthalmic lesions of wegener's granulomatosis. *Arch. Ophthalmol.* 109:1585. doi: 10.1001/archopht.1991.01080110121049

Trocme, S. D., and Aldave, A. J. (1994). The eye and the eosinophil. *Surv. Ophthalmol.* 39, 241–252. doi: 10.1016/0039-6257(94)90197-X

Tsutsumi, C., Sonoda, K.-H., Egashira, K., Qiao, H., Hisatomi, T., Nakao, S., et al. (2003). The critical role of ocular-infiltrating macrophages in the development of choroidal neovascularization. *J. Leukocyte Biol.* 74, 25–32. doi: 10.1189/jlb.0902436

Turner, J.-E. (2017). Natural killers: the bad guys in fibrosis? *Kidney Int.* 92, 9–11. doi: 10.1016/j.kint.2017.03.011

Wang, J., Li, Q., Yin, Y., Zhang, Y., Cao, Y., Lin, X., et al. (2020). Excessive neutrophils and neutrophil extracellular traps in COVID-19. *Front. Immunol.* 11:2063. doi: 10.3389/fimmu.2020.02063

Wang, Y.-Y., Jiang, H., Pan, J., Huang, X.-R., Wang, Y.-C., Huang, H.-F., et al. (2017). Macrophage-to-Myofibroblast transition contributes to interstitial fibrosis in chronic renal allograft injury. *J. Am. Soc. Nephrol.* 28, 2053–2067. doi: 10.1681/ASN.2016050573

Wendisch, D., Dietrich, O., Mari, T., von Stillfried, S., Ibarra, I. L., Mittermaier, M., et al. (2021). SARS-CoV-2 infection triggers profibrotic macrophage responses and lung fibrosis. *Cell* 184, 6243.e–6261.e. doi: 10.1016/j.cell.2021.11.033

Wenkel, H., and Streilein, J. W. (2000). Evidence that retinal pigment epithelium functions as an immune-privileged tissue. *Invest. Ophthalmol. Vis. Sci.* 41, 3467–3473.

Wieghofer, P., Hagemeyer, N., Sankowski, R., Schlecht, A., Staszewski, O., Amann, L., et al. (2021). Mapping the origin and fate of myeloid cells in distinct compartments of the eye by single-cell profiling. *EMBO J.* 40:e105123. doi: 10.15252/embj.2020105123

Wong, K. L., Yeap, W. H., Tai, J. J. Y., Ong, S. M., Dang, T. M., and Wong, S. C. (2012). The three human monocyte subsets: implications for health and disease. *Immunol. Res.* 53, 41–57. doi: 10.1007/s12026-012-8297-3

Wu, Y.-Y., Wang, S.-H., Wu, C.-H., Yen, L.-C., Lai, H.-F., Ho, C.-L., et al. (2020). In silico immune infiltration profiling combined with functional enrichment analysis reveals a potential role for naïve B cells as a trigger for severe immune responses in the lungs of COVID-19 patients. *PLoS One* 15:e0242900. doi: 10.1371/journal.pone.0242900

Wynn, T. (2008). Cellular and molecular mechanisms of fibrosis. *J. Pathol.* 214, 199–210. doi: 10.1002/path.2277

Wynn, T. A., and Vannella, K. M. (2016). Macrophages in tissue repair, regeneration, and fibrosis. *Immunity* 44, 450–462. doi: 10.1016/j.immuni.2016.02.015

Xu, H., and Chen, M. (2016). Targeting the complement system for the management of retinal inflammatory and degenerative diseases. *Eur. J. Pharmacol.* 787, 94–104. doi: 10.1016/j.ejphar.2016.03.001

Xu, H., Chen, M., and Forrester, J. V. (2009). Para-inflammation in the aging retina. *Prog. Retin. Eye Res.* 28, 348–368. doi: 10.1016/j.preteyeres.2009.06.001

Xu, H., Chen, M., Manivannan, A., Lois, N., and Forrester, J. V. (2008). Age-dependent accumulation of lipofuscin in perivascular and subretinal microglia in experimental mice. *Aging Cell* 7, 58–68. doi: 10.1111/j.1474-9726.2007.00351.x

Xu, H., Dawson, R., Forrester, J. V., and Liversidge, J. (2007). Identification of novel dendritic cell populations in normal mouse retina. *Invest. Ophthalmol. Vis. Sci.* 48:1701. doi: 10.1167/iovs.06-0697

Yamamoto, T., Hartmann, K., Eckes, B., and Krieg, T. (2000). Mast cells enhance contraction of three-dimensional collagen lattices by ®broblasts by cell±cell interaction: role of stem cell factor/c-kit. *Immunology* 99, 435–439. doi: 10.1046/j.1365-2567.2000.00973.x

Yang, S., Li, H., Li, M., and Wang, F. (2015). Mechanisms of epithelial-mesenchymal transition in proliferative vitreoretinopathy. *Discov. Med.* 20, 207–217.

Yu, C., Roubeix, C., Sennlaub, F., and Saban, D. R. (2020). Microglia versus monocytes: distinct roles in degenerative diseases of the retina. *Trends Neurosci.* 43, 433–449. doi: 10.1016/j.tins.2020.03.012

Yu, Y., Ren, X. R., Wen, F., Chen, H., and Su, S. B. (2016). T-helper-associated cytokines expression by peripheral blood mononuclear cells in patients with polypoidal choroidal vasculopathy and age-related macular degeneration. *BMC Ophthalmol.* 16:80. doi: 10.1186/s12886-016-0251-z

Zamiri, P., Masli, S., Streilein, J. W., and Taylor, A. W. (2006). Pigment epithelial growth factor suppresses inflammation by modulating macrophage activation. *Invest. Ophthalmol. Vis. Sci.* 47:3912. doi: 10.1167/iovs.05-1267

Zhang, M., and Zhang, S. (2020). T Cells in fibrosis and fibrotic diseases. *Front. Immunol.* 11:1142. doi: 10.3389/fimmu.2020.01142

Zhao, Z., Xu, P., Jie, Z., Zuo, Y., Yu, B., Soong, L., et al. (2014b). γδ T cells as a major source of IL-17 production during age-dependent RPE degeneration. *Invest. Ophthalmol. Vis. Sci.* 55:6580. doi: 10.1167/iovs.14-15166

Zhao, J., Chen, M., and Xu, H. (2014a). Experimental autoimmune uveoretinitis (EAU)-related tissue damage and angiogenesis is reduced in CCL2 —/— CX3CR1gfp/gfp Mice. *Invest. Ophthalmol. Vis. Sci.* 55:7572. doi: 10.1167/iovs.14-15495

Zhou, M., Geathers, J. S., Grillo, S. L., Weber, S. R., Wang, W., Zhao, Y., et al. (2020). Role of epithelial-mesenchymal transition in retinal pigment epithelium dysfunction. *Front. Cell Dev. Biol.* 8:501. doi: 10.3389/fcell.2020.00501

Zhu, L., Fu, X., Chen, X., Han, X., and Dong, P. (2017b). M2 macrophages induce EMT through the TGF-β/Smad2 signaling pathway: M2 macrophages induce EMT in IPF. *Cell Biol. Int.* 41, 960–968. doi: 10.1002/cbin.10788

Zhu, F., Bai, X., and Chen, X. (2017a). B lymphocytes in renal interstitial fibrosis. *J. Cell Commun. Signal.* 11, 213–218. doi: 10.1007/s12079-017-0382-x

Conflict of Interest: The authors declare that the research was conducted in the absence of any commercial or financial relationships that could be construed as a potential conflict of interest.

Publisher's Note: All claims expressed in this article are solely those of the authors and do not necessarily represent those of their affiliated organizations, or those of the publisher, the editors and the reviewers. Any product that may be evaluated in this article, or claim that may be made by its manufacturer, is not guaranteed or endorsed by the publisher.

Copyright © 2022 Szczepan, Llorián-Salvador, Chen and Xu. This is an open-access article distributed under the terms of the Creative Commons Attribution License (CC BY). The use, distribution or reproduction in other forums is permitted, provided the original author(s) and the copyright owner(s) are credited and that the original publication in this journal is cited, in accordance with accepted academic practice. No use, distribution or reproduction is permitted which does not comply with these terms.

frontiers | Frontiers in Cellular Neuroscience

ORIGINAL RESEARCH
published: 15 June 2022
doi: 10.3389/fncel.2022.892197

MicroRNA-124/Death-Associated Protein Kinase 1 Signaling Regulates Neuronal Apoptosis in Traumatic Brain Injury *via* Phosphorylating NR2B

Yingwu Shi†, Wenxing Cui†, Qiang Wang†, Jinpeng Zhou, Xun Wu, Jin Wang, Shenghao Zhang, Qing Hu, Liying Han, Yong Du, Shunnan Ge, Haixiao Liu and Yan Qu**

Department of Neurosurgery, Tangdu Hospital, Fourth Military Medical University, Xi'an, China

Death-associated protein kinase 1 (DAPK1), a Ca^{2+}/calmodulin-dependent serine/threonine-protein kinase, promotes neurons apoptosis in ischemic stroke and Alzheimer's disease (AD). We hypothesized that knockdown DAPK1 may play a protective role in traumatic brain injury (TBI) and explore underlying molecular mechanisms. ELISA, Western blotting, immunofluorescence, dual-luciferase assay, and Reverse Transcription and quantitative Polymerase Chain Reaction (RT-qPCR) were used to determine the mechanism for the role of DAPK1 in TBI. Open field and novel objective recognition tests examined motor and memory functions. The morphology and number of synapses were observed by transmission electron microscopy and Golgi staining. DAPK1 was mainly found in neurons and significantly increased in TBI patients and TBI mice. The dual-luciferase assay showed that DAPK1 was upregulated by miR-124 loss. The number of $TUNEL^+$ cells, expression levels of cleaved caspase3 and p-NR2B/NR2B were significantly reduced after knocking-down DAPK1 or overexpressing miR-124 in TBI mice; and motor and memory dysfunction was recovered. After Tat-NR2B were injected in TBI mice, pathological and behavioral changes were mitigated while the morphology while the number of synapses were not affected. Overall, DAPK1 is a downstream target gene of miR-124 that regulates neuronal apoptosis in TBI mice *via* NR2B. What's more, DAPK1 restores motor and memory dysfunctions without affecting the number and morphology of synapses.

Keywords: traumatic brain injury, DAPK1, miR-124, NR2B, neuronal apoptosis

OPEN ACCESS

Edited by:
Tim-Henrik Bruun, Velvio GmbH, Germany

Reviewed by:
Shasha Yang, Fudan University, China
Iliana Barrera, University of Bristol, United Kingdom

****Correspondence:***
Haixiao Liu
lhxiao@fmmu.edu.cn
Yan Qu
yanqu0123@fmmu.edu.cn

† These authors have contributed equally to this work

Specialty section:
This article was submitted to Cellular Neuropathology, a section of the journal Frontiers in Cellular Neuroscience

Received: *08 March 2022*
Accepted: *16 May 2022*
Published: *15 June 2022*

Citation:
Shi Y, Cui W, Wang Q, Zhou J, Wu X, Wang J, Zhang S, Hu Q, Han L, Du Y, Ge S, Liu H and Qu Y (2022) MicroRNA-124/Death-Associated Protein Kinase 1 Signaling Regulates Neuronal Apoptosis in Traumatic Brain Injury via Phosphorylating NR2B. Front. Cell. Neurosci. 16:892197. doi: 10.3389/fncel.2022.892197

INTRODUCTION

Traumatic brain injury (TBI) is a high disability and fatality disease (Jiang et al., 2019). Approximately 43% of patients with TBI experienced long-term dysfunctions because of overactivated neuronal apoptosis and the non-renewability of neurons (Su et al., 2019; Capizzi et al., 2020). Death-associated protein kinase 1 (DAPK1) is a Ca^{2+}/calmodulin-dependent serine/threonine-protein kinase, which promotes neuronal apoptosis in neurons during various neurological disorders such as ischemic stroke and Alzheimer's disease (AD) (Shu et al., 2016; Kim et al., 2019; Wang et al., 2020). DAPK1 leads to neuronal apoptosis in ischemic stroke *via* phosphorylating NR2B (p-NR2B), P53, or Tau (Tu et al., 2010; Pei et al., 2015; Wang et al., 2017). In AD, activated DAPK1/NDRG2 pathways lead to cell death, and DAPK1 triggers the amyloidogenic

pathway and Aβ production by phosphorylating APP (Kim et al., 2016; Xu et al., 2019). However, it is unclear whether DAPK1 contributes to TBI.

NR2B is a subunit of N-methyl-D-aspartic acid (NMDA) receptors and regulates Ca^{2+} influx in neurons (Brown et al., 2019), which helps maintain of normal cellular functions and neuronal plasticity (Wang et al., 2014); previous evidence demonstrating that inhibiting the NR2B phosphorylation can rescue TBI-induced neurological impairment (Schumann et al., 2008). As showed in the results of this work, the NR2B level was not changed in TBI group nor by any of the rescue strategies. In cerebral ischemia, the phosphorylation of NR2B can cause neuronal apoptosis by promoting excessive Ca^{2+} influx, the downregulation of cAMP-response element binding protein (CREB), the activation of JUN, neuronal nitric oxide synthase (nNOS) and post-synaptic density protein 95 (PSD95) (Sun et al., 2015; Dai et al., 2016). PSD95 is an abundant scaffolding protein located at excitatory synapses, which specifically binds to NR2B through its PDZ domains. The NR2B–PSD95 complex interaction with activated calmodulin-dependent protein kinase II (CaMK II), resulting in excessive Ca^{2+} influx (Irie et al., 1997). However, the interaction between DAPK1 and NR2B in TBI remains unknown.

Recent research has focused on non-coding RNA, particularly miRNA, as it plays a vital role in gene post-transcriptional regulation and RNA silencing (Bushati and Cohen, 2007; Barry, 2014). The role of miR-124 has been reported in various neurological diseases. In AD, miR-124 can mediate synaptic and memory deficits through Potential Enhancers of Cancer Immunotherapy and Type 1 (PTPN1) (Wang et al., 2018). Besides, the early miR-124 treatment-induced neuroprotection and functional improvement in the case of focal cerebral ischemia stroke (Yang et al., 2017). In Parkinson's disease (PD), overexpression of miR-124 could effectively inhibit DAPK1 expressions and alleviate MPP^{+} induced cell apoptosis (Lu et al., 2020), while the interaction between miR-124 and NR2B has not been reported. Previous research found that miR-124 can promote M2 polarization of microglia and increase hippocampus neurogenesis by inhibiting Toll-like receptor 4 (TLR4) (Yang et al., 2019). These findings suggest that miR-124 can be a promising target for TBI therapy.

This study firstly showed that DAPK1 was upregulated in TBI patients and TBI mice due to miR-124 loss. Overexpression of miR-124 or knocking down DAPK1 can rescue TBI-mediated behavioral and pathological changes. Finally, Tat-NR2B that can block the binding between DAPK1 and NR2B was used in TBI mice, and the results indicate that TBI-induced dysfunction was mitigated while normal synapse function was not affected.

MATERIALS AND METHODS

Patients

This study was approved by the Ethics Committee of Tangdu Hospital, Fourth Military Medical University, and was conducted from September 2020 to April 2021. Patients were between the ages of 18 and 80 diagnosed with TBI *via* head computerized tomography (CT) findings at admission were included in this study. Patients with a history of neurological disease or severe systemic disease (uremia, cirrhosis, or malignant cancer) were excluded from the study. Using 6-month Glasgow Outcome Scale (GOS) score to evaluate the neurologic function. GOS scores of 1∼3 were unfavorable outcomes, and scores of 4–5 were considered favorable outcomes. Preoperative medical records were searched for age, gender, pupil reaction, mechanism of injury, and laboratory biochemical examinations. The hematoma volume on admission CT scan was measured by ABC/2 method as reported before (Kothari et al., 1996). All experimental procedure conformed to the Declaration of Helsiniki.

ELISAs

Cubital venous blood samples were collected from TBI patients who were injured within 24 h and met the inclusion/exclusion criteria. Hemolytic samples were excluded from this study. Plasma was obtained by centrifuging of whole blood at 1,500 g for 15 min. An ELISA kit (Jianglaibio, China) was used to measure the expression levels of DAPK1 in the plasma, and all procedures were completed as per the manufacturer's instructions.

Animals

The Fourth Military Medical University's Ethics Committee approved all experimental procedures. All experiments were performed in accordance with the National Institutes of Health Guide for the Care and Use of Laboratory Animals. Eight weeks old, male C57BL/6 mice were purchased from the Animal Center of the Fourth Military Medical University. All animals were housed in specific pathogen-free environment room (*ad libitum* to food and water) with a 12-h light/dark cycle. The experimental holding room had a temperature (23°C) and humidity control (60%).

Controlled Cortical Impact Model of Traumatic Brain Injury

Mice were subjected to either controlled cortical impact (CCI) or sham surgery, as previously described (Shi et al., 2022). First, the mice were deeply anesthetized with isoflurane, and their heads were fixed on a stereotactic device (RWD, China). The position of craniotomy was the right parietal bone window (1.5 mm from the midline and 1.5 mm behind the bregma) and a 2.0 mm diameter dental drill was used. Then, the skull cap was carefully removed while not damaging the underlying leptomeninges. The cortex was struck with a flat metal tip at a speed of 3.0 m/s and a depth of 1.8 mm; the contact time was 2.0 s. Each mouse underwent with single strikes. After CCI the window on the skull was sealed with bone wax, and the incision was sutured. The mice were allowed to recover on a heating pad to maintain their core body temperature at 37°C. A similar surgical procedure was performed on sham mice but without CCI.

Immunofluorescence Staining

The mice were deeply anesthetized with isoflurane and transcardially perfused with 30 ml of 0.01 M PBS followed by 60 ml of 4%(w/v) formaldehyde 7 days after TBI. Then mice brains were removed quickly and postfixed with 4% (w/v) formaldehyde overnight at 4°C. After dehydrating in 10, 20, and

30% (w/v) sucrose solutions, the brains were cut into 30 μm frontal sections. The sections were incubated with 0.01 M PBS containing 0.1% (v/v) Triton X-100 for 10 min and then blocked with 0.01 M PBS containing 5% (w/v) goat serum for 1 h. The sections were incubated for 12 h at room temperature with the following antibodies: Chicken anti-GFAP (1:300; Invitrogen, California, CA, United States), goat anti-Iba1 (1:300; Abcam, Cambridge, United Kingdom), guineapig anti-NeuN antibody (1:300; Millipore, Massachusetts, MA, United States), rabbit anti-DAPK1 (1:300; Cell Signaling Technology, Massachusetts, MA, United States). Then the sections were washed and laster incubated for 1 h at room temperature with 594 anti-goat (1:500; Invitrogen, California, CA, United States), 594 anti-chicken (1:500; Invitrogen, California, CA, United States), 594 anti-guineapig (1:500; Invitrogen, California, CA, United States), or 488 anti-rabbit (1:500; Invitrogen, California, CA, United States). Finally, the sections were dyed in DAPI solution (1 mg/ml) for 10 min before images were captured on a confocal microscope (A1, Nikon, Tokyo, Japan).

TUNEL Staining

Cell apoptosis was measured by *In Situ* Cell Death Detection Kit (Roche, Basel, Switzerland). Briefly, the sections were incubated with 0.01 M PBS containing 0.1% (v/v) Triton X-100 for 10 min. Then the sections were dyed using the TUNEL reaction solution prepared in a humidified dark box for 1 h at room temperature. Finally, the tissues were dyed in DAPI solution (1 μg/ml) for 10 min before images were captured on a confocal microscope (Nikon, Tokyo, Japan).

Western Blotting

The perilesional cortex was collected under a dissecting microscope at 7 days after TBI and extracted in RIPA lysis buffer containing 1% (v/v) protease and phosphatase inhibitor cocktail. The protein samples were separated by SDS-PAGE and transferred to PVDF. After being blocked with 5% (w/v) non-fat milk, the membranes were incubated overnight at 4°C with the following primary antibodies: Rabbit anti-Cleaved caspase 3 (1:1,000, Cell Signaling Technology, United States), Rabbit anti-DAPK1 (1:1,000, Cell Signaling Technology, Massachusetts, MA, United States), Rabbit anti-β-actin (1:1,000, Abcam, Cambridge, United Kingdom), Rabbit anti-NR2B (1:1,000, Abcam, Cambridge, United Kingdom), Rabbit anti-p-NR2B (Ser1303, 1:1,000, Abcam, Cambridge, United Kingdom), Rabbit anti-PSD95 (1:1,000, Proteintech, China), Rabbit anti-ERK1/2 (1:1,000, Cell Signaling Technology, Massachusetts, MA, United States), Rabbit anti-p-ERK1/2 (Thr202/Tyr204, 1:1,000, Cell Signaling Technology, Massachusetts, MA, United States). Afterward, the membranes were incubated with HRP anti-rabbit (1:1,000, Cell Signaling Technology, Massachusetts, MA, United States) for 1 h at room temperature and then scanned with a Bio-Rad (California, United States) gel imaging system.

Dual-Luciferase Reporter Assay

A wild-type and a mutant DAPK1 3′ UTR were cloned into the pSI-Check2 renilla luciferase reporter plasmid (Hanbio Biotechnology, China). HEK (Human embryonic kidney) 293T cells were cotransfected with the negative control (NC) mimics or miR-124 and wild-type (WT) or mutant (Mut) DAPK1 3′ UTR plasmid. The cells were harvested, and cell lysates were assayed for firefly and renilla luciferase activities using the dual-luciferase reporter assay system (Promega, Wisconsin, WI, Untied States). The normalized values (Renilla luciferase/firefly activity) were used for analysis.

Reverse Transcription and Quantitative Polymerase Chain Reaction

Seven days after TBI, total RNA of the cortex was extracted using TRIzol Reagent (Invitrogen, California, CA, United States) according to the manufacturer's protocol. According to the manufacturer's instructions, the miscript cDNA synthesis kit (Tiangen, China) was used for the reverse transcription reaction. Using miRNA isolation kit (Tiangen, China) to extract miRNA, RT–qPCR was performed using an iQ^{TM} 5 Optical Module Real-Time PCR Detection (Bio-rad, California, CA, United States). ChamQ^{TM} SYBR qPCR master mix was used to quantify miRNA, according to manufacturer's instructions. Using the relative CT method to compare different samples. The fold increase or decrease was determined relative to a vehicle-treated control after normalizing to a housekeeping gene using $2^{-\Delta\Delta CT}$. The primers used are listed in **Supplementary Table 1**.

Delivery of Adeno-Associated Viruses

Injection of AAV2-hsyn-shDAPK1-eGFP to knock down DAPK1 or Con AAV (AAV2-hsyn -eGFP) into the right cortex area, and the viral titer was 1.0×10^9 particles/ml. The stereotaxic coordinates for the cortex injection were anterior-posterior 1.80 mm, medial-lateral 2.50 mm, and dorsal-ventral 1.00 mm. The volume of injected virus was 2.0 μl and injection rate was 0.2 μl/min. After 2 weeks, the mice were subjected to either a sham procedure or CCI, followed by behavioral and pathological tests 1 week later.

Intranasal Delivery of Agomir

Two weeks before TBI induction, the mice were grasped from the back every day, and kept their head and abdomen upward (Hanson et al., 2013). The mouse was fixed in this position for 1 min and then administered agomir in 4 μl drops by pipette, alternating between each nostril every 1 min. The mice were administered different doses (0.01, 0.05, 0.10, 0.50, 1.00, and 5.00 nmol) of agomir (sense sequence: 5′-UAAGGCACGCGGUGAAUGCC-3′, antisense sequence: 5′-CAUUCACCGCGUGCCUUAUU-3′) (GenePharma, China) by nasal instillation daily for 7 days after TBI induction. Control mice received an equal volume of solvent.

Open Field Test

The open field chamber was 43.2 × 43.2 cm with opaque walls (30.5 cm). Seven days after TBI, mice were placed into the center of the apparatus individually and allowed to travel freely for 10 min. Locomotor activity and total distance traveled was recorded using an overhead camera connected to a computer

with video tracking software (Noldus Ethovision version 8.0, Wageningen, Netherlands).

Novel Objective Recognition Test

On day 6 after TBI, mice were individually placed in the same open field as described before for 10 min for habituation. On day 7 and 8 (training days) after TBI two identical cylinders (a height of 8 cm and diameter of 4 cm, made of polyethylene) were fixed at one side of open field and 10 cm from both side walls; mice were placed at the center of open field with their backs to two objects and allowed to travel freely for 10 min; their locomotor activity was recorded using an overhead camera linked to a computer running video tracking software (Noldus Ethovision version 8.0, Wageningen, Netherlands). On day 9 (testing day) after TBI, replace one of the cylinders with a cone (a height of 8 cm and diameter of 4 cm, made of polyethylene), repeat the above steps. Object recognizing was defined when the distance between the nose and the object was less than 2 cm (Leger et al., 2013). Time exploring around the objects was measured. Recognition index = (time exploring the novel object)/(time exploring the novel object + time exploring the familiar object) × 100%.

Quantify of Lesion Volume

Seven days after TBI, A 3T small-animal Magnetic Resonance Imaging (MRI) scanner (UMR780, United imaging, China) was used to generate series of brain images. T2-weighted imaging (T2) was performed to assess total lesion volume. The setup parameters were as follows: repetition time (TR) = 1,000 ms, echo time (TE) = 110.5 ms, field of view (FOV) = 90 × 90 mm^2, image matrix = 336 × 446, and 0.7-mm slice thickness. Image J (Version 1.53C, Maryland, MD, United States) was used to calculate the lesion volume in each brain.

Administration of Peptides

After TBI induction, the mice were intravenously administered 10 mg/kg Tat-NR2B (YGRKKRRQRRR-KKNRNKLRRQHSY) or the scramble control peptide (Tat-sNR2B, YGRKKRRQRRR-NRRRNSKLQHKKY) once every day for 7 days. The peptides with 99% purity were synthesized by Sangon Biotech (Shanghai, China).

Transmission Electron Microscope

On the seventh day after TBI, the mice were deeply anesthetized and perfused as before. Cortical brain regions were trimmed into 1 mm wide blocks in ice-cold PBS. After fixation overnight in 4% (v/v) glutaraldehyde and then in 1% (w/v) osmium tetroxide for 1 h, the brain sections were dehydrated in a graded ethanol immersion series and embedded in resin. Brain tissue pieces were cut into 80 nm sections using an ultramicrotome (Leica, Wetzlar, Germany). The micrographs were captured using a charge-coupled device camera (HT7700, HITACHI, Hitachi, Japan).

Golgi Staining

Seven days after TBI, the mice were perfused as before, and the brains were sliced in 150 μm and then incubated in Golgi-Cox solution at room temperature for 5 days. The bleach-section staining was carried out as follows: rinsing with distilled water for 2 × 5 min, dehydrating with 50% (v/v) ethanol for 5 min, incubating with 3:1 (v/v) ratio ammonia for 10 min, incubating with 5% (w/v) sodium thiosulfate for 10 min (light forbidden), dehydrating with gradient ethanol, clearing with xylene for 2 × 10 min, and finally mounting with resinene.

Statistical Analysis

SPSS 21.0 (IBM, New York, NY, United States) and Prism 8 (Graphpad, California, CA, Untied States) were used for statistical analysis and graphing. A two-tailed t-test was used for comparisons between two groups. One-way analysis of variance (ANOVA) was used for comparisons between more than two groups. For comparisons between two independent variables, Two-way ANOVA was used. For dichotomous variables, χ^2 statistics were performed. Data are presented as mean ± SEM. $p < 0.05$ was considered statistically significant.

RESULTS

Elevated Death-Associated Protein Kinase 1 Expression in Traumatic Brain Injury Patient Plasma Correlated With Poor Prognosis

This study included 147 TBI patients, with 46 (31.3%) having an unfavorable outcome. The univariate analysis results showed age, GCS score, abnormal pupil reaction, tracheotomy, abnormal AST, hyperglycemia and the expression of DAPK1 in plasma were significantly correlated with TBI patient's outcome. The expression of DAPK1 in plasma of TBI patients with favorable outcome and unfavorable outcome were 483.99 ± 250.60 pg/ml and 731.58 ± 273.15 pg/ml, respectively. Furthermore, the multivariate analysis revealed that a high level of DAPK1 expression in plasma is an independent risk factor for an unfavorable TBI outcome (**Table 1**).

Upregulation of Death-Associated Protein Kinase 1 in Mouse Brain After Traumatic Brain Injury

Perilesional and center cortex of the TBI are defined as shown in **Figure 1A**. The diameter of center cortex is 2.0 mm and the width of perilesional cortex is 0.5 mm. The expression level of DAPK1 in the perilesional cortex was examined by Western blotting at different time points after TBI. Compared to the sham group, the expression level of DAPK1 continued to rise on days 1, 3, and 7 after TBI. However, no significant increase in expression level was observed after on day 14 compared to day 7 after TBI (**Figure 1B**); thus, we chose day 7 after TBI for the following experiments. Furthermore, the immunofluorescence results showed that DAPK1 was mainly co-labeled with neuron rather than astrocyte or microglia (**Figure 1C** and **Supplementary Figure 1**).

TABLE 1 | Characteristics of the study population.

	Favorable outcome (*n* = 101)	Unfavorable outcome (*n* = 46)	Univariate analysis (*p*-value)	Multivariate analysis (*p*-value)
Age	47 (34, 56)	55 (47, 65)	<0.01	0.044
Male	79 (78.2%)	35 (76.1%)	0.774	
GCS score	11 (7, 13)	9 (8, 10)	<0.01	<0.01
Abnormal pupil reaction	50 (49.5%)	36 (78.3%)	<0.01	0.022
Marshall CT grade >II	70 (69.3%)	34 (73.9%)	0.569	
Tracheotomy	31 (30.7%)	27 (58.7%)	<0.01	
Mechanism of injury			0.247	
Motor vehicle	56 (55.4%)	31 (67.4%)		
Fall	23 (22.8%)	8 (17.4%)		
Strike	8 (7.9%)	5 (10.9%)		
Others	14 (13.9%)	2 (4.3%)		
Laboratory biochemical examinations				
Abnormal RBC	60 (59.4%)	22 (47.8%)	0.190	
Abnormal ALT	46 (45.5%)	28 (60.9%)	0.085	
Abnormal AST	41 (40.6%)	27 (58.7%)	0.041	0.023
Hyperglycaemia	42 (41.6%)	33 (71.7%)	<0.01	<0.01
Coagulopathy	34 (33.7%)	19 (41.3%)	0.371	
DAPK1 levels in plasma	483.99 ±250.60	731.58 ±273.15	<0.01	<0.01

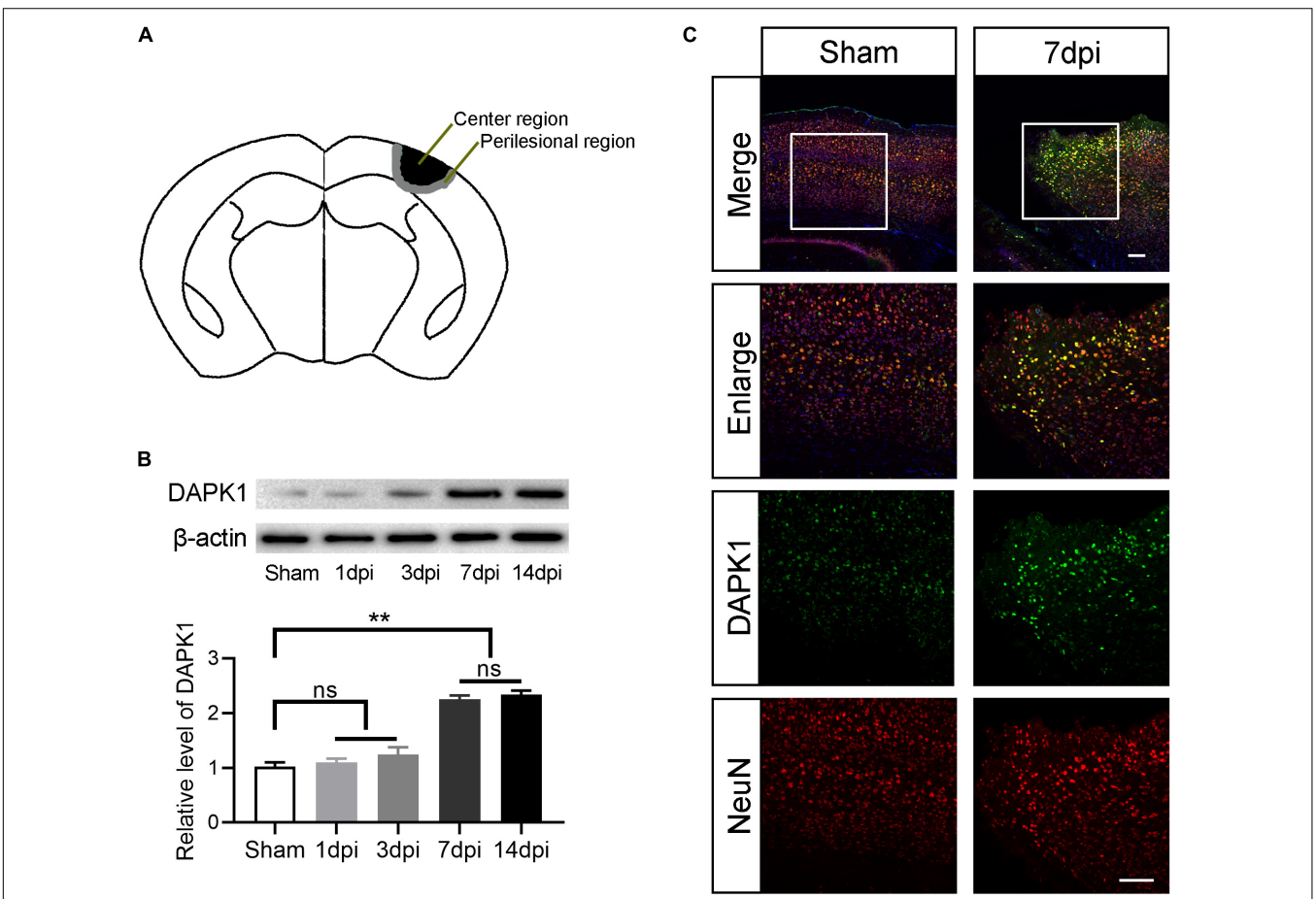

FIGURE 1 | DAPK1 is increase after TBI and mainly expressed in neurons. **(A)** Perilesional of the TBI was indicated in black and center of the TBI was represented in gray. **(B)** Western blotting analysis of the expression level of DAPK1 in the perilesional cortex at different time points after TBI. **(C)** Representative immunofluorescence images in the perilesional cortex at day 7 after TBI. Scale bar, 100 μm. $n = 6$ for each group; $^{**}p < 0.01$; ns, no significance; Values are presented as the mean ± SEM.

Loss of miR-124 in the Traumatic Brain Injury Mice Induces Death-Associated Protein Kinase 1 Upregulation by Post-transcriptional Regulation

The mechanisms underlying DAPK1 upregulation in TBI mice were then investigated. The post-transcriptional regulation of miRNAs has recently received much attention, and we speculate that the increase in DAPK1 expression may be regulated by miRNAs. Firstly, we analyzed the 3′ untranslated regions (3′UTR) of the DAPK1 gene through miRNA.org and TargetScan 7.0; and found that miR-26a, miR-26b, miR-98, miR-124, miR-141, and let-7 family were scored the highest in both predicted outputs. The expression levels of these miRNAs in the perilesional cortex of TBI mice were determined by Reverse Transcription and quantitative Polymerase Chain Reaction (RT-qPCR). The results revealed that the expression levels of miR-98, miR-124, and miR-141 were significantly changed following TBI, whereas the expression levels of the other miRNAs remained unchanged (**Figure 2A**). Only miR-124 was reduced in the plasma of TBI patients with unfavorable outcome compared to patients with favorable outcome (**Supplementary Figure 2**). The post-transcriptional regulation of DAPK1 by miR-124 was determined using a dual-luciferase reporter assay. Our findings demonstrated that miR-124 suppressed luciferase activity in WT constructs but not in mutant constructs (**Figures 2B,C**). These results imply that miR-124 regulates DAPK1 expression and that loss of miR-124 causes DAPK1 upregulation in TBI mice.

Overexpression of miR-124 or Knockdown Death-Associated Protein Kinase 1 Rescued Memory and Motor Change After Traumatic Brain Injury

To investigate the roles of DAPK1 and miR-124 in TBI mice, agomir was used to overexpress miR-124, and AAV-shDAPK1 was used to knock down DAPK1 expression (**Figure 3A**). Agomir of miR-124 was delivered to the brain *via* the intranasal route in this study. Intranasal delivery has been reported to treat neurological diseases since it could effectively cross the blood-brain barrier (Lochhead and Thorne, 2012). At different doses (0, 0.01, 0.05, 0.10, 0.50, 1.00, and 5.00 nmol) and time points (30 min or 24 h after agomir was delivered) the expression level of miR-124 in the cortex was observed by RT-qPCR. The results showed that 1.00 nmol miR-124 agomir could be delivered intranasally to the cortex and achieve a 4.0-fold peak at 30 min and a 1.9-fold peak at 24 h compared to the solvent control (**Figure 3B**), and this does was selected as an optimum dose for the following experiments.

Similarly, shDAPK1 AAV or Con AAV were injected into the prospective injured cortex to reduce the expression level of DAPK1. AAV was injected into the brain two weeks

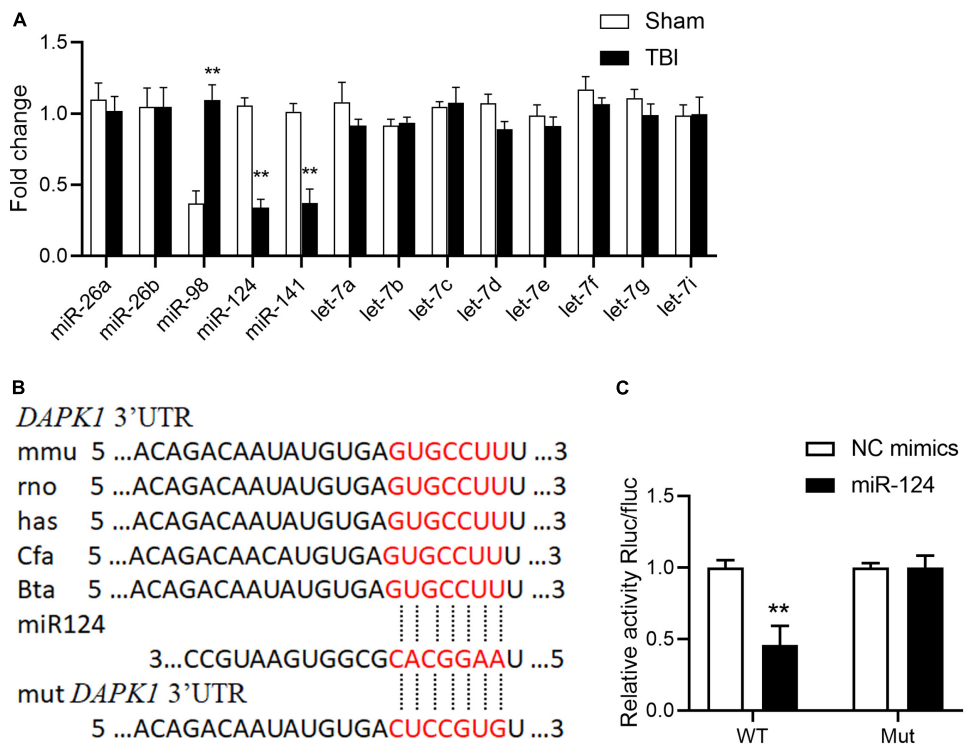

FIGURE 2 | Loss of miR-124 is responsible for DAPK1 elevation in TBI. **(A)** Alterations in predicted miRNAs that target DAPK1 in the perilesional cortex of sham and TBI mice. **(B)** The binding sites of miR-124 with DAPK1 are conserved in mammalians. **(C)** The WT and Mut of DAPK1 were subcloned into the pSI-Check2 vector and transfected into HEK 293T together with miR-124 or NC mimics. The luciferase intensity was measured. $n = 3$ for each group; $^{**}p < 0.01$; Values are presented as the mean ± SEM.

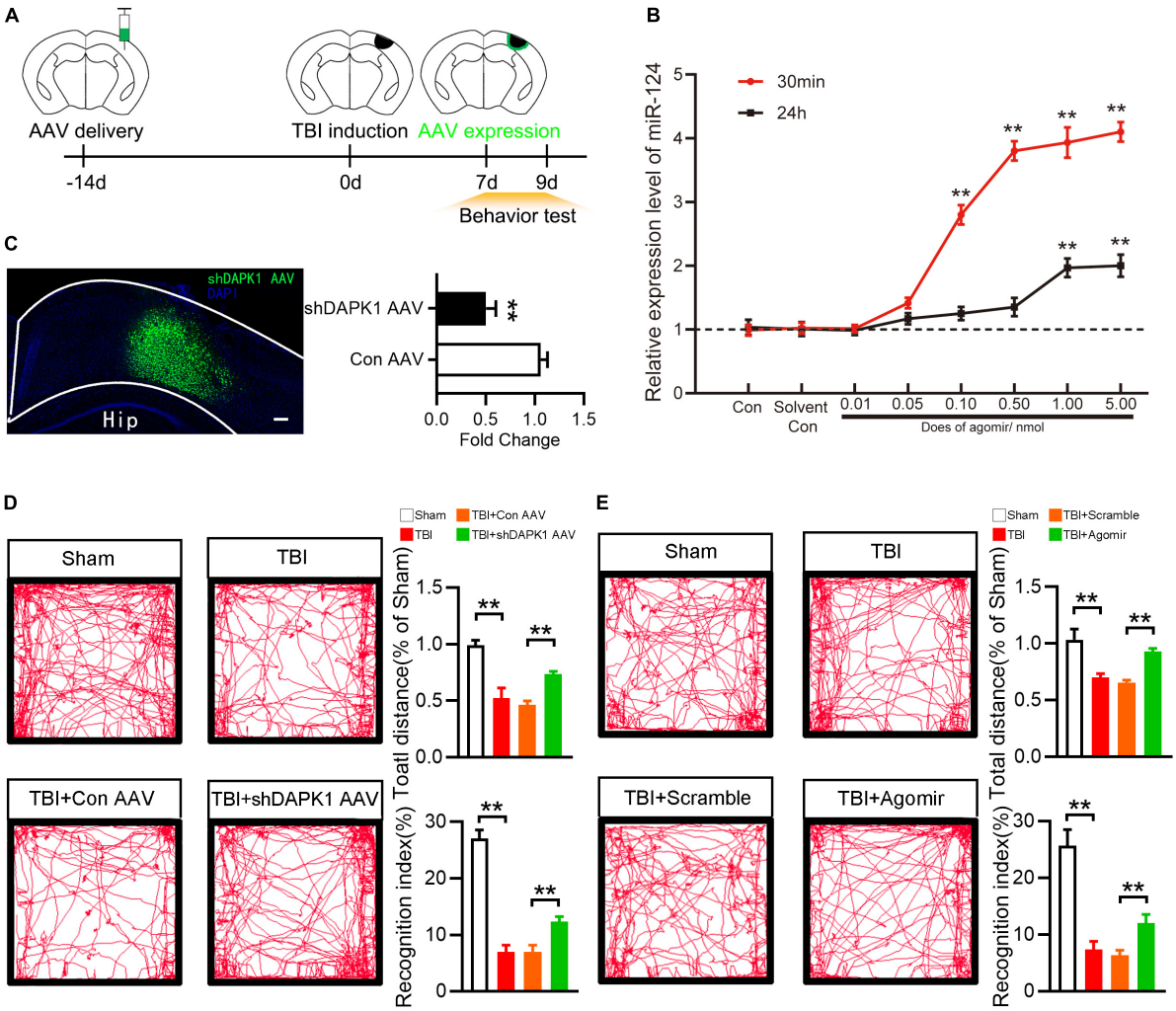

FIGURE 3 | Overexpression of miR-124 or knockdown DAPK1 rescued memory and motor change after TBI. **(A)** Experimental timeline of AAV injection, TBI induction and behavior tests. **(B)** The Expression level of miR-124 in the perilesional cortex at different time points and different dose after agomir delivery. **(C)** Fluorescence image represent expression of AAV-shDAPK1 in the cortex, and quantitative analysis of the expression level of DAPK1 after AAV-shDAPK1 or AAV-Con injection. Scale bar, 100 μm. **(D)** Representative open field activity tracks and statistical analysis of total distance traveled and recognition index after AAV-shDAPK1 or AAV-Con injection. **(E)** The representative open field activity tracks and statistical analysis of total distance traveled and recognition index after agomir or scramble injection. $n = 6$ for each group; $^{**}p < 0.01$; Values are presented as the mean ± SEM.

before TBI induction and was expressed one week later (**Figure 3C**). In this work the damaged brain areas are largely located in sensorimotor cortex. TBI could damage hippocampal-cortex circuits and produces prominent learning and memory deficits (Paterno et al., 2017). Besides, sensorimotor cortex controls whisker movements and contributes to learned, whisker-dependent, goal-directed behaviors, which are involve in learning and object recognition (Petersen, 2019). Thus, the motor and memory behaviors of TBI mice were evaluated using an open field test and a novel object recognition test, respectively. In the open field test, TBI and TBI + Con AAV mice showed impaired ambulation compared to sham mice, whereas TBI + shDAPK1 AAV mice showed rescued ambulation compared to TBI + Con AAV mice; in the object recognition test, TBI and TBI + Con AAV mice showed a lower recognition index than the sham group, while TBI + shDAPK1 AAV mice showed a higher recognition index compared to TBI + Con AAV mice (**Figure 3D**). Similarly, overexpression of miR-124 in the TBI + agomir group could alleviate TBI-induced motor and memory dysfunction (**Figure 3E**).

Overexpression of miR-124 or Knockdown Death-Associated Protein Kinase 1 Reduced Apoptosis and the Expression Level of Phosphorylated NR2B

We then studied how miR-124 and DAPK1 could influence motor and memory dysfunctions after TBI. Initially, the results in TBI mice showed that overexpression of miR-124 or knockdown

of DAPK1 significantly reduced lesion volume (**Figures 4A,B**). Furthermore, Western blotting results revealed that delivering miR-124 agomir or knocking down DAPK1 significantly reduced TBI-induced upregulation of cleaved caspase3 (**Figures 4C,D**). It has been reported that DAPK1 phosphorylates NR2B in stroke (Wang et al., 2017). Whether DAPK1 phosphorylates NR2B in TBI is unknown. As a result, we examined the p-NR2B expression levels in the various groups. The expression level of p-NR2B was significantly higher in TBI and TBI + Con AVV mice than sham mice, whereas TBI + shDAPK1 AAV mice showed a lower expression level of p-NR2B compared to TBI + Con AAV mice (**Figure 4C**). Similarly, in the TBI + agomir group, overexpression of miR-124 could mitigate TBI-induced high p-NR2B expression (**Figure 4D**). Furthermore, the Western blotting results confirmed the downregulation of DAPK1 in mice after agomir or shDAPK1 AAV injection (**Figures 4C,D**). TUNEL staining results showed that decreased apoptosis level in TBI mice after agomir or shDAPK1 AAV injection (**Figures 4E,F**).

Tat-NR2B Could Alleviate Motor and Memory Dysfunction of Traumatic Brain Injury Mice and Reduce Apoptosis and the Expression Level of Phosphorylated NR2B

In this study, a transmembrane peptide called Tat-NR2B was used to specifically inhibit the binding of DAPK1 and NR2B (Tu et al., 2010). Behavioral and pathological changes of the mice were observed, as mentioned before. The TBI mice showed rescued ambulation and higher recognition index after Tat-NR2B injection (**Figure 5A**). Lesion volume was significantly reduced after Tat-NR2B injection (**Figure 5B**). Western blotting results showed that the expression level of cleaved caspase3 was decreased considerably in TBI + Tat-NR2B group compared to TBI + Tat-sNR2B group. Furthermore, after the Tat-NR2B injection, p-NR2B/NR2B expression was significantly reduced in TBI mice, whereas DAPK1 remained unchanged (**Figure 5C**). TUNEL staining results showed decreased apoptosis level in perilesional cortex after Tat-NR2B injection (**Figure 5D**). These findings suggested that DAPK1/NR2B pathways involved neuronal apoptosis following TBI.

Tat-NR2B Didn't Affect the Number and Morphology of Synapse

In addition to participating in neuronal apoptosis, NR2B is also related to synapse structures and functions. It is unclear whether specifically blocking the bind between DAPK1 and NR2B affects the number and morphology of synapses. Golgi staining revealed no significant difference in the number of synapses after Tat-NR2B injection in TBI or sham mice (**Figure 6A**). Transmission electron microscopy results revealed that the depth and length of synapse in TBI or sham mice remained unchanged after Tat-NR2B injection (**Figure 6B**). Furthermore, Western blotting results showed that the expression level of PSD95 was unchanged after Tat-NR2B injection in TBI or sham mice (**Figure 6C**). These results showed that inhibiting the relationship between DAPK1 and NR2B did not affect the number or morphology of synapses.

DISCUSSION

This study reported that the expression level of DAPK1 is upregulated after TBI, which is positively correlated with poor prognosis in TBI patients. We demonstrated that the loss of miR-124 caused DAPK1 upregulation. Then, we found that neuronal apoptosis and NR2B phosphorylation after TBI could be alleviated by knockdown DAPK1 expression in the cortex, which further moderated motor and memory impairment in mice. Finally, neuronal apoptosis and neurological function were improvedby administering Tat-NR2B, specifically blocking DAPK1 binds to NR2B. Golgi staining, Western blotting and transmission electron microscopy showed that the number and morphology of synapse were not affected by Tat-NR2B.

DAPK1 has been shown to play a role in various neurological disorders. Current TBI research has revealed a link between Tau and DAPK1 in the chronic phase (Kim et al., 2021). However, whether and how DAPK1 regulates neuron death in the acute phase is still unknown. We have observed a significant increase of DAPK1 in TBI patients' plasma with unfavorable outcome and in the perilesional cortex of the mice, and DAPK1 is mainly expressed in the neurons. These findings suggested that DAPK1 may play an essential role in neuronal apoptosis of TBI mice.

To begin, we investigate the mechanism of DAPK1 upregulation. miRNA is a short non-coding RNA that binds to mRNA specifically for post-transcriptional regulation (Bartel, 2009). miRNA has been reported to play a role in various neurological disorders (Mehta et al., 2020). For example, In AD, stroke, and TBI, the relationship between neuroprotection and miR-124 has been reported (Wang et al., 2018; Liu et al., 2019; Yang et al., 2019). Clinical research has reported downregulation of miR-124 in the dentate gyrus of TBI patients (Schindler et al., 2020). The primary analysis of miR-124 in TBI models mainly focused on neuronal inflammation and microglia polarization (Huang et al., 2018; Yang et al., 2019). It is unknown whether miR-124 has any other downstream mechanisms in TBI. Our findings confirmed the downregulation of miR-124 in TBI mouse brain tissue and TBI patient plasma. The dual-luciferase assay showed that miR-124 could specifically bind to DAPK1, inhibit the translation of DAPK1 and reduce the expression level of DAPK1 protein. These results showed that DAPK1 is one of the downstream targets of miR-124. We infer that the effect of agomir could be blocked by knocking down DAPK1 prior to the administration of agomir, and this possibility should be addressed in further research.

Agomir is a chemically modified miRNA (Henshall et al., 2016); *in vivo* injection of agomir can significantly increase miR-124 expression and cause pathological and behavioral changes in TBI mice. Intranasal delivery may be a potential route of administration in the future because it is non-invasive and can cross the blood-brain barrier (Erdo et al., 2018). In AD mouse, intranasal administration of miR-146a agomir promotes the pathological process and cognitive impairment

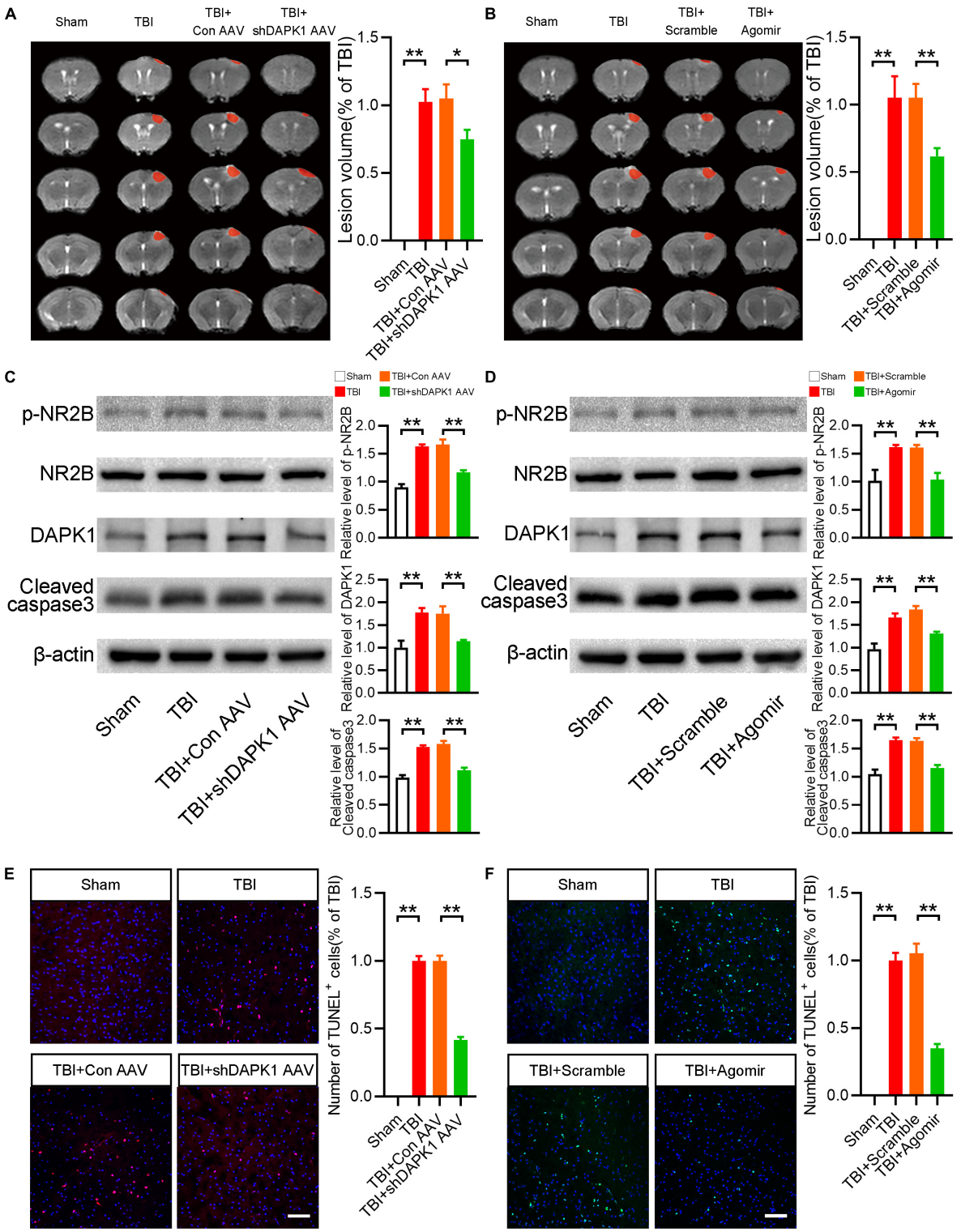

FIGURE 4 | Overexpression of miR-124 or knockdown DAPK1 reduced apoptosis and the expression level of phosphorylated NR2B. **(A)** Representative MRI and statistical analysis of lesion volume after AAV-shDAPK1 or AAV-Con injection. **(B)** Representative MRI and statistical analysis of lesion volume after agomir or scramble injection. **(C)** Western blotting analysis of the expression levels of p-NR2B/NR2B, DAPK1 and cleaved caspase3 after AAV-shDAPK1 or AAV-Con injection. **(D)** Western blotting analysis of the expression levels of p-NR2B/NR2B, DAPK1 and cleaved caspase3 after agomir or scramble injection. **(E)** Representative TUNEL staining images and quantitative analyses of TUNEL$^+$ cells after AAV-shDAPK1 or AAV-Con injection. **(F)** Representative TUNEL staining images and quantitative analyses of TUNEL$^+$ cells after agomir or scramble injection. $n = 6$ for each group; $^{**}p < 0.01$, $^{*}p < 0.05$; Values are presented as the mean ± SEM.

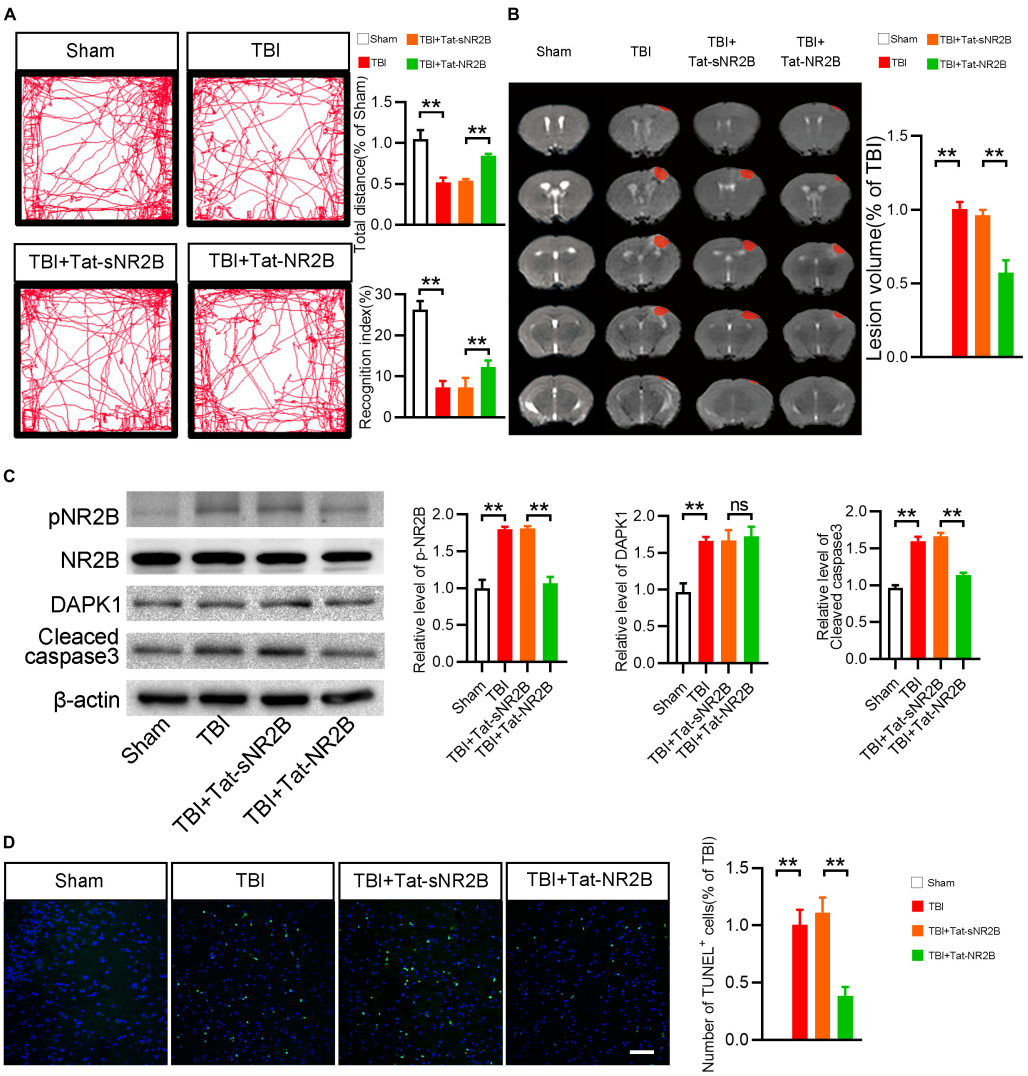

FIGURE 5 | Tat-NR2B could alleviate motor and memory dysfunction of TBI mice and reduce apoptosis and the expression level of phosphorylated NR2B. **(A)** Representative open field activity tracks and statistical analysis of total distance traveled and recognition index in each group. **(B)** Representative MRI and statistical analysis of lesion volume in different groups. **(C)** Western blotting analysis of the expression levels of p-NR2B/NR2B, DAPK1 and cleaved caspase3. **(D)** Representative TUNEL staining images and quantitative analyses of TUNEL$^+$ cells in each group. $n = 6$ for each group; $^{**}p < 0.01$; ns, no significance; Values are presented as the mean ± SEM.

(Mai et al., 2019). Furthermore, intranasal delivery of miR-219 agomir is considered a potential target for treating Theiler's Virus-Induced Demyelinating Disease (Moyano et al., 2018).

The expression of DAPK1 was reduced by injecting AAV-shDAPK1 into the cortex. Later, behavioral tests revealed that overexpression of miR-124 or knockdown of DAPK1 significantly improved TBI mice's motor and memory functions. DAPK1 is the primary key protein kinase that regulates cell death in the brain in various neurodegenerative diseases such as PD and AD (Nair et al., 2013; Kim et al., 2019). To our knowledge, this is the first study to show that DAPK1 can be used to treat TBI-induced cell death in mice.

Further pathological studies revealed that overexpression of miR-124 or knockdown of DAPK1 could reduce lesion volume and the level of apoptosis. Earlier studies have shown that the apoptotic mechanism contributes to the overall pathology of TBI, and the excessive activation of the apoptotic mechanismmay be harmful (Itoh et al., 2013; Akamatsu and Hanafy, 2020). In AD and stroke, DAPK1 is linked to apoptosis (Kim et al., 2019), and these findings show that DAPK1 alsoplays a protective role in TBI by inhibiting the apoptosis of neurons.

The interaction between NR2B and DAPK1 in stroke has been reported (Tu et al., 2010). The expression of NR2B Ser1303 was reduced after overexpression of miR-124 or knockdown of DAPK1, indicating that DAPK1 may be involved in the phosphorylation of NR2B. NR2B is a regulator of Ca^{2+} channels and is closely related to apoptosis and synapse function (Martel et al., 2009). In this study, we are the first to

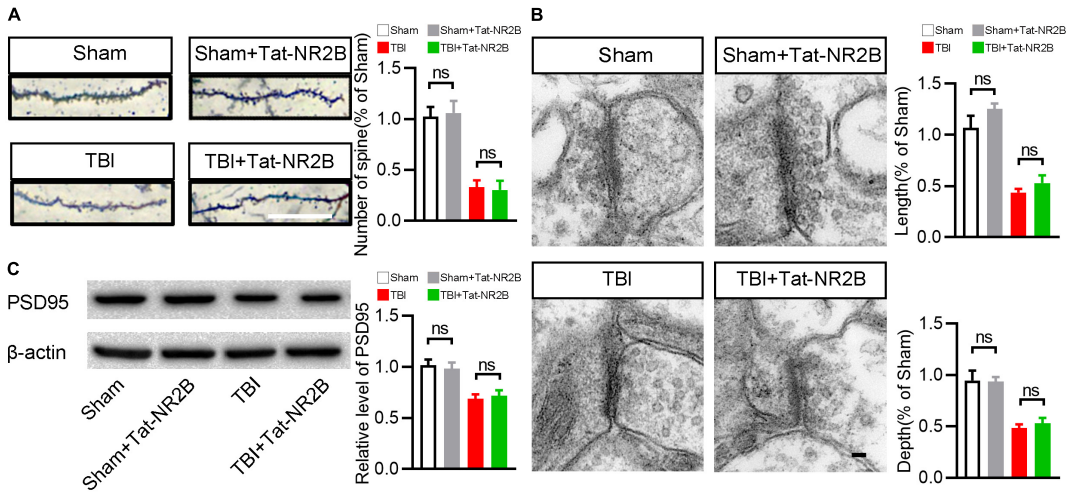

FIGURE 6 | Tat-NR2B didn't affect the number and morphology of synapse. **(A)** Representative Golgi staining images and statistical analysis of dendritic spine number. Scale bar, 10 μm. **(B)** Representative transmission electron microscope images and statistical analysis of length and depth of synapse. Scale bar, 100 nm. **(C)** Western blotting analysis of the expression levels of PSD95. *n* = 6 for each group; ns, no significance; Values are presented as the mean ± SEM.

demonstrate the relation between apoptosis and DAPK1/NR2B in TBI. Phosphorylating NR2B could directly resulting in Ca^{2+} overload; besides, the NR2B–PSD95 complex interaction with CaMK II, could indirectly resulting in excessive Ca^{2+} influx (Irie et al., 1997). Ca^{2+} overload results in excitotoxicity, endoplasmic reticulum stress and mitochondrial dysfunction, which ultimately induced expression of cleaved caspase-3 (Orrenius et al., 2003). In ischemia reperfusion, DAPK1-ERK signal contributing to neuronal apoptosis (Xiong et al., 2018); while in this study the expression level of p-ERK1/2 was not changed in TBI group nor by any of the rescue strategies (**Supplementary Figure 3**), we infer the discordance could be ascribed to various disease models and disparate detection time point.

To demonstrate the role of DAPK1 in the phosphorylation of NR2B in TBI mice, we used Tat-NR2B to block the combination of DAPK1 and NR2B specifically. TBI mice's motor and memory functions were restored after intraperitoneal injection of Tat-NR2B. TBI mice showed a significant decrease in lesion volume and level of apoptosis. These findings suggested that DAPK1 plays an essential role in apoptosis following TBI *via* NR2B. Inhibiting the binding of DAPK1 and NR2B has reduced neuronal apoptosis and restored neuronal functions.

Transcriptional activator protein (Tat) is a transmembrane peptide and has been widely used in drug delivery for diseases because of its low toxicity and high safety (Zou et al., 2013). In animal studies, Tat has been used to bind with multiple neuroprotective proteins to reduce neuron degeneration in PD and protect neurons against cerebral ischemic insults (Tu et al., 2010; Su et al., 2019). Furthermore, Tat-mediated drug delivery has been used in clinical trials and is undergoing phase II trials (Guidotti et al., 2017). Tat peptide could be a future target for the treatment of TBI dysfunction.

Aside from its role in apoptosis, NR2B also plays an essential role in mammalian synapse maturation (Frank et al., 2016); moreover, a rare variant discovered within NR2B C-Terminus in autistic patients affects NMDA receptor surface expression and synapse density (Liu et al., 2017). Furthermore, the stability of NR2B in the nucleus accumbens regulates behavioral and synaptic adaptations to chronic stress (Jiang et al., 2013). It is still unknown whether inhibiting the DAPK1/NR2B pathway affects synaptic number and morphology in TBI mice. In previous study, electrophysiological patch-clamp recording showed that uncoupling of an activated DAPK1 from the NMDA receptor complex protects against brain damage in stroke without affecting the physiological actions of the NMDA receptors (Tu et al., 2010); our results show that after the interaction between DAPK1 and NR2B was blocked by Tat-NR2B, the number and morphology of synapse did not change, which were consistent with above electrophysiological results. We speculated that the phenomenon might be related to the unchanged PSD95 level. PSD95 is a critical synaptic protein that binds to the NMDA receptors and controls synaptic transmission and plasticity (Beique et al., 2006), while overexpression of PSD-95 increases synaptic transmission and blocks long-term depression (Xu et al., 2008; Dore and Malinow, 2021). These findings imply that Tat-NR2B can only influence neuronal apoptosis without affecting number and morphology of synapse, which support the safety of blocking DAPK1/NR2B pathways in TBI treatment to some extent. However, the electrophysiological validation of these findings is lacking, further in electrophysiological patch-clamp recording experiments are awaited to validate these findings in the future.

Overall, our findings indicate that the loss of miR-124 following TBI is associated with increased DAPK1 expression. Inhibiting DAPK1 expression could reduce NR2B phosphorylation, decrease apoptosis in the perilesional cortex,

and improve memory and motor behavioral tests in TBI mice. These studies provide a target for the treatment of TBI-related dysfunction.

DATA AVAILABILITY STATEMENT

The raw data supporting the conclusions of this article will be made available by the authors, without undue reservation.

ETHICS STATEMENT

The studies involving human participants were reviewed and approved by the Ethics Committee of Tangdu Hospital, Fourth Military Medical University. The patients/participants provided their written informed consent to participate in this study. The animal study was reviewed and approved by the Ethics Committee of Tangdu Hospital, Fourth Military Medical University.

AUTHOR CONTRIBUTIONS

YQ and HL developed the hypotheses and designed the experiments. YS, WC, and QW performed the experiments and wrote the manuscript. JZ and XW contributed to the collection and analysis of patient samples. JW and SZ helped to draft the manuscript. QH and LH analyzed the data. YD and SG collected the clinical data. All authors contributed to the article and approved the submitted version.

FUNDING

This work was supported by grants from the State Key Program of National Natural Science Foundation of China (No. 81630027 to YQ) and the National Natural Science Foundation of China (No. 82101379 to HL).

SUPPLEMENTARY MATERIAL

The Supplementary Material for this article can be found online at: https://www.frontiersin.org/articles/10.3389/fncel.2022.892197/full#supplementary-material

Supplementary Figure 1 | Expression pattern of DAPK1 in the cortex; Scale bar, 100 μm.

Supplementary Figure 2 | Alterations of miR-98, miR-124, and miR-141 in the blood plasma of TBI patients.

Supplementary Figure 3 | Expression level of p-ERK/ERK in different groups.

REFERENCES

Akamatsu, Y., and Hanafy, K. A. (2020). Cell Death and Recovery in Traumatic Brain Injury. *Neurotherapeutics* 17, 446–456. doi: 10.1007/s13311-020-00840-7

Barry, G. (2014). Integrating the roles of long and small non-coding RNA in brain function and disease. *Mol. Psychiatry* 19, 410–416. doi: 10.1038/mp.2013.196

Bartel, D. P. (2009). MicroRNAs: target recognition and regulatory functions. *Cell* 136, 215–233. doi: 10.1016/j.cell.2009.01.002

Beique, J. C., Lin, D. T., Kang, M. G., Aizawa, H., Takamiya, K., and Huganir, R. L. (2006). Synapse-specific regulation of AMPA receptor function by PSD-95. *Proc. Natl. Acad. Sci. U. S. A.* 103, 19535–19540. doi: 10.1073/pnas.0608492103

Brown, C. A., Del Corsso, C., Zoidl, C., Donaldson, L. W., Spray, D. C., and Zoidl, G. (2019). Tubulin-Dependent Transport of Connexin-36 Potentiates the Size and Strength of Electrical Synapses. *Cells* 8:1146. doi: 10.3390/cells8101146

Bushati, N., and Cohen, S. M. (2007). microRNA functions. *Annu. Rev. Cell Dev. Biol.* 23, 175–205. doi: 10.1146/annurev.cellbio.23.090506.123406

Capizzi, A., Woo, J., and Verduzco-Gutierrez, M. (2020). Traumatic Brain Injury: An Overview of Epidemiology, Pathophysiology, and Medical Management. *Med. Clin. North. Am.* 104, 213–238. doi: 10.1016/j.mcna.2019.11.001

Dai, H. B., Xu, M. M., Lv, J., Ji, X. J., Zhu, S. H., Ma, R. M., et al. (2016). Mild Hypothermia Combined with Hydrogen Sulfide Treatment During Resuscitation Reduces Hippocampal Neuron Apoptosis *Via* NR2A, NR2B, and PI3K-Akt Signaling in a Rat Model of Cerebral Ischemia-Reperfusion Injury. *Mol. Neurobiol.* 53, 4865–4873. doi: 10.1007/s12035-015-9391-z

Dore, K., and Malinow, R. (2021). Elevated PSD-95 Blocks Ion-flux Independent LTD: A Potential New Role for PSD-95 in Synaptic Plasticity. *Neuroscience* 456, 43–49. doi: 10.1016/j.neuroscience.2020.02.020

Erdo, F., Bors, L. A., Farkas, D., Bajza, A., and Gizurarson, S. (2018). Evaluation of intranasal delivery route of drug administration for brain targeting. *Brain Res. Bull.* 143, 155–170. doi: 10.1016/j.brainresbull.2018.10.009

Frank, R. A., Komiyama, N. H., Ryan, T. J., Zhu, F., O'Dell, T. J., and Grant, S. G. (2016). NMDA receptors are selectively partitioned into complexes and supercomplexes during synapse maturation. *Nat. Commun.* 7:11264. doi: 10.1038/ncomms11264

Guidotti, G., Brambilla, L., and Rossi, D. (2017). Cell-Penetrating Peptides: From Basic Research to Clinics. *Trends Pharmacol. Sci.* 38, 406–424. doi: 10.1016/j.tips.2017.01.003

Hanson, L. R., Fine, J. M., Svitak, A. L., and Faltesek, K. A. (2013). Intranasal administration of CNS therapeutics to awake mice. *J. Vis. Exp.* 74 4440. doi: 10.3791/4440

Henshall, D. C., Hamer, H. M., Pasterkamp, R. J., Goldstein, D. B., Kjems, J., Prehn, J. H. M., et al. (2016). MicroRNAs in epilepsy: pathophysiology and clinical utility. *Lancet Neurol.* 15, 1368–1376. doi: 10.1016/S1474-4422(16)30246-0

Huang, S., Ge, X., Yu, J., Han, Z., Yin, Z., Li, Y., et al. (2018). Increased miR-124-3p in microglial exosomes following traumatic brain injury inhibits neuronal inflammation and contributes to neurite outgrowth *via* their transfer into neurons. *FASEB J.* 32, 512–528. doi: 10.1096/fj.201700673R

Irie, M., Hata, Y., Takeuchi, M., Ichtchenko, K., Toyoda, A., Hirao, K., et al. (1997). Binding of neuroligins to PSD-95. *Science* 277, 1511–1515. doi: 10.1126/science.277.5331.1511

Itoh, T., Imano, M., Nishida, S., Tsubaki, M., Mizuguchi, N., Hashimoto, S., et al. (2013). Increased apoptotic neuronal cell death and cognitive impairment at early phase after traumatic brain injury in aged rats. *Brain Struct. Funct.* 218, 209–220. doi: 10.1007/s00429-012-0394-5

Jiang, B., Wang, W., Wang, F., Hu, Z. L., Xiao, J. L., Yang, S., et al. (2013). The stability of NR2B in the nucleus accumbens controls behavioral and synaptic adaptations to chronic stress. *Biol. Psychiatry* 74, 145–155. doi: 10.1016/j.biopsych.2012.10.031

Jiang, J. Y., Gao, G. Y., Feng, J. F., Mao, Q., Chen, L. G., Yang, X. F., et al. (2019). Traumatic brain injury in China. *Lancet Neurol.* 18, 286–295.

Kim, B. M., You, M. H., Chen, C. H., Suh, J., Tanzi, R. E., and Ho Lee, T. (2016). Inhibition of death-associated protein kinase 1 attenuates the phosphorylation and amyloidogenic processing of amyloid precursor protein. *Hum. Mol. Genet.* 25, 2498–2513. doi: 10.1093/hmg/ddw114

Kim, N., Chen, D., Zhou, X. Z., and Lee, T. H. (2019). Death-Associated Protein Kinase 1 Phosphorylation in Neuronal Cell Death and Neurodegenerative Disease. *Int. J. Mol. Sci.* 20:3131. doi: 10.3390/ijms20133131

Kim, N., Wang, B., Koikawa, K., Nezu, Y., Qiu, C., Lee, T. H., et al. (2021). Inhibition of death-associated protein kinase 1 attenuates cis P-tau and

neurodegeneration in traumatic brain injury. *Prog. Neurobiol.* 203:102072. doi: 10.1016/j.pneurobio.2021.102072

Kothari, R. U., Brott, T., Broderick, J. P., Barsan, W. G., Sauerbeck, L. R., Zuccarello, M., et al. (1996). The ABCs of measuring intracerebral hemorrhage volumes. *Stroke* 27, 1304–1305. doi: 10.1161/01.str.27.8.1304

Leger, M., Quiedeville, A., Bouet, V., Haelewyn, B., Boulouard, M., Schumann-Bard, P., et al. (2013). Object recognition test in mice. *Nat. Protoc.* 8, 2531–2537. doi: 10.1038/nprot.2013.155

Liu, S., Zhou, L., Yuan, H., Vieira, M., Sanz-Clemente, A., Badger, J. D. II, et al. (2017). A Rare Variant Identified Within the GluN2B C-Terminus in a Patient with Autism Affects NMDA Receptor Surface Expression and Spine Density. *J. Neurosci.* 37, 4093–4102. doi: 10.1523/JNEUROSCI.0827-16.2017

Liu, X., Feng, Z., Du, L., Huang, Y., Ge, J., Deng, Y., et al. (2019). The Potential Role of MicroRNA-124 in Cerebral Ischemia Injury. *Int. J. Mol. Sci.* 21:120. doi: 10.3390/ijms21010120

Lochhead, J. J., and Thorne, R. G. (2012). Intranasal delivery of biologics to the central nervous system. *Adv. Drug Deliv. Rev.* 64, 614–628. doi: 10.1016/j.addr.2011.11.002

Lu, Y., Gong, Z., Jin, X., Zhao, P., Zhang, Y., and Wang, Z. (2020). LncRNA MALAT1 targeting miR-124-3p regulates DAPK1 expression contributes to cell apoptosis in Parkinson's Disease. *J. Cell Biochem.* [Epub ahead of print]. doi: 10.1002/jcb.29711

Mai, H., Fan, W., Wang, Y., Cai, Y., Li, X., Chen, F., et al. (2019). Intranasal Administration of miR-146a Agomir Rescued the Pathological Process and Cognitive Impairment in an AD Mouse Model. *Mol. Ther. Nucleic Acids* 18, 681–695. doi: 10.1016/j.omtn.2019.10.002

Martel, M. A., Wyllie, D. J., and Hardingham, G. E. (2009). In developing hippocampal neurons, NR2B-containing N-methyl-D-aspartate receptors (NMDARs) can mediate signaling to neuronal survival and synaptic potentiation, as well as neuronal death. *Neuroscience* 158, 334–343. doi: 10.1016/j.neuroscience.2008.01.080

Mehta, S. L., Dempsey, R. J., and Vemuganti, R. (2020). Role of circular RNAs in brain development and CNS diseases. *Prog. Neurobiol.* 186:101746. doi: 10.1016/j.pneurobio.2020.101746

Moyano, A. L., Steplowski, J., Wang, H., Son, K. N., Rapolti, D. I., Marshall, J., et al. (2018). microRNA-219 Reduces Viral Load and Pathologic Changes in Theiler's Virus-Induced Demyelinating Disease. *Mol. Ther.* 26, 730–743. doi: 10.1016/j.ymthe.2018.01.008

Nair, S., Hagberg, H., Krishnamurthy, R., Thornton, C., and Mallard, C. (2013). Death associated protein kinases: molecular structure and brain injury. *Int. J. Mol. Sci.* 14, 13858–13872. doi: 10.3390/ijms140713858

Orrenius, S., Zhivotovsky, B., and Nicotera, P. (2003). Regulation of cell death: the calcium-apoptosis link. *Nat. Rev. Mol. Cell Biol.* 4, 552–565. doi: 10.1038/nrm1150

Paterno, R., Folweiler, K. A., and Cohen, A. S. (2017). Pathophysiology and Treatment of Memory Dysfunction After Traumatic Brain Injury. *Curr. Neurol. Neurosci. Rep.* 17:52. doi: 10.1007/s11910-017-0762-x

Pei, L., Wang, S., Jin, H., Bi, L., Wei, N., Yan, H., et al. (2015). A Novel Mechanism of Spine Damages in Stroke *via* DAPK1 and Tau. *Cereb. Cortex* 25, 4559–4571. doi: 10.1093/cercor/bhv096

Petersen, C. C. H. (2019). Sensorimotor processing in the rodent barrel cortex. *Nat. Rev. Neurosci.* 20, 533–546. doi: 10.1038/s41583-019-0200-y

Schindler, C. R., Woschek, M., Vollrath, J. T., Kontradowitz, K., Lustenberger, T., Stormann, P., et al. (2020). miR-142-3p Expression Is Predictive for Severe Traumatic Brain Injury (TBI) in Trauma Patients. *Int. J. Mol. Sci.* 21:5381. doi: 10.3390/ijms21155381

Schumann, J., Alexandrovich, G. A., Biegon, A., and Yaka, R. (2008). Inhibition of NR2B phosphorylation restores alterations in NMDA receptor expression and improves functional recovery following traumatic brain injury in mice. *J. Neurotrauma* 25, 945–957. doi: 10.1089/neu.2008.0521

Shi, Y., Wu, X., Zhou, J., Cui, W., Wang, J., Hu, Q., et al. (2022). Single-Nucleus RNA Sequencing Reveals that Decorin Expression in the Amygdala Regulates Perineuronal Nets Expression and Fear Conditioning Response after Traumatic Brain Injury. *Adv. Sci.* 9:e2104112. doi: 10.1002/advs.202104112

Shu, S., Zhu, H., Tang, N., Chen, W., Li, X., Li, H., et al. (2016). Selective Degeneration of Entorhinal-CA1 Synapses in Alzheimer's Disease *via* Activation of DAPK1. *J. Neurosci.* 36, 10843–10852. doi: 10.1523/JNEUROSCI.2258-16.2016

Su, Y., Deng, M. F., Xiong, W., Xie, A. J., Guo, J., Liang, Z. H., et al. (2019). MicroRNA-26a/Death-Associated Protein Kinase 1 Signaling Induces Synucleinopathy and Dopaminergic Neuron Degeneration in Parkinson's Disease. *Biol. Psychiatry* 85, 769–781. doi: 10.1016/j.biopsych.2018.12.008

Sun, Y., Zhang, L., Chen, Y., Zhan, L., and Gao, Z. (2015). Therapeutic Targets for Cerebral Ischemia Based on the Signaling Pathways of the GluN2B C Terminus. *Stroke* 46, 2347–2353. doi: 10.1161/STROKEAHA.115.009314

Tu, W., Xu, X., Peng, L., Zhong, X., Zhang, W., Soundarapandian, M. M., et al. (2010). DAPK1 interaction with NMDA receptor NR2B subunits mediates brain damage in stroke. *Cell* 140, 222–234. doi: 10.1016/j.cell.2009.12.055

Wang, D., Jacobs, S. A., and Tsien, J. Z. (2014). Targeting the NMDA receptor subunit NR2B for treating or preventing age-related memory decline. *Expert Opin. Ther. Targets* 18, 1121–1130. doi: 10.1517/14728222.2014.941286

Wang, S., Chen, K., Yu, J., Wang, X., Li, Q., Lv, F., et al. (2020). Presynaptic Caytaxin prevents apoptosis via deactivating DAPK1 in the acute phase of cerebral ischemic stroke. *Exp. Neurol.* 329:113303. doi: 10.1016/j.expneurol.2020.113303

Wang, S., Shi, X., Li, H., Pang, P., Pei, L., Shen, H., et al. (2017). DAPK1 Signaling Pathways in Stroke: From Mechanisms to Therapies. *Mol. Neurobiol.* 54, 4716–4722. doi: 10.1007/s12035-016-0008-y

Wang, X., Liu, D., Huang, H. Z., Wang, Z. H., Hou, T. Y., Yang, X., et al. (2018). A Novel MicroRNA-124/PTPN1 Signal Pathway Mediates Synaptic and Memory Deficits in Alzheimer's Disease. *Biol. Psychiatry* 83, 395–405. doi: 10.1016/j.biopsych.2017.07.023

Xiong, W., Wu, Y., Xian, W., Song, L., Hu, L., Pan, S., et al. (2018). DAPK1-ERK signal mediates oxygen glucose deprivation reperfusion induced apoptosis in mouse N2a cells. *J. Neurol. Sci.* 387, 210–219. doi: 10.1016/j.jns.2018.01.003

Xu, L. Z., Li, B. Q., and Jia, J. P. (2019). DAPK1: A Novel Pathology and Treatment Target for Alzheimer's Disease. *Mol. Neurobiol.* 56, 2838–2844. doi: 10.1007/s12035-018-1242-2

Xu, W., Schluter, O. M., Steiner, P., Czervionke, B. L., Sabatini, B., and Malenka, R. C. (2008). Molecular dissociation of the role of PSD-95 in regulating synaptic strength and LTD. *Neuron* 57, 248–262. doi: 10.1016/j.neuron.2007.11.027

Yang, J., Zhang, X., Chen, X., Wang, L., and Yang, G. (2017). Exosome Mediated Delivery of miR-124 Promotes Neurogenesis after Ischemia. *Mol. Ther. Nucleic Acids* 7, 278–287. doi: 10.1016/j.omtn.2017.04.010

Yang, Y., Ye, Y., Kong, C., Su, X., Zhang, X., Bai, W., et al. (2019). MiR-124 Enriched Exosomes Promoted the M2 Polarization of Microglia and Enhanced Hippocampus Neurogenesis After Traumatic Brain Injury by Inhibiting TLR4 Pathway. *Neurochem. Res.* 44, 811–828. doi: 10.1007/s11064-018-02714-z

Zou, L. L., Ma, J. L., Wang, T., Yang, T. B., and Liu, C. B. (2013). Cell-penetrating Peptide-mediated therapeutic molecule delivery into the central nervous system. *Curr. Neuropharmacol.* 11, 197–208.

Conflict of Interest: The authors declare that the research was conducted in the absence of any commercial or financial relationships that could be construed as a potential conflict of interest.

Publisher's Note: All claims expressed in this article are solely those of the authors and do not necessarily represent those of their affiliated organizations, or those of the publisher, the editors and the reviewers. Any product that may be evaluated in this article, or claim that may be made by its manufacturer, is not guaranteed or endorsed by the publisher.

Copyright © 2022 Shi, Cui, Wang, Zhou, Wu, Wang, Zhang, Hu, Han, Du, Ge, Liu and Qu. This is an open-access article distributed under the terms of the Creative Commons Attribution License (CC BY). The use, distribution or reproduction in other forums is permitted, provided the original author(s) and the copyright owner(s) are credited and that the original publication in this journal is cited, in accordance with accepted academic practice. No use, distribution or reproduction is permitted which does not comply with these terms.

frontiers | Frontiers in Cellular Neuroscience

ORIGINAL RESEARCH
published: 04 July 2022
doi: 10.3389/fncel.2022.905724

Nicotine Facilitates Facial Stimulation-Evoked Mossy Fiber-Granule Cell Long-Term Potentiation *in vivo* in Mice

Li-Xin Cao[1†], Yan-Hua Bing[1†], Yin-Hua Xu[2†], Guang-Jian Zhang[3], Chun-Ping Chu[4], Lan Hong[1] and De-Lai Qiu[4*]*

[1] Department of Physiology and Pathophysiology, College of Medicine, Yanbian University, Yanji, China, [2] Department of Neurology, Affiliated Hospital of Yanbian University, Yanji, China, [3] Department of Pain, Affiliated Hospital of Yanbian University, Yanji, China, [4] Department of Physiology, College of Basic Medicine, Jilin Medical University, Jilin City, China

OPEN ACCESS

Edited by:
Haruyuki Kamiya,
Hokkaido University, Japan

Reviewed by:
Hiroki Toyoda,
Osaka University, Japan
Ranji Cui,
Second Affiliated Hospital of Jilin University, China

***Correspondence:**
Lan Hong
honglan@ybu.edu.cn
De-Lai Qiu
dlqiu@jlmu.edu.cn;
dlqiu@ybu.edu.cn

[†] These authors have contributed equally to this work

Specialty section:
This article was submitted to Cellular Neurophysiology, a section of the journal Frontiers in Cellular Neuroscience

Received: 27 March 2022
Accepted: 14 June 2022
Published: 04 July 2022

Citation:
Cao L-X, Bing Y-H, Xu Y-H, Zhang G-J, Chu C-P, Hong L and Qiu D-L (2022) Nicotine Facilitates Facial Stimulation-Evoked Mossy Fiber-Granule Cell Long-Term Potentiation in vivo in Mice. Front. Cell. Neurosci. 16:905724. doi: 10.3389/fncel.2022.905724

Nicotine is a psychoactive component of tobacco that plays critical roles in the regulation of neuronal circuit function and neuroplasticity and contributes to the improvement of working memory performance and motor learning function *via* nicotinic acetylcholine receptors (nAChRs). Under *in vivo* conditions, nicotine enhances facial stimulation-evoked mossy fiber-granule cell (MF-GrC) synaptic transmission, which suggests that nicotine regulates MF-GrC synaptic plasticity in the mouse cerebellar cortex. In this study, we investigated the effects of nicotine on facial stimulation-induced long-term potentiation (LTP) of MF-GrC synaptic transmission in urethane-anesthetized mice. Our results showed that facial stimulation at 20 Hz induced an MF-GrC LTP in the mouse cerebellar granular layer that was significantly enhanced by the application of nicotine (1 μM). Blockade of α4β2 nAChRs, but not α7 nAChRs, during delivery of 20 Hz facial stimulation prevented the nicotine-induced facilitation of MF-GrC LTP. Notably, the facial stimulation-induced MF-GrC LTP was abolished by an N-methyl-D-aspartate (NMDA) receptor antagonist, but it was restored by additional application of nicotine during delivery of 20 Hz facial stimulation. Furthermore, antagonism of α4β2 nAChRs, but not α7 nAChRs, during delivery of 20 Hz facial stimulation prevented nicotine-induced MF-GrC LTP. Moreover, inhibition of nitric oxide synthase (NOS) abolished the facial stimulation-induced MF-GrC LTP, as well as the effect of nicotine on it. Our results indicated that 20 Hz facial stimulation induced MF-GrC LTP *via* an NMDA receptor/nitric oxide (NO) cascade, but MF-GrC LTP was enhanced by nicotine through the α4β2 AChR/NO signaling pathway. These results suggest that nicotine-induced facilitation of MF-GrC LTP may play a critical role in the improvement of working memory performance and motor learning function.

Keywords: cerebellar, facial stimulation, mossy fiber-granular cell, long-term potentiation (LTP), nicotine, neuropharmacology, electrophysiology

INTRODUCTION

Nicotine is the main psychoactive component of tobacco and plays an important role in the modulation of brain physiology *via* nicotinic acetylcholine receptors (nAChRs) (Dome et al., 2010). nAChRs are a family of ligand-gated ionic channels, which consist of α2–10 and β2–4 subunits (Gotti et al., 2006; Dani and Bertrand, 2007; Romanelli et al., 2007). A large number of studies have demonstrated that nicotine modulates neuroplasticity, including long-term depression (LTD) and long-term potentiation (LTP), which improves memory and motor learning function *via* nAChRs (Hahn et al., 2002; Kumari et al., 2003; Gonzalez et al., 2006; Heishman et al., 2010; Holschneider et al., 2011, 2013; Hijioka et al., 2012; Grundey et al., 2015; Grundey et al., 2018b). Administration of nicotine produces a focusing effect with an increase in focal LTP-like plasticity *via* a calcium-dependent mechanism (Kuo et al., 2007; Grundey et al., 2018a). Nicotine administration restores paired-associative stimulation-induced LTP-like excitatory neuroplasticity and improves the serial reaction time task performance in deprived smokers (Grundey et al., 2018b). Moreover, chronic administration of low-dose nicotine facilitates recovery and synaptic change after focal ischemia in rats (Gonzalez et al., 2006). Activation of α7 nAChRs or inhibition of cholinesterase improves motor behavior and sensorimotor performance in intracerebral hemorrhage (Hijioka et al., 2012) and ataxic model animals (Wecker et al., 2013). Previous studies have suggested that nicotine can improve motor behavior through modulation of neuronal circuitry function and long-term synaptic plasticity (Grundey et al., 2018b; Alhowail, 2021).

The cerebellar granule cells (GrCs) are assumed to act as a high-pass spatiotemporal filter; these cells receive information from mossy fibers (MFs) and convey them to Purkinje cells (PCs) *via* parallel fibers (D'Angelo and De Zeeuw, 2009; Solinas et al., 2010; Bing et al., 2015). The sensory information coming from MFs induces excitation of GrCs and long-term synaptic plasticity in the cerebellar granular layer (Roggeri et al., 2008; D'Angelo and De Zeeuw, 2009). We recently found that 20 Hz facial stimulation produced LTP of MF-GrC synaptic transmission through an NMDA receptor/nitric oxide (NO) signaling pathway (Lu et al., 2022). The sensory stimulation-induced long-term synaptic plasticity of MF-GrC synaptic transmission is assumed to play an important function during cerebellar adaptation to native MF excitatory inputs and motor learning behavior in living animals (Roggeri et al., 2008; D'Angelo and De Zeeuw, 2009; Lu et al., 2022). In addition, activation of nAChRs facilitates glutamate release at the MF-GrC synapses in cerebellar slices (De Filippi et al., 2001; Reno et al., 2004) and enhances facial stimulation-evoked MF-GrC synaptic transmission *via* activation of α7 and α4β2 nAChRs, which suggests that nicotine modulates sensory information-evoked MF-GrC long-term plasticity *via* nAChRs *in vivo* in mice (Xu et al., 2019). However, the effect of nicotine on MF-GrC long-term synaptic plasticity under *in vivo* conditions is unknown. In this study, we investigated the mechanism of nicotine-modulated facial stimulation-evoked MF-GrC LTP in urethane-anesthetized mice by an extracellular recording technique and pharmacological methods.

MATERIALS AND METHODS

Anesthesia and Surgical Procedures

Anesthesia and surgical procedures have been described previously (Chu et al., 2011). A total of 88 (6- to 8-week-old) male HA/ICR mice were used in this study. The experimental procedures were approved by the Animal Care and Use Committee of Yanbian University and were in accordance with the animal welfare guidelines of the U.S. National Institutes of Health, and the Animal Research: Reporting *In Vivo* Experiments (ARRIVE[1]). The permit number is SYXK (Ji) 2011-006. All mice were housed under a 12-h light/12-h dark cycle with free access to food and water in a colony room under constant temperature (23 ± 1°C) and humidity (50 ± 5%). The mice were anesthetized with urethane (1.3 g/kg body weight, i.p.) and were tracheotomized for avoiding respiratory obstruction. The animals were fixed on a custom-made stereotaxic frame, and soft tissue was stripped to gain access to the dorsal portion of the occipital bone. A watertight recording chamber was created, and a 1- to 1.5-mm craniotomy was drilled to expose the cerebellar surface corresponding to Crus II. The brain surface was constantly superfused with oxygenated artificial cerebrospinal fluid (ACSF: 125 mM NaCl, 3 mM KCl, 1 mM $MgSO_4$, 2 mM $CaCl_2$, 1 mM NaH_2PO_4, 25 mM $NaHCO_3$, and 10 mM d-glucose) with a peristaltic pump (Gilson Minipulse 3; Villiers, Le Bel, France) at 0.5 ml/min. Rectal temperature was monitored and maintained at 37.0 ± 0.2°C using body temperature equipment.

Electrophysiological Recordings and Facial Stimulation

Local field potential recordings from the cerebellar granular layer were performed with an Axopatch 200B amplifier (Molecular Devices, Foster City, CA, United States) under current clamp conditions (I = 0) and acquired through a Digidata 1440 series analog-to-digital interface through a personal computer using Clampex 10.4 software. Recording electrodes were made with a puller (PB-10; Narishige, Tokyo, Japan) from thick-wall borosilicate glass, which were filled with ACSF and with resistances of 3–5 MΩ.

Facial stimulation was performed by air-puff (10 ms, 60 psi) of the ipsilateral whisker pad through a 12-gauge stainless steel tube connected with a pressurized injection system (Picospritzer® III; Parker Hannifin Co., Pine Brook, NJ, United States). The air-puff stimulations were controlled by a personal computer and were synchronized with the electrophysiological recordings and delivered at 0.05 Hz *via* a Master 8 controller (A.M.P.I., Jerusalem, Israel) and Clampex 10.3 software. For obtaining MF-GC synaptic transmission, picrotoxin (100 μM) was added to ACSF during all recordings to prevent $GABA_A$ receptor-mediated inhibitory component. In the presence of picrotoxin (100 μM), air-puff (10 ms, 60 psi) of the ipsilateral whisker

[1]https://arriveguidelines.org

pad evoked a negative component in granular layer of mouse cerebellar cortical folium Crus II (**Figure 1A**). According to our previous studies (Ma et al., 2019; Li et al., 2021; Lu et al., 2022), the facial stimulation-evoked response is identified as MF-GC synaptic transmission in the absence of GABAergic inhibitory inputs. For induction of long-term MF-GrC synaptic plasticity, 20 Hz air-puff stimulation (240 pulses) was delivered 10 min after facial stimulation-evoked response traces became stable (Lu et al., 2022).

Chemicals

The reagents included picrotoxin, D-(-)-2-amino-5-phosphonopentanoic acid (D-APV), NG-Nitro-L-arginine (L-NNA), nitric oxide synthase (NOS) inhibitor, nicotine, methyllycaconitine citrate hydrate (MLA), and dihydro-β-erythroidine hydrobromide (DβEH) bought from Sigma-Aldrich (Shanghai, China). All these chemicals were dissolved in solution and kept in frozen aliquots. For experiments with NOS inhibitor, L-NNA, cerebellar surface was superfused with 200 μM L-NNA for 1 h before recordings were began. The drugs were dissolved in ACSF and applied directly onto the cerebellar surface by a peristaltic pump (0.5 ml/min).

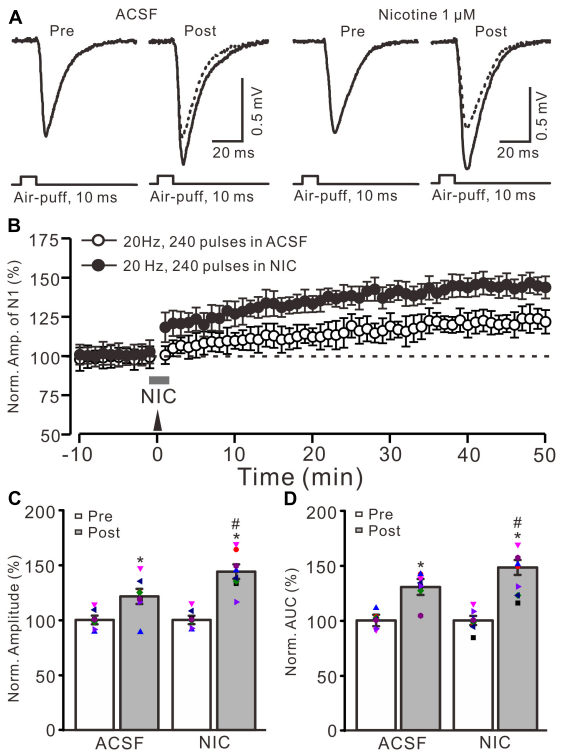

FIGURE 1 | Nicotine enhanced the facial stimulation-induced LTP of MF-GrC synaptic transmission in the mouse cerebellum. **(A)** Representative extracellular recording traces illustrating facial stimulation (10 ms, 60 psi)-evoked MF-GC synaptic transmission before and after delivery of 20 Hz (240 pulses) stimulation in the absence (ACSF; open circle) and the presence (filled circle) of nicotine (NIC; 1 μM). **(B)** Summary of data showing the time course of normalized amplitude of the response before and after delivery of 20 Hz facial stimulation (arrow head) in the absence (ACSF; open circle) and the presence (filled circle) of nicotine (gray bar; NIC; 1 μM). **(C)** Bar graph showing the normalized amplitude before (pre) and after (post) delivery of 20 Hz stimulation in treatment of ACSF and nicotine (NIC; 1 μM). **(D)** Pooled data showing the normalized area under the curve (AUC) of the response before (pre) and after (post) delivery of 20 Hz stimulation in treatment of ACSF and nicotine (NIC). Note that facial stimulation at 20 Hz induced LTP of MF-GC synaptic transmission, which was enhanced by application of nicotine in the mouse cerebellar cortex. Data points are mean ± S.E.M. $n = 8$ recordings from eight mice in each group. $^{*}P < 0.05$ vs. post; $^{\#}P < 0.05$ vs. ACSF.

Statistical Analysis

The electrophysiological data were analyzed using Clampfit 10.6 software (Molecular Devices, Foster City, United States). The amplitude of the evoked field potential responses was maintained constant for an individual experiment before and after delivery of 20 Hz facial stimulation. Values are expressed as mean ± S.E.M. One-way ANOVA, followed by Tukey's *post hoc* test (SPSS software; Chicago, IL, United States), was used to determine the level of statistical significance among groups of data. *P*-values below 0.05 were considered statistically significant.

RESULTS

Cerebellar Surface Perfusion of Nicotine Enhanced the Facial Stimulation-Induced Mossy Fiber-Granule Cell Long-Term Potentiation *in vivo* in Mice

Blockade of $GABA_A$ receptor-mediated inhibition by picrotoxin (100 μM) and facial stimulation with air-puff on the ipsilateral whisker pad induced a negative response in the cerebellar granular layer, which was identified as MF-GrC excitatory synaptic transmission (Ma et al., 2019; Li et al., 2021; Lu et al., 2022). Consistent with our previous study (Lu et al., 2022), facial stimulation at 20 Hz (240 pulse) induced LTP of MF-GrC synaptic transmission. As shown in **Figure 1**, delivery of 20 Hz facial stimulation induced a significant increase in the amplitude of response under control conditions for over 50 min (**Figures 1A,B**). During 40–50 min after 20 Hz facial stimulation, the normalized amplitude of response was 121.4 ± 6.9% of baseline ($F = 32.8$, $P < 0.001$; $n = 8$ experiments; **Figure 1C**), and the normalized area under the curve (AUC) of response was 130.5 ± 8.3% of baseline ($F = 41.6$, $P < 0.001$; $n = 8$ experiments; **Figure 1**). These results indicated that facial stimulation at 20 Hz induced MF-GrC LTP in the mouse cerebellar cortical Crus II.

Cerebellar surface perfusion of low-concentration nicotine (NIC; 1 μM) for 150 s did not change the amplitude of the facial stimulation-evoked response; the normalized amplitude of response was 100.2 ± 1.8% of baseline (ACSF; $F = 0.06$, $P = 0.65$). In the presence of nicotine, delivery of 20 Hz facial stimulation produced a stronger MF-GrC LTP than that under the control condition (**Figures 1A,B**). The normalized amplitude during 40–50 min after 1 Hz facial stimulation was 143.9 ± 6.6% of baseline ($F = 56.1$, $P < 0.001$; $n = 8$ experiments), which was significantly higher than that of the control group (121.4 ± 6.9% of baseline; $F = 8.3$, $P = 0.016$; $n = 8$ experiments; **Figure 1C**), and the

normalized AUC of response was increased to 148.3 ± 7.5% of baseline (F = 48.5, P < 0.001; n = 8 experiments), which was significantly higher than that of the control group (ACSF; 130.5 ± 8.3% of baseline; F = 7.4, P = 0.021; n = 8 experiments; **Figure 1D**). These results indicate that application of nicotine facilitates the facial stimulation-induced MF-GrC LTP, which suggests that nicotine enhances MF-GrC LTP *via* activation of nAChRs *in vivo* in mice.

Nicotine Enhanced the Facial Stimulation-Induced Mossy Fiber-Granule Cell Long-Term Potentiation *via* α4β2 Nicotinic Acetylcholine Receptors, but Not α7 Nicotinic Acetylcholine Receptors

Because α7 nAChRs are expressed in presynaptic regions of the cerebellar granular layer and activation of these nAChRs enhances glutamate release at the MF-GrC synapses in rat cerebellar slices (De Filippi et al., 2001), we further employed a selective α7 nAChR antagonist, MLA (1 μM), to examine whether the nicotine-induced enhancement of MF-GrC LTP occurs through α7 nAChRs. To block α7 nAChRs, MLA was perfused to the cerebellar surface 150 s before the application of nicotine (**Figure 2B**). In the presence of a mixture of MLA (1 μM) and nicotine (1 μM), delivery of 20 Hz facial stimulation still induced a stronger MF-GrC LTP than in the control group (ACSF; **Figure 2A**), which expressed a strong time-dependent increase in amplitude of response (**Figure 2B**). During 40–50 min after 20 Hz facial stimulation, the normalized amplitude of response was 141.8 ± 6.4% of baseline (100.0 ± 4.7%; F = 62.3, P < 0.001; n = 7 experiments), which was significantly higher than that of the control group (121.4 ± 7.1% of baseline; F = 8.2, P = 0.013; n = 7 experiments; **Figure 2C**) but similar to that of nicotine alone (143.9 ± 6.6% of baseline; F = 0.21, P = 0.55; n = 7 experiments). The normalized AUC of response was 146.5 ± 6.8% of baseline, which was also significantly higher than that of the control group (130.4 ± 7.0% of baseline; F = 7.1, P = 0.017; n = 7 experiments; **Figure 2C**) but similar to that of nicotine alone (148.3 ± 7.5% of baseline; F = 0.18, P = 0.47; n = 7 experiments). These results indicate that blockade of α7 nAChRs failed to prevent the nicotine-induced enhancement of MF-GrC LTP, which suggests that nicotine enhancement of MF-GrC LTP is not dependent on α7 nAChRs.

In the cerebellar cortex, α4β2 nAChRs are present in the somas of GrCs and mediate somatic inward currents *in vitro* in rats (De Filippi et al., 2001). Therefore, we employed a selective α4β2 nAChR antagonist, DHβE (1 μM), to observe whether the nicotine-induced facilitation of MF-GrC LTP occurs *via* activation of α4β2 nAChRs. To block α4β2 nAChRs, DHβE (1 μM) was applied to the cerebellar surface 150 s before application of nicotine (**Figure 3B**). In the presence of a mixture of DHβE (1 μM) and nicotine (1 μM), enhancement of MG-GrC LTP was not induced by delivery of 20 Hz (240 pulses) facial stimulation (**Figures 3A,B**). In the presence of a mixture of DHβE and nicotine, the normalized amplitude of response

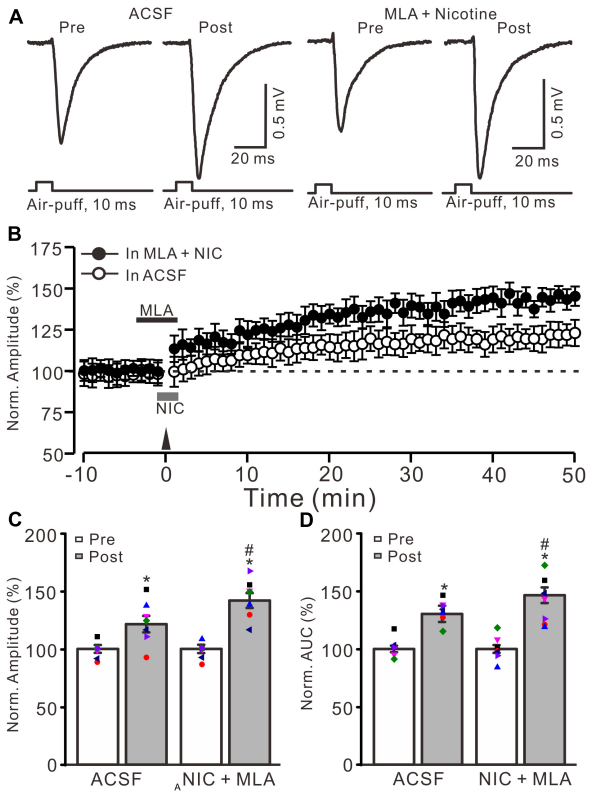

FIGURE 2 | α7 nicotinic acetylcholine receptors antagonist failed to prevent the nicotine-induced enhancement of MF-GrC LTP. **(A)** Representative extracellular recording traces illustrating facial stimulation (10 ms, 60 psi)-evoked responses before and after delivery of 20 Hz (240 pulses) stimulation in the absence (ACSF) and the presence a mixture of α7 nAChR antagonist, MLA (1 μM), and nicotine (NIC; 1 μM). **(B)** Summary of data showing the time course of normalized amplitude of the response before and after delivery of 20 Hz facial stimulation (arrow head) in the absence (ACSF; open circle) and presence (filled circle) a mixture of MLA (1 μM) and nicotine (NIC; gray bar). **(C)** Bar graph showing normalized amplitude before (pre) and after (post) delivery of 20 Hz stimulation in treatment of ACSF and a mixture of MLA and nicotine (NIC). **(D)** Pooled data showing normalized AUC of the response before (pre) and after (post) delivery of 20 Hz stimulation in treatment of ACSF and a mixture of MLA and nicotine (NIC). Note that nicotine enhanced the facial stimulation induced MF-GrC LTP in the presence of α7-nAChR antagonist. Data points are mean ± S.E.M. n = 7 recordings from 7 mice in each group. *P < 0.05 vs. post; #P < 0.05 vs. ACSF.

was 124.1 ± 7.7% of baseline during 40–50 min after 20 Hz facial stimulation, which was similar to that of the control group (121.4 ± 7.2% of baseline; F = 0.15, P = 0.76; n = 8 experiments; **Figure 3C**), but significantly lower than that of nicotine alone (143.9 ± 6.6% of baseline; F = 8.37, P = 0.013; n = 8 experiments; not shown). In addition, the normalized AUC of response was 131.2 ± 7.1% of baseline during 40–50 min after 20 Hz facial stimulation, which was similar to that of control (ACSF: 130.4 ± 7.7% of baseline; F = 0.27, P = 0.61; n = 8 experiments; **Figure 3D**), but significantly lower than that of nicotine alone (148.3 ± 7.5% of baseline; F = 9.85, P = 0.009; n = 8 experiments). These results indicated that blockade of α4β2 nAChRs abolished the nicotine-induced facilitation of facial

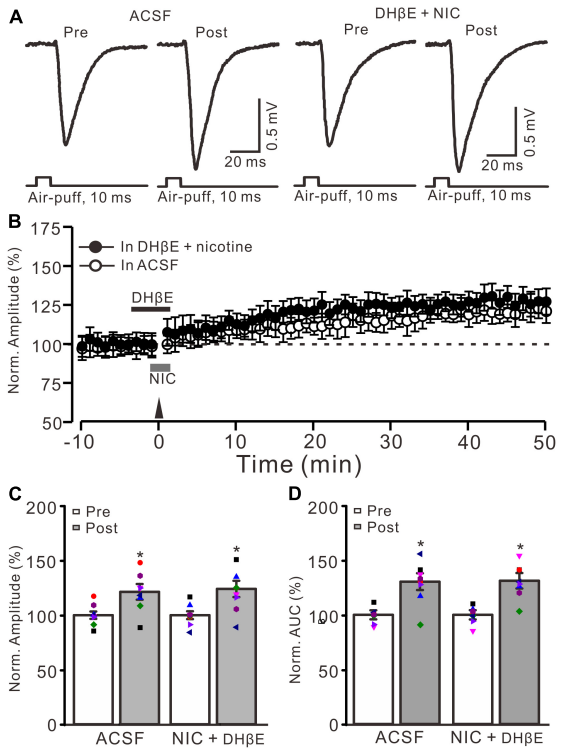

FIGURE 3 | Nicotine-induced enhancement of MF-GrC LTP was abolished by α4β2 antagonist. **(A)** Representative extracellular recording traces illustrating facial stimulation (10 ms, 60 psi)-evoked MF-GrC synaptic response in a mouse cerebellar cortex before and after delivering 20 Hz (240 pulses) stimulation in the absence (ACSF) and the presence of a mixture of α4β2-nAChR blocker, DHβE (1 μM), and nicotine (NIC; 1 μM). **(B)** Summary of data showing the time course of normalized amplitude of the response before and after delivery of 20 Hz facial stimulation (arrow head) in the absence (ACSF, open circle) and the presence of a mixture of DhβE (black bar) and nicotine (NIC; gray bar) (filled circle). **(C)** Bar graph showing normalized amplitude of the response before (pre) and after (post) delivery of 20 Hz facial stimulation in the absence and the presence of a mixture of DHβE and nicotine. **(D)** Pooled data showing normalized AUC of the response before (pre) and after (post) delivery of 20 Hz facial stimulation in the absence and the presence of a mixture of DHβE and nicotine. Note that nicotine failed to enhance the facial stimulation-evoked MF-GrC LTP in the presence of α4β2 nAChR antagonist. Data points are mean ± S.E.M. $n = 8$ recordings from 8 mice in each group. *$P < 0.05$ vs. post.

stimulation-induced MF-GrC LTP, which suggests that nicotine enhances MF-GrC LTP *via* activation of α4β2 nAChRs.

N-Methyl-D-Aspartate Receptor Blockade Abolished Mossy Fiber-Granule Cell Long-Term Potentiation, but Nicotine Restored Mossy Fiber-Granule Cell Long-Term Potentiation *via* Activation of α4β2 Nicotinic Acetylcholine Receptors

Our previous study showed that 20 Hz facial stimulation-induced MF-GrC LTP was dependent on the NMDA receptor. We further investigated whether nicotine could trigger MF-GrC LTP in the presence of the NMDA receptor antagonist. When the NMDA receptor was blocked with D-APV (250 μM), facial stimulation at 20 Hz could not induce MF-GrC LTP (**Figures 4A,B**). The normalized amplitude was 101.5 ± 4.2% of baseline during 45–50 min after 20 Hz facial stimulation ($F = 0.71$, $P = 0.55$; $n = 7$ experiments; **Figure 4C**), and the normalized AUC of response was 102.7 ± 5.3% of baseline during 40–50 min after 20 Hz facial stimulation ($F = 0.75$, $P = 0.68$; $n = 7$ experiments; **Figure 4D**). Notably, MF-GrC LTP was restored when co-application of D-APV and nicotine (1 μM) occurred during delivery of 20 Hz facial stimulation (**Figure 4A**). In the presence of a mixture of D-APV and nicotine, the normalized amplitude was 117.8 ± 6.4% of baseline during 45–50 min after 20 Hz facial stimulation ($F = 45.4$, $P < 0.001$; $n = 7$ experiments; **Figure 4C**), which was significantly higher than that of D-APV alone ($F = 43.1$, $P < 0.001$ versus D-APV; $n = 7$ experiments; **Figure 4C**). The normalized AUC was 123.7 ± 7.7% of baseline during 40–50 min after 20 Hz facial stimulation delivery in the presence of D-APV and nicotine ($F = 52$, $P < 0.001$ versus pre; $n = 7$ experiments; **Figure 4D**), which was significantly higher than that of D-APV alone ($F = 48.3$, $P < 0.001$ versus D-APV; $n = 7$ experiments; **Figure 4D**). However, upon blockade of α4β2 nAChRs, nicotine failed to trigger MF-GrC LTP. In the presence of a mixture of D-APV (250 μM), DhβE (1 μM), and nicotine (1 μM), the normalized amplitude was 103.4 ± 5.8% of baseline during 45–50 min after 20 Hz facial stimulation ($F = 0.13$, $P = 0.51$; $n = 7$ experiments; **Figure 4E**), and the normalized AUC was 103.6 ± 6.2% of baseline during 40–50 min after delivery of 20 Hz facial stimulation in the presence of D-APV and nicotine ($F = 0.26$, $P = 0.62$ versus pre; $n = 7$ experiments; **Figure 4F**). Moreover, blockade of α7 nAChRs did not prevent the nicotine-triggered MF-GrC LTP. In the presence of a mixture of D-APV (250 μM), MLA (1 μM), and nicotine (1 μM), the normalized amplitude was 117.6 ± 6.5% of baseline during 45–50 min after 20 Hz facial stimulation ($F = 43.1$, $P < 0.001$; $n = 7$ experiments; **Figure 4E**), and the normalized AUC was 126.3 ± 6.7% of baseline during 40–50 min after delivery of 20 Hz facial stimulation in the presence of D-APV and nicotine ($F = 50.4$, $P < 0.001$ versus pre; $n = 7$ experiments; **Figure 4F**). These results indicate that blockade of NMDA receptors abolished MF-GrC LTP, which was restored by nicotine through activation of α4β2 nAChRs.

Since facial stimulation at 20 Hz induced MF-GrC LTP in the mouse cerebellar granular layer through the NO cascade (Lu et al., 2022), we further examined whether nicotine enhances the facial stimulation-induced MF-GrC LTP *via* the NO signaling cascade. After perfusion of an NOS inhibitor, L-NNA (200 μM), on the cerebellar surface for 1 h, MF-GrC LTP could not be induced by delivery of 20 facial stimulation under the control condition (L-NNA) and in the presence of nicotine (NIC, 1 μM; L-NNA + NIC) (**Figures 5A,B**). In the presence of L-NNA, the normalized amplitude was 102.3 ± 4.4% of baseline during 45–50 min after 20 Hz facial stimulation ($F = 0.093$, $P = 0.51$; $n = 7$ experiments; **Figure 5C**), and the normalized AUC of response was 102.2 ± 6.4% of baseline during 40–50 min after 20 Hz facial stimulation ($F = 0.11$, $P = 0.58$; $n = 7$ experiments;

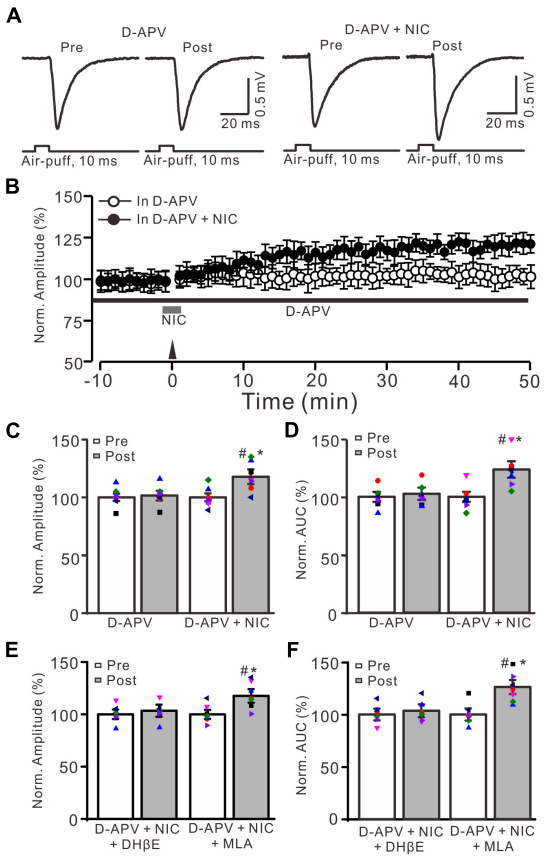

FIGURE 4 | Facial stimulation-induced MF-GrC LTP was prevented by NMDA receptor antagonist, but it was restored by nicotine. **(A)** Representative extracellular recording traces illustrating facial stimulation (10 ms, 60 psi)-evoked MF-GrC synaptic response before (pre) and after (post) delivering 20 Hz (240 pulses) stimulation in the presence of D-APV (50 μM) and a mixture of D-APV + nicotine (D-APV + NIC; 1 μM). **(B)** Summary of data showing the time course of normalized amplitude before and after delivery of 20 Hz facial stimulation (arrow head) in the treatment with D-APV (black bar; open circle) and a mixture of D-APV + nicotine (NIC; gray bar; filled circle). **(C,D)** Bar graphs show normalized amplitude **(C)** and normalized AUC **(D)** of the response before (pre) and after (post) delivery of 20 Hz facial stimulation in treatment with D-APV and a mixture of D-APV + nicotine. Pooled data showing normalized amplitude **(E)** and normalized AUC **(F)** of the response before (pre) and after (post) delivery of 20 Hz facial stimulation in treatment with a mixture of D-APV (250 μM) + nicotine (1 μM) + DHβE (1 μM) (D-APV + NIC + DHβE), and a mixture of D-APV (250 μM) + nicotine (1 μM) + MLA (1 μM) (D-APV + NIC + MLA). Note that the facial stimulation-induced MF-GrC LTP was abolished by NMDA receptor blocker, D-APV, but it was restored by additional application of nicotine. The nicotine triggers the facial stimulation-induced MF-GrC LTP was abolished by DhβE, but not by MLA. Data points are mean ± S.E.M. $n = 7$ recordings from 7 mice in each group. $^{*}P < 0.05$ vs. post; $^{\#}P < 0.05$ vs. post of D-APV.

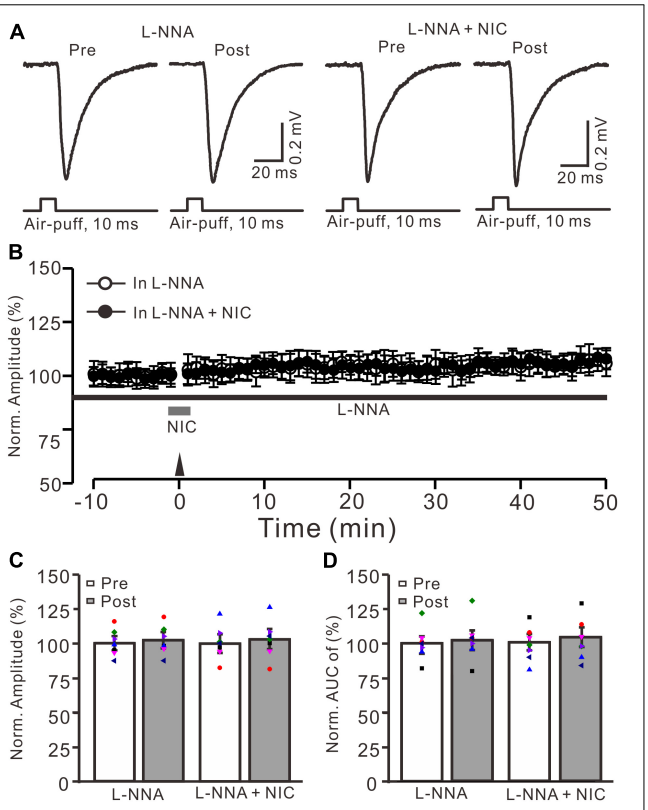

FIGURE 5 | Nicotine-induced enhancement of facial stimulation-induced MF-GrC LTP was prevented by inhibition of NOS. **(A)** Representative extracellular recording traces illustrating facial stimulation (10 ms, 60 psi)-evoked MF-GrC synaptic response before (pre) and after (post) delivering 20 Hz (240 pulses) stimulation in the presence of NOS inhibitor, L-NNA (200 μM), and a mixture of L-NNA (200 μM) + nicotine (NIC; 1 μM). **(B)** Summary of data showing the time course of normalized amplitude before and after delivery of 20 Hz facial stimulation (arrow head) in the treatment with L-NNA (black bar; open circle) and a mixture of L-NNA + nicotine (NIC; gray bar; filled circle). **(C)** Bar graph showing normalized amplitude of the response before (pre) and after (post) delivery of 20 Hz facial stimulation in treatment with L-NNA and a mixture of L-NNA + nicotine (L-NNA + NIC). **(D)** Pooled data showing normalized AUC of the response before (pre) and after (post) delivery of 20 Hz facial stimulation in treatment with L-NNA and a mixture of L-NNA + nicotine (L-NNA + NIC). Note that the nicotine could not trigger MF-GrC LTP in the absence of NOS activity. Data points are mean ± S.E.M. $n = 7$ recordings from seven mice in each group.

Figure 5D). In the presence of a mixture of L-NNA and nicotine, the normalized amplitude was 102.7 ± 6.3% of baseline during 45–50 min after delivery of 20 Hz facial stimulation ($F = 0.28$, $P = 0.45$; $n = 7$ experiments; **Figure 5C**), and the normalized AUC of response was 103.4 ± 6.5% of baseline during 40–50 min after 20 Hz facial stimulation ($F = 0.081$, $P = 0.58$; $n = 7$ experiments; **Figure 5D**). These results indicate that inhibition of NOS abolished the facial stimulation-induced MF-GrC LTP and prevented the nicotine-restored LTP *in vivo* in mice. These results suggest that nicotine enhances MF-GrC LTP *via* the α4β2 nAChR/NO signaling pathway.

DISCUSSION

Cerebellar neuronal circuitry plasticity, including LTD and LTP is presumed to be a mechanism of motor learning (Ito, 1984). We recently found that facial stimulation evokes MF-GrC LTP *via* the NMDA receptor/NO signaling pathway, which suggests that the sensory stimulation-produced MF-GrC long-term plasticity contributes to cerebellar-related motor

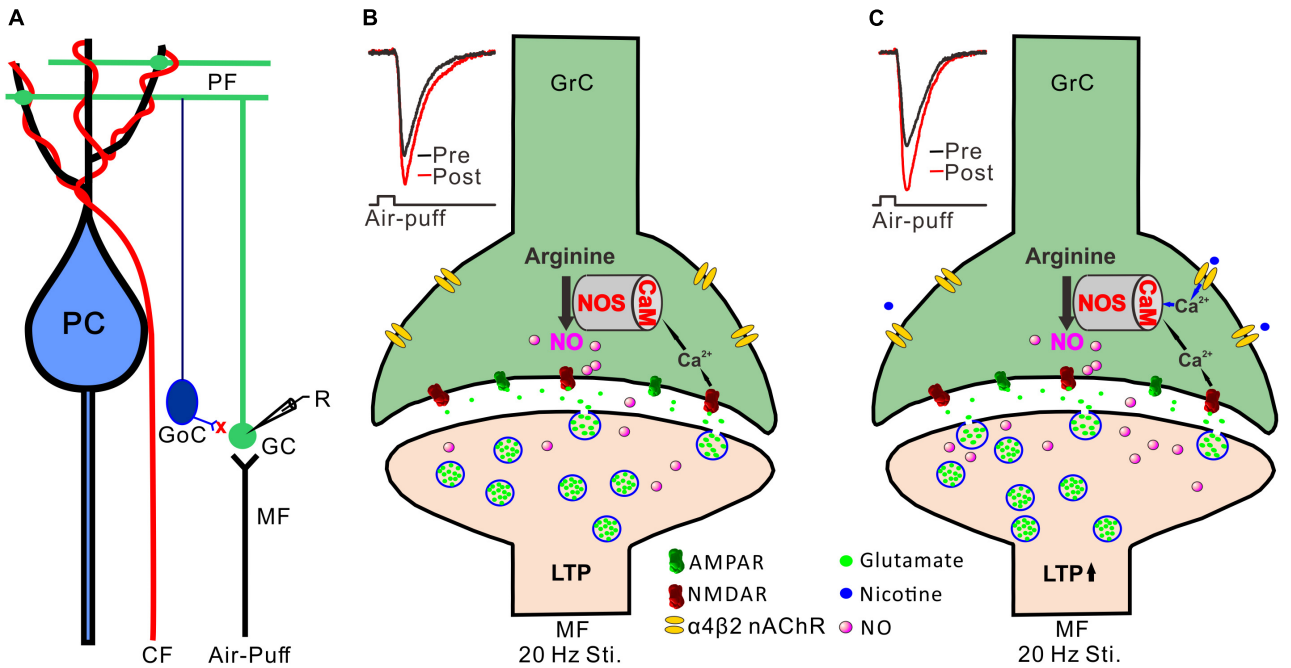

FIGURE 6 | Possible mechanism of nicotine-induced facilitation of MF-GrC LTP. **(A)** Composition of cerebellar cortical microcirculation and the recording diagram of MF-GrC synaptic transmission evoked by facial stimulation. The inhibitory inputs of GoC were blocked by picrotoxin. **(B)** 20 Hz facial stimulation induced MF-GrC LTP *via* the NMDA receptor/NO cascade signaling pathway. Insert, representative traces showing the evoked MF-GrC synaptic transmission before (pre) and after (post) delivery of 20 Hz stimulation. **(C)** Activation of α4β2 nAChR enhanced Ca^{2+} influx and facilitated NO generation in GrC resulting in an enhancement of MF-GrC LTP expression. Insert, representative traces showing the evoked MF-GrC synaptic transmission before (pre) and after (post) delivery of 20 Hz stimulation. PC, Purkinje cell; CF, climbing fiber; MF-mossy fiber; GoC, Golgi cell; GrC, granule cell; R, recording electrode; NOS, nitric oxide synthase; NO, nitric oxide; LTP, long-term potentiation.

learning behavior (Lu et al., 2022). Nicotine plays important roles in modulation of cerebellar neuronal circuitry plasticity and improvement of motor functions *via* nAChRs. Our present results showed that 20 Hz facial stimulation induced an NMDA receptor-dependent MF-GrC LTP, which was significantly enhanced by nicotine *via* α4β2 nAChRs *in vivo* in mice. Blockade of NMDA receptor-dependent MF-GrC LTP revealed a nicotine-trigged MF-GrC LTP through α4β2-nAChR. However, neither the NMDA receptor-dependent nor nicotine-triggered MF-GrC LTP was abolished by inhibition of NOS. These results indicate that nicotine enhanced the MF-GrC LTP *via* the α4β2 nAChR/NO signaling pathway, which suggests that nicotine plays an important role in the modulation of motor learning behavior by regulating sensory-induced MF-GrC plasticity.

Activation of Nicotinic Acetylcholine Receptors Modulate Neuronal Circuitry Activity in the Granular Layer

Nicotinic acetylcholine receptors are found abundantly in the central nervous system and contribute to modulate the release of other neurotransmitters and the synaptic transmission (Gotti et al., 2006; Dani and Bertrand, 2007; Romanelli et al., 2007). Previous studies have demonstrated that mRNAs of the α3, α4, α5, α7, α9, α10, β2, and β4 nAChR subunits are abundantly expressed in developing mouse cerebellar GrCs, and most GrCs express both α4 and β2 nAChRs (Didier et al., 1995; Tribollet et al., 2004; Turner and Kellar, 2005; Lykhmus et al., 2017). The α7 nAChRs are expressed in presynaptic sites of the cerebellar granular layer and contribute to facilitate the release of glutamate at the MF-GrC synapses *in vitro* in rats (De Filippi et al., 2001; Rossi et al., 2003; Reno et al., 2004). By contrast, the α4β2 nAChRs are present in the somas of cerebellar GrCs and contribute to modulate somatic membrane currents (De Filippi et al., 2001). Application of nicotine produces a concentration- and Ca^{2+}-dependent GABA release in mouse cerebellar slices *via* activation of α7 and β2 nAChRs (Pereira da Silva et al., 2018). Cerebellar surface perfusion of nicotine induces an enhancement of facial stimulation-evoked field potential responses in the mouse cerebellar granular layer *via* activation of both α7 and α4β2 nAChR subunits, which suggests that nicotine modulates sensory stimulation-evoked MF-GrC synaptic transmission and plasticity *in vivo* in mice (Xu et al., 2019). Because the 50% effective concentration (EC_{50}) of the nicotine-induced enhancement of the facial stimulation-evoked response in the granular layer is 32.6 μM (Xu et al., 2019), we employed low-concentration nicotine (1 μM) to avoid the direct action of nicotine on facial stimulation evoked MF-GrC synaptic transmission. Our data showed that application of 1 μM nicotine did not significantly change the amplitude of the response. However, delivery of 20 Hz facial stimulation in the presence of

1 μM nicotine induced an LTP of MF-GrC synaptic transmission in the mouse cerebellar cortex, which suggests that physiological activation of nAChRs is involved in facial stimulation-induced MF-GrC LTP *in vivo* in mice.

Nicotine Enhances the Facial Stimulation-Induced Mossy Fiber-Granule Cell Long-Term Potentiation *via* α4β2 Nicotinic Acetylcholine Receptors

It has been well demonstrated that nicotine modulates neuroplasticity and improves working memory performance and motor function in both animals and human subjects (Hahn et al., 2002; Kumari et al., 2003; Heishman et al., 2010; Grundey et al., 2015; Toyoda, 2018, 2019). Application of nicotine produced a focusing effect with increased focal LTP-like plasticity induced by paired associative stimulation and abolished non-focal transcranial direct current stimulation-induced LTP-like plasticity *via* calcium-dependent mechanisms in healthy non-smokers (Kuo et al., 2007; Grundey et al., 2018b). Administration of nicotine restored the excitatory neuroplasticity and was linked to the improvement of implicit motor learning skills in deprived smokers (Grundey et al., 2018a). Furthermore, α4β2 nAChRs were present in the somas of cerebellar GrCs, which mediate somatic membrane currents *in vitro* in rats (De Filippi et al., 2001), and activation of α4β2 nAChRs facilitated long-term plasticity in the mouse insular cortex (Toyoda, 2018, 2019). Moreover, behavioral studies showed that application of nAChR agonists or cholinesterase inhibitor significantly improved the rotarod performance and increased functional activation of the cerebellar vermis in cortical impact injury or ataxic rats (Holschneider et al., 2011, 2013; Wecker et al., 2013). Our present results showed that in the presence of α4β2 nAChR antagonist, delivery of 20 Hz facial stimulation failed to enhance the MF-GrC LTP, which indicated that nicotine facilitated the facial stimulation-induced long-term synaptic plasticity in the cerebellar GrC layer *via* activation of α4β2 nAChRs. In addition, both α7 and α4β2 nAChRs contributed to modulate the facial stimulation-evoked MF-GrC synaptic transmission, but the present data showed that blockade of α7 nAChRs did not prevent the nicotine-induced enhancement of the MF-GrC LTP. The results indicate that nicotine facilitated the facial stimulation-induced MF-GrC LTP in the cerebellar granular layer, but this not occur through α7 nAChRs.

Possible Mechanism of Nicotine-Induced Facilitation of Mossy Fiber-Granule Cell Long-Term Potentiation

Activation of NMDA receptors is required for induction of long-term synaptic plasticity in the cerebellar granular layer (D'Angelo et al., 1999; Roggeri et al., 2008), including the 20 Hz facial stimulation-induced MF-GrC LTP (Lu et al., 2022). It has been proposed that 20 Hz facial stimulation induced Ca^{2+} influx from NMDA receptors and consequently activated calcium-sensitive protein and enzymes, such as calmodulin and NOS, resulting in an increase in NO levels (Kim and Huganir, 1999). Therefore, NO is generated by cerebellar GrCs during the 20 Hz facial stimulation *via* activation of NMDA receptors, resulting in MF-GrC LTP in the mouse cerebellar cortex (**Figures 6A,B**; Lu et al., 2022). Our present results showed that blockade of the NMDA receptor abolished the 20 Hz facial stimulation-induced MF-GrC LTP. However, upon blockade of NMDA receptor-dependent MF-GrC LTP, nicotine induced a kind of MF-GrC LTP through α4β2 nAChRs in response to 20 Hz facial stimulation. Importantly, we found that inhibition of NOS abolished the facial stimulation-induced LTP of MF-GrC synaptic transmission, regardless of the absence or presence of nicotine, which suggests that NOS activation was not only required for induction of the facial stimulation-induced MF-GrC LTP under control conditions but also necessary for the nicotine-induced enhancement of the LTP of MF-GrC synaptic transmission. Previous studies have demonstrated that chronic nicotine administration upregulates NOS expression in the hippocampus (Keser et al., 2011) and contributes to the improvement of motor coordination in female rats (Muñoz-Castañeda et al., 2014). Administration of nicotine significantly improves ethanol-induced impairment of memory, which is abolished by inhibition of NOS, suggesting that the effect of nicotine on ethanol-induced amnesia occurs *via* the NO signaling pathway in the CA1 regions of the dorsal hippocampus in adult mice (Raoufi et al., 2012). It is known that nicotine acts as an agonist of nAChRs with calcium channel properties and can increase intracellular calcium levels and transmitter release *via* both α7 and α4β2 nAChRs (Radcliffe and Dani, 1998; Fujii et al., 1999; Xu et al., 2019). Therefore, administration of nicotine during 20 Hz facial stimulation might induce an increase in calcium influx to achieve sufficient calcium levels and an enhancement of calmodulin activation, resulting in additional activation of NOS in the cerebellar cortical granular layer *via* α4β2 nAChRs (**Figure 6C**; Bredt and Snyder, 1990; Bredt et al., 1991; Garthwaite, 2019). Thus, nicotine facilitates NO release from cerebellar GrCs during 20 Hz facial stimulation *via* activation of α4β2 nAChRs, resulting in an enhancement of MF-GrC LTP in the mouse cerebellum (Garthwaite et al., 1988).

Long-term synaptic plasticity is a type of modification of synaptic strength that is considered to be a synaptic mechanism of motor learning (Ito, 1984). Notably, facial stimulation-evoked long-term synaptic plasticity in the cerebellar granular layer provides the spatiotemporal patterns of activity along the MF-GrC pathway, which is assumed to play important roles in motor coordination and motor learning behavior (Roggeri et al., 2008; D'Angelo and De Zeeuw, 2009; Solinas et al., 2010; Lu et al., 2022). Therefore, the present results may provide new insights for further understanding the mechanisms of nicotine-induced improvement of motor coordination and motor learning ability.

DATA AVAILABILITY STATEMENT

The original contributions presented in this study are included in the article/supplementary material, further inquiries can be directed to the corresponding authors.

ETHICS STATEMENT

The animal study was reviewed and approved by the Animal Care and Use Committee of Yanbian University; the permit number is SYXK (Ji) 2011-006.

AUTHOR CONTRIBUTIONS

D-LQ, C-PC, and Y-HB conceived and designed the experiments. L-XC, Y-HX, and G-JZ performed the experiments. C-PC, Y-HB, and D-LQ analyzed the data. C-PC, LH and D-LQ wrote the manuscript. All authors contributed to the article and approved the submitted version.

FUNDING

This work was supported by the National Natural Science Foundations of China (32070986, 32171005, 82160256, and 31760273) and Scientific and Technological Planning Project of Jilin Province, China (20200201557JC and YDZJ202201ZYTS588).

ACKNOWLEDGMENTS

We thank Emma Longworth-Mills, Ph.D., from Liwen Bianji (Edanz) (www.liwenbianji.cn), for editing the English text of a draft of this manuscript.

REFERENCES

Alhowail, A. (2021). Molecular insights into the benefits of nicotine on memory and cognition. *Mol. Med. Rep.* 23:398. doi: 10.3892/mmr.2021.12037

Bing, Y. H., Zhang, G. J., Sun, L., Chu, C. P., and Qiu, D. L. (2015). Dynamic properties of sensory stimulation evoked responses in mouse cerebellar granule cell layer and molecular layer. *Neurosci. Lett.* 585, 114–118. doi: 10.1016/j.neulet.2014.11.037

Bredt, D. S., and Snyder, S. H. (1990). Isolation of nitric oxide synthetase, a calmodulin-requiring enzyme. *Proc. Natl. Acad. Sci. U. S. A.* 87, 682–685. doi: 10.1073/pnas.87.2.682

Bredt, D. S., Glatt, C. E., Hwang, P. M., Fotuhi, M., Dawson, T. M., and Snyder, S. H. (1991). Nitric oxide synthase protein and mRNA are discretely localized in neuronal populations of the mammalian CNS together with NADPH diaphorase. *Neuron* 7, 615–624. doi: 10.1016/0896-6273(91)90374-9

Chu, C. P., Bing, Y. H., Liu, Q. R., and Qiu, D. L. (2011). Synaptic responses evoked by tactile stimuli in Purkinje cells in mouse cerebellar cortex Crus II in vivo. *PLoS One* 6:e22752. doi: 10.1371/journal.pone.0022752

D'Angelo, E., and De Zeeuw, C. I. (2009). Timing and plasticity in the cerebellum: focus on the granular layer. *Trends. Neurosci.* 32, 30–40. doi: 10.1016/j.tins.2008.09.007

D'Angelo, E., Rossi, P., Armano, S., and Taglietti, V. (1999). Evidence for NMDA and mGlu receptor-dependent long-term potentiation of mossy fiber-granule cell transmission in rat cerebellum. *J. Neurophysiol.* 81, 277–287. doi: 10.1152/jn.1999.81.1.277

Dani, J. A., and Bertrand, D. (2007). Nicotinic acetylcholine receptors and nicotinic cholinergic mechanisms of the central nervous system. *Annu. Rev. Pharmacol. Toxicol.* 47, 699–729. doi: 10.1146/annurev.pharmtox.47.120505.105214

De Filippi, G., Baldwinson, T., and Sher, E. (2001). Evidence for nicotinic acetylcholine receptor activation in rat cerebellar slices. *Pharmacol. Biochem. Behav.* 70, 447–455. doi: 10.1016/S0091-3057(01)00653-0

Didier, M., Berman, S. A., Lindstrom, J., and Bursztajn, S. (1995). Characterization of nicotinic acetylcholine receptors expressed in primary cultures of cerebellar granule cells. *Brain Res. Mol. Brain Res.* 30, 17–28. doi: 10.1016/0169-328X(94)00266-H

Dome, P., Lazary, J., Kalapos, M. P., and Rihmer, Z. (2010). Smoking, nicotine and neuropsychiatric disorders. *Neurosci. Biobehav. Rev.* 34, 295–342. doi: 10.1016/j.neubiorev.2009.07.013

Fujii, S., Ji, Z., Morita, N., and Sumikawa, K. (1999). Acute and chronic nicotine exposure differentially facilitate the induction of LTP. *Brain Res.* 846, 137–143. doi: 10.1016/S0006-8993(99)01982-4

Garthwaite, J. (2019). NO as a multimodal transmitter in the brain: discovery and current status. *Br. J. Pharmacol.* 176, 197–211. doi: 10.1111/bph.14532

Garthwaite, J., Charles, S. L., and Chess Williams, R. (1988). Endothelium derived relaxing factor release on activation of NMDA receptors suggests role as intercellular messenger in the brain. *Nature* 336, 385–388. doi: 10.1038/336385a0

Gonzalez, C. L., Gharbawie, O. A., and Kolb, B. (2006). Chronic low-dose administration of nicotine facilitates recovery and synaptic change after focal ischemia in rats. *Neuropharmacology* 50, 777–787. doi: 10.1016/j.neuropharm.2005.11.018

Gotti, C., Zoli, M., and Clementi, F. (2006). Brain nicotinic acetylcholine receptors: native subtypes and their relevance. *Trends Pharmacol. Sci.* 27, 482–491. doi: 10.1016/j.tips.2006.07.004

Grundey, J., Amu, R., Ambrus, G. G., Batsikadze, G., Paulus, W., and Nitsche, M. A. (2015). Double dissociation of working memory and attentional processes in smokers and non-smokers with and without nicotine. *Psychopharmacology* 232, 2491–2501. doi: 10.1007/s00213-015-3880-7

Grundey, J., Barlay, J., Batsikadze, G., Kuo, M. F., Paulus, W., and Nitsche, M. (2018a). Nicotine modulates human brain plasticity via calcium-dependent mechanisms. *J. Physiol.* 596, 5429–5441. doi: 10.1113/JP276502

Grundey, J., Thirugnasambandam, N., Amu, R., Paulus, W., and Nitsche, M. A. (2018b). Nicotinic Restoration of Excitatory Neuroplasticity Is Linked to Improved Implicit Motor Learning Skills in Deprived Smokers. *Front. Neurol.* 9:367. doi: 10.3389/fneur.2018.00367

Hahn, B., Shoaib, M., and Stolerman, I. P. (2002). Nicotine-induced enhancement of attention in the five-choice serial reaction time task: the influence of task demands. *Psychopharmacology* 162, 129–137. doi: 10.1007/s00213-002-1005-6

Heishman, S. J., Kleykamp, B. A., and Singleton, E. G. (2010). Meta-analysis of the acute effects of nicotine and smoking on human performance. *Psychopharmacology* 210, 453–469. doi: 10.1007/s00213-010-1848-1

Hijioka, M., Matsushita, H., Ishibashi, H., Hisatsune, A., Isohama, Y., and Katsuki, H. (2012). α7 Nicotinic acetylcholine receptor agonist attenuates neuropathological changes associated with intracerebral hemorrhage in mice. *Neuroscience* 222, 10–19. doi: 10.1016/j.neuroscience.2012.07.024

Holschneider, D. P., Guo, Y., Roch, M., Norman, K. M., and Scremin, O. U. (2011). Acetylcholinesterase inhibition and locomotor function after motor-sensory cortex impact injury. *J. Neurotrauma.* 28, 1909–1919. doi: 10.1089/neu.2011.1978

Holschneider, D. P., Guo, Y., Wang, Z., Roch, M., and Scremin, O. U. (2013). Remote brain network changes after unilateral cortical impact injury and their modulation by acetylcholinesterase inhibition. *J. Neurotrauma.* 30, 907–919. doi: 10.1089/neu.2012.2657

Ito, M. (1984). *The Cerebellum and Neural Control*. New York: Raven Press.

Keser, A., Balkan, B., Gozen, O., Kanit, L., and Pogun, S. (2011). Hippocampal neuronal nitric oxide synthase (nNOS) is regulated by nicotine and stress in female but not in male rats. *Brain Res.* 1368, 134–142. doi: 10.1016/j.brainres.2010.10.090

Kim, J. H., and Huganir, R. L. (1999). Organization and regulation of proteins at synapses. *Curr. Opin. Cell. Biol.* 11, 248–254. doi: 10.1016/S0955-0674(99)80033-7

Kumari, V., Gray, J. A., Ffytche, D. H., Mitterschiffthaler, M. T., Das, M., Zachariah, E., et al. (2003). Cognitive effects of nicotine in humans: an fMRI study. *Neuroimage* 19, 1002–1013. doi: 10.1016/S1053-8119(03)00110-1

Kuo, M. F., Grosch, J., Fregni, F., Paulus, W., and Nitsche, M. A. (2007). Focusing effect of acetylcholine on neuroplasticity in the human motor cortex. *J. Neurosci.* 27, 14442–14447. doi: 10.1523/JNEUROSCI.4104-07.2007

Li, B. X., Dong, G. H., Li, H. L., Zhang, J. S., Bing, Y. H., Chu, C. P., et al. (2021). Chronic Ethanol Exposure Enhances Facial Stimulation-Evoked Mossy Fiber-Granule Cell Synaptic Transmission via GluN2A Receptors in the Mouse Cerebellar Cortex. *Front. Syst. Neurosci.* 15:657884. doi: 10.3389/fnsys.2021.657884

Lu, D., Wan, P., Liu, Y., Jin, X. H., Chu, C. P., Bing, Y. H., et al. (2022). Facial stimulation induces a LTP of mossy fiber-granule cell synaptic transmission via GluN2A containing NMDA receptor/nitric oxide cascade in mouse cerebellum. *Front. Cell. Neurosci.* 16:863342. doi: 10.3389/fncel.2022.863342

Lykhmus, O., Voytenko, L. P., Lips, K. S., Bergen, I., Krasteva-Christ, G., Vetter, D. E., et al. (2017). Nicotinic Acetylcholine Receptor α9 and α10 Subunits Are Expressed in the Brain of Mice. *Front. Cell. Neurosci.* 11:282. doi: 10.3389/fncel.2017.00282

Ma, C., Lu, D., Cao, L. X., Bing, Y. H., Chu, C. P., and Qiu, D. L. (2019). Temporal-spacial relationships between facial stimulation-evoked filed potential responses in mouse cerebellar granular layer and molecular layer. *Neurosci. Lett.* 705, 106–111. doi: 10.1016/j.neulet.2019.04.051

Muñoz-Castañeda, R., Díaz, D., Avila-Zarza, C. A., Alonso, J. R., and Weruaga, E. (2014). Sex-influence of nicotine and nitric oxide on motor coordination and anxiety-related neurophysiological responses. *Psychopharmacology* 231, 695–706. doi: 10.1007/s00213-013-3284-5

Pereira da Silva, J. D., Campos, D. V., Nogueira-Bechara, F. M., Stilhano, R. S., Han, S. W., Sinigaglia-Coimbra, R., et al. (2018). Altered release and uptake of gamma-aminobutyric acid in the cerebellum of dystrophin-deficient mice. *Neurochem. Int.* 118, 105–114. doi: 10.1016/j.neuint.2018.06.001

Radcliffe, K. A., and Dani, J. A. (1998). Nicotinic stimulation produces multiple forms of increased glutamatergic synaptic transmission. *J. Neurosci.* 18, 7075–7083. doi: 10.1523/JNEUROSCI.18-18-07075.1998

Raoufi, N., Piri, M., Moshfegh, A., and Shahin, M. S. (2012). Nicotine improves ethanol-induced impairment of memory: possible involvement of nitric oxide in the dorsal hippocampus of mice. *Neuroscience* 219, 82–91. doi: 10.1016/j.neuroscience.2012.06.003

Reno, L. A., Zago, W., and Markus, R. P. (2004). Release of [(3)H]-L-glutamate by stimulation of nicotinic acetylcholine receptors in rat cerebellar slices. *Neuroscience* 124, 647–653. doi: 10.1016/j.neuroscience.2003.12.023

Roggeri, L., Rivieccio, B., Rossi, P., and D'Angelo, E. (2008). Tactile stimulation evokes long-term synaptic plasticity in the granular layer of cerebellum. *J. Neurosci.* 28, 6354–6359. doi: 10.1523/JNEUROSCI.5709-07.2008

Romanelli, M. N., Gratteri, P., Guandalini, L., Martini, E., Bonaccini, C., and Gualtieri, F. (2007). Central nicotinic receptors: structure, function, ligands, and therapeutic potential. *Chem. Med. Chem.* 2, 746–767. doi: 10.1002/cmdc.200600207

Rossi, D. J., Hamann, M., and Attwell, D. (2003). Multiple modes of GABAergic inhibition of rat cerebellar granule cells. *J. Physiol.* 548, 97–110. doi: 10.1113/jphysiol.2002.036459

Solinas, S., Nieus, T., and D'Angelo, E. (2010). A realistic large-scale model of the cerebellum granular layer predicts circuit spatio-temporal filtering properties. *Front. Cell. Neurosci.* 4:12. doi: 10.3389/fncel.2010.00012

Toyoda, H. (2018). Nicotine facilitates synaptic depression in layer V pyramidal neurons of the mouse insular cortex. *Neurosci. Lett.* 672, 78–83. doi: 10.1016/j.neulet.2018.02.046

Toyoda, H. (2019). Nicotinic activity layer specifically modulates synaptic potentiation in the mouse insular cortex. *Eur. J. Neurosci.* 50, 2211–2223. doi: 10.1111/ejn.13857

Tribollet, E., Bertrand, D., Marguerat, A., and Raggenbass, M. (2004). Comparative distribution of nicotinic receptor subtypes during development, adulthood and aging: an autoradiographic study in the rat brain. *Neuroscience* 124, 405–420. doi: 10.1016/j.neuroscience.2003.09.028

Turner, J. R., and Kellar, K. J. (2005). Nicotinic cholinergic receptors in the rat cerebellum: multiple heteromeric subtypes. *J. Neurosci.* 25, 9258–9265. doi: 10.1523/JNEUROSCI.2112-05.2005

Wecker, L., Engberg, M. E., Philpot, R. M., Lambert, C. S., Kang, C. W., Antilla, J. C., et al. (2013). Neuronal nicotinic receptor agonists improve gait and balance in olivocerebellar ataxia. *Neuropharmacology* 73, 75–86. doi: 10.1016/j.neuropharm.2013.05.016

Xu, Y. H., Zhang, B. B., Su, W. H., Wu, M. C., Bing, Y. H., Cui, S. B., et al. (2019). Nicotine modulates the facial stimulation-evoked responses in cerebellar granule cell layer in vivo in mice. *Eur. J. Pharmacol.* 843, 126–133. doi: 10.1016/j.ejphar.2018.11.022

Conflict of Interest: The authors declare that the research was conducted in the absence of any commercial or financial relationships that could be construed as a potential conflict of interest.

Publisher's Note: All claims expressed in this article are solely those of the authors and do not necessarily represent those of their affiliated organizations, or those of the publisher, the editors and the reviewers. Any product that may be evaluated in this article, or claim that may be made by its manufacturer, is not guaranteed or endorsed by the publisher.

Copyright © 2022 Cao, Bing, Xu, Zhang, Chu, Hong and Qiu. This is an open-access article distributed under the terms of the Creative Commons Attribution License (CC BY). The use, distribution or reproduction in other forums is permitted, provided the original author(s) and the copyright owner(s) are credited and that the original publication in this journal is cited, in accordance with accepted academic practice. No use, distribution or reproduction is permitted which does not comply with these terms.

frontiers | Frontiers in Cellular Neuroscience

TYPE Review
PUBLISHED 21 July 2022
DOI 10.3389/fncel.2022.890666

Check for updates

OPEN ACCESS

EDITED BY
Jorg Dietrich,
Harvard Medical School, United States

REVIEWED BY
Marco Mainardi,
Institute of Neuroscience (CNR), Italy
Joëlle Chabry,
UMR7275 Institut de Pharmacologie Moléculaire et Cellulaire (IPMC), France

*CORRESPONDENCE
Xia Bi
bixiash@163.com

SPECIALTY SECTION
This article was submitted to Cellular Neuropathology, a section of the journal Frontiers in Cellular Neuroscience

RECEIVED 06 March 2022
ACCEPTED 29 June 2022
PUBLISHED 21 July 2022

CITATION
Han Y, Yuan M, Guo Y-S, Shen X-Y, Gao Z-K and Bi X (2022) The role of enriched environment in neural development and repair. Front. Cell. Neurosci. 16:890666. doi: 10.3389/fncel.2022.890666

COPYRIGHT
© 2022 Han, Yuan, Guo, Shen, Gao and Bi. This is an open-access article distributed under the terms of the Creative Commons Attribution License (CC BY). The use, distribution or reproduction in other forums is permitted, provided the original author(s) and the copyright owner(s) are credited and that the original publication in this journal is cited, in accordance with accepted academic practice. No use, distribution or reproduction is permitted which does not comply with these terms.

The role of enriched environment in neural development and repair

Yu Han[1,2], Mei Yuan[1,2], Yi-Sha Guo[1,2], Xin-Ya Shen[2,3], Zhen-Kun Gao[2,3] and Xia Bi[2]*

[1]Department of Sport Rehabilitation, Shanghai University of Sport, Shanghai, China, [2]Department of Rehabilitation Medicine, Shanghai University of Medicine and Health Sciences Affiliated Zhoupu Hospital, Shanghai, China, [3]Department of Graduate School, Shanghai University of Medicine and Health Sciences Affiliated Shanghai University of Traditional Chinese Medicine, Shanghai, China

In addition to genetic information, environmental factors play an important role in the structure and function of nervous system and the occurrence and development of some nervous system diseases. Enriched environment (EE) can not only promote normal neural development through enhancing neuroplasticity but also play a nerve repair role in restoring functional activities during CNS injury by morphological and cellular and molecular adaptations in the brain. Different stages of development after birth respond to the environment to varying degrees. Therefore, we systematically review the pro-developmental and anti-stress value of EE during pregnancy, pre-weaning, and "adolescence" and analyze the difference in the effects of EE and its sub-components, especially with physical exercise. In our exploration of potential mechanisms that promote neurodevelopment, we have found that not all sub-components exert maximum value throughout the developmental phase, such as animals that do not respond to physical activity before weaning, and that EE is not superior to its sub-components in all respects. EE affects the developing and adult brain, resulting in some neuroplastic changes in the microscopic and macroscopic anatomy, finally contributing to enhanced learning and memory capacity. These positive promoting influences are particularly prominent regarding neural repair after neurobiological disorders. Taking cerebral ischemia as an example, we analyzed the molecular mediators of EE promoting repair from various dimensions. We found that EE does not always lead to positive effects on nerve repair, such as infarct size. In view of the classic issues such as standardization and relativity of EE have been thoroughly discussed, we finally focus on analyzing the essentiality of the time window of EE action and clinical translation in order to devote to the future research direction of EE and rapid and reasonable clinical application.

KEYWORDS:

enriched environment, CNS disorders, neurodevelopment, neurorestoration, cerebral ischemia

Introduction

Complex genetic backgrounds and epigenetic processes shape the basic structure and function of the mammalian brain at birth for normal neural development. However, in the whole life cycle, the addition of various stimulation from the environment and the interaction with genes form a precise neural circuit structure with complexity far exceeding the content of genomic information, in which highly ordered neuronal activities are the basis of advanced brain function (Sur and Leamey, 2001; Giandomenico et al., 2021). The demonstration that the adaptation of neural networks with the changing environment manifests in subtle diversity, including but not limited to neurogenesis, neurite growth, and synaptic transmission to promote the emergence of optimal phenotypes, has emphasized the importance of environmental factors on neuroplasticity (Guzzetta et al., 2019). However, the complex interaction of numerous signaling pathways and regulatory factors with environmental factors may cause maladaptive plasticity. For instance, stress in the living environment is a risk factor for development-related mental diseases and aging-related neurodegeneration, such as depression, schizophrenia, and Alzheimer's disease (AD; Aznar and Knudsen, 2011). The environmental parameters have attracted far more attention in neurodevelopment and repairing neurological dysfunction due to the limited therapeutic effect of drugs and the relatively uncontrollable genetic background.

Animal models have been widely used to study neurodevelopment and neural restoration, as well as to explore the pathogenesis underlying central nervous system (CNS) disease. Significantly, most animals involved in the study are raised in standard laboratory cages, which are relatively sterile environments without stimulation. The experimental animals receive more physical and social stimulation than standard rearing conditions. Experimental animals can selectively conduct physical movement, exploration, cognition, and social interaction to improve learning and memory by reshaping brain neural network construction, finally presenting better behavior performance (Nithianantharajah and Hannan, 2006). Initially, the EE studies produced impressive changes in neuroanatomy and etiology. Increased cortical thickness (Bennett et al., 1969), dendrite branching, synaptic density (Altschuler, 1979), and glial cell proliferation (Altman and Das, 1964) provide robust evidence to dissect the enhanced learning and memory skills associated with EE (van Praag et al., 2000). During the past two decades, the fundamental studies of EE at behavioral, molecular, and cellular levels have indicated that EE can be regarded as a resultful rehabilitation strategy without side-effect in stroke (Yuan et al., 2021), AD (Rodríguez et al., 2013), Parkinson's disease (PD; Goldberg et al., 2011), Huntington's disease (HD; Couly et al., 2021), spinal cord injury (Hutson et al., 2019), and various neurological disorders.

The implementation of concrete schemes to achieve the transformation of clinical efficacy is the path for any drug or intervention to succeed. A study focused on transforming EE intervention from the laboratory to the clinical setting demonstrated the feasibility of using EE correctly with patients in a rehabilitation setting (Janssen et al., 2012). However, the richness of the environment is relative in virtue of the different social backgrounds that humans come into contact with and the plentiful uncontrollable variables in the environment. In addition, the stimulating patterns of EE are codetermined by the patient's own choice based on interest and the existing environmental facility setting of the hospital. The relativity of environmental richness and the diversity of collocation imply that it is hard to standardize EE, which may be one of the factors contributing to the unstable clinical efficacy of EE owing to the lack of specificity in particular CNS diseases. In this review, the mechanism underlying EE in promoting neurodevelopment and neural repair following CNS disorders is probed, and the classic criticisms and future challenges facing EE.

EE and the rearing condition

The concept of EE was first put forward by Donald Hebb, who found that rats moving freely at home possess better learning and memory capacity than those reared in the laboratory. Such an uncontrolled home environment seems different from the controllability of EE in the laboratory. Still, both reveal the critical feature of enrichment in rearing condition: ensuring the complexity and novelty of the living environment (Nithianantharajah and Hannan, 2006). Although the experimental paradigms and clinical interventions of EE present diversification, they all adopt a complex combination of non-biological and social stimuli to achieve the purpose of enriching the environment with more multi-sensory stimulation, physical activity, and social interaction (Will et al., 2004; **Figure 1**).

Construction of EE in the animal model

Standard conditions for laboratory animals are free of anything other than bedding, adequate food, and water. However, besides primary living conditions, EE provides animals with more motor, sensory, cognitive, and social stimulation, which are four classical mechanisms actuating EE function (Sztainberg and Chen, 2010). Animals are born with the ability to explore. In an exploration environment with abundant and novel toys, including running wheels, tunnels, and building blocks, spontaneous somatic movements such as chasing, running, and jumping can activate motor cortex neurons (Clarke et al., 2014). Colorful, different textures of toys, some can emit music (Li et al., 2021) and unique smells, providing

10.3389/fncel.2022.890666

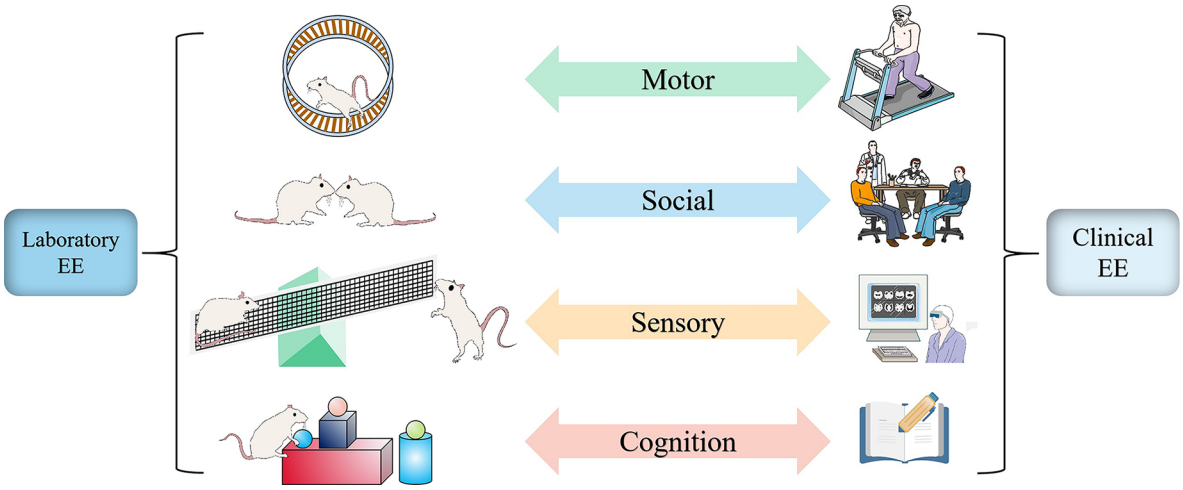

FIGURE 1
Similarity and correspondence between laboratory EE setting and clinical EE intervention. Whether laboratory or clinical, EE always provides motor, sensory, social, and cognitive stimulation to achieve positive changes in function and structure. In physical activity, animals are voluntarily active on a running wheel to match the patient on a treadmill or more diverse exercise (Green); in social stimulation, EE in the laboratory allows for extensive social interaction between animals by increasing the number of animals to match patients in the ward or treatment hall to communicate with other patients or doctors about their conditions or preferred treatment options (Blue). In sensory, animals are involved in touching a series of toys, such as seesaws, swings, and pipes, to match the patient's experience of proprioception, touch, hearing, and other stimuli through virtual reality technology (Yellow). In terms of cognition, Animals recognize the color and shape of objects to match the patient's participation in reading, playing games, and chess according to their interests to improve learning and memory skills (Red).

animals with a full range of multi-sensory stimulation, including vision, proprioception, hearing, and smell (Walsh and Cummins, 1975). In addition to ensuring the complexity of the setting in the environment, the types and locations of the built-in objects constantly change in time and space to create novelty, which improves cognition through spatial perception, object recognition, regulation of attention. Early study has observed that the high proliferation of hippocampal neurons accompanies the improvement of learning and memory ability of EE-fed mice (Kempermann et al., 1997).

Further, the EE cage has more animals and larger activity space to supply social stimulation compared with the standard cage. Properly arranged social environments provide more opportunities for information transmission and emotional exchange among animals. There are differences between social and inanimate stimuli in rearing condition, in which the social environment is relatively uncontrollable under the individual influence. Rich rearing condition provide shared living environments for animals. In contrast, some animals can change their social structure based on their behavior to create unshared environments that affect other individuals in EE cages (Kempermann, 2019). For instance, territorial male rats often fight. Therefore, even with the EE paradigm in the laboratory, environmental factors are not entirely controllable. In general, the standard for EE cage specifications has not been affirmed. However, as long as the living habits of animals are followed and the complexity and novelty of EE rearing condition are satisfied, diverse EE paradigms both produce expected positive benefits on animal behavior and brain structure.

Construction of EE in clinical research

Hospitalized patients with CNS disorders, especially stroke patients with motor and cognitive impairments, spend most of their time with a lack of voluntary activity, if any, as part of routine rehabilitation and are highly dependent on others (Keith and Cowell, 1987; King et al., 2011). In addition, compared to the daily living environment, the ward is a barren environment, with little access to external social stimulation and social activities of inpatients with anxiety accompanied by psychological disorders, even depression (Ayerbe et al., 2013; Campbell Burton et al., 2013). Researches indicate that patients accepting higher levels of physical activity based on impaired body restriction and addition of cognitive (Shimada et al., 2018) and social activity (Lindsay et al., 2019) exert better prognosis and independence (Scrivener et al., 2012).

The forceful rationale that EE has achieved beneficial results in disease models is provided for direct or indirect translation of EE to recovery humans in clinical practice.

A study that has demonstrated 2 weeks of EE can improve activity levels in patients undergoing routine rehabilitation after stroke divided patients' living environment into public and individual areas. Patients entering the communal environment were given access to an internet computer, various reading

materials (newspaper, magazine, and fiction books), games, jigsaw puzzles, and a shared dining hall. Individual enrichment provided participants with special requirements referring to their interests and hobbies, including music, audiobooks, and number puzzles. The choice of activities and equipment was up to patients themselves, without compulsion. Nursing and rehabilitation personnel were only responsible for encouraging inactive patients to enter public areas and providing guided services to resolve operational difficulties if required (Janssen et al., 2012, 2014).

In addition to stroke, EE has also contributed significantly to promoting cognitive function in aging or dementia patients. Train the Brain Consortium has made outstanding dedications to clinical research on EE and cognitive dysfunction. In recent years, they have published clinical data associated with brain health indicators showing that comprehensive physical or cognitive training dramatically decreasing neuropsychiatric symptoms and improved the quality of life to restore cognitive status in patients with mild cognitive impairment (Train the Brain Consortium, 2017; Cintoli et al., 2021). The mechanism may be closely related to improvements in vascular function including amelioration of endothelial function throughout the body, mobilization of $CD34^+$ progenitor cells, and maintenance of carotid artery dilation, especially in patients with hypertension (Bruno et al., 2018). It is well known that dysrhythmia of rest-activity is closely related to cognitive dysfunction for dementia patients (Coogan et al., 2013). One study showed that a small scaled homelike special care unit (SCU), identified as a pattern of EE by the authors, could positively affect the rest-activity rhythms of dementia patients. Compared to a regular SCU, the small scaled homelike SCU provided patients with separate bedrooms and psychosocial treatment, including stimulation of social activities and communication technology, which supplies a more silent environment and alleviates the psychological burden for better rest (Kok et al., 2017). Recent research has really elevated EE to the level of transforming the natural environment in which humans live. The enrichment garden (EG) with 12 stimulation modules, derived from an exceptional renovation of the traditional sensory garden, offers a new treatment for dementia patients in nursing homes. Patients accompanied by caretakers and staff, walking in EG for 10 to 20 min per day, and the path across the EG and location of the stimulus module they tarry can be different each time. For example, the module of sensory amplification achieves the purpose of sensitive stimulation by feeling the sensory gradation of this helicoidal pyramid and possibly modifying planting (Bourdon and Belmin, 2021). Of course, scholars attracted by EE are not limited to research CNS diseases in the elderly. A systematic review hinted that EE seems to be promising for exercise outcomes in cerebral palsy infants (Morgan et al., 2013). EE intervention for infants with cerebral palsy is usually a combination of the following aspects: parent-child interaction with the participation of parents; modification, adjustment, or construction of the treatment room or family environment, including the size, form, placement, and color of facilities to achieve motor skill acquisition; targeted motor skill and cognitive improvement exercises provided by therapists.

Obviously, the clinical application of EE has been carried out in different diseases. Drawing on the construction of experimental EE, clinical EE studies also reflect the combination of sensory stimulation, cognitive training, social activities and exercise. Therefore, it is imperative that a larger sample size and stricter environmental control be put into clinical research on EE.

The effects of EE on neurodevelopment in brain

The maturation of CNS requires the completion of neuroinduction, proliferation, migration, construction of neural circuits, and myelination, with some existing at a particular time, yet some of which span the entire developmental process. During developmental stage, the neural network of the mammalian brain is susceptible to experience and environment, showing high plasticity. Environmental stimulation is associated to a status of increased brain plasticity (Sale et al., 2014). Animal experimental studies have found that EE can affect the anatomical structure, function, and biochemical changes of CNS, promote the neurogenesis process, and improve the positive behavior of animals. The mechanisms involve brain morphology, cytogenetics, molecular biology, neuroendocrinology, and electrophysiological changes.

Environmental stimulation and the brain development

Impact of prenatal environment on development

External stimuli have a strong impact on the brain development of the fetus. The changes in brain plasticity induced by the stimulation of the external environment do not entirely depend on the direct sensory experience of the developing subject. The embryos or fetuses affected by the intrauterine environment are the first to respond to such changes in organogenesis. The nature of the intrauterine environment depends largely on the prenatal environment experienced by the mother.

Prenatal exposure to adverse environments, such as maternal stress, toxic stimulation, viral infection, and substance abuse, can damage normal brain development. Similarly, the prenatal environment determines susceptibility to pathological conditions in later life. Exposure to injuries that cause adverse conditions *in utero* may negatively affect the development

of target organs, destroy the internal microenvironment and enhance the risk of neuropsychiatric disorders in adulthood, including depression, autism and schizophrenia. The biological correlation and mediators between stress and offspring development are mainly related to the hyperactivation of hypothalamic-pituitary-adrenal axis (Gunnar and Quevedo, 2007; Emack and Matthews, 2011), the connection of amygdala and frontotemporal cortex in brain function and microstructure (Favaro et al., 2015), neuronal migration disorders (Hwang et al., 2019), and epigenetic changes (Kundakovic and Jaric, 2017). Numerous animal studies have shown that long-lasting epigenetic changes caused by prenatal stress involve gene encoding BNDF, the corticotropin-releasing factor (Crf), and the glucocorticoid receptor (Nr3c1), which is associated with the HPA axis (Mueller and Bale, 2008; Dong et al., 2015). Recent clinical studies have found that prenatal maternal anxiety predicts accelerated epigenetic age in children in the experimental cohort and reveals increased sensitivity in men rather than woman in regared to the fetal origins of epigenetic age acceleration (Mcgill et al., 2022).

In contrast to adverse stimulation during pregnancy, prenatal positive environment intervention creates favorable conditions for neural development of the embryo and newborn. It is noteworthy that the development of the visual system is sensitive to prenatal EE stimulation. Mice reared in EE showed early eye opening and precocious vision development, which was closely associated with significantly increased precocious cAMP response element-mediated gene expression and higher levels of BDNF and GAD65/67 expression (Cancedda et al., 2004; Sale et al., 2004). Prenatal EE accelerates the migration of neural precursor cells in the retinal ganglion cell layer of the fetus and the natural death of ganglion cells, which depends on the increased insulin-like growth factor-I (IGF-1) induced by enrichment to promote the transfer of nutrients from the placenta to the fetus (Sale et al., 2007). In modern society, pregnant women are extremely vulnerable to active or passive exposure to mobile phone radiation, which will lead to behavioral difficulties in their offspring to varying degrees. Prenatal EE intervention successfully reversed cognitive impairment in elderly offspring caused by long-term radiation exposure during pregnancy through upgrading the synaptic number and the expression of synaptophysin (SYN), postsynaptic density-95 (PSD-95), and BNDF (Hong et al., 2020).

Given that voluntary physical activity is an essential component of EE, we separately analyzed the positive effects of a prenatal exercise intervention on neurodevelopment. More and more studies have shown that reasonable physical exercise during pregnancy is not only conducive to reducing the incidence of gestational diabetes and hypertension and the percentage of body fat in pregnant women but also conducive to promoting fetal development reflected in the increase of placental survival rate and placental hormone secretion (Hopkins et al., 2011; Rosa et al., 2011; Davies and Artal, 2019; Chae et al., 2021). Treadmill training in pregnant rats significantly increased cell proliferation, BNDF, and apoptosis inhibition protein expression in the hippocampus of adolescent and adult progeny rats (Kim et al., 2021), which may explain the high spatial learning ability in neonatal rat pup on the premise of voluntary exercise of maternal rats (Parnpiansil et al., 2003). A meta-analysis of the impact of prenatal exercise on neonatal and child outcomes showed that maternal exercise was associated with a reduced risk of macrosomia, not with neonatal complications or adverse child outcomes (Davenport et al., 2018). In addition to the changes in plasticity of the brain, maternal exercise-induced secretion of Apelin in the placental circulation may provide long-term metabolic benefits to offspring (Son et al., 2022; Wang and Zhu, 2022). These results manifest that prenatal exercise may promote positive development in neonates but may not be effective in inhibiting the occurrence of abnormal diseases, such as those caused by premature birth.

Impact of pre-weaning environment on development

The critical period, also known as the sensitive period, is a specific window period in the early postnatal period. During this time window, the development of the brain is susceptible to external stimuli. The development and maturation of the functional characteristics of the brain and the formation of neural circuits are strongly dependent on its own experience and the influence of the external environment (Sengpiel, 2007). The value of stimulation of postpartum mothers to their offspring is equally worthy of attention as the comfortable living environment and psychological state during pregnancy. In mammals, new mothers respond to infants' unique sounds, touches, and temperatures with attentive responses such as licking and grooming. Infants also enter lactation mode, showing sensitivity to the mother's basic characteristics (Fleming et al., 1999; Pozzi et al., 2021). Maternal behavior is one of the crucial sources for pre-weaning rodents to obtain experience to promote neural development and neural circuit maturation during the critical period.

One of the most pronounced effects of maternal care is the regulation of stress responses in adult offspring. The body's ability to cope with stress depends on the programmed changes of the HPA axis in the neuroendocrine system to promote the release of glucocorticoids that respond to early stress stimuli through multiple intracellular sites and mechanisms. Glucocorticoid receptors (GR) play a central negative feedback regulation role on the HPA axis by changing its expression level in hippocampus. The reduction of the intensity of the stress response at the behavioral and endocrine levels and the improvement in cognitive function in adulthood were found

in pups of mice and rats which received a brief (3–15 min) maternal separation (Meaney et al., 1996). Another interesting explanation for this result is that pups that were briefly separated from their mothers will receive higher levels of maternal care exhibiting fortified behavior of licking/grooming and arched back nursing, which suggests that the effect of early environmental intervention on pre-weaning pups is mediated by maternal behavior (Liu et al., 2000). However, prolonged (3–6 h) daily mother-pup separation produced the opposite effect to short-term separation, with the pups increasing their response to stress factors in adulthood (van Oers et al., 1998). In addition, weight loss, delayed fur growth and eyes opening, and defects in forelimb grasping of pups were found in the model of maternal deprivation recently (Yang et al., 2021). The harmful effects of early maternal isolation on optimal growth and neurobehavioral development of offspring are not only related to the glucocorticoids and secretory signaling pathways described above, but also involve BNDF synthesis disorders (Ströher et al., 2020) as well as the regulation of epigenetics (Borba et al., 2021).

The detction of impairment of memory and cognitive flexibility elicited by maternal deprivation can be avoided by EE intervention prompts that early EE may accelerate the formation of delicate neural circuits (Menezes et al., 2020; Joushi et al., 2021). The fact that pre-weaning pups are largely unable to engage in voluntary physical activity has led to limitations in EE-related studies focusing on early intervention. But existing researches are enough to prove the positive role that early EE plays in neurodevelopment in which dendrite branches (Venable et al., 1989), neuronal differentiation ability (Pascual and Figueroa, 1996), exploration activities, learning and memory ability (Lu et al., 2017), and inhibitory to excitatory balance (Feng et al., 2021) in the hippocampus are improved observably. Especially in the visual system, early EE can not only promote the development of the visual cortex but also accelerate the development of the retina in terms of substantially no plasticity. The mechanism involved is inseparable from the secretion of neurotrophic factors BDNF and IGF-1 (Landi et al., 2007a,b, 2009).

Without considering the element of voluntary physical activity, we continue to explore reliable evidence that other aspects of EE contribute to the neurodevelopment of pre-weaning pups. On the one hand, in a rich housing environment, mouse pups are more receptive to sensory stimuli, including maternal or non-maternal licking and physical contact such as beard stimulation. Massage that mimics maternal care accelerated the development of the rodent brain and the maturation of visual function (Guzzetta et al., 2009) and promoted weight gain in human premature and low-birth-weight infants (Vickers et al., 2004). Furthermore, the discovery that oxytocin enhanced the motor performance of pre-weaning mice associated with beard stimulation (Tabbaa and Hammock, 2020) also demonstrates that tactile sensory stimulation is an indispensable element for the positive effects of early EE on neurodevelopment. On the other hand, studies have highlighted the importance of social contact during pregnancy and breastfeeding for optimal offspring development in terms of behavior and age. The emotional and cognitive benefits offered by EE are primarily dependent on social interaction. Common nesting (CN) is a model of social enrichment in mice during pregnancy and early lactation. In the CN model, multiple mothers raise more pups, meaning that pups are more exposed to diverse social stimuli. Compared to standard reared, the CN offspring in adulthood showed more social interactivity in task activities, less anxious behavior in the open domain, and more escape attempts in the forced swimming task (Curley et al., 2009; Martinez et al., 2015). Therefore, early EE was mainly focused on physical exercise in pregnancy and more targeted sensory and social stimulation in lactation to promote offspring neural development and neural circuit construction.

Impact of environment on development during "adolescence"

Adolescence is the primary postpartum neurodevelopmental period of adult social and cognitive skills maturation, as well as a period of high neuroplasticity of brain development. Rats mature approximately 30 times faster than humans (Quinn, 2005), and the definition of adolescence in animals is based on actual age rather than adolescence, which is roughly divided into early adolescence (P21–34), mid-adolescence (35–46), and late adolescence (47–59; Holder and Blaustein, 2014). The effects of EE on brain plasticity and behavior in adolescent rodents were more significant compared with those before weaning due to the more complex neural circuits and the approaching maturity of the nervous system. In terms of performance of selective and auditory sustained attention, mild adolescent exposure to EE maximizes significant and long-term effects compared to other developmental trajectories such as prenatal or adulthood (Korkhin et al., 2020). EE interventions during adolescence have been used to neutralize the adverse neurodevelopmental hazards of stress during different periods. Postweaned EE can reverse learning and memory impairment in prenatal stress offspring, involving mechanisms associated with lowering plasma corticosterone and increasing the expression of hippocampal IGF-2 and cytoskeletal proteins (Guan et al., 2021). Analogously, spatial learning and memory impairment due to maternal separation before weaning is terminated by enhanced TrkB/BDNF signaling induced by adolescent exposure to EE (Mohammadian et al., 2019; Cordier et al., 2021). Interestingly, new objective recognition of memory and anxiety-like behaviors effects of EE exposure in adolescence appear sex-dependent (Sakhaie et al., 2020).

In addition, we analyzed the contributions of physical exercise and EE to neurodevelopment during adolescence (**Table 1**). Both pubertal exercise and EE ameliorated deficiencies in water maze learning, hippocampal LTP, and BDNF levels elicited by prenatal morphine exposure (Ahmadalipour et al., 2018). In terms of anxiolytic and activity levels, EE and exercise also had comparable effects on CD-1 mice (Aujnarain et al., 2018). Exercise alone can lead to some impacts that appear to be similar to the effects of EE. Still, detailed analysis will reveal how different these seemingly identical effects actually are, such as the the expression of some protein levels in the hippocampus. In the studies of hippocampal plasticity, it was found that IGF-1 responded positively to EE rather than exercise training. The opposite result was obtained in terms of declining corticosterone and parvalbumin expression. Physical activity was superior to EE for an increase in the number of cells in the CA1 (Serra et al., 2020; Rostami et al., 2021). In addition to the changes in the hippocampus, EE was able to regulate leptin sensitivity in young mice and leave metabolic and synaptic imprints to prevent obesity, the mechanism of which involves an increase in activation of STAT3 and a transfer of the excitation/inhibition balance toward the form er in α-melanocyte-stimulating hormone (α-MSH) neurons and toward the latter in agouti-related peptide (AgRP)/Neuropeptide Y (NPY) neurons. However, the above changes produced by physical exercise are not significant as EE and do not involve an effect on synaptic connections (Mainardi et al., 2010). The above results suggest that physical exercise, one of the components of EE, is not in any way weaker than or equal to EE in its impact on neurodevelopment and maturation.

Neural consequences of EE

Brain volume

The early discovery that wild rats and mice living in EE not only have increased active exploration behavior but also possess more outstanding learning and memory abilities and problem-solving abilities than animals in standard rearing cages attract researchers to study the anatomical changes caused by EE Compared with the normal group, male rats exposed to EE for 30 days showed increased dry and wet brain weight and cortical thickness, especially occipital somesthetic and dorsal cortex (Bennett et al., 1969). Subsequent, more detailed study of EE's effects on the cerebral cortex suggested that the changes of cortical thickness were independent of the age of animals, and 30 days instead of a longer time EE had the broader effects on cortex depth (Diamond et al., 1972). This finding may be related to the decline in environmental novelty due to long-term EE. Outside the cortex, EE also aggrandizes the hippocampus, striatum, and midbrain volume (Scholz et al., 2015).

Neurogenesis

Changes in the appearance of the brain have also led scientists to explore microscopic structures. The influence of EE on the number of cells in the adult brain dates back to 1964. A study investigating whether EE enhances the number of neurons found only the genesis of neurogliacyte (Altman and Das, 1964). The probable reason for the failure of new neuron observation was that the research focuses on the cortex rather than the hippocampus. Subsequent studies demonstrated that the increased glial cells were mainly derived from astrocytes (Walsh et al., 1969; Kronenberg et al., 2007) and oligodendrocytes (Szeligo and Leblond, 1977), whose cell morphology was also affected by EE. The 1997 study was the first to suggest that EE increased the number of hippocampal nerve cells in adult mice (Kempermann et al., 1997). Larger hippocampal granulosa cell layers and the 15 percent more granule cell neurons in the dentate gyrus (DG) were discovered in mice living in EE Adult neurogenesis is a crucial mechanism for the beneficial effects of positive living, enabling mice in EE to learn more flexibly (Garthe et al., 2016). Only neurons that undergo a complete process of proliferation, migration, differentiation, and survival can be called successful neurogenesis. Voluntary exercise-induced hippocampal neurogenesis was attributed to cell proliferation, and neuronal survival did not differ from the standard group. Conversely, EE promotes the survival of the neuronal precursors in the hippocampal DG but has no significant effect on the proliferation of neural progenitor cells (van Praag et al., 1999). This means that the mechanism by which new cells are produced in the same genetic context depends on different living environments.

Furthermore, the relationship between the effect of EE on neurogenesis and the age of the target is also quite subtle. Based on the study that EE expedites neurogenesis in adult hippocampus, exposure of adult mice aged 10–20 months to EE showed a fivefold increase in hippocampal neurogenesis (Kempermann et al., 2002). Similarly, comparison of neurogenesis in hippocampal DG area of old and young rats shows that the number of newborn cells of old and young rats is significantly higher than that of control rats after EE, even though the number of newborn cells of old rats is markedly less than that of young rats (Segovia et al., 2006). The above experiments indicate that EE can exert a long but not short effect on neuroplasticity across an extensive age range. However, mice that received EE stimulation 7–21 days after birth was detected with significant differences in autonomic movement but no substantial changes in hippocampal nerve cell proliferation at the age of 4 months compared with the control group (Kohl et al., 2002). This suggests that EE is not highly correlated with hippocampal neurogenesis and the maintenance of neuroplasticity. The reason for this result may be due to the small amount of exercise in mice before weaning and the confusion of EE and maternal effect. Given the age of EE's target

TABLE 1 Effects of physical activity and EE on brain development.

Period	Intervention	Strategy	Mechanisms	Effects	References
Pregnancy	EE	44 × 62 × 28 cm	Increasing expression of precocious cAMP response element-mediated gene, BDNF and GAD65/67	An earlier eye opening, a precocious development of visual acuity, and an accelerated decline of white matter-induced long-term potentiation	Cancedda et al. (2004) and Sale et al. (2004)
	EE	100 × 50 × 82 cm	Increasing expression of IGF-1	Accelerating the migration of neural progenitor cells in the fetal retinal ganglion cell layer and the natural death of ganglion cells and promoting the transfer of nutrients from the placenta to the fetus	Sale et al. (2007)
	EE	60 × 45 × 76 cm	Increasing expression of SYN, PSD-95, an BNDF	Reversing cognitive impairment in elderly offspring caused by long-term radiation exposure	Hong et al. (2020)
	Voluntary exercise	Squat exercise and tower climbing	No found	Heavier and longer mid-uterine horn fetuses and greater placental weight	Rosa et al. (2011)
	Treadmill exercise	At a slope of 0°at 2 m/min for the first 5 min, 5 m/min for the next 5 min, and 8 m/min for the last 20 min	Increasing expression of Bcl-2, BDNF, and TrkB Inhibiting expression of Bax	Promoting hippocampal cell proliferation to improve spatial learning	Kim et al. (2021)
	Treadmill exercise	The intensity of activity in the early, middle and late stages of the embryo was 40% VO_2max, 65% VO_2max, and 50% VO_2max	Activation of apelin-AMPK signaling	Protecting offspring from diet-induced obesity and metabolic disorders	Son et al. (2022)
Pre-weaning	EE	70 × 70 × 40 cm	No found	Increasing basal dendrite branches of pyramidal neurons in occipital cortex	Venable et al. (1989)
	EE	40 × 70 × 100 cm	No found	Promoting differentiation of pyramidal neurons in motor and visual cortex II and III	Pascual and Figueroa (1996)
	EE	62 × 50 × 40 cm	Increasing field excitatory postsynaptic potentials and activation of ERK signaling	Enhancing hippocampal-dependent learning and memory function	Lu et al. (2017)
	EE	60 × 45 × 20 cm	Maintaining the inhibitory to excitatory balance in the hippocampus	Promoting experience-dependent inhibitory plasticity	Feng et al. (2021)
	EE	60 × 50 × 80 cm	Increasing expression of IGF-1 and BDNF	Speeding up the development of the retina	Landi et al. (2007a)
Adolescence	EE	90 × 50 × 60 cm	Increasing expression of IGF-2 and activity-regulated cytoskeletal-associated protein	Repairing learning and memory impairment in offspring of prenatal stress	Guan et al. (2021)
	EE	90 × 60 × 75 cm	Increasing expression of TrkB and BDNF	Improving the effects of maternal separation on spatial learning and memory	Cordier et al. (2021)
	Treadmill exercise	Running at a speed of 2 m/min for the first 5 min, 5 m/min for the next 5 min and then at a speed of 8 m/min for the last 20 min, at a 0° inclination	Enhancing LTP and expression of BDNF	Reversal of spatial learning impairment induced by prenatal morphine exposure	Ahmadalipour et al. (2018)
	EE	100 × 100 × 50 cm			
	Treadmill exercise	Running time and speed started at 8 m/min for 5 min and gradually increased over this period, reaching a maximum of 18 m/min for 60 min	Increasing the total number of parvalbumin cells of subiculumand CA2/3 region (EX>EE)	Promoting early brain development	Aujnarain et al. (2018)

(*Continued*)

TABLE 1 Continued

Period	Intervention	Strategy	Mechanisms	Effects	References
	EE	60 × 30 × 49 cm			
	Combined exercise training	Aerobic and resistance training was performed on even and odd days	Increasing expression of IGF-1 Inhibiting expression of corticosterone and the cell numbers of the hippocampus (EE > EX)	Promoting the downstream plasticity effects on the hippocampus	Rostami et al. (2021)
	EE	40 × 60 × 90 cm			
	EE	44 × 62 × 28 cm	Reducing leptin release and increasing leptin sensitivity and the activation of STAT3 pathway (EE > EX)	Improving glucose tolerance, feeding behavior, and leptin sensitivity to prevent obesity	Mainardi et al. (2010)
	Physical exercise	Free access to a running wheel	Ehancing synaptic connections (Only in EE)		
Adutlhood	EE	86 × 76 cm (No found in height)	No found	Increasing the volume of the hippocampal structure and sensorimotor cortex	Scholz et al. (2015)
	EE	46.2 × 40.3 × 40.4 cm	Promoting the survival of the neuronal precursors in the hippocampal DG	Promoting neurogenesis in the hippocampus	van Praag et al. (1999)
	Physical exercise	Running wheel for voluntary	Accelerating cell proliferation		
	EE	45.5 × 21.5 × 12 inches	Activating FGFR signaling	Promoting neurogenesis in the hippocampus	Grońska-Pęski et al. (2021)
	Physical exercise	Two running wheel for voluntary			
	EE	85 × 75 × 40 cm	Increasing oligodendrocyte-specific RNAs expression	Adding more new axons with sheaths and improving motor coordination	Goldstein et al. (2021)
	EE	24 × 20 × 46 cm	More oligodendrocyte progenitor cells proliferation and oligodendrocyte mature cells in the sensorimotor cortex	Accelerating axon development	Keiner et al. (2017)
	EE	82 × 61 × 45 cm	Increasing spinophilin mRNA expression	Increasing dendritic sprouting and number of dendritic spines	Hu X.-L. et al. (2010)
	EE	36 × 23 × 18 cm	Increasing synaptophysin and PSD-95 expression	Improving synaptogenesis	Nithianantharajah et al. (2004)
Aging	EE	120 × 100 × 60 cm	Enhacing the extracellular concentrations of glutamate and GABA in the hippocampus	Promoting neurogenesis in the hippocampus	Segovia et al. (2006)
	EE	44 × 62 × 28 cm	Reducing the inflammatory chemokine ccl11/eotaxin-1 expression	Improving learning and memory function in elderly mice	Scabia et al. (2021)

Abbreviations: IGF-1, insulin-like growth factors -1; BDNF, brain-derived neurotrophic factor; IGF-2, insulin-like growth factors -2; TrkB, Tyrosine Kinase receptor B; ERK, extracellular regulated protein kinases; LTP, Long-term potentiation; AMPK, AMP-activated protein kinase; Bcl-2, B-cell lymphoma-2; Bax, BCL2-Associated X; DG, dentate gyrus; FGFR, fibroblast growth factor receptor; PSD-95, postsynaptic density-95; EX > EE, the effect of exercise is more significant than EE; EE > EX, the effect of EE is more significant than exercise.

and the specific EE strategies, it remains to be seen whether the impact of enrichment on the plasticity of the CNS is maintained over the long term.

At present, the research on the mechanism of EE affecting neurogenesis is still being explored. Early experiments have shown that EE can enhance the growth factors that promote neurogenesis, including brain-derived neurotrophic factor (BDNF; Zorzin et al., 2021), nerve growth factor (NGF; Pham et al., 1999), glial cell-derived neurotrophic factor (GDNF; Young et al., 1999), vascular endothelial cell growth factor (VEGF; Cao et al., 2004). A recent study suggests that EE and exercise can also enhance adult hippocampal neurogenesis through fibroblast growth factor receptor (FGFR), which induces the proliferation of stem and progenitor cells (Grońska-Pęski et al., 2021).

Neurite growth and synaptogenesis

In addition to affecting the production of new hippocampal DG neurons, EE also leads to further morphological changes. Axon plays a vital role in the functional connection between neurons and target cells at any stage of life. The formation of CNS complex networks is highly dependent on the degree of axon differentiation during normal development. Early

EE intervention extended the axon initial segment of the neocortex to modulate cell excitability (Nozari et al., 2017) and lengthened the axon terminals in the absence of any nerve damage (Fernández-Montoya et al., 2018). Semaphorin-3a of perineuronal nets, a kind of axon growth inhibition factor, was significantly reduced after EE (De Winter et al., 2016). EE for 30 days did not initially increase oligodendrocytes and myelin expression in the white matter. Follow-up studies were surprised to find that 60 days of EE enhanced the g/ratio and more new myelinated axons in 90 days of EE, which suggests that the effects of EE on axons begin with the thickening of myelin fibers followed by an increase in the number of internodes (Goldstein et al., 2021). In addition, more oligodendrocyte progenitor cells proliferation and oligodendrocyte mature cells were detected in the sensorimotor cortex at 10 and 42 days of EE intervention, respectively (Keiner et al., 2017), which indicats EE will accelerate axon development. Unfortunately, there are relatively few studies on EE and positive growth and correct guidance of axons under normal development.

Dendrites, one to more protrusions, emanated from the cell bodies, are responsible for receiving stimuli and transmitting nerve impulses to the cell body of other nuerons. The length, number, branches, and other developmental conditions of dendrites can affect the reception of signals and thus influence the formation of neural circuits. Earlier studies have shown that EE leads to the development of higher-order dendritic branches and denser dendritic spines in vertebral neurons of the occipital (Greenough and Volkmar, 1973), frontotemporal (Greenough et al., 1973), and parietal lobes (Leggio et al., 2005). However, the molecular mechanisms underlying changes in dendritic structural plasticity have rarely been explored. Spinophilin is highly enriched in dendritic spines and is involved in spinal morphology and synaptic plasticity. One week after EE, the density of spinophilin immunoreaction in the hippocampus and cortex augmented instantaneously. In the following 3 weeks of EE intervention, spinophilin mRNA continued to grow (Hu X.-L. et al., 2010).

It is well known that the positive response of dendritic morphology and associated synaptic proteins are strong evidence that EE improves synaptogenesis. EE rats showed a significant increase in SYN, synapsin I, and PSD-95 protein expression (Nithianantharajah et al., 2004; Birch et al., 2013). Interestingly, the distinction between EE physical and social elements was found to have different effects on synaptogenesis. The density of dendritic spines increased in the DG of the social group and the CA1 of the activating group (Gabriel et al., 2020). The reasons for this need to be further explored according to the anatomical characteristics of the hippocampus and different environmental factors. Furthermore, BDNF plays an essential role in EE-induced morphological plasticity of dendritic spines and hippocampal synaptogenesis (von Bohlen und Halbach and von Bohlen und Halbach, 2018). The exact mechanism underlying these effects remains uncertain. The research found that the kinesin superfamily motor protein 1A (KIF1A) was specifically upregulated in the hippocampal region of EE mice. Excitingly, the level of KIF1A and KIF1A mediated cargo transport was positively correlated with BDNF expression. Subsequent studies demonstrated that EE could not induce induced hippocampal synaptogenesis and learning enhancement *via* BDNF in KIFIA knockout mice (Kondo et al., 2012). The result may be applied to explain the mechanism of motion elements of EE in the future.

The effects of EE on CNS disorders

In addition to being widely used in the study of normal animal models, EE is also widely used in the study of various neurological/psychiatric disease models, such as AD, PD, HD, stroke, epilepsy, down syndrome, drug addiction, depression, schizophrenia, attention deficit, and hyperactivity disorder, etc. Studies have shown that EE has beneficial effects on these diseases, and people have even explored the potential of EE as a means of treatment and rehabilitation for these diseases (Kotloski and Sutula, 2015). Here we focus on the neural repair mechanisms of EE in the CNS, especially in stroke.

EE and cerebral ischemia

Stroke is the second leading cause of death and disability worldwide. Cerebral ischemia caused by arterial occlusion is a common type of stroke. The death of neurons in the ischemic core result in irreversible neurodevelopmental damage. Although some molecular mechanisms related to the pathogenesis of cerebral ischemia have been explored in animal experiments, there is still a lack of comprehensive understanding of its pathological process. Due to the current treatment of patients in the subacute stage and acute stage being mainly single drug treatment, more and more scientific research has turned to nonpharmacologic strategies, in which the study of EE on the repair of neurodevelopmental disorders after cerebral ischemia has been carried out in multiple dimensions.

At the level of brain structure, the results of most studies on whether EE can reduce the volume of cerebral infarction are positive (Gonçalves et al., 2018; Deng et al., 2021; Liu et al., 2021). At the same time, the EE group rats showed fewer neurological deficits after ischemia, which hints that EE may save the death of ischemic penumbra neurons. Of course, EE had little effect on the infarct in a subset of ischemic studies (Dahlqvist et al., 1999; Yu et al., 2013a). Surprisingly, premature exercise or administration of EE even enlarged infarct size (Risedal et al., 1999). The results of meta-analysis also support the above view. The reason may be that in the early stage of cerebral infarction, the fear caused by the need for experimental animals to adapt to the new environment results in delayed

tissue injury and increased infarct volume (Janssen et al., 2010). In other words, since most EE interventions are performed 24 h after ischemia, changes in the new environment compared with the initial living environment, including surrounding scene and social interaction may increase the possibility of late tissue loss. The difference of EE on cerebral infarction volume outcome may also be related to various EE settings. Therefore, the relationship between EE and infarct volume needs to be discussed systematically, and the factors such as age, gender, and strain of experimental animals need to be considered.

As with normal neural development, EE also increases neural stem cell and progenitor cell proliferation and neurogenesis of the subventricular zone (Komitova et al., 2005) and hippocampus (Matsumori et al., 2006) after cerebral ischemia. The mechanism of EE promoting neurogenesis after cerebral ischemia is largely related to gliogenesis, especially in astrocytes. On the one hand, EE can comprehensively improve the neurological function of stroke rats through BDNF released by proliferating astrocytes (Chen et al., 2017). On the other hand, EE promotes cytoplasmic to nuclear transfer of nuclear factor κB (NF-κB)/p65 in activated astrocytes, which enhances gene expression of interleukin 17A to facilitate neurogenesis directly (Zhang et al., 2018). It is widely accepted that rehabilitation after stroke requires the cooperation of nerve and vascular tissues. Effective neurovascular reconstruction after ischemia plays a crucial role in the repair of subsequent developmental injury. EE rapidly promotes angiogenesis through different mechanisms to improve physical and cognitive recovery in animal models of ischemic stroke. A significant increase in angiogenesis specific marker CD31 was observed in the cortical area around infarction after EE, and the neurological function was positively correlated with angiogenesis (Yu et al., 2014). When sub-components were isolated to dissect their contribution to the total effect of EE by rearing animals either by stimulating physical exercise, or under social enrichment alone, the results showed that complete EE had a more significant benefit than single sub-components on microvessel density, as manifested by elevated expression of angiopoietin 1, VEGF, and CD31 (Zhang et al., 2021). The mechanism underlying angiogenesis may be mediated by hepatocyte growth factor, a blood-derived factor, which was elevated by EE in cortex and serum after middle cerebral artery occlusion (MCAO). The statement stems from the finding that survival and proliferation of endothelial cells were significantly improved when co-cultured with serum and plasma derived from EE after ischemia (Xie et al., 2019). In addition, magnetic resonance angiography showed selective amplification of basilar, internal carotid, and middle cerebral artery signals after MCAO *via* a three-stage EE paradigm designed according to different stages of cerebral ischemia, which was regulated partially by phosphatidylinositol 3-kinase (PI3K)/protein kinase B (AKT)/glycogen synthase kinase-3 (GSK-3)/β-catenin and the axon guidance molecules (Zhan et al., 2020).

At the molecular level, the repair of damaged brain tissue after cerebral ischemia is dependent on the high release of endogenous growth factors. EE mainly enhances BNDF (Shono et al., 2011; Yu et al., 2020), VEGF (Wu et al., 2018), and NGF (Dahlqvist et al., 2003) to induce neurogenesis, angiogenesis, and synaptogenesis after reperfusion to achieve recovery of physical and cognitive functions. At the functional level, post-stroke cognitive impairment (PSCI) is a major obstacle on the road to neural restoration. We have systematically summarized the recovery mechanism of PSCI after EE paradigms, including cell death, synaptic plasticity, cholinergic circuit, and cerebral blood flow (Yuan et al., 2021). It should be added here that, in addition to classic apoptosis, the latest research shows that EE also alleviates pyroptosis by inhibiting NF-κB/p65 to ameliorate neurological deficits (Liu et al., 2021). Similarly, it is necessary to explore the relationship between other forms of cell death and EE promoting recovery in the future, such as ferroptosis, which occurs largely after cerebral ischemia (She et al., 2020). Brain plasticity is not only the principle of normal brain development, but also plays an irreplaceable role in nerve repair after injury besides spontaneous repair. A recent study has indicated that EE can increase the expression of growth-associated protein (GAP-43) and SYN in bilateral cerebral hemispheres. Interestingly, the incremental expression of synapse-associated proteins on the contralateral side of injury has a higher correlation with cognitive function compared with the ipsilateral side (Wang et al., 2019). In addition to the cholinergic circuit (Wang et al., 2016; Yuan et al., 2020), the upregulation of GABAergic and glutamatergic systems under the effect of EE in the contralateral hippocampus is also committed to the remission of PSCI (Wang et al., 2020), which suggests that EE recovery of PSCI is no longer limited to the damaged hemisphere at least in terms of synaptic plasticity and neurotransmitter system.

Other neurobiological disorders

In addition to cerebrovascular accident, the structural and functional impairment caused by neurodegenerative diseases can be repaired effectively. Studies have found that EE exposure can reduce the probability of hippocampal nerve injury in AD animals, enhance synaptic plasticity, and reduce hyperphosphorylated tau protein and cortical amyloid β-protein in the hippocampus. The abundance level of amyloid improves the decline of memory function (Hu Y.-S. et al., 2010; Valero et al., 2011; Salmin et al., 2017). A study based on resting fMRI found that EE exposure enhanced the functional connection between hippocampal CA1 and cortex of AD transgenic animals (Little et al., 2012). EE exposure can alos reduce the loss of dopaminergic neurons in substantia nigra compacta of PD animals, reduce the expression of dopamine transporter expression (DAT), increase the level of BDNF and

improve motor dysfunction (Goldberg et al., 2011; Fischer, 2016). EE exposure can also restore the level of BDNF in HD animals, improve motor function, restore hippocampal neurogenesis, and alleviate the atrophy of cerebral cortex volume (Nithianantharajah and Hannan, 2006; Fischer, 2016). Three weeks of EE exposure can enhance the resistance of rats to seizures, reduce hippocampal cell apoptosis, promote hippocampal neurogenesis, increase the expression of GDNF and BDNF, increase animal exploration activities and improve spatial learning ability. Even in the absence of neurodegenerative diseases, a decline in cognitive abilities is accompanied by brain aging. Recent studies have demonstrated that EE can improve learning and memory function in elderly mice by reducing pro-inflammatory chemokines ccl11/eotaxin-1, a marker of aging (Scabia et al., 2021).

Moreover, EE exposure can also reduce the strengthening and seeking of psychostimulants (such as cocaine, amphetamine, morphine, nicotine, etc.) and reduce the risk of relapse. These behavioral changes caused by EE are related to the reduction of the functional activities of some brain regions involved in drug seeking and relapse, such as nucleus accumbens, dorsal striatum, amygdala, ventral tegmental area substantia nigra, prefrontal cortex, and cingulate cortex (Solinas et al., 2008, 2010; Thiel et al., 2010; Chauvet et al., 2011; Gill et al., 2014; Sikora et al., 2018) and are related to the reduction of the drug-induced DAT in the striatum and prefrontal cortex, dopamine uptake and the rate-limiting enzyme of dopamine synthesis-tyrosine hydroxylase (Zakharova et al., 2009; Läck et al., 2010; Wooters et al., 2011). In animal models of anxiety and depression, EE also has similar anti-anxiety and anti-depression effects. For example, animals with EE showed lower pleasure deficiency-like behavior in the sugar water preference test, less social withdrawal in the social interaction test and less immobility in the forced swimming test (Zhang et al., 2014).

Challenges and expectations facing EE

Effect weight of stimulus in EE

EE is mainly composed of novel sensory stimulation, sports, and social interaction. A study of perinatal hypoxic-related white matter damage in the brain suggests that a single running wheel, a single novel sensory stimulus, and social interaction have little behavioral and cellular molecular impact on the repair of white matter damage. Only complete EE can have the best effect on neural development and repair, which is basically consistent with the results of the EE element separation experiment mentioned above (Forbes et al., 2020). It shows that the impact of a any factor of EE cannot be isolated easily, and its influence is the interaction between various essential elements nor the result of any single aspect. However, it is unknown whether different factors play different roles in the effects of EE and the weight of the importance of the three factors. Again, this needs to be demonstrated by more rigorous EE element separation experiments.

Window period and duration of EE

Finding the optimal intervention window is critical for CNS recovery. Studies have shown that delayed, late, and prolonged EE do not cause changes in brain plasticity and function in neonatal hypoxia models (Forbes et al., 2020). Early EE intervention for a week only resulted in differential changes at the cellular level, such as promoting oligodendrocyte differentiation and the production of more oligodendrocyte lineage cells. EE intervention lasting 30 days had positive behavioral and cellular molecular effects. Furthermore, EE has made a breakthrough in the research on promoting the visual system's development to explore the intervention window. EE accelerates brain development by acting on the opening and closure of the critical period, as well as being able to reopen the critical period in the adult animal (Morishita and Hensch, 2008). The underlying molecular mechanisms include enhanced serotonin release, decreased inhibitory/excitatory balance, and increased expression of BDNF and IGF-1 (Sale et al., 2014). Reopening the sensitive stage of adult brain plasticity may eventually lead to the restoration of visual function in adult animals with amblyopia at the functional level while improving the plasticity of the visual cortex. Spatially, most EE is performed after the onset of the disease. Encouragingly, EE preconditioning was also associated with injury repair, as demonstrated in models of acute retinal ischemia (González Fleitas et al., 2019) and cerebral ischemia (Yu et al., 2013b). The mechanism of EE preconditioning may be partly related to the reduction of oxidative stress and inflammatory response.

In addition, in terms of time, current animal model studies generally adopt long-term EE exposure, but there are few studies on the impact of a week or a few days of EE expose-related brain. In fact, 24 h of EE exposure was sufficient to improve target recognition memory and was maintained after a more extended period of EE exposure (Kobayashi et al., 2002; Leger et al., 2015). Even dozens of minutes and hours of novel EE exploration can lead to increased activity in multiple brain regions, including the motor cortex, prefrontal cortex, striatum, and hippocampus, etc. (Ali et al., 2009; Rinaldi et al., 2010). A recent study on manganese-enhanced magnetic resonance imaging *in vivo* found that subacute EE exposure at 7 days resulted in volume changes in multiple brain regions. At the same time, EE-related functional changes are not always accompanied by structural changes, and functional changes do not always accompany structural changes. Still, there is a robust structural connection between brain regions with

increased volume and brain regions with increased functional activity (Li et al., 2020). Therefore, subsequent studies on EE should appropriately focus on preconditioning and short-term intervention in order to explore the mechanism of EE from a broader dimension.

Clinical transformation of EE

The classical theory holds that individual phenotype is determined by the interaction of genetic background and environment (Rogers et al., 2019). EE consists of shared environment (such as urban transportation, urban buildings, work units, etc.) and non-shared environment (such as family residence, family background, physical characteristics, etc.). In the same shared environment, individual phenotype differences depend on genetic background and non-shared environment. Individual responses to environmental stimuli are different, which may indicate that the individual steady state has varying degrees of influence on brain plasticity. Recent studies have shown that early EE can lead to persistent individualized changes in behavior, brain plasticity, and epigenetics, even under the condition of controlling genetic background and shared environment (Kempermann, 2019; Zocher et al., 2020). Ethology and epigenetics may be one of the most meaningful topics in future EE exploration.

However, in terms of clinical transformation, it is easier to increase shared environment and reduce non-shared environment as much as possible for inpatients, such as the rehabilitation treatment after stroke in the hospital. However, for out-of-hospital patients, not only the shared environment is variable, but also the non-shared environment is diverse, which is the difficulty of EE transformation. In addition, there are many technical constraints: (1) how the rearing condition in animal experiments correspond to the mode and environment of treatment in clinical practice, and whether the transformation of standardized cages into standardized housing means that life lacks characteristics; (2) it is difficult to achieve standardized environmental conditions between hospitals or between hospital departments let alone the intervention of patients outside hospitals; (3) there is currently a lack of theoretical knowledge on what kind of environmental integration can promote brain plasticity. For the clinical transformation of EE, we can first clarify the molecular mechanism of EE action in animal models, find the critical molecular substrate of EE effect, and develop drugs simulating the action of EE for this molecule. The study demonstrating that reduction of intracortical inhibition can partly restore ocular dominance plasticity in adult rats suggests a possible strategy to mimic the effects of EE (Harauzov et al., 2010). This would lay the ground for reviewing the possible strategies used to reproduce the effects of EE (e.g., by using fluoxetine; Maya Vetencourt et al., 2008) in a more "standardized" manner, with the goal of minimizing the interindividual variations in response to EE. Perhaps elucidating the neural mechanism of EE action and developing devices based on this mechanism to regulate related neural activity is a good choice. Although the road ahead is fraught with difficulties, the future of clinical transformation of EE is still foreseeable.

Conclusion

At present, both animal experiments and clinical studies have proved that environment-dependent brain plasticity is crucial for normal brain neural development and the repair of neurological disorders. EE not only changes basic brain anatomy, but also modulates electrophysiology, neurotrophic factors, and protruding plasticity. At the same time, the multi-dimensional effect of EE on nerve repair in CNS injury has enabled researchers to see therapeutic approaches that do not rely on drugs. However, there are also some contradictory studies, such as the influence of EE on the size of cerebral infarction. Although the level and dimension of EE research are more and more extensive, it still faces many challenges. In the future, window periods and clinical transformation of EE are urgently needed. At the same time, the research direction of EE on neural development and repair should be carried out in a broader direction, among which the study of individuation and epigenetics is worthy of in-depth exploration.

Author contributions

MY and Y-SG designed the structure of the manuscript. X-YS and Z-KG managed the literature searches and analyses. YH wrote the manuscript. XB assisted with the improvement of the manuscript. All authors contributed to the article and approved the submitted version.

Funding

This study was supported by grants from the Featured Clinical Discipline Project of Shanghai Pudong No. PWYts2021-10 (to XB).

Conflict of interest

The authors declare that the research was conducted in the absence of any commercial or financial relationships that could be construed as a potential conflict of interest.

Publisher's Note

All claims expressed in this article are solely those of the authors and do not necessarily represent those of their affiliated organizations, or those of the publisher, the editors and the reviewers. Any product that may be evaluated in this article, or claim that may be made by its manufacturer, is not guaranteed or endorsed by the publisher.

References

Ahmadalipour, A., Ghodrati-Jaldbakhan, S., Samaei, S. A., and Rashidy-Pour, A. (2018). Deleterious effects of prenatal exposure to morphine on the spatial learning and hippocampal BDNF and long-term potentiation in juvenile rats: beneficial influences of postnatal treadmill exercise and enriched environment. *Neurobiol. Learn. Mem.* 147, 54–64. doi: 10.1016/j.nlm.2017.11.013

Ali, A. E.A., Wilson, Y. M., and Murphy, M. (2009). A single exposure to an enriched environment stimulates the activation of discrete neuronal populations in the brain of the fos-tau-lacZ mouse. *Neurobiol. Learn. Mem.* 92, 381–390. doi: 10.1016/j.nlm.2009.05.004

Altman, J., and Das, G. D. (1964). Autoradiographic examination of the effects of enriched environment on the rate of glial multiplication in the adult rat brain. *Nature* 204, 1161–1163. doi: 10.1038/2041161a0

Altschuler, R. A. (1979). Morphometry of the effect of increased experience and training on synaptic density in area CA3 of the rat hippocampus. *J. Histochem. Cytochem.* 27, 1548–1550. doi: 10.1177/27.11.512348

Aujnarain, A. B., Luo, O. D., Taylor, N., Lai, J. K. Y., and Foster, J. A. (2018). Effects of exercise and enrichment on behaviour in CD-1 mice. *Behav. Brain Res.* 342, 43–50. doi: 10.1016/j.bbr.2018.01.007

Ayerbe, L., Ayis, S., Crichton, S., Wolfe, C. D. A., and Rudd, A. G. (2013). The natural history of depression up to 15 years after stroke: the South London Stroke Register. *Stroke* 44, 1105–1110. doi: 10.1161/STROKEAHA.111.679340

Aznar, S., and Knudsen, G. M. (2011). Depression and Alzheimer's disease: is stress the initiating factor in a common neuropathological cascade? *J. Alzheimers Dis.* 23, 177–193. doi: 10.3233/JAD-2010-100390

Bennett, E. L., Rosenzweig, M. R., and Diamond, M. C. (1969). Rat brain: effects of environmental enrichment on wet and dry weights. *Science* 163, 825–826. doi: 10.1126/science.163.3869.825

Birch, A. M., Mcgarry, N. B., and Kelly, A. M. (2013). Short-term environmental enrichment, in the absence of exercise, improves memory and increases NGF concentration, early neuronal survival and synaptogenesis in the dentate gyrus in a time-dependent manner. *Hippocampus* 23, 437–450. doi: 10.1002/hipo.22103

Borba, L. A., Broseghini, L. D. R., Manosso, L. M., De Moura, A. B., Botelho, M. E. M., Arent, C. O., et al. (2021). Environmental enrichment improves lifelong persistent behavioral and epigenetic changes induced by early-life stress. *J. Psychiatr Res.* 138, 107–116. doi: 10.1016/j.jpsychires.2021.04.008

Bourdon, E., and Belmin, J. (2021). Enriched gardens improve cognition and independence of nursing home residents with dementia: a pilot controlled trial. *Alzheimers Res. Ther.* 13:116. doi: 10.1186/s13195-021-00849-w

Bruno, R. M., Stea, F., Sicari, R., Ghiadoni, L., Taddei, S., Ungar, A., et al. (2018). Vascular function is improved after an environmental enrichment program: the train the brain-mind the vessel study. *Hypertension* 71, 1218–1225. doi: 10.1161/HYPERTENSIONAHA.117.10066

Campbell Burton, C. A., Murray, J., Holmes, J., Astin, F., Greenwood, D., and Knapp, P. (2013). Frequency of anxiety after stroke: a systematic review and meta-analysis of observational studies. *Int. J. Stroke* 8, 545–559. doi: 10.1111/j.1747-4949.2012.00906.x

Cancedda, L., Putignano, E., Sale, A., Viegi, A., Berardi, N., and Maffei, L. (2004). Acceleration of visual system development by environmental enrichment. *J. Neurosci.* 24, 4840–4848. doi: 10.1523/JNEUROSCI.0845-04.2004

Cao, L., Jiao, X., Zuzga, D. S., Liu, Y., Fong, D. M., Young, D., et al. (2004). VEGF links hippocampal activity with neurogenesis, learning and memory. *Nat. Genet.* 36, 827–835. doi: 10.1038/ng1395

Chae, S. A., Son, J. S., and Du, M. (2021). Prenatal exercise in fetal development: a placental perspective. *FEBS J.* 289, 3058–3071. doi: 10.1111/febs.16173

Chauvet, C., Lardeux, V., Jaber, M., and Solinas, M. (2011). Brain regions associated with the reversal of cocaine conditioned place preference by environmental enrichment. *Neuroscience* 184, 88–96. doi: 10.1016/j.neuroscience.2011.03.068

Chen, X., Zhang, X., Liao, W., and Wan, Q. (2017). Effect of physical and social components of enriched environment on astrocytes proliferation in rats after cerebral ischemia/reperfusion injury. *Neurochem. Res.* 42, 1308–1316. doi: 10.1007/s11064-016-2172-x

Cintoli, S., Radicchi, C., Noale, M., Maggi, S., Meucci, G., Tognoni, G., et al. (2021). Effects of combined training on neuropsychiatric symptoms and quality of life in patients with cognitive decline. *Aging Clin. Exp. Res.* 33, 1249–1257. doi: 10.1007/s40520-019-01280-w

Clarke, J., Langdon, K. D., and Corbett, D. (2014). Early poststroke experience differentially alters periinfarct layer II and III cortex. *J. Cereb. Blood Flow. Metab.* 34, 630–637. doi: 10.1038/jcbfm.2013.237

Coogan, A. N., Schutová, B., Husung, S., Furczyk, K., Baune, B. T., Kropp, P., et al. (2013). The circadian system in Alzheimer's disease: disturbances, mechanisms and opportunities. *Biol. Psychiatry* 74, 333–339. doi: 10.1016/j.biopsych.2012.11.021

Cordier, J. M., Aguggia, J. P., Danelon, V., Mir, F. R., Rivarola, M. A., and Mascó, D. (2021). Postweaning enriched environment enhances cognitive function and brain-derived neurotrophic factor signaling in the hippocampus in maternally separated rats. *Neuroscience* 453, 138–147. doi: 10.1016/j.neuroscience.2020.09.058

Couly, S., Carles, A., Denus, M., Benigno-Anton, L., Maschat, F., and Maurice, T. (2021). Exposure of R6/2 mice in an enriched environment augments P42 therapy efficacy on Huntington's disease progression. *Neuropharmacology* 186:108467. doi: 10.1016/j.neuropharm.2021.108467

Curley, J. P., Davidson, S., Bateson, P., and Champagne, F. A. (2009). Social enrichment during postnatal development induces transgenerational effects on emotional and reproductive behavior in mice. *Front. Behav. Neurosci.* 3:25. doi: 10.3389/neuro.08.025.2009

Dahlqvist, P., Rönnbäck, A., Risedal, A., Nergårdh, R., Johansson, I. M., Seckl, J. R., et al. (2003). Effects of postischemic environment on transcription factor and serotonin receptor expression after permanent focal cortical ischemia in rats. *Neuroscience* 119, 643–652. doi: 10.1016/s0306-4522(03)00195-7

Dahlqvist, P., Zhao, L., Johansson, I. M., Mattsson, B., Johansson, B. B., Seckl, J. R., et al. (1999). Environmental enrichment alters nerve growth factor-induced gene A and glucocorticoid receptor messenger RNA expression after middle cerebral artery occlusion in rats. *Neuroscience* 93, 527–535. doi: 10.1016/s0306-4522(99)00183-9

Davenport, M. H., Meah, V. L., Ruchat, S.-M., Davies, G. A., Skow, R. J., Barrowman, N., et al. (2018). Impact of prenatal exercise on neonatal and childhood outcomes: a systematic review and meta-analysis. *Br. J. Sports Med.* 52, 1386–1396. doi: 10.1136/bjsports-2018-099836

Davies, G., and Artal, R. (2019). It's time to treat exercise in pregnancy as therapy. *Br. J. Sports Med.* 53:81. doi: 10.1136/bjsports-2018-100360

De Winter, F., Kwok, J. C.F., Fawcett, J. W., Vo, T. T., Carulli, D., and Verhaagen, J. (2016). The chemorepulsive protein semaphorin 3A and perineuronal net-mediated plasticity. *Neural Plast.* 2016:3679545. doi: 10.1155/2016/3679545

Deng, Y.-H., Dong, L.-L., Zhang, Y.-J., Zhao, X.-M., and He, H.-Y. (2021). Enriched environment boosts the post-stroke recovery of neurological function by promoting autophagy. *Neural Regen. Res.* 16, 813–819. doi: 10.4103/1673-5374.297084

Diamond, M. C., Rosenzweig, M. R., Bennett, E. L., Lindner, B., and Lyon, L. (1972). Effects of environmental enrichment and impoverishment on rat cerebral cortex. *J. Neurobiol.* 3, 47–64. doi: 10.1002/neu.480030105

Dong, E., Dzitoyeva, S. G., Matrisciano, F., Tueting, P., Grayson, D. R., and Guidotti, A. (2015). Brain-derived neurotrophic factor epigenetic modifications associated with schizophrenia-like phenotype induced by prenatal stress in mice. *Biol. Psychiatry* 77, 589–596. doi: 10.1016/j.biopsych.2014.08.012

Emack, J., and Matthews, S. G. (2011). Effects of chronic maternal stress on hypothalamo-pituitary-adrenal (HPA) function and behavior: no reversal by environmental enrichment. *Horm. Behav.* 60, 589–598. doi: 10.1016/j.yhbeh.2011.08.008

Favaro, A., Tenconi, E., Degortes, D., Manara, R., and Santonastaso, P. (2015). Neural correlates of prenatal stress in young women. *Psychol. Med.* 45, 2533–2543. doi: 10.1017/S003329171500046X

Feng, T., Alicea, C., Pham, V., Kirk, A., and Pieraut, S. (2021). Experience-dependent inhibitory plasticity is mediated by CCK+ basket cells in the developing dentate gyrus. *J. Neurosci.* 41, 4607–4619. doi: 10.1523/JNEUROSCI.1207-20.2021

Fernández-Montoya, J., Martin, Y. B., Negredo, P., and Avendaño, C. (2018). Changes in the axon terminals of primary afferents from a single vibrissa in the rat trigeminal nuclei after active touch deprivation or exposure to an enriched environment. *Brain Struct. Funct.* 223, 47–61. doi: 10.1007/s00429-017-1472-5

Fischer, A. (2016). Environmental enrichment as a method to improve cognitive function. What can we learn from animal models. *Neuroimage* 131, 42–47. doi: 10.1016/j.neuroimage.2015.11.039

Fleming, A. S., O'day, D. H., and Kraemer, G. W. (1999). Neurobiology of mother-infant interactions: experience and central nervous system plasticity across development and generations. *Neurosci. Biobehav. Rev.* 23, 673–685. doi: 10.1016/s0149-7634(99)00011-1

Forbes, T. A., Goldstein, E. Z., Dupree, J. L., Jablonska, B., Scafidi, J., Adams, K. L., et al. (2020). Environmental enrichment ameliorates perinatal brain injury and promotes functional white matter recovery. *Nat. Commun.* 11:964. doi: 10.1038/s41467-020-14762-7

Gabriel, P., Mastracchio, T.-A., Bordner, K., and Jeffrey, R. (2020). Impact of enriched environment during adolescence on adult social behavior, hippocampal synaptic density and dopamine D2 receptor expression in rats. *Physiol. Behav.* 226:113133. doi: 10.1016/j.physbeh.2020.113133

Garthe, A., Roeder, I., and Kempermann, G. (2016). Mice in an enriched environment learn more flexibly because of adult hippocampal neurogenesis. *Hippocampus* 26, 261–271. doi: 10.1002/hipo.22520

Giandomenico, S. L., Sutcliffe, M., and Lancaster, M. A. (2021). Generation and long-term culture of advanced cerebral organoids for studying later stages of neural development. *Nat. Protoc.* 16, 579–602. doi: 10.1038/s41596-020-00433-w

Gill, M. J., Weiss, M. L., and Cain, M. E. (2014). Effects of differential rearing on amphetamine-induced c-fos expression in rats. *Drug Alcohol Depend.* 145, 231–234. doi: 10.1016/j.drugalcdep.2014.09.779

Goldberg, N. R. S., Haack, A. K., and Meshul, C. K. (2011). Enriched environment promotes similar neuronal and behavioral recovery in a young and aged mouse model of Parkinson's disease. *Neuroscience* 172, 443–452. doi: 10.1016/j.neuroscience.2010.09.062

Goldstein, E. Z., Pertsovskaya, V., Forbes, T. A., Dupree, J. L., and Gallo, V. (2021). Prolonged environmental enrichment promotes developmental myelination. *Front. Cell Dev. Biol.* 9:665409. doi: 10.3389/fcell.2021.665409

Gonçalves, L. V., Herlinger, A. L., Ferreira, T. a. A., Coitinho, J. B., Pires, R. G. W., and Martins-Silva, C. (2018). Environmental enrichment cognitive neuroprotection in an experimental model of cerebral ischemia: biochemical and molecular aspects. *Behav. Brain Res.* 348, 171–183. doi: 10.3389/fmed.2022.860574

González Fleitas, M. F., Aranda, M. L., Dieguez, H. H., Devouassoux, J. D., Chianelli, M. S., Dorfman, D., et al. (2019). Pre-ischemic enriched environment increases retinal resilience to acute ischemic damage in adult rats. *Exp. Eye Res.* 178, 198–211. doi: 10.1016/j.exer.2018.10.007

Greenough, W. T., and Volkmar, F. R. (1973). Pattern of dendritic branching in occipital cortex of rats reared in complex environments. *Exp. Neurol.* 40, 491–504. doi: 10.1016/0014-4886(73)90090-3

Greenough, W. T., Volkmar, F. R., and Juraska, J. M. (1973). Effects of rearing complexity on dendritic branching in frontolateral and temporal cortex of the rat. *Exp. Neurol.* 41, 371–378. doi: 10.1016/0014-4886(73)90278-1

Grońska-Pęski, M., Gonçalves, J. T., and Hébert, J. M. (2021). Enriched environment promotes adult hippocampal neurogenesis through FGFRs. *J. Neurosci.* 41, 2899–2910. doi: 10.1523/JNEUROSCI.2286-20.2021

Guan, S.-Z., Fu, Y.-J., Zhao, F., Liu, H.-Y., Chen, X.-H., Qi, F.-Q., et al. (2021). The mechanism of enriched environment repairing the learning and memory impairment in offspring of prenatal stress by regulating the expression of activity-regulated cytoskeletal-associated and insulin-like growth factor-2 in hippocampus. *Environ. Health Prev. Med.* 26:8. doi: 10.1186/s12199-020-00929-7

Gunnar, M., and Quevedo, K. (2007). The neurobiology of stress and development. *Annu. Rev. Psychol.* 58, 145–173. doi: 10.1146/annurev.psych.58.110405.085605

Guzzetta, A., Baldini, S., Bancale, A., Baroncelli, L., Ciucci, F., Ghirri, P., et al. (2009). Massage accelerates brain development and the maturation of visual function. *J. Neurosci.* 29, 6042–6051. doi: 10.1523/JNEUROSCI.5548-08.2009

Guzzetta, A., Murray, L., Montirosso, R., and Ferrari, P. F. (2019). The role of the social environment on adaptive neuroplasticity in early development. *Neural Plast.* 2019:5375849. doi: 10.1155/2019/5375849

Harauzov, A., Spolidoro, M., Dicristo, G., De Pasquale, R., Cancedda, L., Pizzorusso, T., et al. (2010). Reducing intracortical inhibition in the adult visual cortex promotes ocular dominance plasticity. *J. Neurosci.* 30, 361–371. doi: 10.1523/JNEUROSCI.2233-09.2010

Holder, M. K., and Blaustein, J. D. (2014). Puberty and adolescence as a time of vulnerability to stressors that alter neurobehavioral processes. *Front. Neuroendocrinol.* 35, 89–110. doi: 10.1016/j.yfrne.2013.10.004

Hong, S., Huang, H., Yang, M., Wu, H., and Wang, L. (2020). Enriched environment decreases cognitive impairment in elderly rats with prenatal mobile phone exposure. *Front. Aging Neurosci.* 12:162. doi: 10.3389/fnagi.2020.00162

Hopkins, S. A., Baldi, J. C., Cutfield, W. S., Mccowan, L., and Hofman, P. L. (2011). Effects of exercise training on maternal hormonal changes in pregnancy. *Clin. Endocrinol. (Oxf)* 74, 495–500. doi: 10.1111/j.1365-2265.2010.03964.x

Hu, X.-L., Bergström, S.-A., Brink, M., Rönnbäck, A., and Dahlqvist, P. (2010). Enriched environment increases spinophilin mRNA expression and spinophilin immunoreactive dendritic spines in hippocampus and cortex. *Neurosci. Lett.* 476, 79–83. doi: 10.1016/j.neulet.2010.04.007

Hu, Y.-S., Xu, P., Pigino, G., Brady, S. T., Larson, J., and Lazarov, O. (2010). Complex environment experience rescues impaired neurogenesis, enhances synaptic plasticity and attenuates neuropathology in familial Alzheimer's disease-linked APPswe/PS1DeltaE9 mice. *FASEB J.* 24, 1667–1681. doi: 10.1096/fj.09-136945

Hutson, T. H., Kathe, C., Palmisano, I., Bartholdi, K., Hervera, A., De Virgiliis, F., et al. (2019). Cbp-dependent histone acetylation mediates axon regeneration induced by environmental enrichment in rodent spinal cord injury models. *Sci. Transl. Med.* 11:eaaw2064. doi: 10.1126/scitranslmed.aaw2064

Hwang, H. M., Ku, R. Y., and Hashimoto-Torii, K. (2019). Prenatal environment that affects neuronal migration. *Front. Cell Dev. Biol.* 7:138. doi: 10.3389/fcell.2019.00138

Janssen, H., Ada, L., Bernhardt, J., Mcelduff, P., Pollack, M., Nilsson, M., et al. (2014). An enriched environment increases activity in stroke patients undergoing rehabilitation in a mixed rehabilitation unit: a pilot non-randomized controlled trial. *Disabil. Rehabil.* 36, 255–262. doi: 10.3109/09638288.2013.788218

Janssen, H., Ada, L., Karayanidis, F., Drysdale, K., Mcelduff, P., Pollack, M., et al. (2012). Translating the use of an enriched environment poststroke from bench to bedside: study design and protocol used to test the feasibility of environmental enrichment on stroke patients in rehabilitation. *Int. J. Stroke* 7, 521–526. doi: 10.1111/j.1747-4949.2011.00727.x

Janssen, H., Bernhardt, J., Collier, J. M., Sena, E. S., Mcelduff, P., Attia, J., et al. (2010). An enriched environment improves sensorimotor function post-ischemic stroke. *Neurorehabil. Neural Repair* 24, 802–813. doi: 10.1177/1545968310372092

Joushi, S., Esmaeilpour, K., Masoumi-Ardakani, Y., Esmaeili-Mahani, S., and Sheibani, V. (2021). Effects of short environmental enrichment on early-life adversity induced cognitive alternations in adolescent rats. *J. Neurosci. Res.* 99, 3373–3391. doi: 10.1002/jnr.24974

Keiner, S., Niv, F., Neumann, S., Steinbach, T., Schmeer, C., Hornung, K., et al. (2017). Effect of skilled reaching training and enriched environment on generation of oligodendrocytes in the adult sensorimotor cortex and corpus callosum. *BMC Neurosci.* 18:31. doi: 10.1186/s12868-017-0347-2

Keith, R. A., and Cowell, K. S. (1987). Time use of stroke patients in three rehabilitation hospitals. *Soc. Sci. Med.* 24, 529–533. doi: 10.1016/0277-9536(87)90342-x

Kempermann, G. (2019). Environmental enrichment, new neurons and the neurobiology of individuality. *Nat. Rev. Neurosci.* 20, 235–245. doi: 10.1038/s41583-019-0120-x

Kempermann, G., Gast, D., and Gage, F. H. (2002). Neuroplasticity in old age: sustained fivefold induction of hippocampal neurogenesis by long-term environmental enrichment. *Ann. Neurol.* 52, 135–143. doi: 10.1002/ana.10262

Kempermann, G., Kuhn, H. G., and Gage, F. H. (1997). More hippocampal neurons in adult mice living in an enriched environment. *Nature* 386, 493–495. doi: 10.1038/386493a0

Kim, T.-W., Ko, Y. J., Youn, K.-H., Hwang, B.-G., Bang, H.-S., and Lee, S.-J. (2021). Treadmill exercise improves spatial learning ability by increasing cell proliferation in offspring born to maternal rats receiving stress during pregnancy. *J. Exerc. Rehabil.* 17, 88–95. doi: 10.12965/jer.2142196.098

King, A., Mccluskey, A., and Schurr, K. (2011). The time use and activity levels of inpatients in a co-located acute and rehabilitation stroke unit: an observational study. *Top. Stroke Rehabil.* 18, 654–665. doi: 10.1310/tsr18s01-654

Kobayashi, S., Ohashi, Y., and Ando, S. (2002). Effects of enriched environments with different durations and starting times on learning capacity during aging in rats assessed by a refined procedure of the

Hebb-Williams maze task. *J. Neurosci. Res.* 70, 340–346. doi: 10.1002/jnr.10442

Kohl, Z., Kuhn, H. G., Cooper-Kuhn, C. M., Winkler, J., Aigner, L., and Kempermann, G. (2002). Preweaning enrichment has no lasting effects on adult hippocampal neurogenesis in four-month-old mice. *Genes Brain Behav.* 1, 46–54. doi: 10.1046/j.1601-1848.2001.00009.x

Kok, J. S., Berg, I. J., Blankevoort, G. C.G., and Scherder, E. J.A. (2017). Rest-activity rhythms in small scale homelike care and traditional care for residents with dementia. *BMC Geriatr.* 17:137. doi: 10.1186/s12877-017-0525-1

Komitova, M., Mattsson, B., Johansson, B. B., and Eriksson, P. S. (2005). Enriched environment increases neural stem/progenitor cell proliferation and neurogenesis in the subventricular zone of stroke-lesioned adult rats. *Stroke* 36, 1278–1282. doi: 10.1161/01.STR.0000166197.94147.59

Kondo, M., Takei, Y., and Hirokawa, N. (2012). Motor protein KIF1A is essential for hippocampal synaptogenesis and learning enhancement in an enriched environment. *Neuron* 73, 743–757. doi: 10.1016/j.neuron.2011.12.020

Korkhin, A., Zubedat, S., Aga-Mizrachi, S., and Avital, A. (2020). Developmental effects of environmental enrichment on selective and auditory sustained attention. *Psychoneuroendocrinology* 111:104479. doi: 10.1016/j.psyneuen.2019.104479

Kotloski, R. J., and Sutula, T. P. (2015). Environmental enrichment: evidence for an unexpected therapeutic influence. *Exp. Neurol.* 264, 121–126. doi: 10.1016/j.expneurol.2014.11.012

Kronenberg, G., Wang, L.-P., Geraerts, M., Babu, H., Synowitz, M., Vicens, P., et al. (2007). Local origin and activity-dependent generation of nestin-expressing protoplasmic astrocytes in CA1. *Brain Struct. Funct.* 212, 19–35. doi: 10.1007/s00429-007-0141-5

Kundakovic, M., and Jaric, I. (2017). The epigenetic link between prenatal adverse environments and neurodevelopmental disorders. *Genes (Basel)* 8:104. doi: 10.3390/genes8030104

Läck, A. K., Gill, K. E., and Porrino, L. J. (2010). Local cerebral glucose utilization in rats exposed to an enriched environment: a comparison to impoverishment. *Pharmacol. Biochem. Behav.* 96, 521–525. doi: 10.1002/bmc.5441

Landi, S., Cenni, M. C., Maffei, L., and Berardi, N. (2007a). Environmental enrichment effects on development of retinal ganglion cell dendritic stratification require retinal BDNF. *PLoS One* 2:e346. doi: 10.1371/journal.pone.0000346

Landi, S., Sale, A., Berardi, N., Viegi, A., Maffei, L., and Cenni, M. C. (2007b). Retinal functional development is sensitive to environmental enrichment: a role for BDNF. *FASEB J.* 21, 130–139. doi: 10.1096/fj.06-6083com

Landi, S., Ciucci, F., Maffei, L., Berardi, N., and Cenni, M. C. (2009). Setting the pace for retinal development: environmental enrichment acts through insulin-like growth factor 1 and brain-derived neurotrophic factor. *J. Neurosci.* 29, 10809–10819. doi: 10.1523/JNEUROSCI.1857-09.2009

Leger, M., Paizanis, E., Dzahini, K., Quiedeville, A., Bouet, V., Cassel, J.-C., et al. (2015). Environmental enrichment duration differentially affects behavior and neuroplasticity in adult mice. *Cereb. Cortex* 25, 4048–4061. doi: 10.1093/cercor/bhu119

Leggio, M. G., Mandolesi, L., Federico, F., Spirito, F., Ricci, B., Gelfo, F., et al. (2005). Environmental enrichment promotes improved spatial abilities and enhanced dendritic growth in the rat. *Behav. Brain Res.* 163, 78–90. doi: 10.1016/j.bbr.2005.04.009

Li, J., Li, X., Liu, H., Li, J., Han, Q., Wang, C., et al. (2021). Effects of music stimulus on behavior response, cortisol level and horizontal immunity of growing pigs. *J. Anim. Sci.* 99:skab043. doi: 10.1093/jas/skab043

Li, R., Wang, X., Lin, F., Song, T., Zhu, X., and Lei, H. (2020). Mapping accumulative whole-brain activities during environmental enrichment with manganese-enhanced magnetic resonance imaging. *Neuroimage* 210:116588. doi: 10.1016/j.neuroimage.2020.116588

Lindsay, E. K., Young, S., Brown, K. W., Smyth, J. M., and Creswell, J. D. (2019). Mindfulness training reduces loneliness and increases social contact in a randomized controlled trial. *Proc. Natl. Acad. Sci. U S A* 116, 3488–3493. doi: 10.1073/pnas.1813588116

Little, D. M., Foxely, S., and Lazarov, O. (2012). A preliminary study targeting neuronal pathways activated following environmental enrichment by resting state functional magnetic resonance imaging. *J. Alzheimers Dis.* 32, 101–107. doi: 10.3233/JAD-2012-111508

Liu, D., Diorio, J., Day, J. C., Francis, D. D., and Meaney, M. J. (2000). Maternal care, hippocampal synaptogenesis and cognitive development in rats. *Nat. Neurosci.* 3, 799–806. doi: 10.1038/77702

Liu, J., Zheng, J., Xu, Y., Cao, W., Wang, J., Wang, B., et al. (2021). Enriched environment attenuates pyroptosis to improve functional recovery after cerebral ischemia/reperfusion injury. *Front. Aging Neurosci.* 13:717644. doi: 10.3389/fnagi.2021.717644

Lu, C.-Q., Zhong, L., Yan, C.-H., Tian, Y., and Shen, X.-M. (2017). Effects of preweaning environmental enrichment on hippocampus-dependent learning and memory in developing rats. *Neurosci. Lett.* 640, 117–122. doi: 10.1016/j.neulet.2016.12.053

Mainardi, M., Scabia, G., Vottari, T., Santini, F., Pinchera, A., Maffei, L., et al. (2010). A sensitive period for environmental regulation of eating behavior and leptin sensitivity. *Proc. Natl. Acad. Sci. U S A* 107, 16673–16678. doi: 10.1073/pnas.0911832107

Martinez, A. R., Brunelli, S. A., and Zimmerberg, B. (2015). Communal nesting exerts epigenetic influences on affective and social behaviors in rats selectively bred for an infantile trait. *Physiol. Behav.* 139, 97–103. doi: 10.1016/j.physbeh.2014.11.007

Matsumori, Y., Hong, S. M., Fan, Y., Kayama, T., Hsu, C. Y., Weinstein, P. R., et al. (2006). Enriched environment and spatial learning enhance hippocampal neurogenesis and salvages ischemic penumbra after focal cerebral ischemia. *Neurobiol. Dis.* 22, 187–198. doi: 10.1016/j.nbd.2005.10.015

Maya Vetencourt, J. F., Sale, A., Viegi, A., Baroncelli, L., De Pasquale, R., O'leary, O. F., et al. (2008). The antidepressant fluoxetine restores plasticity in the adult visual cortex. *Science* 320, 385–388. doi: 10.1126/science.1150516

Mcgill, M. G., Pokhvisneva, I., Clappison, A. S., Mcewen, L. M., Beijers, R., Tollenaar, M. S., et al. (2022). Maternal prenatal anxiety and the fetal origins of epigenetic aging. *Biol. Psychiatry* 91, 303–312. doi: 10.1016/j.biopsych.2021.07.025

Meaney, M. J., Diorio, J., Francis, D., Widdowson, J., Laplante, P., Caldji, C., et al. (1996). Early environmental regulation of forebrain glucocorticoid receptor gene expression: implications for adrenocortical responses to stress. *Dev. Neurosci.* 18, 49–72. doi: 10.1159/000111395

Menezes, J., Souto Das Neves, B.-H., Gonçalves, R., Benetti, F., and Mello-Carpes, P. B. (2020). Maternal deprivation impairs memory and cognitive flexibility, effect that is avoided by environmental enrichment. *Behav. Brain Res.* 381:112468. doi: 10.1016/j.bbr.2020.112468

Mohammadian, J., Najafi, M., and Miladi-Gorji, H. (2019). Effect of enriched environment during adolescence on spatial learning and memory and voluntary consumption of morphine in maternally separated rats in adulthood. *Dev. Psychobiol.* 61, 615–625. doi: 10.1002/dev.21808

Morgan, C., Novak, I., and Badawi, N. (2013). Enriched environments and motor outcomes in cerebral palsy: systematic review and meta-analysis. *Pediatrics* 132, e735–e746. doi: 10.1542/peds.2012-3985

Morishita, H., and Hensch, T. K. (2008). Critical period revisited: impact on vision. *Curr. Opin. Neurobiol.* 18, 101–107. doi: 10.1016/j.conb.2008.05.009

Mueller, B. R., and Bale, T. L. (2008). Sex-specific programming of offspring emotionality after stress early in pregnancy. *J. Neurosci.* 28, 9055–9065. doi: 10.1523/JNEUROSCI.1424-08.2008

Nithianantharajah, J., and Hannan, A. J. (2006). Enriched environments, experience-dependent plasticity and disorders of the nervous system. *Nat. Rev. Neurosci.* 7, 697–709. doi: 10.1038/nrn1970

Nithianantharajah, J., Levis, H., and Murphy, M. (2004). Environmental enrichment results in cortical and subcortical changes in levels of synaptophysin and PSD-95 proteins. *Neurobiol. Learn. Mem.* 81, 200–210. doi: 10.1016/j.nlm.2004.02.002

Nozari, M., Suzuki, T., Rosa, M. G. P., Yamakawa, K., and Atapour, N. (2017). The impact of early environmental interventions on structural plasticity of the axon initial segment in neocortex. *Dev. Psychobiol.* 59, 39–47. doi: 10.1002/dev.21453

Parnpiansil, P., Jutapakdeegul, N., Chentanez, T., and Kotchabhakdi, N. (2003). Exercise during pregnancy increases hippocampal brain-derived neurotrophic factor mRNA expression and spatial learning in neonatal rat pup. *Neurosci. Lett.* 352, 45–48. doi: 10.1016/j.neulet.2003.08.023

Pascual, R., and Figueroa, H. (1996). Effects of preweaning sensorimotor stimulation on behavioral and neuronal development in motor and visual cortex of the rat. *Biol. Neonate* 69, 399–404. doi: 10.1159/000244337

Pham, T. M., Ickes, B., Albeck, D., Söderström, S., Granholm, A. C., and Mohammed, A. H. (1999). Changes in brain nerve growth factor levels and nerve growth factor receptors in rats exposed to environmental enrichment for one year. *Neuroscience* 94, 279–286. doi: 10.1016/s0306-4522(99)00316-4

Pozzi, E., Vijayakumar, N., Byrne, M. L., Bray, K. O., Seal, M., Richmond, S., et al. (2021). Maternal parenting behavior and functional connectivity development in children: a longitudinal fMRI study. *Dev. Cogn. Neurosci.* 48:100946. doi: 10.1016/j.dcn.2021.100946

Quinn, R. (2005). Comparing rat's to human's age: how old is my rat in people years. *Nutrition* 21, 775–777. doi: 10.1016/j.nut.2005.04.002

Rinaldi, A., Romeo, S., Agustín-Pavón, C., Oliverio, A., and Mele, A. (2010). Distinct patterns of Fos immunoreactivity in striatum and hippocampus induced

by different kinds of novelty in mice. *Neurobiol. Learn. Mem.* 94, 373–381. doi: 10.1016/j.nlm.2010.08.004

Risedal, A., Zeng, J., and Johansson, B. B. (1999). Early training may exacerbate brain damage after focal brain ischemia in the rat. *J. Cereb. Blood Flow. Metab.* 19, 997–1003. doi: 10.1097/00004647-199909000-00007

Rodríguez, J. J., Terzieva, S., Olabarria, M., Lanza, R. G., and Verkhratsky, A. (2013). Enriched environment and physical activity reverse astrogliodegeneration in the hippocampus of AD transgenic mice. *Cell Death Dis.* 4:e678. doi: 10.1038/cddis.2013.194

Rogers, J., Renoir, T., and Hannan, A. J. (2019). Gene-environment interactions informing therapeutic approaches to cognitive and affective disorders. *Neuropharmacology* 145, 37–48. doi: 10.1016/j.neuropharm.2017.12.038

Rosa, B. V., Firth, E. C., Blair, H. T., Vickers, M. H., and Morel, P. C. H. (2011). Voluntary exercise in pregnant rats positively influences fetal growth without initiating a maternal physiological stress response. *Am. J. Physiol. Regul. Integr. Comp. Physiol.* 300, R1134–R1141. doi: 10.1152/ajpregu.00683.2010

Rostami, S., Haghparast, A., and Fayazmilani, R. (2021). The downstream effects of forced exercise training and voluntary physical activity in an enriched environment on hippocampal plasticity in preadolescent rats. *Brain Res.* 1759:147373. doi: 10.1016/j.brainres.2021.147373

Sakhaie, N., Sadegzadeh, F., Mohammadnia, A., Dadkhah, M., and Saadati, H. (2020). Sex-dependent effects of postweaning exposure to an enriched environment on novel objective recognition memory and anxiety-like behaviors: The role of hippocampal BDNF level. *Int. J. Dev. Neurosci.* doi: 10.1002/jdn.10038 [Online ahead of print].

Sale, A., Berardi, N., and Maffei, L. (2014). Environment and brain plasticity: towards an endogenous pharmacotherapy. *Physiol. Rev.* 94, 189–234. doi: 10.1152/physrev.00036.2012

Sale, A., Cenni, M. C., Ciucci, F., Putignano, E., Chierzi, S., and Maffei, L. (2007). Maternal enrichment during pregnancy accelerates retinal development of the fetus. *PLoS One* 2:e1160. doi: 10.1371/journal.pone.0001160

Sale, A., Putignano, E., Cancedda, L., Landi, S., Cirulli, F., Berardi, N., et al. (2004). Enriched environment and acceleration of visual system development. *Neuropharmacology* 47, 649–660. doi: 10.1016/j.neuropharm.2004.07.008

Salmin, V. V., Komleva, Y. K., Kuvacheva, N. V., Morgun, A. V., Khilazheva, E. D., Lopatina, O. L., et al. (2017). Differential roles of environmental enrichment in Alzheimer's type of neurodegeneration and physiological aging. *Front. Aging Neurosci.* 9:245. doi: 10.3389/fnagi.2017.00245

Scabia, G., Testa, G., Scali, M., Del Turco, S., Desiato, G., Berardi, N., et al. (2021). Reduced ccl11/eotaxin mediates the beneficial effects of environmental stimulation on the aged hippocampus. *Brain Behav. Immun.* 98, 234–244. doi: 10.1016/j.bbi.2021.08.222

Scholz, J., Allemang-Grand, R., Dazai, J., and Lerch, J. P. (2015). Environmental enrichment is associated with rapid volumetric brain changes in adult mice. *Neuroimage* 109, 190–198. doi: 10.1016/j.neuroimage.2015.01.027

Scrivener, K., Sherrington, C., and Schurr, K. (2012). Exercise dose and mobility outcome in a comprehensive stroke unit: description and prediction from a prospective cohort study. *J. Rehabil. Med.* 44, 824–829. doi: 10.2340/16501977-1028

Segovia, G., Yagüe, A. G., García-Verdugo, J. M., and Mora, F. (2006). Environmental enrichment promotes neurogenesis and changes the extracellular concentrations of glutamate and GABA in the hippocampus of aged rats. *Brain Res. Bull.* 70, 8–14. doi: 10.1016/j.brainresbull.2005.11.005

Sengpiel, F. (2007). The critical period. *Curr. Biol.* 17, R742–R743. doi: 10.1016/j.cub.2007.06.017

Serra, F. T., Araujo, B. H. S., Placencia, E. V. D., Henrique, J. S., Dona, F., Torres, L. B., et al. (2020). Enriched environment and exercise effects on parvalbumin expression and distribution in the hippocampal formation of developing rats. *Brain Res. Bull.* 160, 85–90. doi: 10.1016/j.brainresbull.2020.03.021

She, X., Lan, B., Tian, H., and Tang, B. (2020). Cross talk between ferroptosis and cerebral ischemia. *Front. Neurosci.* 14:776. doi: 10.3389/fnins.2020.00776

Shimada, H., Makizako, H., Doi, T., Park, H., Tsutsumimoto, K., Verghese, J., et al. (2018). Effects of combined physical and cognitive exercises on cognition and mobility in patients with mild cognitive impairment: a randomized clinical trial. *J. Am. Med. Dir. Assoc.* 19, 584–591. doi: 10.1016/j.jamda.2017.09.019

Shono, Y., Yokota, C., Kuge, Y., Kido, S., Harada, A., Kokame, K., et al. (2011). Gene expression associated with an enriched environment after transient focal ischemia. *Brain Res.* 1376, 60–65. doi: 10.1016/j.brainres.2010.12.058

Sikora, M., Nicolas, C., Istin, M., Jaafari, N., Thiriet, N., and Solinas, M. (2018). Generalization of effects of environmental enrichment on seeking for different classes of drugs of abuse. *Behav. Brain Res.* 341, 109–113. doi: 10.1016/j.bbr.2017.12.027

Solinas, M., Chauvet, C., Thiriet, N., El Rawas, R., and Jaber, M. (2008). Reversal of cocaine addiction by environmental enrichment. *Proc. Natl. Acad. Sci. U S A* 105, 17145–17150. doi: 10.1073/pnas.0806889105

Solinas, M., Thiriet, N., Chauvet, C., and Jaber, M. (2010). Prevention and treatment of drug addiction by environmental enrichment. *Prog. Neurobiol.* 92, 572–592. doi: 10.1016/j.pneurobio.2010.08.002

Son, J. S., Chae, S. A., Zhao, L., Wang, H., De Avila, J. M., Zhu, M.-J., et al. (2022). Maternal exercise intergenerationally drives muscle-based thermogenesis via activation of apelin-AMPK signaling. *EBioMedicine* 76:103842. doi: 10.1016/j.ebiom.2022.103842

Ströher, R., De Oliveira, C., Stein, D. J., De Macedo, I. C., Goularte, J. F., Da Silva, L. S., et al. (2020). Maternal deprivation and sex alter central levels of neurotrophins and inflammatory cytokines in rats exposed to palatable food in adolescence. *Neuroscience* 428, 122–131. doi: 10.1007/s00117-022-01038-y

Sur, M., and Leamey, C. A. (2001). Development and plasticity of cortical areas and networks. *Nat. Rev. Neurosci.* 2, 251–262. doi: 10.1038/35067562

Szeligo, F., and Leblond, C. P. (1977). Response of the three main types of glial cells of cortex and corpus callosum in rats handled during suckling or exposed to enriched, control and impoverished environments following weaning. *J. Comp. Neurol.* 172, 247–263. doi: 10.1002/cne.901720205

Sztainberg, Y., and Chen, A. (2010). An environmental enrichment model for mice. *Nat. Protoc.* 5, 1535–1539. doi: 10.1038/nprot.2010.114

Tabbaa, M., and Hammock, E. A. D. (2020). Orally administered oxytocin alters brain activation and behaviors of pre-weaning mice. *Horm. Behav.* 118:104613. doi: 10.1016/j.yhbeh.2019.104613

Thiel, K. J., Pentkowski, N. S., Peartree, N. A., Painter, M. R., and Neisewander, J. L. (2010). Environmental living conditions introduced during forced abstinence alter cocaine-seeking behavior and Fos protein expression. *Neuroscience* 171, 1187–1196. doi: 10.1016/j.neuroscience.2010.10.001

Train the Brain Consortium (2017). Randomized trial on the effects of a combined physical/cognitive training in aged MCI subjects: the Train the Brain study. *Sci. Rep.* 7:39471. doi: 10.1038/srep39471

Valero, J., España, J., Parra-Damas, A., Martín, E., Rodríguez-Álvarez, J., and Saura, C. A. (2011). Short-term environmental enrichment rescues adult neurogenesis and memory deficits in app(Sw,Ind) transgenic mice. *PLoS One* 6:e16832. doi: 10.1371/journal.pone.0016832

van Oers, H. J. J., De Kloet, E. R., Li, C., and Levine, S. (1998). The ontogeny of glucocorticoid negative feedback: influence of maternal deprivation. *Endocrinology* 139, 2838–2846. doi: 10.1210/endo.139.6.6037

van Praag, H., Kempermann, G., and Gage, F. H. (1999). Running increases cell proliferation and neurogenesis in the adult mouse dentate gyrus. *Nat. Neurosci.* 2, 266–270. doi: 10.1038/6368

van Praag, H., Kempermann, G., and Gage, F. H. (2000). Neural consequences of environmental enrichment. *Nat. Rev. Neurosci.* 1, 191–198. doi: 10.1038/35044558

Venable, N., Fernández, V., Díaz, E., and Pinto-Hamuy, T. (1989). Effects of preweaning environmental enrichment on basilar dendrites of pyramidal neurons in occipital cortex: a Golgi study. *Brain Res. Dev. Brain Res.* 49, 140–144. doi: 10.1016/0165-3806(89)90068-0

Vickers, A., Ohlsson, A., Lacy, J. B., and Horsley, A. (2004). Massage for promoting growth and development of preterm and/or low birth-weight infants. *Cochrane Database Sys. Rev.* 2004:CD000390. doi: 10.1002/14651858.CD000390.pub2

von Bohlen und Halbach, O., and von Bohlen und Halbach, V. (2018). Bdnf effects on dendritic spine morphology and hippocampal function. *Cell Tissue Res.* 373, 729–741. doi: 10.1007/s00441-017-2782-x

Walsh, R. N., Budtz-Olsen, O. E., Penny, J. E., and Cummins, R. A. (1969). The effects of environmental complexity on the histology of the rat hippocampus. *J. Comp. Neurol.* 137, 361–366. doi: 10.1002/cne.901370309

Walsh, R. N., and Cummins, R. A. (1975). Mechanisms mediating the production of environmentally induced brain changes. *Psychol. Bull.* 82, 986–1000.

Wang, X., Chen, A., Wu, H., Ye, M., Cheng, H., Jiang, X., et al. (2016). Enriched environment improves post-stroke cognitive impairment in mice by potential regulation of acetylation homeostasis in cholinergic circuits. *Brain Res.* 1650, 232–242. doi: 10.1016/j.brainres.2016.09.018

Wang, Y., Wu, J., Xie, H., Wang, L., Wang, C., and Wu, Y. (2020). Enriched environment promotes cognitive function recovery following cerebral

ischemic injury via upregulating gabaergic and glutamatergic systems in the contralateral hippocampus. *Evid. Based Complement. Alternat. Medi.* 2020:8850119. doi: 10.1155/2020/8850119

Wang, C., Zhang, Q., Yu, K., Shen, X., Wu, Y., and Wu, J. (2019). Enriched environment promoted cognitive function bilateral synaptic remodeling after cerebral ischemia. *Front. Neurol.* 10:1189. doi: 10.3389/fneur.2019.01189

Wang, L., and Zhu, L. (2022). Exercise during pregnancy may have more benefits than we thought. *EBioMedicine* 77:103889. doi: 10.1016/j.ebiom.2022.103889

Will, B., Galani, R., Kelche, C., and Rosenzweig, M. R. (2004). Recovery from brain injury in animals: relative efficacy of environmental enrichment, physical exercise or formal training 1990-2002. *Prog. Neurobiol.* 72, 167–182. doi: 10.1016/j.pneurobio.2004.03.001

Wooters, T. E., Bardo, M. T., Dwoskin, L. P., Midde, N. M., Gomez, A. M., Mactutus, C. F., et al. (2011). Effect of environmental enrichment on methylphenidate-induced locomotion and dopamine transporter dynamics. *Behav. Brain Res.* 219, 98–107doi: 10.1016/j.bbr.2011.01.001

Wu, X., Liu, S., Hu, Z., Zhu, G., Zheng, G., and Wang, G. (2018). Enriched housing promotes post-stroke neurogenesis through calpain 1-stat3/hif-1α/vegf signaling. *Brain Res. Bull.* 139, 133–143. doi: 10.1016/j.brainresbull.2018.02.018

Xie, H., Yu, K., Zhou, N., Shen, X., Tian, S., Zhang, B., et al. (2019). Enriched environment elicits proangiogenic mechanisms after focal cerebral ischemia. *Transl. Stroke Res.* 10, 150–159. doi: 10.1007/s12975-018-0629-8

Yang, R., Zhang, M., Xue, Y., Yang, R., Tang, M., and Dang, R. (2021). Effects of maternal deprivation stress and maternal dietary of n-3 polyunsaturated fatty acids on the neurobehavioral development of male offspring. *Nutr. Neurosci.* 24, 865–872. doi: 10.1080/1028415X.2019.1684689

Young, D., Lawlor, P. A., Leone, P., Dragunow, M., and During, M. J. (1999). Environmental enrichment inhibits spontaneous apoptosis, prevents seizures and is neuroprotective. *Nat. Med.* 5, 448–453. doi: 10.1038/7449

Yu, K., Wu, Y., Hu, Y., Zhang, Q., Xie, H., Liu, G., et al. (2013a). Prior exposure to enriched environment reduces nitric oxide synthase after transient mcao in rats. *Neurotoxicology* 39, 146–152. doi: 10.1016/j.neuro.2013.09.002

Yu, K., Wu, Y., Hu, Y., Zhang, Q., Xie, H., Liu, G., et al. (2013b). Neuroprotective effects of prior exposure to enriched environment on cerebral ischemia/reperfusion injury in rats: the possible molecular mechanism. *Brain Res.* 1538, 93–103. doi: 10.1016/j.brainres.2013.09.036

Yu, K.-W., Wang, C.-J., Wu, Y., Wang, Y.-Y., Wang, N.-H., Kuang, S.-Y., et al. (2020). An enriched environment increases the expression of fibronectin type III domain-containing protein 5 and brain-derived neurotrophic factor in the cerebral cortex of the ischemic mouse brain. *Neural Regen. Res.* 15, 1671–1677. doi: 10.4103/1673-5374.276339

Yu, K., Wu, Y., Zhang, Q., Xie, H., Liu, G., Guo, Z., et al. (2014). Enriched environment induces angiogenesis and improves neural function outcomes in rat stroke model. *J. Neurol. Sci.* 347, 275–280. doi: 10.1016/j.jns.2014.10.022

Yuan, M., Guo, Y.-S., Han, Y., Gao, Z.-K., Shen, X.-Y., and Bi, X. (2021). Effectiveness and mechanisms of enriched environment in post-stroke cognitive impairment. *Behav. Brain Res.* 410:113357. doi: 10.1016/j.bbr.2021.113357

Yuan, M., Zhang, X.-X., Fu, X.-C., and Bi, X. (2020). Enriched environment alleviates post-stroke cognitive impairment through enhancing α7-nachr expression in rats. *Arq. Neuropsiquiatr.* 78, 603–610. doi: 10.1590/0004-282X20200081

Zakharova, E., Miller, J., Unterwald, E., Wade, D., and Izenwasser, S. (2009). Social and physical environment alter cocaine conditioned place preference and dopaminergic markers in adolescent male rats. *Neuroscience* 163, 890–897. doi: 10.1016/j.neuroscience.2009.06.068

Zhan, Y., Li, M.-Z., Yang, L., Feng, X.-F., Lei, J.-F., Zhang, N., et al. (2020). The three-phase enriched environment paradigm promotes neurovascular restorative and prevents learning impairment after ischemic stroke in rats. *Neurobiol. Dis.* 146:105091. doi: 10.1016/j.nbd.2020.105091

Zhang, Y., Crofton, E. J., Li, D., Lobo, M. K., Fan, X., Nestler, E. J., et al. (2014). Overexpression of deltafosb in nucleus accumbens mimics the protective addiction phenotype, but not the protective depression phenotype of environmental enrichment. *Front. Behav. Neurosci.* 8:297. doi: 10.3389/fnbeh.2014.00297

Zhang, X., Liu, J.-Y., Liao, W.-J., and Chen, X.-P. (2021). Differential effects of physical and social enriched environment on angiogenesis in male rats after cerebral ischemia/reperfusion injury. *Front. Hum. Neurosci.* 15:622911. doi: 10.3389/fnhum.2021.622911

Zhang, Y., Xu, D., Qi, H., Yuan, Y., Liu, H., Yao, S., et al. (2018). Enriched environment promotes post-stroke neurogenesis through nf-κb-mediated secretion of il-17a from astrocytes. *Brain Res.* 1687, 20–31. doi: 10.1016/j.brainres.2018.02.030

Zocher, S., Schilling, S., Grzyb, A. N., Adusumilli, V. S., Bogado Lopes, J., Günther, S., et al. (2020). Early-life environmental enrichment generates persistent individualized behavior in mice. *Sci. Adv.* 6:eabb1478. doi: 10.1126/sciadv.abb1478

Zorzin, S., Corsi, A., Ciarpella, F., Bottani, E., Dolci, S., Malpeli, G., et al. (2021). Environmental enrichment induces meningeal niche remodeling through trkb-mediated signaling. *Int. J. Mol. Sci.* 22:10657. doi: 10.3390/ijms221910657

frontiers | Frontiers in Neuroscience

TYPE Mini Review
PUBLISHED 29 July 2022
DOI 10.3389/fnins.2022.970350

Check for updates

OPEN ACCESS

EDITED BY
Harold Cremer,
Centre National de la Recherche Scientifique (CNRS), France

REVIEWED BY
Jean-Marie Delalande,
Queen Mary University of London, United Kingdom

*CORRESPONDENCE
Allan M. Goldstein
amgoldstein@partners.org

SPECIALTY SECTION
This article was submitted to Neurogenesis, a section of the journal Frontiers in Neuroscience

RECEIVED 16 June 2022
ACCEPTED 11 July 2022
PUBLISHED 29 July 2022

CITATION
Mueller JL, Stavely R, Hotta R and Goldstein AM (2022) Peripheral nervous system: A promising source of neuronal progenitors for central nervous system repair. *Front. Neurosci.* 16:970350. doi: 10.3389/fnins.2022.970350

COPYRIGHT
© 2022 Mueller, Stavely, Hotta and Goldstein. This is an open-access article distributed under the terms of the Creative Commons Attribution License (CC BY). The use, distribution or reproduction in other forums is permitted, provided the original author(s) and the copyright owner(s) are credited and that the original publication in this journal is cited, in accordance with accepted academic practice. No use, distribution or reproduction is permitted which does not comply with these terms.

Peripheral nervous system: A promising source of neuronal progenitors for central nervous system repair

Jessica L. Mueller, Rhian Stavely, Ryo Hotta and Allan M. Goldstein*

Department of Pediatric Surgery, Massachusetts General Hospital, Harvard Medical School, Boston, MA, United States

With a steadily aging population there is an increasing prevalence of neurological disorders. Given the lack of effective treatment strategies and a limited ability for the central nervous system (CNS) to regenerate endogenously, there is a critical need to better understand exogenous strategies for nervous system repair. Stem cell therapy offers a promising approach to promote the repair of neurologic tissue and function, however studies to date have been limited by various factors including challenges in harvesting donor cells from the CNS, ethical concerns regarding use of embryonic or fetal tissue, tumorigenic potential of induced pluripotent stem cells, and immune-mediated rejection of non-autologous cell sources. Here we review and propose two alternative sources of autologous cells derived from the peripheral nervous system (PNS) for CNS repair: enteric neuronal stem cells (ENSCs) and neural crest-derived Schwann cells found in subcutaneous adipose tissue (termed SAT-NSCs). ENSCs can be successfully isolated from the postnatal enteric nervous system, propagated *in vitro*, and transplanted successfully into models of CNS injury via both direct intracerebral injection and systemic tail vein injection. Similarly, SAT-NSCs can be readily isolated from both human and mouse adipose tissue and, although not yet utilized in models of CNS injury, have successfully been transplanted and restored function in models of colonic aganglionosis and gastroparesis. These unique sources of PNS-derived autologous cells offer an exciting option for stem cell therapies for the CNS as they have proven neurogenic potential and eliminate concerns around tumorigenic risk, ethical considerations, and immune-mediated rejection.

KEYWORDS

regenerative therapies, central nervous system, stem cells, autologous cells, neurologic disorders, peripheral nervous system

Introduction

When damaged, the central nervous system (CNS) has a limited ability to regenerate endogenously. This is clinically important as it results in ineffective treatment strategies for most diseases involving CNS injury. With a steadily aging population, there is an increasing prevalence of CNS disorders, including neurodegenerative diseases, traumatic brain injury, neurotoxicity from cancer therapy, and spinal cord injury. Given the significant public health burden of neurologic diseases and the dearth of effective therapies, recent efforts have focused on regenerative therapy via exogenous stem-cell based therapies (Alessandrini et al., 2018; Andrzejewska et al., 2021).

Stem cells have the unique ability to self-renew and to differentiate into multiple different lineages (Venkei and Yamashita, 2018). Stem cell therapy, or treatment of affected tissue with these regenerative progenitor cells, offers an exciting approach to promote repair of neurologic tissue and restore function in CNS diseases. However, thus far, studies have been limited by various factors including challenges gathering donor cells directly from the CNS, ethical concerns with use of embryonic or fetal tissue, tumorigenic potential of induced pluripotent stem cells, and immune-mediated rejection of non-autologous cell sources.

There are numerous candidate donor cells that have been studied in the context of CNS injury (**Table 1** and **Figure 1**). Neural stem/progenitor cells (NSPCs), which are harvested directly from the neural tissue itself, when utilized in models of spinal cord injury can replace lost neurons and glia and promote a local environment of growth and regeneration (Mothe and Tator, 2013). NSPCs can be harvested from both adult and embryonic brain and spinal cord tissue. These cells are widely considered the ideal cell type for use in CNS injury because they most closely resemble the cells being replaced and may therefore respond best to signals from the surrounding local environment. Unfortunately, NSPCs are located deep within the brain so their harvest requires an invasive procedure (Deng et al., 2018). To overcome the challenge of harvesting donor cells directly from the CNS, efforts have focused on embryonic stem cells (ESCs) and induced pluripotent stem cells (iPSCs). Use of embryonic stem cells in spinal cord injury showed significant potential as they were able to engraft, promote axonal growth, undergo remyelination, promote angiogenesis, and recover locomotor function (Kumagai et al., 2009). Similarly, in both rat (Andres et al., 2011) and gerbil (Ishibashi et al., 2004) models of stroke injury, transplantation of fetal-derived neural progenitor cells resulted in improved axonal rewiring and axonal transport as well as enhanced functional recovery. However, the use of embryonic or fetal tissue is controversial and raises ethical concerns. Additionally, treatment with non-autologous cell sources requires immunosuppressive medications, which are associated with numerous risks, including higher rates of infectious diseases, increased development of lymphoproliferative disorders and cancers, and medication specific toxicities. Furthermore, immune cell infiltration following neurotrauma and during neurodegeneration promotes CNS protection and repair (Schwartz and Moalem, 2001; Simard et al., 2006; Ziv et al., 2006; Beers et al., 2008), and this may be inhibited by the use of immunosuppression (Kulbatski, 2010).

Induced pluripotent stem cells, in which somatic cells are reprogrammed via the introduction of specific transcription factor genes to become pluripotent stem cells that exhibit the proliferation and differentiation capacity analogous to embryonic stem cells, bypass these ethical concerns. These cells are also easily obtained from skin biopsies and are autologous, avoiding some of the accessibility and immunogenic concerns of the cell sources described above. Application of iPSCs in models of spinal cord injury and stroke have shown successful engraftment and improved functional recovery (Oki et al., 2012; Nakamura and Okano, 2013), but there have been concerns regarding their tumorigenic potential (Nakamura and Okano, 2013; Deng et al., 2018).

Given the current obstacles hindering stem cell therapy in the CNS, identification of a readily available, not genetically reprogrammed, and autologous source of neural progenitor cells would be optimal. Other autologous sources of stem cells have been proposed and reviewed, including mesenchymal stem cells (MSCs), hematopoietic stem cells (HSCs), and dental pulp derived stem cells (DPSCs). MSCs can be obtained from multiple sources, including bone marrow, umbilical cord blood, and adipose tissue and demonstrate a high differentiation plasticity including the ability to differentiate into mesodermal lineages, including osteocytes, adipocytes, and chondrocytes, as well as reported abilities to differentiate into non-mesodermal lineages, including the neuronal linage (Hernández et al., 2020). They have been reviewed previously and have shown promise in multiple clinical trials of neurodegenerative diseases, including amyotrophic lateral sclerosis, Alzheimer's disease, and Parkinson's disease (Ullah et al., 2015; Andrzejewska et al., 2021). HSCs can be obtained via peripheral blood, and have been primarily studied in the context of autoimmune neurologic disorders, particularly multiple sclerosis (Balassa et al., 2018; Massey et al., 2018). Dental pulp derived stem cells have been isolated from humans (Gronthos et al., 2000; Nuti et al., 2016) and successfully transplanted into a rat model of spinal cord injury, demonstrating regeneration of transected axons and recovery of hindlimb motor function (Sakai et al., 2012), and have shown promise in models of both retinal and CNS injury and disease (Mead et al., 2017).

Although these cell sources have shown great potential in models of CNS disease, they are not derived from a neuronal niche. Moreover, in the case of MSCs, their therapeutic effects are predominantly reliant on paracrine signaling and neurotrophic support of the injured nervous system, with limited cell survivability. In this review, we therefore propose

TABLE 1 Cell sources for regenerative central nervous system (CNS) therapy.

Source of cells	Accessibility	Ethical concerns	Tumorigenic	Autologous	Nervous system-derived
NSPCs	Low	Moderate	Sometimes	Sometimes	Yes
ESCs	Low	Significant	Yes	No	No
iPSCs	High	None	Yes	Yes	No
MSCs	High	None	No	Yes	No
HSCs	High	None	No	Yes	No
DPSCs	High	None	No	Yes	No
ENSCs	High	None	No	Yes	Yes
SAT-NSCs	High	None	No	Yes	Yes

NSPCs, neural stem/progenitor cells; ESCs, embryonic stem cells; iPSCs, induced pluripotent stem cells; MSCs, mesenchymal stem cells; HSCs, hematopoietic stem cells; DPSCs, dental pulp stem cells; ENSCs, enteric neuronal stem cells; SAT-NSCs, subcutaneous adipose tissue–neural stem cells.

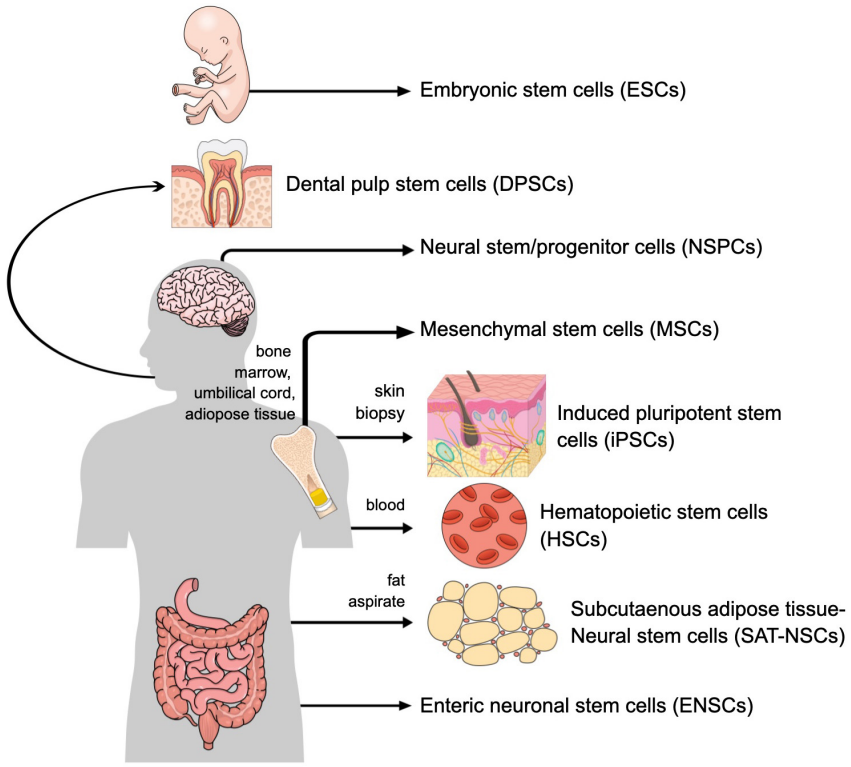

FIGURE 1
Cell sources for regenerative central nervous system (CNS) therapy.

two alternative sources of autologous cells for CNS repair, both directly derived from the peripheral nervous system and therefore with intrinsic neurogenic potential: enteric neuronal stem cells (ENSCs) and neural crest-derived Schwann cells found in subcutaneous adipose tissue (termed SAT-NSCs).

Enteric neuronal stem cells

The enteric nervous system (ENS) is an extensive network of neurons and glia within the wall of the gastrointestinal (GI) tract that regulates many of the GI functions independently from CNS input (Furness, 2012). It has been shown that neural progenitors can be isolated from the GI tract of embryonic and postnatal rodents (Kruger et al., 2002; Almond et al., 2007). Subsequently, these ENSCs have been identified in human gut tissue ranging from embryonic stages to late adulthood, including even an octogenarian (Metzger et al., 2009a). They are easily accessible and have been successfully isolated from neonates (Almond et al., 2007; Lindley et al., 2008), children (Rauch et al., 2006), and adults (Metzger et al., 2009a), from both the small and large intestine (Cheng et al., 2016), and from

full-thickness biopsies and mucosa (Metzger et al., 2009b). Importantly, these cells can be harvested using minimally invasive techniques, including endoscopy (Metzger et al., 2009b). Enteric neuronal stem cells can be propagated *in vitro* as floating neurospheres (clusters of concentrated NSCs) and expanded exponentially (Rauch et al., 2006; Lindley et al., 2009; Metzger et al., 2009a; Cheng et al., 2017). This expansion step is crucial, as it allows a significant increase in the size of the donor cell pool without having to harvest more cells. These neurospheres contain ENSCs that give rise to neurons and glial cells following their transplantation to the embryonic (Lindley et al., 2009; Cheng et al., 2017) and postnatal (Hotta et al., 2013; Hetz et al., 2014; Cheng et al., 2017) mouse gut and restore GI motility in mice with enteric neuropathies (Lindley et al., 2008; McCann et al., 2017). ENSCs have also been transplanted into aganglionic mouse colon generated using diphtheria-toxin mediated ENS ablation (Bhave et al., 2019), where successful cell engraftment, migration, and differentiation of transplanted ENSCs were observed. More importantly, transplantation of ENSCs restored gut architecture changes and reduced mucosal inflammation (Bhave et al., 2019). To build upon the success of ENSCs as a stem cell source for treating enteric neuropathies, two studies have demonstrated their application for the treatment of brain injury (Osman et al., 2014; Belkind-Gerson et al., 2016). ENSCs were transplanted directly into the brains of mice following blunt injury (Belkind-Gerson et al., 2016) or radiation-induced injury (Osman et al., 2014; Belkind-Gerson et al., 2016). The cells survived at least 4 weeks following transplantation, differentiated into neurons and glia, and modulated the local environment to stimulate endogenous neurogenesis (Belkind-Gerson et al., 2016). Additionally, ENSCs delivered via tail vein injection were found to home to the site of injury in the brain where they survived for 10 weeks post-injection, and similarly stimulated endogenous neurogenesis (Belkind-Gerson et al., 2016). The success of systemic injection is clinically appealing compared to a direct approach to the brain or spinal cord.

Other studies have found similar success using ENSCs in models of spinal cord injury (Jevans et al., 2018, 2021). ENSCs were first co-cultured *in vitro* with spinal cord-derived cells, which revealed the formation of extensive cellular connections between the ENSCs and spinal cord-derived cells, as well as the presence of differentiated TuJ1+ neurons, S100+ glia, and Sox10+ stem cells within the transplanted neurospheres. Furthermore, following *in vivo* transplantation of ENSCs to an ablated region of chick spinal cord, donor ENSCs were found to form bridging connections within the injury zone up to 12 days later (Jevans et al., 2018). Combined *in vivo* treatment with ENSCs and chondroitinase ABC, an enzyme that breaks down chondroitin sulfate proteoglycans, which play a role in scar formation following injury, revealed improved regenerative effects compared to treatment with stem cells alone (Jevans et al., 2021). These studies suggest that transplantation of ENSCs can be an exciting treatment option for repair in CNS disorders, particularly when combined with other therapies to enhance their regenerative abilities.

Neural crest-derived Schwann cells in subcutaneous adipose tissue

Adipose tissue has been studied extensively as a potential source for cell based therapies since the isolation of progenitors with mesenchymal trilineage and neuronal differentiation potential were first reported 20 years ago (Zuk et al., 2001, 2002). Specifically, the SAT contains a reservoir of adipose stem cells within the stroma that can be easily obtained via minimally invasive techniques, including simple aspiration or suctioning of the fatty tissue (Zuk et al., 2002). This heterogenous population of progenitor cells are often referred to collectively as mesenchymal stem cells or multipotent stromal cells (MSCs) due to their differentiation potential and presumptive stromal cell origin. From 2007 to 2019 there were over 270 clinical trials worldwide studying this cell population in a variety of diseases, which overall suggested a favorable patient safety profile (Chu et al., 2019). Adipose stem cells have been primarily studied in the context of regenerative medicine and numerous inflammatory diseases including osteoarthritis, degenerative arthritis, cartilage or tendon injury, graft-vs.-host diseases, and chronic kidney diseases (Peng et al., 2019). They have not been well studied in the context of neurologic diseases (Hernández et al., 2020). Recent trials examining the safety of intracerebroventricular (ICV) injection of autologous adipose-derived stromal vascular fraction cells indicate favorable safety profiles across various disease states (24 subjects across 7 diseases) and promising clinical outcomes in the limited data for subjects with Alzheimer's disease (n = 10) and progressive multiple sclerosis (n = 6) (Duma et al., 2019). It was estimated that only 7.5% of the injected cells are adipose stem cells; therefore, these results could be improved upon by administering a more homogenous stem cell population.

Importantly, adipose stem cells can be cultured in conditions favoring the production of a cell population consistent with neural progenitor cells (Zuk et al., 2002; Peterson et al., 2018; Peng et al., 2019) that display a phenotype similar to stem cells derived directly from embryonic brain (Peterson et al., 2018). These adipose-derived neural progenitor cells are thought to arise from the transdifferentiation of isolated MSCs which acquire neural progenitor traits including propagation in culture as neurospheres, and can be induced in neuronal media conditions to become neurons and glia (Peng et al., 2019). When differentiated into neurons, cells derived from adipose tissue have network characteristics and

spontaneous spiking activity similar to primary neuronal cultures (Peterson et al., 2018), suggesting their ability to form a functioning nervous system.

Despite this knowledge of a neural progenitor population within adipose tissue, there have been few studies to date on adipose stem cells in the context of neurologic diseases. In a mouse stroke model, adipose-derived stem cells were found to reduce the size of the infarct and increase neurologic recovery via decreasing autophagy (Kuang et al., 2020). Another study found that the early delivery of adipose-derived stem cells combined with a rehabilitation program improved behavioral recovery, but not infarct size, in a rat stroke model (Mu et al., 2019). Our lab recently studied adipose-derived stem cells in diseases involving the enteric nervous system (Stavely et al., 2022). Importantly, while previously it was thought that the neural progenitors found within adipose tissue were derived from MSCs, we determined that these neural progenitors are likely to be NSCs that are distinct from adipose-derived MSCs and reside within the local nervous system niche of the SAT. These cells become transcriptionally distinct from Schwann cells and acquire features of NSCs during *in vitro* culture, which we anticipate is essential for their expansion and differentiation potential. Following transplantation into the gastrointestinal tract, these SAT-NSCs can successfully engraft, migrate within the muscularis layer, and differentiate into enteric neurons and glia. Transplantation of these cells directly into the gastric antrum in a mouse model of gastroparesis improved gastric emptying of both liquids and solids. Furthermore, transplantation of these cells into the aganglionic distal colorectum of a mouse model of Hirschsprung disease showed successful engraftment, migration, and survival of SAT-NSCs two to 3 weeks after surgery, as well as restoration of neural-evoked smooth muscle contractility. This evidence of functional recovery suggests that SAT-NSCs represent a source of autologous NSCs that could be used for treating enteric nervous system disorders. Given the exciting therapeutic potential of SAT-NSCs in ENS disorders, we believe that these cells offer significant potential for treatment of CNS disorders and further research is warranted.

Discussion

The above data reveal the exciting potential of two alternative sources of autologous stem cells, both of which are easily accessible and can be harvested from the donor with minimal risk. Importantly, they are derived from the nervous system and therefore possess intrinsic neurogenic potential that can be leveraged for CNS applications. ENSCs have been shown numerous times to be easily accessible from donors of all ages, from both small and large intestine, and from full-thickness and mucosal biopsies, making them a feasible source of donor cells for regenerative cell therapy. They engraft, migrate, differentiate, and survive when transplanted into the gut, and have shown restoration of normal gut architecture and improved survival when transplanted into models of ENS injury. Moreover, these cells have been shown to engraft, migrate, differentiate, survive, and promote endogenous neurogenesis when injected intracerebrally into areas of injured brain or when delivered systemically. Furthermore, ENSCs have also successfully engrafted, differentiated, and survived in *in vitro* and *in vivo* models of spinal cord injury. Further research is needed to assess functional recovery following ENSC transplantation in models of CNS injury.

Neural crest-derived Schwann cells found in subcutaneous adipose tissue are even more easily accessible than ENSCs, and can be isolated via simple aspiration or liposuction. These cells can similarly be expanded in culture to form neurospheres, and can engraft, migrate, undergo neuroglial differentiation, and survive when transplanted directly into the gut. Importantly, these cells form functional neuronal networks, as evidenced by the functional recovery following transplantation in two models of ENS disease, gastroparesis and Hirschsprung disease. Given this success, we believe SAT-NSCs offer great potential for treatment of CNS diseases, and further research is certainly warranted. These unique sources of PNS-derived autologous cells offer an exciting option for regenerative cell therapy in the CNS.

Author contributions

JM wrote the manuscript and created the table and figure. RH, RS, and AG helped write the manuscript and reviewed the table and figure. All authors contributed to the article and approved the submitted version.

Conflict of interest

The authors declare that the research was conducted in the absence of any commercial or financial relationships that could be construed as a potential conflict of interest.

Publisher's note

All claims expressed in this article are solely those of the authors and do not necessarily represent those of their affiliated organizations, or those of the publisher, the editors and the reviewers. Any product that may be evaluated in this article, or claim that may be made by its manufacturer, is not guaranteed or endorsed by the publisher.

References

Alessandrini, M., Preynat-Seauve, O., de Bruin, K., and Pepper, M. (2018). Stem cell therapy for neurologic disorders. *S. Afr. Med. J.* 109, 571–578. doi: 10.7196/SAMJ.2019.v109i8b.14009

Almond, S., Lindley, R., Kenny, S. E., Connell, M. G., and Edgar, D. H. (2007). Characterisation and transplantation of enteric nervous system progenitor cells. *Gut* 56, 489–496. doi: 10.1136/gut.2006.094565

Andres, R. H., Horie, N., Slikker, W., Keren-Gill, H., Zhan, K., Sun, G., et al. (2011). Human neural stem cells enhance structural plasticity and axonal transport in the ischaemic brain. *Brain* 134, 1777–1789. doi: 10.1093/brain/awr094

Andrzejewska, A., Dabrowska, S., Lukomska, B., and Janowski, M. (2021). Mesenchymal stem cells for neurological disorders. *Adv. Sci. (Weinh.)* 8, 2002944. doi: 10.1002/advs.202002944

Balassa, K., Danby, R., and Rocha, V. (2018). Haematopoietic stem cell transplants: principles and indications. *Br. J. Hosp. Med. (Lond.)* 80, 33–39. doi: 10.12968/hmed.2019.80.1.33

Beers, D. R., Henkel, J. S., Zhao, W., and Appel, S. H. (2008). CD4+ T cells support glial neuroprotection, slow disease progression, and modify glial morphology in an animal model of inherited ALS. *Proc. Natl. Acad. Sci. U.S.A.* 105, 15558–15563. doi: 10.1073/pnas.0807419105

Belkind-Gerson, J., Hotta, R., Whalen, M., Nayyar, N., Nagy, N., Cheng, L., et al. (2016). Engraftment of enteric neural progenitor cells into the injured adult brain. *BMC Neurosci.* 17:5. doi: 10.1186/s12868-016-0238-y

Bhave, S., Arciero, E., Baker, C., Ho, W. L., Stavely, R., Goldstein, A. M., et al. (2019). Enteric neuronal cell therapy reverses architectural changes in a novel diphtheria toxin-mediated model of colonic aganglionosis. *Sci. Rep.* 9:18756. doi: 10.1038/s41598-019-55128-4

Cheng, L. S., Graham, H. K., Pan, W. H., Nagy, N., Carreon-Rodriguez, A., Goldstein, A. M., et al. (2016). Optimizing neurogenic potential of enteric neurospheres for treatment of neurointestinal diseases. *J. Surg. Res.* 206, 451–459. doi: 10.1016/j.jss.2016.08.035

Cheng, L. S., Hotta, R., Graham, H. K., Belkind-Gerson, J., Nagy, N., and Goldstein, A. M. (2017). Postnatal human enteric neuronal progenitors can migrate, differentiate, and proliferate in embryonic and postnatal aganglionic gut environments. *Pediatric. Res.* 81, 838–846. doi: 10.1038/pr.2017.4

Chu, D. T., Phuong, T. N. T., Tien, N. L. B., Tran, D. K., Minh, L. B., Thanh, V. V., et al. (2019). Adipose tissue stem cells for therapy: an update on the progress of isolation, culture, storage, and clinical application. *J. Clin. Med.* 8:917. doi: 10.3390/jcm8070917

Deng, J., Zhang, Y., Xie, Y., Zhang, L., and Tang, P. (2018). Cell transplantation for spinal cord injury: tumorigenicity of induced pluripotent stem cell-derived neural stem/progenitor cells. *Stem Cells Int.* 2018:5653787. doi: 10.1155/2018/5653787

Duma, C., Kopyov, O., Kopyov, A., Berman, M., Lander, E., Elam, M., et al. (2019). Human intracerebroventricular (ICV) injection of autologous, non-engineered, adipose-derived stromal vascular fraction (ADSVF) for neurodegenerative disorders: results of a 3-year phase 1 study of 113 injections in 31 patients. *Mol. Biol. Rep.* 46, 5257–5272. doi: 10.1007/s11033-019-04983-5

Furness, J. B. (2012). The enteric nervous system and neurogastroenterology. *Nat. Rev. Gastroenterol. Hepatol.* 9, 286–294. doi: 10.1038/nrgastro.2012.32

Gronthos, S., Mankani, M., Brahim, J., Robey, P. G., and Shi, S. (2000). Postnatal human dental pulp stem cells (DPSCs) in vitro and in vivo. *Proc. Natl. Acad. Sci. U.S.A.* 97, 13625–13630. doi: 10.1073/pnas.240309797

Hernández, R., Jiménez-Luna, C., Perales-Adán, J., Perazzoli, G., Melguizo, C., and Prados, J. (2020). Differentiation of human mesenchymal stem cells towards neuronal lineage: clinical trials in nervous system disorders. *Biomol. Ther.* 28, 34–44. doi: 10.4062/biomolther.2019.065

Hetz, S., Acikgoez, A., Voss, U., Nieber, K., Holland, H., Hegewald, C., et al. (2014). In Vivo transplantation of neurosphere-like bodies derived from the human postnatal and adult enteric nervous system: a pilot study. *PLoS One* 9:e93605. doi: 10.1371/journal.pone.0093605

Hotta, R., Stamp, L. A., Foong, J. P. P., et al. (2013). Transplanted progenitors generate functional enteric neurons in the postnatal colon. *J. Clin. Investig.* 123, 1182–1191. doi: 10.1172/JCI65963

Ishibashi, S., Sakaguchi, M., Kuroiwa, T., Yamasaki, M., Kanemura, Y., Shizuko, I., et al. (2004). Human neural stem/progenitor cells, expanded in long-term neurosphere culture, promote functional recovery after focal ischemia in Mongolian gerbils. *J. Neurosci. Res.* 78, 215–223. doi: 10.1002/jnr.20246

Jevans, B., James, N. D., Burnside, E., McCann, C. J., Thapar, N., Bradbury, E. J., et al. (2021). Combined treatment with enteric neural stem cells and chondroitinase ABC reduces spinal cord lesion pathology. *Stem Cell Res. Ther.* 12:10. doi: 10.1186/s13287-020-02031-9

Jevans, B., McCann, C. J., Thapar, N., and Burns, A. J. (2018). Transplanted enteric neural stem cells integrate within the developing chick spinal cord: implications for spinal cord repair. *J. Anat.* 233, 592–606. doi: 10.1111/joa.12880

Kruger, G. M., Mosher, J. T., Bixby, S., Joseph, N., Iwashita, T., and Morrison, S. J. (2002). Neural crest stem cells persist in the adult gut but undergo changes in self-renewal, neuronal subtype potential, and factor responsiveness. *Neuron* 35, 657–669. doi: 10.1016/S0896-6273(02)00827-9

Kuang, Y., Zheng, X., Zhang, L., Ai, X., Venkataramani, V., Kilic, E., et al. (2020). Adipose-derived mesenchymal stem cells reduce autophagy in stroke mice by extracellular vesicle transfer of miR-25. *J. Extracell. Vesicles* 10:e12024. doi: 10.1002/jev2.12024

Kulbatski, I. (2010). Stem/Precursor cell-based CNS therapy: the importance of circumventing immune suppression by transplanting autologous cells. *Stem Cell Rev. Rep.* 6, 405–410. doi: 10.1007/s12015-010-9141-6

Kumagai, G., Okada, Y., Yamane, J., Kitamura, K., Mukaino, M., Tsuji, O., et al. (2009). Roles of ES cell-derived gliogenic neural stem/progenitor cells in functional recovery after spinal cord injury. *PLoS One* 4:e7706. doi: 10.1371/journal.pone.0007706

Lindley, R. M., Hawcutt, D. B., Connell, M. G., Almond, S. L., Vannucchi, M. G., Faussone-Pellegrini, M. S., et al. (2008). Human and mouse enteric nervous system neurosphere transplants regulate the function of aganglionic embryonic distal colon. *Gastroenterology* 135, 205–216. doi: 10.1053/j.gastro.2008.03.035

Lindley, R. M., Hawcutt, D. B., Connell, M. G., Edgar, D. H., and Kenny, S. E. (2009). Properties of secondary and tertiary human enteric nervous system neurospheres. *J. Pediatr. Surg.* 44, 1249–1255. doi: 10.1016/j.jpedsurg.2009.02.048

Massey, J. C., Sutton, I. J., Ma, D. D. F., and Moore, J. J. (2018). Regenerating immunotolerance in multiple sclerosis with autologous hematopoietic stem cell transplant. *Front. Immunol.* 9:410. doi: 10.3389/fimmu.2018.00410

McCann, C. J., Cooper, J. E., Natarajan, D., Jevans, B., Burnett, L. E., Burns, A. J., et al. (2017). Transplantation of enteric nervous system stem cells rescues nitric oxide synthase deficient mouse colon. *Nat. Commun.* 8:15937. doi: 10.1038/ncomms15937

Mead, B., Logan, A., Berry, M., Leadbeater, W., and Scheven, B. A. (2017). Concise review: dental pulp stem cells: a novel cell therapy for retinal and central nervous system repair. *Stem Cells* 35, 61–67. doi: 10.1002/stem.2398

Metzger, M., Bareiss, P. M., Danker, T., Wagner, S., Hennenlotter, J., Guenther, E., et al. (2009a). Expansion and differentiation of neural progenitors derived from the human adult enteric nervous system. *Gastroenterology* 137, 2063–2073. doi: 10.1053/j.gastro.2009.06.038

Metzger, M., Caldwell, C., Barlow, A. J., Burns, A. J., and Thapar, N. (2009b). Enteric nervous system stem cells derived from human gut mucosa for the treatment of aganglionic gut disorders. *Gastroenterology* 136, 2214–2225. doi: 10.1053/j.gastro.2009.02.048

Mothe, A. J., and Tator, C. H. (2013). Review of transplantation of neural stem/progenitor cells for spinal cord injury. *Int. J. Dev. Neurosci.* 31, 701–713. doi: 10.1016/j.ijdevneu.2013.07.004

Mu, J., Bakreen, A., Juntunen, M., Korhonen, P., Oinonen, E., Cui, L., et al. (2019). Combined adipose tissue-derived mesenchymal stem cell therapy and rehabilitation in experimental stroke. *Front. Neurol.* 10:235. doi: 10.3389/fneur.2019.00235

Nakamura, M., and Okano, H. (2013). Cell transplantation therapies for spinal cord injury focusing on induced pluripotent stem cells. *Cell Res.* 23, 70–80. doi: 10.1038/cr.2012.171

Nuti, N., Corallo, C., Chan, B., Ferrari, M., and Gerami-Naini, B. (2016). Multipotent differentiation of human dental pulp stem cells: a literature review. *Stem Cell Rev. Rep.* 12, 511–523. doi: 10.1007/s12015-016-9661-9

Oki, K., Tatarishvili, J., Wood, J., Koch, P., Wattananit, S., Mine, Y., et al. (2012). Human-induced pluripotent stem cells form functional neurons and improve recovery after grafting in stroke-damaged brain. *Stem Cells* 30, 1120–1133. doi: 10.1002/stem.1104

Osman, A. M., Zhou, K., Zhu, C., and Blomgren, K. (2014). Transplantation of enteric neural stem/progenitor cells into the irradiated young mouse hippocampus. *Cell Transplant.* 23, 1657–1671. doi: 10.3727/096368913X674648

Peng, C., Lu, L., Li, Y., and Hu, J. (2019). Neurospheres induced from human adipose-derived stem cells as a new source of neural progenitor cells. *Cell Transplant.* 28(Suppl. 1), 66S–75S. doi: 10.1177/0963689719888619

Peterson, E. D., Zenchak, J. R., Lossia, O. V., and Hochgeschwender, U. (2018). Neural stem cells derived directly from adipose tissue. *Stem Cells Dev*. 27, 637–647. doi: 10.1089/scd.2017.0195

Rauch, U., Hänsgen, A., Hagl, C., Holland-Cunz, S., and Schäfer, K. H. (2006). Isolation and cultivation of neuronal precursor cells from the developing human enteric nervous system as a tool for cell therapy in dysganglionosis. *Int. J. Colorectal Dis*. 21, 554–559. doi: 10.1007/s00384-005-0051-z

Sakai, K., Yamamoto, A., Matsubara, K., Nakamura, S., Naruse, M., Yamagata, M., et al. (2012). Human dental pulp-derived stem cells promote locomotor recovery after complete transection of the rat spinal cord by multiple neuro-regenerative mechanisms. *J. Clin. Invest*. 122, 80–90. doi: 10.1172/JCI59251

Schwartz, M., and Moalem, G. (2001). Beneficial immune activity after CNS injury: prospects for vaccination. *Neuroimmunology* 113, 185–192. doi: 10.1016/S0165-5728(00)00447-1

Simard, A. R., Soulet, D., Gowing, G., Julien, J. P., and Rivest, S. (2006). Bone marrow-derived microglia play a crticial role in restricting senile plaque formation in Alzheimer's disease. *Neuron* 49, 489–502. doi: 10.1016/j.neuron.2006.01.022

Stavely, R., Hotta, R., Picard, N., Rahman, A. A., Pan, W., Bhave, S., et al. (2022). Schwann cells in the subcutaneous adipose tissue have neurogenic potential and can be used for regenerative therapies. *Sci. Transl. Med.* 14:eabl8753. doi: 10.1126/scitranslmed.abl8753

Ullah, I., Subbarao, R. B., and Rho, G. J. (2015). Human mesenchymal stem cells - current trends and future prospective. *Biosci. Rep*. 35:e00191. doi: 10.1042/BSR20150025

Venkei, Z. G., and Yamashita, Y. M. (2018). Emerging mechanisms of asymmetric stem cell division. *J. Cell Biol*. 217, 3785–3795. doi: 10.1083/jcb.201807037

Ziv, Y., Avidan, H., Pluchino, S., Martino, G., and Schwartz, M. (2006). Synergy between immune cells and adult neural stem/progenitor cells promotes functional recovery from spinal cord injury. *Proc. Natl. Acad. Sci. U.S.A*. 103, 13174–13179. doi: 10.1073/pnas.0603747103

Zuk, P. A., Zhu, M., Ashijan, P., De Ugarte, D. A., Huang, J. I., Mizuno, H., et al. (2002). Human adipose tissue is a source of multipotent stem cells. *Mol. Biol. Cell* 13, 4279–4295. doi: 10.1091/mbc.e02-02-0105

Zuk, P. A., Zhu, M., Mizuno, H., Huang, J., Futrell, J. W., Katz, A. J., et al. (2001). Multilineage cells from human adipose tissue: implications for cell-based therapies. *Tissue Eng*. 7, 211–228. doi: 10.1089/107632701300062859

frontiers | Frontiers in Cellular Neuroscience

TYPE Review
PUBLISHED 04 August 2022
DOI 10.3389/fncel.2022.969002

Check for updates

OPEN ACCESS

EDITED BY
Chao Deng,
University of Wollongong, Australia

REVIEWED BY
Igor Jakovcevski,
Witten/Herdecke University, Germany
Lukas Grassner,
Paracelsus Medical University, Austria

*CORRESPONDENCE
Pengxiang Yang
yangpengxiang@163.com
Jing Jie
jiejing1103@126.com
Yumin Yang
yangym@ntu.edu.cn

SPECIALTY SECTION
This article was submitted to Cellular Neuropathology, a section of the journal Frontiers in Cellular Neuroscience

RECEIVED 14 June 2022
ACCEPTED 18 July 2022
PUBLISHED 04 August 2022

CITATION
Feng Y, Peng Y, Jie J, Yang Y and Yang P (2022) The immune microenvironment and tissue engineering strategies for spinal cord regeneration.
Front. Cell. Neurosci. 16:969002.
doi: 10.3389/fncel.2022.969002

COPYRIGHT
© 2022 Feng, Peng, Jie, Yang and Yang. This is an open-access article distributed under the terms of the Creative Commons Attribution License (CC BY). The use, distribution or reproduction in other forums is permitted, provided the original author(s) and the copyright owner(s) are credited and that the original publication in this journal is cited, in accordance with accepted academic practice. No use, distribution or reproduction is permitted which does not comply with these terms.

The immune microenvironment and tissue engineering strategies for spinal cord regeneration

Yuan Feng[1], Yong Peng[1], Jing Jie[2]*, Yumin Yang[1]* and Pengxiang Yang[1,3]*

[1]Key Laboratory of Neuroregeneration of Jiangsu and Ministry of Education, Co-innovation Center of Neuroregeneration, Nantong University, Nantong, China, [2]Department of Clinical Laboratory, The First People's Hospital of Nantong, The Second Affiliated Hospital of Nantong University, Nantong, China, [3]Institute of Cancer Prevention and Treatment, Heilongjiang Academy of Medical Science, Harbin Medical University, Harbin, China

Regeneration of neural tissue is limited following spinal cord injury (SCI). Successful regeneration of injured nerves requires the intrinsic regenerative capability of the neurons and a suitable microenvironment. However, the local microenvironment is damaged, including insufficient intraneural vascularization, prolonged immune responses, overactive immune responses, dysregulated bioenergetic metabolism and terminated bioelectrical conduction. Among them, the immune microenvironment formed by immune cells and cytokines plays a dual role in inflammation and regeneration. Few studies have focused on the role of the immune microenvironment in spinal cord regeneration. Here, we summarize those findings involving various immune cells (neutrophils, monocytes, microglia and T lymphocytes) after SCI. The pathological changes that occur in the local microenvironment and the function of immune cells are described. We also summarize and discuss the current strategies for treating SCI with tissue-engineered biomaterials from the perspective of the immune microenvironment.

KEYWORDS

spinal cord injury, immune microenvironment, regeneration, immune cells, biomaterials

Introduction

Physical injuries of the spinal cord and neurodegenerative diseases often cause irreversible damage and loss of function, and as many as 3.6 to 195.4 cases per million people suffer from spinal cord injury (SCI) each year worldwide (Jazayeri et al., 2015; Kumar et al., 2018; Flack et al., 2022; Varadarajan et al., 2022). At present, SCI is a serious clinical problem that lacks effective treatment, especially secondary injury

caused by the activation and infiltration of immune cells (Ahmed et al., 2018). The harsh microenvironment after SCI greatly hinders nerve regeneration and repair. In this process, the primary influencing microenvironmental cues are complex, including insufficient intraneural vascularization, prolonged immune responses, overactive immune responses, dysregulated bioenergetic metabolism and terminated bioelectrical conduction (Li et al., 2018a; Qian et al., 2021). Successful regeneration of injured nerves requires the intrinsic regenerative capability of the neurons and a suitable microenvironment (Park et al., 2008; Moore et al., 2009; Du et al., 2015). Nerve cells, glial cells, endothelial cells, fibroblasts and immune cells contribute to the formation of the local microenvironment. In addition to these cells, the extracellular matrix (ECM) and factors that produce cell-to-cell signals profoundly influence regeneration (Yang et al., 2021a). Efforts to promote injured nerve regeneration, particularly by removing unfavorable inflammatory factors, have been met with mixed success. The dual roles of immune cells within the inflammatory microenvironment are one key reason. Here, we discuss the structural characteristics of the spinal cord and significant clinical progress. A brief overview of the model systems that are most commonly used to study SCI is described. Importantly, we systematically summarize our current understanding of mammalian SCI responses to injury and highlight key advances in immune cells (neutrophils, macrophages, microglia, and T cells) in reconstructing the immune microenvironment. Moreover, we focus on the effects of biomaterials on SCI regeneration through regulating immune cells because these events have become the new direction of regenerative approaches.

Spinal cord structure

The anatomical structure and cellular composition of the central nervous system are more complex than those of the peripheral nerves, which is one of the reasons why SCI is difficult to overcome. The spinal cord is located in the spinal canal, and the upper end joins the medulla oblongata at the foramen magnum (Shechter et al., 2013). The shape of the spinal cord is slightly flat, and there are two enlargements (cervical and lumbosacral). The spinal cord gradually tapers to form the conus medullaris below the lumbosacral enlargement and terminally forms the filament. The outermost layer of the surface of the spinal cord is wrapped by the hard spinal cord. The upper end is attached to the foramen magnum, and the lower end is attached to the coccyx. The middle layer is a translucent membrane encased by the spinal cord arachnoid. The innermost layer is the pia mater and is filled with cerebrospinal fluid. There is a large gap between the innermost layer and the arachnoid (Canaani et al., 2011; Chen et al., 2017). In addition, the surface of the spinal cord is not smooth and is composed of six longitudinal grooves or fissures. The spinal cord is mainly composed of neurons and glial cells, and the neuron cell body is mostly composed of dendrites, which aggregate to form gray matter. The central canal runs through the spinal cord, connects the fourth ventricle above, and reaches the conus medullaris below to form the terminal chamber, containing cerebrospinal fluid. In adults, the central canal is often regarded as vestigial, with studies showing that it is occluded and disassembled during the second decade of life (Garcia-Ovejero et al., 2015; Saker et al., 2016). The gray matter exhibits an "H" shape surrounding the intermediate canal, which consists of anterior horns, posterior horns and a median zone. White matter is loaded around gray matter and is mainly composed of nerve fibers, glial cells and blood vessels. Longitudinal fiber tracts in the white matter form the connection pathways between the brain and spinal cord. The glial cells are around neurons, and microglia are ependymal cells that line the central lumen of the spinal cord (Bradbury and Burnside, 2019; Courtine and Sofroniew, 2019). The oligodendrocyte initiates multiple processes that contact and wrap around the axon to form the myelin sheath. The soma of astrocytes sends out many long and branched protrusions, which stretch and fill between the soma and the protrusions of nerve cells to support and separate. The ends of astrocytes are attached to adjacent capillary walls (**Figure 1**).

Clinical progress

The central nervous system of adult mammals has limited plasticity, and axons cannot regenerate spontaneously in the harsh microenvironment after severe spinal cord injury (Curcio and Bradke, 2018). At present, most preclinical strategies are only effective in animal models. There is no effective treatment to restore severely damaged spinal cord function. The clinical treatment of SCI is mainly aimed at the acute phase, including early immobilization of the damaged part of the spinal cord, palliative surgical decompression, vasopressors to increase mean arterial pressure (MAP) and selective injection of corticosteroids, such as methylprednisolone (Ahuja et al., 2017; Jutzeler et al., 2018; Samano and Nistri, 2019). It is worth noting that injection of methylprednisolone contributed little to the recovery of nerve function. These treatments are often conservative and do not greatly improve regeneration of the injured nervous system, and high-dose injections of methylprednisolone also increase the risk of adverse events. In addition to these treatments, drug therapy strategies targeting at alleviating secondary SCI have also emerged (Baroncini et al., 2021). Granulocyte-colony stimulating factor (G-CSF) is a glycoprotein that stimulates the bone marrow (BM) to produce granulocytes and stem cells, and it is mainly used in neutropenia. Moreover, G-CSF also has the neuroprotective effect of reducing cell inflammation and apoptosis. In phase I/II clinical trials, G-CSF was administered intravenously for 5 days

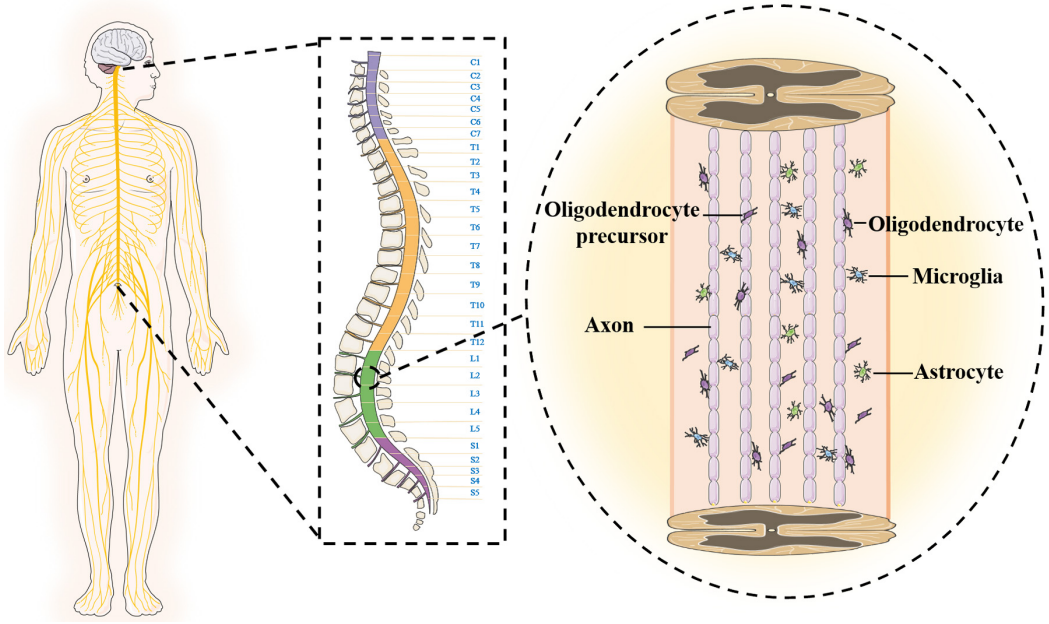

FIGURE 1
The structural characteristics of spinal cord.

in patients with acute SCI, and no serious adverse effects were observed (Koda et al., 2018). In a multicentre, prospective, non-randomized, non-blinded, comparative control study (phase IIb clinical trial), ASIA motor score was significantly improved in the G-CSF group (Inada et al., 2014). Minocycline, as an antibiotic, has properties of reducing inflammation and oxidative stress. Minocycline also exerts neuroprotective effects by inhibiting apoptosis. In a phase II clinical trial, the serum concentration of minocycline was stabilized for 7 days, and there were no obvious adverse reactions after SCI treatment. Furthermore, minocycline was proved to be feasible and safe in the above study, and associated with a trend of improvement in several outcome indicators (Casha et al., 2012). In addition, a variety of drugs can alleviate secondary SCI by reducing excitotoxicity and the inflammatory response, inhibiting apoptosis, promoting angiogenesis and/or supporting neuronal cells. These drugs include riluzole, basic fibroblast growth factor, glyburide, imatinib and AC-105 (Casha et al., 2012; Samano and Nistri, 2019; Takami et al., 2020; Baroncini et al., 2021; Flack et al., 2022). Most of these drugs have demonstrated efficacitive to some extent in animal studies and early clinical trials. Unfortunately, no drugs have been approved for the treatment of SCI (Koda et al., 2018; Takami et al., 2020).

Stem cell treatment

Stem cell transplantation for SCI has significant advantages as follows: (1) Compared with the implantation of inert materials, it avoids the harm caused by the secondary surgical; (2) transplanted cells rapidly fill the defect of the lesion site; and (3) various nutritional factors are secreted and promote the regeneration of axons. Recently, stem cell transplantation has become the most promising preclinical treatment strategy for SCI (Bryukhovetskiy et al., 2005). Human embryonic stem cells (hESCs), induced pluripotent stem cells (iPSCs), ependymal stem/progenitor cells and mesenchymal stem cells (MSCs) have been used frequently in SCI research (Bryukhovetski et al., 2005; Okano, 2009; Blasko et al., 2017; Ning et al., 2019). hESCs have the ability to differentiate into ectodermal cells, such as neurons and glial cells. The transplantation of oligodendrocytes and neuronal progenitors derived from embryonic stem cells has achieved some success in animal models. iPSCs can differentiate into neural progenitor cells, neuronal cells and oligodendrocytes. The transplantation of iPSCs promotes functional recovery in the early stage of injury, but it has a risk of tumorigenicity (Wertheim et al., 2022). At present, stem cells are still controversial due to ethical issues, immune rejection and other issues. MSCs have significant advantages because they are isolated from BM, umbilical cord, fat and other tissues without causing harm to health or ethical controversy (Ma et al., 2018; Li L. et al., 2020; Zhu et al., 2021). The survival rate of MSCs can be improved by loading neurotrophic factors or cytokines with biological material scaffolds, such as hydrogels or ECM.

There are different applications of biological materials in support of stem cell transplantation to treat SCI. One way is to fill spinal cord defects with exogenous stem

cells, which can differentiate into neurons and glial cells to promote spinal cord regeneration. Natural or artificial biological material scaffolds can directly load cells to repair SCI. Wang N. et al., 2018 used functional hydrogels or collagen-loaded MSCs to bridge defects of the spinal cord, which promoted axon growth and regeneration of neurons as well as significantly improved motor function recovery (Wang N. et al., 2018; Yin et al., 2018). The other way is to activate endogenous neural stem cells and induce their differentiation into functional neurons by scaffold loading neurotrophic factors, cytokines or small molecules (Fan et al., 2017; Yang et al., 2021d; Yin et al., 2021). This approach involves fewer ethical issues and is not limited to stem cell sources, stem cell numbers and low survival rates. Yang et al. (2015) used chitosan scaffolds loaded with neurotrophic factor-3 (NT-3) to provide an excellent microenvironment that activates endogenous neural stem cells at the injury site; the slow release of NT-3 promotes spinal cord nerve growth and functional recovery (Duan et al., 2015; Yang et al., 2015; Rao et al., 2018). The nervous injury microenvironment is not conducive to the survival of stem cells. Stem cell-derived exosomes are another way to achieve neural regeneration and protection. Exosomes are evenly dispersed in hydrogels, forming delivery systems that improve spinal cord regeneration in a more precise manner. Mu et al. (2021) coated human MSC-derived exosomes with a peptide-modified adhesive hydrogel to regulate the microenvironment of SCI and reduce inflammation and oxidative reactions, which is conducive to spinal cord regeneration and protection.

Tissue engineering strategy

Approaches that focus on cell transplantation have failed to improve the complex, multilayered and spatiotemporal dynamics of the SCI microenvironment. The difficulty of transplantation and endogenous recruitment cells increases with high levels of reactive oxygen species or nitrogen (ROSN)accumulation under ischemia, excessive tissue remodeling under inflammatory response, excitability and cytotoxicity as well as glial scar formation (Bi et al., 2021). The combination strategy based on scaffolds can provide an excellent microenvironment for nerve regeneration, and it is mainly performed based on the two aspects of promoting growth or eliminating inhibitive factors (Fu et al., 2022). Various studies have been performed to promote spinal cord regeneration through scaffold load cells or nutritional factors. Natural biological materials (chitosan, collagen, gelatin, hyaluronic acid and cell matrix., etc.) or synthetic biodegradable biomaterials (polyglycolic acid, polylactic acid, polylactic acid-glycolic acid and polyepsilon-caprolactone., etc.) mimic the natural structure of the spinal cord for neuron proliferation, migration and differentiation (Chen et al., 2017; Varone et al., 2017; Shen et al., 2022a). Moreover, neurotrophic factor (NT-3), brain-derived neurotrophic factor (BDNF), basic fibroblast growth factor (bFGF) and vascular endothelial growth factor (VEGF) can be used alone or in combination to improve the survival of neurons and promote axonal regeneration (Li et al., 2009, 2019; He et al., 2011; Han et al., 2015; Chen et al., 2018; Wang X. L. et al., 2018; Shang et al., 2019).

During the acute period of SCI, many immune cells (macrophages, neutrophils, microglia and lymphocytes) are activated and infiltrate the lesion site. Severe inflammation and oxidation reactions hinder spinal cord regeneration, and some even persist for the rest of the patient's life. Many researchers use hydrogels, nanoparticles and immunomodulatory scaffolds to deliver anti-inflammatory or antioxidant drugs or factors to treat SCI. These strategies improve the immune microenvironment of the damaged site and enhance regeneration capacity (White-Schenk et al., 2015; Dombrowski et al., 2017; Ham and Leipzig, 2018; Bi et al., 2021; Gao et al., 2021; Shen et al., 2022b). This review focuses on the pathological changes in the local microenvironment and the changes and functions of immune cells after SCI. The current strategies for treating SCI with tissue-engineered biomaterials are also discussed from the perspective of the immune microenvironment.

Model for spinal cord injury regeneration

The animal model should be similar to human pathophysiology, morphological structure, electrophysiology and many other aspects. The ideal experimental animal model of SCI has the following characteristics: (1) ensure repeatability and reliability; (2) similar to anatomical structure and pathophysiology; (3) adjustable SCI degree; and (4) low cost, simple model and strong operability. The application of rats or mice remains optimal for preclinical studies of SCI. A review of 2,209 studies (excluding review articles and unoriginal articles) indicated that 92% of SCI models use rodents with 72.4% of the rodent models being rat models, which is attributed to rat models being easier to operate than mouse models (Sharif-Alhoseini et al., 2017). Moreover, rats are more similar to humans in terms of pathophysiology, morphological structure and electrophysiology. However, 16% of the models are mouse models, and the mouse genome is closer to that of humans. At present, SCI models include contusion, transection injury, compression injury, ischemia injury and photochemical injury models. Among them, the contusion model and transection injury model (partial and

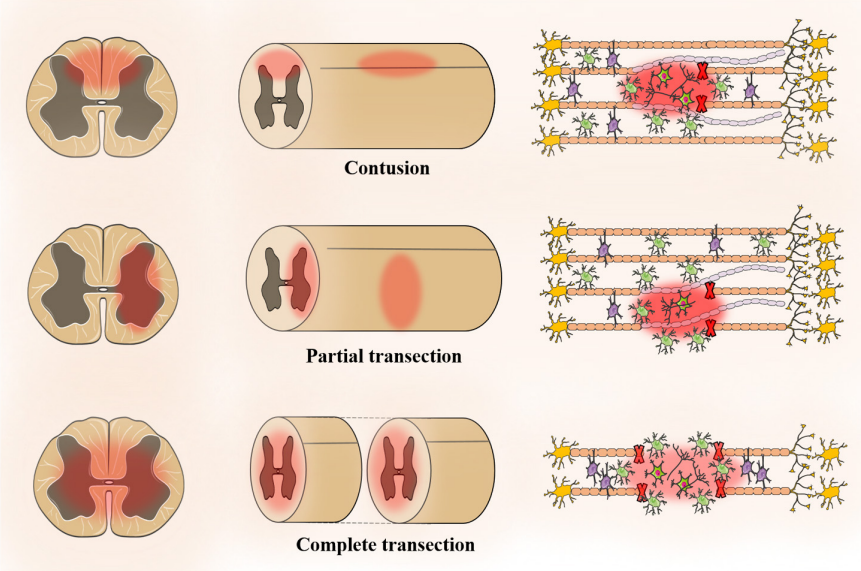

FIGURE 2
The animal model for spinal cord injury regeneration.

complete) account for a large proportion (**Figure 2**; Abdullahi et al., 2017).

Contusion model

Allen (1991) first attempted to create a model of SCI that could be controlled by using an object to fix the height of the spinal cord. Since then, SCI models have undergone design improvements in terms of repeatability and quality control, including height, time and speed (Gruner, 1992). The most common impact method is weight loss (∼37.5% of all studies) followed by impact (∼27.4%) and infinite impact (∼20.6%) (Sharif-Alhoseini et al., 2017). In addition, there is also an air gun for SCI modeling in rats, which avoids lamina resection. However, its repeatability and stability need to be verified (Marcol et al., 2012).

Transverse damage model

Allen (1991) showed that the injury progression of the contusion and transverse fracture have a similar trend in the acute phase within three weeks, but the pathophysiology and tissue morphology of the injury site are completely different (All and Al-Nashash, 2021). There are two types of transverse injuries, namely, partial and complete. In clinical practice, complete spinal cord transection is rare. Although complete spinal cord transection is not suitable for neuroprotective research, it is suitable for testing the performance of multifunctional biomaterial scaffolds, which explore neural regeneration, plasticity and tissue engineering strategies (Kim et al., 2018). The complete transverse injury model is suitable for cell transplantation. Lukovic et al. (2015) proposed a detailed and standard surgical procedure for a complete transect model and restored motor function in the transplant group to support the complete transect model for cell transplantation (All and Al-Nashash, 2021). After the lamina is surgically removed, the spinal cord is transected completely or partially using surgical scissors or blades (Talac et al., 2004). One side of the spinal cord is resected, while the spinal cord bundle is completely or partially preserved on the other side. The complete transect model facilitates the study of different functions of the damaged or non-damaged spinal tract. Neuroanatomic and electrophysiological studies have used a transverse injury model to assess the recovery of spinal motor function.

Compression damage model

The majority of studies have used a spinal cord compression injury model with aneurysm clips (Sharif-Alhoseini et al., 2017). Rivlin and Tator (1978) first removed the rat spinal laminae and then molded them using a modified version of the aneurysm clip, and they quantified the relationship between the duration of compression injury and the severity of SCI by applying compression forces of 180 g or other to the spinal cord area for varying lengths of time. The advantages of the improved model are lower cost and relatively simple operation, but the actual compression force at the clipping

site is difficult to accurately grasp (von Euler et al., 1997; Marques et al., 2014). Tarlov et al. (1953) inserted a balloon catheter into the spinal cord and then injected air or saline to compress and cause injury. Lim et al. (2007) measured the degree of spinal canal occlusion by injecting contrast agent into the catheter based on Tarlov's method, and they also assessed the severity of SCI by HE.

Ischemic injury model

Ischemia injury has been established in primates, large animals and rodents (Awad et al., 2021). It is necessary to block the descending aorta in an ischemia model of the spinal cord (Marsala et al., 1994). Lang-Lazdunski et al. (2000) established a model of spinal cord ischemia in mice by reperfusing the aortic arch and the left subclavicular artery after cross-foraging for different time periods followed by assessment of motor function scores and HE. A reproducible mouse ischemia model has been generated by cross-clipping of the aortic arch and the left subclavian artery. Compared to rats, mouse models have obvious advantages in genomic research.

Pathological changes in the immune microenvironment in spinal cord injury

Primary SCI is a direct injury that shows destruction of spinal cord structure and contents caused by traction, shearing and compression from external forces. A series of complex and interrelated activities occurs at the site of injury, including the oxidative stress response, inflammatory response, delayed apoptosis and glial scar formation, which cause secondary SCI. In these activities, immune cells, such as monocytes, macrophages, neutrophils and microglia, play various roles, and they also interact with oligodendrocytes and astrocytes to guide the transformation between proinflammatory and anti-inflammatory cells in the immune microenvironment. Secondary SCI can be divided into acute, subacute and chronic stages according to the time course (**Figure 3**).

Acute phase

The acute phase usually occurs within 48 h of SCI. The spinal cord structure is severely damaged after being impacted by external forces. The main pathological manifestations are destruction of the BSCB, severe bleeding, sever edema, ion imbalance, increased excitatory toxicity, free radical production and inflammatory reactions caused by activation and infiltration of immune cells.

Severe bleeding and ischemic edema

The blood–spinal cord barrier (BSCB) is composed of astrocytes, microglia surrounding blood vessels and continuous capillary endothelial cells in the basement membrane. These cells insulate and protect the spinal cord from metabolites and harmful substances in the blood and surrounding environment. Damage to the BSCB by mechanical external forces is one of the earliest events in the acute stage of SCI. Bleeding usually occurs in the central part of the spinal cord, occupying a major part of the gray matter and radiating into the white matter (Bartanusz et al., 2011). There is evidence that bleeding causes nerve tissue damage (Noble and Wrathall, 1989). After sustained bleeding, vascular ischemia, hypovolemia, and hyperfusion occur at the site of injury. Various phagocytes are activated and migrate to the site of injury and catalyze the release of metal ions, leading to the formation of free radicals. The nerve of the spinal cord is rich in fatty acid chains, which are sensitive to free radicals, ultimately leading to a large amount of neuronal cell death and tissue destruction (LeBel and Bondy, 1991). At the same time, the blood vessel ruptures, causing a large amount of immune cells (neutrophils, macrophages, microglia and lymphocytes) to extravasate into the blood. These immune cells migrate and ingest myelin fragments by sensing the injury signal. However, these immune cells impair the tight junctions and interstitial junctions of endothelial cells, leading to increased vascular permeability and leakage. Plasma-derived macromolecules penetrate cell membranes and cause edema.

Excitatory toxicity and ion imbalance

Excitatory toxicity and ion imbalance are markers in the acute stage of secondary SCI. Glutamate receptors are involved in the excitatory transmission of the central nervous system and are associated with various chemical changes in synaptic transmission. In primary SCI, neurons and glial cells release a large amount of glutamate, which overactivates ionic glutamate receptors. Calcium and sodium ion influx leads to cell necrosis, apoptosis or autophagy. In addition, the release of ATP and nucleotides activates purinergic receptors and leads to calcium influx.

Inflammatory response

The inflammatory response occurs throughout the process of SCI. Multiple immune cells are activated to rapidly migrate and infiltrate into the damaged spinal cord. Astrocytes, dendritic cells and other cells are also involved in the inflammatory response (Yang et al., 2018; Xing et al., 2019). In the first stage, neutrophils, resident microglia and astrocytes migrate to the site of injury, and they play a dual role in damage and repair during spinal cord regeneration. In the second stage, blood-derived macrophages and T/B lymphocytes produce various cytokines (IL-1α, IL-1β, IL-6 and TNF-α) and aggravate the inflammatory and oxidative reactions of the immune microenvironment. In this review, we will discuss the details in the next chapter. It

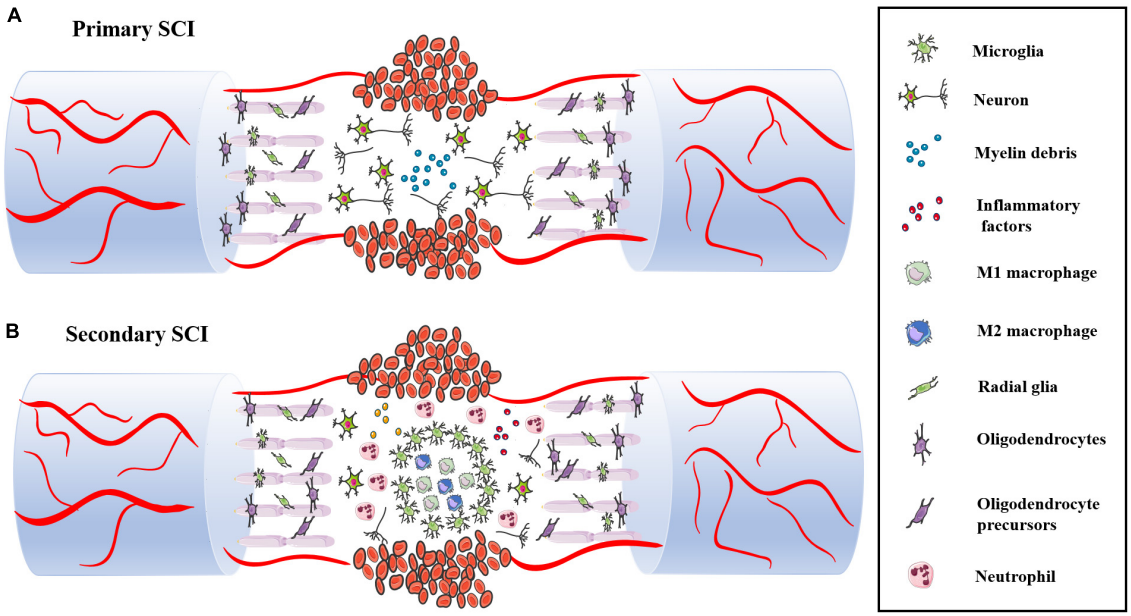

FIGURE 3
(A) The structure and content of spinal cord are destroyed during primary SCI, including neuron body and axon damage and destruction of the BSCB. **(B)** Following SCI, immune cells infiltrate into the damaged spinal cord and release various pro-inflammatory factors, which leads to massive neuronal death.

is important to note that inflammation is more apparent in the acute phase of injury but still continues in subacute and chronic inflammation.

Subacute stage

The subacute phase typically occurs within 48 h to two weeks after SCI. Neuron and oligodendrocyte apoptosis as well as axon demyelination occur in this stage. The appearance of glial scars around the lesion site and the release of axon growth inhibition factor are key events affecting spinal cord regeneration.

Apoptosis and axonal demyelination

Demyelination mainly occurs 2-7 days after SCI, and it initially occurs in the lesion center and then gradually moves to the fiber bundles of spinal white matter (Blight, 1985). Totoiu and Keirstead (2005) conducted a study on chronic pathological processes and found that the number of demyelinated axons peaks within one day of injury and then declines within 1-2 weeks with a process lasting up to 450 days. Therefore, it can be inferred that the pathological process of demyelination mainly occurs within two weeks, but this process may last for a long time. The process of demyelination is often accompanied by the apoptosis and necrosis of oligodendrocytes, which may be one of the important causes (Wu and Ren, 2008). A series of studies have demonstrated this view. Sanchez et al. (1996) showed that locally induced aggregation of neural fiber networks by oligodendrocytes is critical for axon growth. Traka et al. (2016) found that oligodendrocyte death results in extensive myelin and axon loss. Moore et al. (2015) showed that oligodendrocyte progenitor cells at the site of injury are affected by proinflammatory T cells, M1-polarized BM cells and microglia, resulting in reduced differentiation. In addition, other research on oligodendrocyte apoptosis has been reported, including excessive glutamate release, insufficient nutritional factors and activated caspases (Xu et al., 2004). Studies on spinal cord regeneration mainly involve inhibition of demyelination or promotion of myelin regeneration. Armstrong et al. (2002) found that an increase in FGF2 facilitates the proliferation of oligodendrocyte progenitor cells and reduces the number of differentiated mature glial cells (Armstrong et al., 2002). Schwann cells are generally considered to be myelinated cells of the peripheral nervous system, but some studies have shown that Schwann cell remyelination also occurs after central nervous damage. Franklin et al. reported that the Schwann cells in the central system migrate from peripheral nerves after the destruction of glial cells (Franklin and Blakemore, 1993). Keirstead et al. (1999) suggested that Schwann cell remyelination is due to the abnormal differentiation of endogenous precursor cells.

Glial scar formation and axon growth inhibition factor

As immune cells infiltrate, glial cells become activated, proliferate and eventually form glial scars, which blocks the

inflammatory response caused by immune cell infiltration. However, scarring largely prevents neuron regeneration and differentiation. The mechanical barrier of axonal regeneration includes a variety of cells (astrocytes, oligodendrocyte progenitor cells, immune cells fibroblasts) and cell matrix compositions (Bradbury and Burnside, 2019; Lukacova et al., 2021). Activated astrocytes also have two different phenotypes, namely, A1 and A2, similar to macrophages. A1 astrocytes have neurotoxic effects and induce rapid neuronal and oligodendrocyte death, while A2 astrocytes have neuroprotective effects and promote neuronal survival (Wang et al., 2021).

In addition, the injured site microenvironment is a key factor. Growth-related inhibitory factors in the extracellular matrix, including chondroitin sulfate proteoglycan (CSPG), neurite outgrowth inhibitor (NOGO-A), myelin-associated glycoprotein (MAG) and oligodendrocyte myelin glycoprotein (OMgp), inhibit regeneration progression. CSPG is the major component of the glial scar after SCI. CSPG inhibits axon regeneration and plays a leading role in demyelination and axonal degeneration. Removal of glycosaminoglycan chains of CSPG attenuates the inhibitory activity in spinal cord regeneration. The traditional view is that astrocyte scar is not conducive to axon regeneration and its formation is one of the important reasons for the failure of axons regeneration. Anderson et al. (2016) proposed the opposite opinion. They demonstrated that astrocyte glial scarring contributes to rather than prevents axon regeneration in the central nervous system through loss of function. In addition, astrocyte scar formation may play a beneficial role in limiting inflammatory cell infiltration, filling the injured site, rebuilding the BCSC, and protecting neurons and oligodendrocytes (Bush et al., 1999; Sofroniew, 2005, 2015; Kawano et al., 2012; Bradbury and Burnside, 2019). The role of glial scar formation in recovery from spinal cord injury remains controversial.

Chronic phase

In the chronic stage, the glial scar thickens, and regeneration becomes more difficult. In the acute stage, astrocyte scarring alleviates the inflammatory response at the site of SCI, however, it obstructs the regeneration and differentiation of neuron cells to a large extent (Anderson et al., 2016). Li et al. (2018b) reported that glial scars in subacute and chronic stages have different compositions, characteristics and effects. The treatment strategies for glial scars in different stages should also be different. Li et al. (2018b) also suggested that the glial scar has an inhibitory effect on axon regeneration and that removal of the glial scar in the chronic stage significantly increases axon regeneration. Some researchers have attempted to transplant stem cells at the chronic stage. Wertheim et al. removed the scar of the chronic stage and transplanted hydrogel-encapsulated iPSCs to the injured site, resulting in good functional recovery, and they also transplanted neural stem cells/progenitor cells from human olfactory epithelial mucosa, resulting in improved hind limb motor function of rats (Voronova et al., 2020).

At present, few studies have focused on the immune microenvironment of chronic stages after SCI. Beck et al. detected changes in major immune cell types at the early stage (10 days) and later stage (180 days) after SCI with immune cells still detected at 180 days after injury, and they reported that the inflammatory response has a reparative effect (Beck et al., 2010). These findings suggest SCI is a lengthy process, and the associated reactions may persist throughout the patient's life. Dulin et al. reported increased levels of oxidative and inflammatory metabolites in the injured site of rats 9 months after SCI, and they demonstrated that licofelone reduces the expression level in the injured site (Dulin et al., 2013). Hains et al. intrathecally injected the microglial inhibitor, minocycline, in a rat contusion model and showed that activated microglia promote chronic central nerve pain.

Immune cells in the microenvironment of spinal cord injury

Various inflammatory immune cells, such as neutrophils, monocytes and microglia, are activated by cytokines or chemokines, and they rapidly infiltrate through damaged blood vessels and participate in the activities of the immune microenvironment after SCI (Anwar et al., 2016; Yang et al., 2021c). Astrocytes, microglia and oligodendrocyte progenitors subsequently proliferate. Monocytes differentiate into macrophages and engulf damaged tissue or cell debris, and fibroblasts are stimulated and activated to induce fibrosis (Kong and Gao, 2017). To prevent further expansion of the damaged tissue, the fibrotic scar is gradually surrounded by an astrocyte scar, reaching a stable state after injury, which greatly obstructs the regeneration and differentiation of nerve cells (**Figure 4**).

Neutrophils

Neutrophils are derived from BM hematopoietic stem cells and are abundant in the peripheral blood. Neutrophils are short-lived (~24 h) innate immune cells, and they are removed by macrophages. Neutrophils are the first activated inflammatory cells that migrate to the injured spinal cord. Neutrophils cause oxidative and inflammatory responses, but the exact mechanism is still unclear. In addition, the degranulation and phagocytosis of neutrophils against myelin sheath fragments after SCI have become a new research direction.

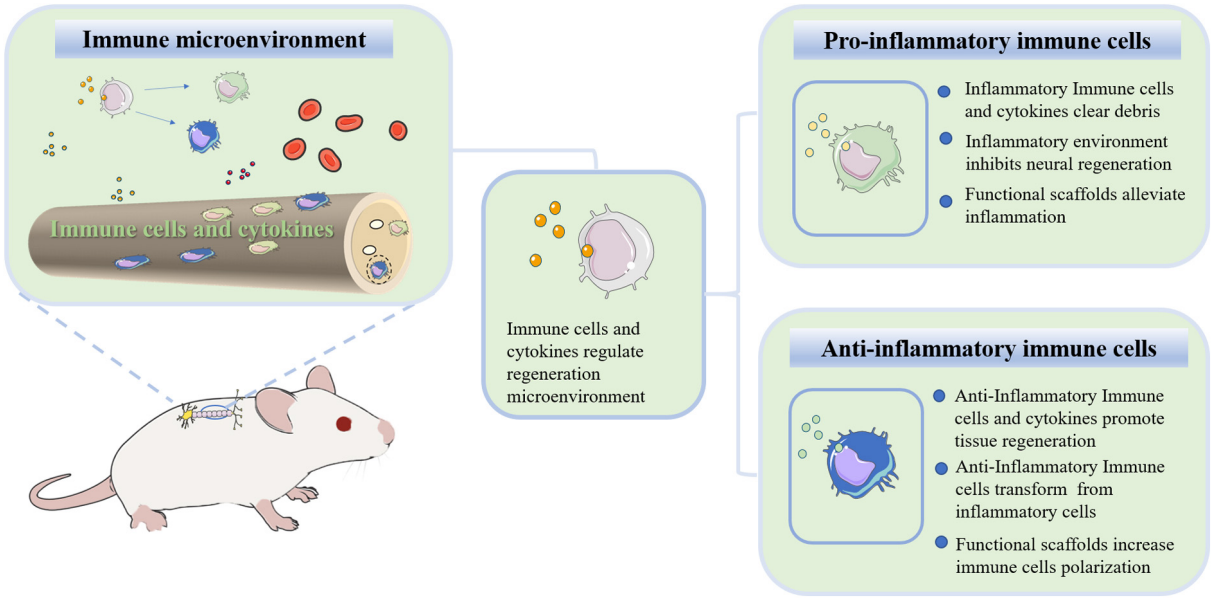

FIGURE 4
Changes of immune cells in the microenvironment of spinal cord injury.

Neutrophil activation and migration

The loss of injured nerve function is associated with neutrophil recruitment and accumulation at the local lesion site. Neutrophil receptors recognize two types of signaling, namely, pathogen-associated molecular patterns (PAMPs) and danger-associated molecular patterns (DAMPs), in response to pathogen invasion or tissue damage. After SCI, injured cells are damaged and release various DAMPs, including DNA, RNA, histones, high mobility group protein 1 (HMGB1) and adenosine triphosphate (ATP). The receptors that sense these signals activate serine-activated protein kinase and NF-κB downstream pathways to express more proinflammatory factors, thereby recruiting more neutrophils (Albrecht et al., 2007). Previous research has found that the expression of CCL2, CXCL1 and CXCL2 in astrocytes from 3 h to 12 h leads to neutrophil infiltration, which is related to the MyD88 and IL-1 receptor signaling pathways (Pineau et al., 2010). Other inflammatory, factors and chemokines included IL-1α, IL-1β, TNF, GCSF, CCL3, CXCL1, CXCL2, and CXCL5, are involved in this process (Zivkovic et al., 2021). Spleen tyrosine kinase (Syk) facilitates specific neutrophil functional responses to SCI, including activation, cytokine expression and cell death. Long-term neurological deficits are exacerbated by Syk signaling in neutrophils independent of acute blood–spinal cord barrier disruption and long-term white matter sparing (McCreedy et al., 2021). Generally, neutrophils begin to infiltrate the injured site within a few hours and peak within three days. Neutrophils produce more inflammatory factors, proteolytic enzymes, ROS and nitrogen substances, which deteriorate the microenvironment of the injured site, resulting in a large amount of cell apoptosis and necrosis (Okada, 2016).

Infiltrating neutrophils induce tissue damage

The adverse effects of neutrophil infiltration in the acute stage of SCI are inflammation, oxidative stress response, proinflammatory factors, hydrolase and other damage to the BSCB, which result in inadequate vascular formation. Neutrophils release harmful substances that are unfavorable to the injury microenvironment. These unfavorable factors include neutrophil matrix traps (NETs), neutrophil elastase (NE), myeloperoxidase (MPO) and metal matrix peptide enzymes (MMPs) (Fiani et al., 2021).

Neutrophil matrix traps are composed of chromatin fibers and granular proteins, including histones, granulocyte enzymes and peptides. Previous research has shown that NETs induce inflammatory responses and damage the BSCB, resulting in axonal degeneration, which is not conducive to neuronal regeneration. The arginine deaminase-4 peptide blocks the formation of NETs by DNAse-1, which reduces cell death and scar formation, thereby promoting functional recovery (Feng et al., 2021). In addition, NETs accelerate endothelial cell injury and destroy the BSCB by increasing the expression of TRPV4. Tonai et al. (2001) used the specific neutrophil protease inhibitor, ONO-5046, to significantly reduce nerve injury in a rat model of compression. MMP is an important extracellular matrix hydrolase that degrades basement membrane components. MMPs damage the BSCB and aggravate the microenvironment. MMPs participating in SCI

mainly include MMP-1, MMP-2, MMP-9 and MMP-12. MMP-9 and MMP-2 are closely related to the loss of nerve function and formation of glial scars (Zhang et al., 2011). The expression of MMP-9 peaks at 12-24 h, which exacerbates secondary SCI (de Castro et al., 2000). In addition, MMP-9 restricts angiogenesis in the early stage of tissue damage (**Figure 5**; Noble et al., 2002).

After spinal cord injury, a large number of neutrophils with blood and other immune cells infiltrate the damaged site and release a large number of pro-inflammatory and chemotactic factors; Neutrophils release cytokines and various harmful enzymes (MMP, NE, mpo.,etc.); Various inflammatory mediators activate monocytes, microglia, astrocytes, etc. to produce reactive oxygen and nitrogen species, resulting in the deterioration of the microenvironment; Macrophages phagocytized apoptotic neutrophils and transformed into M2 macrophages.

Potential regenerative effects of neutrophils

Although most research has focused on the deleterious effects of neutrophils on SCI, neutrophils are heterogeneous, and the recruitment of subsets may not necessarily indicate an exacerbation of injury. Sas et al. (2020) discovered that a new subpopulation of neutrophils ($CD14^+$ $Ly6G^{low}$) promotes neuronal survival and axon regeneration in the central nervous system. Another study has shown that neutrophils activate more immune cells to migrate to the injury site and clear debris by secreting proinflammatory factors. Excessive infiltrating neutrophils are removed by macrophages, which induces their transformation into the M2 anti-inflammatory phenotype and promotes injury repair (Soehnlein and Lindbom, 2010). It has also been demonstrated that neutrophils play a role in inflammation and tissue repair to some extent by releasing secretory leukocyte proteases (Ghasemlou et al., 2010).

Engineered neutrophils promote spinal cord regeneration

Neutrophils activate and migrate to the injured site and release various proinflammatory and oxidative factors. Some researchers have applied these characteristics to loads with drugs or cytokines to improve the immune regeneration microenvironment. Tetramethylpyrazine (TMP) has anti-inflammatory, antioxidative, and neuroprotective effects, but it is not easily soluble in water. Li et al. (2021) developed nanoparticles that can be internalized by neutrophils. These nanoparticles rapidly infiltrate into the injury site of the spinal cord in the acute phase, and the drug-loaded nanoparticles significantly improve the immune regeneration microenvironment (Li et al., 2021). Yihui et al. developed a neutrophil membrane-encapsulated polydopamine nanoparticle, which effectively adsorbs various inflammatory factors and inhibits the production of ROS and nitrogen substances. The improved local immune microenvironment promotes neuronal growth, differentiation and motor recovery in rats (Bi et al., 2021).

Macrophages

At the central site of SCI, macrophages are heterogeneous and mostly derived from BM. Macrophages are responsible for removing debris from damaged cells and tissues, while specialized activated microglia (central nerve resident cells) form boundaries at the damaged site (David and Kroner, 2011). Two sources of macrophages are indistinguishable in tissue sections and are termed microglia/macrophages after staining of the CD11b and IBA-1 markers. Considering some similar features, monocyte-derived macrophages and neuroresident microglia have been discussed together in many studies. However, these cells vary widely in terms of origin, biomarkers and function. After tissue damage, microglia recognize the injury signal from the surrounding environment and thus activate and infiltrate to the injury site following monocyte-derived macrophages (MDMs) (Ding et al., 2021; Sun et al., 2021). In addition, microglia contain fragments of phagocytic tissue 3 days after SCI, which is before MDM migration (David et al., 2018). Microglia and macrophages may have different roles in the injury microenvironment. In the next section, we discuss microglia and macrophages from two different sources. We first introduce monocyte-derived macrophages that migrate to the lesion site after activation from BM or the spleen (**Figure 6**).

Recruitment and polarization of monocyte-derived macrophages

Under the condition of injury, specific cytokines stimulate macrophages to differentiate into different phenotypes, namely, pro-inflammatory M1 and anti-inflammatory M2 macrophages (Kroner and Rosas Almanza, 2019). M1 macrophages are neurotoxic and inflammatory, and they are induced by LPS, IFN-γ and Th1 cytokines. M1 macrophages also produce many inflammatory cytokines and chemokines, such as IL-1β, IL-6, IL-12, IL-23, TNF-α, IFN-γ, CCL5, and iNOS, as well as proteolytic enzymes to clean up myelin sheath fragments and apoptotic cells as well as to promote tissue remodeling. Previous research has shown that chondroitin sulfate proteoglycan is 17 times higher in M1 macrophages than in M2 macrophages. Chondroitin sulfate proteoglycan is an inhibitor of axon growth, suggesting that M1 macrophages are harmful to axons (Tan et al., 2005; Martinez et al., 2006). In addition, M1-derived IL-6 disrupts the tight junctions of endothelial cells, increases vascular permeability and promotes continuous leakage of the BSCB. The consumption of macrophages significantly improves vascular-to-barrier leakage and promotes the functional recovery

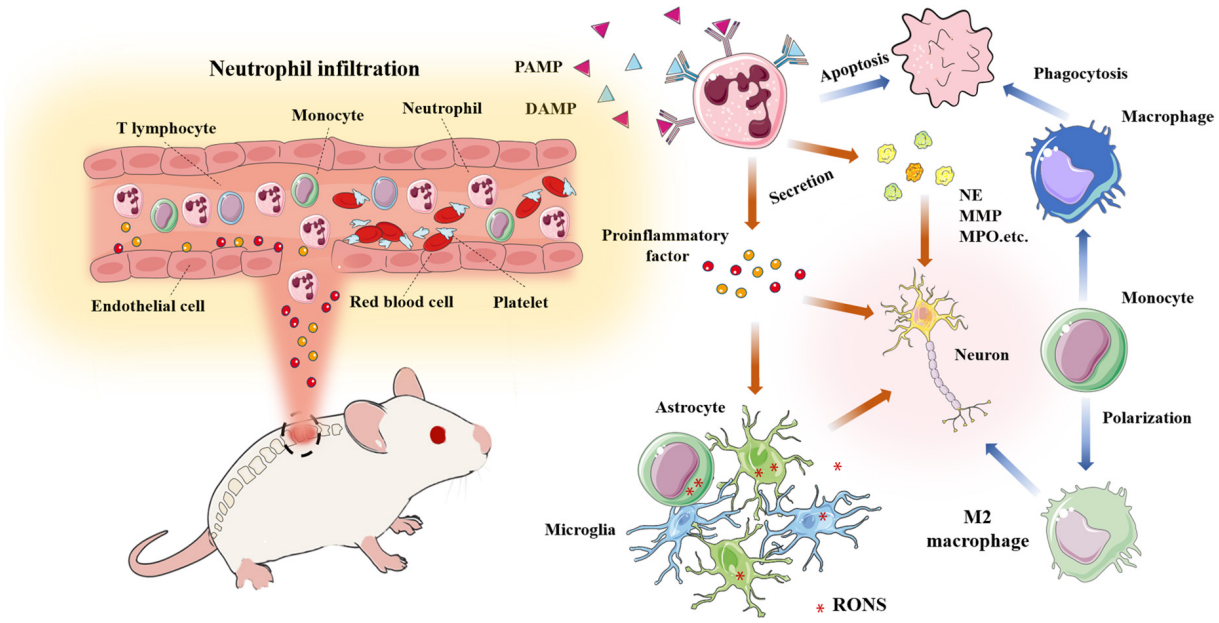

FIGURE 5
A large number of neutrophils infiltrate into the damaged site and release pro-inflammatory factors and chemokines; Neutrophils release various harmful enzymes (MMP, NE, MPO,etc); Activated monocytes, microglia, astrocytes,etc produce RONS, resulting in the deterioration of the microenvironment; Macrophages phagocytize apoptotic neutrophils and transform into M2 macrophages.

of SCI (Luo et al., 2022). Ge et al. (2021) also confirmed that miR-155 from M1-polarized macrophage exosomes impairs the mitochondrial function of vascular endothelial cells and destroys the BSCB in the SCI microenvironment. However, these results do not indicate that M1 macrophages have no role in the repair and regeneration of SCI. M1 macrophages phagocytose and clear damaged tissues and apoptotic cells, and they promote axon growth to a certain extent (Kong and Gao, 2017; Kroner and Rosas Almanza, 2019).

Monocytes polarize to M2 macrophages under the stimulation of the Th2 cytokines, IL-4 and IL-13. There are three subpopulations of M2 macrophages, namely, M2a, M2b and M2c. M2a macrophages are mainly involved in reducing inflammation and enhancing phagocytosis and differentiation of neural stem cells. M2b macrophages produce CCL1, IL-10, ROS and nitrogen substances during the activation of M1 macrophages cells. M2c macrophages clear myelin sheath debris and promote healing (Kong and Gao, 2017). Most studies have suggested that M2-type macrophages promote the regeneration of the injury microenvironment. After adoptive transfer of M2 macrophages into a rat SCI model, Ma et al. (2015) reported that the secreted IL-10 and TGF-β induce polarization of microglia/macrophages and significantly improve the recovery of neurological function. Peng et al. (2021) applied M2-derived exosomes to reduce the proportion of M1 macrophages and increase the proportion of M2 cells, and they found that M2 polarization mainly occurred through the miRNA–mRNA network and that the miR-23a-3p/PTEN/PI3K/AKT axis plays an important role in this process. Yao et al. (2014) demonstrated that PD-1 may play an important role in macrophage polarization, and they reported that increased expression of transcriptional activator-1 in M1 macrophages of PD-1 knockout mice promotes M2 transformation.

Phagocytosis of monocyte-derived macrophages

Macrophages induce a dual role of inflammation and phagocytosis. On the one hand, the removal of myelin sheath fragments and apoptotic cells is conducive to improving the microenvironment of the injury site; on the other hand, inflammation, chemokines, ROS and excessive phagocytosis lead to the formation of harmful foam macrophages. After phagocytosis of myelin after nerve injury, macrophages are filled with lipid droplets and transform into foam-like cells, which lose the ability to clean up residual debris. Kong et al. (2020) reported that scavenger receptor (SR) promotes excessive phagocytosis fragments in macrophages, resulting in foam-like macrophage-induced inflammation (Yao et al., 2014; Kong et al., 2020). Kroner et al., 2014 showed that macrophages accumulate a large amount of iron after phagocytosis and induce the expression of

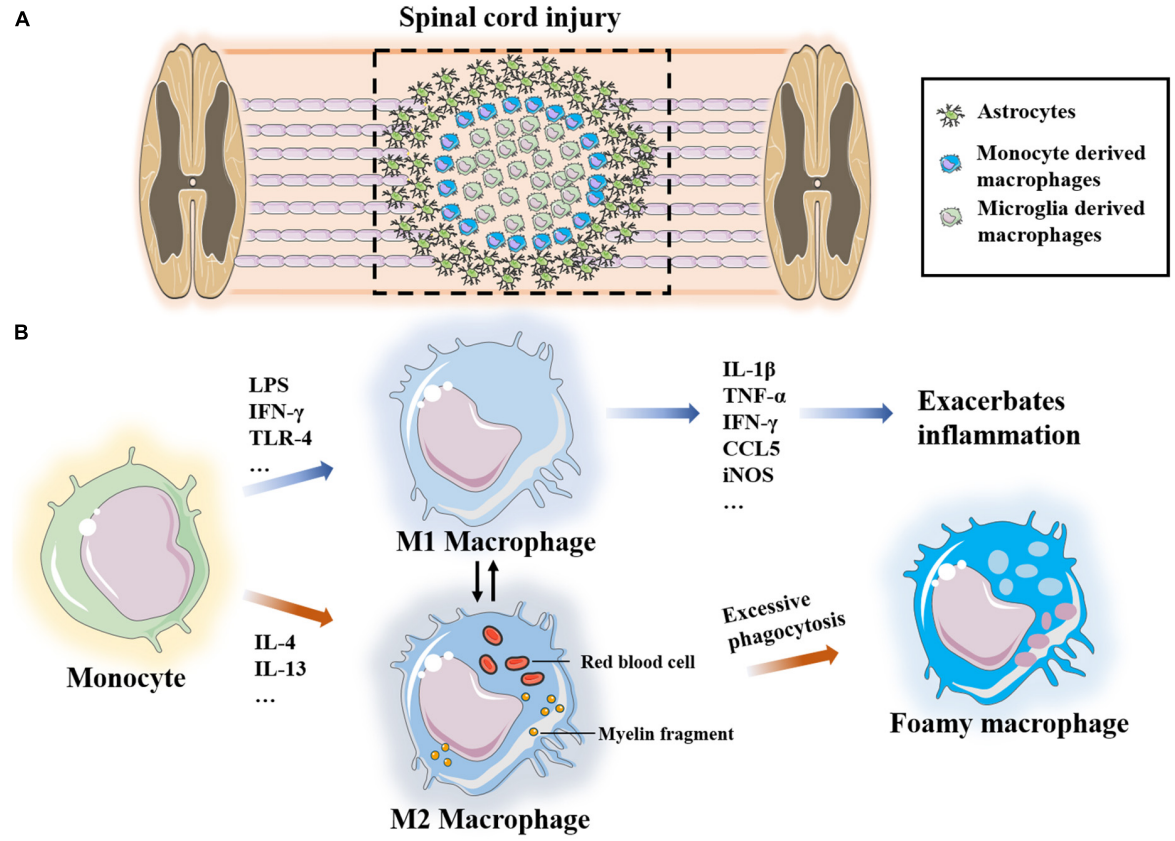

FIGURE 6
(A) Microglia-derived macrophages form boundaries at the site of injury and monocyte-derived macrophages infiltrate into the site of injury. **(B)** Monocytes polarize into two different phenotypes M1 and M2 under the stimulation of different factors, which transform into each other. Excessive phagocytosis of myelin sheath fragments and apoptotic cells induce macrophages transform into foam macrophages.

TNF, which contributes to the maintenance of the M2-induced regeneration microenvironment.

Biomaterials regulate macrophages and improve the immune microenvironment

Shen et al. (2022b) optimized photocrosslinked gelatin hydrogels with polyamine-amine dendritic macromolecules (PAMAM-G3) and IL-10, and they demonstrated that the hydrogels inhibit the inflammatory response of monocytes/macrophages, regulate M2 polarization and promote the differentiation and regeneration of neuronal cells. Jeong et al. (2017) injected PLGA-modified nanoparticles with the macrophage receptor and collagenous structure; these nanoparticles not only significantly reduce macrophage polarization and glial scar formation but also reduce the accumulation of chondroitin sulfate proteoglycan, and the regeneration of axons promotes motor function recovery. Bartus et al. (2014) applied a lentivirus vector to deliver the chondroitin sulfate gene to regulate the phenotype of macrophages and protect injured nerves, and they reported that the polarized M2 macrophages reduce the number of glial cells (astrocytes and microglia) and promote the immune regeneration microenvironment through the expression of TNF-β and IL-10. Kigerl et al. (2009) reported that M2 macrophage-conditioned medium promotes long and extensive neurites of dorsal root ganglion neurons, and they also demonstrated that M1 macrophage-conditioned medium induces short and stunted neurites with multiple branches. Li X. et al., 2020 developed nanofiber hydrogels using maleimide-modified PCL fibers connected to hyaluronic acid, and they reported that these hydrogels induce M2 polarization and significantly reduce inflammation and vascularization as well as promote neuronal cell regeneration and differentiation after SCI.

Microglia

Microglia are derived from the embryonic yolk sac, and they are differentiated from border macrophages distributed around the vascular space outside the spinal cord parenchyma. As innate resident immune cells, microglia rapidly change their morphology after being stimulated by environmental signals,

such as hypoxia or injury. Microglia express high levels of CD86 and MHCII, and they secrete a variety of proinflammatory or chemokines to promote immune cell infiltration. One day after spinal cord contusion, approximately 33% of microglia migrate to the injury site, and this number reaches half of all immune cells within 4 days. Furthermore, the microglia began to release CD68, and the number peaks at 7 days. The phagocytic capacity of microglia decreases after 14 days (Xu et al., 2021). Guo et al. (2013) reported that G-CSF improves the inflammatory response in the microglial environment and increases the expression of trophic factors. Another study has reported that SCI can heal without forming glial scars in newborn mice, in which microglia play an important role (Li Y. et al., 2020).

T lymphocytes

The effect of T cells after nerve injury is often contradictory, which may be due to T cells differentiating into various subpopulations. According to phenotype, T cells are divided into $CD4^+$ T cells and $CD8^+$ T cells (Yang et al., 2021b). Furthermore, the subpopulations of $CD4^+$ T cells include helper T cells (Th1, Th2 and Th17) and regulatory T cells (Tregs) (Yang et al., 2019; Hu et al., 2021). Both $CD4^+$ T and $CD8^+$ T cells migrate to the injured site of the central nervous system to induce inflammation and neurodegeneration. Th1 cells activate macrophages by secreting IL-2 and IFN-γ, and Th2 cells mainly produce IL-4, IL-5, and IL-13. In addition, Tregs secrete high levels of IL-10 and TGF-β to modulate adaptive immune responses. At present, there are few studies on the role of T cells in nerve regeneration and protection. One study has shown that Th1 and Th2 both play protective roles in the central nervous system. Hu et al. (2016) adoptively transferred myelin basic protein to activate Th1 cells and induce higher levels of proinflammatory cells and cytokines in a rat model. In contrast, myelin basic protein-activated Th2 cells are more beneficial to the recovery of motor function in rats through anti-inflammatory cytokines. Studies have also shown that Th2 cells secrete more neurotrophic factors than Th1 and Th17 cells in CNS injury (Hendrix and Nitsch, 2007). Other research has found that Th1 cells are more conducive to regeneration. Ishii et al. (2012) showed that proinflammatory Th1 cells secrete IFN-γ and IL-10 to promote functional recovery after SCI. The more pronounced neuroprotective effect of Th1 cells has been verified in a mouse model of SCI (Ishii et al., 2012). T cells mostly indirectly regulate the regeneration and repair of injured nerves, and few reports have directly demonstrated their effects. One study has shown that Tregs promote the differentiation of oligodendrocyte progenitor cells into mature oligodendrocytes after central nervous system injury, indicating that T cells directly regulate injury nerve regeneration (Dombrowski et al., 2017).

Conclusion and perspectives

Immune cells play an important role in the recognition of SCI, remodeling of the microenvironment and tissue regeneration. Few studies have discussed the immune microenvironment after SCI. In this review, different pathological characteristics and changes in immune cells after SCI were described in detail. Neutrophils, macrophages, microglia and T lymphocytes play a dual role in injury and repair. On the one hand, these cells eliminate adverse factors and promote regeneration. Monocytes and microglia migrate to the damaged site to phagocytose and remove the damaged tissue debris, which is beneficial to the microenvironment. Th2 cells secrete IL-4 and IL-13, mediating M2 macrophage-promoted axon regeneration. The neutrophil subsets and Tregs have the ability to repair injured tissue. On the other hand, the remodeling of the microenvironment caused by immune cells may be highly inflammatory. Immune cell infiltration tends to release a large number of factors that induce inflammation and oxidative responses. Excessive phagocytosis results in the formation of foamy macrophages. Th1 cells release IFN-γ and IL-6 to activate macrophages, which have a proinflammatory role, thereby disrupting the balance of the immune system.

Functional nanoparticles, hydrogels and acellular matrix scaffolds have been widely used in tissue engineering regeneration and repair. Optimizing the physical and chemical properties of biomaterials has been explored. Biomaterial scaffold-loaded immune cells or factors slow inflammatory reactions and rebalance the regenerative microenvironment. There are three ways to regulate the immune response with biomaterials. First, the regulated immune biomaterial itself inhibits the inflammatory response of the microenvironment. Second, biomaterials loaded with inhibitors or anti-inflammatory factors promote nerve regeneration. Third, biomaterials encapsulate stem cells or immune cells that can interact with the immune microenvironment. These strategies effectively improve the microenvironment after SCI and promote the occurrence of new neurons. With the help of various biomaterials, the immunological principles described above show great potential. However, it should be noted that biomaterials loading a single cell or factor cannot solve all the problems in such a complex and spatiotemporal dynamic microenvironment at present. The combination of multiple factors and a precise engineering strategy may provide a promising future.

Author contributions

YF: conceptualization and writing – original draft. YP: writing – original draft. JJ: writing – review editing, project administration, and funding acquisition. YY: supervision. PY: conceptualization, writing – original draft, review

and editing, supervision, project administration, and funding acquisition. All authors contributed to the article and approved the submitted version.

Acknowledgments

We thank to acknowledge the financial support received from the National Natural Science Foundation of China (No. 31900987), Heilongjiang Natural Science Foundation (No. YQ2019H022), Jiangsu Province "Double Innovation Plan" (No. JSSCBS20211603), Research Project of Health Commission of Nantong (No. MB2021011), Science and Technology Project of Nantong city (No. JC2019146), and Nantong University Clinical Medicine Project (No. 2019JZ004).

Conflict of interest

The authors declare that the research was conducted in the absence of any commercial or financial relationships that could be construed as a potential conflict of interest.

Publisher's note

All claims expressed in this article are solely those of the authors and do not necessarily represent those of their affiliated organizations, or those of the publisher, the editors and the reviewers. Any product that may be evaluated in this article, or claim that may be made by its manufacturer, is not guaranteed or endorsed by the publisher.

References

Abdullahi, D., Annuar, A. A., Mohamad, M., Aziz, I., and Sanusi, J. (2017). Experimental spinal cord trauma: a review of mechanically induced spinal cord injury in rat models. *Rev. Neurosci.* 28, 15–20.

Ahmed, A., Patil, A. A., and Agrawal, D. K. (2018). Immunobiology of spinal cord injuries and potential therapeutic approaches. *Mol. Cell Biochem.* 441, 181–189. doi: 10.1007/s11010-017-3184-9

Ahuja, C. S., Nori, S., Tetreault, L., Wilson, J., Kwon, B., Harrop, J., et al. (2017). Traumatic spinal cord injury-repair and regeneration. *Neurosurgery* 80, S9–S22.

Albrecht, U., Yang, X., Asselta, R., Keitel, V., Tenchini, M. L., Ludwig, S., et al. (2007). Activation of NF-kappaB by IL-1beta blocks IL-6-induced sustained STAT3 activation and STAT3-dependent gene expression of the human gamma-fibrinogen gene. *Cell Signal.* 19, 1866–1878. doi: 10.1016/j.cellsig.2007.04.007

All, A. H., and Al-Nashash, H. (2021). Comparative analysis of functional assessment for contusion and transection models of spinal cord injury. *Spinal Cord* 59, 1206–1209.

Allen, A. (1991). Surgery of experimental lesion of spinal cord equivalent to crush injury of fracture dislocation of spinal columm. *JAMA* 57, 878–880. doi: 10.1001/jama.1911.04260090100008

Anderson, M. A., Burda, J. E., Ren, Y., Ao, Y., O'Shea, T. M., Kawaguchi, R., et al. (2016). Astrocyte scar formation aids central nervous system axon regeneration. *Nature* 532, 195–200. doi: 10.1038/nature17623

Anwar, M. A., Al Shehabi, T. S., and Eid, A. H. (2016). Inflammogenesis of secondary spinal cord injury. *Front. Cell. Neurosci.* 10:98. doi: 10.3389/fncel.2016.00098

Armstrong, R. C., Le, T. Q., Frost, E. E., Borke, R. C., and Vana, A. C. (2002). Absence of fibroblast growth factor 2 promotes oligodendroglial repopulation of demyelinated white matter. *J. Neurosci.* 22, 8574–8585. doi: 10.1523/JNEUROSCI.22-19-08574.2002

Awad, H., Efanov, A., Rajan, J., Denney, A., Gigax, B., Kobalka, P., et al. (2021). Histological findings after aortic cross-clamping in preclinical animal models. *J. Neuropathol. Exp. Neurol.* 80, 895–911. doi: 10.1093/jnen/nlab084

Baroncini, A., Maffulli, N., Eschweiler, J., Tingart, M., and Migliorini, F. (2021). Pharmacological management of secondary spinal cord injury. *Expert. Opin. Pharmacother.* 22, 1793–1800.

Bartanusz, V., Jezova, D., Alajajian, B., and Digicaylioglu, M. (2011). The blood-spinal cord barrier: morphology and clinical implications. *Ann. Neurol.* 70, 194–206.

Bartus, K., James, N. D., Didangelos, A., Bosch, K. D., Verhaagen, J., Yanez-Munoz, R. J., et al. (2014). Large-scale chondroitin sulfate proteoglycan digestion with chondroitinase gene therapy leads to reduced pathology and modulates macrophage phenotype following spinal cord contusion injury. *J. Neurosci.* 34, 4822–4836. doi: 10.1523/JNEUROSCI.4369-13.2014

Beck, K. D., Nguyen, H. X., Galvan, M. D., Salazar, D. L., Woodruff, T. M., and Anderson, A. J. (2010). Quantitative analysis of cellular inflammation after traumatic spinal cord injury: evidence for a multiphasic inflammatory response in the acute to chronic environment. *Brain* 133(Pt 2), 433–447. doi: 10.1093/brain/awp322

Bi, Y. H., Duan, W. X., Chen, J., You, T., Li, S. Y., Jiang, W., et al. (2021). Neutrophil decoys with anti-inflammatory and anti-oxidative properties reduce secondary spinal cord injury and improve neurological functional recovery. *Adv. Funct. Mater.* 31:2102912. doi: 10.1002/adfm.202102912

Blasko, J., Szekiova, E., Slovinska, L., Kafka, J., and Cizkova, D. (2017). Axonal outgrowth stimulation after alginate/mesenchymal stem cell therapy in injured rat spinal cord. *Acta Neurobiol. Exp.* 77, 337–350.

Blight, A. R. (1985). Delayed demyelination and macrophage invasion: a candidate for secondary cell damage in spinal cord injury. *Cent. Nerv. Syst. Trauma* 2, 299–315. doi: 10.1089/cns.1985.2.299

Bradbury, E. J., and Burnside, E. R. (2019). Moving beyond the glial scar for spinal cord repair. *Nat. Commun.* 10:3879.

Bryukhovetski, A. S., Yaryghin, V. N., Mentkevich, G. L., Dolgopolov, I., Mheidze, D. M., Zaytsev, A. Y., et al. (2005). Mobilized autologous stem cells in the SCI treatment. *J. Neurol. Sci.* 238, S64–S64.

Bryukhovetskiy, A. S., Yaryghin, V. N., Karakhan, V. B., Lavrentyev, A. V., Mentkevich, G. L., Dolgopolov, I., et al. (2005). Tissue engineering and autologous stem cells in severe SCI treatment in humans. *Eur. J. Neurol.* 12, 26–26.

Bush, T. G., Puvanachandra, N., Horner, C. H., Polito, A., Ostenfeld, T., Svendsen, C. N., et al. (1999). Leukocyte infiltration, neuronal degeneration, and neurite outgrowth after ablation of scar-forming, reactive astrocytes in adult transgenic mice. *Neuron* 23, 297–308. doi: 10.1016/s0896-6273(00)80781-3

Canaani, J., Kollet, O., and Lapidot, T. (2011). Neural regulation of bone, marrow, and the microenvironment. *Front. Biosci.* 3:1021–1031. doi: 10.2741/206

Casha, S., Zygun, D., McGowan, M. D., Bains, I., Yong, V. W., and Hurlbert, R. J. (2012). Results of a phase II placebo-controlled randomized trial of minocycline in acute spinal cord injury. *Brain* 135(Pt 4), 1224–1236.

Chen, B., Xiao, Z. F., Zhao, Y. N., and Dai, J. W. (2017). Functional biomaterial-based regenerative microenvironment for spinal cord injury repair. *Natl. Sci. Rev.* 4, 530–532.

Chen, X., Zhao, Y., Li, X., Xiao, Z., Yao, Y., Chu, Y., et al. (2018). Functional multichannel poly(propylene fumarate)-collagen scaffold with collagen-binding neurotrophic factor 3 promotes neural regeneration after transected spinal cord injury. *Adv. Healthc. Mater.* 7:e1800315. doi: 10.1002/adhm.201800315

Courtine, G., and Sofroniew, M. V. (2019). Spinal cord repair: advances in biology and technology. *Nat. Med.* 25, 898–908. doi: 10.1038/s41591-019-0475-6

Curcio, M., and Bradke, F. (2018). Axon regeneration in the central nervous system: facing the challenges from the inside. *Annu. Rev. Cell Dev. Biol.* 34, 495–521. doi: 10.1146/annurev-cellbio-100617-062508

David, S., and Kroner, A. (2011). Repertoire of microglial and macrophage responses after spinal cord injury. *Nat. Rev. Neurosci.* 12, 388–399. doi: 10.1038/nrn3053

David, S., Kroner, A., Greenhalgh, A. D., Zarruk, J. G., and Lopez-Vales, R. (2018). Myeloid cell responses after spinal cord injury. *J. Neuroimmunol.* 321, 97–108.

de Castro, R. C. Jr, Burns, C. L., McAdoo, D. J., and Romanic, A. M. (2000). Metalloproteinase increases in the injured rat spinal cord. *Neuroreport* 11, 3551–3554.

Ding, Y., Zhang, D., Wang, S., Zhang, X., and Yang, J. (2021). Hematogenous macrophages: a new therapeutic target for spinal cord injury. *Front. Cell Dev. Biol.* 9:767888. doi: 10.3389/fcell.2021.767888

Dombrowski, Y., O'Hagan, T., Dittmer, M., Penalva, R., Mayoral, S. R., Bankhead, P., et al. (2017). Regulatory T cells promote myelin regeneration in the central nervous system. *Nat. Neurosci.* 20, 674–680.

Du, K., Zheng, S., Zhang, Q., Li, S., Gao, X., Wang, J., et al. (2015). Pten deletion promotes regrowth of corticospinal tract axons 1 year after spinal cord injury. *J. Neurosci.* 35, 9754–9763. doi: 10.1523/JNEUROSCI.3637-14.2015

Duan, H., Ge, W., Zhang, A., Xi, Y., Chen, Z., Luo, D., et al. (2015). Transcriptome analyses reveal molecular mechanisms underlying functional recovery after spinal cord injury. *Proc. Natl. Acad. Sci. U.S.A.* 112, 13360–13365.

Dulin, J. N., Karoly, Wang, Y., Strobel, H. W., and Grill, R. J. (2013). Licofelone modulates neuroinflammation and attenuates mechanical hypersensitivity in the chronic phase of spinal cord injury. *J. Neurosci.* 33, 652–664. doi: 10.1523/JNEUROSCI.6128-11.2013

Fan, C., Li, X., Xiao, Z., Zhao, Y., Liang, H., Wang, B., et al. (2017). A modified collagen scaffold facilitates endogenous neurogenesis for acute spinal cord injury repair. *Acta Biomater.* 51, 304–316. doi: 10.1016/j.actbio.2017.01.009

Feng, Z., Min, L., Liang, L., Chen, B., Chen, H., Zhou, Y., et al. (2021). Neutrophil extracellular traps exacerbate secondary injury via promoting neuroinflammation and blood-spinal cord barrier disruption in spinal cord injury. *Front. Immunol.* 12:698249. doi: 10.3389/fimmu.2021.698249

Fiani, B., Kondilis, A., Soula, M., Tao, A., and Alvi, M. A. (2021). Novel methods of necroptosis inhibition for spinal cord injury using translational research to limit secondary injury and enhance endogenous repair and regeneration. *Neurospine* 18, 261–270. doi: 10.14245/ns.2040722.361

Flack, J. A., Sharma, K. D., and Xie, J. Y. (2022). Delving into the recent advancements of spinal cord injury treatment: a review of recent progress. *Neural. Regen. Res.* 17, 283–291. doi: 10.4103/1673-5374.317961

Franklin, R. J., and Blakemore, W. F. (1993). Requirements for schwann cell migration within CNS environments: a viewpoint. *Int. J. Dev. Neurosci.* 11, 641–649. doi: 10.1016/0736-5748(93)90052-f

Fu, Z., Li, W., Wei, J., Yao, K., Wang, Y., Yang, P., et al. (2022). Construction and biocompatibility evaluation of fibroin/sericin-based scaffolds. *ACS Biomater. Sci. Eng.* 8, 1494–1505. doi: 10.1021/acsbiomaterials.1c01426

Gao, J., Khang, M., Liao, Z., Detloff, M., and Lee, J. S. (2021). Therapeutic targets and nanomaterial-based therapies for mitigation of secondary injury after spinal cord injury. *Nanomedicine* 16, 2013–2028. doi: 10.2217/nnm-2021-0113

Garcia-Ovejero, D., Arevalo-Martin, A., Paniagua-Torija, B., Florensa-Vila, J., Ferrer, I., Grassner, L., et al. (2015). The ependymal region of the adult human spinal cord differs from other species and shows ependymoma-like features. *Brain* 138(Pt 6), 1583–1597. doi: 10.1093/brain/awv089

Ge, X., Tang, P., Rong, Y., Jiang, D., Lu, X., Ji, C., et al. (2021). Exosomal miR-155 from M1-polarized macrophages promotes EndoMT and impairs mitochondrial function via activating NF-kappaB signaling pathway in vascular endothelial cells after traumatic spinal cord injury. *Redox Biol.* 41:101932.

Ghasemlou, N., Bouhy, D., Yang, J. X., Lopez-Vales, R., Haber, M., Thuraisingam, T., et al. (2010). Beneficial effects of secretory leukocyte protease inhibitor after spinal cord injury. *Brain* 133, 126–138. doi: 10.1093/brain/awp304

Gruner, J. A. (1992). A monitored contusion model of spinal cord injury in the rat. *J. Neurotrauma* 9, 123–126.

Guo, Y., Zhang, H., Yang, J., Liu, S., Bing, L., Gao, J., et al. (2013). Granulocyte colony-stimulating factor improves alternative activation of microglia under microenvironment of spinal cord injury. *Neuroscience* 238, 1–10. doi: 10.1016/j.neuroscience.2013.01.047

Ham, T. R., and Leipzig, N. D. (2018). Biomaterial strategies for limiting the impact of secondary events following spinal cord injury. *Biomed. Mater.* 13:024105. doi: 10.1088/1748-605X/aa9bbb

Han, S. F., Wang, B., Jin, W., Xiao, Z. F., Li, X., Ding, W. Y., et al. (2015). The linear-ordered collagen scaffold-BDNF complex significantly promotes functional recovery after completely transected spinal cord injury in canine. *Biomaterials* 41, 89–96. doi: 10.1016/j.biomaterials.2014.11.031

He, Q. F., Zhao, Y. N., Chen, B., Xiao, Z. F., Zhang, J., Chen, L., et al. (2011). Improved cellularization and angiogenesis using collagen scaffolds chemically conjugated with vascular endothelial growth factor. *Acta Biomater.* 7, 1084–1093. doi: 10.1016/j.actbio.2010.10.022

Hendrix, S., and Nitsch, R. (2007). The role of T helper cells in neuroprotection and regeneration. *J. Neuroimmunol.* 184, 100–112.

Hu, J. G., Shi, L. L., Chen, Y. J., Xie, X. M., Zhang, N., Zhu, A. Y., et al. (2016). Differential effects of myelin basic protein-activated Th1 and Th2 cells on the local immune microenvironment of injured spinal cord. *Exp. Neurol.* 277, 190–201. doi: 10.1016/j.expneurol.2016.01.002

Hu, W., Wang, Z. M., Feng, Y., Schizas, M., Hoyos, B. E., van der Veeken, J., et al. (2021). Regulatory T cells function in established systemic inflammation and reverse fatal autoimmunity. *Nat. Immunol.* 22, 1163–1174. doi: 10.1038/s41590-021-01001-4

Inada, T., Takahashi, H., Yamazaki, M., Okawa, A., Sakuma, T., Kato, K., et al. (2014). Multicenter prospective nonrandomized controlled clinical trial to prove neurotherapeutic effects of granulocyte colony-stimulating factor for acute spinal cord injury: analyses of follow-up cases after at least 1 year. *Spine* 39, 213–219. doi: 10.1097/BRS.0000000000000121

Ishii, H., Jin, X., Ueno, M., Tanabe, S., Kubo, T., Serada, S., et al. (2012). Adoptive transfer of Th1-conditioned lymphocytes promotes axonal remodeling and functional recovery after spinal cord injury. *Cell Death Dis.* 3:e363.

Jazayeri, S. B., Beygi, S., Shokraneh, F., Hagen, E. M., and Rahimi-Movaghar, V. (2015). Incidence of traumatic spinal cord injury worldwide: a systematic review. *Eur. Spine J.* 24, 905–918.

Jeong, S. J., Cooper, J. G., Ifergan, I., McGuire, T. L., Xu, D., Hunter, Z., et al. (2017). Intravenous immune-modifying nanoparticles as a therapy for spinal cord injury in mice. *Neurobiol. Dis.* 108, 73–82. doi: 10.1016/j.nbd.2017.08.006

Jutzeler, C., Tong, B. B., Cragg, J. J., Geisler, F., and Kramer, J. K. (2018). Acute pharmacological management after spinal cord injury: a secondary analysis of clinical trial data. *J. Neurotraum* 35, A175–A176.

Kawano, H., Kimura-Kuroda, J., Komuta, Y., Yoshioka, N., Li, H. P., Kawamura, K., et al. (2012). Role of the lesion scar in the response to damage and repair of the central nervous system. *Cell Tissue Res.* 349, 169–180.

Keirstead, H. S., Ben-Hur, T., Rogister, B., O'Leary, M. T., Dubois-Dalcq, M., and Blakemore, W. F. (1999). Polysialylated neural cell adhesion molecule-positive CNS precursors generate both oligodendrocytes and Schwann cells to remyelinate the CNS after transplantation. *J. Neurosci.* 19, 7529–7536. doi: 10.1523/JNEUROSCI.19-17-07529.1999

Kigerl, K. A., Gensel, J. C., Ankeny, D. P., Alexander, J. K., Donnelly, D. J., and Popovich, P. G. (2009). Identification of two distinct macrophage subsets with divergent effects causing either neurotoxicity or regeneration in the injured mouse spinal cord. *J. Neurosci.* 29, 13435–13444.

Kim, C. Y., Sikkema, W. K. A., Kim, J., Kim, J. A., Walter, J., Dieter, R., et al. (2018). Effect of graphene nanoribbons (TexasPEG) on locomotor function recovery in a rat model of lumbar spinal cord transection. *Neural. Regen. Res.* 13, 1440–1446. doi: 10.4103/1673-5374.235301

Koda, M., Hanaoka, H., Sato, T., Fujii, Y., Hanawa, M., Takahashi, S., et al. (2018). Study protocol for the G-SPIRIT trial: a randomised, placebo-controlled, double-blinded phase III trial of granulocyte colony-stimulating factor-mediated neuroprotection for acute spinal cord injury. *BMJ Open* 8:e019083. doi: 10.1136/bmjopen-2017-019083

Kong, F. Q., Zhao, S. J., Sun, P., Liu, H., Jie, J., Xu, T., et al. (2020). Macrophage MSR1 promotes the formation of foamy macrophage and neuronal apoptosis after spinal cord injury. *J. Neuroinflammation* 17:62. doi: 10.1186/s12974-020-01735-2

Kong, X. Y., and Gao, J. (2017). Macrophage polarization: a key event in the secondary phase of acute spinal cord injury. *J. Cell Mol. Med.* 21, 941–954. doi: 10.1111/jcmm.13034

Kroner, A., and Rosas Almanza, J. (2019). Role of microglia in spinal cord injury. *Neurosci. Lett.* 709:134370.

Kroner, A., Greenhalgh, A. D., Zarruk, J. G., Passos Dos Santos R., Gaestel M., and David S. (2014). TNF and increased intracellular iron alter macrophage polarization to a detrimental M1 phenotype in the injured spinal cord. *Neuron* 83, 1098–1116. doi: 10.1016/j.neuron.2014.07.027

Kumar, R., Lim, J., Mekary, R. A., Rattani, A., Dewan, M. C., Sharif, S. Y., et al. (2018). Traumatic spinal injury: global epidemiology and worldwide volume. *World Neurosurg.* 113, e345–e363.

Lang-Lazdunski, L., Matsushita, K., Hirt, L., Waeber, C., Vonsattel, J. P., Moskowitz, M. A., et al. (2000). Spinal cord ischemia. Development of a model in the mouse. *Stroke* 31, 208–213. doi: 10.1161/01.str.31.1.208

LeBel, C. P., and Bondy, S. C. (1991). Oxygen radicals: common mediators of neurotoxicity. *Neurotoxicol. Teratol.* 13, 341–346.

Li, J., Wei, J., Wan, Y. J., Du, X. J., Bai, X. S., Li, C. H., et al. (2021). TAT-modified tetramethylpyrazine-loaded nanoparticles for targeted treatment of spinal cord injury. *J. Control Release* 335, 103–116. doi: 10.1016/j.jconrel.2021.05.016

Li, L., Zhang, Y., Mu, J., Chen, J., Zhang, C., Cao, H., et al. (2020). Transplantation of human mesenchymal stem-cell-derived exosomes immobilized in an adhesive hydrogel for effective treatment of spinal cord injury. *Nano Lett.* 20, 4298–4305. doi: 10.1021/acs.nanolett.0c00929

Li, M. L., Zhao, W., Gao, Y. D., Hao, P., Shang, J. K., Duan, H. M., et al. (2019). Differentiation of bone marrow mesenchymal stem cells into neural lineage cells induced by bFGF-chitosan controlled release system. *Biomed. Res. Int.* 2019:5086297. doi: 10.1155/2019/5086297

Li, X., Li, J., Xiao, Z., and Dai, J. (2018a). The role of glial scar on axonal regeneration after spinal cord injury. *Zhongguo Xiu Fu Chong Jian Wai Ke Za Zhi* 32, 973–978.

Li, X., Yang, B., Xiao, Z., Zhao, Y., Han, S., Yin, Y., et al. (2018b). Comparison of subacute and chronic scar tissues after complete spinal cord transection. *Exp. Neurol.* 306, 132–137. doi: 10.1016/j.expneurol.2018.05.008

Li, X., Yang, Z., Zhang, A., Wang, T., and Chen, W. (2009). Repair of thoracic spinal cord injury by chitosan tube implantation in adult rats. *Biomaterials* 30, 1121–1132. doi: 10.1016/j.biomaterials.2008.10.063

Li, X., Zhang, C., Haggerty, A. E., Yan, J., Lan, M., Seu, M., et al. (2020). The effect of a nanofiber-hydrogel composite on neural tissue repair and regeneration in the contused spinal cord. *Biomaterials* 245:119978.

Li, Y., He, X., Kawaguchi, R., Zhang, Y., Wang, Q., Monavarfeshani, A., et al. (2020). Microglia-organized scar-free spinal cord repair in neonatal mice. *Nature* 587, 613–618. doi: 10.1038/s41586-020-2795-6

Lim, J. H., Jung, C. S., Byeon, Y. E., Kim, W. H., Yoon, J. H., Kang, K. S., et al. (2007). Establishment of a canine spinal cord injury model induced by epidural balloon compression. *J. Vet. Sci.* 8, 89–94. doi: 10.4142/jvs.2007.8.1.89

Lukovic, D., Moreno-Manzano, V., Lopez-Mocholi, E., Rodriguez-Jimenez, F. J., Jendelova, P., Sykova, E., et al. (2015). Complete rat spinal cord transection as a faithful model of spinal cord injury for translational cell transplantation. *Sci. Rep.* 5:9640. doi: 10.1038/srep09640

Lukacova, N., Kisucka, A., Kiss Bimbova, K., Bacova, M., Ileninova, M., Kuruc, T., et al. (2021). Glial-Neuronal interactions in pathogenesis and treatment of spinal cord injury. *Int. J. Mol. Sci.* 22:13577. doi: 10.3390/ijms222413577

Luo, Y., Yao, F., Hu, X., Li, Y., Chen, Y., Li, Z., et al. (2022). M1 macrophages impair tight junctions between endothelial cells after spinal cord injury. *Brain Res. Bull.* 180, 59–72. doi: 10.1016/j.brainresbull.2021.12.019

Ma, S. F., Chen, Y. J., Zhang, J. X., Shen, L., Wang, R., Zhou, J. S., et al. (2015). Adoptive transfer of M2 macrophages promotes locomotor recovery in adult rats after spinal cord injury. *Brain Behav. Immun.* 45, 157–170. doi: 10.1016/j.bbi.2014.11.007

Ma, Y. H., Zeng, X., Qiu, X. C., Wei, Q. S., Che, M. T., Ding, Y., et al. (2018). Perineurium-like sheath derived from long-term surviving mesenchymal stem cells confers nerve protection to the injured spinal cord. *Biomaterials* 160, 37–55. doi: 10.1016/j.biomaterials.2018.01.015

Marcol, W., Slusarczyk, W., Gzik, M., Larysz-Brysz, M., Bobrowski, M., Grynkiewicz-Bylina, B., et al. (2012). Air gun impactor-a novel model of graded white matter spinal cord injury in rodents. *J. Reconstr. Microsurg.* 28, 561–568. doi: 10.1055/s-0032-1315779

Marques, S. A., de Almeida, F. M., Mostacada, K., and Martinez, A. M. (2014). A highly reproducible mouse model of compression spinal cord injury. *Methods Mol. Biol.* 1162, 149–156.

Marsala, M., Sorkin, L. S., and Yaksh, T. L. (1994). Transient spinal ischemia in rat: characterization of spinal cord blood flow, extracellular amino acid release, and concurrent histopathological damage. *J. Cereb. Blood Flow Metab.* 14, 604–614. doi: 10.1038/jcbfm.1994.75

Martinez, F. O., Gordon, S., Locati, M., and Mantovani, A. (2006). Transcriptional profiling of the human monocyte-to-macrophage differentiation and polarization: new molecules and patterns of gene expression. *J. Immunol.* 177, 7303–7311. doi: 10.4049/jimmunol.177.10.7303

McCreedy, D. A., Abram, C. L., Hu, Y., Min, S. W., Platt, M. E., Kirchhoff, M. A., et al. (2021). Spleen tyrosine kinase facilitates neutrophil activation and worsens long-term neurologic deficits after spinal cord injury. *J. Neuroinflammation* 18:302. doi: 10.1186/s12974-021-02353-2

Moore, C. S., Cui, Q. L., Warsi, N. M., Durafourt, B. A., Zorko, N., Owen, D. R., et al. (2015). Direct and indirect effects of immune and central nervous system-resident cells on human oligodendrocyte progenitor cell differentiation. *J. Immunol.* 194, 761–772. doi: 10.4049/jimmunol.1401156

Moore, D. L., Blackmore, M. G., Hu, Y., Kaestner, K. H., Bixby, J. L., Lemmon, V. P., et al. (2009). KLF family members regulate intrinsic axon regeneration ability. *Science* 326, 298–301.

Mu, J. F., Wu, J. H., Cao, J., Ma, T., Li, L. M., Feng, S. Q., et al. (2021). Rapid and effective treatment of traumatic spinal cord injury using stem cell derived exosomes. *Asian J. Pharm. Sci.* 16, 806–815.

Ning, G. Z., Song, W. Y., Xu, H., Zhu, R. S., Wu, Q. L., Wu, Y., et al. (2019). Bone marrow mesenchymal stem cells stimulated with low-intensity pulsed ultrasound: better choice of transplantation treatment for spinal cord injury Treatment for SCI by LIPUS-BMSCs transplantation. *CNS Neurosci. Ther.* 25, 496–508. doi: 10.1111/cns.13071

Noble, L. J., and Wrathall, J. R. (1989). Distribution and time course of protein extravasation in the rat spinal cord after contusive injury. *Brain Res.* 482, 57–66. doi: 10.1016/0006-8993(89)90542-8

Noble, L. J., Donovan, F., Igarashi, T., Goussev, S., and Werb, Z. (2002). Matrix metalloproteinases limit functional recovery after spinal cord injury by modulation of early vascular events. *J. Neurosci.* 22, 7526–7535.

Okada, S. (2016). The pathophysiological role of acute inflammation after spinal cord injury. *Inflamm. Regen.* 36:20.

Okano, H. (2009). [Regeneration of the central nervous system using iPS cell-technologies]. *Rinsho Shinkeigaku* 49, 825–826.

Park, K. K., Liu, K., Hu, Y., Smith, P. D., Wang, C., Cai, B., et al. (2008). Promoting axon regeneration in the adult CNS by modulation of the PTEN/mTOR pathway. *Science* 322, 963–966.

Peng, P., Yu, H., Xing, C., Tao, B., Li, C., Huang, J., et al. (2021). Exosomes-mediated phenotypic switch of macrophages in the immune microenvironment after spinal cord injury. *Biomed. Pharmacother.* 144:112311. doi: 10.1016/j.biopha.2021.112311

Pineau, I., Sun, L., Bastien, D., and Lacroix, S. (2010). Astrocytes initiate inflammation in the injured mouse spinal cord by promoting the entry of neutrophils and inflammatory monocytes in an IL-1 receptor/MyD88-dependent fashion. *Brain Behav. Immun.* 24, 540–553. doi: 10.1016/j.bbi.2009.11.007

Qian, Y., Lin, H., Yan, Z., Shi, J., and Fan, C. (2021). Functional nanomaterials in peripheral nerve regeneration: scaffold design, chemical principles and microenvironmental remodeling. *Mater. Today* 51, 165–187.

Rao, J. S., Zhao, C., Zhang, A., Duan, H., Hao, P., Wei, R. H., et al. (2018). NT3-chitosan enables de novo regeneration and functional recovery in monkeys after spinal cord injury. *Proc. Natl. Acad. Sci. U.S.A.* 115, E5595–E5604. doi: 10.1073/pnas.1804735115

Rivlin, A. S., and Tator, C. H. (1978). Effects of duration of acute spinal cord compression in a new acute cord injury model in the rat. *Surg. Neurol.* 10, 38–43.

Saker, E., Henry, B. M., Tomaszewski, K. A., Loukas, M., Iwanaga, J., Oskouian, R. J., et al. (2016). The human central canal of the spinal cord: a comprehensive review of its anatomy. Embryology, molecular development, variants, and pathology. *Cureus* 8:e927. doi: 10.7759/cureus.927

Samano, C., and Nistri, A. (2019). Mechanism of neuroprotection against experimental spinal cord injury by riluzole or methylprednisolone. *Neurochem. Res.* 44, 200–213.

Sanchez, I., Hassinger, L., Paskevich, P. A., Shine, H. D., and Nixon, R. A. (1996). Oligodendroglia regulate the regional expansion of axon caliber and local accumulation of neurofilaments during development independently of myelin formation. *J. Neurosci.* 16, 5095–5105. doi: 10.1523/JNEUROSCI.16-16-05095.1996

Sas, A. R., Carbajal, K. S., Jerome, A. D., Menon, R., Yoon, C., Kalinski, A. L., et al. (2020). A new neutrophil subset promotes CNS neuron survival and axon regeneration. *Nat. Immunol.* 21, 1496–1505.

Shang, J., Qiao, H., Hao, P., Gao, Y., Zhao, W., Duan, H., et al. (2019). BFGF-sodium hyaluronate collagen scaffolds enable the formation of nascent neural networks after adult spinal cord injury. *J. Biomed. Nanotechnol.* 15, 703–716. doi: 10.1166/jbn.2019.2732

Sharif-Alhoseini, M., Khormali, M., Rezaei, M., Safdarian, M., Hajighadery, A., Khalatbari, M. M., et al. (2017). Animal models of spinal cord injury: a systematic review. *Spinal Cord* 55, 714–721.

Shechter, R., Miller, O., Yovel, G., Rosenzweig, N., London, A., Ruckh, J., et al. (2013). Recruitment of beneficial M2 macrophages to injured spinal cord is orchestrated by remote brain choroid plexus. *Immunity* 38, 555–569. doi: 10.1016/j.immuni.2013.02.012

Shen, H., Fan, C. X., You, Z. F., Xiao, Z. F., Zhao, Y. N., and Dai, J. W. (2022a). Advances in biomaterial-based spinal cord injury repair. *Adv. Funct. Mater.* 32:2110628.

Shen, H., Xu, B., Yang, C., Xue, W., You, Z., Wu, X., et al. (2022b). A DAMP-scavenging, IL-10-releasing hydrogel promotes neural regeneration and motor

function recovery after spinal cord injury. *Biomaterials* 280:121279. doi: 10.1016/j.biomaterials.2021.121279

Soehnlein, O., and Lindbom, L. (2010). Phagocyte partnership during the onset and resolution of inflammation. *Nat. Rev. Immunol.* 10, 427–439. doi: 10.1038/nri2779

Sofroniew, M. V. (2005). Reactive astrocytes in neural repair and protection. *Neuroscientist* 11, 400–407.

Sofroniew, M. V. (2015). Astrocyte barriers to neurotoxic inflammation. *Nat. Rev. Neurosci.* 16, 249–263.

Sun, J., Song, Y., Chen, Z., Qiu, J., Zhu, S., Wu, L., et al. (2021). Heterogeneity and molecular markers for CNS glial cells revealed by single-cell transcriptomics. *Cell. Mol. Neurobiol.* doi: 10.1007/s10571-021-01159-3 [Epub ahead of print].

Takami, T., Shimokawa, N., Parthiban, J., Zileli, M., and Ali, S. (2020). Pharmacologic and regenerative cell therapy for spinal cord injury: WFNS spine committee recommendations. *Neurospine* 17, 785–796. doi: 10.14245/ns.2040408.204

Talac, R., Friedman, J. A., Moore, M. J., Lu, L., Jabbari, E., Windebank, A. J., et al. (2004). Animal models of spinal cord injury for evaluation of tissue engineering treatment strategies. *Biomaterials* 25, 1505–1510. doi: 10.1016/s0142-9612(03)00497-6

Tan, A. M., Zhang, W., and Levine, J. M. (2005). NG2: a component of the glial scar that inhibits axon growth. *J. Anat.* 207, 717–725.

Tarlov, I. M., Klinger, H., and Vitale, S. (1953). Spinal cord compression studies. I. Experimental techniques to produce acute and gradual compression. *AMA Arch. Neurol. Psychiatry* 70, 813–819.

Tonai, T., Shiba, K., Taketani, Y., Ohmoto, Y., Murata, K., Muraguchi, M., et al. (2001). A neutrophil elastase inhibitor (ONO-5046) reduces neurologic damage after spinal cord injury in rats. *J. Neurochem.* 78, 1064–1072. doi: 10.1046/j.1471-4159.2001.00488.x

Totoiu, M. O., and Keirstead, H. S. (2005). Spinal cord injury is accompanied by chronic progressive demyelination. *J. Comp. Neurol.* 486, 373–383.

Traka, M., Podojil, J. R., McCarthy, D. P., Miller, S. D., and Popko, B. (2016). Oligodendrocyte death results in immune-mediated CNS demyelination. *Nat. Neurosci.* 19:65.

Varadarajan, S. G., Hunyara, J. L., Hamilton, N. R., Kolodkin, A. L., and Huberman, A. D. (2022). Central nervous system regeneration. *Cell* 185, 77–94.

Varone, A., Knight, D., Lesage, S., Vollrath, F., Rajnicek, A. M., and Huang, W. (2017). The potential of *Antheraea pernyi* silk for spinal cord repair. *Sci. Rep.* 7:13790. doi: 10.1038/s41598-017-14280-5

von Euler, M., Seiger, A., and Sundstrom, E. (1997). Clip compression injury in the spinal cord: a correlative study of neurological and morphological alterations. *Exp. Neurol.* 145(2 Pt 1), 502–510.

Voronova, A. D., Stepanova, O. V., Valikhov, M. P., Chadin, A. V., Semkina, A. S., and Chekhonin, V. P. (2020). Neural stem/progenitor cells of human olfactory mucosa for the treatment of chronic spinal cord injuries. *Bull. Exp. Biol. Med.* 168, 538–541. doi: 10.1007/s10517-020-04749-1

Wang, N., Xiao, Z., Zhao, Y., Wang, B., Li, X., Li, J., et al. (2018). Collagen scaffold combined with human umbilical cord-derived mesenchymal stem cells promote functional recovery after scar resection in rats with chronic spinal cord injury. *J. Tissue Eng. Regen. Med.* 12, e1154–e1163. doi: 10.1002/term.2450

Wang, X. L., Gao, J. Q., Ouyang, X. M., Wang, J. B., Sun, X. Y., and Lv, Y. Y. (2018). Mesenchymal stem cells loaded with paclitaxel-poly(lactic-co-glycolic acid) nanoparticles for glioma-targeting therapy. *Int. J. Nanomed.* 13, 5231–5248. doi: 10.2147/IJN.S167142

Wang, X., Zhang, Z., Zhu, Z., Liang, Z., Zuo, X., Ju, C., et al. (2021). Photobiomodulation promotes repair following spinal cord injury by regulating the transformation of A1/A2 reactive astrocytes. *Front. Neurosci.* 15:768262. doi: 10.3389/fnins.2021.768262

Wertheim, L., Edri, R., Goldshmit, Y., Kagan, T., Noor, N., Ruban, A., et al. (2022). Regenerating the injured spinal cord at the chronic phase by engineered iPSCs-derived 3D neuronal networks. *Adv. Sci.* 9:e2105694. doi: 10.1002/advs.202105694

White-Schenk, D., Shi, R., and Leary, J. F. (2015). Nanomedicine strategies for treatment of secondary spinal cord injury. *Int. J. Nanomed.* 10, 923–938.

Wu, B., and Ren, X. J. (2008). Control of demyelination for recovery of spinal cord injury. *Chin. J. Traumatol.* 11, 306–310.

Xing, L., Yang, T., Cui, S., and Chen, G. (2019). Connexin hemichannels in astrocytes: role in CNS disorders. *Front. Mol. Neurosci.* 12:23. doi: 10.3389/fnmol.2019.00023

Xu, G. Y., Hughes, M. G., Ye, Z., Hulsebosch, C. E., and McAdoo, D. J. (2004). Concentrations of glutamate released following spinal cord injury kill oligodendrocytes in the spinal cord. *Exp. Neurol.* 187, 329–336. doi: 10.1016/j.expneurol.2004.01.029

Xu, L., Wang, J., Ding, Y., Wang, L., and Zhu, Y. J. (2021). Current knowledge of microglia in traumatic spinal cord injury. *Front. Neurol.* 12:796704. doi: 10.3389/fneur.2021.796704

Yang, P., Cao, X., Cai, H., Chen, X., Zhu, Y., Yang, Y., et al. (2021a). Upregulation of microRNA-155 enhanced migration and function of dendritic cells in three-dimensional breast cancer microenvironment. *Immunol. Invest.* 50, 1058–1071. doi: 10.1080/08820139.2020.1801721

Yang, Y., Fan, Y., Zhang, H., Zhang, Q., Zhao, Y., Xiao, Z., et al. (2021d). Small molecules combined with collagen hydrogel direct neurogenesis and migration of neural stem cells after spinal cord injury. *Biomaterials* 269:120479. doi: 10.1016/j.biomaterials.2020.120479

Yang, P., Peng, Y., Feng, Y., Xu, Z., Feng, P., Cao, J., et al. (2021c). Immune cell-derived extracellular vesicles - new strategies in cancer immunotherapy. *Front. Immunol.* 12:771551. doi: 10.3389/fimmu.2021.771551

Yang, P., Cao, X., Cai, H., Feng, P., Chen, X., Zhu, Y., et al. (2021b). The exosomes derived from CAR-T cell efficiently target mesothelin and reduce triple-negative breast cancer growth. *Cell. Immunol.* 360:104262. doi: 10.1016/j.cellimm.2020.104262

Yang, P., Song, H., Feng, Z., Wang, C., Huang, P., Zhang, C., et al. (2019). Synthetic, supramolecular, and self-adjuvanting CD8+T-cell epitope vaccine increases the therapeutic antitumor immunity. *Adv. Ther.* 2:1900010.

Yang, P., Song, H., Qin, Y., Huang, P., Zhang, C., Kong, D., et al. (2018). Engineering dendritic-cell-based vaccines and PD-1 blockade in self-assembled peptide nanofibrous hydrogel to amplify antitumor T-cell immunity. *Nano Lett.* 18, 4377–4385. doi: 10.1021/acs.nanolett.8b01406

Yang, Z., Zhang, A., Duan, H., Zhang, S., Hao, P., Ye, K., et al. (2015). NT3-chitosan elicits robust endogenous neurogenesis to enable functional recovery after spinal cord injury. *Proc. Natl. Acad. Sci. U.S.A.* 112, 13354–13359. doi: 10.1073/pnas.1510194112

Yao, A., Liu, F., Chen, K., Tang, L., Liu, L., Zhang, K., et al. (2014). Programmed death 1 deficiency induces the polarization of macrophages/microglia to the M1 phenotype after spinal cord injury in mice. *Neurotherapeutics* 11, 636–650. doi: 10.1007/s13311-013-0254-x

Yin, W., Li, X., Zhao, Y., Tan, J., Wu, S., Cao, Y., et al. (2018). Taxol-modified collagen scaffold implantation promotes functional recovery after long-distance spinal cord complete transection in canines. *Biomater. Sci.* 6, 1099–1108.

Yin, W., Xue, W., Zhu, H., Shen, H., Xiao, Z., Wu, S., et al. (2021). Scar tissue removal-activated endogenous neural stem cells aid Taxol-modified collagen scaffolds in repairing chronic long-distance transected spinal cord injury. *Biomater. Sci.* 9, 4778–4792. doi: 10.1039/d1bm00449b

Zhang, H., Chang, M., Hansen, C. N., Basso, D. M., and Noble-Haeusslein, L. J. (2011). Role of matrix metalloproteinases and therapeutic benefits of their inhibition in spinal cord injury. *Neurotherapeutics* 8, 206–220. doi: 10.1007/s13311-011-0038-0

Zhu, S., Ying, Y., He, Y., Zhong, X., Ye, J., Huang, Z., et al. (2021). Hypoxia response element-directed expression of bFGF in dental pulp stem cells improve the hypoxic environment by targeting pericytes in SCI rats. *Bioact. Mater.* 6, 2452–2466. doi: 10.1016/j.bioactmat.2021.01.024

Zivkovic, S., Ayazi, M., Hammel, G., and Ren, Y. (2021). For better or for worse: a look into neutrophils in traumatic spinal cord injury. *Front. Cell Neurosci.* 15:648076. doi: 10.3389/fncel.2021.648076

frontiers | Frontiers in Cellular Neuroscience

TYPE Review
PUBLISHED 05 August 2022
DOI 10.3389/fncel.2022.959598

Check for updates

OPEN ACCESS

EDITED BY
Shuxin Li,
Temple University, United States

REVIEWED BY
Regina Armstrong,
Uniformed Services University of the Health Sciences, United States
Gianluca Gallo,
Temple University, United States

*CORRESPONDENCE
Gorazd B. Stokin
gbstokin@alumni.ucsd.edu

SPECIALTY SECTION
This article was submitted to Cellular Neuropathology, a section of the journal Frontiers in Cellular Neuroscience

RECEIVED 07 June 2022
ACCEPTED 18 July 2022
PUBLISHED 05 August 2022

CITATION
Pozo Devoto VM, Onyango IG and Stokin GB (2022) Mitochondrial behavior when things go wrong in the axon. *Front. Cell. Neurosci.* 16:959598. doi: 10.3389/fncel.2022.959598

COPYRIGHT
© 2022 Pozo Devoto, Onyango and Stokin. This is an open-access article distributed under the terms of the Creative Commons Attribution License (CC BY). The use, distribution or reproduction in other forums is permitted, provided the original author(s) and the copyright owner(s) are credited and that the original publication in this journal is cited, in accordance with accepted academic practice. No use, distribution or reproduction is permitted which does not comply with these terms.

Mitochondrial behavior when things go wrong in the axon

Victorio M. Pozo Devoto[1], Isaac G. Onyango[1] and Gorazd B. Stokin[1,2,3]*

[1]Translational Neuroscience and Ageing Program, Centre for Translational Medicine, International Clinical Research Centre, St. Anne's University Hospital, Brno, Czechia, [2]Division of Neurology, University Medical Centre, Ljubljana, Slovenia, [3]Department of Neurosciences, Mayo Clinic, Rochester, MN, United States

Axonal homeostasis is maintained by processes that include cytoskeletal regulation, cargo transport, synaptic activity, ionic balance, and energy supply. Several of these processes involve mitochondria to varying degrees. As a transportable powerplant, the mitochondria deliver ATP and Ca^{2+}-buffering capabilities and require fusion/fission to maintain proper functioning. Taking into consideration the long distances that need to be covered by mitochondria in the axons, their transport, distribution, fusion/fission, and health are of cardinal importance. However, axonal homeostasis is disrupted in several disorders of the nervous system, or by traumatic brain injury (TBI), where the external insult is translated into physical forces that damage nervous tissue including axons. The degree of damage varies and can disconnect the axon into two segments and/or generate axonal swellings in addition to cytoskeletal changes, membrane leakage, and changes in ionic composition. Cytoskeletal changes and increased intra-axonal Ca^{2+} levels are the main factors that challenge mitochondrial homeostasis. On the other hand, a proper function and distribution of mitochondria can determine the recovery or regeneration of the axonal physiological state. Here, we discuss the current knowledge regarding mitochondrial transport, fusion/fission, and Ca^{2+} regulation under axonal physiological or pathological conditions.

KEYWORDS

mitochondria, axonal degeneration, traumatic brain injury, mitochondrial dynamics, mitochondrial transport, calcium homeostasis

Introduction

Mitochondria's main role in the cell is to generate chemically usable energy in the form of ATP (Chang and Reynolds, 2006a). Among several other functions, mitochondria participate in reactive oxygen species (ROS) homeostasis, trigger apoptosis, and intervene in the buffering of the intracellular Ca^{2+}. To ensure their health and proper distribution, mitochondria rely on the processes such as biogenesis, transport, fusion/fission, and recycling, collectively known as mitochondrial dynamics (Mishra and Chan, 2016; Seager et al., 2020).

Mitochondrial DNA (mtDNA) codes for only 13 proteins, which are essential, but not sufficient for respiratory chain function, and thus, mitochondria depend on the nuclear DNA, other organelles, and axonal translation for most of their proteins

(Mishra and Chan, 2014; Shigeoka et al., 2016). In flat, spherical, or elongated shaped cells, mitochondria are localized few micrometers away from the nucleus or the endoplasmic reticulum (ER). Conversely, in neurons, the highly polarized morphology would constitute a constrain to axonal development and function if mitochondrial biogenesis and maintenance would occur only in the soma. At a mean anterograde speed of 0.5 μm/s (Misgeld and Schwarz, 2017), a fully functional mitochondrion in the soma would need almost 23 days to reach the tip of a 1-m axon, whereas in a typical epithelial columnar cell, it would need less than a minute to move from the basal to the apical membrane. Thus, processes responsible for functional maintenance, movement, distribution, and recycling of mitochondrial populations far away from the soma are particularly relevant in a neuron (Amiri and Hollenbeck, 2008). In the axon, the mitochondrial roles are key for neuronal function and include providing energy for the maintenance of the membrane potential, axonal transport, synaptic activity, neurotransmitter uptake and recycling, and buffering of the presynaptic Ca^{2+} (Howarth et al., 2012; Sheng and Cai, 2012).

The cardinal importance of mitochondria in the axons is evidenced by the strong association between mitochondrial homeostasis and axonal degeneration in neurodegenerative diseases. Axonal damage or degeneration manifests in Alzheimer's disease (AD) (Huang et al., 2007), Parkinson's disease (PD) (Cheng et al., 2010), amyotrophic lateral sclerosis (ALS) (Graham et al., 2004), multiple sclerosis (MS) (Ferguson et al., 1997), and Charcot–Marie–Tooth (CMT) disease (Verhoeven et al., 2006). Some of the familial forms of neurodegenerative diseases present mutations in genes that have association with mitochondrial function such as PTEN-induced putative kinase (PINK1), Parkin, DJ-1, alpha-synuclein, mitofusin (MFN) 2, and Cu/Zn superoxide dismutase (SOD1) among others (Schon and Przedborski, 2011). In general, even if these proteins have an impact on energy production, they do not participate directly in oxidative phosphorylation, but in processes linked to mitochondrial recycling, ROS, and fusion/fission. Besides the strong correlation between these diseases and mitochondrial dysfunction, it is not completely clear yet if the dysfunction originates in the axon, or if the pathology begins in the soma and then propagates to the axon. Detailed and extensive reviews are dedicated to these topics (Lingor et al., 2012; Burté et al., 2015; Paß et al., 2021; Wang et al., 2021).

Pathologies that result from direct impact from external insults to the axonal bundles include traumatic brain injury (TBI), spinal cord injury (SCI), and peripheral nerve injury (PNI). TBI is caused by a blow or a shake to the head, with possible long-term consequences such as cognitive deficits, emotional and behavioral problems, and increased risk of developing AD (Wilson et al., 2017). The physical trauma or the acceleration forces applied to the head produce internal pressure gradients that stretch and damage axons. This results in diffuse axonal injury (DAI), characterized by a multifocal damage to white matter tracts in regions such as the corpus callosum, brain stem, and the gray-white matter junctions (Blennow et al., 2016). The main histopathological hallmark of DAI is the presence of axonal dilations along the axonal tracts, known as axonal swellings (Bruggeman et al., 2021). In SCI or PNI, a trauma in the form of contusion, compression, or laceration affects white matter tracts in the spinal cord or peripheral nerves, respectively (McDonald and Sadowsky, 2002; Scheib and Höke, 2013). To a different degree, and depending on the type of injury, TBI, SCI, or PNI all produce also a secondary injury consisting of events that develop as a consequence of the primary impact such as hemorrhage, edema, excitotoxicity, and immune activation. Many experimental models devoted to understanding the molecular events that occur after axonal trauma or axotomy highlight the role of mitochondria as a player in axonal degeneration and regeneration. An increasing number of studies on axonal mitochondrial distribution, fusion/fission, transport, and function under physiological or pathological settings are revealing a strong interconnection among these processes, which not only govern mitochondrial homeostasis but, in several cases, also axonal fate.

In this work, we examine the current knowledge regarding the roles of mitochondrial transport, fusion/fission, and Ca^{2+} handling, when axonal homeostasis is disrupted, emphasizing the studies that focus on axonal mitochondria whenever possible. We focus particularly on the axonal pathological conditions derived from physical traumatic events and to a lesser extent on neurodegenerative disorders that present axonal pathologies.

Mitochondrial transport

Mitochondrial movement and distribution in the axons

Proper mitochondrial distribution along the axon is essential to deliver ATP and Ca^{2+}-buffering capacity to the regions in need. Their movement is relevant to maintain a population of functional and active mitochondria, particularly in axons where extremely long distances from the soma must be reached. In general, movement toward the axonal tip replenishes energy supply that is essential for neuronal viability, whereas the movement back to the soma is required for the elimination of damaged and dysfunctional mitochondria (Chen et al., 2016). A number of studies using different types of neurons observed that mitochondria populate the axonal shaft at a density near to 1 per 10 μm (Shepherd and Harris, 1998; Smit-Rigter et al., 2016; Pozo Devoto et al., 2017). However, the presence of mitochondria is higher in some presynaptic terminals (Palay, 1956; Li et al., 2020), branching regions (Spillane et al., 2013), and the juxtaparanode region of myelinated axons (Figure 1A;

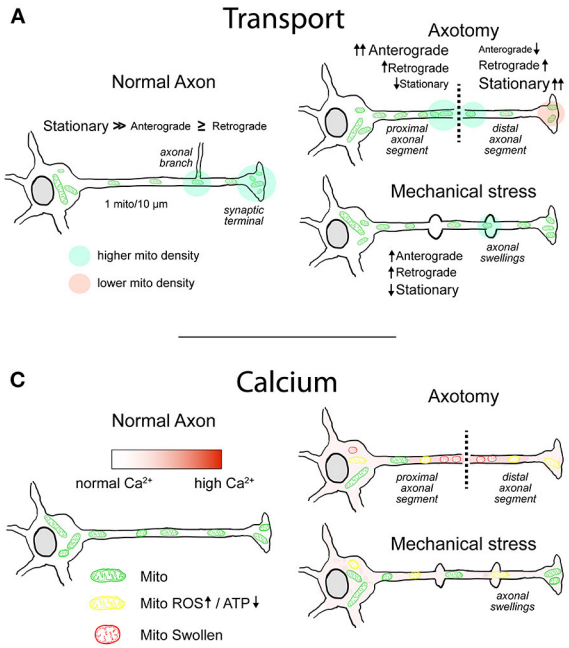

FIGURE 1
Mitochondrial behavior in normal and injured axons. **(A)** Mitochondrial transport. Most of the axonal mitochondria in physiological conditions are stationary, with increased density in axonal branches and in some presynaptic sites. After injury, the axons that have a higher chance of regeneration exhibit an increased mitochondrial motility. In axotomy, the mitochondrial anterograde movement increases in the proximal segment, generating a buildup of ATP near the lesioned region that favors regeneration. Mitochondria in the distal segment are mainly stationary with some increases in retrograde movement, leading to an accumulation in the injury site. Typically, distal segment will go through Wallerian degeneration. Axons that are damaged but maintain their integrity display axonal swellings, which can present disruption or rearrangement of cytoskeletal components. Evidence shows that the transport through axonal swellings is not always impaired and that immediately after injury mitochondrial movement is moderately increased. **(B)** Mitochondrial fusion/fission. In physiological conditions, the rates of fusion/fission in axons are balanced. Fission favors the movement and degradation of mitochondria, whereas fusion favors replenishment of mitochondrial proteins and enhances Ca^{2+}-buffering capacity. Following axonal injury, the fission of mitochondria is enhanced, more notably after axotomy. It is yet not clear whether the enhanced fission in the proximal axonal segment favors regeneration. **(C)** Mitochondria and Ca^{2+}. Mitochondria in the axon play a role in Ca^{2+} buffering, particularly in presynaptic sites. Immediately following axotomy, intra-axonal Ca^{2+} levels rise with a gradient that is maximum at the injury site. Moderate and sustained increase in Ca^{2+} levels lead to an impairment of electron transport chain with decrease in ATP production and increase in ROS generation. High intra-axonal Ca^{2+} levels result in mitochondrial Ca^{2+} overload, activation of the mPTP, and consequent loss of mitochondrial membrane potential. Mitochondria display swollen morphology. After mechanical stress, rise in intra-axonal Ca^{2+} levels varies in magnitude and duration, impairing mitochondrial respiration and ROS generation to varying degrees.

Chang et al., 2006; Ohno et al., 2011; Chavan et al., 2015). Compared to other common axonal cargoes such as lysosomes, vesicles, and endosomes, mitochondrial general mobility is the lowest (Maday et al., 2014; Lewis et al., 2016; Misgeld and Schwarz, 2017). *In vitro*, only 10% of the mitochondria are in movement at any given moment (Obashi and Okabe, 2013), but this proportion can increase to 40% depending on the time window and the model used (Overly et al., 1996; Misgeld and Schwarz, 2017). In addition, factors such as age of the neurons and distance from the soma are among the variables that influence mitochondrial motility. Several studies show that mitochondria move more in young or developing than in mature or older axons (Chang and Reynolds, 2006b; Lewis et al., 2016) and that motility decreases with increasing distance to the soma (Plucińska et al., 2012). Furthermore, electrical activity of the axon modulates its movement, enhancing or reducing mitochondrial mobility depending on the location in the axon (e.g., nodes of Ranvier, presynapses, etc.) (Ohno et al., 2011; Obashi and Okabe, 2013; Sajic et al., 2013). Increased Ca^{2+} and ADP levels that result from electrical activity are at least partially responsible for the inhibition of mitochondrial movement (Mironov, 2007; Wang and Schwarz, 2009).

Proteins responsible for mitochondrial movement

Long-distance movement of mitochondria in the axon is executed by ATP hydrolyzing motor proteins that walk on microtubule tracks. The unique axonal disposition of the microtubules with their plus-ends toward the axonal tips and minus-ends toward the soma (Burton and Paige, 1981) dictates the directionality of the motor protein movement with an

anterograde movement (toward the microtubule plus-end) and a retrograde movement (toward the microtubule minus-end). Kinesin (heavy chains of the kinesin-1 family: KIF5A, B, and C) and dynein motor (cytoplasmic dynein) are responsible for the anterograde and the retrograde movement, respectively (Hirokawa et al., 2010). The link between these motor proteins and mitochondria is mediated by several adaptor proteins such as the mitochondrial Rho-GTPase protein (MIRO) (Guo et al., 2005), syntabulin (Cai et al., 2005), metaxins (MTX) (Zhao et al., 2021), fasciculation, and elongation protein zeta-1 (FEZ) (Ikuta et al., 2007), armadillo repeat-containing genes located in X chromosome (Armcx) (López-Doménech et al., 2012), Ran-binding protein 2 (RanBP2) (Cho et al., 2007), and actin-related protein 10 (Actr10) (Drerup et al., 2017). The interaction between MIRO and the motor heavy chains is mediated by Milton (Stowers et al., 2002), which in mammals has two family members TRAK 1 and 2 that are present in the axons and dendrites, respectively (van Spronsen et al., 2013). Interestingly, MIRO not only has adaptor properties, but it can also regulate mitochondrial movement through intracellular Ca^{2+} levels. MIRO presents two EF-hand motifs that when bound to Ca^{2+} favor the interaction with kinesin heavy chain motor domain. As a result, it abrogates interaction between the motor and microtubules leading to inhibition of mitochondrial movement (Wang and Schwarz, 2009). Additionally, syntaphilin (SNPH) through interactions with microtubules and with kinesin-1 motor participates in the immobilization (docking) of mitochondria in a MIRO-Ca^{2+}-dependent manner (Kang et al., 2008; Chen and Sheng, 2013). Mitochondrial movement in actin filaments, which in many cases acts by opposing microtubule-based movement, is further controlled by myosin motor proteins such as MYO5, MYO6, and MYO19 (Quintero et al., 2009; Pathak et al., 2010; Li et al., 2020). The complexity of the molecular players that participate in this organelle movement and positioning can be found in extensive reviews dedicated to the topic (Saxton and Hollenbeck, 2012; Cheng and Sheng, 2021; Kruppa and Buss, 2021).

Mitochondrial motion in the axons after injury

Direct insults to the axons resulting from SCI, PNI, or TBI can lead to axotomy or to axonal damage without disconnection. Axotomy is a severe process where the axon is cut in a region of the shaft leading to detachment from the soma of the distal segment and regeneration or degeneration of the proximal segment. The detached segment undergoes a process of programmed axonal death called Wallerian degeneration. A number of studies show that mitochondria increase their movement after axotomy in the proximal axon segment (Figure 1A; Misgeld et al., 2007; Mar et al., 2014; Cartoni et al., 2016). The first response is an increase in anterograde movement that starts almost immediately after injury, followed in time by a subsequent increase in retrograde transport (Misgeld et al., 2007; Mar et al., 2014). After intercostal nerve transection in mice, a robust 80% increase in anterograde transport in the proximal segment of the axotomized axons was observed, lasting for 48 h, and declining only slightly in the following weeks. Retrograde transport followed the increase in anterograde transport with a delay of 12 h following transection. In contrast, in the distal segment of the axon, the anterograde mitochondrial transport is almost immediately reduced, whereas retrograde transport lasts between 6 and 12 h after injury (Misgeld et al., 2007). Indeed, delayed Wallerian degeneration caused by JNK inhibition enhances mitochondrial movement in the distal axon segment (Shin et al., 2012). The buildup of mitochondria in the proximal segment of the axon that results from the increased anterograde transport showed to be determinant in the regeneration process (Han et al., 2016; Zhou et al., 2016). In *C. elegans*, axotomy in GABA motoneurons shows a significantly higher regeneration in the axons with more than 10 mitochondria per 100 μm when compared to the axons with lower mitochondrial density. Moreover, regeneration of the axons depends directly on the energy supply that results from increased density of mitochondria (Han et al., 2016; Zhou et al., 2016).

In contrast to axotomy, mechanical stress or stretching applied to the axon can injure the axon without an initial disconnection. Depending on the severity and the location, it has been reported that such injuries produce breakage of microtubules (Tang-Schomer et al., 2010), neurofilament compaction (Chen et al., 1999), and temporary increase in axonal membrane permeability (Farkas et al., 2006), among other effects (Datar et al., 2019). Moreover, following TBI, the formation of focal enlargements of the axonal shaft, called axonal swellings, occurs particularly within the white matter tracts (Ziogas and Koliatsos, 2018). Some studies report the spatial coincidence of the cytoskeletal disruption and the formation of axonal swellings (Chen et al., 1999; Tang-Schomer et al., 2010; Datar et al., 2019), leading to an accumulation of mitochondria and other cargoes in regions with axonal swellings (Maxwell, 1996; Tang-Schomer et al., 2012; Cross et al., 2019). Based on these studies, mitochondria are stuck in axonal swelling regions with less anterograde or retrograde movement across them. Supporting these observations, primary neuronal cultures subjected to fluid shear stress injury show that mitochondria concentrate at the locations of axonal swellings (Kilinc et al., 2008). *In vivo*, axonal swellings that appear after 24 h of a closed cortical impact (CCI) injury show degraded neurofilament or microtubule architecture, and some of them present electron-dense bodies and swollen mitochondria without clearly

delineated cristae (Ziogas and Koliatsos, 2018). However, most of these observations were collected by transmission electron microscopy, which makes it impossible to obtain a complete picture of the mitochondrial distribution across the whole axon. To our knowledge, there is a lack of studies that assess *in vivo* mitochondrial transport or distribution in the axons after a TBI or similar injury. Alternatively, axonal swellings generated after a TBI may present cytoskeletal rearrangement that does not completely impair transport. On the one hand, mitochondria are not always present in the axonal swellings (Stone et al., 2001) whereas on the other hand, the accumulation of organelles does not necessarily mean that they cannot cross through the axonal swellings (Datar et al., 2019; Pozo Devoto et al., 2022). Furthermore, the *in vitro* real-time models of mechanical stress show that there is no drastic impairment on mitochondrial transport immediately after injury (Figure 1A; Gu et al., 2017; Pozo Devoto et al., 2022). Applying a controlled mechanical injury in axons derived from human neurons results in immediate formation of axonal swellings, characterized by microtubule and neurofilament rearrangements. In parallel, anterograde and retrograde proportions of moving mitochondria during and 5 min after injury are significantly increased (Pozo Devoto et al., 2022). These results are in line with mitochondrial behavior after axotomy in proximal axonal segments and suggest that as a result of axonal damage, mobilization of mitochondria favors axonal repair and regeneration.

In contrast, axonal transport of the mitochondria is generally impaired in neurodegenerative diseases. In ALS, motoneurons develop an early decrease in anterograde transport, resulting in a significant reduction of axonal mitochondrial population with the concomitant increase in somatic mitochondrial density (De Vos et al., 2007; Smith et al., 2019). Amyloid-β peptide (Aβ) accumulation observed in AD pathology also reduces mitochondrial anterograde transport and its speed in the axons, causing a reduction in the presynaptic mitochondrial density (Du et al., 2010; Calkins and Reddy, 2011; Guo et al., 2013; Zhang et al., 2018). Moreover, in neurons derived from patients with alpha-synuclein duplication (a model of PD), the proportion of moving axonal mitochondria is significantly decreased due to the oligomerization of alpha-synuclein (Prots et al., 2013). As an exception, in MS models where demyelination of the axons occurs, mitochondrial mobilization is significantly enhanced, particularly the anterograde movement that delivers mitochondria from soma to the axon (Licht-Mayer et al., 2020). Several studies show that the resulting higher mitochondrial density in axons promotes the survival of demyelinated axons (Witte et al., 2009; Zambonin et al., 2011; Ohno et al., 2014). Altogether, the evidence suggests that the impairment in mitochondrial movement observed in neurodegenerative diseases corresponds to a preexisting pathophysiological process that may be affecting their normal function or dynamics.

Molecular signals governing mitochondrial movement in injured axons

The movement behavior of mitochondria in the axon is determined by signaling pathways that target molecular regulators of mitochondrial transport. For example, in axonal injury, modifying different molecular regulators of mitochondrial motility promotes axonal regeneration (Kiryu-Seo et al., 2016; Zhou et al., 2016). The *C. elegans* mutant for ric-7, a gene that is essential for mitochondrial localization in the axons, leads to an impaired mitochondrial transport in injured axons which degenerate rapidly. Such degeneration can be suppressed by forcing mitochondria into axons through a direct link between tomm7 and kinesin-1 (Rawson et al., 2014). Overexpression of Armcx1, an adaptor that promotes mitochondrial motility, also enhances axonal regeneration and neuronal survival *in vivo* (Cartoni et al., 2016). Moreover, if SNPH, a protein that mediates the docking and axonal retention of mitochondria (Kang et al., 2008), is overexpressed, the mitochondrial movement is significantly suppressed. On the other hand, in axonal injury, its downregulation leads to a reduction in stationary mitochondria, contributing to the removal of damaged mitochondria and enhancing nerve regeneration (Zhou et al., 2016; Lin et al., 2017; Han et al., 2020). Physiologically, this response is mediated by AKT signaling. Indeed, after axonal damage due to ischemic injury, there is an activation of AKT, a kinase that acts on several prosurvival signaling pathways. One of the targets activated by AKT is p21-activated kinase 5 (PAK5), which in turn phosphorylates SNPH to release and promote remobilization of anchored mitochondria (Cotteret et al., 2003; Huang et al., 2021). In *C. elegans* neurons, axotomy or axonal breakage is followed by an increase of about 2-folds in mitochondrial density. This effect is mainly a consequence of increased mitochondrial transport from the soma mediated by MIRO and the signaling of dual-leucine zipper kinase-1 (DLK-1) pathway (Han et al., 2016). DLK-1 activation through CEBP-1 is in fact sufficient to increase axonal mitochondrial density in a MIRO-independent manner. DLK-1 injury-signaling pathway is a key determinant of axonal regeneration in *C. elegans*, *Drosophila,* and mice; however, the specific molecular connection to mitochondria remains unknown.

Mitochondrial fusion and fission

Mitochondrial fusion and fission in the axons

Fusion and fission of mitochondria are the processes involved in determining the size, the distribution, and the health of mitochondria. Fusion favors biogenesis through

the exchange of new proteins and mitochondrial DNA between the merging organelles, restoring functional proteins to dysfunctional mitochondria. By splitting one mitochondria into two, the fission process reduces mitochondrial size and leads to enhanced mitochondrial axonal transport, distribution, and mitophagy (Itoh et al., 2013; Chan, 2020).

In physiological conditions, the size of axonal mitochondria is regulated by a balance between fusion and fission (Figure 1B; Amiri and Hollenbeck, 2008), an active process that in axons presents a rate of fission comparable to that of fusion (Cagalinec et al., 2013; Di Meo et al., 2021). In *C. elegans* neurons, this balance is regulated by aging, with a drastic increase in size occurring in early adulthood, followed by a progressive reduction in length through the rest of the lifespan (Morsci et al., 2016). Moreover, modulation of the molecular players of fusion/fission impacts directly on mitochondrial distribution in the axon (Spillane et al., 2013; Berthet et al., 2014). As an example, inhibition of an important component of the fission machinery results in a 50–60% decrease in mitochondrial content in the axon (Spillane et al., 2013). Finally, besides the specific mutations in the fusion/fission molecular machinery that lead to CMT disease or dominant optic atrophy (DOA), changes in mitochondrial size have also been observed in neurodegenerative diseases such as PD, Huntington's disease, and AD (Itoh et al., 2013) and in other neuropathological conditions (Ineichen et al., 2021).

Proteins in charge of fusion/fission

Regulation of mitochondrial morphology is mediated by interactions between the proteins controlling fusion and fission. The fusion process is driven by MFN1 and MFN2, proteins from the dynamin-related GTPase family (Meeusen et al., 2004). MFN is located in the outer mitochondrial membrane (OMM) and expression of MFN2 in the nervous tissue is more abundant when compared to that of MFN1 (Lee et al., 2012; Zhou et al., 2019). MFN is responsible for the fusion of the OMM, whereas optic dominant atrophy 1 (OPA1) is responsible for the fusion of the inner mitochondrial membrane (IMM) (Alexander et al., 2000). Joining together two mitochondria requires the sequential activation of the outer and inner membrane fusion to yield a functional mitochondrion (Song et al., 2009). On the other hand, fission led by the activity of another dynamin-related GTPase protein (DRP1), which oligomerizes and forms a ring-shape structure around mitochondria, acting as a constricting diaphragm at the mitochondrial membrane (Pitts et al., 1999). Given that DRP1 is a cytosolic protein, its recruitment to mitochondria is mediated by different receptor-like proteins including mitochondrial fission factor (Mff), mitochondrial fission 1 (Fis1), and mitochondrial dynamic proteins MiD49s (MiD49) and MiD51 (MiD51) (Osellame et al., 2016). For an in-depth description of the molecular components involved in the mitochondrial fusion/fission, we direct the readers to the following reviews (Chan, 2020; Giacomello et al., 2020).

Fusion disruption affects the mitochondrial size and their distribution and leads to axonal degeneration

The relevance of mitochondrial fusion process in axonal homeostasis is manifested in diseases such as CMT and DOA, caused by mutations in MFN2 and OPA1, respectively (Burté et al., 2015). These mutations have a deleterious effect on the axons, particularly the long ones, with neuropathy in peripheral motor or sensory axons, or degeneration of retinal ganglion cells (RGC) and optic nerves. A plethora of studies shows that loss of function mutations in MFN2 affects several mitochondrial processes occurring in the axon ranging from size reduction and transport impairment to altered distribution, clustering, and functional deficit (Detmer et al., 2008; Cartoni et al., 2010; Byrne et al., 2019; Zhou et al., 2019). Furthermore, the effects can go beyond mitochondria. As an example, knockdown of MFN2 in motoneurons derived from human embryonic stem cells results not only in smaller mitochondria but also in the loss of mitochondrial potential, aggregation of phosphorylated neurofilaments, decreased transport, reduced levels of motor proteins, and formation of axonal swellings (Mou et al., 2021). The impact of these processes increases with age, and in most cases, dysfunction hastens axonal loss (Byrne et al., 2019). The observation that these mutations affect primarily peripheral motor and sensory axons points to the relevance of mitochondrial function and distribution for proper maintenance of the axon throughout all its length. It is not clear, however, whether the wide spectrum of perturbations resulting from disruption in MFN2 can be attributed completely to the decreased fusion of mitochondria. In dorsal root ganglia neurons, the fusion impairment due to the overexpression of MFN2 disease-linked mutant leads to axonal degeneration, whereas fusion impairment due to depletion of OPA1 does not (Misko et al., 2012). The role of MFN2 in mitophagy and mitochondrial transport can be an alternative mechanism underlying the deleterious effects of its mutations (Dorn, 2020).

Fission impairment depletes mitochondria from the axons

In mice, the absence of DRP1 is embryonic lethal, whereas the conditional knockout in the nervous tissue is perinatal lethal (Ishihara et al., 2009). Nevertheless, the ablation of DRP1 in forebrain neurons of adult mice leads to minor changes in the branching of the hippocampal neurites with no reduction in spine or synaptic numbers. At the same time, mitochondria

accumulate in the perikarya of hippocampal neurons, suggesting that the delivery of mitochondria to neurites is impaired (Oettinghaus et al., 2016). In fact, loss of mitochondrial mass in axons due to reduced DRP1 activity has been observed in several settings. For example, in *Drosophila* DRP1 mutant flies, motoneurons show reduced levels of mitochondria in the neuropil and clumps in the somas, with mitochondria largely absent from synapses (Verstreken et al., 2005; El Fissi et al., 2018). DRP1-null mice selective for dopaminergic neurons show a drastic decrease in mitochondrial mass in the axons as well as impaired transport (Berthet et al., 2014). Surprisingly, the consequences of the mitochondrial mass reduction in axons are not always deleterious and depend on the neuronal type (Shields et al., 2015). In dopaminergic neurons of the substantia nigra, the decrease of mitochondria in nerve terminals leads to a progressive degeneration of synaptic terminals and cell loss, whereas dopaminergic neurons in the ventral tegmental area survive, despite the depletion of mitochondria in their axons (Berthet et al., 2014). Furthermore, in *Drosophila,* the lack of mitochondria at presynaptic sites of neuromuscular junctions (NMJ) has no major effect on basal neurotransmission, showing impairments only under intense stimulation (Verstreken et al., 2005). On the other hand, the effects of Mff downregulation are less drastic than the ones observed when DRP1 is downregulated. Mff knockdown increases axonal mitochondrial size, without affecting their localization in pre-synapses (Lewis et al., 2018). The bigger mitochondria in pre-synapses result in enhanced Ca^{2+} buffering, less cytosolic Ca^{2+} and reduced evoked neurotransmitter release. A further effect of reducing Mff levels is the decreased rate at which mitochondria enter the axon, explaining at least in part the diminished axonal mitochondrial mass observed in fission impairment models (Lewis et al., 2018).

The balance between fusion and fission

Size, transport, and distribution of mitochondria are the results of a fine balance between fusion- and fission-dedicated proteins. Depletion of mitochondria in NMJ of motoneurons caused by the MFN R364W mutation, which enhances MFN activity, can be reverted by overexpressing DRP1 (El Fissi et al., 2018), whereas simultaneous disruption of fusion and fission proteins rescues the morphology and the functionality of the neuron (Byrne et al., 2019). MFN or OPA knockdown in flies produces a reduction in motility and density of mitochondria in distal axons, together with a decrease in respiration rate, ATP synthesis, and mitochondrial membrane potential. Simultaneous knockdown of DRP1 with OPA restores morphology and density of mitochondria, but the functional parameters remain impaired. The opposite occurs with simultaneous knockdown of DRP and MFN, where the function of mitochondria is restored, recovering also fly viability and indicating that mitochondrial function is more important for survival than the morphology or the distribution (Trevisan et al., 2018).

Loss of the mitochondrial fusion/fission balance in axonal injury

Several studies report a decrease in the size of axonal mitochondria after axotomy (Figure 1B; Kiryu-Seo et al., 2016; Arrázola et al., 2019; Kedra et al., 2021). As an example, there is a decrease in mitochondrial size in sciatic nerve explants that progress during the 48 h after injury (Arrázola et al., 2019). A similar outcome has been observed in mice after sciatic nerve transection, showing a significant decrease in size 7 days after the injury and recovering to normal sizes 56 days after the injury (Kiryu-Seo et al., 2016). Using the same mouse model, it was shown that mitochondria located in the soma of motoneurons lack significant changes in size after axotomy (Tamada et al., 2017), suggesting that smaller mitochondria in axons are the result of locally enhanced fission process and not of smaller mitochondria delivered from the soma. In support of this finding, it was observed in a SCI model that the size of mitochondria is smaller the closer they are to the injury site (Kedra et al., 2021). However, the linkage between fragmentation of mitochondria and nerve regeneration is not completely clear. Reducing the fragmentation of mitochondria after axotomy *in vitro* by incubation with Mdivi (a pharmacological inhibitor of DRP1) results in a partial but significant decrease in axonal degeneration (Arrázola et al., 2019). In line with this, after a SCI *in vivo*, incubation with Mdivi decreases the lesion size and the number of retraction bulbs present in the axons (Kedra et al., 2021). Furthermore, in *C. elegans,* loss of function for OPA1 shows impairment in axonal regrowth, despite that both show mitochondrial fragmentation (Knowlton et al., 2017). Opposing effects were observed in a mouse model harboring a conditional knockout for DRP1, where after sciatic nerve injury, mitochondria are bigger, show decreased transport, and have lower membrane potential, altogether leading to a significant degeneration of the axons after 14 days (Kiryu-Seo et al., 2016).

Studies of the fusion/fission balance after TBI are scarce. *In vivo*, the effects of TBI related to fusion/fission have not been assessed directly in the axons, but by brain homogenates or in isolated mitochondria. In rats, a mild TBI induces the changes in the protein expression levels within the first 120 h, with upregulation of the fusion-related proteins (MFN1/2, OPA1) and downregulation of the fission proteins (DRP1, FIS1). Surprisingly, the opposite is observed if the TBI is stronger, showing downregulation of fusion and upregulation of fission components (Di Pietro et al., 2017). In line with this last result, a CCI injury in mice produces a mild but significant

increase in the size of hippocampal mitochondria 24 h after injury, evolving to a decrease in size at 72 h. This correlates with an increased localization of DRP1 in the mitochondria at 72 h, which when blocked by the administration of Mdivi results in mitochondria with normal size, decreased death in dentate gyrus neurons and memory improvement (Fischer et al., 2016). Taken together with the observed mitochondrial behavior in axotomy, the evidence suggests that the balance favors the fission of mitochondria after axonal damage (Figure 1B). The increased fission may induce rapid transport (Misgeld et al., 2007) and delivery of mitochondria, as well as their homogenous distribution along the axonal shaft. Furthermore, in an *in vitro* TBI model, phosphoproteomic analysis performed immediately after axonal injury revealed changed regulation of fusion/fission-related proteins in the soma. Among them, mitochondrial elongation factor 1 (MIEF1 or MiD51), a receptor for DRP1, mitochondrial fission regulator 1-like protein (MTFR1L or FAM54B), and HECT, UBA, and WWE domain-containing E3 ubiquitin protein ligase 1 (HUWE1), which ubiquitinates MFN2 to negatively regulate mitochondrial fusion (Pozo Devoto et al., 2022). These fast post-translational modifications of fusion/fission molecular machinery could be interpreted as an early response of the neurons to axonal stress, which could be followed by slower *de novo* synthesis or degradation.

In neurodegenerative diseases, a plethora of studies reports fusion/fission imbalance, which is particularly well-described in PD and ALS (Cho et al., 2009; Zilocchi et al., 2018; Smith et al., 2019). Indeed, most of the studies observe increased fragmentation of mitochondria. For example, in PD, several disease-associated mutations in alpha-synuclein, PINK, Parkin, and LRRK2 have been shown to impact fusion/fission regulators or exert their effects directly by binding to the mitochondrial membrane (Yang et al., 2008; Glauser et al., 2011; Wang et al., 2012; Pozo Devoto et al., 2017). In ALS, models including SOD1 and TDP-43 disease-associated mutations show an expression profile that tilts the balance toward the increased expression of DRP1 or Fis1 (Ferri et al., 2010; Xu et al., 2010). However, these phenomena involve many factors that could be influencing the balance between fusion and fission including the changes in the soma and dendrites to the regulation of mitophagy.

Calcium effects on mitochondria

Calcium homeostasis in axonal mitochondria

Ca^{2+} is a fundamental regulator of axonal function and homeostasis, participating in the processes such as synaptic neurotransmitter release, cargo transport, cytoskeletal remodeling, and axon pathfinding (Henley and Poo, 2004; Sudhof, 2004; Rosenberg and Spitzer, 2011; Niescier et al., 2018). Axonal Ca^{2+} levels also regulate mitochondrial transport as well as fusion/fission (Saxton and Hollenbeck, 2012) and mitochondrial energy metabolism with Ca^{2+} acting as a co-activator for some tricarboxylic acid cycle enzymes (Wan et al., 1989). Importantly, due to its Ca^{2+}-buffering role in presynaptic terminals, mitochondria naturally cope with transient increases in Ca^{2+} concentrations (Devine and Kittler, 2018). However, above a certain threshold, increased intra-mitochondrial Ca^{2+} uncouples the electron transport chain resulting in a greater production of oxidative stress by increasing free electrons, which are easily trapped by oxygen. The increased levels of ROS are responsible for oxidizing mitochondrial membrane phospholipids such as cardiolipin that are essential to maintain the selectivity and permeability of the IMM (Bayir et al., 2007). In cases where high long-lasting Ca^{2+} and ROS levels are present, such as in excitotoxic conditions, mitochondrial Ca^{2+} uptake is overloaded and leads to an activation of the mitochondrial permeability transition pore (mPTP), loss of mitochondrial membrane potential, ATP depletion, and cell loss (Bernardi et al., 2006; Barrientos et al., 2011).

Axonal injury triggers increased intra-axonal calcium levels

Aside from excitotoxicity, the excessive increase in intracellular Ca^{2+} levels has been observed in injuries that produce mechanical damage to the axon as well as in specific pathologies. Several studies have shown an intra-axonal increase in Ca^{2+} levels after TBI in *in vitro* models (Figure 1C; Wolf et al., 2001; Yuen et al., 2009; Staal et al., 2010; Tang-Schomer et al., 2010; Gu et al., 2017; Pozo Devoto et al., 2022). The axonal entry of Ca^{2+} can occur through mechanosensitive channels (Gu et al., 2017), voltage-gated Ca2+ channels (VGCCs) (Yuen et al., 2009), and the Na^{+}-Ca^{2+} exchanger (Wolf et al., 2001) and can even result from Ca^{2+} release from intracellular stores (Staal et al., 2010). *In vivo*, the Ca^{2+} increase observed in TBI models such as CCI or fluid percussion injury (FPI) is supported by indirect evidence from spectrin cleavage by specific Ca^{2+}-dependent proteases (Büki et al., 2000; Johnson et al., 2016) or attenuation of axonal degeneration by Ca^{2+} channel inhibitors (Stirling et al., 2014; Ribas et al., 2017). In axotomy, a Ca^{2+} increase is also detected almost immediately after the ablation (Figure 1C; Villegas et al., 2014), and depending on the model, this increase can happen as a short peak of 100 s (Vargas et al., 2015) or it can be longer than 10 min (Kedra et al., 2021) or even hours (Stirling et al., 2014). Altogether, most of the experimental evidence points to a fundamental role of Ca^{2+} in the axonal collapse, which can be the result of the impact of Ca^{2+} on mitochondrial homeostasis.

Increased calcium levels alter mitochondrial dynamics

The increase in axonal Ca^{2+} impacts the mitochondrial behavior directly. On the one hand, it can modify their transport and localization (Yi et al., 2004). Several experiments have shown that increased cytosolic Ca^{2+} in the axon leads to mitochondrial arrest through MIRO1 (Saotome et al., 2008; Macaskill et al., 2009; Wang and Schwarz, 2009). When cytosolic Ca^{2+} levels are high, the MIRO EF-hand domains that bind Ca^{2+} modify their conformation and promote the interaction with kinesin-1 motor domains leading to mitochondrial arrest (Wang and Schwarz, 2009). The cessation of mitochondrial movement due to high Ca^{2+} levels is particularly relevant to retain mitochondria in presynaptic terminals where they deliver ATP and exert the Ca^{2+}-buffering function. However, under pathological conditions, the arrest of mitochondria due to the elevated Ca^{2+} levels can lead to axonal degeneration. In *Drosophila*, Ca^{2+} elevation triggered by CaMKII significantly reduces mitochondrial transport, resulting in axonal degeneration (Woolums et al., 2020). Surprisingly, the overexpression of a MIRO mutant unable to bind Ca^{2+} reduces axonal degeneration, suggesting that impaired transport contributes to degeneration. It is possible that sustained high Ca^{2+} levels are achieved in the distal axonal segment after axotomy. This part of the axon presents a decrease in mitochondrial transport and coincidentally also requires sustained high Ca^{2+} levels for axonal collapse (Wallerian degeneration) (Misgeld et al., 2007; Coleman and Höke, 2020).

On the other hand, several studies showed that increased cytosolic Ca^{2+} levels in neurites produce an upregulation in DRP1 activity, causing increased mitochondrial fragmentation (Bao et al., 2018). In rat hippocampal neurons, DRP1 becomes phosphorylated as a result of CaMKII activation (Godoy et al., 2014) and in primary neurons, DRP1 becomes activated by MIRO's Ca^{2+}-binding activity (Saotome et al., 2008). Furthermore, blockage of mitochondrial calcium uniporter channel (MCU) inhibits the entry of Ca^{2+} into mitochondria and reduces their fragmentation, indicating that mitochondrial fission can result from Ca^{2+} overload (Kedra et al., 2021).

Injury induced mitochondrial calcium overload as a determinant of axonal fate

The capability of mitochondria to buffer intracellular Ca^{2+} in the axon is well-documented, particularly in the presynapses where it exerts a fundamental role in neurotransmitter release (Guo et al., 2005; Kang et al., 2008; Li et al., 2020; Stavsky et al., 2021). In the axons, evoked action potentials lead to an increased Ca^{2+} concentration in the mitochondrial matrix, a buffer effect even more notable in mature axons than in the young ones (Lewis et al., 2016).

In pathological conditions, the massive rise of Ca^{2+} in the axon resulting from axotomy (Vargas et al., 2015) or from intracellular store release (Villegas et al., 2014) leads to axonal degeneration. It has been shown that Ca^{2+} increase spreads from the injury site through the shaft and is followed by a wave of mitochondrial oxidation which results in mitochondrial swelling and fragmentation (Figure 1C; Gitler and Spira, 1998; Breckwoldt et al., 2014). Molecularly, the Ca^{2+} overload triggers the opening of the mPTP, a protein complex formed mainly by the voltage-dependent anion channel (VDAC) in the OMM, the adenine nucleotide translocase (ANT) in the IMM and cyclophilin D in the mitochondrial matrix. The opening of the pore consists in the interaction of these proteins in an irreversible conformation, leading to the massive release of Ca^{2+}, disruption of the IMM, and loss of mitochondrial membrane potential, resulting in ATP depletion and ROS production (Vargas et al., 2015). The flow of solutes through the IMM that result from the mPTP formation leads to an increase in the volume of the mitochondria, which ultrastructurally can be seen as swollen mitochondria (Arrázola et al., 2015). Diverse methods to block the mitochondrial incorporation and overload of Ca^{2+}, such as blocking the MCU, have proven not only to protect mitochondria, but also to reduce axonal degeneration (Villegas et al., 2014). Alternatively, inhibiting the formation of the mPTP genetically by cyclophilin D knockdown (Barrientos et al., 2011; Breckwoldt et al., 2014) or pharmacologically by cyclosporin A (Villegas et al., 2014) prevents the swelling of mitochondria and protects the axons from degeneration.

In TBI, mitochondria harvested from the forebrain of mice following a CCI present significantly higher Ca^{2+} levels 6 h post-injury, resulting in the impairment of the electron transport chain (Figure 1C; Xiong et al., 1997). The decreased oxidative phosphorylation and ATP production in injured mitochondria occur within 24 h post-injury and can last up to 14 days in experimental models of TBI (Gilmer et al., 2009). In these models, post-injury administration of cyclosporin A or NIM811 (a non-immunosuppressive cyclosporin A analog) has shown to decrease the neuronal and axonal damages, improving both motor skills and cognition when compared to non-treated animals (Büki et al., 1999; Mbye et al., 2009; Readnower et al., 2011). Also *in vitro*, a uniaxial strain on hippocampal axons shows decreased mitochondrial membrane potential 1 h after the injury. However, the mitochondrial potential is maintained if Ca^{2+} entry to mitochondria is reduced by pharmacological incubation with a Na^{+}/H^{+} exchanger inhibitor (Toda et al., 2007; Dollé et al., 2014). These data suggest that the mitochondrial damage in TBI may occur in severe cases and way later after the injury (Hånell et al., 2015).

Ca^{2+} imbalance has a well-studied role in the pathogenesis of the neurodegenerative diseases and extensive reviews dwell on the topic; however, studies directed exclusively to the axons are

more limited (Cali et al., 2012; Schrank et al., 2020; Jadiya et al., 2021). Aβ was shown to interact with several components that can be implicated in the regulation of Ca^{2+} levels in the axon. There is evidence that incubation of hippocampal slices with Aβ increases intracellular Ca^{2+} originating from the extracellular space through different types of VGCC (Ueda et al., 1997; Ramsden et al., 2002). Alternatively, intracellular Ca^{2+} levels have been shown to increase either through ER stores depletion by Aβ (Ferreiro et al., 2008; Sanz-Blasco et al., 2008) or through enhancing the gating of the inositol trisphosphate receptor by presenilin mutations associated with AD (Cheung et al., 2008). Furthermore, Aβ peptides can translocate to the mitochondrial matrix through TOM40 where they interact with specific intra-mitochondrial proteins such as the cyclophilin D (Hansson Petersen et al., 2008). Axons derived from primary hippocampal neurons reveal that after translocation to mitochondria, Aβ induces an opening of mPTP with consequent increase in Ca^{2+} and ROS levels, reducing the number of synapses (Guo et al., 2013). Similarly to Aβ behavior, PD linked mutation in alpha-synuclein modulates the activity of N-type VGCC in the presynapses leading to an increased Ca^{2+} levels and reduced axonal arborization in mouse caudate-putamen (Sgobio et al., 2019). PINK1 deficiency increases Ca^{2+} accumulation in mitochondrial matrix and ROS production by diminishing the Ca^{2+} efflux through the Na^{+}/Ca^{2+} exchanger of the mitochondria (NCLX) (Gandhi et al., 2009).

Discussion

There is an intricate relationship between the axons and mitochondria. Changes in the axons impact mitochondrial transport, fusion/fission, and health, but also the changes in mitochondrial behavior and health contribute to axonal homeostasis. With few exceptions, an axon devoid of mitochondria is destined to degenerate (Kitay et al., 2013; Berthet et al., 2014; Rawson et al., 2014). Immediately after axonal injury, several changes happen in mitochondria. In several models, mitochondrial anterograde transport is enhanced, which is followed by an increase in retrograde transport (Figure 1A; Misgeld et al., 2007; Zhou et al., 2016; Pozo Devoto et al., 2022). Mobilization of mitochondria together with proper delivery of ATP to regions in need (Han et al., 2016; Zhou et al., 2016) seems to be important factors that influence axonal regeneration (Xu et al., 2017; Wang et al., 2019). Favoring the increased movement, the fusion/fission balance tilts to the fission side, thus generating smaller mitochondria that are more prone to move (Figure 1B; Kiryu-Seo et al., 2016). However, not all of the evidence points to a positive role of mitochondrial fragmentation in axonal rescue after injury (Kedra et al., 2021). Even though fission favors the mobilization of mitochondria, the fusion is involved in stability and increased biogenesis (Chen et al., 2016). It is possible that factors such as high local ATP requirements that may need an abundant mitochondrial mass located in specific region would favor a fusion strategy. On the other hand, the need for increased distribution along the axon or the damage of a big number of mitochondria can be the factors defining the fission as a best strategy to promote survival and/or regeneration. The two main organelles involved in Ca^{2+} regulation in the axons are the ER and mitochondria. In contrast to ER, mitochondrial function can be irreversibly impaired by Ca^{2+} overload (Figure 1C). Even more, the loss of mitochondrial potential can trigger signals that result in apoptosis or a degenerative process. For this reason, the pharmacological inhibition of Ca^{2+} influx through the MCU or the blockage of the mPTP formation protects mitochondrial and axonal stability in several cases (Breckwoldt et al., 2014; Villegas et al., 2014). In milder conditions, a surge in intra-axonal Ca^{2+} levels has shown to increase ROS production, which directly results in decreased ATP production through the oxidation of the components of the electron transport chain or increased leakage of the IMM (Xiong et al., 1997; Breckwoldt et al., 2014).

Each of the different pathologies that lead to axonal degeneration presents characteristics that makes them unique. For example, an axon that is either stretched or crushed requires repair of the damaged regions, whereas an axon that is transected requires regrowth of its proximal segment and reinnervation of its target to maintain its previous function. Furthermore, the distal axonal segment that results from axotomy undergoes Wallerian degeneration. The discovery of delayed degeneration of the distal segment of cut axons in the Wallerian degeneration slow (WldS) transgenic mouse model (Lunn et al., 1989) led to the identification of nicotinamide mononucleotide adenylyltransferase 2 (NMNAT2) and sterile alpha and TIR motif-containing protein 1 (SARM1) as the two main players responsible for this delay (Gilley and Coleman, 2010; Osterloh et al., 2012; Gerdts et al., 2015). NMNAT2 is an axonal protein that catalyzes the conversion of nicotinamide mononucleotide (NMN) to nicotinamide adenine dinucleotide (NAD^{+}). Both depletion of NAD^{+} and increase in NMN trigger axonal degeneration through SARM1 (Angeletti et al., 2022). Axotomy reduces the axonal availability of NMNAT2, which is a short-lived enzyme transported from the soma, leading to NAD^{+} depletion and NMN increase. However, the connection between this pathway and mitochondria is not completely clear (Merlini et al., 2022). In *Drosophila* motoneurons, it has been shown that the presence of mitochondria accelerates the axonal Wallerian degeneration but is not necessary for its execution (Kitay et al., 2013). Conversely, in the olfactory receptor neurons of *Drosophila,* the degeneration triggered by mitochondrial depletion from the axon cannot be rescued by NMNAT overexpression (Kitay et al., 2013). The involvement of NMNAT2 or SARM1 as executors in axonal degeneration is well supported (Feng et al., 2010; Ziogas and Koliatsos, 2018), but several studies suggest that axonal homeostasis is further maintained by the pathways

independent of NMNAT2/SARM1 (Kitay et al., 2013; Liu et al., 2021).

In axonal mechanical injury without detachment, axons present microtubule disruption or rearrangement, which can affect mitochondrial mobility. It is generally accepted that an axon that regenerates is an axon that exhibits more mitochondrial movement. So, the integrity of microtubule tracks is a key for proper distribution and delivery of mitochondria to places in need of ATP and Ca^{2+}-buffering capacity. Axonal swellings are present in many pathological settings, from TBI (Weber et al., 2019) to neurodegenerative diseases (Stokin et al., 2005; Adalbert et al., 2009; Nikić et al., 2011; Babij et al., 2013) and last for long periods or immediately precede axonal collapse (Rawson et al., 2014). It is still not clear whether the axonal swellings represent regions of cytoskeletal damage, particularly of microtubules and neurofilaments (Tang-Schomer et al., 2012). Several studies observe that axonal swellings can form and last for a really short period of time (Gu et al., 2017), or that they can present cytoskeletal rearrangement that permits the movement of cargo across them (Datar et al., 2019; Pozo Devoto et al., 2022). It has been proposed that the specific local increases of Ca^{2+} occurring during axonal injury contribute to the formation or maintenance of axonal swellings in time (Staal et al., 2010; Stirling et al., 2014). Mechanistically, this could have an impact not only on cytoskeletal remodeling by Ca^{2+}-dependent signaling, but also on the movement and fission of mitochondria if high Ca^{2+} concentrations are maintained. An important amount of evidence points to a major role of Ca^{2+} as a determinant of axonal fate after injury, with effects that are mitochondria-dependent and mitochondria-independent.

An increasing knowledge on the molecular pathways that regulate and connect processes such as mitochondrial transport and fusion/fission with biogenesis and recycling of mitochondrial components keeps advancing our understanding of the mitochondrial homeostasis in a challenging structure such as the axon.

Author contributions

VMPD: conceptualization, literature research, manuscript writing, and figure. IGO: literature research, manuscript writing, and editing. GBS: conceptualization, supervision, reviewing, and editing. All authors contributed to the article and approved the submitted version.

Funding

This work was supported by the European Regional Development Funds No. CZ.02.1.01/0.0/0.0/16_019/0000868 ENOCH grant and the European Regional Development Fund-Project MAGNET No. CZ.02.1.01/0.0/0.0/15_003/0000492.

Acknowledgments

We would like to thank Ms. Monica Feole and Katja Klosterman for their assistance and feedback.

Conflict of interest

The authors declare that the research was conducted in the absence of any commercial or financial relationships that could be construed as a potential conflict of interest.

Publisher's note

All claims expressed in this article are solely those of the authors and do not necessarily represent those of their affiliated organizations, or those of the publisher, the editors and the reviewers. Any product that may be evaluated in this article, or claim that may be made by its manufacturer, is not guaranteed or endorsed by the publisher.

References

Adalbert, R., Nogradi, A., Babetto, E., Janeckova, L., Walker, S. A., Kerschensteiner, M., et al. (2009). Severely dystrophic axons at amyloid plaques remain continuous and connected to viable cell bodies. *Brain* 132, 402–416. doi: 10.1093/brain/awn312

Alexander, C., Votruba, M., Pesch, U. E., Thiselton, D. L., Mayer, S., Moore, A., et al. (2000). OPA1, encoding a dynamin-related GTPase, is mutated in autosomal dominant optic atrophy linked to chromosome 3q28. *Nat. Genet.* 26, 211–215. doi: 10.1038/79944

Amiri, M., and Hollenbeck, P. J. (2008). Mitochondrial biogenesis in the axons of vertebrate peripheral neurons. *Dev. Neurobiol.* 68, 1348–1361. doi: 10.1002/dneu.20668

Angeletti, C., Amici, A., Gilley, J., Loreto, A., Trapanotto, A. G., Antoniou, C., et al. (2022). SARM1 is a multi-functional NAD(P)ase with prominent base exchange activity, all regulated bymultiple physiologically relevant NAD metabolites. *iScience* 25, 103812. doi: 10.1016/j.isci.2022.103812

Arrázola, M. S., Saquel, C., Catalán, R. J., Barrientos, S. A., Hernandez, D. E., Martínez, N. W., et al. (2019). Axonal degeneration is mediated by necroptosis activation. *J. Neurosci.* 39, 3832–3844. doi: 10.1523/JNEUROSCI.0881-18.2019

Arrázola, M. S., Silva-Alvarez, C., and Inestrosa, N. C. (2015). How the Wnt signaling pathway protects from neurodegeneration: the mitochondrial scenario. *Front. Cell. Neurosci.* 9, 166–166. doi: 10.3389/fncel.2015.00166

Babij, R., Lee, M., Cortés, E., Vonsattel, J.-P. G., Faust, P. L., and Louis, E. D. (2013). Purkinje cell axonal anatomy: quantifying morphometric

changes in essential tremor versus control brains. *Brain* 136, 3051–3061. doi: 10.1093/brain/awt238

Bao, F., Shi, H., Gao, M., Yang, L., Zhou, L., Zhao, Q., et al. (2018). Polybrene induces neural degeneration by bidirectional Ca^{2+} influx-dependent mitochondrial and ER-mitochondrial dynamics. *Cell Death Dis.* 9, 966. doi: 10.1038/s41419-018-1009-8

Barrientos, S. A., Martinez, N. W., Yoo, S., Jara, J. S., Zamorano, S., Hetz, C., et al. (2011). Axonal degeneration is mediated by the mitochondrial permeability transition pore. *J. Neurosci.* 31, 966–978. doi: 10.1523/JNEUROSCI.4065-10.2011

Bayir, H., Tyurin, V. A., Tyurina, Y. Y., Viner, R., Ritov, V., Amoscato, A. A., et al. (2007). Selective early cardiolipin peroxidation after traumatic brain injury: an oxidative lipidomics analysis. *Ann. Neurol.* 62, 154–169. doi: 10.1002/ana.21168

Bernardi, P., Krauskopf, A., Basso, E., Petronilli, V., Blachly-Dyson, E., Blalchy-Dyson, E., et al. (2006). The mitochondrial permeability transition from *in vitro* artifact to disease target. *FEBS J.* 273, 2077–2099. doi: 10.1111/j.1742-4658.2006.05213.x

Berthet, A., Margolis, E. B., Zhang, J., Hsieh, I., Zhang, J., Hnasko, T. S., et al. (2014). Loss of mitochondrial fission depletes axonal mitochondria in midbrain dopamine neurons. *J. Neurosci.* 34, 14304–14317. doi: 10.1523/JNEUROSCI.0930-14.2014

Blennow, K., Brody, D. L., Kochanek, P. M., Levin, H., McKee, A., Ribbers, G. M., et al. (2016). Traumatic brain injuries. *Nat. Rev. Dis. Primers* 2, 16084. doi: 10.1038/nrdp.2016.84

Breckwoldt, M. O., Pfister, F. M., Bradley, P. M., Marinković, P., Williams, P. R., Brill, M. S., et al. (2014). Multiparametric optical analysis of mitochondrial redox signals during neuronal physiology and pathology *in vivo*. *Nat. Med.* 20, 555–560. doi: 10.1038/nm.3520

Bruggeman, G. F., Haitsma, I. K., Dirven, C. M. F., and Volovici, V. (2021). Traumatic axonal injury (TAI): definitions, pathophysiology and imaging-a narrative review. *Acta Neurochir.* 163, 31–44. doi: 10.1007/s00701-020-04594-1

Büki, A., Okonkwo, D. O., and Povlishock, J. T. (1999). Postinjury cyclosporin A administration limits axonal damage and disconnection in traumatic brain injury. *J. Neurotrauma* 16, 511–521. doi: 10.1089/neu.1999.16.511

Büki, A., Okonkwo, D. O., Wang, K. K., and Povlishock, J. T. (2000). Cytochrome c release and caspase activation in traumatic axonal injury. *J. Neurosci.* 20, 2825–2834. doi: 10.1523/JNEUROSCI.20-08-02825.2000

Burté, F., Carelli, V., Chinnery, P. F., and Yu-Wai-Man, P. (2015). Disturbed mitochondrial dynamics and neurodegenerative disorders. *Nat. Rev. Neurol.* 11, 11–24. doi: 10.1038/nrneurol.2014.228

Burton, P. R., and Paige, J. L. (1981). Polarity of axoplasmic microtubules in the olfactory nerve of the frog. *Proc. Natl. Acad. Sci. U.S.A.* 78, 3269–3273. doi: 10.1073/pnas.78.5.3269

Byrne, J. J., Soh, M. S., Chandhok, G., Vijayaraghavan, T., Teoh, J. S., Crawford, S., et al. (2019). Disruption of mitochondrial dynamics affects behaviour and lifespan in *Caenorhabditis elegans*. *Cell. Mol. Life Sci.* 76, 1967–1985. doi: 10.1007/s00018-019-03024-5

Cagalinec, M., Safiulina, D., Liiv, M., Liiv, J., Choubey, V., Wareski, P., et al. (2013). Principles of the mitochondrial fusion and fission cycle in neurons. *J. Cell Sci.* 126, 2187–2197. doi: 10.1242/jcs.118844

Cai, Q., Gerwin, C., and Sheng, Z. H. (2005). Syntabulin-mediated anterograde transport of mitochondria along neuronal processes. *J. Cell Biol.* 170, 959–969. doi: 10.1083/jcb.200506042

Cali, T., Ottolini, D., and Brini, M. (2012). Mitochondrial Ca(2+) and neurodegeneration. *Cell Calcium* 52, 73–85. doi: 10.1016/j.ceca.2012.04.015

Calkins, M. J., and Reddy, P. H. (2011). Amyloid beta impairs mitochondrial anterograde transport and degenerates synapses in Alzheimer's disease neurons. *Biochim. Biophys. Acta* 1812, 507–513. doi: 10.1016/j.bbadis.2011.01.007

Cartoni, R., Arnaud, E., Médard, J. J., Poirot, O., Courvoisier, D. S., Chrast, R., et al. (2010). Expression of mitofusin 2(R94Q) in a transgenic mouse leads to charcot-marie-tooth neuropathy type 2A. *Brain* 133, 1460–1469. doi: 10.1093/brain/awq082

Cartoni, R., Norsworthy, M. W., Bei, F., Wang, C., Li, S., Zhang, Y., et al. (2016). The mammalian-specific protein armcx1 regulates mitochondrial transport during axon regeneration. *Neuron* 92, 1294–1307. doi: 10.1016/j.neuron.2016.10.060

Chan, D. C. (2020). Mitochondrial dynamics and its involvement in disease. *Annu. Rev. Pathol.* 15, 235–259. doi: 10.1146/annurev-pathmechdis-012419-032711

Chang, D. T., Honick, A. S., and Reynolds, I. J. (2006). Mitochondrial trafficking to synapses in cultured primary cortical neurons. *J. Neurosci.* 26, 7035–7045. doi: 10.1523/JNEUROSCI.1012-06.2006

Chang, D. T., and Reynolds, I. J. (2006a). Mitochondrial trafficking and morphology in healthy and injured neurons. *Prog. Neurobiol.* 80, 241–268. doi: 10.1016/j.pneurobio.2006.09.003

Chang, D. T. W., and Reynolds, I. J. (2006b). Differences in mitochondrial movement and morphology in young and mature primary cortical neurons in culture. *Neuroscience* 141, 727–736. doi: 10.1016/j.neuroscience.2006.01.034

Chavan, V., Willis, J., Walker, S. K., Clark, H. R., Liu, X., Fox, M. A., et al. (2015). Central presynaptic terminals are enriched in ATP but the majority lack mitochondria. *PLoS ONE* 10, e0125185. doi: 10.1371/journal.pone.0125185

Chen, M., Li, Y., Yang, M., Chen, X., Chen, Y., Yang, F., et al. (2016). A new method for quantifying mitochondrial axonal transport. *Protein Cell* 7, 804–819. doi: 10.1007/s13238-016-0268-3

Chen, X. H., Meaney, D. F., Xu, B. N., Nonaka, M., McIntosh, T. K., Wolf, J. A., et al. (1999). Evolution of neurofilament subtype accumulation in axons following diffuse brain injury in the pig. *J. Neuropathol. Exp. Neurol.* 58, 588–596. doi: 10.1097/00005072-199906000-00003

Chen, Y., and Sheng, Z. H. (2013). Kinesin-1-syntaphilin coupling mediates activity-dependent regulation of axonal mitochondrial transport. *J. Cell Biol.* 202, 351–364. doi: 10.1083/jcb.201302040

Cheng, H. C., Ulane, C. M., and Burke, R. E. (2010). Clinical progression in Parkinson disease and the neurobiology of axons. *Ann. Neurol.* 67, 715–725. doi: 10.1002/ana.21995

Cheng, X. T., and Sheng, Z. H. (2021). Developmental regulation of microtubule-based trafficking and anchoring of axonal mitochondria in health and diseases. *Dev. Neurobiol.* 81, 284–299. doi: 10.1002/dneu.22748

Cheung, K.-H., Shineman, D., Müller, M., Cárdenas, C., Mei, L., Yang, J., et al. (2008). Mechanism of Ca2+ disruption in Alzheimer's disease by presenilin regulation of InsP3 receptor channel gating. *Neuron* 58, 871–883. doi: 10.1016/j.neuron.2008.04.015

Cho, D. H., Nakamura, T., Fang, J., Cieplak, P., Godzik, A., Gu, Z., et al. (2009). S-nitrosylation of Drp1 mediates beta-amyloid-related mitochondrial fission and neuronal injury. *Science* 324, 102–105. doi: 10.1126/science.1171091

Cho, K. I., Cai, Y., Yi, H., Yeh, A., Aslanukov, A., and Ferreira, P. A. (2007). Association of the kinesin-binding domain of RanBP2 to KIF5B and KIF5C determines mitochondria localization and function. *Traffic* 8, 1722–1735. doi: 10.1111/j.1600-0854.2007.00647.x

Coleman, M. P., and Höke, A. (2020). Programmed axon degeneration: from mouse to mechanism to medicine. *Nat. Rev. Neurosci.* 21, 183–196. doi: 10.1038/s41583-020-0269-3

Cotteret, S., Jaffer, Z. M., Beeser, A., and Chernoff, J. (2003). p21-Activated kinase 5 (Pak5) localizes to mitochondria and inhibits apoptosis by phosphorylating BAD. *Mol. Cell. Biol.* 23, 5526–5539. doi: 10.1128/MCB.23.16.5526-5539.2003

Cross, D. J., Meabon, J. S., Cline, M. M., Richards, T. L., Stump, A. J., Cross, C. G., et al. (2019). Paclitaxel reduces brain injury from repeated head trauma in mice. *J. Alzheimers Dis.* 67, 859–874. doi: 10.3233/JAD-180871

Datar, A., Ameeramja, J., Bhat, A., Srivastava, R., Mishra, A., Bernal, R., et al. (2019). The roles of microtubules and membrane tension in axonal beading, retraction, and atrophy. *Biophys. J.* 117, 880–891. doi: 10.1016/j.bpj.2019.07.046

De Vos, K. J., Chapman, A. L., Tennant, M. E., Manser, C., Tudor, E. L., Lau, K. F., et al. (2007). Familial amyotrophic lateral sclerosis-linked SOD1 mutants perturb fast axonal transport to reduce axonal mitochondria content. *Hum. Mol. Genet.* 16, 2720–2728. doi: 10.1093/hmg/ddm226

Detmer, S. A., Vande Velde, C., Cleveland, D. W., and Chan, D. C. (2008). Hindlimb gait defects due to motor axon loss and reduced distal muscles in a transgenic mouse model of charcot-marie-tooth type 2A. *Hum. Mol. Genet.* 17, 367–375. doi: 10.1093/hmg/ddm314

Devine, M. J., and Kittler, J. T. (2018). Mitochondria at the neuronal presynapse in health and disease. *Nat. Rev. Neurosci.* 19, 63–80. doi: 10.1038/nrn.2017.170

Di Meo, D., Ravindran, P., Sadhanasatish, T., Dhumale, P., and Püschel, A. W. (2021). The balance of mitochondrial fission and fusion in cortical axons depends on the kinases SadA and SadB. *Cell Rep.* 37, 110141. doi: 10.1016/j.celrep.2021.110141

Di Pietro, V., Lazzarino, G., Amorini, A. M., Signoretti, S., Hill, L. J., Porto, E., et al. (2017). Fusion or fission: the destiny of mitochondria in traumatic brain injury of different severities. *Sci. Rep.* 7, 9189. doi: 10.1038/s41598-017-09587-2

Dollé, J. P., Morrison, B., Schloss, R. S., and Yarmush, M. L. (2014). Brain-on-a-chip microsystem for investigating traumatic brain injury: axon diameter and mitochondrial membrane changes play a significant role in axonal response to strain injuries. *Technology* 2, 106. doi: 10.1142/S2339547814500095

Dorn, G. W. (2020). Mitofusin 2 dysfunction and disease in mice and men. *Front. Physiol.* 11, 782. doi: 10.3389/fphys.2020.00782

Drerup, C. M., Herbert, A. L., Monk, K. R., and Nechiporuk, A. V. (2017). Regulation of mitochondria-dynactin interaction and mitochondrial retrograde transport in axons. *Elife* 6, e22234. doi: 10.7554/eLife.22234.021

Du, H., Guo, L., Yan, S., Sosunov, A. A., McKhann, G. M., and Yan, S. S. (2010). Early deficits in synaptic mitochondria in an Alzheimer's disease mouse model. *Proc. Natl. Acad. Sci. U.S.A.* 107, 18670–18675. doi: 10.1073/pnas.1006586107

El Fissi, N., Rojo, M., Aouane, A., Karatas, E., Poliacikova, G., David, C., et al. (2018). Mitofusin gain and loss of function drive pathogenesis in *Drosophila* models of CMT2A neuropathy. *EMBO Rep.* 19, e45241. doi: 10.15252/embr.201745241

Farkas, O., Lifshitz, J., and Povlishock, J. T. (2006). Mechanoporation induced by diffuse traumatic brain injury: an irreversible or reversible response to injury. *J. Neurosci.* 26, 3130–3140. doi: 10.1523/JNEUROSCI.5119-05.2006

Feng, Y., Yan, T., Zheng, J., Ge, X., Mu, Y., Zhang, Y., et al. (2010). Overexpression of Wld(S) or Nmnat2 in mauthner cells by single-cell electroporation delays axon degeneration in live zebrafish. *J. Neurosci. Res.* 88, 3319–3327. doi: 10.1002/jnr.22498

Ferguson, B., Matyszak, M. K., Esiri, M. M., and Perry, V. H. (1997). Axonal damage in acute multiple sclerosis lesions. *Brain* 120, 393–399. doi: 10.1093/brain/120.3.393

Ferreiro, E., Oliveira, C. R., and Pereira, C. M. F. (2008). The release of calcium from the endoplasmic reticulum induced by amyloid-beta and prion peptides activates the mitochondrial apoptotic pathway. *Neurobiol. Dis.* 30, 331–342. doi: 10.1016/j.nbd.2008.02.003

Ferri, A., Fiorenzo, P., Nencini, M., Cozzolino, M., Pesaresi, M. G., Valle, C., et al. (2010). Glutaredoxin 2 prevents aggregation of mutant SOD1 in mitochondria and abolishes its toxicity. *Hum. Mol. Genet.* 19, 4529–4542. doi: 10.1093/hmg/ddq383

Fischer, T. D., Hylin, M. J., Zhao, J., Moore, A. N., Waxham, M. N., and Dash, P. K. (2016). Altered mitochondrial dynamics and TBI pathophysiology. *Front. Syst. Neurosci.* 10, 29. doi: 10.3389/fnsys.2016.00029

Gandhi, S., Wood-Kaczmar, A., Yao, Z., Plun-Favreau, H., Deas, E., Klupsch, K., et al. (2009). PINK1-associated Parkinson's disease is caused by neuronal vulnerability to calcium-induced cell death. *Mol. Cell* 33, 627–638. doi: 10.1016/j.molcel.2009.02.013

Gerdts, J., Brace, E. J., Sasaki, Y., DiAntonio, A., and Milbrandt, J. (2015). Neurobiology. SARM1 activation triggers axon degeneration locally via NAD? destruction. Science 348, 453–457. doi: 10.1126/science.1258366

Giacomello, M., Pyakurel, A., Glytsou, C., and Scorrano, L. (2020). The cell biology of mitochondrial membrane dynamics. *Nat. Rev. Mol. Cell Biol.* 21, 204–224. doi: 10.1038/s41580-020-0210-7

Gilley, J., and Coleman, M. P. (2010). Endogenous Nmnat2 is an essential survival factor for maintenance of healthy axons. *PLoS Biol.* 8, e1000300-. doi: 10.1371/journal.pbio.1000300

Gilmer, L. K., Roberts, K. N., Joy, K., Sullivan, P. G., and Scheff, S. W. (2009). Early mitochondrial dysfunction after cortical contusion injury. *J. Neurotrauma* 26, 1271–1280. doi: 10.1089/neu.2008.0857

Gitler, D., and Spira, M. E. (1998). Real time imaging of calcium-induced localized proteolytic activity after axotomy and its relation to growth cone formation. *Neuron* 20, 1123–1135. doi: 10.1016/S0896-6273(00)80494-8

Glauser, L., Sonnay, S., Stafa, K., and Moore, D. J. (2011). Parkin promotes the ubiquitination and degradation of the mitochondrial fusion factor mitofusin 1. *J. Neurochem.* 118, 636–645. doi: 10.1111/j.1471-4159.2011.07318.x

Godoy, J. A., Arrázola, M. S., Ordenes, D., Silva-Alvarez, C., Braidy, N., and Inestrosa, N. C. (2014). Wnt-5a ligand modulates mitochondrial fission-fusion in rat hippocampal neurons. *J. Biol. Chem.* 289, 36179–36193. doi: 10.1074/jbc.M114.557009

Graham, J. M., Papadakis, N., Evans, J., Widjaja, E., Romanowski, C. A., Paley, M. N., et al. (2004). Diffusion tensor imaging for the assessment of upper motor neuron integrity in ALS. *Neurology* 63, 2111–2119. doi: 10.1212/01.WNL.0000145766.03057.E7

Gu, Y., Jukkola, P., Wang, Q., Esparza, T., Zhao, Y., Brody, D., et al. (2017). Polarity of varicosity initiation in central neuron mechanosensation. *J. Cell Biol.* 216, 2179–2199. doi: 10.1083/jcb.201606065

Guo, L., Du, H., Yan, S., Wu, X., McKhann, G. M., Chen, J. X., et al. (2013). Cyclophilin D deficiency rescues axonal mitochondrial transport in Alzheimer's neurons. *PLoS ONE* 8, e54914. doi: 10.1371/journal.pone.0054914

Guo, X., Macleod, G. T., Wellington, A., Hu, F., Panchumarthi, S., Schoenfield, M., et al. (2005). The GTPase dMiro is required for axonal transport of mitochondria to *Drosophila* synapses. *Neuron* 47, 379–393. doi: 10.1016/j.neuron.2005.06.027

Hånell, A., Greer, J. E., McGinn, M. J., and Povlishock, J. T. (2015). Traumatic brain injury-induced axonal phenotypes react differently to treatment. *Acta Neuropathol.* 129, 317–332. doi: 10.1007/s00401-014-1376-x

Han, Q., Xie, Y., Ordaz, J. D., Huh, A. J., Huang, N., Wu, W., et al. (2020). Restoring cellular energetics promotes axonal regeneration and functional recovery after spinal cord injury. *Cell Metab.* 31, 623–641.e8. doi: 10.1016/j.cmet.2020.02.002

Han, S. M., Baig, H. S., and Hammarlund, M. (2016). Mitochondria localize to injured axons to support regeneration. *Neuron* 92, 1308–1323. doi: 10.1016/j.neuron.2016.11.025

Hansson Petersen, C. A., Alikhani, N., Behbahani, H., Wiehager, B., Pavlov, P. F., Alafuzoff, I., et al. (2008). The amyloid beta-peptide is imported into mitochondria via the TOM import machinery and localized to mitochondrial cristae. *Proc. Natl. Acad. Sci. U.S.A.* 105, 13145–13150. doi: 10.1073/pnas.0806192105

Henley, J., and Poo, M. M. (2004). Guiding neuronal growth cones using Ca2+ signals. *Trends Cell Biol.* 14, 320–330. doi: 10.1016/j.tcb.2004.04.006

Hirokawa, N., Niwa, S., and Tanaka, Y. (2010). Molecular motors in neurons: transport mechanisms and roles in brain function, development, and disease. *Neuron* 68, 610–638. doi: 10.1016/j.neuron.2010.09.039

Howarth, C., Gleeson, P., and Attwell, D. (2012). Updated energy budgets for neural computation in the neocortex and cerebellum. *J. Cereb. Blood Flow Metab.* 32, 1222–1232. doi: 10.1038/jcbfm.2012.35

Huang, J., Friedland, R. P., and Auchus, A. P. (2007). Diffusion tensor imaging of normal-appearing white matter in mild cognitive impairment and early Alzheimer disease: preliminary evidence of axonal degeneration in the temporal lobe. *Am. J. Neuroradiol.* 28, 1943–1948. doi: 10.3174/ajnr.A0700

Huang, N., Li, S., Xie, Y., Han, Q., Xu, X. M., and Sheng, Z. H. (2021). Reprogramming an energetic AKT-PAK5 axis boosts axon energy supply and facilitates neuron survival and regeneration after injury and ischemia. *Curr. Biol.* 31, 3098–3114.e7. doi: 10.1016/j.cub.2021.04.079

Ikuta, J., Maturana, A., Fujita, T., Okajima, T., Tatematsu, K., Tanizawa, K., et al. (2007). Fasciculation and elongation protein zeta-1 (FEZ1) participates in the polarization of hippocampal neuron by controlling the mitochondrial motility. *Biochem. Biophys. Res. Commun.* 353, 127–132. doi: 10.1016/j.bbrc.2006.11.142

Ineichen, B. V., Zhu, K., and Carlström, K. E. (2021). Axonal mitochondria adjust in size depending on g-ratio of surrounding myelin during homeostasis and advanced remyelination. *J. Neurosci. Res.* 99, 793–805. doi: 10.1002/jnr.24767

Ishihara, N., Nomura, M., Jofuku, A., Kato, H., Suzuki, S. O., Masuda, K., et al. (2009). Mitochondrial fission factor Drp1 is essential for embryonic development and synapse formation in mice. *Nat. Cell Biol.* 11, 958–966. doi: 10.1038/ncb1907

Itoh, K., Nakamura, K., Iijima, M., and Sesaki, H. (2013). Mitochondrial dynamics in neurodegeneration. *Trends Cell Biol.* 23, 64–71. doi: 10.1016/j.tcb.2012.10.006

Jadiya, P., Garbincius, J. F., and Elrod, J. W. (2021). Reappraisal of metabolic dysfunction in neurodegeneration: Focus on mitochondrial function and calcium signaling. *Acta Neuropathol. Commun.* 9, 124. doi: 10.1186/s40478-021-01224-4

Johnson, V. E., Stewart, W., Weber, M. T., Cullen, D. K., Siman, R., and Smith, D. H. (2016). SNTF immunostaining reveals previously undetected axonal pathology in traumatic brain injury. *Acta Neuropathol.* 131, 115–135. doi: 10.1007/s00401-015-1506-0

Kang, J. S., Tian, J. H., Pan, P. Y., Zald, P., Li, C., Deng, C., et al. (2008). Docking of axonal mitochondria by syntaphilin controls their mobility and affects short-term facilitation. *Cell* 132, 137–148. doi: 10.1016/j.cell.2007.11.024

Kedra, J., Lin, S., Pacheco, A., Gallo, G., and Smith, G. M. (2021). Axotomy induces Drp1-dependent fragmentation of axonal mitochondria. *Front. Mol. Neurosci.* 14, 668670. doi: 10.3389/fnmol.2021.668670

Kilinc, D., Gallo, G., and Barbee, K. A. (2008). Mechanically-induced membrane poration causes axonal beading and localized cytoskeletal damage. *Exp. Neurol.* 212, 422–430. doi: 10.1016/j.expneurol.2008.04.025

Kiryu-Seo, S., Tamada, H., Kato, Y., Yasuda, K., Ishihara, N., Nomura, M., et al. (2016). Mitochondrial fission is an acute and adaptive response in injured motor neurons. *Sci. Rep.* 6, 28331. doi: 10.1038/srep28331

Kitay, B. M., McCormack, R., Wang, Y., Tsoulfas, P., and Zhai, R. G. (2013). Mislocalization of neuronal mitochondria reveals regulation of Wallerian degeneration and NMNAT/WLD(S)-mediated axon protection independent of axonal mitochondria. *Hum. Mol. Genet.* 22, 1601–1614. doi: 10.1093/hmg/ddt009

Knowlton, W. M., Hubert, T., Wu, Z., Chisholm, A. D., and Jin, Y. (2017). A select subset of electron transport chain genes associated with optic atrophy link mitochondria to axon regeneration in *Caenorhabditis elegans*. *Front. Neurosci.* 11, 263. doi: 10.3389/fnins.2017.00263

Kruppa, A. J., and Buss, F. (2021). Motor proteins at the mitochondria-cytoskeleton interface. *J. Cell Sci.* 134, jcs226084. doi: 10.1242/jcs.226084

Lee, S., Sterky, F. H., Mourier, A., Terzioglu, M., Cullheim, S., Olson, L., et al. (2012). Mitofusin 2 is necessary for striatal axonal projections of midbrain dopamine neurons. *Hum. Mol. Genet.* 21, 4827–4835. doi: 10.1093/hmg/dds352

Lewis, T. L., Kwon, S. K., Lee, A., Shaw, R., and Polleux, F. (2018). MFF-dependent mitochondrial fission regulates presynaptic release and axon branching by limiting axonal mitochondria size. *Nat. Commun.* 9, 5008. doi: 10.1038/s41467-018-07416-2

Lewis, T. L., Turi, G. F., Kwon, S. K., Losonczy, A., and Polleux, F. (2016). Progressive decrease of mitochondrial motility during maturation of cortical axons *in vitro* and *in vivo*. *Curr. Biol.* 26, 2602–2608. doi: 10.1016/j.cub.2016.07.064

Li, S., Xiong, G. J., Huang, N., and Sheng, Z. H. (2020). The cross-talk of energy sensing and mitochondrial anchoring sustains synaptic efficacy by maintaining presynaptic metabolism. *Nat. Metab.* 2, 1077–1095. doi: 10.1038/s42255-020-00289-0

Licht-Mayer, S., Campbell, G. R., Canizares, M., Mehta, A. R., Gane, A. B., McGill, K., et al. (2020). Enhanced axonal response of mitochondria to demyelination offers neuroprotection: implications for multiple sclerosis. *Acta Neuropathol.* 140, 143–167. doi: 10.1007/s00401-020-02179-x

Lin, M. Y., Cheng, X. T., Tammineni, P., Xie, Y., Zhou, B., Cai, Q., et al. (2017). Releasing syntaphilin removes stressed mitochondria from axons independent of mitophagy under pathophysiological conditions. *Neuron* 94, 595–610.e6. doi: 10.1016/j.neuron.2017.04.004

Lingor, P., Koch, J. C., Tönges, L., and Bähr, M. (2012). Axonal degeneration as a therapeutic target in the CNS. *Cell Tissue Res.* 349, 289–311. doi: 10.1007/s00441-012-1362-3

Liu, P., Huang, H., Fang, F., Liu, L., Li, L., Feng, X., et al. (2021). Neuronal NMNAT2 overexpression does not achieve significant neuroprotection in experimental autoimmune encephalomyelitis/optic neuritis. *Front. Cell. Neurosci.* 15, 754651. doi: 10.3389/fncel.2021.754651

López-Doménech, G., Serrat, R., Mirra, S., D'Aniello, S., Somorjai, I., Abad, A., et al. (2012). The Eutherian Armcx genes regulate mitochondrial trafficking in neurons and interact with Miro and Trak2. *Nat. Commun.* 3, 814–814. doi: 10.1038/ncomms1829

Lunn, E. R., Perry, V. H., Brown, M. C., Rosen, H., and Gordon, S. (1989). Absence of wallerian degeneration does not hinder regeneration in peripheral nerve. *Eur. J. Neurosci.* 1, 27–33. doi: 10.1111/j.1460-9568.1989.tb00771.x

Macaskill, A. F., Rinholm, J. E., Twelvetrees, A. E., Arancibia-Carcamo, I. L., Muir, J., Fransson, A., et al. (2009). Miro1 is a calcium sensor for glutamate receptor-dependent localization of mitochondria at synapses. *Neuron* 61, 541–555. doi: 10.1016/j.neuron.2009.01.030

Maday, S., Twelvetrees, A. E., Moughamian, A. J., and Holzbaur, E. L. (2014). Axonal transport: cargo-specific mechanisms of motility and regulation. *Neuron* 84, 292–309. doi: 10.1016/j.neuron.2014.10.019

Mar, F. M., Simões, A. R., Leite, S., Morgado, M. M., Santos, T. E., Rodrigo, I. S., et al. (2014). CNS axons globally increase axonal transport after peripheral conditioning. *J. Neurosci.* 34, 5965–5970. doi: 10.1523/JNEUROSCI.4680-13.2014

Maxwell, W. L. (1996). Histopathological changes at central nodes of Ranvier after stretch-injury. *Microsc. Res. Tech.* 34, 522–535. doi: 10.1002/(SICI)1097-0029(19960815)34:6<522::AID-JEMT4>3.0.CO;2-L

Mbye, L. H., Singh, I. N., Carrico, K. M., Saatman, K. E., and Hall, E. D. (2009). Comparative neuroprotective effects of cyclosporin A and NIM811, a nonimmunosuppressive cyclosporin A analog, following traumatic brain injury. *J. Cereb. Blood Flow Metab.* 29, 87–97. doi: 10.1038/jcbfm.2008.93

McDonald, J. W., and Sadowsky, C. (2002). Spinal-cord injury. *Lancet* 359, 417–425. doi: 10.1016/S0140-6736(02)07603-1

Meeusen, S., McCaffery, J. M., and Nunnari, J. (2004). Mitochondrial fusion intermediates revealed *in vitro*. *Science* 305, 1747–1752. doi: 10.1126/science.1100612

Merlini, E., Coleman, M. P., and Loreto, A. (2022). Mitochondrial dysfunction as a trigger of programmed axon death. *Trends Neurosci.* 45, 53–63. doi: 10.1016/j.tins.2021.10.014

Mironov, S. L. (2007). ADP regulates movements of mitochondria in neurons. *Biophys. J.* 92, 2944–2952. doi: 10.1529/biophysj.106.092981

Misgeld, T., Kerschensteiner, M., Bareyre, F. M., Burgess, R. W., and Lichtman, J. W. (2007). Imaging axonal transport of mitochondria *in vivo*. *Nat. Methods* 4, 559–561. doi: 10.1038/nmeth1055

Misgeld, T., and Schwarz, T. L. (2017). Mitostasis in neurons: maintaining mitochondria in an extended cellular architecture. *Neuron* 96, 651–666. doi: 10.1016/j.neuron.2017.09.055

Mishra, P., and Chan, D. C. (2014). Mitochondrial dynamics and inheritance during cell division, development and disease. *Nat. Rev. Mol. Cell Biol.* 15, 634–646. doi: 10.1038/nrm3877

Mishra, P., and Chan, D. C. (2016). Metabolic regulation of mitochondrial dynamics. *J. Cell Biol.* 212, 379–387. doi: 10.1083/jcb.201511036

Misko, A. L., Sasaki, Y., Tuck, E., Milbrandt, J., and Baloh, R. H. (2012). Mitofusin2 mutations disrupt axonal mitochondrial positioning and promote axon degeneration. *J. Neurosci.* 32, 4145–4155. doi: 10.1523/JNEUROSCI.6338-11.2012

Morsci, N. S., Hall, D. H., Driscoll, M., and Sheng, Z.-H. (2016). Age-Related phasic patterns of mitochondrial maintenance in adult caenorhabditis elegans neurons. *J. Neurosci.* 36, 1373–1385. doi: 10.1523/JNEUROSCI.2799-15.2016

Mou, Y., Dein, J., Chen, Z., Jagdale, M., and Li, X. J. (2021). MFN2 deficiency impairs mitochondrial transport and downregulates motor protein expression in human spinal motor neurons. *Front. Mol. Neurosci.* 14, 727552. doi: 10.3389/fnmol.2021.727552

Niescier, R. F., Hong, K., Park, D., and Min, K. T. (2018). MCU interacts with miro1 to modulate mitochondrial functions in neurons. *J. Neurosci.* 38, 4666–4677. doi: 10.1523/JNEUROSCI.0504-18.2018

Nikić, I., Merkler, D., Sorbara, C., Brinkoetter, M., Kreutzfeldt, M., Bareyre, F. M., et al. (2011). A reversible form of axon damage in experimental autoimmune encephalomyelitis and multiple sclerosis. *Nat. Med.* 17, 495–499. doi: 10.1038/nm.2324

Obashi, K., and Okabe, S. (2013). Regulation of mitochondrial dynamics and distribution by synapse position and neuronal activity in the axon. *Eur. J. Neurosci.* 38, 2350–2363. doi: 10.1111/ejn.12263

Oettinghaus, B., Schulz, J. M., Restelli, L. M., Licci, M., Savoia, C., Schmidt, A., et al. (2016). Synaptic dysfunction, memory deficits and hippocampal atrophy due to ablation of mitochondrial fission in adult forebrain neurons. *Cell Death Differ.* 23, 18–28. doi: 10.1038/cdd.2015.39

Ohno, N., Chiang, H., Mahad, D. J., Kidd, G. J., Liu, L., Ransohoff, R. M., et al. (2014). Mitochondrial immobilization mediated by syntaphilin facilitates survival of demyelinated axons. *Proc. Natl. Acad. Sci. U.S.A.* 111, 9953–9958. doi: 10.1073/pnas.1401155111

Ohno, N., Kidd, G. J., Mahad, D., Kiryu-Seo, S., Avishai, A., Komuro, H., et al. (2011). Myelination and axonal electrical activity modulate the distribution and motility of mitochondria at CNS nodes of Ranvier. *J. Neurosci.* 31, 7249–7258. doi: 10.1523/JNEUROSCI.0095-11.2011

Osellame, L. D., Singh, A. P., Stroud, D. A., Palmer, C. S., Stojanovski, D., Ramachandran, R., et al. (2016). Cooperative and independent roles of the Drp1 adaptors Mff, MiD49 and MiD51 in mitochondrial fission. *J. Cell Sci.* 129, 2170–2181. doi: 10.1242/jcs.185165

Osterloh, J. M., Yang, J., Rooney, T. M., Fox, A. N., Adalbert, R., Powell, E. H., et al. (2012). dSarm/Sarm1 is required for activation of an injury-induced axon death pathway. *Science* 337, 481–484. doi: 10.1126/science.1223899

Overly, C. C., Rieff, H. I., and Hollenbeck, P. J. (1996). Organelle motility and metabolism in axons vs dendrites of cultured hippocampal neurons. *J. Cell Sci.* 109, 971–980. doi: 10.1242/jcs.109.5.971

Palay, S. L. (1956). Synapses in the central nervous system. *J. Biophys. Biochem. Cytol.* 2, 193–202. doi: 10.1083/jcb.2.4.193

Paß, T., Wiesner, R. J., and Pla-Martín, D. (2021). Selective neuron vulnerability in common and rare diseases-mitochondria in the focus. *Front. Mol. Biosci.* 8, 676187. doi: 10.3389/fmolb.2021.676187

Pathak, D., Sepp, K. J., and Hollenbeck, P. J. (2010). Evidence that myosin activity opposes microtubule-based axonal transport of mitochondria. *J. Neurosci.* 30, 8984–8992. doi: 10.1523/JNEUROSCI.1621-10.2010

Pitts, K. R., Yoon, Y., Krueger, E. W., and McNiven, M. A. (1999). The dynamin-like protein DLP1 is essential for normal distribution and morphology of the endoplasmic reticulum and mitochondria in mammalian cells. *Mol. Biol. Cell* 10, 4403–4417. doi: 10.1091/mbc.10.12.4403

Plucińska, G., Paquet, D., Hruscha, A., Godinho, L., Haass, C., Schmid, B., et al. (2012). *In vivo* imaging of disease-related mitochondrial dynamics in a vertebrate model system. *J. Neurosci.* 32, 16203–16212. doi: 10.1523/JNEUROSCI.1327-12.2012

Pozo Devoto, V. M., Dimopoulos, N., Alloatti, M., Pardi, M. B., Saez, T. M., Otero, M. G., et al. (2017). αSynuclein control of mitochondrial homeostasis in human-derived neurons is disrupted by mutations associated with Parkinson's disease. *Sci. Rep.* 7, 5042. doi: 10.1038/s41598-017-05334-9

Pozo Devoto, V. M., Lacovich, V., Feole, M., Bhat, P., Chovan, J., Carna, M., et al. (2022). Unraveling axonal mechanisms of traumatic brain injury cold spring harbor laboratory. *bioRxiv*. doi: 10.1101/2022.03.30.486433

Prots, I., Veber, V., Brey, S., Campioni, S., Buder, K., Riek, R., et al. (2013). α-Synuclein oligomers impair neuronal microtubule-kinesin interplay. *J. Biol. Chem.* 288, 21742–21754. doi: 10.1074/jbc.M113.451815

Quintero, O. A., DiVito, M. M., Adikes, R. C., Kortan, M. B., Case, L. B., Lier, A. J., et al. (2009). Human Myo19 is a novel myosin that associates with mitochondria. *Curr. Biol.* 19, 2008–2013. doi: 10.1016/j.cub.2009.10.026

Ramsden, M., Henderson, Z., and Pearson, H. A. (2002). Modulation of Ca2+ channel currents in primary cultures of rat cortical neurones by amyloid beta protein (1-40) is dependent on solubility status. *Brain Res.* 956, 254–261. doi: 10.1016/S0006-8993(02)03547-3

Rawson, R. L., Yam, L., Weimer, R. M., Bend, E. G., Hartwieg, E., Horvitz, H. R., et al. (2014). Axons degenerate in the absence of mitochondria in *C. elegans*. *Curr. Biol.* 24, 760–765. doi: 10.1016/j.cub.2014.02.025

Readnower, R. D., Pandya, J. D., McEwen, M. L., Pauly, J. R., Springer, J. E., and Sullivan, P. G. (2011). Post-injury administration of the mitochondrial permeability transition pore inhibitor, NIM811, is neuroprotective and improves cognition after traumatic brain injury in rats. *J. Neurotrauma* 28, 1845–1853. doi: 10.1089/neu.2011.1755

Ribas, V. T., Koch, J. C., Michel, U., Bähr, M., and Lingor, P. (2017). Attenuation of axonal degeneration by calcium channel inhibitors improves retinal ganglion cell survival and regeneration after optic nerve crush. *Mol. Neurobiol.* 54, 72–86. doi: 10.1007/s12035-015-9676-2

Rosenberg, S. S., and Spitzer, N. C. (2011). Calcium signaling in neuronal development. *Cold Spring Harb. Perspect. Biol.* 3, a004259. doi: 10.1101/cshperspect.a004259

Sajic, M., Mastrolia, V., Lee, C. Y., Trigo, D., Sadeghian, M., Mosley, A. J., et al. (2013). Impulse conduction increases mitochondrial transport in adult mammalian peripheral nerves *in vivo*. *PLoS Biol.* 11, e1001754. doi: 10.1371/journal.pbio.1001754

Sanz-Blasco, S., Valero, R. A., Rodríguez-Crespo, I., Villalobos, C., and Núñez, L. (2008). Mitochondrial Ca2+ overload underlies Abeta oligomers neurotoxicity providing an unexpected mechanism of neuroprotection by NSAIDs. *PLoS ONE* 3, e2718. doi: 10.1371/journal.pone.0002718

Saotome, M., Safiulina, D., Szabadkai, G., Das, S., Fransson, A., Aspenstrom, P., et al. (2008). Bidirectional Ca2+-dependent control of mitochondrial dynamics by the Miro GTPase. *Proc. Natl. Acad. Sci. U.S.A.* 105, 20728–20733. doi: 10.1073/pnas.0808953105

Saxton, W. M., and Hollenbeck, P. J. (2012). The axonal transport of mitochondria. *J. Cell Sci.* 125, 2095–2104. doi: 10.1242/jcs.053850

Scheib, J., and Höke, A. (2013). Advances in peripheral nerve regeneration. *Nat. Rev. Neurol.* 9, 668–676. doi: 10.1038/nrneurol.2013.227

Schon, E. A., and Przedborski, S. (2011). Mitochondria: the next (neurode)generation. *Neuron* 70, 1033–1053. doi: 10.1016/j.neuron.2011.06.003

Schrank, S., Barrington, N., and Stutzmann, G. E. (2020). Calcium-handling defects and neurodegenerative disease. *Cold Spring Harb. Perspect. Biol.* 12, a035212. doi: 10.1101/cshperspect.a035212

Seager, R., Lee, L., Henley, J. M., and Wilkinson, K. A. (2020). Mechanisms and roles of mitochondrial localisation and dynamics in neuronal function. *Neuronal Signal* 4, NS20200008. doi: 10.1042/NS20200008

Sgobio, C., Sun, L., Ding, J., Herms, J., Lovinger, D. M., and Cai, H. (2019). Unbalanced calcium channel activity underlies selective vulnerability of nigrostriatal dopaminergic terminals in parkinsonian mice. *Sci. Rep.* 9, 4857. doi: 10.1038/s41598-019-41091-7

Sheng, Z.-H., and Cai, Q. (2012). Mitochondrial transport in neurons: impact on synaptic homeostasis and neurodegeneration. *Nat. Rev. Neurosci.* 13, 77–93. doi: 10.1038/nrn3156

Shepherd, G. M., and Harris, K. M. (1998). Three-dimensional structure and composition of CA3–>CA1 axons in rat hippocampal slices: implications for presynaptic connectivity and compartmentalization. *J. Neurosci.* 18, 8300–8310. doi: 10.1523/JNEUROSCI.18-20-08300.1998

Shields, L. Y., Kim, H., Zhu, L., Haddad, D., Berthet, A., Pathak, D., et al. (2015). Dynamin-related protein 1 is required for normal mitochondrial bioenergetic and synaptic function in CA1 hippocampal neurons. *Cell Death Dis.* 6, e1725. doi: 10.1038/cddis.2015.94

Shigeoka, T., Jung, H., Jung, J., Turner-Bridger, B., Ohk, J., Lin, J. Q., et al. (2016). Dynamic axonal translation in developing and mature visual circuits. *Cell* 166, 181–192. doi: 10.1016/j.cell.2016.05.029

Shin, J. E., Miller, B. R., Babetto, E., Cho, Y., Sasaki, Y., Qayum, S., et al. (2012). SCG10 is a JNK target in the axonal degeneration pathway. *Proc. Natl. Acad. Sci. U.S.A.* 109, E3696–E3705. doi: 10.1073/pnas.1216204109

Smith, E. F., Shaw, P. J., and De Vos, K. J. (2019). The role of mitochondria in amyotrophic lateral sclerosis. *Neurosci. Lett.* 710, 132933. doi: 10.1016/j.neulet.2017.06.052

Smit-Rigter, L., Rajendran, R., Silva, C. A., Spierenburg, L., Groeneweg, F., Ruimschotel, E. M., et al. (2016). Mitochondrial dynamics in visual cortex are limited *in vivo* and not affected by axonal structural plasticity. *Curr. Biol.* 26, 2609–2616. doi: 10.1016/j.cub.2016.07.033

Song, Z., Ghochani, M., McCaffery, J. M., Frey, T. G., and Chan, D. C. (2009). Mitofusins and OPA1 mediate sequential steps in mitochondrial membrane fusion. *Mol. Biol. Cell* 20, 3525–3532. doi: 10.1091/mbc.e09-03-0252

Spillane, M., Ketschek, A., Merianda, T. T., Twiss, J. L., and Gallo, G. (2013). Mitochondria coordinate sites of axon branching through localized intra-axonal protein synthesis. *Cell Rep.* 5, 1564–1575. doi: 10.1016/j.celrep.2013.11.022

Staal, J. A., Dickson, T. C., Gasperini, R., Liu, Y., Foa, L., and Vickers, J. C. (2010). Initial calcium release from intracellular stores followed by calcium dysregulation is linked to secondary axotomy following transient axonal stretch injury. *J. Neurochem.* 112, 1147–1155. doi: 10.1111/j.1471-4159.2009.06531.x

Stavsky, A., Stoler, O., Kostic, M., Katoshevsky, T., Assali, E. A., Savic, I., et al. (2021). Aberrant activity of mitochondrial NCLX is linked to impaired synaptic transmission and is associated with mental retardation. *Commun. Biol.* 4, 666. doi: 10.1038/s42003-021-02312-w

Stirling, D. P., Cummins, K., Wayne Chen, S. R., and Stys, P. (2014). Axoplasmic reticulum Ca(2+) release causes secondary degeneration of spinal axons. *Ann. Neurol.* 75, 220–229. doi: 10.1002/ana.24099

Stokin, G. B., Lillo, C., Falzone, T. L., Brusch, R. G., Rockenstein, E., Mount, S. L., et al. (2005). Axonopathy and transport deficits early in the pathogenesis of Alzheimer's disease. *Science* 307, 1282–1288. doi: 10.1126/science.1105681

Stone, J. R., Singleton, R. H., and Povlishock, J. T. (2001). Intra-axonal neurofilament compaction does not evoke local axonal swelling in all traumatically injured axons. *Exp. Neurol.* 172, 320–331. doi: 10.1006/exnr.2001.7818

Stowers, R. S., Megeath, L. J., Górska-Andrzejak, J., Meinertzhagen, I. A., and Schwarz, T. L. (2002). Axonal transport of mitochondria to synapses depends on milton, a novel *Drosophila* protein. *Neuron* 36, 1063–1077. doi: 10.1016/S0896-6273(02)01094-2

Sudhof, T. C. (2004). The synaptic vesicle cycle. *Annu. Rev. Neurosci.* 27, 509–547. doi: 10.1146/annurev.neuro.26.041002.131412

Tamada, H., Kiryu-Seo, S., Hosokawa, H., Ohta, K., Ishihara, N., Nomura, M., et al. (2017). Three-dimensional analysis of somatic mitochondrial dynamics in fission-deficient injured motor neurons using FIB/SEM. *J. Comp. Neurol.* 525, 2535–2548. doi: 10.1002/cne.24213

Tang-Schomer, M. D., Johnson, V. E., Baas, P. W., Stewart, W., and Smith, D. H. (2012). Partial interruption of axonal transport due to microtubule breakage accounts for the formation of periodic varicosities after traumatic axonal injury. *Exp. Neurol.* 233, 364–372. doi: 10.1016/j.expneurol.2011.10.030

Tang-Schomer, M. D., Patel, A. R., Baas, P. W., and Smith, D. H. (2010). Mechanical breaking of microtubules in axons during dynamic stretch injury underlies delayed elasticity, microtubule disassembly, and axon degeneration. *FASEB J.* 24, 1401–1410. doi: 10.1096/fj.09-142844

Toda, T., Kadono, T., Hoshiai, M., Eguchi, Y., Nakazawa, S., Nakazawa, H., et al. (2007). Na+/H+ exchanger inhibitor cariporide attenuates the mitochondrial Ca2+ overload and PTP opening. *Am. J. Physiol. Heart Circ. Physiol.* 293, H3517–H3523. doi: 10.1152/ajpheart.00483.2006

Trevisan, T., Pendin, D., Montagna, A., Bova, S., Ghelli, A. M., and Daga, A. (2018). Manipulation of mitochondria dynamics reveals separate roles for form and function in mitochondria distribution. *Cell Rep.* 23, 1742–1753. doi: 10.1016/j.celrep.2018.04.017

Ueda, K., Shinohara, S., Yagami, T., Asakura, K., and Kawasaki, K. (1997). Amyloid beta protein potentiates Ca2+ influx through L-type voltage-sensitive Ca2+ channels: a possible involvement of free radicals. *J. Neurochem.* 68, 265–271. doi: 10.1046/j.1471-4159.1997.68010265.x

van Spronsen, M., Mikhaylova, M., Lipka, J., Schlager, M. A., Kuijpers, M., Wulf, P. S., et al. (2013). TRAK/Milton motor-adaptor proteins steer mitochondrial trafficking to axons and dendrites. *Neuron* 77, 485–502. doi: 10.1016/j.neuron.2012.11.027

Vargas, M. E., Yamagishi, Y., Tessier-Lavigne, M., and Sagasti, A. (2015). Live imaging of calcium dynamics during axon degeneration reveals two functionally distinct phases of calcium influx. *J. Neurosci.* 35, 15026–15038. doi: 10.1523/JNEUROSCI.2484-15.2015

Verhoeven, K., Claeys, K. G., Züchner, S., Schröder, J. M., Weis, J., Ceuterick, C., et al. (2006). MFN2 mutation distribution and genotype/phenotype correlation in charcot-marie-tooth type 2. *Brain* 129, 2093–2102. doi: 10.1093/brain/awl126

Verstreken, P., Ly, C. V., Venken, K. J., Koh, T. W., Zhou, Y., and Bellen, H. J. (2005). Synaptic mitochondria are critical for mobilization of reserve pool vesicles at *Drosophila* neuromuscular junctions. *Neuron* 47, 365–378. doi: 10.1016/j.neuron.2005.06.018

Villegas, R., Martinez, N. W., Lillo, J., Pihan, P., Hernandez, D., Twiss, J. L., et al. (2014). Calcium release from intra-axonal endoplasmic reticulum leads to axon degeneration through mitochondrial dysfunction. *J. Neurosci.* 34, 7179–7189. doi: 10.1523/JNEUROSCI.4784-13.2014

Wan, B., LaNoue, K. F., Cheung, J. Y., and Scaduto, R. C. (1989). Regulation of citric acid cycle by calcium. *J. Biol. Chem.* 264, 13430–13439. doi: 10.1016/S0021-9258(18)80015-1

Wang, B., Huang, M., Shang, D., Yan, X., Zhao, B., and Zhang, X. (2021). Mitochondrial behavior in axon degeneration and regeneration. *Front. Aging Neurosci.* 13, 650038. doi: 10.3389/fnagi.2021.650038

Wang, Q., Tian, J., Chen, H., Du, H., and Guo, L. (2019). Amyloid beta-mediated KIF5A deficiency disrupts anterograde axonal mitochondrial movement. *Neurobiol. Dis.* 127, 410–418. doi: 10.1016/j.nbd.2019.03.021

Wang, X., and Schwarz, T. L. (2009). The mechanism of Ca2+ -dependent regulation of kinesin-mediated mitochondrial motility. *Cell* 136, 163–174. doi: 10.1016/j.cell.2008.11.046

Wang, X., Yan, M. H., Fujioka, H., Liu, J., Wilson-Delfosse, A., Chen, S. G., et al. (2012). LRRK2 regulates mitochondrial dynamics and function through direct interaction with DLP1. *Hum. Mol. Genet.* 21, 1931–1944. doi: 10.1093/hmg/dds003

Weber, M. T., Arena, J. D., Xiao, R., Wolf, J. A., and Johnson, V. E. (2019). CLARITY reveals a more protracted temporal course of axon swelling and disconnection than previously described following traumatic brain injury. *Brain Pathol.* 29, 437–450. doi: 10.1111/bpa.12677

Wilson, L., Stewart, W., Dams-O'Connor, K., Diaz-Arrastia, R., Horton, L., Menon, D. K., et al. (2017). The chronic and evolving neurological consequences of traumatic brain injury. *Lancet Neurol.* 16, 813–825. doi: 10.1016/S1474-4422(17)30279-X

Witte, M. E., Bø, L., Rodenburg, R. J., Belien, J. A., Musters, R., Hazes, T., et al. (2009). Enhanced number and activity of mitochondria in multiple sclerosis lesions. *J. Pathol.* 219, 193–204. doi: 10.1002/path.2582

Wolf, J. A., Stys, P. K., Lusardi, T., Meaney, D., and Smith, D. H. (2001). Traumatic axonal injury induces calcium influx modulated by tetrodotoxin-sensitive sodium channels. *J. Neurosci.* 21, 1923–1930. doi: 10.1523/JNEUROSCI.21-06-01923.2001

Woolums, B. M., McCray, B. A., Sung, H., Tabuchi, M., Sullivan, J. M., Ruppell, K. T., et al. (2020). TRPV4 disrupts mitochondrial transport and causes axonal degeneration via a CaMKII-dependent elevation of intracellular Ca^2. *Nat. Commun.* 11, 2679. doi: 10.1038/s41467-020-16411-5

Xiong, Y., Gu, Q., Peterson, P. L., Muizelaar, J. P., and Lee, C. P. (1997). Mitochondrial dysfunction and calcium perturbation induced by traumatic brain injury. *J. Neurotrauma* 14, 23–34. doi: 10.1089/neu.1997.14.23

Xu, Y., Chen, M., Hu, B., Huang, R., and Hu, B. (2017). *In vivo* imaging of mitochondrial transport in single-axon regeneration of zebrafish mauthner cells. *Front. Cell. Neurosci.* 11, 4. doi: 10.3389/fncel.2017.00004

Xu, Y. F., Gendron, T. F., Zhang, Y. J., Lin, W. L., D'Alton, S., Sheng, H., et al. (2010). Wild-type human TDP-43 expression causes TDP-43 phosphorylation, mitochondrial aggregation, motor deficits, and early mortality in transgenic mice. *J. Neurosci.* 30, 10851–10859. doi: 10.1523/JNEUROSCI.1630-10.2010

Yang, Y., Ouyang, Y., Yang, L., Beal, M. F., McQuibban, A., Vogel, H., et al. (2008). Pink1 regulates mitochondrial dynamics through interaction with the fission/fusion machinery. *Proc. Natl. Acad. Sci. U.S.A.* 105, 7070–7075. doi: 10.1073/pnas.0711845105

Yi, M., Weaver, D., and Hajnóczky, G. (2004). Control of mitochondrial motility and distribution by the calcium signal: a homeostatic circuit. *J. Cell Biol.* 167, 661–672. doi: 10.1083/jcb.200406038

Yuen, T. J., Browne, K. D., Iwata, A., and Smith, D. H. (2009). Sodium channelopathy induced by mild axonal trauma worsens outcome after a repeat injury. *J. Neurosci. Res.* 87, 3620–3625. doi: 10.1002/jnr.22161

Zambonin, J. L., Zhao, C., Ohno, N., Campbell, G. R., Engeham, S., Ziabreva, I., et al. (2011). Increased mitochondrial content in remyelinated axons: implications for multiple sclerosis. *Brain* 134, 1901–1913. doi: 10.1093/brain/awr110

Zhang, L., Trushin, S., Christensen, T. A., Tripathi, U., Hong, C., Geroux, R. E., et al. (2018). Differential effect of amyloid beta peptides on mitochondrial axonal trafficking depends on their state of aggregation and binding to the plasma membrane. *Neurobiol. Dis.* 114, 1–16. doi: 10.1016/j.nbd.2018.02.003

Zhao, Y., Song, E., Wang, W., Hsieh, C. H., Wang, X., Feng, W., et al. (2021). Metaxins are core components of mitochondrial transport adaptor complexes. *Nat. Commun.* 12, 83. doi: 10.1038/s41467-020-20346-2

Zhou, B., Yu, P., Lin, M. Y., Sun, T., Chen, Y., and Sheng, Z. H. (2016). Facilitation of axon regeneration by enhancing mitochondrial transport and rescuing energy deficits. *J. Cell Biol.* 214, 103–119. doi: 10.1083/jcb.201605101

Zhou, Y., Carmona, S., Muhammad, A. K. M. G., Bell, S., Landeros, J., Vazquez, M., et al. (2019). Restoring mitofusin balance prevents axonal degeneration in a charcot-marie-tooth type 2A model. *J. Clin. Invest.* 129, 1756–1771. doi: 10.1172/JCI124194

Zilocchi, M., Finzi, G., Lualdi, M., Sessa, F., Fasano, M., and Alberio, T. (2018). Mitochondrial alterations in Parkinson's disease human samples and cellular models. *Neurochem. Int.* 118, 61–72. doi: 10.1016/j.neuint.2018.04.013

Ziogas, N. K., and Koliatsos, V. E. (2018). Primary traumatic axonopathy in mice subjected to impact acceleration: a reappraisal of pathology and mechanisms with high-resolution anatomical methods. *J. Neurosci.* 38, 4031–4047. doi: 10.1523/JNEUROSCI.2343-17.2018

frontiers | Frontiers in Cellular Neuroscience

TYPE Original Research
PUBLISHED 15 September 2022
DOI 10.3389/fncel.2022.969261

Check for updates

OPEN ACCESS

EDITED BY
Jason R. Plemel,
University of Alberta, Canada

REVIEWED BY
Brett J. Hilton,
German Center
for Neurodegeneratives (HZ), Germany
Matthew James Broadhead,
University of St Andrews,
United Kingdom

*CORRESPONDENCE
Meifan Chen
meifan.chen@uky.edu
Mark P. Goldberg
goldbergm@uthscsa.edu

SPECIALTY SECTION
This article was submitted to
Non-Neuronal Cells,
a section of the journal
Frontiers in Cellular Neuroscience

RECEIVED 15 June 2022
ACCEPTED 10 August 2022
PUBLISHED 15 September 2022

CITATION
Chen M, Ingle L, Plautz EJ, Kong X,
Tang R, Ghosh N, Romprey MK,
Fenske WK and Goldberg MP (2022)
LZK-dependent stimulation
of astrocyte reactivity promotes
corticospinal axon sprouting.
Front. Cell. Neurosci. 16:969261.
doi: 10.3389/fncel.2022.969261

COPYRIGHT
© 2022 Chen, Ingle, Plautz, Kong,
Tang, Ghosh, Romprey, Fenske and
Goldberg. This is an open-access
article distributed under the terms of
the Creative Commons Attribution
License (CC BY). The use, distribution
or reproduction in other forums is
permitted, provided the original
author(s) and the copyright owner(s)
are credited and that the original
publication in this journal is cited, in
accordance with accepted academic
practice. No use, distribution or
reproduction is permitted which does
not comply with these terms.

LZK-dependent stimulation of astrocyte reactivity promotes corticospinal axon sprouting

Meifan Chen[1,2]*, Laura Ingle[3], Erik J. Plautz[3], Xiangmei Kong[3], Rui Tang[3], Neil Ghosh[3], Megan K. Romprey[1,2], William K. Fenske[1] and Mark P. Goldberg[3,4]*

[1]Spinal Cord and Brain Injury Research Center, College of Medicine, University of Kentucky, Lexington, KY, United States, [2]Department of Neuroscience, College of Medicine, University of Kentucky, Lexington, KY, United States, [3]Department of Neurology and Neurotherapeutics, University of Texas Southwestern Medical Center, Dallas, TX, United States, [4]Department of Neurology, University of Texas Health Science Center San Antonio, San Antonio, TX, United States

Injury to the adult mammalian central nervous system induces compensatory plasticity of spared axons—referred to as collateral axon sprouting—that can facilitate neural recovery. The contribution of reactive astrocytes to axon sprouting remains elusive. Here, we sought to investigate the role of axon degeneration-reactive astrocytes in the regulation of collateral axon sprouting that occurs in the mouse spinal cord after unilateral photothrombotic stroke of the primary motor cortex. We identified astrocytic leucine zipper-bearing kinase (LZK) as a positive regulator of astrocyte reactivity to corticospinal axon degeneration. Remarkably, genetic stimulation of astrocyte reactivity, via LZK overexpression in adult astrocytes, enhanced corticospinal axon sprouting. LZK promoted the production of astrocyte-derived ciliary neurotrophic factor (CNTF) that likely enhanced axon growth in mice with astrocytic LZK overexpression after injury. Our finding that LZK-dependent stimulation of astrocyte reactivity promotes corticospinal axon sprouting highlights the potential of engineering astrocytes to support injury-induced axon plasticity for neural repair.

KEYWORDS

CNS injury, stroke, astrogliosis, reactive astrocytes, LZK/MAP3K13, axon plasticity, axon sprouting, CNTF

Introduction

Injury to the adult mammalian central nervous system (CNS) results in often permanent loss of motor and sensory functions, due to the lack of regenerative capacity of the damaged CNS. Limited spontaneous recovery, however, occurs in both experimental animal models and human survivors of CNS insults, including stroke and spinal cord injury (Hallett, 2001; Fawcett et al., 2007; Cramer, 2008;

Courtine and Sofroniew, 2019). Such spontaneous neurological recovery is associated with injury-induced neural plasticity (Hallett, 2001; Cramer, 2008; Chen and Zheng, 2014; Hutson and Di Giovanni, 2019). One form of neural plasticity is the development of new collateral connections from intact axons, referred to as collateral axon sprouting, that occurs in the spinal cord (Lapash Daniels et al., 2009; Rosenzweig et al., 2010; Chen and Zheng, 2014; Starkey and Schwab, 2014; Carmichael et al., 2017). Intra-spinal sprouting of corticospinal tract (CST) axons, which are important for voluntary motor function, can form new synapses with denervated neuronal targets via direct or relay connections to regain motor control after injury (Bareyre et al., 2004; Rosenzweig et al., 2010; Ueno et al., 2012; Chen and Zheng, 2014; Lindau et al., 2014; Wahl et al., 2014). Experimentally stimulating CST axon sprouting, by increasing neuron-intrinsic potential of axon growth or blocking neuron-extrinsic inhibitors, improves functional recovery after CNS injury (Cafferty and Strittmatter, 2006; Starkey et al., 2012a; Ueno et al., 2012; Lindau et al., 2014; Wahl et al., 2014; Jin et al., 2015; Liu et al., 2017). However, the cellular and molecular events that coordinate axon sprouting remain elusive.

Astrocytes are important modifiers of CNS injury outcomes (Liddelow and Barres, 2017; Pekny et al., 2019). Following CNS injury, astrocytes undergo a range of molecular and functional changes that are collectively referred to as reactive astrogliosis (Sofroniew, 2014). Severe astrogliosis that results in a tissue-protective astrocytic scar at the site of acute focal injury has been extensively studied (Silver and Miller, 2004). Intriguingly, reactive astrocytes have also been suggested to play a role in intra-spinal CST axon sprouting that occurs distal to the injury site (Menet et al., 2003; Liu et al., 2014). Constitutive whole-body deletion of the cytoskeletal proteins glial fibrillary acidic protein and vimentin ($GFAP^{-/-}Vim^{-/-}$) attenuates astrocytes' structural reactivity to injury, and reduces intra-spinal CST axon sprouting after unilateral cortical stroke but increases sprouting after spinal cord lateral hemisection (Menet et al., 2003; Liu et al., 2014). These studies raise the intriguing question of how reactive astrocytes regulate axon plasticity that occurs in undamaged tissue distal to the primary lesion. Given evidence from $GFAP^{-/-}Vim^{-/-}$ mice in the stroke model that suggests a positive role of reactive astrocytes in axon sprouting, would a gain-of-function approach that stimulates astrocyte reactivity promote neural plasticity and functional recovery?

Previously, we identified leucine zipper-bearing kinase (LZK) as an astrocyte-intrinsic, positive regulator of scar-forming astrogliosis at the injury site following spinal cord injury (Chen et al., 2018); we also identified LZK as an activator of STAT3 signaling that is critical to the regulation of astrogliosis (Okada et al., 2006; Herrmann et al., 2008; Chen et al., 2018). In this study, we tested the role of LZK in the regulation of axon degeneration-reactive astrocytes (Wang et al., 2009), which are non-scar forming. We hypothesized that these non-scar forming astrocytes serve as a cellular trigger of axon sprouting.

We used a photothrombotic ischemic model to unilaterally ablate the primary motor cortex containing CST neurons that control forelimb function. This lesion results in remote sprouting of uninjured contra-lesional CST axons in the cervical spinal cord that cross the midline into the denervated hemi-cord (Lapash Daniels et al., 2009; Lindau et al., 2014; Liu et al., 2014; Wahl et al., 2014; Kaiser et al., 2019). In this CST injury model, we deleted or overexpressed LZK in adult astrocytes to test the effects on i) astrocyte reactivity to CST degeneration in the spinal cord, ii) CST sprouting in the spinal cord, and iii) motor recovery. We found that astrocytic LZK is a positive regulator of astrocyte reactivity to CST axon degeneration in the spinal cord, where CST axon sprouting also occurs. While LZK gene deletion in adult astrocytes did not reduce injury-induced CST axon sprouting, stimulation of astrocyte reactivity via LZK overexpression in adult astrocytes enhanced CST axon sprouting. Furthermore, we found that LZK promotes the production of ciliary neurotrophic factor (CNTF), which is an activating ligand and transcriptional target of the JAK/STAT pathway sufficient to enhance CNS axon growth after injury. Our results reveal LZK-dependent, axon growth-supporting function of reactive astrocytes in undamaged tissue that may be harnessed to potentiate neural recovery.

Results

LZK is upregulated in astrocytes reactive to corticospinal axon degeneration

Our previous work identified LZK as a promoter of astrocytic scar formation at the injury site following spinal cord injury, and established genetic mouse models that enable tamoxifen-inducible LZK deletion ($GFAP\text{-}CreER^{T2}$; $LZK^{f/f}$) or LZK overexpression ($GFAP\text{-}CreER^{T2}$; LZK^{OE}) in adult astrocytes (Chen et al., 2018). Here, we sought to assess the contribution of axon degeneration-reactive astrocytes, which are non-scar forming, to CST axon sprouting. In order to do this, we first determined if LZK regulates axon degeneration-reactive astrocytes, which would then allow for their modulation via genetic manipulation of LZK expression (Chen et al., 2018).

We utilized the unilateral photothrombotic (PT) stroke model to examine the interplay between axon degeneration-reactive astrocytes and CST axon sprouting (**Figure 1A**). Unilateral PT to the primary motor cortex is commonly used to experimentally study intra-spinal CST axon sprouting (Lapash Daniels et al., 2009; Lindau et al., 2014; Liu et al., 2014; Wahl et al., 2014; Kaiser et al., 2019). We targeted PT to the forelimb sensorimotor cortex unilaterally, which resulted in degeneration of CST axons originating from the ablated corticospinal neurons (CS neurons) and sprouting of intact CST axons originating

from contra-lesional (uninjured) CS neurons (Figure 1A). CST axon degeneration and axon sprouting were examined at the cervical enlargement of the spinal cord, where forelimb-projecting CST axons innervate spinal motor neurons to control forelimb movement (Figure 1A).

In sham-injured mice, protein kinase C isoform gamma (PKCγ)—a marker of the CST—intensely labeled the intact CST main bundle in the dorsal funiculus of the cervical spinal cord (Figure 1B, *top* panel), with minimally detectable astrocytes positive for the reactivity marker GFAP (Figure 1B, *top* panel). Following unilateral PT stroke, degeneration of CST axons originating from the ablated neurons was evident by reduced PKCγ immunoreactivity on 14 days post injury (dpi), concurrent with the appearance of stellate $GFAP^+$ reactive astrocytes (Figure 1B, *bottom* panel, "deg CST"). Furthermore, these axon degeneration-reactive astrocytes upregulated endogenous LZK protein expression (Figure 1C, *bottom* panel). Compared to the intact CST, the number of LZK^+GFAP^+ cells in the degenerating CST increased by four-fold on 7 dpi, and sustained until at least 28 dpi (Figure 1C, graph). These findings suggest a positive role of LZK in astrocyte reactivity to CST axon degeneration, and that manipulation of LZK gene expression may modulate such reactivity.

LZK is a positive regulator of astrocyte reactivity to corticospinal tract axon degeneration

To test LZK-dependent regulation of astrocyte reactivity to axon degeneration, we used GFAP-$CreER^{T2}$; $LZK^{f/f}$ mice (herein referred to as astrocytic LZK-KO mice) and GFAP-$CreER^{T2}$; LZK^{OE} mice (herein referred to as astrocytic LZK-OE mice) that allow tamoxifen-inducible LZK deletion or overexpression in adult astrocytes, respectively (Chen et al., 2018). Tamoxifen treatment was given one week prior to unilateral PT. Tamoxifen-treated GFAP-$CreER^{T2}$ littermates were used as genotype controls.

We compared astrocyte reactivity to CST axon degeneration based on GFAP immunoreactivity among control, astrocytic LZK-KO, and astrocytic LZK-OE mice in a time course after unilateral PT. In genotype control mice, astrocyte reactivity localized to the degenerating CST increased by 1.5-fold on 7 dpi that further increased by 2–3 fold on 14–28 dpi respectively, compared to sham baseline (Figures 2A,B). These axon degeneration-reactive astrocytes also expressed LZK (Figures 1C, 2A). Astrocytic LZK deletion did not affect the baseline level of GFAP immunoreactivity in the CST without injury (Figure 2B). Following unilateral PT, astrocytic LZK-KO mice showed reduced LZK expression and reactive astrocyte density within the degenerating CST (Figure 2A), though exhibited only a statistically non-significant trend toward lower astrocyte reactivity to CST axon degeneration compared to the genotype control on 7 and 14 dpi (Figure 2B).

In contrast, astrocytic LZK-OE mice showed 50% increase in astrocyte reactivity to CST axon degeneration that was sustained from 14 to 28 dpi, compared to the genotype control at the same timepoints (Figures 2A,B). This was accompanied by a strong upregulation of LZK and its fluorescent reporter tdTomato in $GFAP^+$ cells (Chen et al., 2018; Figure 2A). Interestingly, in spite of this robust stimulation of astrocyte reactivity to CST axon degeneration, there was no difference in baseline astrocyte reactivity within the CST between control and astrocytic LZK-OE mice in the absence of injury (Figures 2B,C). This suggests astrocytic LZK-OE alone is insufficient to induce astrocyte reactivity in the healthy CST without injury.

Following unilateral PT, astrocyte reactivity in the spinal cord was largely localized to the degenerating CST. The level of GFAP immunoreactivity in the spared hemi-CST did not change from sham baseline in the control and astrocytic LZK-KO mice throughout the time course (Figure 2C). Minimal increase was observed in astrocytic LZK-OE mice on 28 dpi (Figure 2C). Lastly, the level of CST degeneration in the cervical spinal cord was verified to be comparable across all genotypes, based on quantification of PKCγ immunoreactivity in the degenerating hemi-CST in the cervical spinal cord (Figure 2D), indicating consistency in injury severity in all animals. Taken together, these findings demonstrate that following unilateral PT stroke to the primary motor cortex, while astrocytic LZK deletion did not abrogate reactive astrocytes localized to the degenerating CST, astrocytic LZK overexpression amplified astrocyte reactivity to CST axon degeneration in the spinal cord.

Astrocytic LZK overexpression enhances intra-spinal corticospinal tract axonal sprouting

Given that LZK promotes astrocyte reactivity to CST axon degeneration in the spinal cord, we next used astrocytic LZK mutant mice to determine the effects of modulating axon degeneration-reactive astrocytes on intra-spinal CST axon sprouting following unilateral PT. As before, LZK gene manipulation in adult astrocytes was achieved by tamoxifen treatment one week prior to unilateral PT. Two weeks after injury, the neuronal tracer biotinylated dextran amine (BDA) was injected into the contra-lesional forelimb sensorimotor cortex to label CST neurons that project to the cervical spinal cord. At the end of a 4 weeks survival period after PT, CST axon sprouting across the midline in the cervical enlargement of the spinal cord was analyzed by BDA immunostaining (Figure 3A).

In the absence of injury, baseline intra-spinal CST axon sprouting was similar among all genotypes (Figures 3B,C).

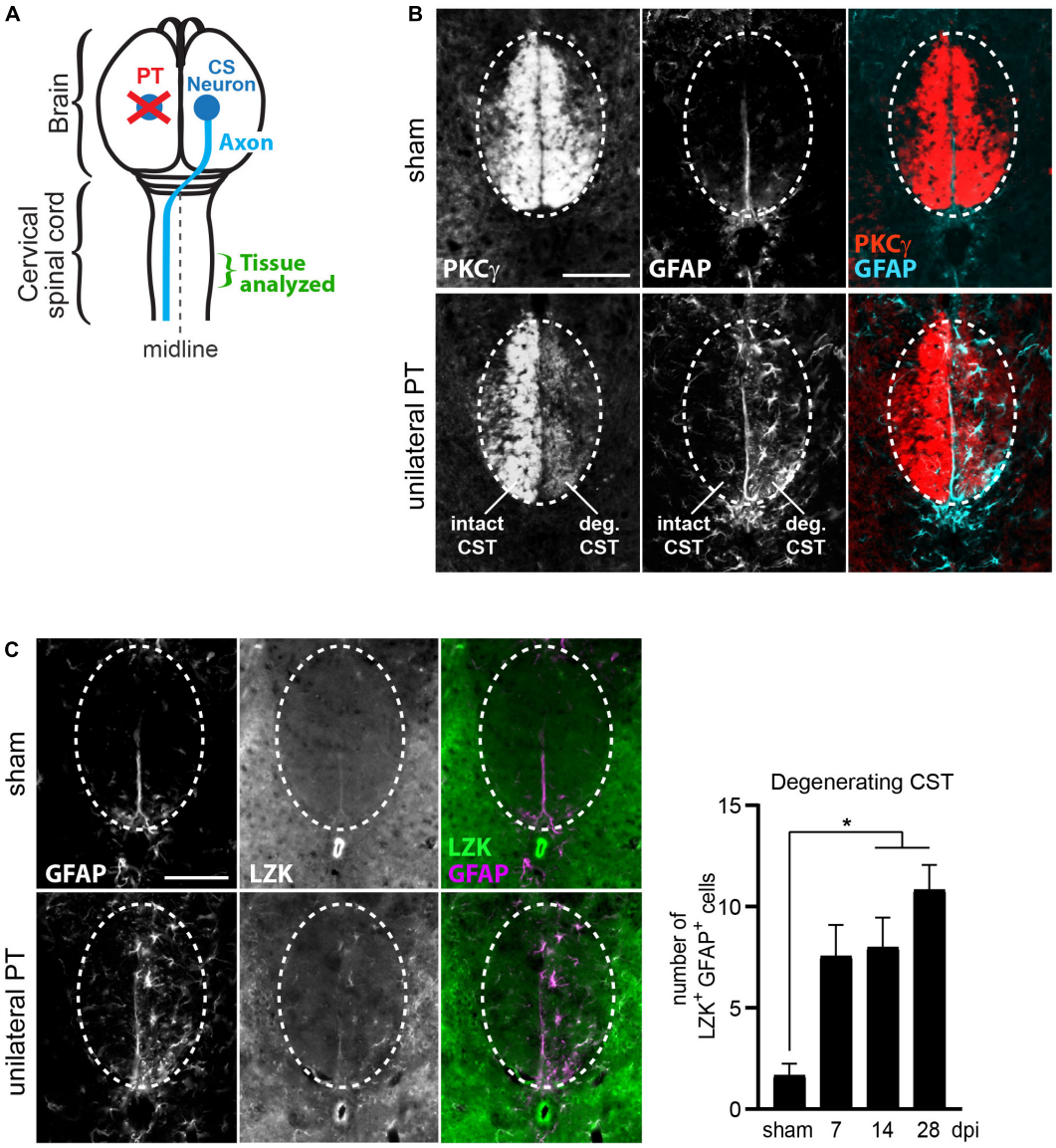

FIGURE 1
Upregulation of LZK expression in reactive astrocytes localized to the degenerating CST. **(A)** Illustration of unilateral photothrombosis (PT, red X) targeted to the forelimb sensorimotor cortex in one hemisphere of the mouse brain. Corticospinal (CS) axons (blue line) originating from CS neurons (blue circle) in the uninjured hemisphere decussate at the medulla and extend down the spinal cord, whereas CS axons originating from neurons ablated by photothrombosis undergo degeneration. Tissues from the cervical enlargement of the spinal cord at C7 were analyzed by immunohistochemistry in this study. **(B)** Immunofluorescence staining of PKCγ and GFAP in the corticospinal tract (CST) at the cervical spinal cords in wildtype mice without injury or 14 days post injury (dpi, unilateral PT). Dotted ovals outline the CST; intact and degenerating (deg) hemi-CSTs are indicated; scale bar represents 100 μm. **(C)** *Left*, immunofluorescence staining of endogenous LZK and GFAP in the CST at the cervical spinal cords of wildtype mice without injury or on 14 dpi. Dotted ovals outline the CST; scale bar represents 100 μm. *Right*, quantification of the number of LZK^+GFAP^+ cells localized to the degenerating CST in the cervical spinal cord on 7, 14, and 28 days after unilateral PT. $n = 3$ per timepoint; graphing mean with SEM. By one-way ANOVA, $p < 0.05$ for main injury effect. Asterisk (*) on graph indicates $p < 0.05$ for *post-hoc* comparison between sham and the post-injury timepoints of 14 dpi or 28 dpi with Bonferroni correction.

Unilateral PT induced CST axon sprouting by approximately two-fold in genotype control and likewise in astrocytic LZK-KO mice on 28 dpi, compared to their respective no injury baseline (Figures 3B,C). The lack of effect of astrocytic LZK deletion on CST axon sprouting correlates with its inability to abrogate astrocyte reactivity to CST axon degeneration (Figures 2A,B, 3B,C). In contrast, astrocytic LZK-OE mice exhibited a four-fold increase in injury-induced CST axon sprouting compared to its own sham baseline (Figures 3B,C), which is a two-fold enhancement compared to the injured genotype control or astrocytic LZK-KO mice (Figures 3B,C). Notably, the ability of astrocytic

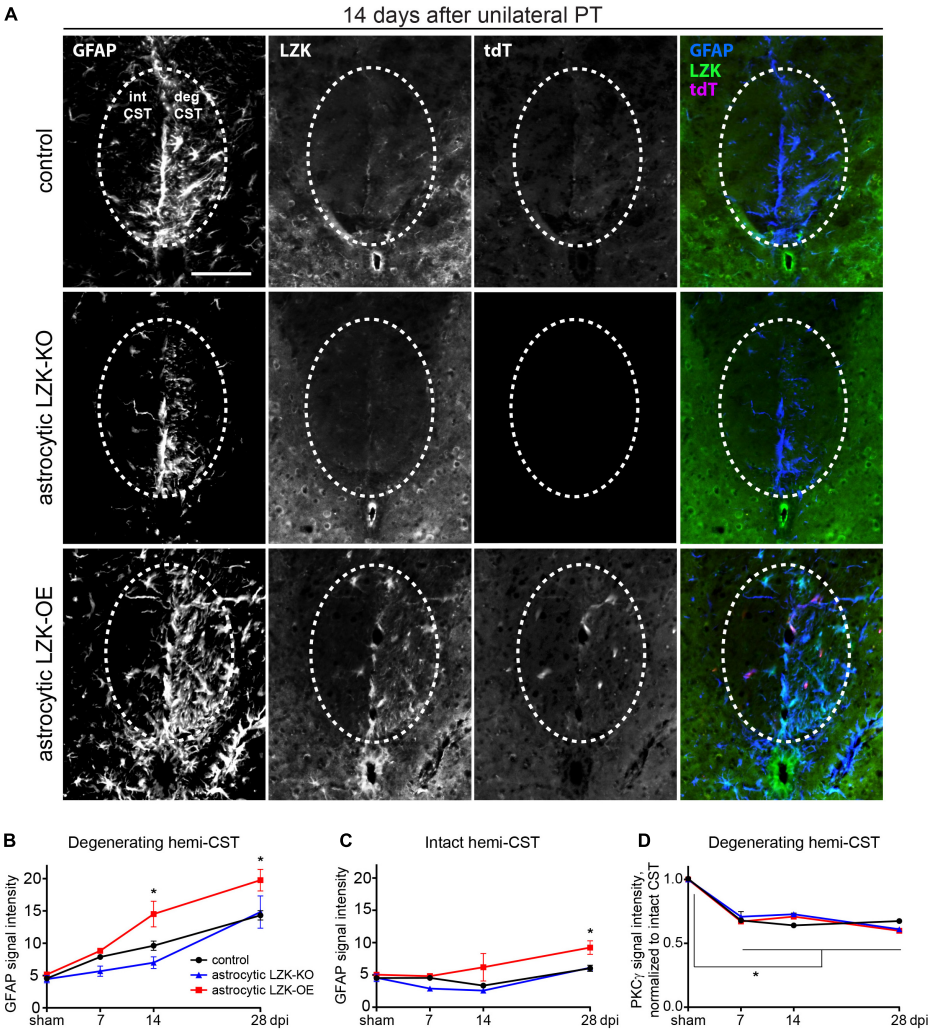

FIGURE 2
LZK is a positive regulator of astrocyte reactivity to CST axon degeneration. **(A)** Immunofluorescence staining of LZK and GFAP in the CST at the cervical spinal cords of tamoxifen treated genotype control, astrocytic LZK-KO (GFAP-CreER^{T2}; LZK$^{f/f}$), and astrocytic LZK-OE (GFAP-CreER^{T2}; LZK^{OE}) mice; 14 days after unilateral PT. Dotted ovals outline the CST; intact and degenerating (deg) hemi-CSTs are indicated in the upper left panel that applies to all images; scale bar represents 100 μm. **(B)** Quantification of astrocyte reactivity within the degenerating hemi-CST, based on GFAP immunofluorescence intensity, in tamoxifen treated genotype control, astrocytic LZK-KO (GFAP-CreER^{T2}; LZK$^{f/f}$), and astrocytic LZK-OE (GFAP-CreER^{T2}; LZK^{OE}) mice without injury and on 7, 14, and 28 days after unilateral PT. $n = 3$ per genotype per timepoint; graphing group mean with SEM. By two-way ANOVA, $p < 0.05$ for main injury effect and genotype effect, no interaction. Asterisk (*) on graph indicates $p < 0.05$ for *post-hoc* comparison between genotype control and GFAP-CreER^{T2}; LZK^{OE} mice at the corresponding timepoints with Bonferroni correction. Not marked on graph: $p < 0.05$ for the following *post-hoc* comparisons of injury effect within each genotype with Bonferroni correction (control—sham vs 14 dpi or 28 dpi; astrocytic LZK-KO—sham vs 28 dpi; astrocytic LZK-OE—sham vs 14 dpi or 28 dpi). **(C)** Quantification of astrocyte reactivity within the intact hemi-CST, based on GFAP immunofluorescence intensity, in the indicated tamoxifen treated groups over a time course after unilateral PT. $n = 3$ per genotype per timepoint; graphing group mean with SEM. By two-way ANOVA, $p < 0.05$ for main injury effect and genotype effect, no interaction. Asterisk (*) on graph indicates $p < 0.05$ for *post-hoc* comparison between genotype control and GFAP-CreER^{T2}; LZK^{OE} mice at the corresponding timepoint with Bonferroni correction. Not marked on graph: $p < 0.05$ between sham vs 28 dpi within LZK-OE group, by *post-hoc* comparison with Bonferroni correction. **(D)** Quantification of CST axon degeneration within the degenerating hemi-CST, based on PKCγ immunofluorescence intensity, in the indicated tamoxifen treated groups over a time course after unilateral PT. $n = 3$ per genotype per timepoint; graphing group mean with SEM. By two-way ANOVA, $p < 0.05$ for injury effect only. Asterisk (*) on graph indicates $p < 0.05$ for *post-hoc* comparison in PKCγ signal intensity between sham injury and all post-injury timepoints with Bonferroni correction.

LZK overexpression to augment CST axon sprouting requires the presence of injury (Figures 3B,C). The stimulatory effects of astrocytic LZK overexpression on CST axon sprouting positively corresponds to its ability to amplify astrocyte reactivity to CST axon degeneration after unilateral PT (Figures 2A,B, 3B,C). Taken together, these results show that LZK deletion in adult astrocytes does not allow for testing of the role of axon degeneration-reactive astrocytes

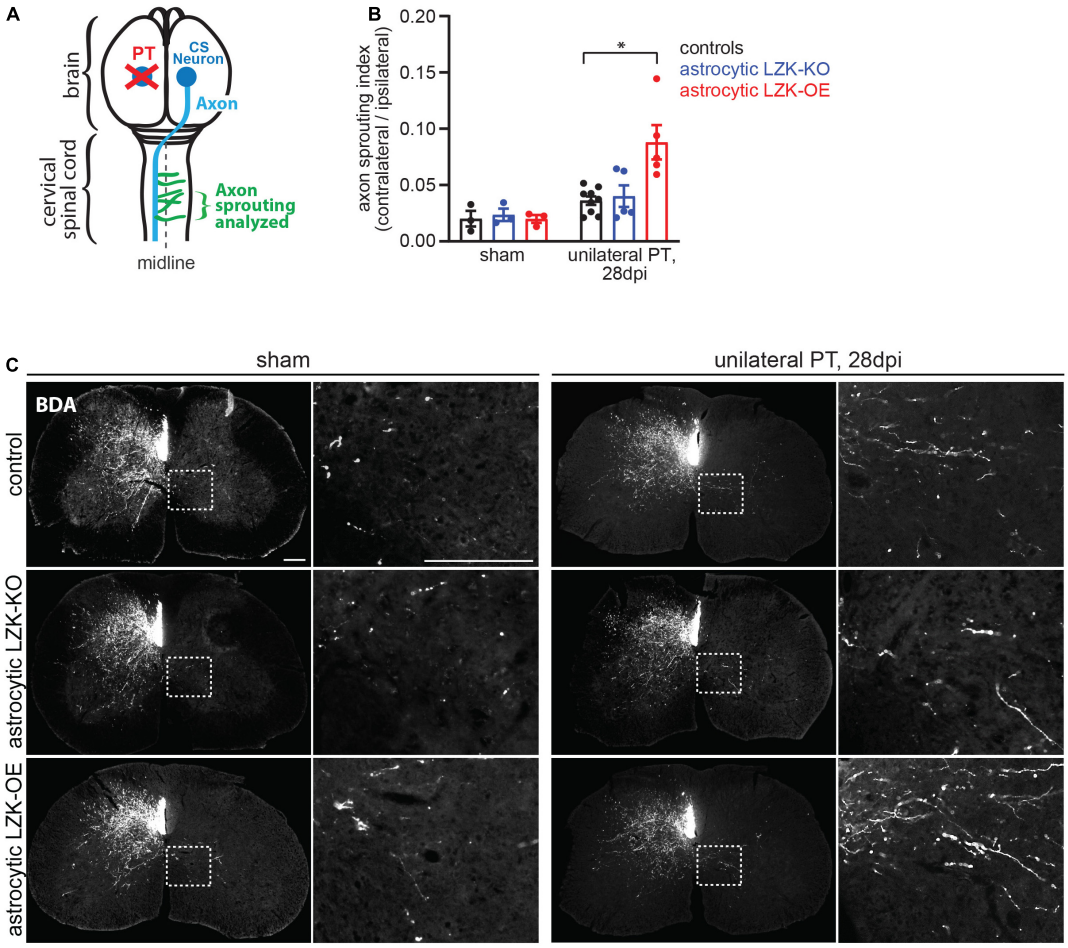

FIGURE 3
LZK overexpression in astrocytes enhanced CST axon sprouting. **(A)** Diagram shows sprouting of intact CST axons (green) that cross the midline (dotted line) in the spinal cord, following unilateral PT (red X) to the forelimb sensorimotor cortex. Tissues from the cervical spinal cord at C7 were used to analyze CST axon sprouting. **(B)** Quantification of CST axon sprouting density index (contra-lesional/ipsi-lesional) in the indicated tamoxifen treated groups. $n = 3$ per group without injury; $n = 5–9$ per group 28 days after unilateral PT; graphing group mean with SEM. By two-way ANOVA, $p < 0.05$ for main injury effect and genotype effect, $p < 0.05$ for interaction between the two variables. Asterisk (*) on graph indicates $p < 0.05$ for *post-hoc* comparison between genotype control and GFAP-CreER^{T2}; LZK^{OE} mice on 28 dpi with Bonferroni correction. **(C)** Biotinylated dextran amine (BDA) was injected into the uninjured cerebral cortex to label intact CST axons in the cervical spinal cord in the indicated tamoxifen treated groups, without or after unilateral PT. Dotted box outlines area magnified in adjacent image to show CST axon sprouting across the midline into the denervated gray matter, quantified in panel **(B)**. Scale bar represents 200 μm in both low and high magnification images.

in axon sprouting by loss-of-function approach; whereas amplification of astrocyte reactivity by LZK overexpression in adult astrocytes stimulates axon sprouting but only in the presence of injury.

Astrocytic LZK overexpression trends toward improved motor coordination, but not skilled stepping

Because CST axon sprouting can facilitate functional recovery, we next assessed motor recovery in control, astrocytic LZK-KO, and astrocytic LZK-OE mice following unilateral PT. We first utilized the rotarod test to examine general motor coordination, balance, and endurance over 8 weeks of recovery period. Unilateral PT resulted in 30–50% deficit in rotarod performance at 1 week after injury (Figure 4A). Compared to genotype control and astrocytic LZK-KO mice that reached 76–78% of their pre-injury performance by 8 weeks after injury respectively, astrocytic LZK-OE mice showed a statistically non-significant trend toward full recovery to their pre-injury level by 8 weeks (Figure 4A).

In addition to assessing gross motor function, we also examined skilled forelimb stepping by regular horizontal ladder. The ladder task detects limb-specific, subtle or chronic deficits in paw placement accuracy and compensatory adjustments

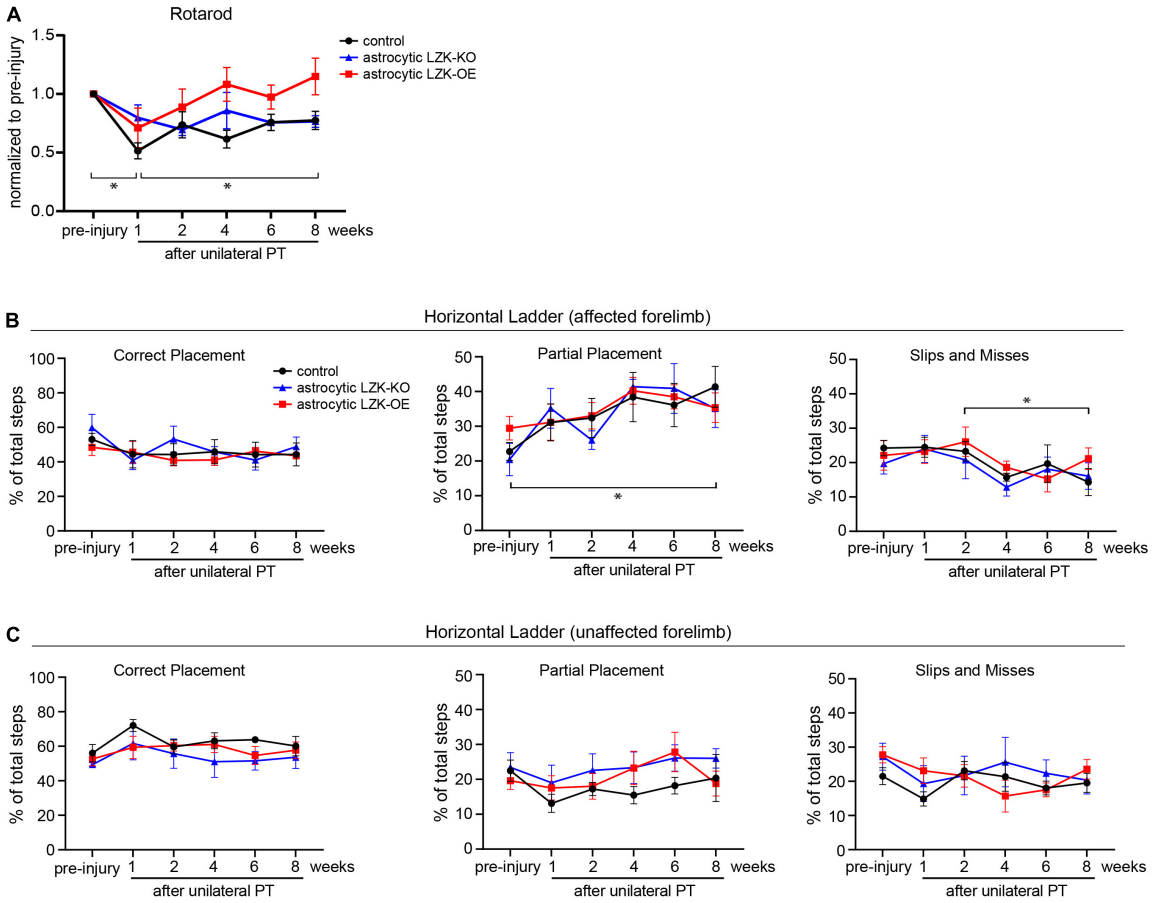

FIGURE 4
LZK overexpression in astrocytes trended toward improved recovery of general motor coordination, but not skilled stepping. **(A)** General motor coordination and balance were assessed by rotarod in the indicated tamoxifen treated groups before and over 8 weeks after unilateral PT. Time on rotarod of each animal was normalized to its own pre-injury performance. $n = 6$ per group; graphing group mean with SEM. By two-way ANOVA with repeated measures, $p < 0.05$ for injury effect and $p = 0.0501$ for genotype effect. Asterisks (*) on graph indicate $p < 0.05$ for *post-hoc* comparison of rotarod performance at the indicated time points in the control group with Bonferroni correction. **(B)** Skilled stepping of the affected forelimb, contralateral to PT, assessed by regular horizontal ladder before and over 8 weeks after unilateral PT. $n = 6$ per group; graphing group mean with SEM. *Left*, percentage of total steps that correctly placed on ladder rungs. *Middle*, percentage of total steps that partially placed on ladder rungs; two-way ANOVA with repeated measures showed $p < 0.05$ for injury effect only; asterisk (*) on graph indicates $p < 0.05$ for *post-hoc* comparison between pre-injury and week 8 after unilateral PT in the control group with Bonferroni correction. *Right*, percentage of total steps that were slips or misses; two-way ANOVA with repeated measures showed $p < 0.05$ for injury effect only; asterisk (*) on graph indicates $p < 0.05$ for *post-hoc* comparison between weeks 2 and 8 after unilateral PT in the control group with Bonferroni correction. **(C)** Skilled stepping of the unaffected forelimb, ipsilateral to PT, assessed by regular horizontal ladder as in panel **(B)**.

(Farr et al., 2006). No difference at baseline performance was observed among control, astrocytic LZK-KO, and astrocytic LZK-OE mice by ladder assessment (Figure 4B). Unilateral PT resulted in subtle deficit and adaptive use of the affected forelimb, shown by a two-fold increase of partially placed steps taken by the affected forelimb at 8 weeks after injury compared to pre-injury baseline in the control group (Figure 4B, *middle* graph). Correspondingly, there was a decrease in correctly placed steps (did not reach statistical significance, Figure 4B, *left* graph) and also a decrease in slips/misses (statistically significant, Figure 4B, *right* graph) following unilateral PT. This injury-dependent adaptation to partial placement in stepping of the affected forelimb was similar across genotypes. No statistically significant change in stepping behavior was observed in the unaffected forelimb (Figure 4C). Taken together, astrocytic LZK-OE mice showed a statistically non-significant trend toward improved recovery of general motor coordination as assessed by rotarod, but did not affect skilled forelimb stepping on horizontal ladder.

LZK promotes production of ciliary neurotrophic factor by astrocytes

We next sought to determine the molecular basis of LZK's ability to augment CST axon sprouting. Our previous

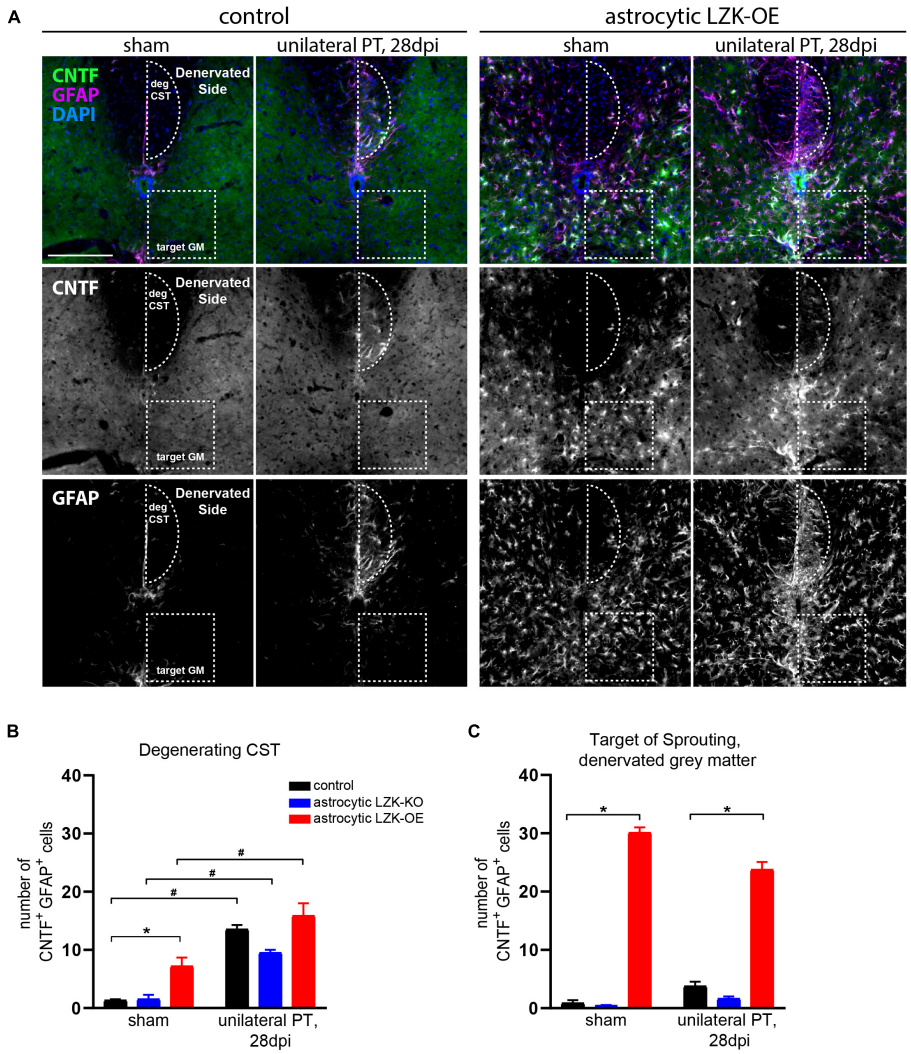

FIGURE 5
Upregulation of astrocyte-derived CNTF following astrocytic LZK overexpression. **(A)** Immunofluorescence staining of CNTF and GFAP in the indicated tamoxifen treated groups, with no injury or 28 days after unilateral PT. Dotted semi-oval outlines the degenerating hemi-CST (labeled as "deg CST") at the cervical spinal cord; dotted box outlines the gray matter in the denervated spinal cord that intact CST axons sprout into (labeled as "target GM," on the "Denervated Side"). Scale bar represents 200 μm. **(B)** Quantification of the number of $CNTF^{+}GFAP^{+}$ cells in the degenerating CST [outlined by dotted semi-oval in panel **(A)**], in the groups indicated, with no injury or 28 days after unilateral PT. $n = 3$ per group; graphing group mean with SEM. By two-way ANOVA, $p < 0.05$ for main injury effect and genotype effect, no interaction. In the sham injury group, asterisk (*) indicates $p < 0.05$ for *post-hoc* comparison between genotype control and GFAP-$CreER^{T2}$; LZK^{OE} mice with Bonferroni correction. Pound sign (#) indicates $p < 0.05$ between sham and 28 dpi within each genotype by *post-hoc* comparisons with Bonferroni correction. Not marked on graph: $p < 0.05$ between astrocytic LZK-KO and LZK-OE mice without injury, by *post-hoc* comparison Bonferroni correction. **(C)** Quantification of the number of $CNTF^{+}GFAP^{+}$ cells in the sprouting target gray matter [outlined by dotted box in panel **(A)**], in the groups indicated, with no injury or 28 days after unilateral PT. $n = 3$ per group; graphing group mean with SEM. By two-way ANOVA, $p < 0.05$ for main genotype effect only. Asterisk (*) indicates $p < 0.05$ for *post-hoc* comparison between genotype control and GFAP-$CreER^{T2}$; LZK^{OE} mice at the corresponding timepoint with Bonferroni correction. Not marked on graph: $p < 0.05$ between astrocytic LZK-KO and LZK-OE mice without injury or on 28 dpi, by *post-hoc* comparison Bonferroni correction.

work identified LZK as an activator of signal transducer and activator of transcription 3 (STAT3) (Chen et al., 2018). One of the transcriptional targets of STAT3 is the secreted neurotrophic cytokine ciliary neurotrophic factor (CNTF) (Keasey et al., 2013), which is in turn an activating ligand of the JAK-STAT pathway (Stahl et al., 1994). Additionally, intra-spinal AAV-mediated overexpression of CNTF is sufficient to increase sprouting of CST axons in the cervical spinal cord following unilateral transection of the CST at the brainstem (Jin et al., 2015).

Based on this evidence supporting LZK as an upstream regulator of CNTF, we tested if astrocytes in LZK-OE mice produce CNTF following unilateral PT. We first examined CNTF expression in astrocytes reactive to CST axon

degeneration in the cervical cord. In genotype controls, unilateral PT induced a ten-fold increase in the number of $CNTF^{+}GFAP^{+}$ cells within the degenerating CST (**Figures 5A,B**). Astrocytic LZK deletion reached only a six-fold increase by the same measurement, but this reduction compared to the genotype control did not reach statistical significance (**Figure 5B**). While astrocytic LZK overexpression increased the number of $CNTF^{+}GFAP^{+}$ cells within the CST at no injury baseline, the number of $CNTF^{+}GFAP^{+}$ cells localized to the degenerating CST was comparable to that observed in genotype control (**Figures 5A,B**). These results suggest that first, astrocytes reactive to axon degeneration express CNTF and therefore have the potential to support axon growth; second, CNTF-producing reactive astrocytes within the degenerating CST, which were present in similar numbers in genotype control and LZK-OE mice, likely do not account for the ability of astrocytic LZK overexpression to enhance CST axon sprouting.

Next, we examined CNTF expression in astrocytes in the spinal gray matter on the denervated side of the spinal cord, where sprouting CST axons cross the midline just below the dorsal column (**Figures 3C**, **5A**). Within this sprouting target in the gray matter, the genotype control had minimally detectable number of $CNTF^{+}GFAP^{+}$ cells in the absence or presence of unilateral PT, likewise for the astrocytic LZK-KO group (**Figures 5A,C**). In contrast, astrocytic LZK overexpression significantly increased the number of $CNTF^{+}GFAP^{+}$ cells within the sprouting target gray matter, by more than six-fold compared to the genotype control at either sham baseline, or following unilateral PT (**Figures 5A,C**). Notably, such increase of CNTF-producing astrocytes was not limited to the sprouting target gray matter, but observed throughout the spinal gray matter of astrocytic LZK-OE mice (**Figures 5A,C**). The unique presence of CNTF-producing astrocytes exclusively in the spinal gray matter of astrocytic LZK-OE mice presents a potential mechanism that promotes axon sprouting in these animals. Despite widespread CNTF-producing astrocytes in the gray matter of astrocytic LZK-OE mice, CST axon sprouting only occurred in the presence of injury (**Figures 3B,C**). These findings together demonstrate that LZK overexpression in adult astrocytes stimulates non-scar forming reactive astrocytes that produce CNTF in the spinal gray matter, which may contribute to enhance CST axon sprouting in astrocytic LZK-OE mice in the presence of unilateral PT stroke.

Discussion

Understanding how astrocytes impact axon growth following injury will open new avenues to potentiate axon plasticity and neural recovery. Current knowledge of reactive astrocytes in acute focal injury is largely based on studies that focused on scar-forming astrocytes at the injury site, which are part of a multicellular glial scar traditionally recognized as inhibitory to axon regeneration in the adult mammalian CNS (Davies et al., 1999; Silver and Miller, 2004; Sofroniew, 2014; Hara et al., 2017; Stern et al., 2021), though regeneration-supporting astrocytes have also been observed at the primary lesion (Lee et al., 2010; Liu et al., 2010; Zukor et al., 2013; Du et al., 2015; Anderson et al., 2016).

Two studies have implicated a role of astrocytes in axon sprouting that occurs distal to the injury site, using mice with constitutive and whole-body knockout of two cytoskeletal proteins GFAP and vimentin ($GFAP^{-/-}Vim^{-/-}$) (Menet et al., 2003; Liu et al., 2014). However, it remained elusive the extent to which astrocyte reactivity *per se* impacts axon sprouting, where or how astrocytes regulate axon sprouting in undamaged tissue, and what effects amplification of astrocyte reactivity would have on axon sprouting.

In this study, we sought to test the role of axon degeneration-reactive astrocytes in the regulation of compensatory axon sprouting that occurs in undamaged tissue away from the injury site. We targeted PT stroke to the primary motor cortex unilaterally to induce CST axon degeneration and collateral CST axon sprouting in the spinal cord. We first determined LZK-dependent regulation of astrocyte reactivity to axon degeneration, using GFAP-CreERT2; $LZK^{f/f}$ (astrocytic LZK-KO) mice and GFAP-CreERT2; LZK^{OE} (astrocytic LZK-OE) mice to respectively delete or overexpress LZK—a key signaling activator of the astrocytic injury response—in adult astrocytes (Chen et al., 2018). Astrocytic LZK deletion did not abolish reactive astrocytes localized to the degenerating CST, and therefore did not allow for testing of the requirement of these reactive astrocytes in CST axon sprouting. In contrast, astrocytic LZK overexpression enhanced astrocyte reactivity to CST axon degeneration and collateral CST axon sprouting. However, because astrocytic LZK overexpression also induced stellate reactive astrocytes throughout the spinal gray matter (Chen et al., 2018) in addition to the degenerating CST, reactive astrocytes from both of these regions may contribute to stimulating axon sprouting in astrocytic LZK-OE mice. Nevertheless, these findings provide exciting first insights into the positive effects of LZK-induced reactive astrocytes on axon plasticity in an injured CNS.

Our previous discovery of LZK as an activator of STAT3 signaling in astrocytes (Chen et al., 2018) guided our identification of astrocyte-derived CNTF as a candidate molecular effector of LZK that promotes axon sprouting. In CNS neurons, STAT3 activation potently stimulates axon regeneration and sprouting after CNS injury (Sun et al., 2011; Lang et al., 2013; Jin et al., 2015), which is in part mediated by the neurotrophic cytokine CNTF (Jin et al., 2015). CNTF alone is sufficient to promote intra-spinal CST axon sprouting (Jin et al., 2015). We found that astrocytes reactive to CST axon degeneration upregulate LZK and CNTF, suggesting an endogenous capacity of these astrocytes

to support axon growth. These CNTF-producing astrocytes reactive to axon degeneration may serve as an endogenous cellular mechanism that promotes spontaneous intra-spinal CST axon sprouting following CNS injury. Production of CNTF by reactive astrocytes *in vivo* also has been observed in other injury models (Park et al., 2000; Muller et al., 2007; Tripathi and McTigue, 2008), and reported to stimulate axon regeneration (Muller et al., 2007).

Within the degenerating CST, astrocytic LZK overexpression did not further increase CNTF-producing astrocytes compared to genotype control. This suggests that CNTF produced by astrocytes in the degenerating CST may not account for LZK-dependent stimulatory effects on axon sprouting. Rather, it may be the unique presence of CNTF-producing astrocytes in the spinal gray matter of astrocytic LZK-OE mice that potentiated CST axon sprouting. This environment rich in astrocyte-derived CNTF resulting from astrocytic LZK overexpression is analogous to intra-spinal AAV-mediated CNTF overexpression reported to augment CST axon sprouting (Jin et al., 2015). Strikingly, astrocytic LZK-OE alone was insufficient to induce CST axon sprouting in the absence of injury. This indicates a requirement for injury-dependent events, such as the loss of neuronal activity (Jiang et al., 2019), to elicit axon growth-enhancing effects of astrocytic LZK overexpression.

In addition to sprouting of CST axons originating from the contra-lesional motor cortex, which we examined here, there are other forms of axon plasticity occurring in the spinal cord that are associated with motor recovery following unilateral cortical injury. For example, CST axons originating from the ipsi-lesional hindlimb motor cortex sprout into the cervical spinal cord following unilateral ischemic injury targeted to the forelimb motor cortex (Starkey et al., 2012b). Several descending brainstem-spinal tracts have also been observed to sprout into the denervated spinal cord. It was estimated that compared to CST neurons, six times more brainstem-spinal neurons project into the affected cervical hemicord following unilateral PT (Bachmann et al., 2014). Brainstem neurons of the medullary raphe and reticular nuclei have been proposed to form relay pathways to enable control of the denervated neuronal targets in the spinal cord by the spared motor cortex (Bachmann et al., 2014). It is possible that these descending tracts can also respond to LZK-induced astrocyte reactivity.

While astrocytic LZK overexpression increased CST axon sprouting, it did not result in statistically significant improvement in post-stroke motor recovery as assessed by rotarod and horizontal ladder. Although postural coordination and skilled paw placement measured by these two tests are commonly used to evaluate motor recovery after unilateral stroke, tests that are more sensitive such as detailed kinematic analysis of forelimb movement, or tests that are more specific to CST-mediated fine motor control such as single pellet grasping may be needed to detect functional alterations in mice with astrocytic LZK overexpression. Additionally, while enhancing axon sprouting is important to promoting neural plasticity after injury, itself alone may not be adequate to result in meaningful functional restoration. Timing of rehabilitative training relative to administration of axon growth-enhancing intervention has been shown to critically affect the motor recovery after cortical stroke modeled by unilateral PT (Wahl et al., 2014). Incorporation of timely rehabilitative training therefore may be required to effect motor improvement in astrocytic LZK-OE mice.

Together with our previous work, we have determined LZK as a positive regulator of two distinct forms of astrocyte reactivity: (i) scar-forming reactive astrocytes at the site of acute focal trauma (Chen et al., 2018); and (ii) non-scar forming reactive astrocytes that are either endogenously responding to axon degeneration or exogenously induced by astrocytic LZK overexpression in undamaged tissue. Our findings point to the capacity of the latter form of reactive astrocytes in supporting axon sprouting. The injury response and physiological impacts of astrocytes are context-dependent, influenced by CNS region, the type of insult, stage of injury, and the local injury environment among other variables (Zhang and Barres, 2010; Zamanian et al., 2012; Khakh and Sofroniew, 2015; Diaz-Castro et al., 2021; Hasel et al., 2021; Burda et al., 2022). While LZK induces astrocyte reactivity as broadly assessed by traditional hallmarks of reactivity here and previously (Chen et al., 2018), it does not mean that reactive astrocytes in general promote axon growth. It remains to be elucidated whether LZK-stimulated astrocytes represent a specific subtype of reactive astrocytes. Their axon growth-supportive potential is likely contextual, given the multitude of factors mentioned above that influence astrocyte functions. The level of LZK induction in astrocytes—whether occurring endogenously following injury or by experimental manipulation—is also an important consideration, as a strong genetic induction of LZK overexpression results in poor survival (Chen et al., 2018). This indicates a delicate balance in eliciting LZK-dependent astrocyte reactivity that is pro-regenerative versus dysfunctional.

The ability of LZK overexpression in adult astrocytes to upregulate CNTF production and stimulate CST axon sprouting highlight the potential of engineering astrocytes for neural repair. CNTF has also been shown to promote survival and proliferation of oligodendrocyte precursor cells (Barres et al., 1996; Linker et al., 2002) and protect the integrity of myelin sheaths in mouse model of multiple sclerosis (Linker et al., 2002). Enhancing axon plasticity in the presence of CNTF, together with interventions that strengthen appropriate reinnervation, would be beneficial to CNS repair not only following acute focal trauma, but conceivably also in CNS diseases involving axonopathy and inflammatory demyelination.

Experimental procedures

Mice. All mouse husbandry and experimental procedures were performed in compliance with protocols approved by the Institutional Animal Care and Use Committee at the University of Texas Southwestern Medical and the University of Kentucky. Tamoxifen inducible and astrocyte-targeted LZK-knockout mice (GFAP-CreER^{T2};LZK$^{f/f}$) and LZK-overexpression mice (GFAP-CreER^{T2};LZK^{OE}) have been previously described (Chen et al., 2018). Both lines were bred into C57BL/6 background ($N > 10$ generations) for this study. Adult male and female mice at the age of 10–12 weeks were used. To delete LZK from astrocytes in adult GFAP-CreER^{T2};LZK$^{f/f}$ mice, 75 mg/kg of tamoxifen was given by oral gavage once daily, consecutively for five days. To induce LZK overexpression in astrocytes of adult GFAP-CreER^{T2};LZK^{OE} mice, 75 mg/kg of tamoxifen was given by oral gavage once daily, consecutively for two days. Tamoxifen dosage was reduced in GFAP-CreER^{T2};LZK^{OE} to prevent severe astrogliosis-associated lethality (Chen et al., 2018). One week after the last dose of tamoxifen treatment, all mice were subjected to unilateral cortical photothrombosis. All surgical procedures, animal dissection, tissue processing, and data analyses were performed blind to genotypes.

Photothrombotic stroke. Unilateral photothrombotic stroke was performed similarly as previously described (Watson et al., 1985; Poinsatte et al., 2019; Becker et al., 2020). Mice were anesthetized with isoflurane (3.5% induction, 2% maintenance in 70% nitrous oxide and 30% oxygen mixture). While fixed in a stereotactic frame (Kopf), the mouse scalp was injected with lidocaine and incised at the midline to expose the intact skull. Rose Bengal (40 mg/kg, 5 mg/ml in saline, Sigma) was injected intraperitoneally one minute before delivery of focused 561 nm laser illumination (Coherent, laser diameter of 3 mm) to the forelimb motor cortex centered at 1.7 mm lateral to bregma under a surgical microscope (Nikon SMZ800), at 45 mW for 15 min. Sham-injured mice received anesthesia, analgesia, scalp incision, Rose Bengal injection, but no laser illumination.

Anterograde labeling of CST axons. Two weeks after photothrombosis, mice used for analyses of CST axon sprouting received BDA injections to anterogradely trace forelimb targeting CST axons originating from the contra-lesional sensorimotor cortex. 0.5 μl of 10% BDA in saline (10,000 MW, Invitrogen D1956) was injected into each of three sites: (AP, ML) in mm from Bregma: (0.5, 1.25), (−0.5, 1.25), (0, 2) at the depth of 0.6 mm. Two weeks after BDA injection (equivalent to 4 weeks after photothrombosis), mice were euthanized for brain and spinal cord dissections.

Histology. Terminal anesthesia was performed by isoflurane overdose. Mice were perfused with 4% paraformaldehyde intracardially, after which brains and spinal cords were dissected and post-fixed at 4°C overnight. Tissues were cryoprotected in 30% sucrose at 4°C overnight before embedding. C4-C7 spinal cord was embedded for transverse sections in O.C.T compound (Scigen Tissue-Plus) on dry ice. Embedded tissue blocks were sectioned at 15 μm thickness on a cryostat (Leica). Free floating sections were collected in PBS with 0.01% sodium azide for further histological examination.

Immunohistochemistry. Staining procedures have been described previously (Chen et al., 2018). Free floating sections were washed twice (0.2% triton in PBS, for 10 min), then blocked and permeabilized (0.4% triton, 5% sera matching species of secondary antibody in PBS) for 1 h at room temperature. Primary antibody incubation (see antibody concentrations below, in 0.2% triton, 1% matching sera, 0.01% sodium azide, in PBS) was carried out at room temperature overnight on a rocking platform. Sections were washed three times and incubated in secondary antibody solution (all secondary antibodies used at 1:500) for 2 h at room temperature on a rocking platform. After three washes, sections were incubated with DAPI (1 μg/ml in PBS) for 10 min, then mounted onto glass slides (Fisher Scientific) and cover slipped with Fluoromount-G (Southern Biotech). BDA staining was done as previously described (Geoffroy et al., 2015). Coronal sections of the cervical spinal cord were incubated in Vectastain ABC solution (Vector Laboratories) at 4°C overnight, washed three times in PBS, then incubated with TSA Plus solution at 1:200 (Perkin Elmer, see below) according to manufacturer's instructions for 10 min, protected from light at room temperature.

Antibodies. Commercially available primary antibodies used were: LZK (1:500, rabbit, Sigma-Aldrich HPA016497), GFAP (1:1,000, rabbit, Dako Z0334), GFAP (1:1,000, rat, Invitrogen 2.2B10), CNTF (1:300, goat, Novus AF-557-SP), PKCγ (1:1,000, mouse, Santa Cruz SC166385). Alexa Fluor-tagged secondary antibodies used were Alexa 488, Alexa 546, and Alexa 647. BDA detection was performed using TSA Plus Cyanine 5 or Cyanine 3 (Perkin Elmer).

Microscopy and quantification. Stained tissue sections were imaged by an epifluorescent slide-scanning microscope (Zeiss Axio Scan.Z1). Image analyses were done using ImageJ software. All quantifications were conducted by observers blind to genotypes. Images of transverse sections from the cervical spinal cord at levels C7 were used for the following quantifications. For exact values of n per group, see figure legends.

To quantify PKCγ immunofluorescence intensity of the degenerating hemi-CST (area labeled as "deg CST" in **Figure 1B**) in the cervical spinal cord, integrated density within a semi-oval region of interest covering the degenerating hemi-CST (about 25,000 μm^2) was normalized to that of the intact hemi-CST (area labeled as "deg CST" in **Figure 1B**). Four transverse sections of C7 spinal cord per animal were averaged to generate PKCγ signal intensity per animal. To quantify GFAP immunofluorescence intensity of the degenerating hemi-CST (area labeled as "deg CST" in **Figure 1B**) or intact hemi-CST (area labeled as "intact CST" in **Figure 1B**), integrated density

within a semi-oval region of interest covering the respective hemi-CST (about 25,000 μm^2) was averaged over five transverse cervical spinal cord sections per animal after subtraction of background signal.

For LZK^+GFAP^+ cell count in the degenerating hemi-CST, the number of cells double positive for LZK and GFAP by co-immunofluorescence staining was quantified within the semi-oval region labeled as "deg CST" (**Figures 1B,C**), where reactive astrocytes localized. Three transverse sections of C7 spinal cord per animal were averaged to generate cell count per animal. For $CNTF^+GFAP^+$ cell count in the degenerating hemi-CST, the number of cells double positive for CNTF and GFAP by co-immunofluorescence staining was quantified within the region outlined as "deg CST" in **Figure 5A** (area of 25,837 μm^2). Three transverse cervical spinal cord sections per animal were averaged to generate cell count per animal. Likewise, $CNTF^+GFAP^+$ cells in the sprouting target area of the denervated gray matter were quantified within the region outlined as "target GM" in **Figure 5A** (area of 40,000 μm^2).

CST axon sprouting was quantified as previously described (Grider et al., 2006). Density of BDA-labeled axons on the denervated side of the spinal cord was quantified within a rectangular area of 0.54 mm^2 in transverse sections of C7 spinal cord, and normalized against the axon density on the innervated side of the spinal cord of the same sections. Axons in the main CST were excluded from analysis. Six sections of C7 spinal cord per animal were averaged to generate the axon sprouting index per animal.

Behavioral analyses. Behavioral tests were done with the observer blind to genotypes. Two motor tasks were used to assess motor function before and after cerebral cortical photothrombosis. To evaluate gross motor coordination, mice were placed on a five-lane elevated rotating rod (IITC Life Science), facing away from the observer while walking on the rod. Rotarod was set with starting speed of 4 rpm, constant acceleration of 0.2 rpm/s, and top speed of 44 rpm. Maximum test duration was 300 s. Mice were scored based on time to fall or holding onto the rod without moving. Three trials were averaged for a final score per mouse per session. Mice had pre-injury rotarod training once a day, consecutively for 5 days before injury. Post-injury testing was done at 1, 2, 4, 6, and 8 weeks after unilateral photothrombosis. Post-injury end time of each animal was normalized to its own pre-injury end time, with the pre-injury baseline performance represented as 1 on quantification. To evaluate skilled forelimb stepping, regular horizontal ladder was used. Mice were filmed (60 fps, interlaced, and rendered to 30 fps playback) walking across an 81 cm horizontal ladder with 1.5 cm regularly spaced rungs (Farr et al., 2006). Paw placement of each forelimb was video-scored and defined as follows: correct placement (score of 6); partial placement (score of 5); misses (scores of 0–4). Each animal had three trials per day of testing. Number of steps from each placement type was expressed as a percentage of total steps. Three trials were averaged per mouse per session. Mice had pre-injury training three days before injury. Post-injury testing was done at 1, 2, 4, 6, and 8 weeks after unilateral photothrombosis.

Statistical analyses. One-way or two-way ANOVA analysis was applied depending on the experimental design (see Figure Legends), using GraphPad Prism software. *Post-hoc* comparisons were performed only when a main effect showed statistical significance. Bonferroni correction was used to adjust *p* value of multiple comparisons. All graphs show mean with SEM. *N* represents the number of mice per genotype or treatment group. See figure legends for exact n and *p* values, and statistical test applied.

Data availability statement

The original contributions presented in this study are included in the article. Further inquiries can be directed to the corresponding authors.

Ethics statement

The animal study was reviewed and approved by Institutional Animal Care and Use Committee, University of Kentucky and UT Southwestern Medical Center.

Author contributions

MC conceived the study. MC and MG organized the study, and wrote the manuscript. MC, LI, and EP planned and performed the experiments. MC, XK, RT, and NG performed sample and data collection. MC, NG, MR, and WF performed the data analyses. All authors contributed to manuscript reading and approved submitted manuscript.

Funding

This work was supported by grants from American Heart Association (18CDA34060059) and NIH/NINDS (RO1NS121193) to MC, Kentucky Spinal Cord & Head Injury Research Trust training fund to Chen Lab, and the Haggerty Center for Brain Injury and Repair to MG.

Conflict of interest

The authors declare that the research was conducted in the absence of any commercial or financial relationships that could be construed as a potential conflict of interest.

Publisher's note

All claims expressed in this article are solely those of the authors and do not necessarily represent those of their affiliated organizations, or those of the publisher, the editors and the reviewers. Any product that may be evaluated in this article, or claim that may be made by its manufacturer, is not guaranteed or endorsed by the publisher.

References

Anderson, M. A., Burda, J. E., Ren, Y., Ao, Y., O'Shea, T. M., Kawaguchi, R., et al. (2016). Astrocyte scar formation aids central nervous system axon regeneration. *Nature* 532, 195–200. doi: 10.1038/nature17623

Bachmann, L. C., Lindau, N. T., Felder, P., and Schwab, M. E. (2014). Sprouting of brainstem-spinal tracts in response to unilateral motor cortex stroke in mice. *J. Neurosci.* 34, 3378–3389. doi: 10.1523/JNEUROSCI.4384-13.2014

Bareyre, F. M., Kerschensteiner, M., Raineteau, O., Mettenleiter, T. C., Weinmann, O., and Schwab, M. E. (2004). The injured spinal cord spontaneously forms a new intraspinal circuit in adult rats. *Nat. Neurosci.* 7, 269–277. doi: 10.1038/nn1195

Barres, B. A., Burne, J. F., Holtmann, B., Thoenen, H., Sendtner, M., and Raff, M. C. (1996). Ciliary neurotrophic factor enhances the rate of oligodendrocyte generation. *Mol. Cell. Neurosci.* 8, 146–156.

Becker, A. M., Betz, D. M., and Goldberg, M. P. (2020). Forelimb cortical stroke reduces precision of motor control in mice. *Neurorehabil. Neural Repair* 34, 475–478. doi: 10.1177/1545968320921825

Burda, J. E., O'Shea, T. M., Ao, Y., Suresh, K. B., Wang, S., Bernstein, A. M., et al. (2022). Divergent transcriptional regulation of astrocyte reactivity across disorders. *Nature* 606, 557–564. doi: 10.1038/s41586-022-04739-5

Cafferty, W. B., and Strittmatter, S. M. (2006). The Nogo-Nogo receptor pathway limits a spectrum of adult CNS axonal growth. *J. Neurosci.* 26, 12242–12250. doi: 10.1523/JNEUROSCI.3827-06.2006

Carmichael, S. T., Kathirvelu, B., Schweppe, C. A., and Nie, E. H. (2017). Molecular, cellular and functional events in axonal sprouting after stroke. *Exp. Neurol.* 287(Pt 3), 384–394.

Chen, M., and Zheng, B. (2014). Axon plasticity in the mammalian central nervous system after injury. *Trends Neurosci.* 37, 583–593.

Chen, M., Geoffroy, C. G., Meves, J. M., Narang, A., Li, Y., Nguyen, M. T., et al. (2018). Leucine zipper-bearing kinase is a critical regulator of astrocyte reactivity in the adult mammalian CNS. *Cell Rep.* 22, 3587–3597. doi: 10.1016/j.celrep.2018.02.102

Courtine, G., and Sofroniew, M. V. (2019). Spinal cord repair: Advances in biology and technology. *Nat. Med.* 25, 898–908. doi: 10.1038/s41591-019-0475-6

Cramer, S. C. (2008). Repairing the human brain after stroke: I. Mechanisms of spontaneous recovery. *Ann. Neurol.* 63, 272–287. doi: 10.1002/ana.21393

Davies, S. J., Goucher, D. R., Doller, C., and Silver, J. (1999). Robust regeneration of adult sensory axons in degenerating white matter of the adult rat spinal cord. *J. Neurosci.* 19, 5810–5822.

Diaz-Castro, B., Bernstein, A. M., Coppola, G., Sofroniew, M. V., and Khakh, B. S. (2021). Molecular and functional properties of cortical astrocytes during peripherally induced neuroinflammation. *Cell Rep.* 36:109508.

Du, K., Zheng, S., Zhang, Q., Li, S., Gao, X., Wang, J., et al. (2015). Pten deletion promotes regrowth of corticospinal tract axons 1 year after spinal cord injury. *J. Neurosci.* 35, 9754–9763. doi: 10.1523/JNEUROSCI.3637-14.2015

Farr, T. D., Liu, L., Colwell, K. L., Whishaw, I. Q., and Metz, G. A. (2006). Bilateral alteration in stepping pattern after unilateral motor cortex injury: A new test strategy for analysis of skilled limb movements in neurological mouse models. *J. Neurosci. Methods* 153, 104–113. doi: 10.1016/j.jneumeth.2005.10.011

Fawcett, J. W., Curt, A., Steeves, J. D., Coleman, W. P., Tuszynski, M. H., Lammertse, D., et al. (2007). Guidelines for the conduct of clinical trials for spinal cord injury as developed by the ICCP panel: Spontaneous recovery after spinal cord injury and statistical power needed for therapeutic clinical trials. *Spinal Cord* 45, 190–205. doi: 10.1038/sj.sc.3102007

Geoffroy, C. G., Lorenzana, A. O., Kwan, J. P., Lin, K., Ghassemi, O., Ma, A., et al. (2015). Effects of PTEN and nogo codeletion on corticospinal axon sprouting and regeneration in mice. *J. Neurosci.* 35, 6413–6428. doi: 10.1523/JNEUROSCI.4013-14.2015

Grider, M. H., Chen, Q., and Shine, H. D. (2006). Semi-automated quantification of axonal densities in labeled CNS tissue. *J. Neurosci. Methods* 155, 172–179. doi: 10.1016/j.jneumeth.2005.12.021

Hallett, M. (2001). Plasticity of the human motor cortex and recovery from stroke. *Brain Res. Brain Res. Rev.* 36, 169–174.

Hara, M., Kobayakawa, K., Ohkawa, Y., Kumamaru, H., Yokota, K., Saito, T., et al. (2017). Interaction of reactive astrocytes with type I collagen induces astrocytic scar formation through the integrin-N-cadherin pathway after spinal cord injury. *Nat. Med.* 23, 818–828. doi: 10.1038/nm.4354

Hasel, P., Rose, I. V. L., Sadick, J. S., Kim, R. D., and Liddelow, S. A. (2021). Neuroinflammatory astrocyte subtypes in the mouse brain. *Nat. Neurosci.* 24, 1475–1487.

Herrmann, J. E., Imura, T., Song, B., Qi, J., Ao, Y., Nguyen, T. K., et al. (2008). STAT3 is a critical regulator of astrogliosis and scar formation after spinal cord injury. *J. Neurosci.* 28, 7231–7243.

Hutson, T. H., and Di Giovanni, S. (2019). The translational landscape in spinal cord injury: Focus on neuroplasticity and regeneration. *Nat. Rev. Neurol.* 15, 732–745. doi: 10.1038/s41582-019-0280-3

Jiang, Y. Q., Armada, K., and Martin, J. H. (2019). Neuronal activity and microglial activation support corticospinal tract and proprioceptive afferent sprouting in spinal circuits after a corticospinal system lesion. *Exp. Neurol.* 321:113015. doi: 10.1016/j.expneurol.2019.113015

Jin, D., Liu, Y., Sun, F., Wang, X., Liu, X., and He, Z. (2015). Restoration of skilled locomotion by sprouting corticospinal axons induced by co-deletion of PTEN and SOCS. *Nat. Commun.* 6:8074. doi: 10.1038/ncomms9074

Kaiser, J., Maibach, M., Salpeter, I., Hagenbuch, N., de Souza, V. B. C., Robinson, M. D., et al. (2019). The spinal transcriptome after cortical stroke: In search of molecular factors regulating spontaneous recovery in the spinal cord. *J. Neurosci.* 39, 4714–4726. doi: 10.1523/JNEUROSCI.2571-18.2019

Keasey, M. P., Kang, S. S., Lovins, C., and Hagg, T. (2013). Inhibition of a novel specific neuroglial integrin signaling pathway increases STAT3-mediated CNTF expression. *Cell Commun. Signal.* 11:35. doi: 10.1186/1478-811X-11-35

Khakh, B. S., and Sofroniew, M. V. (2015). Diversity of astrocyte functions and phenotypes in neural circuits. *Nat. Neurosci.* 18, 942–952.

Lang, C., Bradley, P. M., Jacobi, A., Kerschensteiner, M., and Bareyre, F. M. (2013). STAT3 promotes corticospinal remodelling and functional recovery after spinal cord injury. *EMBO Rep.* 14, 931–937.

Lapash Daniels, C. M., Ayers, K. L., Finley, A. M., Culver, J. P., and Goldberg, M. P. (2009). Axon sprouting in adult mouse spinal cord after motor cortex stroke. *Neurosci. Lett.* 450, 191–195.

Lee, J. K., Chow, R., Xie, F., Chow, S. Y., Tolentino, K. E., and Zheng, B. (2010). Combined genetic attenuation of myelin and semaphorin-mediated growth inhibition is insufficient to promote serotonergic axon regeneration. *J. Neurosci.* 30, 10899–10904. doi: 10.1523/JNEUROSCI.2269-10.2010

Liddelow, S. A., and Barres, B. A. (2017). Reactive astrocytes: Production, function, and therapeutic potential. *Immunity* 46, 957–967.

Lindau, N. T., Banninger, B. J., Gullo, M., Good, N. A., Bachmann, L. C., Starkey, M. L., et al. (2014). Rewiring of the corticospinal tract in the adult rat after unilateral stroke and anti-Nogo-A therapy. *Brain* 137(Pt 3), 739–756. doi: 10.1093/brain/awt336

Linker, R. A., Maurer, M., Gaupp, S., Martini, R., Holtmann, B., Giess, R., et al. (2002). CNTF is a major protective factor in demyelinating CNS disease: A neurotrophic cytokine as modulator in neuroinflammation. *Nat. Med.* 8, 620–624. doi: 10.1038/nm0602-620

Liu, K., Lu, Y., Lee, J. K., Samara, R., Willenberg, R., Sears-Kraxberger, I., et al. (2010). PTEN deletion enhances the regenerative ability of adult corticospinal neurons. *Nat. Neurosci.* 13, 1075–1081.

Liu, Y., Wang, X., Li, W., Zhang, Q., Li, Y., Zhang, Z., et al. (2017). A sensitized IGF1 Treatment restores corticospinal axon-dependent functions. *Neuron* 95, 817–833.e4. doi: 10.1016/j.neuron.2017.07.037

Liu, Z., Li, Y., Cui, Y., Roberts, C., Lu, M., Wilhelmsson, U., et al. (2014). Beneficial effects of gfap/vimentin reactive astrocytes for axonal remodeling and motor behavioral recovery in mice after stroke. *Glia* 62, 2022–2033. doi: 10.1002/glia.22723

Menet, V., Prieto, M., Privat, A., and Gimenez y Ribotta, M. (2003). Axonal plasticity and functional recovery after spinal cord injury in mice deficient in both glial fibrillary acidic protein and vimentin genes. *Proc. Natl. Acad. Sci. U.S.A.* 100, 8999–9004. doi: 10.1073/pnas.1533187100

Muller, A., Hauk, T. G., and Fischer, D. (2007). Astrocyte-derived CNTF switches mature RGCs to a regenerative state following inflammatory stimulation. *Brain* 130(Pt 12), 3308–3320. doi: 10.1093/brain/awm257

Okada, S., Nakamura, M., Katoh, H., Miyao, T., Shimazaki, T., Ishii, K., et al. (2006). Conditional ablation of Stat3 or Socs3 discloses a dual role for reactive astrocytes after spinal cord injury. *Nat. Med.* 12, 829–834.

Park, C. K., Ju, W. K., Hofmann, H. D., Kirsch, M., Ki Kang, J., Chun, M. H., et al. (2000). Differential regulation of ciliary neurotrophic factor and its receptor in the rat hippocampus following transient global ischemia. *Brain Res.* 861, 345–353. doi: 10.1016/s0006-8993(00)02045-x

Pekny, M., Wilhelmsson, U., Tatlisumak, T., and Pekna, M. (2019). Astrocyte activation and reactive gliosis-A new target in stroke? *Neurosci. Lett.* 689, 45–55. doi: 10.1016/j.neulet.2018.07.021

Poinsatte, K., Betz, D., Torres, V. O., Ajay, A. D., Mirza, S., Selvaraj, U. M., et al. (2019). Visualization and quantification of post-stroke neural connectivity and neuroinflammation using serial two-photon tomography in the whole mouse brain. *Front. Neurosci.* 13:1055. doi: 10.3389/fnins.2019.01055

Rosenzweig, E. S., Courtine, G., Jindrich, D. L., Brock, J. H., Ferguson, A. R., Strand, S. C., et al. (2010). Extensive spontaneous plasticity of corticospinal projections after primate spinal cord injury. *Nat. Neurosci.* 13, 1505–1510.

Silver, J., and Miller, J. H. (2004). Regeneration beyond the glial scar. *Nat. Rev. Neurosci.* 5, 146–156.

Sofroniew, M. V. (2014). Astrogliosis. *Cold Spring Harb. Perspect. Biol.* 7:a020420.

Stahl, N., Boulton, T. G., Farruggella, T., Ip, N. Y., Davis, S., Witthuhn, B. A., et al. (1994). Association and activation of Jak-Tyk kinases by CNTF-LIF-OSM-IL-6 beta receptor components. *Science* 263, 92–95. doi: 10.1126/science.8272873

Starkey, M. L., and Schwab, M. E. (2014). How plastic is the brain after a stroke? *Neuroscientist* 20, 359–371.

Starkey, M. L., Bartus, K., Barritt, A. W., and Bradbury, E. J. (2012a). Chondroitinase ABC promotes compensatory sprouting of the intact corticospinal tract and recovery of forelimb function following unilateral pyramidotomy in adult mice. *Eur. J. Neurosci.* 36, 3665–3678. doi: 10.1111/ejn.12017

Starkey, M. L., Bleul, C., Zorner, B., Lindau, N. T., Mueggler, T., Rudin, M., et al. (2012b). Back seat driving: Hindlimb corticospinal neurons assume forelimb control following ischaemic stroke. *Brain* 135(Pt 11), 3265–3281. doi: 10.1093/brain/aws270

Stern, S., Hilton, B. J., Burnside, E. R., Dupraz, S., Handley, E. E., Gonyer, J. M., et al. (2021). RhoA drives actin compaction to restrict axon regeneration and astrocyte reactivity after CNS injury. *Neuron* 109, 3436–3455.e9. doi: 10.1016/j.neuron.2021.08.014

Sun, F., Park, K. K., Belin, S., Wang, D., Lu, T., Chen, G., et al. (2011). Sustained axon regeneration induced by co-deletion of PTEN and SOCS. *Nature* 480, 372–375. doi: 10.1038/nature10594

Tripathi, R. B., and McTigue, D. M. (2008). Chronically increased ciliary neurotrophic factor and fibroblast growth factor-2 expression after spinal contusion in rats. *J. Comp. Neurol.* 510, 129–144. doi: 10.1002/cne.21787

Ueno, M., Hayano, Y., Nakagawa, H., and Yamashita, T. (2012). Intraspinal rewiring of the corticospinal tract requires target-derived brain-derived neurotrophic factor and compensates lost function after brain injury. *Brain* 135(Pt 4), 1253–1267. doi: 10.1093/brain/aws053

Wahl, A. S., Omlor, W., Rubio, J. C., Chen, J. L., Zheng, H., Schroter, A., et al. (2014). Neuronal repair. Asynchronous therapy restores motor control by rewiring of the rat corticospinal tract after stroke. *Science* 344, 1250–1255. doi: 10.1126/science.1253050

Wang, L., Hu, B., Wong, W. M., Lu, P., Wu, W., and Xu, X. M. (2009). Glial and axonal responses in areas of Wallerian degeneration of the corticospinal and dorsal ascending tracts after spinal cord dorsal funiculotomy. *Neuropathology* 29, 230–241. doi: 10.1111/j.1440-1789.2008.00969.x

Watson, B. D., Dietrich, W. D., Busto, R., Wachtel, M. S., and Ginsberg, M. D. (1985). Induction of reproducible brain infarction by photochemically initiated thrombosis. *Ann. Neurol.* 17, 497–504. doi: 10.1002/ana.410170513

Zamanian, J. L., Xu, L., Foo, L. C., Nouri, N., Zhou, L., Giffard, R. G., et al. (2012). Genomic analysis of reactive astrogliosis. *J. Neurosci.* 32, 6391–6410.

Zhang, Y., and Barres, B. A. (2010). Astrocyte heterogeneity: An underappreciated topic in neurobiology. *Curr. Opin. Neurobiol.* 20, 588–594. doi: 10.1016/j.conb.2010.06.005

Zukor, K., Belin, S., Wang, C., Keelan, N., Wang, X., and He, Z. (2013). Short hairpin RNA against PTEN enhances regenerative growth of corticospinal tract axons after spinal cord injury. *J. Neurosci.* 33, 15350–15361. doi: 10.1523/JNEUROSCI.2510-13.2013

frontiers | Frontiers in Cellular Neuroscience

TYPE Original Research
PUBLISHED 03 October 2022
DOI 10.3389/fncel.2022.1000538

Check for updates

OPEN ACCESS

EDITED BY
Tim-Henrik Bruun,
Velvio GmbH, Germany

REVIEWED BY
Jan Bakos,
Slovak Academy of Sciences, Slovakia
Emily Brook,
Curtin University, Australia

*CORRESPONDENCE
Silke Haerteis
silke.haerteis@ur.de

SPECIALTY SECTION
This article was submitted to Cellular Neurophysiology, a section of the journal Frontiers in Cellular Neuroscience

RECEIVED 22 July 2022
ACCEPTED 14 September 2022
PUBLISHED 03 October 2022

CITATION
Jurek B, Denk L, Schäfer N, Salehi MS, Pandamooz S and Haerteis S (2022) Oxytocin accelerates tight junction formation and impairs cellular migration in 3D spheroids: evidence from Gapmer-induced exon skipping. Front. Cell. Neurosci. 16:1000538. doi: 10.3389/fncel.2022.1000538

COPYRIGHT
© 2022 Jurek, Denk, Schäfer, Salehi, Pandamooz and Haerteis. This is an open-access article distributed under the terms of the Creative Commons Attribution License (CC BY). The use, distribution or reproduction in other forums is permitted, provided the original author(s) and the copyright owner(s) are credited and that the original publication in this journal is cited, in accordance with accepted academic practice. No use, distribution or reproduction is permitted which does not comply with these terms.

Oxytocin accelerates tight junction formation and impairs cellular migration in 3D spheroids: evidence from Gapmer-induced exon skipping

Benjamin Jurek[1,2], Lucia Denk[1], Nicole Schäfer[1,3], Mohammad Saied Salehi[4], Sareh Pandamooz[5] and Silke Haerteis[1]*

[1]Institute for Molecular and Cellular Anatomy, University of Regensburg, Regensburg, Germany, [2]Research Group Neurobiology of Stress Resilience, Max Planck Institute of Psychiatry, Munich, Germany, [3]Experimental Orthopaedics, Centre for Medical Biotechnology (ZMB), Bio Park 1, University of Regensburg, Regensburg, Germany, [4]Clinical Neurology Research Center, Shiraz University of Medical Science, Shiraz, Iran, [5]Stem Cells Technology Research Center, Shiraz University of Medical Sciences, Shiraz, Iran

Oxytocin (OXT) is a neuropeptide that has been associated with neurological diseases like autism, a strong regulating activity on anxiety and stress-related behavior, physiological effects during pregnancy and parenting, and various cellular effects in neoplastic tissue. In this study, we aimed to unravel the underlying mechanism that OXT employs to regulate cell-cell contacts, spheroid formation, and cellular migration in a 3D culture model of human MLS-402 cells. We have generated a labeled OXT receptor (OXTR) overexpressing cell line cultivated in spheroids that were treated with the OXTR agonists OXT, Atosiban, and Thr^4-Gly^7-oxytocin (TGOT); with or without a pre-treatment of antisense oligos (Gapmers) that induce exon skipping in the human OXTR gene. This exon skipping leads to the exclusion of exon 4 and therefore a receptor that lost its intracellular G-protein-binding domain. Sensitive digital PCR (dPCR) provided us with the means to differentiate between wild type and truncated OXTR in our cellular model. OXTR truncation differentially activated intracellular signaling cascades related to cell-cell attachment and proliferation like Akt, ERK1/2-RSK1/2, HSP27, STAT1/5, and CREB, as assessed by a Kinase Profiler Assay. Digital and transmission electron microscopy revealed increased tight junction formation and well-organized cellular protrusions into an enlarged extracellular space after OXT treatment, resulting in increased cellular survival. In summary, OXT decreases cellular migration but increases cell-cell contacts and therefore improves nutrient supply. These data reveal a novel cellular effect of OXT that might have implications for degenerating CNS diseases and tumor formation in various tissues.

KEYWORDS

oxytocin, Gapmer-induced exon skipping, spheroid, tight junction, intracellular signaling

Introduction

The neuropeptide oxytocin (OXT) has been implicated in many behavioral and physiological processes, like the formation of parent-offspring bonding, labor and milk-letdown, social interaction, general anxiety, and stress-coping (Jurek and Neumann, 2018). A subset of patients suffering from central nervous system (CNS)-related disorders like autism-spectrum disorder, general anxiety, or schizophrenia could benefit from intranasal applications of OXT (Hurlemann, 2017), potentially by modulating the social salience network (Shamay-Tsoory and Abu-Akel, 2016; Jurek and Meyer, 2020), but with a yet-unknown cellular/molecular mechanism. On a cellular level, OXT induces mitogenic and calcium-related signaling cascades *via* the direct binding to its OXT receptor (OXTR; Busnelli and Chini, 2018), the vasopressin receptors (V1a, V1b, V2; Chini and Manning, 2007), or the TrpV1 channel (Nersesyan et al., 2017). The agonist Thr^4-Gly^7-oxytocin (TGOT) is specific for the OXTR with a very low affinity for the V1a/b/V2 receptors, thus it can serve as an internal control for OXTR activation (Busnelli et al., 2013). Both, OXT and TGOT activate second messenger signaling either by inhibitory $G\alpha_i$, $G\alpha_o$, or bystimulatory $G\alpha_q$-protein coupling to the OXTR, depending on the ligand concentration (Gimpl and Fahrenholz, 2001). Biased agonists, such as Atosiban, bind the OXTR but selectively activate the inhibitory $G\alpha_i$-protein-coupled pathways (Reversi et al., 2005). Upon OXTR activation and in addition to G-protein signaling, β-arrestin also binds the OXTR at the intracellular loops of its transmembrane domains and induces G-protein-independent signaling cascades (Grotegut et al., 2011; Passoni et al., 2016). Signaling cascades that have been linked to the activated OXTR encompass the MAPK pathways (Jurek et al., 2012), calcium-related cascades (Meyer et al., 2022), and the activation of transcription factors like CREB or MEF2A (Winter et al., 2021). Once activated, the OXTR undergoes desensitization, internalization, and either degradation or recycling back to the cell surface (Conti et al., 2009; Passoni et al., 2016). The stability of the OXTR, its ligand-affinity, and its subsequent signaling response depend on hardly manageable factors, like the genetic variant (Meyer et al., 2022), the membrane cholesterol content (Reversi et al., 2006a; Muth et al., 2011), and its location in caveolin-enriched domains in the cellular membrane, which affects the temporal pattern of mitogenic signaling (Rimoldi et al., 2003).

As a consequence of the promiscuous coupling to inhibitory or stimulatory G-proteins, OXT inhibits or stimulates cellular proliferation under physiological and neoplastic conditions (Cassoni et al., 1994, 1996, 2000, 2001, 2004; Reversi et al., 2006b). The cell types in which OXT induces cell proliferation range from primary astrocytes, epithelial adenocarcinoma MCF7 cells, human osteoblast-like cells, small cell lung carcinoma cells, to human dermal microvascular endothelial cells, or endothelial sarcomatous cell lines. Cell types in which OXT inhibits cell proliferation include neuroblastoma cells (IMR32, SH-N-SH, SH-SY5Y), epithelial cells (HUVEC, HAEC, HPAEC), adenocarcinoma of the endometrium, breast cancer cells (T47D, MDA-MB231), ovarian carcinoma (SKOV3), endometrial carcinoma (Colo684, A-MEC, HEC1A), prostate cancer cells (DU145), and osteosarcoma cells (MG-63, U2OS; for an overview of cell-types see Reversi et al., 2006b and references therein). In addition to proliferation, OXT stimulates cellular migration in human endothelial and prostate cancer cells (Cattaneo et al., 2008; Zhong et al., 2010), but inhibits migration in head and neck squamous cell carcinoma cells. Moreover, the same study also found OXT-induced size-reduction and inhibition of 3D-spheroid formation (Kim et al., 2017). In contrast, we have recently shown that OXT increases the spheroid size in rat hypothalamic neurons (Salehi et al., 2021). The spheroid formation, proliferation, and cellular migration are being orchestrated by the cells' ability to perform cell-cell contacts or cell-matrix interactions (Atat et al., 2022), cellular characteristics that are important hallmarks in degenerative disorders of the CNS or tumor formation in the periphery (Stadler et al., 2018; Atat et al., 2022). In this study, we have made use of the liposarcoma cell line MLS-402, which was virally transduced to overexpress a fluorescently labeled OXTR. MLS-402 cells form spheroids and serve as an ideal model system for neoplastic endothelial cells, but also to study general intracellular cascades and cell-cell interactions.

The contrasting effects on proliferation and spheroid formation, which are dependent on above-mentioned highly variable factors, render OXT a suboptimal treatment option for any medical regimen; however, detailed knowledge of the underlying mechanism that allows both pro- and anti-proliferative effects, might provide us with a tool to enforce any desired cellular response. Consequently, the aim of this study is to characterize the intracellular response to OXTR ligands with novel approaches, such as Gapmer-induced exon skipping, to gain a better understanding of the decisive factors that regulate OXT-induced cellular processes.

Antisense oligo (Gapmer)-induced exon skipping is an innovative technique that relies on the blockade of exonic splice enhancer (ESE) and splice acceptor sites by modified oligos (Li et al., 2018; Flynn et al., 2021). Those so-called Gapmers are antisense oligos whose backbones are chemically modified for increased stability, less toxicity, and the ability to enter cells *via* gymnosis (Winter et al., 2021). In this study, we have made use of Gapmers that were designed to bind to ESEs within exon 4 of the *OXTR*, so that exon 4 will be skipped from the mature mRNA. If exon 4 is missing in the mature mRNA due to exon skipping, the resulting receptor lacks the intracellular domain and therefore the ability to activate intracellular signaling cascades *via* G-proteins.

The overall expression level of the OXTR protein in any given cell is generally very low, with some physiological exceptions such as the gestational myometrium

(Akerlund et al., 1999). This fact can be attributed to the general toxicity of overexpressed GPCRs in eukaryotic cells (Rajagopal and Shenoy, 2018). The method of choice to differentiate between wild type and mutated OXTR is digital PCR, a novel and more sensitive form of quantitative PCR that is able to reliably detect the wild type and mutated OXTR in absolute values, without the need for a standard curve (Huggett, 2020). We designed the *OXTR*-detection probes to specifically bind the exon 2–3 boundary, or to bind within exon 4. This approach allows us to differentiate between a wild type and a truncated receptor that is lacking the exon 4 and therefore its intracellular domain.

In summary, this study employed a novel approach to investigate the molecular mechanism underlying the diverse effects of OXT on cell-cell contacts, proliferation, and migration in a 3D spheroid environment, which provides the basis for a better understanding of degenerative diseases and cancer.

Material and methods

Cell culture

Human MLS-402 (liposarcoma cells kindly provided by Prof. Dr. Steffen Eisenhardt, University Hospital Freiburg, and their derivate subclone overexpressing EGFP-OXTR-mCherry (MLS-G2^{OXTR}) and the control subclone MLS-402$^{EGFP\text{-}mCherry}$ were cultured in RPMI-1640 medium, with L-glutamine and sodium bicarbonate (#R8758, Sigma Aldrich, Darmstadt, Germany), supplemented with 10% fetal bovine serum (#S1810, Biowest, Nuaillé, France) at 37°C and 5% CO_2 until 80% confluency. Cells were kept under antibiotic-free sterile conditions and tested for mycoplasmic contamination on a regular basis. Passaging was performed at least once a week by gentle trypsinization. Cell counts were recorded and compared between MLS-402 and MLS-G2^{OXTR} cell lines to extrapolate proliferation rates.

Viral transduction and monoclonal cell line creation

EGFP and mCherry labeled human OXTR under the control of a CMV early enhancer/chicken β-actin promoter was transduced into MLS-402 cells using a lentiviral system (pLV[Exp]-Hygro-CBh > EGFP/hOXTR[NM_001354654.1]/mCherry, VectorBuilder, Berlin, Germany). A control virus (pLV[Exp]-Hygro-CBh > EGFP/mCherry) was used to assess the side effects of transduction and EGF/mCherry expression. 10 MOI of viral particles were used, and 250 μg/ml hygromycin (Sigma Aldrich, H3274) for 3 days to select successfully transduced cells. Vital, proliferating cells were singled out in 96-well plate, and resulting colonies were cryo-preserved until further analysis per digital PCR.

RNA isolation, cDNA synthesis, and digital PCR (dPCR)

Cells were lysed using 1 ml Ambion TRIzol (#15596018, Invitrogen, Carlsbad, USA) per 6-well according to the manufacturer's protocol, the resulting RNA phase was washed and DNA digested using the RNeasy Mini Kit (#74104 and #79254, Qiagen, Hilden Germany), 1 μg/μl of cDNA was synthesized with the iScript cDNA synthesis Kit (#1708890, BioRad, Feldkirchen, Germany), the resulting cDNA was used undiluted for dPCR-based detection of the OXTR transcript with a Qiacuity dPCR cycler (Qiagen) in an 8.5 k 24-well Qiacuity Nanoplate and QuantiNova LNA probe PCR assays (see **Table 1**). Homo sapiens ACTB was used as a reference gene to control for even cDNA content. Cycling conditions were as follows: 2 min at 95°C heat activation, 15 s 95°C denaturation, 30 s 60°C annealing/extension for 40 cycles. Imaging was set to 500 ms exposure and gain of 20.

Spheroid cultivation

MLS-G2 cells were thawed and sub-cultured for at least two times under Hygromycin selection medium (50 μg/ml). Then, 1×10^5 cells were seeded in a 96-well plate sterile-coated with 1.5% agarose for 24 h or 3 days in 200 μl normal growth medium with or without immediate addition of OXTR ligands and Gapmers.

Gapmer transfection and OXTR ligand stimulation

After seeding cells in agarose coated 96-well plates, negative control LNA Gapmer A (referred to as n.c., #339999) or a 1:1:1 mixture of three custom designed LNA Gapmers (see **Table 2**) that bind exonic splice enhancer and acceptor sites are pre-mixed with 1 μl Lipofectamine RNAiMax (Invitrogen) per 200 μl medium and gently added to the forming spheroids. After Gapmer transfection, OXTR ligands OXT (#4016373, Bachem, Bubendorf, Switzerland), Atosiban (#6332, Tocris, Wiesbaden, Germany), and TGOT (#4013837, Bachem) are added at 100 nM or 1 μM for 24 h.

Spheroid volume/area/sphericity assay

After 24 h of Gapmer and ligand stimulation, spheroids are imaged on a Leica DM IL LED microscope and spheroid

TABLE 1 Technical details of the QuantiNova LNA Probe PCR assays (Qiagen).

Probe name	Amplicon start	Exon	Amplicon length	Ensembl Gene ID
HS_OXTR_2484965	423	2–3 boundary	80	ENSG00000180914
HS_OXTR_2484969	1,395	3–4 boundary	228	ENSG00000180914
HS_OXTR_170144	2,203	4	167	ENSG00000180914
HS_ACTB_2476226	433	3–4 boundary	85	ENSG00000075624

TABLE 2 Sequence and binding site of OXTR specific Gapmers and negative control (referred to as n.c. in the figures) Gapmers.

Product name	Target	Product sequence 5'–3'
OXTR-ESE1-V1	Exonic splice enhancer site Exon 4, hOXTR	/Biosg/A*C*A*G*G*A*A*G*C*G*C*T*G*C*A*C*G*A*G*T*T
OXTR-ESE2-V1	Exonic splice enhancer site, Exon 4, hOXTR	/Biosg/A*G*C*A*G*C*T*C*C*T*C*T*G*G*C*T*G*G*A
OXTR-E4ACC-V1	Exonic splice acceptor site, Exon 4, hOXTR	/Biosg/T*G*A*T*G*A*A*G*G*C*C*G*A*G*G*C*T*G*A*G
Negative control A	-	/Biosg/A*C*G*T*C*T*A*T*A*C*G*C*C*C*A

area is assessed by means of Fiji ImageJ (1.53f51, NIH, USA). Spheroid volume is calculated by the formula $4/3\pi$ [(D1 + D2)/4]3, with D1 and D2 being the diameters. Spheroid volume was also recorded on the Keyence VHX7000 digital microscope using the 3D Panorama function. Sphericity was recorded using Fijis "Analyze particles" function with a cut-off of 0.7 being "spherical" and below 0.7 being "aspherical". Spheroids with centric holes (donut-shape) are also classified as "aspherical".

Cellular migration assay

Twenty-four hours after Gapmer transfection and ligand stimulation, spheroids are transferred with their stimulation medium to a standard cell culture flat bottom 96-well plate. The spheroids are allowed to settle for 1 h and imaged as time point 0 on the Leica DM IL LED microscope. After 12 h and 84 h the spheroids are imaged again with identical microscope settings. Spheroids are cropped from time point 0 images and overlayed on time point 84 h to visualize the original spheroid size. Original spheroid size and the size of the migrated cell layer are put into ratio as % increase of migration area. As some of the spheroids are close to one well wall and consequently can only migrate asymmetrically, we assessed the 10 longest distances of cells traveled from the spheroid and recorded that as migration distance.

Cell viability assay

To determine cell viability after 24 h of 100 nM OXT or TGOT, cells were seeded in 6-well plates at 1.5×10^6 cells in normal growth medium. Cell viability was determined by means of the Promega CellTiter-Glo^{TM} cell viability assay according to the manufacturer's instructions and analyzed *via* GloMax plate reader system.

Nucleus size and count in spheroids

Gapmer- and ligand-treated spheroids were fixated using 4% paraformaldehyde for 20 min and nuclei were stained with Hoechst 333342 for nucleus count and size determination using the blue channel, auto threshold, and the "analyze particles" function in Fiji. The same ROI was used between different images, and all images were acquired with identical settings.

Live cell imaging

Live cell imaging was performed on an inverted Zeiss Axiovert 200 M microscope equipped with a heating element to retain 37°C. Cells were cultured on glass cover slides in a 6-well plate under normal growth medium conditions for 24 h. Cover slips were removed and placed inverted on a glass microscope slide (Menzel, Braunschweig Germany) with PBS. Images were processed and analyzed by Fiji ImageJ.

Transmission electron microscopy (TEM) imaging

For electron microscopy, the untreated (VEH) and treated (100 nM OXT) spheroids were primarily fixated in 2% glutaraldehyde (Serva, Heidelberg, Germany) buffered with 100 mM sodium cacodylate, pH 7.4 for 24 h at 4°C. For better handling during the following process, the spheroids were coated with 4% low melting agarose in 100 mM sodium cacodylate. After the addition of 1% osmium tetroxide (Science Services, München, Germany) for a secondary fixation step and 0.5% uranyl acetate for optimal contrast, the spheroids were dehydrated in a graded series of ethanol and embedded in two perpendicular orientations (diagonal and longitudinal) in Epon (Fluka, Taufkirchen, Germany), which was polymerized at 60°C for 3 days.

The ultrathin sections of the embedded spheroids were cut with a diamond knife (Diatome, Nidau, Switzerland) on an ultramicrotome EM UC7 (Leica, Wetzlar, Germany) and then collected on a slot grid coated with 1.5% Pioloform® (Polyvinyl butyral), solved in chloroform (Plano, Wetzlar, Germany). The electron micrographs were taken at 80 kV on an EM 902 transmission electron microscope (Zeiss, Oberkochen, Germany; Minuth and Denk, 2015).

The captured TEM images were background subtracted (30 pixel rolling ball), smoothed, and distortions were corrected using the "distortion correction" plugin in Fiji/ImageJ (Kaynig et al., 2010) with a lambda of 9.51, and stitched using the MosaicJ plugin.

Correlative light electron microscopy (CLEM)

MLS-G2 cells were seeded on 35 mm glass bottom culture dishes with gridded coverslips (MatTek, P35G-1.5-14-CGRD), fixated in 4% paraformaldehyde in 100 mM cacodylate buffer, and imaged for OXTR-EGFP fluorescence at a Zeiss Axiovert 200 MOT. After imaging, the cells were post-fixated with 2% glutaraldehyde in 100 mM cacodylate buffer and treated as described for TEM imaging until alcohol dehydration. Lastly, acetone was used to disconnect the glass cover slip from the cell culture dish, and cells were embedded in 1:1 acetone/Epon for 5 min, and pure Epon for 1.5 h at 30°C. Final polymerization was achieved by incubation for 2 days at 60°C. Images were pre-processed identical to TEM imaging and imaged with the underlying grid for orientation. Fluorescent and TEM images were overlayed by means of the ec-CLEM plugin in ICY Bioimage Analysis software platform.

Digital 3D microscopy

A VHX7000 digital microscope at 200× magnification was used to assess the volume and 3D-surface characteristics of 4% PFA-fixated spheroids covered by 50–100 µl PBS on a black imaging surface, which guarantees that spheroids retain their native shape but are accessible for 3D imaging, undisturbed by surrounding well-walls. The black and flat imaging surface is essential for setting a baseline and subsequent correct volume determination.

Machine learning based image segmentation

TEM micrographs were segmented into four classes: "extracellular space", "cytoplasm", "organelles", and "cell membrane" using the machine learning based Fiji Plugin *trainable WEKA segmentation*. A classifier model was trained using a minimum of eigth traces per class. The resulting probability image of "extracellular space" was auto thresholded (Otsu), converted to binary mask, selection created, and restored to the original probability image. The area was then measured as % of total area.

Cell stimulations for kinase profiler assay

MLS-G2 cells were seeded at 7×10^6 cells per 10 mm^2 cell culture dish in normal growth medium. After 1 h cells were transfected with negative control Gapmers or OXTR-specific Gapmers. After 24 h, the normal growth medium with the Gapmers was removed and for 2 h replaced by a serum-reduced medium (RPMI + 0.1% FCS) containing again Lipofectamine and the according Gapmers in identical concentration. The transfected cells were then stimulated with 100 nM of OXT, Atosiban, or TGOT for 10 min. Non-treated cells are indicated as vehicle (VEH). After 10 min, proteins were isolated and blotted onto a capture-antibody spotted membrane, according to the Kinase Array protocol (ARY003C, R + D Systems, Minneapolis, USA). Images were recorded by a Vilber Western Blot Imager and the membrane was analyzed using Fiji ImageJ.

Data acquisition and analysis

The data about cancer-related OXTR mutations were extracted from the online database cBioPortal for cancer genomics (Cerami et al., 2012; Gao et al., 2013). The term "OXTR" was queried using data from 22,882 patients/23,945 samples from a total of 31 studies as listed in **Supplementary Table 1**.

Statistics

Data were analyzed either by two-way/one-way ANOVA followed by Holm-Sidak *post-hoc* correction or Chi-square test with nominal data (sphericity assay) using GraphPad Prism 8. The variance between groups was similar, normal distribution was tested by Kolmogorov-Smirnov and Shapiro-Wilk test, and statistical significance was accepted at $p < 0.05$. N numbers represent biological replicates, technical replicates are additionally indicated. Data are represented as mean + SEM.

Results

When queried for "OXTR" of approx. 24,000 samples from 31 registered studies, the cancer biology database cBioportal identified 20 exonic missense mutations and one truncation at the end of exon 3 (**Figure 1A**; Cerami et al., 2012; Gao et al., 2013), all of which have been associated with different types of sarcoma/carcinoma/glioma (for a complete list see **Supplementary Table 1**). Twenty out of 35 missense mutations lie within the large transmembrane domains of Exon

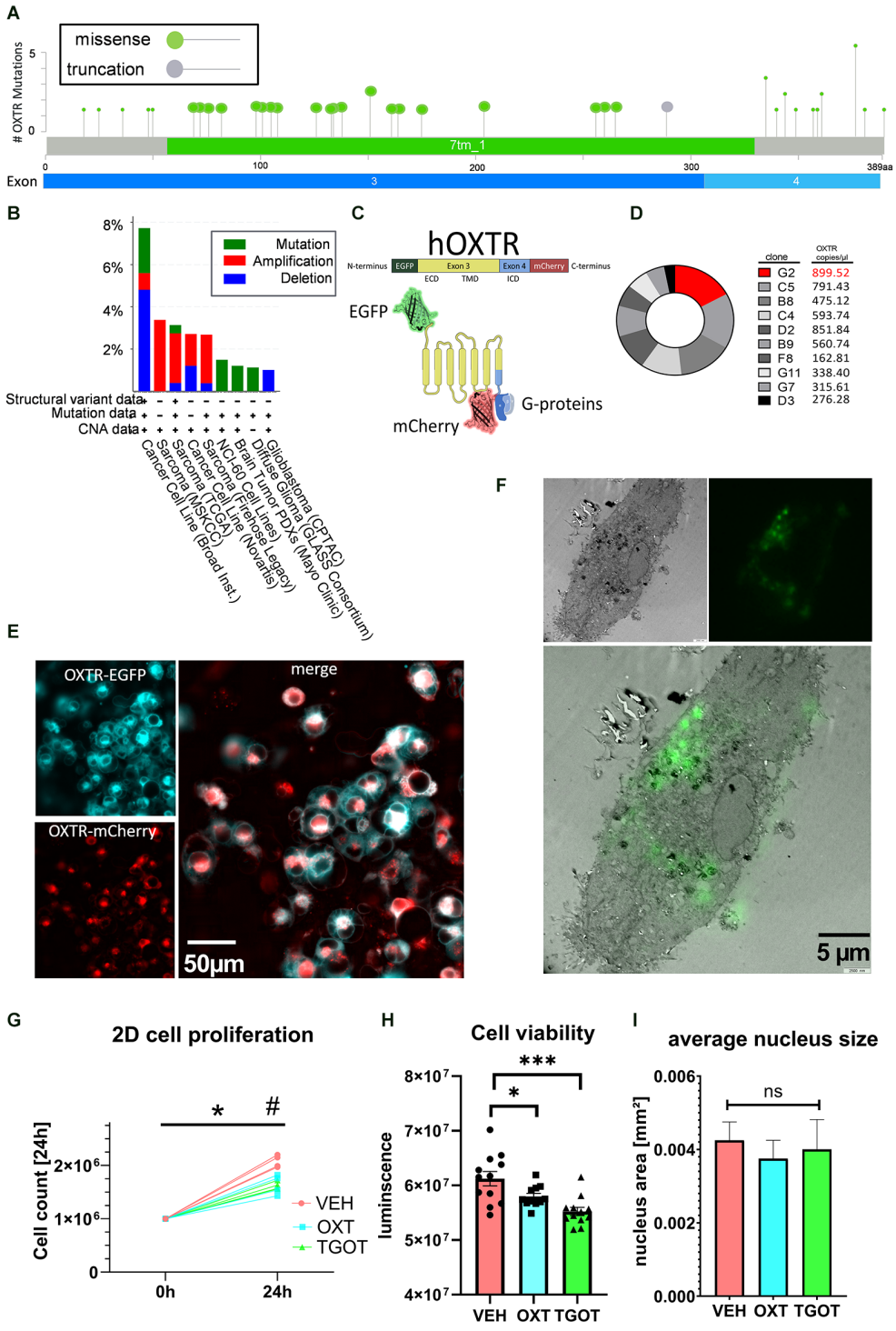

FIGURE 1
Establishment of labeled OXTR-overexpressing liposarcoma cells MLS-G2. **(A)** Localization of exonic sarcoma/carcinoma-related missense mutations or truncation within the human *OXTR* gene. Twenty missense mutations are localized in the transmembrane domain (Exon 3), and 10 missense mutations are localized in the intracellularG-protein-binding C-terminal domain. Source: cBioportal, data extracted from 23,945 samples from 31 different studies. **(B)** cBioPortal-extracted data on the occurrence of *OXTR* variants from different sources. Cancer cell lines and sarcoma tissue are represented with 8% and 3%, respectively, indicating a minor but consistent basis for the use of the liposarcoma cell line MLS-402 for *OXTR* overexpression. **(C)** Schematic representation of the labeled human *OXTR* with N-terminal EGFP and C-terminal mCherry. Exon 3 encodes the extracellular domain (ECD) and the transmembrane domain (TMB), whereas exon 4 encodes most of the intracellular
(*Continued*)

FIGURE 1 (Continued)
domain (ICD) with the G-protein binding site. **(D)** Comparison of the expression levels of the lentiviral *EGFP-OXTR-mCherry* construct in 10 different clones of MLS-402 liposarcoma cells analyzed by dPCR as absolute numbers in copies per microliter. The clone MLS-G2 showed the highest expression of the *OXTR* construct and was therefore chosen for further experiments. **(E)** Visualization of the OXTR N-terminal EGFP (cyan) and C-terminal mCherry (red) labels. The EGFP-fluorescent signal is mainly situated in the cellular periphery, indicating a cell membrane incorporation of the OXTR; the C-terminal mCherry signal is evenly distributed in the cytoplasm, interspersed with perinuclear accumulations. **(F)** Correlative light electron microscopy (CLEM) micrograph (3,000x magnification) of an OXTR-EGFP expressing MLS-G2 cell. OXTR expression is detected perinuclear and at the cell membrane, implying functional expression. **(G)** The cellular proliferation rate of MLS-G2 cells decreases under stimulated (OXT, TGOT, both 100 nM) conditions compared to normal (control) conditions in a 2D culture after 24 h of treatment. Two-way ANOVA, time × treatment, significant interaction $F_{(2, 9)} = 15.45$, $p = 0.0012$, Tukey *post hoc* correction $^{*}p < 0.0001$ vs. time point 0, $^{\#}p = 0.0001$ vs. other treatment groups, $n = 4$ biological replicates. **(H)** Cell viability decreases under stimulated (OXT, TGOT, both 100 nM, 24 h) conditions. One-way ANOVA, $F_{(2, 32)} = 10.26$, $p = 0.0004$. Holm-Sidak *post hoc* correction $^{***}P = 0.0002$, $^{*}p = 0.044$, $n = 12$ biological replicates. **(I)** Average nucleus size is not affected by the OXT or TGOT treatment (100 nM, 24 h) under 2D conditions. ns= not significant.

3. Interestingly, 10 out of 35 missense mutations lie within the relatively short C-terminal intracellular G-protein binding domain, and one truncation mutation occurs at the end of Exon 3, evoking the loss of Exon 4. Although not highly ranked among carcinogenic genes (**Figure 1B**), the OXTR protein does contribute to the regulation of proliferation and migration in a variety of different tissues (Cassoni et al., 2001), with a special emphasis on the Exon 4-encoded C-terminus.

In this study we have made use of the human liposarcoma cell line MLS-402, which we tested for endogenous *OXTR* expression and found it to be below a reliable detection level using qPCR ($C_q > 45$, data not shown). However, basal low-level expression of endogenous *OXTR* cannot be excluded. A lentiviral construct was transduced containing the human *OXTR* (based on the sequence NM_001354654.1). To detect *OXTR* expression and monitor exon 4 expression, we labeled the N-terminus of the *OXTR* sequence with EGFP and the C-terminus with mCherry (**Figure 1C**). Expression efficiency levels between different clones were determined by digital PCR (dPCR). Clone G2 showed the highest level of *OXTR* transcript (**Figure 1D**) and was, therefore, chosen for further experiments. The clonal culture will be from here on referred to as MLS-G2. Correct expression of the OXTR protein was visualized by live cell microscopy (**Figure 1E**), and correlative light electron microscopy (CLEM, **Figure 1F**), showing mostly membrane expression, with some perinuclear vesicular accumulations, representing the normal expression/recycling cycle of the OXTR (Conti et al., 2009). The general proliferation rate and morphology was identical to the mother cell line MLS-402, indicating no deleterious effects of the *OXTR* gene insertion. When stimulated under classical 2D conditions with 100 nM OXT or the specific OXTR agonist TGOT (100 nM), proliferation rates dropped significantly, indicating a correct membrane insertion of a functional receptor (**Figure 1G**). Moreover, cell viability determined by the ATP content decreased significantly compared to vehicle-treated cells (**Figure 1H**), again indicating a functional OXTR and an anti-proliferation effect of OXT in the MLS-G2 cell line. In line with an anti-proliferative effect in 2D culture, average nucleus size, a rough indicator for cell division (Webster et al., 2009) remained constant (**Figure 1I**).

Next, we generated spheroids from MLS-G2 cells to determine the effects of OXT and other OXTR ligands, namely Atosiban and TGOT, on basic cellular processes in a 3D environment. MLS-G2 cells begin spheroid formation already after 6–8 h and show fully formed spheroids after 24 h. Pilot experiments revealed that the spheroids are stable for 7 days and disintegrate thereafter, but already stop responding to treatment after 3 days (**Supplementary Figure 1A**). Based on those data, we designed our experiments accordingly to encompass 24 h of treatment where possible, or 3 days of treatment maximum. Therefore, our treatment (ligands and Gapmers) is present during the formation of spheroids, with Gapmers preceding the presence of ligands for 2 h. To control for transfection artifacts, we employed a non-specific negative control (n.c.) Gapmer and evaluated the Gapmer efficacy by dPCR with Exon 4/or Exon 2–3-specific probes, and mCherry and EGFP-specific quantitative Western blot (**Supplementary Figures 1B,C**).

When transfected with n.c. Gapmers and treated with 100 nM OXT for 24 h, spheroid volume and area increased significantly at 56% and 23%, respectively, compared to n.c./vehicle-treated spheroids (black bars, **Figures 2A,B**). In case spheroids deviate from a sphere-like shape, volume calculation becomes unreliable. However, the spheroid surface area can be accurately measured independent of the spheroid shape and represents a sound method to assess spheroid size. Sphericity, which would allow volume calculation in all spheroids, was not evenly distributed among the groups. When compared between n.c. and Gapmer treated spheroids, regardless of the ligand treatment, the sphericity of spheroids was increased in Gapmer-treated cells (**Figure 2C**). Consequently, vehicle (VEH, H_2O) treatment causes cells to form dense clusters with a macroscopic spherical shape but blocking the OXTR with Gapmers induces a less dense cell cluster displaying an irregular macroscopic shape.

Furthermore, the number of nuclei per spheroid, indicative of cell count, was not increased by the 100 nM OXT treatment (**Figure 2D**). In addition, nucleus size, indicative of increased cell size to account for increased spheroid size, was not increased by 100 nM OXT (**Figure 2E**). If spheroid size increases, but neither cell number nor cell size increases, the only possible explanation is a decreased cell density within the spheroid.

10.3389/fncel.2022.1000538

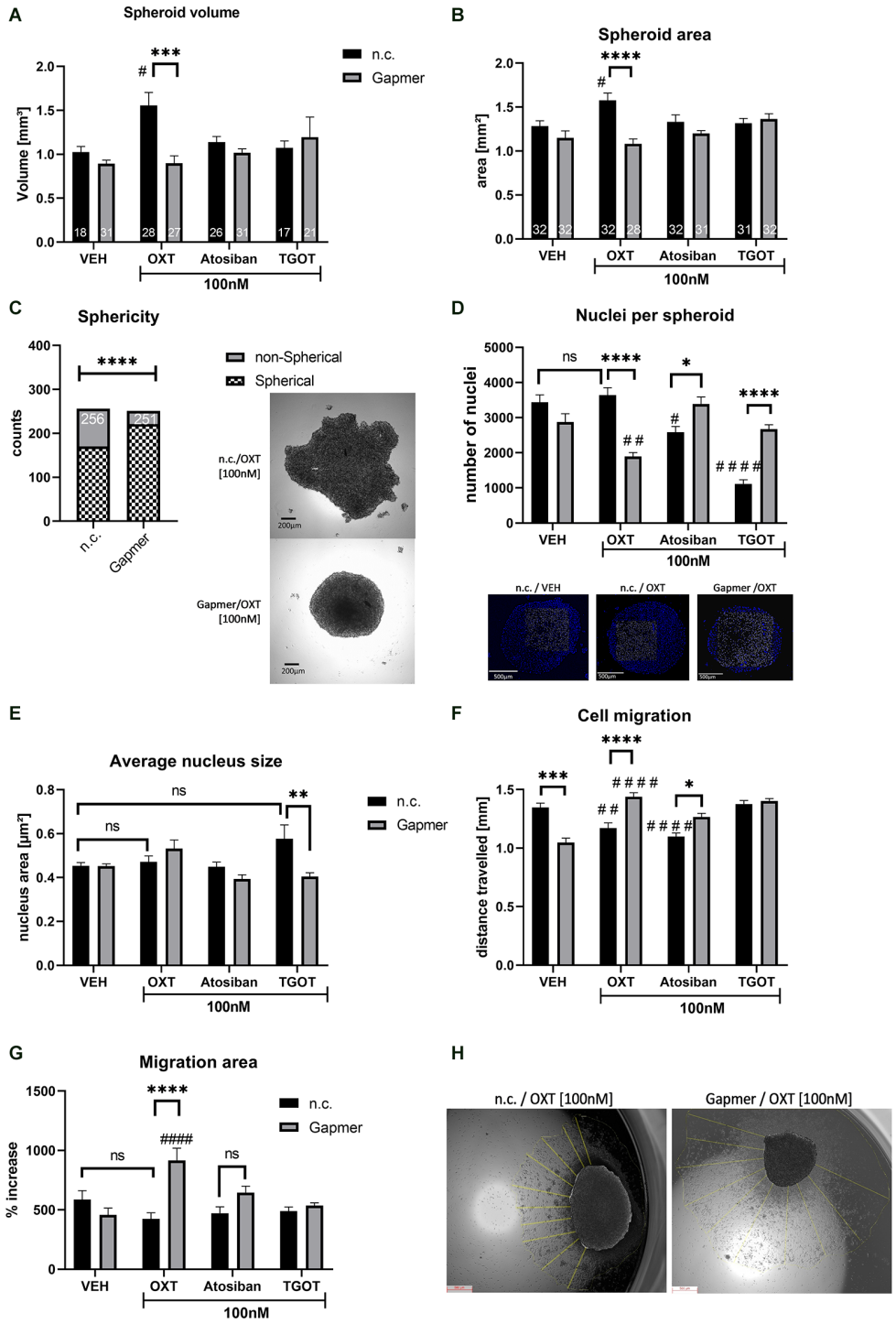

FIGURE 2
Effects of OXTR truncation and ligand treatment (OXT, Atosiban, TGOT) on cells cultured 3D in spheroids. Legend for all graphs: # = significant vs. the respective VEH control; * = significant vs. respective ligand treatment; data represented as mean + SEM; n.s. = not significant; n.c. = negative control Gapmer; Gapmer = OXTR-specific Gapmers inducing exon 4 skipping. **(A)** Spheroid volume is increased 1.5-fold by 100 nM OXT (p = 0.0191), an effect that is reversed by Gapmer pre-treatment (p = 0.0001). 100 nM Atosiban or 100 nM TGOT have no effect on spheroid volume (two-way ANOVA, Gapmer × Ligand treatment, significant interaction $F_{(3,191)}$ = 4.865, p = 0.0028, Tukey *post hoc* correction, only spheroids with sphere-like shape are included, resulting in = 17–31, as indicated in bars). **(B)** Spheroid area corroborates the validity of the spheroid volume data. 100 nM OXT increases the spheroid surface area to ∼1.6 mm^2, Gapmer pre-treatment reverses this increase to basal
(*Continued*)

FIGURE 2 (Continued)
levels (~1.3 mm^2, two-way ANOVA, Gapmer × ligand treatment, significant interaction $F_{(3,242)} = 5.933$, $p = 0.0006$, Tukey *post hoc* correction, $^{\#}p = 0.031$, $^{****}p < 0.0001$, $n = 28–31$, as indicated in bars). 100 nM of Atosiban and TGOT have no effect on the spheroid surface area. **(C)** Sphericity of spheroids indicates the ability to form proper cell-cell contacts and therefore round spheroids. All n.c. treated spheroids combined show a lower number of spherical spheroids than all Gapmer-treated spheroids combined, indicating an overall effect of the OXTR-intracellular domain on cell-cell contacts (Chi-square test, df = 33.64, 1; $p < 0.0001$, $z = 5.8$, two-sided Fisher's exact test $p < 0.0001$; $n = 251–256$, as indicated in bars). **(D)** The number of nuclei in spheroids indicates cell count and therefore proliferation rate. 100 nM n.c./OXT-treated spheroids do not show an increased nucleus count per spheroid, but a significant decrease in Gapmer/OXT-treated spheroids compared to Gapmer/VEH ($p = 0.0057$) and n.c./OXT-treated spheroids ($p < 0.0001$). 100 nM Atosiban decreases cell count significantly ($p = 0.0257$), and Gapmer treatment reversed this effect back to basal levels ($p = 0.043$). 100 nM TGOT exerted the strongest effect on cell count by reducing nuclei per spheroid to one-third of the VEH levels ($p < 0.0001$), but Gapmer treatment reversed this effect to basal levels ($p < 0.0001$ vs. n.c./TGOT). Two-way ANOVA, Gapmer × ligand treatment, significant interaction $F_{(3,72)} = 33.57$, $p < 0.0001$, Tukey *post hoc* correction, $n = 10$. **(E)** Average nucleus size indicates cell proliferation or cell death. No effect of the 100 nM OXT, Atosiban, or TGOT treatment was detectable, however, Gapmer pre-treatment significantly decreased average nucleus size of TGOT treated cells ($p = 0.0044$). Two-way ANOVA, Gapmer × ligand, significant interaction $F_{(3,72)} = 5.127$, $p = 0.0029$, $n = 10$. **(F)** Cell migration is inhibited by OXTR activation. 100 nM of OXT ($p = 0.0067$, black bar) and Atosiban ($p < 0.0001$, black bar) reduce the distance traveled by ~300 μm. Gapmer pre-treatment under VEH conditions reduces cell migration significantly ($p < 0.0001$, gray bar), but increases the distance traveled compared to its respective ligand treatment (OXT $p < 0.0001$; Atosiban $p = 0.01$) and to its respective VEH control (OXT $p = 0.0067$; Atosiban $p < 0.0001$). Two-way ANOVA, Gapmer × ligand treatment, significant Interaction $F_{(3,632)} = 26.93$; $p < 0.0001$, Tukey *post hoc* correction, $n = 8$ biological replicates, 10 technical replicates per biological replicate. **(G)** Migration area is assessed by measuring the area of the outgrown cell layer, which corroborates the cell migration data. Gapmer pre-treatment increases the cells' ability to migrate, resulting in a larger area covered in Gapmer/OXT-treated spheroids compared to the n.c./OXT group ($p < 0.0001$), or to the n.c./VEH group ($p < 0.0001$). Two-way ANOVA, Gapmer × ligand treatment, significant interaction $F_{(3,56)} = 9.298$, $p < 0.0001$, Tukey *post hoc* correction, $n = 8$. **(H)** Visualization of the migrated cell layer originating from the mother spheroid. Cell migration was measured from the overlayed day 0 spheroid border to the border of the cell layer, as indicated by yellow lines.

Indicative of altered cell-matrix attachment, when placed on an adherent surface, OXT-treated cells migrated less far from their spheroid than VEH-treated cells. Decreased cellular migration was determined as the average migration distance the cells traveled from their spheroid (Figure 2F) and as the area of the cell layer surrounding the spheroid (Figures 2G,H).

Interestingly, the effects of OXT on spheroid volume and area were blocked by the OXTR specific Gapmers (gray bars, Figures 2A,B) that induced exon 4 skipping and loss of the intracellular G-protein binding domain of the OXTR. Consequently, the cells' ability to attach to the extracellular matrix was restored, resulting in increased migration distance and area of Gapmer/OXT-treated cells, compared to Gapmer/VEH-treated cells (Figures 2F,G).

Atosiban acts as a biased OXTR agonist that selectively activates the $G\alpha_i$-protein but antagonizes the $G\alpha_q$ OXTR and V1a receptors. In our cell model, n.c./Atosiban [100 nM] treatment does neither alter the spheroid size, nor nucleus size, however, the number of nuclei in a spheroid is reduced, indicating a reduced proliferation rate (Figure 2D). Cellular migration, as measured by distance traveled was also significantly reduced (Figures 2D,F). Taken together, the actions of Atosiban *via* the $G\alpha_i$-protein pathway reduce proliferation in a spheroid and inhibit cellular migration.

When pre-treated with the OXTR-specific Gapmers, Atosiban can no longer activate the $G\alpha_i$-pathway and is unable to reduce proliferation (Figure 2D, gray bars) or cell migration (Figure 2F, gray bars), highlighting the importance of the intracellular G-protein binding domain for this effect. The absence of an effect on spheroid size indicates that the cell-cell attachment, as altered by OXT, depends on an alternative G-protein pathway, e.g., $G\alpha_q$ or $G\alpha_o$.

In contrast to OXT but in accordance with Atosiban, TGOT did not alter spheroid volume or area (Figures 2A,B black bars). This difference indicates slight binding differences between OXTR agonists, as discussed below in the discussion section.

However, 100 nM TGOT was most effective in reducing nuclei count per spheroid to an about three-fold reduction (Figure 2D, black bar), with a non-significant trend towards increased nucleus size (Figure 2E, black bar). Gapmer pre-treatment reversed both effects, i.e., increased the nuclei count to basal levels (Figure 2D, gray bar) and significantly decreased the average nucleus size, compared to n.c./TGOT treated spheroids, back to basal levels (Figure 2E, gray bar).

In contrast to OXT or Atosiban treatment, the concentration of 100 nM TGOT was not effective to alter cellular migration (Figures 2F,G). As shown in the following Figure 3, the higher TGOT concentration of 1 μM decreased cellular migration, indicating that TGOT is indeed effective, but only at higher concentrations.

Similar to the 100 nM treatment regimen (see Figure 2A), treating spheroids with 1 μM OXT increased spheroid volume, but 1 μM Atosiban and TGOT had no effect (Figure 3A). The OXT-induced volume increase was blocked by Gapmer pre-treatment and reversed the volume back to basal levels. However, pre-treatment with Gapmers increased the volume in Atosiban and TGOT treated spheroids. This indicates: (1) that the OXT-induced effect is mediated by the intracellular G-protein domain of the OXTR; and (2) that 1 μM and 100 nM OXT activate a unique pathway that is disregarded by the other ligands in both concentrations. Spheroid area measurements corroborated the spheroid volume

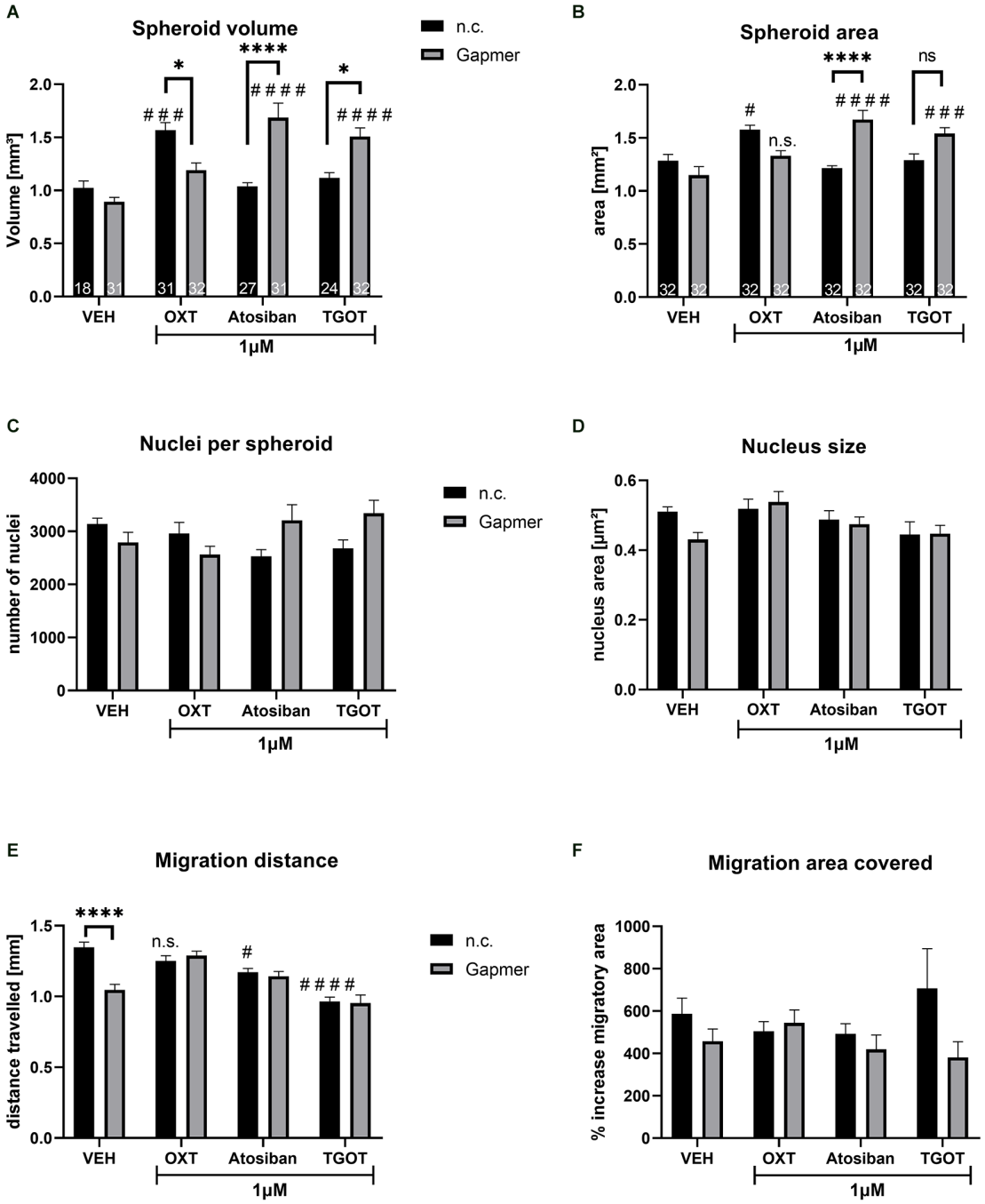

FIGURE 3
Spheroid size, nucleus count and size, and cellular migration caused by 1 μM of ligand treatment (OXT, Atosiban, TGOT) under negative control (n.c.) or OXTR Gapmer (Gapmer) conditions. Legend for all graphs: # = significant vs. the respective VEH control; * = significant vs. respective ligand treatment; n.s. = not significant; data represented as mean + SEM; n.c. = negative control Gapmer; Gapmer = OXTR-specific Gapmers inducing exon 4 skipping. **(A)** Spheroid volume was not affected by Gapmer pre-treatment under VEH conditions. When stimulated by n.c./OXT, spheroid volume increased significantly compared to n.c./VEH ($p = 0.0005$), and Gapmer pre-treatment reversed the spheroid volume back to basal levels ($p = 0.0108$). n.c./Atosiban treatment did not alter spheroid volume, but Gapmer pre-treatment increased it 1.68-fold ($p < 0.0001$) compared to n.c./Atosiban and Gapmer/VEH. The treatment of n.c./TGOT did not affect spheroid volume, but pre-treatment with Gapmers significantly increased it compared to Gapmer/VEH ($p < 0.0001$) and n.c./TGOT ($p = 0.0161$). Two-way ANOVA, Gapmer × ligand treatment, significant interaction $F_{(3,218)} = 18.10$, $p < 0.0001$; $n = 18–27$ as indicated in bars. **(B)** Spheroid area data parallels spheroid volume, with no effect of Gapmer pre-treatment under VEH conditions, but increased spheroid area by n.c./OXT stimulation ($p = 0.0150$) compared to n.c./VEH. Gapmer pre-treatment reversed the effect so that the spheroid area is no longer significantly different from the Gapmer/VEH. However, unlike

(*Continued*)

FIGURE 3 (Continued)
spheroid volume, the effect on the area is too small to be significantly different from the n.c./OXT group. Neither n.c./Atosiban nor n.c./TGOT altered spheroid area, but Gapmer pre-treatment increased it significantly ($p < 0.0001$ and $p = 0.0002$). Two-way ANOVA, Gapmer × ligand treatment, significant interaction $F_{(3, 248)} = 14.94$, $p < 0.0001$; $n = 32$. **(C)** The number of nuclei per spheroid was not affected by 1 μM treatment of OXT, Atosiban, or TGOT. **(D)** The size of nuclei within spheroids was not affected by 1 μM of OXT, Atosiban, or TGOT. **(E)** Migration distance was decreased by the Gapmer treatment ($p < 0.0001$) only in the VEH group, but in none of the other treatment groups. Atosiban ($p = 0.0217$) and TGOT ($p < 0.0001$) reduced the migration distance significantly and Gapmer pre-treatment had no effect on this reduction. **(F)** A significant overall effect of Gapmer treatment on migration area was detected in the two-way ANOVA, however, none of the comparisons after Tukey *post hoc* correction were significant. Two-way ANOVA, ligand × Gapmer treatment, Gapmer treatment $F_{(1,55)} = 4.330$; $p = 0.0421$, $n = 8$.

data (**Figure 3B**), granting the validity of the assessment method. Cellular proliferation within the spheroid was not affected by the 1 μM treatment with OXT, Atosiban, or TGOT, as indicated by the number (**Figure 3C**) and size (**Figure 3D**) of spheroidal nuclei. Migration from the spheroid onto a 2D surface was reduced by the Gapmer pre-treatment under VEH conditions, and by 1 μM Atosiban and TGOT stimulations (**Figure 3E**). However, Gapmer pre-treatment had no effect on the Atosiban and TGOT-induced reduction. This seemingly contradictory result must be taken with caution, as the slightly different assessment method of "migration area covered" (**Figure 3F**) revealed only an overall significant effect of the Gapmer treatment but did not detect any significant difference between the groups. This inconsistency suggests that the mathematical significant effects of the 1 μM OXT, Atosiban, and TGOT treatment are biologically questionable.

A top-down view of spheroids is insufficient to correctly interpret the true 3-dimensional cellular organization of the spheroid, therefore we employed different methods to visualize the shape and consistency of the spheroid. As shown in the schematic illustration of **Figure 4A**, the growth of the spheroids is dependent on the treatment with OXT. These differences can be detected with digital 3D microscopy, which revealed the true surface shape of the spheroids by Z-stack stitching of 200 × magnification images and digital reconstruction in three dimensions. This approach also allows to visualizing ripples and wrinkles on the spheroid surface that would be invisible in a top-down view. As expected, VEH-treated spheroids show a smooth, "ball-like" shape, whereas 100 nM OXT-treated spheroids reveal a rough and uneven surface. As an example of the importance of 3D-imaging, the representative right image in **Figure 4B** of the 100 nM OXT-treated spheroid shows a small hump on the left side, which would have been missed with the other techniques.

For further investigations, the spheroids were cut in ultrathin sections from two perpendicular planes (diagonal and longitudinal) to evaluate them by transmission electron microscopy (TEM). These orientations of the electron micrographs reveal the overall shape of the spheroids, as well as the cell density below the spheroid surface. The untreated (VEH) spheroids show a round, "ball-like" shape, a high cell density, and very minute extracellular space, except for the apoptotic zone at the near-center of the spheroid (red circle, **Figures 4C,D**). The nutrient and oxygen supply decreases towards the inner zones of the spheroid, creating a survival gradient from the proliferating outer zone towards the inner-most apoptotic center (Ryu et al., 2019). In contrast, OXT-treated spheroids show a decreased cellular density and evenly distributed extracellular spaces (see **Supplementary Figure 2** for quantification of the extracellular space and **Supplementary Figure 3** for the spatial distribution of tight junctions within a spheroid). The macroscopic shape of the OXT-treated spheroid deviates from the "ball-like" shape of the VEH-treated spheroids, thereby increasing its surface. In addition, higher magnification reveals the widespread OXT-induced formation of tight junctions and protrusions of the "luminal" side of the cells that reach into an enlarged extracellular space. This indicates well-organized cell-cell contacts, which level out the nutrient and oxygen gradient even further, resulting in an absent apoptotic zone (**Figures 4E,F**).

Lastly, by using a kinase phosphorylation profiler assay we evaluated whether OXT influences the regulation of signaling cascades associated with cell survival and cell-cell adhesion. Most notably, OXT increased the phosphorylation of Akt 1/2/3 S47 by 63%, whilst it dephosphorylated heat shock protein 27 (HSP27) by 47% (**Figure 5A**). For a better understanding, we summarized the OXT-induced intracellular pathways and their outcomes on cell-cell interaction in a schematic overview (**Figure 5B**).

Discussion

The neuropeptide OXT has been implicated in a multitude of behavioral and physiological effects, and our understanding of the intracellular signaling cascades that are responsible for those effects is ever-growing (Grinevich and Neumann, 2021). However, the extent to which OXT affects intracellular processes is yet underappreciated, as evidenced by our and other groups' recent discoveries (Zatkova et al., 2019; Meyer et al., 2020, 2022; Reichova et al., 2020; Salehi et al., 2021). For instance, OXT modulates cellular morphology, which is one important aspect of intercellular communication, especially in neurons and astrocytes (Meyer et al., 2018; Falougy et al., 2019). Cellular ATP content and mitochondrial respiration rate, which support morphological rearrangements, are further enhanced by OXTR-induced signaling cascades (Meyer et al.,

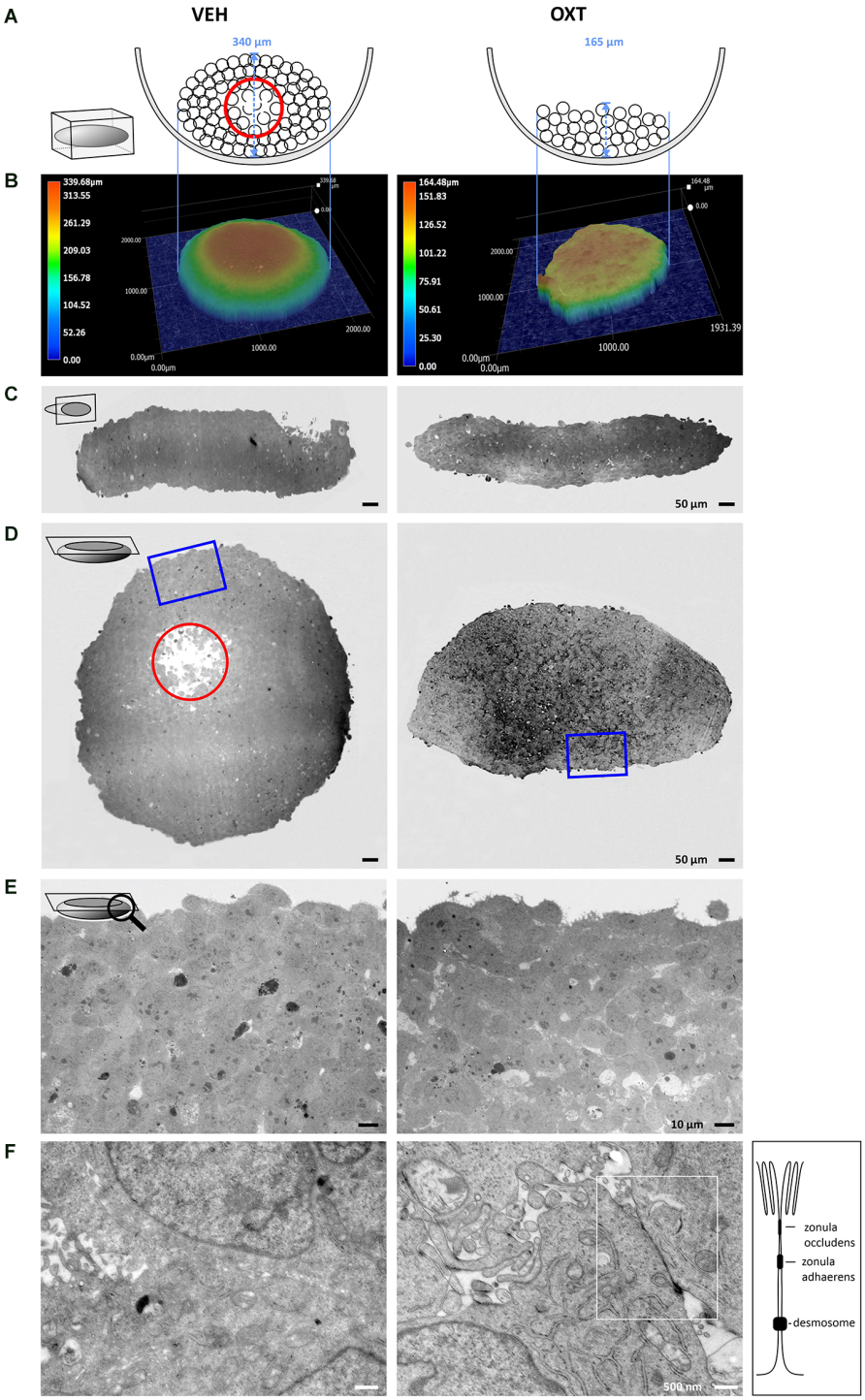

FIGURE 4
Images of VEH-treated (left column) vs. OXT-treated (right column, 100 nM for 24 h) spheroids shown in different orientations and magnification using TEM and digital 3D-microscopy. **(A)** Schematic representation of the OXT-induced effect on spheroid formation. The U-shaped well bottom is shown in the side-view. Black circles represent individual cells, a red circle indicates the apoptotic zone within the round spheroid. Please note the absence of an apoptotic zone in the flat OXT-treated spheroid. **(B)** Representative 3D images of VEH vs. OXT-treated spheroids. VEH-treated spheroids resemble a gravity-condensed ball-shape, whereas OXT-treated spheroids are irregular in shape and less densely packed. **(C)** Diagonal 250× TEM micrographs of 70 nm sections of VEH or OXT-treated spheroids. VEH-treated spheroids appear more uniform, indicating a reduced intercellular space, whereas OXT-treated spheroids show clear intercellular spacing. **(D)** Longitudinal 250× micrographs of 70 nm sections of the
(*Continued*)

FIGURE 4 (Continued)
identical spheroids used in **(C)**. The red circle indicates the apoptotic zone, which is only apparent in the VEH-treated spheroid; the blue square indicates the magnified zone in **(E)**. **(E)** 400x magnified micrographs of the spheroid shown in **(D)**. VEH-treated spheroids show a high cell density with sparse intercellular spacing, whereas OXT-treated spheroids show a less densely packed cell clustering. **(F)** 12,000x magnification reveals atypical and barely distinguishable cell-cell contacts in VEH-treated spheroids, but very regular and evenly-distributed classical tight junctions in OXT-treated spheroids. Additional TEM micrographs showing more OXT-induced tight junctions or the lack thereof in VEH-treated spheroids can be provided upon request.

2020). Those neuron-specific OXT effects are translatable to other cell types, especially cancer cells, where OXT affects proliferation and cellular migration in a cell-type-specific way (Cassoni et al., 2004; Cattaneo et al., 2008). As mentioned in the introduction, it is nearly impossible to predict the effect OXT has on a specific cell type. However, what makes up the difference between cell types that causes OXT to act in sometimes diametrical opposing ways is yet unknown. One aspect to solve this issue could be the removal of culturing artifacts. While most of the early studies on OXT and cancer have been conducted in classical two-dimensional cultures (Cassoni et al., 2004), we know nowadays that a 3D environment and cell-matrix interactions alter basic cellular characteristics and can affect the cellular response to certain stimuli (Jensen and Teng, 2020; Pandamooz et al., 2020). Consequently, we chose in our study a cellular model consisting of a cancer type that shows OXTR dysregulation, i.e., liposarcoma cells, and a 3D spheroid culturing method, which helps to reduce and replace *in vivo* animal experiments, and allows to monitor cell-cell interaction (tight junction formation) in a natural environment. The cellular assays we ran with our liposarcoma spheroids, e.g., proliferation or migration, are not only meaningful for metastases formation in cancer biology, but also for neuronal migration and survival in the brain, wound healing, etc. In that sense, we hope that this study prompts further research into OXT-induced effects in a 3-dimensional culture setting with other cell types.

Since Gerald Gimpls' and Falk Fahrenholzs' review about the oxytocin receptor in 2001 (Gimpl and Fahrenholz, 2001), according to PubMed 240 articles have been published that address "oxytocin receptor signaling" and the binding of different types of G-proteins upon exposure to different ligand concentrations or biased agonists (Busnelli and Chini, 2018; Jurek and Neumann, 2018). Those different types of G-proteins, namely $G\alpha_i$, $G\alpha_q$, and $G\alpha_o$, activate different sets of signaling cascades, including the transactivation of other receptors (EGFR; Blume et al., 2008) or channels (TrpV1; van den Burg et al., 2015). The most commonly studied OXTR-coupled pathway is the MAPK pathway, consisting of ras, raf, MEK1/2, and ERK1/2 (Blume et al., 2008; Jurek et al., 2012, 2015), acting on downstream transcription factors like CREB (Tomizawa et al., 2003; Jurek et al., 2015) and MEF2A (Meyer et al., 2018, 2020; Winter et al., 2021). Here, in this study, we aimed to broaden the scope of OXTR-coupled pathways by using a kinase array, which revealed a strong activation of the Akt (also known as protein kinase B) pathway. Akt is known to phosphorylate the transcription factor CREB, which drives the expression of survival genes (Walton and Dragunow, 2000), but is also involved in proliferation, metabolism, and angiogenesis (Hoxhaj and Manning, 2020). Closely related to the Akt pathway is the heat shock protein 27 (HSP27), which directly orchestrates the formation of filamentous actin (F-actin). F-actin is a prerequisite for coupling to the β-integrin complex that connects the cell to the extracellular matrix (ECM; Gerthoffer and Gunst, 2001). We have previously shown that OXT treatment reduces β-integrin protein expression (Meyer et al., 2020) and that it reduces the formation of F-actin fibers (unpublished personal communication with Prof. Dr. Sareh Pandamooz). Consequently, we can now provide the full pathway from the activated OXTR, to reduced HSP27 phosphorylation, reduced F-actin formation, and reduced β-integrin expression, ultimately causing diminished cellular migration.

In addition, we are able to add another novel aspect to the OXTR-coupled cascades, which are the STAT1–5 transcription factors. The observed OXT-induced downregulation of STAT proteins likely results in a downregulation of HSP27 protein, since HSP27 expression depends on active STAT transcription factors. This adds another layer of regulatory control of OXT-induced signaling cascades over cellular effects like F-actin formation, β-integrin function, and finally cellular migration.

Another aspect of intercellular effects was the OXT-induced formation of tight junctions between cells of the treated spheroid, unlike in VEH-treated spheroids, where densely packed cell clusters seem to only be brought to close proximity by gravity. We also describe for the first time the clear formation of tight junctions in OXT-treated spheroids, indicating a polarization of the cells towards a defined extracellular space, with a "luminal" and a "basal" side of the cells, a process described as mesenchymal to epithelial transition (MET; Jayachandran et al., 2021). This OXT-induced MET counteracts the opposing epithelial to mesenchymal transition (EMT), which generally occurs during the regular (untreated) formation of spheroids (Jeon et al., 2017). Despite the irregular shape of the OXT-treated spheroids on a macroscopic level, 12,000× magnification using TEM reveals regular and functional tight junctions between cells of the spheroid, and no apoptotic zone in the center of the spheroid. It is tempting to speculate that the formation of highly functional tight junctions and a surrounding enlarged extracellular space ("lumen") and consequently a polarized cell morphology accelerates the nutrient transport and gas exchange within the spheroid, preventing the formation of an apoptotic zone at the inner-most

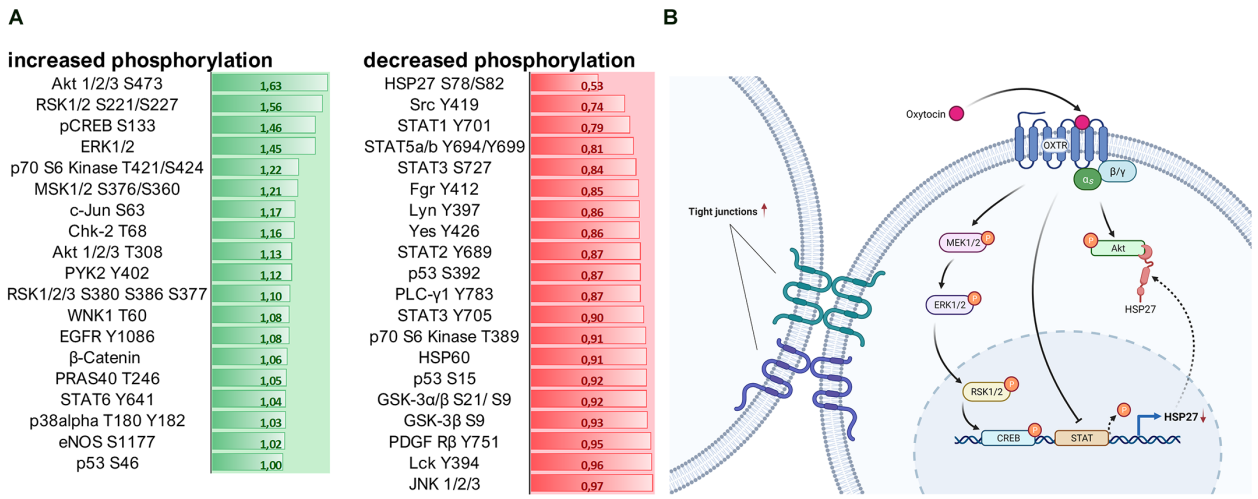

FIGURE 5
(A) Assessment of 100 nM OXT-induced signaling cascade activation by quantification of kinase phosphorylation. Data is shown in fold change (green = increase; red = decrease) compared to basal VEH-treated cells. A fold change of greater than ± 0.2 is considered relevant. Signaling cascades involved in cell survival are upregulated, and cascades involved in cell-cell adhesion and cell-matrix interaction are downregulated. **(B)** Schematic overview of the intracellular signaling cascades activated by the OXTR and their effect on tight junction formation. Created with www.BioRender.com.

core of the spheroid. This process is of special interest for the treatment of degenerative diseases where cells lose polarity, cell-cell contacts, and undergo apoptosis, e.g., as it is the case in the breakdown of the blood-brain barrier (Knox et al., 2022). Another pathological aspect that is affected by cell-cell contacts and cell polarity is metastatic tumor formation, where single cells undergo EMT, detach from the primary tumor, and invade other organs or tissues *via* the bloodstream (Ben Amar et al., 2022). As OXT opposes the EMT by inducing the formation of tight junctions and also inhibits cellular migration, it might be helpful to consider its use as an adjuvant treatment.

Having identified tight junction formation in OXT-treated spheroids by TEM micrographs, this study only contains a limited methodological approach to further analyze tight junctions, a limitation that we will address in subsequent studies.

Despite the clear effect of OXT on our spheroid model, OXT is a promiscuous molecule which can also bind other receptors (Chini et al., 2008; Nersesyan et al., 2017), therefore it is of utmost importance to control for OXTR activation with a specific and highly effective inhibitor. Pharmacological inhibitors are notorious for being unspecific for their intended target (Manning et al., 2008), and a mere knockdown of the OXTR increases the likelihood of OXT or even TGOT binding to vasopressin receptors (Sala et al., 2013) or TrpV1 channels (Nersesyan et al., 2017). In addition, the binding of different OXTR agonists can produce varying outcomes: for instance, in contrast to OXT but in accordance with Atosiban, TGOT did not alter spheroid volume or area (**Figures 2A,B** black bars). As TGOT has a slightly lower receptor affinity than OXT (Ki: 0.79 nM OXT vs. 6.62 nM TGOT; Chini and Manning, 2007), a higher than 100 nM TGOT concentration is required to prompt the same G-protein pathways as OXT. As previously published (Busnelli and Chini, 2018), 90–100 nM OXT is more likely to activate the Gαo-pathway, whereas concentrations between 30 and 90 nM OXT activate the $G\alpha_i$-pathways. As TGOT has a lower affinity for the OXTR (Busnelli et al., 2013), 100 nM TGOT is more likely to activate the $G\alpha_i$-pathway. This pathway, as observed with Atosiban, does not affect cell-cell attachments, and therefore spheroid size.

To overcome those issues, we designed a novel approach to inhibit the OXTR signaling by transiently removing the intracellular G-protein-coupling domain from the receptor *via* Gapmer-induced exon skipping, which leaves the transmembrane and ligand binding domain intact. In that way, we are able to specifically block OXTR-signaling, without increasing the likelihood of the supplemented OXT binding to other receptors. Moreover, this approach is highly selective for the OXTR against the vasopressin receptors, as it relies on Gapmer binding in the *OXTR*-specific sequence of exon 4, unlike pharmacological inhibitors which face the difficult-to distinguish similarities between OXTR and vasopressin receptors on the protein level. We have previously used Gapmers to induce alternative splicing and subsequent exon-skipping to alter the characteristics of another GPCR, the corticotropin releasing factor receptor 2α (CRFR2α) as well asthe TGF-SSreceptor and confirmed their applicability *in vivo* (Peters et al., 2021; Winter et al., 2021). Therefore, we

hope to prompt further use of this highly efficient and specific OXTR inhibitor for basic and applied research *in vitro* as well as *in vivo*.

In summary, this study reveals some novel aspects of OXTR-coupled intracellular signaling (STAT1-5, HSP27, Akt) that determine the ability of cells to form tight junctions within 3-dimensional spheroids and to migrate on a 2-dimensional surface. We have narrowed down the effects of 100 nM and 1 μM OXT to the OXTR, as Gapmer-induced exon skipping efficiently diminished or even reversed the effects of OXT. We also advocate for the use of digital PCR (dPCR) to reliably quantify small amounts of *OXTR* transcript, and the use of CLEM to visualize the OXTR protein on a subcellular level. Taken together, our data lays the foundation for future OXT-related studies in the field of (neuro-) degenerative diseases or tumor formation employing 3D-culturing methods like spheroids or organoids.

Data availability statement

The original contributions presented in the study are included in the article/**Supplementary material**, further inquiries can be directed to the corresponding author.

Author contributions

BJ, NS, and LD contributed to the conception and design of the study. BJ wrote the first draft of the manuscript. LD wrote sections of the manuscript. All authors contributed to the article and approved the submitted version.

Funding

Funding was provided by the Angela Schötz Keilholz foundation (grant number 3/2021).

Acknowledgments

We thank Prof. Michael Krahn for providing nanogold-antibodies, Veronica Kurbel for technical support creating the MLS-G2^{OXTR} cell line (the "Kurbelcells"), Stefanie Stapfer and Nicole Feichtgruber for scientific support with spheroid experiments.

References

Akerlund, M., Bossmar, T., Brouard, R., Kostrzewska, A., Laudanski, T., Lemancewicz, A., et al. (1999). Receptor binding of oxytocin and vasopressin antagonists and inhibitory effects on isolated myometrium from preterm and term pregnant women. *Br. J. Obstet. Gynaecol.* 106, 1047–1053. doi: 10.1111/j.1471-0528.1999.tb08112.x

Atat, O. E., Farzaneh, Z., Pourhamzeh, M., Taki, F., Abi-Habib, R., Vosough, M., et al. (2022). 3D modeling in cancer studies. *Hum. Cell* 35, 23–36. doi: 10.1007/s13577-021-00642-9

Ben Amar, D., Thoinet, K., Villalard, B., Imbaud, O., Costechareyre, C., Jarrosson, L., et al. (2022). Environmental cues from neural crest derivatives act as

Conflict of interest

The authors declare that the research was conducted in the absence of any commercial or financial relationships that could be construed as a potential conflict of interest.

Publisher's note

All claims expressed in this article are solely those of the authors and do not necessarily represent those of their affiliated organizations, or those of the publisher, the editors and the reviewers. Any product that may be evaluated in this article, or claim that may be made by its manufacturer, is not guaranteed or endorsed by the publisher.

Supplementary material

The Supplementary Material for this article can be found online at: https://www.frontiersin.org/articles/10.3389/fncel.2022.1000538/full#supplementary-material.

SUPPLEMENTARY FIGURE 1
(A) Lack of effect of different doses of OXT or TGOT on spheroid volume after 3 days of culturing. N numbers are indicated in bars, ligand concentration is indicated in x-axis. Data represented as mean + SEM. **(B)** dPCR-determined absolute copy numbers of OXTR transcript downregulated 10, 2, or 0.2 nM OXTR Exon 4-specific Gapmers by compared to negative control Gapmer (n.c.). Data represented as mean + SD. **(C)** Western Blot showing EGFP and mCherry expression in Gapmer or negative control (n.c.) treated spheroids. No difference in EGFP expression is detectable, while Gapmer treatment induced a 35% downregulation of mCherry compared to n.c.

SUPPLEMENTARY FIGURE 2
Evaluation of the area occupied between the cell membranes of neighboring cells (=extracellular space in a spheroid). A machine learning image segmenting approach revealed significantly increased extracellular space in OXT-treated spheroids. Normal distribution tested by Kolmogorov-Smirnov and Shapiro-Wilk test, two-tailed, unpaired t-test $p < 0.0001$, $t = 5{,}365$, n(control) = 15, n(OXT) = 35.

SUPPLEMENTARY FIGURE 3
Evaluation of spatial distribution of tight junction formation. The OXT-induced increase in extracellular space and tight junction formation is independent of the position within the spheroid. Tight junctions (OXT) or cell-cell borders (controls) are similar at the center, near center, or periphery of the spheroid.

SUPPLEMENTARY TABLE 1
List of studies queried for "OXTR" and associated sample number per study.

metastatic triggers in an embryonic neuroblastoma model. *Nat. Commun.* 13:2549. doi: 10.1038/s41467-022-30237-3

Blume, A., Bosch, O. J., Miklos, S., Torner, L., Wales, L., Waldherr, M., et al. (2008). Oxytocin reduces anxiety via ERK1/2 activation: local effect within the rat hypothalamic paraventricular nucleus. *Eur. J. Neurosci.* 27, 1947–1956. doi: 10.1111/j.1460-9568.2008.06184.x

Busnelli, M., Bulgheroni, E., Manning, M., Kleinau, G., and Chini, B. (2013). Selective and potent agonists and antagonists for investigating the role of mouse oxytocin receptors. *J. Pharmacol. Exp. Ther.* 346, 318–327. doi: 10.1124/jpet.113.202994

Busnelli, M., and Chini, B. (2018). Molecular basis of oxytocin receptor signalling in the brain: what we know and what we need to know. *Curr. Top. Behav. Neurosci.* 35, 3–29. doi: 10.1007/7854_2017_6

Cassoni, P., Fulcheri, E., Carcangiu, M. L., Stella, A., Deaglio, S., and Bussolati, G. (2000). Oxytocin receptors in human adenocarcinomas of the endometrium: presence and biological significance. *J. Pathol.* 190, 470–477. doi: 10.1002/(SICI)1096-9896(200003)190:4<470::AID-PATH550>3.0.CO;2-G

Cassoni, P., Marrocco, T., Deaglio, S., Sapino, A., and Bussolati, G. (2001). Biological relevance of oxytocin and oxytocin receptors in cancer cells and primary tumors. *Ann. Oncol.* 2, S37–S39. doi: 10.1093/annonc/12.suppl_2.s37

Cassoni, P., Sapino, A., Marrocco, T., Chini, B., and Bussolati, G. (2004). Oxytocin and oxytocin receptors in cancer cells and proliferation. *J. Neuroendocrinol.* 16, 362–364. doi: 10.1111/j.0953-8194.2004.01165.x

Cassoni, P., Sapino, A., Negro, F., and Bussolati, G. (1994). Oxytocin inhibits proliferation of human breast cancer cell lines. *Virchows Arch.* 425, 467–472. doi: 10.1007/BF00197549

Cassoni, P., Sapino, A., Papotti, M., and Bussolati, G. (1996). Oxytocin and oxytocin-analogue F314 inhibit cell proliferation and tumor growth of rat and mouse mammary carcinomas. *Int. J. Cancer* 66, 817–820. doi: 10.1002/(SICI)1097-0215(19960611)66:6<817::AID-IJC18>3.0.CO;2-#

Cattaneo, M. G., Chini, B., and Vicentini, L. M. (2008). Oxytocin stimulates migration and invasion in human endothelial cells. *Br. J. Pharmacol.* 153, 728–736. doi: 10.1038/sj.bjp.0707609

Cerami, E., Gao, J., Dogrusoz, U., Gross, B. E., Sumer, S. O., Aksoy, B. A., et al. (2012). The cBio cancer genomics portal: an open platform for exploring multidimensional cancer genomics data. *Cancer Discov.* 2, 401–404. doi: 10.1158/2159-8290.CD-12-0095

Chini, B., and Manning, M. (2007). Agonist selectivity in the oxytocin/vasopressin receptor family: new insights and challenges. *Biochem. Soc. Trans.* 35, 737–741. doi: 10.1042/BST0350737

Chini, B., Manning, M., and Guillon, G. (2008). Affinity and efficacy of selective agonists and antagonists for vasopressin and oxytocin receptors: an "easy guide" to receptor pharmacology. *Prog. Brain Res.* 170, 513–517. doi: 10.1016/S0079-6123(08)00438-X

Conti, F., Sertic, S., Reversi, A., and Chini, B. (2009). Intracellular trafficking of the human oxytocin receptor: evidence of receptor recycling via a Rab4/Rab5 "short cycle". *Am. J. Physiol. Endocrinol. Metab.* 296, E532–E542. doi: 10.1152/ajpendo.90590.2008

Falougy, H. E., Filova, B., Ostatnikova, D., Bacova, Z., and Bakos, J. (2019). Neuronal morphology alterations in autism and possible role of oxytocin. *Endocr. Regul.* 53, 46–54. doi: 10.2478/enr-2019-0006

Flynn, L. L., Mitrpant, C., Adams, A., Pitout, I. L., Stirnweiss, A., Fletcher, S., et al. (2021). Targeted SMN exon skipping: a useful control to assess in vitro and in vivo splice-switching studies. *Biomedicines* 9:552. doi: 10.3390/biomedicines9050552

Gao, J., Aksoy, B. A., Dogrusoz, U., Dresdner, G., Gross, B., Sumer, S. O., et al. (2013). Integrative analysis of complex cancer genomics and clinical profiles using the cBioPortal. *Sci. Signal.* 6:pl1. doi: 10.1126/scisignal.2004088

Gerthoffer, W. T., and Gunst, S. J. (2001). Invited review: focal adhesion and small heat shock proteins in the regulation of actin remodeling and contractility in smooth muscle. *J. Appl. Physiol. (1985).* 91, 963–972. doi: 10.1152/jappl.2001.91.2.963

Gimpl, G., and Fahrenholz, F. (2001). The oxytocin receptor system: structure, function and regulation. *Physiol. Rev.* 81, 629–683. doi: 10.1152/physrev.2001.81.2.629

Grinevich, V., and Neumann, I. D. (2021). Brain oxytocin: how puzzle stones from animal studies translate into psychiatry. *Mol. Psychiatry* 26, 265–279. doi: 10.1038/s41380-020-0802-9

Grotegut, C. A., Feng, L., Mao, L., Heine, R. P., Murtha, A. P., and Rockman, H. A. (2011). beta-Arrestin mediates oxytocin receptor signaling, which regulates uterine contractility and cellular migration. *Am. J. Physiol. Endocrinol. Metab.* 300, E468–E477. doi: 10.1152/ajpendo.00390.2010

Hoxhaj, G., and Manning, B. D. (2020). The PI3K-AKT network at the interface of oncogenic signalling and cancer metabolism. *Nat. Rev. Cancer* 20, 74–88. doi: 10.1038/s41568-019-0216-7

Huggett, J. F. (2020). The digital MIQE guidelines update: minimum information for publication of quantitative digital PCR experiments for 2020. *Clin. Chem.* 66, 1012–1029. doi: 10.1093/clinchem/hvaa125

Hurlemann, R. (2017). Oxytocin-augmented psychotherapy: beware of context. *Neuropsychopharmacology* 42:377. doi: 10.1038/npp.2016.188

Jayachandran, J., Srinivasan, H., and Mani, K. P. (2021). Molecular mechanism involved in epithelial to mesenchymal transition. *Arch. Biochem. Biophys.* 710:108984. doi: 10.1016/j.abb.2021.108984

Jensen, C., and Teng, Y. (2020). Is it time to start transitioning from 2D to 3D cell culture? *Front. Mol. Biosci.* 7:33. doi: 10.3389/fmolb.2020.00033

Jeon, S., Lee, H.-S., Lee, G.-Y., Park, G., Kim, T.-M., Shin, J., et al. (2017). Shift of EMT gradient in 3D spheroid MSCs for activation of mesenchymal niche function. *Sci. Rep.* 7:6859. doi: 10.1038/s41598-017-07049-3

Jurek, B., and Meyer, M. (2020). Anxiolytic and anxiogenic? How the transcription factor MEF2 might explain the manifold behavioral effects of oxytocin. *Front. Endocrinol. (Lausanne)* 11:186. doi: 10.3389/fendo.2020.00186

Jurek, B., and Neumann, I. D. (2018). The oxytocin receptor: from intracellular signaling to behavior. *Physiol. Rev.* 98, 1805–1908. doi: 10.1152/physrev.00031.2017

Jurek, B., Slattery, D. A., Hiraoka, Y., Liu, Y., Nishimori, K., Aguilera, G., et al. (2015). Oxytocin regulates stress-induced Crf gene transcription through CREB-regulated transcription coactivator 3. *J. Neurosci.* 35, 12248–12260. doi: 10.1523/JNEUROSCI.1345-14.2015

Jurek, B., Slattery, D. A., Maloumby, R., Hillerer, K., Koszinowski, S., Neumann, I. D., et al. (2012). Differential contribution of hypothalamic MAPK activity to anxiety-like behaviour in virgin and lactating rats. *PLoS One* 7:e37060. doi: 10.1371/journal.pone.0037060

Kaynig, V., Fischer, B., Muller, E., and Buhmann, J. M. (2010). Fully automatic stitching and distortion correction of transmission electron microscope images. *J. Struct. Biol.* 171, 163–173. doi: 10.1016/j.jsb.2010.04.012

Kim, J., Kang, S.-M., Lee, H.-J., Choi, S.-Y., and Hong, S.-H. (2017). Oxytocin inhibits head and neck squamous cell carcinoma cell migration by early growth response-1 upregulation. *Anticancer Drugs* 28, 613–622. doi: 10.1097/CAD.0000000000000501

Knox, E. G., Aburto, M. R., Clarke, G., Cryan, J. F., and O'Driscoll, C. M. (2022). The blood-brain barrier in aging and neurodegeneration. *Mol. Psychiatry* 27, 2659–2673. doi: 10.1038/s41380-022-01511-z

Li, D., Mastaglia, F. L., Fletcher, S., and Wilton, S. D. (2018). Precision medicine through antisense oligonucleotide-mediated exon skipping. *Trends Pharmacol. Sci.* 39, 982–994. doi: 10.1016/j.tips.2018.09.001

Manning, M., Stoev, S., Chini, B., Durroux, T., Mouillac, B., and Guillon, G. (2008). Peptide and non-peptide agonists and antagonists for the vasopressin and oxytocin V1a, V1b, V2 and OT receptors: research tools and potential therapeutic agents. *Prog. Brain Res.* 170, 473–512. doi: 10.1016/S0079-6123(08)00437-8

Meyer, M., Berger, I., Winter, J., and Jurek, B. (2018). Oxytocin alters the morphology of hypothalamic neurons via the transcription factor myocyte enhancer factor 2A (MEF-2A). *Mol. Cell. Endocrinol.* 477, 156–162. doi: 10.1016/j.mce.2018.06.013

Meyer, M., Jurek, B., Alfonso-Prieto, M., Ribeiro, R., Milenkovic, V. M., Winter, J., et al. (2022). Structure-function relationships of the disease-linked A218T oxytocin receptor variant. *Mol. Psychiatry* 27, 907–917. doi: 10.1038/s41380-021-01241-8

Meyer, M., Kuffner, K., Winter, J., Neumann, I. D., Wetzel, C. H., and Jurek, B. (2020). Myocyte enhancer factor 2A (MEF2A) defines oxytocin-induced morphological effects and regulates mitochondrial function in neurons. *Int. J. Mol. Sci.* 21:2200. doi: 10.3390/ijms21062200

Minuth, W. W., and Denk, L. (2015). Advanced fixation for transmission electron microscopy unveils special extracellular matrix within the renal stem/progenitor cell niche. *Methods Mol. Biol.* 1212, 21–37. doi: 10.1007/7651_2014_93

Muth, S., Fries, A., and Gimpl, G. (2011). Cholesterol-induced conformational changes in the oxytocin receptor. *Biochem. J.* 437, 541–553. doi: 10.1042/BJ20101795

Nersesyan, Y., Demirkhanyan, L., Cabezas-Bratesco, D., Oakes, V., Kusuda, R., Dawson, T., et al. (2017). Oxytocin modulates nociception as an agonist of pain-sensing TRPV1. *Cell Rep.* 21, 1681–1691. doi: 10.1016/j.celrep.2017.10.063

Pandamooz, S., Jafari, A., Salehi, M. S., Jurek, B., Ahmadiani, A., Safari, A., et al. (2020). Substrate stiffness affects the morphology and gene expression of

epidermal neural crest stem cells in a short term culture. *Biotechnol. Bioeng.* 117, 305–317. doi: 10.1002/bit.27208

Passoni, I., Leonzino, M., Gigliucci, V., Chini, B., and Busnelli, M. (2016). Carbetocin is a functional selective Gq agonist that does not promote oxytocin receptor recycling after inducing β-arrestin-independent internalisation. *J. Neuroendocrinol.* 28:n/a. doi: 10.1111/jne.12363

Peters, S., Kuespert, S., Wirkert, E., Heydn, R., Jurek, B., Johannesen, S., et al. (2021). Reconditioning the neurogenic niche of adult non-human primates by antisense oligonucleotide-mediated attenuation of TGFβ signaling. *Neurotherapeutics* 18, 1963–1979. doi: 10.1007/s13311-021-01045-2

Rajagopal, S., and Shenoy, S. K. (2018). GPCR desensitization: acute and prolonged phases. *Cell. Signal.* 41, 9–16. doi: 10.1016/j.cellsig.2017.01.024

Reichova, A., Bacova, Z., Bukatova, S., Kokavcova, M., Meliskova, V., Frimmel, K., et al. (2020). Abnormal neuronal morphology and altered synaptic proteins are restored by oxytocin in autism-related SHANK3 deficient model. *Mol. Cell. Endocrinol.* 518:110924. doi: 10.1016/j.mce.2020.110924

Reversi, A., Rimoldi, V., Brambillasca, S., and Chini, B. (2006a). Effects of cholesterol manipulation on the signaling of the human oxytocin receptor. *Am. J. Physiol. Regul. Integr. Comp. Physiol.* 291, R861–R869. doi: 10.1152/ajpregu.00333.2006

Reversi, A., Cassoni, P., and Chini, B. (2006b). Oxytocin receptor signaling in myoepithelial and cancer cells. *J. Mammary Gland Biol. Neoplasia* 10:221. doi: 10.1007/s10911-005-9583-7

Reversi, A., Rimoldi, V., Marrocco, T., Cassoni, P., Bussolati, G., Parenti, M., et al. (2005). The oxytocin receptor antagonist atosiban inhibits cell growth via a "biased agonist" mechanism. *J. Biol. Chem.* 280, 16311–16318. doi: 10.1074/jbc.M409945200

Rimoldi, V., Reversi, A., Taverna, E., Rosa, P., Francolini, M., Cassoni, P., et al. (2003). Oxytocin receptor elicits different EGFR/MAPK activation patterns depending on its localization in caveolin-1 enriched domains. *Oncogene* 22, 6054–6060. doi: 10.1038/sj.onc.1206612

Ryu, N. E., Lee, S. H., and Park, H. (2019). Spheroid culture system methods and applications for mesenchymal stem cells. *Cells* 8:1620. doi: 10.3390/cells8121620

Sala, M., Braida, D., Donzelli, A., Martucci, R., Busnelli, M., Bulgheroni, E., et al. (2013). Mice heterozygous for the oxytocin receptor gene ($Oxtr^{+/-}$) show impaired social behaviour but not increased aggression or cognitive inflexibility: evidence of a selective haploinsufficiency gene effect. *J. Neuroendocrinol.* 25, 107–118. doi: 10.1111/j.1365-2826.2012.02385.x

Salehi, M. S., Neumann, I. D., Jurek, B., and Pandamooz, S. (2021). Co-stimulation of oxytocin and arginine-vasopressin receptors affect hypothalamic neurospheroid size. *Int. J. Mol. Sci.* 22:8464. doi: 10.3390/ijms22168464

Shamay-Tsoory, S. G., and Abu-Akel, A. (2016). The social salience hypothesis of oxytocin. *Biol. Psychiatry* 79, 194–202. doi: 10.1016/j.biopsych.2015.07.020

Stadler, M., Scherzer, M., Walter, S., Holzner, S., Pudelko, K., Riedl, A., et al. (2018). Exclusion from spheroid formation identifies loss of essential cell-cell adhesion molecules in colon cancer cells. *Sci. Rep.* 8:1151. doi: 10.1038/s41598-018-19384-0

Tomizawa, K., Iga, N., Lu, Y. F., Moriwaki, A., Matsushita, M., Li, S. T., et al. (2003). Oxytocin improves long-lasting spatial memory during motherhood through MAP kinase cascade. *Nat. Neurosci.* 6, 384–390. doi: 10.1038/nn1023

van den Burg, E. H., Stindl, J., Grund, T., Neumann, I. D., and Strauss, O. (2015). Oxytocin stimulates extracellular $Ca2^{+}$ influx through TRPV2 channels in hypothalamic neurons to exert its anxiolytic effects. *Neuropsychopharmacology* 40, 2938–2947. doi: 10.1038/npp.2015.147

Walton, M. R., and Dragunow, M. (2000). Is CREB a key to neuronal survival? *Trends Neurosci.* 23, 48–53. doi: 10.1016/s0166-2236(99)01500-3

Webster, M., Witkin, K. L., and Cohen-Fix, O. (2009). Sizing up the nucleus: nuclear shape, size and nuclear-envelope assembly. *J. Cell Sci.* 122, 1477–1486. doi: 10.1242/jcs.037333

Winter, J., Meyer, M., Berger, I., Royer, M., Bianchi, M., Kuffner, K., et al. (2021). Chronic oxytocin-driven alternative splicing of Crfr2α induces anxiety. *Mol. Psychiatry* doi: 10.1038/s41380-021-01141-x. [Online ahead of print].

Zatkova, M., Reichova, A., Bacova, Z., and Bakos, J. (2019). Activation of the oxytocin receptor modulates the expression of synaptic adhesion molecules in a cell-specific manner. *J. Mol. Neurosci.* 68, 171–180. doi: 10.1007/s12031-019-01296-x

Zhong, M., Boseman, M. L., Millena, A. C., and Khan, S. A. (2010). Oxytocin induces the migration of prostate cancer cells: involvement of the Gi-coupled signaling pathway. *Mol. Cancer Res.* 8, 1164–1172. doi: 10.1158/1541-7786.MCR-09-0329

frontiers | Frontiers in Cellular Neuroscience

TYPE Original Research
PUBLISHED 11 November 2022
DOI 10.3389/fncel.2022.1012523

Check for updates

OPEN ACCESS

EDITED BY
Ulrich - Bogdahn,
University of Regensburg, Germany

REVIEWED BY
Yasemin Gürsoy-Özdemir,
Koç University, Turkey
Rodolfo Gabriel Gatto,
Mayo Clinic, United States
Muge Yemisci,
Hacettepe University, Turkey
Ayman ElAli,
Laval University, Canada
Aurel Popa-Wagner,
University of Medicine and Pharmacy of Craiova, Romania
Subhra Prakash Hui,
University of Calcutta, India

*CORRESPONDENCE
Ertugrul Kilic
ekilic@medipol.edu.tr;
kilic44@yahoo.com

SPECIALTY SECTION
This article was submitted to Cellular Neuropathology, a section of the journal Frontiers in Cellular Neuroscience

RECEIVED 05 August 2022
ACCEPTED 25 October 2022
PUBLISHED 11 November 2022

CITATION
Balçıkanlı Z, Culha I, Dilsiz P, Aydin MS, Ates N, Beker MC, Baltaci SB, Koc HI, Yigitbasi A, Gündogar M, Doeppner TR, Hermann DM and Kilic E (2022) Lithium promotes long-term neurological recovery after spinal cord injury in mice by enhancing neuronal survival, gray and white matter remodeling, and long-distance axonal regeneration.
Front. Cell. Neurosci. 16:1012523.
doi: 10.3389/fncel.2022.1012523

Lithium promotes long-term neurological recovery after spinal cord injury in mice by enhancing neuronal survival, gray and white matter remodeling, and long-distance axonal regeneration

Zeynep Balçıkanlı[1,2], Irem Culha[1,2], Pelin Dilsiz[1,2], Mehmet Serif Aydin[1,3], Nilay Ates[1,4], Mustafa Caglar Beker[1,2], Saltuk Bugra Baltaci[1,2], Halil I. Koc[1,2], Ahmet Yigitbasi[5], Mustafa Gündogar[1,6], Thorsten R. Doeppner[1,7], Dirk M. Hermann[8] and Ertugrul Kilic[1,2]*

[1]Department of Physiology, Regenerative and Restorative Medical Research Center, Istanbul Medipol University, Istanbul, Turkey, [2]Department of Physiology, School of Medicine, Istanbul Medipol University, Istanbul, Turkey, [3]Research Institute for Health Sciences and Technologies (SABITA), Istanbul Medipol University, Istanbul, Turkey, [4]Department of Pharmacology, School of Medicine, Istanbul Medipol University, Istanbul, Turkey, [5]Department of Hematology, Medical Faculty, Trakya University, Edirne, Turkey, [6]Department of Endodontics, Faculty of Dentistry, Istanbul Medipol University, Istanbul, Turkey, [7]Department of Neurology, University Hospital Gießen, Göttingen, Germany, [8]Department of Neurology, University Hospital Essen, University of Duisburg-Essen, Essen, Germany

Spinal cord injury (SCI) induces neurological deficits associated with long-term functional impairments. Since the current treatments remain ineffective, novel therapeutic options are needed. Besides its effect on bipolar mood disorder, lithium was reported to have neuroprotective activity in different neurodegenerative conditions, including SCI. In SCI, the effects of lithium on long-term neurological recovery and neuroplasticity have not been assessed. We herein investigated the effects of intraperitoneally administered lithium chloride (LiCl) on motor coordination recovery, electromyography (EMG) responses, histopathological injury and remodeling, and axonal plasticity in mice exposed to spinal cord transection. At a dose of 0.2, but not 2.0 mmol/kg, LiCl enhanced motor coordination and locomotor activity starting at 28 days post-injury (dpi), as assessed by a set of behavioral tests. Following electrical stimulation proximal to the hemitransection, LiCl at 0.2 mmol/kg decreased the latency and increased the amplitude of EMG responses in the denervated hindlimb at 56 dpi. Functional recovery was associated with reduced gray and white matter atrophy rostral and caudal to the hemitransection, increased neuronal survival and reduced astrogliosis in the dorsal and ventral horns caudal to the hemitransection, and increased regeneration of long-distance axons proximal and distal to the lesion site

in mice receiving 0.2 mmol/kg, but not 2 mmol/kg LiCl, as assessed by histochemical and immunohistochemical studies combined with anterograde tract tracing. Our results indicate that LiCl induces long-term neurological recovery and neuroplasticity following SCI.

KEYWORDS

axonal plasticity, axonal regeneration, motor coordination, neurological recovery, spinal cord hemitransection, spinal cord trauma

Introduction

Spinal cord injury (SCI) defines the traumatic disruption of neuronal networks at any spinal cord level (Zhang S. et al., 2018), inducing sensorimotor deficits and giving rise to long-term functional impairments (Carelli et al., 2019). Following the acute injury, secondary pathomechanisms, including free radical formation, ischemia, and inflammation, further aggravate the primary tissue damage, inducing secondary neuronal degeneration and spinal cord atrophy (Volarevic et al., 2013; Boyce and Mendell, 2014; Zhang D. et al., 2018). Surgical, pharmacological, and rehabilitative interventions have been studied regarding their capacity of improving functional SCI recovery, so far with limited success (Elizei and Kwon, 2017; Nori et al., 2017). There is an urgent need of treatments that enhance spinal cord remodeling and clinical outcome.

Lithium chloride (LiCl) (in the following referred to as lithium) is widely used for the treatment of bipolar mood disorder. Lithium revealed neuroprotective and anti-inflammatory effects in several neurodegenerative conditions (Young, 2009; Chiu and Chuang, 2011; Huo et al., 2012; Li et al., 2015; Lauterbach, 2016). Thus, lithium was shown to improve neurological recovery and neuronal injury in an ischemic stroke model (Nonaka and Chuang, 1998), to prevent hippocampal neurodegeneration and cognitive decline in an Alzheimer's disease model (De Ferrari et al., 2003) and to decrease neurodegeneration in a Parkinson's disease model (Youdim and Arraf, 2004). Recent studies revealed that lithium elevates central nervous system (CNS) levels of brain-derived neurotrophic factor (BDNF) and its receptor TrkB (Dwivedi and Zhang, 2014; Abdanipour et al., 2019), which promote neuroplasticity and neurological recovery in the injured spinal cord (Keefe et al., 2017). Despite these findings, previous studies focused on the neuroprotective effects of lithium in the early SCI phase. These studies, all done in rats, revealed that lithium reduced structural spinal cord damage and neurological deficits *via* mechanisms involving autophagy activation and antiinflammation (Kim et al., 2017; Liu et al., 2017; Zhang D. et al., 2018; Abdanipour et al., 2019).

The effect of lithium on long-term neurological recovery and neuroplasticity remained to be clarified. This study aimed to evaluate the dose-dependent effect of lithium on disrupted motor coordination after long-term SCI and investigate the effect of long-term lithium administration on post-injury tissue damage, cell survival, and axonal regeneration. We herein exposed mice to spinal cord hemitransection and evaluated lithium's actions on (a) motor coordination recovery using a detailed test battery that involved the Basso mouse scale (BMS), horizontal ladder rung, and open field tests, (b) functional electromyography (EMG) responses of the denervated hindlimb following electrical spinal cord stimulation rostral to the lesion, (c) neuronal degeneration and gray and white matter remodeling using histochemical and immunohistochemical techniques, and (d) the regeneration of anterogradely labeled long-distance spinal cord axons. Our data reveal a neurological recovery- and neuronal plasticity-promoting action of low-dose (0.2 mmol/kg), but not high-dose (2 mmol/kg) lithium which persisted over up to 56 days post-SCI (dpi). The data shown here will provide an understanding of the effects of long-term lithium treatment on motor coordination, neuronal survival, and axonal plasticity in the post-injury spinal cord and offer an alternative and novel approach to the existing treatment options for SCI.

Materials and methods

Animals and experimental groups

The experiments were performed in accordance with National Institutes of Health (NIH) guidelines for the care and use of laboratory animals and were approved by the local government authorities (Istanbul Medipol University Animal Research Ethical Committee). All animals were housed at 22–24°C in a constant 12-h light (07:00–19:00 h) and dark (19:00–07:00 h) cycle. For behavioral analysis and immunohistochemistry, a total of 48 male Balb/c mice (9–12 week-old) were randomly divided into three groups that were intraperitoneally treated with (i) vehicle (0.9% isotonic saline), (ii) 0.2 mmol/kg lithium (dissolved in 0.9% isotonic saline) or (iii) 2 mmol/kg lithium (dissolved in 0.9% isotonic saline) (n = 16 mice/group). To detect plasma lithium concentrations, the same treatment protocol was applied to total of 54 male Balb/c mice (9–12 week-old) (n = 3 mice/group/time point).

Analysis of plasma lithium concentrations

Vehicle, 0.2 mmol/kg or 2 mmol/kg lithium was administered to the animals. A total of 30 min, 3, 6, 12, or 24 h after treatment, the mice were sacrificed, and the blood samples were obtained and centrifuged at 10,000 rpm for 10 min at room temperature (22°C). Sera were collected and stored at −80°C to measure serum lithium concentrations in a clinical biochemistry laboratory (Centro, Istanbul, Turkey) using Roche Cobas C501 instrument (Basel, Switzerland), calibrated (Roche, Kit No: 10759350 190), and analyzed (Kit No: 04679598 190) (Ates et al., 2022).

Induction of spinal cord injury

Animals were anesthetized using 1% isoflurane (30% O_2, remainder N_2O). Rectal temperature was maintained between 36.5 and 37.0°C using a feedback-controlled heating system. Mice were placed in a stereotaxic instrument (World Precision Instruments, FL, USA). SCI was performed as previously described with minor modifications (Chen et al., 2019). Briefly, the skin, subcutaneous fascia layer, muscle, and muscle tendons from T9 to T11 and the bilateral vertebral plate of T10 were removed to expose the T10 segment of the spinal cord. Then, a hemisection was performed on the right side of the spinal cord using a 26G syringe tip. After induction of injury, superficial and deep back muscles and the skin were sutured. All mice exhibited complete paralysis of their right hindlimbs immediately after the surgery.

Lithium administration

Lithium doses were selected based on a previous study (Doeppner et al., 2017; Ates et al., 2022). Animals were intraperitoneally (i.p.) treated with normal saline (vehicle) or LiCl (0.2 mmol/kg or 2 mmol/kg dissolved in normal saline; L4408; Sigma-Aldrich, St. Louis, MO, USA) at 24-h intervals starting 24 h after SCI for 56 days. Animals were sacrificed at 56 dpi (**Supplementary Figure 1**).

Behavioral tests

Functional neurological recovery was assessed using the following tests:

Basso mouse scale

The BMS is an accurate method used to evaluate motor functions after SCI (Basso et al., 2006). The scale consists of a 0–9 point rating scale, which evaluates the hindlimb motor functions. The point scale was divided as follows: 0 = no ankle movement, 1 = slight ankle movement, 2 = extensive ankle movement, 3 = plantar placing of the paw or dorsal stepping, 4 = occasional plantar stepping, 5 = frequent or consistent plantar stepping, no coordination; 6 = frequent or consistent plantar stepping with some coordination; 7 = frequent or consistent plantar stepping with severe trunk instability; 8 = frequent or consistent plantar stepping with mild trunk instability; and 9 = frequent or consistent plantar stepping with normal trunk stability (Basso et al., 2006). Animals were observed in an open field chamber for 4 min and blindly evaluated by two different observers, of which mean scores were obtained. BMS scores were determined at 1, 3, 7, 14, 28, and 42 dpi.

Horizontal ladder rung walking test

The ladder rung test was adapted from a previous study (Farr et al., 2006). The apparatus consists of two 69.5 cm × 15 cm plexiglass walls each containing 121 holes with 0.20 cm diameter placed 3 cm apart to allow mice to walk through the ladder without hesitation. The ladder has 0.10 cm diameter metal bars that are 0.50 cm apart. Before testing, the animals were acclimated to the apparatus by allowing them to freely walk through the ladder for 10 min. After acclimation, the mice were trained to walk through the metal ladder. Animals were recorded using a high-speed camera and correct foot placement was assessed from the recordings. Correct foot placement was defined as the contact of the hindlimb to the rung with either palm or digits around the rung or a weight-bearing step on the rung. Percent of correct foot placement was measured (correct foot placement × 100/total steps). Horizontal ladder rung tests were obtained at baseline and at 3, 14, 28, and 42 dpi.

Open field test

The open field test evaluates spontaneous locomotor activity and exploration behavior of animals in a circular arena (diameter = 150 cm) with a white plastic floor, surrounded by a 35 cm high sidewall made of white polypropylene (Kilic et al., 2014; Kelestemur et al., 2020). The arena was divided into three sections, including an outer wall zone (17.7% of the diameter, close to the wall), an intermediate transition zone (32.3% of the diameter), and an inner zone (50% of the diameter, the center of the arena). Each animal was released near the wall and observed for 10 min using an electronic imaging system (ANY-maze®; Stoelting Co., Wood Dale, IL, USA). The resting and progressing time, the time spent in each of the three zones, and the rotations were recorded. Open field tests were performed at baseline and at 3, 14, 28, and 42 dpi.

Electromyography

Electrophysiological recovery was assessed by the latency and amplitude of gastrocnemius muscle contraction after stimulating the spinal cord above the site of the injury area at the T7 level. At 56 dpi, mice were anesthetized and the hair over the right hindlimb gastrocnemius muscle was shaved. A small skin incision was made to expose the ipsilesional gastrocnemius muscle, in which positive and negative platinum electrodes were inserted. In order to stimulate the spinal cord, laminectomy was performed at the T7 level and the stimulating electrode was inserted into the ipsilesional hemicord, while the ground electrode was placed just below the stimulating electrode above the injury site. Stimulations were performed using 2 V pulses with 10 repeats at 0.2 Hz. Data were obtained using the PowerLab data acquisition system with LabChart 8 software (ADInstruments, Dunedin, New Zealand). The latency, duration, and amplitude of evoked EMG potentials in the gastrocnemius muscle were measured.

Evaluation of spinal cord remodeling and atrophy

For histochemical analysis, mice were deeply anesthetized and perfused with 4% paraformaldehyde (PFA) at 56 dpi. A 1 cm spinal cord sample centered around the hemitransection, was harvested and dehydrated in 30% sucrose solution at 4°C. In caudal to rostral direction, 50 μm-thick coronal sections were serially collected on glass microscope slides using a cryostat (CM1950, Leica Biosystems, Wetzlar, Germany). To evaluate spinal cord atrophy, Cresyl violet staining was performed on spinal cord sections from the level of T8 (Rostral level) and T13 (Caudal level) according to a standard protocol (Beker et al., 2015; Kelestemur et al., 2020). Sections were imaged using a stereo zoom microscope (AxioZoom.V16, Carl Zeiss, Jena, Germany) and besides gray matter and the dorsal, lateral, and ventral funiculus of the white matter was outlined blindly using Zen Blue software (Carl Zeiss, Germany). Ipsilateral areas were calculated as percent of contralateral areas (Caglayan et al., 2022).

Next, we examined the density of surviving neurons and reactive astrocytes. For this purpose, sections from the spinal cord segments were postfixed in 4% paraformaldehyde (PFA)/0.1 M phosphate-buffered saline (PBS), washed and immersed for 1 h in 0.1 M PBS containing 0.3% Triton X-100 (PBS-T)/10% normal goat serum (G9023; Sigma-Aldrich). Sections were incubated overnight at 4°C with Alexa Fluor 647 conjugated monoclonal rabbit anti-neuronal nuclear protein (NeuN; 1:100; 62,994; Cell Signaling, Beverly, MA, USA) and Alexa Fluor 555 conjugated monoclonal mouse anti-glial fibrillary acidic protein (GFAP) (1:100; 3,656; Cell Signaling) antibody. Sections were analyzed using a laser scanning confocal microscope (LSM780, Carl Zeiss) by evaluating regions of interest (ROI) measuring 62,500 μm^2 in the dorsal, intermediate and ventral horns. Cells were counted blindly by two different observers in the ipsilesional and contralesional spinal cord. Mean values were calculated for both counting (Caglayan et al., 2019). Data were presented as the ratio of numbers determined in the ipsilesional and contralesional hemicords.

Tract tracing of axonal regeneration

To detect the axonal plasticity induced by lithium treatment, we traced axons of the lateral spinothalamic tract. Animals were anesthetized at 42 dpi and laminectomy was performed at the L2 level to expose the dorsal segment of the spinal cord (Caglayan et al., 2019). Under visual inspection, 1 μl biotinylated dextran amine (BDA, 10,000 MW; D1956; Invitrogen, Waltham, MA, USA) diluted in 0.01 M PBS was bilaterally injected 0.3 mm lateral to the midline and 0.7 mm deep to the dorsal surface using a Hamilton syringe connected to a glass tip. The syringe tip remained inside the injection area for 1 min to prevent backflow. After 14 days, animals were sacrificed by transcardial perfusion with 4% PFA and coronal sections were collected. Then, sections were washed with PBS, blocked with 10% normal goat serum in PBS for 1 h at room temperature, incubated with Alexa Fluor 555 conjugated streptavidin (S21391; Invitrogen) for 90 min at room temperature and analyzed using confocal microscopy (LSM780, Carl Zeiss). The number of axons crossing the rostral and caudal spinal cord segments were blindly counted in the lateral spinothalamic tract of the ipsilesional and contralesional hemicord in ROI measuring 62,500 μm^2.

Statistical analysis

Statistical analysis was performed using SPSS (version 15; SPSS Inc., Chicago, USA) software. Data were evaluated by one-way analysis of variance (ANOVA) followed by least-significant difference (LSD) tests and expressed as mean ± standard deviation (SD). Throughout the study, p-values < 0.05 were considered statistically significant.

Results

Plasma lithium concentrations following low-dose and high-dose lithium administration

Lithium has a therapeutic range between 0.6 and 1.2 mmol/L in humans (Singer and Rotenberg, 1973; Jope, 1999). Based on our results, we investigated the time and dose-dependent serum concentration of lithium. Although 2 mmol/kg LiCl was previously shown to have neuroprotective activity after ischemic stroke (Ates et al., 2022), we observed that 0.2 mmol/kg LiCl had

a restorative effect after SCI. Our findings also imply that serum lithium concentration decreases below <0.05 when measured 6 h after their administration in 0.2 mmol/kg and 12 h in the 2 mmol/kg group (Table 1).

Low-dose lithium induces long-term motor coordination recovery

To evaluate the effects of lithium on motor coordination, we evaluated ankle movement, plantar placement of the paw with or without a weight support, plantar stepping, gait, and trunk stability in mice exposed to SCI using the BMS. Post-SCI, spontaneous motor movements were absent in ipsilesional (i.e., right-sided) hindlimbs at 1 dpi in all groups (Figure 1A). From 3 to 42 dpi, spontaneous motor movements returned, but directed movements of paretic hindlimbs, stepping and gait were severely impaired in vehicle treated mice (Figure 1A). Lithium at 0.2 mmol/kg, but not 2.0 mmol/kg significantly enhanced motor coordination performance in the BMS at 28 and 42 dpi compared with vehicle (Figure 1A). Likewise, 0.2 mmol/kg lithium significantly increased motor coordination performance in the horizontal ladder rung test, which is widely used post-SCI (Emerick and Kartje, 2004; Ajao et al., 2012; Adkins et al., 2015), at 28 or 42 dpi compared with 2.0 mmol/kg lithium or vehicle, respectively (Figure 1B). As a consequence of the hindlimb impairment, spontaneous locomotor activity assessed by the time of active mobility, the total distance covered, mean speed, and rotation movements in the open field test were markedly reduced post-SCI (Figures 1C–F). Lithium at 0.2 mmol/kg significantly increased the time of active mobility, the total distance covered, mean speed, and rotation movements at 28 and 42 dpi compared with vehicle (Figures 1C–F). Hence, sustained motor coordination recovery was noted in mice receiving 0.2 but not 2.0 mmol/kg lithium.

Low-dose lithium enhances functional electromyography responses evoked by spinal cord stimulation

To further characterize the effects of lithium on functional motor recovery, we next recorded EMG responses of the gastrocnemius muscle (Figure 2A) following electrical stimulation of the spinal cord rostral to the lesion site at 56 dpi (Figure 2B). Lithium at 0.2 mmol/kg significantly reduced the latency of the evoked EMG potential (Figure 2C) without influencing its duration (Figure 2D), and significantly increased the EMG amplitude (Figure 2E). Lithium at 2.0 mmol/kg did not influence evoked EMG responses (Figures 2C–E). Collectively, lithium improved functional EMG responses at the 0.2 mmol/kg dose.

Low-dose lithium prevents spinal cord atrophy rostral and caudal to the lesion

To examine structural correlates of motor coordination recovery, cresyl violet staining was used to analyze gray and white matter atrophy rostral and caudal to the spinal cord lesion. In mice receiving vehicle, significant gray and white matter atrophy was noted in the injured hemicord both rostral (Figures 3A–E) and caudal (Figures 3F–J) to the lesion site at 56 dpi. Rostral to the spinal cord lesion, the white matter atrophy was most pronounced in the dorsal funiculus (Figures 3C–E), while caudal to the spinal cord lesion, spinal cord atrophy more similarly affected the dorsal, lateral and ventral funiculi (Figures 3H–J). Lithium at 0.2 mmol/kg, but not 2.0 mmol/kg significantly reduced gray matter atrophy rostral and caudal to the spinal cord lesion (Figures 3A,F), reduced white matter atrophy in the dorsal funiculus rostral and caudal to the lesion (Figures 3C,H) and reduced white matter atrophy in the ventral funiculus caudal to the lesion (Figure 3J). Hence, lithium at 0.2 mmol/kg protected against spinal cord degeneration.

Low-dose lithium prevents neuronal degeneration in the dorsal and ventral horns caudal to the lesion

We subsequently evaluated the survival of spinal cord neurons rostral and caudal to the hemitransection by immunohistochemistry for the neuronal marker NeuN. SCI markedly reduced the density of $NeuN^+$ neurons in the ipsilesional dorsal and ventral horns caudal to the hemitransection at 56 dpi (Figures 4A–H). Lithium at 0.2 mmol/kg but not at 2 mmol/kg significantly increased the density of surviving $NeuN^+$ neurons in the ipsilesional dorsal

TABLE 1 Serum lithium concentrations measured by ICP-MS and shown in mmol/L.

Vehicle	30 min	1 h	3 h	6 h	12 h	24 h
	N/A	N/A	N/A	N/A	N/A	N/A
0.2 mmol/kg	0.18 ± 0	0.12 ± 0.04	0.09 ± 0.03	<0.05	<0.05	<0.05
2 mmol/kg	0.88 ± 0.12	0.45 ± 0.05	0.39 ± 0.09	0.15 ± 0.04	<0.05	<0.05

N/A, not applicable. Data are expressed as mean ± SD (n = 3 mice/for each time point).

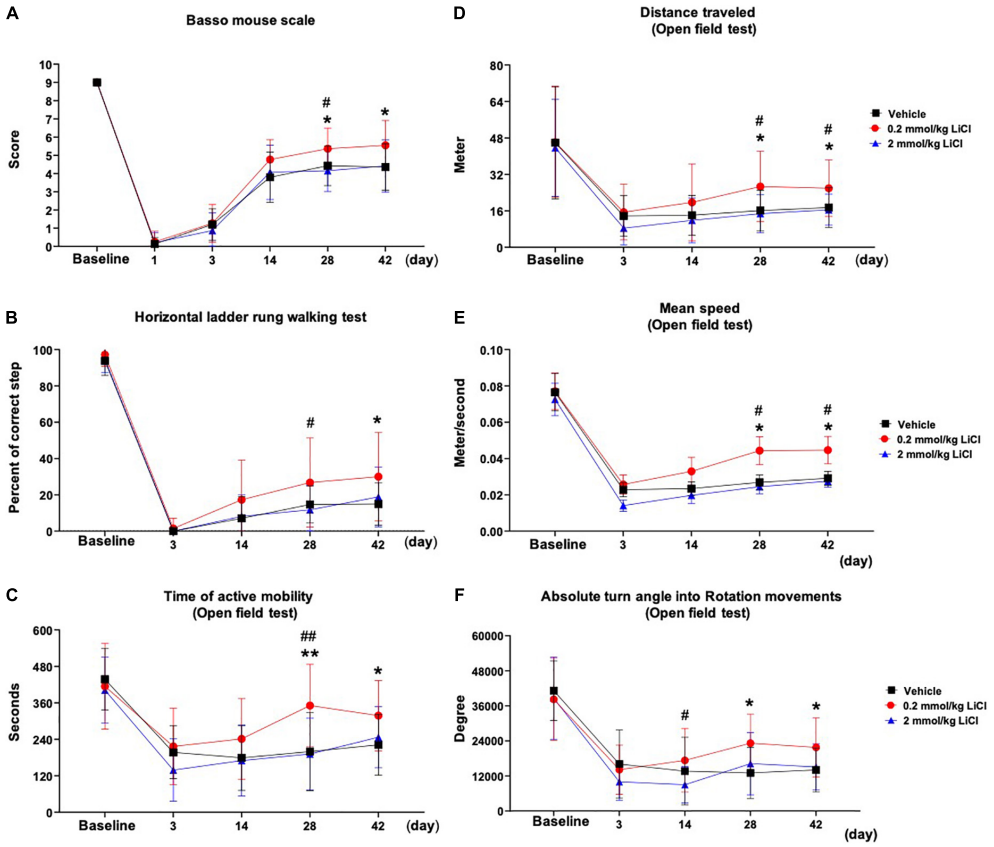

FIGURE 1
Low-dose lithium enhances motor coordination recovery and spontaneous locomotor activity following spinal cord injury (SCI). Motor performance evaluated by **(A)** the Basso mouse scale and **(B)** the horizontal ladder rung walking test of mice exposed to right-sided spinal cord hemitransection at the T10 level, which were treated with vehicle or lithium (0.2 or 2 mmol/kg/day) for 56 days. Spontaneous motor activity evaluated by **(C)** the time of active mobility, **(D)** the total distance traveled, **(E)** mean speed, and **(F)** rotation movements in the open field test of the same mice exposed to spinal cord hemitransection, which were treated with vehicle or lithium (0.2 or 2 mmol/kg/day) for 56 days. Data are expressed as mean ± SD values (n = 16 animals/group). $^{*}p < 0.05/^{**}p < 0.01$ for 0.2 mmol/kg LiCl vs. vehicle; $^{\#}p < 0.05/^{\#\#}p < 0.01$ for 0.2 mmol/kg LiCl vs. 2 mmol/kg LiCl.

and ventral horns caudal to the hemitransection (Figures 4E,G). This neuroprotection also involved the density of large-sized NeuN^{+} motor neurons, which were increased by lithium (Figure 4H). Rostral to the hemitransection, SCI did not influence the density of NeuN^{+} neurons, and neuronal survival was not influenced by lithium (Figures 4A–D).

Low-dose and high-dose lithium reduces reactive astrogliosis in the gray matter caudal to the lesion

We next assessed reactive astrogliosis in the gray and white matter by GFAP immunohistochemistry. Significant reactive astrogliosis was noted in the ipsilesional gray and white matter rostral and caudal to the hemitransection at 56 dpi (Figures 5A–F and Supplementary Figures 2A–F). Lithium at 0.2 and 2 mmol/kg significantly reduced the density of GFAP^{+} astrocytes in the ipsilesional gray matter caudal to the hemitransection (Figures 5D–F), but not the ipsilesional gray matter rostral to the hemitransection (Figures 5A–C). White matter astrogliosis was not influenced by lithium, neither rostral nor caudal to the hemitransection (Supplementary Figures 2A–F).

Low-dose and high-dose lithium enhances axonal regeneration proximal and distal to the lesion

To evaluate the effects of lithium on the regeneration of spinal cord axons, we performed tract tracing experiments, in which the anterograde axonal tracer BDA was bilaterally injected into the spinal cord at the L2 level at 42 dpi (Reitmeir et al., 2011, 2012), followed by the evaluation of BDA-labeled axons in both lateral spinothalamic tracts 14 days

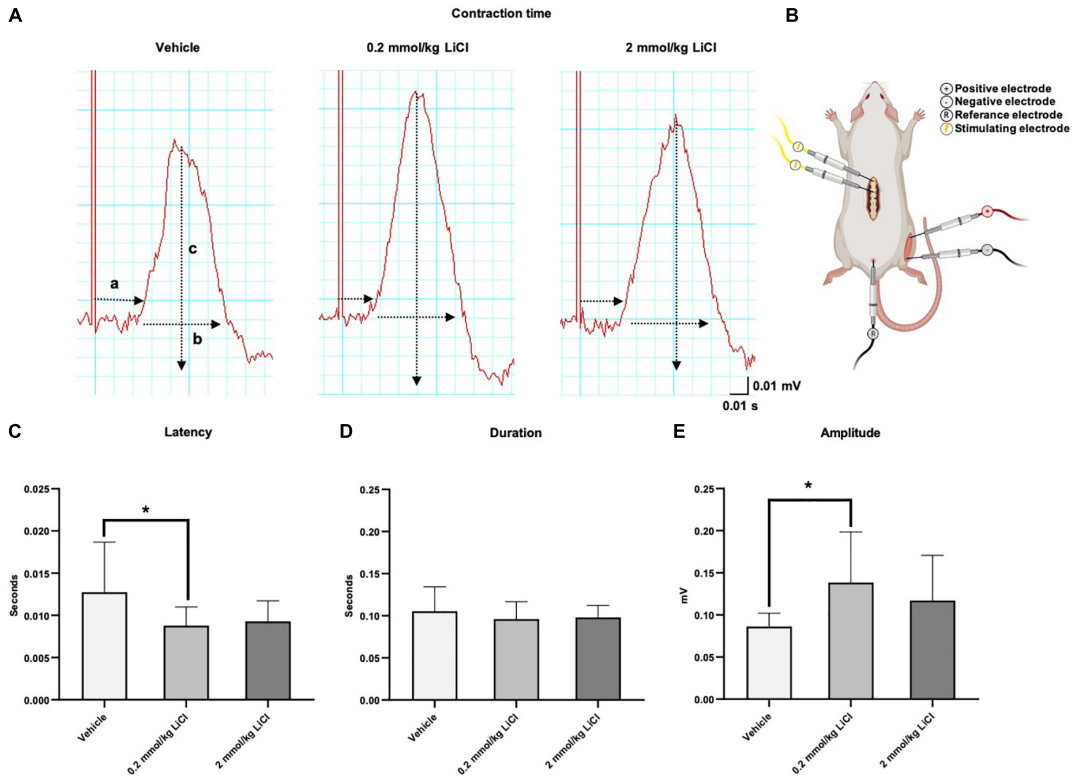

FIGURE 2
Low-dose lithium enhances functional EMG responses evoked by spinal cord stimulation. **(A)** Representative electromyograms (EMG) obtained in the right-sided gastrocnemius muscle after electrical stimulation of the spinal cord of mice exposed to spinal cord hemitransection, which were treated with vehicle or lithium (0.2 or 2 mmol/kg/day) for 56 days (a: Latency, b: Duration, c: Amplitude). **(B)** Schematic illustration of the electrical stimulation site at the T7 level of the spinal cord and the EMG recording site in the gastrocnemius muscle. After lithium treatment at 0.2 mmol/kg/day but not 2 mmol/kg/day, **(C)** the latency of the evoked potential decreased, **(D)** the duration of the potential remained unchanged and **(E)** the amplitude increased. Data are mean ± SD values (n = 16 animals/group). *$p < 0.05$ for 0.2 mmol/kg LiCl vs. vehicle.

later, that is, at 56 dpi (Figures 6A–D). The density of BDA-labeled axons in the ipsilesional lateral spinothalamic tract (Figures 6C,D) was markedly lower than that in the contralesional lateral spinothalamic tract (Figures 6A,B), indicating axonal injury in the lesioned hemicord. Lithium at 0.2 mmol/kg significantly increased the density of ipsilesional lateral spinothalamic tract axons caudal to the hemitransection (i.e., proximal to the site of damage) (Figure 6D). Besides, lithium at 0.2 and 2 mmol/kg significantly increased the density of ipsilesional lateral spinothalamic tract axons rostral to the hemitransection (i.e., distal to the site of damage) (Figure 6B). Hence, lithium restored axonal connections, which were disrupted by SCI.

Discussion

In a model of spinal cord hemitransection, we herein show that lithium, administered i.p. at a dose of 0.2 mmol/kg, enhanced motor coordination recovery over up to 42 dpi, as assessed by the BMS, horizontal ladder rung, and open field tests. Motor coordination improvements were associated with improved functional EMG responses, i.e., an increase in EMG amplitude and a decrease in EMG latency, in the denervated gastrocnemius muscle after spinal cord stimulation rostral to the lesion site. Functional recovery was accompanied by reduced gray and white matter atrophy rostral and caudal to the hemitransection, increased neuronal survival and reduced astrogliosis in the dorsal and ventral horns caudal to the hemitransection, and increased regeneration of long-distance axons proximal and distal to the lesion site, as assessed by histochemical studies combined with anterograde tract tracing at 56 dpi. Lithium at a dose of 2 mmol/kg i.p. did not influence motor coordination recovery, evoked EMG responses, neuronal survival, or spinal cord remodeling. In line with previous studies (Finley, 2016) we conclude that higher dose remained ineffective since lithium has a relatively narrow therapeutic window in which long-term neurological recovery and neuroplasticity are induced.

Previous studies, all performed in rat models, already examined the neuroprotective effects of lithium in the early

10.3389/fncel.2022.1012523

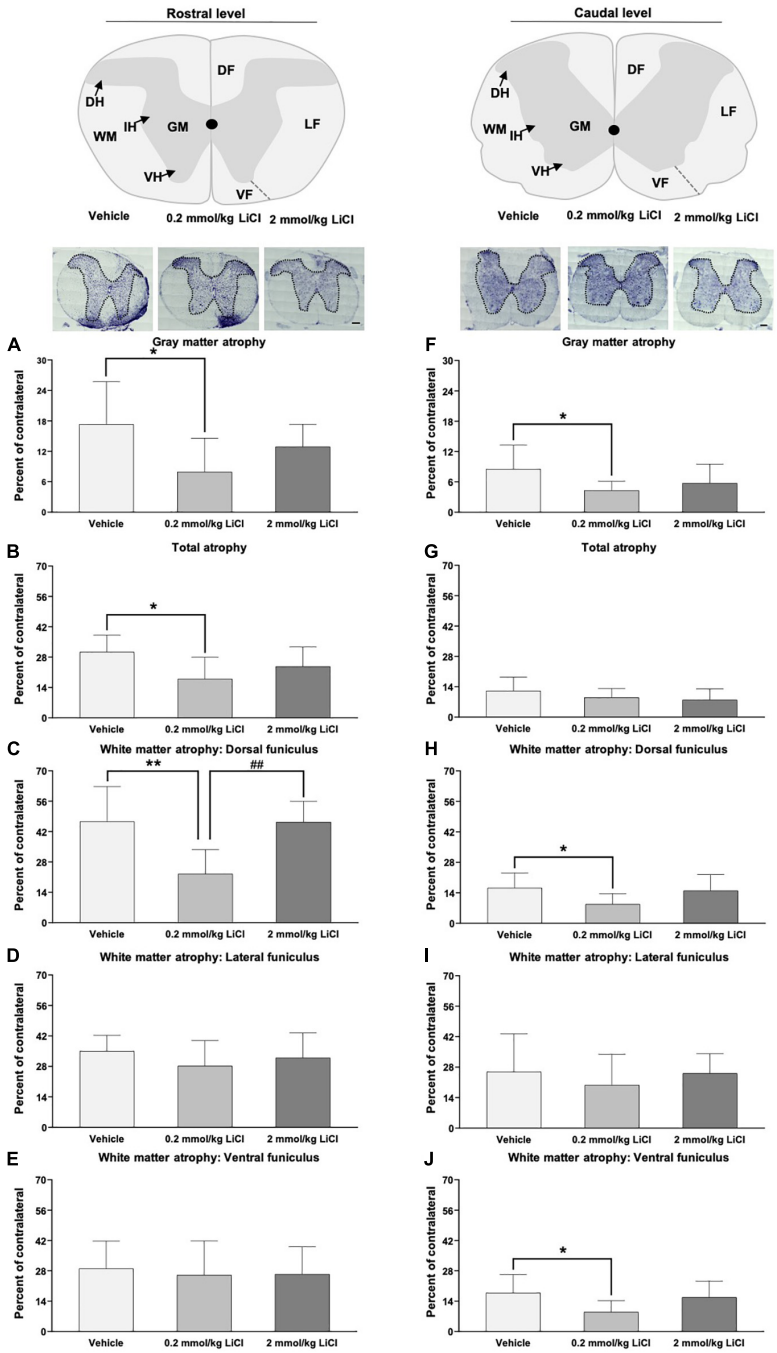

FIGURE 3

Low-dose lithium reduces spinal cord atrophy rostral and caudal to the hemitransection. **(A,F)** Gray matter atrophy, **(B,G)** total atrophy, **(C,H)** white matter atrophy of the dorsal funiculus, **(D,I)** white matter atrophy of the lateral funiculus, and **(E)** white matter atrophy of the ventral funiculus assessed by Cresyl violet staining at **(A–E)** the rostrocaudal level above the hemitransection ("Rostral level") and **(F–J)** the rostrocaudal level below the hemitransection ("Caudal level") of SCI mice, which were treated with vehicle or lithium (0.2 or 2 mmol/kg/day) for 56 days. Representative spinal cord sections are also shown. WM, white matter; GM, gray matter; DH, dorsal horn; IH, intermediate horn; VH, ventral horn; DF, dorsal funiculus; LF, lateral funiculus; and VF, ventral funiculus. Data are mean ± SD values (n = 16 animals/group). *$p < 0.05$/**$p < 0.01$ for 0.2 mmol/kg LiCl vs. vehicle; $^{\#\#}p < 0.01$ for 0.2 mmol/kg LiCl vs. 2 mmol/kg LiCl. Scale bars, 200 μm.

SCI phase, demonstrating that lithium reduced structural spinal cord damage and motor coordination deficits *via* mechanisms including autophagy activation, antiinflammation and neurotrophic factor (specifically, BDNF) formation (Kim et al., 2017; Liu et al., 2017; Zhang D. et al., 2018; Abdanipour et al., 2019). So far, two studies evaluated

10.3389/fncel.2022.1012523

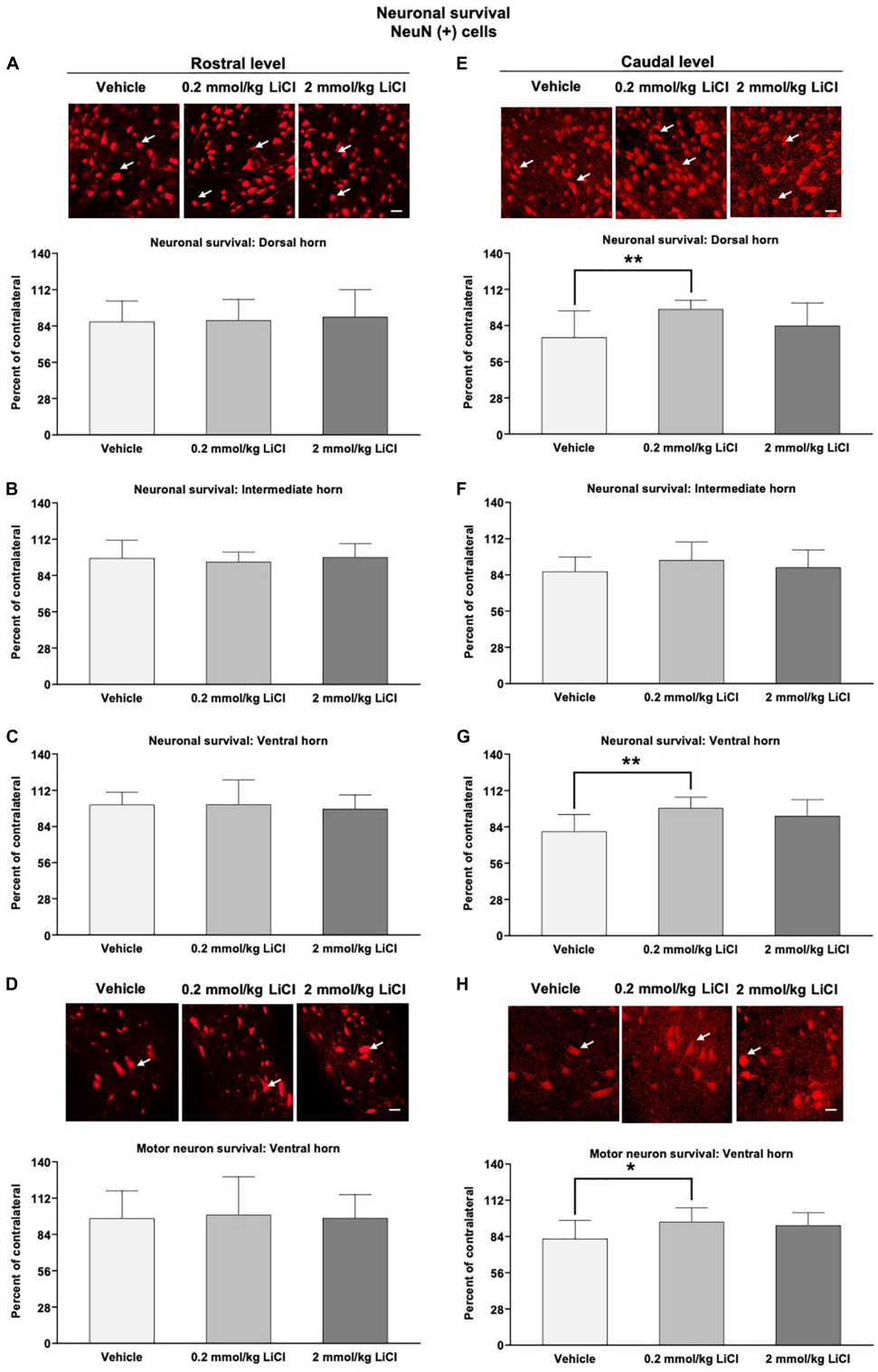

FIGURE 4
Low-dose lithium prevents neuronal degeneration in the dorsal and ventral horns caudal to the hemitransection. Neuronal survival in **(A,E)** the dorsal horn, **(B,F)** the intermediate horn, and **(C,G)** the ventral horn of the spinal cord, as well as **(D,H)** survival of large-sized motor neurons in the spinal cord ventral horn assessed by NeuN immunohistochemistry at **(A–D)** the rostrocaudal level above the hemitransection ("Rostral level") and **(E–H)** the rostrocaudal level below the hemitransection ("Caudal level") of SCI mice, which were treated with vehicle or lithium (0.2 or 2 mmol/kg/day) for 56 days. Representative NeuN stainings are also shown. Data are mean ± SD values (n = 16 animals/group). *$p < 0.05$/**$p < 0.01$ for 0.2 mmol/kg LiCl vs. vehicle. Please note that white arrows indicate representative neurons. Scale bars, 50 μm.

10.3389/fncel.2022.1012523

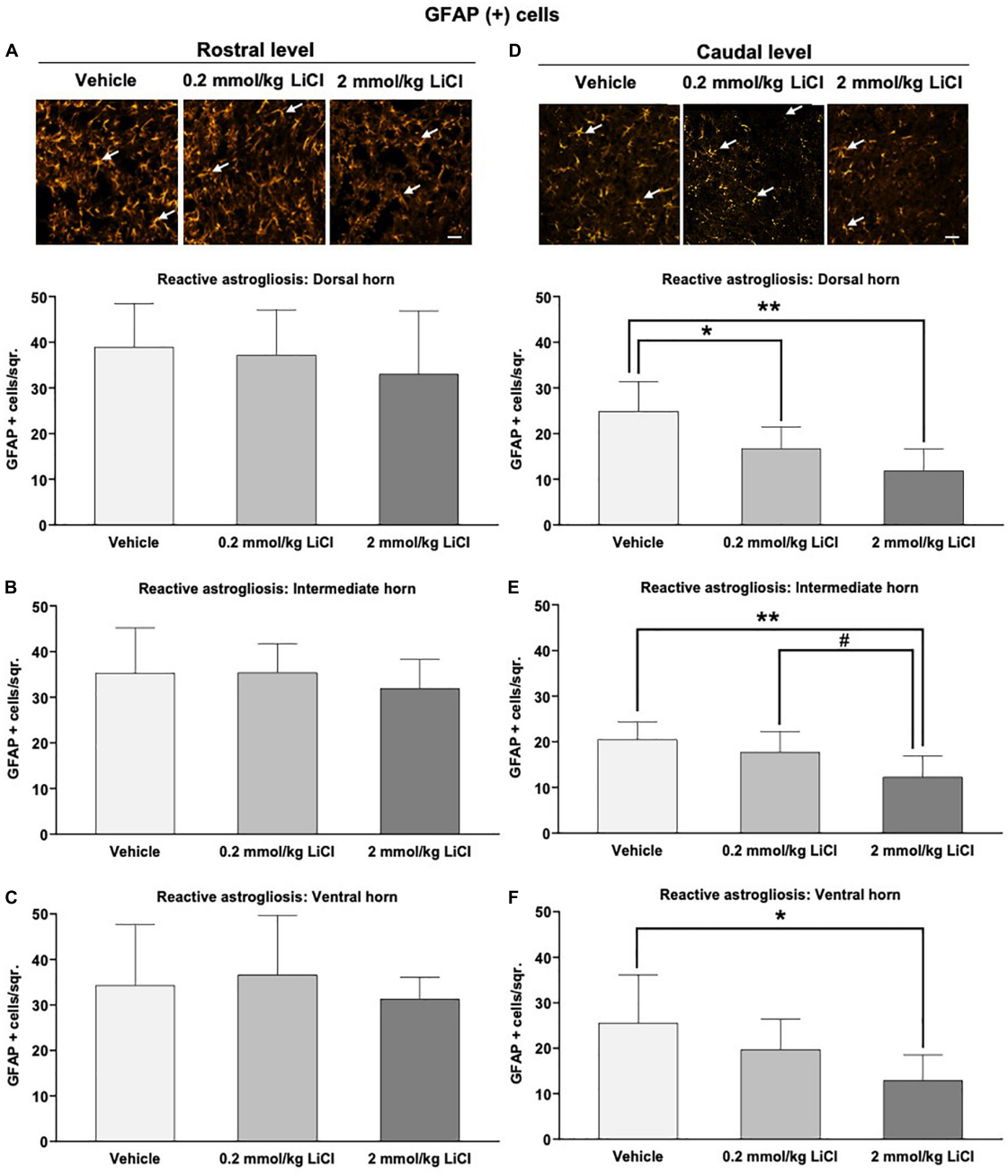

FIGURE 5
Low-dose and high-dose lithium reduces reactive astrogliosis in the gray matter caudal to the hemitransection. Reactive astrogliosis in **(A,D)** the dorsal horn, **(B,E)** the intermediate horn, and **(C,F)** the ventral horn of the spinal cord assessed by GFAP immunohistochemistry at **(A–C)** the rostrocaudal level above the hemitransection ("Rostral level") and **(D–F)** the rostrocaudal level below the hemitransection ("Caudal level") of SCI mice, which were treated with vehicle or lithium (0.2 or 2 mmol/kg/day) for 56 days. Representative GFAP stainings are also shown. Data are mean ± SD values (n = 16 animals/group). *$p < 0.05$/**$p < 0.01$ for 0.2 mmol/kg or 2 mmol/kg LiCl vs. vehicle; $^{\#}p < 0.05$ for 2 mmol/kg LiCl vs. 0.2 mmol/kg LiCl. Please note that white arrows indicate representative glia. Scale bars, 50 μm.

lithium's effects on motor coordination deficits for up to 14 dpi (Kim et al., 2017; Abdanipour et al., 2019) and one study for up to 28 dpi (Zhang D. et al., 2018). The study by Kim et al. (2017), which also studied histopathological sequelae of neuroprotection in a model of clip compression, found that lithium reduced locomotor deficits assessed by the Basso, Beattie, and Bresnahan scale, reduced spinal cord leukocyte infiltrates, reduced microglial activation and reduced spinal cord hemorrhage. On the molecular level, lithium was shown to induce the phosphorylation (i.e., inactivation) of glycogen

10.3389/fncel.2022.1012523

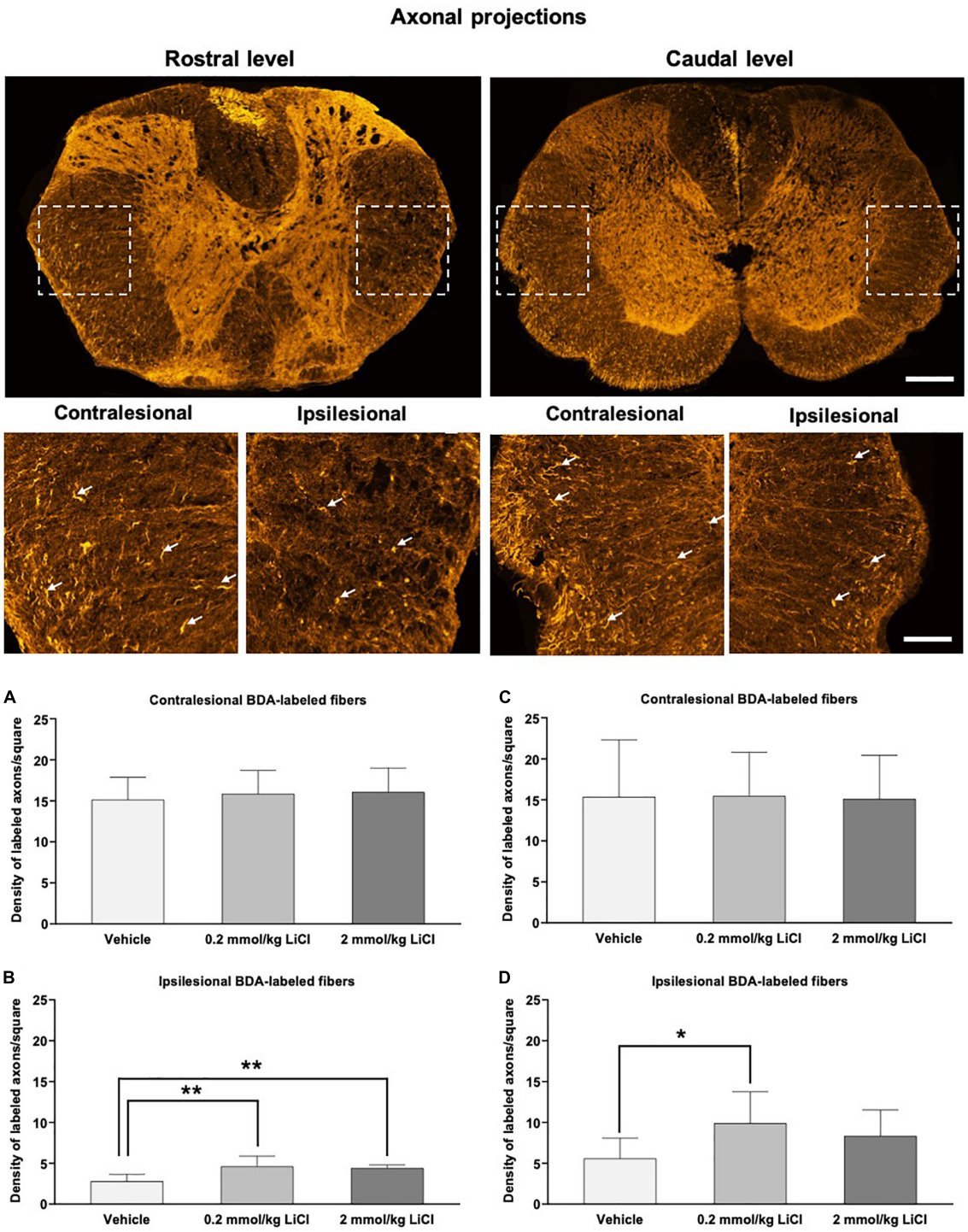

FIGURE 6

Low-dose and high-dose lithium enhances axonal regeneration proximal and distal to the hemitransection. Representative confocal microscopy images with enlargements of BDA-stained fibers ascending through the injured spinal cord at the rostrocaudal levels above the hemitransection ("Rostral level") and below the hemitransection ("Caudal level") of an SCI mouse treated with vehicle, in which BDA had bilaterally been injected into the spinal cord at the L2 level. Quantitative analysis of the density of BDA-labeled fibers in **(A,C)** the contralesional lateral spinothalamic tract and **(B,D)** the ipsilesional lateral spinothalamic tract at **(A,B)** at the rostrocaudal level rostral to the hemitransection ("Rostral level") and **(C,D)** the rostrocaudal level caudal to the hemitransection ("Caudal level") of SCI mice, which were treated with vehicle or lithium (0.2 or 2 mmol/kg/day) for 56 days. Data are mean ± SD values (n = 16 animals/group). *$p < 0.05$/**$p < 0.01$ for 0.2 mmol/kg or 2 mmol/kg LiCl vs. vehicle. Please note that white arrows indicate representative BDA-labeled fibers. Scale bars, 200 μm (lower magnification images)/50 μm (higher magnification images).

synthase kinase-3β (GSK-3β), a known lithium target, which elevated the GSK-3β target nuclear factor erythroid 2-related factor-2 (Nrf-2) and the Nrf-2 target heme oxygenase-1 (HO-1) (Kim et al., 2017). The Basso, Beattie, and Bresnahan scale is an observation scale that was developed for rats (Basso et al., 1995) and resembles the BMS for mice (Basso et al., 2006).

To exclude examiner influences, we combined the BMS with the horizontal ladder rung test and open field test, showing that lithium indeed induces robust motor coordination improvements associated with brain remodeling that persisted in the post-acute SCI phase for up to 56 dpi. Our study expands the test repertoire for studying motor coordination deficits post-SCI. The development of motor coordination tests in mouse SCI models remains a challenge. The vertical ladder climb test and the grid walking test have been shown to be suitable for studying motor coordination improvements with adequate adjustments, while other tests, such as the inclined plane, the plantar test, and the tail-flick test, were not suitable to discriminate motor coordination changes post-SCI (Pajoohesh-Ganji et al., 2010). The horizontal ladder rung test has originally been established for studying motor coordination recovery following motor cortical lesions (Farr et al., 2006). The open field test is widely used for studying spontaneous locomotor activity in brain injury models (Kilic et al., 2008). It provides useful quantitative readouts, such as the time of mobility, the total distance traveled, mean speed, and rotation movements, which can be analyzed investigator independently in an automated way.

In line with the motor coordination improvements, lithium significantly enhanced evoked responses in the ipsilesional gastrocnemius muscle after electrical stimulation rostral to the spinal cord hemitransection. As such, the latency of EMG potentials was reduced and the EMG potential amplitude was increased by lithium on the lesioned side. EMG recordings provide comprehensive information about motor function after SCI (Tysseling et al., 2013), but motor evoked potentials have so far not been used for studying lithium's effects on the recovery of the injured spinal cord. The latency of evoked EMG potentials depends on the integrity of myelin sheaths, whereas the amplitude depends on axonal integrity (Schulz et al., 2014). The observation that lithium reduced the evoked potential latency and increased the evoked potential amplitude indicates that axonal regeneration and remyelination were enhanced by lithium. In a rat model of ventral root avulsion and reimplantation of the brachial plexus, lithium has previously been shown to improve the outgrowth and remyelination of peripheral nerves (Fang et al., 2016).

Following spinal cord hemitransection, motor coordination recovery by lithium was closely associated with reduced gray and white matter atrophy rostral and caudal to the hemitransection, increased neuronal survival in the dorsal and ventral horns caudal to the hemitransection, and reduced astrogliosis in the gray matter caudal to the hemitransection. In rat SCI models, improvements of motor coordination impairments closely go in line with the reduced histopathological injury and enhanced white matter integrity (Cao et al., 2005; Dunham et al., 2010). In rat models of a spinal contusion injury, lithium has previously been shown to reduce the size of the lesion cavity (Abdanipour et al., 2019) and increase neuronal survival at the contusion site (Zhang D. et al., 2018). Our present study expands these earlier data by showing that gray and white matter were equally protected by lithium after spinal cord hemitransection. Indeed, significant tissue preservation was noted by planimetry rostral and caudal to the lesion site, which persisted in the long-term. Effects of lithium on perilesional astrogliosis have not been studied after SCI.

By anterograde tract tracing, we finally found that lithium enhanced the regeneration of long-distance axons both proximal and distal to the lesion site. For this purpose, BDA deposits were administered into the lateral spinal cord caudal to the hemitransection, which allowed us to evaluate axonal regeneration of the lateral spinothalamic tract below and above the lesion site. Anterograde tract tracing techniques have previously been used to study plasticity-promoting treatments in mouse and rat models of ischemic stroke (Reitmeir et al., 2011, 2012) and SCI (Guest et al., 1997; Kartje et al., 1999), but had so far not been used for studying lithium effects in the lesioned spinal cord. The combined evidence of this study suggests that lithium induced robust structural spinal cord remodeling resulting in functional tissue recovery. Due to the narrow therapeutic window of lithium, its clinical utility in human stroke patients with cardiovascular risk factors and comorbidities will be low.

Data availability statement

The original contributions presented in the study are included in the article/**Supplementary material**, further inquiries can be directed to the corresponding author.

Ethics statement

The animal study was reviewed and approved by the Istanbul Medipol University Animal Research Ethical Committee.

Author contributions

ZB, IC, PD, NA, and MB performed the animal experiments and behavioral tests. SB and HK performed EMG analyzes. ZB and MA prepared the histochemical studies. AY and MG

performed biochemical analyzes. EK, TD, and DH analyzed data wrote the manuscript. All authors revised and finalized this manuscript.

Funding

EK was supported by the Turkish Academy of Sciences (TUBA) and this study was by Istanbul Medipol University.

Conflict of interest

The authors declare that the research was conducted in the absence of any commercial or financial relationships that could be construed as a potential conflict of interest.

Publisher's note

All claims expressed in this article are solely those of the authors and do not necessarily represent those of their affiliated organizations, or those of the publisher, the editors and the reviewers. Any product that may be evaluated in this article, or claim that may be made by its manufacturer, is not guaranteed or endorsed by the publisher.

Supplementary material

The Supplementary Material for this article can be found online at: https://www.frontiersin.org/articles/10.3389/fncel.2022.1012523/full#supplementary-material

SUPPLEMENTARY FIGURE 1
Schematic representation of experimental design.

SUPPLEMENTARY FIGURE 2
Lithium does not influence reactive astrogliosis of the white matter. Reactive astrogliosis in **(A,D)** the dorsal funiculus, **(B,E)** the lateral funiculus, and **(C,F)** the ventral funiculus of the spinal cord assessed by GFAP immunohistochemistry at **(A–C)** the rostrocaudal level above the hemitransection ("Rostral level") and **(D–F)** the rostrocaudal level below the hemitransection ("Caudal level") of SCI mice, which were treated with vehicle or lithium (0.2 or 2 mmol/kg/day) for 56 days. Representative GFAP stainings are also shown. Data are mean ± SD values (n = 16 animals/group). No significant group differences were detected. Scale bars, 50 μm.

References

Abdanipour, A., Moradi, F., Fakheri, F., Ghorbanlou, M., and Nejatbakhsh, R. (2019). The effect of lithium chloride on BDNF, NT3, and their receptor mRNA levels in the spinal contusion rat models. *Neurol. Res.* 41, 577–583. doi: 10.1080/01616412.2019.1588507

Adkins, D. L., Ferguson, L., Lance, S., Pevtsov, A., McDonough, K., Stamschror, J., et al. (2015). Combining multiple types of motor rehabilitation enhances skilled forelimb use following experimental traumatic brain injury in rats. *Neurorehabil. Neural Repair* 29, 989–1000. doi: 10.1177/1545968315576577

Ajao, D. O., Pop, V., Kamper, J. E., Adami, A., Rudobeck, E., Huang, L., et al. (2012). Traumatic brain injury in young rats leads to progressive behavioral deficits coincident with altered tissue properties in adulthood. *J. Neurotrauma* 29, 2060–2074. doi: 10.1089/neu.2011.1883

Ates, N., Caglayan, A., Balcikanli, Z., Sertel, E., Beker, M. C., Dilsiz, P., et al. (2022). Phosphorylation of PI3K/Akt at Thr308, but not phosphorylation of MAPK kinase, mediates lithium-induced neuroprotection against cerebral ischemia in mice. *Exp. Neurol.* 351:113996. doi: 10.1016/j.expneurol.2022.113996

Basso, D. M., Beattie, M. S., and Bresnahan, J. C. (1995). A sensitive and reliable locomotor rating scale for open field testing in rats. *J. Neurotrauma* 12, 1–21. doi: 10.1089/neu.1995.12.1

Basso, D. M., Fisher, L. C., Anderson, A. J., Jakeman, L. B., McTigue, D. M., and Popovich, P. G. (2006). Basso mouse scale for locomotion detects differences in recovery after spinal cord injury in five common mouse strains. *J. Neurotrauma* 23, 635–659. doi: 10.1089/neu.2006.23.635

Beker, M. C., Caglayan, A. B., Kelestemur, T., Caglayan, B., Yalcin, E., Yulug, B., et al. (2015). Effects of normobaric oxygen and melatonin on reperfusion injury: Role of cerebral microcirculation. *Oncotarget* 6, 30604–30614. doi: 10.18632/oncotarget.5773

Boyce, V. S., and Mendell, L. M. (2014). Neurotrophic factors in spinal cord injury. *Handb. Exp. Pharmacol.* 220, 443–460. doi: 10.1007/978-3-642-45106-5_16

Caglayan, A. B., Beker, M. C., Caglayan, B., Yalcin, E., Caglayan, A., Yulug, B., et al. (2019). Acute and post-acute neuromodulation induces stroke recovery by promoting survival signaling, neurogenesis, and pyramidal tract plasticity. *Front. Cell. Neurosci.* 13:144. doi: 10.3389/fncel.2019.00144

Caglayan, A. B., Beker, M. C., Sertel Evren, E., Caglayan, B., Kilic, Ü, Ates, N., et al. (2022). The unconventional growth factors cerebral dopamine neurotrophic factor and mesencephalic astrocyte-derived neurotrophic factor promote post-ischemic neurological recovery, perilesional brain remodeling, and lesion-remote axonal plasticity. *Transl. Stroke Res.* 1–15. doi: 10.1007/s12975-022-01035-2

Cao, Q., Zhang, Y. P., Iannotti, C., DeVries, W. H., Xu, X.-M., Shields, C. B., et al. (2005). Functional and electrophysiological changes after graded traumatic spinal cord injury in adult rat. *Exp. Neurol.* 191(Suppl. 1), S3–S16. doi: 10.1016/j.expneurol.2004.08.026

Carelli, S., Giallongo, T., Rey, F., Colli, M., Tosi, D., Bulfamante, G., et al. (2019). Neuroprotection, recovery of function and endogenous neurogenesis in traumatic spinal cord injury following transplantation of activated adipose tissue. *Cells* 8:329. doi: 10.3390/cells8040329

Chen, G., Liang, Y., Chen, F., Wang, H., and Zhu, G. (2019). The effect of lithium chloride on the motor function of spinal cord injury–controlled rat and the relevant mechanism. *Eur. J. Inflamm.* 17:2058739219852855. doi: 10.1177/2058739219852855

Chiu, C.-T., and Chuang, D.-M. (2011). Neuroprotective action of lithium in disorders of the central nervous system. *Zhong Nan Da Xue Xue Bao Yi Xue* 36, 461–476. doi: 10.3969/j.issn.1672-7347.2011.06.001

De Ferrari, G. V., Chacón, M. A., Barría, M. I., Garrido, J. L., Godoy, J. A., Olivares, G., et al. (2003). Activation of Wnt signaling rescues neurodegeneration and behavioral impairments induced by beta-amyloid fibrils. *Mol. Psychiatry* 8, 195–208. doi: 10.1038/sj.mp.4001208

Doeppner, T. R., Kaltwasser, B., Sanchez-Mendoza, E. H., Caglayan, A. B., Bähr, M., and Hermann, D. M. (2017). Lithium-induced neuroprotection in stroke involves increased miR-124 expression, reduced RE1-silencing transcription factor abundance and decreased protein deubiquitination by GSK3β inhibition-independent pathways. *J. Cereb. Blood Flow Metab.* 37, 914–926. doi: 10.1177/0271678X16647738

Dunham, K. A., Siriphorn, A., Chompoopong, S., and Floyd, C. L. (2010). Characterization of a graded cervical hemicontusion spinal cord injury model in adult male rats. *J. Neurotrauma* 27, 2091–2106. doi: 10.1089/neu.2010.1424

Dwivedi, T., and Zhang, H. (2014). Lithium-induced neuroprotection is associated with epigenetic modification of specific BDNF gene promoter and

altered expression of apoptotic-regulatory proteins. *Front. Neurosci.* 8:457. doi: 10.3389/fnins.2014.00457

Elizei, S. S., and Kwon, B. K. (2017). The translational importance of establishing biomarkers of human spinal cord injury. *Neural Regen. Res.* 12, 385–388. doi: 10.4103/1673-5374.202933

Emerick, A. J., and Kartje, G. L. (2004). Behavioral recovery and anatomical plasticity in adult rats after cortical lesion and treatment with monoclonal antibody IN-1. *Behav. Brain Res.* 152, 315–325. doi: 10.1016/j.bbr.2003.10.010

Fang, X.-Y., Zhang, W.-M., Zhang, C.-F., Wong, W.-M., Li, W., Wu, W., et al. (2016). Lithium accelerates functional motor recovery by improving remyelination of regenerating axons following ventral root avulsion and reimplantation. *Neuroscience* 329, 213–225. doi: 10.1016/j.neuroscience.2016.05.010

Farr, T. D., Liu, L., Colwell, K. L., Whishaw, I. Q., and Metz, G. A. (2006). Bilateral alteration in stepping pattern after unilateral motor cortex injury: A new test strategy for analysis of skilled limb movements in neurological mouse models. *J. Neurosci. Methods* 153, 104–113. doi: 10.1016/j.jneumeth.2005.10.011

Finley, P. R. (2016). Drug interactions with lithium: An update. *Clin. Pharmacokinet.* 55, 925–941. doi: 10.1007/s40262-016-0370-y

Guest, J. D., Hesse, D., Schnell, L., Schwab, M. E., Bunge, M. B., and Bunge, R. P. (1997). Influence of IN-1 antibody and acidic FGF-fibrin glue on the response of injured corticospinal tract axons to human Schwann cell grafts. *J. Neurosci. Res.* 50, 888–905. doi: 10.1002/(SICI)1097-4547(19971201)50:5<888::AID-JNR24<3.0.CO;2-W

Huo, K., Sun, Y., Li, H., Du, X., Wang, X., Karlsson, N., et al. (2012). Lithium reduced neural progenitor apoptosis in the hippocampus and ameliorated functional deficits after irradiation to the immature mouse brain. *Mol. Cell. Neurosci.* 51, 32–42. doi: 10.1016/j.mcn.2012.07.002

Jope, R. S. (1999). Anti-bipolar therapy: Mechanism of action of lithium. *Mol. Psychiatry* 4, 117–128. doi: 10.1038/sj.mp.4000494

Kartje, G. L., Schulz, M. K., Lopez-Yunez, A., Schnell, L., and Schwab, M. E. (1999). Corticostriatal plasticity is restricted by myelin-associated neurite growth inhibitors in the adult rat. *Ann. Neurol.* 45, 778–786. doi: 10.1002/1531-8249(199906)45:6<778::aid-ana12<3.0.co;2-b

Keefe, K. M., Sheikh, I. S., and Smith, G. M. (2017). Targeting neurotrophins to specific populations of neurons: NGF, BDNF, and NT-3 and their relevance for treatment of spinal cord injury. *Int. J. Mol. Sci.* 18:548. doi: 10.3390/ijms18030548

Kelestemur, T., Beker, M. C., Caglayan, A. B., Caglayan, B., Altunay, S., Kutlu, S., et al. (2020). Normobaric oxygen treatment improves neuronal survival functional recovery and axonal plasticity after newborn hypoxia-ischemia. *Behav. Brain Res.* 379:112338. doi: 10.1016/j.bbr.2019.112338

Kilic, E., Kilic, U., Bacigaluppi, M., Guo, Z., Abdallah, N. B., Wolfer, D. P., et al. (2008). Delayed melatonin administration promotes neuronal survival, neurogenesis and motor recovery, and attenuates hyperactivity and anxiety after mild focal cerebral ischemia in mice. *J. Pineal Res.* 45, 142–148. doi: 10.1111/j.1600-079X.2008.00568.x

Kilic, E., Reitmeir, R., Kilic, Ü, Caglayan, A. B., Beker, M. C., Kelestemur, T., et al. (2014). HMG-CoA reductase inhibition promotes neurological recovery, peri-lesional tissue remodeling, and contralesional pyramidal tract plasticity after focal cerebral ischemia. *Front. Cell. Neurosci.* 8:422. doi: 10.3389/fncel.2014.00422

Kim, Y., Kim, J., Ahn, M., and Shin, T. (2017). Lithium ameliorates rat spinal cord injury by suppressing glycogen synthase kinase-3β and activating heme oxygenase-1. *Anat. Cell Biol.* 50, 207–213. doi: 10.5115/acb.2017.50.3.207

Lauterbach, E. C. (2016). Six psychotropics for pre-symptomatic & early Alzheimer's (MCI), Parkinson's, and Huntington's disease modification. *Neural Regen. Res.* 11, 1712–1726. doi: 10.4103/1673-5374.194708

Li, G., Jia, Z., Cao, Y., Wang, Y., Li, H., Zhang, Z., et al. (2015). Mitochondrial division inhibitor 1 ameliorates mitochondrial injury, apoptosis, and motor dysfunction after acute spinal cord injury in rats. *Neurochem. Res.* 40, 1379–1392. doi: 10.1007/s11064-015-1604-3

Liu, P., Zhang, Z., Wang, Q., Guo, R., and Mei, W. (2017). Lithium chloride facilitates autophagy following spinal cord injury via ERK-dependent pathway. *Neurotox. Res.* 32, 535–543. doi: 10.1007/s12640-017-9758-1

Nonaka, S., and Chuang, D. M. (1998). Neuroprotective effects of chronic lithium on focal cerebral ischemia in rats. *Neuroreport* 9, 2081–2084. doi: 10.1097/00001756-199806220-00031

Nori, S., Ahuja, C. S., and Fehlings, M. G. (2017). Translational advances in the management of acute spinal cord injury: What is new? What is Hot? *Neurosurgery* 64, 119–128. doi: 10.1093/neuros/nyx217

Pajoohesh-Ganji, A., Byrnes, K. R., Fatemi, G., and Faden, A. I. (2010). A combined scoring method to assess behavioral recovery after mouse spinal cord injury. *Neurosci. Res.* 67, 117–125. doi: 10.1016/j.neures.2010.02.009

Reitmeir, R., Kilic, E., Kilic, U., Bacigaluppi, M., ElAli, A., Salani, G., et al. (2011). Post-acute delivery of erythropoietin induces stroke recovery by promoting perilesional tissue remodelling and contralesional pyramidal tract plasticity. *Brain* 134, 84–99. doi: 10.1093/brain/awq344

Reitmeir, R., Kilic, E., Reinboth, B. S., Guo, Z., ElAli, A., Zechariah, A., et al. (2012). Vascular endothelial growth factor induces contralesional corticobulbar plasticity and functional neurological recovery in the ischemic brain. *Acta Neuropathol.* 123, 273–284. doi: 10.1007/s00401-011-0914-z

Schulz, A., Walther, C., Morrison, H., and Bauer, R. (2014). In vivo electrophysiological measurements on mouse sciatic nerves. *J. Vis. Exp.* 86:51181. doi: 10.3791/51181

Singer, I., and Rotenberg, D. (1973). Mechanisms of lithium action. *N. Engl. J. Med.* 289, 254–260. doi: 10.1056/NEJM197308022890508

Tysseling, V. M., Janes, L., Imhoff, R., Quinlan, K. A., Lookabaugh, B., Ramalingam, S., et al. (2013). Design and evaluation of a chronic EMG multichannel detection system for long-term recordings of hindlimb muscles in behaving mice. *J. Electromyogr. Kinesiol.* 23, 531–539. doi: 10.1016/j.jelekin.2012.11.014

Volarevic, V., Erceg, S., Bhattacharya, S. S., Stojkovic, P., Horner, P., and Stojkovic, M. (2013). Stem cell-based therapy for spinal cord injury. *Cell Transplant.* 22, 1309–1323. doi: 10.3727/096368912X657260

Youdim, M. B. H., and Arraf, Z. (2004). Prevention of MPTP (N-methyl-4-phenyl-1,2,3,6-tetrahydropyridine) dopaminergic neurotoxicity in mice by chronic lithium: Involvements of Bcl-2 and Bax. *Neuropharmacology* 46, 1130–1140. doi: 10.1016/j.neuropharm.2004.02.005

Young, W. (2009). Review of lithium effects on brain and blood. *Cell Transplant.* 18, 951–975. doi: 10.3727/096368909X471251

Zhang, S., Fujita, Y., Matsuzaki, R., and Yamashita, T. (2018). Class I histone deacetylase (HDAC) inhibitor CI-994 promotes functional recovery following spinal cord injury. *Cell Death Dis.* 9:460. doi: 10.1038/s41419-018-0543-8

Zhang, D., Wang, F., Zhai, X., Li, X.-H., and He, X.-J. (2018). Lithium promotes recovery of neurological function after spinal cord injury by inducing autophagy. *Neural Regen. Res.* 13, 2191–2199. doi: 10.4103/1673-5374.241473

COPYRIGHT

© 2022 Balçıkanlı, Culha, Dilsiz, Aydin, Ates, Beker, Baltaci, Koc, Yigitbasi, Gündogar, Doeppner, Hermann and Kilic. This is an open-access article distributed under the terms of the Creative Commons Attribution License (CC BY). The use, distribution or reproduction in other forums is permitted, provided the original author(s) and the copyright owner(s) are credited and that the original publication in this journal is cited, in accordance with accepted academic practice. No use, distribution or reproduction is permitted which does not comply with these terms.

frontiers | Frontiers in Cellular Neuroscience

TYPE Review
PUBLISHED 29 November 2022
DOI 10.3389/fncel.2022.1077441

Check for updates

OPEN ACCESS

EDITED BY
Tim-Henrik Bruun,
Velvio GmbH, Germany

REVIEWED BY
Shiying Li,
Nantong University, China
Lukas Grassner,
Paracelsus Medical University, Austria

*CORRESPONDENCE
Shengwen Liu
liushengwent047@163.com

SPECIALTY SECTION
This article was submitted to Cellular Neuropathology, a section of the journal Frontiers in Cellular Neuroscience

RECEIVED 23 October 2022
ACCEPTED 08 November 2022
PUBLISHED 29 November 2022

CITATION
Wu Y, Tang Z, Zhang J, Wang Y and Liu S (2022) Restoration of spinal cord injury: From endogenous repairing process to cellular therapy. *Front. Cell. Neurosci.* 16:1077441. doi: 10.3389/fncel.2022.1077441

COPYRIGHT
© 2022 Wu, Tang, Zhang, Wang and Liu. This is an open-access article distributed under the terms of the Creative Commons Attribution License (CC BY). The use, distribution or reproduction in other forums is permitted, provided the original author(s) and the copyright owner(s) are credited and that the original publication in this journal is cited, in accordance with accepted academic practice. No use, distribution or reproduction is permitted which does not comply with these terms.

Restoration of spinal cord injury: From endogenous repairing process to cellular therapy

Yaqi Wu, Zhijian Tang, Jun Zhang, Yu Wang and Shengwen Liu*

Department of Neurosurgery, Tongji Hospital, Tongji Medical College, Huazhong University of Science and Technology, Wuhan, China

Spinal cord injury (SCI) disrupts neurological pathways and impacts sensory, motor, and autonomic nerve function. There is no effective treatment for SCI currently. Numerous endogenous cells, including astrocytes, macrophages/microglia, and oligodendrocyte, are involved in the histological healing process following SCI. By interfering with cells during the SCI repair process, some advancements in the therapy of SCI have been realized. Nevertheless, the endogenous cell types engaged in SCI repair and the current difficulties these cells confront in the therapy of SCI are poorly defined, and the mechanisms underlying them are little understood. In order to better understand SCI and create new therapeutic strategies and enhance the clinical translation of SCI repair, we have comprehensively listed the endogenous cells involved in SCI repair and summarized the six most common mechanisms involved in SCI repair, including limiting the inflammatory response, protecting the spared spinal cord, enhancing myelination, facilitating neovascularization, producing neurotrophic factors, and differentiating into neural/colloidal cell lines.

KEYWORDS

spinal cord injury, repair, cell transplantation, mechanism, stem cell

Introduction

Spinal cord injury (SCI) leads to a great burden for the patients and the society (Garcia-Altes et al., 2012; Dorsett et al., 2017; James Spencer and Theadom, 2019; Collaborators et al., 2021). The global incidence of SCI is 10.5 cases per 100,000 people, with an estimated 0.8 million new cases recorded each year (Kumar et al., 2018). Traffic accidents and falls have been considered to be the two most dominant causes all throughout the world (McDonald and Sadowsky, 2002; Alizadeh et al., 2019; Du et al., 2021). The spinal cord underwent two continuous pathophysiological processes after injury before entering a chronic state (McDonald and Sadowsky, 2002; Ahuja et al., 2017; **Figure 1**). The first stage is the primary injury caused by an external force, damaging

the neural pathways and surrounding blood vessels (Alizadeh et al., 2019; Defrin et al., 2022). Then, a cascade of reactions including inflammation, oxidative stress, excitatory toxicity, ischemia, and astrocytic hyperplasia are triggered by the overflowing blood gradients and cellular components (Tran et al., 2018). All these changes lead to fibroglial scarring and cavity formation, as well as a further decrease of neurons and interruption of the neural pathways, which result in allodynia, impaired locomotor and autonomic dysfunction in some populations (Berger et al., 2014; Brommer et al., 2021; Defrin et al., 2022).

The pathological changes after SCI also induce an overproduction of molecules as chondroitin sulfate proteoglycans (CSPGs), Nogo A, myelin-associated glycoprotein, and oligodendrocyte myelin glycoprotein, which are inhibitors for neural regeneration in extracellular matrix (Moeendarbary et al., 2017). In animal models, researchers found that neutralization by functionally blocking antibodies, genetic deletion of Nogo-A, or blockade of Nogo-A receptors induces substantial axonal regeneration, as well as enhanced neuronal plasticity and functional recovery after SCI or stroke (Gonzenbach et al., 2010; Schwab and Strittmatter, 2014; Wahl et al., 2014). Furthermore, due to the lack of growth-promoting factors within the lesion, self-repair of the spinal cord to rebuild the damaged neural circuit is very difficult. So far as we know, effective approaches for the treatment of SCI patients are very limited. However, various strategies have been explored to treat SCI on animal models, including the transplantation of cells and biomaterials (Assinck et al., 2017a; Dumont et al., 2019), administration of medications (Liu et al., 2019) and neurotrophic factors (Xu et al., 2014), locomotor training (Angeli et al., 2018), and electrical stimulation (Formento et al., 2018). A great achievement has been made in animal experiments and some of these approaches have been applied in clinical trials for human subjects (Liu et al., 2019; Bartlett et al., 2020). For instance, in their initial human study published in 2018, Kucher academics assessed the early efficacy of human anti-nogo-A antibodies given intravenously to patients with acute, total traumatic paraplegia and quadriplegia. They discovered that following SCI, human anti-nogo-A antibodies partially recovered motor function. Their discoveries set the stage for the clinical use of anti-nogo-A antibodies. But more extensive studies on the effectiveness of anti-nogo-A antibodies in enhancing neurological recovery following SCI are required (Kucher et al., 2018).

At present, various treatments such as stem cell transplantation, growth factor injection, and biomaterial transplantation promote the repair of spinal cord function by reducing inflammatory response, promoting myelination, reducing cavity area, and promoting axon growth (Lu et al., 2014; Maldonado-Lasuncion et al., 2021). However, the complexity and heterogeneity of the pathophysiology of SCI are the main reasons for the lack of understanding and failure of SCI treatment. It is very crucial to comprehend the repair mechanism of SCI in order to offer a superior repair strategy (O'Shea et al., 2017). In light of this, this review summarizes the role of endogenous cells in the repair of SCI such as astrocyte, macrophages/microglia, oligodendrocyte, pericyte, endogenous neural stem/progenitor cell, Schwann cells, and other cells. In addition, we also summarized the targets of intervention through exogenous treatment of SCI, such as limiting the inflammatory response, protecting the spared spinal cord, enhancing myelination, facilitating neovascularization, producing neurotrophic factors, and differentiating into neural/colloidal cell lines. This review provides a very comprehensive description of the process of endogenous cellular repair in SCI and the associated mechanisms, which provides a solid basis for research strategies for SCI repair.

Cell types involved in spinal cord injury repair

A variety of cell types attempt to aid in the healing of SCI, and these cells interact with one another and take part in the healing process (O'Shea et al., 2017). We can create more efficient treatment plans by better understanding how cells repair it. These cells include astrocytes, macrophages/microglia, oligodendrocytes, pericytes, endogenous neural stem/progenitor cells, Schwann cells, and other cells, as described in **Table 1** and **Figure 2**. The role that each type of cell involved in the repair process of SCI is described as follows.

Astrocyte

During the development of the mammalian nervous system, neurogenesis often occurs in the embryonic stage, while glial are formed after birth (Eze et al., 2021). Astrocytes are the complex and abundant glial cells in the nervous system, which are present throughout the spinal cord (Wiltbank and Kucenas, 2021). When cultured *in vitro*, activated astrocytes can form neurons, oligodendrocytes, and astrocytes under certain factors (Noristani et al., 2016; Xia et al., 2020; Wang et al., 2021). Astrocytes have a variety of functions, including the regulation of blood flow (MacVicar and Newman, 2015; Bazargani and Attwell, 2016), the provision of energy to surrounding neurons (Magistretti and Allaman, 2018), the formation and function of synapses (Klapper et al., 2019), maintenance of extracellular ion balance and the delivery of related neurotransmitters (Parpura et al., 2016).

The role of astrocytes in SCI is still controversial (Escartin et al., 2021). According to the majority of studies, SCI can activate astrocytes, which create glial scars at the site of injury

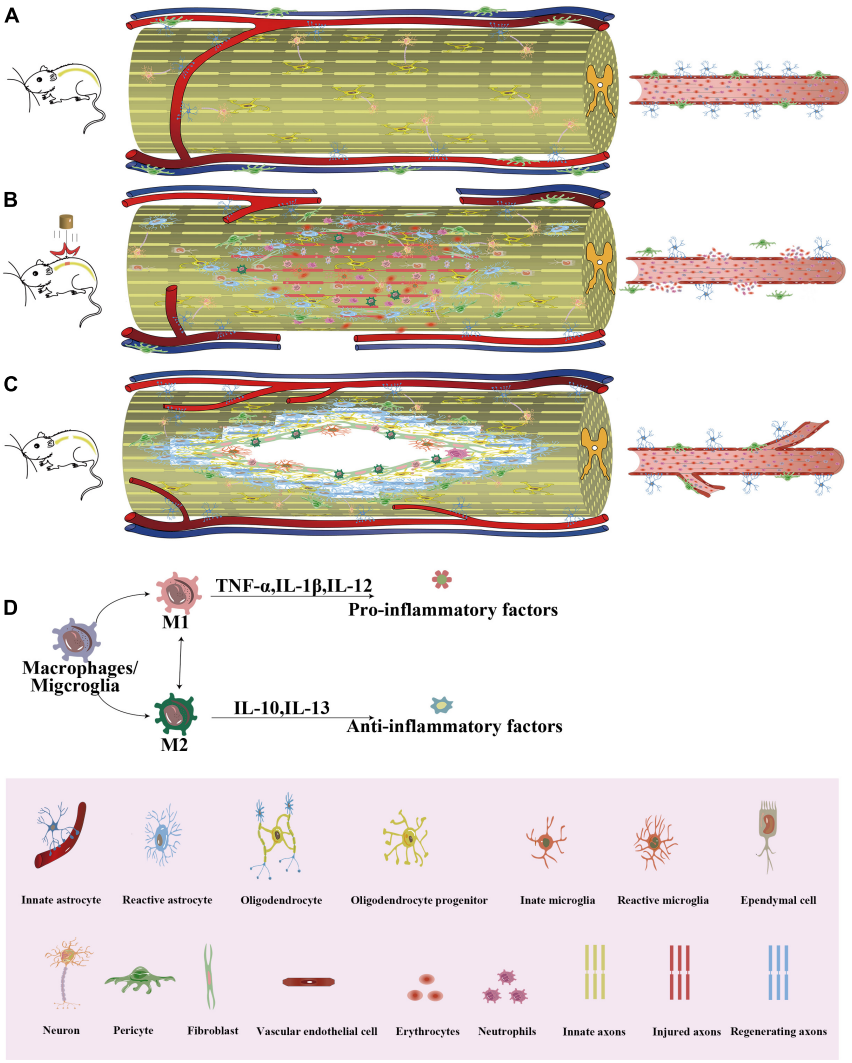

FIGURE 1
The process of cellular repair of SCI. After SCI, a series of repeated cascade responses, including cellular as well as non-cellular reactions, will occur. **(A)** Normal spinal cord and paraspinal vessels in uninjured mice. **(B)** In the acute phase of SCI, the BSCB is disrupted, neuronal death occurs, Wallerian degeneration of distal axons with a demyelinating response, permeability of the vessel wall increases, hematomas form, and hematogenous macrophages and neutrophils are recruited to the core of the lesion. Astrocytes migrate toward the core of the lesion and envelop the damaged tissue, thus protecting the remaining tissue from further damage. Microglia are also activated and morphologically altered to engulf the necrotic tissue along with blood-derived macrophages. Oligodendrocyte precursor cells have a marked ability to proliferate and interact with reactive glial cells at the border of the injury. Fibroblasts induced a marked fibroblast response, with large numbers of fibroblasts depositing around the core of the lesion. Epithelial cells migrated from the central canal of the spinal cord to the site of injury and participated in repair as endogenous stem cells. Pericytes detach from the basement membrane of the vessel wall and migrate to the injury site to participate in glial scar formation and to close the center of the injury. **(C)** In the chronic phase of SCI, the core of the lesion is often not effectively treated, resulting in the formation of a cavity in the lesion area surrounded by a glial scar formed by aggregates of hypertrophic astrocytes, pericytes, fibroblasts, and NG2+ oligodendrocytes, with neovascularization and accompanied by a small amount of myelin and axon formation. **(D)** The inflammatory environment causes changes in the macrophage phenotype. SCI, Spinal cord injury; BSCB, Blood-spinal cord barrier; TNF, Tumor necrosis factor; IL, Interleukin; NG2, Neuron-glial antigen 2.

that can wrap around injured tissue, reduce inflammation and prevent neuronal death, and maintain the integrity of the cells around the lesion (Robel et al., 2011). These reactive astrocytes are important for enveloping the injury site in the early stages of damage. Astrocytes can also play a direct role in synaptic transmission and may even support axonal regeneration by regulating the release of synaptic active molecules such as glutamate, purine (ATP and adenosine), GABA, and D-serine (Gundersen et al., 2015; Boddum et al., 2016; **Figure 2**). However, Yiu and other researchers believed that the persistent role of these glial scars would not only act as a physical barrier but also secrete neuroinhibitory factors that prevent the

regeneration of axons, which is not conducive to the clinical repair of SCI (Silver and Miller, 2004; Yiu and He, 2006). Menet also demonstrated that reducing reactive astrocytes during injury improved axonal regeneration and enhanced functional recovery after SCI in mice lacking both GFAP and vimentin (Menet et al., 2003).

Astrocytes can be reprogrammed and a patient's endogenous glial cells can be converted into neurons to treat SCI. Horner demonstrated that astrocytes lose their ability to form neurons after the second week of formation (Horner et al., 2000), but Vierbuchen et al. found that mature reactive astrocytes can still form neurons (Buffo et al., 2008; Vierbuchen et al., 2010; Caiazzo et al., 2011). Torper also demonstrated that astrocytes can be transformed into neuroblasts with proliferative properties by a single transcription factor SOX2 and further develop into functionally mature neurons *in vivo* (Torper et al., 2013). These findings imply that astrocytes might possess specific stem cell characteristics, opening up fresh avenues for the therapy of SCI. However, cell reprogramming is inefficient and the number of neurons successfully converted is relatively small currently. Due to the regional heterogeneity of astrocytes (Tsai et al., 2012), there are no specific studies of astrocytes in the adult spinal cord that can be reprogrammed *in vivo*. In order to enhance the reprogramming process and produce particular subtypes of neurons that support SCI repair, more study is required in this field, which necessitates the development of a novel, precise programming technique.

Macrophages/microglia

Macrophages and microglia emerge from separate embryonic sources (Ginhoux et al., 2010; Schulz et al., 2012; Kierdorf et al., 2013). Mice's microglia, which are resident macrophages in the central nervous system (CNS), are produced from erythromyeloid progenitors in the fetal yolk sac during embryonic development (Prinz and Priller, 2014; Bian et al., 2020). Macrophages are derived from extravasated monocytes, which are first made by aorta-gonad-mesonephros erythromyeloid progenitors (Perdiguero et al., 2015). Microglia and blood-derived macrophages are the sources of macrophages in the region of the lesion after spinal cord damage (David and Kroner, 2011).

Spinal cord injury induces a powerful and highly coordinated inflammatory response involving rapid activation and migration of microglia, accompanied by infiltration and recruitment of macrophages derived from peripheral blood monocyte within the lesion (David and Kroner, 2011). The damaged spinal cord tissue releases cytokines and chemokines into the circulation, and monocytes then migrate to the site of injury and differentiate into macrophages in response to the chemokines (Shechter et al., 2009). Inflammatory response after SCI is a double-edged sword (Plemel et al., 2014a; Gadani et al., 2015). Along with the death of neurons after SCI, the inflammatory response also causes glial scarring and cavitation. Recent research has however demonstrated that inflammation promotes neuronal regeneration and functional recovery, with activated microglia and blood-derived macrophages playing a crucial part (Cunha et al., 2020). Microglia and blood-derived macrophages primarily phagocytose and remove cellular debris and leftover tissue that accumulate after SCI (**Figure 2**). Microglia rapidly activate and proliferate after SCI, yet in the rat SCI model, blood-derived macrophages do not reach the SCI site until about 3 days after SCI and peak at 7 days after SCI, with two subsequent peaks at day 14 and day 60 after SCI, respectively (Chio et al., 2021). Therefore, compared to blood-derived macrophages, microglia have a much better efficiency and proliferation rate when phagocytosing lesioned myelin. When a mouse's spinal cord was injured, macrophages were found toward the lesion's center, whereas microglia were mostly found at the lesion's perimeter (Shechter et al., 2009; Greenhalgh and David, 2014; Zrzavy et al., 2021; **Figure 1**). Additionally, it has recently been demonstrated that microglia and macrophages interact, and that co-culturing microglia and blood-derived macrophages causes a decrease in the capacity of the microglia to phagocytose myelin and an increase in the ability of the blood-derived macrophages to do so (Greenhalgh and David, 2014; Greenhalgh et al., 2018).

Microglia and blood-derived macrophages in SCI are mainly classified into two phenotypes according to their different cellular markers and functions: M1 type with pro-inflammatory properties and M2 type with anti-inflammatory properties (David and Kroner, 2011; Zhou et al., 2014; Hu et al., 2015; Orihuela et al., 2016; **Figure 1**). After SCI, M1 microglia and blood-derived macrophages upregulate and produce TNF-α, IL-1β, and chemokines, which draw inflammatory cells to the lesion to speed up the removal of necrotic tissue while simultaneously accelerating neuronal death and tissue damage (Liddelow et al., 2017). M2 microglia and blood-derived macrophages secrete TGF-β, IL-4, and IL-10, which suppress excessive immune inflammatory responses and promote the repair of damaged tissues (Cherry et al., 2014). Determining the conditions that will cause the phenotypic flip of M1/M2 macrophages is thus another issue that has to be addressed. One of the key strategies in the treatment of SCI will be to reduce the activation of M1-type cells while preserving the activation of M2-type cells or encouraging the conversion of M1-type to M2-type macrophages. M2 macrophages are important in tissue fibrosis as well (Pechkovsky et al., 2010; Ikezumi et al., 2011), therefore their prolonged presence after SCI may encourage the development of fibrotic scarring, which is harmful to axonal regeneration.

Due to their comparable shape and phenotypic characteristics in the diseased CNS, microglia and blood-derived macrophages are difficult to distinguish from one another. Transcriptomics revealed that specific genes such

TABLE 1 Cells involved in the repair process of SCI and their repair roles.

Types of cells	Study	Journal	Restoration effect
Astrocytes	Noristani et al., 2016	Molecular Neurodegeneration	Forming neurons and oligodendrocytes
	Wang et al., 2021	Cell	
	Xia et al., 2020	Translational Neurodegeneration	
Astrocytes	Bazargani and Attwell, 2016	Nature Neuroscience	Regulating blood flow
	MacVicar and Newman, 2015	Cold Spring Harbor Perspectives in Biology	
Astrocytes	Magistretti and Allaman, 2018	Nature Reviews Neuroscience	Providing energy to the surrounding neurons
Astrocytes	Klapper et al., 2019	Glia	Involving in the formation of synapses
Astrocytes	Parpura et al., 2016	Glia	Maintaining extracellular ion balance and delivering of related neurotransmitters
Astrocytes	Sofroniew and Vinters, 2010	Acta Neuropathologica	Creating glial scars at the site of injury
Astrocytes	Boddum et al., 2016	Nature Communications	Supporting axonal regeneration by regulating the release of synaptic active molecules
	Gundersen et al., 2015	Physiological Reviews	
Astrocytes	Torper et al., 2013	Proceedings of the National Academy of Sciences of the United States of America	Possessing specific stem cell characteristics
Macrophages/microglia	Liddelow et al., 2017	Nature	Secreting pro-inflammatory factors
Macrophages/microglia	David and Kroner, 2011	Nature Reviews Neuroscience	Secreting anti-inflammatory factors
	Hu et al., 2015	Nature Reviews Neurology	
	Orihuela et al., 2016	British Journal of Pharmacology	
	Zhou et al., 2014	Neural Regeneration Research	
Macrophages/microglia	Greenhalgh and David, 2014	Journal of Neuroscience	Phagocyticing and removing accumulated cellular debris and leftover tissue after SCI
	Greenhalgh et al., 2018	PLoS Biology	
Macrophages/microglia	Ikezumi et al., 2011	Histopathology	Promoting tissue fibrosis
	Pechkovsky et al., 2010	Clinical Immunology	
Oligodendrocytes/ oligodendrocyte progenitor cells	Kirby et al., 2019	Nature Communications	Promoting axon regeneration
Oligodendrocytes/ oligodendrocyte progenitor cells	Gibson et al., 2014	Science	Promoting myelin formation
Pericytes	Attwell et al., 2016	Journal of Cerebral Blood Flow and Metabolism	Constricting blood vessels
Pericytes	Fawcett et al., 2011	Nature Medicine	Forming scar tissue
	Goritz et al., 2011	Science	
Pericytes	Dias et al., 2018	Cell	Promoting fibrosis formation and extracellular matrix deposition
Pericytes	Chen et al., 2017a	Proceedings of the National Academy of Sciences of the United States of America	Maintaining the stability of the blood-brain barrier
	Yao et al., 2014	Nature Communications	
Pericytes	Hesp et al., 2018	Journal of Neuroscience	Promoting vascular remodeling
	You et al., 2014	Angiogenesis	Maintaining normal vascular structure Promoting tissue healing
Pericytes	An et al., 2022	Diabetes	Maintaining normal vascular structure
	Santos et al., 2019	Neuroscience Bulletin	
Pericytes	Rustenhoven et al., 2017	Trends in Pharmacological Sciences	Phagocytosis
Pericytes	Cheng et al., 2018	Acta Neuropathologica	Secreting neurotrophic factors
	Nikolakopoulou et al., 2019	Nature Neuroscience	
Pericytes	Nakagomi et al., 2015	Stem Cells	Possessing specific stem cell characteristics
Endogenous neural stem/progenitor cells	McKay, 1997	Science	Self-renewing and differentiating into neurons, astrocytes, and oligodendrocytes
	Reynolds and Weiss, 1992	Science	
	Stenudd et al., 2015	JAMA Neurology	

(Continued)

TABLE 1 (Continued)

Types of cells	Study	Journal	Restoration effect
Schwann cells	Boerboom et al., 2016	Frontiers in Molecular Neuroscience	Promoting myelin formation
	Jessen et al., 2015	Cold Spring Harbor Perspectives in Biology	
	Norrmen et al., 2018	Journal of Neuroscience	
	Soto and Monje, 2017	Glia	
Schwann cells	Min et al., 2021	Glia	Recruiting macrophages
	Yin et al., 2022	Molecular Medicine	
Schwann cells	Jessen and Mirsky, 2016	The Journal of Physiology	Removing Waller degeneration and distal neuronal myelin and stimulating axonal growth
Schwann cells	Catignas et al., 2021	Glia	Secreting neurotrophic factors
	Maugeri et al., 2020	International Journal of Molecular Sciences	
	Selvaraj et al., 2012	Journal of Cell Biology	
	Sukhanov et al., 2021	Journal of Neuroscience	
Schwann cells	Liu et al., 2017a	Acta Biomaterialia	Promoting axon regeneration
Fibroblasts	Lee et al., 2020	Elife	Converting to inducible motor neurons
Microvascular endothelial cells	Zhou et al., 2019	Nature Neuroscience	Engulfing myelin fragments
Immunological T cells	Ishii et al., 2013	Cell Death and Disease	Initiating T cell-mediated autoimmune responses Secreting neurotrophic factors
Platelet cells	Ye et al., 2021	Neural Regeneration Research	Enhancing the performance of the BSCB

as TMEM119 and P2RY12 are highly expressed in microglia compared to blood-derived macrophages, so this can be used as a microglia-specific marker, but the levels of these markers are not stable and constant (Haynes et al., 2006; Bennett et al., 2016), so markers that can stably distinguish between macrophages and microglia need to be further explored by a wide range of scholars. Additionally, in patients who have had SCI, cellular debris may continue to exist for a number of years (Becerra et al., 1995). Therefore, a deeper comprehension of the processes by which microglia and blood-derived macrophages are ingested and digested is essential, and the phagocytosis of microglia and blood-derived monocytes may also be a viable target for the treatment of SCI.

Oligodendrocyte

Myelin, the primary component of the myelin sheath, surrounds axons in the nervous system and is crucial for allowing axonal signaling (**Figures 1**, **2**), which is the exchange of information between neurons (Stadelmann et al., 2019). The gray and white matter of the spinal cord includes oligodendrocyte progenitors that support the growth of endogenous oligodendrocytes and myelin regrowth (Maldonado et al., 2013; Gibson et al., 2014; Huang W. et al., 2020). By preventing inflammatory molecules from being released and secreting neurotrophic substances, oligodendrocyte progenitors aid in axonal regeneration (Kirby et al., 2019). The microenvironment following SCI, however, has an impact on its capacity to develop into oligodendrocytes (Alizadeh and Karimi-Abdolrezaee, 2016; Yalcin and Monje, 2021). Understanding the factors that promote endogenous oligodendrocyte progenitor cell activity in the SCI microenvironment can help to develop more effective repair strategies to achieve myelin regeneration after SCI (Gautier et al., 2015).

After SCI, oligodendrocyte death, a secondary demyelination reaction, causes axonal damage and the loss of sensorimotor function (Plemel et al., 2014b; Duncan et al., 2020; Floriddia et al., 2020). Axonal action potential transmission is dependent on sodium ion channels in the axonal membrane (Berret et al., 2016, 2017). Demyelination decreases the distribution of sodium ion channels in the axonal membrane, which may impede or slow action potential transmission and result in functional defects (Lubetzki et al., 2020). However, there isn't any conclusive direct evidence that demyelination is what's causing the conduction failure following SCI (Duncan et al., 2018). For instance, even when axons are preserved after SCI, there is decreased transmission in the spinal cord, which is clinically referred to as spinal shock (Ziu and Mesfin, 2022). The regeneration of myelin sheath in oligodendrocytes and the recovery of action potential conduction were also inconsistent in time. The partial potential conduction can be recovered within the first two weeks following SCI (Beaumont et al., 2006). But two weeks after SCI, oligodendrocytes began to regenerate their myelin (James et al., 2011).

It is currently unclear how exactly oligodendrocyte apoptosis occurs following SCI, while it may be related to ischemia or an inflammatory reaction at the damage site (Alizadeh and Karimi-Abdolrezaee, 2016). Calcium can accumulate toxically in oligodendrocytes as a result of excitatory toxicity brought on by glutamate or ATP (Voccoli et al., 2014;

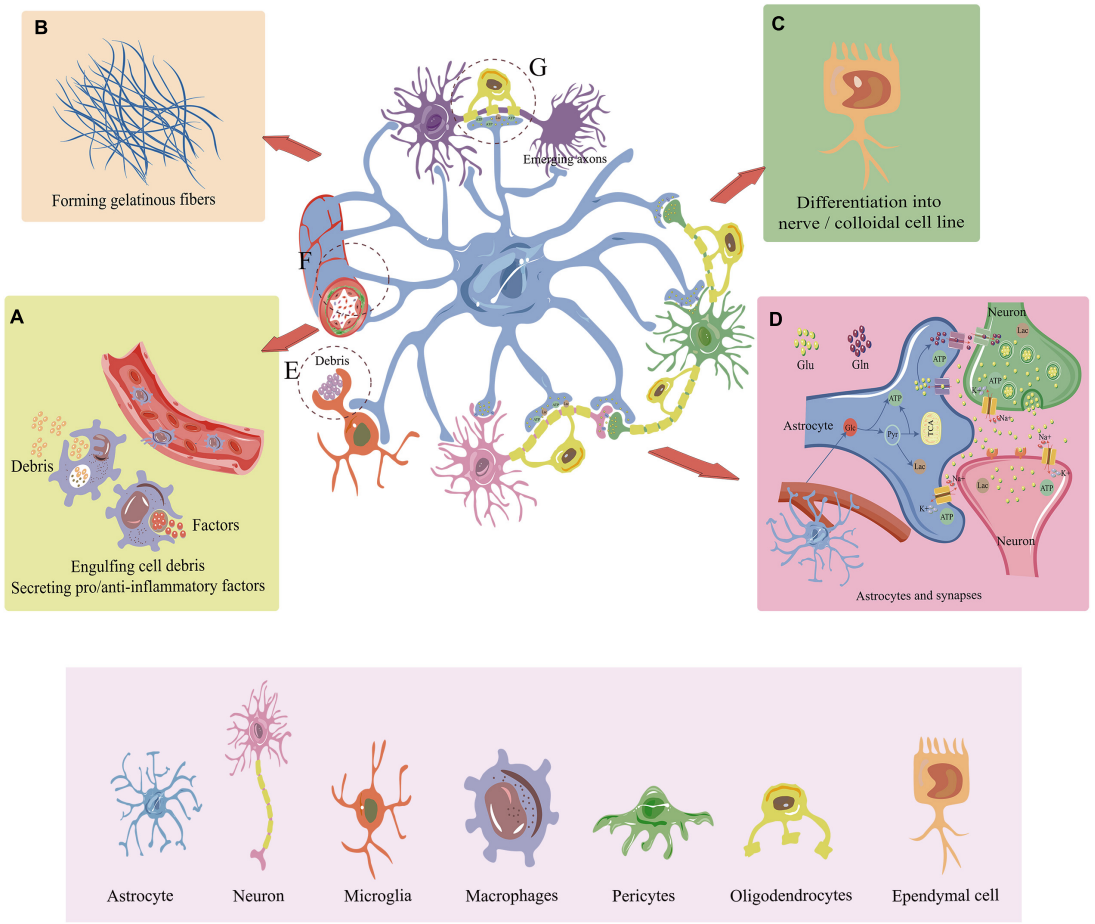

FIGURE 2
Major role of endogenous cells in the repair of SCI. **(A)** Under the influence of chemokines, macrophages migrate to the site of injury with outstretched peduncles to engulf cell debris and remnant tissues. They also stimulate relevant pro-inflammatory and anti-inflammatory molecules involved in the repair of spinal cord injuries. **(B)** Astrocytes and pericytes can secrete fibronectin to promote glial. **(C)** Ependymal cells are the major endogenous stem cells that differentiate into neural/colloidal cell lines that includes neurons, oligodendrocytes, and astrocytes. **(D)** Astrocytes take up glucose from blood vessels and convert it to lactate and ATP to provide energy for peripheral neurons. Astrocytes also facilitate the transmission of neurotransmitters such as glutamate, enhancing the signal communication between neurons. In addition, astrocytes maintain ion homeostasis inside and outside the cell. **(E)** Microglia engulf cellular debris and residual tissue at the site of SCI. **(F)** Astrocytes control blood flow by interacting with blood arteries. Pericyte can promote vascular remodeling, maintain normal vascular structure and stabilize the BSCB during SCI repair. **(G)** Oligodendrocytes help myelin regenerate, and astrocytes also give myelin and axon regeneration energy. SCI, Spinal cord injury; BSCB, Blood-spinal cord barrier; Glu, Glucose; Glu, Glutamate; Gln, Glutamine; TAC, Tricarboxylic acid cycle; Lac, Lactate; Pyr, Pyruvic acid.

Lecca et al., 2016; Barron and Kim, 2019; Paez and Lyons, 2020). Oligodendrocyte death is also facilitated by inflammatory mediators generated by infiltrating neutrophils and microglia (Zirngibl et al., 2022). Therefore, preventing oligodendrocytes from dying or encouraging oligodendrocyte progenitor cells to differentiate following SCI can aid in the recovery of function (Manley et al., 2017; Sankavaram et al., 2019).

Whether mature oligodendrocytes have the ability to promote myelin regeneration has not been unanimously concluded in the scientific community. Some researchers have long believed that oligodendrocytes can neither migrate nor regenerate myelin sheath after SCI since oligodendrocytes are post-mitotic and differentiated (Crawford et al., 2016). Recent research, however, has revealed that mature oligodendrocytes do take a role in myelin repair following injury (Macchi et al., 2020). These variations in outcomes can be attributable to various experimental animal models, cell lines, and demyelination damage types. Regenerated myelin, however, is frequently thinner and less regular than healthy myelin (Duncan et al., 2017). The diameter of the axon and the thickness of the regenerated myelin sheath did not correlate linearly (Ludwin and Maitland, 1984). Additionally, myelin internodes are smaller and more delicate than usual (Griffiths and McCulloch, 1983). But Powers' study contradicts it by arguing that past assessments have underestimated the extent and quality of regenerated myelin (Powers et al., 2013). Therefore, it is

necessary to further confirm the difference between regenerated myelin and normal myelin at a later stage.

Pericyte

Pericytes are also called Rouget cells or parietal cells. Rouget made the initial discovery of pericytes in 1873 while researching the capillaries' ability to contract (Rouget, 1873). In 1923, Zimmermann named them pericytes based on their location around blood vessels (Zimmermann, 1923). Pericytes, which are often embedded and linked to the blood vessel basement membrane, are found on the walls of blood arteries and surround endothelial cells (Attwell et al., 2016). Pericytes have different morphologies at different locations in the vasculature, including "Transitional pericyte," which has more annular protrusions at the ends of small arteries in the capillary bed, "Midcapillary pericyte," which has more longitudinal protrusions, and "Stellate-shaped pericyte," which has more stellate protrusions at the ends of small veins in the capillary bed (**Figure 3**; Hartmann et al., 2015).

Astrocytes promoting scar formation after SCI have been a research hotspot (Anderson et al., 2016; Hara et al., 2017). Goritz and others discovered, however, that after SCI, pericytes detach from the basement membrane, multiply, and go to the SCI site where they take part in the creation of glial scar and seal the damage center (**Figure 1**; Fawcett et al., 2011; Goritz et al., 2011). Within 14 days of SCI in mice, the proliferation of pericytes exceeded that of astrocytes, and inhibition of pericyte proliferation disrupted scar formation and led to open tissue defects, which suggests that pericytes are also key to scar formation after SCI (Goritz et al., 2011). Additionally, it has been demonstrated that preventing pericyte proliferation lessens the fibrotic response and extracellular matrix deposition, which boosts axonal regeneration and encourages sensorimotor recovery after SCI (Dias et al., 2018). These studies have shown the significance of pericytes in the development of scars following SCI. The mechanism of peripheral cell growth and migration from the vascular wall to the scar site following SCI, however, is poorly understood (Dias et al., 2021).

Pericytes come in a variety of subtypes, and each subtype performs a unique function during SCI (Zhu et al., 2022). CD146 pericytes maintain the stability of the blood-brain barrier (Chen et al., 2017a) and secrete cell-adhesion molecules that allow pericytes to attach to endothelial cells (Iacobaeus et al., 2017); NG2 pericytes can not only promote vascular remodeling,

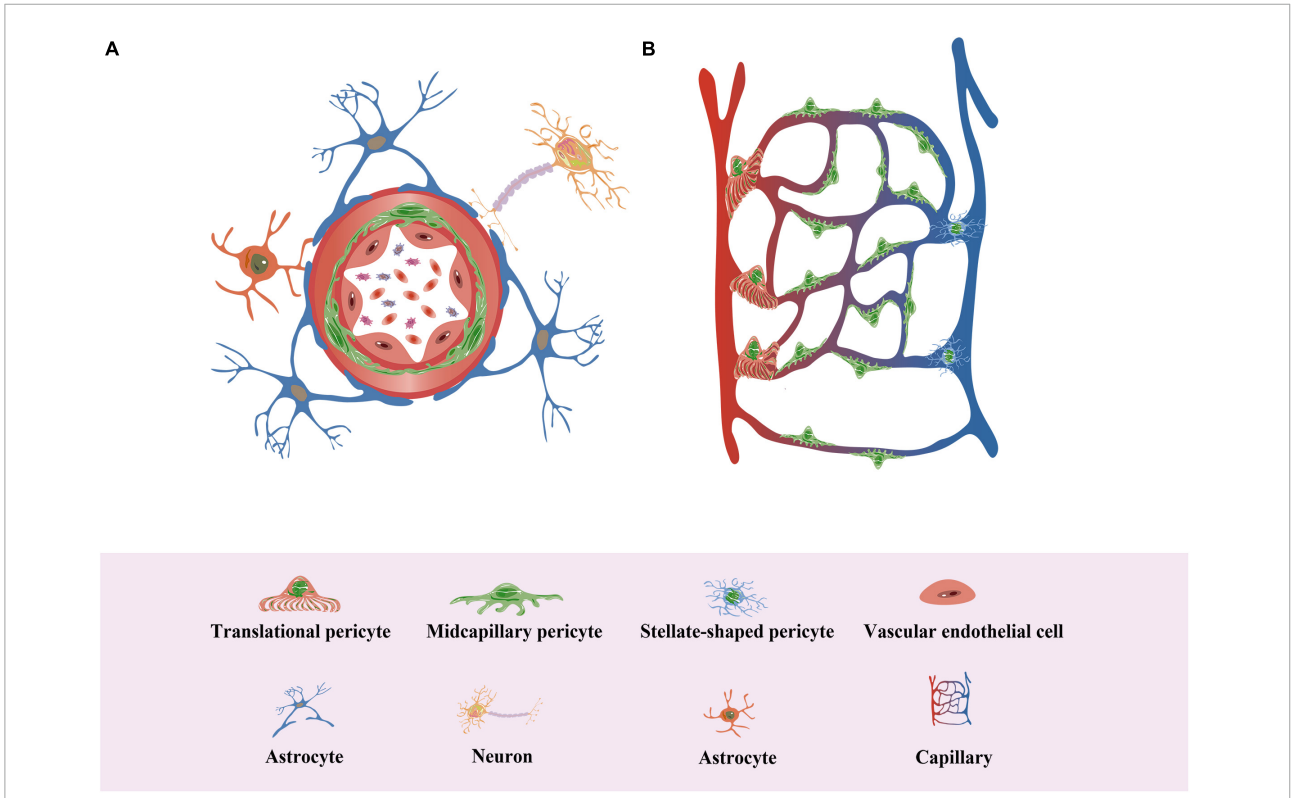

FIGURE 3
Pericytes in neovascularization. **(A)** Pericytes surround the endothelium in the vessel wall and are typically embedded in and linked to the basement membrane of the vessel. **(B)** Pericytes are a population of cells with various subtypes, including "Transitional pericyte", which has more annular protrusions at the ends of small arteries in the capillary bed, "Midcapillary pericyte", which has more longitudinal protrusions, and "Stellate-shaped pericyte", which has more stellate protrusions at the ends of small veins in the capillary bed.

maintain normal vascular structure, but also promote tissue healing (You et al., 2014; Hesp et al., 2018); PDGFR-β pericytes are the source of scar formation after SCI and have the potential to block lesions (Dias et al., 2021). However, conducting specialized study on pericytes is challenging since there is no one marker that can identify the entire pericyte population.

Pericytes play a very intricate role in SCI. It not only affects the integrity of the blood-brain barrier by influencing the role of AQP4 at the end of foot processes of astrocytes (Gundersen et al., 2014; Yao et al., 2014) but also plays a key role in angiogenesis (Caporali et al., 2017; Teichert et al., 2017). At the same time, pericytes play a crucial part in the stability and structural maintenance of blood vessels; otherwise, the blood vessels have a different shape and are more likely to burst as microaneurysms (Santos et al., 2019; An et al., 2022). Pericytes phagocytosis has been shown by Rustenhoven to be effective in clearing harmful materials from the microcirculation (Rustenhoven et al., 2017). Neurotrophic factors including NGF, BDNF, and NT-3 are produced by pericytes, and these substances can help neurons develop (Cheng et al., 2018; Nikolakopoulou et al., 2019). Pericytes also possess stem cell properties and can differentiate into neurons, astrocytes, and oligodendrocytes (Nakagomi et al., 2015). Research continues into the mediators and process governing pericyte directional differentiation. After SCI, severe demyelination frequently takes place, which impairs the transmission of motor signals (Orr and Gensel, 2018). Fuente discovered that pericytes would alter the CNS's myelin regeneration process and that abnormalities in pericytes would cause a delay in myelin production through the research of a mouse model missing pericytes (De La Fuente et al., 2017). These results suggest that pericytes may be the key cells involved in the SCI repair process.

Pericytes are therefore possible therapeutic targets for SCI. The therapeutic use of pericytes is somewhat constrained since there is no reliable way to recognize and separate the many subtypes of pericytes. In order to implement appropriate targeted therapeutics, researchers can expand pertinent studies in this field and investigate the precise functions played by various pericyte subtypes throughout the development of SCI.

Endogenous neural stem/progenitor cells

In the adult spinal cords of rodents and primates, a region known as the neurogenic region has recently been identified. This region is made up of cells that surround the central canal, proliferate, and generate a range of cell types *in vivo* while acting similarly to neural stem cells *in vitro* (Weiss et al., 1996; Johansson et al., 1999; Horner et al., 2000; Meletis et al., 2008; Bamabé-Heider et al., 2010). Endogenous neural stem/progenitor cells are present in the nervous system with the ability not only to self-renew but also to differentiate into neurons, astrocytes, and oligodendrocytes (**Figure 4**; Reynolds and Weiss, 1992; McKay, 1997). Cells with endogenous neural stem/progenitor cells potential in the adult spinal cord, which lie dormant in the uninjured spinal cord, are activated and migrate to the injury center once the spinal cord is injured (Morest and Silver, 2003; Horky et al., 2006; Duncan et al., 2020). Activated neural stem cells (NSCs) can self-renew and differentiate into astrocytes and oligodendrocytes for tissue repair (Stenudd et al., 2015). Meletis has identified endogenous NSCs as ependymal cells through genetic profiling (Meletis et al., 2008). Ependymal cells are present in the ventricular system and the central canal of the spinal cord (Sabelstrom et al., 2014). In the mouse spinal cord, ependymal cells originate in the middle embryo and are already present completely around the central canal at birth (Li X. et al., 2016).

There are three main types of cells involved in uninjured spinal cord division, of which 80% were derived from NG2+/Olig2+ oligodendrocytes, <5% from GFAP+/CX30+/Sox9+ astrocytes and <5% from FoxJ1+ ependymal cells (Bamabé-Heider et al., 2010). Meletis divides ependymal cells into three basic types according to the form of them by Foxj1-Creer transgenic mice: Cuboidal ependymal cell, tanycyte, and radial ependymal cell (Meletis et al., 2008).

In animals with SCI, endogenous neurogenesis has almost completely repaired the damaged spinal cord, showing strong repair potential (Llorens-Bobadilla et al., 2020). After SCI, ependymal cells can proliferate, differentiate and migrate due to the change of microenvironment, such as the increase of some soluble factors, hypoxia, immune response, and so on (Perez Estrada et al., 2014; Covacu and Brundin, 2017). Activated ependymal cells mainly differentiate into astrocytes to form glial scar tissue that protects the integrity of remaining tissue and provides nutritional support for surviving neurons, making endogenous NSCs a potential therapeutic target in SCI. However, the ability of ependymal cells to differentiate into neurons is limited and the direction of differentiation is not controllable. At the same time, several studies claim that within the second decade of life, the whole cord almost completely lacks a patent central canal (Kasantikul et al., 1979; Milhorat et al., 1994; Yasui et al., 1999). In 2015, Garcia-Ovejero found by MRI, histology and immunohistochemistry, and laser capture microdissection that the central canal is predominantly absent in the adult human spinal cord, replaced by a structure that is morphologically and molecularly different from those described in rodents and other primates (Garcia-Ovejero et al., 2015). Therefore, the use of stem cell differentiation of ependymal cells for repair of SCI may be useful in immature adults, but not in adults. Additionally, the translation of therapeutic strategies for repairing SCI by ependymal cells in animal models to clinical studies should be approached with caution.

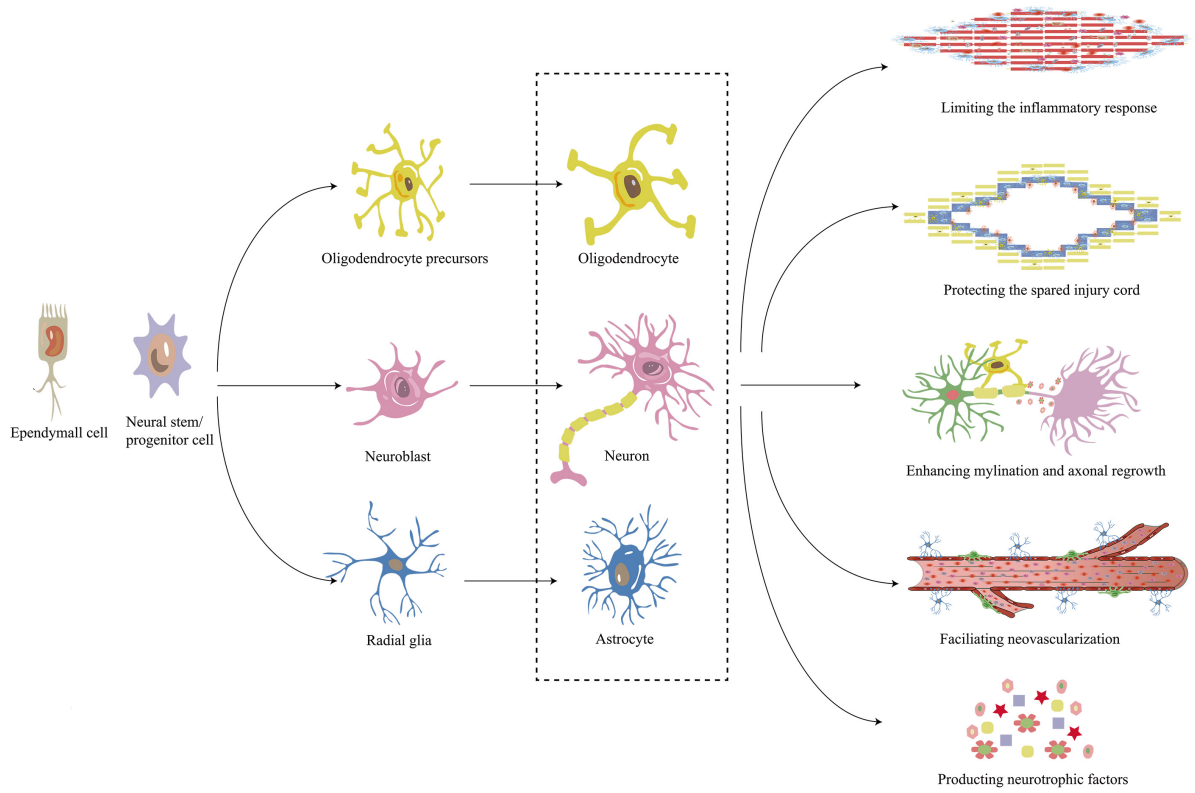

FIGURE 4
Mechanism of neural stem/progenitor cell and ependymal cell in repair of SCI. Neural stem/progenitor cell and ependymal cell differentiate into neural/colloidal cell lines including oligodendrocytes, neurons, and astrocytes. These differentiated cells work together to limit the inflammatory response, protect the spared spinal cord, encourage myelination, promote neovascularization and produce neurotrophic factors to promote the repair of SCI. SCI, Spinal cord injury.

Schwann cells

The neural crest is the origin of spinal nerve Schwann cells (Shi et al., 2016). Schwann cells are glial cells in the peripheral nervous system, which are distributed along with the processes of neurons and wrapped in nerve fibers to form myelinated nerve fibers (Nave and Werner, 2014; Salzer, 2015).

Because Schwann cells have the ability to dedifferentiate and re-differentiate and then re-myelinate when the nerve is damaged (Jessen et al., 2015; Boerboom et al., 2016; Soto and Monje, 2017; Norrmen et al., 2018). Therefore, transplantation of Schwann cells has been widely used in spinal cord demyelination models of rodents and primates to repair SCI and re-form myelin sheath to promote functional repair (Plemel et al., 2014b; Assinck et al., 2017a). Severe neurological problems can result from myelination disorders such demyelination, delayed myelination, or poor myelination (Duncan and Radcliff, 2016; Stadelmann et al., 2019). Despite these significant developments, transplanting Schwann cells only partially enhanced myelin regeneration (Assinck et al., 2017a; Monje et al., 2021), for which there are still no obvious explanations. Inadequate stimulation or inhibitory signals on re-differentiated Schwann cells may be the cause of hypomyelination. Furthermore, Sherman demonstrated that Schwann cells may have lost their normal response to myelin inducible factor (Sherman and Brophy, 2005). During the development of the peripheral nervous system, it is the axonal neuregulin-1 III that almost adjusted to all stages of the stem cell line, and the number of axial expressions of NRG1 III is determined to determine myeloid thickness (Bartus et al., 2016; Clark et al., 2017). Ruth showed that overexpression of axonal neuregulin-1 (NRG1) type III and NRG1 type I can restore normal myelination in transgenic mouse models of SCI (Stassart et al., 2013).

In addition to having a poor capacity for axon regeneration after SCI, the CNS also has a limited capacity for functional recovery. This might be the result of SCI-induced Waller's degeneration of the distal nerve and demyelination of the nerve fibers, which causes an accumulation of numerous organelles and cell fragments at the lesion site and results in fluid-filled cavities and glial scars that prevent the regeneration of axons (Wozniak et al., 2018). Axonal regeneration is also hampered by the development of glial scars or matrix suppressors after SCI (Ghosh et al., 2012), in part because the buildup of

CSPGs inhibits the migration of Schwann cells to the Waller degeneration region, which in turn affects immune cell response (Silver and Miller, 2004; Tran et al., 2018). Chondroitinase ABC can enhance the growth of axons in lesion sites and promote functional recovery by degrading the glycosaminoglycan (GAG) side chains of CSPGs (Kosuri et al., 2022). During Waller degeneration, chemokines and cytokines produced by Schwann cells can recruit macrophages, such as TNF-α, iNOS, and MCP-1 (Min et al., 2021; Yin et al., 2022), which help Schwann cells to clear Waller degeneration and distal neuronal myelination and stimulate axon growth to restore nerve conduction and function (Jessen and Mirsky, 2016).

Despite the fact that there are many other transplantable cells (Assinck et al., 2017a), Schwann cells are commonly regarded by researchers as the promising transplantation cell type for regeneration of spinal (Monje et al., 2021). Schwann cells have a long history of being transplanted, and the first transplantation experiment using pure Schwann cells was performed in 1981 (Duncan et al., 1981). The sensory function of the damaged spinal cord can be more effectively restored by Schwann cells (Poplawski et al., 2018; Rinwa et al., 2021). Schwann cells can secrete a variety of factors necessary to promote the survival of damaged neurons and axon regeneration, which can protect the residual tissue and promote the growth of axons. Such as ciliary neurotrophic factor (CNTF), cell adhesion molecules, pituitary adenylyl cyclase-activating peptide, and integrins (Selvaraj et al., 2012; Maugeri et al., 2020; Catignas et al., 2021; Sukhanov et al., 2021). Williams has demonstrated how transplanting Schwann cells may serve as a bridge and interact with astrocytes to encourage the outgrowth of axons in the lesion area (Williams et al., 2015). Our early research also demonstrated that the co-action of Schwann cells with regulated viral BDNF enhances axon regeneration in alginate hydrogels after SCI (Liu et al., 2017a). In 2017, Anderson scholars from the Miami Project to Cure Paralysis conducted a phase I clinical trial in which autologous human Schwann cells were transplanted into six patients with subacute SCI (Anderson et al., 2017). One year after transplantation, the patients had no surgical, medical, or neurological complications, and some patients with clinically significant neuropathic pain or muscular spasms were able to find some relief. In 2022, Gant again demonstrated the use of autologous Schwann cells for the treatment of chronic SCI, and they found that Schwann cells had significant efficacy in shrinking the diseased cystic cavity in patients with SCI (Gant et al., 2022). This confirms the great potential of Schwann cells for the treatment of SCI. Despite the fact that Schwann cells are found in the peripheral nervous system and not the CNS, following an SCI, these cells can migrate to the location of the damage through the spinal cord dorsal root (Zhang et al., 2013). The process by which Schwann cells enter the SCI region is unclear, nevertheless. People hypothesize that it might be caused by a variety of variables, including the development of blood vessels and an immunological response. In the early stages of Schwann cell transplantation for SCI, the functional recovery of SCI is not significant, and the therapeutic effect is not optimal (Hill et al., 2007), which may cause Schwann cells to die from necrosis and apoptosis due to damage to the microenvironment, low oxygen levels, M1-type macrophage-mediated inflammatory response, and cell-mediated immune response (Pearse et al., 2007). Existing evidence also suggests that axons rarely regenerate in the myelopathy area or in the area of cell transplantation during SCI. Even if the axon is regenerated, it cannot establish an effective connection with normal spinal cord tissue (Deng et al., 2013; Lee et al., 2016). This is one of the reasons why the region of SCI cannot be adequately improved by the implantation of Schwann cells. These studies also showed that Schwann cell transplantation alone was not enough to repair the regeneration of brainstem spinal cord axons. Therefore, researchers developed a number of elements that utilize combination treatment to boost the recovery of motor function (Anderson et al., 2018; Yang et al., 2021).

Other cells

Fibroblasts, microvascular endothelial cells, neuron, and immunological T cells are additionally engaged in SCI repair in addition to the aforementioned cells (**Table 1**). By successively inducing POU5F1(OCT4) and LHX3, Lee demonstrated that human fibroblasts can be transformed into induced motor neurons (Lee et al., 2020). In mice with SCI, the transplantation of induced motor neurons into the injured area can aid in the recovery of motor function (Lee et al., 2020). Myelin sheath removal is very important to the function of nerve injury recovery, Zhou proved that IgG opsonization of myelin debris is required for microvascular endothelial cells engulfment myelin debris, myelin debris engulfment can induce endothelial-to-mesenchymal transition and the process to make the endothelial cells have the ability to stimulate the endothelial-derived production of fibrotic components (Zhou et al., 2019). The development of fibrotic scarring can help to reduce the inflammatory response to SCI and aid in the healing of spinal cord damage. Following SCI, CNS myelin-associated autoantigens (including myelin basic protein) can initiate T cell-mediated autoimmune responses, which can then produce a range of neurotrophic factors and cytokines in accordance with tissue requirements to aid in tissue repair (Ishii et al., 2013). Additionally, platelet cells might help the spinal cord heal from injury. Because Ye demonstrated that platelet-derived growth factor can enhance the blood-spinal cord barrier (BSCB)'s performance, boost the recovery of locomotor function following SCI, and promote endothelial cell regeneration by regulating autophagy (Ye et al., 2021).

Cellular repair mechanisms of spinal cord injury

Schwann cells, NSCs, oligodendrocyte progenitors, olfactory sheathing cells, and mesenchymal stem cells (MSCs) are among the cell types that have been extensively researched for the therapy of SCI (Assinck et al., 2017a; Zipser et al., 2022). Ceto and his colleagues have also shown that transplanting neural or embryonic stem cells into damaged spinal cords can promote functional recovery (Assinck et al., 2017a; Ceto et al., 2020). Cell transplants were usually viable to treat SCI, according to clinical studies conducted in 2018 (Curtis et al., 2018). In this section, we outline six strategies by which cellular grafts repair SCI, including limiting the inflammatory response, protecting the spared spinal cord, enhancing myelination, facilitating neovascularization, producing neurotrophic factors, and differentiating into neural/colloidal cell lines (**Figure 4**). With a greater knowledge of these pathways, we may conduct pertinent research and potentially deliver matching targeted therapy, leading to better SCI treatment options.

Limiting the inflammatory response

After SCI, the BSCB is breached (Jin et al., 2021), activating astrocytes (Karimi-Abdolrezaee and Billakanti, 2012), microglia/macrophages (Chen et al., 2017b), fibroblasts and other glial cells to encourage immune cell infiltration (Fernandez-Klett and Priller, 2014), as well as inducing complex inflammatory responses (Orr and Gensel, 2018; Hellenbrand et al., 2021), which leads to severe SCI.

Early inflammatory response, according to Cunha, is advantageous because it can assist eliminate tissue and cell debris and raise the amount of nutritional factors (Cunha et al., 2020). The large release of inflammatory factors, reactive oxygen species, proteolytic enzymes, and matrix metalloproteinases by inflammatory cells, however, can cause further harm to the surrounding normal spinal cord tissues when the inflammatory response persists (Neirinckx et al., 2014; Gadani et al., 2015). The fact that macrophages and microglia exhibit two opposing phenotypes, namely, neurotoxic M1 and anti-inflammatory M2, is proof of the complexity of the inflammatory response (Kigerl et al., 2009; David and Kroner, 2011; Miron et al., 2013). Kigerl reported that the number of M2-type macrophages would gradually decrease over time (Kigerl et al., 2009) and M1-type macrophages would play a dominant role after SCI, causing secondary SCI.

Drug administration, cell transplantation, and the use of biomaterials can change the microenvironment of SCI and create an anti-inflammatory state that can protect remaining tissue, promote repair, and enhance functional recovery (Gensel et al., 2017; Liu et al., 2017b). However, clinical measures to limit inflammation after SCI are very limited. The FDA has authorized the therapeutic medication methylprednisolone sodium succinate for SCI. However, due to its hazardous side effects, including gastrointestinal bleeding, aseptic necrosis of the femoral head, and wound infection, its clinical usage gradually decreased (Liu et al., 2019). Cell transplantation can promote the repair of spinal cord anatomy and function by alleviating adverse inflammatory responses. MSCs have been extensively researched in this area recently (Cofano et al., 2019; Andrzejewska et al., 2021). Professor Li implanted MSCs into the NT-3 gel sponge scaffold he invented and loaded it with neurotrophic factors, which enhanced the survival rate and anti-inflammatory effect of transplanted cells and thus promoted the regeneration of the spinal cord (Li G. et al., 2016). Exosomes from MSCs have the function of regulating the microenvironment. Li implanted exosomes secreted by MSCs into self-made hydrogels, making exosomes continuously released and effectively reducing inflammatory and oxidative reactions (Li et al., 2020). The use of biomaterials to control the diseased microenvironment is a potential approach to treating SCI (Lv et al., 2021; Silva et al., 2021).

Mesenchymal stem cells are multipotent progenitor cells with significant anti-apoptotic capabilities as well as the capacity to release a variety of neurotrophic and anti-inflammatory compounds. In this way, inflammation at SCI can be reduced and functional recovery can be promoted (Liau et al., 2020). When rats' spinal injuries were treated with bone marrow MSCs, Nakajima's team observed a switch from M1- to M2-type macrophages (Nakajima et al., 2012). The number of M1-type macrophages dramatically dropped at the same time that the number of M2-type macrophages significantly rose. In addition, the secretion of TNF-α and IFN-γ decreased while the secretion of IL-4 and IL-10 increased, which contributed to the reduction of cytotoxicity in the pathological microenvironment (Nakajima et al., 2012). Limiting inflammation may primarily be seen as a result of changes in macrophage phenotype following mesenchymal stem cell implantation (Bernardo and Fibbe, 2013). Future study will focus on determining the precise mechanism of action between them in order to determine if the limitation of the inflammatory response following SCI is caused by the transplanted cells, immunological control, or a combination of the two.

Protecting the spared spinal cord

Primary SCI can cause complex secondary injury (O'Shea et al., 2017; Tran et al., 2018). Through many ways, cell transplantation may promote neuroprotective (Assinck et al., 2017a). The increase in normal tissue volume, the decrease in diseased tissue volume, and the release of neurotrophic factors are typical parameters used to assess the presence of neuroprotective effects. Numerous cell transplantation types, including Schwann cells, MSCs, and olfactory sheath cells, have

been shown to have neuroprotective properties (Assinck et al., 2017a).

Cantinieaux et al. proved that transplantation of bone marrow MSCs in a rat model of SCI can not only reduce the size of spinal cord sac but also protect white matter tracts and reduce the inflammatory response, contributing to better motor function recovery (Cantinieaux et al., 2013; Kumagai et al., 2013; Mohammad-Gharibani et al., 2013; Wang et al., 2014). Transplantation of bone marrow MSCs after SCI can promote functional recovery to a certain extent, partly because of their neuroprotective ability to preserve neural tissues (Ritfeld et al., 2012). Transplantation of Schwann cells and olfactory sheath cells increased the number of spinal cord neurons and promoted the preservation of axons (Bunge, 2016; Gomez et al., 2018). Continuous spinal cord contraction occurs after SCI, resulting in increased volume of the damaged spinal cord (Ziegler et al., 2018). Lee believed that macrophage depletion and Schwann cell transplantation after SCI can also reduce cyst size (Lee et al., 2018). Laura's team treated SCI with a combination of Schwann cells and gel significantly improved the spatial distribution of transplanted cells in the endogenous tissue. A reduction in cyst cavitation and neuronal loss was also observed, as well as a substantial increase in forelimb strength and coordination in mice (Marquardt et al., 2020).

Therefore, it is debatable whether lesion volume changes should be used to gauge the neuroprotective impact of transplanted cells. Many transplanted cells promote axonal regeneration and myelin sheath formation to increase the volume of remaining tissue (Powers et al., 2012; Hawryluk et al., 2014). Increased residual tissue is often associated with improved motor function (Basso et al., 1996; Schucht et al., 2002; Plemel et al., 2008). Therefore, the increase of residual tissue near the injury site can better explain the protective effect of cell transplantation on the injured spinal cord. At the same time, more researchers are needed to explore whether different stem cell types differ in their ability to increase the volume of tissue near the injury and protect the remaining tissue.

Encouraging myelination

The tubular outer membrane that surrounds the axon of myelinated nerve fibers is referred to as the "myelin sheath" since myelin is its primary constituent. Insulation provided by myelin allows it to conduct impulse orientation by preventing interference between nerve impulses. In the event that an axon is destroyed, myelin can help direct the regeneration of the damaged axon. In the demyelinating disease, the nutritional support provided by myelin is essential for the survival of axons (Suminaite et al., 2019; Bolino, 2021).

In vertebrates, myelin loss and oligodendrocyte apoptosis (Crowe et al., 1997) that impair the conduction of nerve impulses (Funfschilling et al., 2012; Lee et al., 2012) can be seen in a few weeks after SCI. In an incomplete SCI, some degree of spontaneous re-myelination can be seen, which may be the result of myelination re-sheathed by transplanted Schwann cells or by oligodendrocyte precursors from other places (Duncan et al., 1981; Salzer, 2015; Assinck et al., 2017b). Duncan demonstrated that it is feasible to stimulate the development of endogenous progenitor cells into mature myelin-forming oligodendrocytes (Duncan et al., 2020).

Spinal cord injury in mammals has a limited ability to recover and to re-establish functional neural connections. Cell transplantation is currently a great way to repair myelin deficiency. After studying several biomaterials, we discovered that anisotropic alginate hydrogels can encourage axonal development and restore action potential conduction after SCI (Schackel et al., 2019; Huang L. et al., 2020). Oligodendrocytes are myelinated glial cells in the CNS, which can maintain the long-term integrity of axons (Simons and Nave, 2015). The majority of research have shown that the transplantation of NSCs or oligodendrocyte progenitor cells (OPCs) after SCI can improve myelin repair and functional recovery (Keirstead et al., 2005; Assinck et al., 2017a). These studies were unable to distinguish whether the restoration of function was due to neurotrophic support decreasing demyelinating harm or to transplanted cells remyelinating demyelinated axons. In 2005, Hofstetter's research team transplanted adult NSCs into a rat model of thoracic SCI, which promoted the recovery of motor function and reduced myelin formation in the injured area, while leading to abnormal axonal growth and increasing the effect of ectopic pain (Hofstetter et al., 2005). This raises the possibility of substantial adverse effects from stem cell transplantation following SCI, raising doubts about the causal link between myelin regeneration and increased function. At the same time, most researchers believe that treating SCI with stem cell transplantation can alleviate neuropathic pain to some extent (Fandel et al., 2016; Hu et al., 2021). Since the experimental results are generally judged by the researchers based on the pain behavior of the mice, there is a lack of uniform standards for the mice's response to pain, and the experimental results are also influenced by the subjective factors of the researchers and the heterogeneity of the mice.

Keirstead found that after transplantation of OPCs on day 7 or 10 months after SCI, only animals given OPCs on day 7 showed increased remyelination and improved motor function (Keirstead et al., 2005). This shows that the therapeutic window for remyelination is only available during the first few weeks following damage. This could also be because late astrocyte scarring prevents Schwann cell migration and axon regeneration, which affects re-myelination (O'Shea et al., 2017; Bradbury and Burnside, 2019). It's intriguing that astrocytes can promote axon growth when they extend in a linear path to the site of the lesion (Matthews et al., 1979).

Most researchers studying spinal cord remyelination are unable to discriminate between intact and injured axons' myelin state and their function. There are also three possible sources of remyelination after SCI: remyelination of endogenous NSCs (Powers et al., 2012; Hesp et al., 2015), myelination of transplanted cells (Sankavaram et al., 2019), and myelin preservation at the site of injury. The precise source of myelin regeneration following SCI is unclear at this time. Nashmi and Fehlings found in SCI models that most regenerated myelin sheaths were also incomplete, with new myelin sheaths being very thin and leading to conduction failure (Nashmi and Fehlings, 2001). Therefore, promoting myelin formation after SCI is not an accurate criterion for assessing functional recovery, unless there is an accurate method to determine the specific source of myelin in the tissue.

Facilitating neovascularization

Spinal cord injury results in structural and functional changes of micro-vessels around the tissue (Li et al., 2017). Tao demonstrated that SCI was brought on by mechanical and physical action that cut off the spinal cord's blood supply (Wang et al., 2018). The destruction of blood vessels not only reduces the perfusion of the remaining spinal parenchyma and destroys the BSCB, but also aggravates the ischemia, hypoxia, and inflammatory response of the injured spinal cord (McDonald and Sadowsky, 2002; Ahuja et al., 2017), which both hinder the repair of endogenous nerve tissue and aggravate SCI (Figley et al., 2014). Bearden and Rauch proved that the growth of blood vessels would guide the growth of axons (Bearden and Segal, 2004; Rauch et al., 2009). Lu's research team also enlarged blood vessel diameter by atorvastatin, which increased blood perfusion and reduced neuron damage (Lu et al., 2004). Thus, increased blood flow appears to reduce neuron damage and provide better perfusion to damaged tissue (Yamaya et al., 2014). Vascular formation is also prior to functional recovery after SCI. Increased vascular density has been observed to be associated with improved recovery in many SCI models (Fassbender et al., 2011; Rocha et al., 2018; Hong et al., 2022). These studies indicated that the generation of spinal blood vessels may be a potential mechanism for spinal cord repair.

The expression of vascular endothelial growth factor (VEGF) can inhibit the apoptosis of vascular endothelial cells and promote the differentiation and migration of vascular endothelial cells (Sondell et al., 1999). It is a highly effective angiogenesis stimulator and vascular permeability regulator (Ferrara et al., 2003; Brockington et al., 2004). VEGF can not only directly protect neurons (Ku et al., 2017) and promote the growth of axons (Cattin et al., 2015), but also contribute to the survival and proliferation of a variety of glial cells (Sondell et al., 1999; Mani et al., 2005). In a mouse model of SCI, Deng observed that 3D human placenta-derived MSCs could produce trophic factors like VEGF and induce angiogenesis, indicating neuroprotective benefits (Deng et al., 2021). In addition, IL-8 can significantly increase the production of VEGF in BMSCs through PI3K/Akt and MAPK/ERK signaling pathways, which can enhance the angiogenic potential of BMSCs (Hou et al., 2014).

Mesenchymal stem cells have been used in clinical and preclinical trials for their role in promoting angiogenesis (Mathew et al., 2020). The treatment of human placental mesenchymal stem cell transplantation has also been proved by Kong to promote the repair of cerebral ischemia (Kong et al., 2018). Marrotte combined NSCs and endothelial cells with biomaterial hydrogel and successfully induced the generation of nerves and blood vessels in the rat SCI model (Marrotte et al., 2021). This biomaterial of biomimetic hydrogel has been proved by researchers to be able to induce the generation of blood vessels *in vivo* and *in vitro* (Sokic and Papavasiliou, 2012; Schweller et al., 2017). More and more studies have shown that stem cell transplantation for SCI is mainly mediated by exosomes secreted by stem cells (Mendt et al., 2019; Cao et al., 2021). Zhang extracted exosomes derived from human embryonic MSCs by centrifugation and injected them into the SCI model. They found that the number of blood vessels, vascular connectivity, and vascular volume fraction in the spinal cord significantly increased and improved motor and sensory function (Zhang et al., 2020).

The development and regeneration of blood vessels are associated to functional recovery after SCI, according to the results of the available study; however, the pertinent particular mechanism research is insufficient. Future study might go in this route because there is no pertinent literature to support the idea that the transplanted cell types affect vascular development differently.

Producing neurotrophic factors

Neurotrophic factor and cytokines may play a part in the neurotrophic process of cell transplantation for SCI (Hawryluk et al., 2012a,b; Garcia et al., 2016). *In vitro*, trophic factors and cytokines can be secreted by MSCs, neural precursor cells (NPCs), Schwann cells, and microglia. After transplantation, these cells can also enhance the amount of these substances in the host (O'Shea et al., 2017; Maldonado-Lasuncion et al., 2018; Maugeri et al., 2020). Numerous healing effects are produced by neurotrophic factors and associated trophic factors. For example: apoptosis prevention (Zhang et al., 2014), axon regeneration promotion (Anderson et al., 2018), myelination enhancement (Bartus et al., 2016), and regulate of NPCs proliferation and differentiation (Gao et al., 2022). These healing effects are mostly interconnected. However, NGF can also have adverse effects, such as causing neuropathic pain (Dai et al., 2020).

The nutritional factors most commonly examined by researchers include NGF, BDNF, and NT-3 (Nieto-Sampedro et al., 1982; Dougherty et al., 2000; Widenfalk et al., 2001; Tokumine et al., 2003). After SCI, the expression of nutrient factors NGF, BDNF, GDNF, and so on are upregulated (Mocchetti and Wrathall, 1995; Dougherty et al., 2000; Widenfalk et al., 2001), while there are research works that show the opposite changes (Uchida et al., 2003; Gulino et al., 2004), which may be related to the SCI model, the severity of the damage, and the various nutritional factor detection times. Therefore, future research in this area may be better able to identify changes in nutritional factor expression following SCI using the same criteria.

Since cell transplantation has pleiotropic effects and neurotrophic advantages for the surrounding tissues, it is essentially a combined treatment for SCI healing. Hawryluk discovered that cell transplantation and the neurotrophic medications minocycline and cyclosporine worked best together to treat SCI (Hawryluk et al., 2012a). The use of neurotrophic factors incorporated into biomaterials to improve NSPCs transplantation for SCI has also shown impressive results (Li G. et al., 2016). However, there is little direct evidence that cells supporting transplantation produce nutritional factors. Different transplanted cells also produce different nutritional factors (Hawryluk et al., 2012b). The mechanism by which transplanted cells produce nutritional factors is unclear, and there have been few systematic research works on the association between the kind of transplanted cells and the cell-derived nutrients required for SCI healing. Therefore, it would be important to further understand in detail whether the secretion of nutritional factors and cytokines by transplanted cells is necessary for SCI repair.

Differentiating into nerve/colloidal cell line

Neurons, astrocytes, and oligodendrocytes can all develop from NSCs, which are pluripotent stem cells (McKay, 1997; Barnabe-Heider and Frisen, 2008; Assinck et al., 2017a). The differentiation of NSCs is regulated by both the environment and its own characteristics. *In vivo* and *in vitro* NSC modulation is mediated by Notch and Rho signaling pathways (Ben-Shushan et al., 2015; Hosseini et al., 2022). There are more differentiated astrocytes than neurons in endogenous NSCs when Notch1 and Hes1 genes are highly expressed. Notch can inhibit, delay, or induce differentiation and can promote cell division and apoptosis through multiple pathways. When the Notch pathway is activated, stem cells would be proliferated; however, when the Notch signal is suppressed, stem cells would differentiate (Kageyama and Ohtsuka, 1999; Lai, 2004; Bhat, 2014; Pinto-Teixeira and Desplan, 2014). Meletis proved that transfection of Ngn2 and OligO2 can promote the differentiation of NSCs into motor neurons and oligodendrocytes, respectively (Meletis et al., 2008). This suggests that the process and proportion of stem cell differentiation into neural functional cells can be precisely regulated by changing the relevant signals.

Research has recently shifted its attention to the variables influencing the proliferation and development of NSCs. There have been numerous research works on how to induce stem cells to develop into neurons. We combined NSCs with alginate hydrogel cross-linked by Ca2+ and found that approximately one-third (38.3%) of the NSCs survived after transplantation into acute T8 complete spinal cord transection sites in adult rats and differentiated into neurons (40.7%), astrocytes (26.6%), and oligodendrocytes (28.4%) at 8 weeks post-transplantation (Zhou et al., 2022). Johe and Massey found that the complex interaction between matrix, medium and cells could affect the proliferation and differentiation of NSCs (Johe et al., 1996; Tsai and McKay, 2000). Li, Hung and Wang also proved that some matrix can guide the extension of nerve cells to the target (Hung et al., 2006; Wang et al., 2006; Li et al., 2009). BDNF and GDNF are two major neurotrophic factors, which are essential for the proliferation and differentiation of NSCs (Deng et al., 2013; Wakeman et al., 2014; Chang et al., 2021). Platelets-derived growth factor, ciliary neurotrophic factor, and sonic hedgehog have been shown to play an important role in stem cell survival and differentiation into specific neural lineages (Lachyankar et al., 1997; Caldwell et al., 2001; Bambakidis et al., 2003; Kondo et al., 2005; Li et al., 2005). These results indicate that neurotrophic factors and stroma can control the proliferation and differentiation of NSCs to a certain extent (Lachyankar et al., 1997; Wang et al., 2006).

Prospect

The repair of SCI is a complex pathophysiological process. In recent years, a lot of research has been conducted and a certain degree of success has been achieved through strategies such as stem cell transplantation, biomaterials, and exosomes to promote SCI repair. However, due to the heterogeneity of SCI and the complexity of the repair process, no ideal repair strategy has been found for the repair and regeneration of SCI.

With stem cell therapy for SCI, people should pay attention to the variations among study methodologies, the effectiveness and purity of stem cell differentiation, and the development of teratomas (Nori et al., 2015). Low differentiation and survival rates of stem cells are typical issues with stem cell transplantation for SCI (Gericota et al., 2014; Iwai et al., 2014; Lee et al., 2014; Tuszynski et al., 2014). NSCs transplanted into the injured spinal cord differentiated mainly into glial cells (Cao et al., 2001; Zhou et al., 2022). More research is needed to achieve targeted differentiation of NSCs. Therefore, these challenges further exacerbate the heterogeneity of patients with SCI and hinder clinical research on stem cell therapy

for SCI, which also needs to be addressed in basic research. Treatment of SCI by biomaterials requires consideration of biodegradation rate, biocompatibility, and safety of the material to facilitate better clinical translation. In addition, exosome therapy faces many challenges. To date, ultracentrifugation remains the most commonly used method for exosome isolation and concentration, and although there are various methods for exosome extraction, the recovery rate and specificity of exosome isolation still need to be improved, and ultracentrifugation destroys the integrity of exosomes and has a high rate of protein contamination. In clinical applications, the development of accurate and effective standard methods for the identification, isolation, and quantification of exosomes is still an urgent issue to be addressed. Combination therapy might be superior to single therapeutic approaches. Combination therapies like "biomaterials + stem cells + growth factors," "exosomes + stem cells + growth factors," and "biomaterials + exosomes + stem cells" have been successful in animal models, but the majority of the current animal experiments have been done in the acute and subacute phases of SCI, and the treatment of the chronic phase of SCI needs more research.

This review summarizes the cell types involved in the repair process of SCI and the common repair mechanisms of SCI, which can be very helpful for the clinical translation of SCI treatment. This review can provide a better understanding of the pathophysiological processes involved in SCI repair and help them to develop more targeted strategies for SCI repair.

Author contributions

YqW illustrated the figures and wrote the manuscript. All authors provided the input and approved the submitted version.

Funding

This work was supported by the National Natural Science Foundation of China (Grant No. 81901895 to SL).

Conflict of interest

The authors declare that the research was conducted in the absence of any commercial or financial relationships that could be construed as a potential conflict of interest.

Publisher's note

All claims expressed in this article are solely those of the authors and do not necessarily represent those of their affiliated organizations, or those of the publisher, the editors and the reviewers. Any product that may be evaluated in this article, or claim that may be made by its manufacturer, is not guaranteed or endorsed by the publisher.

References

Ahuja, C. S., Wilson, J. R., Nori, S., Kotter, M. R. N., Druschel, C., Curt, A., et al. (2017). Traumatic spinal cord injury. *Nat. Rev. Dis. Primers* 3:17018. doi: 10.1038/nrdp.2017.18

Alizadeh, A., Dyck, S. M., and Karimi-Abdolrezaee, S. (2019). Traumatic Spinal Cord Injury: An Overview of Pathophysiology, Models and Acute Injury Mechanisms. *Front. Neurol.* 10:282. doi: 10.3389/fneur.2019.00282

Alizadeh, A., and Karimi-Abdolrezaee, S. (2016). Microenvironmental regulation of oligodendrocyte replacement and remyelination in spinal cord injury. *J. Physiol.* 594, 3539–3552. doi: 10.1113/JP270895

An, D., Tan, B., Yu, D. Y., and Balaratnasingam, C. (2022). Differentiating Microaneurysm Pathophysiology in Diabetic Retinopathy Through Objective Analysis of Capillary Nonperfusion Inflammation, and Pericytes. *Diabetes* 71, 733–746. doi: 10.2337/db21-0737

Anderson, K. D., Guest, J. D., Dietrich, W. D., Bartlett Bunge, M., Curiel, R., Dididze, M., et al. (2017). Safety of Autologous Human Schwann Cell Transplantation in Subacute Thoracic Spinal Cord Injury. *J. Neurotrauma* 34, 2950–2963. doi: 10.1089/neu.2016.4895

Anderson, M. A., Burda, J. E., Ren, Y. L., Ao, Y., O'Shea, T. M., Kawaguchi, R., et al. (2016). Astrocyte scar formation aids central nervous system axon regeneration. *Nature* 532, 195–200. doi: 10.1038/nature17623

Anderson, M. A., O'Shea, T. M., Burda, J. E., Ao, Y., Barlatey, S. L., Bernstein, A. M., et al. (2018). Required growth facilitators propel axon regeneration across complete spinal cord injury. *Nature* 561, 396–400. doi: 10.1038/s41586-018-0467-6

Andrzejewska, A., Dabrowska, S., Lukomska, B., and Janowski, M. (2021). Mesenchymal Stem Cells for Neurological Disorders. *Adv. Sci.* 8:2002944. doi: 10.1002/advs.202002944

Angeli, C. A., Boakye, M., Morton, R. A., Vogt, J., Benton, K., Chen, Y., et al. (2018). Recovery of Over-Ground Walking after Chronic Motor Complete Spinal Cord Injury. *N. Engl. J. Med.* 379, 1244–1250. doi: 10.1056/NEJMoa1803588

Assinck, P., Duncan, G. J., Hilton, B. J., Plemel, J. R., and Tetzlaff, W. (2017a). Cell transplantation therapy for spinal cord injury. *Nat. Neurosci.* 20, 637–647. doi: 10.1038/nn.4541

Assinck, P., Duncan, G. J., Plemel, J. R., Lee, M. J., Stratton, J. A., Manesh, S. B., et al. (2017b). Myelinogenic Plasticity of Oligodendrocyte Precursor Cells following Spinal Cord Contusion Injury. *J. Neurosci.* 37, 8635–8654.

Attwell, D., Mishra, A., Hall, C. N., O'Farrell, F. M., and Dalkara, T. (2016). What is a pericyte? *J. Cereb. Blood Flow Metab* 36, 451–455. doi: 10.1177/0271678X15610340

Bambakidis, N. C., Wang, R. Z., Franic, L., and Miller, R. H. (2003). Sonic hedgehog-induced neural precursor proliferation after adult rodent spinal cord injury. *J. Neurosurg.* 99, 70–75. doi: 10.3171/spi.2003.99.1.0070

Barnabe-Heider, F., and Frisen, J. (2008). Stem cells for spinal cord repair. *Cell Stem Cell* 3, 16–24. doi: 10.1016/j.stem.2008.06.011

Bamabé-Heider, F., Goritz, C., Sabelstrom, H., Takebayashi, H., Pfrieger, F. W., Meletis, K., et al. (2010). Origin of new glial cells in intact and injured adult spinal cord. *Cell Stem Cell* 7, 470–482. doi: 10.1016/j.stem.2010.07.014

Barron, T., and Kim, J. H. (2019). Neuronal input triggers Ca (2+) influx through AMPA receptors and voltage-gated Ca (2+) channels in oligodendrocytes. *Glia* 67, 1922–1932. doi: 10.1002/glia.23670

Bartlett, R. D., Burley, S., Ip, M., Phillips, J. B., and Choi, D. (2020). Cell Therapies for Spinal Cord Injury: Trends and Challenges of Current Clinical Trials. *Neurosurgery* 87, E456–E472. doi: 10.1093/neuros/nyaa149

Bartus, K., Galino, J., James, N. D., Hernandez-Miranda, L. R., Dawes, J. M., Fricker, F. R., et al. (2016). Neuregulin-1 controls an endogenous repair mechanism after spinal cord injury. *Brain* 139, 1394–1416. doi: 10.1093/brain/aww039

Basso, D. M., Beattie, M. S., and Bresnahan, J. C. (1996). Graded histological and locomotor outcomes after spinal cord contusion using the NYU weight-drop device versus transection. *Exp. Neurol.* 139, 244–256. doi: 10.1006/exnr.1996.0098

Bazargani, N., and Attwell, D. (2016). Astrocyte calcium signaling: The third wave. *Nat. Neurosci.* 19, 182–189. doi: 10.1038/nn.4201

Bearden, S. E., and Segal, S. S. (2004). Microvessels promote motor nerve survival and regeneration through local VEGF release following ectopic reattachment. *Microcirculation* 11, 633–644. doi: 10.1080/10739680490517659

Beaumont, E., Onifer, S. M., Reed, W. R., and Magnuson, D. S. (2006). Magnetically evoked inter-enlargement response: An assessment of ascending propriospinal fibers following spinal cord injury. *Exp. Neurol.* 201, 428–440. doi: 10.1016/j.expneurol.2006.04.032

Becerra, J. L., Puckett, W. R., Hiester, E. D., Quencer, R. M., Marcillo, A. E., Post, M. J., et al. (1995). MR-pathologic comparisons of wallerian degeneration in spinal cord injury. *AJNR Am. J. Neuroradiol.* 16, 125–133.

Bennett, M. L., Bennett, F. C., Liddelow, S. A., Ajami, B., Zamanian, J. L., Fernhoff, N. B., et al. (2016). New tools for studying microglia in the mouse and human CNS. *Proc. Natl. Acad. Sci. U S A.* 113, E1738–E1746. doi: 10.1073/pnas.1525528113

Ben-Shushan, E., Feldman, E., and Reubinoff, B. E. (2015). Notch Signaling Regulates Motor Neuron Differentiation of Human Embryonic Stem Cells. *Stem Cells* 33, 403–415. doi: 10.1002/stem.1873

Berger, M. J., Hubli, M., and Krassioukov, A. V. (2014). Sympathetic skin responses and autonomic dysfunction in spinal cord injury. *J. Neurotrauma* 31, 1531–1539. doi: 10.1089/neu.2014.3373

Bernardo, M. E., and Fibbe, W. E. (2013). Mesenchymal stromal cells: Sensors and switchers of inflammation. *Cell Stem Cell* 13, 392–402. doi: 10.1016/j.stem.2013.09.006

Berret, E., Barron, T., Xu, J., Debner, E., Kim, E. J., and Kim, J. H. (2017). Oligodendroglial excitability mediated by glutamatergic inputs and Nav1.2 activation. *Nat. Commun.* 8:557. doi: 10.1038/s41467-017-00688-0

Berret, E., Kim, S. E., Lee, S. Y., Kushmerick, C., and Kim, J. H. (2016). Functional and structural properties of ion channels at the nerve terminal depends on compact myelin. *J. Physiol.* 594, 5593–5609. doi: 10.1113/JP272205

Bhat, K. M. (2014). Notch signaling acts before cell division to promote asymmetric cleavage and cell fate of neural precursor cells. *Sci. Signal.* 7:ra101. doi: 10.1126/scisignal.2005317

Bian, Z. L., Gong, Y. D., Huang, T., Lee, C. Z. W., Bian, L. H., Bai, Z. J., et al. (2020). Deciphering human macrophage development at single-cell resolution. *Nature* 582, 571–576. doi: 10.1038/s41586-020-2316-7

Boddum, K., Jensen, T. P., Magloire, V., Kristiansen, U., Rusakov, D. A., Pavlov, I., et al. (2016). Astrocytic GABA transporter activity modulates excitatory neurotransmission. *Nat. Commun.* 7:13572. doi: 10.1038/ncomms13572

Boerboom, A., Dion, V., Chariot, A., and Franzen, R. (2016). Molecular Mechanisms Involved in Schwann Cell Plasticity. *Front. Mol. Neurosci.* 10:38. doi: 10.3389/fnmol.2017.00038

Bolino, A. (2021). Myelin Biology. *Neurotherapeutics* 18, 2169–2184. doi: 10.1007/s13311-021-01083-w

Bradbury, E. J., and Burnside, E. R. (2019). Moving beyond the glial scar for spinal cord repair. *Nat. Commun.* 10:3879. doi: 10.1038/s41467-019-11707-7

Brockington, A., Lewis, C., Wharton, S., and Shaw, P. J. (2004). Vascular endothelial growth factor and the nervous system. *Neuropath. Appl. Neuro.* 30, 427–446. doi: 10.1111/j.1365-2990.2004.00600.x

Brommer, B., He, M., Zhang, Z., Yang, Z., Page, J. C., Su, J., et al. (2021). Improving hindlimb locomotor function by Non-invasive AAV-mediated manipulations of propriospinal neurons in mice with complete spinal cord injury. *Nat. Commun.* 12:781. doi: 10.1038/s41467-021-20980-4

Buffo, A., Rite, I., Tripathi, P., Lepier, A., Colak, D., Horn, A. P., et al. (2008). Origin and progeny of reactive gliosis: A source of multipotent cells in the injured brain. *Proc. Natl. Acad. Sci. U S A.* 105, 3581–3586. doi: 10.1073/pnas.0709002105

Bunge, M. B. (2016). Efficacy of Schwann cell transplantation for spinal cord repair is improved with combinatorial strategies. *J. Physiol.* 594, 3533–3538. doi: 10.1113/JP271531

Caiazzo, M., Dell'Anno, M. T., Dvoretskova, E., Lazarevic, D., Taverna, S., Leo, D., et al. (2011). Direct generation of functional dopaminergic neurons from mouse and human fibroblasts. *Nature* 476, 224–227. doi: 10.1038/nature10284

Caldwell, M. A., He, X., Wilkie, N., Pollack, S., Marshall, G., Wafford, K. A., et al. (2001). Growth factors regulate the survival and fate of cells derived from human neurospheres. *Nat. Biotechnol.* 19, 475–479. doi: 10.1038/88158

Cantinieaux, D., Quertainmont, R., Blacher, S., Rossi, L., Wanet, T., Noel, A., et al. (2013). Conditioned medium from bone marrow-derived mesenchymal stem cells improves recovery after spinal cord injury in rats: An original strategy to avoid cell transplantation. *PLoS One* 8:e69515. doi: 10.1371/journal.pone.0069515

Cao, Q. L., Zhang, Y. P., Howard, R. M., Walters, W. M., Tsoulfas, P., and Whittemore, S. R. (2001). Pluripotent stem cells engrafted into the normal or lesioned adult rat spinal cord are restricted to a glial lineage. *Exp. Neurol.* 167, 48–58. doi: 10.1006/exnr.2000.7536

Cao, Y., Xu, Y., Chen, C., Xie, H., Lu, H., and Hu, J. (2021). Local delivery of USC-derived exosomes harboring ANGPTL3 enhances spinal cord functional recovery after injury by promoting angiogenesis. *Stem Cell Res. Ther.* 12:20. doi: 10.1186/s13287-020-02078-8

Caporali, A., Martello, A., Miscianinov, V., Maselli, D., Vono, R., and Spinetti, G. (2017). Contribution of pericyte paracrine regulation of the endothelium to angiogenesis. *Pharmacol. Ther.* 171, 56–64. doi: 10.1016/j.pharmthera.2016.10.001

Catignas, K. K., Frick, L. R., Pellegatta, M., Hurley, E., Kolb, Z., Addabbo, K., et al. (2021). alpha(V)integrins in Schwann cells promote attachment to axons, but are dispensable in vivo. *Glia* 69, 91–108. doi: 10.1002/glia.23886

Cattin, A. L., Burden, J. J., Van Emmenis, L., Mackenzie, F. E., Hoving, J. J. A., Calavia, N. G., et al. (2015). Macrophage-Induced Blood Vessels Guide Schwann Cell-Mediated Regeneration of Peripheral Nerves. *Cell* 162, 1127–1139. doi: 10.1016/j.cell.2015.07.021

Ceto, S., Sekiguchi, K. J., Takashima, Y., Nimmerjahn, A., and Tuszynski, M. H. (2020). Neural Stem Cell Grafts Form Extensive Synaptic Networks that Integrate with Host Circuits after Spinal Cord Injury. *Cell Stem Cell* 27, 430–440.e5. doi: 10.1016/j.stem.2020.07.007

Chang, D. J., Cho, H. Y., Hwang, S., Lee, N., Choi, C., Lee, H., et al. (2021). Therapeutic Effect of BDNF-Overexpressing Human Neural Stem Cells (F3.BDNF) in a Contusion Model of Spinal Cord Injury in Rats. *Int. J. Mol. Sci.* 22:6970. doi: 10.3390/ijms22136970

Chen, J., Luo, Y., Hui, H., Cai, T., Huang, H., Yang, F., et al. (2017a). CD146 coordinates brain endothelial cell-pericyte communication for blood-brain barrier development. *Proc. Natl. Acad. Sci. U S A.* 114, E7622–E7631. doi: 10.1073/pnas.1710848114

Chen, J., Wang, Z. G., Zheng, Z. M., Chen, Y., Khor, S. N., Shi, K. S., et al. (2017b). Neuron and microglia/macrophage-derived FGF10 activate neuronal FGFR2/PI3K/Akt signaling and inhibit microglia/macrophages TLR4/NF-kappa B-dependent neuroinflammation to improve functional recovery after spinal cord injury. *Cell Death Dis.* 8:e3090. doi: 10.1038/cddis.2017.490

Cheng, J., Korte, N., Nortley, R., Sethi, H., Tang, Y., and Attwell, D. (2018). Targeting pericytes for therapeutic approaches to neurological disorders. *Acta Neuropathol.* 136, 507–523. doi: 10.1007/s00401-018-1893-0

Cherry, J. D., Olschowka, J. A., and O'Banion, M. K. (2014). Neuroinflammation and M2 microglia: The good, the bad, and the inflamed. *J. Neuroinflammation* 11:98. doi: 10.1186/1742-2094-11-98

Chio, J. C. T., Xu, K. J., Popovich, P., David, S., and Fehlings, M. G. (2021). Neuroimmunological therapies for treating spinal cord injury: Evidence and future perspectives. *Exp. Neurol.* 341:113704. doi: 10.1016/j.expneurol.2021.113704

Clark, A. J., Kaller, M. S., Galino, J., Willison, H. J., Rinaldi, S., and Bennett, D. L. H. (2017). Co-cultures with stem cell-derived human sensory neurons reveal regulators of peripheral myelination. *Brain* 140, 898–913. doi: 10.1093/brain/awx012

Cofano, F., Boido, M., Monticelli, M., Zenga, F., Ducati, A., Vercelli, A., et al. (2019). Mesenchymal Stem Cells for Spinal Cord Injury: Current Options, Limitations, and Future of Cell Therapy. *Int. J. Mol. Sci.* 20:2698. doi: 10.3390/ijms20112698

Collaborators, G. U. N. D., Feigin, V. L., Vos, T., Alahdab, F., Amit, A. M. L., Barnighausen, T. W., et al. (2021). Burden of Neurological Disorders Across the US From 1990-2017: A Global Burden of Disease Study. *JAMA Neurol.* 78, 165–176. doi: 10.1001/jamaneurol.2020.4152

Covacu, R., and Brundin, L. (2017). Effects of Neuroinflammation on Neural Stem Cells. *Neuroscientist* 23, 27–39. doi: 10.1177/1073858415616559

Crawford, A. H., Tripathi, R. B., Foerster, S., McKenzie, I., Kougioumtzidou, E., Grist, M., et al. (2016). Pre-Existing Mature Oligodendrocytes Do Not Contribute to Remyelination following Toxin-Induced Spinal Cord Demyelination. *Am. J. Pathol.* 186, 511–516. doi: 10.1016/j.ajpath.2015.11.005

Crowe, M. J., Bresnahan, J. C., Shuman, S. L., Masters, J. N., and Beattie, M. S. (1997). Apoptosis and delayed degeneration after spinal cord injury in rats and monkeys. *Nat. Med.* 3, 73–76. doi: 10.1038/nm0197-73

Cunha, M. I., Su, M. H., Cantuti-Castelvetri, L., Muller, S. A., Schifferer, M., Djannatian, M., et al. (2020). Pro-inflammatory activation following demyelination is required for myelin clearance and oligodendrogenesis. *J. Exp. Med.* 217:e20191390. doi: 10.1084/jem.20191390

Curtis, E., Martin, J. R., Gabel, B., Sidhu, N., Rzesiewicz, T. K., Mandeville, R., et al. (2018). A First-in-Human, Phase I Study of Neural Stem Cell Transplantation for Chronic Spinal Cord Injury. *Cell Stem Cell* 22, 941–950.e6. doi: 10.1016/j.stem.2018.05.014

Dai, W. L., Yan, B., Bao, Y. N., Fan, J. F., and Liu, J. H. (2020). Suppression of peripheral NGF attenuates neuropathic pain induced by chronic constriction injury through the TAK1-MAPK/NE-kappa B signaling pathways. *Cell Commun. Signal.* 18:66. doi: 10.1186/s12964-020-00556-3

David, S., and Kroner, A. (2011). Repertoire of microglial and macrophage responses after spinal cord injury. *Nat. Rev. Neurosci.* 12, 388–399. doi: 10.1038/nrn3053

De La Fuente, A. G., Lange, S., Silva, M. E., Gonzalez, G. A., Tempfer, H., van Wijngaarden, P., et al. (2017). Pericytes Stimulate Oligodendrocyte Progenitor Cell Differentiation during CNS Remyelination. *Cell Rep.* 20, 1755–1764. doi: 10.1016/j.celrep.2017.08.007

Defrin, R., Gruener, H., Gaidukov, E., Bondi, M., Rachamim-Katz, O., Ringler, E., et al. (2022). From acute to long-term alterations in pain processing and modulation after spinal cord injury: Mechanisms related to chronification of central neuropathic pain. *Pain* 163, e94–e105. doi: 10.1097/j.pain.0000000000002315

Deng, J., Li, M., Meng, F., Liu, Z., Wang, S., Zhang, Y., et al. (2021). 3D spheroids of human placenta-derived mesenchymal stem cells attenuate spinal cord injury in mice. *Cell Death Dis.* 12:1096. doi: 10.1038/s41419-021-04398-w

Deng, L. X., Deng, P., Ruan, Y. W., Xu, Z. C., Liu, N. K., Wen, X. J., et al. (2013). A Novel Growth-Promoting Pathway Formed by GDNF-Overexpressing Schwann Cells Promotes Propriospinal Axonal Regeneration, Synapse Formation, and Partial Recovery of Function after Spinal Cord Injury. *J. Neurosci.* 33, 5655–5667.

Dias, D. O., Kalkitsas, J., Kelahmetoglu, Y., Estrada, C. P., Tatarishvili, J., Holl, D., et al. (2021). Pericyte-derived fibrotic scarring is conserved across diverse central nervous system lesions. *Nat. Commun.* 12:5501. doi: 10.1038/s41467-021-25585-5

Dias, D. O., Kim, H., Holl, D., Werne Solnestam, B., Lundeberg, J., Carlen, M., et al. (2018). Reducing Pericyte-Derived Scarring Promotes Recovery after Spinal Cord Injury. *Cell* 173, 153–165.e22. doi: 10.1016/j.cell.2018.02.004

Dorsett, P., Geraghty, T., Sinnott, A., and Acland, R. (2017). Hope, coping and psychosocial adjustment after spinal cord injury. *Spinal Cord Ser. Cases* 3:17046. doi: 10.1038/scsandc.2017.46

Dougherty, K. D., Dreyfus, C. F., and Black, I. B. (2000). Brain-derived neurotrophic factor in astrocytes, oligodendrocytes, and microglia/macrophages after spinal cord injury. *Neurobiol. Dis.* 7, 574–585. doi: 10.1006/nbdi.2000.0318

Du, J., Hao, D., He, B., Yan, L., Tang, Q., Zhang, Z., et al. (2021). Epidemiological characteristics of traumatic spinal cord injury in Xi'an China. *Spinal Cord* 59, 804–813.

Dumont, C. M., Carlson, M. A., Munsell, M. K., Ciciriello, A. J., Strnadova, K., Park, J., et al. (2019). Aligned hydrogel tubes guide regeneration following spinal cord injury. *Acta Biomater.* 86, 312–322. doi: 10.1016/j.actbio.2018.12.052

Duncan, G. J., Manesh, S. B., Hilton, B. J., Assinck, P., Liu, J., Moulson, A., et al. (2018). Locomotor recovery following contusive spinal cord injury does not require oligodendrocyte remyelination. *Nat. Commun.* 9:3066. doi: 10.1038/s41467-018-05473-1

Duncan, G. J., Manesh, S. B., Hilton, B. J., Assinck, P., Plemel, J. R., and Tetzlaff, W. (2020). The fate and function of oligodendrocyte progenitor cells after traumatic spinal cord injury. *Glia* 68, 227–245. doi: 10.1002/glia.23706

Duncan, I. D., Aguayo, A. J., Bunge, R. P., and Wood, P. M. (1981). Transplantation of rat Schwann cells grown in tissue culture into the mouse spinal cord. *J. Neurol. Sci.* 49, 241–252. doi: 10.1016/0022-510X(81)90082-4

Duncan, I. D., Marik, R. L., Broman, A. T., and Heidari, M. (2017). Thin myelin sheaths as the hallmark of remyelination persist over time and preserve axon function. *Proc. Natl. Acad. Sci. U S A.* 114, E9685–E9691. doi: 10.1073/pnas.1714183114

Duncan, I. D., and Radcliff, A. B. (2016). Inherited and acquired disorders of myelin: The underlying myelin pathology. *Exp. Neurol.* 283, 452–475. doi: 10.1016/j.expneurol.2016.04.002

Escartin, C., Galea, E., Lakatos, A., O'Callaghan, J. P., Petzold, G. C., Serrano-Pozo, A., et al. (2021). Reactive astrocyte nomenclature, definitions, and future directions. *Nat. Neurosci.* 24, 312–325. doi: 10.1038/s41593-020-00783-4

Eze, U. C., Bhaduri, A., Haeussler, M., Nowakowski, T. J., and Kriegstein, A. R. (2021). Single-cell atlas of early human brain development highlights heterogeneity of human neuroepithelial cells and early radial glia. *Nat. Neurosci.* 24, 584–594. doi: 10.1038/s41593-020-00794-1

Fandel, T. M., Trivedi, A., Nicholas, C. R., Zhang, H., Chen, J., Martinez, A. F., et al. (2016). Transplanted Human Stem Cell-Derived Interneuron Precursors Mitigate Mouse Bladder Dysfunction and Central Neuropathic Pain after Spinal Cord Injury. *Cell Stem Cell* 19, 544–557. doi: 10.1016/j.stem.2016.08.020

Fassbender, J. M., Whittemore, S. R., and Hagg, T. (2011). Targeting microvasculature for neuroprotection after SCI. *Neurotherapeutics* 8, 240–251. doi: 10.1007/s13311-011-0029-1

Fawcett, J. W., Duffield, J. S., and Silver, J. (2011). Starting the scar: A primary role for pericytes? *Nat. Med.* 17, 1052–1053. doi: 10.1038/nm0911-1052

Fernandez-Klett, F., and Priller, J. (2014). The Fibrotic Scar in Neurological Disorders. *Brain Pathol.* 24, 404–413. doi: 10.1111/bpa.12162

Ferrara, N., Gerber, H. P., and LeCouter, J. (2003). The biology of VEGF and its receptors. *Nat. Med.* 9, 669–676. doi: 10.1038/nm0603-669

Figley, S. A., Khosravi, R., Legasto, J. M., Tseng, Y. F., and Fehlings, M. G. (2014). Characterization of vascular disruption and blood-spinal cord barrier permeability following traumatic spinal cord injury. *J. Neurotrauma* 31, 541–552. doi: 10.1089/neu.2013.3034

Floriddia, E. M., Lourenco, T., Zhang, S. P., van Bruggen, D., Hilscher, M. M., Kukanja, P., et al. (2020). Distinct oligodendrocyte populations have spatial preference and different responses to spinal cord injury. *Nat. Commun.* 11:5860. doi: 10.1038/s41467-020-19453-x

Formento, E., Minassian, K., Wagner, F., Mignardot, J. B., Le Goff-Mignardot, C. G., Rowald, A., et al. (2018). Electrical spinal cord stimulation must preserve proprioception to enable locomotion in humans with spinal cord injury. *Nat. Neurosci.* 21, 1728–1741. doi: 10.1038/s41593-018-0262-6

Funfschilling, U., Supplie, L. M., Mahad, D., Boretius, S., Saab, A. S., Edgar, J., et al. (2012). Glycolytic oligodendrocytes maintain myelin and long-term axonal integrity. *Nature* 485, 517–521. doi: 10.1038/nature11007

Gadani, S. P., Walsh, J. T., Lukens, J. R., and Kipnis, J. (2015). Dealing with Danger in the CNS:The Response of the Immune System to Injury. *Neuron* 87, 47–62. doi: 10.1016/j.neuron.2015.05.019

Gant, K. L., Guest, J. D., Palermo, A. E., Vedantam, A., Jimsheleishvili, G., Bunge, M. B., et al. (2022). Phase 1 Safety Trial of Autologous Human Schwann Cell Transplantation in Chronic Spinal Cord Injury. *J. Neurotrauma* 39, 285–299. doi: 10.1089/neu.2020.7590

Gao, X., Cheng, W., Zhang, X., Zhou, Z., Ding, Z., Zhou, X., et al. (2022). Nerve Growth Factor-Laden Anisotropic Silk Nanofiber Hydrogels to Regulate Neuronal/Astroglial Differentiation for Scarless Spinal Cord Repair. *ACS Appl. Mater. Interfaces* 14, 3701–3715. doi: 10.1021/acsami.1c19229

Garcia, E., Aguilar-Cevallos, J., Silva-Garcia, R., and Ibarra, A. (2016). Cytokine and Growth Factor Activation In Vivo and In Vitro after Spinal Cord Injury. *Mediators Inflamm.* 2016:9476020. doi: 10.1155/2016/9476020

Garcia-Altes, A., Perez, K., Novoa, A., Suelves, J. M., Bernabeu, M., Vidal, J., et al. (2012). Spinal cord injury and traumatic brain injury: A cost-of-illness study. *Neuroepidemiology* 39, 103–108. doi: 10.1159/000338297

Garcia-Ovejero, D., Arevalo-Martin, A., Paniagua-Torija, B., Florensa-Vila, J., Ferrer, I., Grassner, L., et al. (2015). The ependymal region of the adult human spinal cord differs from other species and shows ependymoma-like features. *Brain* 138, 1583–1597. doi: 10.1093/brain/awv089

Gautier, H. O. B., Evans, K. A., Volbracht, K., James, R., Sitnikov, S., Lundgaard, I., et al. (2015). Neuronal activity regulates remyelination via glutamate signalling to oligodendrocyte progenitors. *Nat. Commun.* 6:8518. doi: 10.1038/ncomms9518

Gensel, J. C., Kopper, T. J., Zhang, B., Orr, M. B., and Bailey, W. M. (2017). Predictive screening of M1 and M2 macrophages reveals the immunomodulatory effectiveness of post spinal cord injury azithromycin treatment. *Sci. Rep.* 7:40144.

Gericota, B., Anderson, J. S., Mitchell, G., Borjesson, D. L., Sturges, B. K., Nolta, J. A., et al. (2014). Canine epidermal neural crest stem cells: Characterization and potential as therapy candidate for a large animal model of spinal cord injury. *Stem Cells Transl. Med.* 3, 334–345. doi: 10.5966/sctm.2013-0129

Ghosh, M., Tuesta, L. M., Puentes, R., Patel, S., Melendez, K., El Maarouf, A., et al. (2012). Extensive cell migration, axon regeneration, and improved function with polysialic acid-modified Schwann cells after spinal cord injury. *Glia* 60, 979–992. doi: 10.1002/glia.22330

Gibson, E. M., Purger, D., Mount, C. W., Goldstein, A. K., Lin, G. L., Wood, L. S., et al. (2014). Neuronal activity promotes oligodendrogenesis and adaptive myelination in the mammalian brain. *Science* 344:1252304. doi: 10.1126/science.1252304

Ginhoux, F., Greter, M., Leboeuf, M., Nandi, S., See, P., Gokhan, S., et al. (2010). Fate mapping analysis reveals that adult microglia derive from primitive macrophages. *Science* 330, 841–845. doi: 10.1126/science.1194637

Gomez, R. M., Sanchez, M. Y., Portela-Lomba, M., Ghotme, K., Barreto, G. E., Sierra, J., et al. (2018). Cell therapy for spinal cord injury with olfactory ensheathing glia cells (OECs). *Glia* 66, 1267–1301. doi: 10.1002/glia.23282

Gonzenbach, R. R., Gasser, P., Zörner, B., Hochreutener, E., Dietz, V., and Schwab, M. E. (2010). Nogo-A antibodies and training reduce muscle spasms in spinal cord-injured rats. *Ann. Neurol.* 68, 48–57. doi: 10.1002/ana.22009

Goritz, C., Dias, D. O., Tomilin, N., Barbacid, M., Shupliakov, O., and Frisen, J. (2011). A pericyte origin of spinal cord scar tissue. *Science* 333, 238–242. doi: 10.1126/science.1203165

Greenhalgh, A. D., and David, S. (2014). Differences in the phagocytic response of microglia and peripheral macrophages after spinal cord injury and its effects on cell death. *J. Neurosci.* 34, 6316–6322. doi: 10.1523/JNEUROSCI.4912-13.2014

Greenhalgh, A. D., Zarruk, J. G., Healy, L. M., Baskar Jesudasan, S. J., Jhelum, P., Salmon, C. K., et al. (2018). Peripherally derived macrophages modulate microglial function to reduce inflammation after CNS injury. *PLoS Biol.* 16:e2005264. doi: 10.1371/journal.pbio.2005264

Griffiths, I. R., and McCulloch, M. C. (1983). Nerve fibres in spinal cord impact injuries. Part 1. Changes in the myelin sheath during the initial 5 weeks. *J. Neurol. Sci.* 58, 335–349. doi: 10.1016/0022-510X(83)90093-X

Gulino, R., Lombardo, S. A., Casabona, A., Leanza, G., and Perciavalle, V. (2004). Levels of brain-derived neurotrophic factor and neurotrophin-4 in lumbar motoneurons after low-thoracic spinal cord hemisection. *Brain Res.* 1013, 174–181. doi: 10.1016/j.brainres.2004.03.055

Gundersen, G. A., Vindedal, G. F., Skare, O., and Nagelhus, E. A. (2014). Evidence that pericytes regulate aquaporin-4 polarization in mouse cortical astrocytes. *Brain Struct. Funct.* 219, 2181–2186. doi: 10.1007/s00429-013-0629-0

Gundersen, V., Storm-Mathisen, J., and Bergersen, L. H. (2015). Neuroglial Transmission. *Physiol. Rev.* 95, 695–726. doi: 10.1152/physrev.00024.2014

Hara, M., Kobayakawa, K., Ohkawa, Y., Kumamaru, H., Yokota, K., Saito, T., et al. (2017). Interaction of reactive astrocytes with type I collagen induces astrocytic scar formation through the integrin-N-cadherin pathway after spinal cord injury. *Nat. Med.* 23, 818–828. doi: 10.1038/nm.4354

Hartmann, D. A., Underly, R. G., Grant, R. I., Watson, A. N., Lindner, V., and Shih, A. Y. (2015). Pericyte structure and distribution in the cerebral cortex revealed by high-resolution imaging of transgenic mice. *Neurophotonics* 2:041402. doi: 10.1117/1.NPh.2.4.041402

Hawryluk, G. W., Mothe, A., Wang, J., Wang, S., Tator, C., and Fehlings, M. G. (2012a). An in vivo characterization of trophic factor production following neural precursor cell or bone marrow stromal cell transplantation for spinal cord injury. *Stem Cells Dev.* 21, 2222–2238. doi: 10.1089/scd.2011.0596

Hawryluk, G. W., Mothe, A. J., Chamankhah, M., Wang, J., Tator, C., and Fehlings, M. G. (2012b). In vitro characterization of trophic factor expression in neural precursor cells. *Stem Cells Dev.* 21, 432–447. doi: 10.1089/scd.2011.0242

Hawryluk, G. W., Spano, S., Chew, D., Wang, S., Erwin, M., Chamankhah, M., et al. (2014). An examination of the mechanisms by which neural precursors augment recovery following spinal cord injury: A key role for remyelination. *Cell Transplant.* 23, 365–380. doi: 10.3727/096368912X662408

Haynes, S. E., Hollopeter, G., Yang, G., Kurpius, D., Dailey, M. E., Gan, W. B., et al. (2006). The P2Y12 receptor regulates microglial activation by extracellular nucleotides. *Nat. Neurosci.* 9, 1512–1519. doi: 10.1038/nn1805

Hellenbrand, D. J., Quinn, C. M., Piper, Z. J., Morehouse, C. N., Fixel, J. A., and Hanna, A. S. (2021). Inflammation after spinal cord injury: A review of the critical timeline of signaling cues and cellular infiltration. *J. Neuroinflammation* 18:284. doi: 10.1186/s12974-021-02337-2

Hesp, Z. C., Goldstein, E. Z., Miranda, C. J., Kaspar, B. K., and McTigue, D. M. (2015). Chronic oligodendrogenesis and remyelination after spinal cord injury in mice and rats. *J. Neurosci.* 35, 1274–1290. doi: 10.1523/JNEUROSCI.2568-14.2015

Hesp, Z. C., Yoseph, R. Y., Suzuki, R., Jukkola, P., Wilson, C., Nishiyama, A., et al. (2018). Proliferating NG2-Cell-Dependent Angiogenesis and Scar Formation Alter Axon Growth and Functional Recovery After Spinal Cord Injury in Mice. *J. Neurosci.* 38, 1366–1382. doi: 10.1523/JNEUROSCI.3953-16.2017

Hill, C. E., Hurtado, A., Blits, B., Bahr, B. A., Wood, P. M., Bartlett Bunge, M., et al. (2007). Early necrosis and apoptosis of Schwann cells transplanted into the injured rat spinal cord. *Eur. J. Neurosci.* 26, 1433–1445. doi: 10.1111/j.1460-9568.2007.05771.x

Hofstetter, C. P., Holmstrom, N. A., Lilja, J. A., Schweinhardt, P., Hao, J., Spenger, C., et al. (2005). Allodynia limits the usefulness of intraspinal neural stem cell grafts; directed differentiation improves outcome. *Nat. Neurosci.* 8, 346–353. doi: 10.1038/nn1405

Hong, J. Y., Kim, S. H., Seo, Y., Jeon, J., Davaa, G., Hyun, J. K., et al. (2022). Self-assembling peptide gels promote angiogenesis and functional recovery after spinal cord injury in rats. *J. Tissue Eng.* 13:20417314221086491. doi: 10.1177/20417314221086491

Horky, L. L., Galimi, F., Gage, F. H., and Horner, P. J. (2006). Fate of endogenous stem/progenitor cells following spinal cord injury. *J. Comp. Neurol.* 498, 525–538. doi: 10.1002/cne.21065

Horner, P. J., Power, A. E., Kempermann, G., Kuhn, H. G., Palmer, T. D., Winkler, J., et al. (2000). Proliferation and differentiation of progenitor cells throughout the intact adult rat spinal cord. *J. Neurosci.* 20, 2218–2228. doi: 10.1523/JNEUROSCI.20-06-02218.2000

Hosseini, S. M., Alizadeh, A., Shahsavani, N., Chopek, J., Ahlfors, J. E., and Karimi-Abdolrezaee, S. (2022). Suppressing CSPG/LAR/PTPa Axis Facilitates Neuronal Replacement and Synaptogenesis by Human Neural Precursor Grafts and Improves Recovery after Spinal Cord Injury. *J. Neurosci.* 42, 3096–3121. doi: 10.1523/JNEUROSCI.2177-21.2022

Hou, Y., Ryu, C. H., Jun, J. A., Kim, S. M., Jeong, C. H., and Jeun, S. S. (2014). IL-8 enhances the angiogenic potential of human bone marrow mesenchymal stem cells by increasing vascular endothelial growth factor. *Cell Biol. Int.* 38, 1050–1059. doi: 10.1002/cbin.10294

Hu, X., Leak, R. K., Shi, Y., Suenaga, J., Gao, Y., Zheng, P., et al. (2015). Microglial and macrophage polarization-new prospects for brain repair. *Nat. Rev. Neurol.* 11, 56–64. doi: 10.1038/nrneurol.2014.207

Hu, X. C., Lu, Y. B., Yang, Y. N., Kang, X. W., Wang, Y. G., Ma, B., et al. (2021). Progress in clinical trials of cell transplantation for the treatment of spinal cord injury: How many questions remain unanswered? *Neural Regen. Res.* 16, 405–413. doi: 10.4103/1673-5374.293130

Huang, L., Wang, Y., Zhu, M., Wan, X., Zhang, H., Lei, T., et al. (2020). Anisotropic Alginate Hydrogels Promote Axonal Growth across Chronic Spinal Cord Transections after Scar Removal. *ACS Biomater. Sci. Eng.* 6, 2274–2286. doi: 10.1021/acsbiomaterials.9b01802

Huang, W., Bhaduri, A., Velmeshev, D., Wang, S., Wang, L., Rottkamp, C. A., et al. (2020). Origins and Proliferative States of Human Oligodendrocyte Precursor Cells. *Cell* 182, 594–608.e11. doi: 10.1016/j.cell.2020.06.027

Hung, C. H., Lin, Y. L., and Young, T. H. (2006). The effect of chitosan and PVDF substrates on the behavior of embryonic rat cerebral cortical stem cells. *Biomaterials* 27, 4461–4469. doi: 10.1016/j.biomaterials.2006.04.021

Iacobaeus, E., Sugars, R. V., Tornqvist Andren, A., Alm, J. J., Qian, H., Frantzen, J., et al. (2017). Dynamic Changes in Brain Mesenchymal Perivascular Cells Associate with Multiple Sclerosis Disease Duration, Active Inflammation, and Demyelination. *Stem Cells Transl. Med.* 6, 1840–1851. doi: 10.1002/sctm.17-0028

Ikezumi, Y., Suzuki, T., Karasawa, T., Hasegawa, H., Yamada, T., Imai, N., et al. (2011). Identification of alternatively activated macrophages in new-onset paediatric and adult immunoglobulin A nephropathy: Potential role in mesangial matrix expansion. *Histopathology* 58, 198–210. doi: 10.1111/j.1365-2559.2011.03742.x

Ishii, H., Tanabe, S., Ueno, M., Kubo, T., Kayama, H., Serada, S., et al. (2013). ifn-gamma-dependent secretion of IL-10 from Th1 cells and microglia/macrophages contributes to functional recovery after spinal cord injury. *Cell Death Dis.* 4:e710. doi: 10.1038/cddis.2013.234

Iwai, H., Nori, S., Nishimura, S., Yasuda, A., Takano, M., Tsuji, O., et al. (2014). Transplantation of neural stem/progenitor cells at different locations in mice with spinal cord injury. *Cell Transplant.* 23, 1451–1464. doi: 10.3727/096368913X670967

James, N. D., Bartus, K., Grist, J., Bennett, D. L., McMahon, S. B., and Bradbury, E. J. (2011). Conduction failure following spinal cord injury: Functional and anatomical changes from acute to chronic stages. *J. Neurosci.* 31, 18543–18555. doi: 10.1523/JNEUROSCI.4306-11.2011

James Spencer, L., and Theadom, A. (2019). Global, regional, and national burden of traumatic brain injury and spinal cord injury, 1990-2016: A systematic analysis for the Global Burden of Disease Study 2016. *Lancet Neurol.* 18, 56–87. doi: 10.1016/S1474-4422(18)30415-0

Jessen, K. R., and Mirsky, R. (2016). The repair Schwann cell and its function in regenerating nerves. *J. Physiol.* 594, 3521–3531. doi: 10.1113/JP270874

Jessen, K. R., Mirsky, R., and Lloyd, A. C. (2015). Schwann Cells: Development and Role in Nerve Repair. *Cold Spring Harb. Perspect. Biol.* 7:a020487. doi: 10.1101/cshperspect.a020487

Jin, L. Y., Li, J., Wang, K. F., Xia, W. W., Zhu, Z. Q., Wang, C. R., et al. (2021). Blood-Spinal Cord Barrier in Spinal Cord Injury: A Review. *J. Neurotraum.* 38, 1203–1224. doi: 10.1089/neu.2020.7413

Johansson, C. B., Momma, S., Clarke, D. L., Risling, M., Lendahl, U., and Frisén, J. (1999). Identification of a neural stem cell in the adult mammalian central nervous system. *Cell* 96, 25–34. doi: 10.1016/S0092-8674(00)80956-3

Johe, K. K., Hazel, T. G., Muller, T., Dugich-Djordjevic, M. M., and McKay, R. D. (1996). Single factors direct the differentiation of stem cells from the fetal and adult central nervous system. *Genes Dev.* 10, 3129–3140. doi: 10.1101/gad.10.24.3129

Kageyama, R., and Ohtsuka, T. (1999). The Notch-Hes pathway in mammalian neural development. *Cell Res.* 9, 179–188. doi: 10.1038/sj.cr.7290016

Karimi-Abdolrezaee, S., and Billakanti, R. (2012). Reactive astrogliosis after spinal cord injury-beneficial and detrimental effects. *Mol. Neurobiol.* 46, 251–264. doi: 10.1007/s12035-012-8287-4

Kasantikul, V., Netsky, M. G., and James, A. E. (1979). Relation of age and cerebral ventricle size to central canal in man. Morphological analysis. *J. Neurosurg.* 51, 85–93. doi: 10.3171/jns.1979.51.1.0085

Keirstead, H. S., Nistor, G., Bernal, G., Totoiu, M., Cloutier, F., Sharp, K., et al. (2005). Human embryonic stem cell-derived oligodendrocyte progenitor cell transplants remyelinate and restore locomotion after spinal cord injury. *J. Neurosci.* 25, 4694–4705. doi: 10.1523/JNEUROSCI.0311-05.2005

Kierdorf, K., Erny, D., Goldmann, T., Sander, V., Schulz, C., Perdiguero, E. G., et al. (2013). Microglia emerge from erythromyeloid precursors via Pu.1- and Irf8-dependent pathways. *Nat. Neurosci.* 16, 273–280. doi: 10.1038/nn.3318

Kigerl, K. A., Gensel, J. C., Ankeny, D. P., Alexander, J. K., Donnelly, D. J., and Popovich, P. G. (2009). Identification of two distinct macrophage subsets with divergent effects causing either neurotoxicity or regeneration in the injured mouse spinal cord. *J. Neurosci.* 29, 13435–13444. doi: 10.1523/JNEUROSCI.3257-09.2009

Kirby, L., Jin, J., Cardona, J. G., Smith, M. D., Martin, K. A., Wang, J., et al. (2019). Oligodendrocyte precursor cells present antigen and are cytotoxic targets in inflammatory demyelination. *Nat. Commun.* 10:3887. doi: 10.1038/s41467-019-11638-3

Klapper, S. D., Garg, P., Dagar, S., Lenk, K., Gottmann, K., and Nieweg, K. (2019). Astrocyte lineage cells are essential for functional neuronal differentiation and synapse maturation in human iPSC-derived neural networks. *Glia* 67, 1893–1909. doi: 10.1002/glia.23666

Kondo, T., Johnson, S. A., Yoder, M. C., Romand, R., and Hashino, E. (2005). Sonic hedgehog and retinoic acid synergistically promote sensory fate specification from bone marrow-derived pluripotent stem cells. *Proc. Natl. Acad. Sci. U S A.* 102, 4789–4794. doi: 10.1073/pnas.0408239102

Kong, T., Park, J. M., Jang, J. H., Kim, C. Y., Bae, S. H., Choi, Y., et al. (2018). Immunomodulatory effect of CD200-positive human placenta-derived stem cells in the early phase of stroke. *Exp. Mol. Med.* 50:e425. doi: 10.1038/emm.2017.233

Kosuri, S., Borca, C. H., Mugnier, H., Tamasi, M., Patel, R. A., Perez, I., et al. (2022). Machine-Assisted Discovery of Chondroitinase ABC Complexes toward Sustained Neural Regeneration. *Adv. Healthc. Mater.* 11:2102101. doi: 10.1002/adhm.202102101

Ku, Z., Han, K. W., Chen, J. G., Wang, C. H., Dong, Y., Yu, M. K., et al. (2017). Vascular endothelial growth factor is neuroprotective against ischemic brain injury by inhibiting scavenger receptor A expression on microglia. *J. Neurochem.* 142, 700–709. doi: 10.1111/jnc.14108

Kucher, K., Johns, D., Maier, D., Abel, R., Badke, A., Baron, H., et al. (2018). First-in-Man Intrathecal Application of Neurite Growth-Promoting Anti-Nogo-A Antibodies in Acute Spinal Cord Injury. *Neurorehabil. Neural Repair* 32, 578–589. doi: 10.1177/1545968318776371

Kumagai, G., Tsoulfas, P., Toh, S., McNiece, I., Bramlett, H. M., and Dietrich, W. D. (2013). Genetically modified mesenchymal stem cells (MSCs) promote axonal regeneration and prevent hypersensitivity after spinal cord injury. *Exp. Neurol.* 248, 369–380. doi: 10.1016/j.expneurol.2013.06.028

Kumar, R., Lim, J., Mekary, R. A., Rattani, A., Dewan, M. C., Sharif, S. Y., et al. (2018). Traumatic Spinal Injury: Global Epidemiology and Worldwide Volume. *World Neurosurg.* 113, e345–e363. doi: 10.1016/j.wneu.2018.02.033

Lachyankar, M. B., Condon, P. J., Quesenberry, P. J., Litofsky, N. S., Recht, L. D., and Ross, A. H. (1997). Embryonic precursor cells that express Trk receptors:induction of different cell fates by NGF, BDNF, NT-3, and CNTF. *Exp. Neurol.* 144, 350–360. doi: 10.1006/exnr.1997.6434

Lai, E. C. (2004). Notch signaling: Control of cell communication and cell fate. *Development* 131, 965–973. doi: 10.1242/dev.01074

Lecca, D., Fumagalli, M., Ceruti, S., and Abbracchio, M. P. (2016). Intertwining extracellular nucleotides and their receptors with Ca2+ in determining adult neural stem cell survival, proliferation and final fate. *Philos. Trans. R. Soc. Lond. B Biol. Sci.* 371:20150433. doi: 10.1098/rstb.2015.0433

Lee, H., Lee, H. Y., Lee, B. E., Gerovska, D., Park, S. Y., Zaehres, H., et al. (2020). Sequentially induced motor neurons from human fibroblasts facilitate locomotor recovery in a rodent spinal cord injury model. *Elife* 9:e52069. doi: 10.7554/eLife.52069

Lee, Y., Lee, S., Lee, S. R., Park, K., Hong, Y., Lee, M., et al. (2014).), Beneficial effects of melatonin combined with exercise on endogenous neural stem/progenitor cells proliferation after spinal cord injury. *Int. J. Mol. Sci.* 15, 2207–2222. doi: 10.3390/ijms15022207

Lee, Y., Morrison, B. M., Li, Y., Lengacher, S., Farah, M. H., Hoffman, P. N., et al. (2012). Oligodendroglia metabolically support axons and contribute to neurodegeneration. *Nature* 487, 443–448. doi: 10.1038/nature11314

Lee, Y. I., Li, Y., Mikesh, M., Smith, I., Nave, K. A., Schwab, M. H., et al. (2016). Neuregulin1 displayed on motor axons regulates terminal Schwann cell-mediated synapse elimination at developing neuromuscular junctions. *Proc. Natl. Acad. Sci. U S A.* 113, E479–E487. doi: 10.1073/pnas.1519156113

Lee, Y. S., Funk, L. H., Lee, J. K., and Bunge, M. B. (2018). Macrophage depletion and Schwann cell transplantation reduce cyst size after rat contusive spinal cord injury. *Neural Regen. Res.* 13, 684–691. doi: 10.4103/1673-5374.230295

Li, G., Che, M. T., Zhang, K., Qin, L. N., Zhang, Y. T., Chen, R. Q., et al. (2016). Graft of the NT-3 persistent delivery gelatin sponge scaffold promotes axon regeneration, attenuates inflammation, and induces cell migration in rat and canine with spinal cord injury. *Biomaterials* 83, 233–248. doi: 10.1016/j.biomaterials.2015.11.059

Li, L., Zhang, Y., Mu, J., Chen, J., Zhang, C., Cao, H., et al. (2020). Transplantation of Human Mesenchymal Stem-Cell-Derived Exosomes Immobilized in an Adhesive Hydrogel for Effective Treatment of Spinal Cord Injury. *Nano Lett.* 20, 4298–4305. doi: 10.1021/acs.nanolett.0c00929

Li, X., Floriddia, E. M., Toskas, K., Fernandes, K. J. L., Guerout, N., and Barnabe-Heider, F. (2016). Regenerative Potential of Ependymal Cells for Spinal Cord Injuries Over Time. *EBioMedicine* 13, 55–65. doi: 10.1016/j.ebiom.2016.10.035

Li, X., Yang, Z., Zhang, A., Wang, T., and Chen, W. (2009). Repair of thoracic spinal cord injury by chitosan tube implantation in adult rats. *Biomaterials* 30, 1121–1132. doi: 10.1016/j.biomaterials.2008.10.063

Li, X. J., Du, Z. W., Zarnowska, E. D., Pankratz, M., Hansen, L. O., Pearce, R. A., et al. (2005). Specification of motoneurons from human embryonic stem cells. *Nat. Biotechnol.* 23, 215–221. doi: 10.1038/nbt1063

Li, Y. Q., Lucas-Osma, A. M., Black, S., Bandet, M. V., Stephens, M. J., Vavrek, R., et al. (2017). Pericytes impair capillary blood flow and motor function after chronic spinal cord injury. *Nat. Med.* 23, 733–741. doi: 10.1038/nm.4331

Liau, L. L., Looi, Q. H., Chia, W. C., Subramaniam, T., Ng, M. H., and Law, J. X. (2020). Treatment of spinal cord injury with mesenchymal stem cells. *Cell Biosci.* 10:112. doi: 10.1186/s13578-020-00475-3

Liddelow, S. A., Guttenplan, K. A., Clarke, L. E., Bennett, F. C., Bohlen, C. J., Schirmer, L., et al. (2017). Neurotoxic reactive astrocytes are induced by activated microglia. *Nature* 541, 481–487. doi: 10.1038/nature21029

Liu, S., Sandner, B., Schackel, T., Nicholson, L., Chtarto, A., Tenenbaum, L., et al. (2017a). Regulated viral BDNF delivery in combination with Schwann cells promotes axonal regeneration through capillary alginate hydrogels after spinal cord injury. *Acta Biomater.* 60, 167–180. doi: 10.1016/j.actbio.2017.07.024

Liu, S., Schackel, T., Weidner, N., and Puttagunta, R. (2017b). Biomaterial-Supported Cell Transplantation Treatments for Spinal Cord Injury: Challenges and Perspectives. *Front. Cell. Neurosci.* 11:430. doi: 10.3389/fncel.2017.00430

Liu, Z., Yang, Y., He, L., Pang, M., Luo, C., Liu, B., et al. (2019). High-dose methylprednisolone for acute traumatic spinal cord injury: A meta-analysis. *Neurology* 93, e841–e850. doi: 10.1212/WNL.0000000000007998

Llorens-Bobadilla, E., Chell, J. M., Le Merre, P., Wu, Y., Zamboni, M., Bergenstrahle, J., et al. (2020). A latent lineage potential in resident neural stem cells enables spinal cord repair. *Science* 370:eabb8795. doi: 10.1126/science.abb8795

Lu, D., Mahmood, A., Goussev, A., Schallert, T., Qu, C., Zhang, Z. G., et al. (2004). Atorvastatin reduction of intravascular thrombosis, increase in cerebral microvascular patency and integrity, and enhancement of spatial learning in rats subjected to traumatic brain injury. *J. Neurosurg.* 101, 813–821. doi: 10.3171/jns.2004.101.5.0813

Lu, P., Woodruff, G., Wang, Y., Graham, L., Hunt, M., Wu, D., et al. (2014). Long-distance axonal growth from human induced pluripotent stem cells after spinal cord injury. *Neuron* 83, 789–796. doi: 10.1016/j.neuron.2014.07.014

Lubetzki, C., Sol-Foulon, N., and Desmazieres, A. (2020). Nodes of Ranvier during development and repair in the CNS. *Nat. Rev. Neurol.* 16, 426–439. doi: 10.1038/s41582-020-0375-x

Ludwin, S. K., and Maitland, M. (1984). Long-term remyelination fails to reconstitute normal thickness of central myelin sheaths. *J. Neurol. Sci.* 64, 193–198. doi: 10.1016/0022-510X(84)90037-6

Lv, B., Zhang, X., Yuan, J., Chen, Y., Ding, H., Cao, X., et al. (2021). Biomaterial-supported MSC transplantation enhances cell-cell communication for spinal cord injury. *Stem Cell Res.* 12:36. doi: 10.1186/s13287-020-02090-y

Macchi, M., Magalon, K., Zimmer, C., Peeva, E., El Waly, B., Brousse, B., et al. (2020). Mature oligodendrocytes bordering lesions limit demyelination and favor myelin repair via heparan sulfate production. *Elife* 9:e51735. doi: 10.7554/eLife.51735

MacVicar, B. A., and Newman, E. A. (2015). Astrocyte regulation of blood flow in the brain. *Cold Spring Harb. Perspect. Biol.* 7:a020388. doi: 10.1101/cshperspect.a020388

Magistretti, P. J., and Allaman, I. (2018). Lactate in the brain: From metabolic end-product to signalling molecule. *Nat. Rev. Neurosci.* 19, 235–249. doi: 10.1038/nrn.2018.19

Maldonado, P. P., Velez-Fort, M., Levavasseur, F., and Angulo, M. C. (2013). Oligodendrocyte precursor cells are accurate sensors of local K+ in mature gray matter. *J. Neurosci.* 33, 2432–2442. doi: 10.1523/JNEUROSCI.1961-12.2013

Maldonado-Lasuncion, I., Haggerty, A. E., Okuda, A., Mihara, T., de la Oliva, N., Verhaagen, J., et al. (2021). The Effect of Inflammatory Priming on the Therapeutic Potential of Mesenchymal Stromal Cells for Spinal Cord Repair. *Cells* 10:1316. doi: 10.3390/cells10061316

Maldonado-Lasuncion, I., Verhaagen, J., and Oudega, M. (2018). Mesenchymal Stem Cell-Macrophage Choreography Supporting Spinal Cord Repair. *Neurotherapeutics* 15, 578–587. doi: 10.1007/s13311-018-0629-0

Mani, N., Khaibullina, A., Krum, J. M., and Rosenstein, J. M. (2005). Astrocyte growth effects of vascular endothelial growth factor (VEGF) application to perinatal neocortical explants: Receptor mediation and signal transduction pathways. *Exp. Neurol.* 192, 394–406. doi: 10.1016/j.expneurol.2004.12.022

Manley, N. C., Priest, C. A., Denham, J., Wirth, E. D., and Lebkowski, J. S. (2017). Human Embryonic Stem Cell-Derived Oligodendrocyte Progenitor Cells: Preclinical Efficacy and Safety in Cervical Spinal Cord Injury. *Stem Cell Transl. Med.* 6, 1917–1929. doi: 10.1002/sctm.17-0065

Marquardt, L. M., Doulames, V. M., Wang, A. T., Dubbin, K., Suhar, R. A., Kratochvil, M. J., et al. (2020). Designer, injectable gels to prevent transplanted Schwann cell loss during spinal cord injury therapy. *Sci. Adv.* 6:eaaz1039. doi: 10.1126/sciadv.aaz1039

Marrotte, E. J., Johnson, K., Schweller, R. M., Chapla, R., Mace, B. E., Laskowitz, D. T., et al. (2021). Induction of Neurogenesis and Angiogenesis in a Rat Hemisection Spinal Cord Injury Model With Combined Neural Stem Cell, Endothelial Progenitor Cell, and Biomimetic Hydrogel Matrix Therapy. *Crit. Care Explor.* 3:e0436. doi: 10.1097/CCE.0000000000000436

Mathew, S. A., Naik, C., Cahill, P. A., and Bhonde, R. R. (2020). Placental mesenchymal stromal cells as an alternative tool for therapeutic angiogenesis. *Cell Mol. Life Sci.* 77, 253–265. doi: 10.1007/s00018-019-03268-1

Matthews, M. A., St Onge, M. F., Faciane, C. L., and Gelderd, J. B. (1979). Axon sprouting into segments of rat spinal cord adjacent to the site of a previous transection. *Neuropathol. Appl. Neurobiol.* 5, 181–196. doi: 10.1111/j.1365-2990.1979.tb00618.x

Maugeri, G., D'Amico, A. G., Musumeci, G., Reglodi, D., and D'Agata, V. (2020).), Effects of PACAP on Schwann Cells: Focus on Nerve Injury. *Int. J. Mol. Sci.* 21:8233. doi: 10.3390/ijms21218233

McDonald, J. W., and Sadowsky, C. (2002). Spinal-cord injury. *Lancet* 359, 417–425. doi: 10.1016/S0140-6736(02)07603-1

McKay, R. (1997). Stem cells in the central nervous system. *Science* 276, 66–71. doi: 10.1126/science.276.5309.66

Meletis, K., Barnabe-Heider, F., Carlen, M., Evergren, E., Tomilin, N., Shupliakov, O., et al. (2008). Spinal cord injury reveals multilineage differentiation of ependymal cells. *PLoS Biol.* 6:e182. doi: 10.1371/journal.pbio.0060182

Mendt, M., Rezvani, K., and Shpall, E. (2019). Mesenchymal stem cell-derived exosomes for clinical use. *Bone Marrow Transplant.* 54, 789–792. doi: 10.1038/s41409-019-0616-z

Menet, V., Prieto, M., Privat, A., and Ribotta, M. G. Y. (2003). Axonal plasticity and functional recovery after spinal cord injury in mice deficient in both glial fibrillary acidic protein and vimentin genes. *Proc. Natl. Acad. Sci. U S A.* 100, 8999–9004. doi: 10.1073/pnas.1533187100

Milhorat, T. H., Kotzen, R. M., and Anzil, A. P. (1994). Stenosis of central canal of spinal cord in man: Incidence and pathological findings in 232 autopsy cases. *J. Neurosurg.* 80, 716–722. doi: 10.3171/jns.1994.80.4.0716

Min, Q., Parkinson, D. B., and Dun, X. P. (2021). Migrating Schwann cells direct axon regeneration within the peripheral nerve bridge. *Glia* 69, 235–254. doi: 10.1002/glia.23892

Miron, V. E., Boyd, A., Zhao, J. W., Yuen, T. J., Ruckh, J. M., Shadrach, J. L., et al. (2013). M2 microglia and macrophages drive oligodendrocyte differentiation during CNS remyelination. *Nat. Neurosci.* 16, 1211–1218. doi: 10.1038/nn.3469

Mocchetti, I., and Wrathall, J. R. (1995). Neurotrophic factors in central nervous system trauma. *J. Neurotrauma* 12, 853–870. doi: 10.1089/neu.1995.12.853

Moeendarbary, E., Weber, I. P., Sheridan, G. K., Koser, D. E., Soleman, S., Haenzi, B., et al. (2017). The soft mechanical signature of glial scars in the central nervous system. *Nat. Commun.* 8:14787. doi: 10.1038/ncomms14787

Mohammad-Gharibani, P., Tiraihi, T., Delshad, A., Arabkheradmand, J., and Taheri, T. (2013). Improvement of contusive spinal cord injury in rats by co-transplantation of gamma-aminobutyric acid-ergic cells and bone marrow stromal cells. *Cytotherapy* 15, 1073–1085. doi: 10.1016/j.jcyt.2013.05.002

Monje, P. V., Deng, L., and Xu, X. M. (2021). Human Schwann Cell Transplantation for Spinal Cord Injury: Prospects and Challenges in Translational Medicine. *Front. Cell. Neurosci.* 15:690894. doi: 10.3389/fncel.2021.690894

Morest, A. K., and Silver, J. (2003). Precursors of neurons, neuroglia and ependymal cells in the CNS: What are they? Where are they from? How do they get where they are going? *Glia* 43, 6–18. doi: 10.1002/glia.10238

Nakagomi, T., Kubo, S., Nakano-Doi, A., Sakuma, R., Lu, S., Narita, A., et al. (2015). Brain Vascular Pericytes Following Ischemia Have Multipotential Stem Cell Activity to Differentiate Into Neural and Vascular Lineage Cells. *Stem Cells* 33, 1962–1974. doi: 10.1002/stem.1977

Nakajima, H., Uchida, K., Guerrero, A. R., Watanabe, S., Sugita, D., Takeura, N., et al. (2012). Transplantation of mesenchymal stem cells promotes an alternative pathway of macrophage activation and functional recovery after spinal cord injury. *J. Neurotrauma* 29, 1614–1625. doi: 10.1089/neu.2011.2109

Nashmi, R., and Fehlings, M. G. (2001). Changes in axonal physiology and morphology after chronic compressive injury of the rat thoracic spinal cord. *Neuroscience* 104, 235–251. doi: 10.1016/S0306-4522(01)00009-4

Nave, K. A., and Werner, H. B. (2014). Myelination of the nervous system: Mechanisms and functions. *Annu. Rev. Cell Dev. Biol.* 30, 503–533. doi: 10.1146/annurev-cellbio-100913-013101

Neirinckx, V., Coste, C., Franzen, R., Gothot, A., Rogister, B., and Wislet, S. (2014). Neutrophil contribution to spinal cord injury and repair. *J. Neuroinflammation* 11:150. doi: 10.1186/s12974-014-0150-2

Nieto-Sampedro, M., Lewis, E. R., Cotman, C. W., Manthorpe, M., Skaper, S. D., Barbin, G., et al. (1982). Brain injury causes a time-dependent increase in neuronotrophic activity at the lesion site. *Science* 217, 860–861. doi: 10.1126/science.7100931

Nikolakopoulou, A. M., Montagne, A., Kisler, K., Dai, Z., Wang, Y., Huuskonen, M. T., et al. (2019). Pericyte loss leads to circulatory failure and pleiotrophin depletion causing neuron loss. *Nat. Neurosci.* 22, 1089–1098. doi: 10.1038/s41593-019-0434-z

Nori, S., Okada, Y., Nishimura, S., Sasaki, T., Itakura, G., Kobayashi, Y., et al. (2015).), Long-term safety issues of iPSC-based cell therapy in a spinal cord injury model: Oncogenic transformation with epithelial-mesenchymal transition. *Stem Cell Rep.* 4, 360–373. doi: 10.1016/j.stemcr.2015.01.006

Noristani, H. N., Sabourin, J. C., Boukhaddaoui, H., Chan-Seng, E., Gerber, Y. N., and Perrin, F. E. (2016). Spinal cord injury induces astroglial conversion towards neuronal lineage. *Mol. Neurodegener.* 11:68. doi: 10.1186/s13024-016-0133-0

Norrmen, C., Figlia, G., Pfistner, P., Pereira, J. A., Bachofner, S., and Suter, U. (2018). mIORC1 Is Transiently Reactivated in Injured Nerves to Promote c-Jun Elevation and Schwann Cell Dedifferentiation. *J. Neurosci.* 38, 4811–4828. doi: 10.1523/JNEUROSCI.3619-17.2018

Orihuela, R., McPherson, C. A., and Harry, G. J. (2016). Microglial M1/M2 polarization and metabolic states. *Br. J. Pharmacol.* 173, 649–665. doi: 10.1111/bph.13139

Orr, M. B., and Gensel, J. C. (2018). Spinal Cord Injury Scarring and Inflammation: Therapies Targeting Glial and Inflammatory Responses. *Neurotherapeutics* 15, 541–553. doi: 10.1007/s13311-018-0631-6

O'Shea, T. M., Burda, J. E., and Sofroniew, M. V. (2017). Cell biology of spinal cord injury and repair. *J. Clin. Invest.* 127, 3259–3270. doi: 10.1172/JCI90608

Paez, P. M., and Lyons, D. A. (2020). Calcium Signaling in the Oligodendrocyte Lineage: Regulators and Consequences. *Annu. Rev. Neurosci.* 43, 163–186. doi: 10.1146/annurev-neuro-100719-093305

Parpura, V., Sekler, I., and Fern, R. (2016). Plasmalemmal and mitochondrial Na(+) -Ca(2+) exchange in neuroglia. *Glia* 64, 1646–1654. doi: 10.1002/glia.22975

Pearse, D. D., Sanchez, A. R., Pereira, F. C., Andrade, C. M., Puzis, R., Pressman, Y., et al. (2007). Transplantation of Schwann cells and/or olfactory ensheathing glia into the contused spinal cord: Survival, migration, axon association, and functional recovery. *Glia* 55, 976–1000. doi: 10.1002/glia.20490

Pechkovsky, D. V., Prasse, A., Kollert, F., Engel, K. M., Dentler, J., Luttmann, W., et al. (2010). Alternatively activated alveolar macrophages in pulmonary fibrosis-mediator production and intracellular signal transduction. *Clin. Immunol.* 137, 89–101. doi: 10.1016/j.clim.2010.06.017

Perdiguero, E. G., Klapproth, K., Schulz, C., Busch, K., Azzoni, E., Crozet, L., et al. (2015). Tissue-resident macrophages originate from yolk-sac-derived erythro-myeloid progenitors. *Nature* 518, 547–551. doi: 10.1038/nature13989

Perez Estrada, C., Covacu, R., Sankavaram, S. R., Svensson, M., and Brundin, L. (2014). Oxidative stress increases neurogenesis and oligodendrogenesis in adult neural progenitor cells. *Stem Cells Dev.* 23, 2311–2327. doi: 10.1089/scd.2013.0452

Pinto-Teixeira, F., and Desplan, C. (2014). Notch activity in neural progenitors coordinates cytokinesis and asymmetric differentiation. *Sci. Signal.* 7:e26. doi: 10.1126/scisignal.2005980

Plemel, J. R., Duncan, G., Chen, K. W., Shannon, C., Park, S., Sparling, J. S., et al. (2008). A graded forceps crush spinal cord injury model in mice. *J. Neurotrauma* 25, 350–370. doi: 10.1089/neu.2007.0426

Plemel, J. R., Wee Yong, V., and Stirling, D. P. (2014a). Immune modulatory therapies for spinal cord injury–past, present and future. *Exp. Neurol.* 258, 91–104. doi: 10.1016/j.expneurol.2014.01.025

Plemel, J. R., Keough, M. B., Duncan, G. J., Sparling, J. S., Yong, V. W., Stys, P. K., et al. (2014b). Remyelination after spinal cord injury: Is it a target for repair? *Progress Neurobiol.* 117, 54–72. doi: 10.1016/j.pneurobio.2014.02.006

Poplawski, G., Ishikawa, T., Brifault, C., Lee-Kubli, C., Regestam, R., Henry, K. W., et al. (2018). Schwann cells regulate sensory neuron gene expression before and after peripheral nerve injury. *Glia* 66, 1577–1590. doi: 10.1002/glia.23325

Powers, B. E., Lasiene, J., Plemel, J. R., Shupe, L., Perlmutter, S. I., Tetzlaff, W., et al. (2012). Axonal thinning and extensive remyelination without chronic demyelination in spinal injured rats. *J. Neurosci.* 32, 5120–5125. doi: 10.1523/JNEUROSCI.0002-12.2012

Powers, B. E., Sellers, D. L., Lovelett, E. A., Cheung, W., Aalami, S. P., Zapertov, N., et al. (2013). Remyelination reporter reveals prolonged refinement of spontaneously regenerated myelin. *Proc. Natl. Acad. Sci. U S A.* 110, 4075–4080. doi: 10.1073/pnas.1210293110

Prinz, M., and Priller, J. (2014). Microglia and brain macrophages in the molecular age: From origin to neuropsychiatric disease. *Nat. Rev. Neurosci.* 15, 300–312. doi: 10.1038/nrn3722

Rauch, M. F., Hynes, S. R., Bertram, J., Redmond, A., Robinson, R., Williams, C., et al. (2009). Engineering angiogenesis following spinal cord injury: A coculture of neural progenitor and endothelial cells in a degradable polymer implant leads to an increase in vessel density and formation of the blood-spinal cord barrier. *Eur. J. Neurosci.* 29, 132–145. doi: 10.1111/j.1460-9568.2008.06567.x

Reynolds, B. A., and Weiss, S. (1992). Generation of neurons and astrocytes from isolated cells of the adult mammalian central nervous system. *Science* 255, 1707–1710. doi: 10.1126/science.1553558

Rinwa, P., Calvo-Enrique, L., Zhang, M. D., Nyengaard, J. R., Karlsson, P., and Ernfors, P. (2021). Demise of nociceptive Schwann cells causes nerve retraction and pain hyperalgesia. *Pain* 162, 1816–1827. doi: 10.1097/j.pain.0000000000002169

Ritfeld, G. J., Nandoe Tewarie, R. D., Vajn, K., Rahiem, S. T., Hurtado, A., Wendell, D. F., et al. (2012). Bone marrow stromal cell-mediated tissue sparing enhances functional repair after spinal cord contusion in adult rats. *Cell Transplant.* 21, 1561–1575. doi: 10.3727/096368912X640484

Robel, S., Berninger, B., and Götz, M. (2011). The stem cell potential of glia: Lessons from reactive gliosis. *Nat. Rev. Neurosci.* 12, 88–104. doi: 10.1038/nrn2978

Rocha, L. A., Sousa, R. A., Learmonth, D. A., and Salgado, A. J. (2018). The Role of Biomaterials as Angiogenic Modulators of Spinal Cord Injury: Mimetics of the Spinal Cord, Cell and Angiogenic Factor Delivery Agents. *Front. Pharmacol.* 9:164. doi: 10.3389/fphar.2018.00164

Rouget, C. (1873). Memoire sur le developpement, la structure et les proprietes physiologiques des capillaries sanguins et lymphatiques. *Arch. Physiol. Norm. Path.* 5, 603–663.

Rustenhoven, J., Jansson, D., Smyth, L. C., and Dragunow, M. (2017). Brain Pericytes As Mediators of Neuroinflammation. *Trends Pharmacol. Sci.* 38, 291–304. doi: 10.1016/j.tips.2016.12.001

Sabelstrom, H., Stenudd, M., and Frisen, J. (2014). Neural stem cells in the adult spinal cord. *Exp. Neurol.* 260, 44–49. doi: 10.1016/j.expneurol.2013.01.026

Salzer, J. L. (2015). Schwann cell myelination. *Cold Spring Harb. Perspect. Biol.* 7:a020529. doi: 10.1101/cshperspect.a020529

Sankavaram, S. R., Hakim, R., Covacu, R., Frostell, A., Neumann, S., Svensson, M., et al. (2019). Adult Neural Progenitor Cells Transplanted into Spinal Cord Injury Differentiate into Oligodendrocytes, Enhance Myelination, and Contribute to Recovery. *Stem Cell Rep.* 12, 950–966. doi: 10.1016/j.stemcr.2019.03.013

Santos, G. S. P., Magno, L. A. V., Romano-Silva, M. A., Mintz, A., and Birbrair, A. (2019). Pericyte Plasticity in the Brain. *Neurosci. Bull.* 35, 551–560. doi: 10.1007/s12264-018-0296-5

Schackel, T., Kumar, P., Gunther, M., Liu, S., Brunner, M., Sandner, B., et al. (2019). Peptides and Astroglia Improve the Regenerative Capacity of Alginate Gels in the Injured Spinal Cord. *Tissue Eng. Part A* 25, 522–537. doi: 10.1089/ten.tea.2018.0082

Schucht, P., Raineteau, O., Schwab, M. E., and Fouad, K. (2002). Anatomical correlates of locomotor recovery following dorsal and ventral lesions of the rat spinal cord. *Exp. Neurol.* 176, 143–153. doi: 10.1006/exnr.2002.7909

Schulz, C., Gomez Perdiguero, E., Chorro, L., Szabo-Rogers, H., Cagnard, N., Kierdorf, K., et al. (2012). A lineage of myeloid cells independent of Myb and hematopoietic stem cells. *Science* 336, 86–90. doi: 10.1126/science.1219179

Schwab, M. E., and Strittmatter, S. M. (2014). Nogo limits neural plasticity and recovery from injury. *Curr. Opin. Neurobiol.* 27, 53–60. doi: 10.1016/j.conb.2014.02.011

Schweller, R. M., Wu, Z. J., Klitzman, B., and West, J. L. (2017). Stiffness of Protease Sensitive and Cell Adhesive PEG Hydrogels Promotes Neovascularization In Vivo. *Ann. Biomed. Eng.* 45, 1387–1398. doi: 10.1007/s10439-017-1822-8

Selvaraj, B. T., Frank, N., Bender, F. L. P., Asan, E., and Sendtner, M. (2012). Local axonal function of STAT3 rescues axon degeneration in the pmn model of motoneuron disease. *J. Cell Biol.* 199, 437–451. doi: 10.1083/jcb.201203109

Shechter, R., London, A., Varol, C., Raposo, C., Cusimano, M., Yovel, G., et al. (2009). Infiltrating blood-derived macrophages are vital cells playing an anti-inflammatory role in recovery from spinal cord injury in mice. *PLoS Med.* 6:e1000113. doi: 10.1371/journal.pmed.1000113

Sherman, D. L., and Brophy, P. J. (2005). Mechanisms of axon ensheathment and myelin growth. *Nat. Rev. Neurosci.* 6, 683–690. doi: 10.1038/nrn1743

Shi, H., Gong, Y., Qiang, L., Li, X., Zhang, S., Gao, J., et al. (2016). Derivation of Schwann cell precursors from neural crest cells resident in bone marrow for cell therapy to improve peripheral nerve regeneration. *Biomaterials* 89, 25–37. doi: 10.1016/j.biomaterials.2016.02.029

Silva, D., Sousa, R. A., and Salgado, A. J. (2021). Hydrogels as delivery systems for spinal cord injury regeneration. *Mater. Today Bio* 9:100093. doi: 10.1016/j.mtbio.2021.100093

Silver, J., and Miller, J. H. (2004). Regeneration beyond the glial scar. *Nat. Rev. Neurosci.* 5, 146–156. doi: 10.1038/nrn1326

Simons, M., and Nave, K. A. (2015). Oligodendrocytes: Myelination and Axonal Support. *Cold Spring Harb. Perspect. Biol.* 8:a020479. doi: 10.1101/cshperspect.a020479

Sofroniew, M. V., and Vinters, H. V. (2010). Astrocytes: Biology and pathology. *Acta Neuropathol.* 119, 7–35. doi: 10.1007/s00401-009-0619-8

Sokic, S., and Papavasiliou, G. (2012). Controlled Proteolytic Cleavage Site Presentation in Biomimetic PEGDA Hydrogels Enhances Neovascularization In Vitro. *Tissue Eng. Part A* 18, 2477–2486. doi: 10.1089/ten.tea.2012.0173

Sondell, M., Lundborg, G., and Kanje, M. (1999). Vascular endothelial growth factor has neurotrophic activity and stimulates axonal outgrowth, enhancing cell survival and Schwann cell proliferation in the peripheral nervous system. *J. Neurosci.* 19, 5731–5740. doi: 10.1523/JNEUROSCI.19-14-05731.1999

Soto, J., and Monje, P. V. (2017). Axon contact-driven Schwann cell dedifferentiation. *Glia* 65, 864–882. doi: 10.1002/glia.23131

Stadelmann, C., Timmler, S., Barrantes-Freer, A., and Simons, M. (2019). Myelin in the Central Nervous System: Structure, Function, and Pathology. *Physiol. Rev.* 99, 1381–1431. doi: 10.1152/physrev.00031.2018

Stassart, R. M., Fledrich, R., Velanac, V., Brinkmann, B. G., Schwab, M. H., Meijer, D., et al. (2013). A role for Schwann cell-derived neuregulin-1 in remyelination. *Nat. Neurosci.* 16, 48–54. doi: 10.1038/nn.3281

Stenudd, M., Sabelstrom, H., and Frisen, J. (2015). Role of Endogenous Neural Stem Cells in Spinal Cord Injury and Repair. *JAMA Neurol.* 72, 235–237. doi: 10.1001/jamaneurol.2014.2927

Sukhanov, N., Vainshtein, A., Eshed-Eisenbach, Y., and Peles, E. (2021). Differential Contribution of Cadm1-Cadm3 Cell Adhesion Molecules to Peripheral Myelinated Axons. *J. Neurosci.* 41, 1393–1400.

Suminaite, D., Lyons, D. A., and Livesey, M. R. (2019). Myelinated axon physiology and regulation of neural circuit function. *Glia* 67, 2050–2062. doi: 10.1002/glia.23665

Teichert, M., Milde, L., Annegret, H. W., Stanicek, L., Gengenbacher, N., Savant, S., et al. (2017). Pericyte-expressed Tie2 controls angiogenesis and vessel maturation. *Nat. Commun.* 8:16106. doi: 10.1038/ncomms16106

Tokumine, J., Kakinohana, O., Cizkova, D., Smith, D. W., and Marsala, M. (2003). Changes in spinal GDNF, BDNF, and NT-3 expression after transient spinal cord ischemia in the rat. *J. Neurosci. Res.* 74, 552–561. doi: 10.1002/jnr.10760

Torper, O., Pfisterer, U., Wolf, D. A., Pereira, M., Lau, S., Jakobsson, J., et al. (2013). Generation of induced neurons via direct conversion in vivo. *Proc. Natl. Acad. Sci. U S A.* 110, 7038–7043. doi: 10.1073/pnas.1303829110

Tran, A. P., Warren, P. M., and Silver, J. (2018). The Biology of Regeneration Failure and Success After Spinal Cord Injury. *Physiol. Rev.* 98, 881–917. doi: 10.1152/physrev.00017.2017

Tsai, H. H., Li, H., Fuentealba, L. C., Molofsky, A. V., Taveira-Marques, R., Zhuang, H., et al. (2012). Regional astrocyte allocation regulates CNS synaptogenesis and repair. *Science* 337, 358–362. doi: 10.1126/science.1222381

Tsai, R. Y., and McKay, R. D. (2000). Cell contact regulates fate choice by cortical stem cells. *J. Neurosci.* 20, 3725–3735. doi: 10.1523/JNEUROSCI.20-10-03725.2000

Tuszynski, M. H., Wang, Y., Graham, L., McHale, K., Gao, M., Wu, D., et al. (2014). Neural stem cells in models of spinal cord injury. *Exp. Neurol.* 261, 494–500. doi: 10.1016/j.expneurol.2014.07.011

Uchida, K., Baba, H., Maezawa, Y., Furukawa, S., Omiya, M., Kokubo, Y., et al. (2003). Increased expression of neurotrophins and their receptors in the mechanically compressed spinal cord of the spinal hyperostotic mouse (twy/twy). *Acta Neuropathol.* 106, 29–36. doi: 10.1007/s00401-003-0691-4

Vierbuchen, T., Ostermeier, A., Pang, Z. P., Kokubu, Y., Sudhof, T. C., and Wernig, M. (2010). Direct conversion of fibroblasts to functional neurons by defined factors. *Nature* 463, 1035–1041. doi: 10.1038/nature08797

Voccoli, V., Tonazzini, I., Signore, G., Caleo, M., and Cecchini, M. (2014). Role of extracellular calcium and mitochondrial oxygen species in psychosine-induced oligodendrocyte cell death. *Cell Death Dis.* 5:e1529. doi: 10.1038/cddis.2014.483

Wahl, A. S., Omlor, W., Rubio, J. C., Chen, J. L., Zheng, H., Schröter, A., et al. (2014). Neuronal repair. Asynchronous therapy restores motor control by rewiring of the rat corticospinal tract after stroke. *Science* 344, 1250–1255. doi: 10.1126/science.1253050

Wakeman, D. R., Redmond, D. E. Jr., Dodiya, H. B., Sladek, J. R. Jr., Leranth, C., Teng, Y. D., et al. (2014). Human neural stem cells survive long term in the midbrain of dopamine-depleted monkeys after GDNF overexpression and project neurites toward an appropriate target. *Stem Cells Transl. Med.* 3, 692–701. doi: 10.5966/sctm.2013-0208

Wang, J. H., Hung, C. H., and Young, T. H. (2006). Proliferation and differentiation of neural stem cells on lysine-alanine sequential polymer substrates. *Biomaterials* 27, 3441–3450. doi: 10.1016/j.biomaterials.2006.02.002

Wang, L. J., Zhang, R. P., and Li, J. D. (2014). Transplantation of neurotrophin-3-expressing bone mesenchymal stem cells improves recovery in a rat model of spinal cord injury. *Acta Neurochir.* 156, 1409–1418. doi: 10.1007/s00701-014-2089-6

Wang, L. L., Serrano, C., Zhong, X., Ma, S., Zou, Y., and Zhang, C. L. (2021). Revisiting astrocyte to neuron conversion with lineage tracing in vivo. *Cell* 184, 5465–5481.e16. doi: 10.1016/j.cell.2021.09.005

Wang, T., Fang, X., and Yin, Z. S. (2018). Endothelial progenitor cell-conditioned medium promotes angiogenesis and is neuroprotective after spinal cord injury. *Neural Regen. Res.* 13, 887–895. doi: 10.4103/1673-5374.232484

Weiss, S., Dunne, C., Hewson, J., Wohl, C., Wheatley, M., Peterson, A. C., et al. (1996). Multipotent CNS stem cells are present in the adult mammalian spinal cord and ventricular neuroaxis. *J. Neurosci.* 16, 7599–7609.

Widenfalk, J., Lundstromer, K., Jubran, M., Brene, S., and Olson, L. (2001). Neurotrophic factors and receptors in the immature and adult spinal cord after mechanical injury or kainic acid. *J. Neurosci.* 21, 3457–3475.

Williams, R. R., Henao, M., Pearse, D. D., and Bunge, M. B. (2015). Permissive Schwann cell graft/spinal cord interfaces for axon regeneration. *Cell Transplant.* 24, 115–131. doi: 10.3727/096368913X674657

Wiltbank, A. T., and Kucenas, S. (2021). Diversity and convergence within peripheral glia development. *Trends Neurosci.* 44, 930–932. doi: 10.1016/j.tins.2021.10.004

Wozniak, K. M., Vornov, J. J., Wu, Y., Liu, Y., Carozzi, V. A., Rodriguez-Menendez, V., et al. (2018). Peripheral Neuropathy Induced by Microtubule-Targeted Chemotherapies: Insights into Acute Injury and Long-term Recovery. *Cancer Res.* 78, 817–829. doi: 10.1158/0008-5472.CAN-17-1467

Xia, X. H., Li, C. H., Wang, Y., Deng, X. B., Ma, Y. Z., Ding, L., et al. (2020). Reprogrammed astrocytes display higher neurogenic competence, migration ability and cell death resistance than reprogrammed fibroblasts. *Transl. Neurodegener.* 9:6. doi: 10.1186/s40035-020-0184-6

Xu, J., Lacoske, M. H., and Theodorakis, E. A. (2014). Neurotrophic natural products: Chemistry and biology. *Angew. Chem. Int. Ed Engl.* 53, 956–987. doi: 10.1002/anie.201302268

Yalcin, B., and Monje, M. (2021). Microenvironmental interactions of oligodendroglial cells. *Dev. Cell* 56, 1821–1832. doi: 10.1016/j.devcel.2021.06.006

Yamaya, S., Ozawa, H., Kanno, H., Kishimoto, K. N., Sekiguchi, A., Tateda, S., et al. (2014). Low-energy extracorporeal shock wave therapy promotes vascular endothelial growth factor expression and improves locomotor recovery after spinal cord injury. *J. Neurosurg.* 121, 1514–1525. doi: 10.3171/2014.8.JNS132562

Yang, Y. M., Fan, Y. H., Zhang, H. P., Zhang, Q., Zhao, Y. N., Xiao, Z. F., et al. (2021). Small molecules combined with collagen hydrogel direct neurogenesis and migration of neural stem cells after spinal cord injury. *Biomaterials* 269:120479. doi: 10.1016/j.biomaterials.2020.120479

Yao, Y., Chen, Z. L., Norris, E. H., and Strickland, S. (2014). Astrocytic laminin regulates pericyte differentiation and maintains blood brain barrier integrity. *Nat. Commun.* 5:3413. doi: 10.1038/ncomms4413

Yasui, K., Hashizume, Y., Yoshida, M., Kameyama, T., and Sobue, G. (1999). Age-related morphologic changes of the central canal of the human spinal cord. *Acta Neuropathol.* 97, 253–259. doi: 10.1007/s004010050982

Ye, L. X., An, N. C., Huang, P., Li, D. H., Zheng, Z. L., Ji, H., et al. (2021). Exogenous platelet-derived growth factor improves neurovascular unit recovery after spinal cord injury. *Neural Regen. Res.* 16, 765–771. doi: 10.4103/1673-5374.295347

Yin, G., Lin, Y. F., Wang, P. L., Zhou, J., and Lin, H. D. (2022). Upregulated lncARAT in Schwann cells promotes axonal regeneration by recruiting and activating proregenerative macrophages. *Mol. Med.* 28:76. doi: 10.1186/s10020-022-00501-9

Yiu, G., and He, Z. (2006). Glial inhibition of CNS axon regeneration. *Nat. Rev. Neurosci.* 7, 617–627. doi: 10.1038/nrn1956

You, W. K., Yotsumoto, F., Sakimura, K., Adams, R. H., and Stallcup, W. B. (2014). NG2 proteoglycan promotes tumor vascularization via integrin-dependent effects on pericyte function. *Angiogenesis* 17, 61–76. doi: 10.1007/s10456-013-9378-1

Zhang, C., Zhang, C., Xu, Y., Li, C., Cao, Y., and Li, P. (2020). Exosomes derived from human placenta-derived mesenchymal stem cells improve neurologic function by promoting angiogenesis after spinal cord injury. *Neurosci. Lett.* 739:135399. doi: 10.1016/j.neulet.2020.135399

Zhang, H., Wu, F., Kong, X., Yang, J., Chen, H., Deng, L., et al. (2014). Nerve growth factor improves functional recovery by inhibiting endoplasmic reticulum stress-induced neuronal apoptosis in rats with spinal cord injury. *J. Transl. Med.* 12:130. doi: 10.1186/1479-5876-12-130

Zhang, S. X., Huang, F., Gates, M., and Holmberg, E. G. (2013). Role of endogenous Schwann cells in tissue repair after spinal cord injury. *Neural Regen. Res.* 8, 177–185.

Zhou, J., Wu, Y., Tang, Z., Zou, K., Chen, J., Lei, Z., et al. (2022). Alginate hydrogel cross-linked by Ca(2+) to promote spinal cord neural stem/progenitor cell differentiation and functional recovery after a spinal cord injuryhh. *Regen. Biomater.* 9:rbac057. doi: 10.1093/rb/rbac057

Zhou, T., Zheng, Y., Sun, L., Badea, S. R., Jin, Y., Liu, Y., et al. (2019). Microvascular endothelial cells engulf myelin debris and promote macrophage recruitment and fibrosis after neural injury. *Nat. Neurosci.* 22, 421–435. doi: 10.1038/s41593-018-0324-9

Zhou, X., He, X., and Ren, Y. (2014). Function of microglia and macrophages in secondary damage after spinal cord injury. *Neural Regen. Res.* 9, 1787–1795. doi: 10.4103/1673-5374.143423

Zhu, S., Chen, M., Ying, Y., Wu, Q., Huang, Z., Ni, W., et al. (2022). Versatile subtypes of pericytes and their roles in spinal cord injury repair, bone development and repair. *Bone Res.* 10:30. doi: 10.1038/s41413-022-00203-2

Ziegler, G., Grabher, P., Thompson, A., Altmann, D., Hupp, M., Ashburner, J., et al. (2018). Progressive neurodegeneration following spinal cord injury: Implications for clinical trials. *Neurology* 90, e1257–e1266. doi: 10.1212/WNL.0000000000005258

Zimmermann, K. W. (1923). Der feinere Bau der Blutcapillaren. *Z. Anat. Entwickl. Gesch* 68, 29–109 doi: 10.1007/978-3-642-92456-9

Zipser, C. M., Cragg, J. J., Guest, J. D., Fehlings, M. G., Jutzeler, C. R., Anderson, A. J., et al. (2022). Cell-based and stem-cell-based treatments for spinal cord injury: Evidence from clinical trials. *Lancet Neurol.* 21, 659–670. doi: 10.1016/S1474-4422(21)00464-6

Zirngibl, M., Assinck, P., Sizov, A., Caprariello, A. V., and Plemel, J. R. (2022). Oligodendrocyte death and myelin loss in the cuprizone model: An updated overview of the intrinsic and extrinsic causes of cuprizone demyelination. *Mol. Neurodegener.* 17:34. doi: 10.1186/s13024-022-00538-8

Ziu, E., and Mesfin, F. B. (2022). *Spinal Shock StatPearls, vol. Treasure Island (FL): StatPearls Publishing*. Florida: StatPearls Publishing LLC.

Zrzavy, T., Schwaiger, C., Wimmer, I., Berger, T., Bauer, J., Butovsky, O., et al. (2021). Acute and non-resolving inflammation associate with oxidative injury after human spinal cord injury. *Brain* 144, 144–161. doi: 10.1093/brain/awaa360

Frontiers in
Cellular Neuroscience

Leading research in cellular mechanisms underlying brain function and development

Part of the world's most cited neuroscience journal series that advances our understanding of the cellular mechanisms underlying cell function in the nervous system across all species.

Discover the latest Research Topics

See more →

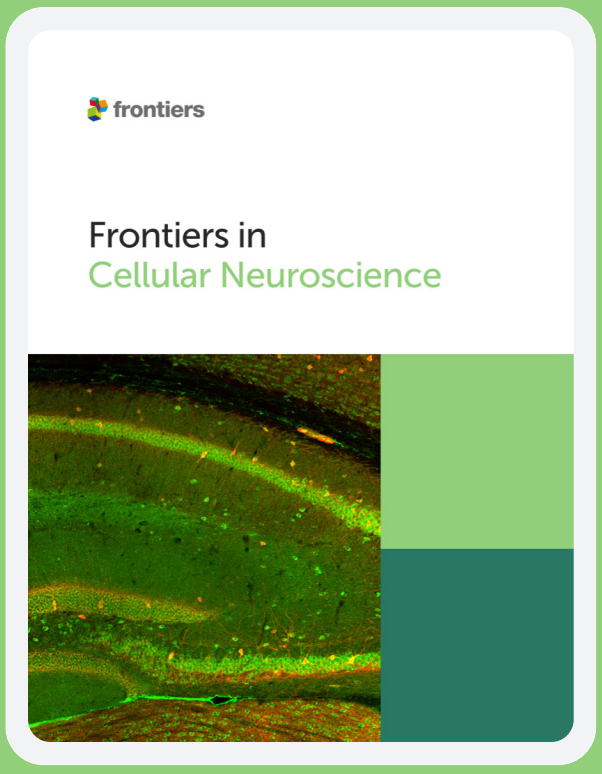

Frontiers

Avenue du Tribunal-Fédéral 34
1005 Lausanne, Switzerland
frontiersin.org

Contact us

+41 (0)21 510 17 00
frontiersin.org/about/contact